EFFICIENT, SUSTAINABLE, AND FULLY

COMPREHENSIVE SMART CITIES

II IBERO-AMERICAN CONGRESS OF SMART CITIES (ICSC-CITIES 2019)

EFFICIENT, SUSTAINABLE, AND FULLY

COMPREHENSIVE SMART CITIES

II IBERO-AMERICAN CONGRESS OF SMART CITIES (ICSC-CITIES 2019)

Soria, Spain
October 7th to 9th, 2019

Proceedings

CITIES
CIUDADES INTELIGENTES TOTALMENTE INTEGRALES, EFICIENTES Y SOSTENIBLES

PROGRAMA IBEROAMERICANO
CYTED
CIENCIA Y TECNOLOGÍA PARA EL DESARROLLO

UVa

VIGILADA MINEDUCACIÓN
USC
UNIVERSIDAD SANTIAGO DE CALI
EDITORIAL

Zúñiga Cañón, Claudia Liliana
Efficient, Sustainable, and Fully Comprehensive Smart Cities / Claudia Liliana Zuñiga Cañón, Luis Hernández Callejo. -- Cali : Universidad Santiago de Cali, 2020.
889 páginas : fotos ; 24 cm.
Incluye índice de contenido.
ISBN 978-958-5583-78-8
1. Generación de energía fotovoltaica 2. Producción de energía eléctrica 3. Ingeniería sostenible 4. Convertidores de energía solar
5. Arquitectura ecológica I. Hernández Callejo, Luis, autor II. Tí
621.31 cd 21 ed.
A1660683

CEP-Banco de la República-Biblioteca Luis Ángel Arango

Efficient, Sustainable, and Fully Comprehensive Smart Cities. II Ibero-American Congress of Smart Cities (ICSC-CITIES 2019).

© 2019 Universidad Santiago de Cali.
©Universidad de Valladolid, España.
© I Ibero-American Congress of Smart Cities (ICSC-CITIES 2018).

© Conference Chairs: Vicente Leite, Luis Hernández Callejo, Javier Prieto, Claudia Liliana Zuñiga Cañón, Ângela Ferreira, Sergio Nesmachnow y Fabián Castillo Peña.
1a. Edición.
Cali, Colombia - 2019.

ISBN (Libro digital): 978-958-5583-78-8

Fondo Editorial University Press Team

Carlos Andrés Pérez Galindo
Rector
Rosa del Pilar Cogua Romero
Directora General de Investigaciones
Edward Javier Ordóñez
Editor en Jefe

Proceso de arbitraje doble ciego:
"Double blind" peer-review

Recepción/Submission:
Agosto (August) de 2019

Evaluación de contenidos/ Peer-review outcome:
Septiembre (September) de 2019

Correcciones de autor/ Improved version submission:
Noviembre (November) de 2019

Aprobación/Acceptance:
Febrero (February) de 2020

Diseño de portada

Juan Diego Tovar Cardenas
Universidad Santiago de Cali
Tel. 5183000 - Ext. 9130
Cel. 301 439 7925

Distribución y Comercialización

Universidad Santiago de Cali
Publicaciones
Calle 5 No. 62 - 00
publica@usc.edu.co
Tel: 518 3000, Ext. 323 - 324 - 414

La editorial de la Universidad Santiago de Cali se adhiere a la filosofía de acceso abierto. Este libro está licenciado bajo los términos de la Atribución 4.0 de Creative Commons (http://creativecommons.org/licenses/by/4.0/), que permite el uso, el intercambio, adaptación, distribución y reproducción en cualquier medio o formato, siempre y cuando se dé crédito al autor o autores originales y a la fuente https://creativecommons.org/licenses/by/4.0/

About The Conference

The infrastructures of the cities are changing, and this evolution is the result of the need for energy, water and the reduction of CO_2 emissions. **Smart City** is a consequence of the need to achieve efficient and sustainable cities.

Being a strategic issue that brings new challenges, the organizers request participation in the I**I Ibero-American Congress of Smart Cities (ICSC-CITIES 2019)**, which will be a discussion forum that will create synergies among different research groups to favor the development of Smart Cities, and contribute to their knowledge and integration in different scenarios, their possible development and the strategies to address them.

ICSC-CITIES 2019 will take place on October 7-9, 2019 in the Auditorium of University of Valladolid (UVa), Duques de Soria Campus (Soria, Spain), with the sponsorship of the **Ibero-American Program of Science and Technology for Development (CYTED)**.

Articles written in English submitted to the conference will be considered for publication in the **conference proceedings at Springer Communications in Computer and Information Science (CCIS)**. In addition, authors of selected articles will be invited to expand their contribution for publication in a **Special Issue of the Journal of the University of Antioquia** (indexed in Scopus Q3 and Web of Science ESCI), and in a **Special Issue of the Journal of the Smart Cities (MDPI)**.

Welcome from the local committee

We are pleased to welcome you to the **II Ibero-American Congress of Smart Cities (ICSC-CITIES 2019)**. The forum for the latest achievements in *Smart Cities* is visiting this year the town of Soria (Spain).

The technical program has been carefully designed to offer a fresh and balanced selection of advances and results in topics, encouraging the presence of fresh and interdisciplinary topics. The proposals for the conference should be based on the subject areas that have been defined by the Conference's Committee of Experts:

- Energetic Efficiency and Sustainability.
- Infrastructures, Energy and the Environment.
- Mobility and IoT.
- Governance and Citizenship.

In addition, an attractive social program is proposed among a sample of selected interesting places. The Welcome Reception will take place at Auditorium of University of Valladolid (UVa), Duques de Soria Campus (Soria, Spain) on Monday 7th. Besides, the Gala Dinner will be at the Hotel Leonor Mirón on Monday 7th.

We are really thankful to all members of the Organizing Committee for their continuous help to organize every detail of this outstanding conference. Finally, we are in debt to the more than 111 members of Technical Program Committee (TPC) for their hard and anonymous work to care for the highest quality of papers and splendid coordination of TPC Chairs.

Sincerely hoping you enjoy ICSC-CITIES 2019 in Soria and this experience to last in your memory for a long time, receive our warmest welcome.

Dr. Luis Hernández Callejo
Dra. Claudia Zúñiga Cañón
Dr. Sergio Nesmachnow
Dr. Vicente Leite
Dra. Ângela Ferreira
Dr. Javier Prieto
Dr. Fabián Castillo Peña

UVa

EIFAB
Escuela de Ingeniería de la Industria Forestal, Agronómica y de la Bioenergía

CITIES
CIUDADES INTELIGENTES TOTALMENTE INTEGRALES, EFICIENTES Y SOSTENIBLES

PROGRAMA IBEROAMERICANO
CYTED
CIENCIA Y TECNOLOGÍA PARA EL DESARROLLO

Supporting companies

CI-RTI 30

UNIVERSIDAD LIBRE
SCIENTIA FONS LIBERTATIS
COLOMBIA

USC
UNIVERSIDAD SANTIAGO DE CALI

Excmo. Ayuntamiento de Almazán

GrantThornton

Diputación de Soria

AYUNTAMIENTO Soria

ipb INSTITUTO POLITÉCNICO DE BRAGANÇA

UNIVERSIDAD DE LA REPÚBLICA URUGUAY

Conference Chairs

Dr. Luis Hernández Callejo – Universidad de Valladolid (Spain)

Dr. Vicente Leite – Instituto Politécnico de Braganza (Portugal)

Dra. Claudia Liliana Zuñiga Cañón – Universidad Santiago de Cali (Colombia)

Dr. Javier Prieto – Universidad de Salamanca (España)

Dr. Sergio Nesmachnow – Universidad de la República (Uruguay)

Dra. Ângela Ferreira – Instituto Politécnico de Braganza (Portugal)

Dr. Fabián Castillo Peña – Universidad Libre Seccional Cali (Colombia)

Organizing Committee

Adriana Correa - Universidad de Valladolid (Spain)

Ángel L. Zorita - Universidad de Valladolid (Spain)

Begoña Asenjo Martín - Universidad de Valladolid (Spain)

Daniel Moríñigo - Universidad de Valladolid (Spain)

Daphne Hermosilla - Universidad de Valladolid (Spain)

Epifanio Díez - Universidad de Valladolid (Spain)

Ignacio de Godos - Universidad de Valladolid (Spain)

Lilian J. Obregón - Universidad de Valladolid (Spain)

Luis Hernández Callejo - Universidad de Valladolid (Spain)

Oscar Duque - Universidad de Valladolid (Spain)

Pablo Jiménez Rodríguez - Universidad de Valladolid (Spain)

Teodoro Calonge - Universidad de Valladolid (Spain)

Víctor Alonso Gómez - Universidad de Valladolid (Spain)

Technical Program Committee

Adolfo Ruelas
Universidad Autónoma de Baja California (México)

Adriana Correa Guimaraes
Universidad de Valladolid (Spain)

Albert Rego
Universitat Politècnica de València (Spain)

Alberto López
Diputación de Ávila (Spain)

Alejandro paz Parra
Pontificia Universidad Javeriana, Cali (Colombia)

Alejandro Otero
Universidad de Buenos Aires (Argentina)

Alfredo Cristobal
Universidad Veracruzana (México)

Alexis Acuña
Universidad Autónoma de Baja California (México)

Ana Ruíz
Universidad de San Jorge (Spain)

Andrei Tchernykh
CICESE Research Center (México)

Andrés Adolfo Navarro Newball
Pontificia Universidad Javeriana, Cali (Colombia)

Andrés Felipe Fuentes
Pontificia Universidad Javeriana, Cali (Colombia)

Ángel Luis Zorita Lamadrid
Universidad de Valladolid (Spain)

Ángel M. García Pedrero
Universidad de Valladolid (Spain)

Ângela Ferreira
Polytechnical Institute of Bragança (Portugal)

Antonio Javier García Sánchez
Universidad Politécnica de Cartagena (Spain)

Beethoven Zuleta
Universidad de Valladolid (Spain)

Carlos Meza Benavides
Costa Rica Institute of Technology (Costa Rica)

Carlos A. Méndez
INTEC (UNL-CONICET) (Argentina)

Claudia L. Zúñiga Cañón
Universidad Santiago de Cali (Colombia)

Claudia P. Murcia Zorrilla
Universidad Cooperativa de Colombia (Colombia)

Cleonilson Protasio
Federal University of Paraíba (Brasil)

Cristina Sáez Blázquez
Universidad de Salamanca (Spain)

Daniel Moríñigo Sotelo
Universidad de Valladolid (Spain)

Daphne Hermosilla
Universidad de Valladolid (Spain)

David de la Vega
Universidad del País Vasco (Spain)

Diego Loaiza
Universidad Santiago de Cali (Colombia)

Diego Vilches Antao
Universidad Nacional de la Plata (Argentina)

Diego González Aguilera
Universidad de Salamanca (Spain)

Diego Alberto Godoy
Universidad Gastón Dachary (Argentina)

Diego Fernando Marín
Universidad Libre, Cali (Colombia)

Diego Gabriel Rossit
Universidad Nacional del Sur (Argentina)

Edgardo Aníbal
Universidad Gastón Dachary (Argentina)

Eduardo Omar Sosa
Universidad Gastón Dachary (Argentina)

Esteban Mocskos
Universidad de Buenos Aires (Argentina)

Emmanuel Luján
Universidad de Buenos Aires (Argentina)

Estefanía Alfaro
Universidad del Valle (Colombia)

Euler Cássio Tavares de Macedo
Federal University of Paraíba (Brasil)

Fabián Castillo Peña
Universidad Libre, Cali (Colombia)

Fabián Favret
Universidad Gastón Dachary (Argentina)

Fabricio Carvalho
Federal University of Paraíba (Brasil)

Félix Santos García
CEETA (Cuba)

Fernando Vélez Varela
Universidad Libre, Cali (Colombia)

Francisco Valbuena
Universidad de Valladolid (Spain)

Francisco David Moya
Universidad Santiago de Cali (Colombia)

Francisco Javier Finat Codes
Universidad de Valladolid (Spain)

Fredy Vélez
CARTIF (Spain)

Gregorio López
Universidad Politécnica de Madrid (Spain)

Guadalupe Ramos Truchero
Universidad de Valladolid (Spain)

Hortensia Amarís
Universidad Carlos III de Madrid (Spain)

Ignacio Martín Nieto
Universidad de Salamanca (Spain)

Itziar Angulo
University of the Basque Country (Spain)

Iván García Magariño
Universidad de Zaragoza (Spain)

Jaime Lloret Mauri
Universitat Politècnica de València (Spain)

Javier Prieto
Universidad de Salamanca (Spain)

Javier Rocher
Universitat Politècnica de València (Spain)

Jesús Vegas
Universidad de Valladolid (Spain)

Jorge Mírez
Universidad Nacional de Ingeniería (Perú)

Jorge J. Gómez Sanz
Universidad Complutense de Madrid (Spain)

José Aguerre
Universidad de la República (Uruguay)

José Antonio Ferrer
CIEMAT (Spain)

José Ramón Aira Zunzunegui
Universidad de Valladolid (Spain)

Juan Espinoza
Universidad de Cuenca (Ecuador)

Juan Mauricio
Federal University of Paraíba (Brasil)

Juan Peralta
Escuela Superior Politécnica del Litoral (Ecuador)

Juan De Dios Benítez
Universidad Gastón Dachary (Argentina)

Laura Fava
LINTI (Argentina)

Liliana Gutierrez Rancruel
Universidad Cooperativa de Colombia (Colombia)

Lorena Parra
Universitat Politècnica de València (Spain)

Luis Hernández Callejo
Universidad de Valladolid (Spain)

Luis Marrone
Universidad Nacional de la Plata (Argentina)

Luis Cano
CIEMAT (Spain)

Luis Claudio García Santander
Universidad de Concepción (Chile)

Luis Manuel Navas Gracia
Universidad de Valladolid (Spain)

Luisena Fernández
Universidad del Zulia (Venezuela)

Luiz Angelo Steffenel
Université de Reims Champagne-Ardenne (France)

Manuel González
Universidad de Valladolid (Spain)

Manuel Álvarez
Universidad Politécnica de Madrid (Spain)

Marcia Eugenio Gozalbo
Universidad de Valladolid (Spain)

María del Rosario Heras Celemín
CIEMAT (Spain)

María Pilar Lisbona
Universidad de Valladolid (Spain)

Miguel Rodelgo Lacruz
CUD-ENM (Spain)

Mónica Alonso
Universidad Carlos III de Madrid (Spain)

Mónica Montoya
CIDET (Colombia)

Nicolás Velasquez
Universidad Autónoma de Baja California (México)

Noelia Uribe Pérez
TECNALIA (Spain)

Noelia Soledad Pinto
Universidad Tecnológica Nacional (Argentina)

Oscar Duque Pérez
Universidad de Valladolid (Spain)

Oscar Izquierdo
CIEMAT (Spain)

Oscar Carpintero
Universidad de Valladolid (Spain)

Pablo Monzón
Universidad de la República (Uruguay)

Francisco Rodríguez
Föra Förest Technologies (Spain)

Paulo Godim
Universidad de Brasil (Brasil)

Pedro Luis González Ramírez
Universidad Central (Colombia)

Ponciano Jorge Escamilla Ambrosio
CIC-IPN (México)

Rafael Asorey Cacheda
CUD-ENM (Spain)

Renzo Massobrio
Universidad de la República (Uruguay)

Ricardo Quijano
Universidad Nacional de Colombia (Colombia)

Roberto Best Brown
Universidad Nacional Autónoma de México (México)

Roberto Villafáfila Robles
Universidad Politècnica de Catalunya (Spain)

Roberto Getino De La Mano
EREN (Spain)

Ronney Arismel Mancebo
CEFET/RJ (Brasil)

Sandra Sendra
University of Granada (Spain)

Santiago Egea Gómez
Universidad de Valladolid (Spain)

Santiago Iturriaga
Universidad de la República (Uruguay)

Santiago Hernán Bareiro
Universidad Gastón Dachary (Argentina)

Sara Gallardo Saavedra
Universidad de Valladolid (Spain)

Sergio Nesmachnow
Universidad de la República (Uruguay)

Susana Del Pozo
Universidad de Salamanca (Spain)

Teodoro Calonge
Universidad de Valladolid (Spain)

Vanessa Gimaraes
CEFET/RJ (Brasil)

Vicente Leite
Polytechnical Institute of Bragança (Portugal)

Vicente Canals
Universidad de las Islas Baleares (Spain)

Víctor Alonso Gómez
Universidad de Valladolid (Spain)

Yuri Percy Molina
Federal University of Paraíba (Brasil)

Companies and Other Initiatives

During the day of October 7-8, the congress has invited experts from the sector of *Smart Cities* to organize a sectoral debate.

This debate will be composed of prestigious companies in the sector, Public Administration, as well as specialized consultants. The aim is to give a business point of view around *Smart Cities*.

Members of the debate:

- D. Francisco Valbuena, Arquitecto Director de Unidad Técnica de Arquitectura de la Universidad de Valladolid (España).
- Dª. Rosario Chávez, Concejala de Innovación, Desarrollo Económico, Empleo y Comercio Ayuntamiento de Valladolid (España).
- D. Carlos González, Grant Thornton.
- Dr. Jorge J. Gómez-Sanz, Vicerrector de Tecnología y Sostenibilidad Universidad Complutense de Madrid (España).
- D. Enrique Morgades, Secretario Técnico de FutuRed (España).
- D. Diego Edinson Sánchez, Centro de Innovación y Desarrollo Tecnológico (Colombia).
- Dra. Mª Rosario Heras Celemín, CIEMAT (España).
- Dª. Mar Garcia, Grant Thornton (España).
- D. Alejandro Jimenez Benitez, Acciona (España).
- D. Miguel Ángel Pérez, ZIGOR (España).
- D. Gonzalo Fernández, VODANE (España).
- D. Luis Miguel Diez, Elivere Innovación SL. (España).

Technical Program

CITIES CIUDADES INTELIGENTES TOTALMENTE INTEGRALES, EFICIENTES Y SOSTENIBLES

CYTED PROGRAMA IBEROAMERICANO DE CIENCIA Y TECNOLOGÍA PARA EL DESARROLLO

II Ibero-American Congress of Smart Cities (ICSC-CITIES2019)

Soria, Spain, October 7-9, 2019

	Monday - 07/10/2019	Tuesday - 08/10/2019	Wednesday - 09/10/2019
09:00 - 09:30	**Registration ICSC-CITIES2019**		
09:30 - 10:00	**Opening Session**	**Registration ICSC-CITIES2019**	**Registration ICSC-CITIES2019**
10:00 - 11:30	**Special Session** Governance and Citizenship	**Special Session** Tech Day Smart Utilities	**Track 2** Mobility and IoT
11:30 - 12:00	Coffee break and Poster Session	Coffee break and Poster Session	Coffee break and Poster Session
12:00 - 14:00	**Track 1** Infrastructures, Energy and the Environment	**Track 3** Energy Efficiency and Sustainability	**Track 3** Energy Efficiency and Sustainability
14:00 - 15:00	Lunch and Poster Session	Lunch and Poster Session	Lunch and Poster Session
15:00 - 17:00	**Track 2** Mobility and IoT	**Track 1** Infrastructures, Energy and the Environment	**Closing Session**

Social Program

Monday, 7th October

In these dates, there are numerous activities that the city of Soria celebrates. In addition, Romanesque churches can be visited at any time of the year.

The train travels the main points of interest of the Soria's culture, being able to visit the main jewels of the classic Romanesque that exist in Spain: http://www.trenturisticosoria.com

Visit the Romanesque art of the city of Soria






Gala Dinner

The gala dinner will take place at Hotel Leonor Mirón. Attendees will have the opportunity to enjoy some of Soria's best gastronomy.

After the Gala Dinner the attendees will be invited to have a drink and share a pleasant moment, enjoying Soria's night atmosphere.

Hotel Leonor Mirón
Paseo el Mirón, 10, 42005 Soria




Coordination

Meeting: CITIES (CYTED)

CYTED is the Ibero-American Program of Science and Technology for Development, created by the governments of Ibero-American countries to promote cooperation on issues of science, technology and innovation for the harmonious development of Ibero-America.

CYTED achieves its objectives through different financing instruments that mobilize Ibero-American entrepreneurs, researchers and experts and allow them to be trained and generate joint research, development and innovation projects. Thus, the countries that make up the CYTED Program are able to keep up to date with the most recent advances and scientific-technological developments.

Since its creation in 1984, more than 28,000 Ibero-American businessmen, researchers and experts in priority areas of knowledge have participated in the Program.

The results of the Programme include the generation of strategic R&D projects in which companies and experts participate, who from the CYTED cooperation platform have access to important international funds.

The **Thematic Networks** are **clusters of research and development** (R&D) formed by public or private entities and **corporations** from the member countries of the CYTED Programme, whose scientific or technological activities are related within a common area of interest and included in one of the Programme Areas. Their main objective is the exchange of knowledge between R&D groups and the strengthening of cooperation as a work method.

Dr. Luis Hernández Callejo, Professor/Researcher at the University of Valladolid (UVa), coordinates a CYTED Thematic Network called CITIES (CIUDADES INTELIGENTES TOTALMENTE INTEGRALES, EFICIENTES Y SOSTENIBLES).

The objectives of CITIES are:

- To strengthen the technical and professional training of research centres and participating companies in the cities of the future and, therefore, the improvement of the quality of life and the environment of Latin American citizens.
- Promote new investment opportunities in the sectors covered by CITIES that lead to economic diversification and commercial openness of their companies through the identification of barriers and competitive advantages.
- To promote the environmental and economic benefits produced by the incorporation of CITIES among members of the public administration, group of architects, builders, financing institutions, companies, research centres, society in general, etc., by means of the realization of specific activities directed to these groups in a clear bet for the sustainable development of the cities.

- Search for strengths and weaknesses among the participating entities to consolidate a continuous and active exchange of scientific knowledge that allows the development of an action procedure in the cities of Iberoamerica, as well as the formulation of future R&D projects that will lead to consolidate a future line of work around CITIES.
- To promote the meeting of the different researchers who make up the research groups in the annual conferences/congresses, in order to identify potential implementation projects in the following areas: Intelligent Infrastructure (II), solutions for the monitoring and conservation of cultural and environmental heritage, applications aimed at efficient and sustainable mobility, promotion of renewable generation sources and energy efficiency in the new IC, development of solutions for IC management based on IoT.
- Disseminate the results acquired during the project in the usual frameworks (congresses, seminars, conferences, etc.).
- Carrying out specific courses in the different areas of the project: Climate change and the environment, Integral Urban Development, Taxation and governability.
- Encourage networking, to address issues common to Latin American countries in the scope of the project. In the same way, this network will serve to identify new partners participating in the R&D sector, commercial, productive and institutional. End users (public administrations and companies) will participate.

The two main activities of CITIES in 2019 are the development of the II Ibero-American Congress (ICSC-CITIES 2019) and the holding of the coordination meeting. This meeting will be held on the 7th, 8th and 9th of October, coinciding with the congress event. In the meeting will be reviewed the activities carried out so far, and the 2020 activities will be proposed.

Table of Contents

Monday: 10/07/2019

Track 1: Infrastructures, Energy and the Environment

Track 2: Mobility and IoT

Tuesday: 10/08/2019

Track 3: Energy Efficiency and Sustainability

Track 1: Infrastructures, Energy and the Environment

Wednesday: 10/09/2019

Track 2: Mobility and IoT

Track 3: Energy Efficiency and Sustainability

Poster Session

Assessment of demand response programs by using self-organizing maps and elasticity of substitution to reduce cost of energy supply in the wholesale electricity market. Máximo Alberto Domínguez Garabitos, René Báez Santana, Victor Ocaña Guevara and Félix Santos García

Eficiencia energética en edificación. Opciones para el gobierno local de ámbito forestal. Un marco conceptual. Miguel Broto-Cartagena, Epifanio Díez and Luis Bonilla

Arquitectura de un Sistema de Telemonitorización para Adultos Mayores en salud y movilidad de su silla de ruedas apoyada en Tecnologías de Internet de las cosas (IoT). RobotUp_IoT. Nancy E. Ochoa Guevara, Juan S. Sanchez Arteta, David A. Almesiga Riaño, Diego A. Sarmiento Vargas, Bryan E. Tunarosa Naranjo, Oscar Daniel Diaz Castillo and Javier A. Rios Suarez

Monthly meteorological data interpolation variability. Blas Manuel Franco, Luis Hernández-Callejo and Luis Manuel Navas-Gracia

Metodología de planificación energética territorial (PET) en Suiza; caso de aplicación. Javier Trespalacios, Claudia Blanquicett and Paulo Carrillo

Clasificación de perfiles de comportamientos de clientes residenciales a partir de información aportada por medidores inteligentes. Luis GarcÍa-Santander, Lester Marrero, Guillermo Zarate, Fernando Ulloa and Dante Carrizo

Monitorización Energética y Medioambiental en la Iniciativa de Campus Sostenible del Proyecto RES2+U. Sonia Solera Cotanilla, Manuel Alvarez-Campana and Gregorio López

Energía eólica implementada en Metro – Caso de Estudio: Trenes en Línea 1 del Metro de Lima. Jorge Luis Mírez Tarrillo and Estefani Gabriela Mendoza Guerra

Hacia una solución tecnológica basada en realidad virtual para el entrenamiento del personal de salud en la atención de víctimas de un evento sísmico. Lina M. Salguero, Diego F. Loaiza, Mérida Rodríguez-López, Juan C. Martínez, Laureano Qunitero, Juan F. Millán and Andrés A. Navarro-Newball

Energy management platform based on a smart microgrid of distributed generation with renewables. Miguel Euclides Aybar Mejía, Lesyani León Viltre, Felix Santos, Iosvani López and Atilio De-Frías

Measurement of the environmental impact determined in the Goods, Networks and Services of an ICT infrastructure. Fernando Velez Varela, Diego Fernando Marin Lozano and Fabian Castillo Peña

Estudio del Potencial de Contribución 2018 – 2022 de la energía eólica en el cambio climático. Jorge Luis Mírez Tarrillo and Victoria Matos

Comparación entre diferentes estudios de caracterización de RSU para aplicación de tecnologías WTE: Metodolo-gía, y variación estadística de resultados. Alejandro Paz and Gildardo Chavez

Aerogeneradores Urbanos integrados a Transporte Masivo - Un caso de estudio: Tramo Estaciones Honorio Delgado - El Milagro del Metropolitano, Lima. Jorge Luis Mírez Tarrillo and Jhonatan Tafur Llaja

Autonomous navigation of unmanned aerial vehicles using markers. Santiago Díaz, Bruno Garate, Sergio Nesmachnow and Santiago Iturriaga

Building Energy Management Based on Predictive Control for Energy Efficient in the Dominican Republic. Deyslen Mariano-Hernández, Félix Santos García, Iosvani Lopez, Luis Hernández-Callejo and Lesyani León Viltre

Ecosistema Territorial Tecnológico estructurante de gobernanza y desarrollo integrador. Fabián Zuleta and Santiago Vásquez

Cómo la tecnología 5G cambiará las ciuda-des y la gestión de los servicios públicos. Gonzalo Fernández Espeso and Jose Manuel Laustalet

Towards a Visual Grammar for IoT Systems Representation and their Cybersecurity Issues. Alain Gómez-Cabrera, Ponciano Jorge Escamilla Ambrosio, Jassim Happa and Abraham Rodríguez-Mota

Communications for the Smart City - An updated review of technologies and future trends within the framework of IoT. Noelia Uribe-Perez, Luis Hernandez-Callejo and David de la Vega

General purpose I-V tester developed to measure a wide range of photovoltaic systems

Bhishma Hernández-Martínez[1[0000-0001-5577-209X]], Sara Gallardo-Saavedra[1[0000-0002-2834-5591]], Luís Hernández-Callejo[1[0000-0002-8822-2948]], Víctor Alonso-Gómez[1[000-0001-5107-4892]] and José Ignacio Morales-Aragonés[1[0000-0002-9163-9357]]

[1] University of Valladolid, Campus Universitario Duques de Soria, Soria (Spain):
bhishma.hernandez@alumnos.uva.es, B.H-M.;
sara.gallardo@uva.es, S.G-S.;
luis.hernandez.callejo@uva.es, L.H-C.;
victor.alonso.gomez@uva.es, V.A-G.;
ziguratt@coit.es, J.I.M-A.

Abstract. Within this paper it is proposed the design and development of an instrument with extended capabilities for photovoltaic (PV) devices I/V tracing. Commercial instruments that measure I-V curves from PV devices are suitable for a wide range of applications. However, more specific research and measurements require developing customized equipment. Custom-made development provides flexibility, and allows to implement tailored algorithms and to have accurate control of obtained information. Full control offers better flexibility for testing and extends the measurement possibilities. Designed I-V tester is capable to measure low voltages and manages very low resistance load to provide short circuit current values with voltages close to zero.

Keywords: I-V tracer, I-V tester, measurement instrument, Arduino.

1 Introduction

To date, cities have been consumers of resources (energy, water, food, etc.), but recently, under the concept of Smart City (SC), cities begin to be resource producers. In the case of energy, the SC is integrating renewable generation sources into existing infrastructure [1-2].

In recent years, renewable systems are being integrated into electrical grids in a massive way. Specifically, renewable technology with the greatest boom and interest is PVs, and it is likely that the next few years will continue to be the most installed [3]. This trend is followed by cities, which will integrate PV technology into their spaces [4-5].

But PV systems present problems. These problems can be caused in manufacturing, but most of them are caused by the operation of the system. As shown in [6], numerous problems occurred during the operation of the plant, so maintenance work is critical.

The detection of failures in PV systems is a very broad topic [7-8]. For example, it is possible to use thermographic images for fault detection [9], or electroluminescence

images [10]. However, the classic detection of loss of efficiency in a PV module is by means of instruments such as I-V plotter [11-12].
Commercial I-V devices have some limitations, for example, they are not able to operate with very low currents and voltages. Therefore, these devices cannot make partial measurements within a module (set of cells embraced by a bypass diode) or a single cell. In this sense, this work presents the electronic architecture and software to have an I-V device capable of covering the lack of commercial devices.

2 Methodology and resources

This section explains the current commercial I-V testers, their limitations found on field measurements and how developed I-V tester overcome those limitations. At the end of the chapter, it is presented some measurements that cannot be performed with commercial I-V tracers.

2.1 Commercial I-V Tester

PV testers allow field measurements of I-V Curve and determination of the main characteristic parameters both of a single module and of strings of modules for PV installations up to a maximum of 1500V and 15A. Some of them, manages an internal database of the modules, which can be updated at any time by the user and comparison between the measured data with the rated values allows immediately evaluating whether the string or the module fulfills the efficiency parameters declared by the manufacturer. I-V Curve can be adjusted also by decentralizing irradiation and temperature measurements by using an optional remote unit to measure reference temperature and irradiation. The display, once finishes the I-V Curve measurement, shows the measured parameters and compare it with the specifications declared by the PV module manufacturer.

2.2 Commercial I-V tester. Specifications.

Table 1 represents some of the main useful parameters measured by PV testers. The majority of PV modules could be analyzed accordingly.

Symbol	Description	Range	Resolution
Pmax	Maximum nominal power of a module	50 - 4800W	1W
Voc	Open circuit voltage	15 – 99.99V 100-320.0V	0.01V 0.1V
Vmpp	Voltage on point of maximum power	15 – 99.99V 100-320.0V	0.01V 0.1V
Isc	Short circuit current	0.5 - 15A	0.01A
Impp	Current on point of maximum power	0.5 - 15A	0.01A

Table 1 Typical parameters of PV modules tester.

Information provided by PV tester corresponds with raw information. Information measured is used to be analyzed to obtain further conclusions on PV research. Fig. 1 PV module measured with PV tester Fig. 1 represents information obtained from the

standard PV module measured on a field installation. Full I-V curve is shown, and short circuit current (Isc), open circuit voltage (Voc) and maximum power (Pmax) can be inferred.

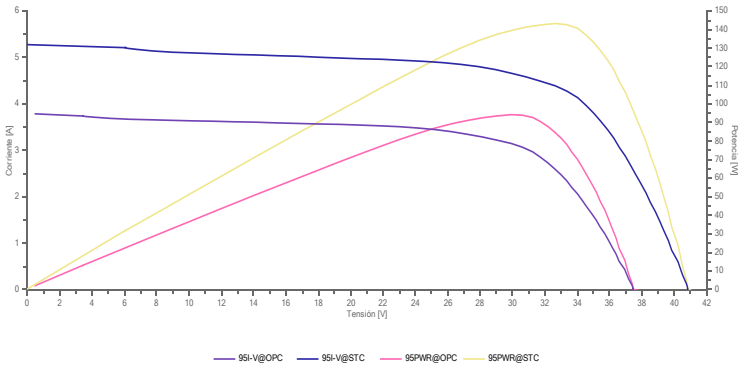

Fig. 1 PV module measured with PV tester.

2.3 Commercial I-V tester. Limitations.

PV modules are composed of different cell string layout. Different cells configurations provide electrical characteristics that the PV modules datasheet specify.

Detailed measurements of different systems and cell configurations are needed to understand some PV module failures. In this situation is when instrument limitation appears. Usually, a minimum input voltage of 15 V is required, and this value, limits measurements to full PV module. Therefore, the instrument does not provide capability to measure one PV string independently, which usually presents a voltage under this minimum value.

In some situations, is important to increase the level of detail and measure cell by cell. This is the most restrictive situation. PV cell electrical specifications are around 10 Amps and 0.6 V. Hence, the measuring instrument should be compliant with very restrictive electrical requirements. There are no instruments that could cover module measurements, string measurements and cell measurements at the same time.

Another important limitation is the I-V tester specifications. In most situations, algorithms used to measure and process measurements are not public. It becomes a limitation when an investigator needs to understand testing process from end-to-end and needs to have a full understanding of results obtained.

2.4 General purpose I-V Tester.

In order to overcome measurement limitations and to continue with researching and results, it was decided to develop a customized I-V tester to extend measurement needs. The instrument was developed based on Arduino platform.

Using open hardware and open software platforms, provide us well-documented information to grow the new functionality that was needed. It was decided to design a new layer for Arduino M0 motherboard. Arduino PCB provides a connector to be

used as link between boards which parameters are standard. Common connectivity provides needed functionality and a simple method for scale designs.
Fig. 2 presents the connectivity that most of Arduino devices have as general-purpose connectivity provided for user applications. Connectors are placed to ensure Pokayoke usability in order to avoid mistakes once the user-created layer (or skin) is placed.

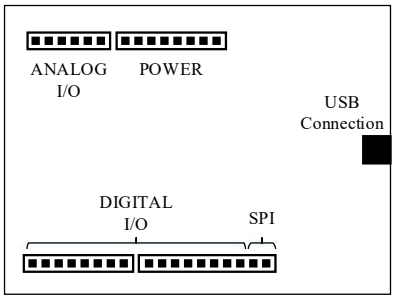

Fig. 2 Arduino general-purpose pinout.

The proposed development could be designed for simple Arduino M0 motherboard and used in other motherboards with more peripherals like Ethernet connectivity, SD memory card or Bluetooth.
Fig. 3 and Fig. 4 show two motherboard that use same connector with same functionality but, providing different hardware solution. Different blocks represented show the functionality available on each accessible pin: Ground connection (GND), analog to digital conversion (ADCx), digital pins and their functions (Pxyy, x = port name, yy = port number, PWM, Serial, SPI and I2C digital communications, etc.).
If needed, the compatibility provided for the same platform, simplify changing the motherboard from one to other with different specifications.

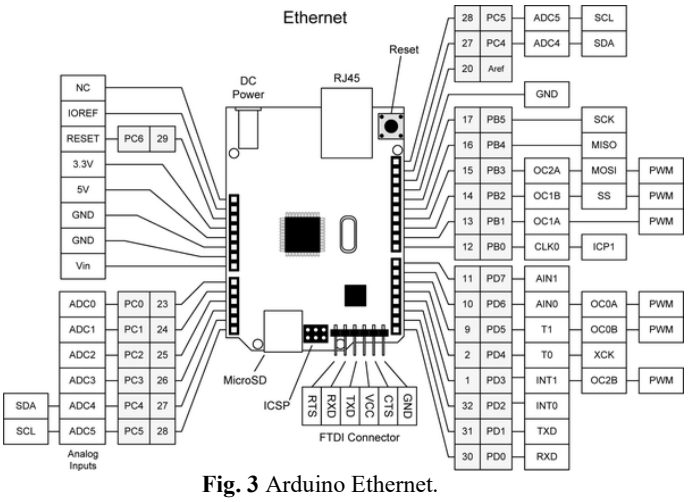

Fig. 3 Arduino Ethernet.

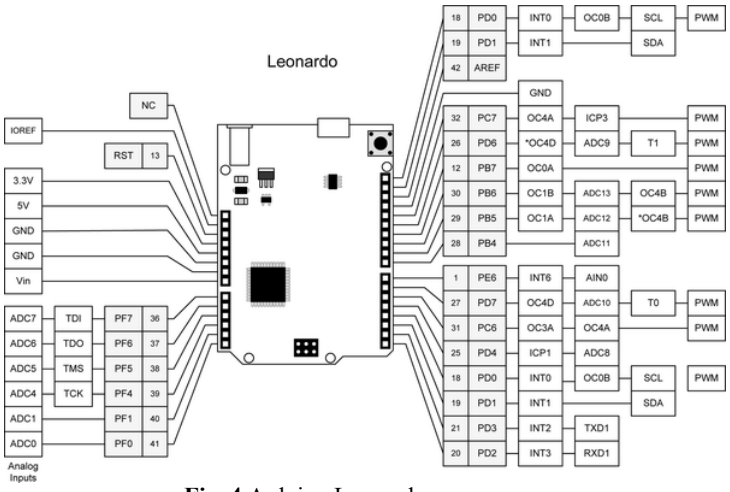

Fig. 4 Arduino Leonardo.

2.5 General purpose I-V Tester. Specifications.

Numatia is the code name used for the general purpose I-V tester developed. Before design, the instrument is very important to define the characteristics and limitations that it should meet. In Numantia's case, two different inputs were defined.

Firs input used to measure high power elements up to 600W (60V@10A). It is a useful input to characterize PV modules or strings that could be on those PV modules. It covers a big dynamic voltage range from 0V to 60V ensuring sensibility between measurements below 60mV.

The second input is defined for low voltage and high current cells up to 10W (1V@10A). This input needs to ensure a low resistance to ensure the capability to measure Isc with accuracy. To measure cells it should ensure a low resistance on fill measurement system due to a low voltage provided by standalone PV cells. The instrument provides by design on full measurement path the resistance lower than 5mΩ.

Measure information is sent to the laptop through USB connection provided by Arduino that can manage ADC and DAC that system needs to configure to provide different measurements. Fig. 5 represents topology that measurement system has.

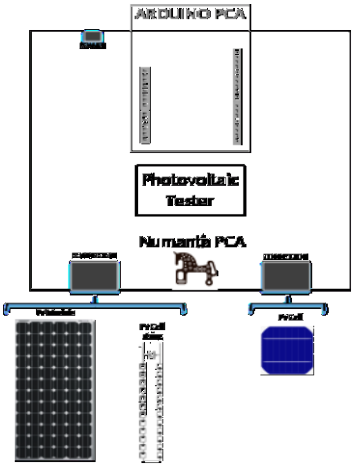

Fig. 5 General purpose PV tester.

The procedure used to measure I-V curve is based on variable resistor obtained configuring the MOSFET gate voltage. It was selected a low channel resistor to ensure reducing loses due to measurement system itself. Fig. 6 represents the simplified block diagram of the custom I-V tracer.

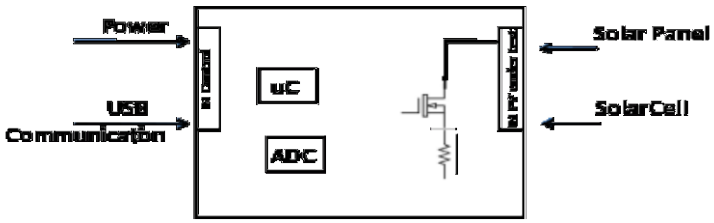

Fig. 6 General purpose PV tester block diagram.

2.6 General purpose I-V Tester. Software and hardware configuration.

Hardware devices defined to be involved on measurement system are critical. Instrument performance will depend on the quality and specifications of each component.

By definition, the MOSFET channel resistance is a maximum of 1.9mΩ. The shunt resistor selected is different for both systems. To measure high power PV devices is used a 200mΩ shunt resistor. However, to measure PV cells, it was needed to use 2mΩ shunt resistor. Thanks to using different shunt resistors for different measurements it is obtained the capability to measure wide range of PV systems using same device and procedure.

Code is the second important part of the design. Arduino's open-source provides us the capability to do fast developments and test design instrument performance. In the specific case of I-V tracer is important to include in the code a few different variables in order to calibrate full system. We have obtained positive results using one constant to adjust the gain that electronics provide and second variable to remove offset. Using

both constants defined at the beginning of the microcontroller firmware, instrument provides a high accuracy value.
All measurements are radiometric, it means that are linearly dependents on the power used to supply instrument. Power provided by USB is very stable, but there is uncertainty around exact value. The system could use USB batteries that could have voltage drift during full measurement procedure. To overcome this limitation, we define a double voltage cross-check. We measure power supply using Arduino and the voltage reference it has. The ADC in the instrument has one channel used to measure their own voltage as well. Both voltages are compared and use to adjust measures.
Fig. 7 represents graphically how to adjust measure value to obtain better approach to real measures removing undesired effect from own measurement process.

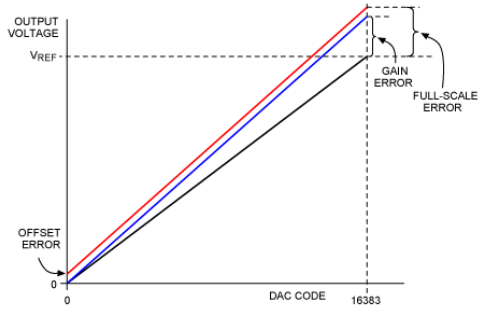

Fig. 7 Gain and offset.

Fig. 8 and Fig. 9 presents the hardware-implemented for developed I-V tester and the user interface design to facilitate measurements and user interaction on testing procedure.

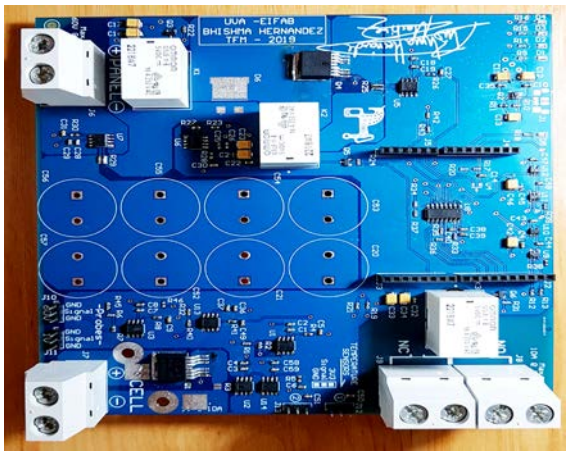

Fig. 8 Numantia PCA photo.

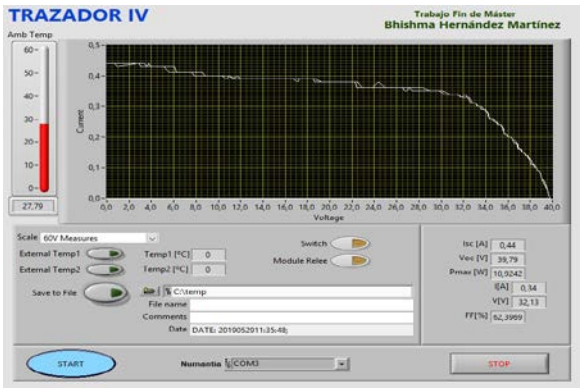

Fig. 9 User interface for I-V tester.

3 Results

Field measurements were performing on a monocrystalline PV module which specifications are P=175W, Voc=44.35V, Isc=5.35A. It is a monocrystalline PV module, it composes by 3 different strings with 24 PV cells each.
The main results obtained are summarized in Table 2. The differences in values obtained with both instruments come due to different irradiation values registered during both measurements.

	Voc[V]	**Isc[A]**	**Pmax[W]**	**Irradiation [W/m^2]**
Develop I-V tester	42.19	4.25	63.2	739
Commercial I-V tester	37.91	4.2	59.84	718

Table 2 PV module field measurement using commercial I-V tester and developed I-V tester

Fig. 10 and Fig. 11 present the field failure PV failure measurement result. It is seen reviewing detail I-V curves a failure in some string. The shape obtained on both I-V measurements demonstrates good performance of developing I-V tracer has to compare with commercial calibrate instrument. Similar peaks and valleys are measured providing similar figures.
To improve PV module performance is needed to fully understand behavior that PV module is providing and their failure modes. Investigations will prove improvements and weaknesses that will be implemented in future manufacturing procedures.

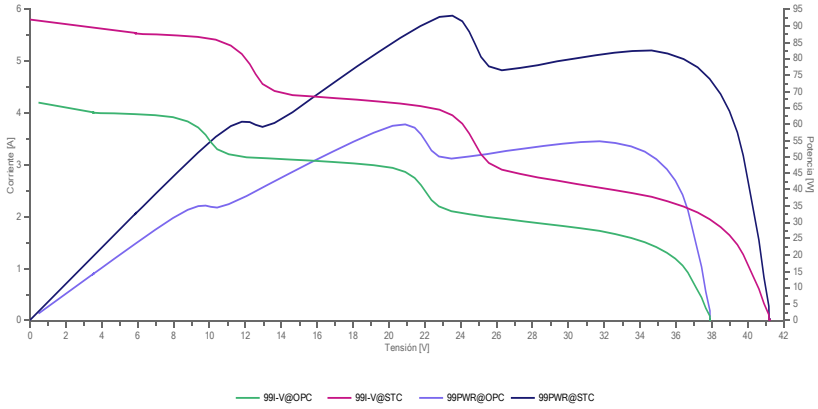

Fig. 10 Failure PV module measured with PV tester.

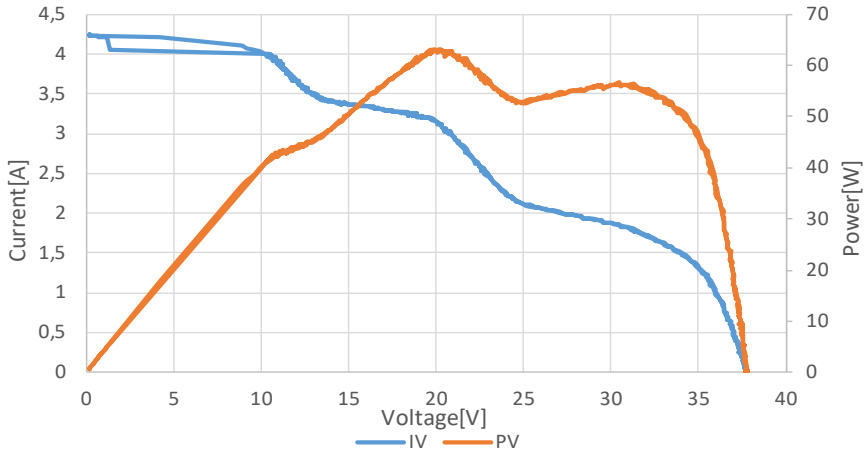

Fig. 11 Faulty PV module measured on field with I-V PV tester developed.

By means of the developed instrument, we obtained the different string measurements that are present in Fig. 12, Fig. 13 and Fig. 14. Is not possible to present string measurements to be compared due to limitation that commercial instrument has. Using those measurements, there is new information from field that could use on current investigations.

Different performances of 3 string included on same PV module create the poor performance saw. On ideal PV module, strings included on it should perform in a similar way. Represent values obtain on 3 different string and the big variation they have.

Table 3 summarize measurements perform using developed I-V tester. Due to open circuit voltage below 15V (commercial I-V tester limitation, see Table 1), the table only reflects result obtained with custom I-V tester.

	Voc[V]	Isc[A]	Pmax[W]	Irradiation [W/m^2]
String 1	12.9	2.21	16.11	718
String 2	11.91	3.28	28.14	723
String 3	13.5	4.19	36.20	724

Table 3 Failure PV module strings measured with PV tester developed.

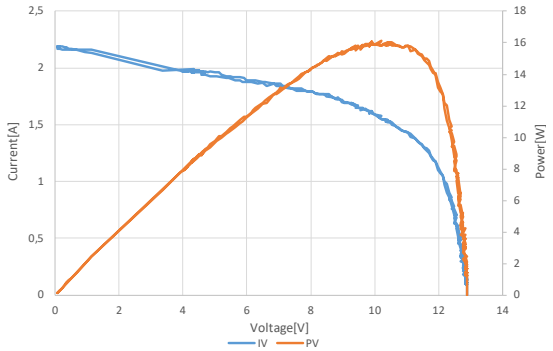

Fig. 12 Faulty PV module (string 1) measured on field with I-V PV tester developed

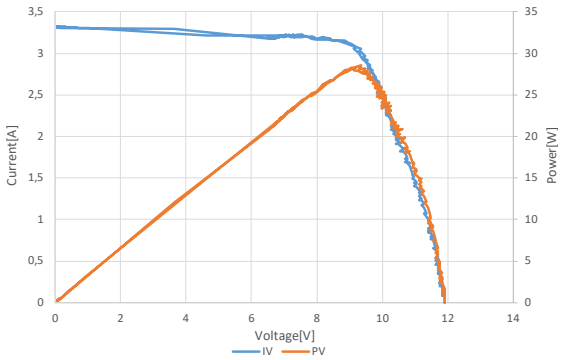

Fig. 13 Faulty PV module (string 2) measured on field with I-V PV tester developed

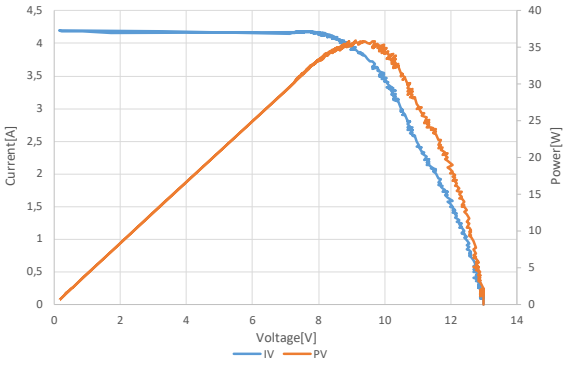

Fig. 14 Faulty PV module (string 3) measured on field with I-V PV tester developed

4 Conclusions

The new custom instrument developed helps the research group to go further on field PV module failure analysis and to obtain new values for future studies.
Minimum voltage limits from commercial instruments are overcome, and brig new capability on field measurements to analyze PV panels, PV string and PV cells. Having information from all components represents the advantage of handling full functionality from all components.
It is valued very positively the flexibility provided by a tailored instrument in terms of the capability to modify algorithms and hardware for investigation requirements. To have full control over instrument functions and specifications facilitates adapting test procedures to different working conditions and enlarge the usability that it has.

Acknowledgments

The authors thank the CYTED Thematic Network “INTELLIGENT CITIES FULLY INTEGRAL, EFFICIENT AND SUSTAINABLE (CITIES)” nº 518RT0558. In addition, the work has been possible thanks to the "DOCTOR-PV" project Ref .: RTC-2017-6712-3, which has been funded by the “Ministry of Industry, Economy and Competitiveness, State R + D + i Program Oriented to the Challenges of the Society (Collaboration Challenges)”.

References

[1]. Brenna, M., Calvo. M.C., Foiadelli, F., Martirano, L., Massaro, F., Poli, D., Vaccaro, A.: Challenges in Energy systems for the smart-cities of the future. In: *2012 IEEE International Energy Conference and Exhibition (ENERGYCON)*, 9-12 Sep. 2012, Florence (Italy).

[2]. Al-Nory, M.T.: Optimal Decision Guidance for the Electricity Supply Chian Integration With Renewable Energy: Aligning Smart Cities Research With Sustainable Development Goals. IEEE Access, 7(May), 74996-75006 (2019).

[3]. Hernández-Callejo, L., Gallardo-Saavedra, S., Alonso-Gómez, V.: A review of photovoltaic systems: Design, operation and maintenance. Solar Energy, 188(August), 426-440 (2019).

[4]. Olowu, T.O., Sundararajan, A., Moghaddami, M., Sarwat, A.I.: Future Challenges and Mitigation Methods for High Photovoltaic Penetration: A Survey. Energies, 11(7), 1782-1814 (2018).

[5]. Gercek, C., Reinders, A.: Smart Appliances for Efficient Integration of Solar Energy: A Dutch Case Study of a Residential Smart Grid Pilot. Applied Sciences, 9(3), 581-595 (2019).

[6]. Gallardo-Saavedra, S., Hernández-Callejo, L., Duque-Pérez, O.: Quantitative failure rates and modes analysis in photovoltaic plants. Energy, 183(September), 825-836 (2019).
[7]. Ashwini, P., Geethanjali, P. Parameter estimation for photovoltaic system under normal and partial shading conditions: A survey. Renewable and Sustainable Energy Reviews, 84(March), 1-11 (2018).
[8]. Mellit, A., Tina, G.M., Kalogirou, S.A. A survey. Renewable and Sustainable Energy Reviews, 91(August), 1-17 (2018).
[9]. Gallardo-Saavedra, S., Hernández-Callejo, L., Duque-Pérez, O.: Technological review of the instrumentation used in aerial thermographic inspection of photovoltaic plants. Renewable and Sustainable Energy Reviews, 93(October), 566-579 (2018).
[10]. Deitsch, S., Christlein, V., Berger, S., Buerhop-Lutz, C., Maier, A., Gallwitz, F., Riess, Ch.: Automatic classification of defective photovoltaic module cels in electroluminescence images. Solar Energy, 185(June), 445-468 (2019).
[11]. Szabo, R., Gontean, A. Photovoltaic Cell and Module I-V Characteristic Approximation Using Bézier Curves. Applied Sciences, 8(5), 655-678 (2018).

A hybrid energy storage system for renewable-based power plants

Francisco Díaz-González[1], Francesc Girbau-Llistuella[1], Mònica Aragüés-Peñalba[1], Cristian Chillón-Antón[1], and Marc Llonch-Masachs[1]

Centre d'Innovació Tecnològica en Convertidors Estàtics i Accionaments (CITCEA-UPC), Universitat Politècnica de Catalunya ETS d'Enginyeria Industrial de Barcelona, C. Avinguda Diagonal, 647, Pl. 2, 08028 Barcelona, Spain,
francisco.diaz-gonzalez@upc.edu

Abstract. This paper presents an hybrid energy storage system for the integration of renewable-based power plants in power networks. A hybrid energy storage system is defined as that able to integrate and maximize the contribution of a heterogeneous grouping of storage systems. The services which this hybrid solution is able to perform are identified and then related to a specific storage technology which have the best potential to solve the issues created by the intermittent renewable generation. The presented solution combines three different storage technologies, a lead-acid battery pack, a flywheel and a set of supercapacitors. The description of the system is complemented by a study case, for the performance analysis of the set of supercapacitors.

Keywords: Smart grids, hybrid energy storage systems, renewable-based power plants.

1 Introduction

The installation of renewable generation presents a growing tendency worldwide over the last decades, being mainly motivated by the need for reducing the dependency from fossil fuels and coal, as well as the the required drastic decrease of pollutant emissions. According to IRENA (International Renewable Energy Agency) [1], at the end of 2019, global renewable generation capacity was 2351 GW, dominated by hydro (1172 GW), wind (564 GW) and solar (486 GW). More than 80 % of the new capacity that was built in 2018 came from solar and wind installations. Therefore, it is clear wind and solar power plants play a key role for contributing to the power system decarbonisation. However, their generation presents variability and uncertainty, which are a barrier to a constant and predictable power output from this power plants. In this sense, Energy Storage Systems (ESS) can help to integrate large amounts of renewable generation. Furthermore, energy storage can also provide a fast response to large variations in demand.

The services that energy storage systems can provide in grids with large penetration of renewable generation are described in [2]. They are classified

in three categories in terms of power rating, energy rating and main type of beneficiary of the service. Small scale ESS (from a few tens of kW to a few MW in power and few tens of kWh to a hundreds of MWh in energy) is specially used for services for end-user or customer level. Mid scale ESS (from a few tens of kW to a few MW in power and few tens of kWh to a few MWh in energy) have applications for services at distribution level. Large scale ESS (from a few to hundreds of MW in power and time response up to several hours) are the ones that provide services to large scale renewable power plants.

The focus of this paper is on mid scale ESS and, in particular, on hybrid mid scale ESS. Hybrid ESS combine different energy storage technologies so as to benefit from the technical and economical advantages each one can offer depending on the response required in different operational situations. Depending on the type of battery selected, a large amount of energy can be available but with reduced power, or high power peaks for less time (low power); not both at the same time. Similarly, superconductors and flywheels offer high power peaks, but for a short time (low stored energy). The design of storage systems capable of offering good performance in power, energy, life expectancy, response times, ease of operation, scalability, reliability, security, etc., is possible through the concept of hybridization. Additionally, a hybridization can also allow lower costs and lower size for the ESS solution to be developed. For instance, a lead-acid battery supports instantaneous electrical currents of up to 100 % of the nominal, without affecting dramatically the useful life of it. In contrast to lead-acid batteries, lithium-ion batteries (especially those of lithium-iron-phosphate) can exchange currents of up to ten times their nominal value for 30 seconds [3]. These maximum currents are even larger for supercapacitors [4]. Thus, hybrid solutions that provide high instantaneous currents can be configured without having to install in parallel a high number of batteries with low power performance, with the consequent reduction in cost and size.

In this study, a hybrid ESS is here proposed, which consists of a front-end inverter and three parallel DC/DC modules, each one integrating a different energy storage technology: electrochemical (lead-acid battery), electrical (supercapacitor) and electromechanical (flywheel). The objective of this device is to enable a large penetration of renewable generation in distribution grids, while guaranteeing the accomplishment of grid code requirements [7] and ensuring power quality in these networks. The paper is structured as follows. In Section 2, the type of services provided by ESS in combination with renewable based generation are detailed. Then, in Section 3, the conceptual design of the hybrid ESS is presented, explaining the advantages and drawbacks of the power electronics and energy storage technologies selected. The experimental characterization of the behavior of the supercapacitor is shown in Section 4. Finally, conclusions are drawn.

2 Services from energy storage in renewable-based power plants

ESS can provide numerous services to electrical networks. Literature on this matter is extensive [5], [6], providing approaches from various perspectives, from the technology to the market sides.

The energy and power ratings of an ESS greatly determine the services it can provide in electrical networks. For instance, a flywheel cannot store large amounts of energy because it would imply to apply an unrealistic rotating disk. In addition to ratings, suitable services for ESSs are constrained by other inherent characteristics of the technology, such as cyclability, time response and ageing mechanisms. So each technology fits best for a particular catalogue of services.

In general terms, as introduced in [2], services can be classified in three main categories. A brief summary is offered in the following. The first category is that requiring small-scale ESSs. Energy storage here can be exploited to improve the self-consumption performance and to provide services to the end user. In this case, the storage device is installed at local residences or small facilities. Services in this regard can be that for maximizing self-consumption, off-grid operation of neighbourhoods and in synergy with demand management.

Small-scale storage devices can be sized here considering the local consumption and generation profiles and the desired service level. The size of these systems are in the scale of few kW to hundreds of kW in power and of few tens of kWh to hundreds of kWh (for community scale installations). Suitable ESSs for end user centered applications are mainly secondary batteries, specially lead-acid ones, because of their low cost; and progressively gaining momentum, lithium-ion ones, because of their great performance.

The second category of services is that requiring mid-scale ESSs. These technologies, aimed to be installed in low and medium voltage networks, will help to trigger vast deployment of distributed generation and electrical vehicles. In particular, services here include various keywords, such as power quality improvement, congestion alleviation in networks, and improvement of security of supply. Thus, these storages may provide services to the grid operator and end users.

The power and energy ratings for eligible energy storage systems in this category will depend on the type of customers willing to profit from these service. The power rating of the power electronic equipment will be in the range of a few tens kW to few MW. The energy storage capacity will depend on the interruption time allowed in the installation and is in the range of tens of kWh to few MWh and this depends on the time a grid congestion occurs and its severity, for instance. Thus, the most suitable storage technologies are secondary batteries and flow batteries. Also, short-term storages offering high cyclability and power ramp rates such as flywheels and supercapacitors are well addressed for power quality improvement related services.

Finally, the third category of services is that requiring large-scale ESSs. These technologies, aimed to be installed in large renewable power plants or primary substations may be operated to provide grid ancillary services and to improve

the controllability of power flows within the power network. Grid ancillary services refer to the provision of primary and secondary power reserves, voltage control, power ramp-rate limitation and black start capability of power plants. In regard of the application of energy storage in renewable-based power plants, operational rules and related control algorithms should be explored according to the corresponding regulations, or namely grid codes. The applicable grid code regulation in Europe that determines the requirements for the grid connection of renewable-based power plants and the ancillary services they should provide is the European Commission Regulation 2016/631 of 14 April 2016 [7]. The controllability of power flows within the network, specifically refers to the time shifting and compensation of forecasting errors for renewables, thus facilitating the grid integration of such bulk renewable generation.

Usual capacity requirements for these services are between few MW to hundreds of MW in power. The most suitable technologies are compressed-air energy storage, pumped-hydro installations, hydrogen and secondary batteries, especially lithium-ion, lead-acid or sodium ones for systems rated at tens of MW. Flywheels, because of their easy scalability, enabling the realization of systems rated at tens of MW in power can be also suitable for these services.

3 The hybrid energy storage solution

The hybridization of ESSs permit to provide various services with a unique device. The proposed hybrid solution for the purposes of the present work, i.e. the grid integration of renewable-based power plants, is presented in this section.

The aim of the solution is to maximize the integration of renewable generation into the distribution grid. It has to contribute to the fulfilment of the grid code requirements for the renewable-based power plants, as well as those related to the participation in grid ancillary services. Moreover, it pursues the improvement of voltage waveform, compensating the slow variations, smoothing the fluctuations and eliminating the flicker generated by the intermittent generation.

The solution is designed as an hybrid energy storage system. The main idea behind the hybridization is to combine complementary storage systems for taking advantage of their strengths, and facilitate the renewable accommodation at a reasonable cost. Figure 1 depicts a conceptual scheme of the hybrid energy storage solution. In particular, the adopted solution is composed by a front-end inverter and three parallel DC/DC modules. Each one of these DC/DC modules integrates a different energy storage technology.

Figure 1 also presents the architecture of the solution. It is selected because it offers excellent performance in regard of efficiency, flexibility and fault tolerance, with the potentiality of configuring a solution with less volume than others architectures, according to a quantitative comparison realized in [8]. However, it also has the following limitations:

– The front-end inverter is a bottleneck. In other words, there is only a way to exchange power with the external grid, i.e. through the unique front-end

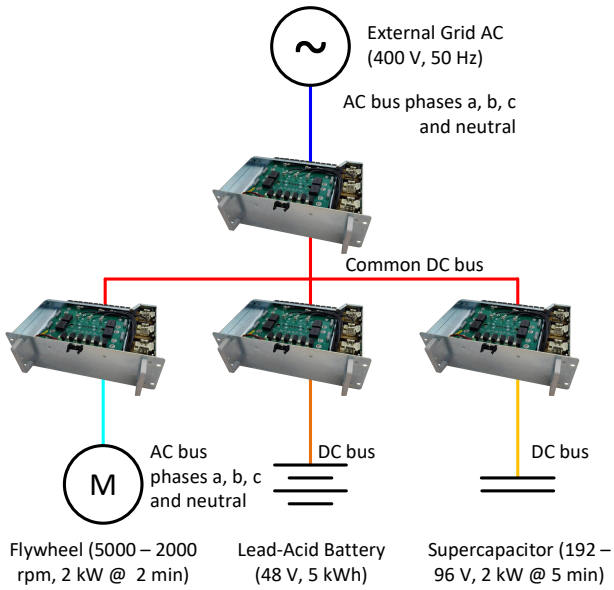

Fig. 1. Conceptual scheme of the hybrid energy storage solution.

inverter, therefore, the whole power of the solution is limited by the rated power of this inverter.
- The power electronics performance is higher when the output power reach the rated value. Therefore, if the inverter is oversized to cover the whole storage systems (or at least the highest storage system) rated power, the performance will be lower some occasions.
- The front-end inverter requires that the voltage of the common DC bus is at least $400\frac{2\sqrt{2}}{\sqrt{3}}$. It is really high voltage in comparison with the rated DC voltage of the storage systems, so the difference between them is notably large, and therefore, the duty will be veritably small and its range will be also short.

The particular hybrid energy storage system combines three different technologies: an electrochemical technology, a lead-acid battery; an electrical, a super-capacitor; and electromechanical technology, a flywheel. Following a short revision of technologies is performed.

The lead-acid batteries are featured by:

- Its reduced cost and hazard level.
- They can provide instantly a so high short-circuit current.
- They are used in stationary applications which do not require to cycle them many times, to estimate their state of charge, and to calculate their performance.

– In addition, there is a high complexity to estimate the previous points because the internal resistance is remarkably high (in comparison other battery technologies) which makes it difficult and extremely dependent of the current.
– It is not common find accurate BMS solutions in the market.
– Both power-weight and energy-weight ratios are typically lower than lithium batteries.

Flywheels and super-capacitors are two similar technologies which stores energy via inertia and voltage, respectability, both are characterized by:

– Their reduced cost and long life.
– They are faster technologies and are much more suitable for cycling than batteries.
– However, it is necessary to oversized them because it is not possible to operate them at the whole range. By way of example, the flywheel has to be able to supply 2 kW during 2 minutes. If it is presented the power curve for this flywheel (see Fig. 2) it is appreciated that it can only exchange 2 kW in the range between 2000 to 5000 rpm. Therefore, if it required to supply this power during 2 minutes, the flywheel will decrease its velocity from 5000 to 2000 rpm. Similarly, the super-capacitor has to be able to supply 2 kW during 5 minutes, so it will decrease its voltage from 192 V to 96 V.

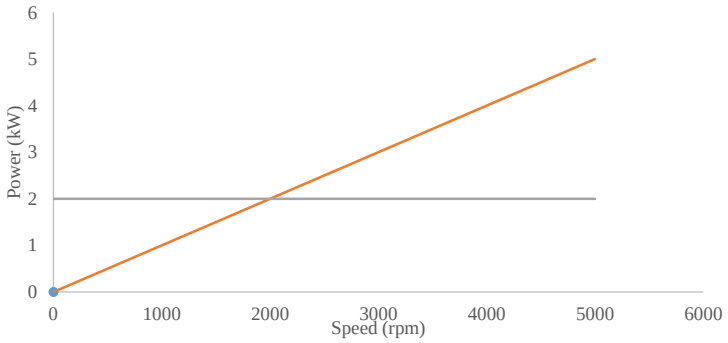

Fig. 2. Flywheel operation range. The power characteristic of the motor is under a constant torque condition.

– Their self-discharging is higher than batteries. As Fig. 2 it is appreciated that the flywheel operates at least 2000 rpm, so it is continuously rotating, therefore, it is always required and a small torque input in order to ensure that its angular velocity does not decrease from 2000 rpm. Similarly, it happens with the super-capacitors, so a small current is always required to avoid its completely discharge.
– In addition, in case of flywheel technology, the bearings are also a source of losses and can create problems.

As traditional energy storage system solutions, the proposed solution is composed by two main parts: i) a so-called power plane; and ii) a management plane. The power plane includes the components actually exchanging electrical power with the network. This plane defines how the system is connected, i.e. storage systems and power electronics are linked according to previous architecture. In turn, the management plane is composed by algorithms and related hardware managing the aforementioned system. In this sense, the management the front-end inverter is the responsible of maintaining the voltage in the common DC bus while the DC/DC modules exchanges power with the external grid, in order to provide the expected response. In this sense, apart from the implementation of grid services in the device, it is necessary to develop a power sharing algorithm that ensures the proper functioning of the whole system.

Finally, the Fig. 3 depicts the prototype designed. The whole power electronic solution is contained in the same cabinet, except from the storage units which are directly connected to it. Inside the cabinet, there is a holder for the modules. In this holder there are the four independent power converter which constitute the hybrid storage solution. The holder provides all the connections for the power and controls, in front of this holder, there is the control and measurement equipment. Finally, below the modules holder cabinet, there are all the power interconnections and the protection equipment.

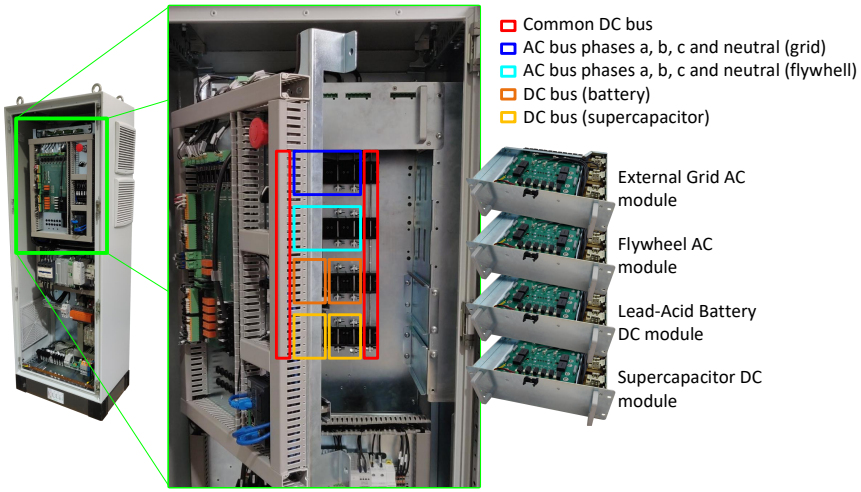

Fig. 3. Hybrid energy storage solution demo platform.

4 Study case: Experimental characterization of supercapacitors

After the presentation of the hybrid energy storage solution and the discussion of the complementarity of the storage technologies embedded into it, this section presents laboratory tests to characterize the supercapacitor modules.

There are three supercapacitor modules connected in series from the manufacturer Maxwell Technologies, model BMOD0141 P064 B04 (see Figure 4).

Fig. 4. The three supercapacitor modules connected in series. The maximum voltage is 192 V and the capacitance per each module is 141 F.

Supercapacitors are well suited for providing power during relatively short time (few minutes at most), accounting on low degradation. This way, they can be cycled hundreds of thousands times till reaching the end of life condition.

A test has been performed to the set of three supercapacitor modules connected in series to characterize the energy ratings and efficiency. Results are plotted in Figure 5. The upper subplot presents the voltage per each of the three modules and the lower subplot depicts the driving current. As can be observed, the supercapacitors are charged from a minimum operating voltage of 30 V to the rated voltage per each of the modules (64 V), and then discharged back to the minimum state of charge. The following conclusions are derived from the test:

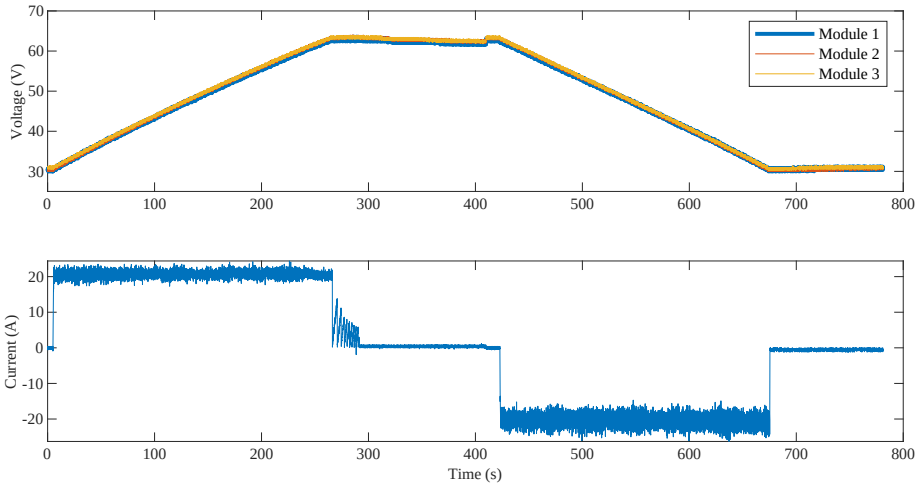

Fig. 5. The upper subplot presents the voltage per each of the three supercapacitor modules connected in series. The lower subplot shows the charge (positive) and discharge (negative) current for the test.

- Setting a minimum operating voltage for each supercapacitor module of 30 V and the maximum one to 64 V, and while charging at 20 A, the energy consumed in this process is 330 Wh. While discharging back to 30 V per module and, again, at constant current of 20 A, the energy provided is 318 Wh. Therefore, the round trip energy efficiency for the set of supercapacitor modules is 96.3 %. This implies a small internal resistance for the cell, as determined by the manufacturer.
- The practical energy storage capacity of a supercapacitor is bounded by the minimum operating voltage, and this should be determined by the designer. Very low voltages, although admissible for the supercapacitors, are not practical. This is because excessive currents through the supercapacitors would be required to develop the required power.
- Negligible voltage unbalances among supercapacitor cells are experienced. This can be observed in Figure 5, in the upper subplot: all three voltage profiles are almost identical. Such small voltage unbalances among different modules in series is a clear advantage of supercapacitors over batteries.

5 Conclusions

This paper presented a hybrid energy storage system for the provision of services in renewable-based power plants. The system is hybrid, since combining through a single power-electronics cabinet, three types of energy storage technologies: a lead-acid battery pack, a flywheel and a supercapacitor. The complementarity of the storage technologies trigger the provision of various services simultaneously,

i.e. the provision of energy-based services through the battery, and power-based services by the management of the supercapacitor and the flywheel. The modularity of the power-electronics cabinet permit to operate differently each of the storage technologies, even triggering a power sharing among them if necessary. Complementing the description of the solution, one of the storage technologies embedded into the hybrid solution, the supercapacitor, has been tested in laboratory. Results derive a round trip efficiency of 96.3 %, and minimum voltage unbalances among the modules connected in series. Such performance serve to identify supercapacitors as well suited for services requiring frequent charge and discharge.

6 Acknowledgments

This work was supported by the Ministerio de Economia, Industria y Competitividad (Spanish government), under the grant agreement number ENE2017-86493-R.

References

1. Renewable Capacity Statistics 2019, International Renewable Energy Agency (IRENA), March 2019 URL: https://www.irena.org/publications/2019/Mar/Renewable-Capacity-Statistics-2019. [Accessed on July 2019]
2. Díaz-González F., Bullich-Massagué E., Vitale C., Gil-Sánchez M., Aragüés-Peñalba M., Girbau-Llistuella F. (2019) Services of Energy Storage Technologies in Renewable-Based Power Systems. In: Nesmachnow S., Hernández Callejo L. (eds) Smart Cities. ICSC-CITIES 2018. Communications in Computer and Information Science, vol 978. Springer, Cham.
3. A123 Systems (2017) AMP20M1HD-A Prismatic Cell datasheet.
4. Maxwell Technologies (2017) BMOD0094 P075 B02 datasheet. URL: http://www.maxwell.com/
5. Díaz-González F, Sumper A, Gomis-Bellmunt O (2016). Energy Storage in Power Systems, John Wiley & Sons
6. Energy Storage Association (2000). Energy Storage, Case Studies. URL: http://energystorage.org/energy-storage/case-studies/delivering-100-commercial-reliability-aes-los-andes-battery-energy. [Accessed June 2018].
7. European Commission (2016). Commission Regulation (EU) 2016/631 of 14 April 2016 establishing a network code on requirements for grid connection of generators. URL: https://eur-lex.europa.eu/legal-content/EN/TXT/?uri=OJ\%3AJOL_2016_112_R_0001. [Accessed on June 2018]
8. F. Díaz-González, D. Heredero-Peris, A. Sumper, F. Girbau-Llistuella, M. Aragüés-Peñalba; S. Marksteiner; L. Candido, R. Gallart-Fernandez (2017). D2.1 – Power electronics device design specifications and models for the architectures. URL: https://resolvd.eu/documents/. [Accessed on July 2019]

Pieles y Envolventes Eólicas en Arquitectura: Una aproximación de su diseño

Luis Sánchez-Loayza[1] and Jorge Mírez[2][0000-0002-5614-5853]

[1] Faculty of Sciences, Universidad Nacional de Ingeniería (UNI). Lima, PERU.
[2] Grupo de Modelamiento Matemático y Simulación Numérica (GMMNS), Facultad de Petróleo, Gas y Petroquímica, Universidad Nacional de Ingeniería. Lima, PERU
jmirez@uni.edu.pe

Abstract. Este documento presenta una aproximación de una metodología de diseño de fachadas arquitectónicas que incluya variables climatológicas, cuyos valores están en constante cambio, con diversos grados de actividad. Además Se aborda el dinamismo y respuesta al medio ambiente, utilizando múltiples parámetros ambientales que afectan las condiciones internas y la eficiencia energética del lugar en donde se van a implementar éstos diseños arquitectónicos.

Keywords: Pieles, Envolventes, Arquitectura, Eólica, Smart Cities.

1 Introducción

Comúnmente se usa el término "adaptación" en arquitectura para designar las morfologías (configuraciones) cambiantes del artefacto arquitectónico. Estas configuraciones variables han sido el resultado de cambios pertinentes y de la evolución de la arquitectura como entidad social, producto tecnológico y como práctica.

Las configuraciones arquitectónicas se adaptan al tiempo en que se crean y se ejecutan. Estas morfologías adaptativas son el resultado de los tiempos cambiantes: la forma social, el apoyo económico, las necesidades del usuario y los efectos ambientales.

Durante el día ocurren transformaciones ambientes que influyen en el objeto arquitectónico, lo que lleva a adaptaciones locales.

Las mejoras en la tecnología, el apoyo económico y el proceso de pensamiento humano contribuyen a la respuesta adaptativa más acertada en la arquitectura.

La edificación no solo brinda sombra y protección contra el ambiente externo, sino que tiene una multitud de funciones a realizar con una variedad de condiciones para adaptarse y responder. La arquitectura ha pasado de ser funcional a inteligente (manejando variables ambientales cambiantes).

2 Pieles y Envolventes

"Junto con la llegada de la arquitectura contemporánea se produce un cambio de paradigma en cuanto la fachada deja de ser un elemento pesado y estructural de un edificio, para transformarse en una envolvente, piel o membrana, capaz de proteger su interior, actuar como filtro del sol o el viento, mejorar las condiciones térmicas interiores, ser vegetal e incluso, ser móvil y tecnológica." [1]

"Hoy, la transformación de la arquitectura además de estar vinculada a un aspecto cultural, se relaciona intrínsecamente con el avance de la tecnología y nuevos materiales. De esta manera es importante mantenerse informados en cuanto a la serie de posibles soluciones a la hora de proyectar. La piel es filtro, transparencia, protección, privacidad, movimiento, cortina, amortiguador y bienestar interior." [1]

3 ¿Adaptarnos a la naturaleza o competir con ella?

"Una envolvente de un edifico significa una separación entre interior y exterior, el cual proporcionan las funciones de; soporte, control, acabado (estético) y distribución de servicios, sin embargo, resulta más interesante pensar en una interfaz y no en una separación, entre los factores ambientales externos y las demandas interiores de los ocupantes; la envolvente es un moderador ambiental." [3]

Al contrario de esta idea de envolvente como interfaz reguladora encontramos, que los cerramientos de los edificios son construido con grandes restricciones que excluyen la interacción con el entorno, la eficiencia energética y la optimización de materiales; a pesa que las características climáticas de cada zona son paramentos variables, las fachadas son en su mayoría estática y suplen esa falta de interacción mediante sistemas dinámicos que utilizan grandes cantidades de energía para controlar el confort interno, "el consumo de energía destinadas a las instalaciones de calefacción y refrigeración representa un 60% del total de la energía consumida en el edificio"[4].

"El confort ambiental es el rango de las condiciones del entorno consideradas aceptables dentro de un espacio habitable, en el que el ser humano desarrolla sus actividades" [5]. La ausencia de confort implica una sensación de incomodidad o molestia, ya sea por frío, calor, deslumbramiento, exceso de ruido o falta de iluminación, entre otros.

"El espacio climático es un espacio complejo ya que además de las tres dimensiones espaciales, hay que considerar otra que es el tiempo. El clima no solo cambia cuando nos desplazamos en sentido vertical u horizontal, también conforme pasa el tiempo,…." [3]

La Tierra, debido al cambio climático, aumentará notablemente de temperatura y llegará a un punto en que ésta registrará niveles insostenibles, "Lo más importante que podemos hacer es adaptarnos a los cambios que se avecinan" [6]

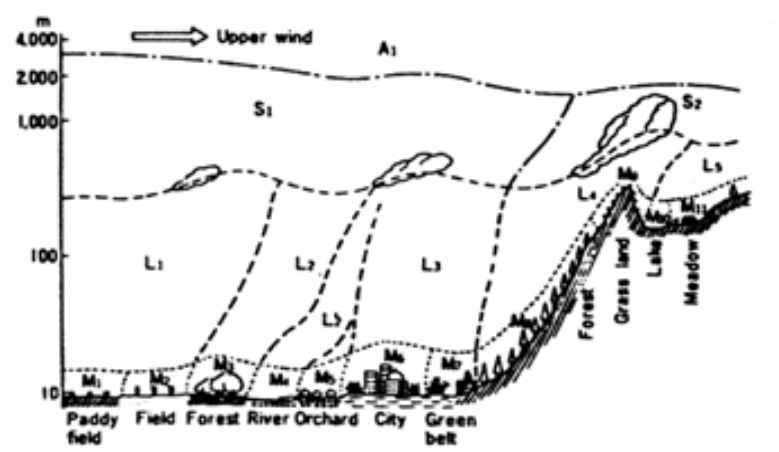

Fig. 1. Ilustración Esquemática de las Escalas Climaticas: Micro (M), Local (S) y macro (M) [1],

4 Criterios arquitectónicos que afectan al rendimiento y a la eficiencia energética

Con el fin de optimizar el comportamiento energético y el confort térmico y visual de los ocupantes se adecuación las condiciones medio ambientales siendo uno de los objetivos más importantes en los edificios durante su vida útil.

Entre los "criterios arquitectónicos, actualmente la producción arquitectónica tiende a dividir las funciones sobreentendidas de los elementos arquitectónicos según sus formas, estructuras y materiales a lo largo de la historia de la Arquitectura" [8], al contrario de la herencia del estilo Internacional que ha repartido por todas las ciudades del mundo, grandes prismas acristalado que no corresponden a los valores estéticos locales, ni a las condiciones climáticas.

Un edificio manifiesta una materialidad definida a través de "criterios constructivos: este tipo de criterio actualmente apunta hacia los procesos de fabricación industrial en serie, siendo una causa para que los edificios sean funcionalmente inertes, irresponsables y perjudiciales para el medio ambiente cambiante" [8], en lugar de producciones personalizadas para para cada lugar en particular

5 Adaptabilidad de las envolventes arquitectónicas

Sin olvidar la naturaleza, pero creando soluciones adecuadas podemos garantizar una mayor integración entre el edificio y el entorno construido (contexto).

Las innovaciones recientes en el diseño, la recopilación y el seguimiento de los datos climáticos permiten aprovechar al clima: temperatura, humedad, luz, dióxido de carbono (parámetros ambientales). Un diagrama de funciones según los desafíos que tienen que hacer frente la envolvente en cada clima se muestra en la Fig. 2.

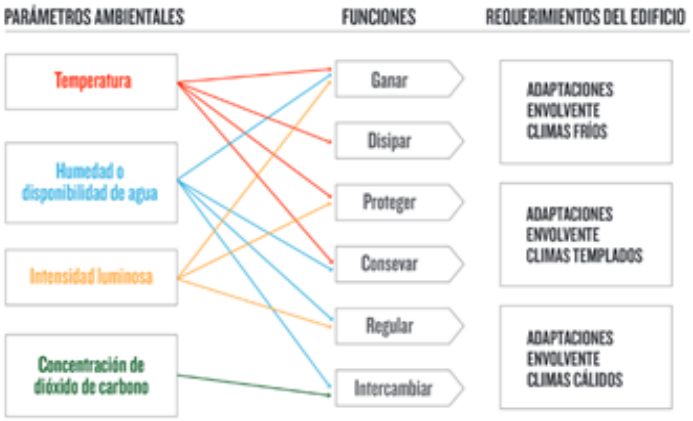

Fig. 2. Diagrama de funciones según los desafíos que tienen que hacer frente la envolvente en cada clima

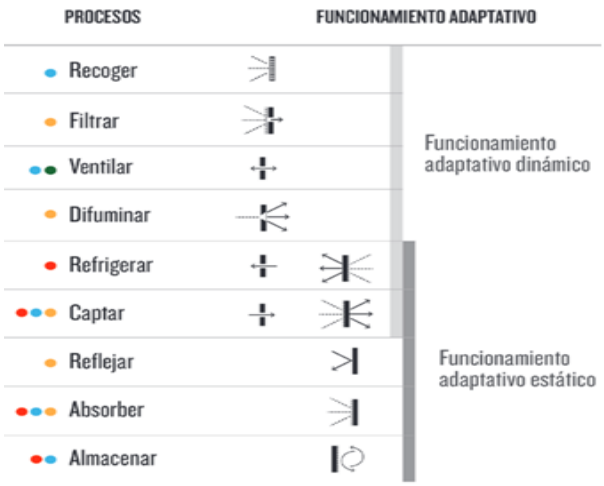

Fig. 3. Diagrama de los tipos de funcionamiento identificado en una envolvente arquitectónica

Las innovaciones recientes en el diseño, la recopilación y el seguimiento de los datos climáticos permiten aprovechar al máximo los recursos naturales y optimizarlos para una mayor eficiencia. Todo ello sin olvidar la naturaleza, pero trabajando para que podamos garantizar una mayor integración entre el entorno construido.

El síguete diseño conceptual (Figura 4), muestra los retos que se deben afrontar las envolventes arquitectónicas en climas como Lima

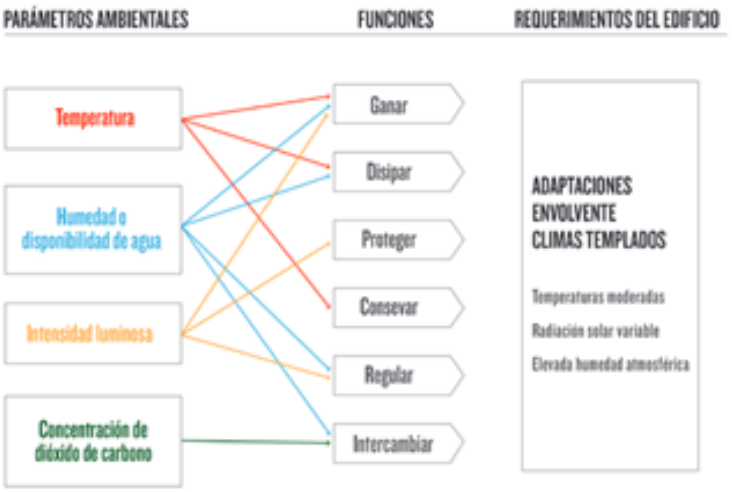

Fig. 4. Diagrama conceptual de los desafíos de las envolventes en la ciudad de Lima

El diseño de la envolvente tiene una serie de criterios que preceden a las decisiones de las características de forma de la envolvente.

Los parámetros que definen el diseño y la caracterización de envolventes arquitectónicas son: localización, posición relativa, morfología superficial, escala, configuración estructural, mallado, secciones de trabajo estructural, uniones y anclajes, materiales de estructura, tipología de cerramiento, grado de permeabilidad, materiales para cerramiento y soporte vegetal.

6 Programación del modelo paramétrico

Parametrizar, consiste en adaptar automáticamente una forma mediante la introducción de unos determinados valores o parámetros definidos.

Grasshopper™, es un lenguaje de programación visual desarrollado por David Ruten en Robert McNell & Associates. Grasshopper es un plug-in que corre dentro de la aplicación CAD Rhinoceros 3D. Los programas son creados arrastrando componentes en el área de trabajo. Los componentes tienen entradas y salidas, las salidas se conectan a las entradas de los componentes subsecuentes. Es utilizado principalmente para programar algoritmos generativos. Los programas pueden también contener otro tipo de algoritmos, tales como los numéricos y textuales audio-visuales 3D y aplicaciones hapticas.

Con los parámetros establecidos se crean componentes en Grasshopper para crear una geometría que genera una forma.

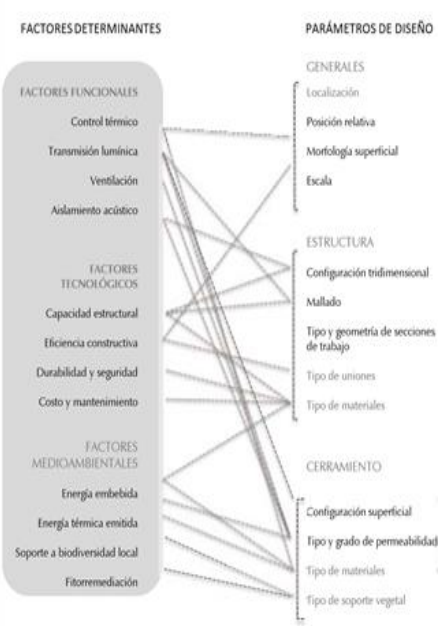

Fig. 5. Factores determinantes y parámetros propuestos.

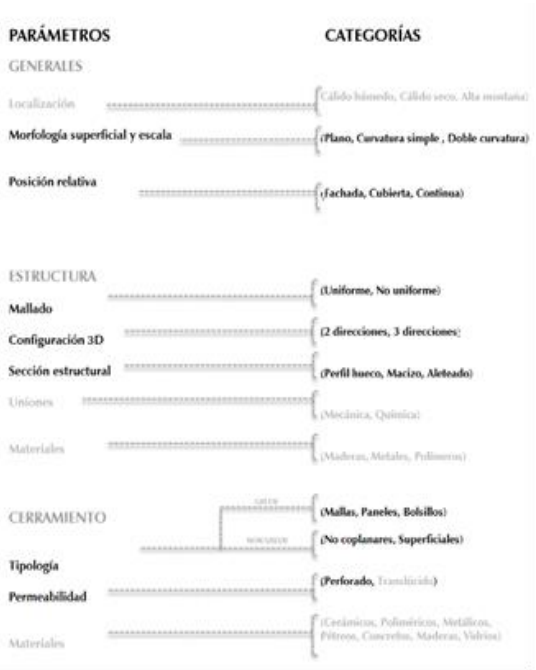

Fig. 6. Variables de la programación.

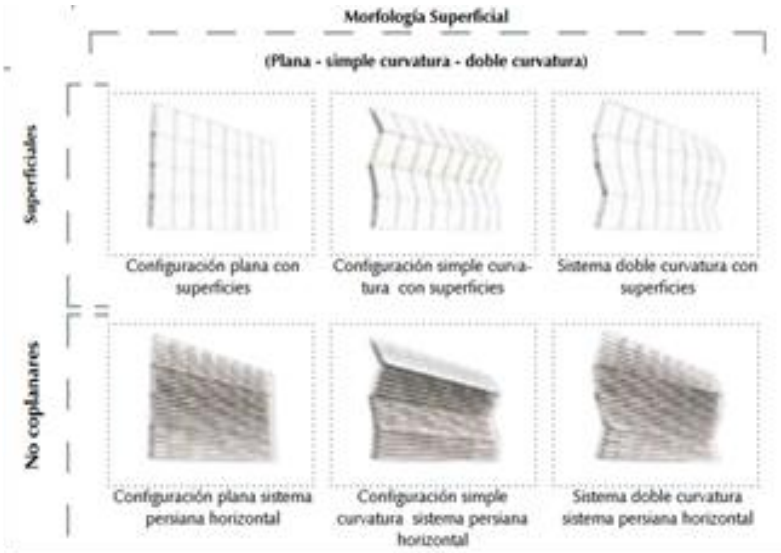

Fig. 7. Posibilidades constructivas.

7 Conclusiones

Esta propuesta adaptativa [en que se usa pieles arquitectónicas] cuestiona la naturaleza estática de los espacios arquitectónicos usuales y los vuelve un entorno (contexto) complejo y dinámico que conlleva a mejoras en la estética y la eficiencia energética, así mismo, crea nuevas oportunidades de negocio y trabajo, y contribuye a la modernización de las ciudades inteligentes.

Además se ha abordado un problema mayor, al considerar el dinamismo y respuesta al medio ambiente, utilizando múltiples parámetros ambientales que afectan las condiciones internas y la eficiencia energética del lugar en donde se van a implementar éstos diseños arquitectónicos.

References

1. ArchDaily Perú 2019. "Nuevos Materiales: Pieles y Envolventes". [Online]. Available: https://www.archdaily.pe/pe/02-101408/nuevos-materiales-pieles-y-envolventes [Accessed: 25- Aug- 2019]
2. Geiger, R., Aron, R. H., Todhunter, P. "The Climate Near The Ground", 5ª Edición. Vieweg & Sohn. Weisbaden, 1995.
3. Wang J, Beltrán LO, Kim J., (2012) "From static to kinetic: a review of acclimated kinetic building envelopes". Denver, CO.
4. Omrany, Hossein & Ghaffarianhoseini, Ali & Ghaffarianhoseini, Amirhosein & Raahemifar, Kaamran & Tookey, John, 2016. "Application of passive wall systems for improving the energy efficiency in buildings: A comprehensive review," Renewable and Sustainable Energy Reviews, Elsevier, vol. 62(C), pages 1252-1269.

5. Bustamante W., (2009) Guía de Diseño para la Eficiencia Energética en la Vivienda Social, Ministerio de Vivienda y Urbanismo. División Técnica de Estudio y Fomento Habitacional (MINVU) y Programa País de Eficiencia Energética (CNE), Santiago de Chile, 2009.
6. S. Científicas, ""El ser humano debe adaptarse a los cambios que se avecinan"", Agenciasinc.es, 2019. [Online]. Available: https://www.agenciasinc.es/Reportajes/El-ser-humano-debe-adaptarse-a-los-cambios-que-se-avecinan. [Accessed: 25- Aug- 2019].
7. Oxman, N., (2012) Computación material, Fabvolution: Avances en la Fabricación Digital. Ajuntament de Barcelona, Barcelona pp. 57-64.
8. Soar, R., Andreen, D. "The Role of Additive Manufacturing and Physiomimetic Computational Design for Digital Construction. Material Computation: Higher Integration in Morphogenetic Design Architectural Design". Vol. 82. Wiley Academy, London (2011).

Over-Voltage Protection for Pico-Hydro Generation Using PV Microinverters

Isabella Cristina Scotta[1,3][0000−0002−7401−0979], Gabriela Moreira Ribeiro[1,4][0000−0003−3434−578X], Wellington Maidana[1,2][0000−0002−5361−3850], and Vicente Leite[1,2][0000−0002−8790−519X]

[1] Instituto Politécnico de Bragança, Bragança, Campus Santa Apolónia, Portugal
[2] Research Centre in Digitalization and Intelligent Robotics (CeDRI)
[3] Universidade Tecnológica Federal do Paraná, Campus Toledo, Paraná, Brazil
[4] CEFET/RJ, Campus Maracanã, Rio de Janeiro, Brazil
isahcs9@gmail.com; gribeiro.eletronica@gmail.com; maidana@ipb.pt; avtl@ipb.pt

Abstract. Innovative, low-cost, environmentally friendly and renewable resource-based solutions are emerging to meet growing global energy demand. Hydroelectric technology is quite old and mature. Despite its importance, it is associated with large plants, with environmental impact. On contrary, small-scale systems, called pico-hydro systems (up to 5 kW) are not yet explored. Anyway, the exploration of pico-hydro systems has been increasing consistently, from the first off-grid applications in remote places to distributed generation, with the injection of the generated energy in the main grid or microgrids. Very recently, there have been advances in grid connection of these small-scale systems, using off-the-shelf components. Indeed, pico-hydro systems can be connected to the grid using off-the-shelf components, namely photovoltaic inverters. Thus, grid-connected pico-hydro systems have gained an enormous potential in distributed production. However, in situations of over-power, or whenever the generator is under no load, there is a need for effective over-voltage protection, unlike photovoltaic systems. The goal of this paper is to propose an over-voltage protection circuit, designed to ensure the integration of low-power pico-hydro systems connected to the grid using conventional photovoltaic microinverters. Extensive tests were performed on an experimental platform using three microinverters easily found on the market and a low power generator (300 W) developed for small wind turbines. The experimental results, demonstrated the performance of the proposed over-voltage protection circuit in four different situations, presented in this work, thus avoiding irreversible damages of generators and microinverters, in the context of the above described grid connection approach.

Keywords: Microgrids · Distributed Generation · Photovoltaic Microinverters.

1 Introduction

The growing need for energy from renewable resources is undeniable today as a consequence of the increase in energy consumption, besides environmental commitments made by many countries to reduce greenhouse gases [3]. The new technologies to be developed for micro-generation based on green energy allow the creation of solutions that currently facilitate the electrification in developing countries [16], as well as promoting self-sustaining, growing systems in developed countries [5, 11]. Distributed generation (DG), through different renewable resource plants, despite the low power, may contribute significantly to the increase in sustainability at the local and global levels [8, 14].

According to [6], small hydropower plants can be considered one of the best methods for producing renewable energy, as long they are based on cheap, reliable, mature technologies and do not cause significant environmental changes where installed. Pico-hydro systems generate up to 5 kW [1] and have potential in meeting growing energy demand, once they allow widespread exploitation of small rivers, shallow water reservoirs, and wastewater [6, 13].

Recent studies have shown the integration of low power wind generators with pico-hydro applications, in which they are connected to the grid through the use of photovoltaic (PV) inverters [9]. PV inverters are mature technologies widely available on the market. Its combination with a permanent magnet synchronous generator (PMSG) is an alternative for energy generation. Although PV inverters have been created to operate with PV modules, a PMSG and a bridge rectifier can be used as DC source, instead of those modules [9, 10].

As is the case with large hydropower plants, in order to provide a stable voltage output, mechanical devices are generally used for water flow adjustments. Afterwards, the rotation of the turbine is controlled so as to reduce voltage and frequency deviation [15]. Hydraulic dynamics, with the seasonal variations of water flow, influence these parameters in a generation. The energy production efficiency is improved with turbines or water wheels performing at variable speed. Therefore, the characteristics of the generators and inverters require that they be integrated. Furthermore, to prevent damage to the electrical system, a protective circuit is required. Indeed, an over-voltage protection circuit is necessary to ensure that, during grid synchronization or disconnection and overpower generation, the generator does not damage the inverter [10].

This paper proposes a simple and low-cost over-voltage protection circuit that limits the rectified DC voltage of the generator by dissipating the energy in a power resistor or by short-circuiting the generator if over-power generation is detected. The reliability of the designed circuit is demonstrated with numerous tests carried out on a laboratory workbench and an experimental platform. The connection of low power PMSGs to the electrical grid through PV microinverters is also demonstrated.

2 Over-Voltage Protection

2.1 Integration Between Generator and PV Inverter

PV inverters, up to 5 kW, are widely diffused, have a competitive cost and are very widespread. There is also a significant set of manufacturers that provide a wide offer of generators, for that power range, namely for small wind turbines. Although the compatibility between PMSGs and PV inverters is not always guaranteed, their integration is possible by combining the safe operating areas of both, shown in Fig. 1.

Three parameters that establish the operating limits in which the inverter can operate, V_{DCmax}, I_{DCmax} and P_{DCmax} which are voltage, current and maximum power, respectively. In Fig. 2, the green lines represent the voltage and current characteristics of a generator after rectifying on the DC side, when it operates with constant speed. The brown area marks the safe operating area of the PV inverter [9].

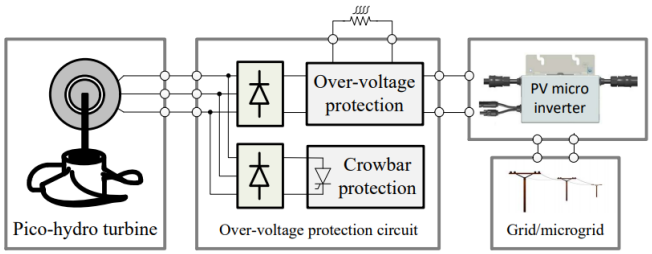

Fig. 1. Design topology for grid-connected pico-hydro systems.

To ensure the generator will work in the safe operating area of the inverter, certain conditions must be guaranteed. First, the no-load DC voltage of the generator, or the one imposed by the protection circuit, must be greater than the voltage $V_{PV_{start}}$ which enables the inverter to start operating. Also, the nominal power of the generator should be in the range of 0,4 P_{DCmax} to P_{DCmax} of the inverter and the output DC voltage of the generator must be within the input voltage range of the inverter, thus less than V_{DCmax}. Finally, the rated current of the generator must be equal to or less than I_{DCmax}. Moreover, a current greater than P_{DCmax}/V_{DCmax} is recommended to ensure that the inverter will be able to process the available power without overloading the generator [10].

An over-voltage protection circuit is required to ensure the operation within the limits V_{DCmax} and P_{DCmax} allowed at the PV inverter input. Another important feature in PV inverters is their internal maximum power point tracking MPPT algorithm, which is the selection of a point of operation where the current and voltage pair allows the process of maximum power available from the connected power source. Unlike PV modules, generators have their maximum power point when their current approaches their rated value $I_{G_{DCrated}}$ [10].

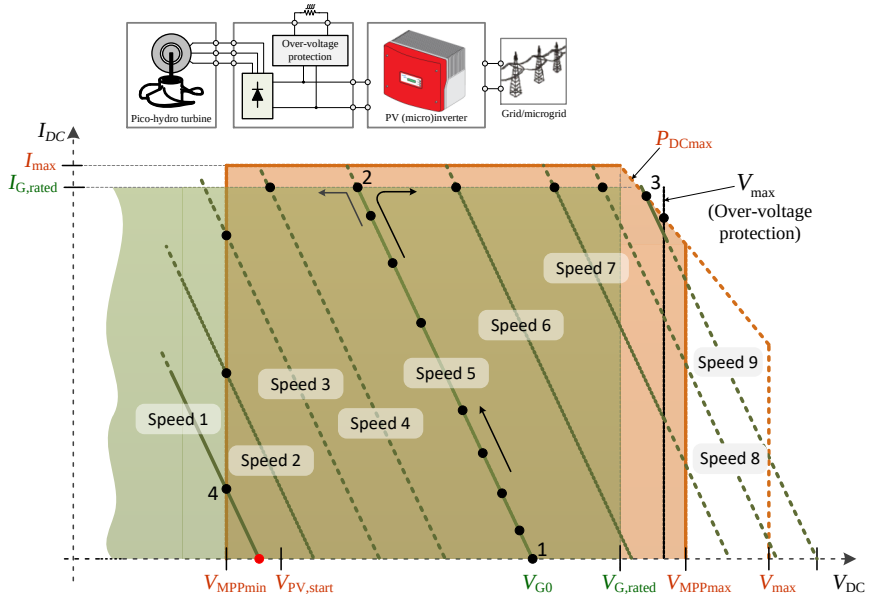

Fig. 2. Overlapping of the operating areas of PV inverter and generator.

Taking into account all of the conditions above and also the MPPT algorithm, the green lines in the graph show the behaviour of the inverter for different speeds of a generator. At "Speed 5", for example, the point at which the generator is operating guarantees that the inverter will turn on, that the MPPT will start at point 1 and it will increase to the maximum current at point 2. If the speed and, consequently, the power increase to "Speed 9", the operating point is defined by point 3 and does not exceed this value, because at that point the protection comes into action and the excess energy is dissipated in the auxiliary resistor. In contrast, if the power and speed decrease to "Speed 1", the inverter operates at point 4, where there is the minimum voltage for which it can operate [10].

2.2 Over-Voltage Protection Circuit

This section presents an over-voltage protection circuit to limit the speed and, consequently, the output DC voltage of the generator. This is done by dissipating the energy in a power resistor or by short-circuiting the generator if the power is too high. The protection circuit is fundamental to ensure that the inverter will not be damaged and whenever the generator runs at no load. This can occur due to:

- Low power demand or high power delivered by the generator;
- Grid failure (e.g. due to frequency or voltage outside the limits) that turns off the inverter;
- The time required by the inverter for synchronization with the grid.

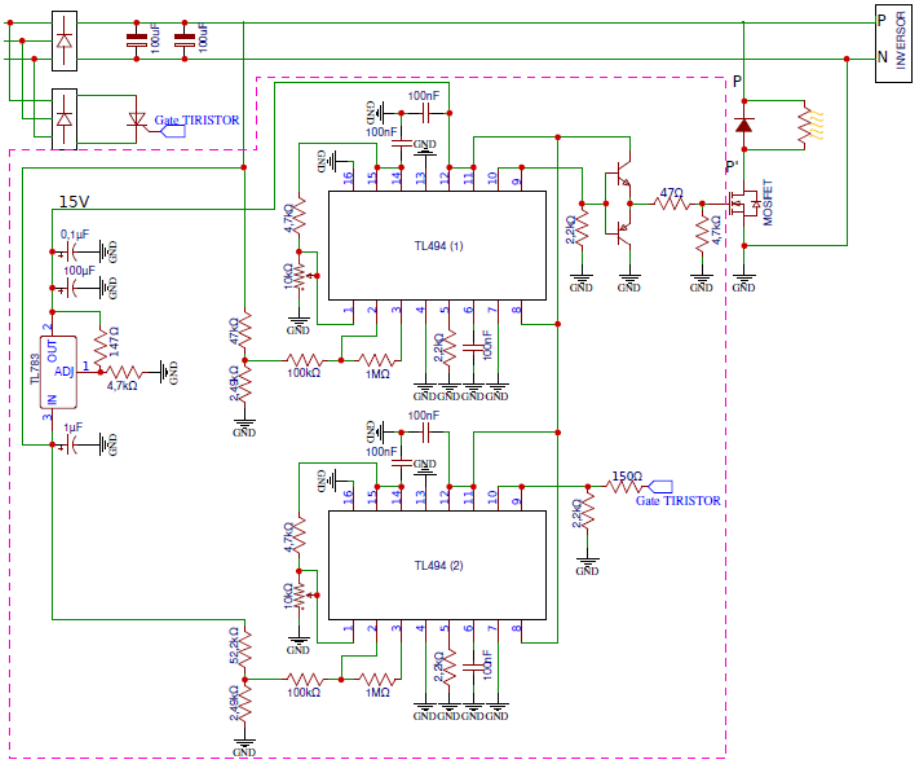

Fig. 3. Over-voltage protection circuit schematic.

The protection circuit schematic is shown in Fig. 3. It is based on a step-down converter with a power MOSFET and a free-wheeling diode to dissipate the energy in a power resistor. The control is performed by Pulse-Width-Modulation (PWM) using the PWM controller TL494(1). A voltage divider (at pin 1), with a 4k7 resistor and a 10k potentiometer, sets the threshold voltage for which the TL494(1) starts the generation of pulses. Another voltage divider (at pin 2) is used to measure the DC output voltage of the generator. The deviation between these two inputs is amplified by one of the two error amplifiers of the TL494. The error controls the generated duty-cycle. The resistor and capacitor connected to pins 5 and 6, respectively, set the switching frequency at approximately 4,54 kHz.

The microinverters used in this work have a V_{DCmax} of 50 V and the V_{MPP} is 40 V as it will be presented later. Therefore, upon reaching a voltage value equal to 45 V on the DC bus, the TL494(1) starts generating pulses with a duty-cycle proportional to the DC voltage. The MOSFET activates the part of the circuit that dissipates the energy in an external resistor R to avoid the no-load operation of the generator and, thus, limiting the DC output voltage. The power resistor must be sized to withstand the P_{DCmax} and at V_{DCmax}, hence:

$$R = \frac{V_{DCmax}^2}{P_{DCmax}}. \quad (1)$$

However, if the PMSG speed or power continues to increase and, therefore, the voltage goes beyond 48 V on the DC bus, a second PWM controller, TL494(2), starts generating pulses, triggering a power thyristor. This action short-circuits the generator and, thus, avoids the destruction of the microinverter by over-voltage. This crowbar protection is a second level of protection and it is expected to operate only in extreme conditions. In normal operating conditions the protection is ensured by the over-voltage protection described above.

3 Experimental Results

This section presents the experimental results achieved with the proposed over-voltage protection circuit. Different operating conditions requiring protection were tested: (a) during the inverter synchronization with the grid, moving from no load to load operation; (b) when the microinverter disconnects from the grid due to a grid failure; (c) when generated power is above P_{DCmax}; and (d) when the PMSG short circuit is required.

For the first two cases, (a) and (b), the test is done using an emulation platform for pico-hydro systems. This structure has a water reservoir, at the height of 3,5 m and 4 pipes with a total water flow of 40 l/s [4]. The pipes have their outlets equally spaced around the blades of a horizontal water wheel prototype. The wind generator 1 (gen. 1), with the characteristics presented in Table 1, is coupled to the water wheel by a 1:5 mechanical transmission.

Table 1. PMSG technical data.

Gen.	**Speed** (rpm)	V_{DCo} (V)	V_{DC} (V)	I_{DC} (A)	P_{DC} (W)
1	300	45	28	10.7	300
2	630	30	24	12.5	300

In the third and fourth cases, (c) and (d), the tests were done on a workbench that has a three-phase induction motor driven by a conventional frequency converter. The PID macro, usually available in the frequency converters, was used to perform a closed-loop control of the shaft (mechanical) power of the generator. For these tests, it was used the wind generator 2 (gen. 2) presented in Table 1. This PMSG was directly connected to the shaft of the induction motor.

The microinverters presented in Table 2 were used in both experimental platforms.

Table 2. Microinverter technical data [2], [12] and [7].

Characteristic	Unit	Microinverter		
		1	**2**	**3**
P_{DCmax}	W	300	300	280
I_{DCmax}	A	11.5	9.5	10
V_{DCmax}	V	50	50	50
V_{DCmin}	V	20	18	22
V_{MPPrange}	V	24-40	20-40	28-40
P_{ACmax}	W	250	235	245

3.1 Results Obtained With an Emulation Platform

As said above, an emulation platform for pico-hydro systems, consisting of a horizontal water wheel, was used for evaluation tests in real conditions. The synchronization test (a) aims to show the performance of the protection circuit when the generator starts with no load and the microinverter initiates the synchronization procedure before connecting to the grid. At first, the generator is loaded by the protection circuit while waiting for the PV microinverter to be able to process the power generated by the turbine (water wheel). During this synchronization time the protection circuit operates and limits the voltage set point as designed. The energy is dissipated in a power resistor preventing damage of the PV microinverter.

During the start-up of the generator shown in Fig. 4(a), the microinverter sought to connect a few times. However, it was unsuccessful at first and the protection circuit actions were required. The microinverter of Fig. 4(b), connects the generator to the grid after about 15 seconds. The protection circuit operates during the last 5 seconds, limiting the DC voltage to 47,2 V. Both figures show the PWM operating as soon as the DC voltage reaches 45 V. For Fig. 4(c), the microinverter was very agile as it started and achieved the steady-state voltage value of approximately 28,8 V, even before the protection circuit was activated.

Similar to what occurs during grid synchronization, a grid failure causes the increase on generator voltage, unless the protection circuit limits the voltage. Test (b) is shown in Fig.5, where the voltage, which was being maintained at an approximately constant operating point by the microinverters, passed to the value limited by the protection circuit, immediately after the grid failure simulation.

3.2 Results Obtained With a Work Bench

The over-power test (c), is performed with a generated power higher than the maximum input power of the microinverter. Fig.6 plots the power dissipated by the protection circuit in the resistive load and the power at the input of the microinverter. The tests were performed increasing the power. As soon as the

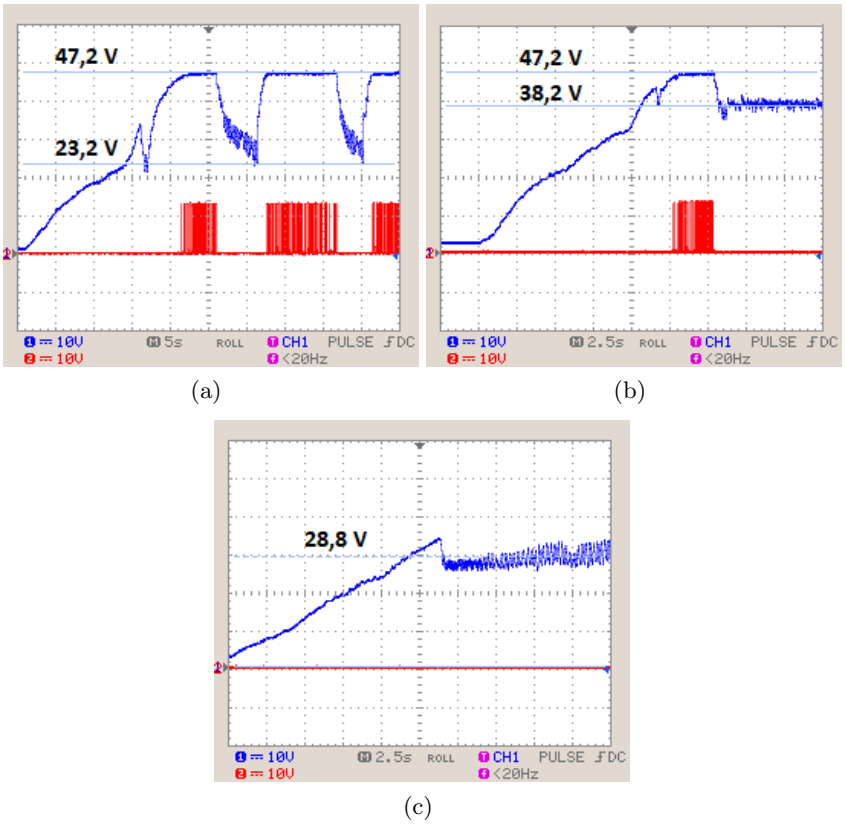

Fig. 4. Over-voltage protection circuit behaviour during generator start-up and grid synchronization tests with (a) Microinverter 1, (b) Microinverter 2 and (c) Microinverter 3.

input power of the microinverter reaches its limit, the protection circuit starts dissipating in the power resistor.

The crowbar test (d) was performed increasing the power until the voltage reached the value designed to short circuit the generator.

Fig.7 illustrates the moment when the short-circuit occurs. First, PWM pulses (in blue) are generated by the over-voltage protection when the DC voltage reaches 45 V. Subsequently, when it catches up 47,2 V, the thyristor is turned on and the voltage falls drastically to a value corresponding to a voltage drop across the thyristor (2,4 V). The final value of short circuit current (for the maximum generated power) was 18 A.

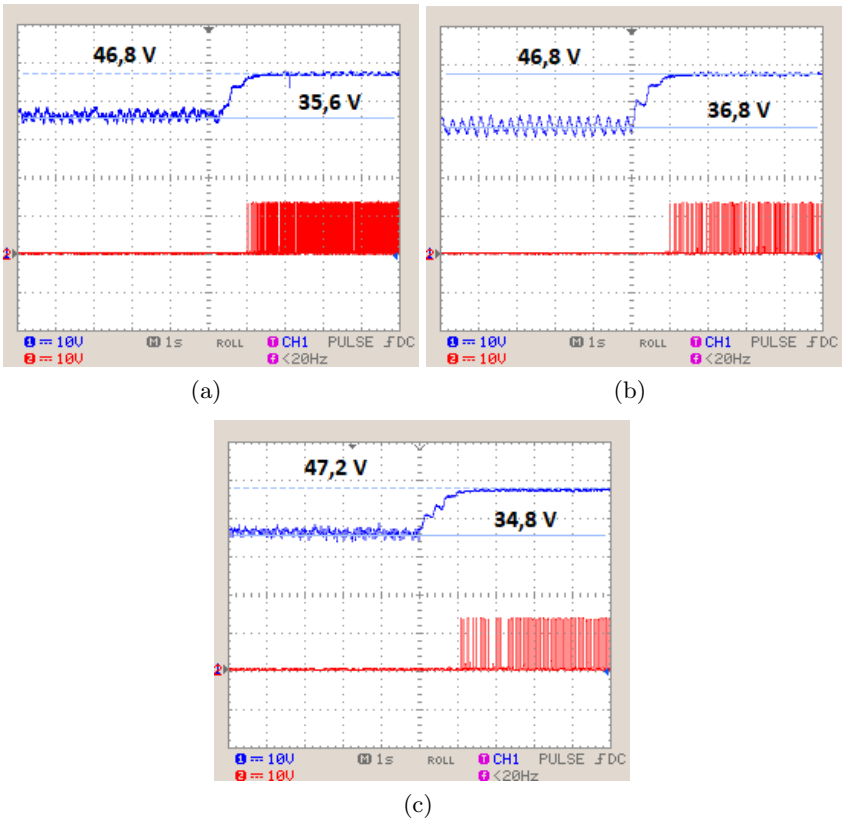

Fig. 5. Over-voltage protection circuit behavior in failure tests with (a) Microinverter 1, (b) Microinverter 2 and (c) Microinverter 3.

4 Discussion

The evaluation results using a benchwork and real emulation platform proved the effectiveness of the protection circuit. Tests with the emulation platform, consisting of a horizontal water wheel, showed that the start-up of the generator (and water wheel) is slow enough for the Microinverter 3 to connect to the grid, even before the protection circuit action is required. Microinverter 2 connected to the grid after about 15 s, but the action of the protection circuit was required during about 5 s to limit the voltage. Microinverter 1 took several seconds to connect to the grid. In this case, the protection circuit limited the DC voltage conveniently.

The performance of the protection was demonstrated when the DC voltage reached the value of 45 V and then limited it to 47,2 V, waiting for the Microinverters 1 and 2 connect the generator to the grid. After the starting transient all microinverters operated with a DC voltage defined by the MPP tracking algo-

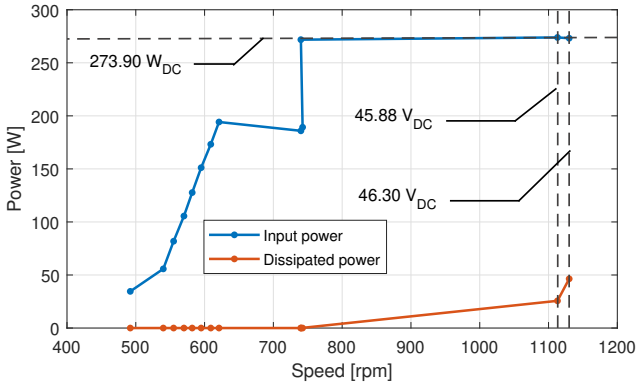

(a)

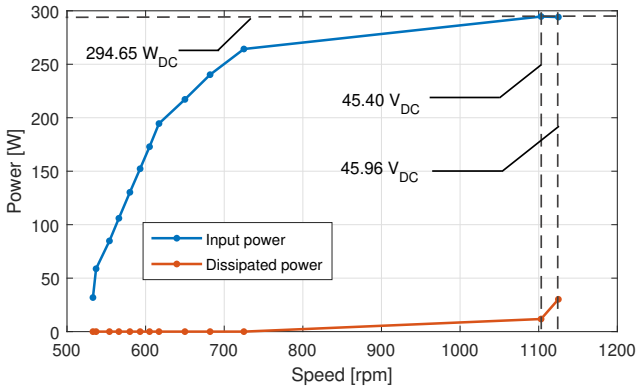

(b)

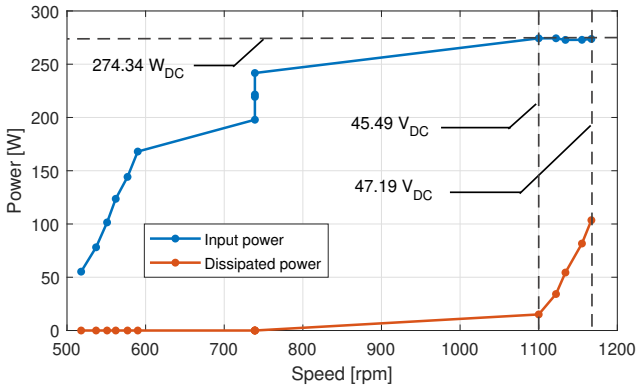

(c)

Fig. 6. Over-voltage protection circuit behaviour with over-power generation tests with (a) Microinverter 1, (b) Microinverter 2 and (c) Microinverter 3.

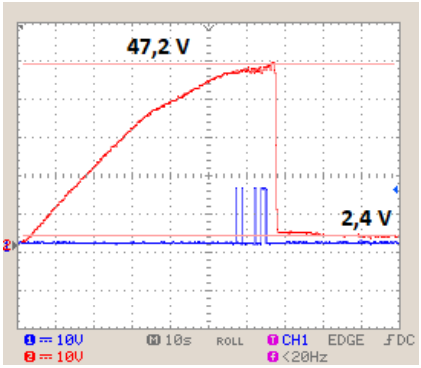

Fig. 7. Over-voltage protection circuit behaviour with a short-circuit test.

rithm (below the protection threshold) and the action of the protection circuit was terminated.

When simulating the grid failure, the protection circuit limited the DC voltage to 46,8 V with the first and second Microinverters and to 47,2 V with the third one. Once again, the developed circuit has proved effectiveness in protecting the devices.

Tests made on a workbench, showed that as the generator power increased, the speed and, therefore, the DC voltage also rose, as seen in Fig. 6. At a certain point, a P_{DCmax} value was reached and the microinverters were no longer able to process the generated power. In this case, the excess was dissipated in the auxiliary power resistor. Notably, the moment when maximum input power is reached, the resistor starts to dissipate. For all cases, the DC voltage protection threshold was approximately 45,50 V.

Moreover, when the generated power (and voltage) is too high, further protection is needed. This is done by short-circuiting the generator. During the test (d) it was demonstrated two protections (dissipation in the resistor and the short-circuit itself) working properly. The generator breaks and the speed is significantly reduced. The voltage in the DC bus is limited to the voltage on the thyristor. This additional protection prevents damage of the devices in extreme situations. In this situation, for the system to resume normal operation, operator intervention may be required. In effect, the thyristor will no longer turn off while there is voltage on the DC bus.

5 Conclusion

Small-scale pico-hydro systems are an interesting energy generation opportunity because they run 24 hours a day. These systems can be easily exploited if standard technology widely available on the market is used, such as generators designed for small wind turbines and photovoltaic microinverters. The integration of this equipment, as distributed energy sources connected to the grid, is

possible with the over-voltage protection circuit proposed and developed in this work. Experimental tests were performed for validation purposes, both in real context with a water wheel or on a workbench. The results demonstrated the usefulness and efficacy of the developed circuit. Two permanent magnet synchronous generators were connected to the grid using three different microinverters. The protection has proved to be effective in the expected situations: during the turbine (generator) starting, while the microinverter is connecting to the grid; when the generator is at no load due to grid failures; and in cases of excessive power. Thus, the developed circuit effectively protects the generator against too high speeds and, consequently, it limits the DC voltage at the input of PV microinverters, whenever these are used for grid connection of pico-hydro turbines.

Acknowledgments. The authors would like to thank FCT (Foundation of Science and Technology, Portugal) for the financial support through the contract SAICT-POL/24376/2016 (POCI-01-0145-FEDER-024376), and to the partnership among IPB, CEFET/RJ and UTFPR in the teaching and research program.

References

1. Basar, M.F., Ahmad, A., Hasim, N., Sopian, K.: Introduction to the pico hydro power and the status of implementation in malaysia. In: 2011 IEEE Student Conference on Research and Development. pp. 283–288 (12 2011). https://doi.org/10.1109/SCOReD.2011.6148751
2. BeOn Energy Ltd., De Timor Street, 35, 7400-214, Ponde de Sor, Portugal: Data Sheet: BeON 1 Microinverter (3 2019)
3. Commission, E.: Novel carbon capture and utilisation technologies. https://ec.europa.eu/research/sam/pdf/ sam_ccu_report.pdf#view=fit&page mode=none, accessed: June, 2019
4. Dalmarco, I., Araujo, P., Leite, V., Queijo, L., Lima, L.: Prototyping a horizontal water wheel for electricity generation in a small museum: The house of silk. In: I Ibero-American Congress of Smart Cities (ICSC-CITIES 2018) (9 2018)
5. Gaius-obaseki, T.: Hydropower opportunities in the water industry. International Journal of Environmental Sciences **1**(3), 392–402 (2010)
6. Hatata, A., El-Saadawi, M., Saad, S.: A feasibility study of small hydro power for selected locations in egypt. Energy Strategy Reviews **24**, 300–313 (2019)
7. INVOLAR Corporation Ltd.: Installation and Operations Manual: INVOLAR MAC250 Photovoltaic Micro-Iverter, 1.2 edn. (8 2011)
8. Lahimer, A., Alghoul, M., Sopian, K., Amin, N., Asim, N., Fadhel, M.: Research and development aspects of pico-hydro power. Renewable and Sustainable Energy Reviews **16**(8), 5861–5878 (2012)
9. Leite, V., Couto, J., Ferreira, Â., Batista, J.: A practical approach for grid-connected pico-hydro systems using conventional photovoltaic inverters. In: 2016 International Energy Conference (ENERGYCON). pp. 1–6. IEEE (2016)

10. Leite, V., Ferreira, Â., Couto, J., Batista, J.: Compatibility analysis of grid-connected pico-hydro systems using conventional photovoltaic inverters. In: 2016 18th European Conference on Power Electronics and Applications (EPE'16 ECCE Europe). pp. 1–9. IEEE (2016)
11. Leite, V., Figueiredo, T., Pinheiro, T., Ferreira, Â., Batista, J.: Dealing with the very small: first steps of a picohydro demonstration project in an university campus. Renewable Energy & Power Quality Journal pp. 683–685 (2012)
12. Logistic, G.W.: Micro-inverters technical details and specifications (6 2019), https://www.ev-power.eu/Micro-Inverters-Tech/
13. Machado, M., et al.: Microturbinas em redes de abastecimento de água. Ph.D. thesis, tese de mestrado, Universidade de Aveiro (2015)
14. Maidana, W., Leite, V., Ferreira, A., Bonaldo, J., Gonçalves, E., Batista, J.: Design of a self-sustainable system based on renewable energy sources for a small museum of science dissemination - the house of silk. in III Congresso Ibero-Americano de Empreendedorismo, Energia, Meio Ambiente e Tecnologia - CIEEMAT 2017, Bragança, Portugal (7 2017)
15. Mhlambi, B.A., Kusakana, K., Raath, J.: Voltage and frequency control of isolated pico-hydro system. In: 2018 Open Innovations Conference (OI). pp. 246–250 (10 2018). https://doi.org/10.1109/OI.2018.8535603
16. Yah, N.F., Oumer, A.N., Idris, M.S.: Small scale hydro-power as a source of renewable energy in malaysia: A review. Renewable and Sustainable Energy Reviews **72**, 228–239 (2017)

Análisis de un microsistema de generación solar fotovoltaico bajo el esquema de balance neto de electricidad (Net Metering): Caso Ecuador

Analysis of a photovoltaic solar generation microsystem under the Net Metering scheme: Ecuador Case

J. Romero[1], J. Flores[1], Luis Hernández-Callejo[2][0000-0002-8822-2948], J.L. Espinoza[1][000-0002-7450-2084] and L.G. González[1][0000-0001-9992-3494]

[1] Universidad de Cuenca, Campus Central, 010104 Cuenca, Ecuador
[2] Universidad de Valladolid, Campus Universitario Duques de Soria, 42004 Soria, Spain
Corresponding author: juan.espinoza@ucuenca.edu.ec, J.L.E.; luis.hernandez.callejo@uva.es, L.H-C.

Abstract: This paper shows a case study of a photovoltaic solar generation microsystem (μPVS) applied to a single-family house in the city of Cuenca, Ecuador under the regulation ARCONEL 003/18, which is based on the Net Metering scheme. The system has a capacity of 550Wp, and allows an estimated monthly generation of 57,91 kWh, which represents 18,1% of the consumption of electricity in the house under study. According to the economic analysis, the system could have a profitability after 11 years, time that seems high but it could be reduced by an eventual increase in the electricity price, by a fall in the cost of the solar system or by an additional incentive to the photovoltaic self-generator. The macroeconomic or environmental benefits offered by the mass installation of μPVS are not considered in the analysis. The study highlights the benefit of applying the Regulation under study, as a policy for promoting photovoltaic solar energy, allowing the use of the national power grid an ideal storage system, without any additional cost.

Keywords: ARCONEL No. 003/18, net metering, Photovoltaic Microgeneration System, solar energy, Ecuador.

Resumen. En el presente trabajo se muestra un caso de estudio de un microsistema de generación solar fotovoltaico (μSFV) instalado en una vivienda unifamiliar en la ciudad de Cuenca, Ecuador, en el marco de la regulación ARCONEL 003/18, misma que se basa en el esquema Net Metering. El sistema utilizado presenta una capacidad de 550Wp, y permite una generación mensual estimada de 57,91 kWh, lo que representa un 18,1% el consumo de energía eléctrica en la vivienda. De acuerdo al análisis económico el sistema podría tener una rentabilidad económica al cabo de 11 años, tiempo que pudiese parecer elevado pero que podría reducirse ante un eventual incremento del precio de la electricidad, por

una reducción del costo del µSFV o por un incentivo adicional al autogenerador fotovoltaico. En el análisis no se contemplan los beneficios macroeconómicos o ambientales que ofrecería la instalación masiva de µSFV. Del estudio, se destaca el beneficio que puede representar la aplicación la Regulación bajo estudio, como política de promoción de la energía solar fotovoltaica, permitiendo el uso del sistema eléctrico nacional como un sistema de almacenamiento ideal, sin ningún costo adicional.

Palabras Clave: Regulación ARCONEL No. 003/18, balance neto, Sistema de Microgeneración Fotovoltaica, energía solar, Ecuador.

1 Background

CO_2 emissions produced by the use of fossil fuels increase year by year, which contributes to accelerating global warming. According to [1] it will be necessary to reduce emissions by 3.5% per year in order to reach the targets set out by the Paris Agreement. To mitigate this problem, many countries, through their energy policies, promote the use of non-conventional renewable energy, where photovoltaic solar energy stands out for its aggressive price reduction in the last decade, in addition to its great scalability. Ecuador presents an important potential for the use of this technology due to its geographical location and its high levels of solar radiation. Despite the availability of solar resources in the country, aspects such as reduced electricity costs (including public subsidies), ignorance of the subject, and complex administrative procedures are some of the aspects that have prevented, or at least slowed down, the development of photovoltaic projects. In addition, hydroelectricity, a cheap energy source, has an important contribution to the Ecuadorian generation matrix. In 2017, the nominal installed power capacity, at the national level, was 8.036,34 MW of which 4.715,15 MW (58,67%) corresponded to renewable energy sources and 3.321,19 MW (41,33%) to non-renewable energy sources. Of the total generation with renewable sources, hydroelectricity, with an installed power of 4.515,96 MW, represented 95,78%, while photovoltaic power capacity (parks connected to the grid) was 26,48 MW, barely 0,56%. [2].

Despite the fact that the country's energy policies aim to promote non-polluting alternative energies, in accordance with higher level legal norms such as the Constitution of the Republic (e.g., Article 15) [4], the Organic Law of the Public Service of Electricity (e.g., Article 26), [5], or the Energy Efficiency Law (e.g., Article 3) [6], the efforts of the State have focused on large-scale renewable generation. Low importance is giving to the potential that cities, through their inhabitants, have to develop their own small-scale generation projects, particularly at the residential level. One of the advantages of solar photovoltaic technology is that it can also be used on a small scale in so-called generation microsystems. Currently, Ecuador does not have precise information on the number of distributed solar generation microsystems, since only photovoltaic projects with capacities between 0,37 MW and 1 MW are considered by national statistics. [3]

Due to the foregoing, on October 22, 2018, the Board of Directors of the Electricity Regulation and Control Agency of Ecuador (ARCONEL) approved Regulation No. ARCONEL 003/18: *"Photovoltaic Generation for Self-Supply of Final Consumers of Electricity"* in order to make photovoltaic microgeneration viable in the country. The norm will allow final users to have their own electrical energy systems for self-consumption. Among other things, the Regulation establishes the technical, commercial, and legal conditions for users to develop their own photovoltaic generation microsystems, with a nominal installed capacity of up to 100kW. These systems may be located on roofs, residential surfaces, or in buildings for the residential and general categories determined in the tariff specifications at low or medium voltage [7].

The objective of this paper is to analyze a photovoltaic solar generation microsystem (µPVS) implemented in a home for self-consumption purposes. To this end, section 2 presents an analysis of the development of photovoltaic solar energy in the Latin American region, with emphasis on the Ecuadorian case. In section 3, the main energy policies to promote small renewable energy systems in the region are briefly described and Arconel Regulation 003/18 is analyzed in detail. In order to know the effect that the cited regulation would have on a residential user who decides to install a µPVS, section 4 presents the tariff scheme in force in Ecuador and section 5 shows a real case study, analyzing a single-family house in the city of Cuenca-Ecuador where a µPVS has been installed. In section 6 the analysis of results is carried out, finally in section 7 the conclusions of the study are presented.

2 Photovoltaic Development in Latinoamerica

As in many other regions of the world, photovoltaic (PV) solar energy has made important advances in the last decade in Latin America, particularly with grid-connected systems (photovoltaic farms). A recent report indicates that the Latin American PV market is on track to grow exponentially, with a cumulative forecast of 41 GW of installed demand by 2020, so by the end of the decade the region is expected to account for 10% of global PV demand [8]. In Latin America, each country has different economic models, policies, regulations, and environmental challenges to face but thanks to its solar potential, there are a large number of photovoltaic projects throughout the region. For example, Honduras went from having 5MW installed in 2014 to 460MW in 2015, Chile had 4,9MW installed in 2012 and reached more than 1.600MW in 2017 [9]. Brazil went from 1MW installed in 2010 to 2.296 MW in 2018, making it the leader in solar power in South America according to [10]. Mexico is another country that in the last decade has grown in solar power capacity as the country went from 25 MW in 2009 to have 3.364 MW of installed capacity in the first quarter of 2019, thanks to its 44 solar farms in which the PV Villanueva Solar Farm stands out with 828 MW, the largest in Latin America [11].

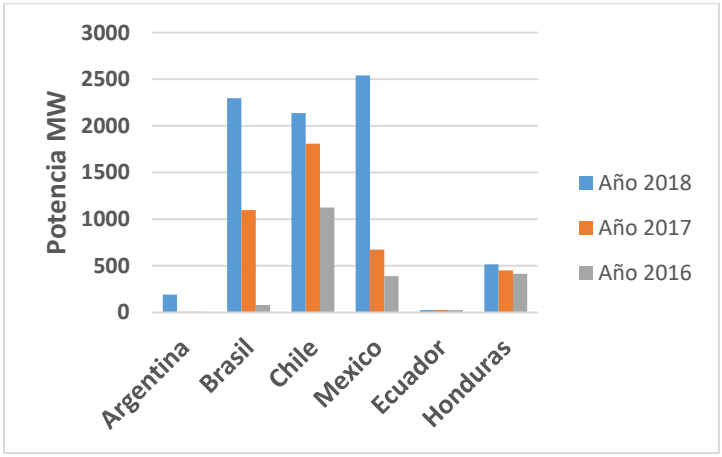

Fig. 1. Photovoltaic Solar Power installed per year in Latin America [12].

An important factor that is helping to integrate solar PV systems into the power generation grids is the reduction of commercial equipment costs. Currently, the price of PV panels per watt peak (Wp) is in the order of 21,5¢USD [13]. However, it is important to note that within the leveled energy costs (LCOE), residential solar PV generation is among the highest as compared to other technologies. In addition, by 2018 residential PV energy had a range of 160-270USD/MWh, while large-scale grid-connected PV systems cost about 50 USD/MWh [14].

2.1 Photovoltaic Energy in Ecuador

Ecuador has a privileged geographical position for reception of solar energy since radiation falls almost perpendicularly on its surface throughout the year, which does not occur elsewhere on the planet. This is why Ecuador has relatively constant insolation, on average approximately 4,574kWh /m^2/day, as shown in Figure 2[3]. In other countries, where solar rays do not strike perpendicularly, this insolation can fall significantly, such as Argentina which, despite having sites with very good radiation, has an average solar radiation of 3 kWh /m^2/day [15].

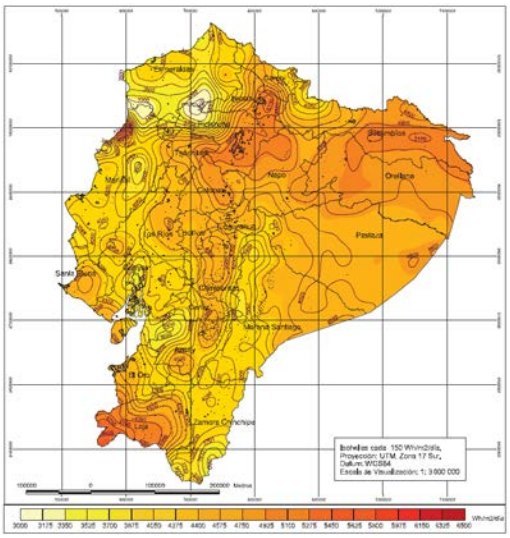

Fig. 2. Average global radiation in Ecuador [3].

From a dynamic point of view, in Ecuador there are great variations of the solar resource, mainly due to the typical cloudiness of the Andes Mountains. Figure 3 shows the solar radiation (in W/m^2) of a typical day in the Andean area, which is the area of the case study (section 5), presenting variations of more than 10% of the power per minute. Faced with this behavioral profile, the massification of residential PV generation systems could cause instability problems in electric power systems with relatively low inertia. However, within Ecuador's power generation matrix, this scenario is not that real due to the strong dependence on hydroelectricity, a power source with high inertia.

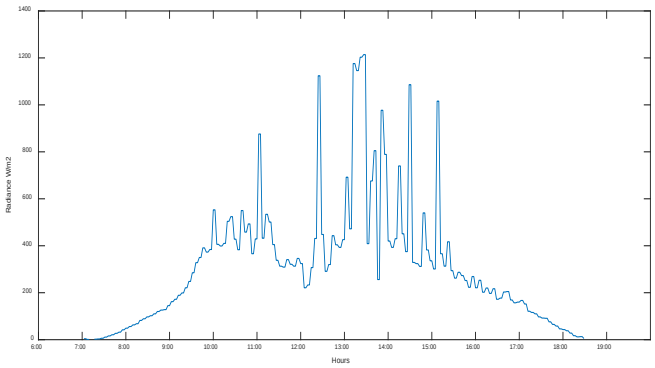

Fig. 3. Typical daily behaviour of solar radiation in the Ecuadorian Andes (August).

3 Energy policies for promoting self-generation with photovoltaic solar energy.

Although Latin American countries have different levels of growth, investment, and development capacity for non-conventional renewable energies, all face common challenges and seek two main objectives in their power sectors: 1) to promote new technologies, diversifying the supply of generation; and 2) to give users the possibility of generating their own energy. For this reason, Latin American countries are implementing policies for the promotion of non-conventional renewable energies and, particularly, for self-generation by users of the distribution grid. Some of the policies implemented for this purpose are summarized below.

Uruguay

In July 2010, thanks to Decree 173/010, Uruguay became the first Latin American country to allow users of the low-voltage distribution grid to generate their own energy, with the possibility of selling it to the electricity grid [16]. This decree establishes that at the end of the month a net balance must be made between the energy generated and consumed by the user. If the user generates more than what she consumes, she can either saves the surplus to discount from future consumption or charges for the energy injected at the same price sold by the power utility.

Brazil

Brazil allows the self-generation of electricity from renewable sources of up to 5 MW of power capacity for final customers under the Normative Resolution ANEEL 482/2012 and 687/2015[17]. This norm establishes that if the client generates more than it consumes, this surplus can be inserted into the grid, and the distributor will return this energy to the client through credits directly on the energy bill. This credit can be used up to 60 months after generation. A great support for microgeneration is that the National Economic and Social Development Bank (BNDES) has financed people interested in microgeneration with loans with an interest rate between 4.03% and 4.55% per year, with a grace period of 3 to 24 months, and 12 years for payment. [18]

Mexico

Mexico has boosted the small-scale solar photovoltaic generation industry thanks to its new regulation for Distributed Generation approved by Mexico's Energy Regulatory Commission (CRE) [19], which states that users can become both consumers and producers of electricity at the same time. The regulation establishes that the installation must be less than 500 kW of capacity under the schemes of Net Metering, Net billing, and total compensation of sale. One of the main advantages of the Mexican policy is that the user takes control of the generation of their own electricity. This seeks to lead to the reduction of demand for electricity generation in peak hours, less infrastructure for the generation and transmission of electricity, and less use of fossil fuels.

Chile

In Chile, the operation of electricity generation equipment that uses non-conventional renewable energy for self-consumption of customers is regulated by the General Law of Electrical Services (Law 21.118) [20], which establishes that the installed power capacity for each individual system must not exceed 300kW. If the generation capacity is higher than the consumption, the surplus energy may be injected into the power grid under the Net billing format. The cost of the energy injected will depend on the price established by each of the distribution companies published in the document Electricity Supply Tariffs [21]. The value that the user receives for the energy injected into the grid will be discounted from the value of his electricity bill corresponding to the month in which the energy injection was made.

Table 1. Average electricity price (resid.) in some Latin American countries [22].

COUNTRY	ECUADOR	MEXICO	CHILE	BRAZIL	URUGUAY
COSTS (USD/ kWh)	0,0983	0,0615	0,1562	0,105	0,2128

It is worth to mention that the predominant energy policy or scheme in the cases cited has to do with Net Metering or Net billing, which leads to total sales compensation at the end of a given period of time. According to Table 1, Uruguay has the highest electricity price per kWh in the group of countries, being the place where the application of these policies would have a higher impact on the end consumer. This scheme, which is summarized in section 3.1, is also applied in the Ecuadorian Regulation ARCONEL 003/18, as explained in section 3.2.

3.1 NET METERING

Net Metering is a system that allows consumers to generate electricity on their own from non-conventional renewable energy sources. Net Metering was born in the U.S. in the 1980s as a response to the request of several self-producers with small renewable power stations in order to get an energy credit for future use. The principle of operation is simple, the owner of a house can have his own energy system and can also receive electricity from the public power grid; the surplus of energy that he may have is delivered to the power grid for future use or sale, all this recorded in a bidirectional type meter that register these values [23]. Figure 4 shows the net metering scheme.

Advantages of Net Metering [23].

- Reduces electricity bills immediately
- Supports the development of non-conventional renewable energy sources and energy saving at household level.
- Longer time use of self-generation electricity without the need for storage.
- It is not required to install another meter for energy sale.
- Lower investment risk.

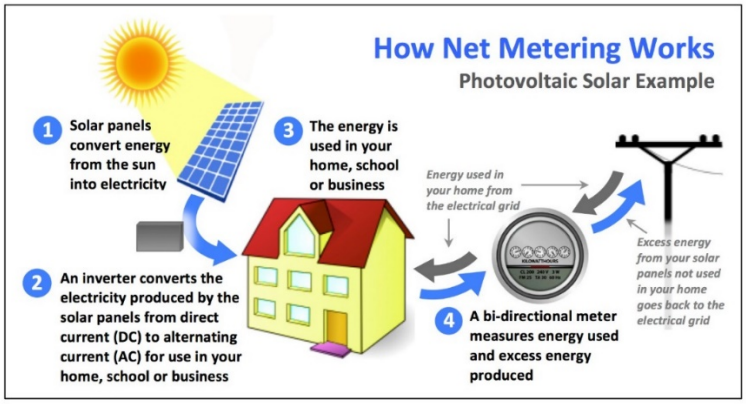

Fig. 4. Net Metering Scheme [24]

3.2 Regulation ARCONEL - 003/18

This regulation allows the use of the µPVS for 20 years from its installation, and applies to distribution companies and regulated users who have installed a system with a nominal capacity of up to 100 kW. The norm will be applicable temporarily for residential consumers who are interested in installing µPVS up to 300 kW nominal capacity and up to 1000 kW for commercial or industrial consumers, operating in synchronism with the power grid [7].

The Regulation establishes the administrative procedures to be considered for its application, emphasizing that they require duly certified studies and authorizations by national and regional energy agencies. The administrative processes may require more than 45 days. Within the Regulation, the µPVS installation contemplates a bidirectional meter that allows to count the energy consumed and delivered to the public electric grid. The meter monthly register the net balance of the energy delivered and consumed by the user with the µPVS, by means of equation (1):

$$\Delta E = (Energy\ consumed\ from\ the\ grid - Energy\ injected\ into\ the\ grid) \quad (1)$$

If the result of the monthly net energy balance (ΔE) is positive, it represents a balance in favor of the power company, it will not be subject to the subsidies (detailed in section 4) or any other subsidy. Conversely, if there is a negative remaining balance, this is considered energy delivered to the grid in favor of the consumer with µPVS. This will be an energy credit in favor of the user that will be carried forward to the following month and so on up to a maximum period of 2 years, after this, the accumulated credit will be lost and started again at zero. According to the regulation, the hourly demand is not discriminated, so, in terms of the energy balance, the energy delivered by the photovoltaic solar system, during the hours of solar radiation, can be used at another time without any restriction. In this context, the national power grid could be considered as an ideal storage system, where neither efficiency in the "load cycle" nor the "number of load cycles" are accounted for determining the “useful life” of this storage system.

4 Electricity tariff scheme in Ecuador

In Ecuador, as a national policy, the strategic sectors (including energy) are managed by the State. Electricity prices are regulated and these values may contain an important subsidy from the State, stratified according to demand. The residential tariff applies to all consumers subject to this category, regardless of the connected load, having a stratified cost according to Table 1. The tariff is ruled by national policies according to [25], while the marketing cost presents a fixed charge of 1,414 USD per consumer.

The Ecuadorian State grants a subsidy to the country's residential users located in terms of energy consumption in quintiles 1 and 2 of population (low income sectors), which currently represent a monthly consumption of up to 110 kWh-months. This subsidy called "Dignity Tariff Subsidy" provides an exemption of US$0.04/kWh and US$0.07/consumer [26].

Table 2, Tariff Schedule (residential sector) applied by the distribution company in the study area [25].

Consumption Range (kWh)	USD/kWh	Consumption Range (kWh)	USD/kWh
1-50	0,091	351-500	0,105
51-100	0,093	501-700	0,1285
101-150	0,095	701-1000	0,1450
151-200	0,097	1001-1500	0,1709
201-250	0,099	1501-2500	0,2752
251-300	0,101	2501-3500	0,4360
301-350	0,103	Higher	0,6812

Within the pricing policies, the residential sector does not contemplate the cost of hourly demand, which is not the case for the rest of consumption sectors. Therefore, Regulation ARCONEL 003/18 does not discriminate against hourly demand in its application.

5 Case study: µPVS in a single-family residence.

In order to analyze the impact that Regulation No. ARCONEL -003/18 could have, a house located on the outskirts of the city of Cuenca was selected. Cuenca is the third city of Ecuador, with an approximate population of 500,000 inhabitants and is located in the south of the Andean region of the country, at an altitude of 2,500 meters above sea level. The house in study belongs to a middle-class family of four people, has a construction area of approximately 200 m^2, where a single-phase µPVS was installed. The system has a nominal power of 550Wp and consists of two photovoltaic solar panels, both with nominal power of 275Wp [27], connected to a microinverter with nominal power of 600W, with maximum efficiency of 91% and harmonic distortion of maximum current (THDmax) of 5% [28]. The single-family house has a two-phase power supply (220 V) from the electricity distribution company, and the µPVS has been connected to the circuit containing loads with higher daytime consumption such as the refrigerator and other household appliances. From the aesthetic point of view, the photovoltaic panels are integrated into the architecture of the dwelling, presenting harmony with the facade (figure 5).

Fig. 5. Side view of the house with the photovoltaic system under study.

5.1 Energy analysis in µPVS

With the implementation of the µPVS under study, a set of electrical variables of the system was recorded as well as the energy consumed by the home. For the study, the energy measurement equipment (PW3337) of the manufacturer HIOKI was used. In August 2019, the values of energy generated by the panels were recorded in the interval from 06:00AM to 06:00PM, a period where solar radiation allows the generation of

electricity as a complement to the electricity demanded by the home. Figure 3 shows the behavior of solar radiation on one day of the month under study, taken at a distance of 2,7 km from the residence, using the weather station available at [29]. Figure 6 shows the dynamic behavior of the µPVS and the consumption of the house on a typical day of the month under analysis.

In figure 6, it is observed that the consumption behavior of the house presents specific loads higher than 1,500 W, in the time slot between 7:30AM and 8:30AM due to the habits of the family (use of microwave oven, washing machine, etc.). In the same figure it is observed that the power from the photovoltaic system does not exceed 520W, presenting energy injection into the grid during the coincidence of solar radiation rise and reduction of the house demand. From the energy point of view, Figure 7 shows the energy profile during a typical day of August. At the end of this month, the µPVS generated 49 kWh, which allows 3.29 Peak Sun-Hours (PSH), similar to the study [30]. For an annual projection for the installed system, with an efficiency of 90% and an average value of 3,9 PSH according to [30], 57,915 kWh could be generated monthly. Considering this last value generated by the µPVS, the power consumption of the house from the electricity grid (with the contribution of the µPVS) would drop from 320 kWh to 262.1kWh during the month under analysis. It is important to highlight that the surplus of energy that is injected into the national power grid during the analysis period reached 5.94kWh, which represents 10.26% of the energy generated by the µPVS.

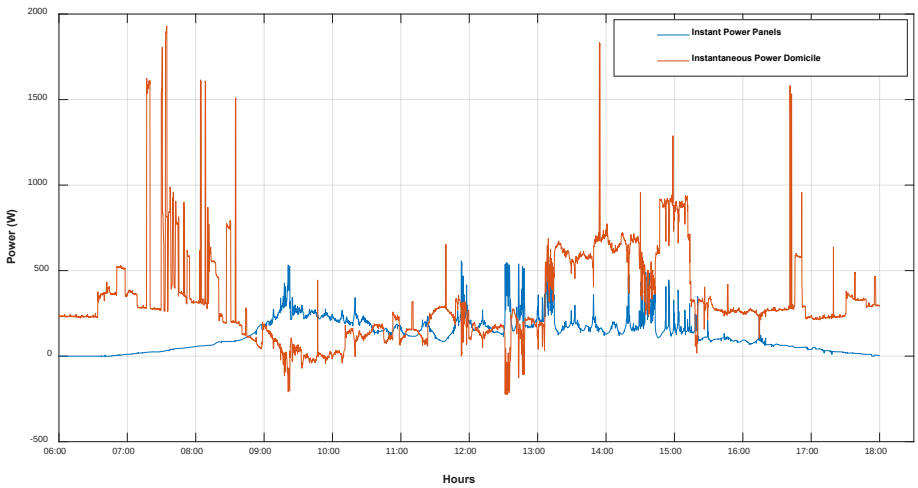

Fig. 6. Power curves: consumed by the home (red); produced by the panels (blue).

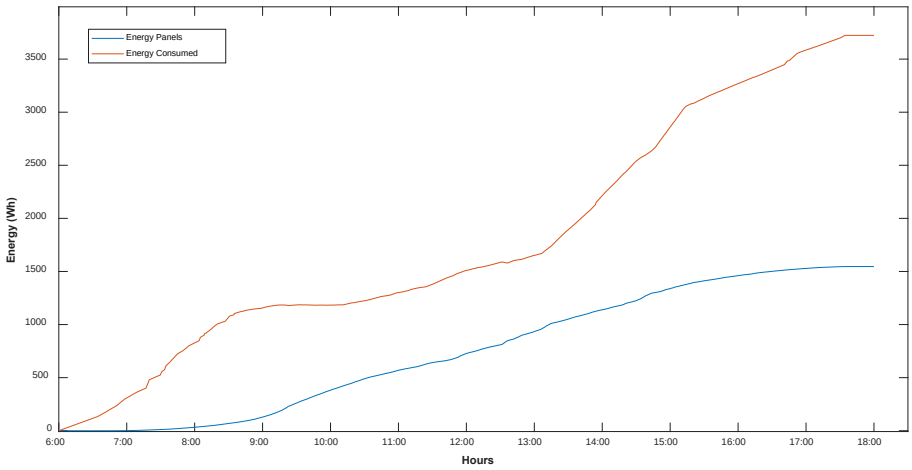

Fig. 7. Curves of the energy consumed by the home (red) and the energy produced by the panels (blue).

6 Analysis of Results

For the study of energy consumption, the electricity bill of the selected house presents an average monthly consumption of 320kWh. By means of the µPVS installed, monthly electricity consumption could be reduced to 262,1 kWh, which represents a drop of approximately 18,1%.
In environmental terms, the reduction in electricity consumption represents approximately 28,37kg of CO_2 per month considering an emission factor of 0.49 tCO2 / MWh [31]. In economic terms, the cost of electricity consumed by the home, whose tariff stratum is between 301-350 kWh/month, at a price of 0.103USD/kWh, would be reduced by 2.06 USD of monthly expenditure. The remaining kWh saved would fall in the segment between 251-300 kWh/month, at a price of 0.101USD/kWh, which would reduce an additional 3.82 USD. Therefore, if the user consumes between 301-350 kWh/month he would have a total saving of 5.88 USD per month with the µPVS installed. With an annual projection the installed system could save a total of 70.56 USD. In relation to the investment made, the analyzed µPVS has an approximate cost of 600 USD, which represents 1.1 USD/Wp.

Projecting these values over time, and with a cost of money at 5% per year, the owner of the installed system could get back the investment in approximately 11 years. In the event of an increase in the cost of energy to an average of 0.15 USD/kWh, the system could be amortized over a period close to 6.5 years. This scenario could take the form of either a reform of the current tariff scheme (tariff increase) or an additional incentive

to the photovoltaic self-generator consisting of an extra payment ("premium") over the cost of the conventional kWh.

7 Conclusions

The present paper shows a case study of a photovoltaic solar generation microsystem applied to a single-family house located in Cuenca, Ecuador, within the context of the ARCONEL 003/18 regulation, in force since the end of 2018, and which is based on the net metering scheme. The photovoltaic system has a capacity of 550Wp, and allows an estimated monthly generation of 57,91 kWh, which represents 18,1% of electricity consumption in the house under study. According to the economic analysis, the system would be profitable after 11 years, a time that seems high but that can be reduced by an increase in the price of electricity, by a reduction in the cost of the µSFV, or by an additional incentive to the photovoltaic self-producer. However, the analysis does not consider the benefits for the Ecuadorian electricity system in macroeconomic terms (e.g. avoided investment in new generation) as well as environmental terms (e.g. reduction of CO_2 emissions) that the massive installation of µPVS would present. The study highlights the benefit that the application of the Regulation under study can offer, as a policy to promote photovoltaic solar energy, allowing the use of the national power grid as an ideal storage system, without any additional cost.

References

1. IRENA, Global energy transformation: A roadmap to 2050 (2019 edition), International Renewable Energy Agency, Abu Dhabi (2019).
2. ARCONEL, Atlas del Sector Eléctrico Ecuatoriano, pp. 1-168(2017)
3. Consejo Nacional de Electricidad (CONELEC), Atlas solar del Ecuador con fines de generación eléctrica, pp. 2-51 (2008).
4. Asamblea Nacional, Constitución de la República del Ecuador, pp. 24-25 (2008).
5. Asamblea Nacional, Ley orgánica del servicio público de energía eléctrica, pp. 12 (2015).
6. Asamblea Nacional, Ley orgánica de eficiencia energética, pp. 1-8 (2019).
7. Agencia de Regulación y Control de Electricidad (ARCONEL), Regulación Nro. ARCONEL-003/18, pp. 1-42 (2018).
8. GTM Research, https://www.greentechmedia.com/articles/read/explaining-latin-americas-impending-solar-boom1#gs.wtkai1, 2017/03/10.
9. Energía Limpia XXI, https://energialimpiaparatodos.com/2019/08/02/argentina-chile-brasil-y-mexico-lideran-energia-eolica-solar-y-biomasa-4/, 2019/08/02.
10. Renovables Verdes, https://www.renovablesverdes.com/boom-fotovoltaico-latinoamerica/, 2017/04/21
11. IRENA, Estadística de energía renovable 2019, pp. 1-398 (2019).
12. GTM Research, https://www.greentechmedia.com/articles/read/explaining-latin-americas-impending-solar-boom1#gs.wtkai1, 2017/03/10.
13. ANEEL, resolução normativa N 687, pp. 1-25 (2015).
14. Global Market Outlook For Solar Power, http://www.solarpowereurope.org/wp-content/uploads/2019/05/SolarPower-Europe-Global-Market-Outlook-2019-2023.pdf(2019).

15. Energías Sustentables, http://www.energiasustentables.com.ar/energia%20solar/argentina.html.
16. Dirección Nacional de Energía (DNE), Guía para microgeneración en Uruguay, pp. 1-9 (2013).
17. ANEEL, resolução normativa N 482, pp. 1-12 (2011).
18. ANEEL, resolução normativa N 687, pp. 1-25 (2015).
19. Comisión Reguladora de Energía, http://www.dof.gob.mx/nota_detalle_popup.php?codigo=5474790, 2017/03/07
20. Ministerio de Energía, Ley Núm. 21.118, pp. 1-4 (2018).
21. Ministerio de Energía, Tarifas de Suministro Eléctrico, pp. 1-12 (2019).
22. Osinergmin, http://observatorio.osinergmin.gob.pe/tarifas-electricas-residenciales-latinoamerica.
23. S.W.H. group, http://www.swhgroup.eu/sp-net-metering.html,2018/01/15
24. Ministerio de Energía, Ley de Generación Distribuida, pp. 1-32(2017).
25. ARCONEL, Pliego Tarifario para las empresas eléctricas de distribución codificado, pp. 1-38 (2019).
26. ARCONEL, Resolución Nro. ARCONEL-040/18, pp. 1-6(2018).
27. JinKo Solar, https://www.jinkosolar.com/ftp/SP-MKT-275PP-60(4BB).pdf (2015).
28. Kaideng Microinverters, https://heliomotion.com/app/uploads/wvc-600-manual.pdf (2014).
29. J. L. Espinoza, L. G. Gonzalez, and R. Sempertegui, “Micro grid laboratory as a tool for research on non-conventional energy sources in Ecuador,” in *2017 IEEE International Autumn Meeting on Power, Electronics and Computing (ROPEC)*, 2017, pp. 1–7.
30. Marcelo Cárdenas, Estudio técnico económico de la energía solar fotovoltaica y mini eólica a pequeña escala, pp. 1-152(2019).
31. Operador Nacional de Electricidad CENACE, Informe Anual 2018, pp. 124(2018).

Short term load forecasting of industrial electricity using machine learning

Rodrigo Porteiro[1], Sergio Nesmachnow[2], and Luis Hernández-Callejo[3]

[1] UTE
rporteiro@ute.com.uy
[2] Universidad de la República, Uruguay
sergion@fing.edu.uy
[3] Universidad de Valladolid, Spain
luis.hernandez.callejo@uva.es

Abstract. Forecasting the day-ahead electricity load is beneficial for both suppliers and consumers. The reduction of electricity waste and the rational dispatch of electric generator units can be significantly improved with accurate load forecasts. This article is focused on studying and developing computational intelligence techniques for electricity load forecasting. Several models are developed to forecast the electricity load of the next hour using real data from an industrial pole in Spain. Feature selection and feature extraction are performed to reduce overfitting and therefore achieve better models, reducing the training time of the developed methods. The best of the implemented models is optimized using grid search strategies on hyperparameter space. Then, twenty four different instances of the optimal model are trained to forecast the next twenty four hours. Considering the computational complexity of the applied techniques, they are developed and evaluated on the computational platform of the National Supercomputing Center (Cluster-UY), Uruguay. Standard performance metrics are applied to evaluate the proposed models. The main results indicate that the best model based on ExtraTreesRegressor obtained has a mean absolute percentage error of 2.55% on day ahead hourly forecast which is a promising result.

1 Introduction

Decision making in the energy sector was historically supported by information that allows predicting, with certain degree of uncertainty, the variables that affect these decisions [8, 22]. Much of the useful information is related to natural variables (e.g., temperature, wind speed, humidity). Other information is related to the energy consumption profile of users. In recent years, the sources of energy generation have diversified in the world. Many renewable sources that are directly related to natural variables have been incorporated [16].

All of aforementioned issues implies that for making decisions is necessary to take into account a large number of stochastic variables, to ensure that they are feasible/optimal from the economic point of view. The increase in complexity

associated with the number of variables to be considered is mitigated by two factors. On the one hand, the sources of data on the variables have multiplied, since many technological components of measurement have emerged in all disciplines and the hardware infrastructure that supports these components has developed strongly. On the other hand, multiple new uses for energy have emerged.

The new reality presents the challenge of developing new tools that allow taking advantage of available data as much as possible. Classic statistical models that were always useful for making predictions have clear limitations in this new context. Computational intelligence algorithms have shown in recent years to perform excellently for forecasting in different areas [11, 13, 15]. These methods are able to learn the most relevant features of the data to be taken into account in order to provide a precise forecast, thus providing excellent results by excluding information of little relevance and considering the most relevant one.

In this line of work, this article presents the application of several prediction algorithms based on computational intelligence to forecast the electricity demand of an industrial pole for the next hour. The modeled scenario is based on historical demand data of an industrial pole in Spain from 2014 to 2017. From the study and comparison of the results of the algorithms developed for the next hour, a model is constructed to forecast the next 24 hours. This model is based on optimizing the algorithm that presented the best results for the one hour forecast and extending it to 24 hours forecast. The major contributions of this research are: *i*) the evaluation and comparison of computational intelligence models applied to forecasting the demand of an industrial pole in Spain, and *ii*) the optimization of the model using the infrastructure of the National Supercomputing Center, in Uruguay.

The article is organized as follows. Section 2 presents the formulation of the day ahead forecasting problem and a review of related works. Section 3 describes the proposed approach to solve the problem proposed. Section 4 presents Experimental Analysis of the problem. In section 4.5 analysis of the best method and extension to 24 hour load forecast is presented. Finally, section 5 formulates the main conclusions and lines for future work.

2 Load Forecasting

This section introduces the load forecasting problem, describes forecasting techniques, and reviews related works.

2.1 General considerations

The load forecasting problem is usually approached applying mathematical methods using historical data to predict the demand of electric power. In general, there is no method that can be used in all types of load forecasting. Thus, an appropriate method must be found for each load profile. Using historical data of a particular load profile is common in practice to determine the most effective algorithm. Electric load forecasting can be classified by time horizon to forecast:

i) ultra short-term load forecasting: up to a few minutes ahead; ii) short-term load forecasting: up to few days ahead; iii) medium-term load forecasting: up to few month ahead; and long-term load forecasting: years ahead. Different techniques are applied when considering each time horizon. This work focuses in short-term load forecasting using historical data.

The energy management and operation of grids becomes highly difficult and uncertain, particularly when new technologies were incorporated. The power demand of end customers is versatile and is changing on hourly, daily, weekly, and seasonally basis. Hence, there is a real need of developing a model for precise and accurate forecasting at different time horizons, depending on the management goals. Day ahead hourly power load prediction is considered a short term forecasting problem, and it is very important to develop very precise models for solving this particular problem.

This work focuses on industrial power consumption. Residential (domestic) power profiles are usually very variable, mainly dependent on the time of the day and the day of the week, but it also dependent on occasional vacations and other particular factors. On the other hand, industrial users power profile tends to be more stable due to the needs of the industrial process itself.

There are two classes of forecasting models for predicting power profile: statistical and physical models. The main purpose of both classes of models is to predict the power profile at a future time frame. Statistical models can be built for time series analysis. Computationally, statistical models are less complex than physical models and are suitable for short term prediction. Physical models are based on differential equations for relating the dynamics of the environment and generally are applied for long term forecasting. In the present work, statistical models are selected for short term forecasting due to their very good prediction accuracy and lower complexity.

2.2 Problem formulation and strategies

Relation between one hour and 24 hour forecasting. The main goal of the study reported in this article is to apply computational intelligence methods to develop a model for electricity load 24 hours ahead forecasting. When historical data are available with hourly frequency is natural to develop a model that predicts next hour. From that model, a multi-step time forecasting model can be constructed, in this case 24 steps in the future.

Four strategies are typically applied for multi-step forecasting starting from a one-step model:

– *Direct strategies* develop a different model for each time step to be predicted. Assuming past observations of the variable to be predicted are used, this strategy implies, in case of 24 steps, developing 24 models with the structure defined in Eq. 1, where $pred_t$ is the prediction of time t value and obs_t is the observed value at time t.

$$
\begin{aligned}
pred_{(t+1)} &= model_1(obs_t, obs_{(t-1)}, ..., obs_{(t-n)}) \\
pred_{(t+2)} &= model_2(obs_t, obs_{(t-1)}, ..., obs_{(t-n)}) \\
&\dots \\
pred_{(t+24)} &= model_{24}(obs_t, obs_{(t-1)}, ..., obs_{(t-n)})
\end{aligned} \tag{1}
$$

Unfortunately, a direct strategy implies developing a model for each time step to be predicted and consequently is very expensive computationally. In addition, temporary dependencies are not explicitly preserved between consecutive time steps.

– *Recursive strategies* apply a one-step model (recursively), multiple times. The predictions for previous time steps are used as input for making a prediction on the following time step. The structure to develop for a recursive strategy is presented in Eq. 2.

$$
\begin{aligned}
pred_{(t+1)} &= model_1(obs_t, obs_{(t-1)}, ..., obs_{(t-n)}) \\
pred_{(t+2)} &= model_1(pred_{(t+1)}, obs_t, obs_{(t-1)}, ..., obs_{(t-n+1)}) \\
&\dots \\
pred_{(t+24)} &= model_1(pred_{(t+23)}, pred_{(t+22)}, ..., pred_{(t+1)}, obs_{(t-n+23)})
\end{aligned} \tag{2}
$$

In this strategy predictions are used instead of observations. A single model is trained, but the recursive structure allows prediction errors to accumulate and the performance of the model can quickly degrade as the time horizon increases.

– *Hybrid strategies* combine the previously described to get benefits form both methods. A separate model is constructed for each time step to be predicted. Each model may use the predictions made by models at prior time steps as input values. For example, using all known prediction, a hybrid strategy produces the structure in Eq. 3.

$$
\begin{aligned}
pred_{(t+1)} &= model_1(obs_t, obs_{(t-1)}, ..., obs_{(t-n)}) \\
pred_{(t+2)} &= model_1(pred_{(t+1)}, obs_t, ..., obs_{(t-n)}) \\
&\dots \\
pred_{(t+24)} &= model_1(pred_{(t+23)}, pred_{(t+22)}, ..., obs_t, ..., obs(t-n))
\end{aligned} \tag{3}
$$

– *Multiple output strategies* develop a model that has as output all time steps to be predicted (in this case 24). Multiple output models are more complex as they can learn the dependence structure between inputs and outputs as well as between outputs. For this reason, they are slower to train and require more data to avoid overfitting. Eq. 4 shows the corresponding structure.

$$
pred_{(t+1,...,t+24)} = model_1(obs(t), obs(t-1), ..., obs(t-n)) \tag{4}
$$

In this work, hybrid strategies are applied for solving the forecasting problem.

One hour forecasting model training. Section 2.3 reviews different approaches and methods for short term load forecasting. This work explores the use of machine learning techniques, mainly those based on model ensembles. Feature selection is commonly applied in this kind of problems due to several reasons. Simpler models are easier to interpret, and have shorter training times. Also, the size of the model using less features is smaller, mitigating the *curse of dimensionality* [3]. But the main reason to apply feature selection is to reduce overfitting, enhancing generalization of the model to unseen data.

Once established the strategy to extend the next hour forecasting models to twenty four hours model, the main issue is to obtain the best possible model for the next hour. With this purpose, standard steps are taken: i) data gathering, ii) data preparation, iii) choosing a model, iv) training, v) evaluation, vi) parameter tuning, and vii) testing. Each of these steps is described in detail in section 3.

Complete model. After obtaining a one hour model with optimized parameters, it is trained for the next hour taking all steps mentioned. Thus, 24 four different instances of this model are trained, one for each of the next 24 hours. Then, the hybrid strategy described in Eq. 3 is applied to build a 24 hour forecasting model. The complete model is evaluated on testing data and results are reported.

2.3 Related works

Several methods support electricity demand forecasting, applying short, medium and long-term predictions. These methods are classified in statistical models and machine learning models. This work focuses on short-term load forecasting using machine learning.

Most used forecasting techniques include auto regressive models (AR), moving average models (MA), auto regressive moving average models (ARMA) and auto regressive integrated moving average (ARIMA) models [24]. These kind of models are easy to implement. ARIMA models for short term load forecasting were initially proposed by Hagan and Behr [12]. Taylor and McSharry [26] compared different ARIMA implementations using load data from multiple countries. Linear regression technique was described by Dudek [10]. However, linear models are inadequate to represent the non-linear behavior of electricity load series and fail to predict the accurate future demand values. Thus, their forecasting accuracy tends to be poor.

Several studies have been conducted on short-term load forecasting using non-linear models. For example, Do et al. [9] described a model for predicting hourly electricity demand considering temperature, industrial production levels, daylight hours, day of the week, and month of the year to forecast electricity consumption. Results suggested that consumption is better modeled considering each hour separately. In our work, this strategy is developed and applied. Son and Kim [25] proposed a method based on support vector regression preceded by feature selection for the short-term forecasting of electricity demand for the residential sector. For feature selection, twenty influential variables were considered and the quality of the model improved substantially.

Peak load estimation is also crucial to determine future demand, in order to assist future investment decisions [21]. In this article, the decision to consider ensemble models was taken based in the work presented by Burger and Moura [5], who applied a gated ensemble learning method for short-term electricity demand forecasting and showed that the combination of multiple models yielded better results than the use of a single model. Silva [23] presented a complex feature engineering to build gradient boosted decision trees and linear regression models for wind forecasting; in our work several similar ideas were developed for demand forecasting. De Felice et al. [7] applied several separate models for each hourly period. Each of those models measure variations in electricity demand based on multiple variables.

The analysis of the related works allowed to conclude that two main issues impact on the forecasting capabilities and the results quiality: the model itself and other preparation and pre-processing techniques. Several works applied techniques like data normalization, filtering of outliers, clustering of data or decomposition by transformations [1,2,6,14] in order to improve the results. In our research, several data preparation techniques are applied for building a robust approach for short term energy utilization forecasting. Next section describes the proposed approach.

3 The proposed approach for day ahead industrial load forecasting

This section describes the proposed approach to solve the day-ahead electricity load forecasting for an industrial pole in Spain, applying the strategies described in Section 2.2.

3.1 General approach

Data description, data preparation, and metrics. The analysis reported in this article considers historical hourly energy consumption data from an industrial pole in Spain. This data was collected between January 2014 and December 2017. The dataset studied in the research is formed by industrial energy consumption measurements. Each measurement is composed of:

- *Year* (integer), representing the year on which the measure was taken.
- *Month* (integer), indicating the month on which the measure was taken.
- *Day* (integer), indicating the day on which the measure was taken.
- *Hour* (integer), indicating the hour on which the measure was taken.
- *Dayofweek* (integer), indicating the day on which the measure was taken.
- *Workingday* (boolean), indicating whether the measure was taking in a working day or not.
- *Useful* (boolean), indicating whether the measure is valid.
- *Demand* (float), indicating the real power measured.

The data preparation consists in replacing useless measures or outliers using information from neighboring hours. A few useless measures and outliers were found (less than 0.0001%), and none of this measueres corresponded to consecutive hours. Thus, useless measures were replaced with the average measure of the previous and next hour. Outliers were replaced by the value of the mean of the measures plus 3 standard deviations. A measure is considered an outlier when its signed number of standard deviations by which is above the mean value of what is being measured is greater than 3. Feature standardization was applied to avoid scale problems. Finally, from the dataset, new features were generated associated with past demand measures to train the models. In particular, the last 48 measures were considered for each record to capture at least two days of consumption pattern directly in the features.

Several visualization analysis were performed to gain an intuitive insight of the information contained in each feature. The most relevant fact confirmed in this preliminary analysis was the daily periodicity of the demand value. The correlation diagram shown in Fig. 1 presents the high correlation between actual demand and the demand of the same hour of two days before. Data preprocessing was performed using pandas library [18]. The dataset from 2014 to 2017 was extended to include all lag features of the last 24 past hours. The training set included all data from 2014 to 2016, and the testing set included data from 2017. A linear regression model M_{sim} was trained using the sklearn toolkit [20], configured with default parameters as benchmark model. New training and test datasets were produced keeping only the relevant features, according to the analysis performed to determine the relative importance of each feature.

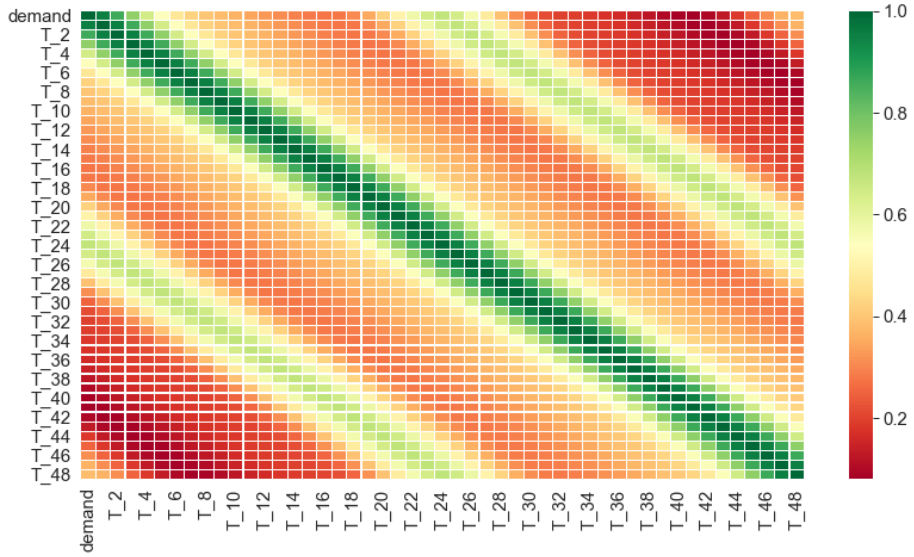

Fig. 1: Correlation diagram between actual demand and 48 last demand measures

Three standard metrics were used for evaluation: Mean absolute percentage error (*MAPE*, Eq. 5), root mean square error (*RMSE*, Eq. 6) and mean absolute error (*MAE*, Eq. 7); $real_i$ represents the measured value for $t = i$, $pred_i$ represents the predicted value and n represents the predicted horizon length.

$$MAPE = 100 \times \frac{\sum_{i=1}^{n} |\frac{real_i - pred_i}{real_i}|}{n} \tag{5}$$

$$RMSE = \sqrt{\frac{\sum_{i=1}^{n} (real_i - pred_i)^2}{n}} \tag{6}$$

$$MAE = \frac{\sum_{i=1}^{n} |real_i - pred_i|}{n} \tag{7}$$

Training one hour ahead forecasting models. Once all data was prepared for model training, a four-step procedure was applied for training and evaluation. The four steps are:

1. Training and test sets were generated in a 3:1 proportion. In this case, the training set considered data from 2014 to 2016 and the test set considered data from 2017.
2. A simple base model was trained for benchmarking. Using the trained model, a recursive feature elimination process was performed. The ten most important features are preserved.
3. Several models were trained and compared with the benchmark model.
4. The best model according to *MAPE*, *RMSE* and *MAPE* metrics was chosen.
5. An optimization of hyperparameters of the best model was performed using grid search techniques.

Finally, the best model found with the optimized hyperparameters was used as a reference to train the 24 hour forecasting model.

Twenty four hour model. The best model configured with the best hyperparameters obtained in the previous step, was used to generate twenty four models $M_1, M_2, ..., M_{24}$ to forecast day ahead hours, applying the following procedure:

1. Training and test sets were generated in a 3:1 proportion. the training set considered data from 2014 to 2016 and the test set considered data from 2017.
2. Model M_i was trained using y_i as output, where y_i consists of the demand value corresponding to i hours ahead, and input X is enriched for models $M_i,\ i > 2$ with a new column consisting of the $i - 1$ prediction obtained by the trained model M_{i-1}
3. Models M_i are assembled to get a complete model M to forecast the next 24 hours altogether.

3.2 Implementation

This section describes the implementation of the approach described in section 3.1.

Computational platform and software environment. Experiments were performed in an HP ProLiant DL380 G9 server with two Intel Xeon Gold 6138 processors (20 cores each) and 128 GB RAM, from the high performance computing infrastructure of National Supercomputing Center Cluster-UY [19].

The proposed approach was implemented in Python. Several scientific packages were used to handle data, train models and visualize results. Used packages included pandas, sklearn, and keras. A generic module was implemented to train various type of models following a pipeline processing. Parameter tuning of the studied models were performed using RandomizedSearchCV and GridSearchCV modules from sklearn. The main details of the implementation of the studied models are provided in the following subsections.

Implementation of one hour model. Data preprocessing was already described in section 3.1. All one hour models described in this section use a training set containing data from 2014 to 2016 and a test set containing data from 2017.

Base model: Linear regression. A linear regression model was trained to be used as benchmark for the results comparison. A recursive feature selection strategy [4] was also applied on this model to determine the most important features (the rest of features were removed from the dataset).

Ten features were selected based on their relative importance:

- T_1, T_2, T_{24}, T_{25}: demand values lagged.
- *workingday*: flag indicating whether the day of measured value is a working day
- *month*: month on which the measure was taken.
- *hour*: hour of the day on which the measure was taken.
- *dayofweek*: day of the week on which the measure was taken.
- *day*: day of month on which the measure was taken.
- *year*: year on which the measure was taken.

The most relevant past demand values are T_1, T_2, T_{24}, and T_{25} because the current demand is highly correlated with the immediate past demands and also with the demands of the previous day at the same time due to the daily periodicity. The full analysis is presented and discussed in Section 4.1.

Selection of the best method. Seven regression models were trained including the base model considering the ten most important features, and default parameters, using the scikit-learn API [4]: Linear Regression, MLP, Extra Trees, Gradient Boosting, Random Forest, K-Neighobors and Ridge. These models were evaluated using the *MAPE* metric and the linear regression model was used to determine a baseline performance value. The most accurate method was chosen for further evaluation (this method is called M_{best}).

Optimization of the best method Parameter search techniques were applied to optimize a model based on the best method obtained (M_{best}). The model M_{best} trained with default parameters was optimized using two standard sklearn tools:

- GridSearchCV: The user specify a parameters grid selecting a discrete set of values for each parameter and a model. The tool trains the model in each point of the multidimensional grid generated and finds the best parameters setting according to a predetermined metric.
- RandomizedSearchCV: The user specify a parameter probability distribution and the number of points that must be draw. The tool samples according to the distribution and train the model in each of this points. Then finds the best parameters setting according to a predetermined metric.

The best parameter set obtained for M_{best} results in an optimal model M_{opt}. The main details of the implementation of the complete model based on M_{opt} are described in the next subsection.

3.3 Implementation of the complete model

Model M_{opt} was optimized for predicting the next hour and used for predicting any of the following 24 hours to build the complete model. This decision was adopted assuming that the forecasting quality of the parameter setting obtained in the previous phase is independent of the hour used as output.

To build the complete model, 24 instances of the optimized model M_{opt} were trained. These instances are called $M_{opt,i}$, defining the model trained to forecast the i_{th} hour ahead. The output y_i used to train the model consisted in the demand value for the i-th hour ahead. For $i > 2$, the input X_i is enriched with a new set of columns consisting of all predictions obtained by models $M_{opt,1}, ..., M_{opt,i-1}$. Eq. 8 describes the hybrid strategy applied to M_{opt}.

$$\begin{aligned} pred_{(t+1)} &= M_{opt,(t+1)}(obs_t, obs_{(t-1)}, ..., obs_{(t-n)}) \\ pred_{(t+2)} &= M_{opt,(t+2)}(M_{(t+1)}, obs_t, ..., obs_{(t-n)}) \\ &\dots \\ pred_{(t+24)} &= M_{opt,(t+24)}(M_{(t+23)}, M_{(t+22)}, ..., obs_t, ..., obs(t-n)) \end{aligned} \tag{8}$$

The complete model M_{opt} is computed by Eq. 9. Output of the model is a 24 valued vector, one prediction for each hour.

$$M_{opt}(t) = (pred_{(t+1)}, pred_{(t+2)}, ..., pred_{(t+24)}) \tag{9}$$

4 Experimental analysis

This section presents the results of the experimental analysis of the proposed computational intelligence methods for day ahead industrial electricity load forecasting.

4.1 Recursive Feature Elimination

A feature selection analysis was performed using the recursive feature elimination tool in sklearn. A model and a number of features are selected, and the tool works by recursively removing features and building a new model (of the type selected) on those remaining features. The accuracy of the new model is used to identify the features or combination of features that contribute the most to predicting the target attribute. The recursive feature selection tool was applied over the linear regression method described in subsection 3.2 and studying up to ten features. Fig. 2 presents the results of the analysis, reporting the relative importance of the ten most important features.

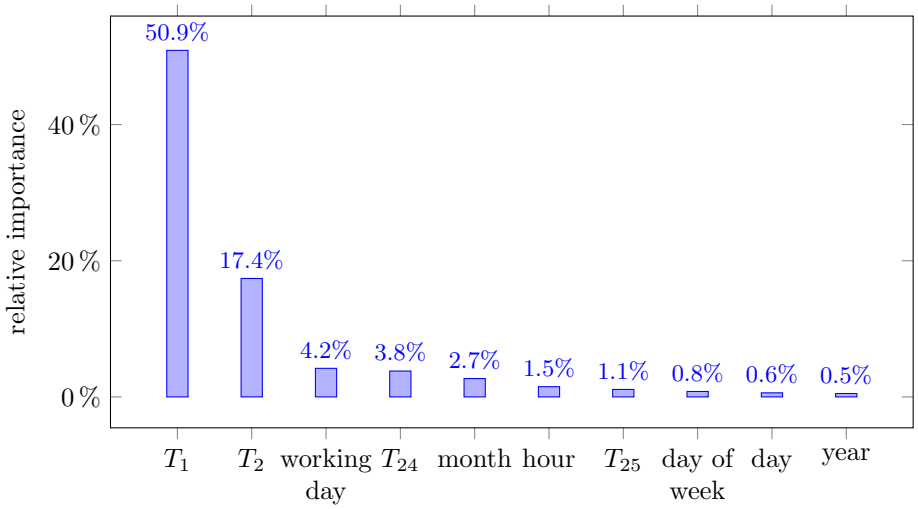

Fig. 2: Relative importance of most important features (percentage values)

4.2 Experimental results on preliminary models

Performance metrics defined in Section 3.1 were used to evaluate implementation of one hour models as described in Section 3.2. Table 1 reports the obtained results for the studied forecasting models. The best results are reported in cells with green background. Results reported in Table 1 indicate that three methods achieved the best results regarding the analyzed metrics. Focusing on *MAPE*, Extratreesregressor improved over MLP by 4.16% and over RandomForest by 6.54%. Additionally, the training time of Extratreesregressor was approximately three times shorter than RandomForest and six times smaller than MLP. Overall, ExtraTreesRegressor was the most effective model for forecasting the next hour, outperforming all the other methods regarding the three standard metrics studied. According to this result, ExtraTrees was selected as the best method for showing the best performance and a low training time. M_{best}=*ExtraTreesRegressor*.

Table 1: Results for each regression method.

Regression method	*MAE*	*MAPE*	*RMSE*	*Score*	*Time (s)*
LinearRegression	127.63	3.60	176.00	0.96	1.72
Ridge	127.63	3.60	176.00	0.97	0.09
KNeighbors	180.54	5.03	253.20	0.93	0.07
RandomForest	108.20	3.21	151.54	0.98	3.1
GradientBoosting	121.97	3.38	166.17	0.97	1.99
MLP	111.08	3.13	154.23	0.97	6.21
ExtraTrees	105.44	3.00	148.61	0.99	1.2

4.3 Parameter tuning

Parameter tuning techniques described in Section 3.2 were applied on the best model M_{best}. The following grid was generated as input for both studied techniques: *n_estimators*: [10, 50, 75, 100, 150], *max_features*: [auto, sqrt, log2], and *max_depth*: [50, 100,150, 200, 250]. GridSearchCV achieved the best results. The best parameter setting found by the algorithm was *n_estimators*=50, *max_features*=auto and *max_depth*=250, improving 14% on the *MAPE* results over the second best configuration.

4.4 Experimental results after parameter tuning

Table 2 reports results of the *ExtraTreesRegressor* model before and after parameter tuning. The best results are highlighted (cells with green background).

Results show that the numerical results improved considerably for the three studied metrics. In particular, *MAPE* reduced from 3.00% to 1.79%. The performance improvement just demanded a negligible increase on training time increases after parameter tuning from 1.2 s to 1.7 s.

Table 2: Comparative results of ExtraTrees before and after parameter tuning.

Regression method	*MAE*	*MAPE*	*RMSE*	*Score*	*Time(s)*
ExtraTrees before tuning	105.44	3.00	148.61	0.99	1.2
ExtraTrees after tuning	87.52	1.79	111.08	0.99	1.7

4.5 Experimental results of the complete model

The forecast accuracy of the final model was validated by applying a metric that extends *MAPE*. Let $MAPE_h$ be the *MAPE* value for a predicted horizon h, the extension of *MAPE* to the complete testing set is defined by Eq 10.

$$MAPE_{tot} = \frac{\sum_{i=1}^{k} MAPE_h}{k} \tag{10}$$

Table 3 reports the results for each of the 24 models. The expected behaviour is that the models trained for highly correlated hours in the future respect to the current hour, perform best. This fact is due to predictability, and it s enhanced when the correlation between input features and predicted values is higher. According to Fig. 1, highly correlated demand values correspond to the immediately preceding hours and from the same hours of the day before.

Analyzing the obtained results for the $MAPE_{tot}$ metric for each one of the 24 hourly models, the performance got worse from $i = 1$ to $i = 17$ and then improved from $i = 18$ to $i = 24$. These results show that highly correlated demand values performed better, as expected.

Table 3: $MAPE_{tot}$ score for each $ET_{opt,i}$ single hour model.

	hour											
	1	2	3	4	5	6	7	8	9	10	11	12
$MAPE_{tot}$	1.79	1.84	1.90	1.97	2.09	2.19	2.39	2.52	2.68	2.75	2.80	2.86
	hour											
	13	14	15	16	17	18	19	20	21	22	23	24
$MAPE_{tot}$	2.93	3.02	3.05	3.08	3.09	3.02	2.88	2.77	2.63	2.49	2.32	2.17

Finally, the complete model ET_{opt} was applied. A day-ahead hourly forecast load curve was generated for each time window for the testing set and the $MAPE_{tot}$ value was calculated.

The final result for the complete model was $MAPE_{tot} = 2.55\%$. This result implies that the model obtained for the day ahead demand forecasting of the industrial pole analyzed incurs in an error that is considered very low for most of the studies that rely on these types of models [13,15]. Fig. 3 presents an example of the real demand curve and the predicted demand curve using the best model, for the testing set considered in the experiments.

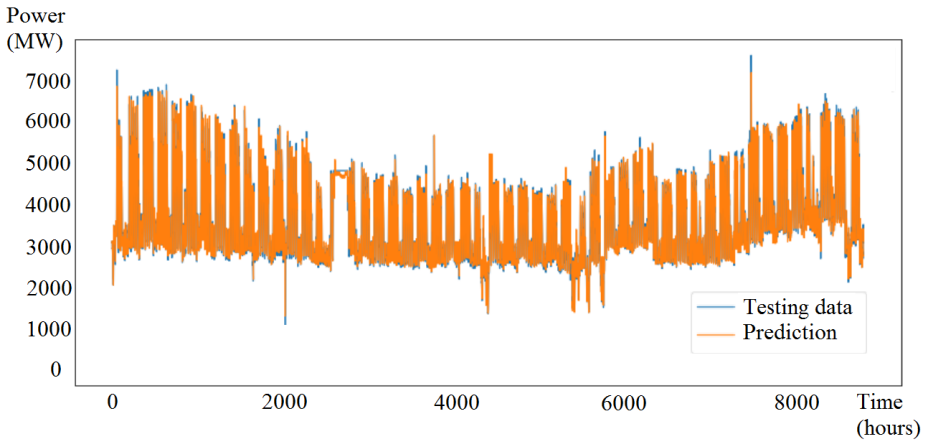

Fig. 3: Predicted demand and testing data curves

5 Conclusions and future work

This article presented an approach to address the problem of day ahead electricity load forecasting. Several machine learning models was presented and studied for next hour forecasting. Recursive feature selection was applied to select most relevant features to train the studied models. After a comparative evaluation, the best model was optimized using random search and grid search techniques. With the optimized model for single hour prediction, an hybrid strategy (direct and recursive) was applied to build a complete day ahead electricity load hourly forecasting model.

An extension of *MAPE* metric was used to evaluate this complete model for the testing set, obtaining a value of $MAPE_{tot} = 2.55\%$. This result shows that the proposed algorithm is effective for addressing the problem of day-ahead industrial demand forecasting.

The main lines for future work are related to extend the analysis to other data sets of industrial poles with different demand profiles, and apply the proposed approach to residential demand forecasting, including other relevant features (e.g., related to weather, such as temperature, humidity, and wind speed, which have impact on residential demand [17]). Deep learning techniques (e.g., recurrent/long-short term memory neural networks) should be considered for future work, since they can provide accurate results in scenarios that are difficult for other simpler methods, i.e. when handling large volumes of historical data.

References

1. Amjady, N., Keynia, F.: Short-term load forecasting of power systems by combination of wavelet transform and neuro-evolutionary algorithm. Energy 34(1), 46–57 (2009)
2. Bashir, Z., El-Hawary, M.: Applying wavelets to short-term load forecasting using pso-based neural networks. IEEE Transactions on Power Systems 24(1), 20–27 (2009)
3. Bellman, R.: Dynamic programming. Princeton University Press (1957)
4. Buitinck, L., Louppe, G., Blondel, M., Pedregosa, F., Mueller, A., Grisel, O., Niculae, V., Prettenhofer, P., Gramfort, A., Grobler, J., Layton, R., VanderPlas, J., Joly, A., Holt, B., Varoquaux, G.: API design for machine learning software: experiences from the scikit-learn project. In: ECML PKDD Workshop: Languages for Data Mining and Machine Learning. pp. 108–122 (2013)
5. Burger, E., Moura, S.: Gated ensemble learning method for demand-side electricity load forecasting. Energy and Buildings 109, 23–34 (2015)
6. Chen, Y., Luh, P., Rourke, S.: Short-term load forecasting: Similar day-based wavelet neural networks. In: 7^{th} World Congress on Intelligent Control and Automation. pp. 3353–3358 (2008)
7. De Felice, M., Alessandri, A., Ruti, P.M.: Electricity demand forecasting over italy: Potential benefits using numerical weather prediction models. Electric Power Systems Research 104, 71–79 (2013)
8. Diniz, A., Costa, F., Maceira, M., dos Santos, T., Dos Santos, L., Cabral, R.: Short/mid-term hydrothermal dispatch and spot pricing for large-scale systems-the case of Brazil. In: Power Systems Computation Conference. pp. 1–7 (2018)

9. Do, L., Lin, K.H., Molnár, P.: Electricity consumption modelling: A case of germany. Economic Modelling 55, 92–101 (2016)
10. Dudek, G.: Pattern-based local linear regression models for short-term load forecasting. Electric Power Systems Research 130, 139–147 (2016)
11. Fan, S., Chen, L., Lee, W.J.: Machine learning based switching model for electricity load forecasting. Energy Conversion and Management 49(6), 1331–1344 (2008)
12. Hagan, M., Behr, S.: The time series approach to short term load forecasting. IEEE Transactions on Power Systems 2(3), 785–791 (1987)
13. Karrthikeyaa, S., Vijayaraghavan, V.: A two-fold machine learning approach for efficient day-ahead load prediction at hourly granularity for nyc. In: Advances in Information and Communication. vol. 2, p. 84 (2019)
14. Kim, C., Yu, I., Song, Y.: Kohonen neural network and wavelet transform based approach to short-term load forecasting. Electric Power Systems Research 63(3), 169–176 (2002)
15. Lahouar, A., Slama, J.: Day-ahead load forecast using random forest and expert input selection. Energy Conversion and Management 103, 1040–1051 (2015)
16. Lazos, D., Sproul, A., Kay, M.: Optimisation of energy management in commercial buildings with weather forecasting inputs: A review. Renewable and Sustainable Energy Reviews 39, 587–603 (2014)
17. Luján, E., Otero, A., Valenzuela, S., Mocskos, E., Steffenel, L., Nesmachnow, S.: An integrated platform for smart energy management: the CC-SEM project. Revista Facultad de Ingeniería (2019)
18. McKinney, W.: Data structures for statistical computing in python. In: Proceedings of the 9^{th} Python in Science Conference. pp. 51–56 (2010)
19. Nesmachnow, S., Iturriaga, S.: Cluster-UY: scientific HPC in Uruguay. In: Int. Supercomputing in Mexico (2019)
20. Pedregosa, F., Varoquaux, G., Gramfort, A., Michel, V., Thirion, B., Grisel, O., Blondel, M., Prettenhofer, P., Weiss, R., Dubourg, V., Vanderplas, J., Passos, A., Cournapeau, D., Brucher, M., Perrot, M., Duchesnay, E.: Scikit-learn: Machine learning in Python. Journal of Machine Learning Research 12, 2825–2830 (2011)
21. Qamber, I.: Peak load estimation studies in several countries. Electric Power Systems Research 1(2) (2017)
22. Resende, L., Soares, M., Ferreira, P.: Electric power load in Brazil: view on the long-term forecasting models. Production 28, 83–99 (2018)
23. Silva, L.: A feature engineering approach to wind power forecasting: GEFCom 2012. International Journal of Forecasting 30(2), 395–401 (2014)
24. Soliman, A., Al-Kandari, A.: Electrical load forecasting: modeling and model construction. Elsevier (2010)
25. Son, H., Kim, C.: Short-term forecasting of electricity demand for the residential sector using weather and social variables. Resources, conservation and recycling 123, 200–207 (2017)
26. Taylor, J., McSharry, P.: Short-term load forecasting methods: An evaluation based on European data. IEEE Transactions on Power Systems 22(4), 2213–2219 (2007)

Segmentation of thermographic images of solar cells and panels*

Estefanía Alfaro-Mejía[1][0000−0002−7986−7170], Humberto Loaiza-Correa[1][0000−0001−7206−7333], Edinson Franco-Mejía[1][2222−−3333−4444−5555], and Luis Hernández-Callejo[2][0000−0002−8822−2948]

[1] Universidad del Valle, Calle 13 100-00 Cali, Colombia
{estefania.alfaro,humberto.loaiza,edinson.franco}@correounivalle.edu.co
[2] Universidad de Valladolid, Campus Universitario Duques de Soria, 42004, Soria-Spain
luis.hernandez.callejo@uva.es

Resumen Diagnosis of solar panel failures from thermographic aerial imaging (ITIR) techniques using unmanned aerial vehicles (UAV) is not a trivial task; a first problem is in the techniques of acquisition of thermal images, the selection of instruments such as the UAV and the camera is essential to ensure an adequate diagnosis in photovoltaic systems. The relevant charateristics for the UAV are discussed, such as flight autonomy, operating temperature, wind resistance and for the thermal imager, resolution, spectral band, operating temperature ranges and the compatibility with the communication protocols of the UAV. Another problem is the acquisition of the images considering environmental conditions that affect the data and the performance of the panels and indirectly the usefulness of the data to be processed. In this work, two segmentation techniques for solar panels (PPV) are explored, the first corresponds to the filtering by area and the second to the method of active contours level sets (MCA LS). The tuning of these techniques allows to obtain the contours of the PPV, once the contours are ob-tained, morphological operations are used to refine the obtained edges and the Hough transform is used to find the main lines in the image. Later the vertices are found from the possible intersections between the lines. Finally, the vertices are brought to the desired position at scale according to the reference of the PPVs using projection transformations. The extraction of the region of interest is evaluated from the DICE, IOU, and recall segmentation metrics.

Keywords: Photovoltaic · Thermography imaging · Unmanned aerial vehicles UAV · Image segmentation · Degradation.

1. Introduction

Photovoltaic solar installations continue to increase as part of the solution to mit-igate climate change problems, proving to be economically viable by increa-

* Funded by the Universidad del Valle-Colombia

sing the production of panels and inverters [9],[8]. In 2017, there was an increase from 98 GW to 402 GW in overall clean generation capacity. Investments are large and the risks of production loss are appreciable if there are system failures. The high levels of irradiance, necessary for the photovoltaic effect to occur, generate temperature increases in the cells that reduce the efficiency of the solar panels. Anomalies or defects may occur during the manufacture, installation, and operation of the solar panels [7]. Manufacturers guarantee a lifespan of approximately 25 years for photovoltaic panels; however, damage to any cell in the chain or from a panel in the chain can sharply decrease energy production; it is for this reason of great importance to investigate techniques to detect anomalies in time and take correctives that reduce the negative economic impact. There are different techniques for inspecting PPVs, including electrical tech-niques such as the I-V curve and image analysis generated by Electroluminescence (EL), photoluminescence (PL), and Thermography infrared (TIR) [1].

Most of the faults in the solar panels are imperceptible to the human eye, manual inspection is not effective since it is not a simple task because usually, the panels are in high areas, difficult to access and with little space between them; added to the fact of exposure to electrical risk to circuits with continuous current of several amps. The use of Unmanned Aerial Vehicles (UAV) is a solution alternative for the inspection of photovoltaic modules [8], [10], [2], [6], etc. The UAVs must be guided remotely and manually to capture the images taking into account multiple considerations such as the height of the UAV, the angles of the camera and the weather conditions that alter the image acquisition procedure. Once TIR is acquired, it is necessary to employ processing methods for IRRs and pattern recognition techniques that allow the classification of the state of the solar panels.

2. Benchmark

The equipment used for the acquisition of solar panel thermal imaging (PPV) is described in the Table 1. The acquisition of the images through controlled flights of the UVA was carried out with the Drone Matrice 100 DJI, which has an A2 flight controller, and an SDK open to development; the capture of thermal imaging was carried out with the camera Zenumuse XT resolution 336×256, (see [5]). The solar panels studied are configured in a string of 4 PPV of monocrystalline silicon, connected to an electronic load that emulates the consumption generated by a resistive load. The data of the collected images are recorded in [3].

UAV Matrice 100		Camera IR Zenmuse XT		ERDM-85 PPV	
Flight endurance (min)	18	Resolution (pixels)	336 × 256	Open circuit voltage (V)	21.78
Full payload (g)	1000	Weight (g)	270	Optimal operating voltage (V)	17.95
Flight speed (m/s)	10	Spectral Band (μm)	7-13.5	Maximum Power	85

Table 1. Equipment for IR inspection photovoltaic.

3. Method

The proposed method for segmenting aerial thermal imaging is illustrated in the Fig. 1.

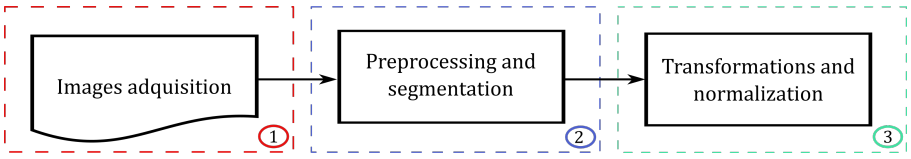

Figura 1. Acquisition and segmentation method IR images.

The method consists of three phases and each phase is described with stages, the phases are image acquisition; preprocessing and segmentation; transformation and normalization. The image acquisition phase consists of a definition of initial condition stages that let establish some restrictions to a correct capture procedure, such as the acquisition time from 10 : 00 am to 3 : 00 pm due to in the city of Cali-Colombia registering irradiance peaks of more than $600W/m$; the time slot from 12 : 00 m to 1 : 00 pm is excluded to avoid the shadow projections generated by the UAV over the analyzed PPVs, the catches are only made if there is no apparent rain or cloudiness. In order to have the panel working near to the MPPT point, the condition-stage of operation of the solar panels were adjusted to be delivering 80 % Voc. The environmental variables such as external temperature, wind speed, and irradiance are measured to verify that they are in operating ranges used in similar experiments and that the acquired images can be analyzed. The irradiance must be greater than $500W/m^2$ [4], and wind speed $3m/s < F.S \leq 5m/s$ [10]. Finally, it initiates the procurement procedure by estimating the acquisition height and the capture angle of the camera so that the emission and reflection remain constant.

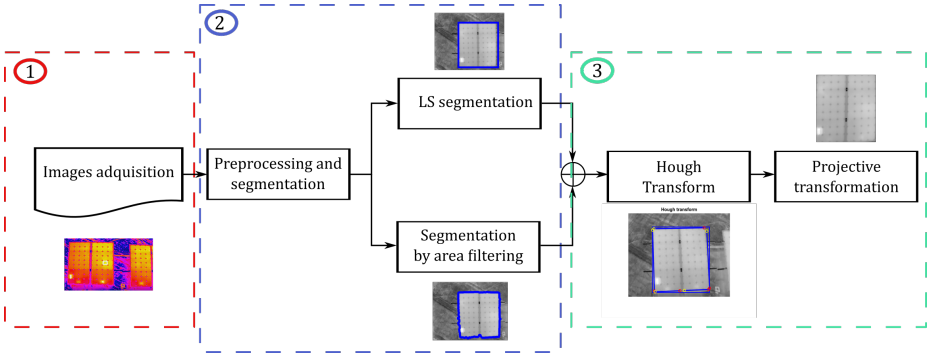

Figura 2. Acquisition and segmentation method detailed for the IEEE scenario.

Once captured the aerial thermal imaging, starts the preprocessing phase; here the thermal imaging enters a step-low filtering process (medium filter) to decrease the noise present in the image. The window selection is 25x25 and is done heuristically with a sequence of test images, then starts the binarization process of the filtered image by applying the Otsu method. Once this procedure is finished, the segmentation method is chosen as illustrated in fig. 3 between the method of active contours LS (MCA LS) and segmentation by area filtering. The segmentation methods return the contours, then an edge detector is used and with a morphological operation from the use of a square structural element, the main lines on the image that are analyzed from the Hough transform are obtained; Finally, a projection transformation operation is used to generate a normalization of segmented PPVs.

4. Results

The solar panels are segmented from two proposed techniques, the MCA level sets active contour method and the area filtering approach. For the MCA LS method, an initial surface with the size of the image 336×256 is defined. To tune the convergence parameters of the implicit surface, ranges are defined for the variables like this: $-1{,}5 < \sigma \leq 1{,}5$, $-7 < \alpha \leq 7$ and $-3 < \epsilon \leq 3$ and compared with a *ground truth*, according to the initial tests defined as adjustment parameters in the method of active contours $\sigma = 1{,}5$, $\alpha = 1{,}7$ and $\epsilon = 1{,}5$. Finally the surface converges to the contour of the solar panels and subsequently an edge detector with a square structural element is used. The FA segmentation method consists of the definition of the minimum search area of 0,1 and maximum of 0,9, related to the size of the images, then the possible objects that meet the search criteria are labeled. A dilation operation with a square structural element of 7×7 is used on the contours obtained from both segmentation methods. Once the defined contours are obtained, the Hough transform is used to find the

main lines in the contours and from the equations in polar coordinates there are possible intersections between all the combinations of lines found in the images as illustrated in ec.1. Late the equation 1 is resolved in terms of the angle θ it is replaced in ec.1, with (r,θ) the x-y coordinate system is used to assign an address to the vertices.

$$\frac{A_1}{A_2} = \frac{(\theta - \phi_1)}{(\theta - \phi_2)} R = \frac{A_1}{(\theta_R - \phi_1)} \tag{1}$$

With the information of the vertices obtained, a projection transformation is used to ensure that the images have the same composition 4. The vertices are taken to the desired position values obtained from the scale ratio of the PPV *datasheet* as illustrated in fig. 3.

$$xt_1 yt_1 1 = H xr_1 yr_1 1 \tag{2}$$

$$\begin{aligned} xt &= H_{(1,1)} \cdot xr_1 + H_{(1,2)} \cdot yr_1 + H_{(1,3)} \cdot 1 \\ yt &= H_{(2,1)} \cdot xr_1 + H_{2,2)} \cdot yr_1 + H_{(2,3)} \cdot 1 \\ 1 &= H_{(3,1)} \cdot xr_1 + H_{(3,2)} \cdot yr_1 + H_{(3,3)} \cdot 1 \end{aligned} \tag{3}$$

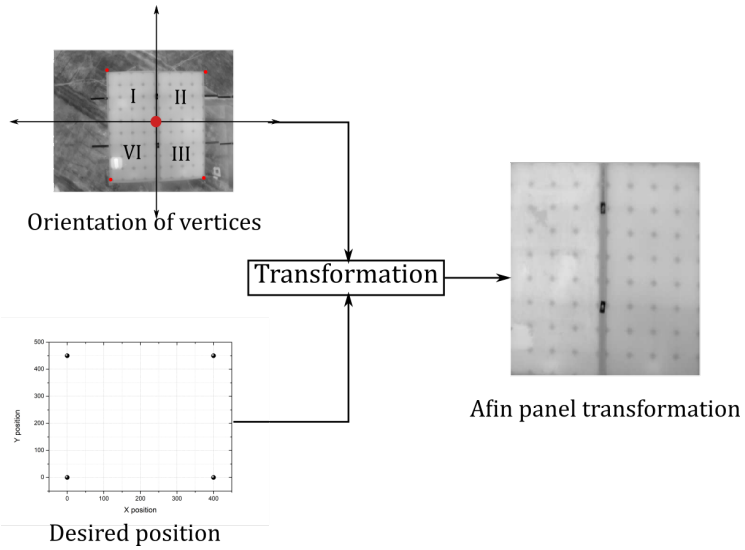

Figura 3. Affine transformation.

The segmentation methods implemented were tested based on the DICE and IOU metrics.

segmentation method	IOU	DICE	RECALL
FA	0.97	0.94	0.70
MCA LS	0.92	0.96	0.69

Table 2. Segmentation Metrics.

The DICE or IOU measurement is done with a representative sample of 60 images to compare both FA and MCA KS methods.

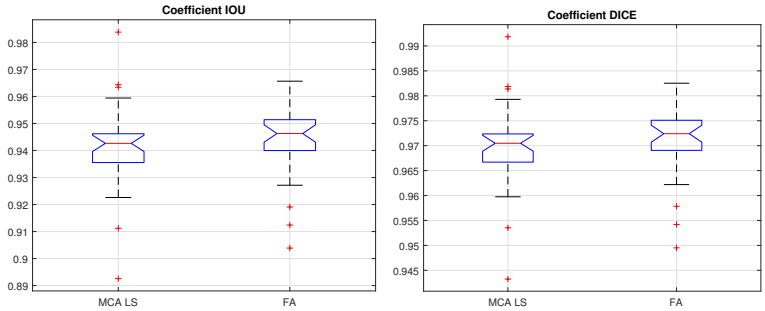

(a) IOU metric. (b) DICE metric.

Figura 4. Metric to measure segmentation performance.

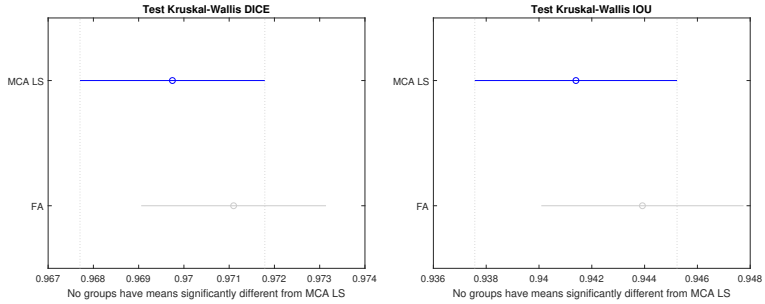

(a) DICE metric. (b) IOU Metric.

Figura 5. Kruskall-Wallis Test.

5. Conclusions

The image acquisition phase allowed establishing the relevant variables in the selection of the equipment used for thermographic inspection of PPV. For

the UAV: flight autonomy > 18 min and operating temperature $\leq 40^{o}$C. For the thermal camera the spectral range between 7,5 to 13μm, resolution 336×256 or higher and compatibility with the UAV communication protocols.

On the other hand, the definition of capture conditions establishes the minimum ranges suitable for the correct processing of the images, among which are: environmental conditions (such as absence of rain), the acquisition schedule in the time slot of 11:00 am at 12:00 pm and 1:00 pm to 3:00 pm (specific case of Santiago de Cali), irradiance levels $< 600W/m^2$, wind speed $> 5m/s$.

In the pre-processing phase, medium filters, Otsu thresholding, morphological operations were explored to refine the contours obtained from the proposed methods. With a representative sample of 40 images selected by acquisition folders, the medium filter windows were varied from 3×3 to 35×35. The search lets us a better performance with the 25×25 window.

FA and MCA LS techniques were used for segmentation, which was evaluated from the *Sorensen Dice* metrics of 0.92 and IOU of 0.96 for MCA LS and for the area approach 0.97 with Dice and 0.94 with IOU. It was found that the FA segmentation method found specific statistical differences using the Kruskal-Wallis test (see fig. fig: kruskall-wallis) in the comparison with the MCA LS method of $P < 0{,}51$. Finally, we found that FA is better for segmenting panels than MCA LS but without a big difference.

The morphological operation that improved the edges obtained was the expansion with a square structural element of dimensions 5×5.

Finally, the tuned Hough transform is used to detect the main lines on the image and all its possible intersections to find the vertices. The vertices found are brought to a desired position from a related transformation or normalization.

The segmentation method implemented will allow the state of the photovoltaic system to be analyzed per cell.

Referencias

1. Abdelhamid, M., Singh, R., Omar, M.: Review of microcrack detection techniques for silicon solar cells. IEEE Journal of Photovoltaics **4**(1), 514–524 (Jan 2014). https://doi.org/10.1109/jphotov.2013.2285622, https://doi.org/10.1109/jphotov.2013.2285622
2. Addabbo, P., Angrisano, A., Bernardi, M.L., Gagliarde, G., Mennella, A., Nisi, M., Ullo, S.: A UAV infrared measurement approach for defect detection in photovoltaic plants (jun 2017). https://doi.org/10.1109/metroaerospace.2017.7999594, https://doi.org/10.1109/metroaerospace.2017.7999594
3. Alfaro-Mejía, E., Loaiza-Correa, H., Franco-Mejía, É., Restrepo-Girón, A., Nope-Rodríguez, S.: Dataset for recognition of snail trails and hot spot failures in monocrystalline si solar panels. Data in Brief p. 104441 (Aug 2019). https://doi.org/10.1016/j.dib.2019.104441, https://doi.org/10.1016/j.dib.2019.104441
4. Dotenco, S., Dalsass, M., Winkler, L., Wurzner, T., Brabec, C., Maier, A., Gallwitz, F.: Automatic detection and analysis of photovoltaic modules in aerial infrared imagery. In: 2016 IEEE Winter Conference on Applications of Computer

Vision (WACV). IEEE (Mar 2016). https://doi.org/10.1109/wacv.2016.7477658, https://doi.org/10.1109/wacv.2016.7477658
5. Gallardo-Saavedra, S., Hernandez-Callejo, L., Duque-Perez, O.: Image resolution influence in aerial thermographic inspections of photovoltaic plants. IEEE Transactions on Industrial Informatics **14**(12), 5678–5686 (Dec 2018). https://doi.org/10.1109/tii.2018.2865403, https://doi.org/10.1109/tii.2018.2865403
6. Li, X., Yang, Q., Chen, Z., Luo, X., Yan, W.: Visible defects detection based on UAV-based inspection in large-scale photovoltaic systems. IET Renewable Power Generation **11**(10), 1234–1244 (aug 2017). https://doi.org/10.1049/iet-rpg.2017.0001, https://doi.org/10.1049/iet-rpg.2017.0001
7. Mellit, A., Tina, G., Kalogirou, S.: Fault detection and diagnosis methods for photovoltaic systems: A review. Renewable and Sustainable Energy Reviews **91**, 1–17 (Aug 2018). https://doi.org/10.1016/j.rser.2018.03.062, https://doi.org/10.1016/j.rser.2018.03.062
8. Pursiheimo, E., Holttinen, H., Koljonen, T.: Inter-sectoral effects of high renewable energy share in global energy system. Renewable Energy **136**, 1119–1129 (Jun 2019). https://doi.org/10.1016/j.renene.2018.09.082, https://doi.org/10.1016/j.renene.2018.09.082
9. Sundaram, S., Benson, D., Mallick, T.K.: Overview of the PV Industry and Different Technologies. Elsevier (2016). https://doi.org/10.1016/b978-0-12-802953-4.00002-0, https://doi.org/10.1016/b978-0-12-802953-4.00002-0
10. Zhang, P., Zhang, L., Wu, T., Zhang, H., Sun, X.: Detection and location of fouling on photovoltaic panels using a drone-mounted infrared thermography system. Journal of Applied Remote Sensing **11**(1), 016026 (Feb 2017). https://doi.org/10.1117/1.jrs.11.016026, https://doi.org/10.1117/1.jrs.11.016026

Monthly characterization of the generation of photovoltaic arrays. Microgrid case CEDER, Soria, Spain

López-Meraz R. A. [1[0000-0002-3236-3709]], Hernández-Callejo L. [2[0000-0002-8822-2948]], Jamed-Boza L. O. [1[0000-0002-6378-758X]] and Alonso-Gómez V. [2[000-0001-5107-4892]]

[1] Universidad Veracruzana, Circuito Universitario Gonzalo Aguirre Beltrán s/n, 91000, Mexico
[2] Universidad de Valladolid, Campus universitario Duques de Soria s/n, 42004, Spain
meraz_raul@hotmail.com: R.L-M.; luis.hernandez.callejo@uva.es: L.H-C.; lojb33@gmail.com: L.J-B.; victor.alonso.gomez@uva.es: V.A-G.

Abstract. The implicit difficulties (resources and intermittent generation) of renewable energies prevent their insertion with greater security and reliability in electricity networks. However, as the priority of favoring environmental issues and represent one of the main axes of the electricity sector, it is essential to make efforts that characterize the behavior of the effective production of photovoltaic systems in real applications. In this way, the objective of this article is to propose a methodology where the monthly profile of future facilities is estimated. To this end, the received solar radiation (based on the Gamma probability distribution) is modeled along with the generation of seven photovoltaic arrays of different technology, connected to the microgrid of the Center for the Development of Renewable Energies (CEDER), belonging to the Center of Energy, Environmental and Technological Research (CIEMAT), located in Soria, Spain. The measurement of the solar resource was made with a Baseline Surface Radiation Network, and the injection of photovoltaic power to the microgrid was acquired with the help of smart meters. The verification of the procedure was carried out with simulations in Matlab and the statistical analyzes were confirmed with the JMP software. The results may be helpful in sizing a backup model and will collaborate in the proper management of the case study energy.

Keywords: Gamma Distribution, Microgrid, Radiation, Simulated Power.

1 Introduction

In recent years, humanity demands a large amount of electricity; Latin America, for example, has a growth rate of 5% [1,2]. The use of raw materials, the cornerstone of technical progress in the middle of the twentieth century, to satisfy consumption contributes to the erosion of nature and to promote anthropogenic climate change. In this scenario, renewable energies are incorporated as a new actor trying to cover what society requests in a less polluting way.

There are essentially two schemes where renewable production is present. The first, distributed energy resources (DER), includes different aspects such as generation, storage and demand response. On the other hand, the new paradigms and the latest developments in the electricity sector are based on the introduction of distributed generation (DG), which is a philosophy where energy is not produced exclusively in large centralized plants, but also in smaller locations taking advantage of local conditions in order to minimize transmission/distribution losses, as well as optimizing production and consumption. This represents an opportunity for renewable energies, where elements such as photovoltaic panels and wind turbines, scattered throughout the network, supply installations on-site or sell energy depending on their generation/consumption conditions [3]. Consequently, according to data from the European Commission, DG penetration into the European network is estimated to be around 20-25% of the total generation by 2020, and by 2030 this figure will be set at 30-35%.

However, electricity generation based on renewable resources, mainly wind and solar, has highlighted additional challenges in the management of the electricity system, primarily due to the dispersion of this type of generators, the energy of changing output and to the inefficient coordination of the conditions of the electrical grid. These complications have created technical obstacles such as energy management, architecture design of electrical systems, voltage and frequency support, means of protection and low voltage aspects [4]. They also increase the computation difficulty due to the more complex and asymmetrical probability distributions associated with the intermittent plant [5]. In addition, given the considerable number of plants, there is the challenge of obtaining energy production data in real-time [6]. Other relevant issues are the difference, in statistical terms, between the availability of intermittent source resources and conventional generation, as well as the contribution that oscillating production can make to satisfy the peak demand of the system while maintaining its reliability [7].

Complications caused by photovoltaic generation are dependent on solar radiation, promoting the interest of different studies to find a probability model that best fits your measurement. Thus, [8] performs a radiation analysis in Taiwan with Weibull distributions, logistics, Normal and logNormal without detecting bimodal behavior. Also, in [9] they claim that the variation in radiation does not follow bimodal behavior. In addition, the study of the behavior of global radiation in the M'Sila region (Algeria) is developed in [10], using 6 individual frequency distributions finding that the Weibull distribution best matches the measured data for all months, that is, they did not find a bimodal fit either. On the other hand, [11,12] argue bimodal performance in the distribution of radiation observations, [13] they analyze solar radiation records and similarly detect bimodal behavior in the distribution of data for intervals less than 60 minutes.

Given the importance of photovoltaic generation, this work attempts to approximate the quantification of the real power supplied from photovoltaic arrays (PVA) to the microgrid of the Center for the Development of Renewable Energies (CEDER) belonging to the Center for Environmental and Technological Energy Research (CIEMAT) located in Soria, Spain. The analysis focuses on modeling, on a monthly basis, the radiation with the Gamma probability distribution and, at the same time, finding relationships between it and the individual production in days with the best solar resource finding the profile of each PVA. The text is structured as follows: section 2 describes the

components of the case study and methodology used to model the radiation and determine the association functions between the solar resource and the PV power, the following part, with the help of the software JMP version 2.0, shows the results of the monthly radiation characterization and the reasons that represent the behavior of the Afvs are found to estimate the monthly power achieved by the solar array, the verification of the proposed has been achieved with the simulation in Matlab 2005a. Finally, the most relevant conclusions are presented.

2 Materials and methods

In order to facilitate the understanding of the methodology developed and the variables involved in it, Fig. 2 shows the corresponding flow chart. Lines below deepen these sections.

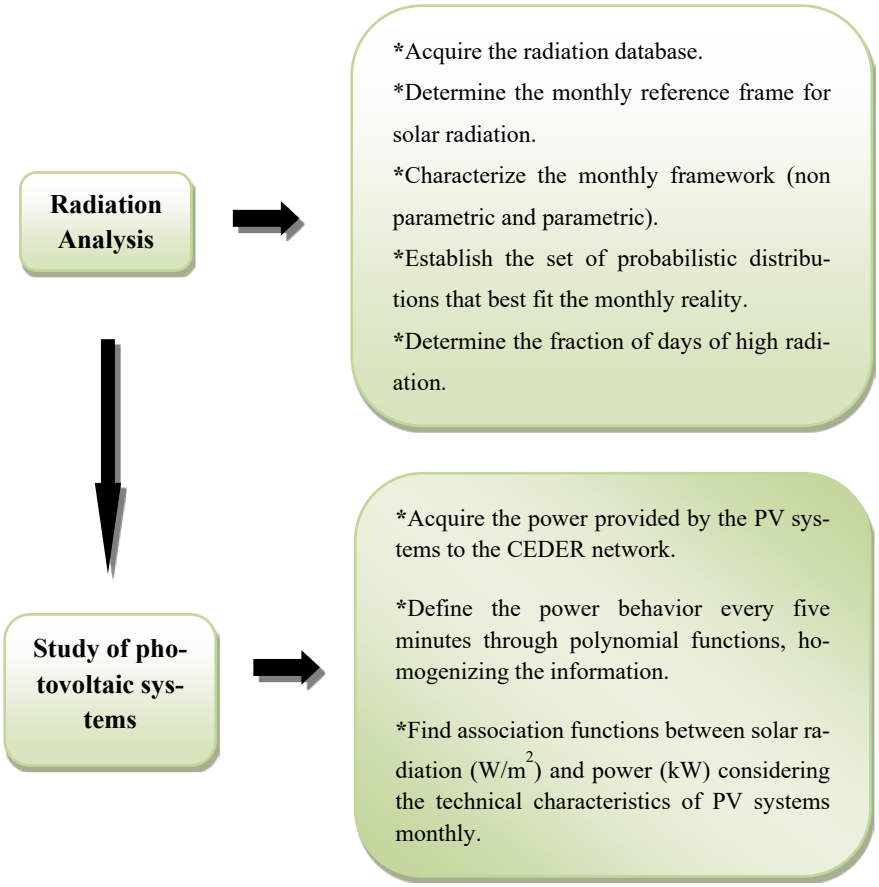

Fig. 1. Methodological flow chart.

2.1 Case of study

Of all the manageable components of CEDER's microgrid, this work focuses on a photovoltaic generation whose total peak power is of 78 kW. As shown in Fig. 2, the PVAs are assembled into five generation groups [14], three of them are on roofs and the rest are at floor level.

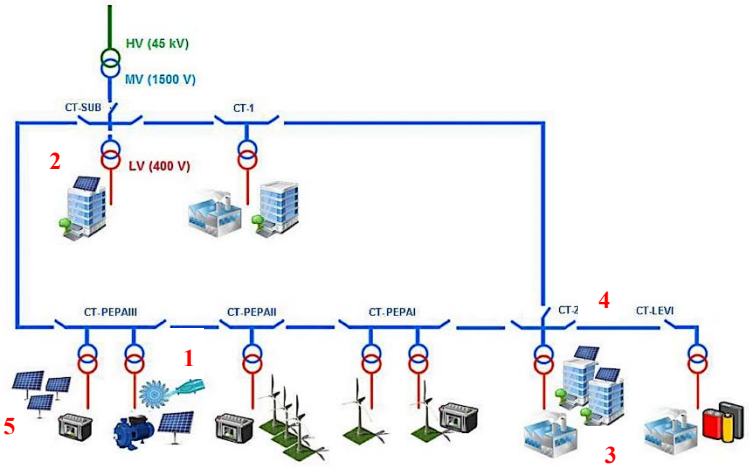

Fig. 2. Distribution of RES in CEDER microgrid.

The five solar sets are briefly described.

1. Turbine zone: the installation consists of 16 kW distributed in 64 panels of monocrystalline silicon of 250 W each, housed in two structures, forming four series (two series per structure) of 16 panels each. The output is connected to a 15 kW inverter and connected to the three-phase network.
2. Roof photovoltaic building E01 Arfrisol: this generator of 12 kW is made up of 80 monocrystalline silicon panels of 150 W, distributed in five series of 16 modules each. They arrive at a three-phase inverter of 10 kW.
3. Building roof E03: the arrangement has a power of 12.5 kW in 54 panels of monocrystalline silicon of two different brands. Some give 230 W and the other 240 W, with very similar characteristics, there are 36 of the first type and 18 of the second. They are connected to a 10 kW three-phase inverter.
4. Building roof E09, Grinding: plant divided into two groups, one of 84 and the other of 154 modules, arranged in 17 series of 14 panels each, with a peak capacity of 23.5 kW. The 238 panels are thin film (CdTe) with a power of 97 W and discharge to a three-phase inverter of 20 kW.
5. PEPA III: consists of three facilities called park 1, park 2 and park 3. They deliver their generation to single-phase inverters of 5 kW, connecting each park to a phase. Structures 2 and 3 are the same. Park 1: consists of 24 modules of polycrystalline silicon distributed in four series of 6 panels, its

peak power is 5 kW. Parks 2 and 3: generators of 32 modules of monocrystalline silicon of 140 W, grouped in four series of 8 panels, providing a maximum power of 4.5 kW.

The measurement of the solar radiation in situ was made with a Baseline Surface Radiation Network (BSNR), being the period recorded from May 30, 2012 to March 3, 2015, in total 442,905 records of 5 minutes. The monitoring of the power injection produced by the photovoltaic plants to the CEDER network was done through intelligent meters, their acquisition is exported to a database formed at different granularity, 5 minutes and hourly, respectively. The correspondence between the measuring equipment and its respective PVA is presented in Table 1.

Table 1. Smart Meters with your generation plant.

Smart Meter	PV generator	Meter	PV generator
AE1037	Park 1	AE2005	E03
AE1038	Park 2	AE2010	Turbine zone
AE1044	Park 3	AE4360	E09 grinding
AE2000	E01 Arfrisol		

2.2 Radiation modeling

Gamma distribution

Since the behavior of a random variable is described by its probability distribution the closest to the measured monthly radiation was sought. Among the most useful for representing atmospheric parameters is Gamma, which is suitable for modeling when bias, positive asymmetry and time is involved. Such environmental measures include precipitation, wind speed and relative humidity, all restricted by a physical limit.

In short, the Gamma distribution is the one where the random variable occurs α times until there is a certain event [15]. Its density function is given by:

$$f(x) = \begin{cases} \frac{1}{\beta^{\alpha}\Gamma(\alpha)}\ x^{\alpha-1}e^{\frac{-x}{\beta}}, & \text{for } x > 0;\ \alpha, \beta > 0 \\ 0 \end{cases} \quad (1)$$

Where α is the shape parameter and β the scale parameter. When large values of α occur, distributions result in less bias and a shift in the probability of density to the right. For very large values of α ($50 < \alpha < 100$) the distribution approximates, in its form, the normal. The parameter β "extends" or "squeezes" the function to the right or to the left, when β is large the curve is more elongated [16]. The main cases of this distribution are as follows: with $\alpha < 1$ it is strongly skewed to the right. For $\alpha = 1$ the function cuts the vertical axis in $1/\beta$ with $x = 0$ (in this scenario is called exponential distribution). With $\alpha > 1$ the distribution begins at the source, $f(0)=0$.

To model the radiation the analysis was carried out with the Normal and Gamma distribution, individually and in combination, that is, two Normal distributions and two Gamma, respectively. The JMP software was used, filtering the information for each

month, with a granularity of 5 minutes and limiting the records to the existence of radiation. In the first two analyzes the Kolmogorov - Smirnov - Lilliefors (KSL) and Cramer-Von Mises (CVM) goodness of fit tests are applied to determine whether or not the null hypothesis is rejected. In the case of Gamma behaviors, goodness of curve fit test was developed using the Pearson statistic with the simultaneous quantification of four parameters, obtaining the observed frequency directly from the measurements and testing the parameter values adjusting them to create minimization of the statistic of χ^2. The process of obtaining the parameters, for each month, was carried out in the Excel program so that said test maximized the probability of the right tail of the χ^2 itself. The hypothesis test applied in the adjustment of the goodness of fit is:

- Create classes in the histogram. There are as many classes as 5 minute measurements exist in each month.
- Locate the original data in each class, ie, the observed frequency (*ofr*) is found.
- Create the hypothesis test (HT). H0: Do the original data follow two Gamma distributions with their parameters α_a, β_a and α_b, β_b? H1: does not comply with the above.
- Prepare the expected frequency table (*efr*).
- Calculate the statistical χ^2_ν: $\chi^2_0 = \sum_{i=1}^{k} \frac{(ofr_i - efr_i)^2}{efr_i}$. Where: ν represents the degrees of freedom (DF). $\nu = k - P - 1$, with k the number of classes and P the parameters to be determined.
- The criterion for rejection of H0 is: $\chi^2_0 > \chi^2_{\nu,\alpha}$
- If it is not possible to reject, we can assume, with confidence of (1-α) % that the data set does meet the double Gamma distribution.

Approach index to measurements

In order to demonstrate the reliability of radiation simulation, an indicator was established to demonstrate proximity to measured data. The proximity index to measurements (Ipm) is defined with the help of the following expressions:

$$\phi = \frac{dr_{pS}}{dr_{pT}} \tag{2}$$

$$f_{dif} = (\phi - 1)\left[\frac{fda_T}{fda_S}\right](f) \tag{3}$$

$$I_{am} = (1 - f_{dif})(100) \tag{4}$$

Where ϕ is the ratio of the simulated reference splines (dr_{pS}) and the theoretical one obtained with the information (dr_{pT}) [17], f_{dif} is the fraction of difference and is a function of the fractions of days of good theoretical radiation (fda_T), of that provided by the simulation (fda_S) and of the random factor $f = \frac{1}{\sigma^2}$ where σ^2 is the variance of the combined simulation of the crossed gamma adjusted to the nearest integer.

Fraction of high radiation days

To determine the percentage of days with better radiation were found two monthly values, these are: reference distance (rd) represented by the radiation peak measured from the spline reference frame and high distance (hd) estimated from the points observed with the highest magnitude. In this way the fraction of high radiation days was found: $F_{hr} = \frac{\mathrm{rd}}{\mathrm{hd}}$. When there are days of higher radiation the spline "rises", thus both distances are close, indicating the presence of a greater number of days where the radiation is considered high.

Radiation conformation

The structure of the monthly radiation matrix (Rad), which represents the 12 months of the year, consists of 192 elements consisting of 12 rows and 16 columns. Its configuration is as follows: the elements located in the first six positions correspond to the β's of the polynomials of each month, obtained from the characterization of radiation [17]; the number of days (nd) is found in column seven, the following three parameters are the maximum reached value, that is, the peak radiation (pr), the magnitude of the reference spline (rd) and the minimum value (mv). The start (sr) and end (er) readings of the radiation measurement form columns eleven and twelve and the last four are the coefficients of α and β of the two Gammas distributions; in this way, α_a and β_a equal the simulation on sunny days and α_b and β_b represent the cloudy days.

2.3 Photovoltaic systems

Standardization of PV power

The analysis of the solar systems was carried out in two parts. In the first one the radiation was directly related, in the days with the best resource (the PV systems in their design are independent of environmental variations in their operation), and the production of the PVAs measured by the following equipment: AE1037, AE1038, AE1044, AE2000 AND AE2005. It is important to remember that the systems measured by AE1038 and AE1044 correspond to exactly the same facilities in their architecture and type of technology. However, power variations were found in four months, and consequently, the analysis of the park two only covers the months of July, August, September and October. The second section corresponded to the characterization of the power obtained by the meters AE2010 and AE4360; different polynomial adjustments without transformation were tested finding few correlations, so it was decided to analyze the transformation with logarithm base 2 in the response (power) to improve the experimental space of measurements and to clearly represent its behavior. The reason for using transformation with base logarithm 2 instead of the traditional natural logarithm was to observe improvement in correlation by reducing the base exponent e to 2, better adjusting both curves to the "m" type characteristic.

In the absence of congruence in the measured time interval, the equivalence of power was thus obtained every five minutes on the basis of the radiation collected. This results in their behavior over that period of time, homogenizing the information between generated power and measured radiation.

Association Functions (r's)

The monthly relationship between the measurements of energy produced and radiation received is found with polynomial functions in the form of reasons that allow it to be segmented to any granularity. This intrinsically characterization links other particularities such as type of technology, connections between cells, geometric construction, etc. In addition, since each PV system has its nominal power referenced at 1,000 W/m^2, the peak functions (rp) are obtained. Thus we have equations 5 and 6:

$$r = \frac{E}{R} \tag{5}$$

$$r_p = \frac{E_p}{R_p} \tag{6}$$

Where E is the energy produced by each PVA, R represents the measured radiation, E_p and R_p describe the energy and radiation in maximum conditions, respectively. It is worth mentioning that in the PVAs of higher production the functions r and r_p were converted again with the help of the following property of the logarithms: $log_a N = \frac{InN}{In_a}$. Where a is the basis of logarithm and N is the number to be transformed.
From the above, it is possible to determine the simulated power (kW) of each of the PVA by means of equation 7.

$$P_{sim} = \left(\frac{P_n}{1000}\right) Rad_{sim} \left(\frac{r}{r_p}\right) \tag{7}$$

Where P_{sim} is the simulated power (kW), P_n is the rated power (kW) of each FV system, Rad_{sim} is the radiation (W/m^2) that the simulator generates, r and r_p are the associations between the energy produced and the radiation at a certain instant and in peak conditions, respectively. However, where radiation exceeds 1 kW/m^2 the PV production shall be higher than the nominal one.

3 Results

3.1 Radiation

Normal and Gamma Distributions

First of all, the adjustment with the normal distribution was developed, the KSL test was applied and the H0 was rejected, later, the Gamma distribution was tested, and this, without a doubt, is better approached to reality; however, the CVM goodness test also rejected H0. For simplicity, it has been decided to show only the radiation behavior of January through a histogram with their respective classes. Fig. 3 shows the adjustment of the Normal distribution and Fig. 4 the corresponding analysis with the Gamma distribution, each with their respective tests of goodness of fit.

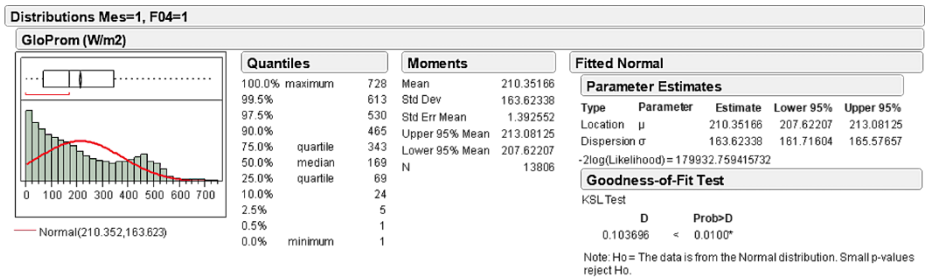

Fig. 3. Normal distribution for the month of January.

The reason for rejecting the adjustment of the normal distribution lies in the following fact: under this behavior, the average and the standard deviation of the data represent the possible best fit, clearly in the figure the null approach is observed.

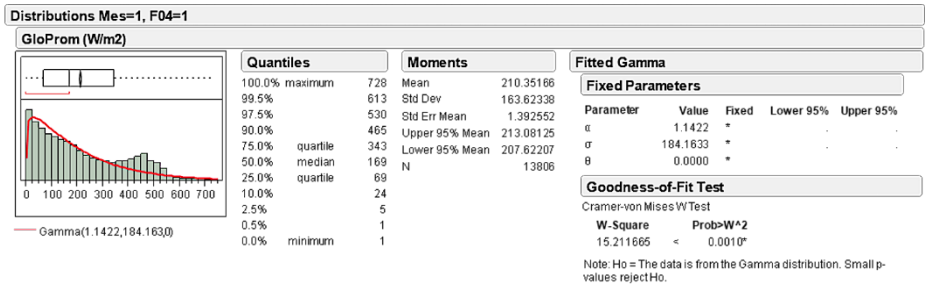

Fig. 4. Gamma distribution for the month of January.

When an asymmetric distribution, such as Gamma, is applied to the information, the methodology for achieving the best possible adjustment consists in optimizing the shape parameter (α) since it represents the region of greatest probability (area under the curve) and obtaining the average of the data to estimate the value of the scale parameter (σ), due to the above, in the figure there is a better visual adjustment in the upper part and in the asymptotic low zone there is a mismatch. However, the proximity is greater compared to the normal distribution.

By reviewing the behaviors of the experimental points and histograms, it was detected that there is no single distribution; that is, there are two different probabilistic behaviors. Visually the first behavior, between 0 and 350 W/m^2, tends to be a gamma with $\alpha = 1$ (exponential) and the second to a normal one, its combined effect would generate the histogram of the data.

The previous combination was tested without the expected response. Due to this, two normal curves were associated, being equally rejected. When this possibility was ruled out, two crossed Gamma distributions were tested: the first represents the days of greatest radiation and the crossed one the low ones. When performing different tests, combining them and varying their characteristic parameters, the strong approximation

with the radiations measured in each month is observed, generating them without spaces that serve as the input of the photovoltaic systems.

Radiation simulation with Gamma distributions

In order to find the parameters of the Gamma distributions that reflect an approach to radiation, four simulations were made, creating four years of radiation. Fig. 4 warns the fourth simulation for the month of January.

In Fig. 5, 15,000 simulated points are observed every five minutes of the radiation, as well as the spline adjustment that reaches a correlation factor ($r = \sqrt{R^2}$) of 0.7141, exceeding that found in the observed data. The main difference is presented in the number of points, that is, in the acquisition of information there are absences of records. A criterion taken into account to approach reality was to maintain the spline function at the same original value, for January the peak is 350 W/m^2 and the original is 346.157 W/m^2, that is, there is a difference of 1.11% from the measured. They were simulated 10 times each month to determine the Ipm; Table 2 shows the values of this indicator.

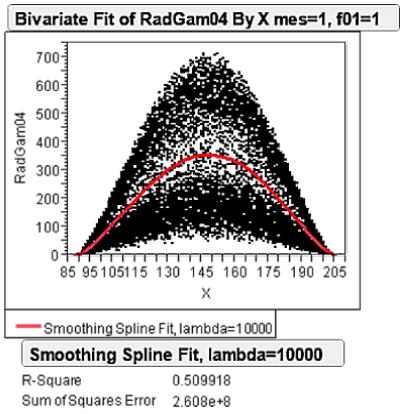

Fig. 5. Radiation simulation with two Gamma distributions with their corresponding spline fit for the month of January.

Table 2. Radiation measurement approach index.

Month	Ipm(%)	Month	Ipm(%)
January	98.9	July	94.9
February	98.6	August	95.4
March	98.1	September	98.7
April	93.4	October	97.6
May	97.3	November	98.1
June	97.6	December	96.9

As shown in the table, no Ipm exceeds the measured by 10%. April is the month where the difference is greater with 6.6%, due to intermittences of great duration, and in the months with low temperatures the simulator is closer to the measurements.

Matrix Rad

The matrix that was formed for the simulation of the particular radiation of each month is presented in Table 3.

The simulator, automatically, decides the section of the matrix from which it will take the information when requesting the generation of a certain month. As a characteristic of the polynomials, a majority of negative odd coefficients are observed in contrast to the pairs, this means that, being the horizontal axis always positive, odd-order contributions compensate for ever increasing increases in even contributions. Since all functions are of 4^{th} and 5^{th} order, at least 3 curvature changes are possible, reflecting the radiation behavior. The parameters α and β of the Gamma distributions are highlighted in the matrix.

Table 3. Matrix Rad

β_0	β_1	β_2	β_3	β_4	β_5	nd	hd	rd	mv	sr	er	$\propto_a$	β_a	$\propto_b$	β_b
$5.4e^3$	-184. 1	2.2	$-1.06\ e^{-2}$	$1.79e^{-5}$	0	31	750	346.1	25	89	204	4.6	42	5.8	28
$4.0e^3$	-147.1	1.8	$-9.08e^{-3}$	$1.53e^{-5}$	0	28	975	445.2	60	84	210	5.6	48	5.7	45
$1.8e^3$	-83.1	1.2	$-6.17e^{-3}$	$1.06e^{-5}$	0	31	1000	537.3	30	79	216	6.2	48	7	45
$2.0e^3$	-89.0	1.3	$-6.63e^{-3}$	$1.14e^{-5}$	0	30	1280	654.4	30	69	226	5.7	47	7.5	45
$3.1e^3$	-143.0	2.3	$-1.52e^{-2}$	$4.51e^{-5}$	$-5.0e^{-8}$	31	1300	739.9	5	64	231	3.5	85	7.8	58
$4.8e^2$	-40.2	0.8	$-4.37e^{-3}$	$7.65e^{-6}$	0	30	1325	838.6	5	62	236	3	95	8.5	65
$2.6e^3$	-126.4	2.1	$1.37e^{-2}$	$3.93e^{-5}$	$-4.1e^{-8}$	31	1380	861.4	0	64	231	3.2	110	0	0
$3.7e^3$	-168.4	2.7	$-1.75e^{-2}$	$5.11e^{-5}$	$-5.\ 6e^{-8}$	31	1350	834.2	0	69	226	3.3	100	0	0
$5.4e^3$	-232.7	3.5	$-2.32e^{-2}$	$6.99e^{-5}$	$-7.9e^{-8}$	30	1100	677.4	5	74	220	2.8	84	8.5	50
$6.2e^3$	-240.6	3.3	$-2.02e^{-2}$	$5.57e^{-5}$	$-5.6e^{-8}$	31	975	509.3	5	84	213	5	60	8.5	42
$5.2e^3$	-177.7	2.1	$-1.01e^{-2}$	$1.71e^{-5}$	0	30	800	339.5	5	89	204	5.1	62	8.2	30
$6.7e^3$	-224.1	2.6	$-1.26e^{-2}$	$2.14e^{-5}$	0	31	650	346.9	5	93	200	4.7	45	6.1	31

3.2 Photovoltaic generation

r's function

With the intention of exposing the three typical behaviors, it has been decided to present models of the functions found with their statistical analyzes. For this, Fig. 6, show the reasons of three AFVs measured by AE1037 (March), AE1044 (June) and AE2000 (March), respectively.

The characterization of the functions r's of the first PVA shows, on the one hand, the best adjustments in the months of March and December, with coefficients R^2 of 0.97 and 0.92 respectively; on the other hand, the approaches with less quality in the prediction are the months of May, July and September. Relations in parks 2 and 3 show better correlations between 0.91 and 0.99. In the three PVAs of lower power perfectly marked behaviors of "U" prevail in the "cold" and "M" in the "hot" months. The best correlations, in general, coincide in the fourth PVA and at the same time, their characterizations are more complex (4° and 5°), in the months where the temperature is low

they are perceived behaviors in the form of "Ω" and under this trend the reasons are better. The latter system has greater diversity in the behaviors found, however, it is still the high order functions that best fit.

It is emphasized that in each of the analyzes meaningful relationships ($\alpha \leq 0.05$) are met and all the estimated parameters satisfy the tests of statistical behavior causing the regression.

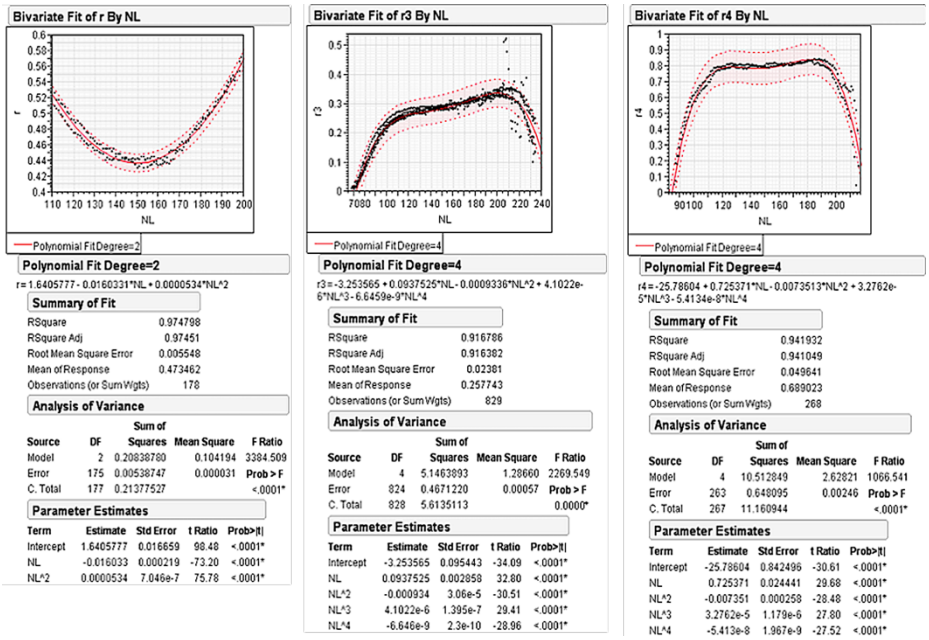

a) b) c)

Fig. 6. r's function. a) Park 1 for the month of March, b) Park 3 for the month of June, c) E01 Arfrisol for the month of March.

Photovoltaic power simulation

Although the simulator has an interval where the user can request different powers of the PVA it was decided to use the CEDER nominals to compare the simulation with its consumption, the period requested was one year. Table 4 shows two of the most important characteristics: F_{hr} is the factor of days where the radiation is greater than the reference spline and P_{pmed} corresponds to the average peak photovoltaic power of all PVAs.

The table shows three months that would not cover, on average, the maximum power of the CEDER (40 kW). For its part, the summer months would supply this requirement without any difficulty, it would even be necessary to define which solar generators would interrupt its connection to the micro network. The above is clearly reflected in the F_{hr}, with an exceptional case being December, reaching 8.3% of days above the

expected. During the months of June-August, P_{pmed} reached the nominal PV power installed. As the simulation reflects, lower production is frequently present in November.

Table 4. General monthly behavior of radiation and PV power.

Month	F_{hr}	P_{Pmed} (kW)
January	0.452	28.160
February	0.536	42.110
March	0.548	52.260
April	0.500	56.078
May	0.581	66.735
June	0.633	77.341
July	0.613	79.299
August	0.677	79.150
September	0.567	53.346
October	0.484	50.560
November	0.267	27.404
December	0.613	29.776

4 Conclusions

For the approach of the behavior of the monthly radiation is proposed a double distribution of probability Gamma, reaching a strong approximation to the reality shown by the Ipm, standing out as one of the few investigations that silver a double simulation. Moreover, achieving these results required only four simulations.

On the other hand, the PVAs have a similarity in the form of their regression curves according to the ambient temperature existing in each month, favoring the electric production cold climatic conditions. With the help of the relationships, under the best conditions between PV power and radiation, factors such as the geometry of PVAs, wiring losses, soil degradation and aging have been included in the characterization, which is not present in the measurements. Functions were also established at any granularity of time for future analysis. In all regression studies, the parameters meet the significance tests achieving a 95% confidence interval. In addition, the functions with the best correlations are independent of their degree.

All of the above has allowed us to establish, approximately, the capacity of the backup system needed in each month to meet the demand of the CEDER. Likewise, the results obtained will be raw material in the development of an energy management system of the same microgrid.

5 Acknowledgments

We would like to thank the CEDER by providing information for the development of this work.

References

1. Rudnick, H., Barroso, L., Skerk, C. y Blanco, A.: South American reform lessons - twenty years of restructuring and reform in Argentina, Brazil, and Chile. Power and Energy Magazine 3, 49-59 (2005).
2. Mocarquer, S., Barroso, L., Rudnick, H, Bezerra B. y Pereira, M.: Balance of power. Power and Energy Magazine 7, 26-35 (2009).
3. Hernández, L., Baladrón, C., Aguiar, J., Calavia, L., Carro, B., Sánchez-Esguevillas, A., Pérez, F &Lloret, J.: Artificial neural network for short-term load forecasting in distribution systems. Energies 7, 1576-1598 (2014).
4. The Royal Academy of Engineering.: The cost of generation electricity. Published by The Royal Academy of Engineering, London (2004).
5. Anderson, D.: Power system reserves and costs with intermittent generation. UK Energy Research Centre Working Paper (2006).
6. Lin, S. y Chen, J.: Distributed optimal power flow for smart grid transmission system with renewable energy sources. Energy 56, 184-192 (2013).
7. Skea, J., Anderson, D., Green, T., Gross, R., Heptonstall, P., and Leach, M.: Intermittent renewable generation and maintaining power system reliability. IET Generation, Transmission & Distribution 2, 82 - 89 (2008).
8. Chang, T.: Investigation on Frequency Distribution of Global Radiation Using Different Probability Density Functions, Int. J. Appl. Sci. Eng. 8(2), 99-107 (2010).
9. Sánchez, R., Aguirre, G., Sánchez, S., Alcalá, J.: Investigando variaciones aleatorias de radiación solar en Guadalajara, México. Revista Iberoamericana de Ciencias. (2016).
10. Razika, I., Nabila, I.: Modeling of monthly global solar radiation in M'sila region (Algeria). IEEE. 978-1-4673-9768-1/16 (2016).
11. Assunção, H., Escobedo, J., Oliveira, A.: Modelling frequency distributions of 5 minute-averaged solar radiation indexes using Beta probability functions. Theor. Appl. Climatol.75, 213–224 (2003).
12. Soubdhan, T., Emilion, R., Calif, R.: Classication of daily solar radiation distributions using a mixture of Dirichlet distributions. Aricle soumis à Solar Energy (2008).
13. Jurado, M., Caridad, J., Ruiz, V.: Statistical distribution of the clearness index with radiation data integrated over five minute intervals. Solar Energy 55, 469–473 (1995).
14. Uribe-Pérez, N., Latorre, M., Angulo, I., De la Vega, D.: Aprovechamiento de los recursos renovables e integración de las TICs: ejemplo práctico de una Microred eléctrica. In: III Congreso Ibero-Americano de Empreendedorismo, Energía, Ambiente e Tecnología, pp. 161-166. Instituto Politécnico de Braganca, Portugal (2017).
15. Arroyo, I., Bravo, C., Llinás, H., Muñoz, F.: Distribuciones Poisson y Gamma: una discreta y continua relación. Prospect 12 (1), 99-107 (2014).
16. Bidegain, M., Diaz, A.: Análisis estadístico de datos climáticos. Universidad de la República. Uruguay. p. 15. (2011).
17. López, R., Hernández, L., Jamed, L., Alonso, V.: Solar intermittency with Spline fit modeling. Microgrid case CEDER, Soria, Spain. In: I Ibero-American Congress of Smart Cities, pp. 592-601. Universidad Santiago de Cali, Colombia (2018).

Electric Microgrid in Smart Cities: CEDER-CIEMAT a case study

Luis Hernández-Callejo[1], Oscar Izquierdo Monge[2] y Lilian J. Obregón[1]

[1] University of Valladolid, Campus Universitario Duques de Soria, Soria, Spain. L.H-C: luis.hernandez.callejo@uva.es; L.J.O.: liliancitaobregon@gmail.com
[2] CEDER-CIEMAT, Autovía de Navarra A15 sal. 56, 42290 Lubia (Soria), Spain. M.L.Z: oscar.izquierdo@ciemat.es

Abstract. The increase in the penetration of renewable generation sources is fundamental in Smart Cities. But these renewable sources can be integrated with distributed electrical storage and intelligence for the management of all assets through electric microgrids. Therefore, these new generation and consumption environments will be present in the Smart City. In this sense, this paper presents one of the most versatile and interesting electric microgrid that exists today, specifically the microgrid of the Center for the Development of Renewable Energies (CEDER) located in Soria (Spain).

Keywords: Electric Microgrid, Smart City, Energy Efficiency, Sustainability.

1 Introduction

As it appears in [1], a *Smart City* (*SC*) is a sustainable urban environment, which tries to provide a high quality of life to its residents, for which it requires an optimal management of resources. Therefore, one of the main challenges of the *SC* will be to carry out an optimal and efficient management of the available resources.

Therefore, it is possible to say that the *SC* is faced with a challenge similar to that of micro-networks, specifically the management of existing assets [2]. In the case of the microgrid, these assets are: *Distributed Generation* (*DG*), distributed electrical storage and loads. These elements also appear in the scenario of the *SC*, so it must face a problem similar to that of the microgrid.

One of the benefits of the electric microgrid is its guarantee of efficiency and sustainability in the global network infrastructure. In this sense, in [3] it is shown how microgrids can be the future of cities in Europe and, therefore, throughout the world.

Other authors [4] focus on the importance of the integration of the electric microgrid in the SC in distributed electrical storage. The storage not only seen as support elements to the renewable *DG*, but as an integrating and agglutinating element of the electric vehicle.

The *SC* presents another great challenge, its management. When talking about management, not only must we think about the elements described as members of a microgrid, but also the circulation [5], parking [6-7], infrastructures [8], etc.

In the case of the microgrid, management mainly focuses on distributed resources (generators and storage) [9-10]. This management is independent of whether the microgrid is designed in alternate or continuous [11-12].

What it can affirm is that the electric microgrids will be part of the *SC*, for which the management of those will be their responsibility [13]. This coexistence makes it interesting that there are microgrid test environments, since the integration of these in the *SC* will depend on the degree of control and management of the microgrids.

Numerous are the test scenarios in electric microgrid environments, both real and simulated. However, the authors have selected a special environment in Spain, as it has special conditions in terms of *DG* elements and distributed electrical storage, which makes this environment likes a unique microgrid.

After this introduction the publication is as follows: Section 2 presents the selected microgrid environment; Section 3 lists the objectives that are intended to be covered by this electrical microgrid; and Section 4 ends with some conclusions and future work to be able to develop in this test scenario.

2 Test Scenario: CEDER-CIEMAT

As already mentioned, there are many scenarios in the world based on electric microgrids [14]. Some of these environments are based on simulation, others on emulation, but the vast majorities are real environments.

Without underestimating the simulated and emulated scenarios, it is in the real environments where the validation of the hypotheses takes a decisive character. The transition from simulated/emulated models to the real world is critical and fundamental, since this is where most of the problems or restrictive situations that are over- looked in computational environments appear.

In this sense, this work is centered on a scenario with electric microgrid, which undoubtedly represents one of the most interesting locations found in the literature. Specifically, we are talking about the Center for the Development of Renewable Energies (CEDER) of Lubia (Soria - Spain), created in 1987 as a national center for the re- search and development of renewable energies. CEDER presents a microgrid on a real scale, and this facility is in Castilla y León, and is owned by the Center for Energy, Environmental and Technological Research (CIEMAT), Public Research Organization, currently under the Ministry of Economy, Industry and Competitiveness.

As will be seen later, CEDER is an ideal environment for the validation and experimentation of the application and integration of *DG*, electrical storage, power electronics and intelligence technologies applied to the operation and control of electric microgrids. All the elements that make up the microgrid (substation, transformers, DG, storage, loads, etc.) of CEDER are owned by CIEMAT, allowing any type of maneuver and operation.

Figure 1 shows an area image of the entire CEDER complex. The research center is deployed in some 640 ha, where, as already said, there is a real microgrid, operated and managed in real time, and where the charges and generators are real, and its operation has consequences on the energy flow of the microgrid.

Fig. 1. Aerial image of CEDER. The center is located on 640 ha of land. Courtesy of CEDER.

CEDER has a medium voltage grid (15kV) and 8 transformation centers can be identified, which adjust the voltage from 15 kV to 400 V three-phase low voltage. CEDER has a contracted power of 115 kW, and the distribution company supplies electrical power at a voltage level of 45 kV which, through a transformer at the entrance to the center, is conditioned to 15 kV. The input transformer element is 45/15 kV and 1,000 kVA. Next, the center deploys a medium voltage network of about 3 km, interspersing transformation centers to supply low voltage to the consumptions and generators.

All *DG* elements, distributed electrical storage and loads, are connected at low voltage. With regard to demand, the center presents different consumption profiles, which are similar to those that can be found in an industrial environment, in the service sector or even in the domestic sector.

2.1 Elements of *Distributed Generation*

As it could not be otherwise, a microgrid must integrate elements of *DG*, therefore, CEDER presents an interesting variety of these elements, besides being all of them renewable. The electric microgrid installed in CEDER presents the following *DG* elements:

- Wind generation systems: horizontal axis and leeward wind turbine with 50 kW of installed capacity. In addition, it integrates a wind turbine with a hori zontal and windward axis with 3.5 kW of installed capacity.

- Photovoltaic generation system: the center integrates 6 photovoltaic systems. The first installation consists of 16 kW distributed in 64 monocrystalline panels of 250 W each, connected to a three-phase inverter of 15 kW. A second roof system consisting of 80 panels of monocrystalline silicon, distributed in 5 arrays connected in parallel, where each array, consists of 16 panels connected in series each, to make a total of 12 kW of power and connected to an inverter three-phase of 10 kW. The third system is another installation on roof of 12.6 kW in 54 monocrystalline photovoltaic panels of two different brands, there are 36 of the brand LDK of 230 W and another 18 of the brand SACLIMA of 240 W, all of them connected to a three-phase inverter of 10 kW in 3 series of 18 panels each. A fourth roof installation of 23 kW is divided into two groups of modules, which form a first series of 84 and another of 154 modules, forming a total of 238 thin-film panels of 97 W per panel, distributed in 17 series of 14 panels each, feeding a three-phase inverter of 20 kW. The fifth installation (5.04 kW) is on ground distributed in 24 polycrystalline panels of 210 W each. The sixth installation is on roof, divided into three blocks (one of 48, another of 30 and another of 48 modules), to form a set of 126 polycrystalline photovoltaic modules of 310 W, connected to 2 three-phase inverters of 20 kW.

- Microcentral hydraulics with Pelton turbine (Figure 2) and three-phase asynchronous generator coupled directly to the impeller of the turbine, with maxi- mum electrical power generated 40 kW. The installation is completed with a bank of capacitor banks to compensate the power factor of the installation. The system is controlled by means of a system of supervision, control and acquisition of its own data, with instructions for active power and regulation through flow through injectors.

Fig.2. Pelton hydraulic microcentral installation. Courtesy CEDER.

2.2 Distributed Electrical Storage Elements

Achieving a balance in power in a microgrid is necessary. In order to achieve this, it is imperative that the *DG* elements are supported with distributed electrical storage. In this sense, CEDER integrates different storage technologies, which make the center a flexible environment for demand management. The electric microgrid installed in CEDER presents the following elements of distributed electrical storage:

- Mechanical storage: associated to the hydraulic microcentral, the center has 3 water reservoirs (2.000 m^3 and 70 m head) and a hydraulic pumps system by means of two centrifugal pumps of 18 kW of power each, which can be managed independently.

- Pb-acid storage: the center also integrates electrochemical storage through three banks of Pb-acid batteries. There are 3 batteries banks: The first bank is composed of 150 elements (2V) and with capacity of 1080Ah (C_{120}), the second has 120 elements (2V) and 765 Ah (C_{120}) and the third one 24 elements (2V) and 660 Ah (C_{120}).

- Lithium-ion storage: they also integrate another electrochemical storage technology, specifically a lithium-ion battery with a capacity of 2 x 50 Ah. Figure 3 shows the Li-ion battery bank and its corresponding bi-directional inverter.

Fig. 3. Lithium-ion battery and bi-directional inverter. Courtesy CEDER.

2.3 Existing Demand

A microgrid must be completed with charges, which will request energy to perform its functions (motors, lighting, boilers, laboratories, etc.). To guarantee the supply of said loads, or at least of the priority ones, will be the responsibility of the manager of the microgrid.

In this sense, CEDER has loads that must be fed. In addition, these loads are what allow the day to day operation of the center, or in other words, the different buildings that make up the center are those that demand energy for its operation.

In addition, these real charges have different consumption patterns, so some facilities behave as an industrial environment, while others do so as a domestic consumer or the service sector. In this way, the microgrid has different consumption profiles, which will allow different adjustments to generation and storage, based on the varied behavior of the existing demand.

3 Monitoring of Microgrid

The control center of CEDER is in charge of monitoring the entire microgrid. All the loads (buildings and installations) of CEDER are connected to this centralized manager by means of ethernet technology, so that the data can be sent and received at any point of the center, to be processed in a decentralized way later. The monitoring also reaches the *DG* elements and distributed electrical storage.

To fulfill this purpose of monitoring, CEDER has a total of 53 single-phase and three-phase smart meters, and 9 data concentrators to record the measurements taken by them. Each transformation center integrates a data concetrator, and those with a

double transformer incorporate a second data concentrator, in master-slave configuration. Smart meters obtain current and voltage data, active power, reactive power in the four quadrants, bidirectional active energy, reactive energy in the four quadrants and instantaneous power factor. All mentioned devices incorporate communications technology through *PoweRline Intelligent Metering Evolution* (*PRIME*). Figure 4 shows a display of three-phase smart meters and a data concentrator of a transformation center.

Fig. 4. a) Smart meters for the measurement of consumption and *DG*; b) Data concentrator in transformation center to monitor smart meters in low voltage.

4 Objectives of the CEDER-CIEMAT Electric Microrgrid

The main objective of the micro-network of CEDER is to approach the energy sustainability. For this, it is essential to integrate sources of renewable generation, small- scale and as *DG*, and in this way reduce the dependence on foreign energy.

In addition, the communications displayed in CEDER allow achieving clear objectives, namely:

- Monitoring: thanks to the advanced measurement it is possible to monitor the network topography, as well as its evolution over time through web services and specific software. In addition, it is possible to analyze the evolution of the different roles of the devices that make up the measure (smart meter and data concentrator), availability of the network, availability of smart meters, registered/deregistered devices and operation of the protocol *PRIME*.

- Intelligent measurement and management: the data coming from the measure are sent daily through scheduled tasks through web services implemented in the data concentrators. In this way, the data concentrators interrogate the smart meters of their subnet to obtain the specified information. The information is sent, in xml files, via FTP to the control center, where they are stored in databases. This information can be used for multiple offline processes: verification of simulations, training of models for predicting electricity demand or renewable generation, design of consumption and generation patterns, etc.
- Demand management: by comparing the tariff and electricity bills of CEDER with simulated tariffs and load profiles, it is possible to design behavior patterns with the objective of reducing costs and improving energy efficiency. Figure 5 shows the measurement of different buildings of the CEDER.
- Quality of service (noise and interference): from a communication perspective, in an electrical microgrid a reliable means of communication is necessary for proper data management. In this case, the electrical cable can be affected by interferences, which can cause alterations in the configuration of the network, as well as loss of data and the impossibility of controlling remote devices.

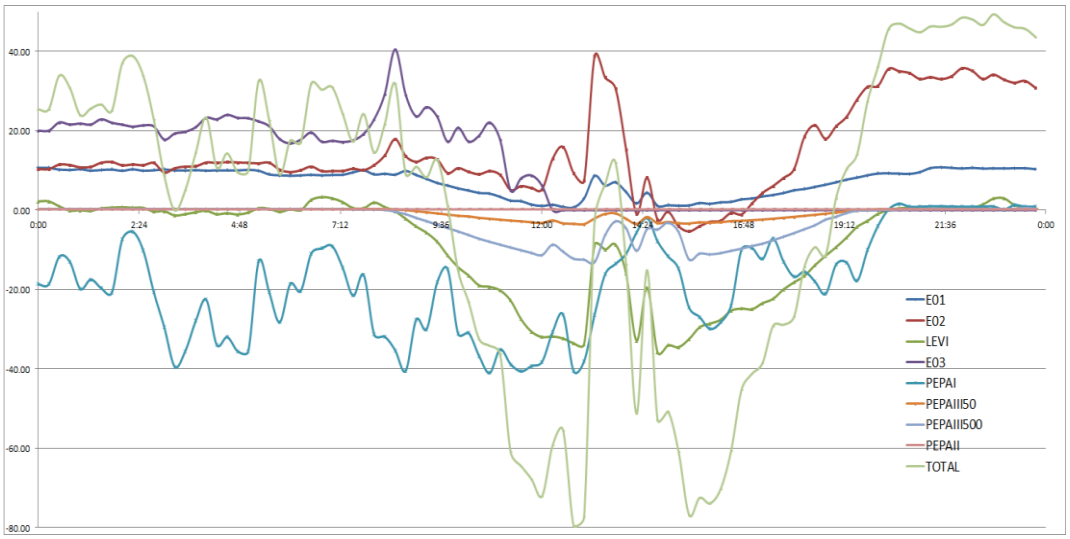

Fig. 5. a) Daily consumption data collected

5 Conclusions and Future Jobs

The integration of renewable generation sources is a reality today. The integration is present in all the levels: transport and distribution in the electrical grids, and in the *SC*. In addition, the *SC* is also an integrator of the new paradigm that supposes the electric microgrid, being this in turn a *DG* integrator (renewable or not), distributed electrical storage and intelligence.

In this sense, the existence of demonstration environments and technology validators are crucial in the technological development. Electric microgrids position them- selves as integrating spaces of different technologies, and of very different areas (energy, communications, systems, social, etc.).

This work has presented the electric microgrid of CEDER, located in Soria (Spain), which can be considered one of the most complete of the real microgrids in the world, mainly due to its great variety of *DG* and storage technologies.

Based on a very efficient and robust communications and monitoring layer, CEDER's microgrid effectively manages all its assets under its responsibility. In addition, this demonstration environment allows the addition of any other *DG* or storage element, since the CEDER dimensions allow it.

CEDER is presented as a perfect test scenario for the validation of electric micro-grid technologies. The multiple possibilities that this environment allows, positions this microgrid as one of the most interesting in the world.

Acknowledgent

The authors thank the CYTED Thematic Network "CIUDADES INTELIGENTES TOTALMENTE INTEGRALES, EFICIENTES Y SOSTENIBLES (CITIES)" nº 518RT0558.

References

1. Calvillo, C.F., Sánchez-Miralles, A., Villar, J.: Energy management and planning in smart cities. Renewable and Sustanaible Energy Reviews 55(March), 273-287 (2016).
2. Hernández-Callejo, L., Mirez, J., Horn, M., Bonilla, L.M.: Simulation of Direct Current Microgrid and Study of Power and Battery Charge/Discharge Management. Dyna 92 (November), 673-679 (2017).
3. Schmitt, L., Kumar, J., Sun, D., Kayal, S., Mani Venkata, S.S.: Ecocity Upon a Hill: Mi crogrids and the Future of the Europeai City. IEEE Power and Energy Magazine 11(4), 59- 70 (2013).
4. Coelho, V.N., Coelho, I.M., Coelho, B.N., de Oliveira, G.C., Barbosa, A.C., Pereira, L., de Freitas, A., Santos, H.G., Ochi, L.S., Guimaraes, F.G.: A communitarian microgrid storage planning system inside the scope of a smart city. Applied Energy 201(September), 371-381 (2017).

5. Mwasilu, F., Justo, J.J., Kim, E-K., Do, T.D., Jung, J-W.: Electric vehicles and smart grid interaction: A review on vehicle to grid and renewable energy sources integration. Renewable and Sustanaible Energy Reviews 34(June), 501-516 (2014).
6. Giuffre, T., Siniscalchi, S.M., Tesoriere, G.: A Novel Architecture of Parking Management for Smart Cities. Procedia – Social and Behavioral Sciences 53(October), 16-28 (2012).
7. Barone, R.E., Giuffre, T., Siniscalchi, S.M., Morgano, M.A., Tesoriere, G.: Architecture for parking management in Smart cities. IET Intelligent Transport Systems 8(5), 445-452 (2014).
8. Al-Hader, M., Rodzi, A.: The Smart City Infrastructure Development & Monitoring. Theoretical and Empirical Researches in Urban Management 4(2), 87-94 (2009).
9. Katiraei, F., Iravani, M.R.: Power Management Strategies for a Microgrid With Multiple Distributed Generation Units. IEEE Transactions on Power Systems 21(4), 1821-1831 (2006).
10. Zhou, H., Bhattacharya, T., Tran, D., Terence, T.S., Khambadkone, A.M.: Composite Energy Storage Involving Battery and Ultracapacitor With Dynamic Energy Management in Microgrid Applications. IEEE Transactions on Power Electronics 26(3), 923-930 (2011).
11. Chen, Y-K., Wu, Y-Ch., Song, Ch-Ch., Chen, Y-S.: Design and Implementation of Energy Management System With Fuzzy Control for DC Microgrid Systems. IEEE Transactions on Power Electronics 28(4), 1563-1570 (2013).
12. Nejabatkhah, F., Li, Y.W.: Overview of Power Management Strategies of Hybrid AC/DC Microgrid. IEEE Transactions on Power Electronics 30(12), 7072-7089 (2015).
13. Hernández, L., Baladrón, C., Aguiar, J.M., Calavia, L., Carro, B., Sánchez-Esguevillas, A., Cook, D.J., Chinarro, D., Gómez, J.: A study of the relationship between weather variables and Electric power demand inside a Smart grid/Smart world framework. Sensors 12(9), 11571-11591 (2012).
14. Hernández, L.: Microrredes Eléctricas: Integración de generación renovable distribuida, almacenamiento distribuido e inteligencia. Garceta Grupo Editorial: 2018.

Comparativa a nivel de barrio de los porcentajes de ahorro energético como resultado de transformar los edificios de viviendas a NZEB en Zaragoza.

García-Ballano, Claudio Javier[1][0000-0002-9328-3841], Ruiz-Varona, Ana[2][0000-0001-8807-4917], y Casas-Villarreal, Luis[3][0000-0001-8429-5456]

[1, 2, 3] Escuela de Arquitectura y Tecnología, Universidad San Jorge, Zaragoza, España
nruiz@usj.es

Abstract. Este artículo recoge los resultados obtenidos de haber aplicado una metodología de análisis que permite evaluar los ahorros de costes energéticos obtenidos como resultado de adaptar la envolvente exterior de las viviendas para transformarlas en edificios de consumo casi nulo (NZEB) en Zaragoza, de acuerdo con la normativa vigente en materia de eficiencia energética. Se han tomado las bases de datos del catastro como fuentes de información y los cálculos se han realizado aplicando tecnologías de información geográfica (SIG). La investigación evidencia las diferencias de ahorro entre barrios de acuerdo a variables como la antigüedad, factor de forma y tipo edificatorio y concluye sobre la importancia que tienen estos valores en términos de pobreza energética y, en este sentido, como parte integrante de los índices de vulnerabilidad urbana integral.

Keywords: rehabilitación urbana integral, SIG, catastro, eficiencia energética, sostenibilidad.

1 Adaptación normativa de la fachada a edificios de consumo casi nulo

Desde un punto de vista histórico, comprobamos que la primera normativa publicada en España en materia de regulación sobre medidas a adoptar en las edificaciones con objeto de reducir el consumo de energía se publica en 1975. En ella no se definían condiciones unitarias por cerramiento, sino que se establecía, en términos generales, un coeficiente global máximo de la vivienda (K_G), en función de su factor de forma y de su ubicación en la península [1].

Esta normativa fue derogada en 1979 al aprobarse la Norma Básica de la Edificación sobre Condiciones Térmicas en los edificios (NBE-CT-79), documento que establecía unos valores máximos para la envolvente de la vivienda, en función del tipo de cerramiento y de la zona climática donde esté ubicada la edificación [2]. Además del aludido factor de forma de la edificación, este documento diferenciaba el tipo de combustible utilizado para la calefacción de la misma.

La publicación en 2006 del Código Técnico de la Edificación [3] incorpora una visión que prioriza la estrategia de ahorro y eficiencia energética no sólo de los edificios

sino también de los espacios urbanos donde se ubican. Esto se traduce en lo siguiente: por un lado, los edificios deberán disponer de una envolvente de características tales que limite adecuadamente la demanda energética necesaria para conseguir el bienestar térmico (DB-CTE-HE), cuestión que fijaría reducciones de la demanda de hasta un 25 por ciento con respecto a la norma de 1979; por otro lado, una mayor discriminación entre zonas peninsulares, fijando cinco valores de transmitancias máximas según emplazamiento y, además, 6 valores para cada uno de los grupos anteriores en función del tipo de cerramiento.

En 2013 esta norma sufre modificación y se incorpora una sección que aborda la limitación al consumo energético, introduciendo valores más restrictivos y una nueva zona. Estos valores se mantienen sin variación hasta la publicación del borrador de la revisión prevista del CTE, teóricamente objeto de aprobación durante el 2019.

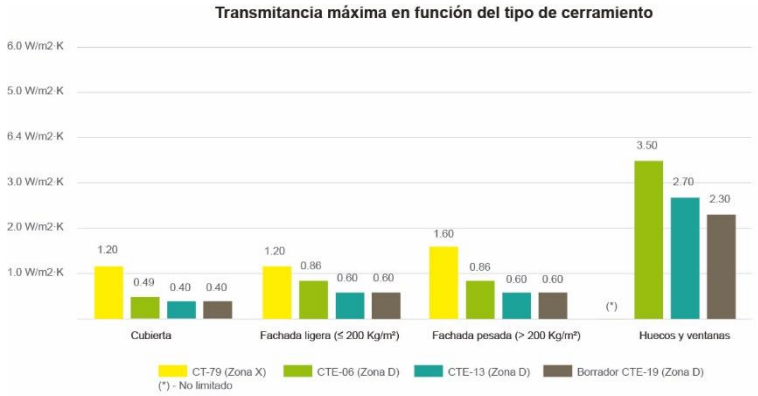

Fig. 1. Transmitancia máxima en función del tipo de cerramiento. Fuente: elaboración propia, 2019.

Conviene reseñar que, aunque se observa durante este periodo una reducción en las transmitancias máximas exigidas por la normativa nacional (Fig. 1), durante un periodo extenso, hasta 2017, España no fijó ningún criterio de cumplimiento de eficiencia energética de los edificios que refiere la Directiva Europea 2010/31/UE. Como es sabido, en el año 2010 la citada Directiva Europea relativa a la eficiencia energética de los edificios fija que para el año 2020 todos los edificios deben ser de consumo casi nulo (NZEB). España, a diferencia de otros países que concretan los criterios a cumplir por un edificio de consumo casi nulo, ha incluido una definición poco rigurosa de qué se entiende por NZEB, afirmando que éste es aquel "que cumple con las exigencias reglamentarias establecidas para edificios de nueva construcción en las diferentes secciones de este documento básico [DB-HE 'Ahorro de Energía']" [4].

Esta cuestión es importante, puesto que la directriz se enmarca en la estrategia UE 20/20/20, por la que se pretende reducir en un 20% la emisión de gases de efecto invernadero, ampliar la eficiencia energética en 20% y uso del 20% de energías renovables. Contar con unos criterios estrictos de cumplimiento en los edificios supone ampliar la

eficiencia energética en línea no sólo con dicha directiva sino con el horizonte 2030 a nivel de edificio y de espacio urbano.

Esta cuestión relativa a la eficiencia energética a nivel de edificio y de barrio va a ser estudiada en el presente trabajo. En concreto vamos a estudiar cuál sería el porcentaje de ahorro energético a nivel de barrio que se obtiene como resultado de transformar los actuales edificios de viviendas a NZEB, según los criterios fijados en el borrador del CTE 2019. Los resultados permiten comparar los porcentajes de ahorro entre dos barrios de la ciudad de Zaragoza, evidenciando sobre qué variables conviene actuar para obtener los mayores porcentajes de ahorro y detectando si los actuales criterios fijados en le CTE son adecuados a la hora de garantizar que se obtienen unas mejoras del 20 % de la eficiencia energética de los edificios.

1.1 Valores de transmitancia máximos que debe cumplir un edificio para transformarse en NZEB

Las pérdidas de energía del edificio que se producen por la envolvente exterior suponen, en general, entre un 60 a 65 % del total del edificio [5]. Una de las acciones a aplicar para transformar los edificios hacia el consumo casi nulo (NZEB) es la mejora constructiva de estos elementos que forman la envolvente exterior [6]. Como ya ha sido referido, en España, la normativa actual define NZEB como aquel que cumple lo referido en los documentos básicos de ahorro de energía y salubridad desarrollados en el código técnico de la edificación [4]. Es decir, los valores de transmitancia máximos que debe cumplir un NZEB dependen del tipo de cerramiento y, como consecuencia, de la antigüedad de los edificios.

Así, si adecuamos la envolvente de los edificios a las actuales exigencias normativas [7], podemos conocer cuál es el porcentaje de ahorro energético que obtenemos como resultado de transformar los edificios de viviendas a NZEB.

Para ello, consideramos que cada uno de los edificios actuales cumplen con la normativa en materia energética que estaba vigente en la fecha de su construcción. Así, las demandas exigidas al tipo de cerramiento dependerán de la antigüedad de los edificios. Teniendo esta acotación presente, podemos calcular cuál es la diferencia de transmitancias que debe hacer frente una mejora constructiva de la envolvente exterior de cada edificio para cumplir con los valores fijados por la normativa actual.

La antigüedad de los edificios también condiciona las soluciones constructivas en términos de cambios en las técnicas aplicadas, que han sido distinta según épocas. Así, hay estudios que refieren, para cada época, los elementos que componen las soluciones tipo de fachadas, cubiertas y huecos [8]. El periodo correspondiente a las décadas de 1940 a 1960 supone un punto de inflexión con respecto a los valores de transmitancia, puesto que se pasa de estructura de muro de carga a estructura porticada de hormigón. La fachada se libera de la capacidad portante y, como consecuencia, la envolvente alcanza valores mayores de transmitancia. Frente a periodos anteriores, los edificios construidos en estas décadas presentan peor eficiencia energética de su envolvente.

Si tomamos como referencia los cambios en los sistemas constructivos, junto con los cambios normativos, podemos determinar una divisoria en torno a 8 grupos (Tabla 1).

Tabla 1. Definición de los 8 grupos de estudio.

Grupo	Antigüedad	Justificación de divisoria	
1	<1900	Cambios sistemas constructivos	
2	1900 a <1940	Cambios sistemas constructivos	
3	1940 a <1960	Cambios sistemas constructivos	
4	1960 a <1979	Cambios sistemas constructivos	
5	1979 a <1990	Cambios normativos CT-79	Cambios sistemas constructivos
6	1990 a <2006		Cambios sistemas constructivos
7	2006 a <2013	Cambios normativos CTE-2006	
8	> 2013	Cambios normativos CTE-2013	

El estudio de las soluciones constructivas para cada uno de los grupos de edad nos permite obtener los valores de transmitancia, tanto para fachada (parce ciega y huecos) como cubierta. Conocidos estos valores, podemos determinar qué tipo de operaciones de mejora deben realizarse para alcanzar los valores de transmitancia exigidos en la actualidad.

Valores de transmitancia en fachadas, partes ciegas. Hasta el año 1900, la envolvente ciega de fachada se realizaba a través de un muro de carga de un pie de ladrillo macizo, acompañado por mortero de cemento y enlucido de yeso [8]. El cálculo de los valores medios de transmitancia que obtenemos referido a esta solución constructiva es de 2,66 W/m2·K.

Esto significa que, para que este cerramiento alcance los valores de transmitancia máximo exigidos en la actualidad, las acciones de mejora para la fachada deben de contemplar la incorporación de un aislamiento de lana de roca de 6 centímetros, junto con una capa de mortero acrílico. Como solución propuesta para las fachadas se plantea un sistema de aislamiento térmico por el exterior (SATE), ya que la actuación es más sencilla de implementar en edificios habitados, no se pierde superficie útil de vivienda y se resuelve la problemática de los puentes térmicos existentes [9]. Además, aunque energéticamente no existen diferencias sustanciales entre aislar por el exterior o por el interior [10], estudios recientes apuntan que el consumo energético de las viviendas rehabilitadas con aislamiento por el interior alcanza peores valores que las rehabilitadas por el exterior [11].

Esta solución constructiva de fachada sufre alguna variación en décadas posteriores, caracterizándose por incluir, además de lo anterior, medio pie de ladrillo macizo entre 1900 a 1940 o por reducir el pie inicial por medio pie de ladrillo macizo durante las décadas de 1940 a 1960, alcanzando unos valores medios de transmitancia de 2,01 y

3,06 W/m2·K, respectivamente. En cualquier caso, la operación de mejora para alcanzar los valores de transmitancia máxima fijados por la actual normativa contempla la incorporación de los mismos elementos que en el caso anterior.

A partir de 1960 se incluye una cámara de aire de 5 centímetros de espesor sin ventilar, junto con una fábrica de ladrillo hueco sencillo durante el periodo de 1960 a 1979 a, además, una capa de poliuretano proyectado de 2 centímetros de espesor entre 1979 y 2006. La capa de poliuretano proyectado alcanza los 3 a 4 centímetros durante el periodo 2006 a 2013, a la que acompaña una cámara de aire sin ventilar de 2 centímetros. Estas soluciones alcanzan unos valores de transmitancia considerablemente menores que en épocas anteriores, llegando a 1,68, 1,18 y 0,75 W/m2·K, respectivamente. En cualquier caso, para adaptar la fachada a los valores de transmitancia máxima fijados por normativa se precisa incorporar un aislamiento SATE de lana de roca de 4 centímetros, de menor espesor que en los casos anteriores.

Desde 2013, los espesores de la cámara de aire sin ventilar y del poliuretano proyectado alcanzan los 2 y 5 centímetros respectivamente, obteniendo unos valores de transmitancia menores de 0,6 W/m2·K. En este caso no es necesario intervenir en este tipo de solución constructiva, pues cumple con los valores máximos de transmitancia fijados por la actual normativa.

Valores de transmitancia en fachadas, huecos. El estudio de los huecos refleja que hasta la entrada en vigor de la NBE CT-79, las ventanas utilizadas se caracterizaban por un marco de madera o metal sin rotura de puente térmico con vidrio sencillo de 4 a 6 milímetros de espesor [8], alcanzando unos valores de transmitancia medio de 4,4 W/m2·K para un porcentaje de ocupación del marco de madera en el hueco del 35 por ciento y de 5,7 W/m2·K para un porcentaje de ocupación del marco metálico en el hueco del 26 por ciento. Estos valores se mantienen hasta el año 1990, puesto que durante el periodo 1990-2006 la solución constructiva anterior cambia, sustituyendo el vidrio sencillo por un vidrio doble, alcanzando unos valores de transmitancia de 4,38 W/m2·K. Para adaptar las transmitancias de las partes huecas de la envolvente a los valores previstos para 2019 debe sustituirse la carpintería y el vidrio por un marco de aluminio con rotura de puente térmico mayor de 12 milímetros (o PVC de dos cámaras) y vidrio doble 4 + 16 + 6 bajo emisivo.

Nuestro estudio propone la sustitución total del conjunto marco-vidrio para las viviendas construidas antes del 2006, o la sustitución del vidrio si la construcción es posterior, al considerar que dichas viviendas cuentan con marcos apropiados con rotura de puente térmico.

A partir de 2006, los huecos de ventana, con marco de madera, aluminio o PVC, incorporan rotura de puente térmico con vidrios dobles de 4 milímetros y cámara de 6 milímetros, obteniendo una transmitancia media de 3,51 W/m2·K. Este valor se reduce hasta el máximo de 2,3 W/m2·K previsto para 2019 mediante la sustitución de la parte acristalada por un vidrio doble 4 + 16 + 6 bajo emisivo que proponemos.

Desde 2013 los huecos disponen de vidrios con cámaras de aire de mayor espesor, entre 10 y 12 milímetros, además de marcos con cámaras intermedias. A pesar de que la transmitancia de estos huecos se reduce hasta alcanzar valores medios de 2,55

W/m2·K, es necesario sustituir la parte acristalada por un vidrio doble 4 + 16 + 6 bajo emisivo para alcanzar los valores de transmitancia máximo previstos en 2019.

La elección del tipo de vidrio con cámara de 16 milímetros que reemplace el anterior viene respaldada por ser esta cámara la que establece el mejor equilibrio entre transmisión por radiación/conducción y convección en el interior del vidrio [12]. Asimismo, la selección de los diferentes espesores del vidrio (4 y 6 milímetros) viene justificada por la mejora en términos de aislamiento acústico [13]. La carpintería seleccionada para reemplazar a la anterior queda justificada por las características que debe cumplir, garantizando, por un lado, una adecuada colocación del vidrio doble de 26 milímetros de espesor final y, por otro lado, disponiendo de rotura de puente térmico para alcanzar los valores de transmitancia máximos exigidos y de permeabilidad al aire máxima permitida.

Valores de transmitancia en cubiertas. Por su parte, la evolución de la ejecución de las cubiertas es similar a la de las fachadas. Hasta 1900, la construcción típica se caracterizaba por la colocación de elementos cerámicos, como soportes para tejas, sobre cerchas de madera, generando un espacio abuhardillado que se cerraba por cañizo y yeso [8]. Las transmitancias medias de esta solución constructiva alcanzaban unos valores de 2,25 W/m2·K. Para cumplir con la transmitancia máxima actualmente exigida el cerramiento de cubierta debe incorporar, sustituyendo a la tierra y la tabla conífera ligera anterior, una capa de poliestireno extruido (XPS) de 8 centímetros de espesor, además de una capa de mortero y un tablero cerámico de 3 y 4 centímetros respectivamente, obteniendo una transmitancia de 0,36 W/m2·K.

A partir de 1900 y hasta 1940, los cálculos que obtenemos de los valores de transmitancia se reducen hasta un valor de 1,53 W/m2·K, debido al uso de estructuras porticadas de hormigón, apoyando los tabiques palomeros de las cubiertas ventiladas sobre forjados unidireccionales de 20 centímetros de espesor con bovedillas cerámicas acabadas con enlucido de yeso [8]. La transmitancia se reducía hasta 1,40 W/m2·K durante el periodo 1940 a 1960 al aumentar hasta 25 centímetros el espesor del forjado. La misma solución de XPS con 8 centímetros de espesor –junto con el mortero y tablero cerámico, que sustituyen a la tierra y tabla conífera ligera– se emplea en estos dos casos para alcanzar los valores máximos de transmitancia exigidos.

Ante la mayor exigencia normativa, se incorpora una cámara de aire a los cerramientos de cubierta. Así, desde 1960 a 1980 el cerramiento obtiene unos valores medios de transmitancia de 1,57 W/m2·K al contemplar una cámara de aire junto con un tablero cerámico de 4 centímetros de espesor. Además, el forjado unidireccional pasa a ser de bovedillas de hormigón. Durante el periodo de 1980 a 2006, el cerramiento de cubierta incluye un aislamiento de lana de roca (MW) de 3 centímetros de espesor, reduciendo la transmitancia máxima hasta valores de 0,81 W/m2·K. La mejora de cubierta para el periodo 1960 a 1980 contempla, de nuevo, incorporar una capa de XPS de 8 centímetros de espesor para cumplir con la transmitancia máxima exigida, mientras que para el periodo de 1980 a 2006 el espesor se reduce a 6 centímetros.

A pesar de que los elementos que componen el cerramiento de cubierta no van a cambiar en años posteriores, el espesor del aislamiento MW aumenta durante los periodos 2006 a 2013 y 2013 a actualidad, desde los 3 centímetros anteriores hasta los 8 y

10 centímetros, alcanzando una transmitancia máxima de 0,45 y 0,38 W/m2·K respectivamente. En este caso, para cumplir con los actuales valores máximos de transmitancia debe incluirse una capa de XPS de 6 centímetros de espesor en aquellas soluciones constructivas de cubierta pertenecientes al periodo de 2006 a 2013, no siendo necesaria ninguna mejora para aquellas correspondientes al periodo 2013 en adelante.

Teniendo en cuenta todo lo anterior, las operaciones de mejora necesarias para cada uno de los grupos definidos, de manera que alcancen los valores máximos exigidos de transmitancias en los edificios NZEB, son las siguientes:

Tabla 2. Intervenciones de mejora necesarias en los edificios para transformarse en NZEB.

<table>
<tr><th rowspan="2">Grupo</th><th>U actual [W/m2·K]</th><th>U propuesta vs. CTE 2019 [W/m2·K]</th><th colspan="2">Fachada (F)</th><th>Cubierta (C)</th></tr>
<tr><th>F-PC / F-PH / C</th><th>F-PC / F-PH / C</th><th>Parte ciega (PC)</th><th>Huecos (PH)</th><th></th></tr>
<tr><td>1</td><td>2,66/4,4/2,25</td><td>0,47<0,6/2,11<2,3/ 0,36<0,4</td><td rowspan="3">SATE, 6 cm.</td><td rowspan="5">Sustitución ventana</td><td rowspan="3">XPS, 8 cm.</td></tr>
<tr><td>2</td><td>2,01/4,4/1,53</td><td>0,44<0,6/2,11<2,3/ 0,33<0,4</td></tr>
<tr><td>3</td><td>3,06/5,07/1,40</td><td>0,48<0,6/2,11<2,3/ 0,33<0,4</td></tr>
<tr><td>4</td><td>1,68/5,7/1,57</td><td>0,57<0,6/2,11<2,3/ 0,34<0,4</td><td rowspan="4">SATE, 4 cm.</td><td rowspan="2"></td></tr>
<tr><td>5</td><td>1,18/5,7/0,81</td><td>0,50<0,6/2,11<2,3/ 0,33<0,4</td><td rowspan="3">XPS, 6 cm.</td></tr>
<tr><td>6</td><td>1,18/4,38/0,81</td><td>0,50<0,6/2,11<2,3/ 0,33<0,4</td><td></td></tr>
<tr><td>7</td><td>0,75/3,51/0,45</td><td>0,40<0,6/2,11<2,3/ 0,25<0,4</td><td rowspan="2">Sustitución vidrio</td></tr>
<tr><td>8</td><td>0,54/2,55/0,38</td><td>0,54<0,6/2,11<2,3/ 0,38<0,4</td><td>-</td><td>-</td></tr>
</table>

2 Diseño de la metodología para calcular los porcentajes de ahorro energético en las envolventes de los edificios de vivienda

Conocidas las medidas a aplicar en cada edificio en función de su antigüedad, el cálculo de los ahorros energéticos dependerá de la superficie de envolvente exterior de cada uno de ellos, puesto que no será lo mismo actuar sobre un edificio cuya envolvente de cubierta supone la mitad de superficie con respecto a la fachada que el de otro edificio

cuya superficie de cubierta es igual al de fachada. También debe considerarse el porcentaje de huecos de fachada que caracteriza a los edificios, y que, en términos generales, depende de la época de construcción.

A este respecto, estudios existentes establecen unos rangos variables entre el 5 y hasta el 40 por ciento según tipos edificatorios [14] o un valor medio fijo del 16 por ciento [15] independiente del periodo de construcción, en cualquier caso, para localizaciones comparables a nuestro caso de estudio (zona climática D3, según CTE 2017). Sin embargo, el análisis detallado de los resultados para el caso de Zaragoza demuestra que el porcentaje medio de huecos en fachada no alcanza valores superiores al 34 % para ninguno de los ocho grupos definidos (Tabla 3).

Tabla 3. Porcentaje de huecos según antigüedad

Grupo	Antigüedad	Porcentaje medio de hueco en fachada
1	<1900	28 %
2	1900 a <1940	34 %
3	1940 a <1960	20 %
4	1960 a <1979	25 %
5	1979 a <1990	22 %
6	1990 a <2006	23 %
7	2006 a <2013	16 %
8	> 2013	29 %

La investigación ha desarrollado una metodología de cálculo (explicada en detalle en otras contribuciones, en vías de ser publicadas) que permite, de manera automatizada, la consulta de datos catastrales para calcular la superficie de cubierta y de fachada exterior de cada uno de los edificios considerados.

La información necesaria para realizar el cálculo de la superficie de fachada exterior y de cubierta del conjunto de los edificios de Zaragoza se obtiene a través de los servicios que ofrece la Dirección General de Catastro, bien desde su sede electrónica digital o bien de los servicios de cartografía catastral, según la directiva Inspire. También se puede realizar la descarga a través de diferentes complementos que se han diseñado para obtener a través de SIG de escritorio la información referida a la cartografía catastral, tanto la base espacial como su información alfanumérica asociada. En este caso, se ha optado por el complemento del software informático QGIS para la descarga de datos catastrales de parcelas, edificios y direcciones de España.

El tratamiento de la información catastral se realiza teniendo en cuenta las siguientes acotaciones de la investigación:

En primer lugar, se ha considerado únicamente aquellos edificios de uso residencial, obviando los de agricultura, industria, oficina, comercio y servicios públicos.

En segundo lugar, dado que el interés del proyecto se centra en determinar el ahorro energético generado al transformar la envolvente exterior de los edificios de acuerdo

con la normativa actual, se reclasifica la antigüedad de cada unidad constructiva según los ocho grupos de anteriores.

En tercer lugar, se estima una altura de tres metros entre plantas para calcular la altura de los edificios y no se considera la planta baja de aquellas construcciones con un número de plantas superior a dos. Esto se explica porque se entiende que las primeras plantas de los edificios, en términos generales, no van a estar dedicadas a uso vivienda sino a usos complementarios al residencial. No obstante, sí que se considera la planta baja para aquellas construcciones con un número de plantas igual o inferior a dos, contemplando en este caso la tipología de vivienda unifamiliar de uso residencial.

En cuarto y último lugar, se incorpora información sobre la pertenencia de los edificios a los diferentes barrios de la ciudad de Zaragoza. Frente a la posibilidad de realizar dicha delimitación en función de divisiones administrativas (juntas municipales, códigos postales, unidades de distrito o unidades censales, se ha optado por tomar el barrio como referencia y unidad de análisis. La justificación reside en que es a esta escala de barrio donde se producen las relaciones vecinales que logran cierto nivel de autosuficiencia en el desarrollo de la vida cotidiana [16] y, en consecuencia, es a esta escala desde donde se ha venido abordando con una mayor precisión los estudios sobre vulnerabilidad urbana y la definición de políticas públicas en torno a ello [17].

La figura 2 da razón de la edad de las edificaciones según su pertenencia a los 8 grupos anteriormente definidos.

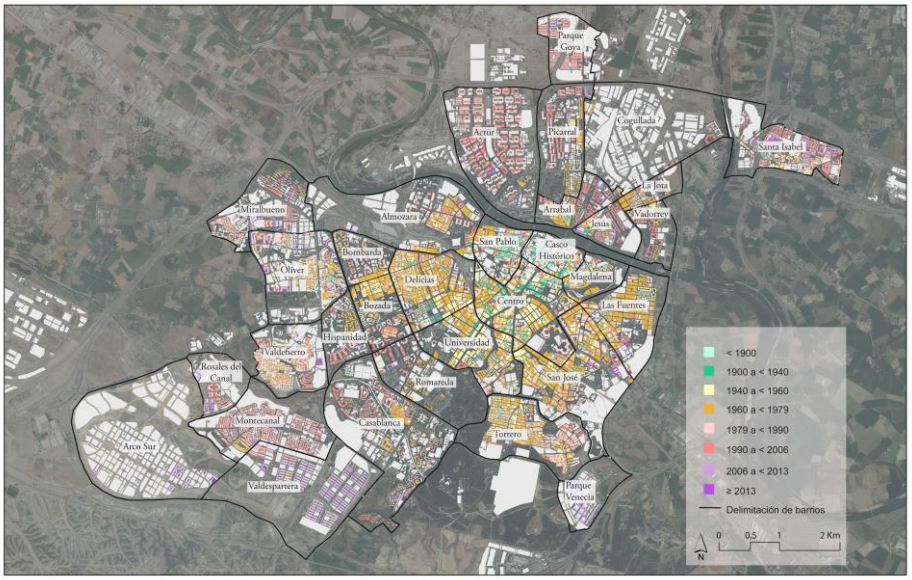

Fig. 2. Edad de los edificios de uso residencial en Zaragoza por barrios. Fuente: elaboración propia, 2019.

3 Comparativa de resultados a nivel de barrio para la ciudad de Zaragoza

Las pérdidas por transmisión que se producen a través de la envolvente exterior pueden ser calculadas mediante la siguiente ecuación:

$$Q_T = [\sum_{i=1}^{n} A_i U_i] G_T \quad \text{[kWh/a]},$$

siendo A_i el área de la envolvente (bien fachada ciega, hueco o cubierta), U_i la transmitancia de dichas envolventes, respectivamente, y G_T los grados hora año [18].

Según lo anterior, como el área y los grados hora año se mantienen en los mismos valores tras haber aplicado soluciones de mejora constructiva en las envolventes de los edificios, el ahorro energético calculado dependerá, en este caso, de la variación de transmitancia entre la situación inicial y final.

Al haber calculado estos valores de transmitancias para cada uno de los grupos, podemos obtener una media ponderada de la superficie de envolvente de fachada, huecos y cubierta de los edificios. Estos valores obtenidos pueden presentarse a diferentes niveles de agregación, de tal manera que podamos evaluar los porcentajes de ahorro energético no sólo por vivienda, sino por edificio, manzana, barrio o, incluso, ciudad.

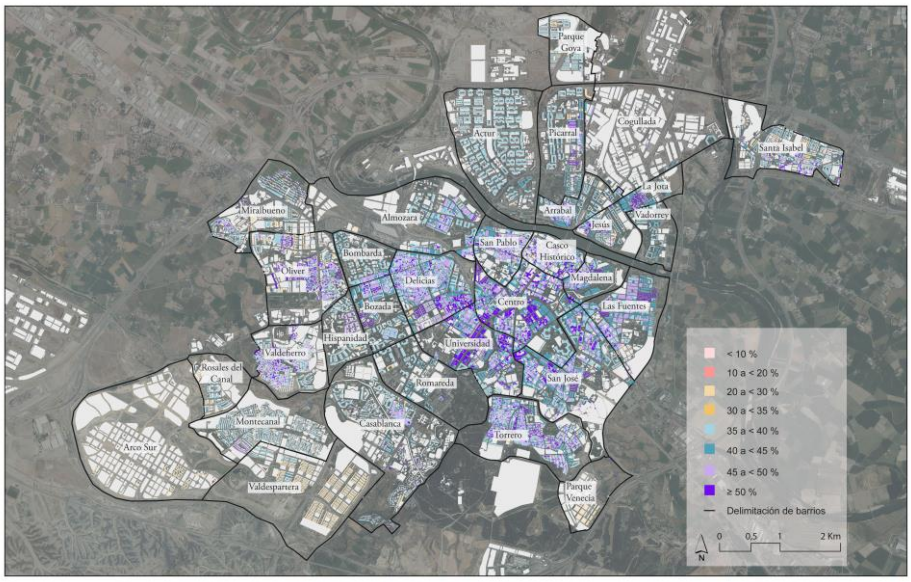

Fig. 3. Porcentaje de ahorro energético real de los edificios de uso residencial en Zaragoza por barrios. Fuente: elaboración propia, 2019.

En este caso, nosotros presentamos los porcentajes de ahorro energético por edificio y barrio. Como las pérdidas energéticas que se producen por la envolvente exterior so-

bre la que actuamos suponen un 65 % del total de las pérdidas del edificio [5], aplicamos el coeficiente corrector del 0,65 para conocer el porcentaje de ahorro energético real del edificio (Figura 3).

La figura 4 compara, a nivel de barrio los valores medios de antigüedad y de porcentajes de ahorro energético a nivel de barrio.

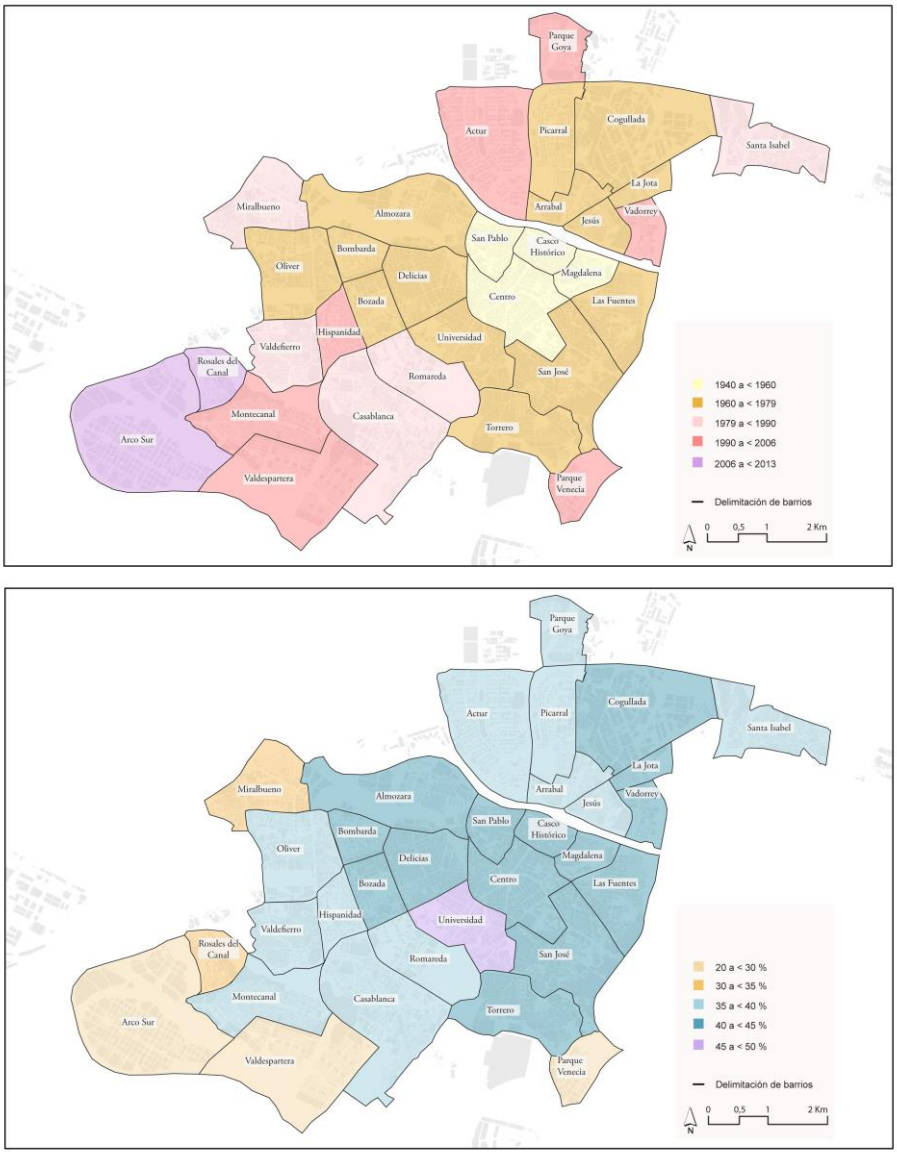

Fig. 4. Promedio de la antigüedad y de los porcentajes de ahorro energético a nivel de barrio en Zaragoza. Fuente: elaboración propia, 2019.

Los resultados obtenidos evidencian que los porcentajes de ahorro varían entre un 1% al 52,8% a nivel de edificio, si bien la gran mayoría de edificios obtienen ahorros entre el 35 al 52,8 %. Por su parte, si el nivel de agregación se establece en el barrio, los porcentajes medios de ahorro oscilan entre el 21,8 y 45,6 %.

La comparativa entre barrios ofrece resultados interesantes en términos no sólo de antigüedad de los edificios, sino, también, de otras variables como son el factor de forma y el tipo edificatorio. En este sentido, si comparamos el barrio con el porcentaje medio de mayor antigüedad (Casco Histórico, 44,7 % de ahorro total, antigüedad media de 1943,3 años) con respecto al barrio con mayor porcentaje de ahorro energético (Universidad, más del 45% de ahorro total y antigüedad media fijada en 1961,3 años), obtenemos resultados que conviene tener en consideración (Fig. 5). Los resultados obtenidos permiten concluir que barrios que han sido construidos en épocas más recientes se adecuan en peor medida en términos energéticos que barrios construidos en épocas anteriores.

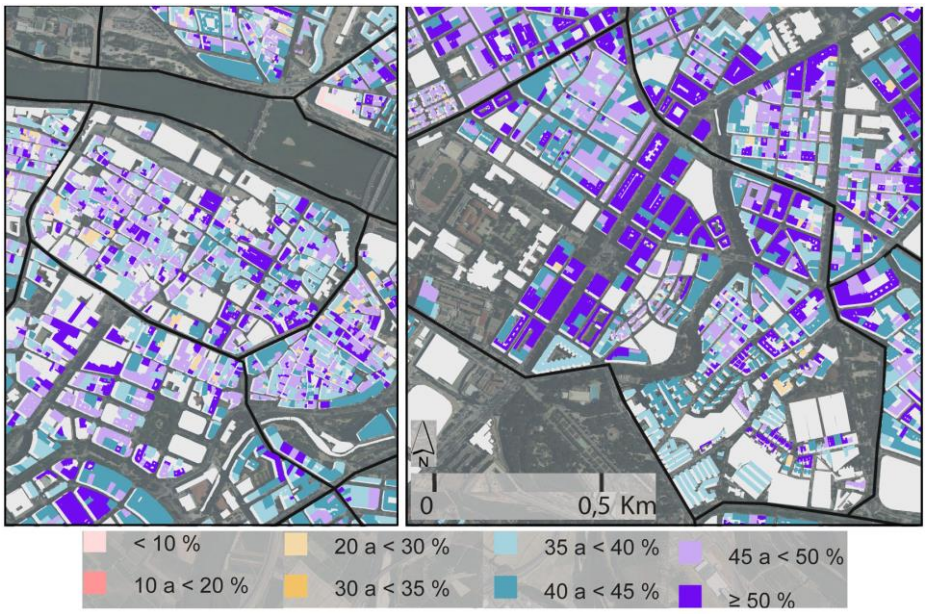

Fig. 5. Porcentaje de ahorro energético real de los edificios de uso residencial de los barrios de Casco Histórico (izquierda) y de Universidad (derecha) en Zaragoza. Fuente: elaboración propia, 2019.

4 Discusión y reflexiones conclusivas

Los porcentajes de ahorro que se alcanzan permite un conocimiento preciso del panorama actual del parque de viviendas con respecto a las posibles medidas pasivas que pueden aplicarse en determinados sectores de la ciudad. Teniendo esto en cuenta, la

metodología de análisis aquí presentada puede servir como herramienta útil a la hora de evaluar los niveles de pobreza energética en la ciudad [19]. Las medidas planteadas en el marco de esta investigación han sido pasivas, por lo que, una vez ejecutadas, no suponen una obligación de uso en términos económicos, como podría llegar a pasar con las medidas para rehabilitación energética de tipo activo [20]. Asimismo, se comprueba que los porcentajes de ahorro alcanzan y, en términos generales, superan el valor del 20 % de mejora de la eficiencia energética definida por la estrategia europea 20/20/20.

Por ello, esta metodología puede ser útil para la definición de políticas públicas y acciones en materia de rehabilitación urbana integral a diferentes niveles de desagregación, desde vivienda, edificio, manzana, barrio, centros históricos o, incluso, a nivel de ciudad [21]. En última instancia, conocer el porcentaje de ahorro energético de la envolvente de las viviendas constituye una vía útil a la hora de considerar la vulnerabilidad energética como caracterización de los índices de vulnerabilidad integral a nivel de barrio.

Este trabajo ha sido apoyado por el Programa Operativo FEDER Aragón 2014-2020, "Construyendo Europa desde Aragón", Grupo de Investigación Arquitecturas OpenSource.

Referencias

1. DECRETO 1490/1975, de 12 de junio, por el que se establecen medidas a adoptar en las edificaciones con objeto de reducir el consumo de energía, 1975.
2. Real Decreto 2429/1979, de 6 de julio por el que se aprueba la norma básica de edificación NBE-CT-79, sobre condiciones térmicas en los edificios.
3. Real Decreto 314/2006, de 17 de marzo por el que se aprueba el Código Técnico de la edificación.
4. Orden FOM/588/2017, Boletín Oficial del Estado, viernes 23 de junio de 2017, número 149, pp. 51621-51626.
5. El-Darwish, I; Gomaa, M. (2017). Retrofitting strategy for building envelopes to achieve energy efficiency. Alexandria Engineering Journal, 56(4), p. 579-589.
6. Directive 2010/31/EU of the European Parliament and of the Council of 19 May 2010 on the energy performance of buildings. 2010.
7. Proyecto de Real Decreto por el que se modifica el RD 314/2006, de 17 de marzo, por el que se aprueba el Código Técnico de la Edificación. Versión para trámite de audiencia e información pública. 2018.
8. Instituto Valenciano de la Edificación. Catálogo de tipología edificatoria residencial para España. 2016.
9. Alonso, C.; Oteiza I.; García-Navarro, J,: Martín-Consuegra, F. (2016). Energy consumption to cool and heat experimental modules for energy refurbishment of façades. Three studies in Madrid. Energy and Buildings, 126, p. 252-262.
10. Pérez Fargallo, A.; Calama Rodríguez, J. M.; Flores Alés, V. (2016). Comparativa de resultados de rehabilitación energética para viviendas en función del grado de mejora. Informes de la Construcción, 68(541): e134, doi: http://dx.doi.org/10.3989/ic.15.048.

11. Đukanović, l.; Radivojević, a.; Rajčić, A. (2016) Potentials and limitations for energy refurbishment of multi-family residential buildings built in Belgrade before the World War One. Energy and Buildings, 115, p. 112-120.
12. IDAE (2019). Soluciones de acristalamiento y cerramiento acristalado, Madrid: Instituto para la Diversificación y Ahorro de Energía
13. Catálogo de elementos constructivos del CTE, Ministerio de Fomento, https://itec.cat/cec/
14. de Luxan, M.,Barbero, M.; Gómez G.; Román E. (2010) Estudio para la elaboración del Plan Renove de acristameinto en viviendas de la Comunidad de Madrid. SB10mad. Congreso Internacional Sustainable Building 2010, SB10mad.
15. Martín-Consuegra, Frutos, F.; Oteiza I.; Hernández de Aja, A. (2018). Use of cadastral data to assess urban scale building energy loss. Application to a deprived quarter in Madrid. Energy and Buildings, 171, p. 50-63.
16. Obst, P. L. & White, K. M. (2004). Revisiting the Sense of Community Index: A confirmatory factor analysis. Journal of Community Psychology, 32(6), 691-705. https://doi.org/10.1002/jcop.20027
17. Ruiz, A. & Alfaro, P. (2017). Áreas de rehabilitación en la ciudad de Zaragoza: noción, encaje urbanístico y criterios de selección. Clivatge. Estudios y testimonios sobre el conflicto y el cambio social, (5), 170-198.
18. Orden FOM/588/2017, de 15 de junio, por la que se modifican el Documento Básico DB-HE «Ahorro de energía» y el Documento Básico DB-HS «Salubridad», del Código Técnico de la Edificación, aprobado por Real Decreto 314/2006, de 17 de marzo.
19. Directive 2010/31/EU of the European Parliament and of the Council of 19 May 2010 on the energy performance of buildings.
20. Luxán García de Diego, M.; Gómez Muñoz, G.; Román López, E. (2015). Cuentas energéticas no habituales en edificación residencial. Informes de la Construcción, 67(EXTRA-1): m028, doi: http://dx.doi.org/10.3989/ic.14.059.
21. Rubio de Val, J. (2015). Potencial del nuevo marco normativo para el impulso de la rehabilitación y la regeneración urbana en los ámbitos autonómico y local. Informes de la Construcción, 67(Extra-1): m023 doi: 10.3989/ic.14.072.

Detecting hot spots in photovoltaic panels using low-cost thermal cameras

Miguel Dávila-Sacoto[1[0000-0001-6318-2137]], Luis Hernández-Callejo[2[0000-0002-8822-2948]], Víctor Alonso-Gómez[2[000-0001-5107-4892]], Sara Gallardo-Saavedra[2[0000-0002-2834-5591]] and L.G. González[1[0000-0001-9992-3494]]

[1] Universidad de Cuenca, Campus Central, 010104 Cuenca, Ecuador
[2] Universidad de Valladolid, Campus Universitario Duques de Soria, 42004 Soria, Spain
M.D-S. miguela.davila@ucuenca.edu.ec;
L.H-C. luis.hernandez.callejo@uva.es;
V.A-G. victor.alonso.gomez@uva.es;
S.G-S. sara.gallardo@uva.es;
Corresponding author: L.G.G. luis.gonzalez@ucuenca.edu.ec

Abstract. One of the most important challenges to mitigate global climate change is to move towards replacing petroleum-based energy sources. In this idea, non-conventional renewable energy sources such as photovoltaic (PV) solar and wind power are the most used worldwide. In the case of the massification of PV solar generation systems due to its low cost, it has resulted in the use of large-scale supervision techniques that allow a quick and effective determination of the health status of its main components. This study, performs an analysis of the performance of different low-cost cameras for thermography. The analysis compares the accuracy of the thermal images obtained and the error is quantified by means of an image dispersion analysis in each of them. Three-dimensional meshes and contours figures are also made to determine the temperature of a faulty cell. The study shows that the performance obtained with low-cost cameras presents errors below 10% in costs and less than 0.015USD/pixel.

Keywords: Thermography, PV panel, low cost, thermal camera, image processing.

1 Introduction

Thermography in PV panels is a technique that has been used in Operation and Maintenance (O&M) of PV solar generation systems for more than a decade [1]. It is used to determine hot spots in cells that can be originated as a result of cell deterioration or partial shading, and can compromise panel performance in a solar farm. Thermography is used to obtain representative images of temperature on the surface of solar panels, generally using high-resolution thermal cameras in order to obtain detailed information on the temperature of each part of the PV panel under study.

Nowadays most of the cameras used for thermography of solar panels are expensive, which is an inconvenience for the massification of this technology. However, there are low-cost thermal cameras in the market. Although they do not have the technical characteristics and advantages offered by the most sophisticated alternatives, they can be used for small-scale analysis providing information that allows initial actions to be taken in case of any anomaly observed.

This study shows the use of low-cost cameras for thermography, making measurements on solar panels under operation, detailing the most important features and emphasizing its cost. The analysis of the images obtained with both temperature tables and static images is carried out, and the corresponding temperature measurement error between cameras is obtained.

2 Thermal Cameras

2.1 Cameras used in thermography studies

Thermal cameras capture the radiation emitted by an object [2], converting it into an image that represents the temperature pattern of the area of interest. The use of thermal cameras for analysis of equipment and machinery is known as thermography and is currently part of the non-invasive techniques to observe the temperature of an object [2]. Since last decade, the advance on new energy sources and especially the adoption of PV solar energy, mainly due to its rapid worldwide price reduction, has allowed the incorporation of techniques such as thermography that allows to identify failures in PV cells or in electrical connections [3]-[9], providing relevant information that facilitates the O&M of PV sites. However the equipment normally used is expensive. Table 1 shows the most important characteristics and costs of a set of thermal imaging cameras commonly used today.

Table 1. Features and prices of thermal cameras used in the thermographic analysis in PV panels.

Brand	Flir	Flir	Testo	Flir
Model	SC655	TAU2	870-2	i3
Thermal image quality (pixels)	640x480	640x512	160x120	60x60
Thermal sesitivity	<0.1ºC	<0.1ºC	<0.1ºC	<0.15ºC
Price (USD)	$26,990.00	$6,000.00	$2,528.00	$1,295.00
Price/Resolution (USD/pixel)	0.0875	0.0183	0.1316	0.3597

Although the costs of the options presented in Table 1 are high, the resolution of the sensors is higher and allows detailed analysis. Regarding the relationship between cost and resolution, the most expensive options generally have a smaller cost per reso-

lution ratio. Among them, the Flir TAU2 camera stands out with a lower cost per pixel.

2.2 Low-cost thermal cameras

In the market, there are options of low-cost thermal cameras with technical characteristics suitable for its usage in thermography, in particular, those shown in Table 2. These are the cameras used in this paper.

Table 2. Features and prices of options for low-cost thermal cameras.

Brand	Caterpillar	Flir
Model	CAT s60	One Pro
Thermal image quality (pixels)	80x60	160x120
Thermal sensitivity	<0.15ºC	<0.15ºC
Price (USD)	$428.00	$388.92
Price/Resolution (USD/pixel)	0.089	0.015

It is observed that the selected cameras have a similar price, below $500, which makes them easily accessible compared to others more expensive. In Figure 1, images captured with the cameras under study are observed. They present similar behaviors, however, as expected, the one taken with the higher resolution camera (Flir One Pro) presents sharper or more defined edges.

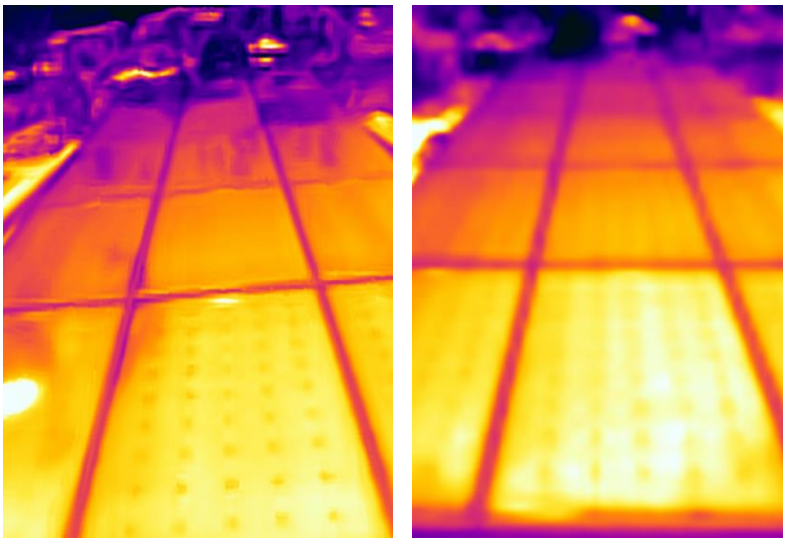

(a) (b)

Fig. 1. Thermal image of a PV panel captured by (a) FLIR One Pro camera, (b) Caterpillar Cat S60 camera.

3 Thermography with low-cost cameras

The low-cost cameras in Table 2 were used to perform a thermographic analysis of the 35kWp installation described in [10]. After manual inspection of 160 solar panels, two were found with anomalies identified as hot spots. One of these anomalies captured using the Flir One Pro camera and processed with the FLIR Tools software [11], in which measurement points were added, is shown in Figure 2,. Two points identified as T1 and T2 are observed with temperatures of 43.0ºC and 29.6ºC, respectively.

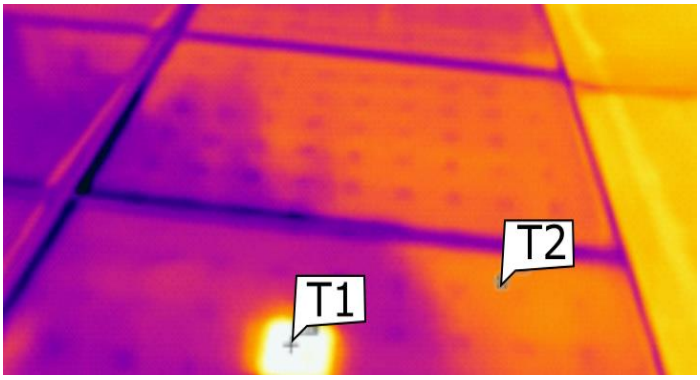

Fig. 2. Thermal image of a PV panel captured by a FLIR One Pro camera.

The FLIR One Pro camera and the Cat S60 embed into their images metadata corresponding to the temperature of each pixel. This information can be extracted with the thermal camera software and allows an analysis of the temperature at each point of the image, permitting the use of this information in the data processing software. Table 3 shows part of the metadata in Figure 2 (rows and columns headers are only for reference).

Table 3. Metadata of figure 2, with Flir One Pro camera.

Row/column	Pixel [1,2]	Pixel [1,3]	Pixel [1,4]	Pixel [1,5]	Pixel [1,n]
Pixel [2,1]	25.331	25.331	25.331	25.331	…
Pixel [3,1]	25.338	25.338	25.338	25.338	…
Pixel [4,1]	25.354	25.354	25.354	25.346	…
Pixel [5,1]	25.376	25.376	25.376	25.369	…
Pixel [6,1]	25.407	25.407	25.399	25.392	…
Pixel [7,1]	25.437	25.437	25.43	25.422	…
Pixel [8,1]	25.468	25.46	25.46	25.445	…
…	…	…	…	…	…

Other types of cameras display only an image that does not contain metadata, making necessary the use of image processing techniques that allow the temperature estimation to be determined based on the intensity of the color.

3.1 Thermal image analysis and temperature tables

First, was established a panel that showed considerable thermal variations, in which three points of interest were identified (see Figure 3); the defective cell, the unaffected area and the junction box. Using the Flir One Pro camera, these points were identified as T1, T2, and T3, with temperatures of 51.3ºC, 35.3ºC, and 35.2ºC, respectively (Figure 3a).

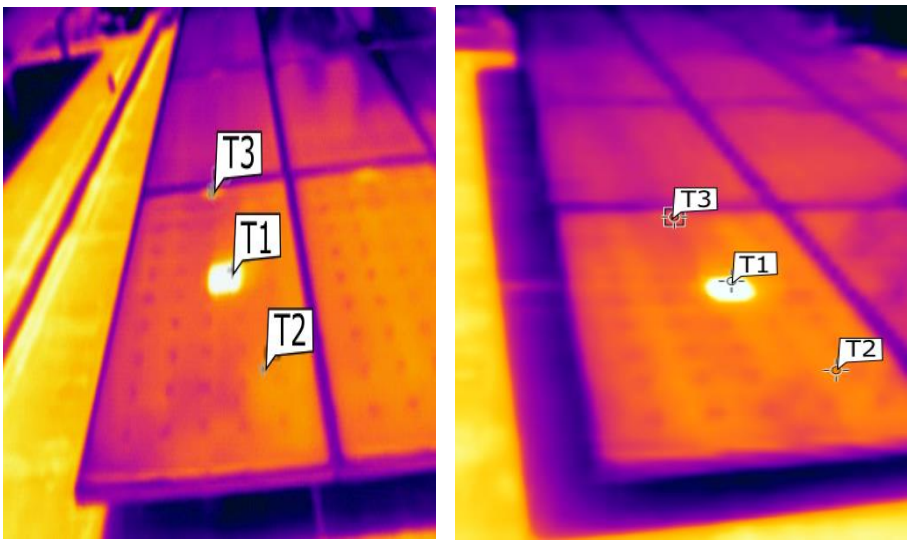

(a) (b)

Fig. 3. Thermal image of a defective PV panel captured by (a) Flir One Pro camera (b) Cat S60 camera.

The temperature difference between the faulty cell and a different point on the panel in Figure 3a, defined as $\Delta T = T1-T2$, reaches 15.9°C. The maximum temperature of the image under study is 52°C. Studies indicate that 51.3°C reached on the cell could be considered as a major fault [8], so short term maintenance is required. In addition, according to [4] the value obtained of ΔT indicates a "medium failure". On the other hand, Figure 3b, captured with a Cat S60 camera, shows three points identified as T1, T2, and T3, with temperatures of 53.6ºC, 36.9ºC, and 38.4ºC, respectively. Here the temperature difference of points of interest reaches $\Delta T=14.8$°C between the faulty cell and a different point of the panel, with a maximum temperature of the image under study at 53.2°C.

Using the temperature table obtained with Flir Tools tool, the thermal image (Figure 4) was reconstructed as an intensity graph, where each pixel is given by equation (1):

$$pixel = (X\ position, Y\ position, temperature) \quad (1)$$

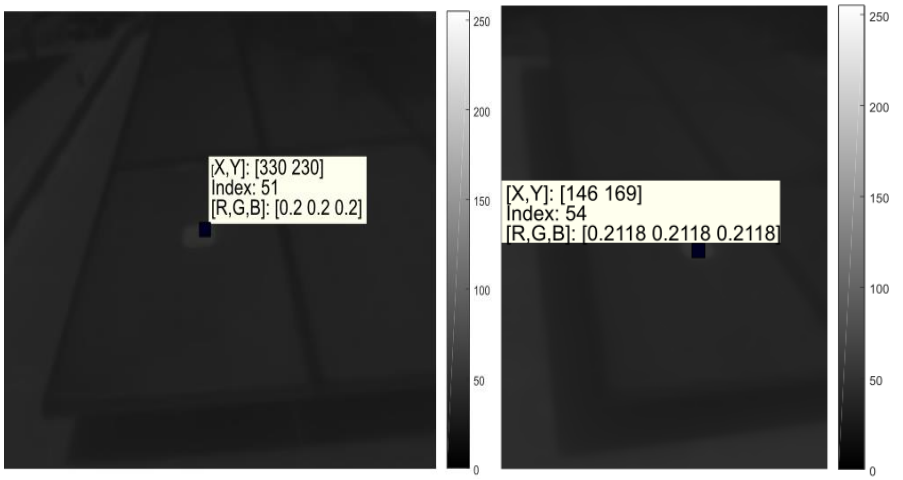

(a) (b)

Fig. 4. Image reconstructed from the temperature table (a) Flir One Pro camera (b) Cat S60 camera.

The intensity graph in Figure 4 has the "appearance" of a grayscale image, however, it is not the result of applying a grayscale algorithm, but on the contrary, it is the direct graph of the pixel intensity information, that is, the graph of the temperature measured by the thermal camera. This presents an important advantage because the exact temperature of each element in the image can be obtained without the need of any type of normalization or further processing.

From data in Figure 4, an X-Y graph was made in Matlab® (see Figure 5), where the dispersion of the temperature values is obtained. This allows identifying the maximum temperature value corresponding to the faulty cell, which shows the highest pixel temperature in that area, in this case, 52°C, and a maximum temperature of 43°C for the highest temperature area near the cell (ΔT = 9°C). According to [4] this could mean a "light failure".

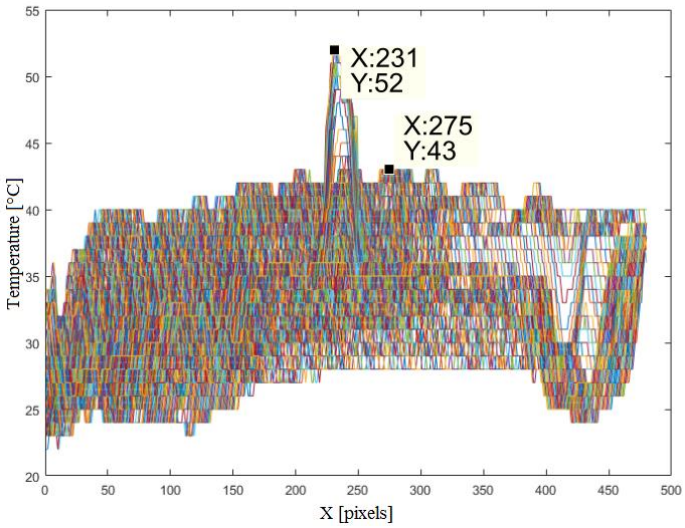

Fig. 5. X-Y dispersion of the thermal image of the panel with a hot spot.

Visualizing the data in a three-dimensional domain, Figure 6, shows the representation of the temperature from the temperature table, where the arrangement of the thermal image intensities can be observed. The mesh obtained allows to easily identify the hottest point of the image.

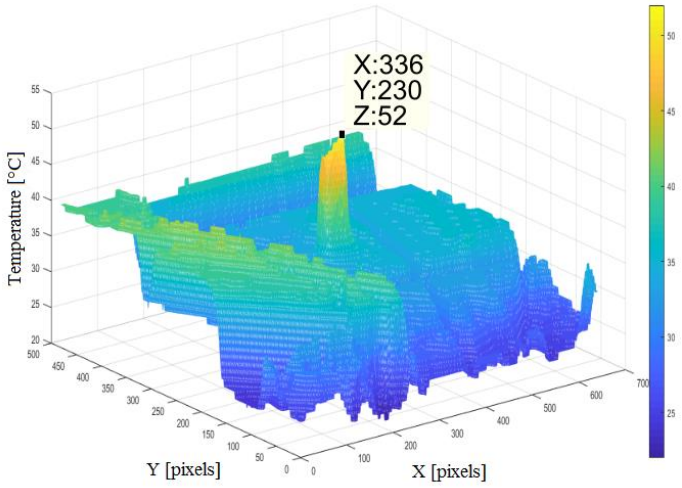

Fig. 6. A three-dimensional mesh of the thermal image of the panel with a hot spot.

Performing a contour analysis, Figure 7 shows the projection of the Z-axis (temperatures) of the three-dimensional function on a two-dimensional image, and it can be used as an edge detection approach.

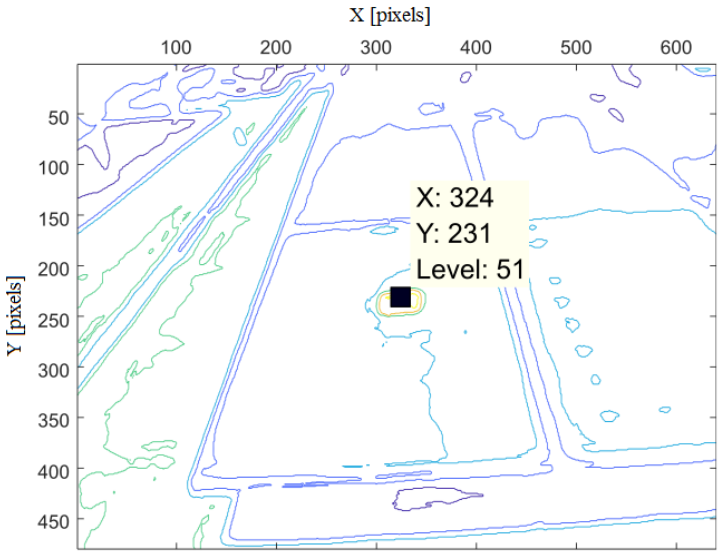

Fig. 7. The contour of the three-dimensional mesh of the thermal image.

3.2 Static Image Analysis

Because static images are common in low-cost cameras (without metadata), their analysis is studied to observe their validity in thermographic applications on PV solar panels. The static image is taken with its color map (sidebar that indicates the relationship between the color of the image and the temperature) to be able to have a reference of the temperature of each pixel without necessarily having the metadata, showing the maximum and minimum temperatures at the top and bottom of the bar (see Figure 8). Through the tests performed it was observed that in the case of FLIR cameras these values do not correspond to the maximum and minimum recorded previously in the image. Here a maximum of 46°C is observed, which does not agree with the 52°C observed in the data in the temperature table.

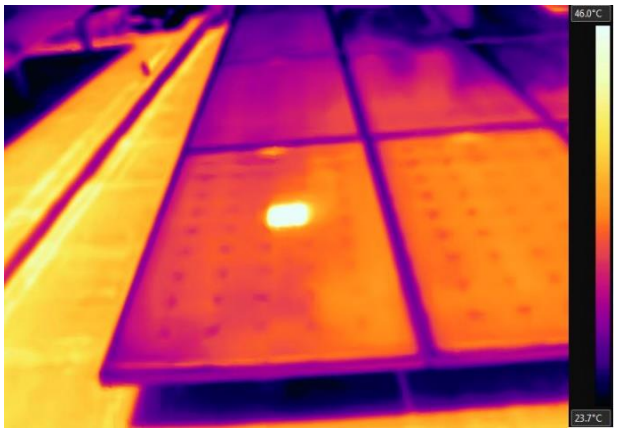

Fig. 8. Static image obtained from a thermal camera with the color map on the left side.

In order to obtain the estimated pixel temperature, the image is initially converted to grayscale, and then the intensity values are normalized to find the new pixel value using equation (2):

$$Temperature_{pixel} = T_{min} + (T_{max} - T_{min}) \times Intensity \quad (2)$$

With this, a grayscale image is obtained, where the new pixel intensity value corresponds to a normalized temperature as shown in Figure 9.

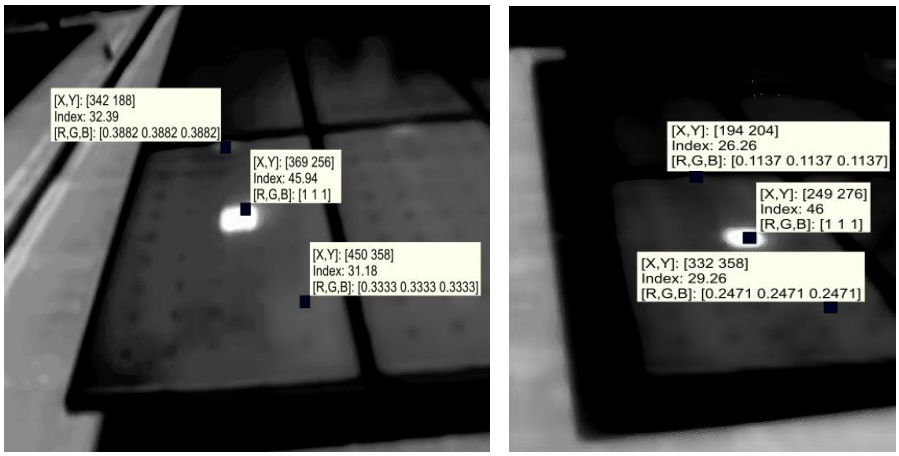

(a) (b)

Fig. 9. Standard grayscale static image showing pixel temperature (a) Flir One Pro (b) Cat S60.

In the XY scatter plot shown in Figure 10, the maximum pixel temperature can be found, however, there is a loss of details due to the normalization and the accuracy decreases due to the conversion of this type of image. It is also observed that the am-

plitude of the pixel values increases for areas other than the faulty cell and that there are more pixels with low temperatures.

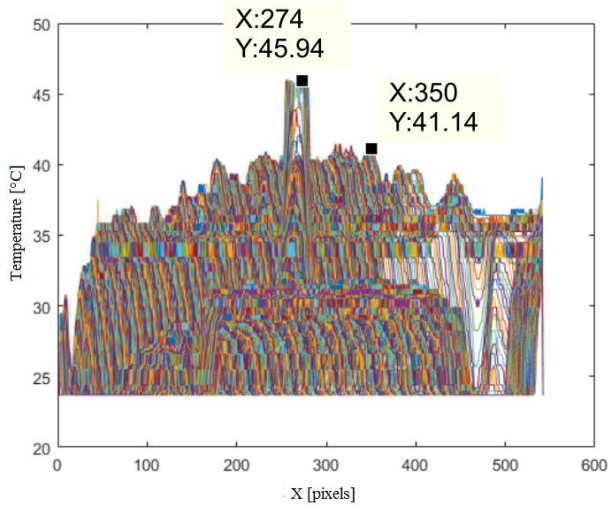

Fig. 10. Dispersion of the static image obtained from a Flir One Pro camera.

By repeating the procedure described above for the mesh graphic in the static image, Figure 11, is obtained. A similar behavior of the thermal image is shown with the Cat S60 camera, with the difference in the maximum temperature achieved. In the same way, as in the dispersion, a greater amount of values is observed in the base of the graph within the lower temperatures of the image.

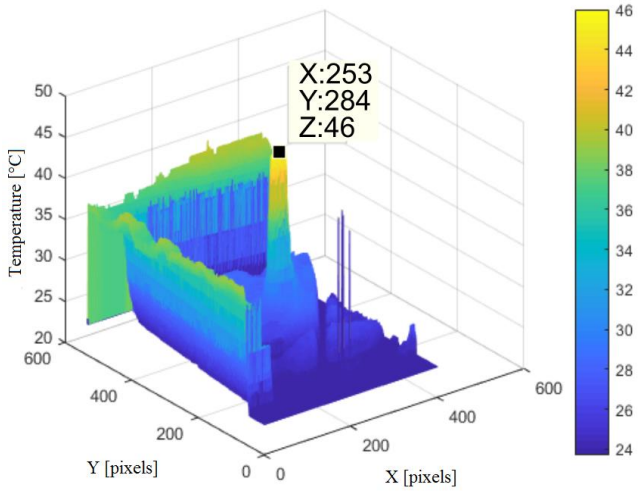

Fig. 11. A three-dimensional mesh of the static image of the panel with a hot spot obtained from the Cat S60 camera.

Finally, by repeating the contour of the mesh, Figure 12a is obtained, where it is observed that, due to the normalization of the image, there are marked areas of the temperature gradient, which can make it difficult to use geometry identification algorithms in image processing. This variation between the different techniques is shown in Figure 12b.

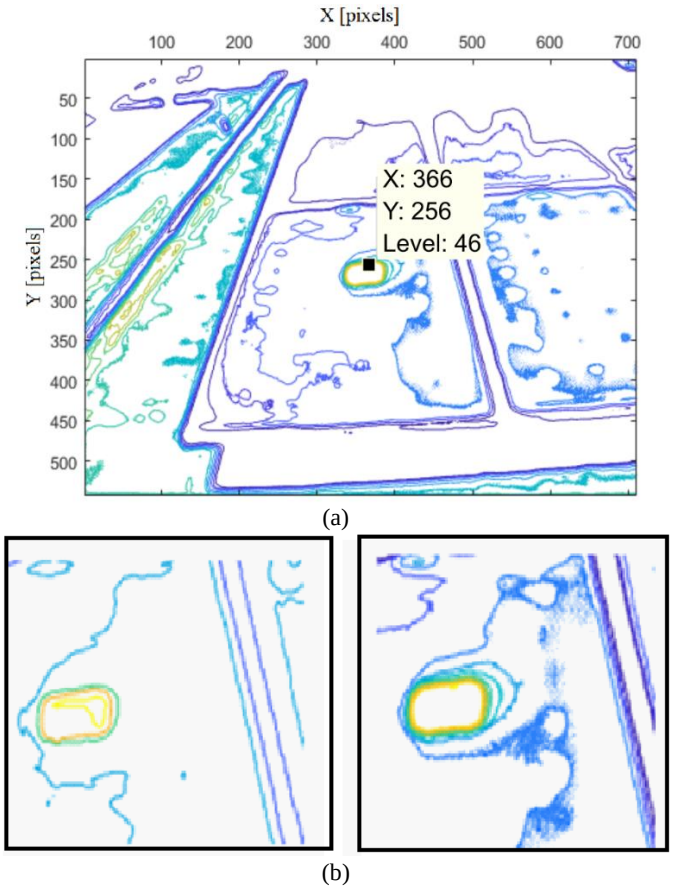

Fig. 12. The contour of the three-dimensional mesh of the panel with hot spot (a) obtained from the static image, (b) comparison between thermal image contour (left) and static image (right).

3.3 I-V/P-V curves analysis

The faulty PV modules under study are monocrystalline ATERSA A-250P of 250Wp [12]. Figure 13a shows the I-V curves of the panel that has a hot spot and a panel without faults. The curves were captured with a Solmetric PVA-600 tracer [13]. It is observed that the voltage of the panel with failure falls at around 16Vdc, showing a typical behavior of a damaged or "shaded" cell [14]-[17]. When reviewing the P-V curve of the panels (Figure 13b), the decrease in the maximum power point is ob-

served, obtaining a 25% less power in the panel with the hot point compared to a panel without failures.

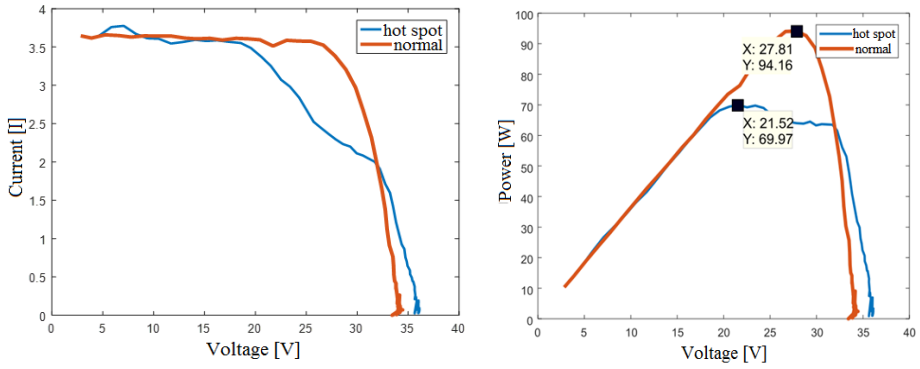

(a) (b)

Fig. 13. Characteristic curves of the panel with failure and another without anomalies (a) I-V curves (b) P-V curves.

3.4 UAV and low-cost camera tests

Inspections with low-cost cameras can be carried out with the help of remote-operated mobile systems. Further information about this kind of onboard termal inspections can be found in [18] and [19]. In this research the behavior of the Cat S60 camera is tested. The camera was mounted on a DJI Mavic Pro drone (Figure 14a) and used as proof of concept in order to verify that this camera can show the hot spot on the faulty panel. The drone was flown at three meters above the panel, obtaining the image shown in Figure 14b. It is noted that the hot spot in the image can be clearly identified. However, this camera does not deliver a heat map or a temperature table in video capture mode, so its use should be limited to manual hot spots detection.

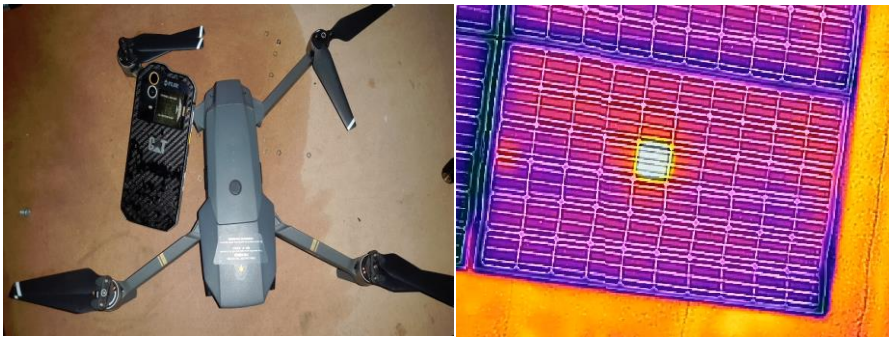

(a) (b)

Fig. 14. Solar panel thermography with drone (a) Cat s60 thermal camera and DJI Mavic Pro drone (b) captured the image.

3.5 Technical advantages of low-cost thermal cameras

Low-cost thermal cameras could be used for thermal inspection on small or mid-sized solar farms but considering their limitations. High-end or professional-grade thermal cameras are specifically designed to perform in challenging environments and record high-resolution images with high accuracy and confidence. General advantages of using professional thermal cameras include IP rating so using them in harsh environments is not a problem, higher framerate enabling smooth video analysis and included ethernet or industrial communication protocols.

On the other hand, low-cost alternatives are becoming widely used by hobbyists, students and contractors, while high-end cameras are used mainly by research institutes or by industries with large budgets. Some of the advantages of using low-cost thermal cameras include lower energy consumption (very important to embedded systems, or UAVs), standard and commercial communication protocols (USB) and wide community behind its use and development. The latter of these advantages for low-cost cameras is very important to independent researchers or too small research groups because when developing solutions or carrying out study cases, technical support is an important issue, especially if the camera manufacturer is from other country or speaks a different language than the user. With low-cost cameras (or nearly all low-cost solutions in hardware thanks to the open-source community), it is possible to find support within users. With high-end cameras users generally need to contact the manufacturer directly and wait for support or even pay for it.

Table 4 shows a technical comparison of 2 high-end thermal cameras and the 2 low-cost alternatives discussed in this document.

Table 4. Results.

Parameter	Low-Cost		High-End			
	Flir One Pro	Cat S60	Testo 870-2	Flir i3	Flir SC655	Flir Tau 2
Power [W]	1.1	1.2	2.3	1.6	24	1.3
Framerate [Hz]	8.7	8.7	9	9	50	60
Accuracy	+-3°C 5%	+-5°C 5%	+-2°C 2%	+-2°C 2%	+-2°C 2%	+-2°C 2%
IP grade	No	IP68	IP54	IP54	IP67	IP67

It is shown that low-cost cameras tend to have a lower power consumption than high-end ones, but also have lower framerates and accuracy. This could be a problem depending on the application. For example, if the research needs a real-time temperature monitoring system with instant readings, high-end cameras with high framerates are the best choice.

3.6 Results comparison

Table 5 shows a comparison of the parameters obtained from the thermography analysis of both, the thermal image and the static image. It is observed that in the image analysis a relative error of 10.45% is obtained for the measured temperature of the

faulty cell, and a relative error of 7.75% for ΔT between the cell and an adjacent panel point. For the analysis of the X-Y dispersion, an error of 46.67% is observed for the faulty cell, while for the mesh analysis there is a 11.54% error and for the three-dimensional contour a 9.80% error. This indicates that contour analysis and mesh analysis are better candidates than scatter analysis in image processing in cases where the temperature table is not available.

Table 5. Results.

Parameter	Thermal image	Static image	Absolute error	Relative error
T connection box	35.20ºC	32.39ºC	2.81ºC	7.98%
T panel	35.30ºC	31.18ºC	4.12ºC	11.67%
T faulty cell	51.30ºC	45.94ºC	5.36ºC	10.45%
ΔT faulty cell	16.00ºC	15.00ºC	1.24ºC	7.75%
Scatter				
T max faulty cell	52.00ºC	45.94ºC	6.06ºC	11.65%
T max adjacent area	43.00ºC	41.14ºC	1.86ºC	4.33%
ΔT faulty cell	9.00ºC	4.80ºC	4.20ºC	46.67%
Mesh				
T max faulty cell	52.00ºC	46.00ºC	6.00ºC	11.54%
Contour				
T max faulty cell	51.00ºC	46.00ºC	5.00ºC	9.80%

The errors observed in dispersion and contour analysis are less than 10%, so they can be used in the thermographic analysis by extrapolating the temperature [20]. Previous studies [21]-[23] show that the error can be improved with image processing techniques and neural networks. Table 6 shows a comparison of the cameras used and the limitations found according to on-site tests.

Table 6. Comparison of characteristics of low-cost thermal cameras

Camera	Flir One Pro	Cat S60
Temperature table	Yes	Yes
Connection	USB-C with Android / iOS smartphones	Included inside the smartphone
Weight	36.5g	223g
Outdoor use	No	No
Drone use	Yes (lighter)	Yes

4 Conclusions

This paper presents a description of the characteristics of low-cost thermal imaging cameras, emphasizing its cost/resolution relationship. It is observed that the analysis of thermography using low-cost cameras is viable considering the established errors, which can be less than 10%.

From the analysis of static images, it is shown that a three-dimensional contour is a valid tool with less than 10% error, which can be improved with artificial intelligence techniques and neural networks.

The thermal cameras used in this document cost 10% less than professional cameras (taking as reference a Flir TAU2), without compromising the detection of hot spots in PV panels, which allows these low-cost cameras to be used in thermographic studies considering the limitations in terms of its construction and its feasibility of outdoor use.

References

1. R. Usamentiaga, P. Venegas, J. Guerediaga, L. Vega, J. Molleda, and F. G. Bulnes, "Infrared thermography for temperature measurement and non-destructive testing," Sensors (Switzerland), vol. 14, no. 7, pp. 12305–12348, 2014.
2. P. Battalwar, J. Gokhale, and U. Bansod, "Infrared Thermography and IR Camera," Int. J. Res. Sci. Eng., vol. 1, no. 3, pp. 9–14, 2015.
3. E. Ruggeri, B. B. Van Aken, O. Isabella, and M. Zeman, "Electroluminescence and Dark Lock-In Thermography for the Quality Assessment of Metal-Wrap-Through Solar Devices," IEEE J. Photovoltaics, vol. 8, no. 5, pp. 1174–1182, 2018.
4. C. Toledo, L. Serrano, J. Abad, A. Lampitelli, and A. Urbina, "Measurement of Thermal and Electrical Parameters in Photovoltaic Systems for Predictive and Cross-Correlated Monitorization," Energies, vol. 12, no. 4, p. 668, 2019.
5. R. L. Santos, J. S. Ferreira, G. E. Martins Jr, K. C. A. de Souza, and E. M. Sá Jr, "Low Cost Educational Tool to Trace the Curves PV Modules," IEEE Lat. Am. Trans., vol. 15, no. 8, pp. 1392–1399, 2017.
6. M. Dhimish, V. Holmes, B. Mehrdadi, M. Dales, and P. Mather, "PV output power enhancement using two mitigation techniques for hot spots and partially shaded solar cells," Electr. Power Syst. Res., vol. 158, no. January, pp. 15–25, 2018.
7. H. Amiry et al., "Design and implementation of a photovoltaic I-V curve tracer: Solar modules characterization under real operating conditions," Energy Convers. Manag., vol. 169, pp. 206–216, 2018.
8. Z. A. Jaffery, A. K. Dubey, Irshad, and A. Haque, "Scheme for predictive fault diagnosis in photo-voltaic modules using thermal imaging," Infrared Phys. Technol., vol. 83, pp. 182–187, 2017.
9. A. M. Salazar and E. Q. B. Macabebe, "Hotspots Detection in Photovoltaic Modules Using Infrared Thermography," MATEC Web Conf., vol. 70, p. 10015, 2016.
10. J. L. Espinoza, L. G. Gonzalez, and R. Sempertegui, "Micro grid laboratory as a tool for research on non-conventional energy sources in Ecuador," 2017 IEEE Int. Autumn Meet. Power, Electron. Comput. ROPEC 2017, vol. 2018-Janua, no. Ropec, pp. 1–7, 2018.

11. FLIR, “FLIR Tools Thermal Analysis and Reporting (Desktop) | FLIR Systems.” [Online]. Available: https://www.flir.com/products/flir-tools/. [Accessed: 11-Aug-2019].
12. Atersa, “Atersa A-250M datasheet.” pp. 0–1, 2019.
13. Solmetric, “Solmetric PVA-600 PV Analyzer User’s Guide.” .
14. P. Garcia De La Cruz, “Trazador De Curvas V-I Para Seguimiento De Módulos Solares,” no. Plan, p. 122, 1996.
15. A. Hemza, H. Abdeslam, C. Rachid, and N. Aoun, “Simplified methods for evaluating the degradation of photovoltaic module and modeling considering partial shading,” Meas. J. Int. Meas. Confed., vol. 138, pp. 217–224, 2019.
16. J. E. Quiroz, J. S. Stein, C. K. Carmignani, and K. Gillispie, “In-situ module-level I-V tracers for novel PV monitoring,” 2015 IEEE 42nd Photovolt. Spec. Conf. PVSC 2015, 2015.
17. K. A. Kim, G. S. Seo, B. H. Cho, and P. T. Krein, “Photovoltaic Hot-Spot Detection for Solar Panel Substrings Using AC Parameter Characterization,” IEEE Trans. Power Electron., vol. 31, no. 2, pp. 1121–1130, 2016.
18. Gallardo-Saavedra, S. et al., “Aerial thermographic inspection of photovoltaic plants: Analysis and selection of the equipment,” ISES Solar World Congress 2017 - IEA SHC International Conference on Solar Heating and Cooling for Buildings and Industry 2017, Proceedings, doi: 10.18086 / swc.2017.20.03.
19. S. Gallardo-Saavedra, L. Hernández-Callejo, and O. Duque-Pérez, “Image Resolution Influence in Aerial Thermographic Inspections of Photovoltaic Plants,” IEEE. Trans. Industrial Informatics, vol. 14, pp.5678-5686, 2018.
20. W. Zaaiman, “Solar Irradiance and Photovoltaic Measurements From Solar Radiation to PV Arrays,” 2012.
21. J. A. Tsanakas, L. Ha, and C. Buerhop, “Faults and infrared thermographic diagnosis in operating c-Si photovoltaic modules: A review of research and future challenges,” Renew. Sustain. Energy Rev., vol. 62, pp. 695–709, 2016.
22. R. Koprowski, “Some selected quantitative methods of thermal image analysis in Matlab,” J. Biophotonics, vol. 9, no. 5, pp. 510–520, 2016.
23. W. Chine, A. Mellit, V. Lughi, A. Malek, G. Sulligoi, and A. Massi Pavan, “A novel fault diagnosis technique for photovoltaic systems based on artificial neural networks,” Renew. Energy, vol. 90, pp. 501–512, 2016.

Merged images for fault detection in photovoltaic panels

Sara Gallardo-Saavedra[1[0000-0002-2834-5591]], Luis Hernández-Callejo[1[0000-0002-8822-2948]], Ponciano Jorge Escamilla-Ambrosio [2[0000-0003-3772-3651]] and Víctor Alonso-Gómez[1[0000-0001-5107-4892]].

[1] University of Valladolid, Campus Duques de Soria, 42004 Soria, España
[2] Instituto Politécnico Nacional: Mexico, Distrito Federal, MX
sara.gallardo@uva.es, S.G-S.;
luis.hernandez.callejo@uva.es, L.H-C.;
pjorgeea@googlemail.com, P.J.E-A.;
victor.alonso.gomez@uva.es, V.A-G.

Abstract. Photovoltaic systems are of great interest throughout the world. Its installation, operation and maintenance are crucial for achieving energy sustainability worldwide. In recent years, the inspection of defects in photovoltaic modules using images (thermography, electroluminescence, visible, etc.) is increasing considerably. Therefore, this work presents the experience of merging images to detect faults in photovoltaic modules.

Keywords: image merging, photovoltaic inspections, photovoltaic defects.

1 Introduction

Actual cities have evolved towards a new approach known as Smart City (SC), which must progress towards new intelligent infrastructures, which will integrate new sensors and advanced communications. In this new scenario, renewable energies and their integration have a leading place. Newly installed renewable power capacity set new records in 2018, with 181 GW added, increasing the global total by more than 8% relative to 2017. Solar photovoltaic (PV) was the star performer in 2018, accounting for 55.2% of the total additions, followed by wind power at 28.2% and hydropower at 11.0%. The total Solar PV capacity at the end of 2018 was set in 505 GW. In 2018, renewables accounted for about two-thirds of global investment in power generation and for about the same share of new net electricity generation capacity. For the fourth consecutive year, more renewable power capacity was installed than net additions to fossil fuel capacity. Renewables now represent more than one-third of the global installed electricity generation capacity [1].

Like any other technology, PV production is never faultless. Due to the dominant position that this technology is getting on the market, it is essential that it produces reliable, efficient and safety energy. The main component of these facilities is the PV module, responsible for the conversion of sunlight into electrical energy, through the photoelectric effect. Being able to detect, to identify and to quantify the severity of

defects that appear within a module or a string is essential to constitute a reliable, efficient and safety system. In this way, it would be possible to avoid energy losses, mismatches and safety issues, especially in case of building integrated systems (in roofs or façades), as overheated anomalies could generate a fire risk or an electrical hazard.

Different techniques can be used to detect and quantify PV modules anomalies. Traditionally, faulty modules or cells within a PV plant have been located by applying visual inspections, electrical tests like the I-V curve (current versus voltage curve) test or manual thermography. However, technological developments have made it possible to obtain more efficient sensors that facilitate the maintenance of PV plants, such as aerial thermography or electroluminescence (EL). Each of them has some advantages and disadvantages. For instance, visual inspection is efficient, cheap and quick, but only reveals some of the failures. The I-V curve provides important information about the electrical performance of the system and its main parameters, the module failures, revealing degradation, mismatched modules, cracked cells, improper resistance, shadings or bypass diodes malfunction [2], but it cannot be performed in normal operation. Thermography is not intrusive, and possible thermographic defects detected in a PV module are: cell hotspot, overheated bypass circuit, junction box, connection or whole module [3]. In addition, it can be performed with aerial cameras. Finally, EL can be used in manufacturing process, shipped to a lab after unmounting the modules from the site or on the field, with a structure or specific tripod or also by means of EL cameras mounted on UAVs. The high resolution of the EL images enables resolving some defects more precisely than in IR images [4].

Results provided by each of them are usually studied separately, by different research groups. However, these methods can provide complementary results, losing interesting information about the PV site state in case of using just one of the inspection techniques [5]. In order to simplify the analysis and reporting of results, it could be interesting to use image processing techniques to align multiple scenes in a single fused image. The main objective of this research is to analyze the state of photovoltaic modules using fused images of frames captured by means of different sensors. This work is divided in four sections, starting with an introduction to the topic addressed, followed by the methodology used in the research, that leads onto the results and discussion of the outcomes to conclude with the main findings.

2 Methodology

2.1 EL and thermographic images acquisition

The images used for the fusion have been captured in the School of Forestry, Agronomic and Bioenergy Industry Engineering (EIFAB) in Soria, Spain. EL has been performed in controlled ambient conditions simultaneously than thermography in the

fourth quadrant. For these tests, the University has a temperature and humidity controlled chamber, which is shown in ***Fig. 1***.

Fig. 1. Temperature and humidity controlled chamber at the EIFAB in Soria, Spain

In this chamber, each module is continuously fed with its short circuit current using a laboratory source during 72 hours. EL images are captured with a pco. 1,300 camera each 30 minutes with an exposure of 5,000 ms. Themal images had been captured with a Flir C2 camera with a resolution of 80x60 pixels. This capturing system is presented in ***Fig. 2***, in which can be seen the EL camera, the IR camera, the PC and the screens that control the acquisition.

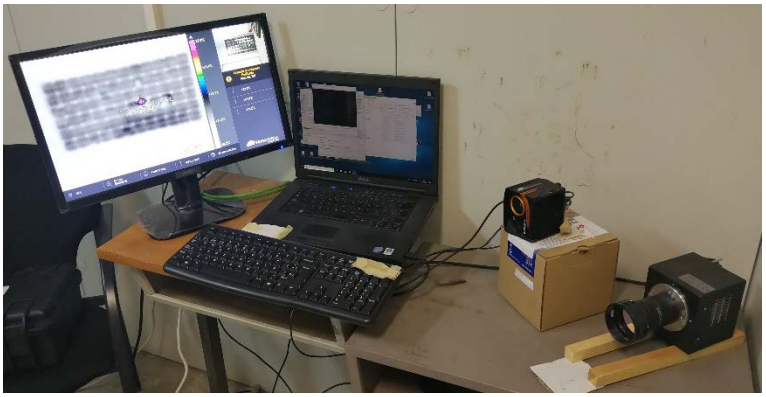

Fig. 2. EL and IR imaging capturing system used in the temperature and humidity controlled chamber.

The module used for the research is called SE-2, and its visual image is presented in ***Fig. 3***. It is an Eoplly mono-crystalline module of 175W, with 72 cells, Voc 44.35 V and Isc 5.45 A.

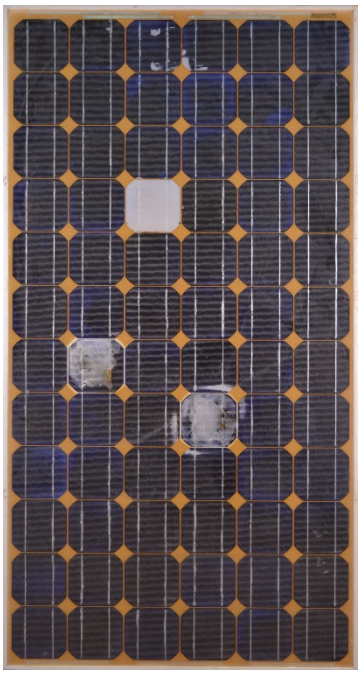

Fig. 3. Visual image of the PV module SE-2 used in the research

2.2 Image processing and fusion

In this section the image fusion process is presented. In general terms, image fusion is the process of combining different information from several images (sensors) taken from the same scene to obtain a composite image, which will contain the best information coming from the original images [6]. In that sense, it is expected that the fused image will have better quality (or more information) than any of the original images.

The image fusion process can be performed at various levels, depending on information representations and applications. Usually, these levels are categorized into signal, feature and symbol levels. Image signal level fusion is performed at pixel-level, which is the lowest-level type of fusion and involves the combination of raw source images into a single composite image. Image feature level fusion involves combining information in the form of image feature extracted properties, for example, edges, shapes, textures or regions. While image symbol-level fusion combines information given in the form of several symbolic representations, based on decision rules that produce common interpretation and resolve differences [7].

In this work a pixel-level fusion is adopted. In order to be able to fuse images at this level, it is essential that the images are adequately aligned prior to be fused. This process is known as image registration, which is the process of overlaying two or more images of the same scene taken at different times, from different viewpoints, and/or by different sensors. In general terms, it geometrically aligns two images,

which are usually referred to as the reference image and the sensed image [8]. Image registration helps to correct problems such as image rotation, scale and inclination, which are common when overlaying images.

The initial available images in their original format are presented in ***Fig. 4***. Note that in one image the panel is placed vertically and in the other horizontally, in addition to being in different formats, EL and thermal image. Hence, image registration of these images is needed.

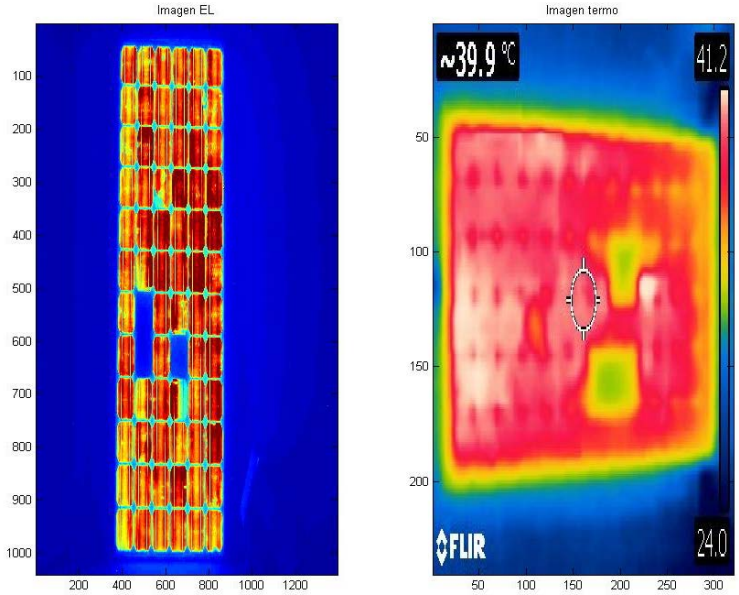

a) b)

Fig. 4. Initial available (a) EL and (b) thermographic images in their original format.

The registration and image fusion processes were implemented using Matlab 9.3 [9] on a PC. Firstly, for the image alignment process to be performed in a better and automatic way, cropping followed by a rotation of both images was performed manually. Once this is performed, it was observed that two images to be merged are of different sizes. Therefore, the images were resized to have the same size, in this case the thermo image is resized to the size of the EL image. Also, both images were transformed to grey scale. The resized and transformed images are presented side by side in ***Fig. 5***.

The registration process was then performed using the Matlab function imregister(). The description of this function is provided below:

"MOVING_REG = imregister(MOVING, FIXED, TRANSFORMTYPE, OPTIMIZER, METRIC) transforms the moving image MOVING so that it is spatially registered with the FIXED image. TRANSFORMTYPE is a string that defines the type of transformation to perform. OPTIMIZER is an object that describes the method for optimizing the metric. METRIC is an object that defines the quantitative measure of similarity between the images to optimize. The output MOVING_REG is a transformed version of MOVING."

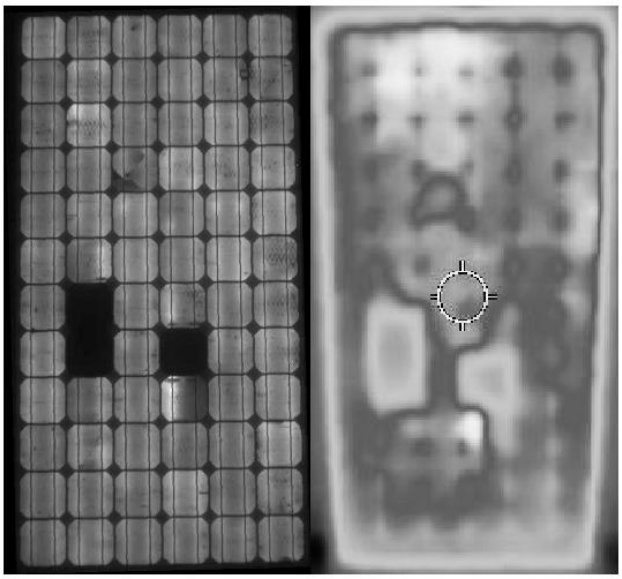

Fig. 5. EL and thermo resized grey scale images placed side by side.

The TRANSFORMTYPE value specifies the geometric transformation to be applied to the moving image can be one of the following values: 'translation', (x,y) translation in 2-D, or (x,y,z) translation in 3-D; 'rigid', rigid transformation consisting of translation and rotation; 'similarity', nonreflective similarity transformation consisting of translation, rotation, and scale; 'affine', affine transformation consisting of translation, rotation, scale, and shear.

The OPTIMIZER and METRIC values are obtained using the Matlab function imreconfig():

"[OPTIMIZER, METRIC] = imregconfig(CONFIGNAME) creates a metric and optimizer configuration to perform a typical image registration. OPTIMIZER contains settings used to configure the intensity similarity optimization. METRIC configures the image similarity metric to be used during registration."

The parameter CONFIGNAME can be ‘monomodal’ and ‘multimodal’. In the present case the ‘multimodal’ parameter was used as is preferred when the images come from different sensors or have different intensity levels.

Thereafter, nine different fusing image algorithms were performed as diff, blend, fpde, ifm, gff.

The algorithms diff and blend, where performed using the Matlab function imfuse():

“C = imfuse(A,B,METHOD,PARAM1,VAL1) creates a composite image of two images A and B. If A and B are different sizes, the smaller dimensions are padded with zeros such that the two images are the same size before computing the composite. The output, C, is a numeric matrix containing a fused version of images A and B.”

In this case, the A and B images are the moving and fixed images obtained from the image registration process (EL and thermo images, respectively). Values of METHOD can be: ‘falsecolor’, create a composite RGB image showing A and B overlayed in different color bands; ‘blend’, overlay A and B using alpha blending; ‘checkerboard’, create image with alternating rectangular regions from A and B; ‘diff’, difference image created from A and B; and ‘montage’, put A and B next to each other in the same image. Parameter1 is ‘Scaling’, which can take the values (VAL1): ‘independent’, images are scaled independently from each other; ‘joint’, images are scaled as a single data set; ‘none’, no additional scaling.

The fpde (Fourth Order Partial Differential Equations) image fusion algorithm is described in [10]. The algorithm is a process of five stages: 1) fourth order partial differential equations on each source image to obtain approximation and detail images; 2) principal component analysis is applied on detail images to obtain optimal weights; 3) final detail image is obtained by fusing these detail images with help of optimal weights; 4) final approximation image is obtained by employing an average operation on approximation images; 5) resultant fused image is calculated by combining the final approximation and detail images. Matlab code for this algorithm is available online [11].

The ifm (Image matting for fusion method) algorithm is described in [12]. The algorithm consists of three steps: first, the focus information of each source image obtained by morphological filtering is used to get the rough segmentation result which is one of the inputs of image matting. Second, image matting technique is applied to obtain the accurate focused region of each source image. Third, the focused regions are combined to construct the fused image. Matlab code for this algorithm is available online [13].

The gff (Image fusion with guided filtering) algorithm is detailed in [14]. First, an average filter is utilized to get two-scale representations. Then, the base and detail

layers are fused through using a guided filtering based weighted average method. Matlab code for this algorithm is available online [15].

3 Results and discussion

This section presents the results obtained in the image processing and merging process detailed in the previous section. The inspection techniques selected for the merging process have been EL and thermography in the fourth quadrant as they can be both performed simultaneously in the temperature and humidity controlled chamber. This study could also be extended with other images, as thermography in the second quadrant (revealing hot spot under ordinary operation of the system) or visual images. However, thermography in the second quadrant should be performed outdoor or indoor with a controlled light source. The initial available images in their original format are presented in ***Fig. 4***. Note that in one image the panel is placed vertically and in the other horizontally, in addition to being in different formats, EL and thermal image. The foregoing necessitates a process of registering or aligning images, as it has been previously detailed. The treated final merged images are presented from ***Fig. 6*** to ***Fig. 14.***

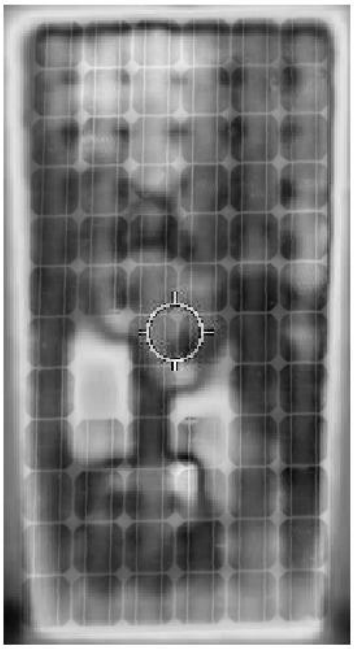

Fig. 6. Merged images using 'diff' algorithm.

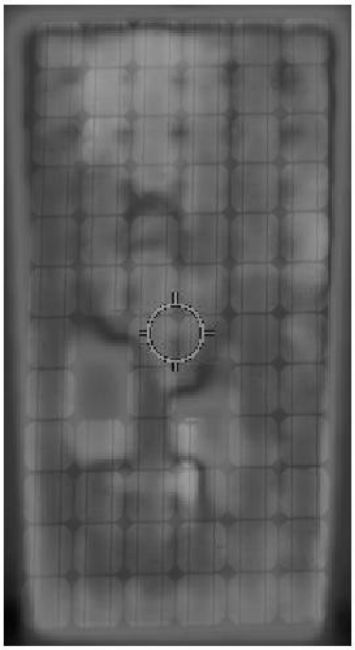

Fig. 7. Merged images using 'blend' algorithm.

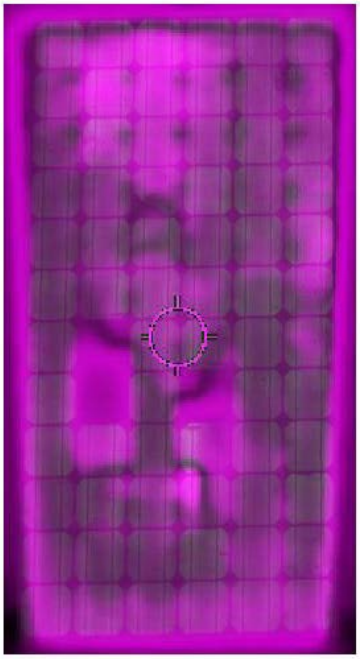

Fig. 8. Merged images using 'diff' algorithm.

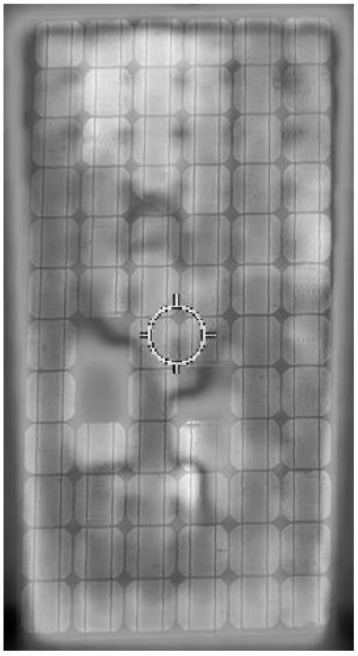

Fig. 9. Merged images using "fpde_fusion" algorithm.

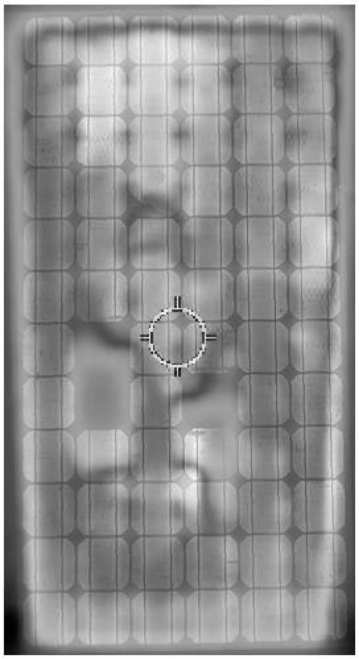

Fig. 10. Merged images using "fpde_fusion" algorithm for color images.

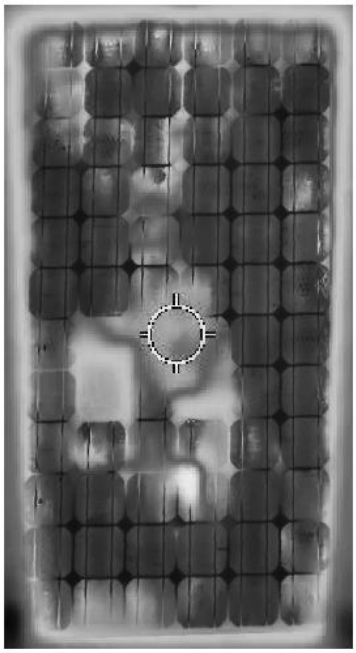

Fig. 11. Merged images using "ifm_fusion" algorithm.

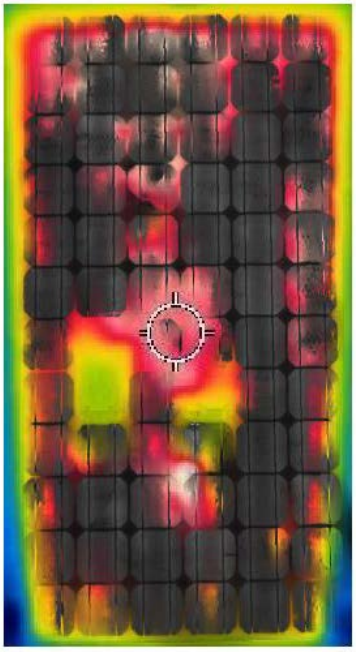

Fig. 12. Merged images using "ifm_fusion" algorithm for color images.

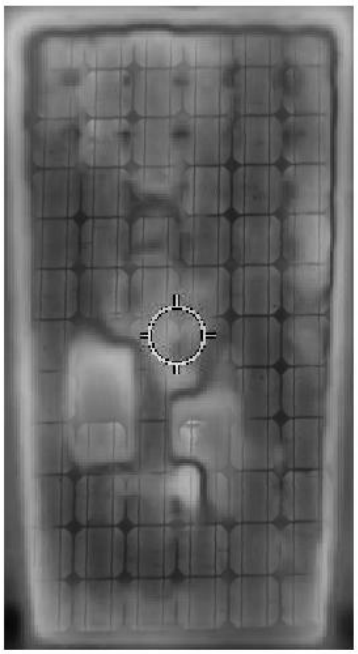

Fig. 13. Merged images using "gff_fusion" algorithm.

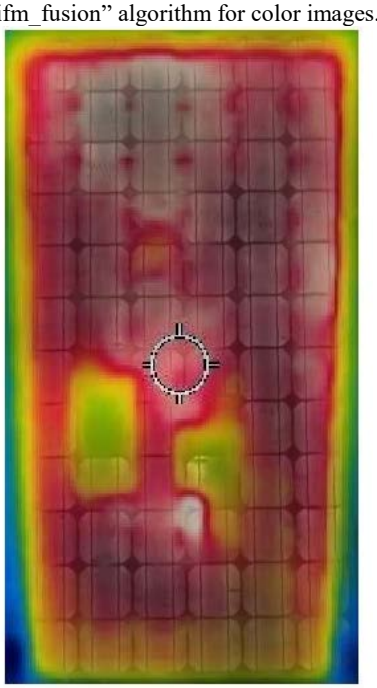

Fig. 14. Merged images using "gff_fusion" algorithm for color images.

As presented in the results, nine different merging images algorithm have been performed in order to determine the more suitable solutions to combine the information given by thermography and EL. The results presented could be improved if a higher sensor resolution was used, as it can be seen in ***Fig. 4***. b). The EL image ***Fig. 4***. a) shows one partially inactive cell (row four - column three) and three total inactive cells appearing completely black, as they do not emit (row seven and eight - column two and row eight – column four). The total inactive cells can be seen as cooler cells in thermography in the fourth quadrant during the current injection for the EL. Therefore, it can be concluded that these cells are short-circuited, allowing the current passing but not producing energy. Additionally, it has been observed that when there is an inactive area within a cell partially active, the active area is revealed as an overheated area. Therefore, it can be concluded that thermographic images during the EL tests also gives important information. This information is clearly shown in the merged images presented. For instance, it is interesting how in ***Fig. 5*** the cooler inactive areas appear in brightly flat white while hotter partially inactive areas are revealed as darker areas. This phenomenon is also evidenced in the colored images.

4 Conclusions

The paper presents nine different possible algorithms to analyze the state of photovoltaic modules using merged images of frames captured by means of EL and thermography in the fourth quadrant. It has been proved how using image processing techniques to align multiple scenes in a single integrated image simplifies the analysis and reporting of results of inspections of PV plants.

It has been shown that merging images for determining the PV modules impact is very interesting. It helps to detect faults. Additionally, other types of merged images could be done to visualize other patterns, such as thermography in the second quadrant.

Acknowledgments

The authors thank the CYTED Thematic Network “INTELLIGENT CITIES FULLY INTEGRAL, EFFICIENT AND SUSTAINABLE (CITIES)” nº 518RT0558. In addition, the work has been possible thanks to the "DOCTOR-PV" project Ref .: RTC-2017-6712-3, which has been funded by the “Ministry of Industry, Economy and Competitiveness, State R + D + i Program Oriented to the Challenges of the Society (Collaboration Challenges)”.

References

1. Renewable Energy Policy Network for the 21st Century (REN21). Renewables 2019 global status report 2019. 2019.
2. Deviations IT. Solar I-V Curves Interpreting I-V 2014
3. Gallardo-Saavedra S, Hernádez-Callejo L, Duque-Pérez Ó. Analysis and characterization of thermographic defects at the PV module level. Rev Fac Ing from Univ Antioquia 2019:1–16
4. Jahn U, Herz M, Köntges M, Parlevliet D, Paggi M, Tsanakas I, et al. Review on Infrared and Electroluminescence Imaging for PV Field Applications. 2018
5. Gallardo-Saavedra, S. et al: Failure diagnosis on photovoltaic modules using thermography, electroluminescence, RGB and I-V techniques. In: 36th European PV Solar Energy Conference and Exhibition EU PVSEC 19, Marseille, France (2019).
6. Pajares, G., De La Cruz, J. M. A wavelet-based image fusion tutorial. Pattern recognition 37(9), 1855-1872 (2004).
7. Ma, J., Chen, C., Li, C., Huang, J. Infrared and visible image fusion via gradient transfer and total variation minimization. Information Fusion 31, 100-109 (2016).
8. Zitova, B., Flusser, J. Image registration methods: a survey. Image and vision computing 21(11), 977-1000 (2003).
9. Matlab Homepage, https://www.mathworks.com/, last accessed 2019/08/25.
10. Bavirisetti, D. P., Xiao, G., Liu, G. (2017, July). Multi-sensor image fusion based on fourth order partial differential equations. In: Proceedings of the 20th International Conference on Information Fusion, (pp. 1-9). IEEE, 2017.
11. Fpde algorithm, https://la.mathworks.com/matlabcentral/fileexchange/63570-multi-sensor-image-fusion-based-on-fourth-order-partial-differential-equations, last accessed 2019/08/25.
12. Li, S., Kang, X., Hu, J., Yang, B. Image matting for fusion of multi-focus images in dynamic scenes. Information Fusion 14(2), 147-162 (2013).
13. Ifm fusion algorithm, https://la.mathworks.com/matlabcentral/fileexchange/68963-a-demo-for-image-fusion, last accessed 2019/08/25.
14. Li, S., Kang, X., Hu, J. Image fusion with guided filtering. IEEE Transactions on Image processing 22(7), 2864-2875 (2013).
15. Gff fusion algorithm, https://la.mathworks.com/matlabcentral/fileexchange/68962-a-demo-for-image-fusion, last accessed 2019/08/25.

Assessing the environmental impact of car restrictions policies: Madrid Central case

Irene Lebrusán[1] and Jamal Toutouh[2]

[1] Harvard University, IGLP, MA, USA
ilebrusan@law.harvard.edu
[2] Massachusetts Institute of Technology, CSAIL, MA, USA
toutouh@mit.edu

Abstract. With the increase of population living in urban areas, many transportation-related problems have grown very rapidly. Pollution causes many inhabitants health problems. A major concern for the International Community is pollution, which causes many inhabitants health problems. Accordingly, and under the risk of fines, countries are required to reduce noise and air pollutants. As a way to do so, road restrictions policies are applied in urban areas. Evaluating objectively the benefits of this type of measures is important to asses their real impact. In this work, we analyze the application of Madrid Central (MC), which is a set of road traffic limitation measures applied in the downtown of Madrid (Spain), by using smart city tools. According to our results, MC significantly reduces the nitrogen dioxide (NO_2) concentration in the air and the levels of noise in Madrid, while not arising any border effect.

1 Introduction

According to the United Nations Populations Division, today, 55% of the world's population lives in urban areas. This proportion is expected to increase to 68% by 2050 [23]. This urban aglomerations are giving shape to new challenges from a social, economical, and environmental point of view, being mobility one of them. The fact is that mobility inside the city and inter-cities is a key aspect that determines the development of the urban areas.

The design of most of our cities prioritizes the use of motorized vehicles. This relegates the rest of uses and users with different negative impact over safety and health, as well as over well-being and development, especially for children and the elderly. For example, it has been demonstrated the causal link between the growth of car use and the reduction of children's access to public space in urban contexts, which critically affects their social and physical development [12]. Other authors demonstrate that eldery improve their independence and well-being in environments with safety walking access [13].

Another major concern derived of the rapid development of car oriented cities is the high generation of emisions (air pollutants and noise) and their impact on the inhabitants health [19]. Air pollution is the top health hazard in the European Union (EU) [8, 26] as it reduces life expectancy, loss of years of healthy life, and

diminishes the quality of health. In the EU, it causes more than 400,000 premature deaths, being primarily associated with heart disease and strokes, followed by lung diseases and lung cancer. Noise pollution is also a major environmental health question; the European Environment Agency (EEA) estimates that environmental noise causes at least 16,600 cases of premature death in Europe each year [7]. Exposure to prolonged noise pollution can cause a range of health problems including annoyance, sleep disturbance, increasing hypertension, and cardiovascular diseases [2]. It can also have effects on children's cognition including communication difficulties, impaired attention, increased arousal, frustration, noise annoyance, and consequences of sleep disturbance on performance [10, 11].

As road traffic generates the referred problems (e.g., about 80% of the noise pollution is caused by cars [20]), reducing it seems to be an efficient strategy to improve urban livability and their inhabitants health. Accordingly, pedestrianization is a commonly implemented approach to this challenge. Pedestrianization can be defined as to convert a street into a car free space by excluding motor vehicles. It should be coupled with creation of effective public and non-motorized transportation facilities. Absolute pedestrianization is difficult to be implemented. Instead, authorities define road transportation limitation policies. For example,distribution and commercial vehicles may be allowed to enter in a pedestrianized area [16].

Many cities around the world started to shift toward non-car friendly access by implementing different plans and measures [16, 19]. However, changes on the spatial configuration of the city requires of a big investment that not all the council can afford. There are several studies that evaluate the impact of pedestrianization implementations [18, 19, 21, 24]. The findings of these studies highlight that this kind of measures have not only environmental health impacts. They positively affect tourism development, job creation, improving safety, enhancing the appearance of urban areas, etc. Fig. 1 shows the main benefits of pedestrianization in urban areas. Their conclusions are principally based on the use of surveys and urban simulation.

In this study, we analyze Madrid Central (MC) which has been implemented in Madrid (Spain), as a case study [1]. This low emissions zone (LEZ) gives continuity to dissuasive measures such as fine-tuning the circulation of certain license plates on alternate days or limitations of access to vehicles considered to be the most polluting, among others. But, does this measure have a positive impact over the reduction of pollution? How can we use smart city tools to take the best decision to evaluate benefits of this measure? The interest of this analysis is even bigger as there exists a controversial political use of this measure. Thanks to the virtues of smart city tools, we can analyze objectively the results of this kind of plans. Specifically, we take advantage of smart governance and transparency services to get data shared through open data platforms.

The main contributions of this work are: *i)* pointing out the potential of open data sources to evaluate the effect of car restrictions implemented in the cities; *ii)* analysing the environmental impact of the measures applied in MC; and *iii)* applying a multidisciplinary approach to assess mobility policies embedded in an

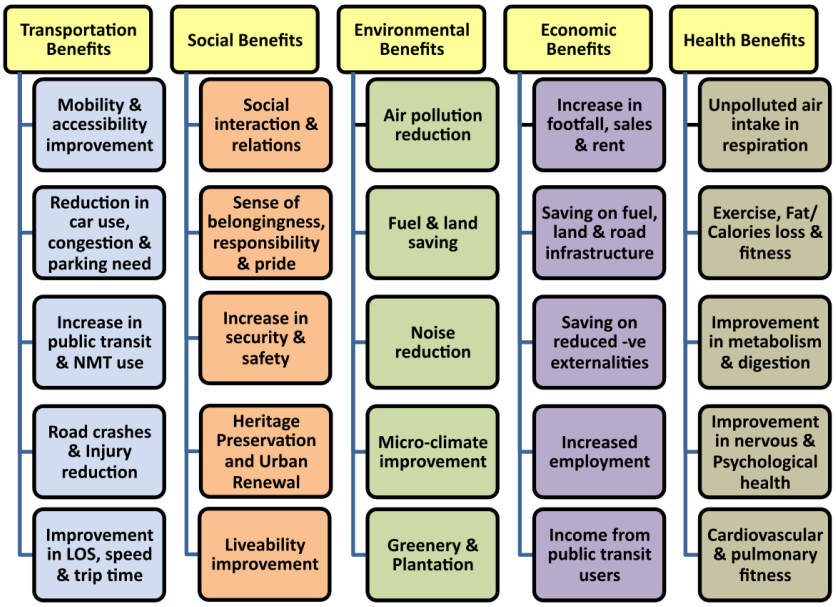

Fig. 1: Summary of pedestrianization benefits. Image created by Soni & Soni [19].

international framework of regulations and guidelines. Finally, nothing prevent us to apply the same approach to analyze other initiatives to deal with air quality, noise, and other challenges derived from urban growth.

The rest of the paper is orgaized as follows: first, we describe the goals, strategies and contextualization of MC, paying especial attention to the directives in which is embedded. Section 3 introduces the materials and methods used in this analysis. The evaluation of the air quality and noise based on the shared open data is shown in Section 4. Finally, Section 5 presents the conclusions and the main lines of future work.

2 Madrid Central: purpose, description and controversia

The concern over the air quality and noise across the EU leads to the adoption of different environmental and health directives. Those policies have the object to safeguard EU citizens from environment-related pressures and risks to health and wellbeing. Accordingly, emissions are monitored in every member state.

The European Commission adopted in 2013 a Clean Air Policy Package based on `Directive 2008/50/EC` [6] and `2004/107/EC` [5]. It points to the full compliance with the established air quality standards and set different objectives for 2020 and 2030. This EU air quality policy rests on three pillars: *i)* air quality standards; *ii)* national emission reduction targets established in the National Emissions Ceiling Directive; and *iii)* emissions standards for key sources of pollution, as the vehicles.

The EU directive about noise (`Directive 2002/49/EC`) [4] focuses on the determination of three main points: *i)* exposure to environmental noise; *ii)* ensuring that information on environmental noise and its effects is made available to the public; and *iii)* preventing and reducing environmental noise where necessary and preserving environmental noise quality where it is good. The directive of noise is not as exigent as the air quality one, leaving the limit or target values at the discretion of the States. However, it does clearly require the creation of noise maps and noise management plans for agglomerations with more than 100,000 inhabitants. In Spain, 63 municipalities have more than 100,000 inhabitants, being Madrid the biggest of them (3,266,126 people).

Regarding to the air quality and based on latest available data, the EU points that the transport sector is the largest contributor to nitrogen oxide emissions, and a significant contributor to particulate matter emissions. Several countries have exceeded repeteadly the PM_{10} and the NO_2, being Spain one of them. More specifically, the levels of pollution admitted by the EU were exceeded in the Spanish biggest cities (Barcelona, Madrid and Valencia). The main source of NO_2 is road traffic [14].

The EU demanded to Spain the reduction of these pollutants in the air, under the threat of taking the case before the European Court and the risk of important economic sanctions. This process is paralized in May of 2018 thanks to the adoption of certain measures to reduce pollutants, such as MC.

MC is a LEZ in Madrid, consisting in car access restrictions in a delimited area of the downtown (see Fig. 2). Those restrictions exclude residents of MC and authorized cars[3]. Otherwise, the access to this area requires vehicles to have an environmental sticker[4]. In other words, the measure seeks to eliminate transit traffic, which crosses but has no origin or destination in *Madrid Central*.

Fig. 2: MC area and the location of the sensor installed in Plaza del Carmen.

[3] People with reduced mobility; public transport; security and emergency services; car-sharing or moto-sharing; specific workers; distribution and commercial vehicles.
[4] There are no restrictions for vehicles labeled as 0 and ECO, but parking in the street for ECO vehicles is limited. B and C vehicles can only use car parks.

MC aims at improving air quality, but also responds to the idea of changing the uses of spaces in the city center, prioritizing the pedestrian one and reducing noise pollution. But as we said, its conformation mainly responds to ensure the objectives demanded by the EU. It should be pointed out that, thanks to this measure, Spain avoided to be brought to the European Court of Justice.

MC convers an area of 4,720,000 m^2, almost the entire *Centro* district, which is formed by the neighborhoods of *Palacio*, *Embajadores*, *Cortes*, *Justicia*, *Universidad*, and *Sol*. *Centro* district has 134,881 inhabitants, of which 12,377 are less than 17 years of age and 21,645 people are 65 years old or more. Those groups are more affected by noise and pollutants. Among other benefits referred to citizenship education, to stablish the perimeter of MC facilitates the understanding of zonal delimitation and aspires to introduce a behavioral change regarding the use of the car. MC is created by the *Ordenanza de Movilidad Sostenible* (October 5th, 2018) and the traffic restriction started on November 30, 2018. However, the fines for noncompliance did not started until March 16, 2019.

However, and despite of the fact that the European Union have told Spain to reduce their emissions under risk of fine, this restriction to the car use is suspended. After the elections (held on May, 26th 2019) the new goverment decided to apply a moratorium on fines from July 1st to September 30th 2019, approved under art. 247 of the *Ordenanza de Movilidad Sostenible*. This suspension leaded to the emergence of social movements claiming the paralization of this reversal based on the negative effects over health and environment, and a warning from the EU. After a contentious-administrative appeal filed by environmental groups, a judge has provisionally paralyzed this reversal of MC.

3 Materials and methods

In order to know more about the objective effects of MC, we analyze different indicators applicable to the dimensions of environmental pollution and noise. The source of data used in this study is provided by the Open Data Portal (ODP) offered by the Madrid City Council[5]. The data gathered by the sensor located in MC (*Plaza del Carmen*) is analyzed to evaluate the impact of the measures carried out (see Fig. 2). The temporal range of this study starts in December of 2016 and finishes in May of 2019, i.e., 30 months grouped in two periods: the 24 months previous to MC (named *Pre-MC*) and six months with the car restrictions (named *Post-MC*).

Following, we introduce the air pollutants evaluated, the outdoor noise metrics studied, and the methodology applied in the evaluation.

3.1 Air quality evaluation

The ODP provides the daily mean concentration of different air pollutants. The sensor located in MC evaluates six air pollutants: carbon monoxide (CO), SO_2, nitrogen monoxide (NO), NO_2, oxides of nitrogen (NOx), and O_3.

[5] Madrid Open Data Portal url: `https://datos.madrid.es/`

The pollutants with the strongest evidence for a public health concern, include particulate matter, SO_2, NO_2, and O_3 [26]. In fact, NO_2 itself caused 241,000 premature deaths among European citizens in 2015 and 2,515,000 of years of life lost [9]. Those pollutants (SO_2, NO_2, and O_3), are the ones we analyze, since those are the ones referred to in the guidelines published by the WHO [26] and in the regulations promoted by EU [8] (see Table 1). We have not data regarding particulate matter.

Table 1: WHO and EU maximum concentration of pollutants in the air.

pollutant	period	WHO guideliness	EU regulations
SO_2	24 hours	20 $\mu g/m^3$	125 $\mu g/m^3$
	1 hour	-	350 $\mu g/m^3$
	10 minutes	500 $\mu g/m^3$	-
NO_2	1 year	40 $\mu g/m^3$	40 $\mu g/m^3$
	1 hour	200 $\mu g/m^3$	200 $\mu g/m^3$
O_3	8 hours	100 $\mu g/m^3$	120 $\mu g/m^3$

3.2 Outdoor noise evaluation

As there is not a clear international regulation about the outdoor noise, we decided to evaluate this concern taking into account three variants of noise measurements: the equivalent sound pressure, the percentile noise, and the noise pollution (NPL) [17] levels.

The equivalent sound pressure levels (L_{eq}) can be described as the average sound level over a selected period. We study the L_{eq24}, that corresponds to the L_{eq} measured during the whole day (24 hours). The L_{eq} measurements are also required for intermediate periods (normally three within a 24 hour period) to determine how noise varies with time and hence community activities. Here, we evaluate the L_{eqD}, L_{eqE}, and L_{eqN}, which represent the L_{eq} during the day (from 7:00h to 19:00h), the evening (from 19:00h to 23:00h), and the night (from 23:00h to 7:00h), respectively. According to the Comunity of Madrid regulations [3], L_{eqD} and L_{eqE} should be lower than 65 dB and L_{eqN} lower than 55 dB.

The percentile noise levels (L_x) are the levels exceeded for x percent of the time, where x is between 0.1% and 99.9%. We evaluate the L_{10}, L_{50}, and L_{90}. The L_{10} takes account of any annoying peaks of noise. The L_{90} is extensively used for rating the outdoor background noise.

The NPL estimates the dissatisfaction caused by road traffic noise comprising the continuous noise level (L_{eq}) and the annoyance caused by fluctuations in that level. It serves as an indicator of the physiological and psychological disturbance of the human system due to the noise pollution in the environment [17]. NPL is equal to L_{eq} plus 2.56 times the standard deviation of the noise distribution. However, it is approximated by $NPL \approx L_{eq} + (L_{10} - L_{90})$.

From the OPD, we get monthly mean values of each metric. This data reports the A-weighted sound level readings to replicate the response of the human ear to the annoyance caused by road traffic noise. Thus, all sound levels referred here are in terms of A-weighted decibel (dBA).

3.3 Methodology

In order to evaluate the impact of MC, we compare the data sensed during Pre-MC and during Post-MC. As MC measures started in December of 2018, this would be consider the first month of every row (number 1). Consequently, November becomes the last one of every year considered (number 12).

The impact on the studied indicators is calculated according to the *gap* for the months M that MC has been active (Eq. 1). The set M is defined as M={*December, January, February, March, April, May*}. The $x_m^{Post-MC}$ and $\overline{x_m^{Pre-MC}}$ represent the average value of the indicator x sensed during month $m \in M$. The gap returns the average percentage of decrease or increase for the indicator x.

$$gap = \frac{1}{|M|} \sum_{m \in M} \frac{x_m^{Post-MC} - \overline{x_m^{Pre-MC}}}{x_m^{Post-MC}} \ \% \tag{1}$$

We use pairwise statistical tests to compare between both periods with a statistical significance of 99% (i.e., p-value<0.01). When the samples data sets are normally distributed, we use the *Student's t-test*, otherwise, we apply the *Mann-Whitney* non-parametric one.

Giving this data in a specific temporal ordering, it is possible to raise questions about how the indicators are likely to behave in the future [25]. Polynomial regression, which have been successfully used in road traffic prediction [22], is applied here to predict the general future trend in pollution (air and noise) after the implementation of the road traffic restrictions in MC.

These last type of analyses, i.e., statistical tests and regressions, use the highest granularity of the data provided by the ODP: daily concentration of air pollutants and monthly levels of noise.

Finally, there are cases (data sensed) in which the concentration of the air pollutants exceed the maximum/threshold defined by WHO and/or EU (see Table 1). and the mean excess quantity. In this cases, we evaluate both dimensions in which this value is exceeded: the period of time and the mean excess quantity.

4 Results and discussion

This section evaluates the results of the actions taken in MC in terms of air quality and noise based on the data sensed.

4.1 Air quality

Table 2 reports the minimum (min), the maximum (max), the mean, the normalized standard deviation, and the gap for the concentration of the pollutants sensed in MC. As these measures are normally distributed, we apply the Student's t-test to asses the statistical significance of the difference between Pre-MC and Post-MC air quality. Fig. 3 shows the mean and the standard deviation of the concentration of the pollutants by months. Notice that for the Pre-MC months (in red), the results cover a wider amount of time, corresponding to two different years. Fig. 3 also shows the bloxplot of the concentration of the air pollutants for the months that coincide Pre-MC and Post-MC (i.e., from December to May).

Table 2: Summary of the air pollutants sensed. The star($\star$) in the last column indicates there is statistical difference between periods analized (p-value<0.01).

metric	**Pre-MC**			**Post-MC**			**gap**
	min	**mean±stdev**	**max**	**min**	**mean±stdev**	**max**	
SO_2	1.00	7.82±50.37%	22.00	10.00	13.97±21.28%	24.00	$\star$56.14%
NO_2	15.00	46.92±31.27%	96.00	8.00	39.60±50.42%	96.00	$\star$-35.65%
O_3	1.00	39.31±52.32%	89.00	5.00	41.20±48.94%	84.00	22.67%

The concentration of SO_2 increases during Post-MC months in comparison to Pre-MC (gap=56.14%). Fig. 3.a1 shows the concentration of SO_2 for the time previous to MC (from June to November) is close to the Post-MC one. This may be explained by the influence of the meteorological conditions (i.e., wind direction and speed, atmospheric pressure, temperature, and relative humidity) possibly affecting the result in unexpected directions.

For both periods, the mean concentration does not exceed the threshold defined by WHO and EU (20 $\mu g/m^3$), however the maxima values do (see Table 2). In Pre-MC the threshold is exceeded during 0.43% of the time by 0.01 $\mu g/m^3$ and in Post-MC during 3.91% of time by 0.09. Thus, this excess is exceptional and negligible, so the EU has not found it problematic in Spain.

Focusing on NO_2, which is the pollutant that almost lead Spain to the European Court, its concentration is significantly reduced in more than one third (gap=-35.65% and Student's t-test p-value<0.01). The mean NO_2 concentration for Post-MC is 39.60$\mu g/m^3$, below the threshold established by WHO and EU (40 $\mu g/m^3$). As it can be seen in Fig. 3.b1, the concentration of NO_2 exceeds during several months the maximum one allowed by WHO and EU for both periods (Pre-MC and Post-MC) but with important diferences. During Pre-MC the threshold is exceeded during 64.01% of the time by 9.72 $\mu g/m^3$. During Post-MC the threshold is exceeded, but it does during less time and with a smaller value: 45.81% of the time by 8.26 $\mu g/m^3$. However, it is notizeable that there is a clear downward trend in the concentration of NO_2 after the application of road traffic limitation (see Fig. 3.b1). Taking into account independently each month, the maximum reduction of NO_2 occurs in April with a concentration of 22.54 $\mu g/m^3$ (gap=-93.93%).

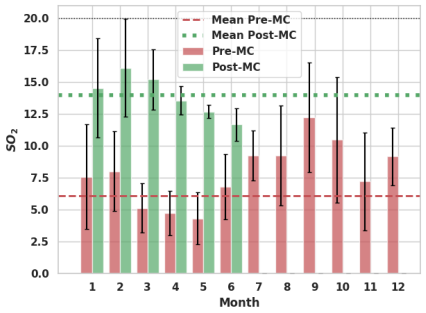

a1) SO_2 mean and standard deviation.

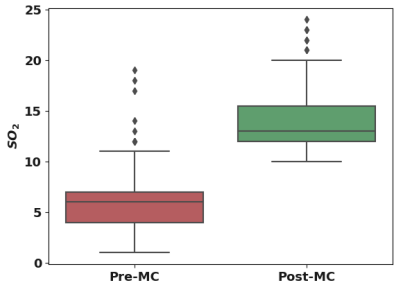

a2) SO_2 boxplot.

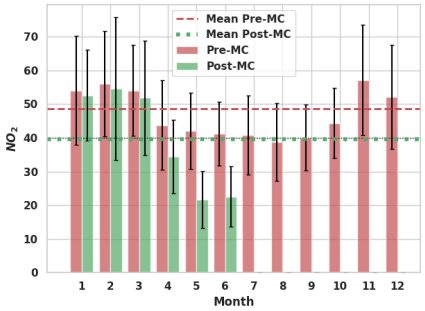

b1) NO_2 mean and standard deviation.

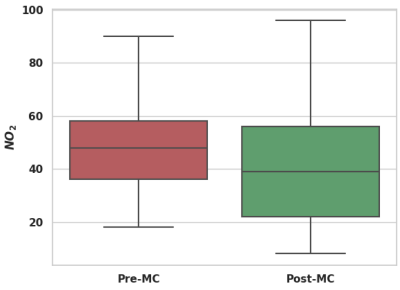

b2) NO_2 boxplot.

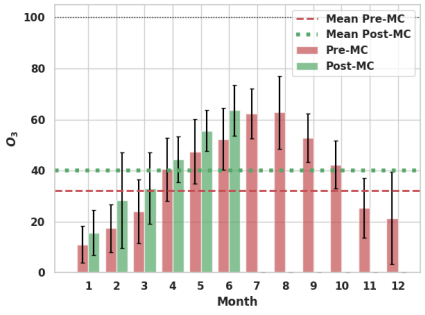

c1) O_3 mean and standard deviation.

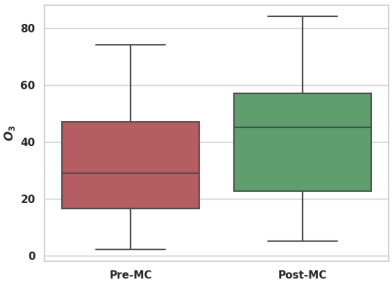

c2) O_3 boxplot.

Fig. 3: Mean and standard deviation of the concentration of the air pollutants gropued by months (left side). The red dashed and greed doted lines show the mean value for the months from one to six for Pre-MC and Post-MC, respectivelly. Boxplot of the concentration of the pollutants (right side).

Fig. 4 illustrates the trend of NO_2 using the data grouped by weeks. According to the polynomial regression of grade 10 (black dashed line), NO_2 concentration increases during colder seasons and decreases in warmer ones. In turn, the linear regression (black line) shows a declined trend over time for this air pollutant. The behaviour of this variable (concentration of NO_2 in the air) under the application of MC measures point that the traffic restriction has a positive effect in the air quality. Therefore, MC is effective both for this environmental dimension and to avoid fines from the international community.

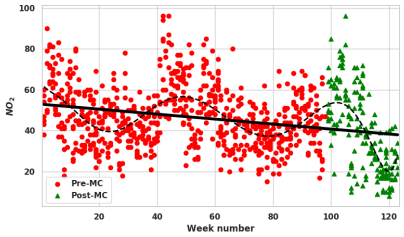

Fig. 4: NO_2 concentration linear regression. Red dots represent the Pre-MC data and the green triangles show Post-MC data grouped in weeks. The black line represents the general trend according to the linear regression.

The concentration of O_3 does not show a significant difference for both periods of time (see Fig. 3.c1 and c2). All the O_3 measures are bellow the maximun defined by WHO and EU (100 and 120 $\mu g/m^3$, respectively). The concentration of this pollutant shows an increase during Post-MC (gap=22.67%). This increment can be due by the oxidation of NO, i.e., the chemical reaction of O_3 and NO that forms NO_2 and O_2, which occurs in urban areas [15]. As the road traffic limitation reduces the concentration NO, the portion of O_3 that reacts with NO is lower. Therefore, the levels of O_3 do not decrease, and subsequenty, the concentration of NO_2 produced by the oxidation of NO is lower. In short, this upturn can be a chemical consequence of the reduction in the air of other components concentration.

Finally, the evaluation of the SO_2, NO_2, and O_3 indicates that the final environmental balance may not always coincide with what was intuitively expected.

4.2 Noise polution

Table 3 reports the min, max, the mean, the normalized standard deviation, and the gap for the levels of noise in MC. As the levels of noise are not normally distributed and the size of the samples is low (>30), we apply the Mann-Whitney test to asses the statistical significance of the difference between Pre-MC and Post-MC noise pollution. Fig. 5 illustrates the mean of a representative set of different levels (L_{eq24}, L_{10}, L_{90}, and NPL) grouped by months. Fig. 6 shows the boxplots of the L_{eq24}, L_{10}, and L_{90} levels of noise.

Table 3: Summary of the sensed levels of noise. The star($\star$) in the last column indicates that there is statistical difference (p-value<0.01).

metric	Pre-MC			Post-MC			gap
	min	mean±stdev	max	min	mean±stdev	max	
L_{eqD}	61.30	63.68±3.56%	68.70	62.10	63.63±2.01%	65.70	-0.72%
L_{eqE}	60.40	61.96±1.24%	63.80	60.60	61.18±0.65%	61.80	$\star$-1.51%
L_{eqN}	59.00	60.57±1.32%	62.80	59.70	60.30±0.80%	61.00	-0.47%
L_{eq24}	60.50	62.70±2.66%	66.50	61.40	62.40±1.27%	63.60	-0.96%
L_{10}	63.10	64.53±1.60%	68.60	63.40	63.88±0.66%	64.50	$\star$-1.51%
L_{50}	57.60	58.66±0.77%	59.60	57.20	57.78±0.78%	58.60	$\star$-1.47%
L_{90}	52.40	53.46±1.46%	55.00	51.30	51.82±0.97%	52.70	$\star$-2.92%
NPL	70.70	73.77±3.40%	80.90	72.60	74.47±1.69%	76.50	-0.07%

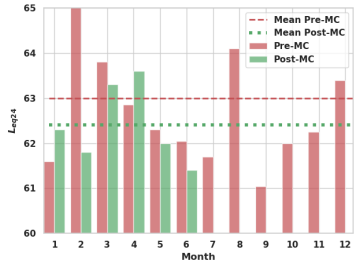

a) L_{eq24}

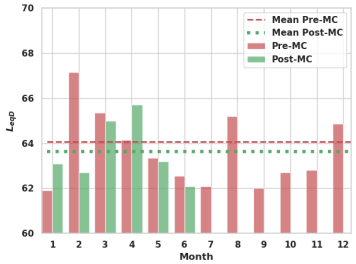

b) L_{eqD}

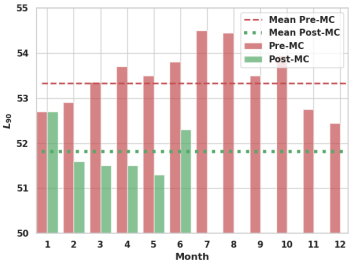

c) L_{90}

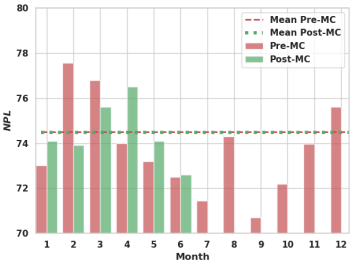

d) NPL

Fig. 5: Mean levels of noise analyzed here gropued by months. The red dashed and greed doted lines show the mean values for Pre-MC and Post-MC, respectivelly.

Regarding the equivalent sound pressure levels (L_{eqD}, L_{eqE}, L_{eqN}, and L_{eq24}), the highest difference between Pre-MC and Post-MC is given by the evening noise (L_{eqE}). This noise is reduced by 1.51% and it is statistically lower than evaluated one during Pre-MC (see Table 3). Among them, the L_{eqN} levels show the lowest decrease. This is mainly explained by the different car affluence during night time, as the nights experience the lightest road traffic flows.

As it can be seen in Fig 6.a, even if there is not a statistical difference regarding to the L_{eq24} level of noise between both periods, during Post-MC this level of noise is generally lower than during Pre-MC. This metric *averages* the whole noise evaluated during the 24 hours of the day. Therefore, in general the noise is lower during MC.

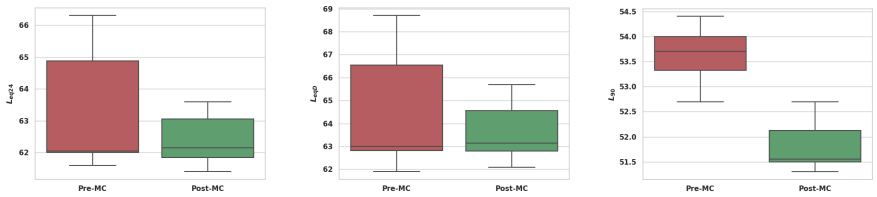

a) L_{eq24} b) L_{eqD} c) L_{90}

Fig. 6: Boxplots of the noise data metrics for both periods of time analized.

During Post-MC, the reduction of the day noise pollution allows the L_{eqD} be lower than 65 dB, which is the threshold proposed by Comunity of Madrid regulations (see Section 3.2). This value is exceeded just during some periods of March (month number 4 in Fig. 5b).

Focusing on the percentile noise levels (L_{10}, L_{50}, and L_{90}), Pre-MC and Post-MC differences are statistically significant. The highest improvement is shown by L_{90} (see Fig. 6.c), which represents the residual background levels of noise of the urban area analyzed (gap=-2.92%). As the continuous road traffic flow is one of the main sources of the backgroung noise, its reduction provoques a decrease on this type of noise. According to the Mann-Whitney test results, the significance reduction of L_{10} is lower than for the other two percentile levels (p-value<0.05). The L_{10} considers annoying peaks of noise. This type of maxima levels of noise are reduced by 1.51% with a mean value during Post-MC of 63.88 dBA.

There is not a significant reduction of NPL (see Table 3). This is principally because this metric depends on L_{eq24} and the difference between L_{10} and L_{90}. On the one hand, there is not a significant difference in the L_{eq24}. On the other hand, both percentile noise levels are reduced during Post-MC. However, the reduction of L_{90} is grater, and therefore, the difference between them L_{10} and L_{90} increases. For example, if we substract the mean values of L_{10} and L_{90} we get that for Pre-MC 64.53-53.46=11.07 dBA and for Post-MC 63.88-51.82=12.06 dBA.

Fig. 7 illustrates the trend of some representative levels of sound (L_{eq24}, L_{eqD}, L_{90}, and NPL). According to the polynomial regression of grade 10 (black dashed line), there is a reduction of the equivalent levels of noise during the months between 19 and 22. In turn, according to the linear regression (black line), the noise in MC is being reducing over the time with MC actions.

Finally, it is clear that the limitation of road traffic flows reduces all the different noise pollution metrics in MC, according to the sensed data.

4.3 Global discussion

According to the analysis carried out, MC has reduced concrete pollutants in the air and in the sensed levels of noise. Specifically, regarding the air quality, the lowering of NO_2 is a very positive result. As we stated in Section 2, this is the component of pollution which affects health the most, increassing bronchitis,

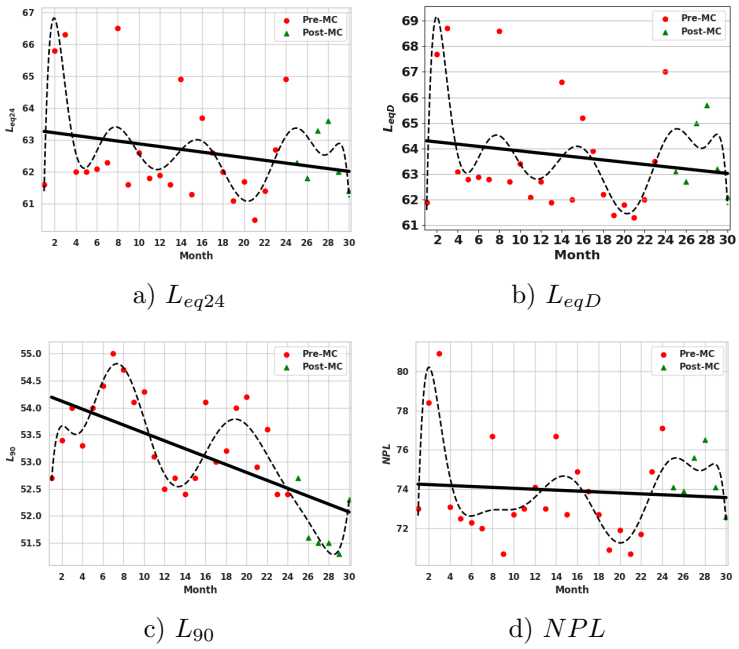

a) L_{eq24} b) L_{eqD}

c) L_{90} d) NPL

Fig. 7: Noise sensed linear regression. Red dots represents the data sensed during Pre-MC and green triangles the ones sensed during Post-MC grouped in months. The black line represents the general trend according to the lineare regression.

asthma and lung problems especially among the children and the older people. Besides, this is the component which lowering was specifically required to Spain by the EU. Accordingly, the reduction of this pollutant is extremely positive, not just having a positive effect for health but fulfilling so the international directions and so, avoiding the risk of fine.

Secondly, as the road traffic is the predominant source of noise pollution in urban areas, it was expected a reduction on all the levels of noise. This was proved to be true. However, and this is relevant, the levels of noise during the night are still higher than the threshold proposed by the Comunity of Madrid [3]. This should be a question to consider in the development of future actions.

5 Conclussions and future work

The quickness of the urbanization process brings new pollution problems, among others. This requires quick responses to create sustainable societies from an environmental, economical, and social points of view, as well to create inclusive spaces. A reliable diagnosis is key to address such challenges. Smart city initiatives, along with open data solutions and smart technologies have proved to be invaluable tools of analysis, helping decision making and leading to the best outcome for the city.

In this work, we evaluate data from ODP to evaluate the real impact of MC in terms of environmental benefits and acomplishment of international directives. Despite of the lifespan of MC, the measures proved to be effective addressing emission problems (reducing NO_2 and noise). These results may be used as a point to oppose the decission of removing MC by the new government.

The lack of use of open data standards in OPD and the poor documentation found hardeness the analysis capacity for this type of studies. For example, we have found data with different granularity for the same indicators (i.e., noise).

The future research lines are: *i)* analysing the impact of MC not just in the downtown but in the whole city of Madrid *ii)* new multivariable analysis taking into account new data (e.g., metheorological conditions); *iii)* evaluating MC (or MC-like) measures considering new dimenssions (such as, morbidity, economical impact, use of spaces, mobility behavioural changes); and *iv)* studying effects on espcific population groups (e.g., children and the elderly).

Acknowledgements

Irene Lebrusán has been partially funded by RCC Harvard program. Jamal Toutouh has been partially funded by European Union's Horizon 2020 research and innovation programme under the Marie Skłodowska-Curie grant agreement No 799078. This research has been partially funded by the Spanish MINECO and FEDER projects TIN2017-88213-R (`http://6city.lcc.uma.es`) and TIN2016-81766-REDT (`http://cirti.es`). Universidad de Málaga, Campus Internacional de Excelencia Andalucía TECH.

References

1. Ayuntamiento de Madrid: Madrid Central- Zona de Bajas Emisiones. `https://tinyurl.com/y2jch2qb` (2018), Accessed: 2019-07-07
2. Basner, M., Babisch, W., Davis, A., Brink, M., Clark, C., Janssen, S., Stansfeld, S.: Auditory and non-auditory effects of noise on health. The lancet 383(9925), 1325–1332 (2014)
3. Counidad de Madrid: Compendio de Normativa de Ruido y Vibraciones. `http://www.madrid.org/bdccm/normativa/PDF/Ruidos%20y%20vibraciones/Compilacion/CPRUID.pdf` (2004), Accessed: 2019-07-07
4. European Commission: Directive 2002/49/ec of the european parliament and the council of 25 june 2002 relating to the assessment and management of environmental noise. Official Journal of the European Union, L 189(18.07), 2002 (2002)
5. European Commission: Directive 2004/107/ec of the european parliament and of the council of 15 december 2004 relating to arsenic, cadmium, mercury, nickel and polycyclic aromatic hydrocarbons in ambient air. Official Journal of the European Union, L 23, 3–16 (2004)
6. European Commission: Directive 2008/50/ec of the european parliament and of the council of 21 may 2008 on ambient air quality and cleaner air for europe. Official Journal of the European Union, L 152, 1–44 (2008)
7. European Environment Agency: Noise pollution is a major environmental health concern in Europe. `https://www.eea.europa.eu/themes/human/noise` (2016), accessed: 2019-07-07

8. European Environment Agency: Air quality in Europe - 2018. https://www.eea.europa.eu/publications/air-quality-in-europe-2018 (2018), Accessed: 2019-07-07
9. European Environment Agency: Air quality in Europe: 2018 report. https://www.eea.europa.eu/publications/air-quality-in-europe-2018, institution = European Environment Agency , note = Accessed: 2019-07-07 (2018)
10. Evans, G., Hygge, S., Luxon, L., Prasher, D.: Noise and its effects (2007)
11. Evans, G.W.: Child development and the physical environment. Annu. Rev. Psychol. 57, 423–451 (2006)
12. Fotel, T., Thomsen, T.U.: The surveillance of children's mobility. Surveillance & Society 1(4) (2003)
13. Lawton, M.P., Nahemow, L.: Ecology and the aging process. (1973)
14. Ministerio de Agricultura y Pesca, Alimentación y Medio Ambiente: Evaluación de la Calidad del Aire de Espa na 2016. https://tinyurl.com/y2jch2qb (2017), Accessed: 2019-07-07
15. Palmgren, F., Berkowicz, R., Hertel, O., Vignati, E.: Effects of reduction of nox on the no2 levels in urban streets. Science of The Total Environment 189-190, 409 – 415 (1996), highway and Urban Pollution
16. Parajuli, A., Pojani, D.: Barriers to the pedestrianization of city centres: perspectives from the global north and the global south. Journal of Urban Design 23(1), 142–160 (2018)
17. Robinson, D.W.: The concept of noise pollution level. Journal of Occupational and Environmental Medicine 13(12), 602 (1971)
18. Sobková, L.F., Čertickỳ, M.: Urban mobility and influence factors: A case study of prague. WIT Transactions on The Built Environment 176, 207–217 (2017)
19. Soni, N., Soni, N.: Benefits of pedestrianization and warrants to pedestrianize an area. Land Use Policy 57, 139 – 150 (2016)
20. Steele, C.: A critical review of some traffic noise prediction models. Applied acoustics 62(3), 271–287 (2001)
21. Tobon, M., Jaramillo, J.P., Sarmiento, I.: Pedestrianization and semi-pedestrianization: A model for recovery public space in the medellín downtown. In: MOVICI-MOYCOT 2018: Joint Conference for Urban Mobility in the Smart City. pp. 1–7 (April 2018)
22. Toutouh, J., Arellano, J., Alba, E.: Bipred: A bilevel evolutionary algorithm for prediction in smart mobility. Sensors 18(12), 4123 (2018)
23. United Nations: World Urbanization Prospects: The 2018 Revision: key facts. https://population.un.org/wup/Publications/Files/WUP2018-KeyFacts.pdf. (2018), Accessed: 2019-07-07
24. Ward, S.V.: What did the germans ever do for us? a century of british learning about and imagining modern town planning. Planning Perspectives 25(2), 117–140 (2010)
25. Witten, I.H., Frank, E., Hall, M.A., Pal, C.J.: Data Mining: Practical machine learning tools and techniques. Morgan Kaufmann (2016)
26. World Health Organization: Ambient (outdoor) air quality and health. https://www.who.int/en/news-room/fact-sheets/detail/ambient-(outdoor)-air-quality-and-health (2018), Accessed: 2019-07-07

Planejamento estratégico do transporte de soja como suporte a efetivação das cidades inteligentes no Brasil

Vanessa de Almeida Guimarães[1,2], Gustav Carl Skroder[3], Glaydston Mattos Ribeiro[2], Pedro Henrique González Silva[4,5]

[1] Centro Federal de Educação Tecnológica Celso Suckow da Fonseca – Angra dos Reis/RJ[2] COPPE/UFRJ – Programa de Engenharia de Transportes, Rio de Janeiro/RJ
[3] POLI/UFRJ –Engenharia de Civil, Rio de Janeiro/RJ
[4] COPPE/UFRJ – Programa de Engenharia em Sistemas e Computação, Rio de Janeiro/RJ
[5]Centro Federal de Educação Tecnológica Celso Suckow da Fonseca – Maracanã/RJ (Departamento de Informática)

Abstract. O transporte de cargas pode impactar na efetividade do desenvolvimento de cidades inteligentes, caso não seja bem planejado. Mercadorias com fluxos internacionais, como a soja, podem causar congestionamentos nas áreas urbanas em que os portos estão instalados, impactando negativamente as dimensões econômicas (e.g. atrasos e multas), sociais (e.g. qualidade de vida da população) e ambientais (e.g. intensificação das emissões). Dessa forma, este trabalho tem como objetivo aplicar um modelo matemático de localização-alocação para determinar a localização ideal de centros de integração logística - CILs voltados para o transporte de soja. Entende-se que, ao localizar adequadamente estruturas que permitam intermodalidade, reduzir-se-ia o uso de transporte rodoviário substituindo-o por alternativas intermodais de menor impacto ambiental e que permitiriam a redução dos congestionamentos rodoviários nos centros urbanos sob influência portuária. Além disso, haveria otimização dos custos totais da rede, promovendo impactos econômicos positivos nas cadeias logística da soja. Para tanto, foram estabelecidos seis cenários variando parâmetros de entrada do modelo (como investimento e volume mínimo de movimentação). O modelo foi implementado na linguagem Mosel, usando o *solver Xpress IVE*, versão 1.24.24. Ao final, foi possível observar que o modelo aplicado pode ser suporte ao planejamento estratégico governamental (incluindo, aqui, o *design* de cidades inteligentes).

Keywords: smart cities, otimização, planejamento estratégico, soja

1 Introdução

O conceito de cidades inteligentes envolve o uso de tecnologia intensiva no *design* de cidades visando conectar pessoas, informações e elementos urbanos com o objetivo de desenvolver ambientes urbanos sustentáveis, competitivos e inovadores, melho-

rando a qualidade de vida da população (Bakici, Almirral e Wareham *et al*., 2013; Cunha *et al*. 2016).

Sabe-se que para uma cidade ser considerada "inteligente" diversos outros fatores, além do transporte, precisam ser considerados (como educação e governança). No entanto, o transporte de carga brasileiro lida com ineficiências estruturais que impactam negativamente tanto o setor econômico (competitividade de produtos, elevação do custo Brasil etc.), quanto o ambiental (este setor foi a principal fonte de emissão antrópica de CO_2 no ano de 2017, respondendo por 45,8% – EPE, 2018) e o social (diretamente – e.g. pelos congestionamentos – e indiretamente, por reflexos dos impactos ambientais – e.g. poluição aumenta os gastos públicos com o sistema único de saúde – e econômicos – a ineficiência reflete na empregabilidade e distribuição de renda, por exemplo).

O trabalho de Guimarães, Leal Junior e Pereira (2017) sobre portos, por exemplo, aborda os impactos econômicos, sociais e ambientais oriundos de instalações portuárias (que, por conceito, são centros de integração logística - CILs). Dessa forma, entende-se que o uso de modelos matemáticos de localização voltados para o transporte de carga pode auxiliar, ainda que indiretamente, no planejamento governamental e de políticas públicas que visem o desenvolvimento de *smart cities*.

Assim, o objetivo deste trabalho é determinar a localização ótima de centros de integração logística voltados para o transporte de soja a partir da aplicação modelo matemático de Guimarães (2015). Entende-se que a localização de facilidades, que permitam a integração modal e o uso de alternativas de maior capacidade, pode proporcionar melhorias nos planejamentos das cidades, redução de congestionamentos nas principais zonas portuárias voltadas para o escoamento de soja, dando suporte, assim, ao planejamento de *smart cities* no contexto brasileiro.

Escolheu-se aplicar o modelo a soja, tendo em vista a relevância deste produto na matriz econômica brasileira: de acordo com a Companhia Nacional de Abastecimento - CONAB, a soja foi responsável por 52% da produção total de grãos no Brasil na safra de 2017/18 e, com o aumento da produção na safra 2018/19, o país se tornou o maior produtor mundial de soja, ultrapassando os Estados Unidos (CONAB, 2018).

Já o contexto brasileiro se justifica pelo fato do custo logístico representar 12,3% do Produto Interno Bruto - PIB brasileiro, frente a um custo de 7,8% dos Estados Unidos (ILOS, 2017). Sendo que o transporte responde pela maior parcela deste custo (CNT, 2016), tendo consumido 6,8% do PIB no ano de 2015 (CNT, 2016) e 6,6% no ano de 2016 (ILOS, 2017). Além disso, o BNDES (2018) defende que a melhoria da infraestrutura logística é fator fundamental para recuperação da economia brasileira, tendo em vista seu impacto sistêmico nos demais setores, especialmente na indústria extrativa-mineral, agropecuária e de bebidas.

Assim, a partir desta seção, são apresentados: o modelo matemático de Guimarães (2015), a descrição do estudo, aplicação e discussão dos resultados, considerações finais, agradecimentos e referências.

2 Modelo matemático de Guimarães (2015)

Trata-se de um modelo de localização-alocação capacitado, multiproduto e multicamada (embora admitam-se fluxos diretos entre O/D, sem utilização das estruturas de integração logística), que busca otimizar os custos logísticos por meio da instalação de CILs que promovam a intermodalidade. Para tanto, adotam-se os seguintes pressupostos:

1) O CIL é uma estrutura simplificada que permite única e exclusivamente a transferência modal. Desta maneira, não há qualquer tipo de agregação de valor ao produto (seja transformação, embalagem, etiquetagem etc.);

2) Os CILs serão selecionados a partir de um conjunto de candidatos pré-definidos, com base em critérios estabelecidos de acordo com o estudo de caso. Assim, embora não haja nenhuma exigência de abertura (como nos modelos de p-mediana), há um número máximo, pré-fixado, de estruturas que poderão ser abertas;

3) O fluxo entre a zona de produção e consumo só será intermediado por um CIL, caso isto proporcione redução no custo total da rede. Ou seja, se a opção pelo transporte direto apresentar um custo menor do que àquele associado à utilização do CIL, opta-se pelo transporte direto (da origem para o destino final, sem passar pela estrutura de integração);

4) Se nenhum produtor for beneficiado pela instalação dos CIL com redução do custo total de transporte, o CIL não deverá ser aberto;

5) Há uma capacidade mínima estabelecida para abertura do CIL, visando assegurar a viabilidade econômica desta facilidade. Caso contrário, uma estrutura de integração poderia ser aberta para movimentar pequenos volumes (e.g. 2 toneladas), os quais poderiam não justificar o montante de recursos investido. Assim, um determinado CIL só será habilitado quando o volume total de carga atraída pela estrutura atingir (ou superar) a capacidade mínima;

6) De forma análoga, considera-se que cada CIL tem uma capacidade máxima de movimentação relacionada a limitações físicas/estruturais, visto que qualquer facilidade tem capacidade limitada. Assim, caso a quantidade movimentada alcance o limite máximo do CIL, nenhuma unidade adicional poderá ser enviada para esta estrutura;

7) Em relação ao fluxo direto, estabelece-se que um determinado produto pode ser enviado diretamente a um ponto de consumo, a partir do ponto de produção, por meio de um único modo. Já o fluxo que passa por um CIL precisa, obrigatoriamente, realizar, pelo menos, uma transferência modal.

Uma vez conhecidos os pressupostos que embasaram o desenvolvimento da proposta de Guimarães (2015), a Tabela 1 detalha os índices, parâmetros e variáveis que compõem este modelo. Salienta-se que o modelo de Guimarães (2015) é um refinamento do trabalho de Costa (2014), pois impõem o atendimento explícito das demandas par-a-par, tornando-o aderente a uma realidade econômica em que fornecedores de bens e serviços preocupam-se em atender clientes específicos e/ou a respeitar contratos já estabelecidos; e pode haver relação de confiança entre produtores e consumidores, não estando os clientes dispostos a ter sua demanda satisfeita por outros fornecedores (Guimarães et al, 2018).

Tabela 1: Conjuntos, índices, parâmetros e variáveis de decisão do modelo de Guimarães (2015)

Notação	Descrição
I	Conjunto de zonas de produção, onde i ∈ I
J	Conjunto de zonas de consume, onde j ∈ J
P	Conjunto de produtos, onde $p \in P$
K	Conjunto de candidates a CIL, onde $k \in K$
M_{pij}^{dir}	Conjunto de modos disponíveis para transporte direto do produto p ∈ P de um ponto de produção i ∈ I a um ponto de consumo j ∈ J
M_{pik}^{ent}	Conjunto de modos disponíveis para transporte do produto p ∈ P de um ponto de produção i ∈ I a um CIL k ∈ K
M_{pkj}^{sai}	Conjunto de modos disponíveis para transporte do produto p ∈ P de um CIL k ∈ K a um ponto de consumo j ∈ J
C_{pijm}^{dir}	Custo unitário de transportado produto p ∈ P de uma origem i ∈ I para um ponto de consumo j ∈ J por um modo de transporte m ∈ M_{pij}^{dir}
C_{pikm}^{ent}	Custo unitário de transporte do produto p ∈ P de uma origem i ∈ I para um CIL k ∈ K por um modo de transporte m ∈ M_{pik}^{ent}
C_{pkjm}^{sai}	Custo unitário de transporte do produto p ∈ P de um CIL k ∈ K para um ponto de consumo j ∈ J por um modo de transporte m ∈ M_{pkj}^{sai}
CT_{pkjm}^{sai}	Custo do transbordo do produto p ∈ P entre um CIL k ∈ K e um ponto de consumo j ∈ J para o modo de transporte m ∈ M_{pkj}^{sai}
g_{pk}	Custo fixo de utilização do candidato a CIL k ∈ K pelo produto p ∈ P
v_{pk}	Custo variável de utilização do candidato a CIL k ∈ K pelo produto p ∈ P
V_k^{min}	Volume mínimo para abertura do candidato a CIL k ∈ K
V_k^{max}	Capacidade máxima para abertura do candidato a CIL k ∈ K
P_{pi}	Oferta máxima do produto p ∈ P no ponto i ∈ I
d_{pj}	Demanda do produto p ∈ P na zona j ∈ J
x_{pijm}^{dir}	Volume do produto p ∈ P transportado diretamente entre o ponto i ∈ I e o ponto j ∈ J por um modo m ∈ M_{pi}^{dir}
x_{pikm}^{ent}	Volume do produto p ∈ P transportado entre o ponto i ∈ I e o candidato a CIL k ∈ K por um modo de transporte m ∈ M_{pi}^{ent}
x_{pkjm}^{sai}	Volume do produto p ∈ P transportado entre o candidato a CIL k ∈ K e o ponto j ∈ J por um modo de transporte m ∈ M_{pk}^{sai}
z_k	Binário que indica a abertura (assume 1) ou não (assume 0) do CIL k ∈ K
y_{pikj}	Volume de produto p ∈ P transportado de i ∈ I para j ∈ J que utiliza o candidato a CIL k ∈ K

Fonte: Adaptado de Guimarães (2015).

O modelo matemático de Guimarães (2015) está descrito a seguir:

Minimizar:

$$Min\ v(Guimarães2015) = \sum_{p\in P}\sum_{i\in I}\sum_{j\in J}\sum_{m\in M_{pij}^{dir}} C_{pijm}^{dir} x_{pijm}^{dir} + \sum_{p\in P}\sum_{i\in I}\sum_{k\in K}\sum_{m\in M_{pik}^{ent}} C_{pikm}^{ent} x_{pikm}^{ent} + \sum_{p\in P}\sum_{k\in K}\left(g_{pk} z_k + v_{pk}\sum_{i\in I}\sum_{m\in M_{pkj}^{sai}} x_{pkjm}^{sai}\right) + \sum_{p\in P}\sum_{k\in K}\sum_{j\in J}\sum_{m\in M_{pkj}^{sai}} \left(CT_{pkjm}^{sai} + C_{pkjm}^{sai}\right) x_{pkjm}^{sai} \quad (1)$$

Sujeito a:

$$\sum_{m\in M_{pij}^{dir}} x_{pijm}^{dir} + \sum_{k\in K} y_{pikj} = d_{pij} \qquad \forall\, p\in P, i\in I, j\in J \quad (2)$$

$$v_k^{min} z_k \le \sum_{p\in P}\sum_{i\in I}\sum_{m\in M_{pik}^{ent}} x_{pikm}^{ent} \le v_k^{max} z_k \qquad \forall\, k\in K \quad (3)$$

$$\sum_{j\in J} y_{pikj} = \sum_{m\in M_{pik}^{ent}} x_{pikm}^{ent} \qquad \forall\, p\in P, k\in K, i\in I \quad (4)$$

$$\sum_{i\in I} y_{pikj} = \sum_{m\in M_{pkj}^{sai}} x_{pkjm}^{sai} \qquad \forall\, p\in P, k\in K, j\in J \quad (5)$$

$$x_{pijm}^{dir} \ge 0 \qquad \forall\, p\in P, i\in I,\ j\in J, m\in M_{pij}^{dir} \quad (6)$$

$$x_{pikm}^{ent} \ge 0 \qquad \forall\, p\in P, i\in I, k\in K, m\in M_{pik}^{ent} \quad (7)$$

$$x_{pkjm}^{sai} \ge 0 \qquad \forall\, p\in P, k\in K,\ j\in J, m\in M_{pkj}^{sai} \quad (8)$$

$$y_{pikj} \ge 0 \qquad \forall\, p\in P,\ i\in I, k\in K,\ j\in J \quad (9)$$

$$z_k \in \{0,1\} \qquad \forall\, k\in K \quad (10)$$

A Função Objetivo (1) busca minimizar o custo total do transporte na rede, alocando os fluxos para os CILs que forem abertos ou diretamente para as zonas de demanda. Consideram os custos operacionais (fixos e variáveis) destas estruturas e seus custos de transbordo. As Restrições (2) garantem que a demanda total de cada zona de consumo seja atendida somando-se o fluxo transportado diretamente de uma zona $i \in I$ com aquele que passou por um CIL $k \in K$. Garante, ainda, que as demandas par-a-par sejam respeitadas independente do CIL eventualmente utilizado.

As Restrições (3) consideram os volumes mínimos e capacidade máxima de utilização de um candidato a CIL, impactando diretamente na decisão de abri-los ou não. As Restrições (4) impõem que o volume total de um produto que deixa uma zona de produção e se destina a uma zona de consumo passando por um CIL seja exatamente igual ao volume total do produto que entra no CIL tendo como origem a zona de produção. As Restrições (5) complementam as Restrições (4) e estão associadas aos flu-

xos de saída. As demais restrições estão relacionadas ao domínio de definição das variáveis.

Existem, ainda, duas restrições que podem ser adicionadas ao modelo: Restrição (11), que limita os investimentos na abertura de CILs caso haja restrição de orçamento; e Restrição (12), caso deseja-se definir uma quantidade máxima p de CILs abertos.

$$\sum_{k \in K} f_k z_k \leq F \tag{11}$$

$$\sum_{k \in K} z_k \leq p \tag{12}$$

Onde: f_k: valor de investimento para abertura de um CIL; F: valor máximo disponível para o investimento; e, p: quantidade de CILs a serem abertos (problema semelhante ao p-medianas).

3 Descrição do Estudo

Os dados foram obtidos a partir da base de dados georreferenciada do Plano Nacional de Logística e Transporte - PNLT prevista para o ano de 2031, devido a sua relevância no planejamento de transporte e logística no Brasil. O zoneamento (pontos de produção e consumo) é constituído por 558 zonas dentro do território nacional e uma zona representando o exterior, totalizando 559 zonas, denominadas de microrregiões. Foram pré-selecionadas 80 microrregiões (Figura 1) que pudessem receber as instalações de um CIL (conhecidas como microrregiões candidatas). Tais regiões foram escolhidas por disporem de entroncamentos modais, ou seja, locais onde se possa efetivamente realizar o transbordo e a intermodalidade.

A rede multimodal do PNLT sugerida para o ano 2031 já considera os projetos de infraestrutura previstos no plano, conforme mostra a Figura 2. Arbitrou-se que, no transporte direto, a opção a ser usada seria totalmente rodoviária. Já no transporte por meio de um CIL, a carga seria destinada do ponto de produção ao CIL pelo modo rodoviário e, ao ser consolidada, partiria desta facilidade para o ponto de destino por meio de uma opção intermodal. A matriz de produção e consumo da soja utilizada neste estudo, também proveniente do PNLT, representa seus fluxos de produção e consumo projetados para o ano 2031, com base nas expectativas de crescimento dos mercados interno e externo e no aumento de produtividade.

As matrizes de custo entre os pares de produção e consumo e as informações de custos fixos e variáveis dos CILs foram obtidas em Guimarães (2015), onde o custo variável é de R$ 8,17/tonelada que realiza transbordo no CIL. Não foi considerada capacidade máxima para que se pudessem estabelecer, em um primeiro momento, todas as possíveis zonas produtoras que escoariam suas produções por CILs.

Para que a economia obtida com a abertura de CILs possa ser avaliada, é necessário conhecer o Cenário 0. Neste cenário, não há abertura de CILs (a Restrição (12) considera $p = 0$), ou seja, é o pior caso utilizado para efeitos comparativos, pois representa o custo em 2031 do escoamento de soja se não houverem os devidos investimentos na otimização da rede logística brasileira (e todo o impacto que isso pode

causar no planejamento e operacionalização de *smart cities*). Assim, verificou-se que este custo seria de R$ 7,3 bilhões de reais. Partindo deste princípio, cinco cenários foram estabelecidos:

Cenário 1: o CIL possui um custo simbólico de abertura de R$1,00, dada sua importância estratégica na concepção da malha de transportes do país e não possui volume mínimo para abertura;

Cenário 2: impõe ao Cenário 1 o volume mínimo para abertura de um CIL equivalente a 1 milhão de toneladas. Este valor foi arbitrado em Costa (2014) e Guimarães (2015).

Cenários 3: considera que o custo para abertura de um CIL pode variar de 30 e a 100 milhões de reais, não havendo volume mínimo para abertura de uma facilidade;

Cenário 4: impõem ao Cenário 3 o volume mínimo de 1 milhão de toneladas para abertura de um CIL; e

Cenário 5: Consiste no Cenário 2, porém o número de CILs abertos foi pré-fixado em valores que variam de 1 a 11.

Fig. 1. Microrregiões candidatas à instalação de um CIL. Fonte: Elaboração própria (2018)

Fig. 2. Rede de modelagem de transportes do PNLT – nacional. Fonte: MT, MD (2007).

4 Aplicação e discussão dos resultados

O modelo implementado na linguagem Mosel (FICO, 2013) a partir dos parâmetros aos parâmetros apresentados na seção anterior (base georreferenciada do PNLT para o horizonte de 2031). No processo de solução de cada um dos cenários propostos, utilizou-se o *solver Xpress IVE*, versão 1.24.24, em uma máquina com *Windows 10*, com processador *Intel® Core™i7* CPU@3,40GHz e 12 GB de RAM instalada. Os cená-

rios levaram aproximadamente 30 minutos para serem solucionados e os resultados foram exibidos com auxílio de mapas que foram produzidos no *software* TransCAD.

As microrregiões habilitadas nos Cenários 1 e 2 podem ser observadas nas Figuras 3 e 4, respectivamente. Nota-se que, no primeiro caso 68 microrregiões (das 80 candidatas) foram indicadas para abertura de CILs. Este valor reduziu para 37, quando se impôs um limitante inferior ao volume movimentado pelas estruturas. Isso significa que, no Cenário 1, quase metade das facilidades foram abertas para movimentar menos de 1 milhão de toneladas de soja. Entende-se que isso pode não ser economicamente viável, tendo em vista que as instalações têm custos de abertura. Mesmo que nestes cenários o custo tenha sido simbólico (equivalente a R$ 1,00), tendo em vista que o CIL seria de interesse governamental e este iria financiar a implementação das estruturas – sabe-se que, muitas vezes, são feitas parcerias público-privadas ou financiamentos públicos para construção de tais obras e, as mesmas, precisam atrair quantidades suficientes que viabilizem o retorno do projeto.

Fig3. CILs habilitados no Cenário 1

Fig4. CILs habilitados no Cenário 2

Quanto aos custos de implantação dos CILs, o custo total no Cenário 1 foi de 4,38 bilhões de reais, aumentando para 4,47 bilhões de reais no Cenário 2. Este aumento era esperado tendo em vista que, ao não permitir a abertura de CILs com movimentação inferior a 1 milhão de toneladas, o custo com transporte aumentaria uma vez que o transporte intermodal por meio de um CIL seria substituído pelo transporte direto, feito unicamente de maneira rodoviária.

Os resultados dos Cenários 3 por sua vez, estão apresentados nas Figuras 5 e 6. Como era de se esperar, ao impor custos de instalação dos CILs (investimento inicial). O número de facilidades habilitadas se reduz para 11 regiões selecionadas (ao custo de 5,10 bilhões) quando o investimento é de R$ 30 milhões; caindo para 6 CILs (ao custo de 5,67 bilhões) quando o investimento é equivalente a R$ 30 milhões.

Fig5. CILs habilitados no Cenário 3 (investimento igual a R$ 30 milhões)

Fig6. CILs habilitados no Cenário 3 (investimento igual a R$ 100 milhões)

Adicionalmente, a Tabela 2 faz um comparativo entre as regiões habilitadas quando o investimento varia de R$ 30 milhões a R$ 100 milhões, em intervalos de R$ 10 milhões. Verifica-se que apenas quatro microrregiões permanecem indicadas como ótimas, independente do custo de implantação dos CILs: Gerais de Balsas, Cruz Alta, Aripuanã e Alto Teles Pires.

De maneira análoga, há regiões habilitadas apenas quando o investimento pequeno, como Guarapuva. Anápolis, por sua vez, só se viabiliza quando o custo de instalação é de, pelo menos, 60 milhões (pois, provavelmente, concentra fluxos de outras regiões e CILs que deixaram de ser abertos).

Tabela 2. Regiões habilitadas considerando diferentes valores de investimento

	Investimento (R$ milhões)							
Regiões habilitadas	30	40	50	60	70	80	90	100
Gerais de Balsas (MA)	X	X	X	X	X	X	X	X
Maringá (PR)	X	X	X	X	X	X		X
Toledo (PR)	X	X	X				X	
Guarapuava (PR)	X							
Cruz Alta (RS)	X	X	X	X	X	X	X	X
Dourados (MS)	X	X	X	X				
Aripuanã (MT)	X	X	X	X	X	X	X	X
Alto Teles Pires (MT)	X	X	X	X	X	X	X	X
Cuiabá (MT)	X	X	X	X	X	X		
Anápolis (GO)				X	X	X	X	X
Entorno de Brasília (GO)	X	X	X					
Sudoeste de Goiás (GO)	X	X	X					

Nota: as siglas se referem aos estados brasileiros, sendo: MA – Maranhão, MT – Mato Grosso, GO – Goiás, PR – Paraná e RS – Rio Grande do Sul.

Em relação ao Cenário 4 esclarecem-se que foram habilitadas as mesma microrregiões ao mesmo custo total do encontrado no Cenário 3. Isso significa que o custo de abertura de CILs é um fator determinante na localização das facilidades, já impondo, de maneira indireta, que a abertura só seria viável para um volume de movimentação maior, cuja economia da rede proporcionada pelo uso de CILs superasse o investimento. Dessa forma, ainda que no Cenário 3 não houvesse sido imposto nenhum limitante inferior para a movimentação nos CILs, o modelo matemático indicou a abertura apenas de estruturas que atraísse volume superior ou igual a 1 milhão de toneladas.

Por fim, os resultados obtidos no Cenário 5 podem ser observados na Tabela 3. Este cenário avalia como a rede se comportaria caso o governo definisse a priori, por meio de alguma política pública visando estabelecer *smart cities* ou por conta de restrições de recurso, o número de CILs a serem abertos. Vale ressaltar que neste o custo de abertura volta a ser simbólico (igual a R$ 1).

Tabela 3 - Custos no Cenário 5

Quantidade de CILs (p)	Custo global (R$ bilhões)	Δ Custo	Regiões ótimas
1	R$ 6,53	-	Anápolis
2	R$ 5,92	-9,46%	Anápolis e Alto Teles Pires
3	R$ 5,67	-13,17%	Anápolis, Alto Teles Pires e Gerais das Balsas
4	R$ 5,45	-16,53%	Anápolis, Alto Teles Pires, Gerais das Balsas e Aripuanã
5	R$ 5,24	-19,75%	Anápolis, Alto Teles Pires, Gerais das Balsas, Aripuanã e Guarapuava
6	R$ 5,07	-22,36%	Anápolis, Alto Teles Pires, Aripuanã, Gerais das Balsas, Cruz Alta e Maringá
7	R$ 4,98	-23,72%	Anápolis, Alto Teles Pires, Aripuanã, Gerais das Balsas, Cruz Alta, Maringá e Cuiabá
8	R$ 4,92	-24,78%	Anápolis, Alto Teles Pires, Aripuanã, Gerais das Balsas, Cruz Alta, Maringá, Cuiabá e Dourados
9	R$ 4,88	-25,29%	Alto Teles Pires, Aripuanã, Gerais das Balsas, Cruz Alta, Maringá, Cuiabá, Dourados, Entorno de Brasília e Sudoeste de Goiás
10	R$ 4,80	-26,48%	Alto Teles Pires, Aripuanã, Gerais das Balsas, Cruz Alta, Maringá, Cuiabá, Dourados, Entorno de Brasília, Sudoeste de Goiás e Toledo
11	R$ 4,77	-27,05%	Alto Teles Pires, Aripuanã, Gerais das Balsas, Cruz Alta, Maringá, Cuiabá, Dourados, Entorno de Brasília, Sudoeste de Goiás, Toledo e Guarapuava

Fonte: Elaboração própria

No que diz respeito às regiões habilitadas, verifica-se que até cinco CILs, mantém-se a configuração anterior, adicionando uma nova região. Em p = 6, as regiões divergem das anteriores. Anápolis se mantém habilitada até p = 8. Entorno de Brasília e Sudoeste de Goiás só são indicadas a partir de p = 8, enquanto Toledo só recebe CILs a partir de p = 10. Guarapuava, por sua vez, é habilitada em dois momentos específicos: p = 5 e p = 11. Ressalta-se que a frequência em que determinada região é indicada para abertura pode ser utilizada para a criação de um plano de investimentos, incluindo prioridades de implantação (para casos específicos em que se adota a restrição semelhante à p-mediana).

Quanto aos custos totais, observa-se redução conforme o número de CILs indicados para abertura aumenta, variando entre -9,46% e – 27,05%. Salienta-se que não foi avaliado o ponto de inflexão, em que a abertura de CILs adicionais proporcionaria aumento nos custos de transporte, sendo, portanto, não ideal. Contudo, tendo em vista que o número de CILs ótimos no Cenário 2 é equivalente a 37 facilidades, pode-se afirmar que a partir desta quantidade, há um distanciamento do custo ótimo. Por fim, a Tabela 4 sintetiza os valores obtidos em todos os cenários.

Destaca-se que, analisando a variação nos custos globais em relação ao número de CILs abertos, observa-se que diferença de custo quando 11 CILs (Cenário 5, p = 11) e 37 CILs (Cenário 2, p livre) estão em operação é muito baixa para que se justifique a construção e operação de novos 26 CILs. Quando se observa apenas o custo de transporte, essa diferença é quase irrisória.

Avaliando especificamente os Cenários 3 e 4, realize-se a mesma constatação quando 6 ou 11 CILs estão abertos. Tendo em vista que a diferença nos custos de transporte está na ordem de R$ 310 milhões, o governo deveria avaliar se abertura de 5 CILs adicionais seria viável ou se o recursos deveria ser destinado a viabilização de outras tecnologias e políticas públicas direcionadas para o *design* de *smart cities*.

Ainda, ressalta-se que, do ponto de vista prático, desconsiderar um volume mínimo que garanta a viabilidade econômica de cada CIL (como foi realizado no Cenário 1), também não é realistico. Além disso, observa-se que a variação dos custos global não é tão inferior ao Cenário 2, mas são habilitados quase o dobro de CILs. A Figura 7 destaca a desaceleração na variação dos custos e economias gerados a partir do número crescente de CILs sendo operados, caracterizado pela horizontalidade da curva.

Com base na Figura 7, pode-se constatar que a variação na economia sofre uma desaceleração a partir do 6º CIL aberto, considerando apenas o custo com transporte (ignorando, portanto, o custo de abertura das estruturas). Salienta-se que, ao se adotar o valor de investimento equivalente a R$ 100 milhões (maior valor investigado nos cenários), apenas 6 CILs foram indicados para abertura. Isso sugere que, em um eventual plano estratégico, p = 6 poderia ser um ponto de partida para o planejamento estratégico governamental.

Tabela 4 - Resumo dos resultados

Cenários	Quantidade de CILs (p)	Custo global (R$ bilhões)	Investimento no CIL (R$)	Custo logístico (R$ bilhões)[1]	Custo com transporte (R$ bilhões)	Volume transportado diretamente (t)	Volume transportado por meio de um CIL (t)
C0	0	7,30	-	7,30	7,30	85.881.600	-
C1	68	4,38	1,00	4,38	3,91	28.887.800	56.993.800
C2	37	4,47	1,00	4,47	4,00	28.618.500	57.263.100
C3	11	5,10	30 milhões	4,77	4,34	33.255.900	52.625.700
	10	5,20	40 milhões	4,80	4,38	33.863.200	52.018.400
	10	5,30	50 milhões	4,80	4,38	33.863.200	52.018.400
	8	5,40	60 milhões	4,92	4,51	35.197.200	50.684.400
	7	5,47	70 milhões	4,98	4,57	35.869.100	50.012.500
	7	5,55	80 milhões	4,99	4,58	35.965.900	49.915.700
	6	5,62	90 milhões	5,08	4,69	38.488.400	47.393.200
	6	5,67	100 milhões	5,07	4,67	36.374.500	49.507.100
C4	11	5,10	30 milhões	4,77	4,34	33.255.900	52.625.700
	10	5,20	40 milhões	4,80	4,38	33.863.200	52.018.400
	10	5,30	50 milhões	4,80	4,38	33.863.200	52.018.400
	8	5,40	60 milhões	4,92	4,51	35.197.200	50.684.400
	7	5,47	70 milhões	4,98	4,57	35.869.100	50.012.500
	7	5,55	80 milhões	4,99	4,58	35.965.900	49.915.700
	6	5,62	90 milhões	5,08	4,69	38.488.400	47.393.200
	6	5,67	100 milhões	5,07	4,67	36.374.500	49.507.100

Tabela 4 - Resumo dos resultados

Cenários	Quantidade de CILs (p)	Custo global (R$ bilhões)	Investimento no CIL (R$)	Custo logístico (R$ bilhões)[1]	Custo com transporte (R$ bilhões)	Volume transportado diretamente (t)	Volume transportado por meio de um CIL (t)
C5	11	4,77	1,00	4,77	4,34	33.255.900	52.625.700
	10	4,80	1,00	4,80	4,38	33.863.200	52.018.400
	9	4,88	1,00	4,88	4,46	34.549.100	51.332.500
	8	4,92	1,00	4,92	4,51	35.197.200	50.684.400
	7	4,98	1,00	4,98	4,57	35.869.100	50.012.500
	6	5,07	1,00	5,07	4,66	36.169.100	49.712.500
	5	5,24	1,00	5,24	4,86	39.643.200	46.238.400
	4	5,45	1,00	5,45	5,15	49.652.800	36.228.800
	3	5,67	1,00	5,67	5,38	50.054.700	35.826.900
	2	5,92	1,00	5,92	5,63	50.272.000	35.609.600
	1	6,53	1,00	6,53	6,27	54.511.000	31.370.600
	0	7,30	-	7,30	7,30	85.881.600	-

Nota: (1) São os custos globais descontados os investimentos para abertura dos CILs.
Fonte: Elaboração própria

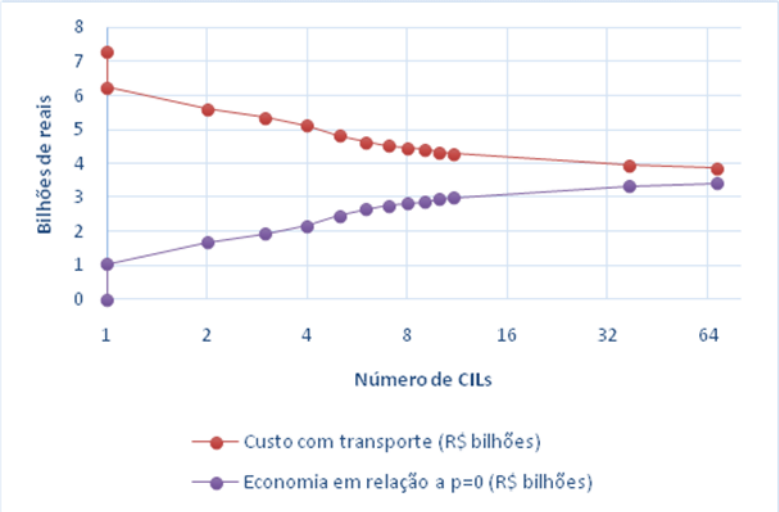

Fig7. Número de CILs habilitados versus custos e economias registradas (gráfico logarítmico - base 2)

Fonte: Elaboração própria

Por fim, cabe salientar que se entende que diversos outros fatores são fundamentais para que se desenvolvam "cidades inteligentes". No entanto, o transporte pode ser um fator chave, especialmente no contexto brasileiro: país de proporções continenais, cuja matriz de transporte é majoritariamente rodoviária – tanto para carga, quanto para passageiros – MT, 2007, 2009 e 2019, que sofre com as ineficiências logísticas (Ilos, 2017 e Fundação Dom Cabral, 2018).

Considerações finais

Ao longo deste trabalho foi possível observar como o planejamento estratégico governamental do setor de transportes pode impactar na efetivação de cidades inteligentes. Embora haja escassez de literatura sobre o tema, entende-se que o transporte é fundamental para circulação de pessoas e mercadorias. Dessa maneira, avaliar estratégias para diminuir o impacto do transporte no *design* e operação das áreas urbanas torna-se fundamental para o desenvolvimento de cidades inteligentes e integradas.

Pode-se afirmar que os objetivos foram atingidos uma vez que foi determinar a localização ótima de centros de integração logística voltados para o transporte de soja a partir da aplicação modelo matemático de Guimarães (2015) para os diferentes cenários desenvolvidos. Além disso, as discussões apresentadas sobre custos e número de estruturas abertas podem auxiliar na definição de políticas públicas e da distribuição dos recursos entre projetos de transporte (ex. que facilitem a mobilidade e reduzam os congestionamentos) e demais dimensões que compõem uma cidade inteligente.

Como limitação, esclarece-se que os resultados são altamente dependentes da base de dados utilizadas e que a última atualização do PNLT foi feita no ano de 2031. Não

foram encontrados planos governamentais mais recentes com as mesmas características (especialmente o fomento à intermodalidade) nem base de dados disponíveis para atualização dos parâmetros de entrada do modelo.

Como sugestão para novos estudos, recomenda-se a adoção de modelos matemáticos de localização sustentáveis ou, pelo menos, que incorporem a dimensão ambiental, tendo em vista a dificuldade em mensurar a dimensão social e a escassez de literatura apresentada em Guimarães (2018) e Guimarães, Ribeiro e Azevedo-Ferreira (2018).

Agradecimentos

Os autores agradecem à Capes pela bolsa de doutorado concedida, ao CEFET/RJ e ao projeto “Ciudades Inteligentes, totalmente integrales, eficiente y sostenibles (CITIES), n. de processo: 518RT0557 pelo fomento.

Referências

1. Bakıcı, T., Almirall, E., Wareham, J.A smart city initiative: the case of Barcelona, *J. Knowl. Econ.*, vol. 4, no. 2, pp. 135–148, 2013.
2. Cunha, M. A., Przeybilovicz, E., Macaya, J. F. M., dos Santos, F. B. P.. Smart cities: transformação digital de cidades. Programa Gestão Pública e Cidadania, 2016.
3. Empresa de Pesquisa Energética - EPE. Balanço Energético Nacional 2018: Relatório Síntese: ano base 2017. Relatório Técnico, 2018
4. Guimarães, V. A.; Leal Junior, I. C.; Pereira, N. N. Conjunto de indicadores para avaliação do desempenho sustentável em portos. Agência Nacional de Transporte Aquaviário - Prêmio Antaq de sustentabilidade Aquaviária, Brasília, 2017.
5. CONAB, 2018, Acompanhamento da safra brasileira de grãos 2018/19 - Primeiro levantamento, v. 6, n. 1. Brasília.
6. CNT. Custo logístico consome 12,7% do PIB do Brasil, Confederação Nacional dos Transportes, 2016.
7. ILOS. Brochura - Panorama ILOS Custos Logísticos no Brasil. Relatório Técnico, 2014.
8. BNDES. Panoramas setoriais 2030: desafios e oportunidades para o Brasil. Rio de Janeiro: BNDES, 2017.
9. COSTA, M.B.B., Utilização de modelo de localização-alocação para identificação de zoneamento logístico integrado ao planejamento estratégico de transportes. [Tese]. COPPE/ Universidade Federal do Rio de Janeiro (UFRJ).
10. GUIMARÃES, V.A., 2015,Modelagem matemática para localização-alocação de centros de integração logística considerando as demandas par-a-par. [Dissertação]. COPPE/ Universidade Federal do Rio de Janeiro (UFRJ)
11. Ministério dos Transportes – MT. Plano Nacional de Logística e Transportes. Brasília, 2007, 2009 e 2012.
12. Guimarães, V. A. Localização-alocação de centros de integração logística considerando critérios econômicos e ambientais. Qualificação de doutorado em Engenharia de Transportes, 2018.
13. Guimarães, V. A.; Ribeiro, G. M. ; Azevedo – Ferreira. Mapping of the Brazilian scientific publication on facility location. pesquisa operacional (impresso), v. 38, p. 307-330, 2018.

LoRa-based IoT Data Monitoring and Collecting Platform

Andres Felipe Fuentes[0000−0003−4687−9316] and Eugenio Tamura[0000−0002−1718−1691]

Universidad Libre Seccional Cali – Cali. Carrera 109 No. 22-00, Cali, Colombia
Pontificia Universidad Javeriana – Cali. Calle 18 No 118-250, Cali, Colombia
andresf.fuentesv@unilibre.edu.co, tek@javerianacali.edu.co

Abstract. IoT (Internet of Things) refers to an integration concept of different communication systems used for connecting heterogeneous devices with constraints on processing, storage capabilities and power consumption to the Internet, with the purpose of data collecting for analysis and decision making about the measurements of data collected. This new paradigm can be applied in different fields to wirelessly measure variables through mobile devices, laptops and wireless devices having in mind restrictions in terms of battery lifetime, capacity, and cost. This paper describes the implementation of a flexible and low-cost monitoring and data collecting platform using sensors based on open hardware such as Arduino, interconnected through a LoRa network and a cloud-based data storage system developed using open source code. The main objective is to quickly collect different types of variables based on a flexible monitoring and collecting platform adaptable to different types of sensors which could be used in both rural and urban areas in applications that require long-range transmission and low energy consumption. In the future, research on the analysis of performance and improvement solutions will be carried out, as well as the use of other types of devices and protocols in order to compare performance and expand the field of implementation of the proposed platform.

Keywords: LoRa WAN · Wireless Sensor Networks (WSN) · Internet of Things (IoT) · Monitoring System · Web Services

1 Introduction

The fast development of IoT and WSN applications and its associated growth of connected devices, which is predicted to be in the order of billions for the coming years [1], make necessary to take advantage of flexible and scalable technologies that allow collection and storage of data from devices like sensors, that take information from the real world and send it to repositories for further processing, analysis and/or identification of patterns for making smart decisions in real-time or according to the required application.

The application scenarios of IoT technologies include smart cities, smart agriculture, pollution monitoring, manufacturing automation, remote health care,

and more [2]. These kind of applications demands a platform that allows the interconnection of devices and systems for collecting data from different types of sensors considering specific requirements such as long-range, low data rate, low energy consumption, and cost-effectiveness. Short-range radio technologies (e.g., ZigBee, Bluetooth) are not adapted for long-range transmission. The cellular communications (e.g., 2G, 3G, and 4G) can provide larger coverage, but energy efficiency is low. Therefore, in this scenario, Low Power Wide Area Network (LPWAN) characteristics offer a solution adaptable to the IoT applications requirements [3]. LPWAN is increasingly gaining popularity in industrial and research communities because of its low power, long-range, and low-cost communication characteristics. It provides long-range communication up to 1040 km in rural zones and 15 km in urban zones [4]. An LPWAN example is LoRa, a wireless communication technology for long-range applications, whose use is rapidly increasing and could be considered a complement of Wi-Fi, Bluetooth, and Cellular.

In addition to the above, for IoT applications there exist different types of platforms for the interconnection of devices, and different types of protocols such as Constrained Application Protocol (CoAP) or Message Queue Telemetry Transport (MQTT) are used as well. These platforms have data acquisition and analytic components, device management components, integration components, and security components [5] [6].

Consequently, when WSN are integrated with platforms of this type, it is necessary to identify the different layers that make up these architectures, classifying the components to determine the options that better fit the requirements of the problem, including the cost and a balance between performance, latency, energy efficiency, scalability, and implementation complexity.

Therefore, in order to understand how these platforms work, it becomes necessary to identify the different blocks that compose them. This paper analyzes the main components of an IoT platform including Sensing component, Communication component, Computation and Cloud component, and Services and Applications components [7].

Once the different components of an IoT platform are analyzed, a platform based on open source components is proposed. Using open hardware devices and using open source software allows faster combination of new integrated IoT solutions towards the development and implementation of different kind of applications [8]. The platform will be designed and implemented using the LoRa protocol[9] for communication between devices; also open hardware devices like Arduino are used as sensor devices. Besides, the data collection and storage platform is also based on open-source software, i.e., PHP and MySQL[10]. Thus, the integration of these components offer a low-cost platform for the quick development of IoT applications for data acquisition and can be adapted for use in applications like smart farming in rural areas where neither cellular coverage nor other networks are available.

2 Related Work

Since IoT has become a subject of research and development, new fields of application for domains such as health, mobility, agriculture or smart cities [11] [12] have been increasing in an exponential manner. Hence, the demand for deploying these kind of systems has being grown lately. This trend implies a faster yet robust development of WSN-based systems in scenarios where different needs are constrained by hardware and software resources [13].

Shinde and Bhagat presented a paper on Industrial Process Monitoring Using IoT. In this paper, a basic platform of IoT is presented through which an industrial monitoring system is implemented using industry-standard protocols on IoT modules, and data conversion mechanisms for different industrial applications, which can also be used for monitoring different real-time applications in industries according to the requirements as well. The principal advantages of using a specific platform were modularity in system, scalability, adaptability, and ease of maintenance [14].

A LoRa-based renewable energy monitoring system is described by Choi, Jeong, and Park. This system is developed using open hardware and an overall platform of the implemented energy IoT monitoring system is showed, focusing on low-cost and quick- construction. The platform shown in this work could be adapted for different applications according to the needs [15].

On the other hand, works like [16] and [17] expose the development of IoT projects based on LoRa, where a specific platform is designed for each project. Both works expose the relevance of a platform for the development of IoT applications.

In the reviewed papers, the use of different kind of open hardware and open software, including wireless communication technologies such as LoRa, is frequent. Also is notorious that each project includes a platform scheme that classifies the functional structure of the hardware, software, and protocols used, as it becomes a fundamental aspect for understanding the IoT applications developed.

3 IoT Platform Components

An IoT platform is an integrated service that offers the necessary technologies to connect heterogeneous devices, such as sensors or actuators, to the Internet. Through an IoT platform, it is possible to interconnect several devices simultaneously, collect the information that these devices generate and manage each one of them.

In order to understand an IoT platform, it can be expressed in several layers such as (1) sensing layer, (2) communication layer, (3) computation and cloud layer, and (4) services and applications layer [5].

Sensing Layer. Different types of sensors, meters, actuators, and controllers are connected in this layer. The node sensors collect data including temperature, humidity, lightness, energy consumption. The controllers and actuators execute actions to generate some kind of effect on a process.

Communication Layer. This layer contains the IoT communication protocols for sending and receiving data. The different IoT devices use communication technologies such as Wi-Fi, ZigBee, NFC, BLE, LTE, LoRa, SigFox or NB-IoT. Usually, in a WSN configuration, the sensors collect the data and send it to a device configured as a gateway which sends the collected data to the Internet.

Computation and Cloud Layer. This layer stores and processes the raw data collected by the sensors. The Computation and Cloud Layer represents the computing and processing capacity of the IoT platform and interacts with the connected devices and the different data processing applications.

Services and Applications Layer. It has the function of exposing the different indicators resulting from the processing, analysis, and diagnosis of the data collected; it also performs as the user interface for monitoring, controlling and feedback data to WSN through the Communication Layer.

4 LoRa-based IoT Data Platform Development

Thus, having in mind the different layers exposed above as components of an IoT platform, a design for the development of a LoRa-based IoT Data Platform, the main objective of this work, is proposed in Figure 1. The proposed platform includes a layer that integrates the Sensing Layer and the Communication Layer, which is called the *Front Layer*. The Computation and Cloud Layer and the Services and Applications Layer, are integrated into a layer called *Back Layer*.

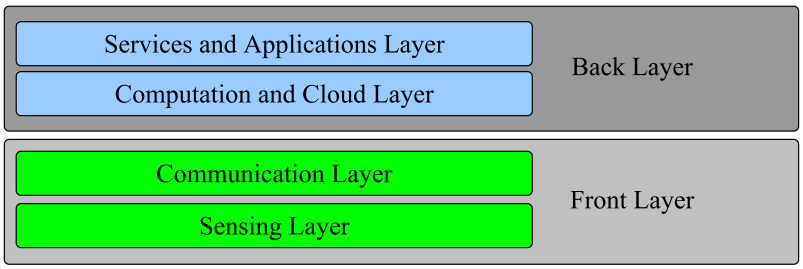

Fig. 1. Proposal of layers for an IoT Platform layer-based design [5]

Figure 2 depicts a diagram with a more detailed view of the components of the LoRa-based IoT Platform proposed in this paper.

For the implementation of the Front Layer, nodes that enable integration with sensors modules and include a LoRa radio (LoRa-Nodes in the following) are used. On the other hand, a gateway (LoRa-Gateway in the following) is

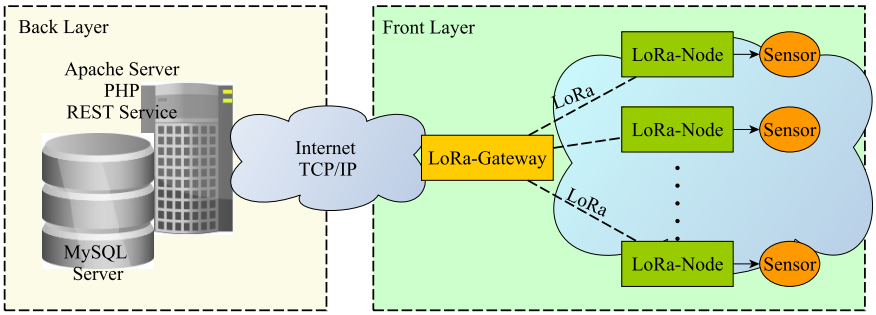

Fig. 2. Proposed LoRa-based IoT Platform

used to receive the data from LoRa-Nodes in order to send it to the Back Layer through the Internet using a TCP/IP stack.

The Back Layer, receives the data from the Front Layer and stores it in a Web Server and the data is exposed to the final users through a web application.

The description of the technologies chosen for the development of the IoT platform proposed in Figure 2 are described below, indicating the advantages they offer regarding IoT applications, including battery efficiency, scalability, coverage, range, deployment, and cost.

LoRaWAN. LoRaWAN is an open standard communication solution, it is relatively new and became the focus of several research centers across the world. LoRa (Long Range) is a modulation technique that enables the long-range transfer of information with a low transfer rate [18].

A LoRaWAN network (Long Range Network Protocol) is a Low Power Wide Area Network (LPWAN) standard, based on battery-powered devices including bidirectional communication. The LoRaWAN specification ensures high interoperability between IoT devices, without the need for complex implementations [19].

LoRaWAN technology advantages are [20]:

1. Uses the unlicensed ISM frequency band (868 MHz in Europe, 915 MHz in North America, and 433 MHz in Asia).
2. Range 5 km (urban), 20 km (rural).
3. It is scalable.
4. It supports bi-directional communication provided by the Chirp Spread Spectrum (CSS).
5. Provides a high level of security due to encryption algorithms.
6. Maximum data rate 50 Kbps.

LoRa implements six spreading factors (SF7 to SF12) to adapt the data rate and range compensation. A higher spreading factor allows a longer range at the

expense of lower data rate, and vice versa. The LoRa data rate is between 300 bps and 50 kbps depending on the spreading factor and channel bandwidth [3].

LoRa devices implement a sleep mode since most of the time they do not need to operate, thus increasing the battery life.

When comparing LoRa with other LPWAN technologies like SigFox or NB-IoT, each technology has advantages for IoT applications. Sigfox and LoRa offer lower-cost devices, with very long-range (high coverage), and very long battery lifetime. NB-IoT offer very low latency and high quality of service [3]. However, LoRa is the lower-cost device, with very long-range (high coverage) and very long battery lifetime.

Back-End Technologies. For the development of the Back Layer proposed, an integration of different technologies was done.

These technologies include development using Representational State Transfer (REST) services which is an interface between systems that uses the HTTP protocol to obtain data or generate operations on that data in several possible formats, such as XML and JSON [21]. REST services offer integration with heterogeneous devices, technologies, and systems, giving flexibility in the development of an IoT platform.

Other elements used for the development of the Back Layer were the MySQL database and the PHP language. PHP is oriented to the development of dynamic web applications with access to information stored in a database. In the PHP language, REST services can be developed by establishing subscription mechanisms in order to receive data from external applications and store them in a database, using their capabilities to connect with database engines like MySQL [22] [14] [23]. The PHP language can also be useful for the development of web pages in order to show data and information to the final user.

4.1 LoRa-based IoT Monitoring And Collecting System Development.

According to the design in Figure 2, both the Front Layer and the Back Layer compose the architecture for the development of the LoRa-based IoT Monitoring and Collecting System, which is developed by integrating the technologies exposed above in the corresponding layer.

Front Layer The Front Layer integrates the LoRa-Nodes and the LoRa-Gateway modules to collect data from different kinds of sensors and send it to the Back Layer. The Front Layer network is configured in a star network topology, where LoRa-Nodes do not have routing capabilities and each LoRa-Node message reaches the LoRa-Gateway in just one hop.

LoRa-Node. The core of the LoRa-Node is the LoRa32u4 II board, which is a light, low consumption, low-cost and commercially available board, based on the Atmega32u4 with 868MHZ/915Mhz. It is a high-quality LoRa module, with

transfer rates range between 0.018 kbps and 37.5 kbps and includes a USB LiPO battery charging circuit [24]. The LoRa32u4 II board can be used as both node or gateway and its architecture is similar to that of the Arduino UNO module. This board includes the LoRaWAN Protocol library [25] and can be programmed with the Arduino IDE, including the LoRa library by BSFrance.

The LoRa-Node's main process is to take data from external sensor modules and send it directly to the LoRa-Gateway through a one-hop communication, calling the send API function from the LoRa protocol stack. The external sensor modules are connected to the LoRa32u4 II board through both Analog to Digital Converter or Digital Inputs provided in the board.

In order to maximize the battery life span a function that detects changes in the data that is being collected, is included in the main program, thus using the LoRA wireless module only when a change in a data collected magnitudes is detected.

Each LoRa-Node is configured with a unique identification (ID) to discriminate the origin of the messages in the LoRa-Gateway. The LoRa-Nodes messages sent can include the ID, the collected data, the timestamp, the battery level and a sequential message number that allows detecting whether a message has been missed.

LoRa-Gateway. The LoRa-Gateway consists of two parts: (1) a LoRa32u4 II board configured like a sink node that receives the messages from every LoRa-Node connected to the network and (2) a mechanism developed in an Android-based application (App) running on a smartphone, that takes the messages received by the sink node and uploads them to the Back Layer.

The messages received from the LoRa-Nodes are taken by the sink node and are sent, via a serial USB interface [26], to an Android-based application (App) deployed in an Android-based mobile device. The data received in the LoRa-Gateway module is then sent to the Back Layer, through an Internet connection, using a REST service exposed by the Back Layer. The App decodes the messages sent from each LoRa-Node and packs them using a JSON format and the uplink messages exchange to the Back Layer is carried out by using the Volley library [27]. The App is developed in the Java language.

Regarding the LoRa modulation capability of the sink node, it can communicate simultaneously on different channels and can have on the same channel signals modulated with different modulation Spreading Factors [28]. In case of collisions, the strongest signal is decoded. Using this feature offers the possibility of increasing the number of sink nodes thus increasing the networks capacity [25].

For the IoT platform proposed, the LoRa network works on the European frequency band of 867-869 MHz.

Back Layer The core of the Back Layer is a web application developed using PHP and MySQL. Additional languages as Javascript, Cascade Style Sheets (CSS), and libraries like JQuery and AJAX were used as well. To deploy the

Back Layer web application an Apache HTTP server was configured on a Ubuntu server, including PHP and MySQL Server.

A REST service was developed in PHP, which receives and decodes the JSON encoded messages coming from the Front Layer. Once the message is decoded, a PHP function sends the message content to a MySQL database created to store the data using the LoRa-Node's ID that collected the data as a key together with the data collected and the timestamp.

Therefore, when the data is stored in the database, it is available to other PHP functions that create a web graphical user interface in order to show the collected data to the end user. At this moment, it is possible to create charts to make a graphical representation of data and show trends or create additional functions to process, transform and interpret data, even apply statistical formulas, data analytic algorithms or machine learning algorithms.

The Back Layer web application was developed in PHP using Object-Oriented Programming; no framework was used. Access from PHP functions to MySQL database is done through the PHP Data Objects (PDO) extension.

5 Experimental Results

In order to test the proposed IoT Data Monitoring and Collecting Platform, a simple prototype to collect data was mounted for the purpose of measuring soil moisture.

Three LoRa-Nodes and one LoRa-Gateway were utilized for this test. The FC-28 soil moisture sensor was used to collect humidity data. The FC-28 sensor can be connected to the LoRa-Node in two modes: analog mode and digital mode. For the test the analog mode was used; the sensor works in the range from 0-1023 (the higher the value, the more dry is the soil). Moisture is measured in percentage; then, the values are mapped from 0-100.

Figure 3 shows the deployed components for the experimental setup.

An FC-28 sensor is connected to the LoRa32u4 II board ADC input, in each LoRa-Node; see Figure 3(B). A script written in C for the LoRa32u4 II board, takes the data from the ADC input and calls the LoRa API to send it as a message to the sink node in the LoRa gateway. A 3.7V 3000 mA polymer Lithium-Ion battery is used as a power supply for the LoRa-Node.

The LoRa-Gateway sink node receives data from the three LoRa-Nodes and sends it to an Android-based Tablet through a serial connection using an OTG cable connector; see Figure 3(A). The App running in the Android-based Tablet parses the messages received and formats them using JSON and sends them to the Back Layer. The App can show the data values collected by each LoRa-Node as well as the time that it was received; see Figure 3(A).

On the other hand, the Back Layer receives the messages from the Front Layer, decodes the messages and stores the data in the MySQL database. A simple web page was developed in order to show a tabulation and a chart of the soil moisture data collected by each LoRa-Node; see Figure 4.

Fig. 3. Front Layer components. (A) Lora-Gateway, (B) Lora-Node, (C) Lora-Node on a cloudy day at 30°C

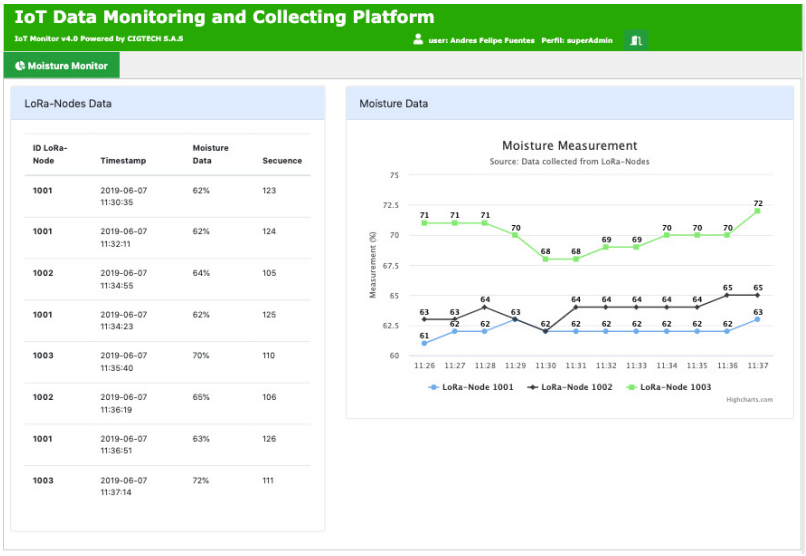

Fig. 4. Web page at the Back Layer to show the soil moisture data collected by each LoRa-Node

Measurements for the proposed IoT Data Monitoring and Collecting Platform were done at different distances both in urban and rural environments. In urban conditions with medium dense buildings and no Line Of Sight (LOS) between the LoRa-Nodes and LoRa-Gateway, the communication range lies between 300 to 600 meters. For the urban test, the LoRa-Gateway was located in the Research Lab in the School of Engineering at Libre University Sectional Cali and the LoRa-Nodes around the campus. On the other hand, in a rural environment with Line Of Sight between the LoRa-Nodes and LoRa-Gateway, the communication range was from 600 meters to 1.5 km. For the rural test LoRa-Nodes were placed in a sugar cane farm near Cali, Colombia, where there is no coverage for neither cellular nor other networks.

The setup values in the LoRa32u4 II module of the LoRa-Gateway and each LoRa-Node are listed in Table 1.

Table 1. Setup values in LoRa-Nodes and LoRa-Gateway.

LoRa Module Parameters	**LoRa API Function** [29].
Power transmission: 20dBm	`LoRa.setTxPower(17);`.
Bandwidth: 125kHz	`LoRa.setSignalBandwidth(125E3);`.
Radio frequency: 868MHz	`LoRa.begin(868E6);`.
Coding rate: 4/8	`LoRa.setCodingRate4(8);`.
Spreading Factor (SF): 7	`LoRa.setSpreadingFactor(7);`.

On the LoRa32u4 II wireless module of each LoRa-Node, the Spreading Factor (SF) values were changed to 7, 9 and 12 and measurements were made at the same distances [28]. When the SF is increased, the package size will be reduced, resulting in higher power over the channel and a longer communication distance. The LoRa spreading factors for 125 kHz bandwidth are listed in Table 2.

Table 2. LoRa Spreading Factors for 125 kHz Bandwidth

Spreading Factor	**Bit rate (bit/s)**
7	5469
9	1758
12	293

The Data Rate column in Table 3, shows the configured values for SF and the Transmission Time column shows the time values that the data transmission takes, observed from the LoRa-Gateway. Messages with an SF equal to 7 take a transmission time of around 40-60 milliseconds, depending on the size of the data. Messages with an SF equal to 9 take a transmission time of more than 164 ms and with an SF equal to 12 they take a transmission time of 1482 ms, more than 20 times the amount of time required to send the same message with SF set to 7.

As shown in Table 3, a higher SF has an enormous effect on battery life, which will be shorted around 20 times if SF 12 is used compared to SF 7.

Table 3. LoRa messages received by LoRa-Gateway using various spreading factors

Frequency	CR	Data Rate	Transmission Time	ID LoRa-Node	Message Size
868.3	4/5	SF 7 BW 125	41.2	1001	12 bytes
868.3	4/5	SF 7 BW 125	61.7	1001	24 bytes
868.5	4/5	SF 9 BW 125	165.3	1002	17 bytes
868.5	4/5	SF 12 BW 125	1379.5	1003	24 bytes

6 Concluding Remarks

This paper proposes a platform for data collection and monitoring applicable to IoT projects based on LoRa, which is a wireless communication technology that is currently applied in the development of IoT [3]. The proposed platform brings a framework for the development of IoT projects by appropriating open hardware and software technologies, as well as low-cost components with a balanced performance.

In addition to the LoRa communication components, this work integrates different technologies, including Web Services and databases engines, for the storage and visualization of the data collected, with the aim of contributing to the development of different projects that require adoption and inclusion of mechanisms of this kind to enhance the use and interpretation of data coming from wireless sensor networks.

Although this work focuses its efforts on the definition of a basic platform for LoRa-based IoT systems, other types of communication schemes based on LPWAN technologies such as Sigfox or NB-IoT, could be used, in order to expand the proposed platform.

Eventually, in order to show the applicability of the LoRa-based platform proposed, an IoT application for moisture measurement is developed, where basic communication tests were carried out identifying the factors that affect the platform performance like LoRa spreading factor.

In future works, it is possible to expand the number of nodes in the network to further analyze aspects of performance, latency and energy efficiency, as well as include different types of sensors for data collection, different LPWAN technologies, as well as the improvement of Web services for data analysis such as machine learning algorithms.

References

1. Sam Lucero et al. IoT platforms: enabling the Internet of Things. *IHS Technology white paper*, 2016.

2. Andrea Zanella, Nicola Bui, Angelo Castellani, Lorenzo Vangelista, and Michele Zorzi. Internet of things for smart cities. *IEEE Internet of Things journal*, 1(1):22–32, 2014.
3. Kais Mekki, Eddy Bajic, Frederic Chaxel, and Fernand Meyer. A comparative study of lpwan technologies for large-scale iot deployment. *ICT express*, 5(1):1–7, 2019.
4. Marco Centenaro, Lorenzo Vangelista, Andrea Zanella, and Michele Zorzi. Long-range communications in unlicensed bands: The rising stars in the iot and smart city scenarios. *IEEE Wireless Communications*, 23(5):60–67, 2016.
5. Hamdan Hejazi, Husam Rajab, Tibor Cinkler, and László Lengyel. Survey of platforms for massive iot. In *2018 IEEE International Conference on Future IoT Technologies (Future IoT)*, pages 1–8. IEEE, 2018.
6. Ala Al-Fuqaha, Mohsen Guizani, Mehdi Mohammadi, Mohammed Aledhari, and Moussa Ayyash. Internet of things: A survey on enabling technologies, protocols, and applications. *IEEE communications surveys & tutorials*, 17(4):2347–2376, 2015.
7. Shashank Agrawal and Dario Vieira. A survey on internet of things. *Abakós*, 1(2):78–95, 2013.
8. Julien Mineraud, Oleksiy Mazhelis, Xiang Su, and Sasu Tarkoma. A gap analysis of internet-of-things platforms. *Computer Communications*, 89:5–16, 2016.
9. LoRa Alliance. Lorawan regional parameters v1. 0. *LoRa Alliance: Fremont, CA, USA*, 2016.
10. Sharvari Rautmare and DM Bhalerao. Mysql and nosql database comparison for iot application. In *2016 IEEE International Conference on Advances in Computer Applications (ICACA)*, pages 235–238. IEEE, 2016.
11. J. Wan and S. Tang. Software-Defined Industrial Internet of Things in the Context of Industry 4.0. *IEEE Sensors Journal*, 16(20):7373–7380, 2016.
12. Y. Seungjun and J. Hyojung. Issues and Implementation Strategies of the IoT Industry. In *10th International Conference on Innovative Mobile and Internet Services in Ubiquitous Computing*, pages 503–508, 2016.
13. Andres Felipe Fuentes Vasquez and Eugenio Tamura. From sdl modeling to wsn simulation for iot solutions. In *Workshop on Engineering Applications*, pages 147–160. Springer, 2018.
14. K. S. Shinde and P. H. Bhagat. Industrial process monitoring using lot. In *2017 International Conference on I-SMAC (IoT in Social, Mobile, Analytics and Cloud) (I-SMAC)*, pages 38–42, Feb 2017.
15. Chang-Sic Choi, Jin-Doo Jeong, Il-Woo Lee, and Wan-Ki Park. Lora based renewable energy monitoring system with open iot platform. In *2018 International Conference on Electronics, Information, and Communication (ICEIC)*, pages 1–2. IEEE, 2018.
16. Michal Wydra, Pawel Kubaczynski, Katarzyna Mazur, and Bogdan Ksiezopolski. Time-aware monitoring of overhead transmission line sag and temperature with lora communication. *Energies*, 12(3):505, 2019.
17. José Miguel Paredes-Parra, Antonio Javier García-Sánchez, Antonio Mateo-Aroca, and Ángel Molina-García. An alternative internet-of-things solution based on lora for pv power plants: Data monitoring and management. *Energies*, 12(5):881, 2019.
18. Emiliano Sisinni, Dhiego Fernandes Carvalho, Paolo Ferrari, Alessandra Flammini, Diego Rodrigo Cabral Silva, and Ivanovitch MD Da Silva. Enhanced flexible lorawan node for industrial iot. In *2018 14th IEEE International Workshop on Factory Communication Systems (WFCS)*, pages 1–4. IEEE, 2018.

19. LoRa Technology. https://www.lora-alliance.org/what-is- lora/technology.
20. Semtech, AN1200. Lora modulation basics, application note, 22.
21. Bo Cheng, Shuai Zhao, Junyan Qian, Zhongyi Zhai, and Junliang Chen. Lightweight service mashup middleware with rest style architecture for iot applications. *IEEE Transactions on Network and Service Management*, 15(3):1063–1075, 2018.
22. J. M, S. M, N. V, P. V. M, and L. K. Monitoring system in industry using iot. In *2019 5th International Conference on Advanced Computing Communication Systems (ICACCS)*, pages 745–748, March 2019.
23. V. Hans, P. S. Sethi, and J. Kinra. An approach to iot based car parking and reservation system on cloud. In *2015 International Conference on Green Computing and Internet of Things (ICGCIoT)*, pages 352–354, Oct 2015.
24. LoRa32u4 II. https://bsfrance.fr/lora-long-range/1345-lora32u4-ii-lora-lipo-atmega32u4-sx1276-hpd13-868mhz-eu-antenna.html.
25. Alexandru Lavric and Valentin Popa. Internet of things and lora low-power wide-area networks: a survey. In *2017 International Symposium on Signals, Circuits and Systems (ISSCS)*, pages 1–5. IEEE, 2017.
26. Felipe Herranz felHR85. https://github.com/felhr85/usbserial.
27. Yang Shulin and Hu Jieping. Research and implementation of web services in android network communication framework volley. In *2014 11th International Conference on Service Systems and Service Management (ICSSSM)*, pages 1–3. IEEE, 2014.
28. S. Sar, . Kaya, C. iman, Y. Baltac, and S. nal. Evaluation of low-power long distance radio communication in urban areas: Lora and impact of spreading factor. In *2019 Seventh International Conference on Digital Information Processing and Communications (ICDIPC)*, pages 68–71, May 2019.
29. Sandeep Mistry. https://github.com/sandeepmistry/arduino-lora.

Bus stops as a tool for increasing social inclusiveness in Smart Cities

Víctor Manuel Padrón Nápoles[1], Diego Gachet Páez[1], José Luis Esteban Penelas[1], Germán García García[1], María José García Santacruz[2]

[1]Escuela de Arquitectura, Ingeniería y Diseño
[2]Facultad de Ciencias Sociales y de la Comunicación
Universidad Europea de Madrid. c/ Tajo s/n, Villaviciosa de Odón, Madrid
victor.padron@universidadeuropea.es, diego.gachet@universidadeuropea.es, jluis.esteban@universidadeuropea.es, gerggcl@gmail.com, mariajose.garcia3@universidadeuropea.es

Abstract. In the last years, the concept of Smart City has moved from a predominantly technological perspective towards a more human based approach, where terms as sustainability and inclusiveness are presents and are part of a new concept referred as Human Smart Cities. In this context, the mobility of people and services represents one of the major challenges that cities must solve. Therefore, urban mobility policies must integrate new mobility needs as well as minimize the impact transportation has on the environment and the quality of life in our cities. Urban areas need to develop new sustainable urban mobility systems integrating traffic state, transport users demand, transport capacity providers, etc. These requirements involve the use of new techniques and methods as Big Data and IoT, but it is necessary to include a social component to ensure social inclusion and inclusiveness, sustainability and inclusiveness. In this paper, we describe some challenges regarding barriers to access new mobility systems and their relevant information. Therefore, we propose a smart bus stop taking into account cultural and socioeconomics characteristics of the transport users employing as a basis the access to information systems.

Keywords: Smart Cities, inclusive transport, smart bus stops, mobility systems.

1 Introduction

When designing Socially Sustainable Cities, we are doubtlessly faced with the opportunity to achieve social accessibility. Sustainability is related to two basic principles: a robust ecosystem and an equally strong social fabric [1]. The relationship between the social and ecological dimensions of unsustainability creates a vicious circle. In this context the transportation and mobility systems plays a major role in the context of sustainable and inclusive smart cities.

In April 2018, European Commission published the document “Transport in the European Union. Current Trends and Issues”, which highlights the importance of

social aspects in the development of an advanced European transport system: “From a social perspective, affordability, reliability and accessibility of transport are key. However, this has not been achieved across the board. Addressing these challenges will help pursue sustainable growth in the EU” [2].

The concepts of social inclusion and the digitalization of transport have to be harmonized in terms of accessibility, affordability, reliability and inclusiveness. Public transport plays a crucial role for mitigating the social exclusion of vulnerable and disadvantaged groups, affecting their access to basic services and their social and employment relationships. Accessibility should include all the stages of the journey, including the walking environment, so that people with mobility impairment can reach and use transport services; the design of transport facilities, addressing the specific needs of vulnerable groups; and safety and security in public transport, crucial issues which disproportionately affect women and the elderly.

It is clear the potential of new transport technologies and social innovation in mitigating social exclusion and providing flexible cost-effective transport services. Currently, there are identified specific policies, research priorities and recommendations for local transport, long-distance transport and tourism. They address problems such as: the need to combat low awareness of disabled passengers’ rights; lack of information on accessibility of local transport; information presented not in accessible formats or not concise and reliable; low use of mobile apps and social media in the sector; low accessibility in suburban and rural areas; generally and major access barriers in interchanges and intermodal hubs.

2 Related Work and Background

In the context of smart cities there is an abundant literature related to transport and mobility as mentioned in [3]. As part of whole transportation in a smart cities several authors mention as an important component a smart traffic management system, including dynamic control of traffic signal lights based on traffic flow using technologies as wireless networks or powerful fiber-optic backbone [4], also there is an important volume of scientific literature describing the use of IoT (Internet of Things) technologies for quality of life improvement of citizens in smart cities through measures that leads to a healthy, green and sustainable environment. The potential benefits and challenges with the IoT service implementation for cities is visible for example in smart bus stops in Barcelona’s (Spain) that are connected to the city’s fiber-optic network offering services as online bus running schedule, information for foreign visitors, shows advertising, USB charging points for mobile gadgets and provide free Wi-Fi hotspots, giving waiting people access to the Internet using their mobile devices [5][6].

As we aforementioned, the scientific literature in relation to the technological systems used in the transportation systems and their main elements is wide, however there is relatively little information available about social aspects of transportation and mobility and particularly referred to public transportation systems and their in-

fluence in the quality of life of groups of people at risk of social exclusion as for example immigrants, refugees, elders, people with disabilities etc.

2.1 Transportation and Social Inclusion

Social inclusion is a very complex concept. The EU defines social inclusion as a tendency to enable people at risk of poverty or social exclusion to have the opportunity to participate fully in social life, and thus enjoy an adequate standard of living considered normal in the society in which they live [7]. Social inclusion is especially concerned about people or groups of people who are in risk of deprivation, segregation or marginalization. Especially susceptible to exclusion are people or groups of people in situations of precariousness or belonging as a collective, stigmatized, either by their origin, gender (male or female), physical condition (disabilities), or sexual orientation, among other things.

In particular, groups of citizens who are especially vulnerable to exclusion, include persons with disabilities and older citizens (many of whom live alone), as well as persons on low incomes and the unemployed. As shown in Fig.1, deserving special attention the situation of women, as some studies reveal that women have different travel patterns from men and that public transportation plays a crucial role in empowerment, access to opportunities and independence [8].

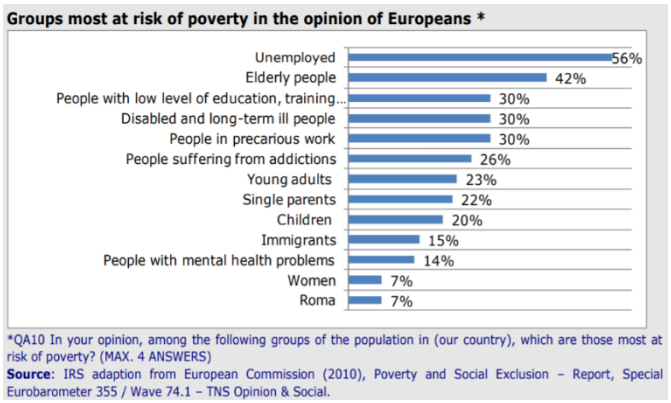

Fig. 1. Vulnerable and disadvantaged groups of citizens.

From the point of view of mobility and transportation the definition of social exclusion provided in [9] is particularly important due mobility in modern cities is an important factor in the people's life and that the reduced accessibility to opportunities, services or social networks are in partly due to insufficient mobility. The role of transport as a potential factor in creating social exclusion is well accepted and documented. Some identified barriers with which transport services can impact on social exclusion are for example, spatial, temporal, personal, psychological, cost and information access.

In order to successfully connect people to opportunities, public transport system should fulfil some criteria, as for example, it must be available, i.e. the public transport network should be easy reachable from people and offer good timetables and frequencies corresponding to patterns of social and working life, this is especially important for elder and handicapped persons. People also need to be kept informed of the services that are available both at smart stop and a whole transportation system. It must be accessible, i.e. vehicles, stops and the walking routes must be designed in such a way that everyone is able to use them without unreasonable difficulty and it must be affordable in the sense that people should not be paid a high fare for using public transport, at last public transport must be comfortable, safe and convenient.

It is clear that social inclusion and the digitalization of transport, have to be harmonized in terms of accessibility, affordability, reliability and inclusiveness. As mentioned in the study about "Social inclusion and EU public transport" [10] for the European Parliament's Committee on Transport and Tourism, public transport plays a crucial role for mitigating the social exclusion of vulnerable and disadvantaged groups, affecting their access to basic services and their social and employment relationships. Accessibility, for example, should include all the stages of the journey, including the walking environment, so that people with mobility impairment can reach and use transport services; the design of transport facilities, addressing the specific needs of vulnerable groups; and safety and security in public transport, crucial issues which disproportionately affect women and the elderly.

2.2 Smart Bus Stops to decrease the risk of social exclusion

Advances in transport systems are tightly related to the digitalization of physical transport assets, through the uses of Internet-of-Things, Big Data and Artificial Intelligence applications that joined with social innovation are producing new services such as shared mobility, multimodal transport planners, Mobility As A Service and public transport on demand. This combination of transportation assets, technological and social innovations is defined, in the scope of this paper, as a "Digitized Transport System" (DTS). An important component related with a DTS and social inclusion is a Smart Bus Stop described in detail in the following sections of this paper.

The concept of Smart Stop is recently new as part of the developments related to "Smart Cities" [11]. Several European cities have launched Smart Stops pilot projects. That is the case of Paris (one stop, Boulevard Diderot, 85 m2, accessible to persons with disabilities, and providing free WiFi and USB charge, among other services), London (100 ClearChannel bus shelters, using Google Outside service to provide information) and Barcelona (around 10 stops, with mobile based payment system). Other cities have incorporated some smart elements to traditional stops to supply more information to users, as arrival time of buses or other general information, without providing more interactivity.

Fig. 2. Aquis Innovo's Smart-Stop (Source: https:// https://europa.eu/investeu/projects/smart-bus-stop_es. EU Invest).

Another example is the Smart Bus Stop (SBS) prototype of Hungarian company Aquis Innovo in Budapest. The design and development of the prototype (Fig. 2) was funded by EC (41000€). This prototype, which includes ticket vending, parcel delivery, passenger counting, passenger information, wireless, USB charging, bike rental, air condition, taxi order, tourist info, news, advertisement, weather forecast, reverse vending, surveillance and others services [12]. On the other hand, there are other smart furniture options, as outdoor bus ticket-kiosk (Portuguese OEMKIOSK) or information providing smart furniture (not a Smart Stop) adapted to people with disabilities as Portuguese TOMI as shown in Fig. 3.

Fig. 3. Outdoor TOMI accessible information kiosk (Courtesy TOMI World).

Another example of advanced pilot project regarding Smart-Stop is the case of Aizuwakamatsu city, Japan. There, low consumption, bistable E-paper (only consumed power when the message changes) is solar powered and communicated with low power wide area (LPWA) wireless technology to provide information to users. This allows replacing paper timetables and improving user experience. Managed remotely through the Papercast data management platform, the multilingual displays will present live bus arrivals, timetables, route data, route transfers, service alterations (planned and unplanned) and a range of other travel advice [13]. Despite the huge potential of this technology, its penetration in many European cities is very limited and its adaptation to inclusiveness just is starting to be developed. One of the possible causes of this is the high mobile phone penetration.

The following sections describe in detail the architecture of a smart Bus Stop developed under the context of the MUSA (Advanced Sustainable Urban Furniture – Mobiliario Urbano Sostenible y Avanzado) project, a long-term project oriented to the development of smart bus stops based on the provision of information services with focus in inclusive, and social driven transport aspects.

3 MUSA Smart Stop Architecture

The MUSA project is being developed to start applying the aforementioned ideas in Madrid transport system, starting from a very popular point of interest: bus stops.

Our Smart Stop is a physical stop equipped with an interactive display and a computer system communicating with a set of cloud systems to provide different services to travelers publically available at the stop. The main of these services is a multimodal trip planner including options for walking, cycling, taxi, private and public transport. The interface to this urban equipment will be customized to increase the accessibility for those citizens that are at risk of exclusion. Smart stops will work as public access points and as travel assistants for low-income or disadvantaged groups of users; improving planning in real time and taking into account the unexpected events that can improves or disrupt transport operations. A Smart Stop, from inclusiveness point of view, is:

a) An interactive bus stop available to the whole population. It is a public access point to a digitized transport system, which allow access to persons without apps or even without a smart phone

b) It can work as a public access point and as a travel assistant for low-income or disadvantaged groups of users.

c) It can improve the accessibility to DTS through customization of interfaces and reduction of cognitive demand.

d) It can improve planning in real time taking into account unexpected events that can improves or disrupt transport operations.

e) Through an attractive and customized interface it can foster the penetration of travel planning apps and its use by different users' segments.

f) These Smart-Stops can be implemented as "small" smart furniture providing a robust, essential electronic equipment that convert traditional stops into accessible Smart-Stops minimizing the modernization cost and having a wide use in the cities and rural areas.

The planning from users' point of view helps to characterize the demand on transport systems. This identified demand jointly with sensorization of transport means can be used by transport providers to customize and fine tuning their services in order to meet user requirement (Fig. 4) and increase satisfaction of their clients.

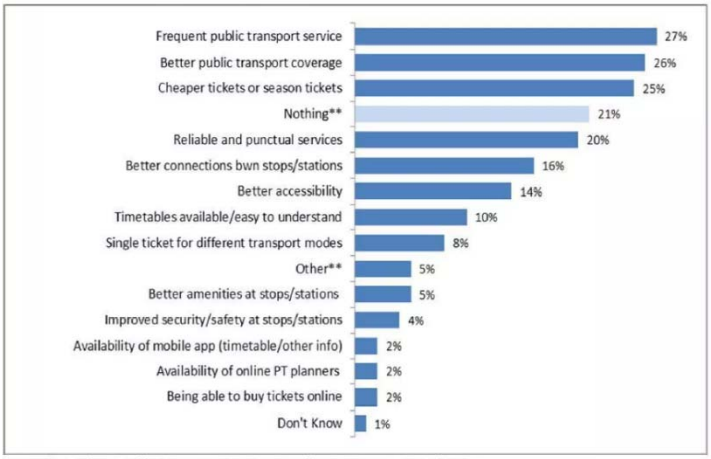

Fig. 4. Factors that can encourage the use of public transport.

3.1 Sensorization of buses.

The efficiency of planning, from users' as well as from transport providers' point of view, is highly correlated to the level sensorization of transport means. For these reasons, two directions were taken. First, increasing sensorization of buses installing Automatic Passenger Counters (APC) to know the occupancy of the bus in real time, the availability of free places for wheelchairs and baby-strollers, as well as the flow of passengers in each bus stop [14]. Second, the design of a smart bus stop, which actually provides a public, accessible entry point to a digitized transport system.

The use of APC for transport providers is very important in order they can analyze the performance of buses in real time, the most demanded segment of routes or routes in highest demand and accordingly re-plan them, if deemed necessary, so as to increase efficiency of service and users' satisfaction. From users' point of view, the bus

occupancy (or its probability) is crucial for an effective planning (it is useless, if the planed bus comes full and passengers cannot get on board).

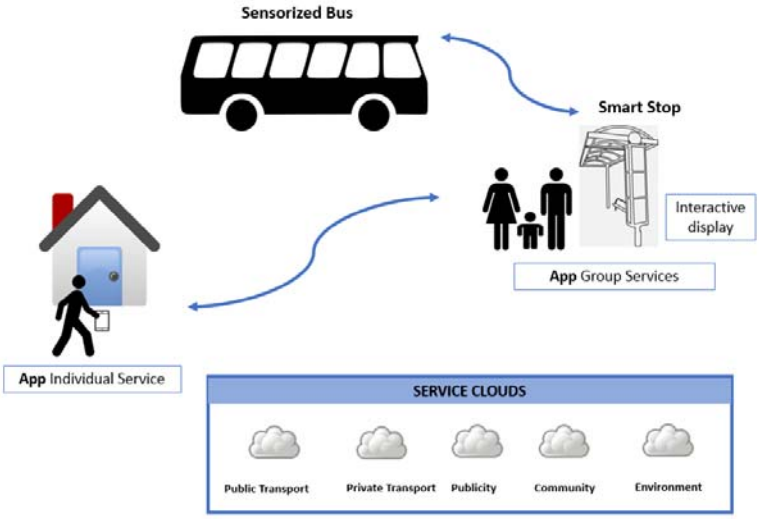

Fig. 5. Main components of MUSA architecture.

Buses normally include ALV (Automatic Vehicle Location) using GPS and SC-AFC (Smart Card Automatic Fare). For a flat-fare service (where nowadays passengers do not check out when alighting the bus, as e.g. in Madrid), the next level of sensorization was the use of APC or Automatic Passenger Counters. There are different technologies for APC, infrared and vision systems (video cameras, stereo cameras and time-of-flight cameras).

The use of the latter can be adapted to detect free available places for wheel chairs and baby strollers, thereby supporting increased inclusiveness. Research about possible smart stop services are being performed. This can include not only public and private transport services, but also community communication services, publicity services, environment and health services, among others. Fig. 5 shows the MUSA architecture.

Though for this project, infrared systems and stereo cameras were studied, we used simple video cameras from Retail Sensing, a Manchester company, to evaluate their performance in real-life conditions (Fig. 6). The cameras located on top of front and rear door use artificial vision algorithms to count in and out passengers. This information was sent through a 4G router to an MQTT server to make it globally available.

First, we tested them on Lab, then we installed then on buses and then we testing during daily operation of a bus in the center of Madrid (Figs. 7 and 8).

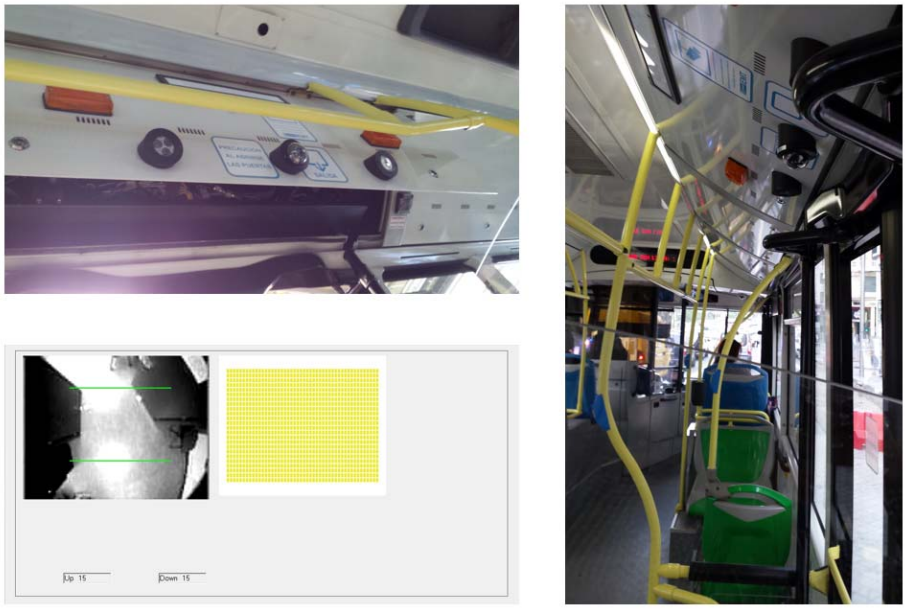

Fig. 6. Installing and testing APC based on video cameras.

Fig. 7. Number of daily passengers entering in the bus (Courtesy Retail Sensing).

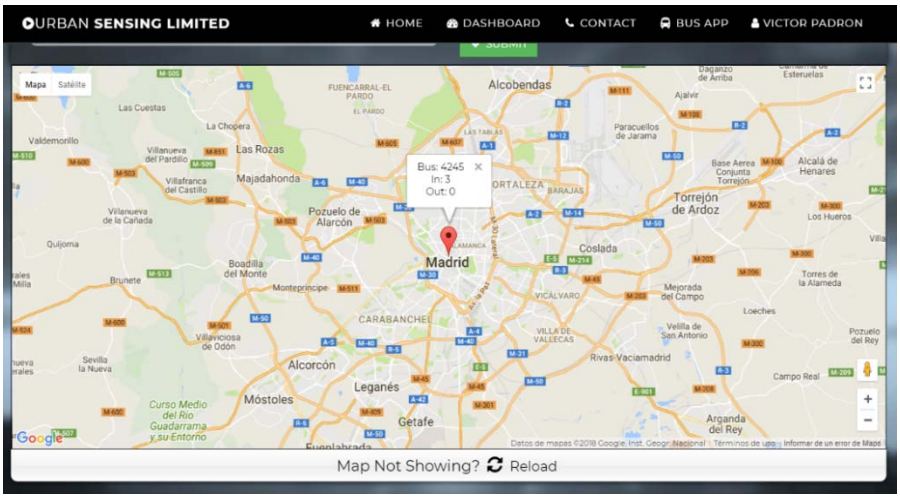

Fig. 8. Behavior of passengers' flow on one bus stop (Courtesy Retail Sensing).

Currently, a massive installation of APC systems using time-of-flight and Artificial Intelligence systems is taking place in Madrid buses. It is foreseeable that information about real-time occupancy of buses and availability of wheelchairs and baby stroller will be public available as Open Data.

3.2 Smart stop services.

The smart bus stop is being designed as a smart furniture, which provides different services: information about public and private transport, reservation of trips, as well as publicity services, community communication services, environment awareness information and delivering point for e-commerce. These services can be accessed from a screen available in the stop which will connect passengers to a set of cloud services. The works on smart stop are currently in progress. Designed as a special software layer (Fig. 9), it can run on a commercial travel planner, such as Google Maps. This has two advantages; it allows the customization of interfaces for different users' segments and the collection of traveling data, which can be used anonymously for building mobility models and develop social innovation solutions. In addition, it can be adapted to different commercial planners.

The prototype of the Smart Stop and its interface are shown in Fig. 10. Advertisement is running on the background (in this case for musicals in the center of Madrid), different services are available in the lower carrousel. To intuitively attract user to different interfaces, two type of icons are available. A traditional picture is used to attract more serious and direct users. Let's call it the "conservative interface". And, a more playful icon is used to attract more skillful and playful users. Let's call this the "playful interface". Other future special services for assisting traveler with special needs (elder, reduced mobility, easier travel with kids or pregnant women) are also

included in the interface. Other services as Community Services and Environment information are available following the already mentioned two icon policy.

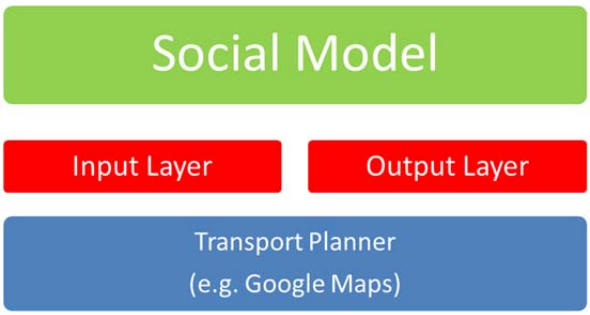

Fig.9. Layering smart stop multimodal planning application.

The "conservative interface" of the public transport app is shown in Fig. 11. A box with the most frequently used destination from current stop is shown on top right corners, increasing the probabilities of reducing the interaction to minimum. Below, a box shows time and duration of the selected trip (cost will be available soon). Also, there is an option to select private or other type of alternative transport without leaving conservative mode of interaction.

Fig. 10. Main interface of the smart bus stop prototype.

A third box allows user to select any origin and destination, using a tactile keyboard on the screen. Finally, information about nearest bus stops can be searched. Typical interactive features of Google Maps are disabled, so conservative user cannot be distracted from their simple, direct interaction with the app.

.

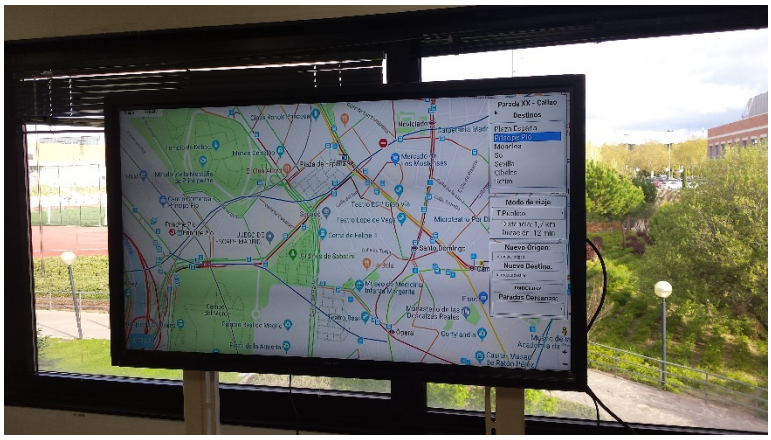

Fig. 11. Multimodal planner using public transport.

Fig. 12 shows the "conservative interface" fostering physical exercises by means of walking. In this case, time and duration of a trip walking and using public transport are similar, so the option of walking can be healthier for the user. This feature can be very interesting for elder people.

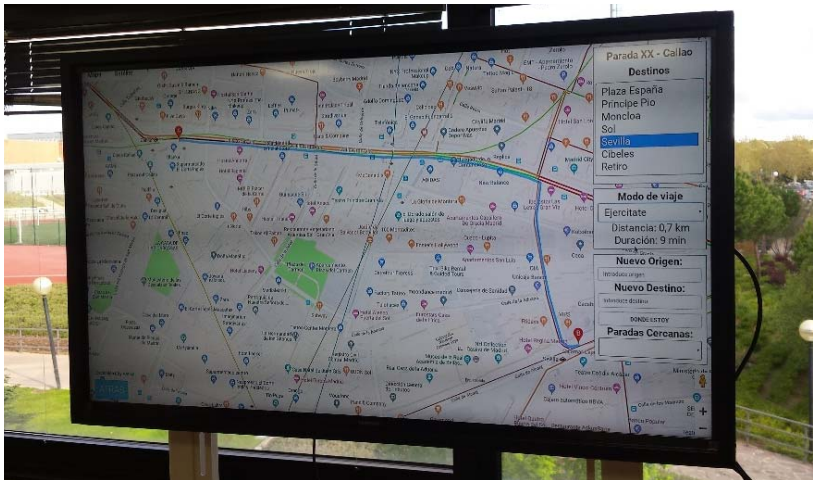

Fig. 12. Fostering physical exercise

4 Conclusions

This paper describes the first steps of development of a smart stop designed to increase social inclusiveness of modern, advanced, smart transport systems (digitized transport systems). Ensuring inclusiveness is crucial for ensuring that people not only can access and get full profit of advanced transport systems. It also helps characterize demand and allow transport providers a better planning and optimization of their resources increasing users' satisfaction.

Next step in the Smart Stop development is the study of more advanced interfaces, as those provided by the Voice Activated Personal Assistants or VAPA (e.g. Alexa) taking into account privacy concerns [15]. The design of this interface in the smart furniture creating a micro-space that isolates user and makes easier the interaction. This type of planning also can foster the use of VAPAs at home. Furthermore, VAPA systems have the potential to increase general accessibility of disabled people in general [16] and other target segments of users as well as decrease of the cognitive load and the effort of planning travels in the context of modern digitized transport systems. Taking into account privacy concerns and cybersecurity, it can be an effective double-approach to lack of digital competences and to reduce the impact of passivity of users.

Acknowledgments: This research was funded by Universidad Europea de Madrid grant number 2018/UEM06. We want to express our deep gratitude to all those persons and institutions that are helping and supporting us in the realization of this project. We want to thank the institutional support from the Municipal Transport Company (EMT) of Madrid, for the kindly support of its executives and technical staff; and at last, but not at least, to Asad Syed from Retail Sensing for his kindly support and sponsorship with the APC system. To all of you, thank you very much.

References

1. T. Verebes, Master Planning The Adpative City, London and New York: outledge Taylor & Francis Group, 2014.
2. Transport in the European Union: Current Trends and Issues, https://ec.europa.eu/transport /sites/transport/files/2018-transport-in-the-eu-current-trends-and-issues.pdf, last accessed July 2019.
3. Kehua Su, Jie Li, and Hongbo Fu. Smart city and the applications. In Electronics, communications and Control (ICECC), 2011 International Conference on, pages 1028{1031. IEEE, 2011
4. Zhiping Wang. The application of wireless city technology in public administration. Journal of Chinese People's Armed Police Force, 24, 2008.
5. Cisco España. Internet of things world forum Barcelona 2013 (video, november 2013).
6. P Wallbank. A geek's tour of Barcelona. 2013.
7. Poverty and social exclusion, https://ec.europa.eu/social/main.jsp?catId=751&langId=en, last accessed July 2019

8. Manuela Samek, Flavia Pesce, Patrizia Malgieri, Silvia Maffi and Caterina Rosa. The Role of Women in the Green Economy. The Issue of Mobility, http://www.europarl.europa.eu/RegData/etudes/note/join/2012/462453/IPOL-FEMM_NT(2012)462453_EN.pdf, last accessed July 2019.
9. Kenyon, K., Lyons G., Rafferty, J. (2003), Transport and social exclusion: investigating the possibility of promoting social exclusion through virtual mobility, Journal of Transport Geography, Vol. 10, pp. 207-219.
10. Social Inclusion in EU Public Transport, http://www.docutren.com/pdf/boletin/[IIIA% 201440].pdf, last acceded July 2019.
11. Gretzel, Ulrike & Sigala, Marianna & Xiang, Zheng & Koo, Chulmo. (2015). Smart tourism: foundations and developments. Electronic Markets. 25. 10.1007/s12525-015-0196-8.
12. Aquis Innovo. https://europa.eu/investeu/projects/smart-bus-stop_es, last accessed July 2019
13. Papercast 2018. https://www.papercast.com/epaper_bus_stop_passenger_information_solutions/products_e-paper_displays/, last accessed July 2019
14. Nápoles, V.M.P.; Rodríguez, M.B.; Páez, D.G.; Penelas, J.L.E.; García-Ochoa, A.G.; Pérez, A.L. MUSA–I. towards New Social Tools for Advanced Multi-Modal Transportation in Smart Cities. *Proceedings* **2018**, *2*, 1215.
15. Aarthi Easwara Moorthy & Kim-Phuong L. Vu (2015) Privacy Concerns for Use of Voice Activated Personal Assistant in the Public Space, International Journal of Human–Computer Interaction, 31:4, 307-335, DOI: 10.1080/10447318.2014.986642
16. Alisha Pradhan , Kanika Mehta , Leah Findlater, "Accessibility Came by Accident": Use of Voice-Controlled Intelligent Personal Assistants by People with Disabilities, Proceedings of the 2018 CHI Conference on Human Factors in Computing Systems, p.1-13, April 21-26, 2018, Montreal QC, Canada DOI 10.1145/3173574.3174033.

Noise and ozone continuous monitoring in an industrial urban area of northeastern Portugal

Leonardo Campestrini Furst [1] [0000-0002-0313-4915], Manuel Feliciano [2] [0000-0002-3147-4511], Artur Gonçalves [2] [0000-0002-4825-6692] and Felipe Romero [3]

[1] Instituto Politécnico de Bragança, Campus de Santa Apolónia, 5300-253 Bragança, Portugal.
[2] Centro de Investigação de Montanha (CIMO), Instituto Politécnico de Bragança, Campus de Santa Apolónia, 5300-253 Bragança, Portugal.
[3]Instituto de la Construcción de Castilla y León (ICCL), Valladolid, Spain
msabenca@ipb.pt

Abstract. The major environmental pressures associated with urban centers are noise and air pollution, making its monitoring of utmost importance to evaluate and reduce the exposure of the population to these environmental risk factors. In this study, continuous monitoring of sound pressure levels, ozone, nitric oxides, carbon monoxide concentrations, and local meteorological variables were performed during the winter and spring months of 2019 at the Mirandela industrial park. Ozone and nitric oxide levels followed a characteristic daily cycle, consistent with the diurnal evolution of radiation and the intensity of the main air pollution sources prevailing in the local. Hourly ozone levels were highest in July, reaching magnitudes of approximately 80 ppb. Ozone concentrations in the industrial park had a strong local influence, mainly related to the local nitric oxides emissions. The results also showed high influence of meteorological parameters on ozone production, especially during daytime. Regarding noise, typical daily and weekly patterns were observed, and sound pressure levels were compatible with those defined for mixed zones according to the Portuguese General Noise Regulation.

Keywords: Air quality, Noise, Monitoring, Industrial Parks.

1 Introduction

The rapid urban expansion, associated with a high population growth rate over the last centuries, tends to influence and modify various environmental aspects, producing impacts on the air, water, soil, and biodiversity [1–4]. Under such circumstances, it is evident that the increase in urban traffic, expansion of industrial zones and suppression of vegetation are the main degradation factors of urban air quality and local meteorological changes [5]. In addition, a large part of the population is exposed to different levels of environmental noises, capable of producing diverse effects on human health and well-being [6]. Therefore, air pollution and environmental noise are the two major environmental pressures associated with decreased quality of life in cities [7].

Air pollution is defined as a condition where one or more substances are present in the atmosphere at concentrations above normal ambient levels and particularly during a sufficiently long period to produce adverse effects on the health of humans, animals, and plants, or to cause material damage [8, 9]. According to the European Directive, noise corresponds to any unwanted sound or set of sounds that cause annoyance or may have an impact on human health, emitted by human activities, such as road traffic, rail traffic, air traffic and industrial sites [10].

Several studies emphasize the adverse effects of these components on human health [7, 11, 12], including respiratory and heart diseases [13, 14], causing annoyance and decreasing the cognitive ability [15, 16]. Thus, one of the great challenges of modern cities managers is providing quality of life to their inhabitants by improving the urban environment. To achieve this purpose, the monitoring of noise levels and air quality are extremely important to assess environmental risks, as well as to maintain or improve the environmental quality in urban centers [15, 17].

The main aim of this study was to study ozone, carbon monoxide, nitrogen oxides, and noise levels in the industrial park of Mirandela - Portugal. Since ozone is a very unstable secondary pollutant, its presence in the troposphere is partially related to the transport from the stratosphere, but the main contribution is its photochemical production, which occurs through the oxidation of hydrocarbons and carbon monoxide in the presence of nitric oxides and solar radiation [18]. For this reason, nitric oxides, carbon monoxide and, meteorological parameters were monitored in this research.

For the study, a monitoring system composed by one weather station, three gas analyzers and one noise sensor were installed in the Mirandela industrial park. The data collected during the winter and spring months of 2019 was used to correlate the different variables monitored with ozone production, and the system allowed further monitoring of the daily noise levels and the identification of the week noise profile. In the next sections of this paper a brief characterization of the industrial park, the methodological details of the study and the main air quality and noise results are presented and discussed.

2 Methodology

2.1 Industrial Park of Mirandela - Brief Description

This study was carried out in the urban industrial park of Mirandela (41°29'N / 7° 9'W), located in the northeastern region of Portugal, in the region known as Trás-os-Montes. The Industrial Park has an area of 33 hectares with 97 lots distributed to different industrial and commercial sectors. It comprises approximately 65 companies of different typologies such as sausage and granite factories, oil mills, carpentry, locksmiths and car repair shops. The Industrial Park is mostly surrounded by rural areas with olive trees plantations and open grassy spaces and is bounded by roadways to the west and south. The Mirandela downtown is southwest of the industrial Park.

2.2 Monitoring and Analyses

The air quality monitoring started in December 2018, with the collection of hourly data for carbon monoxide (CO), nitrogen oxides (NO, NO_2, NO_x) and ozone (O_3). All these gaseous pollutants were monitored according to the reference methods described by the Directive 2008/50/EC, using three gas analyzers: one ozone analyzer HORIBA APOA-370 (non-dispersive ultra-violet-absorption), one nitrogen oxides analyzer HORIBA APNA-370 (chemiluminescence) and one carbon monoxide analyzer HORIBA APMA-370 (non-dispersive infrared absorption). Noise monitoring started in February 2019 using the CESVA TA120 noise sensor, with measurements taken every minute. The noise sensor has class 1 accuracy according to IEC 61672-1 and was deployed outdoors due to the weather protection cover. In addition, a meteorological station was used to characterize the prevailing local weather conditions, measuring the direction and wind speed, solar radiation, temperature, relative humidity, and precipitation. The gas analyzers, weather station and, noise sensor showed in Figure 1 have the capacity to send data remotely via GPRS system, enabling the data to be accessed through a remote server.

Fig. 1. Set of the monitoring equipment used in the study: (A) Weather station; (B) air intake; (C) smart noise sensor; (D) gas analyzers container.

Based on the solar radiation data, the days were divided into daytime (8:00-19:00) and nighttime (20:00-7:00) to determine the correlation coefficient between the variables and the local and regional contribution to the prevailing O_3 levels. These separate timeframes were chosen considering the ozone formation and depletion mechanisms that have a strong dependence on solar radiation. It should be mentioned that in this study it was adopted the Coordinated Universal Time (UTC).

Concerning noise, a daily and weekly profile were evaluated based on hourly average data observed during the spring months. Additionally, the noise assessment was based on the Portuguese General Noise Regulation (RGR) (Decree-Law No. 9/2007 of 17 January). The RGR does not set noise limits to industrial parks itself, but any activity located in an industrial park has to comply with criteria established in RGR for sensitive

receivers (i.e., spaces where people live or stay) near industrial areas. The criteria set for those receivers depend on the classification established in the municipal master plan for the area where they are located. These areas can be classified into sensitive and mixed zones. The RGR defines sensitive zones as areas for residential use, schools, hospitals or similar, and recreational or leisure spaces, and may also contain small shops and services that do not operate at night, while mixed zones in addition to the uses for sensitive zones may contain shops, services, and industries working all day.

In the master plan of Mirandela the residential areas near the industrial park are classified as mixed zones. For these areas, the RGR specify the limit value of 55 dBA for the night noise indicator (Ln) and a 65 dBA for the day-evening-night noise indicator (Lden). Based on this, for research purpose, the monitoring point was evaluated as a mixed zone.

3 Results and Discussion

3.1 Daily Profile of Ozone Levels and its Precursors

Figure 2 shows the variation of solar radiation, ozone and its precursors throughout the day.

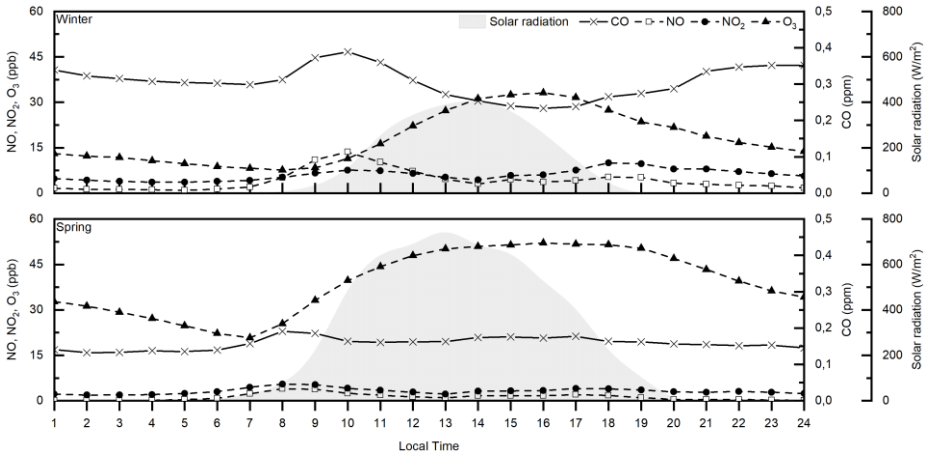

Fig. 2. Average hourly variation of NO_2, NO, CO, O_3 and solar radiation during winter (top) and spring (bottom).

The higher concentrations of the primary pollutants (CO and NOx) registered between 8:00 and 10:00 and between 17:00 and 18:00, coincides with the greatest intensity of traffic associated with the beginning and end of the daily activities inside and outside the industrial park. The higher levels of these primary pollutants in winter show clearly the influence of other combustion sources, such as domestic combustion for heating water and ambient air in dwellings.

In winter, ozone concentrations increase from 8:00 until they reach a peak of 33 ppb at 16:00. It is also noted that during rush hour (about 18:00), the increase in NO and NO_2 concentrations did not imply a significant increase in ozone concentration, partially explained by the prevailing low solar radiation. The ozone pattern in spring and winter was similar, however as the days are longer and the incidence of solar radiation is higher, there are some differences. At spring, ozone concentrations rise from 7:00 to reach its peak at 14:00, remaining stable until 19:00. Considering also that O_3 production depends on the concentration of NO, NO_2, CO, and volatile organic compounds, these gases are consumed as the O_3 concentration increases.

The reactions between O_3, NO, and NO_2 (R1 - R3) are part of a well-established null-cycle [18]. Thus, during daylight hours (R1 - R2), NO, NO_2 and O_3 are typically balanced on a condition referred to photostationary state [19]. For this reason, it is possible to observe in winter an ozone concentration near 30 ppb between 14:00 and 17:00 and in spring a concentration near 50 ppb between 13:00 and 19:00.

$$NO + O_3 \rightarrow NO_2 + O_2 \quad (R1)$$

$$NO_2 + hv \rightarrow NO + O \quad (R2)$$

$$O + O_2 + M \rightarrow O_3 + M \quad (R3)$$

An atmosphere only with nitrogen oxides do not favor the ozone production, as ozone can be recycled during the reactions. However, in the presence of other precursor gases such as carbon monoxide (R4 – R6) and volatile organic compounds (R7-R11), new reactions are triggered, resulting in excess of ozone production [20, 21]. These reactions lead to the formation of the hydroxyl (OH), hydroperoxyl (HO_2) and organo-peroxyl (RO_2) radicals, which results in the formation of nitrogen dioxide without ozone consumption and, consequently, leading to higher ozone production rates by reactions 2 and 3.

$$CO + OH \rightarrow H + CO_2 \quad (R4)$$

$$H + O_2 + M \rightarrow HO_2 + M \quad (R5)$$

$$HO_2 + NO \rightarrow OH + NO_2 \quad (R6)$$

$$CH_4 + OH \rightarrow CH_3 + H_2O \quad (R7)$$

$$CH_4 + O_2 + M \rightarrow CH_3O_2 + M \quad (R8)$$

$$CH_3O_2 + NO \rightarrow CH_3O + NO_2 \quad (R9)$$

$$CH_3O + O_2 \rightarrow HCHO + HO_2 \quad (R10)$$

$$HO_2 + NO \rightarrow OH + NO_2 \quad (R11)$$

3.2 Relation Between Air Quality and Meteorological Variables

Tables 1 and 2 show the daytime and nighttime correlation coefficients between hourly means of individual pollutants (CO, NO, NO_2, NO_x and O_3) and the meteorological parameters for winter and spring. The values in bold were those that show a significant correlation at the 0.05 level (2-tailed). Similar to Agudelo–Castaneda et al. [22], a positive correlation was found between nitrogen oxides and carbon monoxide during daylight, indicating that both gases have the same source, mainly related to combustion processes (e.g motor vehicles and industries).

Ozone showed a significant positive correlation with solar radiation and temperature during the daylight hours. This relation reverses during the night, due to the lack of solar radiation for ozone synthesis. This trend is observed in other studies [23, 24], showing that a favorable temperature and high solar radiation increase the photochemical reactions that generate ozone [25]. Moreover, based on reactions 1 to 3, an inverse relationship between ozone and nitrogen oxides is also observed, which can be confirmed by the negative correlation between these gases.

The results also showed a negative correlation between CO and O_3, since carbon monoxide reacts with hydroxyl radicals (R4) producing HO_2 radicals (R5) and, consequently, NO_2 (R6) which is photo-dissociated to produce O_3 through the reactions 2 and 3.

Table 1. Spearman correlation coefficients between hourly mean CO, NO, NO_2, NO_x, O_3 and meteorological parameters for winter nighttime and daytime

Winter Daytime								
	CO	***NO***	***NO_2***	***O_3***	***T.***	***R.H.***	***W.S.***	***S.R.***
CO	1	**0,780**	**0,693**	**-0,688**	**-0,685**	**0,629**	**-0,559**	**-0,246**
NO		1	**0,800**	**-0,622**	**-0,543**	**0,502**	**-0,410**	**-0,154**
NO_2			1	**-0,356**	**-0,281**	**0,238**	**-0,380**	**-0,251**
O_3				1	**0,852**	**-0,901**	**0,715**	**0,518**
T.					1	**-0,895**	**0,586**	**0,485**
R.H.						1	**-0,554**	**-0,543**
W.S.							1	**0,474**
S.R.								1
Winter Nighttime								
	CO	***NO***	***NO_2***	***O_3***	***T.***	***R.H.***	***W.S.***	***S.R.***
CO	1	**0,771**	**0,840**	**-0,791**	**-0,568**	**0,608**	**-0,358**	**0,160**
NO		1	**0,802**	**-0,672**	**-0,391**	**0,443**	**-0,346**	**0,134**
NO_2			1	**-0,518**	**-0,283**	**0,304**	**-0,300**	**0,076**
O_3				**1**	**0,739**	**-0,860**	**0,458**	**-0,295**
T.					1	**-0,702**	**0,328**	**-0,177**
R.H.						1	**-0,288**	**0,392**
W.S.							1	**0,088**
S.R.								1

T. – Temperature R.H. - Relative Humidity W.V. - Wind Speed S.R. – Solar Radiation

It is also observed in Tables 1 and 2 that the wind speed has a positive correlation with ozone concentration and a negative correlation with nitrogen oxides and carbon monoxide. Agudelo–Castaneda et al. [22] explain that this phenomenon may occur due to high wind speeds, which leads to the dispersion and mixing the gases from local

sources, favoring ozone transport and formation reactions taking place in the atmosphere. Moreover, Markovic and Markovic [26] also justify the positive correlation between wind speed and ozone levels due to the transport of ozone produced on the main roads to the measurement point. There is also an expected negative correlation between ozone and relative humidity, since as relative humidity increases the major photochemical paths of O_3 removal will be lowered [27]. High humidity levels are associated with cloudy days and less sunshine, thus reducing photochemical processes [27].

Table 2. Spearman correlation coefficients between hourly mean CO, NO, NO_2, NO_x, O_3 and meteorological parameters for spring nighttime and daytime

Spring Daytime								
	CO	***NO***	***NO₂***	***O₃***	***T.***	***R.H.***	***W.V.***	***S.R.***
CO	1	**0,675**	**0,781**	**-0,091**	**-0,375**	**0,330**	-0,031	**-0,223**
NO		1	**0,906**	**-0,402**	**-0,340**	**0,369**	0,001	**-0,211**
NO₂			1	**-0,211**	**-0,325**	**0,296**	**-0,096**	**-0,327**
O₃				1	**0,531**	**-0,706**	**0,313**	**0,328**
T.					1	**-0,825**	**0,159**	**0,498**
R.H.						1	**-0,175**	**-0,528**
W.V.							1	**0,160**
S.R.								1
Spring Nighttime								
	CO	***NO***	***NO2***	***O3***	***T.***	***R.H.***	***W.V.***	***S.R.***
CO	1	**0,142**	**0,458**	-0,032	**-0,302**	**0,164**	**-0,069**	-0,009
NO		1	**0,684**	**-0,369**	**0,071**	**0,178**	**-0,193**	**0,403**
NO₂			1	**-0,392**	-0,033	**0,113**	**-0,377**	**0,200**
O₃				1	**0,450**	**-0,715**	**0,702**	**-0,059**
T.					1	**-0,681**	**0,345**	-0,013
R.H.						1	**-0,482**	0,057
W.V.							1	0,058
S.R.								1

T. – Temperature R.H. - Relative Humidity W.V. - Wind Speed S.R. – Solar Radiation

3.3 Local and Regional Contributions to Ozone Formation

To determine the local and regional contribution to ozone formation, potential ozone levels ($O_3 + NO_2$), also called total oxidant levels (OX), were related to NOx, following the same analysis used in other studies [19, 28, 29]. For this purpose, daily average values (day and night) of OX were evaluated against the values of NO_X. For each data distribution, a linear regression was applied, thus providing an equation, in which the slope represents the local contribution (NO_x-dependent), while the intersection represents the regional contribution (NO_x-independent). Figure 3 presents the linear regressions lines obtained for each of the studied months. The regional contribution represents the background OX concentration, while the local contribution is related to the local production/destruction [28].

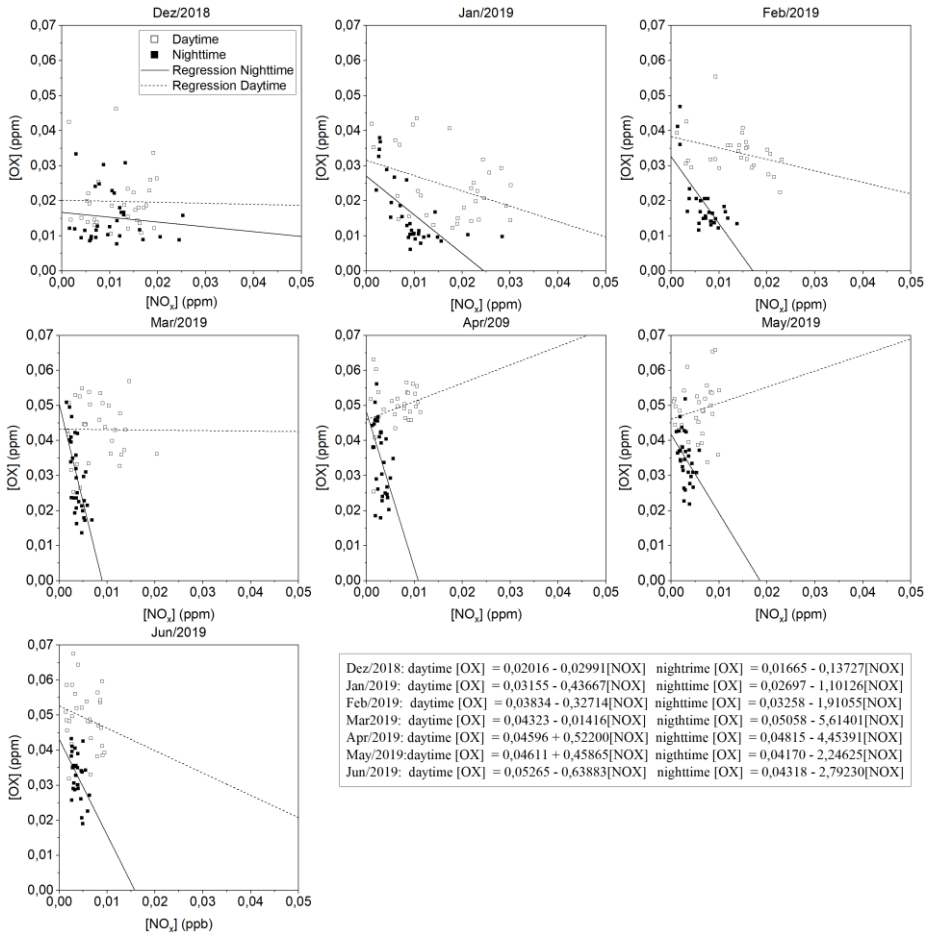

Fig. 3. Daily variation means of regional [OX] with NOx during the months of winter and spring for daytime and nighttime.

When OX levels increase as a function of NO_X, the NO_X contributes mainly to ozone production; when the OX levels decrease, means that NO_X influences the processes of ozone depletion; and when OX levels remain relatively constant as a function of NO_X, indicate that NO_X contributes in equal parts to the production and depletion of ozone.

Based on the regression analysis from December 2018 to June 2019, it was possible to obtain the slope and intersection for each period. These results are presented in Figure 4 showing the monthly local and regional dependence of OX. It is noticeable that values of the local contribution are higher than the values of the regional contribution, thus indicating that for the industrial park of Mirandela OX production occurs mainly locally due to primary pollutants emissions.

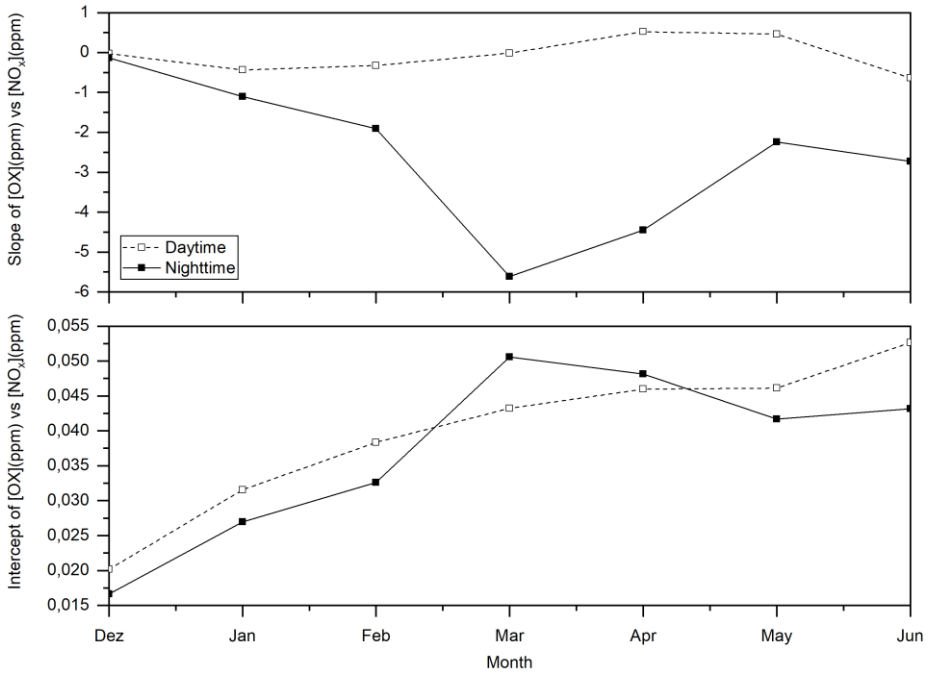

Fig. 4. Monthly variation of regional (intercept) and local (slope) OX in the Industrial Park of Mirandela.

For the regional component, there is a tendency to an increase in the concentration of OX, because the intensification of solar radiation helps photochemical processes. This same tendency was observed in the study of Notario et al. [29]. Regarding the local component, for daytime, an increase in OX concentration is observed from January to May, indicating that during this period NO_X favors ozone production. For the nighttime the relationship is inverse, suggesting that that NO_X is mainly related to ozone depletion mechanisms.

3.4 Noise monitoring

Figure 5 shows the hourly averages values during the spring months. Between Monday and Friday, the noise profile throughout the day is very similar, with the lowest averages observed between 1:00 and 3:00 at night. Subsequently, noise rises until 8:00, when activities start in the industrial zone, remaining relatively stable until 12:00. At his time, there is a decrease in noise levels due to lunchtime, where most activities stop in the industrial zone. After 18h00 the noise level decreases due to the finish of the work hours. During the weekend, noise levels are lower than during working days, although Saturday levels are higher than those registered on Sundays because some activities operate on Saturday.

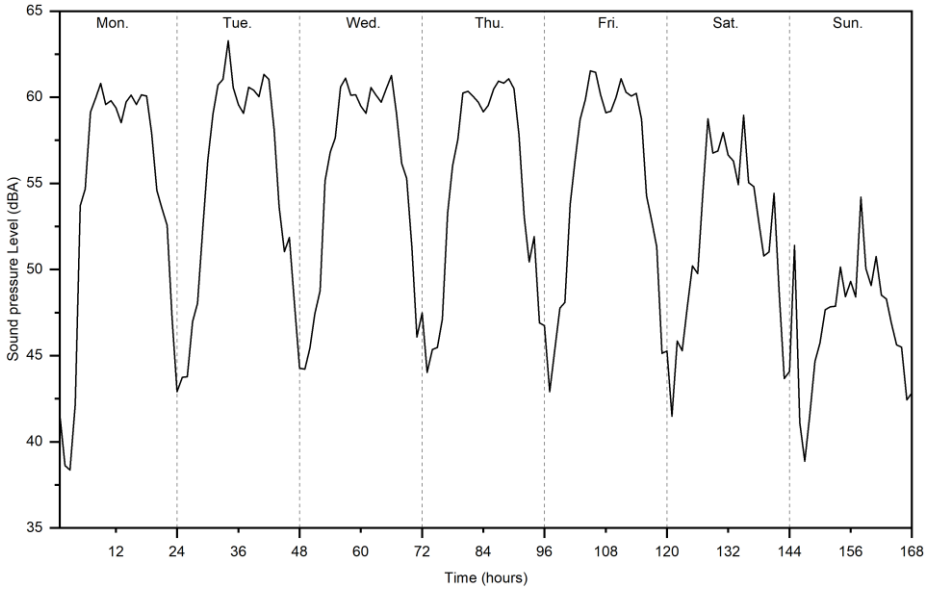

Fig. 5. Average hourly variation of sound pressure levels true for spring weeks.

Figure 6 presents the daily average night noise levels (Ln) and the day-evening-night-noise (Lden) levels during the spring days. The Portuguese Decree-Law No. 9/2007 of 17 January establishes for Lden a limit of 65 dBA and for Ln a limit of 55 dBA for mixed zones. During the evaluation time the night indicator was exceeded on April 4th, 15th, and 24th, and May 8th and 24th, reaching the values of 57.0, 56.7, 56.4. 56.0 and 55.6 dBA respectively. As the values of Ln are very close to the established limit and observing that only occurred five days in three months, it can be inferred that a singular event resulted in this phenomenon, so they are values not very relevant for the acoustic characterization of the industrial zone.

It should also be noted that although there are no legal limits for industrial parks, the observed values are within the legal limits for mixed zones, meaning that noise generated by activities developed in industrial park of Mirandela, including traffic road have little impact on the acoustic environment of the sensitive receivers located in its vicinity.

During working days, noise remains relatively stable, close to 60 dBA, thus indicating that the noise sources in the industrial park have a typical behavior over the week.

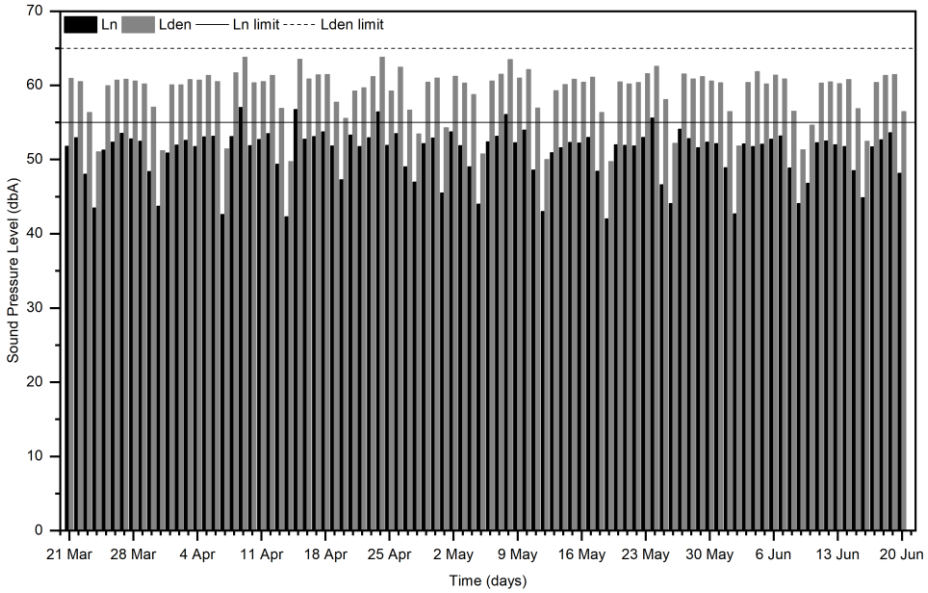

Fig. 6. Ln and Lden levels for Spring

It is noteworthy that only one fixed noise sensor was used in this study, and, for a better acoustic characterization of the industrial zone, it would be necessary to install more noise sensors, considering that the sound is attenuated due to the obstacles and the distance traveled. Additional monitoring points would also add useful information on the diversity of noise sources.

4 Conclusions

The monitoring of atmospheric pollution in the industrial park of Mirandela was useful for the identification of the main components related to the local ozone production, and it was possible to verify that besides the ozone precursors, the meteorological variables have a great influence on its production, especially the solar radiation.

CO and NO emissions were also related mainly to urban traffic because their concentration increased at the same time during the rush hours in the industrial zone. Regarding the analysis of OX vs NO_x, it was found that the ozone present in the region derives mainly from local influence, and the negative relationship found for the local component indicates that NO_x favors ozone depletion mechanisms. Thus, in future studies, it is suggested to monitor VOCs and hydrocarbons to know the different ozone production routes and verify which pollutant has the highest impact on ozone synthesis. Also, by monitoring noise, it was possible to create the daily and weekly sound pressure level profiles and, verify that during the observation period in five occasions the night limit was exceeded.

Continuous monitoring will continue in the industrial park of Mirandela, in order to obtain the ozone and noise profile for all seasons of the year.

Acknowledgments

This study was part of the Trans-National Project Rehabind. The authors would like to thank the Spain-Portugal Transnational Program (POCTEP), with the Financial Support from the European Union under Program FEDER (Euro-pean Regional Development Fund). The authors acknowledge all the support provided by the Mirandela City Council for the execution of this work.

References

1. Molina MJ, Molina LT (2004) Megacities and Atmospheric Pollution. J Air Waste Manage Assoc 54:644–680 . doi: 10.1080/10473289.2004.10470936
2. Ren W, Zhong Y, Meligrana J, Anderson B, Watt WE, Chen J, Leung H-L (2003) Urbanization, land use, and water quality in Shanghai: 1947–1996. Environ Int 29:649–659 . doi: 10.1016/S0160-4120(03)00051-5
3. Imperato M, Adamo P, Naimo D, Arienzo M, Stanzione D, Violante P (2003) Spatial distribution of heavy metals in urban soils of Naples city (Italy). Environ Pollut 124:247–256 . doi: 10.1016/S0269-7491(02)00478-5
4. Seto KC, Güneralp B, Hutyra LR (2012) Global forecasts of urban expansion to 2030 and direct impacts on biodiversity and carbon pools. Proc Natl Acad Sci U S A 109:16083–8 . doi: 10.1073/pnas.1211658109
5. Romero H, Ihl M, Rivera A, Zalazar P, Azocar P (1999) Rapid urban growth, land-use changes and air pollution in Santiago, Chile. Atmos Environ 33:4039–4047 . doi: 10.1016/S1352-2310(99)00145-4
6. Morel J, Marquis-Favre C, Viollon S, Alayrac M (2012) A laboratory study on total noise annoyance due to combined industrial noises. Acta Acust united with Acust 98:286–300
7. Hänninen O, Knol AB, Jantunen M, Lim T-A, Conrad A, Rappolder M, Carrer P, Fanetti A-C, Kim R, Buekers J, Torfs R, Iavarone I, Classen T, Hornberg C, Mekel OCL (2014) Environmental Burden of Disease in Europe: Assessing Nine Risk Factors in Six Countries. Environ Health Perspect 122:439–446 . doi: 10.1289/ehp.1206154
8. Seinfeld JH, Pandis SN (2016) Atmospheric chemistry and physics : from air pollution to climate change
9. Jacobson MZ (2016) Atmospheric Pollution. Cambridge University Press, Cambridge
10. European Parliament and of the Council (2002) Directive 2002/49/EC of the European Parliament and of the Council of 25 June 2002 relating to the assessment and management of environmental noise
11. Linares C, Díaz J, Tobías A, Miguel JMD, Otero A (2006) Impact of urban air pollutants and noise levels over daily hospital admissions in children in Madrid: a time series analysis. Int Arch Occup Environ Health 79:143–152 . doi: 10.1007/s00420-005-0032-0

12. Muzet A (2007) Environmental noise, sleep and health. Sleep Med Rev 11:135–142 . doi: 10.1016/J.SMRV.2006.09.001
13. Ji M, Cohan DS, Bell ML (2011) Meta-analysis of the association between short-term exposure to ambient ozone and respiratory hospital admissions. Environ Res Lett 6:024006 . doi: 10.1088/1748-9326/6/2/024006
14. Gan WQ, Davies HW, Koehoorn M, Brauer M (2012) Association of Long-term Exposure to Community Noise and Traffic-related Air Pollution With Coronary Heart Disease Mortality. Am J Epidemiol 175:898–906 . doi: 10.1093/aje/kwr424
15. Jacquemin B, Sunyer J, Forsberg B, Götschi T, Bayer-Oglesby L, Ackermann-Liebrich U, de Marco R, Heinrich J, Jarvis D, Torén K, Künzli N (2007) Annoyance due to air pollution in Europe. Int J Epidemiol 36:809–820 . doi: 10.1093/ije/dym042
16. Basner M, Babisch W, Davis A, Brink M, Clark C, Janssen S, Stansfeld S (2014) Auditory and non-auditory effects of noise on health. Lancet 383:1325–1332 . doi: 10.1016/S0140-6736(13)61613-X
17. Hossam Eldien H (2009) Noise mapping in urban environments: Application at Suez city center. In: 2009 International Conference on Computers & Industrial Engineering. IEEE, pp 1722–1727
18. Jacob DJ (2000) Heterogeneous chemistry and tropospheric ozone. Atmos Environ 34:2131–2159 . doi: 10.1016/S1352-2310(99)00462-8
19. Clapp LJ, Jenkin ME (2001) Analysis of the relationship between ambient levels of O3, NO2 and NO as a function of NOx in the UK. Atmos Environ 35:6391–6405 . doi: 10.1016/S1352-2310(01)00378-8
20. Hewitt CN, Jackson A V. (2009) Atmospheric science for environmental scientists. Wiley-Blackwell
21. Wallace JM (John M, Hobbs PV (2006) Atmospheric science : an introductory survey. Elsevier Academic Press
22. Agudelo–Castaneda DM, Calesso Teixeira E, Norte Pereira F (2014) Time–series analysis of surface ozone and nitrogen oxides concentrations in an urban area at Brazil. Atmos Pollut Res 5:411–420 . doi: 10.5094/APR.2014.048
23. De la Guardia M, Armenta S (Sergio) (2016) Quality of air. Elsevier
24. Teixeira EC, de Santana ER, Wiegand F, Fachel J (2009) Measurement of surface ozone and its precursors in an urban area in South Brazil. Atmos Environ 43:2213–2220 . doi: 10.1016/J.ATMOSENV.2008.12.051
25. Pudasainee D, Sapkota B, Shrestha ML, Kaga A, Kondo A, Inoue Y (2006) Ground level ozone concentrations and its association with NOx and meteorological parameters in Kathmandu valley, Nepal. Atmos Environ 40:8081–8087 . doi: 10.1016/J.ATMOSENV.2006.07.011
26. Markovic D, Markovic D (2005) The relationship between some meteorological parameters and the tropospheric concentrations of ozone in the urban area of Belgrade. J Serbian Chem Soc 70:1487–1495 . doi: 10.2298/JSC0512487M
27. Nishanth T, Satheesh Kumar MK, Valsaraj KT (2012) Variations in surface ozone and NOx at Kannur: a tropical, coastal site in India. J Atmos Chem 69:101–126 . doi: 10.1007/s10874-012-9234-5
28. Jenkin ME (2004) Analysis of sources and partitioning of oxidant in the UK—Part 2: contributions of nitrogen dioxide emissions and background ozone at a kerbside location

in London. Atmos Environ 38:5131–5138 . doi: 10.1016/J.ATMOSENV.2004.05.055

29. Notario A, Bravo I, Adame JA, Díaz-de-Mera Y, Aranda A, Rodríguez A, Rodríguez D (2012) Analysis of NO, NO2, NOx, O3 and oxidant (OX = O3 + NO2) levels measured in a metropolitan area in the southwest of Iberian Peninsula. Atmos Res 104–105:217–226 . doi: 10.1016/J.ATMOSRES.2011.10.008

Novel machine learning algorithms for cybersecurity in IoT networks

Manuel Lopez-Martin[1[0000-0003-3550-560X]], Belen Carro [1[0000-0001-7051-8479]] and Antonio Sanchez-Esguevillas [1[0000-0003-3620-1106]]

[1] Dpto. TSyCeIT, ETSIT, Universidad de Valladolid, Paseo de Belén 15, Valladolid 47011, Spain

Abstract. With the growing social and economic importance of IoT networks they are becoming the target of cybersecurity attacks, making it necessary to identify and detect changing and sophisticated intrusions through the application of novel detection techniques. Machine learning is currently an area of active research in cybersecurity, since it can learn complex patterns of intrusions directly from real data without relying on assumptions about the structure of such patterns (complex and ever changing) or the need to maintain an updated database of known patterns of attacks. In this paper, we present a review of novel approaches for intrusion detection using current developments in machine learning, such as convolutional and recurrent neural networks, generative models, kernel methods and deep reinforcement learning. We also show the necessary data transformation to apply these models.

Keywords: Machine learning, Cybersecurity, IoT networks

1 Introduction

In recent years there has been a very significant increase in the presence of IoT networks and services in many technologically advanced areas i.e. smart cities, cyber-physical systems, new production processes [1]. This importance increases the risk of attacks on these networks as part of the activities of cyber criminals. Intrusion detection systems (IDS) are an important element to prevent these attacks. An IDS identifies intrusions inside the security perimeter (e.g. established by a firewall). In a first classification, they can be differentiated into host-based IDS (HIDS) and network-based IDS (NIDS), depending on whether they detect threats at the network level or are deployed on a particular host, detecting intrusions only for that host. It is also possible to classify IDS by different detection approaches as: signature-based detection and anomaly-based detection. Signature-based detection methods use a database of previously identified bad patterns to identify and report an attack, while anomaly-based detection uses a model to classify (label) traffic as good or bad, based mainly on supervised or unsupervised machine learning (ML) methods.

Supervised ML methods employ the usual models: Support Vector Machine (SVM), Logistic Regression [2,3]. Unsupervised methods can be set-up in different

ways [4], adopting different approaches: probabilistic methods, clustering methods or deviation methods. In probabilistic methods, we characterize the probability distribution of normal data and define as an anomaly any data with a given probability lower than a threshold. In clustering methods, we cluster the data and categorize as an anomaly any data too far away from the desired normal data cluster. In deviation methods, we define a generative model able to reconstruct the normal data, in this setting we consider as an anomaly any data that is reconstructed with an error higher than a threshold.

In this work we will review novel architectures for supervised ML and unsupervised ML based on generative models, plus an additional new paradigm based on reinforcement learning models which are also recently applied to intrusion detection [5].

The location of the IDS inside the network is a difficult problem, since it requires an agile access to the communication data packets, which allows a classification of the traffic that needs to be fast an efficient [6]. The new modular and highly configurable networks (e.g. Software Defined Networks (SDN) and edge computing) provide a solution, since they facilitate the choice of deployment location for network security services [7]. As an example, Fig 1 presents a high-level view of data distribution and processing services for IoT devices in a Smart City application. In this example, the middle layer (Fig 1) can provide real-time local data analysis (e.g. security services) at the edge of the network, near the source of the data. In parallel with this improvement in data access at the network level, there has been advances in new processing platforms (e.g. GPUs) that can be deployed at the edge layer [8] and new detection algorithms that make use of these platforms (deep learning models). All these elements together provide a promising horizon for future advances in IDS for highly demanding networks such as IoT networks.

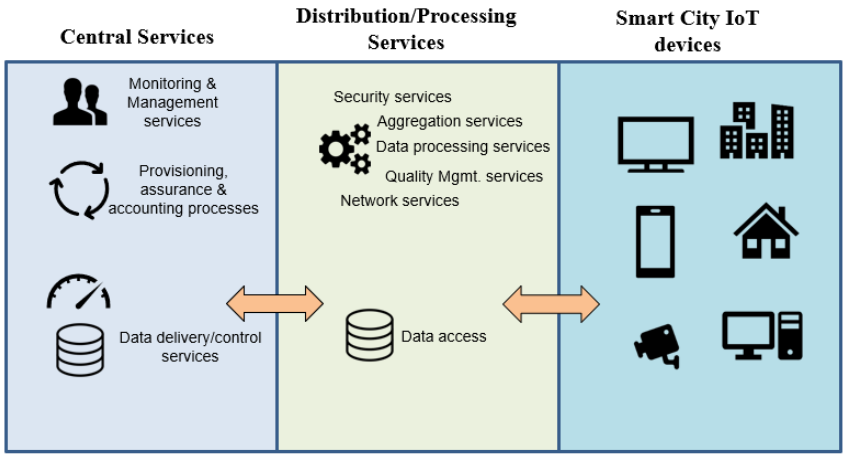

Fig. 1. High level view of data distribution and processing services for IoT devices in a Smart City application.

In this work, we will focus on the new proposals made for intrusion detection using deep learning architectures, with a perspective on related works, but mainly trying to provide an overview of the proposed new methods and their most important characteristics. In particular, we will summarize the required preprocessing of the datasets [9] used to train the models, which is a critical issue but one that is generally overlooked.

The models analyzed will be:1D and 2D convolutional neural networks (CNN), recurrent neural networks (RNN), fully connected networks (FCN) aka multilayer perceptron (MLP), variational autoencoders (VAE) and conditional variational autoencoders (CVAE), kernel approximation (KA) methods and reinforcement learning models (RL).

The structure of the paper is the following: Related works are presented in Section 2. The description of the models is introduced in Section 3, and, finally, Section 4 provides discussion and conclusions.

2 Related works

There are excellent recent reviews that classify, analyze and present the current advances of ML for cybersecurity in general and intrusion detection in particular [1,2]. We can consider intrusion detection as a sub-field of the more generic application of ML to the analysis and prediction of network traffic [10,11] which is an important area of new developments and research.

ML supervised [12] and unsupervised [13] methods have been widely applied to intrusion detection for data networking. The classic ML models applied to IDS have been [14,15]: Support Vector Machine (SVM), Multilayer Perceptron (MLP), K-Nearest Neighbors (KNN), Decision Trees (DT), Naive Bayes (NB) and Random Forest.

It is important to mention the increasing reference in the literature to the new deep learning models, in particular convolutional and recurrent networks and generative models, applied to intrusion and anomaly detection, with updated reviews available [16,17,18].

3 Novel ML models for intrusion detection

In this work we will review the main novel algorithms applied to supervised network traffic classification, and in particular to intrusion detection.

These algorithms are mostly based on deep learning models which employ a lego-like sequence structure of different models with the basic restriction of being able to apply an end-to-end iterative optimization process of a loss function based on gradient descent.

3.1 Data transformation

All the models presented in this work require a prior data transformation applied to a dataset of explanatory features which are used to infer the intrusion label. This features are obtained from the data packets transmitted in the network.

As presented in Fig 2 the dataset is usually obtained from the sequence of packets associated to each communication flow between two communication parties. The data of interest of these sequence of packets are usually the packet headers. In this way, for each communication flow we have a vector time-series composed of a sequence of packet headers (features). To use this vector time-series in a ML model we can perform several formatting actions (Fig 2, right part): (A) To flatten the vector time-series of features and to obtain a long single vector of features. (B) To reshape the vector time-series into a matrix structure (2D array). (C) To keep the vector time-series as it is.

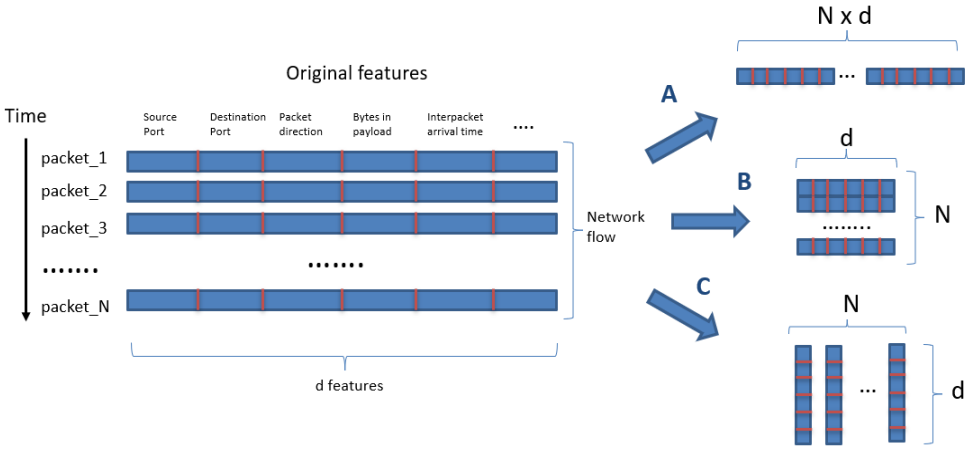

Fig. 2. Possible format transformations applied to the packets of a communication flow.

In other cases, the original sequence of packets is already processed using statistical/aggregation functions (i.e. mean and standard deviation of interarrival times between packets, mean/median of packet lengths…). In this case, we already start from a vector of features associated to each communication flow (Fig 3). Similarly, to the previous case, some data formatting can be applied in this case (Fig 3, right part): (A) To keep the vector of features as it is (1D array). (B) To reshape the vector of features (1D array) into a matrix structure (2D array).

The different data formatting presented in both Fig 2 and 3 will be used for different models. The format to be used is defined by the initial model in the lego-like sequence of models of the deep learning framework. The format identified as A will be used in deep learning frameworks whose initial model is an FCN or CNN-1D. Format B will be required for CNN-2D initial models and format C for RNN models.

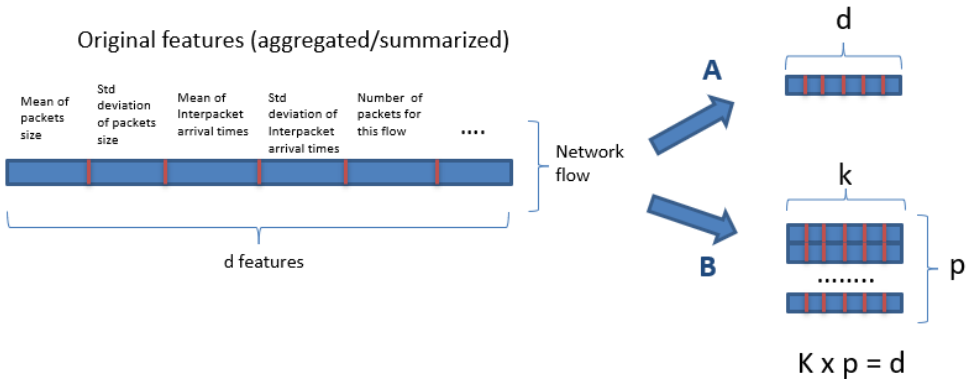

Fig. 3. Possible format transformations applied to summary features of a communication flow.

3.2 Convolutional and recurrent NNs

There are several very extensive reviews of deep learning models applied to intrusion detection [11,16] that present the models in detail and the use of those models in current research works. Of all the models presented, there are two models: CNN and RNN, which are among the most cited.

Fig 4 shows the basic frameworks that can be used for intrusion detection using deep learning models based on CNN and RNN networks [16]. We can see that the usual combinations are: a CNN-2D followed by a fully connected network (FCN) (Fig 4, upper diagram), a CNN-2D followed by an RNN (one or several layers) and a FCN (Fig 4, middle diagram), and, finally an RNN (one or several layers) followed by an FCN (Fig 4, lower diagram) [16,19,20].

Depending on the initial network, the data must be transformed into a 2D matrix format or a sequence of vector time series. In all cases, it is necessary to apply several data transformations within the network to adapt to the data formats needed by different networks in the transitions between the network models.

An important finding is that the inclusion of a CNN-2D improves the classification performance of the models, even when the initial dataset has a time-series structure [19,20]. This is quite remarkable since time-series data have the RNN models as their reference models. In some cases, a single CNN-2D provides better results, without the inclusion of any RNN model.

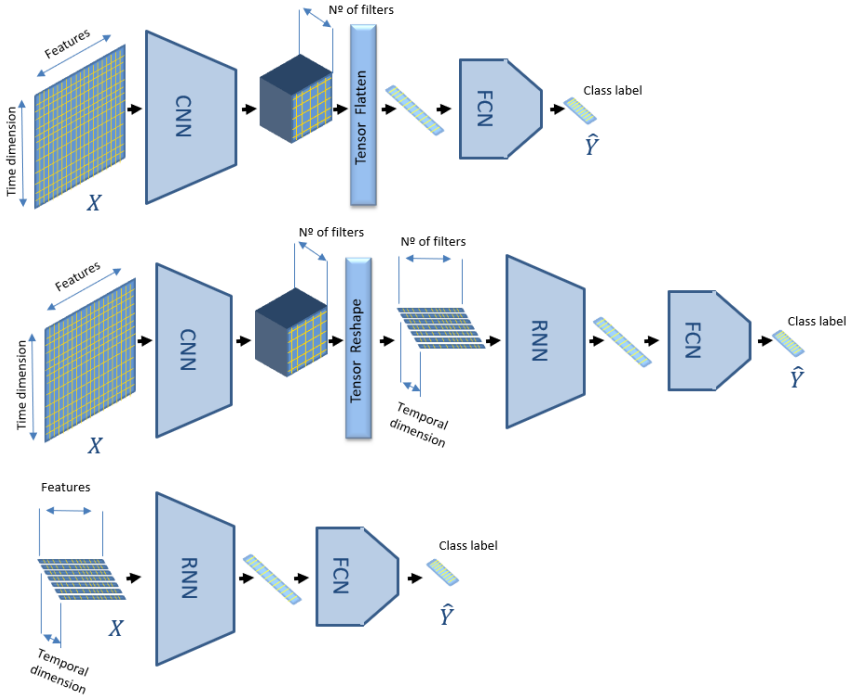

Fig. 4. Deep learning architectures to implement intrusion detection classifiers using CNN, RNN and FCNs.

3.3 Generative models

We can consider two types of classification models in a supervised scenario: discriminative and generative models. In a supervised model we have a set of features (X) and a set of labels (Y) to predict. In a discriminative model we try to learn directly P(Y/X) and prediction is made by choosing the value of Y that maximises it. In this case, the intention is to learn the decision boundary between features/labels. In a generative model we try to learn P (X,Y) and prediction is made by choosing the value of Y that maximizes P(X,Y) given an X. That is, in the discriminative case we try to find the Y that maximizes P(Y/X). Meanwhile, in the generative case we try to find the Y that maximizes P(X/Y)*P(Y), that is P(X,Y). An important consequence is that once P(X, Y) is known, we can take samples of this joint probability distribution.

A particularly interesting architecture for generative models is a variational auto-encoder (VAE) (Fig 5, upper diagram) which is a neural network that tries to reconstruct the input with an intermediate layer (x) that learns the mean and standard deviation of a random generated latent space. A VAE is an evolution of the autoencoder (AE), which, based on different principles, also tries to learn an intermediate representation of the data. In this case, the intermediate representation is deterministic rather than stochastic, as was the case for the VAE model. An AE is not a generative

model. AE based models have been widely used in unsupervised anomaly detection [21], using the reconstruction error as an indication of an 'anomalous' input when the AE has been trained exclusively with 'normal' inputs.

The VAE architecture [22] supports an interesting variant that consists in adding the labels to the decoder (Fig 5, lower diagram), this variant is called a conditional VAE (CVAE) [22].

Both VAE and CVAE can be used for intrusion detection. In the case of VAE, we need to train as many models as different values have the class/label (one VAE per class value), where each training step uses exclusively the samples of a particular label value. The prediction is based on finding the model that best reconstructs the test input (X). In the case of CVAE, we need a unique model that is trained with all the input data and its associated label values. The prediction is based on iterating the model with all the class values to find the one that produces the best reconstruction results. In both cases, the process followed is similar, but in the case of the CVAE we need a single model with a single training step, while a VAE requires k models with k training steps (where k is the number of values of the class/intrusion label) [22].

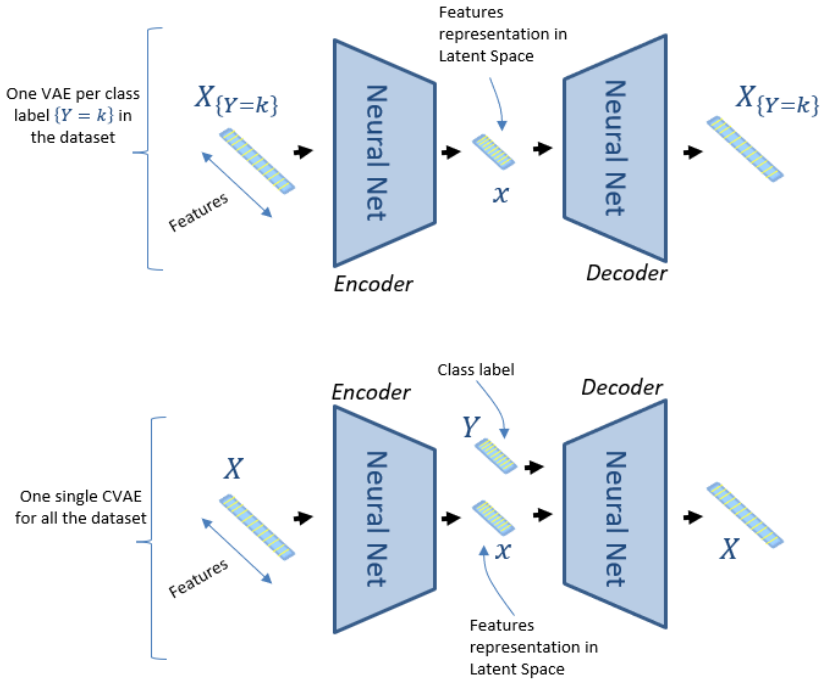

Fig. 5. Generative model architectures to implement intrusion detection classifiers using variational autoencoders (upper diagram) and conditional variational autoencoders (lower diagram).

3.4 Kernel methods combined with shallow NNs

In the models presented in Section 3.3, we try to achieve a data representation in a latent space with a dimensionality much lower than the input space.

There is another way of proceeding, which is to make a representation of the data in a vector space with a dimensionality much greater than the input space [23]. This is obtained with a data transformation called 'kernel approximation'. The interesting result is that with this mapping to a higher dimensional space we can then use a shallow neural network based on a single linear layer, achieving a final result similar to an SVM with a radial basis function kernel [23]. An overview of the architecture is presented in Fig 6.

The architecture in Fig 6 presents many advantages that consist of being fast and requiring fewer resources than similar non-linear models, while being able to fit highly non-linear datasets [23].

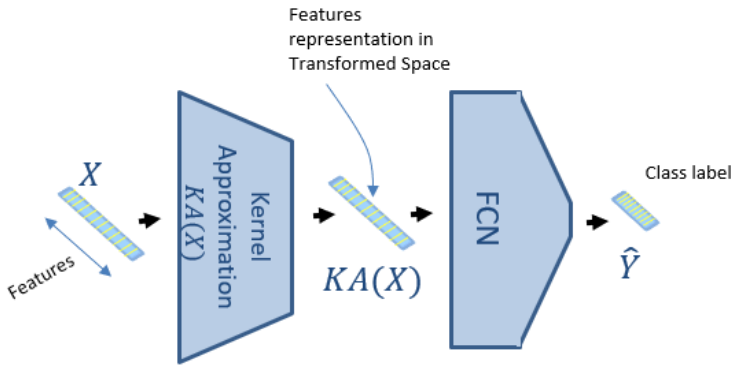

Fig. 6. Shallow network architecture to implement intrusion detection classifiers using kernel approximation methods and a shallow neural network.

3.5 Reinforcement learning

Reinforcement learning (RL) [24] is a framework often used by cybersecurity systems [5] a state-of-the-art technique that allows an algorithm to learn while interacting with a live environment, where we do not start from a training dataset of samples with preassigned ground-truth intrusion labels.

In a classic RL scenario, the RL model learns from a score function (rewards) that the environment uses to provide an indication of how good or bad the current action provided by the agent (classifier) is. In addition to the rewards, the environment provides the agent with a new state (information about the environment variables) each time the agent delivers a new action to the environment (Fig 7, upper diagram). The learning process consists of making the agent maximize the total sum of rewards by

delivering the best possible sequence of actions to the environment. The nature of actions, states and rewards can be quite different for different applications.

In relation to intrusion detection, it is interesting the recent tendency to use several agents in an adversarial configuration with the intention of improving the learning process by allowing the agents to compete under opposite optimization criteria [25]. In this line, it is appealing the application of these ideas to intrusion detection when using a dataset of logged intrusions with their associated intrusion labels [26]. In this case, the RL environment is replaced by an additional agent that performs an intelligent sampling of the dataset with the intention of delivering to the classifier the samples that are more difficult to classify (Fig. 7, lower diagram). The final model [26] presents very interesting properties and is especially suitable for unbalanced data sets, as is the usual case in IDS.

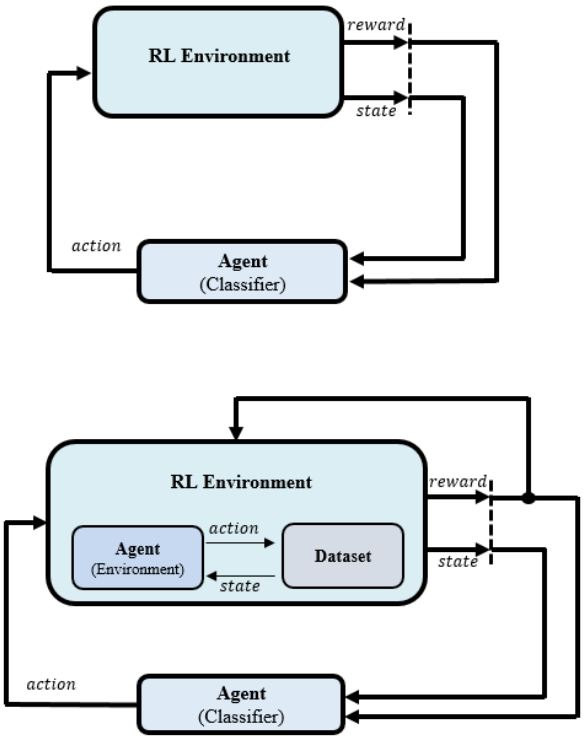

Fig. 7. Classic use of an RL model with a live environment (upper diagram), and alternative framework where the environment is replaced by an intelligent sampling of a dataset (lower diagram)

4 Future challenges

Intrusion detection is an unsolved, complex and challenging subject that requires as many new approaches and novel models as possible. The application of new ML models to this topic presents interesting perspectives, but nevertheless there are still many challenges, which could be summarized, without any intention of being exhaustive:

- Need for better datasets: balanced datasets, less noisy, with more samples of the minority attacks and with updated attacks.
- Need for standardized datasets to compare results between algorithms in a sensible and homogeneous way.
- Improve the interpretation of results. This is especially important with the use of the new deep learning models which present excellent results but with a black box paradigm that prevents providing a plausible interpretation of the prediction logic.
- Prepare against the use of adversarial examples that cause an intentional malfunction of deep learning models by adding slight modifications to the input data.
- Improve the speed of prediction and learning of the algorithms, considering the additional requirements imposed by highly demanding data networks.
- Expand the application of generative models with algorithms such as Generative Adversarial Networks (GAN) and of RL models.

5 Conclusion

This paper provides a review of the new machine learning models applied to intrusion detection with a special focus on IoT networks. It is shown that these models can be conveniently integrated into modern network architectures that use new high-performance platforms (e.g. TensorFlow).

We offer a review of the data transformations necessary for the models and a general description of the main network architectures and their characteristics when applied to intrusion detection problems.

We pay special attention to the new advances in deep learning, generative and reinforcement learning models. With a particular reference to proposals that seek improvements in performance and reduction in training and prediction times, so a special mention is made of the new techniques based on ‘kernel approximation’ methods combined with shallow linear neural networks.

References

1. Hussain F. et al. (2019). Machine Learning in IoT Security: Current Solutions and Future Challenges. arXiv:1904.05735v1 [cs.CR]

2. Bhuyan, M.H.; Bhattacharyya, D.K. & Kalita, J.K. (2014). Network Anomaly Detection: Methods, Systems and Tools. IEEE Communications Surveys & Tutorials, IEEE, Vol 16, pp. 303–336. https://doi.org/10.1109/SURV.2013.052213.00046
3. Mahdavinejad M.S. et al. (2017). Machine learning for Internet of Things data analysis: A survey. Digital Communications and Networks.
4. Aggarwal, C.C. (2013). Outlier Analysis; Springer: New York, NY, USA,. pp. 10–18, ISBN 978-1-4614-639-5.
5. Nguyen T.T. & Reddi V.J. (2019). Deep Reinforcement Learning for Cyber Security, arXiv:1906.05799 [cs.CR]
6. Zarpelao, B.B. et al. (2017). A survey of intrusion detection in Internet of Things. Journal of Network and Computer Applications. Vol. 84. 2017. pp. 25-37. https://doi.org/10.1016/j.jnca.2017.02.009
7. Wang J, Pan J. & Esposito F. (2017). Elastic urban video surveillance system using edge computing. *Proceedings of the Workshop on Smart Internet of Things (SmartIoT '17).* ACM, New York, NY, USA, 2017, Article 7
8. Abadi M. et al. (2016). TensorFlow: Large-Scale Machine Learning on Heterogeneous Distributed Systems. arXiv:1603.04467v2 [cs.DC]
9. Ring M. et al. (2019). A survey of network-based intrusion detection data sets. Computers & Security. Vol. 86. pp. 147-167. https://doi.org/10.1016/j.cose.2019.06.005
10. Wang M. et al. (2018). Machine Learning for Networking: Workflow, Advances and Opportunities. IEEE Network, vol. 32, no. 2, pp. 92-99. https://doi.org/10.1109/MNET.2017.1700200
11. Boutaba R. et al. (2018). A comprehensive survey on machine learning for networking: evolution, applications and research opportunities. Journal of Internet Services and Applications (2018) 9:16. https://doi.org/10.1186/s13174-018-0087-2
12. da Costa K.A.P. et al. (2019). Internet of Things: A survey on machine learning-based intrusion detection approaches. Computer Networks. Vol. 151. pp. 147-157. https://doi.org/10.1016/j.comnet.2019.01.023
13. Nisioti A. et al. (2018). From Intrusion Detection to Attacker Attribution: A Comprehensive Survey of Unsupervised Methods. *IEEE Communications Surveys & Tutorials*, vol. 20, no. 4, pp. 3369-3388. https://doi.org/10.1109/COMST.2018.2854724
14. Tsai Ch-F. et al. (2009) Intrusion detection by machine learning: A review. Expert Systems with Applications. Vol 36. Issue 10. pp. 11994-12000. https://doi.org/10.1016/j.eswa.2009.05.029
15. Yavanoglu O. & Aydos M. (2017). A review on cyber security datasets for machine learning algorithms. *2017 IEEE International Conference on Big Data (Big Data)*, Boston, MA, pp. 2186-2193. https://doi.org/10.1109/BigData.2017.8258167
16. Berman D.S. et al. (2019). A survey of deep learning methods for cyber security. Information, 10(4), 122. https://doi.org/10.3390/info10040122
17. Kim K. & Aminanto M.E. (2017). Deep learning in intrusion detection perspective: Overview and further challenges. 2017 International Workshop on Big Data and Information Security (IWBIS), Jakarta, pp. 5-10. https://doi.org/10.1109/IWBIS.2017.8275095
18. Chalapathy R. & Chawla S. (2019). Deep Learning for Anomaly Detection: A Survey. arXiv:1901.03407 [cs.LG]
19. Lopez-Martin, M., Carro, B., Sanchez-Esguevillas, A., & Lloret, J. (2017). Network Traffic Classifier With Convolutional and Recurrent Neural Networks for Internet of Things. *IEEE Access*, vol. 5, pp. 18042-18050. https://doi.org/10.1109/ACCESS.2017.2747560
20. Lopez-Martin, M., Carro, B., Lloret, J., Egea S. & Sanchez-Esguevillas, A. (2018). Deep Learning Model for Multimedia Quality of Experience Prediction Based on Network Flow

Packets. *IEEE Communications Magazine*, vol. 56, no. 9, pp. 110-117. https://doi.org/10.1109/MCOM.2018.1701156

21. Chen Z. et al. (2018). Autoencoder-based network anomaly detection. *2018 Wireless Telecommunications Symposium (WTS)*, Phoenix, AZ, pp. 1-5. https://doi.org/10.1109/WTS.2018.8363930
22. Lopez-Martin, M., Carro, B., Sanchez-Esguevillas, A., & Lloret, J. (2017). Conditional variational autoencoder for prediction and feature recovery applied to intrusion detection in IoT. Sensors, 17 (9), 1967. https://doi.org/10.3390/s17091967
23. Lopez-Martin, M., Carro, B., Sanchez-Esguevillas, A., & Lloret, J. (2019). Shallow neural network with kernel approximation for prediction problems in highly demanding data networks. Expert Systems with Applications. Vol 124, pp 196-208. https://doi.org/10.1016/j.eswa.2019.01.063
24. Sutton R. S. & Barto A. G. (1998). Reinforcement Learning: An Introduction. A Bradford Book; Second Edition. https://mitpress.mit.edu/books/reinforcement-learning-second-edition
25. Servin A. (2009). Multi-Agent Reinforcement Learning for Intrusion Detection. PhD Thesis, University of York. UK. http://etheses.whiterose.ac.uk/id/eprint/690
26. Caminero G., Lopez-Martin M & Carro B. (2019). Adversarial environment reinforcement learning algorithm for intrusion detection. Computer Networks. Vol 159, pp 96-109. https://doi.org/10.1016/j.comnet.2019.05.013.

Energy Storage Systems for power supply of ultrahigh speed Hyperloop trains

Marcos Lafoz[0000-0002-8196-8958], Gustavo Navarro[0000-0002-5169-9080], Marcos Blanco[0000-0003-3641-1867] and Jorge Torres[0000-0001-7524-9925]

Centro de Investigaciones Energéticas, Medioambientales y Tecnológicas (CIEMAT), Av. Complutense, 40. 28040 Madrid (Spain)
marcos.lafoz@ciemat.es
gustavo.navarro@ciemat.es
marcos.blanco@ciemat.es
jorgejesus.torres@ciemat.es

Abstract. The paper analyses the alternatives for the power supply of a Hyperloop type railway transport. The particular case of the technology of the Spanish company ZELEROS is studied. Specifications related to both a first prototype and a commercial system are presented and the power supply requirements analysed. After considering different alternatives, energy storage based on supercapacitors is obtained as a feasible and competitive solution for the power supply of this application due to the power/energy ratio and the cycles capability. A preliminary design methodology for the energy storage requirements is presented in the paper. Once selected the type of linear motor, the power supply scheme is presented, based on a motor-side power electronic converter and a DC/DC converter which connects to the energy storage devices. An additional low power grid-tie converter for the recharge of the energy storage system is also used. Different track sections are defined, connected to the power electronic converter through corresponding switches, being supplied sequentially when the capsule presence is detected along the track. The number of track sections depends on the limitations of voltage and current, defined by the power electronic converter selected and particular issues like current density selection and the evaluation of skin effect are very important for this application.

Keywords: Energy Storage, Hyperloop, power supply, power electronics.

1 Introduction, historical reference and concept.

According to the European Environmental Agency, in 2016, the transport sector contributed 27 % of total EU-28 greenhouse gas emissions [1]. Emissions need to fall by around two thirds by 2050, compared with 1990 levels, in order to meet the long-term 60 % greenhouse gas emission reduction target as set out in the 2011 Transport White Paper. Beyond the particular vehicles and the freight traffic, which means 72% of them, it is remarkable the pollution levels achieved by the air traffic, reaching even a higher level of pollution than the railway traffic in the range of distances of 500 km.

On the other hand, railway traffic results not as competitive as air traffic for distances higher than 1,000 km.

In this scenario, in 2013, the American entrepreneur Elon Musk, owner of Tesla and SpaceX [2] companies, launched the idea of a new ultrafast train, magnetically levitated and travelling along a low pressure tube. This mean of transport was named Hyperloop and it is considered as the 5th mean of transport, although is sustainability has been sometimes questioned.

Currently there are several projects to be mentioned [3], some other particular projects in America [4], some in Europe [5] and some in Asia [6] to develop this technology. In the case of Europe, a Commission has been created to define the operational specifications of this mean of transport, with the aim to ensure the interoperability between the different systems in operation across Europe.

The concept could be related to some very high speed trains developed in the 20th century, the magnetic levitation (maglev) trains [7][8][9]. In fact, the idea of the Hyperloop concept is not new, but it has some references from the 18th century, when the French inventor Denis Papin developed the idea of a tubular vehicle moving inside a tube as a result of the pressure difference between the front and rear parts of the vehicle. In the 19th century, this idea was materialized in England, in 1827, when the English inventor George Medhurst developed a vehicle moving along a rectangular pipe by the effect of a 1.07 atm pressure. It was named Atmospheric Railway. In 1867, in New York (USA), Alfred Ely Beach invented a similar device (see Fig.1) which would become the first concept of suburban transport.

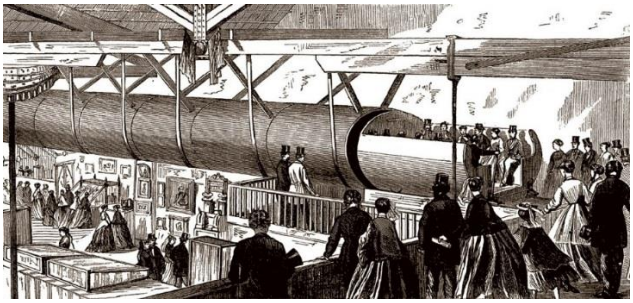

Fig. 1. Neumatic tube by Alfred Ely Beach, in New York (USA), 1867.

Back to the present time, the current operational requirements of the named system are related to the application both of freight railway traffic and of passenger traffic, connecting distances in the range of 1,000 km and maximum speed in the range of 700-1,000 km/h. At this range of speed the use of catenary and pantograph based systems is not possible since technology is does not support such conditions. Alternative systems need to be used for the traction of the moving part along the rails.

The technology is based on a railway line inside a pressurized tube, where several moving parts, hereafter capsules, are travelling between two points, with an utilization period estimated in the range of 1 and 5 minutes between capsules. The rail line can be divided in three areas: firstly, an acceleration area, between 5 and 10 km, where

the capsule is accelerated with the help of a linear motor installed along the rail. Although different options are possible as traction motor, it is preferred the one with less weight in the moving part and more simplicity in the coils supplied along the track line. During this area, the capsule is accelerated to maximum speed. Secondly, the area where the capsule maintains the maximum speed. The losses are compensated by means of an on-board propulsion system that can be also based on different technological solutions. In the case of study, a compressor gets the air in front of the capsule, compresses it and subsequently it is expanded in a reaction turbine, in a similar way than in an aircraft. This air is not only used for the propulsion of the capsule but also for the levitation, in order to minimize the mechanical friction. The energy used for this process is covered by a set of batteries located on-board of the capsule. Finally, when the capsule arrives to the destination, it needs to be braked, using regenerative braking to recuperate part of the kinetic energy of the capsule. Additional braking systems are installed at the capsules in order to act in case of emergency.

Several studies have been accomplished in order to analyse the economic viability of this solution both in passengers and cargo [10].

Fig. 2 shows the technology developed by the Spanish company ZELEROS [11], winner of the 2016 SpaceX competition in the category of best design and best propulsion system.

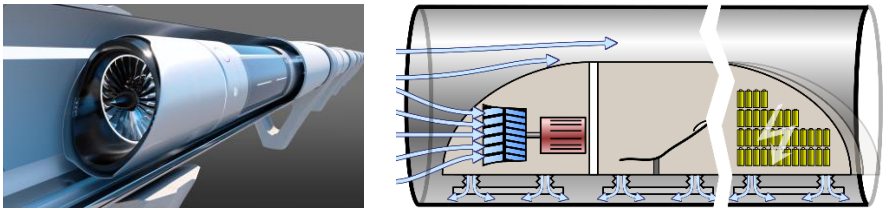

Fig. 2. Technology for Hyperloop form the Spanish company ZELEROS.

CIEMAT Institute is collaborating with the Spanish company ZELEROS in the development of the acceleration device and the power supply of the technological solution proposed. This paper will be focused in the study of the power supply for the acceleration of the capsules within the first area previously described.

2 Analysis of the options for the power supply of the capsules.

The technical specifications for the acceleration device required by the system developed by ZELEROS are compiled in Table.1.

Table 1. Technical specifications for the acceleration area.

Maximum speed	Average acceleration	Acceleration time	Acceleration length	Maximum force	Mass
700 km/h (194 m/s)	2 m/s^2	97 sec	10 km	100 kN	40,000 Kg

First decision is the acceleration profile along the acceleration area. It is possible to choose a constant acceleration, applying a constant force, but it produces a maximum power level very high (around 15 MW in the study case) or, on the contrary, to select a more typical profile in industrial electric drives consisting of a first section of constant force and another section of constant power. In this case, the maximum power is lower (10 MW for the study case) and therefore more convenient for the design of electric equipment, although it requires a higher force value in the first section. The two options are presented in Fig. 2, but the second one is preferred since it gets a better dynamics for the moving capsule and allows to reduce the power, as well as the current intensity during the acceleration process.

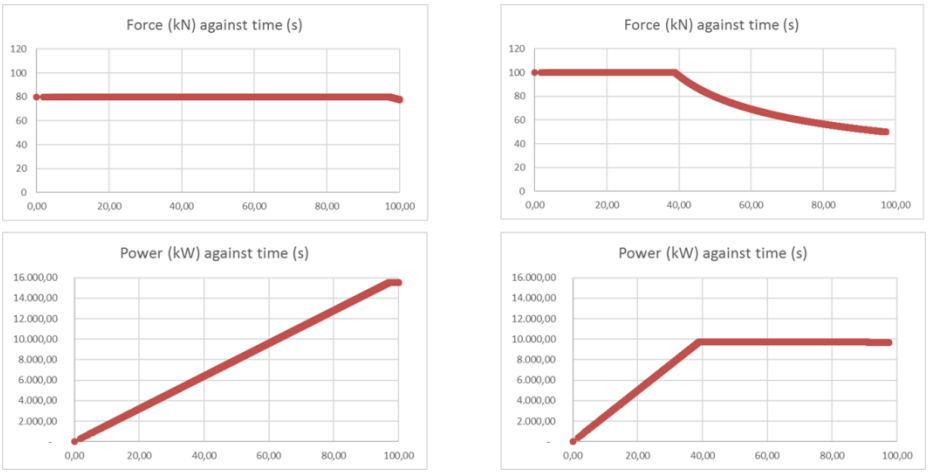

Fig. 3. Constant force profile (left) and constant power profile (right).

According to the constant power profile from Fig. 3 (right), the theoretical amount of energy required for the acceleration of the moving capsule (not considering the efficiency of the system neither the additional power consumption of the auxiliary systems involved) with a maximum power of 10 MW can be estimated as the area under the red curve:

$$Energy = \frac{1}{2}(P_{max} \cdot T1) + P_{max} \cdot (\text{T-T1}) = \frac{1}{2}(10MW \cdot 38sec.) + 10\text{MW} \cdot (97\text{sec-}38\text{sec}) = 780\text{MJ} = 217\text{kWh} \quad (1)$$

A value of 217 kWh has been obtained, used in the following calculations.

2.1 Power supply options for the acceleration linear motor.

Different options for the power supply of the linear motor installed in the acceleration area to achieve the maximum speed of the capsules are presented as following:

a) Direct connection to the electric grid

The first option is the direct connection to the electric grid. The advantages of this scheme are that: allows the use of a high voltage, very convenient for the supply of the linear motor coils, since the voltage level can be transformed easily in the voltage level required; the connection is quite simple; the power supply is guaranteed. On the other hand, as inconvenient there is a higher cost of the infrastructure, the power consumption and the payment for the use of the grid, although the utilization time is quite low.

This is why it makes sense to consider the use of energy storage systems as an alternative.

b) Connection through an energy storage system

Among the different energy storage technologies already existing in the market, nowadays three of them have been selected according to their maturity level and the characteristics of high power, not very high energy and very fast response.

b.1) Batteries

Batteries have emerged as the leading energy storage system for providing a wide variety of grid services as well as for their extensive use in the electric vehicle sector. However, this technology presents two important disadvantages when considering this application: firstly, the ratio power/energy of most of batteries is in the range of 1MW/1MWh, resulting in a very excessive amount of energy for a Hyperloop supply, considering that it is required for the case under analysis 10MW, 0.217MWh. Secondly, the number of charge-discharge cycles required by the application is very high (several hundred cycles per day), and the cycles supported by the batteries before an important loss of capacity is in the range of 5,000-25,000 cycles. That would lead to replace the batteries quite often (every few months) with the consequent high cost.

b.2) Supercapacitors

This technology results quite appropriate when considering the ratio power/energy offered by the commercial solutions, in the order of 1MW/(5-10kWh), very similar to the level required by this application.

On the other hand, the most important limitation is the isolation limit offered by the modules, allowing a voltage of 1,500V. By using a topology with a middle point grounded it is possible to increase the voltage level to 3,000V, still a quite low voltage level for the power level required.

A study based on three commercial solutions of supercapacitors have been accomplished and presented in Fig. 3. The three of them provide the same conclusion, which is that the most restrictive parameter for designing is the energy capacity, remaining some power capability underused, especially considering the low operation time, which does not increase the thermal necessities.

Nevertheless, the market trend for this technology goes towards getting supercapacitors cells with double the energy very soon (by 2020). In that case, the use of supercapacitors would be very suitable for this application, resulting economically competitive comparing with grid connection or batteries.

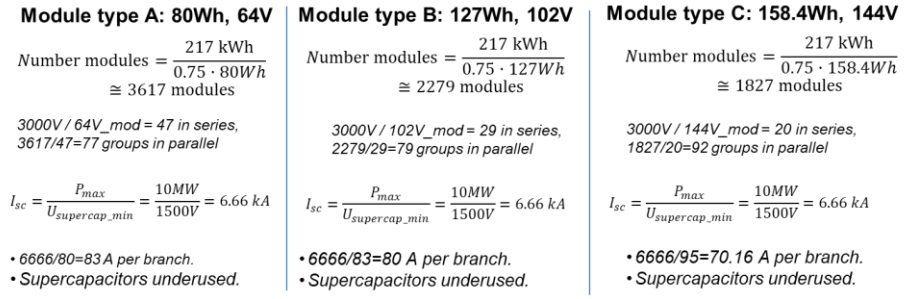

Fig. 4. Dimensioning of energy storage systems required for the acceleration of a capsule, using three types of supercapacitor commercial solutions: A, B and C.

b.3) Flywheels

Other technologies as flywheels could be also used from the point of view of power/energy ratio and number of cycles capacity. However, the required high voltage level for the linear motor has a negative influence in the feasibility of using flywheels for this application since it would increase very much the cost.

3 Development of a 1/3 reduced scale prototype of linear motor and power supply.

First step before the opening of a commercial train line is the development of a test line for validation of the technology. A 1/3 reduced scale prototype of linear motor and power supply system is being currently accomplished. The technical specifications for this system are presented in Table 2. The power supply profile with the scheme of a constant power is shown in Fig. 5.

Table 2. Technical specifications for the acceleration area of the 1/3 scale prototype.

Maximum speed	Average acceleration	Acceleration time	Acceleration length	Maximum force	Mass
500 km/h (139 m/s)	20 m/s^2	7 sec	0.5 km	80 kN	2,000 Kg

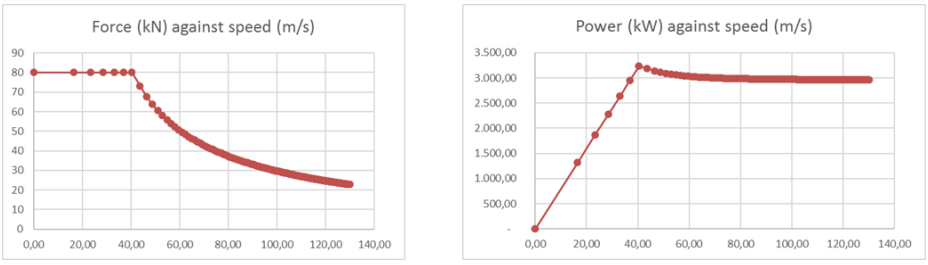

Fig. 5. Profile of force vs speed and power vs speed for the 1/3 reduced scale prototype.

3.1 Preliminary design of an energy storage system for the power supply

Considering the previous specifications, a preliminary design of an energy storage system has been carried out. The methodology followed gets firstly a dimensioning based on the energy required, secondly on the voltage by associating the storage cells and finally validating the current required by the application.

a) Energy Dimensioning

The energy required during the acceleration process can be calculated based on the kinetic energy associated to the maximum speed of the capsule. For this preliminary calculation, efficiency from electric to mechanic conversion has been considered 100% but it must be upgraded with the different efficiencies involved in the conversion process (mainly aerodynamic losses, magnetic levitation losses and Joule effect losses at the linear motor and the power distribution line along the acceleration area).

The energy value is given by (2).

$$E_{kinetic} = \frac{1}{2} \cdot mass \cdot v_{max}^2 = \frac{1}{2} \cdot 2{,}000 \cdot 139^2 = 19.32MJ \tag{2}$$

Selecting one of the commercial modules with an energy of 80Wh (64V,141F) and taking into account a deep of discharge of half of the total voltage, which means 75% of the total energy, the number of modules required to fulfill the energy is 90, as it is obtained from (3).

$$\text{Number modules} = \frac{Energy_{required}\,(J)}{deep_{of_{discharge(p.u)}} \cdot Energy_{module\,(Wh)} \cdot \frac{3.6kJ}{Wh}}$$

$$\text{Number modules} = \frac{19.32MJ}{0.75 \cdot 80Wh \cdot 3.6\,J/W\,h} \cong 90 \tag{3}$$

b) Voltage Dimensioning

The voltage selection depends on the maximum isolation voltage supported by the supercapacitor modules. Considering the same 64V modules, and taking into account a middle point grounded topology (supports maximum of 3,000 V), splitting the previously calculated 90 modules in three branches of 30 series connected modules each, it is achieved a maximum voltage of 1,920V. It remains the possibility to connect other 15 modules more in series per branch, increasing the energy of the complete system in 50% from the point of view of voltage limitation. The voltage of the storage system when reaching the discharge point is 690 V, voltage used to calculate the maximum current.

As a consequence, the already calculated 90 cells are distributed as explained above to fulfill the voltage requirements.

c) Current Dimensioning

The most restrictive current occurs when the voltage is minimum in the energy storage system.

$$I_{supercaps\ \ P=cte} = \frac{P_{max}}{U_{supercap\_min}} = \frac{2.96MW}{690V} = 4{,}289A \tag{4}$$

That implies 1,429 A per each supercapacitor branch.

Considering that the maximum current of the module is 2,000A and that the average current during the operation is in the range of 1,000A, there is no limitation by current. However, it is very important to analyze the thermal effects of the current, since the temperature increase could lead to an important loss of capacitance in the supercapacitors. A thermal model is required to do an accurate study of the transient, not facing it at this point, but considering that the operating time is only 7 seconds, and although this is an important time from the point of view of the power electronics, it is not important for the supercapacitors due to their relatively high thermal inertia.

The already selected modules are therefore validated in terms of current.

3.2 Scheme of the power supply for the reduced scale system.

As a result of section 3.1, the prototype can be supplied by means of a set of series connected supercapacitors. The supercapacitors would be connected through a DC/DC converter to a DC-link and then, a power electronic converter supply the linear motor required for the acceleration. The recharge of the supercapacitors is done by means of a grid-tie converter (GTC), connected to the DC-link, but of much less power than the DC/DC converter. A 50kW grid-tie converter is enough to replace the full energy of the system in less than 10 minutes. These elements are depicted in the scheme of Fig. 6.

As previously stated, the acceleration section needs a linear motor along 500 m in the reduced scale prototype. The design of this motor, although not accomplished in this paper, is based on the definition of a required maximum force, a velocity profile and some dimensional restrictions. Several solutions for the linear motor have been studied in the literature and most of them are based on permanent magnet machines [12]. However, a solution based on reluctance machine has been selected in this case because of the robustness, simplicity and reduced cost [13-15]. A decision of how to split the ampere·turns parameter into number of coil turns and the current has been considered, taking into account the voltage drop and the power electronics design.

On the other hand voltage requirements are also defined in order to compensate the electromagnetic force, the resistive voltage drop and the inductance transient, required to reach the current reference during the operation. As a result, the most suitable solution for the linear motor is to use different types of coils along the acceleration section. That is the best way to take advantage of the number of turns of the coil in order to adapt it to the electromagnetive force, according to the speed. The higher the speed,

the lower the number of turns of the coil. Five different types of coils have been considered in this particular case of study, with a number of turns varying from 12 to 4 as increasing the speed or the distance along the track.

A set of different track sections are calculated after considering the voltage and current limitations. For the prototype of study, a voltage of 4,000V and current of 3,000A have been selected due to the power electronic converter design. The methodology consists in adding a number of coils together, to be supplied at the same time by the power electronic converter, until a limit is reached in terms of voltage or current. Then, a new track section is defined. If a voltage limit is reached, a new track section with the same type of coil is considered. If the current limit is achieved, a new track section with a different type of coil is considered.

Other important issue related to the current is the selection of the current density at the linear motor coils (in order to determine the coils cable section), and the selection of the different track sections to be supplied at the same time by the power converter. Two current densities are being analysed for the calculation, 20 and 40 A/mm^2.

After running the procedure of track section calculation, the results are presented in Table 3, and the scheme of how the track sections are connected to the power electronic converter are described in Fig. 6.

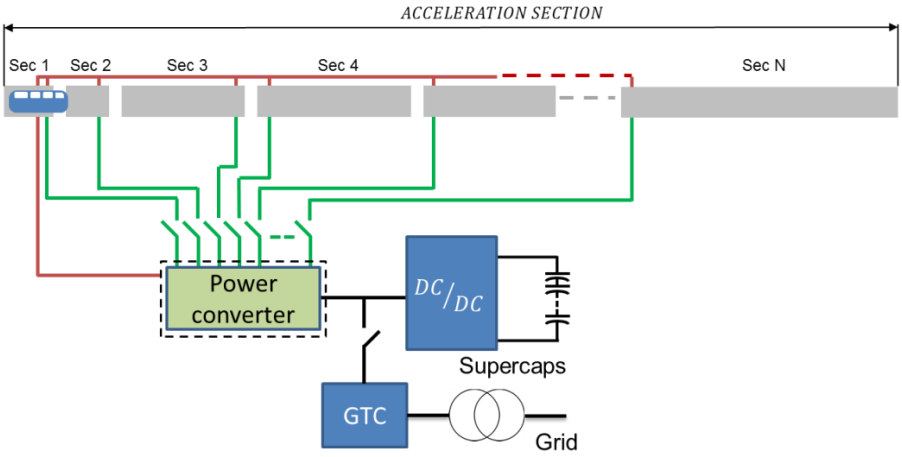

Fig. 6. Scheme of the power supply system proposed and the distribution in track sections.

Table 3. Number of track sections with different current density.

Current density	N=12	N=10	N=8	N=6	N=4	Total number
20 A/mm^2	2	1	2	6	17	**28**
40 A/mm^2	2	1	2	6	19	**30**

Table 4 complements the information of Table 3 with the length of the different track sections along the acceleration area for one of the study cases, using 20A/mm^2.

Table 4. Length associated to the different track sections for the case of J=20 A/mm^2.

Section	Coil Type	Start (m)	End (m)	Section	Coil Type	Start (m)	End (m)
1	N=12	1	4	15	N=4	192	216
2	N=12	4	12	16	N=4	216	238
3	N=10	12	18	17	N=4	238	261
4	N=8	18	25	18	N=4	261	284
5	N=8	25	37	19	N=4	284	306
6	N=6	27	42	20	N=4	306	329
7	N=6	42	58	21	N=4	329	350
8	N=6	58	74	22	N=4	350	372
9	N=6	74	89	23	N=4	372	393
10	N=6	89	104	24	N=4	393	414
11	N=6	104	118	25	N=4	414	436
12	N=6	118	144	26	N=4	436	457
13	N=4	144	168	27	N=4	457	478
14	N=4	168	192	28	N=4	478	500

Skin effect needs to be also considered in this application since quite high frequencies are operating at the high speed area. Fig. 7 presents how the ohmic resistance increases with the speed. The effect is even more important when the current density is lower, since the cable section is bigger.

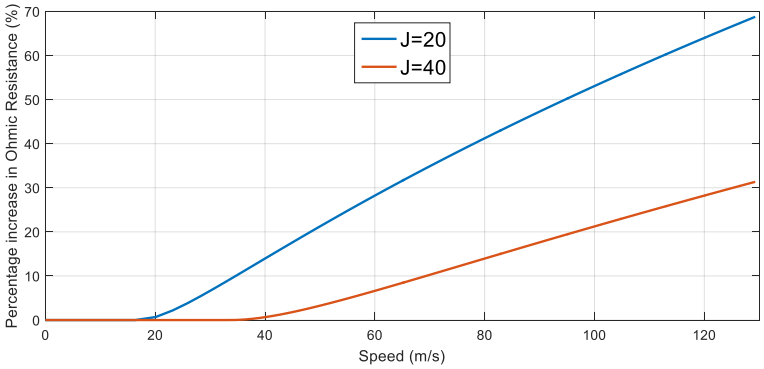

Fig. 7. Increase of the ohmic resistance due to skin effect for two values of current density (J).

Position sensors will be deployed along the acceleration track in order to detect the presence of the capsule. That will provide the closing of switches, connecting each track section to the power electronics converter. Only one track section is supplied by the power converter at the same time being necessary only one power converter to supply the complete linear motor. That is an advantage compared to the power supply of previous similar concepts as maglev [16][17], where different power converters

need to be installed along the track for the power supply, requiring high voltage equipment.

Fig. 8 shows a scheme of how the different track sections are connected to the power electronic converter through the corresponding switches. During the transition of the capsule from one track section to the next (Fig. 9), only part of the coils are providing force, since only part of the supplied coils have their magnetic circuit closed [18]. The force will drop to ½ during a very short time each track section transition.

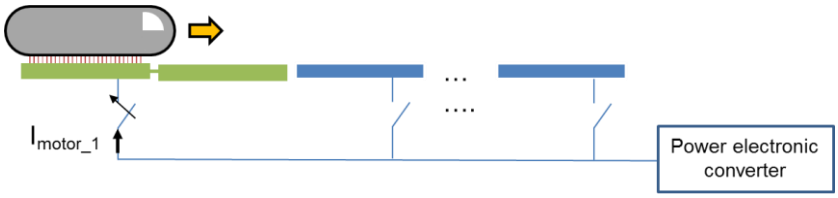

Fig. 8. Commutation of the different track sections switches from the power converter.

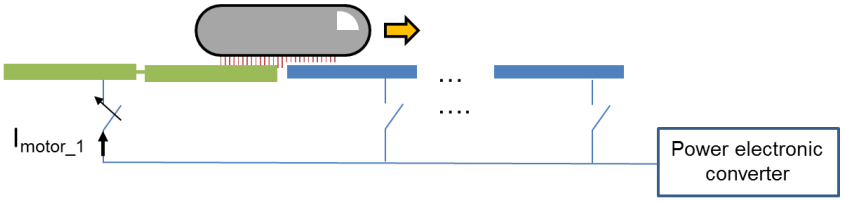

Fig. 9. Transition of the capsule from one track section to the next.

4 Conclusions and next steps

The conclusions of this study can be summarized in three points:

1. The particular characteristics of a quite short acceleration section compared to the total track length for the application of a Hyperloop type railway, including a close deceleration section, implies that the use of energy storage is a viable solution for the power supply. Supercapacitors results a quite convenient technology due to the power/energy ratio as well as the cycling capability.
2. The voltage limitation defined by the modules isolation voltage of 1,500V for the supercapacitor modules force to high current levels or using complicated power electronics topologies to increase the voltage. Voltage of 4,000V is a recommended value to use conventional power electronics.
3. For a very short operation cycles the definition of the maximum current must be obtained from the study with a thermal model, in order to determine the most appropriate current density to be used, avoiding a premature loss of capacity in the supercapacitors. A tradeoff between the material cost and the performance need to be found.

The next steps of the collaboration between CIEMAT and ZELEROS in the development of the 1/3 reduced scale prototype for technology validation are related to the manufacturing of the linear motor, power electronic converters and energy storage based on supercapacitors, as well as the deployment of the equipment in a 500m testing track in Sagunto (Spain), as presented in Fig. 10 by 2020.

Fig. 10. Experimental test facility for the ZELEROS 1/3 reduced scale prototype in Sagunto (Spain).

References

1. European Environment Agency. Greenhouse gas emissions from transport. Retrieved from https://www.eea.europa.eu/data-and-maps/indicators/transport-emissions-of-greenhouse-gases/transport-emissions-of-greenhouse-gases-11
2. Musk, E. (2013). Hyperloop Alpha. Retrieved from http://www.spacex.com/sites/spacex/files/hyperloop alpha-20130812.pdf
3. V. Chesteron, D. Kelvin (2018) Hyperloop-Opportunity For UK Supply Chain, Final Report from https://s3-eu-west-1.amazonaws.com/media.ts.catapult/wp-content/uploads/2018/10/08153525/00601_Hyperloop-Report.pdf
4. Hyperllop One. https://hyperloop-one.com/global-challenge
5. Hardt. (2018). European Hyperloop Program. Retrieved from https://ec.europa.eu/eipp/desktop/en/projects/project-print-9401.html
6. Hyperloop Transportation Technologies. Retrieved from https://www.hyperloop.global/about
7. Motoharu Ono, Shunsaku Koga and Hisao Ohtsuki, Japan's Superconducting MAGLEV TRAIN. IEEE Instrumentation & Measurement Magazine. March 2002, pp. 9-15.
8. H. Ikeda, S. Kaga, Y. Osada, K. Ito, Y. Mugiya and K. Tutumi, "Development of power supply system for Yamanashi Maglev Test Line," Proceedings of Power Conversion Conference - PCC '97, Nagaoka, Japan, 1997, pp. 37-41 vol.1.
9. E.R.A. European Union Agency for Railways: Hyperloop – an Innovation for Global Transportation? from https://www.era.europa.eu/sites/default/files/library/docs/hyperloop_innovation_for_global_transportation_en_1.pdf

10. ZELEROS Hyperloop Technology. Retrieved from https://hyperloopupv.com/projects/
11. Werner, M., Eissing, K., & Langton, S. (2016). Shared Value Potential of Transporting Cargo via. Hyperloop. Frontiers in Built Environment, 2. https://doi.org/10.3389/fbuil.2016.00017
12. S. Chevailler. “Comparative Study & Selection Criteria of Linear Motors” These nº3569. Ecole Polytecnique Federal de Lausanne 2006.
13. P. Moreno Torres, M. Lafoz, M. Blanco, G. Navarro, J. Torres, L. García-Tabarés “ Switched Reluctance Drives with Degraded Mode for Electric Vehicles”. Modeling & Simulation for Electric Vehicle Applications. Chapter 5. INTECH 2016.
14. Kolomeitsev, L.; Kraynov, D.; Pakhomin, S.; Rednov, F.;Kallenbach, E.; Kireev, V.; Schneider, T.; Böcker, J.: Linear Switched Reluctance Motor as a High Efficiency Propulsion System for Railway Vehicles. Proc. Int. Symp. on Power Electronics, Electrical Drives, Automation and Motion (SPEEDAM), Ischia, Italy, 2008, pp. 155-160.
15. L. Kolomeitsev et al., "Control of a Linear Switched Reluctance Motor as a Propulsion System for Autonomous Railway Vehicles," 2008 13th International Power Electronics and Motion Control Conference, Poznan, 2008, pp. 1598-1603.
16. K. Lee, "Advances in the Application of Power Electronics to Railway Traction," 2015 6th International Conference on Power Electronics Systems and Applications (PESA), Hong Kong, 2015, pp. 1-4. doi: 10.1109/PESA.2015.7398960
17. H. Ikeda, S. Kaga, Y. Osada, K. Ito, Y. Mugiya and K. Tutumi, "Development of power supply system for Yamanashi Maglev Test Line," Proceedings of Power Conversion Conference - PCC '97, Nagaoka, Japan, 1997, pp. 37-41 vol.1.
18. Sanket R. Kale1 , Yogesh N. Laghane2 , Akash K. Kharade3 , Supriya B. Kadus, “Hyperloop: Advance Mode of Transportation System and Optimize Solution on Traffic Congestion,” International Journal for Research in Applied Science & Engineering Technology (IJRASET) ISSN: 2321-9653, Volume 7 Issue VII, July 2019

Aplicaciones de IoT en la Monitorización Energética en Smart Cities: Perspectivas de Investigación

Fernando Velez Varela[1] and Diego Fernando Marin Lozano[2] and Fabian Castillo Peña[3]

[1, 2 & 3] Facultad de Ingeniería, Universidad Libre Seccional Cali, Valle del Cauca, COLOMBIA
fernando-velezv@unilibre.edu.co [1], diegof.marinl@unilibre.edu.co [2], fabian.castillo@unilibre.edu.co[3]
Diagonal 37A No. 3 -29, Cali – Valle – Colombia

Abstract. El término "Smart City", se asocia actualmente a una iniciativa de desarrollo y convergencia técnica, moral y social. Dicho término se relaciona con los entornos y contextos urbanos en los que la capacidad computacional, la interconectividad lógica y física, y la capacidad para gestionar los objetos inteligentes que la componen, son referidos y ubicados por medios de interfaces que no necesariamente son los computadores personales. Todo esto debe permitir que lo que se considere parte del entorno y sea representado por estos objetos dentro del sistema generen, intercambien y consuman datos para ser procesados en información útil con conceptos como Big Data.

La tendencia es que las ciudades se conviertan en entornos de convergencia, lo cual implica que estén en la categoría de "Smart City". Esto se está logrando con el uso de conceptos de tecnologías igual de convergentes, y se hace para lograr el objetivo de mejorar los servicios y la calidad de vida de los ciudadanos. Se puede decir que esto genera una revolución en referencia el espectro de aplicación de IoT. Esta iniciativa está ayudando a ciudades pequeñas o grandes, y que están en vías de convertirse de Smart Cities, conectadas de manera física y funcional.

Es probable que las iniciativas sean muy propias de cada cultura y entorno social, pero lo cierto es que a nivel de investigación y desarrollo se puede hablar de modelamientos, metodologías y procesos de normalización, que pueden ser usados como elementos de desarrollo en los proyectos de integrales que se encargan de dar las respectivas soluciones que incidan en la transformación de ciudades en entornos digitales inteligentes, en los que se considere como una directiva la seguridad de la información de forma vertical en el ciclo de vida de desarrollo de estos entornos.

Keywords: Smart City, IoT, Objeto Inteligente, gestión, Telecomunicaciones, Interfaz.

1 Antecedentes Formales

1.1 Consideraciones en la iniciativa de "Smart City"

El IoT -Internet of Things, Internet de las Cosas- proporciona la infraestructura para la introducción de mejoras significativas en la confiabilidad, la producción, los servicios y la satisfacción del cliente, dentro de los entornos tipo campus y ciudades [1]. En el mediano plazo se espera contar con una estructura de beneficios a partir de estas mejoras, que están en relación con los procesos de ahorro de costos iniciando con la identificación de nuevos modelos de negocio y de ofertas de servicios, que determinan la forma de transformación de los factores de consumo, como las redes de bienes y servicios tradicionales se transforman en servicios que proveen información y son seguidos en su comportamiento por los sistemas de gestión dispuestos para cada caso. A largo plazo dejará impuesto como se estará haciendo la transformación de los datos (desde procesos industriales hasta los CRM comerciales) en información gestionable, y convertir esto en conocimientos útiles [2].

1.2 Descriptivas conceptuales

De forma básica, una Smart City empieza por una infraestructura pública inteligente que garantiza agua limpia, un suministro eléctrico fiable, gas seguro y alumbrado público eficiente. A medida que la prestación de servicios esenciales adopta procedimientos inteligentes, se liberan recursos que puede invertir en otros servicios que mejoran la calidad de vida.

Los aspectos como la medición de consumo energético, los estados operacionales y la información que emiten las redes, bienes y servicios dentro del entorno de una ciudad, los desarrollos al respecto referenciados en IoT se cimentan en las normas especificadas para el uso y referencia que son aplicables en la relación existente que hay para los sistemas de bienes, redes y servicios inmersos dentro de una ciudad, y que componen esquemas que se unen con arquitecturas de telecomunicaciones que son parte estructural de un entorno de tecnologías de la información [3] [4].

La razón fundamental para establecer este punto es el definir la referencia fundamental en cuanto a las labores que buscan considerar todo lo referente en cuanto estados, señales, datos y métricas de rendimiento para calificar y cuantificar el gasto y la medición de recursos que se referencian con la disposición de composición metodológica de IoT, y medible por medio de normas como la ITU-T L1440 [5]. Actualmente concebir el desarrollo de un método aplicable a la observación, medición y procesamiento de la información aportada por los esfuerzos de los recursos, depende de la información más la obtención de un modelo que se especifique como marco de referencia, esto requiere hacer un barrido conceptual entre los análisis estructurales y funcionales de dispositivos y mecanismos más los sistemas interrelacionados. Es así, que en primera instancia se debe invocar a todo aquello que esté relacionado con el concepto de gestión aplicable para los sistemas que se relacionan por medio de un componente conceptual

de telecomunicaciones, esto no va buscar a que se verifiquen que límites se deben imponer antes de determinar lo que posiblemente se pueda gestionar o no, y ser parte de cómo se disponga todo para ser gestionado [6].

La búsqueda de entornos eficientes en cuanto al uso de recursos energéticos para producir funcionalidades dentro de una ciudad, hace que se entre en materia de entender a través de modelos como poder relacionar una arquitectura de telecomunicaciones o un entorno externo de tecnologías de la información, que en concreto se soporta mediante sistemas de alimentación o de potencia [7]. Desde el punto de vista funcional se convierte en el objetivo de las labores hechas por los entes a nivel mundial, que se encargan de llevar a cabo los procedimientos de regulación y normalización, los cuales salen a partir en todos los análisis inicialmente de modelos, es por eso que para desarrollar un modelo de gestión que lleve a cabo la sinergia entre los modelos de consumo energético y los modelos de servicios interrelacionados en las arquitecturas de tecnologías de la información [8], hace que sea necesario entrar en los siguientes detalles como:

- Tener en cuenta que los modelos aplicables y funcionales de redes son muy diferentes de los modelos teóricos.
- Los modelos de gestión aplicables en esta parte están más cercanos a los modelos de telecomunicaciones que a los modos de consumo energético.
- El diseño de un esquema funcional de red necesariamente involucra la presencia de un sistema de alimentación asociado que le permita desempeñarse para los objetivos marcados.
- La mayoría de los sistemas actuales buscan ser especificados como eficientes, parten del hecho de usar intrínsecamente un reglaje que los haga desempeñarse en el uso racional energético.
- Las tendencias actuales buscan que se refine las formas con las cuales se pueda medir el consumo energético alto nivel.

Según lo realizado hasta el momento se puede hacer referencia al desarrollo de reportes, informes y revistas que publican iniciativas en este tema y artículos científicos que anuncian teorías, modelos, y métodos propuestos en la comunidad científica internacional [9]; que, con sus objetivos, se limitan sólo a referenciarse en lo especificado por las normas pertinentes de aplicación del caso, considerando que algunas de estas están muy sesgadas por cada fabricante. Esto indica la posibilidad de aplicar estas normativas sobre los objetivos de tener información de todo esto, desde que se halle en la etapa de proyectos, ya que de esta manera se puede partir asegurando y teniendo en cuenta las referencias funcionales, de consumo y estadísticas. La otra instancia es hacer la revisión exhaustiva y el debido análisis del comportamiento que refleje un sistema objetivo ante la óptica de la convergencia, gestionabilidad, pervasividad, ubicuidad y la ecológica. Por estas razones, es aquí donde realmente la palabra gestión, toma significancia dentro del concepto de IoT.

En la parte gestión de redes, se busca aplicar y extrapolar de forma metodológica y teniendo en cuenta los modelos de referencia, un protocolo estándar y extensible, es por eso que se menciona al protocolo SNMP, el cual se usa como mecanismo indicado para

leer información por el comportamiento de los elementos de red especificados por medio de los parámetros. Las normas que llegan a relacionarse con este protocolo van a tomar de la información sólo algunos parámetros que interesen en la funcionalidad, el estado operativo y el rendimiento energético, no se trata de saber cuántos bits se han transmitido sino el estado operacional, características comportamentales funcionales y esfuerzo necesario a nivel energético que se requiere para que éstos se hayan transportado o procesado información y estén en estado operativo provisionando servicios [10]. El desarrollo lleva a delinearse en los parámetros característicos de IoT, que pueden ser obtenidos a través de las interfaces de cada dispositivo, entregando así los estados lógicos, valores medidos de los parámetros energéticos que se han especificados en los modelos de normalización.

Los aspectos claves para el desarrollo de IoT para el concepto de "Smart City" son:

- Tener definida la existencia de una infraestructura de telecomunicaciones, que técnicamente se determine con los conceptos y elementos convergentes del caso, que soporte y determine lo referente a la presencia de los servicios inteligentes que representen a Internet, sensores, aplicaciones y redes sociales, aplicaciones móviles, etc., en combinación con un marco de políticas e iniciativas de acceso normal, estándar y abierto a los usuarios para el consumo y la generación de información masiva y pública.
- Definir los aspectos funcionales y procedimentales de los servicios desde la gestación con sus modelos, y que estén en una alta cohesión con las necesidades primarias y finales del ciudadano-usuario.
- Considerar procesos y conceptos de normalización, presencia y transparencia en el aspecto de comunicación a los ciudadanos de los resultados de los procesos ofrecidos y el rendimiento alcanzado dentro del entorno IoT, por los servicios inteligentes.
- Determinar el necesario aspecto de seguridad en la comunicación de los elementos y componentes de la infraestructura convergente y en la transmisión de datos para IoT.

2 Networking para Smart Cities

Dentro del concepto de Smart City, están definidas por las conexiones entre las múltiples situaciones o las relaciones entre las unidades organizacionales y están compuestas por una variedad de dispositivos que usan protocolos similares y procedimientos para facilitar un intercambio seguro de IoT [11]. En una Smart City cuando la Gestión de políticas y procedimientos no están conformes a las normas requeridas que se tienen de referencia y relacionan sus interacciones cuando se trata de manejar la información en la parte de sus redes de datos de soporte, se llega a los ámbitos de las redes en las que se identifican susceptibilidad a riesgos y que puedan presentar impactos por las políticas tecnológicas aplicadas y por la conformidad aplicada, y esta relaciona los siguientes aspectos: la integridad de los datos, la seguridad, la encriptación protocolar, la autenticación, y la vulnerabilidad en el HW asociado.

2.1 Estándares de Redes para Convergencia

Según lo que se está definiendo para IoT, en conjunto con los estándares de ITU, se pueden definir de forma conjunta para llevar a cabo el Networking y las labores en redes de datos dentro de una Smart City, esto se permite definir con la disposición de las siguientes guías:

- LLN - Low Power & Lossy Network, Capacidades inalámbricas basadas en tecnología convergentes.
- IEEE 802.15.4, uso del espectro en las bandas 2.4 GHz y 900 MHz.
- IEEE 802.15.4g, Smart Utility Network PHY, uso e implementación de tecnologías de RF.
- RFC5548, ROLL Routing Over Low power and Lossy networks, requisitos de enrutamiento LLN (Low Power Lossy Network) específicos de la aplicación para sistemas Urbanos.
- AMI (Advanced Metering Infrastructure), sistemas de medición avanzados hardware y software para datos en comunicaciones remotas, que permiten la medición de información detallada basada en el tiempo y la recopilación y transmisión frecuente de dicha información a varias partes.
- AMR (Automated Meter Reading), que es una tecnología utilizada en los medidores de servicios públicos para recopilar los datos que se necesitan con fines de facturación.
- CVR (Conservation Voltage Reduction), que es una tecnología probada para reducir la energía y la demanda pico
- DR (Demand Response), que cubre el espectro de medidas despachables, que cuando se dispone, reduce la carga durante períodos específicos.
- RFC 6272, Protocolos de INTERNET para Smart Grid – Guía para la configuración de redes IP para Smart (PAP01).
- NISTIR 7764, Directrices para el acceso a estándares inalámbricos para aplicaciones de Smart Grid.
- NISTIR 911198, Guía para la aplicación de los mecanismos de coexistencia para BPLS (Broadband Power Line Systems) con estándares de comunicaciones convergentes.

3 Tópicos de networking a considerar para una Smart City

3.1 Uso seguro de COTS/Sistemas y Redes Públicamente Disponibles

Los indicadores económicos y otros factores hacen que se disponga actualmente del uso de mecanismos como los COTS (Commercial Off-The-Shelf: Componente sacado del Estante), de las redes públicas como el Internet, o de los sistemas empresariales disponibles. El asunto apunta a investigar y/o evaluar si se pueden usar los tales recursos de forma confiable y segura en el despliegue de una Smart City, y cómo ellos se implementarían.

3.1.1 Uso de Internet en una Smart City

Un caso específico es el uso del Internet existente en las comunicaciones relacionadas dentro de una Smart City en donde se disponga la presencia de IoT, en tanto sea posible incluir una infraestructura redundante como mecanismo de emergencia. Actualmente el Internet se tiene disponible y evolucionando, pero para los intereses de una Smart City, debe ser tolerante a fallos. Esta consideración la puede afectar numerosos casos de malwares malévolos y las actividades que pueden poner en riesgo un sistema en producción. Las investigaciones en los métodos para tratar con los ataques tipo DoS, así como identificar otros problemas críticos, sirven para comprender las debilidades y fortalezas, así como las medidas cautelares inherentes que se deben tomar cuando se use al Internet existente para los tipos específicos de aplicaciones de una Smart City con IoT.

3.1.2 Características de Seguridad y Confiabilidad de TCP/IP

Las características de Seguridad/Confiabilidad que se tienen en relación con la adopción de TCP/IP para las redes de una Smart City con IoT, es un tema de la investigación relacionado separado del tema de usar Internet. Es una directiva actual que se considere al uso de Internet, el cual es un mecanismo de convergencia, como una iniciativa de investigación, ya que la adopción de los protocolos de este para las redes de una Smart City con la convergencia de IoT, traen incluida la comprensión del estado actual de los planes de seguridad propuestos para las redes avanzadas. Las características como la calidad de servicio (QoS), la movilidad, el multi-homing, el broadcasting/multicasting, y otras extensiones necesarias para las aplicaciones para una Smart City, debe ser adecuadamente aseguradas y bien gestionadas si TCP/IP va a ser adoptado.

3.1.3 Networking Avanzado

La noción predominante es que las comunicaciones de una Smart City para la aplicación de IoT, está principalmente basada en TCP/IP. El desarrollo del Networking avanzado se perfila hacia obtener aproximaciones más simples hacia infraestructuras de networking que resuelven el asunto por medio del diseño de algunas cosas que se relacionan ahora con los protocolos de Internet.

La iniciativa debe proporcionar esquemas de redes seguras con bajos niveles de complejidad que puedan ser más fácilmente gestionadas y que puedan ofrecer comportamientos más predecibles. Existe una amplia variedad de medios de comunicación que están actualmente disponibles y que se utilizan hoy en día (sistemas WiFi, LiFi, enlaces de microondas, WPAN, WLAN, etc). Cualquier tecnología de red avanzada que tiene como objetivo proporcionar una abstracción uniforme para la comunicación de red inteligente, también necesita soporte de la definición de la incidencia de sus capas de aplicación protocolar.

3.1.4 IPv6

Es muy difícil predecir las consecuencias de las implementaciones a gran escala de las redes. La directiva inicial es que una Smart City con IoT, probablemente se basará en IPv6 en un futuro, y se prevé que se agregarán millones de dispositivos a la red eléctrica inteligente, no es evidente que la columna vertebral vaya a funcionar perfectamente [17]. Por esto, se necesita investigación para asegurar que la red basada en IPv6 vaya a ser estable, confiable y segura. En particular, estos serían los temas que necesitan más investigación y ser revisados:

- ¿Serán escalados los protocolos actuales y futuros para los millones de dispositivos?
- ¿Son actualmente las tecnologías de modelado, simulación y emulación suficientes para modelar las futuras redes utilizando IPv6?
- ¿Cómo se valida la precisión del rendimiento previsto?
- ¿Cuáles dispositivos interactuarán correctamente en entornos de multi-proveedor?
- ¿Son adecuados los protocolos de enrutamiento? ¿Se necesita desarrollar nuevas normas?
- ¿Hay alguna preocupación de seguridad? ¿Cómo se segmentaría la red?
- ¿Se debe utilizar NAT/PAT?
- ¿Es una red fundamentalmente nueva?

3.1.5 Seguridad en la Nube

Con la llegada del Cloud Computing para una Smart City, debe prestarse especial atención a la utilización de recursos de Cloud Computing y las implicaciones de aprovechar esos recursos. Hay organizaciones que se centran en la seguridad y el uso adecuado de estos, como lo es el Cloud Security Alliance. Como con cualquier recurso compartido que contenga información importante, se deben implementar mecanismos de seguridad que proporcionen la protección adecuada y las capacidades determinadas en la nube. El Cloud Computing debe evaluarse de acuerdo con las restricciones y parámetros de los sistemas de control en el contexto de una Smart City con IoT [18]. Los problemas de seguridad de datos deben abordarse con la debida propiedad a nivel de la protección de estos dentro y fuera del Cloud para las acciones de almacenamiento y tránsito, control de acceso a los datos y al Cloud, y manejo de niveles de acceso al sistema. También deben abordarse las cuestiones de seguridad y optimización a nivel WAN dependiendo de los patrones de acceso a datos y de los flujos de información en el Cloud [19]. Esto podría incluir un nuevo trabajo de encriptación, administración de claves, almacenamiento de datos y modelos de disponibilidad.

3.1.6 Seguridad Distribuida vs Centralizada

Actualmente se cuenta con varios modelos para el diseño de acciones autónomas para una Smart City con IoT, especialmente en la gestión de distribución automatizada. Estos se han desplegado donde se consideran a las funciones de medición avanzada, donde por ejemplo el proceso debe llevarse a cabo por un medidor, frente a los sistemas

centralizados (como las aplicaciones de administración de datos de medición o las aplicaciones de control de carga en el centro de Control). Algunos enfoques ofrecen controles de seguridad heredados, mientras que algunos externalizan la seguridad y algunos otros ofrecen combinaciones de ambos enfoques. En el contexto más amplio de la automatización de la distribución avanzada, hay un debate similar sobre cuánta "inteligencia" se debe implementar dentro de los entornos convergentes, los terminales de generación distribuida, etc., en comparación con los sistemas centralizados. También hay sistemas tipo WASA (Wide Area Situational Awareness) y actores distribuidos por naturaleza, sin embargo, la mayoría de los mecanismos de seguridad son casi en su totalidad centralizados [20]. Por esto, se trata tema propuesto y que debe ser abordado conceptualmente con la convergencia más IoT, y se debe realizar una investigación sobre seguridad avanzada para determinar un modelo de seguridad que soporte apoyar estos distintos enfoques distribuidos versus inteligencia centralizada de la seguridad y funcionalidad en una Smart City. Mientras que no esté tener claro qué funciones de seguridad deban ser centralizadas o descentralizadas para una aplicación en particular, como una buena práctica se debe hacer investigación en modelos de referencia coherentes y taxonomías por capas de estos. El modelo debe contener un enfoque estándar en el cual los actores inmersos dentro de una Smart City con IoT, puedan tomar mejores decisiones dentro y en referencia a la arquitectura de seguridad basadas en riesgos para su medio ambiente y la eficiencia de las operaciones de seguridad.

4 Hardening de sistemas de redes de datos para una Smart City

4.1 Introducción conceptual

El desarrollo de procedimientos de Hardening en las arquitecturas de redes es una práctica que se ha considerado más que necesaria, debido a la importancia que refieren los actuales sistemas de networking. Para poner en práctica esta clase acciones conlleva a considerar las formas bajo las cuales las redes se han modelado o desarrollado, o más bien esto indica el punto de partida. En especial lo más formal seria considerar el uso de los modelos OSI o TCP/IP para considerar cuales son aquellas partes que deben protegerse y que deben soportar la implementación de esquemas de seguridad que protejan la integridad de las arquitecturas de servicios que a su vez están desplegadas en las arquitecturas de red. Cabe aclarar que existen muchas formas de Hardening, pero aquí se hará énfasis en lo que tiene que ver con los elementos que conforman el backbone de una red de una Smart City con IoT [21].

Actualmente, con la ejecución de prácticas de Hardening en las arquitecturas de networking se determina inmediatamente los elementos que deben ser objeto de las prácticas de seguridad, en este caso se tratarían de los equipos de red, entre los cuales se debe mencionar a los Routers, Swicthes, Access Points, etc. Cada uno de estos define una estela de parámetros característicos para ser funcionales. Ellos involucran esquemas de datos y estructuras de información, que determinan como debe ser la lógica que en ellos debe obrar y que a su vez determina como deben funcionar las estructuras hardware que se disponen en estos a través de sus puertos de red [22].

A partir de esto es que se determina la necesidad de buscar métodos de fortalecimiento para su normal funcionamiento, en otras palabras, se adiciona seguridad. Este escrito contiene la información necesaria que puede ayudar a asegurar un dispositivo de red, en especial la de aquellos dispositivos que disponen de una infraestructura complementaria entre su lógica utilizada y su hardware. Un hacker que devela estos detalles rápidamente precipita a que un cracker los pueda aprovechar. Las arquitecturas de red son de importancia para un esquema de seguridad, ya que de ellas dependen las estructuras funcionales de la totalidad de los servicios [23]. Conocer los detalles de la conformación de una red es como conocer cómo piensan las personas y que tan cautas son. La aplicación de estas técnicas va a depender de las interfaces que disponga la red desplegada en una Smart City, con sus dispositivos heterogéneos y nativos. Lo ideal es considerar una arquitectura que maneje la información de esta y que sea independiente de las tecnologías de las redes de acceso y que se perfile hacia modelos de convergencia en cuanto a la parte del manejo de los flujos de información, con lo cual se apunta a las redes IP.

4.2 Definiciones de Hardening.

El Hardening es una estrategia para robustecer los niveles de defensa reactivos y proactivos en un sistema arquitectural que involucre a todo lo relacionado en la pila de un sistema que se conforme referencialmente a OSI o funcionalmente a TCP/IP, como en el caso de una Smart City, se busca es traer a este contexto las interfaces y mecanismos de interacción que se relacionen e interoperen. Este conjunto de procedimientos debe proteger a la infraestructura de servicios y/o telecomunicaciones de ataques, así como a los elementos objetivo que conforman el concepto de la adquisición de los datos, denotados por la pervasividad y ubicuidad, que son los Smart Objects, que son parte del concepto de IoT, por medio de la aplicación de las estrategias concebidas de eliminación y/o desactivación de procesos de aplicación o de servicios que son considerados innecesarios, logrando con esto como resultado el cerramiento de lo que se considera un hueco de seguridad y determinando así el potencial control de acceso. Los procedimientos de Hardening son ejecutados por expertos en el tema y no por dummies.

En la gran mayoría de las veces la especificación de este procedimiento en cuanto a su aplicación lleva inmediatamente a ejecutar procesos de observación y análisis en las arquitecturas de servicios, como la que se tiene en una Smart City, las prácticas involucran desde tener en cuenta los procedimientos de tunning de sistemas lógicos que buscan afinar parámetros de comportamiento para mejorar su rendimiento, pasando por los procesos de afinamiento que se llevan a cabo en base a la función que desempeñe el equipo dentro de la infraestructura de servicios y de red, llegando hasta los procesos de personalización, que son los resultados de los esquemas de evaluación y dimensionamiento de la arquitectura de software y en especial para el caso objetivo que es la de red [24]. Esto indica cual será alcance del proyecto y el desarrollo de los procesos personalizados.

5 Seguridad en las operaciones de una red de servicios para una Smart City.

No es nada raro que se piense que para que el concepto de Smart City se disponga, este debe ser implementado para resistir algún nivel de manipulación en sus sistemas de metrología y que otros sistemas no puedan ser asegurados físicamente, así como los grados de invalidez o la falsificación de datos desde las redes de área de Hogar (HAN) accedidas por una simple computadora. La Smart City sería un blanco para cualquiera que se considere malicioso, y que esté bien motivado y fundamentado. La dependencia aumentada en la información y los sistemas de gestión de información en red y distribuidos como en los sistemas SCADA, WAMS, y PLCs implican que el concepto aplicado de Smart City, necesitará mucha más autenticación de dispositivos, encriptación, manejos de fallas, y tener de referencia a modelos de comportamiento normal y anormal, que se pueden contar como un requerimiento explícito [26]. Se considera que una Smart City es como un esquema de sistemas, dispuesto de recursos con niveles de costo que a largo plazo deben construirse para adaptarse a las necesidades cambiantes en términos de la escala y la funcionalidad, y al mismo tiempo, necesita ser construido para tolerar y sobrevivir a los ataques que ahora ni siquiera se puedan prever. Es por esto que se requiere de hacer investigación para desarrollar una arquitectura de protección avanzada que sea claramente dinámica (y que pueda evolucionar), y que además se enfoque en la resiliencia (como es el tolerar fallas).

El Diseño de un esquema de red de servicios para una Smart City debe estar compuesto por elementos que proporcionen independencia protocolar y funcional en su aspecto implementacional y de funcionamiento. Todas las redes son vulnerables a ataques y es por esto que sin la planificación, implementación, operaciones y mantenimiento de red no se tiene un margen de conformidad con los estándares de seguridad operacional impuestos por los conceptos de IoT aplicados a una Smart City. Normalmente, se determina que las operaciones de la seguridad comienzan en el proceso de planificación e implementación de una red, Ver Fig. 2.

Fig. 1. Servicios de seguridad de una plataforma de red segura integrada a una Smart City

5.1 Comunicaciones Seguras en una Smart City

Las comunicaciones definidas en las redes de datos de este tipo de redes se pueden definir dependiendo de cómo se lleven a cabo, por lo general dentro del Sistema, las implementaciones de seguridad a nivel de networking son convencionales, pero cuando se trate de trasladar datos entre ambiente WAN-a-WAN, se deben considerar los siguientes esquemas de comunicación:

- **Comunicaciones Seguras para Accesos Remotos:** Se Proporciona acceso altamente seguro y personalizable a redes corporativas y aplicaciones del entorno de IoT de la Smart City, mediante el establecimiento de túneles cifrados a través de INTERNET.
- **Comunicaciones Seguras para Accesos Sitio-a-Sitio:** Se provee una infraestructura WAN basada en INTERNET para la conexión de sucursales, oficinas o sitios empresariales para la totalidad o para algunas partes del sistema dispuesto de IoT para la captura de información de la Smart City.

5.2 Arquitecturación de los procesos de recuperación y reacción para seguridad

La recuperación eficaz requiere contener el impacto de una falla (que será accidental o provocada); de hecho, hay que dimensionar una solución con los suficientes recursos e información posicionada (por ejemplo, la información estatal a nivel de estadísticas) para regenerar la capacidad perdida; se deben disponer de mecanismos de toma de decisiones de tiempo real que dispongan y señalicen al sistema para que actúe con los mecanismos de reconfiguración y disponga los pasos de recuperación. Incluso aun cuando se deba garantizar la recuperación dentro de un tiempo límite es un problema extremo y sólo puede lograrse bajo ciertas condiciones.

Con la presencia de fuentes de energía renovables en que pueden estar bajo normal operación o por fuera de funcionamiento de forma imprevisible y con la futura demandante carga de energía para los móviles (como los vehículos híbridos) cuyos movimientos no pueden controlarse de forma centralizada, le impone a Smart City una exigencia para que se convierta en un concepto de red más dinámico en su comportamiento operacional. Su fiabilidad dependerá cada vez más de la habilidad de reaccionar a eventos dentro de un tiempo limitado mientras se pueda limitar el impacto de los cambios dentro de cierta región o ámbito de uso. Para esto será bueno considerar y contestar los siguientes interrogantes: ¿Cómo hace a un arquitecto un sistema distribuido de área extensa de la escala de una Smart City tal que sus componentes importantes y los eventos designados tengan una recuperación y reacción definidas en tiempo y espacio? ¿Qué recursos se necesitan tener disponibles? ¿Qué necesidades de seguridad se requiere tener disponible? ¿Cuál es el círculo de influencia que necesita considerarse para facilitar la recuperación y la reacción? De considerar, éstas son las preguntas que la tarea de R&D en I+D en las Smart Cities se deben resolver y contestar.

5.3 Arquitectura de la Seguridad en Tiempo Real

Para la aplicación de IoT al contexto de las Smart Cities, la industria energética hace énfasis en confiar en los sistemas de tiempo real de control avanzados. Estos sistemas deben reunir los requisitos para aplicaciones que tengan una ventana específica de tiempo para ejecutarse correctamente. Algunas aplicaciones de tiempo real planas se deben ejecutar dentro de márgenes de milisegundos. Los sistemas de protección de área extensa y los sistemas de control requerirán comunicaciones seguras que deben encontrar su punto de convergencia [27]. La mezcla de sistemas lógicos y físicos que en este contexto se conocerán como Cyber Sistemas físicos y lógicos, traen consigo a menudo estos factores temporalmente, ya que pueden estar dimensionados para rastrear los cambios dinámicos en un proceso físico. Hasta el momento, típicamente tales sistemas se han tratado autónomamente y libres de amenazas a su Cyber Seguridad. Sin embargo, la funcionalidad e interoperabilidad, combinados en los ambientes bajo amenaza de hoy, requieren que tales sistemas incorporen varias medidas de seguridad que van desde de la autenticación de dispositivos y aplicaciones, control de acceso, redundancia y manejo de fallas para funcionamiento continuo. La inserción de estos mecanismos tiene el potencial para violar los requisitos de tiempo real por la introducción de retardos no controlados o no limitados.

5.4 Implementación de la seguridad en una Smart City

La investigación de la Cyber Seguridad para una Smart City con IoT, normalmente se centra en una variabilidad de componentes. Una muestra de esto es que os primeros trabajos relacionados con una Smart City, está en la seguridad de Sistemas de Control de Procesos (PCS). El Trabajo de seguridad de una Smart City se ha hecho con la privacidad de los usuarios, medidores inteligentes, estimación de estado de sistema de energía eléctrica, comunicaciones de componentes y análisis de ataques cibernéticos. Un PCS es un sistema automatizado que monitorea y controla un proceso usando computadoras. Normalmente funcionan como sistemas aislados que tienen limitadas o no conexiones de red. Estos se pueden utilizar para controlar algunos aspectos de la producción. Su relación en entornos aislados para ser conectados a redes más grandes va a introducir nuevos riesgos de seguridad porque estos (los PCSs tradicionales) fueron diseñados con seguridad limitada.

En el entorno de una Smart City, se colectan muchos más tipos de datos de usuario y nuevos tipos de información. Estos nuevos datos en conjunto con la interconectividad han causado preocupaciones en cuanto a la privacidad del usuario [28]. Existen leyes y reglamentos que protegen la privacidad de estos, que tendrán que ampliarse para proteger a los usuarios de una Smart City con IoT. Los nuevos tipos de datos deberán ser identificados y analizados, por lo que se pueden identificar los riesgos de seguridad y se pueden tomar medidas para asegurar la privacidad del usuario. Los Contadores inteligentes son una versión digital de los medidores de potencia actual, estos se instalarán en el lado del cliente, y se utilizarán para tomar medidas del uso de la potencia de la energía eléctrica llamadas lecturas. Los contadores y dispositivos de medición inteligentes se conectarán a la Smart City, y enviarán periódicamente sus lecturas [29] [30].

Dichas lecturas se utilizan para la estimación del estado funcional y de consumo, que pueden definir parámetros para saber la potencia de la energía eléctrica consumid, o para fines de facturación. Hay unos problemas de seguridad con los medidores inteligentes que van desde la alteración de la funcionalidad del dispositivo a problemas de comunicación entre el medidor y el proveedor de la potencia eléctrica.

La integridad del modelo de estimación de estado es un tema importante en la seguridad de una Smart City con IoT. El networking de los diferentes componentes de Smart City, implica que muchos de estos deben interactuar con otros componentes, porque deben comunicarse, y en lo que respecta existen diferentes requisitos de cada par de componentes de comunicación, en los que se incluyen latencia, ancho de banda, confiabilidad y las necesidades de seguridad; lo que implica que sea necesario tener dispuestos una gran variedad de protocolos que deban ser usados en una Smart City, para permitir la comunicación entre los componentes. Existen muchas consideraciones de diseño diferentes para ser evaluadas antes de que se pueda construir un sistema Smart City. Lo que significa que se necesitan métodos que sean desarrollados para analizar los diferentes diseños, que buscan simular la red inteligente usando software y hardware, con esto se pueden realizar la ejecución de simulaciones y hacer algunas pruebas iniciales de los diferentes diseños de Smart City con IoT. Uno de los aspectos de diseño de esta clase de red que se puede probar con estos sistemas, es la Cyber Seguridad, en la cual por medio de un Análisis de impacto se pueden realizar acciones para evaluar los riesgos potenciales de seguridad.

6 Conclusiones

- Hacer acciones de Colaboración con otras Organizaciones de Desarrollo de Estándares (Standards Developing Organization – SDO) si es necesario.
- La seguridad debe diseñarse en inicio de todo proyecto, y esto debe ser un esfuerzo continuo.
- Abordar sistemáticamente las vulnerabilidades (propiedades intrínsecas de las redes/sistemas). Es importante para que puede se pueda proporcionar protección independiente de lo que pueden ser las amenazas (que están cambiando constantemente y pueden ser desconocidas), se trate la norma X.805, la cual resulta útil aquí.
- La investigación de la Cyber Seguridad de para una Smart City con IoT se divide en cinco diferentes categorías: seguridad de PCS, Seguridad inteligente para medición, seguridad de estimación de estados del sistema de energía, seguridad de protocolo de comunicación de una Smart City y Simulación de IoT para análisis de seguridad.
- La presencialidad de los mecanismos de convergencia dentro de una Smart City, han estado en uso desde tiempo, pero la idea es hacer una sinergia dentro del de dicho entorno como el de una Smart City con IoT. Los sistemas y mecanismos de convergencia tradicionalmente han estado diseñados en relación con la cobertura y la aplicabilidad de estos con o sin seguridad, para que un conjunto completo de herramientas de seguridad y políticas se encargue, esto tendrá que ser desarrollado para estos sistemas. Las vulnerabilidades de seguridad y los métodos de evaluación de riesgos se pueden utilizarse en toda su extensión para elaborar políticas y herramientas de

seguridad para los mismos sistemas que vayan a ser parte del concepto de IoT dentro de una Smart City.

- Ha habido varios riesgos de seguridad identificados con medidores inteligentes, y muchos de estos riesgos deben abordarse antes de la medición inteligente, y antes de aplicarlos en entornos a gran escala.
- Uno de los ataques contra los modelos que implican usar IDS's, es el ataque de inserción de datos falsos. Desde el modelo de estimación de estado del sistema de alimentación se compone de una sección crítica de la funcionalidad de una Smart City, una de las iniciativas utiliza el modelo de estimación de estado del sistema de alimentación para determinar la capacidad de canal de comunicación que se necesitará para garantizar las comunicaciones seguras. Hay muchos otros tipos de ataques que pueden realizarse contra el modelo de estimación de estado y por esto tendrá que ser investigado.
- El Sistema definido de una Smart City con IoT tendrá que usar muchos protocolos de comunicación debido a los diferentes requisitos de los muchos componentes de esta red. Hasta el momento hay iniciativa que han dispuesto guías de diseño de protocolos de autenticación que se pueden ser utilizar por parte de los diseñadores de protocolos.
- Los trabajos de Simulación definidos de IoT en una Smart City, pueden utilizarse para evaluar la Cyber Seguridad. La simulación de una Smart City se divide en dos tipos: software y hardware. Se recomienda por ello trabajar en el desarrollo viable de simuladores de aplicables a contextos urbanos y masivos, ya que esto ayudará a mejorar el proceso de diseño de este nuevo modelo de red.

7 Referencias

[1] A. Gaura, B. Scotneya, G. Parra y S. McCleana, «Smart City Architecture and its Applications based on IoT - The 5th International Symposium on Internet of Ubiquitous and Pervasive Things (IUPT 2015),» *Procedia Computer Science,* nº 52, pp. 1089-1094, 2015.

[2] B. Nguyen y L. Simkin, «The Internet of Things (IoT) and marketing: the state of play, future trends and the implications for marketing,» *Journal of Marketing Management,* vol. 33, nº 1-2, pp. 1-6, 2017.

[3] J. Jin, J. Gubbi, S. Marusic y M. Palaniswami, «An Information Framework for Creating a Smart City Through Internet of Things,» *IEEE Internet of Things Journal,* vol. 1, nº 2, pp. 112-121, 2014.

[4] F. Shroufab y G. Miragliottaa, «Energy management based on Internet of Things: practices and framework for adoption in production management,» *Journal of Cleaner Production,* vol. 100, pp. 235-246, 2015.

[5] ITU International Telecommunication Union, «L.1440: Methodology for environmental impact assessment of information and communication technologies at city level,» ITU, 2015.

[6] J. Gubbi, R. Buyya, S. Marusic y P. Marimuthu, «Internet of Things (IoT): A vision, architectural elements, and future directions,» *Future Generation Computer Systems,* vol. 29, nº 7, pp. 1645-1660, 2013.

[7] W. Ejaz, M. Naeem, A. Shahid, A. Anpalagan y M. Jo, «Efficient Energy Management for the Internet of Things in Smart Cities,» *IEEE Communications Magazine,* vol. 55, nº 1, pp. 84-91, 2017.

[8] F. Tao, W. Yiwen, Z. Ying, Y. Haidong y Z. Meng, «Internet of Things in product life-cycle energy management,» *Journal of Industrial Information Integration,* vol. 1, pp. 26-39, 2016.

[9] J. A. Stankovic, «Research Directions for the Internet of Things,» *IEEE Internet of Things Journal,* vol. 1, nº 1, pp. 3-9, 2014.

[10] P. Sethi y S. R. Sarangi, «Internet of Things: Architectures, Protocols, and Applications,» *Journal of Electrical and Computer Engineering,* vol. 2017, pp. 1-25, 2017.

[11] J. Jin, J. Gubbi, T. Luo y M. Palaniswami, «Network architecture and QoS issues in the internet of things for a smart city,» *2012 International Symposium on Communications and Information Technologies (ISCIT),* 2012.

[12] M. Kuzlu, M. Pipattanasomporn y S. Rahman, «Communication network requirements for major smart grid applications in HAN, NAN and WAN,» *Computer Networks,* vol. 67, pp. 74-88, 2014.

[13] A. Riahi, Y. Challal, E. Natalizio, Z. Chtourou y A. Bouabdallah, «A Systemic Approach for IoT Security,» *2013 IEEE International Conference on Distributed Computing in Sensor Systems,* 2013.

[14] M. U. Farooq, M. Waseem, A. Khairi y S. Mazhar, «A Critical Analysis on the Security Concerns of Internet of Things (IoT),» *International Journal of Computer Applications (0975 8887),* vol. 111, nº 7, pp. 1-6, 2015.

[15] M. Nawir, A. Amir, N. Yaakob y O. B. Lynn, «Internet of Things (IoT): Taxonomy of security attacks,» *2016 3rd International Conference on Electronic Design (ICED),* 2016.

[16] D. Chasaki y C. Mansour, «Security challenges in the internet of things,» *International Journal of Space-Based and Situated Computing,* vol. 5, nº 3, 2015.

[17] D. Minoli, Building the Internet of Things with IPv6 and MIPv6: The Evolving World of M2M Communications, New Jersey: John Wiley & Sons, 2013.

[18] H.-L. Truong y S. Dustdar, «Principles for Engineering IoT Cloud Systems,» *IEEE Cloud Computing,* vol. 2, nº 2, pp. 68-76, 2015.

[19] A. Botta, W. de Donato, V. Persico y A. Pescapé, «Integration of Cloud computing and Internet of Things: A survey,» *Future Generation Computer Systems,* vol. 56, pp. 684-700, 2016.

[20] J. R. Gupta, «Significance of Satellites in IoT,» *International Research Journal of Engineering and Technology (IRJET),* vol. 4, nº 6, pp. 2690-2695, 2017.

[21] M. P. Pawlowski, A. J. Jara y M. J. Ogorzalek, «Harvesting Entropy from On-board Sensors of Constrained Devices for Hardening Security of IoT Communication Mechanisms,» *6th International Workshop on Managing Insider Security Threats (MIST 2014),* pp. 1-13, 2014.

[22] S.-K. Choi, C.-H. Yang y J. Kwak, «System Hardening and Security Monitoring for IoT Devices to Mitigate IoT Security Vulnerabilities and Threats,» *KSII Transactions on Internet and Information Systems,* vol. 12, nº 2, pp. 906-918, 2018.

[23] RAPID7, «HACKING IoT: A Case Study on Baby Monitor Exposures and Vulnerabilities,» RAPID7, Boston, 2015.

[24] S. L. Keoh, S. S. Kumar y H. Tsch, «Securing the Internet of Things: A Standardization Perspective,» *IEEE Internet of Things Journal,* vol. 1, nº 3, pp. 265-275, 2014.

[25] K. Lee, D. Kim, D. Ha, U. Rajput y H. Oh, «On security and privacy issues of fog computing supported Internet of Things environment,» *2015 6th International Conference on the Network of the Future (NOF),* 2015.

[26] N. Kayastha, D. Niyato, E. Hossain y Z. Han, «Smart grid sensor data collection, communication, and networking: a tutorial,» *Wireless Communications and Mobile Computing,* vol. 14, p. 1055–1087, 2012.

[27] O. Flauzac, C. Gonzalez y F. Nolot, «New Security Architecture for IoT Network,» *International Workshop on Big Data and Data Mining Challenges on IoT and Pervasive Systems (BigD2M 2015),* pp. 1028-1033, 2015.

[28] P. Porambage, M. Ylianttila, C. Schmitt, P. Kumar, A. Gurtov y A. V. Vasilakos, «The Quest for Privacy in the Internet of Things,» *IEEE Cloud Computing,* vol. 3, nº 2, pp. 36-45, 2016.

[29] J. Lloret, J. Tomas, A. Canovas y L. Parra, «An Integrated IoT Architecture for Smart Metering,» *IEEE Communications Magazine,* vol. 54, nº 12, pp. 50-57, 2016.

[30] A. R. Al-Ali y R. Aburukba, «Role of Internet of Things in the Smart Grid Technology,» *Journal of Computer and Communications,* vol. 3, pp. 229-233, 2015.

Designing a backbone trunk for the public transportation network in Montevideo, Uruguay

Claudio Risso and Sergio Nesmachnow

Universidad de la República, Uruguay,
{crisso,sergion}@fing.edu.uy

Abstract. Massive public infrastructure is usually structured into hierarchical levels, where different technologies handle different scales of requirements allowing most efficient and scalable implementations. In opposition to the aforementioned architecture, the public transport system in Montevideo (Uruguay) uses a single/flat level, with buses as the only means. This work explores the performance benefits and the cost feasibility of a new hierarchically segmented metropolitan trunk network for the public system in Montevideo, a problem that is tackled through combinatorial optimization approaches. The reference structure assumes light railway trams (LRTs) are used to massively transfer passengers between remote points of the city, while buses are reassigned as feeders of the new backbone in the network. The real-world example integrates demands information, realistic travel and waiting times as well as standard deployment costs. Results show that this new structure is economically competitive and significantly better in terms of quality of service.

Keywords: smart cities; public transportation; network design

1 Introduction

Public transportation is a key element of nowadays societies, which directly impacts over several aspects of daily activities of citizens [16]. Moreover, it has a direct implication on sustainability, as the higher the rate of passengers using a public transportation system, the lesser the air pollution, the most efficient the use of energy, the most livable the city [13, 15]. Public transportation is a very relevant problem in Latin American countries. Overall, public transportation serves a higher interest and delivers more benefits than private transportation. However, having a good public transportation system is not only a matter of good will. In order to succeed, public system travel times should plenty beat those of private vehicles, but the system also has to be economically competitive, reliable, and it has to provide seamless connectivity. There are many trade-offs to balance in such a design, which is not an easy task [2].

Public transportation systems are studied within the concept of *smart mobility* [1] under the novel paradigm of smart cities [3]. In this context, Intelligent Transportation Systems (ITS) make use of technology to develop and enhance transportation [5], usually focusing on public media (e.g., bus, train, etc.)

In large cities, a successful public transportation system comprises different media, which compound a massive infrastructure. Paris Métro and London Underground move around 1.5 billion passengers per year; Moscow Metro is even larger with 2.5 billion. The problem of designing a public transportation system falls in the category of network design problems. As a general rule, large networks are structured into hierarchical levels that use different technologies to handle different scales of requirements. For example, consider access and backbone in telecommunications; high, medium and low voltage in electrical networks; or even subways, surface trains and buses in public transportation systems.

Regarding public transportation networks design, the related literature somehow integrates those technologies, aiming at having the higher *passenger per hour peak direction* media strategically connecting distant points within a city. Most reference works state the problem as a superposition of transportation technologies, where portions of the legacy infrastructure are considered definite. Most cities with massive transportation systems have designed their services correctively, adding elements to address specific situations, progressively improving the result without a coordinated design for the whole of the variables. The result of such a process is generally suboptimal.

This work explores the design of the trunk backbone network of a hierarchically integrated public transportation system. Design premisses are inspired in basic characteristics of resilient and scalable networks. The underlying model assumes a planning-from-scratch approach, where a few stations are set in accordance to demand data and other strategical concerns, while most of the trunk network topology is designed to minimize infrastructure costs and at the same time being competitive in terms of travel times. The design also assumes a two stages approach. First stage precisely comprises the backbone trunk or Rapid Transit System (RTS), which has the highest infrastructure investment. Buses are reassigned to the access function, i.e., they work as feeders for the previously planned backbone network. Thus, the layout of their lines is to be tackled in a second stage, which is out of the scope of this work. Variants of this model can integrate access times of users as a part of the problem.

The strict hierarchy of media intrinsic to the formulation of this problem, turns the new backbone network critical, since an interruption in a line operation could actually disconnect zones of the city. Thus, the design integrates topological constraints to minimize those risks, what constitutes an innovation of this work regarding existing literature. The work uses the city of Montevideo (Uruguay) as a real-world application case, a previously unexplored instance, which constitutes another contribution. The main results indicate that the proposed approach is economically able of being implemented in Montevideo.

This article is organized as follows. Section 2 presents the problem formulation, a description of the case study in Montevideo, and a review of related works. The proposed approach for the backbone transportation network design is also described in Section 2. Section 3 summarizes resolution details, while experimental analysis is reported in Section 4. Finally, Section 5 presents the conclusions and the main lines of future work.

2 Problem formulation and case study in Montevideo

This section introduces the proposed approach to solve the problem of designing a backbone for a public transportation network, the mathematical formulation, and the case study of Montevideo, Uruguay.

2.1 General considerations and related works

From an abstract point-of-view, the planning and location of new transport infrastructure must consider diverse urban or strategic affairs, such as: environmental issues, metropolitan land-use plans, integration of satellite cities into a larger metropolis, and even speculative real-estate concerns, because a better connectivity turns more desirable certain zones of a city. Many of these concerns are analyzed in the related literature [4, 9, 17]. The proposed approach integrates those high-level constraints in the analysis, but most of them are part of the design premisses rather than entities in the optimization model.

One of the advantages of having a transportation network hierarchically structured into two media (LRTs and buses) is that long-haul portions of most travels are carried out using trams/trains, which have the highest *passenger per hour peak direction*. Besides, for a given number of passengers to move, the road congestion and maintenance costs caused by a fleet of LRTs are much lower than buses, as buses are regarding private motor vehicles. Furthermore, electrical engines of LRTs feed directly from the electric grid. Having a mostly electrical public transportation system directly translates into environmental friendliness. Nowadays, electric buses are an available technology, but they use batteries, and the distance a bus can go with a full charge is incompatible with significant portion of current bus lines alignments. Reassigning buses to the access function minimizes distances and fosters the spreading of a fleet of electric buses. Finally, remote terminals serve as gateways to important urban centers nearby.

According to the literature [10], the design of a Rapid Transit System or RTS consists of two intertwined problems: a careful placement for stations and the crafting of the alignments for lines to connect them. Those entities are clearly interdependent, and optimally, the problem should be solved as a whole. However, a sequential approach helps to tackle the problem. A first step is *selecting key nodes* as main stations by their importance as origin or destination for trips. Designing an *optimized core network* is a second stage. This stage aims at connecting key-nodes with a good performance-to-cost ratio, which causes system effectiveness to be achieved while the overall efficiency is maximized. Finally, in order to optimally increase the total coverage of the lines, one might run a third step for *setting secondary stations* as a derived result from the previous alignments. A dual approach [9] analyses the problem as perceived from the user point-of-view. Hence, the attributes regard with *attraction accessibility*: the ease of reaching a station using any mode of transport; and *radiation accessibility*: the proficiency to reach a far-endpoint location.

This article combines both infrastructure and user perspectives of the problem. First of all, key-nodes are selected by the computation of the number of trips starting in each zone, referred to as *trip generation analysis* [10]. By considering those zones that add up to a significant percentage of the total trips, a good overall *attraction accessibility* is sustained. The number of lines to be deployed between those points is set from the number of trips starting and ending at each node/zone, what in turn is referred to as *trip distribution analysis*.

Potential edges for the alignments are selected by the broadness of streets and avenues. Such graph of potential corridors is planar and plenty connected, so secondary stations in this approach are defined as a collateral result of the backbone network, which is the main object of design in this work. Further details and considerations of literature [10], such as *Modal Choice Analysis*: allocation of trips among the currently available transportation systems; and *Trip Assignment Analysis*: assignment of trip flows for the specific routes on each transportation system that will be selected by the users, are appointed as future research. *Radiation accessibility* in this work relies upon the existence of a spread RTS connecting most important demand points in the city at very good end-to-end travel times.

In this work, two formulations of the problem are used to determine a reference topology for the backbone of a public transportation network in Montevideo. The case study and the two formulations are described next.

2.2 Case study: public transportation network in Montevideo

The case study solved in this article is the public transportation network of Montevideo, Uruguay. Public transportation in Montevideo is comprised of 1528 buses operated by four companies. The bus network consists of 145 bus lines with different variants, accounting for outward and return trips, as well as shorter versions of the same line. The total number of bus lines when considering each variant individually is 1383, a remarkably large number. The leftmost of Fig. 1 shows the bus lines of the system, on top of a road map (data from `sig.montevideo.gub.uy`). The city centre, marked as `B` in the rightmost of Fig. 1 is a hub in the bus network, with most lines converging to that area.

Bus lines are significantly large: the average bus line length is 16.7 km (standard deviation 7.1 km) and the median length is 16.4 km, with the longest line spreading over 39.6 km. Intuitively, these figures strike as remarkably large, considering that the total area of Montevideo is 530 km^2 and can be circumscribed to a rectangle of 26×37 km. This work follows literature recommendations: the design aims at integrating Montevideo with its metropolitan area [9] and key-nodes are mostly chosen according with their importance as traffic sources [10]. Table 1 shows the daily origin-destination trips matrix per-zone, considering not only Montevideo municipalities (`A` to `G`) but also demand from satellite cities, which are connected by national routes `R1` to `RInt`. Table 1 accounts total trips by any means. A recent survey [12] details how those trips are performed: *by-foot* 34%, *private vehicles* 32%, using *public buses* 25%, *motorcycles* 4%, *bicycles* 3%,

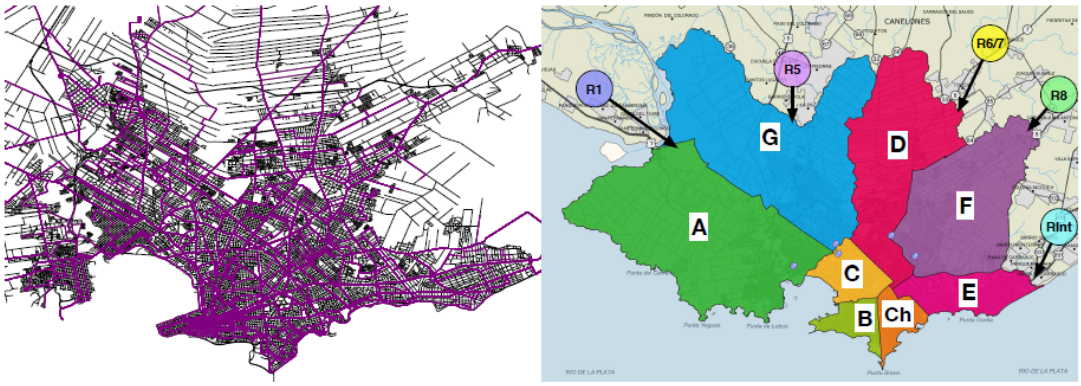

Fig. 1. Bus lines of the public transportation system of Montevideo, Uruguay.

taxis, Uber and other apps 1%, *other medias* 1%. These figures show how much space to grow public transport has.

space to grow public transport has.

Destination / Origin	A	B	C	Ch	D	E	F	G	R1	R5	R6/7	R8	Rint	Total
A	249,690	31,578	20,632	15,239	6,493	4,074	4,224	26,308	1,121	915	140	0	1,285	361,699
B	30,040	395,971	58,687	108,525	22,695	50,501	21,039	21,939	2,686	10,342	3,240	1,321	19,775	746,761
C	22,523	60,039	179,910	23,949	22,213	12,420	10,507	27,319	1,082	2,541	3,940	234	3,693	370,370
Ch	15,770	99,818	25,244	239,919	24,776	53,164	17,432	12,108	1,690	3,067	1,986	318	12,639	507,931
D	4,492	25,010	19,156	23,617	214,225	13,484	41,526	10,877	801	398	2,362	349	2,935	359,232
E	4,216	53,784	15,085	51,642	14,511	97,917	19,354	5,346	158	995	1,184	162	27,726	292,080
F	4,505	20,462	10,637	18,560	39,957	19,330	209,980	5,553	137	1,333	777	166	6,958	338,355
G	23,200	19,480	29,574	13,017	7,510	8,850	4,897	136,145	684	6,979	312	0	0	250,648
R1	966	3,803	1,172	639	727	78	137	684	67,299	405	90	0	285	76,285
R5	915	9,394	2,615	3,384	398	1,365	1,402	8,057	405	235,823	1,999	462	789	267,008
R6/7	152	3,326	3,723	2,142	2,275	1,114	561	381	90	2,369	70,024	3,129	3,352	92,638
R8	0	861	234	318	349	401	327	0	0	599	3,178	35,342	9,421	51,030
Rint	1,669	19,161	3,827	11,876	3,027	28,998	7,083	0	205	858	3,082	10,073	350,559	440,418
Total	358,138	742,687	370,496	512,827	359,156	291,696	338,469	254,717	76,358	266,624	92,314	51,556	439,417	4,154,455

Table 1. Origin-destination matrix for daily trips in Montevideo, Uruguay [12]

Data in Table 1 are taken from a polling of the *Banco de Desarrollo de América Latina* [12]. As it counts in Table 1, the most important internal municipality is the city centre `B`, followed by `Ch`, which is geographically contiguous. Considering municipalities over the city border as connected with near cities, we conclude that areas in order of importance are the following: `E+RInt`, `G+R5`, `D+R6/7` and `A+R1`. Thus, the case of study considered in this article for the LRT design defines five zones to be connected and seven key-nodes, which are definite for the optimization purposes. Design premisses for the backbone of the public transportation network in Montevideo include:

- the backbone architecture is to be of *hub type*, with the city centre (zone `B`) as concentrator, since that zone is the main destination of trips in the city and its location as urban geographic centre makes it a natural candidate to articulate demands;
- three nodes are identified in the city centre: *Plaza Independencia* (`PIN`, node_1), *Tres Cruces* (`XXX`, node_id 2), and *Palacio Municipal* (`PAM`, node_id 3) for whom is supposed to exist a fast interconnection media, that allows to rapidly reach any of these nodes, whose far-end points are closer than 4km;

– four *remote terminals* complete the set of key-nodes. They are *Carrasco* (`CAR`, node_id 4), *Cerro* (`CRO`, node_id 5), *Pocitos* (`POC`, node_id 6) and *Colón* (`TCO`, node_id 7). `POC` and `CAR` are introduced as new stations in the city, and they were included because of the number of trips of their zones, which respectively are `Ch` and `E+RInt`. `CRO` and `TCO` are actual bus stations by this date, and they are also among the most important origin-destination trips. They respectively correspond to `A+R1` and `G+R5`.
– All lines connect the city centre (node_ids from 1 to 3) with some remote terminal (node_ids from 4 to 7). Trips between zones are assumed to relay in the centre. Besides, `CAR`, `TCO` and `CER` serve as gateway respectively terminals towards: East, North and West directions.

Fig. 2. Potential LRT network for the case study in Montevideo

Fig. 2 shows the network of terminal and optional stations as well as potential connections between them. As we previously mentioned edges are select by the importance of streets and avenues. Optional stations are mostly defined by intersections of edges. In the chosen architecture, the remote terminals must be connected to the Centre by means of LRT lines to be displayed on the city. Remaining locations can be part of the solution (i.e., being a *station* of the proposed LRT) or not, depending on the convenience of their utilization. The *hub* architecture is that a passenger whose destination is not the Centre or any of

the intermediate nodes of the line that he boarded, just makes a transfer in the Centre to the final destination.

Since buses are to be reassigned as feeders of the backbone, the last one becomes critical to keep trips running. That issue combined with the fact that LRTs operate at the surface (in opposition to a subway/underground service) and superficial vehicles are exposed to failures, induced to choose an organically robust design. Rather than using preset geometric pattern to assemble the network topology [11], the proposed approach relies upon typical criteria for network design: resiliency as a consequence of the degree of connectivity, i.e., of the number of physically independent paths connecting points. Thus, a specific condition of the design is that there is more than one physically independent line between each concentrator and the hub. In the case study, that number is 2 for terminals `CAR`, `CRO` and `TCO`, and 3 for `POC`, due to the larger number of passengers. In any case, the problem formulation is general, as the number of lines in each case is a specific parameter of the problem instance. Since a rapid transport mean is assumed to exist connecting stations in the city centre, reaching `PIN`, `PAM` or `XXX` is indifferent from the performance point-of-view.

2.3 Problem formulation

The general goal of the problem is to find the optimal subnetwork of a given network of potential tram connections, and the lines assignment to connect a set of locations. The formulation of the problem models the transportation network as an undirected graph $G = (V, E)$, where V is the set of relevant stations and E is the set of possible connections between those stations. Some of these nodes compound the city centre $\mathcal{C}$, other are remote terminals $\mathcal{T}$. The remaining nodes $V \backslash \mathcal{C} \backslash \mathcal{T}$ are optional nodes, also called Steiner nodes. For the instance represented in Fig. 2, $\mathcal{C} = \{1, 2, 3\}$ and $\mathcal{T} = \{4, 5, 6, 7\}$. Previous information is complemented with functions for cost and delay: $C : E \to \mathbb{R}^+$ and $D : E \to \mathbb{R}^+$. We also assume a length function $L : E \to \mathbb{R}^+$. Costs and lengths are related but not necessarily linearly. They can be precisely adjusted to local conditions such as: rivers, lakes, built up areas, or urbanization density. As we see in Section 4, this work takes geographical lengths as a basis to compute trip delays as well as costs. Therefore, rail stretches costs, delays and lengths are precomputed as edges attributes; they respectively are: c_{ij}, d_{ij} and l_{ij} for every segment $ij \in E$.

Two versions of the problem are considered: *maximum resilience* and *maximum travel time limits* models. The main details and the formulation of each problem variant are presented next.

Maximum resilience problem. A simple version of the problem considers a given number of lines from every remote terminal towards the Centre, and it imposes that no line shares any edge with other. Consider the (realistic) case of requiring two lines from `CAR` (id 4), `CRO` (id 5) and `TCO` (node 7) to the Centre, and three from `POC` (node 6). Formally, given the non-directed graph $G = (V, E)$, a directed graph $\widetilde{G} = (V, \widetilde{E})$ is built by duplicating every edge in E considering both directions, except for those edges with nodes `PIN` (id 1), `XXX` (id 2) or `PAM`

(id 3) as endpoints, for which only the incident edge is used. Let x_{ij} be a variable that accounts how much *flow* traverses the edge ij in $\widetilde{E}$.

$$\begin{cases} \min \sum_{ij\in\widetilde{E}} c_{ij}x_{ij} & \\ \text{s.t.} \sum_{jk\in\widetilde{E}} x_{jk} - \sum_{ij\in\widetilde{E}} x_{ij} = 2,\ j = 4,5,7 & (i) \\ \sum_{6k\in\widetilde{E}} x_{6k} - \sum_{i6\in\widetilde{E}} x_{i6} = 3, & (ii) \\ \sum_{ij\in\widetilde{E}} x_{ij} - \sum_{jk\in\widetilde{E}} x_{jk} = 0,\ \forall j \geq 8 & (iii) \\ 0 \leq x_{ij} \leq 1, \quad \forall ij \in \widetilde{E} & (iv) \end{cases} \tag{1}$$

A formulation for this problem instance is that of Eq. 1. The idea is that a set of *flow paths* determine the sequence of edges used by each line. Equations group (i) in Eq. 1 force an outgoing net-flow of 2 units coming from nodes 4,5 and 7. That number is 3 for node 6 because of equation (ii). Equations group (iii) imposes flow balance for every Steiner node, so traffic in this network can only drain out throughout nodes 1, 2 and 3. It is a well-known theoretical result that extreme points in the feasible region of network flow problems are integer, so we do not need to explicitly impose integrity to variables x_{ij}. Thus, equations group (iv) guarantees that any arc is either used ($x_{ij} = 1$) or not ($x_{ij} = 0$), and by at most one unit of flow (a line). The objective function aims at minimizing the total railway investments, which are the most significative in such a project.

Theorem 1. *The maximum resilience problem is within the polynomial time complexity class.*

Proof. Observe that formulation Eq. 1 is a pure linear programing problem, for whose kind there is at least one algorithm [8] of polynomial-time complexity. □

Maximum travel time problem. Although simple to solve, the problem in Eq. 1 pushes physical independence beyond problem premisses, since it does not allow any two lines to use a same edge. We only need such independence for lines coming from the same terminal, but lines from different terminals can share tram yards. Therefore, physical independence can be relaxed to allow lower costs without violating our design goals. Besides, we integrate some passengers Quality-of-Experience concerns to the formulation by setting maximum end-to-end travel times from terminals. The parameter TD_p specifies a threshold on the travel times between the terminal $p \in \mathcal{T}$ and the centre $\mathcal{C}$.

The problem formulation is presented in Eq. 2. The binary variable x_{ij} ($ij \in E$) indicates whether the edge connecting stations i and j is to be included in the solution ($x_{ij} = 1$) or not ($x_{ij} = 0$). Binary variable y_{ij}^{pr} only activates when the r-th line of terminal $p \in \mathcal{T}$ uses the segment $ij \in E$ on its way to-from the city centre. Variables θ_j^{pr} indicate whether or not the node (station) j is part of the route of the r-th line of the terminal station p.

$$
\begin{cases}
\min \sum_{ij \in E} c_{ij} x_{ij} & & \\
\text{s.t.} \sum_{pj \in E} y_{pj}^{pr} = 1, & 4 \le p \le 7, 1 \le r \le 2(3) & (i) \\
\sum_{ij \in E} y_{ij}^{pr} + \sum_{jk \in E} y_{jk}^{pr} = 2\theta_j^{pr}, & j \ge 4, j \ne p, 4 \le p \le 7, \; 1 \le r \le 2(3) & (ii) \\
\sum_{r=1}^{2(3)} y_{ij}^{pr} \le 1, & ij \in E, 4 \le p \le 7, & (iii) \\
\sum_{ij \in E} d_{ij} y_{ij}^{pr} \le TD_p, & 4 \le p \le 7, 1 \le r \le 2(3), & (iv) \\
4x_{ij} \ge \sum_{p=4}^{7} \sum_{r=1}^{2(3)} y_{ij}^{pr}, & ij \in E, & (v) \\
x_{ij}, y_{ij}^{pr}, \theta_j^{pr} \in \{0,1\} & \forall ij \in E, 4 \le p \le 7, \; 1 \le r \le 2(3) & (vi)
\end{cases}
\tag{2}
$$

Equations in group (i) in Eq. 2 set to exactly one the number of edges used by the r-th line of terminal p to come out from it. The index r can range from 1 to 2, or 3 when $p = 6$ (`POC` station). Equations in group (ii) force intermediate nodes to be used twice (inward and outward edges) or not at all. The combined effect of (i) and (ii) is to craft paths for each line of each terminal. Equations in group (iii) prevent from any two (or three) lines of the same terminal to use the same edge, which conveys physical independence. The left-hand side of equations in group (iv) accounts for the end-to-end traveling times for each line of each terminal p, which must be bounded by TD_p. The right-hand side of equations in group (v) counts how many times an edge is used by any line. Since lines from the same terminal cannot share an edge, and there are only four terminals, equations in group (v) are always satisfiable by setting x_{ij} to 1. That, however, increases the cost in the objective function to minimize. Suffices that a line is using edge ij to force the activation of the associated variable x_{ij}. For values of TD_p sufficiently large, travel times do not apply, and problem Eq. 2 becomes a relaxation of Eq. 1 that allows some additional degree of physical dependence. This fact can be used to estimate lower bound to the investments in tram yards.

Theorem 2. *The maximum travel time problem is within the NP-Hard time complexity class.*

Proof. Consider the Resource Constrained Shortest Path Problem (RCSP). Given graph $G{=}(V, E)$, a cost function $C{:}E{\to}\mathbb{R}^+$, a pair source "s" and target "t" nodes in V, resources usage functions $R_k{:}E{\to}\mathbb{R}^+$ for different kinds of resources $k \in \{1, \ldots, K\}$ and resource limits RL_k, the goal is on finding the minimum cost path from s to t in G that keeps the resources usage of each kind below RL_k. RCSP is proven NP-Hard in general [7], even for a unique resource.

Consider now a particular case of Eq. 2 where $\mathcal{C} = \{s\}$, $\mathcal{T} = \{t\}$ while set to 1 the number of lines connecting s and t (Eq. 2 allows in general to have more than one independently physical line from terminals, but it doesn't force it). This subproblem of the Maximum travel time problem is actually a RCSP variant where resources are link delays d_{ij} and the resource limit for that sole kind is TP_t, so single-resource RCSP is a polynomial reduction of Maximum travel time problem and the last one must be NP-Hard as well. □

3 The proposed resolution approach

This section describes the optimization methods applied for solving the two versions of the problem presented in the previous section.

Theorem 1 evidences the reduced intrinsic complexity of the maximum resilience problem version. State of the art linear programming solvers are able to tackle such problems for instances with hundreds of thousands of variables and constraints in very short times. The instantiation of the problem formulation in Eq-1 for the problem instance described in Fig. 2 results in a linear programming problem with just 189 variables and 52 constraints. The problem instance was solved with the `linprog` solver of `Matlab` version 8.5.0 to find the optimum solution, using the interior point method. The problem was solved in 0.04 s executing in an `Intel Core i5@1.8GHz` processor with 8GB RAM.

Due to the intrinsic complexity of the maximum travel time problem version (as proven by Theorem 2), it is not expected to find exact solution for large instances of the problem, regardless of particularities of the formulation. The instantiation of the problem formulation in Eq-2 for the problem instance described in Fig. 2 results in an integer programming problem with 1515 variables and 987 constraints. The `linprog` solver of `Matlab 8.5.0` was not able to find the optimum solution within a time limit of one hour. In order to tackle that much harder problem, our approach relied upon `IBM ILOG CPLEX(R) Interactive Optimizer` version 12.6.3 as the optimization software. A significantly more powerful hardware was also needed, in this case a `HP ProLiant DL385 G7` server, with 24 `AMD Opteron` processor 6172@2.1GHz and 64GB of RAM. The overall execution time required for the resolution in that hardware was 30 s.

Empirical evidence demonstrated that for the real-world case study in Montevideo, even the harder version of the problem is possible of being solved with existing software and hardware. In consequence, we disregarded implementing ad-hoc heuristic algorithms to find good-quality solutions, being that the exact solution can be easily found in a matter of few seconds. However, we acknowledge that heuristic or metaheuristic approaches [14] must be needed in order to address more sophisticated problem variants and/or larger scenarios.

4 Experimental analysis

This section presents the experimental analysis of the proposed approach for the transport system of Montevideo.

4.1 Problem instance

The problem instance models the public transportation network in Montevideo, according to the values reported in Table 2 for the topology presented in Fig. 2.

i	j	c_{ij}	l_{ij}	d_{ij}	i	j	c_{ij}	l_{ij}	d_{ij}	i	j	c_{ij}	l_{ij}	d_{ij}
1	52	24	263	84	12	13	34	3448	275	30	42	81	1478	157
1	53	65	1133	136	12	23	64	3218	262	31	32	36	509	99
1	54	45	690	110	12	25	82	4679	349	32	33	32	460	96
1	55	33	476	97	13	14	29	3283	265	32	41	38	772	115
2	25	116	2660	228	13	22	48	5500	398	34	35	12	410	93
2	33	49	821	118	14	22	30	3103	255	35	36	28	1231	142
2	34	135	2660	228	15	16	26	3037	251	35	39	126	2495	218
2	36	166	4203	321	15	20	27	2676	229	36	37	27	1182	139
2	39	97	2167	199	15	22	20	1888	182	36	39	107	2069	193
2	40	10	82	73	16	17	19	1822	178	37	38	118	2758	234
3	39	78	1642	167	17	19	29	2807	237	37	39	126	2463	216
3	40	100	1921	184	18	19	24	2282	205	38	39	37	542	101
3	49	103	1986	188	18	37	71	3727	292	38	54	31	410	93
3	51	54	1248	143	19	20	14	460	96	39	55	81	1543	161
3	55	31	410	93	19	21	23	1198	140	40	41	25	279	85
4	8	17	2380	211	20	21	26	1100	134	40	49	73	1297	146
4	9	14	1231	142	21	34	84	4728	352	41	42	72	1281	145
4	10	22	3267	265	21	37	31	1478	157	42	45	43	673	109
5	17	36	3776	295	22	23	78	3924	304	42	49	42	640	107
5	18	18	1707	171	22	36	74	4022	310	43	44	33	460	96
6	29	5	230	82	23	24	16	591	104	43	45	42	624	106
6	30	5	279	85	23	35	19	739	113	45	46	28	345	89
6	43	7	460	96	24	25	26	1116	135	46	47	31	410	93
6	44	4	230	82	24	34	10	279	85	46	48	71	1264	144
7	14	154	3185	260	25	26	10	279	85	47	49	55	1018	130
7	15	160	3201	261	26	27	59	1018	130	47	50	61	1379	151
7	16	186	3956	306	26	33	74	1445	155	48	49	99	1872	181
8	9	7	493	98	27	28	38	1806	177	48	50	74	1789	176
8	28	88	4712	351	27	31	52	1395	152	49	51	78	1740	173
9	10	12	1166	138	27	33	81	1527	160	50	51	49	1001	129
10	11	104	6600	464	28	29	21	1018	130	51	52	93	1806	177
10	27	98	5040	371	28	30	68	1395	152	52	53	62	1248	143
11	12	24	4285	326	29	44	29	361	90	53	54	99	2233	202
11	26	61	3300	266	30	31	37	542	101	54	55	38	542	101

Table 2. Reference costs (c_{ij}) [million USD], lengths (l_{ij}) [meters] and delays (d_{ij}) [seconds] in the case study (public transportation system of Montevideo).

Values in Table 2 were defined according to the following procedures:

- Path lengths were taken from Google Maps service (`maps.google.com`).
- Travel times between stations (d_{ij} in Table 2) were computed applying the following start/stop model: i) the LRT acceleration is $1.96m/s^2$ (0.2g), so standing passengers maintain equilibrium; ii) deceleration is also of $1.96m/s^2$ by the same comfort reason; iii) the time required for passengers board/alight the train at each station is 60s, which is added as a fixed per-stop delay to every edge; iv) cruise speed is $60km/h$, so it takes 8.5s to the LRT to get it.
- Regarding rail stretches costs, our approach relies on the study by Flyvbjerg et al. [6], adopting the worst per-kilometer value, since we are assuming elevated crossing point at some intersections.

– Constructions costs are based on lengths, but they are penalized by the urbanization density.

After computing the optimal solution for the *maximum resilience problem* variant for the case study (see Section 4.2), the resulting cost values were corrected by a coefficient so that the average per-kilometer cost to be 30 million USD, following the reference work by Flyvbjerg et al. [6]. Since the objective function in formulation Eq. 1 is linearly scalable, proportional modifications on the function change the objective value, but not the solution where it is attained.

4.2 Maximum resilience problem

The computed optimal solution for the maximum resilience problem variant has a cost of 2 744 million USD. Fig. 3 sketches the solution for the maximum resilience variant of the problem, considering the reference values in Table 2.

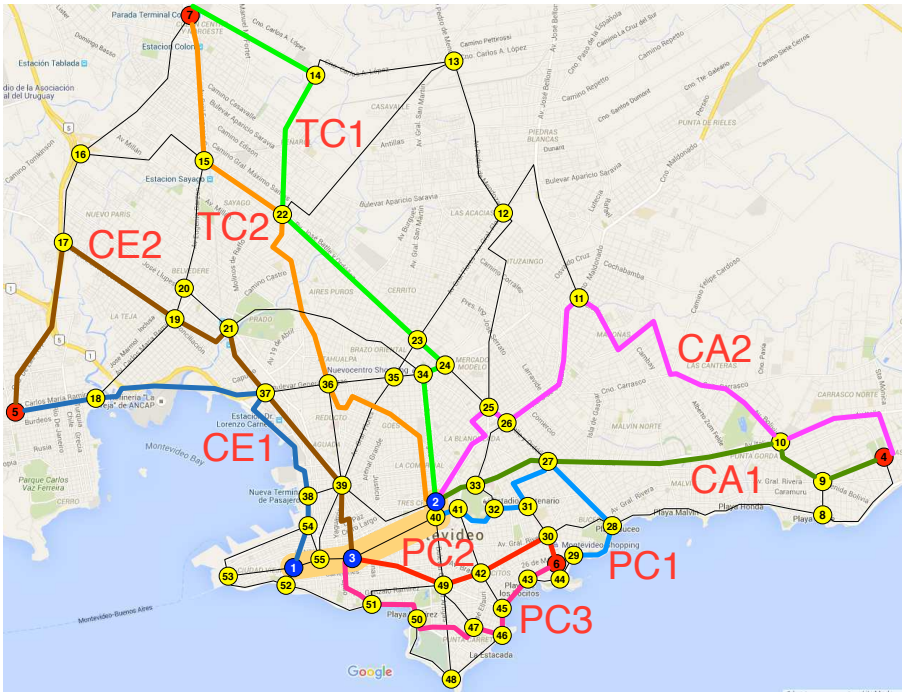

Fig. 3. Optimal solution for the maximum resilience problem

Even though the solution for the maximum resilience problem finds rail stretches costs optimally, it allows more than one configuration for lines. For instance, swapping sub-tours between node 4 and 10 for lines `CA1` and `CA2` still gets a feasible solution with the same cost. Overall, the formulation in Eq. 1 does not determine configuration for lines. Nonetheless, it guarantees that at least a feasible configuration can always be crafted, and that whatever the features of the configuration, lines are independent and rails cost is optimal.

Fig. 3 includes a proposal for the configuration of lines, chosen so that end-to-end travel times between lines of the same terminal are as balanced as possible. The attributes for each line are presented in Table 3

Line ID	CA1	CA2	CE1	CE2	PC1	PC2	PC3	TC1	TC2
Cost (m.USD)	254	313	283	323	225	231	272	423	420
Length (m)	9785	16106	9292	13364	6091	4383	5467	13742	13314
Delay (s)	929	1308	900	1212	913	537	807	1236	1074

Table 3. Lines attributes for the reference alignment

4.3 Maximum travel time problem

Consider the problem formulation in Eq. 2 with end-to-end traveling times bounds TD_p of infinite value, i.e., without limits of time. This eliminates equations group (iv) in Eq. 2, so the result is a relaxation of the general formulation. The solution to that problem is a cycle spanning all terminals and node XXX (id 2), plus an additional path the for third line of Pocitos. That cycle borders the map in Fig. 2 and it is not suitable for passengers, since they would never use the secondary line because of its prohibitive traveling time. However, the cost of that solution is important, because it constitutes a lower bound for more realistic solutions. The solution of the relaxation of Eq. 2 has a cost of 1383 million USD.

Reference values of TD_p are based on Fig. 3, since travel times in Table 3 are much better than those of the actual public transportation system in Montevideo. To allow a wide exploration of solutions, TD_p for a terminal p is defined as the end-to-end time of the worst lines configuration over railways associated to terminal p. For instance, for CAR that configuration is 4, 9, 10, 11, 26, 25 and 2, whose end-to-end travel time is 1323 s. By repeating that procedure upon remaining terminals, the other bounds result: 1266s for CER, 913 s for POC and 1236 s for TCO. Using these TD_p values, line configurations in Fig. 3 are feasible in Eq. 2, so the solution cost computed for the maximum resilience problem is an upper bound for this problem variant. Thus, the optimal cost for this problem is between 1383 and 2744 million dollars. The exact solution for the maximum travel times problem is in fact below the average of those values, with a total cost of 1890 million USD. By prorating this amount among tickets annually sold (300 million) and considering a 30-year repayment period, a per-ticket cost of 0.21 USD over an actual average ticket cost of 1.12 USD (August 2019) is obtained.

Fig. 4 sketches the optimal line configurations and Table 4 presents the main attributes for lines. In this case, the concept of *per-line cost* does not apply, because in this problem version lines share important portions of the tram rails.

Line ID	CA1	CA2	CE1	CE2	PC1	PC2	PC3	TC1	TC2
Length (m)	12264	10951	12412	15169	2611	3399	7011	14513	14365
Delay (s)	1079	1273	1223	1252	499	614	832	1146	1204

Table 4. Lines attributes for the resilient and traveling time bounded problem

End-to-end travel times in the solution of this problem version are better than in the previous one in three out of nine lines: CA2, PC1 and TC1. Per-terminal

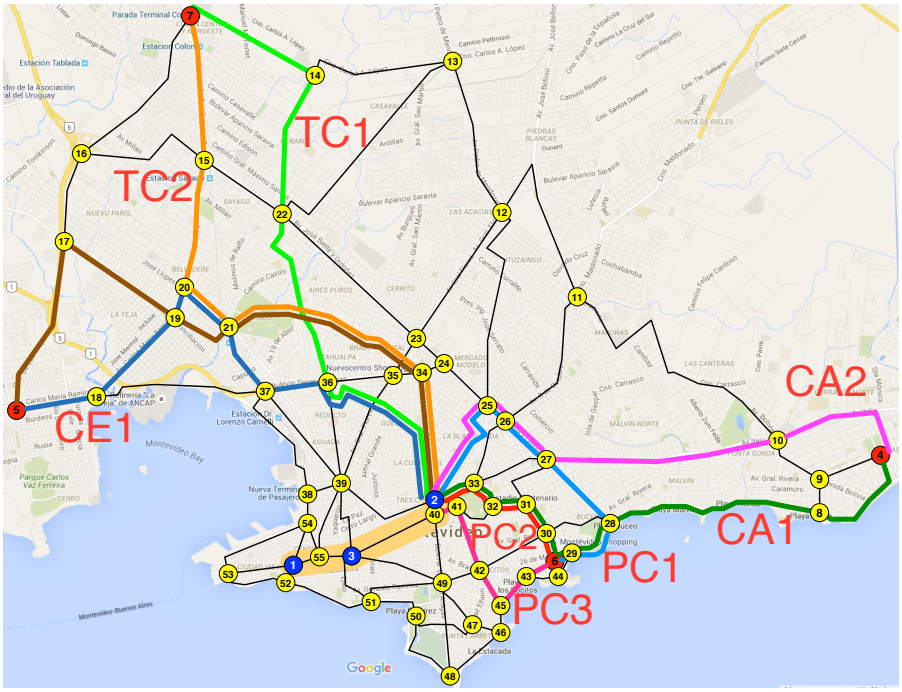

Fig. 4. Optimal solution for the maximum travel time problem

average traveling costs in the new solution are higher for Carrasco (5.1%), Colón (1.7%) and Cerro (17.2%), but they are lower for Pocitos (-13.8%), which moves much more passengers. In either case, differences are relatively low. A notorious difference is observed on the rail stretches cost, since the maximum time solution is 45.2% cheaper than the maximum resilience solution.

The average speed in both solutions are practically the same: 36.9 km/h vs. 36.6 km/h. Average travel times between remote terminals and the city Centre are significantly lower than in the current public bus system: 20 minutes vs. 55 minutes for Carrasco, 21 minutes vs. 61 minutes for Cerro, 11 minutes vs. 31 minutes for Pocitos, and 20 minutes vs. 65 minutes for Colón. Overall, the average speed-up provided by the new system is near to 3.

5 Conclusions and future work

This article presented a combinatorial optimization approach for the problem of designing a backbone trunk public transportation network for Montevideo.

Two variants of the problem were studied, accounting for maximum resilience and maximum travel time solutions. The best computed design balances investments costs with end-to-end travel times, getting to a reference solution with a cost of 1890 million USD, which can be assumed with a low increase of the ticket cost. The overall quality of service provided by the computed solution is

significantly better than in the current bus system of Montevideo, with speedups of around three in the travel times between terminals and the city center.

The main lines for future work include integrating detailed distributions about inter-zone travel times and adding up the access portion of the network, not only to compute such additional travel times but also to estimate reduction in costs coming from reassigning busses to shorter trips.

References

1. Benevolo, C., Dameri, R.P., D'Auria, B.: Smart mobility in smart city. In: Empowering Organizations. pp. 13–28. Springer International Publishing (2016)
2. Ceder, A., Wilson, N.: Bus network design. Transportation Research Part B: Methodological 20(4), 331–344 (1986)
3. Deakin, M., Waer, H.A.: From intelligent to smart cities. Intelligent Buildings International 3(3), 140–152 (2011)
4. Dodson, J., Mees, P., Stone, J., Burke, M.: The principles of public transport network planning: A review of the emerging literature with select examples. Tech. Rep. 15, Griffith University (2011)
5. Figueiredo, L., Jesus, I., Tenreiro, J., Ferreira, J., Martins, J.: Towards the development of intelligent transportation systems. In: IEEE Intelligent Transportation Systems. pp. 1206–1211 (2001)
6. Flyvbjerg, B., Bruzelius, N., van Wee, B.: Comparison of capital costs per route-kilometre in urban rail. European Journal of Transport and Infrastructure Research 8(1), 17–30 (2008)
7. Handler, G.Y., Zang, I.: A dual algorithm for the constrained shortest path problem. Networks 10(4), 293–309 (1980), `https://onlinelibrary.wiley.com/doi/abs/10.1002/net.3230100403`
8. Karmarkar, N.: A new polynomial-time algorithm for linear programming. Combinatorica 4(4), 373–395 (1984)
9. Król, A., Król, M.: The design of a metro network using a genetic algorithm. Applied Sciences 9(3) (2019)
10. Laporte, G., Marín, Á., Mesa, J., Ortega, F.A.: An integrated methodology for the rapid transit network design problem. In: Geraets, F., Kroon, L., Schoebel, A., Wagner, D., Zaroliagis, C.D. (eds.) Algorithmic Methods for Railway Optimization. pp. 187–199. Springer, Berlin, Heidelberg (2007)
11. Laporte, G., Pascoal, M.: Path based algorithms for metro network design. Computers & Operations Research 62, 78–94 (2015)
12. Mauttone, A., Hernández, D.: Encuesta de movilidad del área metropolitana de Montevideo. Principales resultados e indicadores. Online: `http://scioteca.caf.com/handle/123456789/1078` (2019-08-20) (2017)
13. Miller, P., de Barros, A., Kattan, L., Wirasinghe, S.: Public transportation and sustainability: A review. KSCE Journal of Civil Engineering 20(3), 1076–1083 (2016)
14. Nesmachnow, S.: An overview of metaheuristics: accurate and efficient methods for optimisation. International Journal of Metaheuristics, 3(4), 320–347 (2014)
15. Rassafi, A., Vaziri, M.: Sustainable transport indicators: Definition and integration. International Journal of Environmental Science & Technology 2(1), 83–96 (2005)
16. Stjernborg, V., Mattisson, O.: The role of public transport in society—a case study of general policy documents in sweden. Sustainability 8(11), 1120 (2016)
17. Škorupa, M., Kendra, M.: Proposal of backbone public transport lines in the upper Šariš region. Procedia Engineering 192, 800–805 (2017)

Monitorización de espacios urbanos, como herramienta educativa para el apoyo en el cumplimiento de los Objetivos de Desarrollo Sostenible para una Smart University.

Juan Antonio Rodríguez Rama[1][0000-0002-3817-2399], Javier Maroto Lorenzo[2], Clara Godoy Morales[3][0000-0001-9992-3523], Domingo A. Martín Sánchez[4][0000-0002-3179-2245], Ana García Laso[5][0000-0002-3310-2674]

[1] Universidad Politécnica de Madrid
jrodriguez@alumnos.upm.es
[2] Universidad Politécnica de Madrid
javier.maroto@upm.es
[3] Universidad Politécnica de Madrid
cgodoy@alumnos.upm.es
[4] Universidad Politécnica de Madrid
domingoalfonso.martin@upm.es
[5] Universidad Politécnica de Madrid
ana.garcia.laso@alumnos.upm.es

Abstract. El mundo está en plena transformación. Los ciudadanos, las empresas, las universidades, etc. necesitan cada vez más actuar bajo una Responsabilidad Social (RS) que les permita encontrar e incorporar soluciones efectivas al cambio climático, la pobreza, el hambre, etc. Es decir, cumplir con los Objetivos de Desarrollo Sostenible adoptando como eje transversal de su actividad y líneas de desarrollo la Agenda 2030 propuesta por la ONU. En la Escuela Técnica Superior de Ingenieros de Minas y Energía se está trabajando desde hace varios años en el proyecto "AulaEnergía" que facilita un espacio colaborativo de difusión, formación y desarrollo tecnológico como hilo conductor para la aplicación de los ODS en la universidad. Una de sus líneas de trabajo principales (Tellus) es la monitorización de espacios urbanos con sistemas de software y hardware libre. La validación de los prototipos y la calidad los datos generados en condiciones reales de trabajo son una herramienta educativa y de análisis científico con un gran potencial para apoyar la evolución hacia un modelo de Smart University.

Keywords: Tellus, Sostenibilidad, Monitorización, Medio Ambiente, AulaEnergía, Resiliencia, Ciudades, Res2+U, Ciencia de Datos, Objetivos de Desarrollo Sostenible, Smart University

1 Antecedentes

El Cambio Climático se ha convertido, por derecho propio, en uno de los problemas que más incertidumbre está generando en las sociedades y economías de todo el mundo

[1][2] y combatirlo es uno de los ejes de actuación de la mayoría de los gobiernos a través de la adopción de la Agenda 2030 y los 17 Objetivos de Desarrollo Sostenible (ODS) con sus consecuentes metas [3] (Fig. 1).

Las ciudades o entornos urbanos, representan menos del 2% de la superficie de la Tierra, pero despuntan como agentes aceleradores del Cambio Climático, siendo consumidores del 78% de la energía mundial, produciendo más del 60 % de las emisiones de los gases del efecto invernadero y a la vez, se muestran como lugares muy expuestos y vulnerables a sus efectos, ya que en ellas vive el 50 % de la población mundial, cifra que para el 2050 alcanzará el 70% según las previsiones [4].

Debido a ello, son ambientes estratégicos que pondrán a prueba su resiliencia. Su habilidad para mantener su continuidad ante las actuales y futuras alteraciones, mientras contribuyen positivamente a la adaptación y la transformación, por lo que existe la imperiosa necesidad de desarrollar un uso más eficientes de las tecnologías y políticas ya implementadas, así como el desarrollo de otras nuevas, para incrementar la capacidad de las urbes del mundo, de manera que se puedan afrontar nuevos desafíos protegiendo a su población, infraestructuras, y sus activos económicos y naturales [5].

Fig. 1. Objetivos de Desarrollo Sostenible (ODS). Fuente: ONU.

2 Proyecto AulaEnergía

El mundo está en plena transformación, busca cada vez más, una ética detrás de las cosas, que las instituciones y corporaciones presenten una Responsabilidad Social (RS) desde la que encuentren e incorporen soluciones efectivas al cambio climático, la desigualdad social, la pobreza, el hambre, etc. y por ello los ODS se han convertido en una prioridad en todas las agendas, y las universidades deben estar a la vanguardia [6][7], evolucionando hacia un modelo de Smart University [8] creando un ecosistema que mejore la calidad de vida de la comunidad, haciendo uso global, eficiente y sostenible de la tecnología, así como del análisis racional de los datos que generan e interconectando a todos los actores y servicios en beneficio de todos.

La Escuela Técnica Superior de Ingenieros de Minas y Energía (ETSIME) de la Universidad Politécnica de Madrid (UPM) no es ajena a estas inquietudes, desde el 2015 se empezó a conformar el Proyecto AulaEnergía. El cual, en sus diferentes etapas, ha estado siempre ligado a la Responsabilidad Social Universitaria (RSU) de la ETSIME, que se coordina desde la Unidad de Emprendimiento Social, Ética y Valores en la Ingeniería (UESEVI), la cual lleva trabajando en este centro más de 10 años para incorporar sensibilidades Medioambientales, Sociales y de Gobernanza al día a día de la universidad, además de contribuir al desarrollo de la sociedad, entendiendo esta RS como una dimensión ética que toda institución debería tener como visión.

Siendo por tanto una apuesta estratégica y multipropósito capaz de generar impactos positivos y perdurables a nivel educativo, formativo, divulgativo, medioambiental y social, a los que se suma el compromiso de cumplimiento de los ODS, para construir un ecosistema de innovación en colaboración con otros centros de la UPM, instituciones y asociaciones interesadas.

Esta estrategia define tres grandes líneas de trabajo (Fig.2) :

- Optimización de la ETSIME y su entorno mediante el estudio, desarrollo e implementación de sistemas de monitorización que permitan elaborar medidas de eficiencia. Esta rama es denominada Tellus.

- Convertirse en un vivero y plataforma para el desarrollo de proyectos multidisciplinares y sostenibles.

- Dar a conocer las alternativas energéticas existentes a partir de los proyectos que se desarrollen a los estudiantes del Centro, las empresas colaboradoras y el público en general a través de un área expositiva o showroom.

Fig. 2. Líneas de trabajo de AulaEnergía.

3 Monitorización

Poder evaluar, de forma argumentada y justificada, las soluciones precisas que se deban adoptar para el incremento de la resiliencia en las ciudades, hace preciso medir y monitorizar, entre otros aspectos, sus distintas variables físicas de forma periódica y sustentada en el tiempo [9], las cuales tienen un impacto directo en la salud humana, economía y en el calentamiento global, siendo hoy en día, una de las herramientas imprescindibles para garantizar la calidad de vida de sus ciudadanos, proteger el medio ambiente y asegurar la capacidad de adaptación al Cambio Climático [10].

Esto ha llevado a los gobiernos a realizar mediciones y recopilar, durante años, información de variables ambientales en las ciudades, tales como: temperatura, humedad, radiación o calidad del aire. Estas medidas son tomadas mediante estaciones fijas de alta calidad calibradas según los estándares de cada zona [11].

Estas redes de monitorización en tiempo real presentan elevados costes de implantación y mantenimiento, por lo que su número suele ser limitado y, por tanto, sólo se estudian estas variables en localizaciones específicas, lo que lleva a que sólo pueden establecerse estudios por extrapolación. En consecuencia, hace que su desarrollo en ciudades más pequeñas, pueblos o áreas más deprimidas, sea muy escaso. Cómo alternativa, en diferentes partes del mundo, se están dando proyectos basados en tecnologías de software y hardware libre, principalmente usando como base las plataformas Raspberry Pi [12] y Arduino [13], sumado a una gran variedad de sensores que analizan parámetros ambientales de todo tipo (temperatura, humedad, presión atmosférica, ruido, radiación, partículas en suspensión, CO2 velocidad del viento, lluvia, temperatura del suelo, etc.) con una interesante eficiencia-precio y el apoyo de inmensas comunidades que colaboran entre sí, dando acceso a ideas y soluciones a infinidad de situaciones.

3.1 Tellus

La monitorización de los espacios de la ETSIME y su entorno, es parte integral del proyecto y una de las líneas de trabajo fundamentales de AulaEnergía desde 2016. Atendiendo a las diferentes actuaciones realizadas se puede dividir en las siguientes etapas:

Primera Etapa: Sistemas Ambientales (SA´s). Una ciudad resiliente y sostenible es compleja y está altamente interconectada, además alcanza su máxima eficiencia teniendo en consideración sus múltiples relaciones y dimensiones de vinculación, por lo que la implantación de redes de sensores que cubren todos los niveles (Aéreo, Social y Subterráneo) (Fig.3) permitirá obtener numerosos datos del entorno, que sumado a su adecuado procesado hará posible extraer un valor añadido, que permita una gestión fundamentada, más eficiente e inteligente de las ciudades. Con esta filosofía se desarrolló la primera generación de prototipos denominados Sistemas Ambientales Exteriores (SAE´s) como apoyo a los laboratorios, museos y proyectos de la ETSIME [14] [15].

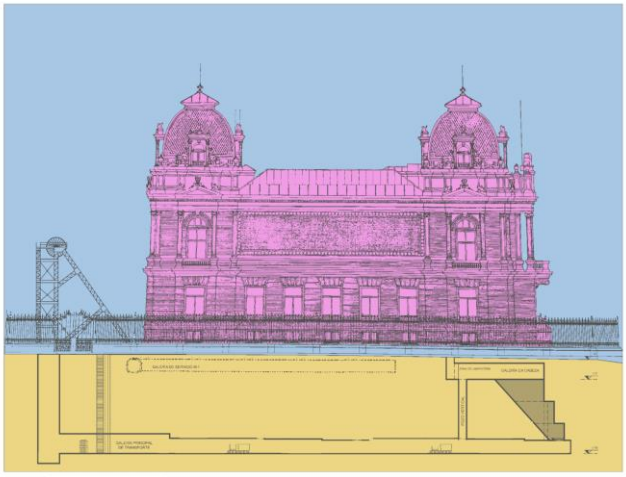

Fig. 3. Ejemplo de distribución de niveles de monitorización en nuestro Centro. En azul se muestra el Nivel Aéreo o Exterior, en morado el Nivel Social o Interior y en naranja el Nivel Subterráneo.

Como primera plataforma de desarrollo se utilizó una placa UNO de Arduino, por su reducido coste y su extendido uso, lo cual permite contar con el apoyo de una gran comunidad de desarrollo. Pero se descartó su uso por los fallos de comunicación que se detectaron debidos a la infraestructura de red del Centro, lo que imposibilita su uso más allá de unos primeros prototipos como el que se usó en la Mina Museo de la ETSIME para conocer la humedad (H) y temperatura (Tª) de su galería en varios puntos (Imagen 1).

Imagen. 1. Ejemplos de SAE´s en base a Arduino [10]

Como segunda opción de trabajo se eligió la plataforma Raspberry Pi 2B. Su utilización es algo más compleja, ya que requiere de un proceso de instalación y de unos conocimientos en sistemas UNIX algo más avanzados, pero aporta versatilidad.

Tras comprobar que era compatible con la red del Centro, el primero de los prototipos en el que se trabajó, fue el montaje de una garita exterior protectora para sensores de Tª/H, instalada en el techo del edificio de despachos y exámenes (M3) (Imagen 2) en la que implementar el hardware y aprender sobre su funcionamiento, estudiando su viabilidad y escalabilidad en condiciones reales para otros proyectos de monitorización de la ETSIME y hacer las pruebas de conexión para la visualización de los datos en la web del proyecto.

Se utilizó Debian 7 como sistema base (Raspbian en Raspberry-Pi) y se eligió el sensor DHT22, que incorpora en la misma sonda los sensores de Tª/H, por su bajo coste, su calibración ya realizada y su sencillez de uso. Este primer acercamiento al funcionamiento de esta plataforma será útil y educativo de cara a poder comparar con datos ambientales de espacios interiores que aportarían los Sistemas Ambientales Interiores (SAI´s), que serían desarrollados a partir de una simplificación de los SAE´s, posibilitando así el estudio de las calidades de los materiales utilizados, medidas de aislamiento, condiciones de habitabilidad, puntos de actuación y mejoras en eficiencia a realizar.

Desde un primer momento se vio el valor añadido de almacenar estos datos para estudios posteriores y no sólo su visualización en tiempo real en la web del proyecto (http://tellus.minasyenergia.upm.es), por lo que todo el desarrollo se orientó a almacenar la información en una Base de Datos (BBDD), escogiendo MySQL por ser relacional y SQL como lenguaje de programación de gestión de la BBDD.

Para poder visualizar los datos en tiempo real de forma pública a través de la web del proyecto se creó un servidor HTTP Apache, escogiendo un framework PHP ya que una web como la que se estaba desarrollando era algo que evolucionaría con el futuro, y necesitaba capacidad de escalarse a medida que se le incorporaran nuevas funcionalidades y características.

Para acceder a los datos del sensor se utilizó un script en PYTHON que leía los datos del sensor y los insertaba en la BBDD cada 5 minutos. Aunque puede considerarse excesivo tomar datos ambientales tantas veces a lo largo del día, se consideró que era lo más adecuado para dotar a los datos de versatilidad a la hora de ser tratados.

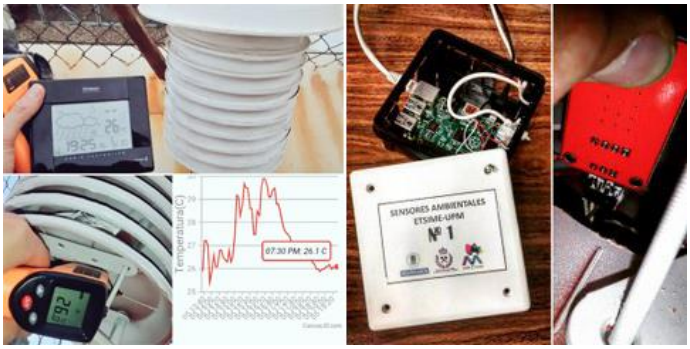

Imagen. 2. SAE en base a Raspberry Pi y comprobación de funcionamiento.

Segunda Etapa: Estaciones Ambientales (EA´s). A partir del 2018 nos sumamos a la sección de monitorización de RES2+U (Responsables, Sostenibles y Universitarios) proyecto estratégico de la UPM, que busca trabajar para contribuir a alcanzar los ODS de la ONU. Se trata de un proyecto pionero que une, iniciativas de sus diferentes centros, a profesores y estudiantes con el fin de alcanzar una universidad sostenible, fomentar la investigación interdisciplinaria mejorando la resiliencia de nuestras infraestructuras y siendo un ejemplo a seguir para estudiantes y ciudadanos de Madrid.

Se alcanza durante este periodo un nuevo estado de madurez y complejidad, con el desarrollo de la segunda y tercera generación de prototipos. Corresponde a este periodo también el cambio de designación de los equipos, que pasan a denominarse; Estaciones Ambientales Exteriores (EAE), Estaciones Ambientales Interiores (EAI), Estaciones Ambientales de Calibración (EAC) y Estaciones Ambientales Subterráneos (EAS), unificando el sistema de nomenclatura según su función y niveles de cobertura.

Gracias a la experiencia obtenida en la primera etapa del proyecto con los SA´s, se vio el interés de ampliar la red de sensores en la ETSIME para cubrir todos los niveles en los que se ha subdividido el entorno del Centro. Para ello se cambió la arquitectura para permitir pasar de tener un único servidor, a una red de estaciones recolectoras de datos y un servidor centralizado de almacenamiento y visualización de datos. Como plataforma de trabajo se escogieron las Raspberry Pi 3B+ (segunda generación), con servidor web APACHE y como servidor de visualización y tratamiento de datos, se escogió un servidor LINUX, con una BBDD MariaDb , servidor web APACHE , como framework PHP de SYMFONY.

En este caso la información no es accesible directamente desde el servidor, sino que hay que tomarla de cada estación. El servidor es el encargado de acceder a las estaciones, y vía HTTP, recoger un fichero JSON generado en la propia estación en el mismo intervalo de tiempo. En las estaciones, cada cinco minutos mediante un programa en PYTHON, se generan dos ficheros; uno para poder visualizar la información vía página web con formato HTML compatible con cualquier navegador y otro con formato JSON para una fácil manipulación de la información. El servidor es el que, desde los ficheros JSON, guarda la información en la BBDD y para poder visualizarla hay un servidor web desarrollado con SYMFONY que permite el acceso en tiempo real de los datos medidos (Fig. 4.).

Las sondas seleccionadas fueron la DHT22, que ya se había utilizado en la etapa anterior pero sólo usando las del fabricante AOSONG [16] que habían tenido mejor desempeño y estabilidad, ya que las sondas genéricas no duraron más de 7 meses sin presentar fallo. Además, se sumó el uso de la BME280 de Bosch [17], que se eligió por incorporar en la misma sonda los sensores de Tª/H/Presión (P), por su bajo coste y por su calibración mucho más fiable y mejor desempeño a lo largo del tiempo [18], que las demás sondas de este tipo presentes en el mercado.

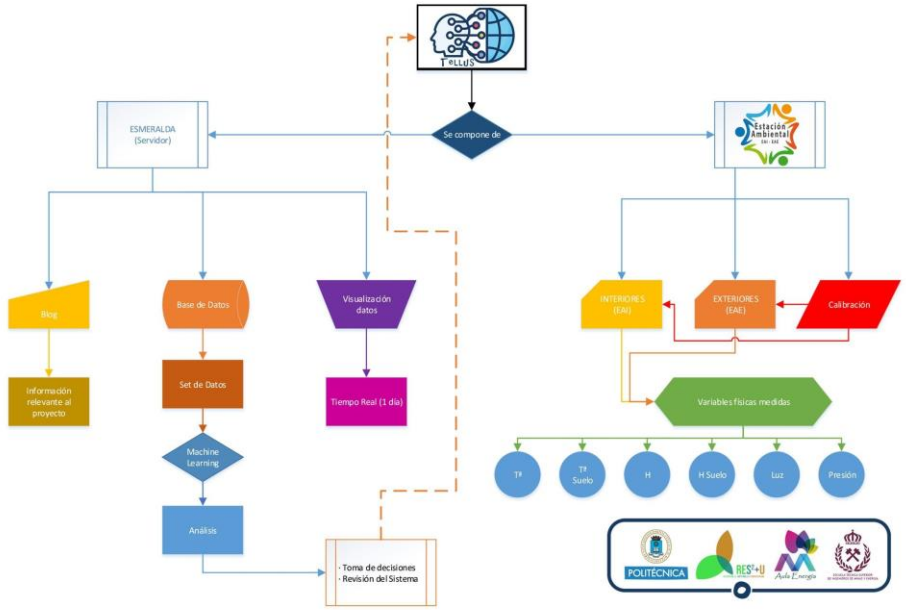

Fig. 4. Actual esquema organizativo del proyecto Tellus de AulaEnergía.

Actualmente están funcionando prototipos en el tejado del aulario (edificio M-2) denominado EAE-1, se trata de una garita meteorológica (Imagen 3) de mejor acceso para la revisión y mantenimiento de los componentes electrónicos, permite ampliar el número de sondas de medición de variables ambientales a medida que se escale el proyecto y fue construida siguiendo las especificaciones oficiales de la AEMET, con lo que se busca un entorno de medición en condiciones reales más adecuado con la menor alteración posible. Esta estación proporciona los datos ambientales que se visualizan en la web del proyecto y que se pueden descargar libremente en http://tellus.minasyenergia.upm.es/salidas. En el siguiente apartado serán analizados los datos aportados por el BME280, ya que se consideran los de mejor calidad obtenidos hasta la fecha.

También, se han dispuesto EAI´s en el IBERCOM y los racks de comunicaciones de la ETSIME para controlar y dar alerta de anomalías ambientales en estos espacios, asegurando el buen funcionamiento de estos equipos. En colaboración con la Cátedra-Empresa CLH de Metrología de los Hidrocarburos se está trabajando en la EAC para asegurar la calibración y trazabilidad de las mediciones de los sensores utilizados, aunque, estos puedan ser sean sustituidos debido a labores de mantenimiento por unidades similares.

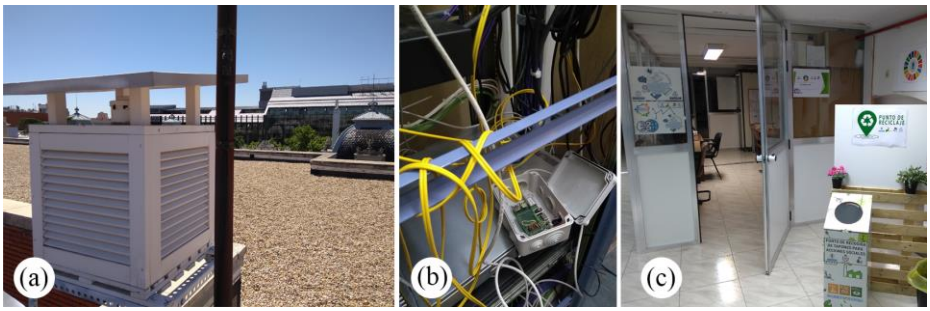

Imagen. 3. EAE-1 en el tejado del aulario de la ETSIME (a), instalación de la EAI del IBERCOM (b) y La Pecera, espacio de trabajo y desarrollo de los prototipos de Tellus (c).

Finalmente, se está trabajando en la primera variante EAS que se instalará en los espacios subterráneos, bajo la denominación de proyecto MESEME auspiciado por RES2+U de la UPM. Se sitúa en la primera galería de la Mina Museo Marcelo Jorissen y permitirá, cuando entre en funcionamiento, analizar el confort térmico de este museo universitario, así como medir la evolución de la temperatura en el terreno a lo largo del año para distintas profundidades, permitiendo crear curvas de Tª con las que conocer cuando alcanza la estabilidad, las mínimas en verano y máximas en invierno de la ciudad de Madrid.

La tercera generación, en la que actualmente se está trabajando se basa en las placas NodeMCU 1.0 LOLIN (V3) que integran el procesador ESP8266. Son plataformas de trabajo mucho más pequeñas y permiten no depender del acceso a red ya que se pueden conectar por la red wifi de la UPM al servidor del proyecto, por lo que su impacto en las instalaciones es mucho menor, permitiendo su progresiva instalación en los espacios de la ETSIME, incluidos aquellos de carácter histórico, como la biblioteca, donde se quiere instalar la primera red de esta 3ª generación, para monitorizar los libros y documentos antiguos recientemente restaurados y servir de herramienta de apoyo a la conservación del patrimonio histórico. Además, su coste es más contenido que el de las Raspberry Pi 3B+, por lo que su implementación permite instalar más estaciones de medición con el mismo presupuesto y disponer así de un volumen de datos más representativo.

3.2 Los datos

Una vez obtenidos datos durante un tiempo representativo, se han querido visualizar y analizar para así comprobar el correcto funcionamiento de los sensores.

Para ello se ha utilizado la plataforma ANACONDA [19], una distribución de código abierto que permite realizar ciencia de datos con el uso de PYTHON, y más en concreto JUPYTER NOTEBOOK, entorno computacional interactivo basado en la web para crear documentos de tipo JSON, que siguen un esquema versionado y que contienen una lista ordenada de celdas de entrada/salida que pueden contener código, texto (usando MARKDOWN), matemáticas, tramas y medios enriquecidos [20].

Una vez leídos, se representaron los datos para comenzar el análisis y poder filtrar errores de medición. Como se puede observar en la Fig. 5, durante este último curso, la toma de datos de la EAE-1 ha tenido tres etapas muy bien diferenciadas. La primera, muestra un periodo de temperatura ambiente bajo y humedades relativas muy elevadas que llega hasta la primera semana de febrero de 2019, momento en el que el sensor BME280 genérico sufre daños junto con parte de la electrónica del proyecto. Sustituir estos componentes y reparar el cableado supuso no poder volver a tomar datos hasta mediados de mayo de 2019, momento en el que vuelve a estar operativa la EAE-1.

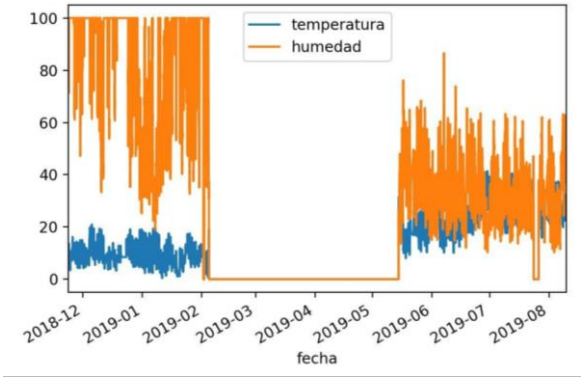

Fig. 5. Visualización de los últimos 9 meses de la EAE-1

Tras analizar el periodo completo y ver que los datos anteriores a mayo de 2019 no servían, se descartan y se toma el periodo de mayo de 2019 hasta agosto de 2019 como el nuevo periodo a analizar En la Figura 6 se puede comprobar que desde ese momento hasta la actualidad, la toma de datos ha funcionado correctamente, salvo por tres episodios, A y B son debidos a actualizaciones del sistema que hicieron que no se recopilaran datos (se identifican por una anomalía en forma de recta corta en la toma de datos diarios) y C es debido a la sustitución de un cable (se identifica por una anomalía muy marcada que llega a 0 hasta que se soluciona, en la toma de datos diarios).

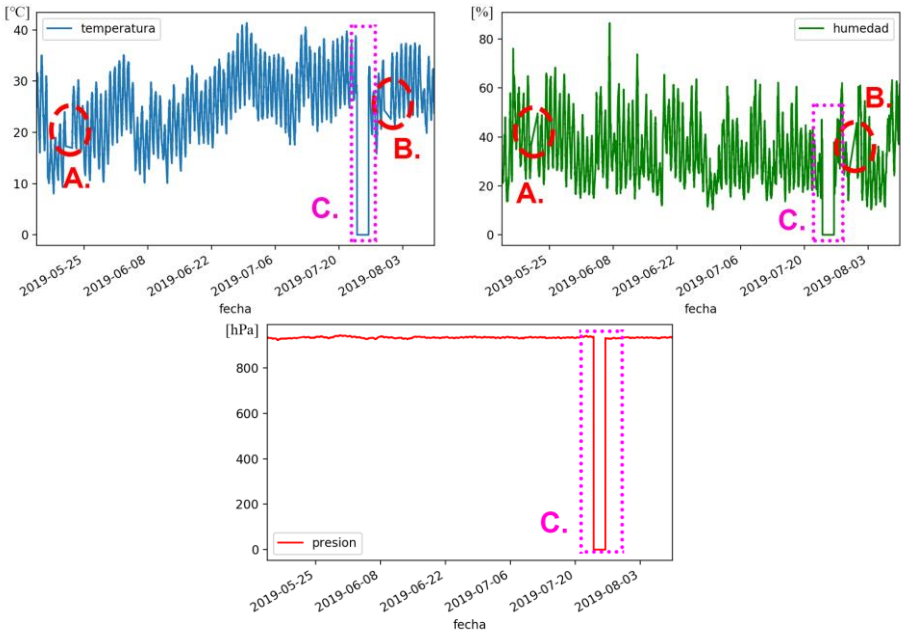

Fig. 6. Visualización de las anomalías y sus causas.

La geometría de estos fallos nos permite aprender de ellos para identificarlos y solucionarlos más rápidamente. En este caso son huecos en los datos, que al estar representando una línea continua une el último dato antes del hueco con el primer dato desde la reactivación (Fig. 7).

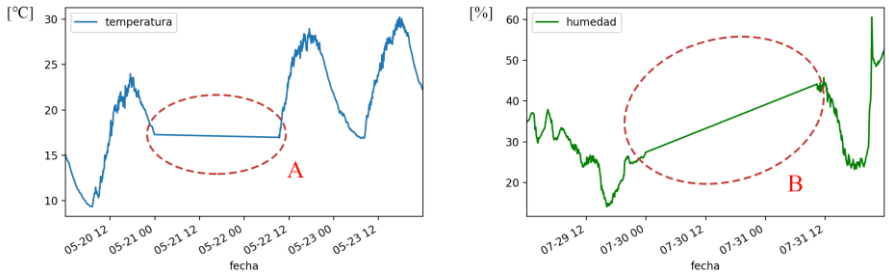

Fig. 7. Detalle de las anomalías A y B. en los datos de la Figura.6.

Con los datos ya filtrados, se comprobará con mediciones reales de estaciones homologadas del Sistema Integral de la Calidad del Aire del Ayuntamiento de Madrid [21] del mismo periodo, para así validarlos. En concreto usaremos los datos aportados por la estación situada en la Avd. Pablo Iglesias esq. C/ Marqués de Lema a menos de 700 m de este proyecto.

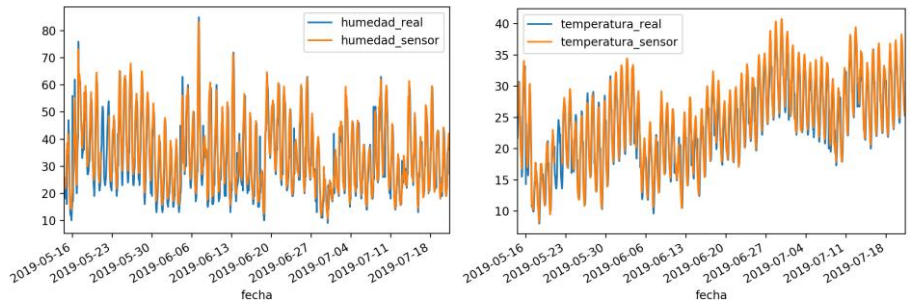

Fig. 8. Comparación Tª/H real (estación del Sistema Integral de la Calidad del Aire del Ayuntamiento de Madrid descrita) con las de Tª/H sensores EAE-1.

Como primer análisis se ha representado la Tª y H de la estación de medida (real) frente a la del sensor (EAE-1), para ello se han tomado datos desde mayo de 2019, primeros datos válidos del sensor, y hasta finales de julio de 2019, últimos datos disponibles de la estación del Ayuntamiento de Madrid. Se puede ver como los datos correlacionan y siguen la misma tendencia. (Fig. 8).

Posteriormente se ha hecho un análisis estadístico basado en regresiones lineales para validar los datos. Un buen estimador de la relación lineal que hay entre ambas variables es el Coeficiente de Correlación de Pearson (R), en este caso, son las variables de Tª y H del EAE-1 comparadas con las mismas variables reales aportadas por la estación de medición anteriormente definida.

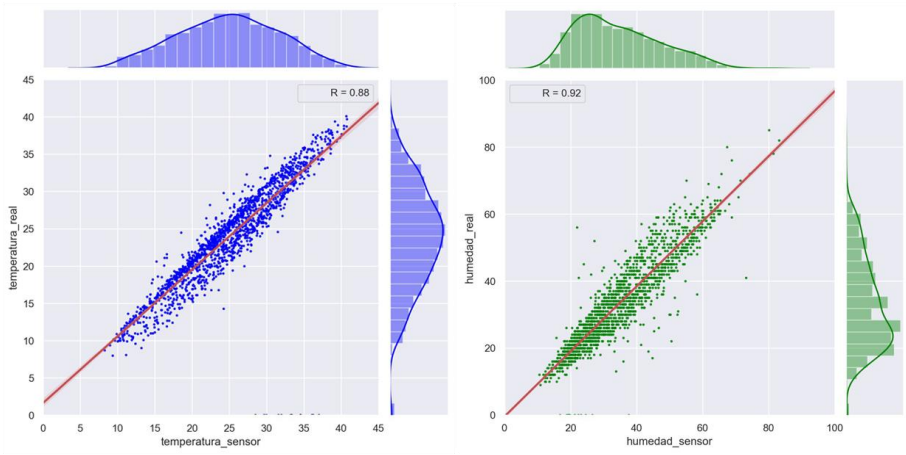

Fig. 9. Regresión entre datos de la estación de medida (real) frente datos de sensor (EAE-1)

Como se puede ver en la Fig. 9, el coeficiente de correlación es de 0.88 para temperatura y 0.92 para humedad, lo que significa que las diferencias entre datos son mínimas, su

relación es muy fuerte y, por tanto, el funcionamiento de los sensores de la EAE-1 es correcto.

4 Transferencia del conocimiento

Uno de los compromisos de AulaEnergía es hacer llegar a la sociedad y especialmente a los estudiantes de la comunidad educativa de la UPM este "know how".

Uno de los medios más directos fue participando en las clases del módulo 2 de la asignatura "Emprendimiento e Innovación Social: Interéticas y Valores" centrado en el emprendimiento e innovación, en ellas se instruyó en la creación de un blog y se les presentaron las plataformas Arduino y Raspberry Pi de manera teórica y fundamentalmente práctica a los estudiantes (Imagen 4a,4b y 5a), animándoles a implementar estos conocimientos en proyectos propios.

Imagen 4. Fotos de las clases del curso 2016 (a) y 2017 (b).

Además de las periódicas publicaciones en la web del proyecto, se hace uso de redes sociales (rrss) como herramientas fundamentales de difusión del día a día e hitos que se van alcanzando. Actualmente se tienen cuentas en Twitter (@aulaenergia) y en Facebook (@aulaenergia). A las que se suman las rrss de UESEVI, ETSIME y RES2+U desde las que se hace eco del proyecto periódicamente.

Finalmente, a lo largo del curso 2019 se ha colaborado en la 1ª Exposición Itinerante de Grupos de Cooperación y Plataformas de la UPM (iEXI) que ha recorrido todos los centros universitarios de la UPM dando a conocer los proyectos (Imagen 5b).

Imagen 5. Fotos de las clases del curso 2018 (a) y de la iEXI (b).

5 Conclusiones

La capacidad de AulaEnergía como hilo conductor para dar a conocer los ODS de manera aplicada, permitiendo a la comunidad universitaria ser partícipe de los mismos e incorporarlos a su día a día es enorme. Además, el gran espectro de colaboraciones que se abren entre centros de la universidad, y con otras instituciones y empresas para su desarrollo es muy enriquecedor. Gracias a proyectos como Tellus, se ponen en valor objetivos como el ODS 4 (Educación de Calidad), el ODS 11 (Ciudades y Comunidades Sostenibles) y el ODS 17 (Alianzas para lograr los Objetivos).

Una vez validados los primeros meses de datos, es preciso continuar con la toma de los mismos y volverlos a analizar periódicamente para estudiar su evolución y tendencias. Esto da impulso además a la expansión de la red de monitorización para cubrir, en su totalidad, el centro y su entorno, trabajando para alcanzar una Smart University, .

La recogida de datos de calidad ha de ser una prioridad, por lo que la calibración de los sensores y su mantenimiento son claves para asegurar que los datos son de calidad y tienen un volumen suficiente que permita realizar análisis cada vez mejores.

Líneas de futuro

Continuar fomentando la línea divulgativa y formativa con la colaboración en sus asignaturas y con la organización de cursos y jornadas dedicadas a la divulgación de las nuevas tecnologías y la industria 4.0. Animando a más estudiantes a sumarse al proyecto y desarrollar sus TFG y TFM en las líneas de trabajo del mismo.

Desarrollo y mejora de capacidades del espacio de trabajo de Tellus, conocido como La Pecera, con la incorporación de nuevos componentes y colaboradores.

Creación de documentación gráfica y divulgativa del proyecto. Mejora e incorporación de nuevos desarrollos a la web del proyecto.

Bibliografía

1. AEMET y OECC. Cambio Climático: Calentamiento Global de 1,5ºC. Agencia Estatal de Meteorología y Oficina Española de Cambio Climático. Ministerio para la Transición Ecológica, Madrid. 2018
2. Intergovernmental Panel on Climate Change. IPCC: Summary for Policymakers. In: Global warming of 1.5°C. 2018
3. ONU. Objetivos de Desarrollo Sostenible, http://www.undp.org/content/undp/es/home/sustainable-development-goals.html
4. ONU HABITAT, https://es.unhabitat.org/temas-urbanos/cambio-climatico/
5. ONU HABITAT, http://www.onuhabitat.org.mx/index.php/ciudades-resilientes
6. Muñoz, E., García-Laso, A., & Martín-Sánchez, D. A. (2018). The Challenge of Transversal Education Through Teaching Ethics in Engineering: From Hubris to Hybrid. In Spanish Philosophy of Technology (pp. 239-249). Springer, Cham.
7. François Vallaeys. ¿Qué es la Responsabilidad Social Universitaria?. Pontificia Universidad Católica del Perú.
8. Jose Manuel Sánchez Bernabeu, Francisco Maciá Pérez, Jose Vicente Berna-Martinez, Andrés Fuster Guilló. Smart University: hacia una universidad más abierta. Marcombo S.A. ISBN: 978-84-267-2328-4. 2016.
9. ONU HABITAT, https://unhabitat.org/urban-initiatives/initiatives-programmes/city-resilience-profiling-programme/
10. The World Bank Group. Guía para la Adaptación al Cambio Climático en Ciudades.
11. Ministerio para la Transición Ecológica. Gobierno de España. https://www.miteco.gob.es/es/calidad-y-evaluacion-ambiental/temas/atmosfera-y-calidad-del-aire/calidad-del-aire/evaluacion-datos/redes/default.aspx
12. Raspberry Pi Foundation. https://www.raspberrypi.org/
13. Arduino Company. https://www.arduino.cc
14. J.A. Rodríguez Rama,.A. García Laso , D.A. Martín Sánchez, J.Maroto Lorenzo, C. García de la Noceda y A.J. Moraño Rodríguez. AulaEnergía ETSIME-UPM. Un espacio colaborativo de difusión, formación tecnológica y desarrollo de la energía: Geotermia. GeoEner 2017: IV Congreso de Energía Geotérmica en la Edificación y la Industria. Madrid (2017)
15. J.A. Rodríguez Rama. PFC: Estudio del subsuelo y diseño de una instalación geotérmica para el Proyecto AulaEnergía de ETSIME-UPM. Madrid (Julio 2018)
16. AOSONG. Temperature and humidity module AM2302 (DHT 22) Product Manual
17. Bosch Sensortec. Final data sheet BME280 (Combined humidity and pressure sensor)
18. Robert-AT-kandrsmith.org. http://www.kandrsmith.org/RJS/Misc/Hygrometers/calib_many.html
19. Anaconda, Inc. https://www.anaconda.com/
20. Jupyter Notebook. Project Jupyter. https://jupyter.org/
21. Ayuntamiento de Madrid. Portal de datos abiertos. Datos meteorológicos. Estaciones de control. https://datos.madrid.es

Sistema de Monitoramento de Chuvas como Ferramenta de Gestão de Desastres em Cidades Inteligentes

Douglas de F. Medeiros
Filipe C.M. de Freitas
Juan M. Mauricio. Villanueva
Yuri P. Molina Rodriguez

Federal University of Paraiba, Brazil
{douglas.medeiros, filipe.freitas, jmauricio, molina.rodriguez}@cear.ufpb.br

Abstract. In the last decades, natural disasters have become more impacting and present in the daily lives of the world's populations. These disasters can be triggered by various phenomena, such as floods, erosion, earthquakes, hurricanes, among others. Coupled with these physical events, accelerated urban growth can potentiate the effects of a natural disaster, since many homes are built in inappropriate places and can directly affect the lives of many people and communities. In this way, the monitoring of risk areas in vulnerable locations has become a very important tool for effective decision making and assistance in the face of natural disasters, such as rainfall, which can cause flooding, slopes, floods, and other impacts to local communities. Although Civil Defense and the competent bodies are systematically carrying out this kind of tasks, the infrastructure used for such activities is always limited, not effectively exploiting the technology available today. Thus, in this paper, the aim is to contribute to the rainfall monitoring infrastructure, in order to reduce the effects on human losses and financial losses caused by natural phenomena. Complementarily, it is intended to establish initiatives for the management of smart cities. To reach these objectives, a rainfall intensity measurement system was developed using a scale type sensor called a rain gauge alongside an electronic prototyping platform. The system consists of the sensor nodes, which are installed in the places where the monitoring is being carried out and the measurements are transmitted by means of SMS messages (Short Message Service) for a central station, located at the Federal University of Paraíba, using GSM cell phone communication technology, for later routing to a database using the internet connection. In this way, any user, through a web application that can be accessed from the browser of a personal computer or a smartphone application, can have access to rainfall information collected by the developed measurement system.

Keywords: Alerts, Emergency, Monitoring, Pluviometer, Rains.

1 Introdução

Os desastres naturais mostram-se cada vez mais presentes e impactantes no cotidiano das pessoas ao redor do mundo. Segundo a Estratégia Internacional das Nações

Unidas para Redução de Desastres (tradução do inglês para *United Nations International Strategy of Disaster Reduction* – UNISDR) (2009), o termo desastre pode ser caracterizado por um distúrbio no cotidiano de uma comunidade ou população, podendo gerar diversos tipos de perdas, tais como perdas humanas, financeiras, materiais, etc. Quando as perdas de uma determinada comunidade estão relacionadas com fenômenos naturais, tais como inundações, erosão, terremotos, furacões, entre outros, são caracterizados como desastres naturais [1]. Além disso, as mudanças climáticas aliadas ao rápido crescimento populacional são fatores que impulsionam as consequências geradas pelo acontecimento destes eventos que tem impacto direto na vida da população.

Sob o mesmo ponto de vista, estes impactos são sentidos até mesmo pelas grandes nações, as quais possuem um maior preparo para enfrentar tais situações, como, por exemplo, os Estados Unidos da América, que vivenciaram no ano de 2017 o furacão Harvey, o qual deslocou mais de um milhão de pessoas das suas casas no estado do Texas e deixou mais de sessenta mortos [2]. Assim também, a região Nordeste do Japão foi impactada no ano de 2011 por um forte terremoto de magnitude 9, ocasionando o tsunami de Tohoku, deixando quase 16.000 mortos [2]. No Brasil, dentre os principais desastres associados aos fenômenos naturais, os mais frequentes são os causados pelos efeitos das chuvas, seja por sua abundância ou por sua falta. Segundo dados da UNISDR e do Centro de Pesquisas de Epidemiologia em Desastres Naturais (CEPED) (2015), o Brasil está entre os 10 países mais atingidos por desastres naturais nos últimos 20 anos, tendo mais de 51 milhões de pessoas afetadas pelos efeitos das mudanças do clima (Defesa Civil, 2016). Embora a maioria dos desastres naturais ocorrentes no Brasil esteja relacionada com aspectos pluviométricos, segundo indica o Atlas Brasileiro de Desastres Naturais, devido ao fato do país possuir dimensões continentais, tais eventos ocorrem de formas diferenciadas nas diferentes regiões do país.

Os desastres relacionados com grandes índices pluviométricos estão concentrados em sua maioria na região Norte do Brasil, por outro lado, a região Nordeste enfrenta a situação da seca e da estiagem [3]. Particularmente no estado da Paraíba, estando situado na região Nordeste do Brasil, a maioria dos problemas enfrentados está relacionada também com a falta das chuvas de acordo com estudo realizado pelo Centro Universitário de Estudos e Pesquisas sobre Desastres Naturais da Universidade Federal de Santa Catarina e a Secretaria Nacional de Defesa Civil e publicado no ano de 2013 no Atlas Brasileiro de Desastres Naturais – Versão Paraíba.

Apesar de grande parte dos registros de ocorrências estar relacionada com a estiagem, existem também dados neste documento de enxurradas e inundações ocorridas no estado da Paraíba entre os anos de 1991 e 2012, um intervalo de 21 anos. Segundo o Atlas, dos 223 municípios do estado, cerca de 70% registraram ocorrências de enxurradas, destacando-se as cidades de Aroeiras e Santa Rita. Além disso, também existem dados referentes à inundações compreendidos no mesmo período, totalizando 136 registros oficiais que podem ser caracterizados por desastres. Desse modo, os impactos dos eventos naturais têm ganhado cada vez mais repercussão nas agendas de governos e instituições internacionais. As estratégias de ação, que se centravam na resposta a esses impactos, têm se direcionado ao estudo, planejamento e intervenção sobre situações e contextos de risco, antes da materialização do impacto [4]. Diante

desse cenário, iniciativas de monitoramento de variáveis climáticas possuem significativa importância no auxílio de sistemas de alertas para a população. No ano de 2017 foi realizado um monitoramento de áreas de risco no município de João Pessoa-PB através de um projeto de extensão do Departamento de Engenharia Elétrica da Universidade Federal da Paraíba em parceria com os órgãos AESA e Defesa Civil e constatou-se a real necessidade de ações de monitoramento em locais desse tipo.

Ainda que a Defesa Civil e os órgãos estejam constantemente acompanhando a ocorrência de desastres naturais, a infraestrutura utilizada para realizar tais atividades é limitada se comparada à tecnologia disponível atualmente. Já existem iniciativas de alertas para população em funcionamento no estado da Paraíba, um exemplo é o serviço de alertas de desastres naturais por mensagens de texto (SMS), esse serviço é oferecido pelo Centro Nacional de Gerenciamento de Riscos e Desastres (CENAD) a partir dos dados fornecidos pela Defesa Civil. Este mesmo serviço está disponível também em outros estados das regiões Norte e Nordeste. Com uma abrangência territorial mais ampla, o aplicativo intitulado “SOS Chuvas” é disponibilizado pelo Governo Federal e oferece um serviço de previsão de chuvas e tempestades baseado em imagens do satélite geoestacionário GOES-16, o qual cobre toda a América do Sul, possibilitando ao usuário acompanhar o volume de chuvas em diversas regiões e receber alertas se desejar. Outra iniciativa que visa auxiliar no acompanhamento das chuvas é o Sistema Integrado de Informações sobre Desastres (S2ID), criado pelo Ministério da Integração com o objetivo de informatizar e disponibilizar registros associados aos desastres naturais no Brasil.

Neste artigo, tem-se como objetivo desenvolver um sistema embarcado de medição de chuvas, o qual será instalado nas zonas de risco no município de João Pessoa-PB, visando auxiliar na infraestrutura utilizada pelos órgãos competes (Defesa civil, AESA) e gerar alertas para redução das consequências de desastres naturais causados pelo grande volume das chuvas, tais como inundações, enxurradas, deslizamentos de terra, etc.

2 Definições Fundamentais

Esta seção trará uma revisão bibliográfica a respeito do tema abordado. Serão apresentados alguns conceitos relativos à precipitações, quais equipamentos são utilizados convencionalmente para realizar suas medidas e qual é a unidade. Mais adiante será feita uma revisão sobre sistemas de monitoramento e alertas de emergências e cidades inteligentes.

2.1 Precipitações - Conceitos

O processo de precipitação é definido como sendo a queda de água em estado líquido ou sólido e é resultado da condensação do vapor de água existente na atmosfera. As chuvas são caracterizadas pela aleatoriedade espacial e temporal. Normalmente o volume de chuvas é medido utilizando um equipamento chamado pluviômetro e a unidade para esta medida é o mm (milímetro), que corresponde a queda de um litro de água por metro quadrado da projeção da superfície terrestre. Existem outras maneiras

de realizar as medições, tais como aquelas baseadas em radares meteorológicos ou imagens de satélite [5].

2.2 Sistema de Monitoramento

Os sistemas de monitoramento têm ganhado bastante importância atualmente, auxiliando na tomada de decisões de ajuda e suporte diante de desastres naturais. Estes sistemas permitem monitorar determinadas áreas a fim de que se possa minimizar as perdas humanas e econômicas decorrentes de eventos causados pelos fenômenos naturais. No Brasil, uma iniciativa neste sentido desenvolvido pelo Centro de Previsão de Tempo e Estudos Climáticos do Instituto Nacional de Pesquisas Espaciais (CPTEC/Inpe), em parceria com o Governo Federal, foi a implantação do sistema chamado "SOS Chuvas". Este sistema consiste em um aplicativo gratuito para celular (Android ou IOS) que fornece informações a respeito da previsão de chuvas e tempestades em curto prazo e pode gerar alerta para os usuários.

Essas previsões são baseadas nos conhecimentos adquiridos sobre as propriedades físicas das nuvens no projeto CHUVA, utilizando as imagens do satélite geoestacionário GOES-16 na cidade de Campinas no período de dois anos. Além das imagens de satélite, a base de dados é composta por medições de estações meteorológicas do Departamento de Controle do Espaço Aéreo (DECEA) e do Centro de Meteorologia de Bauru (IPMET/Unesp). Apesar dos relatórios de precipitação estarem disponíveis para todo o Brasil, a previsão de chuvas ainda está restrita aos estados de São Paulo, Rio de Janeiro e sul de Minas Gerais [6].

No ano de 2018, foi publicado um estudo realizado na cidade de Dakar, capital de Senegal, sul da África, a respeito de um sistema de monitoramento de chuvas de baixo custo. A região é um importante centro administrativo e econômico do país, possuindo pouco mais de 2 milhões de habitantes e sofre constantemente com os efeitos das chuvas, apesar de estar localizada em uma região de clima predominantemente seco. Dessa forma, o estudo objetivou desenvolver um pluviômetro autônomo e conectado a um *gateway* que possui conexão com a internet [7]. A arquitetura deste sistema está exposta na Fig. 1 e exemplifica o caso de dois tipos de estações de medição, a primeira realiza a transferência de dados através de rádio frequência, enquanto que a segunda é utilizada em regiões onde o sinal de telefonia celular está disponível.

Os principais blocos que compõem este sistema são: Unidade de sensoriamento, processador, unidade de alimentação e unidade de transmissão de dados. Este estudo mostrou, por meio de uma comparação com uma estação industrial, sua eficácia na aquisição correta dos dados.

Um estudo análogo ao apresentado para a cidade de Dakar, também realizado na região africana (Namibia), foi publicado no ano de 2017 no evento *Global Wireless Summit* e propõe a criação de um sistema de monitoramento de chuvas de baixo custo utilizando a tecnologia de comunicação da rede celular GPRS (do inglês, *General Pocket Radio Service*). O sistema implementado possui sua arquitetura semelhante ao sistema da cidade de Dakar, porém não possui uma estação central para recepção dos dados. A aquisição de dados é transferida diretamente para o servidor por meio do módulo de comunicação GPRS SIM900. Sendo assim, o sistema é formado apenas

pela estação de medição que contém uma plataforma de prototipagem eletrônica, um sensor em conjunto com um circuito de condicionamento, um módulo de comunicação SIM900 e a unidade de alimentação que utiliza como fonte primária, a energia solar fotovoltaica [8]. Em ambos os estudos realizados nas cidades de Dakar e Namibia, foram utilizados sensores pluviométricos do tipo báscula.

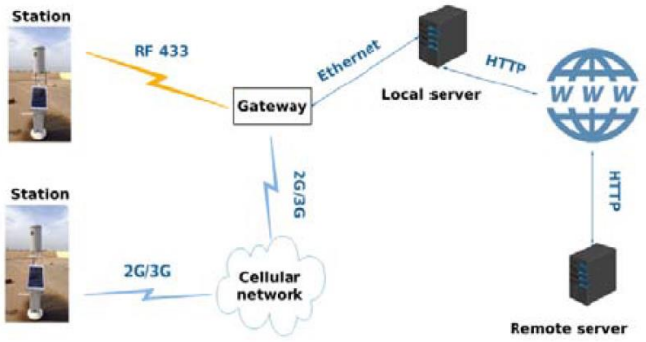

Fig. 1. Arquitetura do sistema de medição de chuvas desenvolvido na cidade de Dakar (Fonte: KAMA, 2018).

2.3 Cidades inteligentes ou *smart cities*

Um conceito que está ganhando bastante repercussão, diante do enorme avanço tecnológico das últimas décadas e da predominante migração da população para as zonas urbanas, é o de cidades inteligentes ou *smart cities*. Como resultado do grande aumento populacional urbano, os serviços públicos tornam-se cada vez mais difíceis de gerir com eficácia de forma que atenda satisfatoriamente toda a população [9]. Sendo assim, pode-se utilizar a tecnologia como ferramenta para auxiliar na gestão dos grandes centros urbanos e melhorar a qualidade de vida dos seus habitantes utilizando os recursos naturais de forma mais eficiente, contribuindo com a manutenção do meio ambiente.

De acordo com a Forbes, conforme citado por Coelho (2015, p. 9), uma cidade pode ser considerada *smart* ou inteligente caso contenha pelo menos cinco das oito características apresentadas na Fig. 2. Este mesmo estudo indica uma projeção do estabelecimento de pelo menos 26 cidades inteligentes até o ano de 2025, onde 50% estejam localizadas na América do Norte e Europa [9]. As cidades inteligentes proporcionam aos seus habitantes uma qualidade de vida muito melhor, que em conjunto com a tecnologia utilizada nelas, promove um desenvolvimento acelerado e inteligente. Além disso, aliado a tecnologia, podem-se gerir também aspectos relacionados aos desastres naturais.

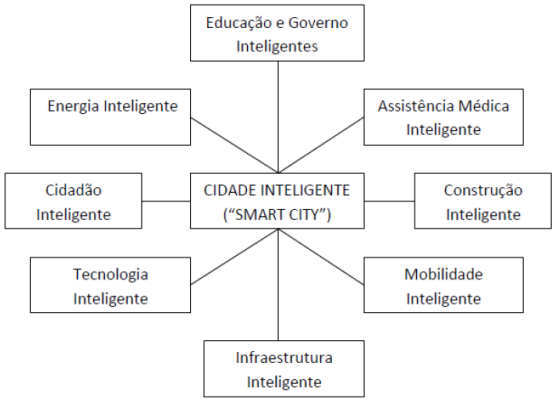

Fig. 2. Principais características de uma cidade inteligente. (Fonte: COELHO, 2018).

3 Descrição Geral do Sistema

Nesta seção será apresentado o sistema de medição de chuvas que foi desenvolvido, assim como uma descrição geral do sistema e logo após uma descrição individual de cada componente do sistema expondo suas principais características e funcionalidades.

A Fig. 3 ilustra os principais blocos que compõem o sistema embarcado de medição pluviométrica. O primeiro bloco, denominado "Medições de intensidade de chuva", corresponde ao módulo de transmissão do sistema que será detalhado nas próximas seções, chamado nó sensor. Este módulo está disponível no local onde serão feitas as medições e é composto por um sensor pluviômetro, pela plataforma de *hardware* Arduino e pelos módulos de GPS (do inglês, *Global Positioning System*), cartão de memória SD e comunicação GSM (do inglês, *Global System for Mobile Communications*).

Fig. 3. Diagrama geral do sistema de medição pluviométrica.

Os dados desse nó sensor são enviados por meio de uma mensagem de texto SMS (com significado da sigla, *Short Message Service*, em português, serviço de mensagens curtas) para um módulo central, chamado de *gateway*, que está localizado na Universidade Federal da Paraíba, em João Pessoa-PB. A partir dos dados recebidos

pelo *gateway*, as informações são processadas pela plataforma de prototipagem eletrônica e posteriormente inseridas em um banco de dados no servidor online. Dessa forma, estas informações poderão ser acessadas pelos usuários que instalarem o aplicativo "Monitoramento de Chuvas - UFPB" e dependendo dos níveis de chuva, receberão um alerta em seu celular para procurar uma área segura. Além disso, os dados também estão disponíveis para consulta em uma página web com acesso restrito.

Um dos componentes do sistema de medição pluviométrica é o nó sensor, também chamado de módulo de transmissão. Este nó sensor está apresentado em forma de diagrama de blocos na Fig. 4 e é formado pela plataforma de prototipagem eletrônica Arduino, pelo sensor e pelos módulos de comunicação GPS e GSM. A plataforma de prototipagem permite gerenciar as informações coletadas pelo sensor pluviômetro e enviar para uma estação central (módulo de recepção). Este componente do sistema ficará instalado nos locais onde está sendo realizado o monitoramento e as medições são enviadas por meio de mensagens SMS para a estação central, localizada na Universidade Federal da Paraíba, utilizando a rede de comunicação de telefonia celular GSM, para um posterior encaminhamento das informações para um banco de dados. Em paralelo a isto, todos os dados obtidos nas medições são gravados também em um cartão de memória SD para garantir que a aquisição de dados não seja perdida e eles sejam salvos mesmo no caso da rede de telefonia celular ficar indisponível. As informações de localização e de data e hora das medições são obtidas por meio do módulo de comunicação GPS e são enviadas juntamente com a indicação do sensor de intensidade de chuva pela mensagem de texto SMS para estação central.

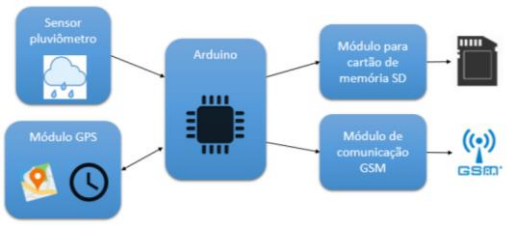

Fig. 4. Diagrama geral do modulo transmissor ou nó sensor.

O módulo de recepção do sistema desenvolvido neste trabalho é um dispositivo *gateway* que pode ser entendido como um *hardware* que funciona como interface entre duas redes que usam protocolos distintos, pois os dados são recebidos por meio do protocolo de comunicação GSM, processados pela plataforma de prototipagem eletrônica NodeMCU-32S e enviados para a nuvem por meio de uma requisição do tipo GET utilizando o protocolo HTTP. Na Fig. 5 se ilustra o diagrama do módulo receptor. Desta maneira, qualquer usuário por meio de uma aplicação web que pode ser acessada através do navegador de um computador pessoal ou por um aplicativo para *smartphones*, poderá ter acesso às informações de chuvas coletadas pelo sistema de medição desenvolvido.

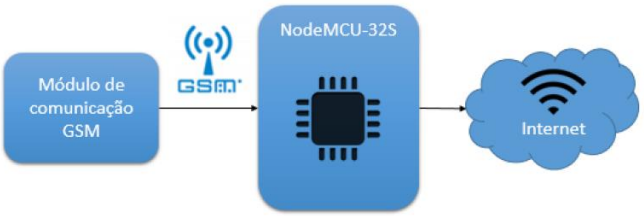

Fig. 5. Diagrama geral do modulo receptor ou *gateway*.

Para medição da intensidade das chuvas foi utilizado um sensor do tipo báscula denominado pluviômetro. Este sensor é fornecido pelo fabricante *Davis Instruments* e possui uma resolução de medição de 0,2 mm de chuva, estando ilustrado na Fig. 6. O funcionamento deste dispositivo é análogo ao de uma gangorra, durante o acontecimento de um período chuvoso a água penetra no furo que está localizado na parte superior de sua estrutura e escorre até a parte interna, onde existe uma estrutura em forma de gangorra com um pequeno reservatório. Quando este reservatório enche, a posição da gangorra é modificada, registrando um volume de chuva de 0,2 mm naquele instante. Normalmente o volume de chuvas em um local é medido utilizando a unidade mm. Exemplificando o uso desta unidade, se em determinado local apresentar um volume de chuvas de 100 mm, significa que ao final da precipitação, um recipiente plano com 1 metro quadrado de base vai conter 100 litros de água por metro quadrado, desconsiderando as gotas que pingaram para fora do recipiente e o efeito da evaporação.

Fig. 6. Pluviômetro do tipo báscula (Fonte: *Davis Instruments*).

Este sensor, além da parte mecânica, é formado por um dispositivo chamado *reed switch*, que funciona como um interruptor elétrico que é acionado por um campo magnético aplicado. Para que a sua correta leitura seja realizada pela plataforma de *hardware* utilizada (Arduino), foi necessário realizar uma montagem na configuração *pull-up*, dessa forma o Arduino receberá um nível lógico alto quando o sensor for ativado e um nível lógico baixo quando o sensor não estiver conduzindo, evitando,

assim, que o pino do entrada do Arduino fique flutuando em algum momento. Essa montagem está exposta na Fig. 7.

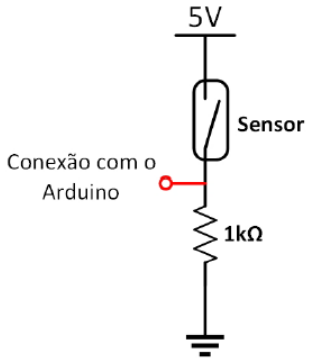

Fig. 7. Condicionamento de sinais do sensor *reed-switch*.

4 Resultados

Esta seção aborda os testes dos componentes do sistema de medição de chuvas de forma individual e ao final, mostram-se os resultados para os testes com o sistema completo em funcionamento, desde o pulso do sensor até a inserção e verificação dos dados no banco de dados utilizando o aplicativo e a página web para consultas. Por fim, serão mostrados os esquemáticos finais para os módulos de recepção e transmissão e o desenvolvimento das placas.

4.1 Verificação do Sensor

Ao ter sua posição modificada e passar pela posição central, o sensor pluviômetro fecha o contato magnético formado pelo *reed-switch* e fornece ao pino digital de entrada do Arduino um nível lógico alto até que o sensor saia desta posição central. Visando obter um valor médio para duração desse pulso de tensão, foram realizadas medições com o auxílio de um instrumento osciloscópio e constatou-se que ao ter sua posição modificada, o sensor fornece uma tensão de saída com amplitude de aproximadamente 5 V e com duração média de 419 mili-segundos, porém, esta duração pode variar de acordo com a intensidade da chuva. O resultado desta medição pode ser observado na Fig. 8. Dessa forma, quando acontece uma borda de subida, o sensor dispara a função de interrupção do Arduino que executa a função de envio de mensagem de texto SMS e realiza as demais funções.

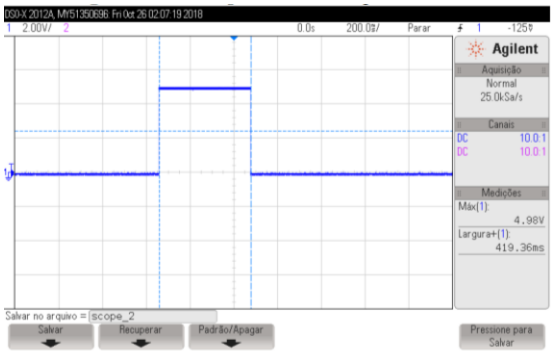

Fig. 8. Verificação do sensor pluviométrico.

4.2 Teste do módulo GPS

O funcionamento do módulo GPS foi verificado para permitir a observação dos seus valores de saída e seus respectivos formatos. Inicialmente, na rotina *setup* do programa gravado no Arduino, foram iniciadas a comunicação serial e do módulo GPS, escrevendo uma mensagem de inicialização, conforme mostram as duas primeiras linhas da Fig. 9.

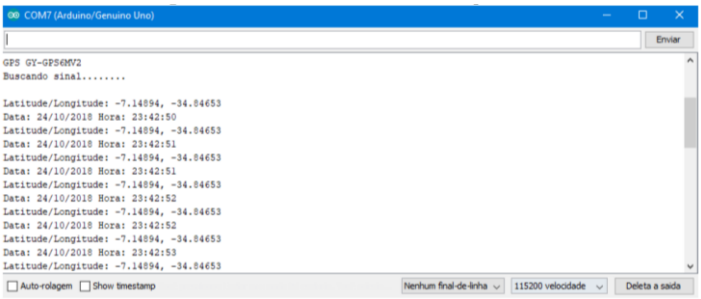

Fig. 9. Teste do módulo de comunicação GPS.

4.3 Comunicação – Envio de Pacotes

Um teste geral do sistema foi realizado simulando o acontecimento de um período chuvoso, para tanto, a posição do sensor pluviométrico foi modificada manualmente e o comportamento do sistema foi observado. Ao modificar a posição do sensor, o código gravado no Arduino ativará a função de leitura do GPS no módulo transmissor por meio de uma interrupção. O Arduino permite utilizar alguns pinos para tal finalidade por meio de interrupções que podem ser ativadas por bordas de subida, bordas de descida, mudança de estado e quando for detectado um nível lógico baixo. Posteriormente, os dados são gravados no cartão de memória para ao final enviar as informações para o módulo de recepção por meio de uma mensagem de texto SMS. O forma-

to padrão definido para envio das mensagens de texto está exemplificado conforme mostra abaixo:

```
UFPB&local&dia&mes&ano&hora&minuto&segundo&medicao&probex
```

Para separação das informações, utilizou-se o caractere "&". O primeiro e o último valor desta mensagem de texto são as duas senhas definidas previamente para que a mensagem seja válida no receptor, "UFPB" e "probex". Caso o usuário não informe estas senhas corretamente, o módulo receptor irá apagar todas as mensagens contidas no chip celular e ignorar a mensagem. Ao detectar que o sensor modificou de posição, o Arduino salvará nas variáveis as informações de interesse e fará a gravação destas informações no cartão de memória SD. A Fig. 10 mostra os dados gravados em um arquivo nomeado "leituras.txt" que está no diretório raíz do cartão de memória.

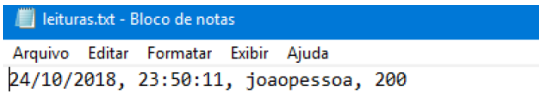

Fig. 10. Teste de gravação no cartão de memória SD.

A Fig. 11 mostra um acesso a página web para consulta dos dados no servidor. Este acesso é restrito por senha e é liberado apenas para os membros do projeto de extensão "Contribuição à infraestrutura de monitoramento de áreas de risco no município de João Pessoa-PB". Neste endereço, que foi implementado com o *framework* Django na linguagem de programação Python, é possível realizar a verificação dos dados do banco de dados, bem como realizar ações de alteração, exclusão e inserção. A imagem do lado esquerdo ilustra a tela onde são listados os registros do banco de dados, nessa tela o usuário pode clicar no nome do registro para obter mais detalhes ou selecionar vários registros para realizar uma ação em conjunto, como uma exclusão, por exemplo.

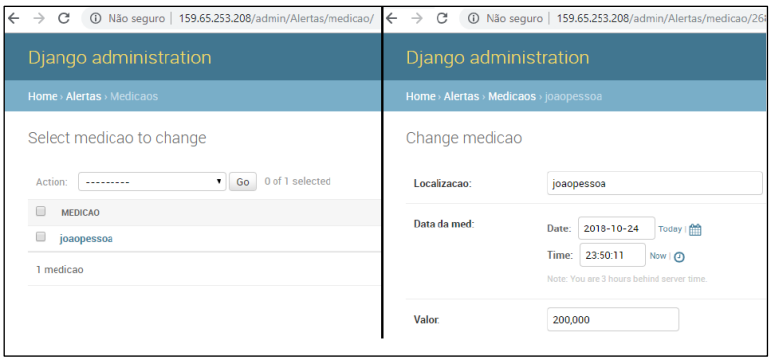

Fig. 11. Teste do banco de dados.

Como o acesso a esta página é restrito, os moradores das comunidades terão acesso apenas ao aplicativo para celular, que está ilustrado na Fig. 12. Inicialmente este aplicativo contém apenas duas funcionalidades a fim de verificar a recepção e transmissão dos dados, a primeira refere-se à exibição dos dados das medições, possibilitando acompanhar em tempo real as últimas medições inseridas pelo módulo transmissor e caso alguma delas apresente um alto risco para a localidade, o aplicativo gerará uma notificação *push* no celular do usuário, sendo esta a segunda funcionalidade. A medição que está sendo mostrada na Fig. 12 refere-se a mensagem enviada pelo módulo de transmissão ilustrado na início desta subseção.

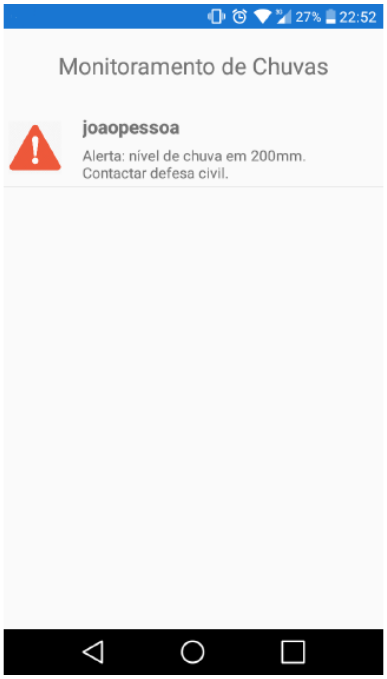

Fig. 12. Teste do aplicativo para Android.

4.4 Circuitos eletrônicos

Nas Fig. 12 e 13 são apresentados os protótipos dos circuitos eletrônicos para os módulo de recepção e transmissão, desenvolvidos neste projeto. Atualmente este desenvolvimento se encontra em fase de aprimoramento e teste na Universidade Federal da Paraíba em conjunto com comunidades do município de João Pessoa, Paraíba, Brasil.

Fig. 13. Protótipo do circuito de recepção.

Fig. 14. Protótipo do circuito de transmissão.

5 Conclusões

Os desastres naturais impactam de forma muito negativa o cotidiano de pessoas e comunidades ao redor do mundo. Até mesmo as grandes nações estão susceptíveis aos impactos causados por estes fenômenos, dessa forma, as ferramentas de monitoramento mostram-se como uma alternativa para minimização dos impactos que podem gerar perdas humanas e financeiras e estão cada vez mais presentes nas discussões e medidas ao redor do planeta. O estado da Paraíba, apesar de estar localizado em uma região onde possui histórico de seca e estiagem, possui registros de inundações, desabamentos e enchentes. Tendo em vista que existem muitas áreas vulneráveis no município de João Pessoa-PB, este trabalho propôs um sistema de monitoramento de chuvas de baixo custo que deverá ser instalado em uma comunidade de área de risco.

O sistema proposto funciona em conjunto com um aplicativo com um servidor online onde ficam armazenados todos os dados da aquisição. Este sistema foi testado em laboratório na Universidade Federal da Paraíba e foi observado que funciona de acordo com as funcionalidades requeridas para o sistema de monitoramento de chuvas, os módulos de transmissão e recepção estão se comunicando através do envio de mensagens de texto SMS e os dados estão se integrando com o servidor online. Foi observado que esses dados estão disponíveis para consulta na página web de administração do banco de dados e também através do aplicativo, o qual está gerando alertas por meio

de notificações *push* de acordo com o volume de chuvas medido para determinada localidade.

Referências

1. Tominaga, L.; Santoro J.; Amaral R.: Desastres naturais: conhecer para prevenir. São Paulo. Instituto Geológico, 2009. 196 p.
2. Atlas brasileiro de desastres naturais: 191 a 2012. Florianópolis: CEPED UFSC, 2013.
3. Relatório de danos materiais e prejuízos decorrentes de desastres naturais no Brasil. CEPED UFSC 2016.
4. Sulaiman, S. N.; Aledo A.: Desastres naturais: convivência com o risco. São Paulo, 2016
5. Andrade F.: Precipitação: definição, métodos de medição e grandezas características. 2014
6. Governo do Brasil. Aplicativo alerta para tempestades em tempo real. 2017
7. Kama, A.; Diallo, M.: Low cost connected and autonomous rain gauge for real time rainfall monitoring in Dakar. IEEE 25th International Conf. on Telecommunications ICT, 2018
8. Mangundu E.M.; Mateus J.N.; Zodi L.; Johson J.: A wireless sensor network for rainfall monitoring, using cellular network: A case for Namibia. IEEE Global Wireless Summit GWS, 2017.
9. Coelho N.: Cidades inteligentes – Infraestrutura tecnológica: caracterização, desafios e tendências. Faculdade de Engenharia Universidade do Porto. 2015.

Sustainable mobility in the public transportation of Montevideo, Uruguay

Silvina Hipogrosso[0000−0003−2124−7267] and
Sergio Nesmachnow[0000−0002−8146−4012]

Universidad de la República, Montevideo, Uruguay,
{silvina.hipogrosso,sergion}@fing.edu.uy

Abstract. Sustainable mobility is a very relevant approach within the novel paradigm of smart cities. This article presents an analysis of sustainable mobility initiatives recently developed in the public transportation of Montevideo, Uruguay. The case study is analyzed considering the main concepts from related works and well-known quantitative and qualitative indicators. Three initiatives are studied: electric bus, public bicycles, and electric scooters. They constitutes novel and promising ways for public transportation in the city. The reported results for each mean of transportation suggest that the first initiatives focus on specific sectors of the population and should be improved in order to extend their accessibility and affordability. Specific recommendations are formulated to develop and improve sustainable mobility in Montevideo.

Keywords: sustainable mobility; public transportation; smart cities

1 Introduction

In modern cities, the participation of citizens in social, economic, and cultural activities requires people to travel, sometimes over long distances and involving long periods of time [8]. The ability of individuals to overcome the limitations imposed by distances and other mobility-related difficulties is critical to guarantee an active participation in city life [4].

Sustainable mobility is a subject that studies the development and use of means of transportation that are sustainable regarding several matters, mostly economic, environmental, and social [11]. Assessing sustainability and studying alternative means of transportation is very important considering that transportation largely contributes to environmental pollution with direct negative implications in health and quality of life of citizens. This is a relevant subject of study under the novel paradigm of smart cities [3].

Public transportation provides the most sustainable mean for mobility [21]. This is the case in Montevideo, Uruguay, where just a few initiatives to promote sustainable private mobility (e.g., electric vans for last mile distribution of people and goods [22]) have been developed recently.

In this line of work, this article presents a study of sustainable mobility initiatives recently developed in Montevideo, Uruguay. Three initiatives are studied: electric bus, public bicycles, and electric scooters, which are novel and promising ways for public transportation in the city. The main motivation of the study is to analyze and characterize the current reality regarding sustainable public transportation in Montevideo, in order to reduce problems in the city and redirect mobility towards a better sustainability. Specific suggestions and recommendations are provided to develop and improve sustainable mobility in Montevideo.

The main contributions of this article are: i) a review of the related literature about sustainable mobility and those proposals that can be developed in Montevideo; ii) the analysis of current initiatives of sustainable mobility in the public transportation system of Montevideo regarding several quantitative and qualitative indicators; and iii) the proposal of suggestions and recommendations to develop and improve sustainable mobility in Montevideo.

The article is structured as follows. Section 2 presents the main concepts related to sustainable mobility. A review of the main related work is presented in Section 3. The analysis of current initiatives in Montevideo is reported in Section 4. The suggestions and recommendations for developing and improving sustainable mobility in Montevideo are described in Section 5. Finally, Section 6 presents the conclusions and the main lines of future work.

2 Sustainable mobility

Sustainability has been a major concern of society since the last decades of the XX century. In 1987, the Brundtland Report for the World Commission on Environment and Development introduced the term *sustainable development*, to define "*the development that meets the needs of the present without compromising the ability of future generations to meet their own needs*" [26]. This concept has become a paramount rule for modern sustainable mobility, a concept related to guarantee the movement of people with minimal environmental impact.

Several concepts are integrated in the sustainable mobility paradigm [2]. A new approach is proposed for designing and planning transportation systems, based on social processes, accessibility, reduction of motorized transportation, integration of people and traffic, and other factors oriented to consider mobility as a valued activity and regarding environmental and social concerns [17]. The World Business Council for Sustainable Development defined sustainable mobility as the ability of a society to fulfill requirements related to the movement of people without sacrificing fundamental human or ecological values [27].

Many researches on sustainable mobility focused on the impacts on environment, but recently, other aspects have also been analyzed, such as the relation with equity and the impact on economy, safety, health, and quality of life in general. In his regard, technology has been identified as one of the main tools that helps ensuring energy efficiency, using alternative and renewable energy sources, reducing contamination (e.g., pollutants emissions, noise, etc.), and provide environmental friendliness.

Furthermore, measures oriented to sustainable mobility put special emphasis on raising awareness and involving citizens, in order to foster a behavioural change. The ultimate goal is that citizens realize that means of transportation proposed by the sustainable mobility paradigm helps society, thus citizens choose to use more sustainable options by their own.

Specific indicators have been proposed and developed to study sustainable mobility in urban scenarios [7]. Furthermore, they have been applied to analyze different means of transportation in many cities around the world. Some of the main related works on the topic are reviewed on next section.

3 Related work

Several means of transportation coexist and share the urban space in modern cities. These means are supposed to be well integrated and connected, in order to provide citizens with efficient and effective mobility [28]. However, administrators often apply traditional urban planning processes that only focus on few parts of the transportation system, instead of providing holistic plans accounting for all means operating in the city and including a comprehensive decision-making to consider indirect and interrelated impacts of the implemented solutions.

The approach that does not consider the city and transportation systems as a whole, leads to isolated actions that usually result in poor and inefficient policies, which fails to solve the main problems related to mobility. Litman and Burwell [13] acknowledged the aforementioned issues and recognized that in order to achieve sustainability, transportation must be conceived from a broad point of view to consider energy efficiency, health, economic and social welfare, and other relevant aspects related to sustainable development. A paradigm shift was proposed for rethinking transportation, in order to consider different integrated solutions to achieve sustainable transportation systems.

Sustainable urban mobility planning begins with designing a strategic plan for the community. Banister [2] put special emphasis on the participation of stakeholders in the planning process in order to involve them in the reasoning and implementation of specific initiatives for sustainable mobility. Several articles [7,12,25] studied indicators and methodological analysis as tools to evaluate the situation of sustainable mobility in cities, understand the evolution towards sustainable transportation systems, and evaluate the impact of selected solutions. Indicators simplify complex phenomena and they often just provide hints of a specific issue or situation [16]. However, the combination of multiple indicators allows capturing different dimensions and aspects of sustainable mobility.

The main concepts about indicators and performance measurement for sustainable transportation were presented in the book by Gudmundsson at el. [7], focusing on the role and importance of quantitative and qualitative indicators for stakeholders (including decision-makers, planners, and operators). A review of frameworks for assessing sustainability metrics and a proposal towards a framework for sustainability transportation were also presented. Two case studies were presented: European transportation and high speed rail in England.

Miiler et al. [21] studied the role of public transportation regarding sustainability and reviewed articles that analyzed case studies of sustainable transportation. A set of recommendations were provided for developing and planning sustainable public transportation systems.

Rodrigues et al. [25] developed an index of sustainable urban mobility including several important features identified by Litman [14] for comprehensive and sustainable transport planning. The index is based on data obtained from planners and includes weights for different criteria, defined by experts. An application on the city of São Carlos, Brazil, demonstrated that the proposed index was relatively easy-to-compute and flexible enough to be applied to characterize sustainable mobility. The approach was extended by performing a multiple criteria decision analysis to determine variables that capture the main features of the reality in Brazilian cities concerning sustainable mobility. The analysis was performed over eleven cities in different states of Brazil. Several dimensions of sustainability were studied and results allowed identifying key elements to be used for proposing public policies for improving sustainable mobility.

Johnston [12] developed a comprehensive method for modeling the impacts of transportation, to be included in an integrated urban model of California. Several major transportation scenarios were studied, evaluating greenhouse gas emissions, economic welfare and equity, air pollution, Results of the analysis were reported as relevant to state and regional transportation plans

The successful case of Bogotá, Colombia was studied by Lyons [15], focusing on the actions taken to address environmental protection and both, economic and social sustainability via a non automobile-centric approach. The integration between transportation planning and social planning was highlighted, especially for the case of new houses and open spaces that complemented transportation, restriction to vehicles during rush hours, and the TransMilenio BRT system. Several outcomes related to sustainability were reported and analyzed. The author concluded that the case study can be replicated in other developing countries in the path towards sustainable transportation.

In Uruguay, project URU/17/G32 “Towards a sustainable and efficient urban mobility system in Uruguay” was launched in 2017, as a joint effort of government and transportation companies. The main goals of the project are defining regulations for low carbon transportation systems, evaluating clean technologies (e.g., electric cars) in Montevideo, and promoting a cultural change towards sustainable transportation modes (e.g, bicycles). Other recent initiatives for studying and developing sustainable transportation in Montevideo are project MOVES [22], which aims at promoting an effective transition towards inclusive, efficient, and low-carbon urban mobility in Uruguay, and project ’Public transportation planning in smart cities’ [24], funded by Fondo Conjunto de Cooperación Uruguay–México (2018–2019).

The research reported in our article constitutes a novel proposal for Uruguay and is oriented to the evaluation of current sustainable mobility initiatives in Montevideo, both included and not in the aforementioned project URU/17/G32.

4 Analysis of sustainable mobility initiatives in Montevideo

This section describes and analyzes sustainable mobility initiatives that are operating in Montevideo through public or private transportation companies.

4.1 Sustainable mobility initiatives

Three sustainable mobility initiatives have been developed recently in Montevideo: electric bus, public bicycles, and electric scooters. The main details of each initiative are presented next.

Electric bus (pilot plan). The main bus transportation company operating in Montevideo (CUTCSA, accounting for about two thirds of the market share and also of the buses operating in the city) has conducted tests of mobility using electric buses, with incentives and support from the Ministry of Energy and the City Hall of Montevideo. Since 2017, a pilot plan is in course, using one electric bus that operates rotatively in different lines to test the performance of this new mean of transportation. The company is working in a financing proposal to be evaluated for the Green Climate Fund in order to buy 100 electric buses and integrate them to the transportation system.

Public bicycles. In 2015, the City Hall of Montevideo introduced a public bicycle system, called *Movete*, as part of the urban transportation system to promote green mobility and a healthy way to know the city, move to workplaces, or simply extend the accessibility of public transportation systems to final destinations. The service consists of a fleet of 80 bicycles spread in a network of eight automated stations, distributed from the Old City to the Center neighborhoods. Bicycles can be rented at one station and returned in another station in the coverage area . A card of the integrated Metropolitan Transportation System (STM) is required to rent a bicycle in Movete and people that do not own a STM card, e.g. tourists, can obtain it with no charge in the center office of Movete. Users cannot use the bicycle service for more than four hours per day. Public bicycle service is planning to expand the coverage area of operation in 2020, to include 60 stations and 600 bicycles in order to increase accessibility and promote active mobility.

Electric scooters. The electric scooter is a new mode of urban transportation that has gained popularity all over the world as an alternative to driving. Electric scooters provides an environmentally friendly alternative for short journeys that are either too far to walk, or too close to drive a car, to be a cost-effective option. Three companies of electric scooter (Grin, Lime, and Movo) have been operating in Montevideo since 2018. The service provides a practical and easy way to use electric scooters: by simply downloading a mobile application and setting up a payment method, users have access to a network of scooters that they can use at any time. Electric scooters have GPS blue tracking, so users are never too far from picking up a electric scooter and they can leave it anywhere within the area where the service operates.

4.2 Indicators to assess sustainable mobility

The analysis considers sustainable mobility indicators proposed by the World Business Council for Sustainable Development [27]. Indicators were separated in two groups; *quantitative indicators*, for which the available data in Montevideo allows computing a numerical value for the specific criteria, and *qualitative indicators*, for which only a qualitative analysis can be performed, since some of the relevant pieces of information are not available for the studied initiatives.

Quantitative indicators. The quantitative indicator group includes: coverage, access to mobility service, affordability, and commuting travel time. The corresponding definitions are presented next.

Coverage. The coverage (cov) is defined as the ratio of the area covered by each sustainable mobility service (ci) and the total urbanized area of the city (ta), according to Eq. 1. The total urbanized area of Montevideo is considered to extend for 200 km^2. The scale for this indicator is straightforward, 0 correspond to 0% of coverage and 10 correspond to 100% of coverage.

$$cov = \frac{ci}{ta} \tag{1}$$

Access to mobility service. Acces to mobility service (am) is defined as the share of population with appropriate access to each service, according to Eq. 2, where nh is the number of citizens living in the city, and $PR(i)$ is the percentage of people living within 400 meters from a public transportation stop or from a possible renting point of a shared mobility system.

$$am = \frac{\sum_i PR(i)}{nh} = 1 - \frac{\overline{PR}}{nh} \tag{2}$$

The methodology for calculation implies determining the percentage of people living within the service areas by using spatial data analysis. Service area are limited by a distance of 400 meters of a sustainable mobility service, which is considered as the maximum distance that a person considers to walk to use a public transportation service [1]. The scale for the am indicator is: 0 represents 0% of the population in the city and 10 represents 100% of the population.

Affordability of sustainable mobility transportation. Affordability (af) is defined as the expenses on transportation made by persons as a percentage of their income. The calculation is based on the methodology by Carruthers et al. [5], considering the cost of performing 45 and 60 trips on each transportation mode and on existing socio-economic data. The indicator is computed for two different relevant social groups, considering the minimum income and the middle income per capita, according to values reported for 2019 by National Institute of Statistics, Uruguay (INE) [10]. The calculation method is described by Eq.3, where nt is the number of trips, p is the cost of a single trip, and is is the income per capita. The scale for the af indicator is: 0 indicates affordability index is over 35% and 10 indicates that is less than 3.5%

$$af = \frac{nt \times p}{is} \tag{3}$$

Commuting travel time. This indicator is defined as the average time spent by a person when travelling from origin to destination of a trip performed in the public transportation system. The methodology applied for calculation considers that: i) (for bus) the average commuting travel time includes the time for a person to walk to the bus stop and the time waiting for the bus to arrive; persons are supposed to walk from the centroid of the zone and the average walking speed is assumed to be 5 km/h; ii) (for bicycles) the average speed is 13.5 km/h and the average walking time to a bicycle station is 4 minutes (walking up to 400 meters); and iii) (for scooters) the average speed is 10 km/h and the walking time a person takes to find a scooter is less than 3 minutes.

Commuting travel times are computed for two relevant distances: i) a *short travel* of 3 km, a reasonable distance for travels to nearby locations such as offices, shopping, education, etc. It is also the average travel distance for electric scooters, considering an average speed of 12 km/h; and ii) a *medium distance* of 10 km, a reasonable average distance for travels to work, according to data from the urban mobility survey for Montevideo [20]. It is also the average travel distance on public transportation, considering an average bus speed of 13 km/h [23].

Two scales are considered for this indicator, for 3 and 10 km. Both considers as lower limit the time to travel the corresponding distance at the average human walking speed of 5 km/h, and as upper limit the time to travel the corresponding distance at the limit speed of bicycles and electric scooters (25 km/h). Thus, for the 3 km distance, 0 represent a trip duration of over 36 minutes and 10 represents a trip duration of 7 minutes; and for the 10 km distance, 0 represent a trip duration of over 2 hours and 10 represents a trip duration of 24 minutes.

Qualitative indicators. The qualitative indicator group includes: net public finance, energy efficiency, intermodal connectivity, intermodal integration, and confort and pleasure. The corresponding definitions are presented next.

Net public finance: Percentage of the cost of each mobility service that the government grants as subsidy to transportation companies.

Energy efficiency: Energy consumption in public transportation, usually evaluated in oil equivalent. The efficiency indicator considers the total energy demand from clean (i.e., renewable) and non-renewable sources.

Intermodal connectivity: Number of locations where users can change from one mode of transportation to another.

Intermodal integration: Quality of the intermodal facilities between the different transport modes.

Comfort and pleasure: Satisfaction perceived by citizens about comfort and pleasure of moving in the city using different transportation modes. Comfort and pleasure indicator is analyzed through access to information, quality of the service, and security.

4.3 Analysis and results

This subsection reports the results of the study to characterize the sustainable mobility initiatives. The study applies a urban data analysis approach [18], accounting for relevant data from each initiative, obtained from public sources.

Quantitative indicators

Coverage. The electric bus operated in several lines during 2017–2018. Table 1 summarizes the number of days of operation on the most relevant lines.

line	*days*	*percentage*
128	78	14.0%
142	16	2.9%
169	47	8.4%
180	303	54.4%
181/183 (circular)	45	8.1%
187	20	3.6%
other lines	less than 6 days	less than 1%

Table 1: Lines operated by the electric bus service in Montevideo (2017–2018)

According to the results in Table 1, the area considered to calculate the coverage of the electric bus service is the one corresponding to the buffer area defined by parallel segments located at 400m of the most used lines routes: 128, 169, 180, and 181/183. For public bicycle, the coverage of the actual service and the projected coverage of the service are reported. The overall area for electric scooters is the one defined by the Grin service, which covers the area of service of the other two companies (Lime and Movo).

The area covered by each studied sustainable mobility initiative in Montevideo and the value of the *cov* indicator is reported in Table 2. Results were computed based on open data from each service.

initiative	area	coverage	*cov* indicator
electric bus	51.4 km^2	25.7%	2.57
public bicycle	3.5 km^2	1.75%	0.175
public bicycle (projected)	13 km^2	6.5%	0.65
electric scooter (Grin)	23.5 km^2	11.75%	1.175
electric scooter (Lime)	15 km^2	7.5%	0.75
electric scooter (Movo)	7 km^2	3.5%	0.35
electric scooter (overall)	23.5 km^2	11.75%	1.175

Table 2: Coverage and the *cov* indicator for sustainable mobility initiatives

The coverage maps for electric bus, public bicycles, and electric scooters services are presented in Fig. 1. The analysis of the coverage indicator demonstrate that the area of service of each sustainable mobility initiatives is represents a small fraction of the total area of the city. The best coverage is for the electric bus service, which covers 25.7% of the city.

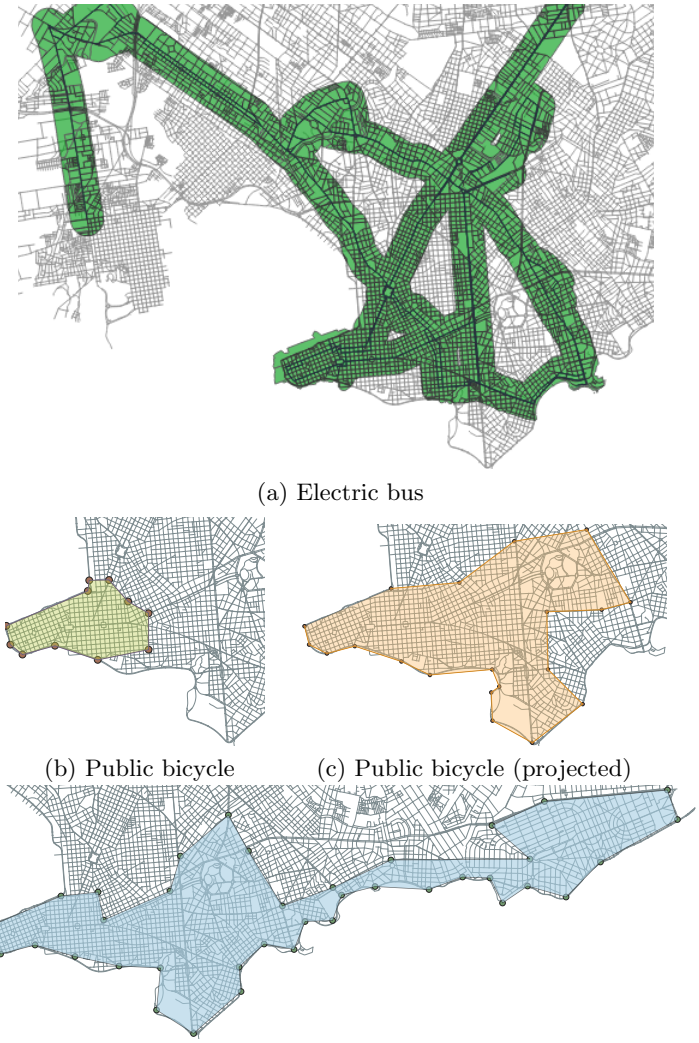

(a) Electric bus

(b) Public bicycle

(c) Public bicycle (projected)

(d) Electric scooters

Fig. 1: Coverage of sustainable mobility initiatives in Montevideo

Coverage results are somehow expected, as the studied initiatives are new and public bicycles were introduced mainly for tourist. For electric scooters, coverage is also limited to zones with highest income (coast area).

Overall, the three studied modes provides a service that covers an area of 67.6 km^2, which represents a 33.8 % of the urbanized area of Montevideo, for a coverage index of 3.8. In conclusion, two thirds of the the citizens who live in the urbanized area are not covered by these sustainable modes of transportation.

Access to mobility service. The population served by each service was computed by intersecting coverage areas with the population map and counting the total population in each zone. The urban population of Montevideo is 1 305 082.

The electric bus service covers 429 269 citizens (32.9% of the population), accounting for the largest access index ($am = 3.29$). Public bicycles cover 86 917 citizens ($am = 0.67$) and the planned expansion is set to cover 193 368 citizens ($am = 1.48$). The electric scooters companies provides service to 285 445 citizens ($am = 2.19$). Overall, sustainable transportation modes cover 554 172 citizens (42.5% of the population, $am = 4.25$). As a consequence, most of the urban population have no access to these sustainable modes of transportation.

Affordability of sustainable mobility. The affordability index was computed for the three studied transportation modes considering *short trips* with a length of 15 minutes (the most frequent travel duration for scooters) and long trips length of 45 minutes (the average time travelled in bus [20]).

Income per capita in Montevideo is USD 691 (middle) and USD 423 (minimum) (as of August, 2019, 1 USD = 37 Uruguayan pesos). The cost of a standard ticket (allowing one transfer trip in one hour) in electric bus is 0.85 USD. Electric scooters and public bicycles apply a time-based fare. The cost of using the public bicycles is 0 (free service) up to 30 minutes and after that, the rental cost is 0.74 USD for 30 minutes. The cost of a 15-minutes rent (average time of utilization) for the electric scooter is 2.1 USD and for one hour is 5.4 USD.

Table 3 reports the affordability index of each sustainable transportation mode for middle and minimum income people.

Results indicate that for 15 minutes, public bicycle has the maximum *af* value (10) for both income groups, since it is a free service. Affordability do not reduce significantly when considering 45 minutes trips. Buses are cheaper than scooters for both short and long periods of time. Furthermore, the *af* indicator for buses is the same, while electric scooters downgrade to $af = 0.0$ for one hour trips. Overall, public bicycle is the most affordable mode of transportation.

trip length: 15 minutes						
income	*45 trips*			*60 trips*		
	bus	*bicycle*	*scooter*	*bus*	*bicycle*	*scooter*
minimum	9.1% (8.2)	0 (10.0)	22.7% (3.9)	12.0% (7.3)	0 (10.0)	30.2% (1.5)
middle	5.5% (9.5)	0 (10.0)	13.9% (6.7)	7.3% (8.8)	0 (10.0)	18.5% (5.2)
trip length: 45 minutes						
income	*45 trips*			*60 trips*		
	bus	bicycle	scooter	bus	bicycle	scooter
minimum	9.1% (8.2)	4% (9.8)	57.2% (0.0)	12.0% (7.3)	5.4% (9.4)	76.2% (0.0)
middle	5.5% (9.5)	2.5% (10.0)	35.0% (0.0)	7.3% (8.8)	3.3% (10.0)	46.7% (0.0)

Table 3: *af* indicator for minimum and middle income in Montevideo

Commuting travel time. Table 4 reports the commuting travel times for distances of 3 km, 10 km, and from end-to-end (*EtoE*) of the coverage areas for each mobility service. Speed and average times for bus were computed according to the methodology by Massobrio and Nesmachnow [19], using the Open Street Map service, estimations of average speed, and public applications.

bus			*bicycle*			*scooter*		
3 km	*10 km*	*EtoE (17.3 km)*	*3 km*	*10 km*	*EtoE (3.5 km)*	*3 km*	*10 km*	*EtoE (17.5 km)*
17.8	49.3	116.0	13.3	44.4	15.6	20.0	60.0	102.0

Table 4: Commuting travel times (minutes)

Results show that bicycle is the fastest option for both short and long distance, followed by the bus, and in third place the electric scooter. Differences between bicycle and bus reduce for 10 km. EtoE bus trips takes longer than traveling on scooter, so in between 10 and 17.5 km travels on scooter become faster than on bus. Overall travel times suggest that sustainable mobility modes do not allow traveling faster on the city.

4.4 Qualitative indicators

Net public finance. Electric buses are benefited from three subsidies: a municipal contribution for students and retirees, fuel subsidy (from the Ministry of Transportation) and contributions to keep the price stable (from the Ministry of Economy and Finance). Furthermore, electric buses are granted a total of 100.000 USD to promote the substitution of 4% of diesel bus to electric.

The public bicycles service is completely financed by the city Hall of Montevideo to promote active and sustainable mobility. Electrics scooters do not received any subsidy as they are run by private companies.

Energy efficiency. All the studied transportation modes use clean renewable energy. Public bicycle is the most efficient of the initiatives, since it does not requires energy of external sources. Electric buses provides a significant improvement over the current diesel vehicles regarding energy efficiency. They produce no CO_2 emissions and have an iron phosphate battery that consumes 100KWh each 100 km, which is a good rate for public transportation. Regarding electric scooters, the energy of operation represents a very low percentage of the total emissions generated (e.g., 4.7% according to the study by Hollingsworth for the city of Raleigh, North Carolina [9]). However, several other concerns arise, such as the non-clean energy required for collecting and distributing scooters, and the short life cycle of batteries, which can have negative environmental impacts.

Intermodal connectivity. The studied sustainable mobility initiatives operate in a common area of 2.8 km^2 (with the projected expansion for bicycles, 7.3 km^2). Within this common area, public bicycles offer full connectivity with buses and scooters, since stations are located less than 100 meters of bus stops and scooters are available nearby. Electric scooters facilitates door-to-door mobility, allowing users to leave scooters anywhere within the operation area, thus providing a valid alternative for intermodal connectivity. Buses also allows intermodal connectivity, limited to the availability of bicycles or scooters near the bus stops.

Intermodal integration. Even though the three transportation modes studied provides intermodal connectivity, the system lacks of intermodal integration. Each service focuses on their own operation, without facilitating integration with others: no information or route guidance is provided to users, terminal bus stations do not provide parking lots for public bicycles or scooters, etc. The only integration is regarding the payment method for buses and public bicycles, which can be paid using the same public transportation card (STM). All these facts are specific drawbacks for intermodal mobility. Overall, integration should be improved to provide efficient mobility.

Comfort and pleasure. Available information of public buses is recognized as one of the best features offered to citizens, according to the recent mobility survey for Montevideo [20]. On the other hand, trip comfort (43,9%) and bus stop comfort (46.4%) were the worst rated attributes of the bus system.

Users have presented multiple claims about the poor service of Movete and bad conditions of the bicycles [6]. Furthermore, the city lacks of a proper infrastructure (e.g., exclusive lanes) for connecting stations of the system.

Finally, users perceive many benefits of electric scooters: they are easy to locate, ride effortlessly, dock-less, and can be parked anywhere. On the other hand, electric scooters are vulnerable to road risks, as they are driven on the same lane as automobiles, and are an uncomfortable mean of transportation with bad weather conditions.

5 Suggestions and recommendations for sustainable mobility in Montevideo

This section provides some recommendations and suggestions that can be implemented in the city of Montevideo to promote sustainable mobility. Recommendations and suggestions are based on the review, analysis, and main results of the study of the three initiatives for public sustainable mobility.

One of the main facts from the analysis is that the initiatives for sustainable mobility are not widespread through the city, but provide a limited coverage and poor access to citizens. In this regard, one of the main recommendation is related to expand the coverage area, by introducing more bicycle stations, operating new lines of the electric bus, covering different routes or extending the routes offered, and expand the areas available to operate electric scooters. To improve coverage, more vehicles must be introduced and an articulated network of exclusive lanes, which will help to improve other indicators too.

Specific suggestions to increase accessibility are extending the bus and ciclying network and the electric scooters operation area by previously evaluating the real demand for each transportation mode via direct and indirect methods, e.g. mobility data analysis approach.

Other suggestion to increase accesibilty is to do a viability study in order to offer these mobility services to areas of lower social incomes.

Concerning affordability, the study demonstrated that electric bus is expensive and electric scooters are prohibitive for low-income citizens. In this regard, a specific suggestion for mobility services is to provide ticket packages for frequently users, offering a lower price and combination with other services, to facilitate intermodality. The public finance can be reviewed to contribute to affordability, mainly by redirecting the assistance to reduce operation and maintenance costs, to guarantee a lower ticket price.

Several suggestions are related to improve travel time, in order to provide more useful and efficient sustainable transportation systems. In this regard, both city administration and transportation companies must focus on providing accurate information to citizens and guaranteeing a quick access to relevant information for travel planning. Electric bus should provide a high frequency service, by redesigning or updating existing timetables, and a better effort must be done in order to provide good synchronization between different bus lines. For public bicycles and electric scooters, travel times are related to availability of vehicles and also on the available interconnection network, so specific improvements on the fleets size and on infrastructure can contribute in this regard.

To take advantage of the modal shift from diesel to electric buses to improve energy efficiency, smart planning of battery charge is needed, by properly locating charge stations in strategic points of the operation area or planning the use of external batteries. Electric scooters also need to review their operation efforts for collecting and distributing vehicles, which demands non-clean energy. A specific suggestion to improve efficiency is installing secure parking stations to charge scooters batteries while parked.

A certain recommendation to enhance sustainable mobility is to promote intermodal connectivity between transportation modes.

In this regard, services should work on providing real time data information (e.g., vehicles available, location, bus stops information, timetabling, etc.) and on installing shared stations for at least two services. A specific suggestion is to integrate the ticketing system, allowing users to share modes within a ride, maybe linked with the aforementioned offers to improve affordability.

In terms of comfort and pleasure, companies can offer a better quality service by improving the comfort of the vehicle, and particularly adopting security measures to guarantee safe travels. Bicycles and electric scooters can incorporate helmet to their service and buses can include seat belts for passengers. Related to the overall quality of experience, companies and city administration can improve access to information providing users with mobile applications, oriented to reduce walking time, waiting time, and the overall travel times.

6 Conclusions and future work

This article studied three recent sustainable mobility initiatives implemented in Montevideo, Uruguay. The study reviewed the main concepts of sustainable mobility from related work and analyzed the three modes of transportation (elec-

tric bus, public bicycles, and electric scooters) through quantity and qualitive indicators of sustainable mobility.

The results of the study indicate that the area of service of each sustainable mobility initiatives represents a small fraction of the total area of the city. Consequently, a significant part of the urban population have no access to these sustainable modes of transportation.

Public bicycle is not only the most affordable mode of transportation, but also the fastest and ecological option to travel for short and long distance. Electric bus is the second best option. These two services have public finance, so the can keep a reasonable price or even reduce it. Electric scooters have prohibitive prices for low income citizens. On the other hand, the service quality of public bicycle is the worst of the three modes in terms of comfort and pleasure. Finally, although the three modes provides intermodal connectivity between them, there is a lack of intermodal integration between services.

Taking into account the result of the analysis, specific suggestions are provided in order to improve sustainable mobility in Montevideo.

The main lines for future work are related to extend the analysis by considering other sustainable mobility indicators and study best practices implemented on other cities in order to contribute to the improvement of urban sustainable mobility in Montevideo.

References

1. Atash, F.: Redesigning suburbia for walking and transit: Emerging concepts. Journal of Urban Planning and Development 120(1), 48–57 (1994)
2. Banister, D.: The sustainable mobility paradigm. Transport Policy 15(2), 73–80 (2008)
3. Barrionuevo, J., Berrone, P., Ricart, J.: Smart cities, sustainable progress. IESE Insight 14(14), 50–57 (2012)
4. Cardozo, O., Rey, C.: La vulnerabilidad en la movilidad urbana: aportes teóricos y metodológicos. In: Foschiatti, A.M.H. (ed.) Aportes conceptuales y empíricos de la vulnerabilidad global, pp. 398–423. Editorial Universitaria de la Universidad Nacional del Nordeste (2007)
5. Carruthers, R.: Affordability of public transport. International Conference Series on Competition and Ownership in Land Passanger Transport pp. 1–15 (2005)
6. El País: IMM licita 60 estaciones para 600 bicicletas en Montevideo (June 24, 2019), `https://www.elpais.com.uy/informacion/sociedad/licitan-bases-bicicletas-montevideo.html`, (August 2019)
7. Gudmundsson, H., Hall, R., Marsden, G., Zietsman, J.: Sustainable Transportation. Springer Berlin Heidelberg (2016)
8. Harvey, D.: Social justice, postmodernism and the city. International Journal of Urban and Regional Research 16(4), 588–601 (1992)
9. Hollingsworth, J., Copeland, B., Johnson, J.X.: Are scooters polluters? the environmental impact of shareddockless electric scooters. Environmental Research Letters 14(8), 1–10 (2019)
10. Instituto Nacional de Estadística, Uruguay: Ingresos de los hogares y de las personas. `https://www.ine.gub.uy/gastos-e-ingresos-de-las-personas-y-los-hogares`, (August 2019)

11. Jeon, C., Amekudzi, M.: Addressing sustainability in transportation systems: Definitions, indicators, and metrics. Journal of Infrastructure Systems 11(1), 31–50 (2005)
12. Johnston, R.: Indicators for sustainable transportation planning. Transportation Research Record: Journal of the Transportation Research Board 2067(1), 146–154 (2008)
13. Litman, T., Burwell, D.: Issues in sustainable transportation. International Journal of Global Environmental Issues 6(4), 331–347 (2006)
14. Litman, T.: Exploring the paradigm shifts needed to reconcile transportation and sustainability objectives. Transportation Research Record 1670(1), 8–12 (1999)
15. Lyons, W.: Sustainable transport in the developing world: A case study of bogota's mobility strategy. In: International Conference on Sustainable Infrastructure (2017)
16. Maclaren, V.: Exploring the paradigm shift needed to reconcile sustainability and transportation objectives. Journal of the American Planning Association 62(2), 184–202 (1999)
17. Marshall, S.: The challenge of sustainable transport. In: Layard, A., Davoudi, S., Batty, S. (eds.) Planning for a Sustainable Future, pp. 131–147 (2001)
18. Massobrio, R., Nesmachnow, S.: Urban data analysis for public transportation systems. In: 2^{nd} Iberoamerican Congress on Smart Cities (2019)
19. Massobrio, R., Nesmachnow, S.: Urban mobility data analysis for public transportation systems: a case study in montevideo, uruguay. Environment and Planning B: Urban Analytics and City Science (2019)
20. Mauttone, A., Hernández, D.: Encuesta de movilidad del área metropolitana de Montevideo. `https://scioteca.caf.com/bitstream/handle/123456789/1078/EncuestadeMovilidadMVD-documentocompleto-final.pdf` (2017), (August 2019)
21. Miller, P., de Barros, A., Kattan, L., Wirasinghe, S.: Public transportation and sustainability: A review. KSCE Journal of Civil Engineering 20(3), 1076–1083 (2016)
22. Ministry of Industry, Energy, and Mining, Uruguay: Proyecto Movés: Movilidad urbana eficiente y sostenible. `https://www.miem.gub.uy/energia/proyecto-moves-movilidad-urbana-eficiente-y-sostenible` (2017), (August 2019)
23. Nesmachnow, S., Bana, S., Massobrio, R.: A distributed platform for big data analysis in smart cities: combining intelligent transportation systems and socioeconomic data for montevideo, uruguay. EAI Endorsed Transactions on Smart Cities pp. 1–18 (2017)
24. Nesmachnow, S., Tchernykh, A., Cristóbal, A.: Planificación de transporte urbano en ciudades inteligentes. In: I Ibero-american Conference on Smart Cities. pp. 204–218 (2018)
25. Rodrigues, A., Costa, M., Macedo, M.: Multiple views of sustainable urban mobility: The case of Brazil. Transport Policy 15(6), 350–360 (2008)
26. United Nations General Assembly: Report of the world commission on environment and development: Our common future (1987), `http://www.un-documents.net/wced-ocf.htm`, (August 2019)
27. World Business Council for Sustainable Development: Methodology and indicator calculation method for sustainable urban mobility. Tech. Rep. 978-2-940521-26-5 (2015)
28. Xiong, Z., Sheng, H., Rong, W., Cooper, D.: Intelligent transportation systems for smart cities: a progress review. Science China Information Sciences 55(12), 2908–2914 (2012)

Stand-alone performance for hybrid solar inverter. A real life Net-Metering vs. Self-consumption comparison

Carlos Martínez de Guereñu[1], Jorge de la Serna[1] and Álvaro Díaz de Guereñu[1]

[1] Zigor Research and Development A.I.E, Vitoria-Gasteiz, Spain

Abstract. This presentation outlines performance results of hybrid solar inverter (PV+storage) working in Stand Alone mode. Both Net-Metering and Self consumption scenarios have been considered.
The information has been obtained from HIS Gridex and HIT Gridex systems working in Borkum island in the course of NETfficient[1] project, where 40 devices had been working for 18 months.

Keywords: Storage, hybridization, solar inverter, Lithium batteries, Net-Metering, Self-consumption

1 Introduction

Adding storage to an on-grid solar inverter (commonly known as Hybrid solar inverter) opens a new outlook to the introduction of renewable energy in domestic, buildings and light industry applications. This small change means a revolution in the paradigm of electricity use [1], turning non-manageable energy sources into manageable ones.

This technological shift matches the European Commission declaration: "… our vision is of an Energy Union with citizens at its core, where citizens take ownership of the energy transition, benefit from new technologies to reduce their bills, …" [2].

NETfficient[1] project deployed more than 40 energy systems in houses, buildings and secondary substations on the German island of Borkum. Both aggregated and stand-alone systems were tested. The objective in mind was to improve the exploitation of renewable energy. The tool was energy storage: ultra-capacitors, lithium batteries, hydrogen and water tanks.

[1] European Union's Horizon 2020 research and innovation program under grant agreement No 646463, project NETfficient, Energy and economic efficiency for today's smart communities through integrated multi-storage technologies.

2 Inverter description

For the project Zigor developed and deployed 37 home (5kW) and 5 building (20kW) sized hybrid solar inverter, named HIS Gridex and HIT Gridex respectively. These inverters are composed of three DC-linked converters: PV solar converters (2 independent MPPTs), multi-chemistry storage converter (some systems included battery and ultra-capacitors) and AC inverter, with a common control.

The inverters had communication with installation billing (smart) meter, battery BMS and supervisor/aggregator. Integrating utility smartmeter allowed the inverter to follow Point-Of-Connection (POC) power setpoints. The setpoints could be internal (stand-alone mode) or external (aggregated mode).

3 Stand Alone mode

In Stand Alone mode, the inverter is optimizing self-consumption of the house or building where it is installed. That means that during day time, when photovoltaic (PV) energy is available from roof-top solar panels, the inverter feeds power into the house trying to avoid home to consume energy from point of connection (POC); any excess of power will charge the batteries, and, being the case (if more PV power is available), some power is fed into island distribution grid.

During night time or, in general, when solar power is not enough to compensate the consumption of the home, the batteries are discharged; the objective is, again, that no power have to be taken from distribution grid.

Once the batteries are depleted, the home will be powered from grid. As well, a small quantity of power will be consumed by inverter for its own electronics and to avoid deep discharge of the battery.

3.1 Sizing and performance

The performance of the whole system will be affected mainly by the sizing of the battery, solar panels and inverter nominal power, in comparison to house or building consumed power and energy.

In case low PV panel power is installed, low energy can be obtained for free, so the final impact of the system will be hardly noticed.

If the battery capacity is reduced, only a small portion of house/building energy can be obtained from battery, limiting again the performance of the system.

Another key point is the huge variability of solar irradiance along different seasons; this is especially critical in high latitude installations such as the ones of our study. In such cases, the correct sizing of battery capacity is not obvious; when optimized for a certain period of the year, it leads to non-optimal performance of the system during several months per year.

Table 1 shows the sizing of the installation for the two different systems analyzed. PV power and Battery capacity are shown in SI units and normalized to inverter nominal power.

Table 1. Component sizing.

	HIT Gridex (Building)	HIS Gridex (House)
Home/building peak power (measured)	11 kW	5.5 kW
Inverter power (kW)	20 kW	5 kW
Installed PV power (kW / p.u)	20 kW / 1.00 p.u.	4 kW / 0.8 p.u.
Battery capacity (kWh / p.u)	61 kWh / 3.05 p.u.	5.12 kWh / 1.02 p.u.

As it can be seen in the table, the battery energy capacity is three times lower in house system, compared to building one. It would affect the performance as it will be shown later.

3.2 Scenarios analyzed

Two different scenarios have been analyzed: Net-Metering and Self-consumption. A third scenario, feed-in tariff (FIT), doesn't fit the type of installations we are focusing on. Anyway this FIT scenario will be difficult to analyze because it will be very sensitive to the prize difference between energy consumed and energy injected.

According to [3], FIT started to lose its power as driver of renewable energy growth since 2011. As far as grid parity became a reality, Net-Metering and Self-consumption will be the only option for smart-grid concept.

Net-Metering
Net Metering is defined as netting of PV production in excess and additional electricity demand over a long period (month/year) (in effect, to spin their meters in reverse) [4].

Self-consumption.
The user produces a percentage of his instantaneous (or on a short period) power directly from solar panels or batteries.

If there is any excess of internal production, exporting to grid is (generally) allowed. In some cases, this grid injected energy is paid, while in others, like for NET-fficient users, are not paid for it.

4 Building use case. HIT Gridex

Only one of the building installations has been operated in Stand Alone working mode. It has been in aggregated mode (EMP operated) up to July 2018 and from them

to the end of the project in Stand Alone. The system analyzed it's located near the harbor.

The final analysis has been performed for the period from August to November 2018. Basically, it represents second half of summer and nearly full autumn. Therefore it can be demonstrative of the overall year performance.

4.1 Real Performance

As an example, the following graph shows the system performance during three days last week of October 2018.

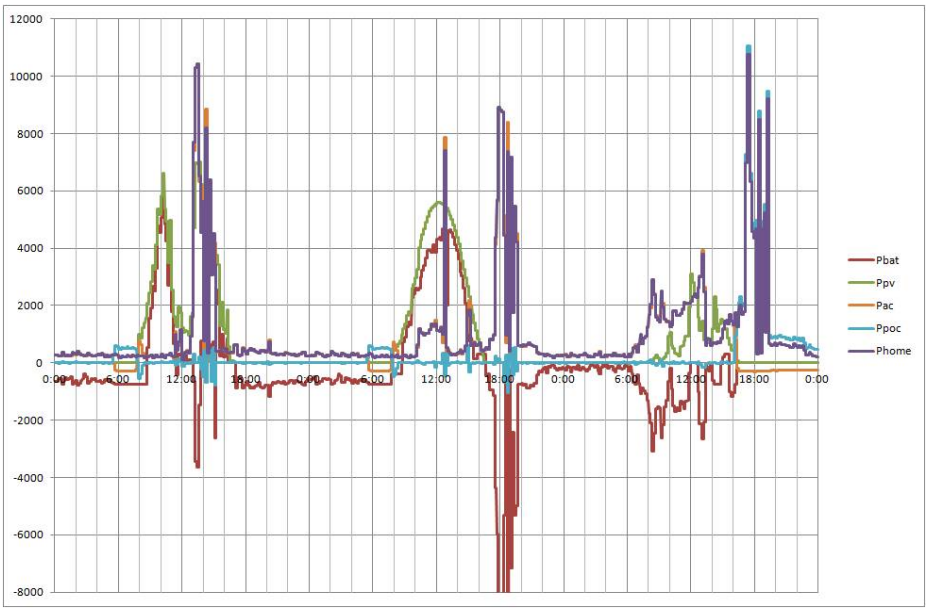

Fig. 1. Real building power.

The purple curve is the building power consumption. As it can be seen, it is quite flat during night time with recurrent peaks at around 18:00. The third day, a higher consumption in the morning can be seen.

The green curve represents solar power from PV panels. The second day is a sunny day, while the third day was a cloudy day (peak power along the whole day is only 3 kW).

The blue curve is the power in the Point-of-Connection (POC); a positive value means power consumed from grid, while a negative value means power injected into the grid. As it's shown, (except the last part of the third day) there is neither consumption nor injection into the grid. It means that, at real time, the power consumed by the building is injected by inverter (orange curve); and it comes from solar panel (green

curve) or from battery (red curve). The last one is charged (positive value) only when solar power exceeds building power.

Analyzing in further detail the behavior of the third day (Fig. 2), it can be observed clearly how the flow of power is optimized with the aim of avoid consuming from grid (flat blue curve at 0w); maximizing the saving to the user. As it can be seen, at around 16:00 the battery is exhausted; from that moment all the power is taken from grid.

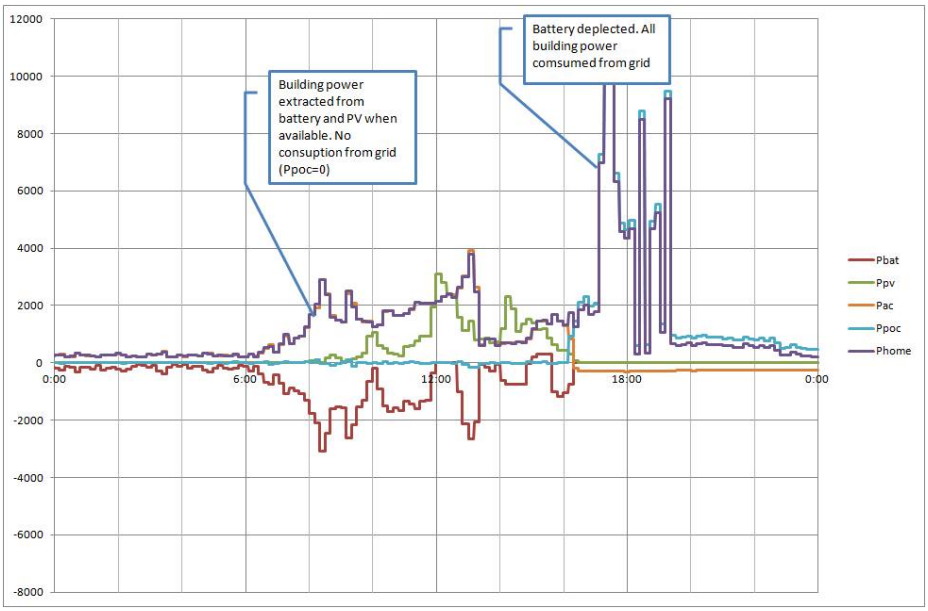

Fig. 2. Building power. Third day

4.2 Simulated non-storage performance

With recorded data, a simulated performance analysis has been carried out assuming a situation with a standard online inverter, without storage. All the solar power is injected into the building.

From recorded data, building consumption and PV power has not been modified. Inverter AC power is then computed from PV power (multiplied by efficiency) and then emulated power in POC is worked out.

The results are shown below in Fig 3. As it can be seen, the generation and consumption of energy is not correlated at all. On one hand, when solar energy is available, building consumption is low; on the other hand, the power peaks of building are provided by the grid.

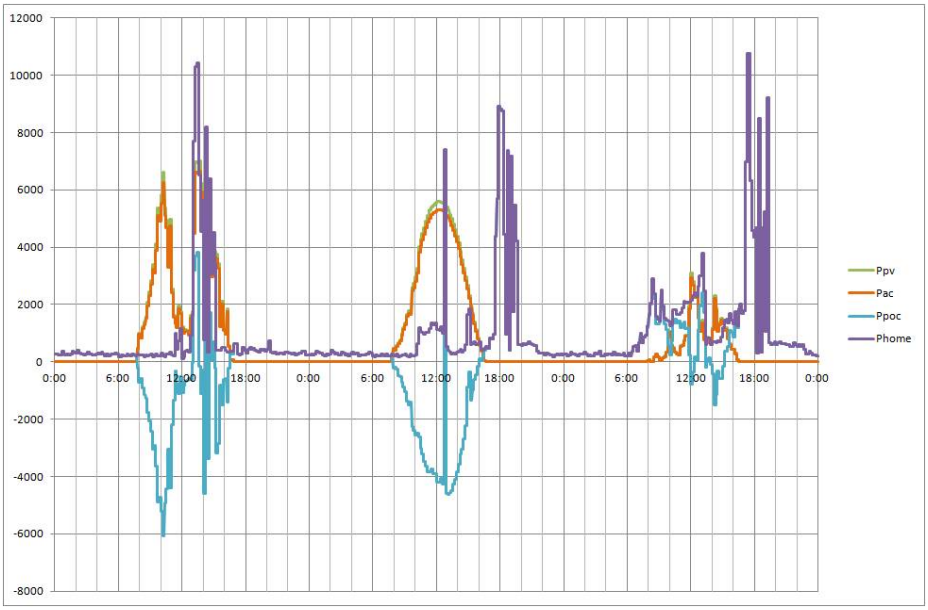

Fig. 3. Simulated "only PV" in building system

4.3 Results and analysis

Table 2 shows the figures resulting of the different scenarios (NET metering vs. Self consumption) and configuration:

- building without solar panels or batteries
- building with only solar panels (no storage)
- building with hybrid system (solar + storage)

The presented values are the monthly average of recorded data.

Table 2. Performance of building system.

	Building energy consumption	Energy consumed from grid	Energy injected to grid	Net metering	Self-consumption (without bonus for injected energy)
No PV/Storage	747 Wkh	747 kWh	0 kWh	747 kWh	747 kWh
Only PV	747 kWh	523 kWh	386 kWh	137 Wh	523 Wh
PV + Storage	747 kWh	218 kWh	15 kWh	204 Wh	218 Wh

In self-consumption scenario (the one in Borkum), as it can be observed, the building has consumed from grid 29% (218 kWh/747 kWh) of its energy needs. This is a big saving for the user. If no storage were installed (so only PV production), the energy bill had been 70%, 2.5 times more compared to the systems with storage. This is

due to the fact that PV production and building consumption are not happening at the same moment of the day.

Therefore, the use of solar energy provides a significant energy saving, but addition of storage really means a huge step in performance.

In scenarios of Net metering, the use of storage really doesn't help because the energy modulation which it provides has not real effect; and, taking into account the electrochemical and electrical conversion losses, storage has no sense.

5 Houses use case. HIS Gridex

Seven systems in Borkum have worked in Stand Alone from April 2018 until the end of the project, December 2018. The performance is analysed from April to November data; therefore it's representative of the complete year's one.

5.1 4.1. Real Performance

The following graphs show the system performance of one of the systems, located in a residential area, in the outskirts of Borkum city.

Here two specific periods of the year are presented. The first one was obtained the third week of June 2018. Therefore the data represent the system behavior at the maximum of the performance, during the summer solstice. The other set were obtained the last week of November 2018, when the solar irradiance is around the yearly minimum one.

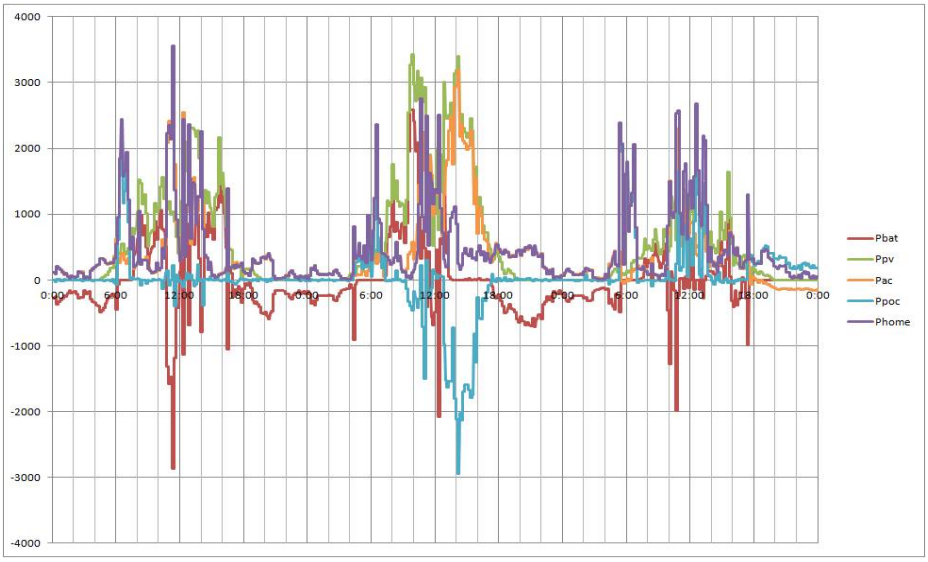

Fig. 4. Real house power during summer period

The purple curve is the house power consumption. As it can be seen, there are some peak consumption in the morning and then around noon, with hardly consumption during night time.

The green curve represents solar power form PV panels. Even being summer, the PV power available barely exceed 3kW (4kWp installed); PV panels tilt and orientation should be far from optimum values.

The blue curve is the power in the Point-of-Connection (POC); a positive value means power consumed from grid, while a negative value means power injected into the grid. As it's shown, mainly there is neither consumption nor injection into the grid. It means that, at real time, the power consumed by the house is injected by inverter (orange curve); and it comes from solar panel (green curve) or from battery (red curve). The last one is charged (positive value) only when solar power exceeds house power; when the battery is fully charged (i.e. in the afternoon of the second day), energy is injected into the grid. On the other side, if the battery is fully depleted (i.e. at 6:00 the first and third day) house energy is consumed directly from grid.

One interesting point to mention is that, in summer, during three days, the battery has been exhausted two times and, then, it has been easily fully charged. This leads to the conclusion that the battery capacity is undersized.

Next graph (Figure 5) shows the performance in winter. Solar power is limited and short; the battery is discharged every day; accordingly, the inverter really works as an additional consumption for the house. For this reason also, the sizing of the battery should be increased.

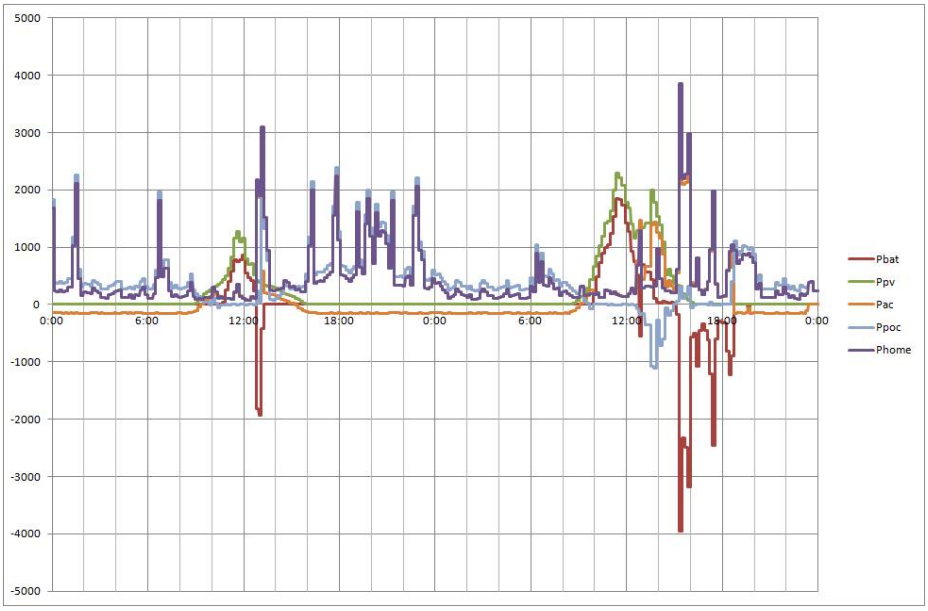

Fig. 5. Real house power during winter period

5.2 Simulated non-storage performance

With recorded data, a simulated performance analysis has been carried out supposing that a standard online inverter, without storage, is used. All the solar power is injected into the house.

House consumption and PV power has not been modified. As in buildings use case, inverter AC power and POC power are then computed.

The results are shown below in Figure 6 and Figure 7. As it can be seen, the energy generation and consumption is not correlated at all. On one hand solar energy is available, building consumption is low; on the other hand the power peaks of building are provided by the grid.

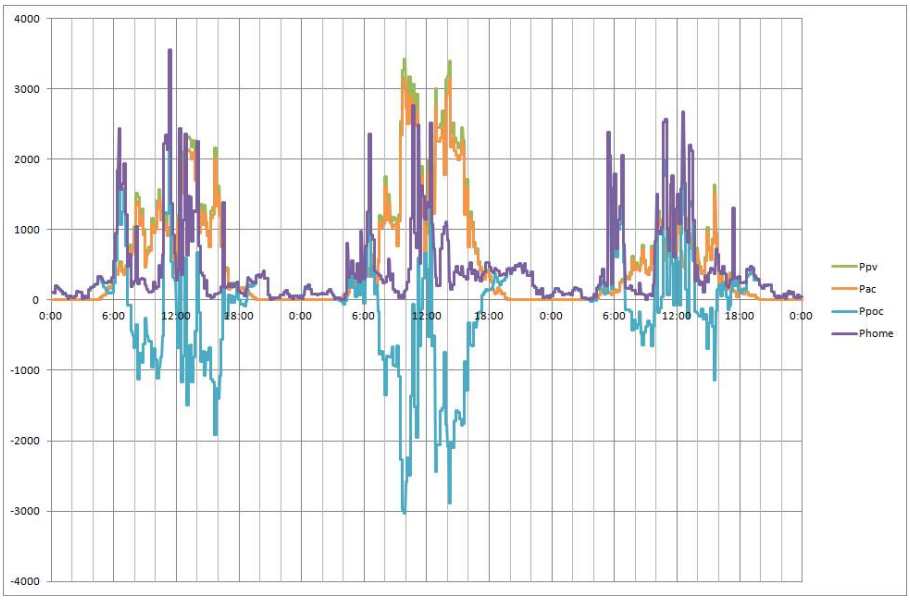

Fig. 6. Simulated "only PV" in house system during summer period

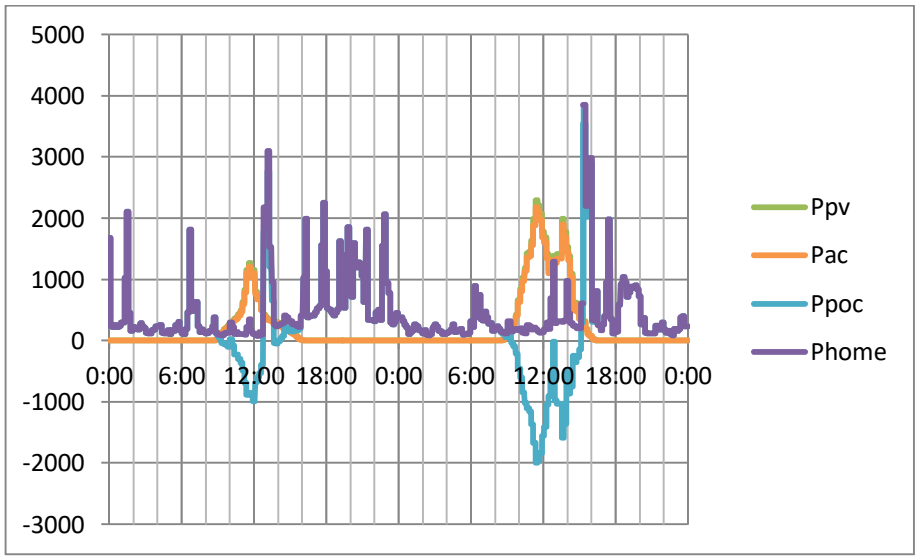

Fig. 7. Simulated "only PV" in house system during winter period

5.3 Results and analysis

The table 3 shows the figures resulting of the different scenarios (NET metering vs. Self consumption) and configuration:

- house without solar panels or batteries
- house with only solar panels
- house with solar + storage

The presented values are the monthly average of recorded data.

Table 3. Performance of house system.

	Building energy consumption	Energy consumed from grid	Energy injected to grid	Net metering	Self-consumption (without bonus for injected energy)
No PV/Storage	332 kWh	332 kWh	0 kWh	332 kWh	332 kWh
Only PV	332 kWh	224 kWh	187 kWh	37 kWh	224 kWh
PV + Storage	332 kWh	210 kWh	79 kWh	131 kWh	210 kWh

In self-consumption scenario, in contrast to the building case studied before, the savings associated to the use of storage are not so noteworthy. Remembering Figure 4, the battery is charged quite fast in summer, and then the solar power is injected (but not got paid) into grid. Once the battery is exhausted, that injected energy should be taken (consumed) from grid. While in Net metering this behavior is acceptable, in self-consumption scenario, it's ineffective.

This indicates probably an undersizing of the storage capacity.

In scenarios of Net metering, as well as in building use case, the estimated case of inverter without storage ("only PV") is a better option.

6 Conclusions

Real performance of hybrid (PV + storage) solar inverter has been presented. The (economic) performance of the system depends vastly on the use or not of storage. The other key parameter is the renewable energy regime or policies to be considered: self-consumption or net metering.

One of the conclusions we can draw is that storage makes sense in self-consumption scenario; the less time correlation between (solar) production and user consumption, the more profitable is the application of storage.

One the other hand, for the net metering scenario, the introduction of storage is not worth.

The second big conclusion to be learnt is that the sizing of the battery is crucial to obtain benefits from storage. In the cases analyzed, while an installed battery capacity of 1C has barely impact on energy bill (compared to only PV inverter), a 3C capacity leads to remarkable savings. Of course the optimum sizing of storage should be evaluated on a case-by-case basis.

References

1. Zahedi, A.: Maximizing solar PV energy penetration using energy storage technology. Renewable and Sustainable Energy Reviews, vol. 15, Issue 1, January 2011, pp 866-870. doi:10.1016/j.rser.2010.09.011
2. 52015DC0080. COMMUNICATION FROM THE COMMISSION TO THE EUROPEAN PARLIAMENT, THE COUNCIL, THE EUROPEAN ECONOMIC AND SOCIAL COMMITTEE, THE COMMITTEE OF THE REGIONS AND THE EUROPEAN INVESTMENT BANK A Framework Strategy for a Resilient Energy Union with a Forward-Looking Climate Change Policy /* COM/2015/080 final */. https://eur-lex.europa.eu/legal-content/EN/TXT/HTML/?uri=CELEX:52015DC0080&from=IT
3. Renewable Market Watch™. Europe Net Metering and Self-Consumption Solar PV Market Outlook 2016 – 2025. Inea Consulting Ltd (2018).
4. Jacobs, D., Sovacool, B.K.: 1.06 - Feed-In Tariffs and Other Support Mechanisms for Solar PV Promotion. Comprehensive Renewable Energy, vol 1, pp. 73-109 (2012). doi:/10.1016/B978-0-08-087872-0.00104-9

Household energy disaggregation based on pattern consumption similarities

Juan Chavat[0000−0001−9925−2651], Jorge Graneri, and Sergio Nesmachnow[0000−0002−8146−4012]

Universidad de la República, Montevideo, Uruguay,
{juan.pablo.chavat,jgraneri,sergion}@fing.edu.uy

Abstract. Non-intrusive load monitoring allows breaking down the aggregated household consumption into a detailed consumption per appliance, without installing extra hardware, apart of a smart meter. Breakdown information is very useful for both users and electric companies, to provide an accurate characterization of energy consumption, avoid peaks, and elaborate special tariffs to reduce the cost of the electricity bill. This article presents an approach for energy consumption disaggregation in residential households, based on detecting similar patterns of recorded consumption from labeled datasets. The proposed algorithm is evaluated using four different instances of the problem, which use synthetically generated data based on real energy consumption. Each generated dataset normalize the consumption values of the appliances to create complex scenarios. The `nilmtk` framework is used to process the results and to perform a comparison with two built-in algorithms provided by the framework, based on combinatorial optimization and factorial hidden Markov model. The proposed algorithm was able to achieve accurate results, despite the presence of ambiguity between the consumption of different appliances or the difference of consumption between training appliances and test appliances.

1 Introduction

Electricity utilization in homes has shown an uninterrupted increase worldwide, as detailed in the World Energy Outlook report, prepared by the International Energy Agency [6]. The electric power demanded in 2050 is expected to be twice as much as that demanded in 2010 [11]. Under this premise, many investigations have been carried out to achieve an efficient use of electricity in factories, buildings, and homes.

One of the approaches implemented to achieve a more efficient use of electric energy in homes is based on encouraging users to have a behavior change, favorable to saving. The incentives for behavioral changes are derived from the analysis of electricity utilization. For this analysis, Non Intrusive Load Monitoring (NILM) techniques are applied.

NILM allows determining the energy consumption of individual devices that are turned on and off, based on the detailed analysis of the current and voltage of the total load, measured at the interface with the source of the load. This approach was developed to simplify the collection of energy consumption data by utilities, but it also has other applications. It is called non-intrusive to contrast it with techniques previously used to collect load data, which requires placing sensors on every appliance and, therefore, an intrusion on the user energy consumption. In particular, NILM techniques are applied in residential households.

NILM uses only the aggregate signal to disaggregate the signal of each appliance, providing an easier way of generating detailed information about household energy consumption. The disaggregated information is useful to provide breakdown bill information to the consumer, schedule the activation of appliances, detect malfunctioning, and suggest actions that can lead a significant reduction in consumption (e.g., up to about 20% in some cases [12]), among other uses.

In this line of work, this article presents a first approach for solving the dissagregation problem by applying a simple algorithm for recognizing on/off appliances states using the aggregate consumption signal, and determine energy consumption patterns. The experimental evaluation of the proposed algorithm is performed over synthetic datasets, specifically built using real energy consumption data from the well-known UK-DALE repository [8]. Experiments are set to analyze the accuracy of the method varying the power consumption of appliances varies and generating complex scenarios including ambiguities between the power consumption of appliances. Experimental results are compared with two built-in methods of the `nilmtk` toolkit: Combinatorial Optimization (CO) and Factorial Hidden Markov Model (FHMM). Results shows that the proposed algorithm is able to achieve accurate results, accounting for an average of 0.95 on the F-score metric, in the most complex problem instances.

The proposal is developed within the project "Computational intelligence to characterize the use of electric energy in residential customers", funded by the Uruguayan government-owned power company (UTE) and Universidad de la República, Uruguay. The project proposes the application of computational intelligence techniques for processing household electricity consumption data to characterize energy consumption, determine the use of appliances that have more impact on total consumption, and identify consumption patterns in residential customers. The main contribution of this article is a simple approach to solve the problem of energy consumption dissagregation in residential households, conceived to be adapted to the main features of the Uruguayan system, and the experimental evaluation over a set of problem instances and the comparison with existing techniques.

The article is structured as follows. Section 2 presents the formulation of the problem addressed in the work. A review of the main related work is presented in Section 3. The proposed algorithms for solving the problem are described in Section 4. The experimental analysis is reported in Section 5. Finally, Section 6 presents the conclusions and the main lines of future work.

2 The energy consumption dissagregation problem

The problem consists of dissagregating the overall energy consumption of a house into the individual consumption of a number of appliances.

Consider a set of appliances available in a house $A = \{a_i\}, i = 1, \ldots, m$, and let x_t be the aggregate power consumption of the house at a given time slice t. x_t can be expressed as the sum of the individual power consumption x_t^i of each appliance in use in that time slice. The status of each time slice is indicated by the binary variable y_t^i, that takes value 1 when appliance i is ON and 0 when it is OFF. The simplest (binary) variant of the problem assumes just two possible values for the power consumption of each appliance, i.e., $x_t^i = c_i \times y_t^i$, that is to say that the power consumption of appliance i is constant and does not depend on the activity being performed by the appliance.

The total power consumption is described as a function $f{:}\{0,1\}^m \rightarrow R$ defined by the expression in Eq. 1.

$$x_t = f((y_t^1, y_t^2, \cdots, y_t^m)) = c_1 y_t^1 + c_2 y_t^2 + \cdots + c_m y_t^m \tag{1}$$

If function f is injective (one-to-one), the problem is trivial. Otherwise, the times series $\{x_t\}_{t \in T}$ must be studied in order to deduce from the variation of power consumption on time, the signatures of the individual appliances.

For instance, suppose the appliances are: fridge (power consumption 250 W), washing machine (2000 W), dish washer (2500 W), kettle (2500 W), and home theater (80 W). The aggregate power consumption is a non-injective function. There is ambiguity between the power consumption of dish washer and kettle, as defined by Eq. 2. The variation of the aggregate power consumption in time must be studied to deduce if the kettle or the dish washer is ON.

$$f((0,0,1,0,0)) = f((0,0,0,1,0)) = 2500 \tag{2}$$

Several attributes and patterns can be studied to solve ambiguities. In the previous example, additional information can be used to solve the ambiguity: e.g., the mean time of utilization of each appliance (it is a couple of minutes for kettle and longer than an hour for the dish washer). Other more sophisticated patterns can be detected to solve problem instances with more complex ambiguities.

3 Related works

The analysis of the related literature allows identifying several proposals on the design and application of software-based methods for energy consumption dissagregation. The main related works are reviewed next.

Hart [5] presented the concept of Nonintrusive Appliance Load Monitoring (NALM). The author stated that the previously presented approaches on the subject had a strong hardware component, installing intrusively monitoring

points in each household appliance connected to a central information collector. Hart proposed an approach based on using a simple hardware and complex software for the analysis, thus eliminating permanent intrusion in homes.

The model proposed by Hart considers that electrical appliances are connected in parallel to the electrical network and that the power consumed is additive (Eq. 3), where $a_i(t)$ represents the ON/OFF state of an appliance at time t.

$$a_i(t) = \begin{cases} 1 \text{ if appliance } i \text{ is ON at time } t \\ 0 \text{ otherwise} \end{cases} \tag{3}$$

Multiphase loads with p phases are modeled as vectors of dimension p where each component is the load in each phase. The total charge of the vector is the sum of the p components. P_i is defined as a vector representing the power consumed by device i when it is turned on (Eq. 4), where $P(t)$ is the corresponding to time t, and $e(t)$ represents the noise or the recorded error for time t.

$$P(t) = \sum_{i=1}^{n} a_i(t).P_i + e(t) \tag{4}$$

The proposed model involves solving a combinatorial optimization problem to determine vector $a(t)$ from P_i and $P(t)$, in order to minimize the error (Eq. 5).

$$\hat{a}(t) = \arg\min_{a} \left| P(t) - \sum_{i=1}^{n} a_i(t).P_i \right| \tag{5}$$

However, the resulting combinatorial optimization problem is NP-hard and therefore computationally intractable for large values of n. Heuristic algorithms allow computing solutions of acceptable quality, but their applicability is limited because in practice the set of vectors P_i is not fully known, the value n is not fixed, and unknown devices tends to be described as a combination of those already known. Furthermore, a small variation in the measurement of $P(t)$ can cause large changes in $a(t)$, mistakenly predicting simultaneous on and off events.

In recent works, NILM has been treated as a machine learning problem, applying supervised and unsupervised learning methods. Supervised learning approach is based on a data set of the consumption of each circuit device and the aggregate signal, and the objective is to generate models that learn to disaggregate the signal of the devices from the added signal. The techniques most commonly applied in this approach are Bayesian learning and neural networks. The unsupervised approach seeks to learn signatures of possible devices from the aggregate signal without knowing *a priori* what devices are inside the circuit. Bonfigli et al. [2] presented a survey of the test data sets available to researchers and the main techniques used for the unsupervised NILM approach. The most used unsupervised learning techniques are those based on Hidden Markov Models (HMM), which define a number of hidden states in which the model can be moved, representing the operating conditions of the device (e.g., on, off and possible intermediate states) and an observable result, which depends on the real state that represents the analyzed consumption data.

Kelly and Knottenbelt [7] analyzed three deep neural networks for disaggregation in the NILM problem. The proposed neural networks had between one and 150 million trainable parameters, so large amounts of training data was needed. The data set used was UK-DALE. The approach consisted of training a neural network for each household appliance, taking as input a sequence of aggregate total consumption and returning as a result the prediction of the power demanded by the associated appliance. Three architectures of neural networks were studied: i) long short-term memory (LSTM) recurrent neural network, suitable for working with data sequences because of its ability to associate the entire history of the inputs to an output vector; ii) a self-coding for noise elimination (denoising autoencoder, dAE) that cleans the aggregate consumption signal to obtain only that corresponding to the target appliance; and iii) a rectangle network to detect the start and end of the use of the target appliance, and its average power demanded at that time. The networks were trained using 50% of real data and 50% of synthetic data, generated with the signatures of the UK-DALE appliances using the nilmtk tool. Results were compared with CO and FHMM. The dAE and the rectangle networks outperformed the results of both CO and FHMM in F1 score, precision, proportion of total energy correctly assigned, and mean absolute error; while LSTM outperformed CO and FHMM in on/off appliances but was behind in multi-state appliances.

Several related works have used the `nilmtk` tool [1], a framework for NILM analysis implemented in Python that facilitates using multiple data sets by converting them to a standard data model. `nilmtk` implements algorithms for data preprocessing, statistics to describe the data sets, two disaggregation algorithms (CO and FHMM), and metrics for evalaution. Within the preprocessing algorithms are *downsample*, to normalize the frequency of consumption signals; and *voltage normalization*, to solve the problem of the variation of voltage between different countries [5], which implements a method to normalize the data and is able to combine different sets of household data from different countries.

Kolter and Johnson [10] introduced the REDD dataset and studied the performance of a FHMM algorithm for dissagregation using the available data. FHMM was evaluated using two weeks of data from five households, subsampled in ten-second intervals. Results showed that FHMM was able to disaggregate the total consumption, observing a clear degradation of the results when going from the prediction in the training set to the prediction in the evaluation set. The FHMM for the training set correctly classified 64.5% of the consumption, while for the evaluation set the correct classification was reduced to 47.7%. The authors posed the challenge of finding a way to combine REDD with the massive amount of untagged data generated daily by public energy service companies.

4 The proposed algorithm

This section describes the proposed algorithm to solve the problem of energy consumption disaggregation based on similar consumption patterns.

4.1 Algorithm description

Function $f : \{0,1\}^m \rightarrow R$ gives the aggregate power consumption of a house for a set of appliances. A function $g : R^{2d+1} \rightarrow R^m$ is considered, where the positive number d determines a time neighbourhood for the predictions (Eq. 6).

$$(\hat{y}_t^1, \hat{y}_t^2, \cdots, \hat{y}_t^m) := g_{W,Z}(x_{t-d}^i, \cdots, x_t^i, \cdots, x_{t+d}^i) \tag{6}$$

In Eq. 6, $(\hat{y}_t^1, \hat{y}_t^2, \cdots, \hat{y}_t^m)$ is the estimated configuration of the set of house appliances. Function $g_{W,Z}$ has random elements; it is defined using the information of a training database $\{W, Z\} = \{w_t, z_t\}$ such that for $t = 1, \cdots, n$, $w_t \in \{0,1\}^m$, $z_t \in R$ and Eq. 7 holds.

$$z_t = f((w_t^1, w_t^2, \cdots, w_t^m)) \tag{7}$$

The parameters of function $g_{W,Z}$ are chosen empirically to maximize the sum given in Eq. 8, where A is the set of ambiguous configurations $A = \{y \in \{0,1\}^m / \exists y' \in \{0,1\}^m, y' \neq y, f(y') = f(y)\}$. This is equivalent to maximize the number of time slices $t \in T$ for which every appliance status is correctly detected.

$$\sum_{y_t \in A} \prod_{i=1}^{m} 1_{\{\hat{y}_t^i = y_t^i\}} \tag{8}$$

The proposed algorithm, named *Pattern Similarities* (PS), consists of two parts, training and testing (prediction), which are described next.

The output of the algorithm is y, the vector of disaggregated power consumption, computed using the following input:

- The vector x containing the aggregate power consumption of one house measured over a period of time with a certain time frequency.
- A training set z containing the aggregate power consumption of one or several houses measured over a period of time with the same time frequency as x.
- A training set w containing the disaggregated power consumption of the house (houses) described in z over the same period of time and with the same frequency as x is measured.
- The parameter d that defines an power consumption neighbourhood.
- The parameter δ that defines a time interval neighbourhood.
- The parameter H that separates high from low power consumption.

Algorithm 1 describes the processing on the training stage. The goal is to build an array (M_Z) with information relating each consumption record with its neighbour records. The information act as a feature of each appliance signature, for each sample. The main loop (lines 2–10) iterates over each sample in the training set. In each iteration step, the algorithm check if the neighbour samples has similar consumption values to the current analyzed sample (lines 4–8); if they have, then a counter is incremented. At the end, the array with the processed values is generated for each testing sample. That array is used in the testing stage to find samples whose consumption is similar to the sample being processed.

Algorithm 1 PS algorithm: training stage

```
1: M_Z ← array of lenght Z
2: for all z_i ∈ Z do
3:    counter ← 0
4:    for all {z_j ∈ Z : |j − i| < d} do
5:       if z_j > z_i − φ then
6:          counter ← counter + 1
7:       end if
8:    end for
9:    M_Z[i] ← counter
10: end for
```

Algorithm 2 PS algorithm: testing stage

```
1: M_X ← array of lenght X
2: for all x_i ∈ X do
3:    counter ← 0
4:    for all {x_j ∈ X : |j − i| < d} do
5:       if x_j > x_i − φ then
6:          counter ← counter + 1
7:       end if
8:    end for
9:    M_X[i] ← counter
10: end for
11: for all x_i ∈ X do
12:    I ← ∅
13:    for all z_j ∈ Z do
14:       if |z_j − x_i| ≤ δ and x_i > H then
15:          I ← I ∪ {j}
16:       end if
17:       if |I| ≥ 1 then
18:          J ← argmin{|M_Z(I(·)) − M_X(i)|}
19:       else
20:          J ← argmin{|z(·) − x(i)|}
21:       end if
22:       k ← rand{1, ..., length(J)}
23:       y(i, ·) ← w(I(J(k)), ·)
24:    end for
25: end for
```

Algorithm 2 presents the testing stage. The first loop (lines 1–10) is similar to the main loop in the training stage, but applied to the testing dataset. This loop builds an array (M_X) with the processed value of signature feature for each testing sample. It is used to compare with the array built into the training stage. The second loop (lines 11–26) iterates over each testing sample to find similarities with the samples of the training dataset. In line 13, each training sample is compared to the consumption of the sample being processed, if the difference between both is lower than a threshold (δ) and the testing sample have a consumption value greater than a minimum (H), it is added to set I, to

be considered for next comparisons. If the set I is not empty, i.e., at least one training sample was found similar to the processing sample, the samples that minimize the difference between signature features (the difference between M_Z and M_X) are selected, and one of them is chosen randomly (line 18 and 22). If set I is empty, i.e., no training samples were found similar to the processing sample, the algorithm select the training samples that minimize the difference of consumption with the sample that is being processed, and one of them is chosen randomly (lines 20 and 22). Once the algorithm have found a similar training sample, it maps the consumption per appliance at the time of the training sample to the prediction results (line 23).

4.2 Implementation

A first version of the proposed algorithm was developed on Matlab, version 8.3.0.532 (R2014a), as a proof of concept. After that, it was re-implemented on python version 3, using `pandas` and `numpy`, which allows the implementation to be included as part of a pipe of execution in `nilmtk`. For this stage, several modifications were included in the metrics and utils files of the framework.

Two scripts were implemented for generating the synthetic datasets. The first script reads the UK-DALE dataset (HDF5 file), normalizes the values for the indicated houses and appliances, and builds a directory structure that contains metadata and the normalized data in CSV files. The normalization replaces all records over a given threshold by an indicated value, and set all other values to zero. The second script reads the directory structure and its content to generate a new HDF5 file with the synthetic dataset. In the resulting dataset, data have the same sample rate than in the original dataset, with the particularity that it does not present gaps, i.e., if original sample rate is six seconds, the generated dataset will have a record each six seconds. The gaps presented in the original dataset are filled by zeros. The algorithm implementation, the scripts for generating the datasets and the modified nilmtk files are available on a public repository (`https://gitlab.com/jpchavat/nilm-scripts`).

5 Experimental analysis

This section presents the experimental analysis of the proposed algorithm. In the experiments, the algorithm was executed in a `nilmtk` pipeline of execution, using a synthetic dataset based on UK-DALE dataset as input. Results were compared with CO and FHMM algorithms executed in same settings.

5.1 Problem instances and datasets

The synthetic datasets used for the experiments are based on house #1 of the UK-DALE dataset, considering the following appliances: fridge, washing machine, kettle, dish washer, and home theater. These appliances are representative of devices that contributes the most to household energy consumption [14].

Four different instances were generated for the experimental analysis. All datasets were generated by downsampling the UK-DALE dataset period to 5 minutes. A *datetime* range limit was established for training and testing data. For training data, the limits were set from 2013-01-01 at 00:00:00 to 2013-07-01 at 00:00:00, while for the testing data the limits were set from 2013-07-01 at 00:00:00 to 2013-12-31 at 23:59:59. A threshold of minimum consumption was applied in the normalization, which was set to 5.0 W. This value allows discarding standby power consumption records. Instances were generated to analyze the efficacy of the proposed algorithm to solve different cases of energy consumption ambiguity. A description of each problem instance and the motivation of using it is provided next.

Instance #1. The generated dataset normalizes the consumption of each appliance using the median of maximum consumption per activation (i.e., periods of time in which an appliance remains in state ON). Outliers were filtered by lower and upper limits defined by the standard deviation. The generated dataset is used for training and testing. This instance aims at working with values close to the real ones but keeping constant consumption values over time.

Instance #2 The generated dataset normalizes the consumption values to generate ambiguity between the consumption of kettle and dish washer. The same dataset is used for training and testing the algorithms. This instance aims at testing how the algorithms solves the most basic case of ambiguity.

Instance #3. The dataset normalizes consumption values like instance #2, but including ambiguities between the sum of consumption of fridge, home theater, and washing machine with the consumption of the dish washer. The same dataset is used for training and testing the algorithms. This instance aims at studying how the algorithms solves a more sophisticated case of ambiguity.

Instance #4 The training dataset is the same than in instance #2; but a new dataset was generated for the testing step, introducing small variations in the consumption of every appliance, but the washing machine. For example, the consumption of the fridge was normalized to 260 instead of 250. This instance aims at testing the algorithm in an scenario where testing appliances are similar but not equal to the appliances used for the training.

Table 1 reports the normalized value of the datasets used for training and testing for each instance, and Figure 1 shows the percentage of records when each appliance is in state ON/OFF, which is the same for all the generated datasets.

instance	*appliance*				
	fridge	*washing machine*	*kettle*	*dishwasher*	*home theater*
#1 (testing, training)	117	3325	2390	2741	93
#2 (testing, training)	250	2000	2500	2500	80
#3 (testing, training)	300	1800	2200	2300	200
#4 (testing)	250	2000	2500	2500	80
#4 (training)	260	2000	2400	2600	70

Table 1: Normalized values per appliance for each instance

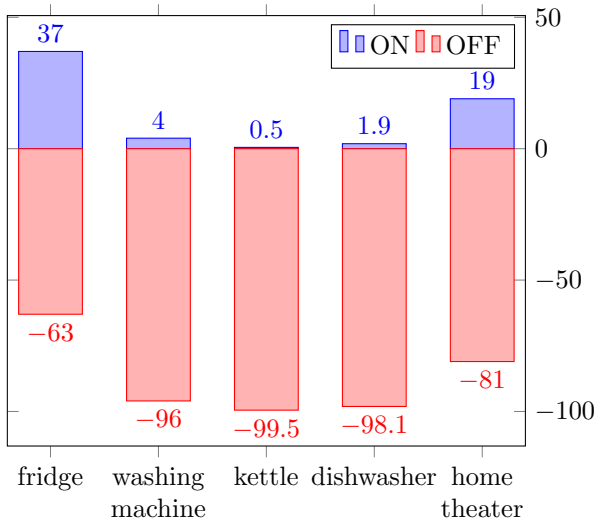

Fig. 1: Percentage of operating time of each appliance

5.2 Software and hardware platform

The `nilmtk` framework was used to implement the pipeline of execution for the experiments, as described in Fig. 2.

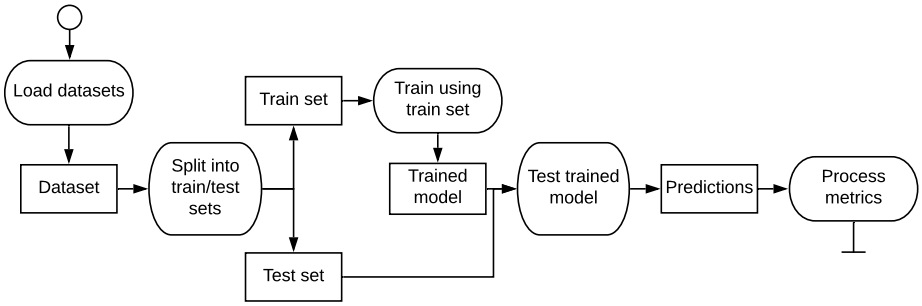

Fig. 2: Execution pipeline implemented in nilmtk

The first stage of the pipeline loads the dataset while the second splits the dataset into a training set and a testing set. The training set is used to train each algorithm and after that, the testing set is used to obtain the results of dissagregation. Finally, results are compared with the ground truth data (i.e. the test set) to compute a set of metrics.

The experimental evaluation was performed on National Supercomputing Center (Cluster-UY) infrastructure that counts with Intel Xeon-Gold 6138 nodes (up to 1120 CPU cores), 3.5 TB RAM, and 28 GPU Nvidia Tesla P100, connected by a high-speed 10 Gbps Ethernet network (`cluster.uy`) [13].

5.3 Baseline algorithms for comparison

Two methods from the related literature were considered as baseline for the comparison of the results obtained by the proposed algorithm: CO and FHMM.

The CO method was first presented by Hart [5], and included in the `nilmtk` framework. The approach of CO is to find the optimal combination of appliance states that minimises the difference between the total sum of aggregated consumption and the sum of the consumption of the predicted state on of appliances. CO searches for a vector $\hat{a}$ that minimises the expression on Eq. 5 Given the complexity of the CO algorithm, which is exponential in the number of appliances, it is not useful to address scenarios with a large number of appliances. The complexity of the CO algorithm is exponential in the number of appliances. Thus, it is not useful to address scenarios with a large number of appliances.

FHMM was introduced by Gharamani and Jordan [4]. Different variations of the original method were developed by Kim et al. [9] to solve the disaggregation problem. HMM are mixture models that encode historical information of a temporal series in a unique multinomial variable, represented as a hidden state; FHMM extends HMM to allow modeling multiple independent hidden state sequences simultaneously. FHMM scales worst than CO in scenarios with a large number of appliances.

5.4 Metrics for results evaluation

Standard metrics were applied to evaluate the efficacy of the studied algorithms. Being $x_i^{(n)}$ the actual status series for appliance n and $\hat{x}_i^{(n)}$ the status predicted by the algorithm, True Positive (TP), False Positive (FP), True Negative (TN) and False Negative (FN) ratios are defined by Eqs. 9–12.

$$TP = \sum_i AND(x_i^{(n)} = 1, \hat{x}_i^{(n)} = 1) \tag{9}$$

$$FP = \sum_i AND(x_i^{(n)} = 0, \hat{x}_i^{(n)} = 1) \tag{10}$$

$$TN = \sum_i AND(x_i^{(n)} = 0, \hat{x}_i^{(n)} = 0) \tag{11}$$

$$FN = \sum_i AND(x_i^{(n)} = 1, \hat{x}_i^{(n)} = 0) \tag{12}$$

Five metrics are considered in the analysis:

- *precision* of the prediction, defined as an estimator of the conditional probability of predicting ON given that the appliance is ON (Eq. 13).
- *recall*, defined as the conditional probability that the appliance is ON given that the prediction is ON (Eq. 14).
- *F–Score*, defined as the harmonic mean of precision and recall (Eq. 15).
- *Error in Total Energy Assigned* (TEE), defined as the error of the total assigned consumptions (Eq. 16).
- *Normalized Error in Assigned Power* (NEAP), defined as the mean normalized error in assigned consumptions (Eq. 17).

$$precision = \frac{TP}{TP + FN} \quad (13) \qquad recall = \frac{TP}{TP + FP} \quad (14)$$

$$F\text{–}Score = \frac{2 \times precision \times recall}{precision + recall} \quad (15)$$

$$\text{TEE}^{(n)} = \left| \sum_t y_t^{(n)} - \sum_t \hat{y}_t^{(n)} \right| \quad (16) \qquad \text{NEAP}^{(n)} = \frac{\sum_t \left| y_t^{(n)} - \hat{y}_t^{(n)} \right|}{\sum_t y_t^{(n)}} \quad (17)$$

5.5 Results

Tables 2–5 report the results of the proposed algorithm (PS) and the baseline algorithms (CO and FHMM), on instances #1 to #4. All results were obtained using the following parameter configuration, set by a rule-of-thumb and empirical evaluation: $\delta = 100$, $d = 10$, $H = 500$ and $\varphi = 250$.

CO					
metric	*fridge*	*washing machine*	*kettle*	*dishwasher*	*home theater*
TEE (kW)	292.18	2318.84	2767.39	6651.69	1118.64
NEAP	0.8663	0.7644	5.9284	2.6279	2.1975
precision	0.8324	0.9863	0.7153	0.9758	0.8413
recall	0.5584	0.4827	0.0228	0.2301	0.2814
F-score	0.6684	0.6481	0.0442	0.3724	0.4218
FHMM					
metric	*fridge*	*washing machine*	*kettle*	*dishwasher*	*home theater*
TEE (kW)	306.46	3209.08	3399.42	5371.37	948.72
NEAP	0.8843	0.8367	6.8117	2.7134	2.3119
precision	0.7576	0.9817	0.7810	0.9768	0.5799
recall	0.5408	0.5078	0.0258	0.2377	0.2199
F-score	0.6311	0.6694	0.0500	0.3823	0.3188
PS					
metric	*fridge*	*washing machine*	*kettle*	*dishwasher*	*home theater*
TEE (kW)	23.87	0.00	0.00	0.00	29.67
NEAP	0.0218	0.0000	0.0000	0.0000	0.1497
precision	0.9839	1.0000	1.0000	1.0000	0.9409
recall	0.9942	1.0000	1.0000	1.0000	0.9121
F-score	0.9891	1.0000	1.0000	1.0000	0.9263

Table 2: Results of CO, FHMM, and PS on instance #1

Results in Table 2 indicate that *PS* was able to accurately solve problem instances without ambiguity between power consumption of appliances. F-score values between 0.92 and 1.0 were obtained. Both *CO* and *FHMM* got F-score values around 0.6 for fridge and washing machine, around 0.3 for dish washer and home theater, and 0.04 (i.e., almost null) for kettle. In all cases, F-score values were lower than the obtained with *PS*.

Results in Table 3 indicate that F-score values of *PS* for appliances with ambiguities decreased up to 9%, while the rest of the F-score values remains similar to instance #1. Regarding the baseline algorithms, *CO* showed a decrease of 50% in the prediction of appliances with ambiguity, while results of *FHMM*

CO					
metric	*fridge*	*washing machine*	*kettle*	*dishwasher*	*home theater*
TEE (kW)	2228.32	1701.36	5595.52	7206.13	685.29
NEAP	1.0053	1.5412	9.8478	3.0491	1.6285
precision	0.6973	0.8271	0.6715	0.9807	0.7781
recall	0.5123	0.2457	0.0111	0.1184	0.2907
F-score	0.5907	0.3789	0.0219	0.2113	0.4233
FHMM					
metric	*fridge*	*washing machine*	*kettle*	*dishwasher*	*home theater*
TEE (kW)	1401.84	962.88	7904.24	5016.79	431.27
NEAP	0.9007	1.1175	13.2448	2.1841	1.7049
precision	0.7687	0.9149	0.7007	0.9787	0.6649
recall	0.5573	0.4790	0.0084	0.2379	0.2850
F-score	0.6461	0.6288	0.0166	0.3828	0.3990
PS					
metric	*fridge*	*washing machine*	*kettle*	*dishwasher*	*home theater*
TEE (kW)	0.00	0.00	42.50	42.50	14.88
NEAP	0.0000	0.0000	0.1788	0.0473	0.1264
precision	1.0000	1.0000	0.9416	0.9681	0.9460
recall	1.0000	1.0000	0.8866	0.9843	0.9289
F-score	1.0000	1.0000	0.9133	0.9761	0.9374

Table 3: Results of CO, FHMM, and PS on instance #2

CO					
metric	*fridge*	*washing machine*	*kettle*	*dishwasher*	*home theater*
TEE (kW)	1690.42	2194.13	6298.06	6720.05	949.90
NEAP	0.9386	1.6483	12.1919	3.0818	1.7343
precision	0.8217	0.8678	0.5876	0.9826	0.8432
recall	0.5754	0.2400	0.0073	0.1212	0.3250
F-score	0.6768	0.3760	0.0145	0.2157	0.4692
FHMM					
metric	*fridge*	*washing machine*	*kettle*	*dishwasher*	*home theater*
TEE (kW)	2069.24	1655.52	6273.13	6895.43	1561.12
NEAP	1.1036	1.2927	12.1388	3.1483	2.0024
precision	0.4318	0.9067	0.6387	0.9797	0.7645
recall	0.4512	0.3677	0.0087	0.1380	0.2942
F-score	0.4413	0.5232	0.0171	0.2419	0.4249
PS					
metric	*fridge*	*washing machine*	*kettle*	*dishwasher*	*home theater*
TEE (kW)	4.50	82.80	15.40	89.70	13.60
NEAP	0.0221	0.0668	0.5000	0.1092	0.0377
precision	0.9893	0.9771	0.7372	0.9266	0.9845
recall	0.9886	0.9570	0.7566	0.9629	0.9780
F-score	0.9889	0.9670	0.7468	0.9444	0.9812

Table 4: Results of CO, FHMM, and PS on instance #3

remained similar to the ones computed for instance #1, with exception of the kettle (F-score decreased 66%).

Results in Table 4 indicates that the F-score values of *PS* decreased for washing machine (3%), dish washer (6%), and kettle (the worst value, 25% less than for instance #1), increased for home theater (6%), and did not vary for fridge. *CO* decreased for washing machine (42%), kettle (67%), and dish washer (42%), compared with instance #1. F-score values for FHMM decreased for all the appliances (up to 66% for kettle), but the home theater (increased 33%).

CO					
metric	*fridge*	*washing machine*	*kettle*	*dishwasher*	*home theater*
TEE (kW)	2543.42	2239.86	5208.68	7414.75	637.84
NEAP	0.9819	1.7824	9.6185	3.0921	1.8408
precision	0.6597	0.7653	0.6533	0.9826	0.7895
recall	0.5202	0.1823	0.0121	0.1193	0.3205
F-score	0.5817	0.2944	0.0238	0.2128	0.4559
FHMM					
metric	*fridge*	*washing machine*	*kettle*	*dishwasher*	*home theater*
TEE (kW)	1829.65	699.35	8567.56	5080.58	560.53
NEAP	0.9218	1.1591	14.6967	2.2034	1.9148
precision	0.7209	0.8403	0.6971	0.9797	0.6961
recall	0.5453	0.4634	0.0083	0.2383	0.2931
F-score	0.6210	0.5974	0.0163	0.3834	0.4125
PS					
metric	*fridge*	*washing machine*	*kettle*	*dishwasher*	*home theater*
TEE (kW)	182.69	62.00	42.60	111.00	145.00
NEAP	0.0440	0.0142	0.3221	0.0821	0.2720
precision	0.9985	1.0000	0.8066	0.9758	0.9666
recall	0.9957	0.9860	0.8984	0.9787	0.9166
F-score	0.9971	0.9930	0.8500	0.9773	0.9409

Table 5: Results of CO, FHMM, and PS on instance #4

Finally, results in Table 5 demonstrate that *PS* has a robust behavior when using different normalized datasets for training and testing steps. The F-score for *PS* was over 0.99 for fridge and washing machine, over 0.97 for dish washer, and over 0.94 for home theater. The lowest F-score value was obtained for kettle (0.85) With respect to instance #1, the F-score of the kettle decreased 15%. The rest of the appliances experienced a decrease/increase lower than 2%. For *CO*, F-score values decreased for all appliances but the home theater For *FHMM*, F-score values of fridge and dish washer varied less than 1.6% with respect to instance #1, and decreased for washing machine and kettle (up to 67%).

Overall, the proposed *PS* algorithm achieved satisfactory results for all the studied instances. Improvements on F-score were 60% over *CO* and 57% over *FHMM* in average, and up to 64% over *CO* in problem instance #4 and up to 60% over *FHMM* in problem instance #3. Furthermore, *PS* systematically obtained the lowest values of both TEE and NEAP metrics for all instances. Degraded results obtained for kettle in problem instances with ambiguity suggest that the lower percentage of operating time (0.5% for kettle) affects the results negatively and the more complex the dataset is, the more consumption samples are needed in the testing dataset.

6 Conclusions and future work

This article presented an approach to address the problem of household energy dissagregation. An algorithm based on pattern similarities was proposed. The experimental evaluation performed over realistic problem instance showed that, overall, the proposed algorithm is effective for addressing the problem of energy consumption disaggregation. Results can be applied to household energy planning by using intelligent recommendation systems [3].

The main lines for future work are related to study instances with different sample rates and noise in the power consumption, and extend the parameter analysis of the proposed algorithm. In addition, more sophisticated computational intelligent methods can be evaluated to solve the problem.

References

1. Batra, N., Kelly, J., Parson, O., Dutta, H., Knottenbelt, W., Rogers, A., Singh, A., Srivastava, M.: NILMTK: an open source toolkit for non-intrusive load monitoring. In: 5^{th} International Conference on Future Energy Systems. pp. 265–276 (2014)
2. Bonfigli, R., Squartini, S., Fagiani, M., Piazza, F.: Unsupervised algorithms for non-intrusive load monitoring: An up-to-date overview. In: 15^{th} International Conference on Environment and Electrical Engineering (2015)
3. Colacurcio, G., Nesmachnow, S., Toutouh, J., Luna, F., Rossit, D.: Multiobjective household energy planning using evolutionary algorithms. In: Iberoamerican Congress on Smart Cities (2019)
4. Ghahramani, Z., Jordan, M.: Factorial hidden Markov models. In: Advances in Neural Information Processing Systems. pp. 472–478 (1996)
5. Hart, G.: Nonintrusive appliance load monitoring. Proceedings of the IEEE 80(12), 1870–1891 (1992)
6. International Energy Agency: World Energy Outlook 2015. White paper (2015)
7. Kelly, J., Knottenbelt, W.: Neural NILM: Deep Neural Networks Applied to Energy Disaggregation. In: 2^{nd} ACM International Conference on Embedded Systems for Energy-Efficient Built Environments. pp. 55–64 (2015)
8. Kelly, J., Knottenbelt, W.: The UK-DALE dataset, domestic appliance-level electricity demand and whole-house demand from five UK homes. Scientific Data 2 (2015)
9. Kim, H., Marwah, M., Arlitt, M., Lyon, G., Han, J.: Unsupervised disaggregation of low frequency power measurements. In: SIAM international conference on data mining. pp. 747–758. SIAM (2011)
10. Kolter, J., Johnson, M.: Redd: A public data set for energy disaggregation research. In: Workshop on Data Mining Applications in Sustainability. pp. 59–62 (2011)
11. Larcher, D., Tarascon, J.: Towards greener and more sustainable batteries for electrical energy storage. Nature Chemistry 7(1), 19–29 (2015)
12. Neenan, B., Robinson, J., Boisvert, R.: Residential electricity use feedback: A research synthesis and economic framework. Electric Power Research Institute (2009)
13. Nesmachnow, S., Iturriaga, S.: Cluster-UY: High Performance Scientific Computing in Uruguay. In: International Supercomputing Conference in Mexico (2019)
14. Orsi, E., Nesmachnow, S.: Smart home energy planning using IoT and the cloud. In: IEEE URUCON (2017)

Planeamiento de la distribución de energía eléctrica considerando incertidumbre en la demanda y recursos energéticos distribuidos

Diego Sanchez[1], Rubén Cruz[1] Ernesto Pérez[2] y Mónica Montoya[1]

[1] CIDET. Medellín 050012, Colombia
[2] Universidad Nacional de Colombia. Medellín 050012, Colombia
diego.sanchez@cidet.org.co

Abstract. This document contains a methodology for the planning of electricity distribution networks considering demand uncertainty and distributed energy resources. In the first place, a demand characterization model is proposed that takes into account the behavior of distributed generation, demand response programs, energy storage and connection of electric vehicles. Subsequently, the planning methodology is based on three principles, optimizing the use of infrastructure, deferring network investment and finally expanding when necessary. The planning problem is solved using a hybrid algorithm GA-PSO, and the results are presented when applying the methodology in an IEEE 33 radial bus test system, obtaining reductions between 30 and 40% compared to the expansion with traditional alternatives. In addition, an analysis is made of different levels of penetration of distributed energy resources.

Keywords: Planeamiento de sistemas de distribución – redes inteligentes – incertidumbre – recursos energéticos distribuidos

1 Introducción

En el contexto de las ciudades inteligentes, en el cual este tipo de sistemas están en la capacidad de responder adecuadamente a las necesidades básicas de instituciones, empresas, y de los propios habitantes, tanto en el plano económico, como en los aspectos operativos, sociales y ambientales [1] [2]. El planeamiento de la expansión de redes de distribución juega un papel preponderante, gracias a la necesidad de atender la demanda de energía eléctrica de forma sostenible; dicho planeamiento consiste en la elección de alternativas para atender la demanda en el mediano y largo plazo; minimizando los costos y atendiendo a criterios de confiabilidad y seguridad de la red. Los plazos de ejecución de los proyectos de esta naturaleza, regularmente entre 2 y 5 años, hacen necesario contar con un plan de inversión de manera anticipada, ocasionando que el planeador deba pronosticar variables con alta incertidumbre como la demanda de energía eléctrica y la conexión de generación distribuida [3].

No obstante, el cambio tecnológico está transformando la manera en que se conciben los sistemas eléctricos, debido a la transformación de los equipos de uso final de la

energía y la disponibilidad de alternativas tecnológicas con impacto tanto en la operación como en la planeación de los sistemas. Quizás la más renombrada de las tendencias, son las redes inteligentes (Smart Grid en inglés), debido a sus implicaciones en la operación de los sistemas, abriendo la posibilidad de optimizar los recursos y operar en regiones cercanas a los limites térmicos de los conductores. Es decir, usando soluciones alternativas las redes de distribución instaladas pueden ser explotadas de forma óptima, evitando o atrasando inversiones en nuevas instalaciones [4].

Dentro de las tendencias tecnológicas derivadas de las redes inteligentes se encuentran los Recursos Energéticos Distribuidos (DER por sus siglas en inglés), dichos recursos energéticos se encuentran conectados cerca al usuario final, y tienen la capacidad de inyectar, reducir o almacenar energía eléctrica. Su comportamiento depende de la disponibilidad de la fuente primaria de energía y del comportamiento estratégico de su propietario, aumentando así la incertidumbre en el comportamiento de la demanda [5] [6]. Sin embargo, los DER con una estrategia de control adecuada pueden disminuir los picos de demanda, al inyectar energía o reducir consumos, evitando que ésta tenga que ser transportada desde zonas lejanas, descongestionando las redes de distribución y optimizando las nuevas inversiones [7].

Por otro lado, se espera el aumento en la penetración de vehículos eléctricos, que tienen la posibilidad de ser conectados directamente en las instalaciones de uno final, principalmente las residencias o zonas comerciales; además, tienen la posibilidad de consumir o inyectar potencia a la red eléctrica, situación que es agravada por las características móviles de los vehículos, que dificultan el pronóstico tanto del tiempo, como de la ubicación en la que éstos realizarán su carga o venderán energía almacenada en sus baterías al sistema eléctrico. Bajo estas condiciones, es necesario contar con redes de distribución lo suficientemente robustas para atender la demanda de energía de los vehículos eléctricos, así como recibir sus excedentes [8].

Otra alternativa tecnológica asociada a los DER, con el potencial de atrasar o evitar las inversiones en la red de distribución es la respuesta a la demanda, que consiste en la disminución o traslado del consumo de los usuarios bajo incentivos del sistema [9]. A diferencia de la generación distribuida o del almacenamiento, esta alternativa no tiene costos de inversión obligatoriamente, contando con la instalación de dispositivos de medición inteligente con la capacidad de conexión o desconexión remota, comunes a todas las alternativas tecnológicas descritas [10]. Sin embargo, la respuesta a la demanda tiene costos fijos, con los cuales se le remunera al usuario final la disponibilidad para ser desconectado cuando el sistema lo necesite, dependiendo el mecanismo en el que participe [11].

Si bien es cierto que estas alternativas tecnológicas, poseen características que, de ser explotadas adecuadamente pueden ayudar a solucionar los problemas de las redes de distribución, una inadecuada planeación de las redes de distribución y la ubicación de este tipo de alternativas, pueden profundizar los problemas de congestión, y estabilidad de los sistemas, ocasionadas por el comportamiento estocástico de la demanda [12]. Así, contar con un plan de expansión cubriendo la totalidad de los riesgos, requiere grandes inversiones en infraestructura, ya que resulta imperioso considerar el peor escenario; esto es, cuando los recursos energéticos distribuidos están fuera de servicio, tanto las baterías estáticas como los vehículos eléctricos estén realizando su ciclo de

carga; y se presente el pico de demanda convencional [13]. Bajo este escenario la demanda de energía eléctrica aumentaría indiscriminadamente, y resultaría inviable la expansión del sistema de distribución manteniendo niveles tarifarios asequibles para los usuarios finales. A continuación, se describe una metodología para el planeamiento de la red distribución, en primer lugar, se describe el modelo de caracterización de demanda, posteriormente se presenta la metodología, el modelo de optimización y los resultados al aplicarlo en un caso de estudio.

2 Caracterización de la demanda

El modelo utilizado para proyectar la demanda de energía eléctrica en un sistema de distribución, parte de la caracterización del comportamiento típico de las cargas; el modelo de curvas en S, utilizado para predecir la penetración de la generación distribuida, principalmente de origen fotovoltaico, y de vehículos eléctricos, además del aporte de los mecanismos de respuesta de la demanda. Finalmente, el comportamiento horario de la demanda está dado como la combinación de los modelos anteriores.

De acuerdo con lo expresado, la demanda de energía eléctrica en cada nodo n del sistema y cada periodo t, en el año del horizonte de planeamiento p, es el resultado de la sumatoria de los efectos citados anteriormente, entre los que se pueden distinguir la línea base de demanda $LBD_{n,t,p}$ resultado de la caracterización del comportamiento de las cargas, la inyección de energía por fuentes de autogeneración y generación distribuida $\mathrm{AGD}_{n,t,p}$, el impacto de los mecanismos de respuesta de la demanda en la línea base de consumo $ERD_{n,t,p}$, y la inyección o consumo de energía por parte de los dispositivos almacenadores instalados detrás de los medidores de los usuarios finales $EALM_{n,t,p}$; por último, el comportamiento de la carga de los vehículos eléctricos $\mathrm{AVE}_{n,t,p}$, como se expresa a continuación:

$$DEE_{n,t,p} = LBD_{n,t,p} - \mathrm{AGD}_{n,t,p} - ERD_{n,t,p} + EALM_{n,t,p} + \mathrm{AVE}_{n,t,p} \quad (1)$$

3 Metodología de planeamiento

La metodología de planeamiento propuesta mantiene la filosofía de seguridad del suministro del planeamiento tradicional manteniendo límites de violación de los criterios técnicos; sin embargo, flexibiliza las soluciones para las problemáticas de la red, al tiempo que considera incertidumbres tanto en la demanda como en la penetración de generación distribuida, almacenamiento, mecanismos de respuesta de la demanda y vehículos eléctricos. La metodología sustentada en tres principios; el primero de ellos consistente en la optimización del uso de la infraestructura existente, dando señales a los usuarios por medio de programas de eficiencia energética y gestión de la demanda de largo plazo, que permitan modificar las características de la curva de carga y eviten la expansión de la red por la reducción o traslado de la carga en horas pico. El segundo principio de la metodología es aplazar las inversiones en la red, mediante la instalación de recursos energéticos distribuidos por parte del distribuidor que permitan gestionar la

operación de las redes eléctricas y aplazar las inversiones. Por último, solo se expande la red cuando con ningunas de las alternativas anteriores fue posible asegurar la operación confiable del sistema en el horizonte de planeamiento.

Nótese, que, en el primer principio de la metodología de planeamiento, el distribuidor juega un papel pasivo, brindando señales para que el usuario modifique su consumo, esto trae variaciones en la proyección de las características de la curva de carga. Sin embargo, en mercados liberalizados, con la desintegración vertical de las compañías es necesario que dichas señales provengan de agentes externos al distribuidor. En el segundo principio, el distribuidor toma un papel más activo, instalando equipos en las redes de distribución cerca a los usuarios.

En la Fig 1, se presenta el diagrama de la metodología propuesta, iniciando con la definición del problema de planeamiento, que debe responder requerimientos regulatorios y del mercado, se delimita el problema en recursos, tiempo, población, entre otros criterios, e identifican las variables que el inversionista considera relevantes para tomar decisiones. En la segunda etapa, se realiza la caracterización y posterior proyección de la demanda de energía eléctrica por usuario de acuerdo con el modelo planteado anteriormente.

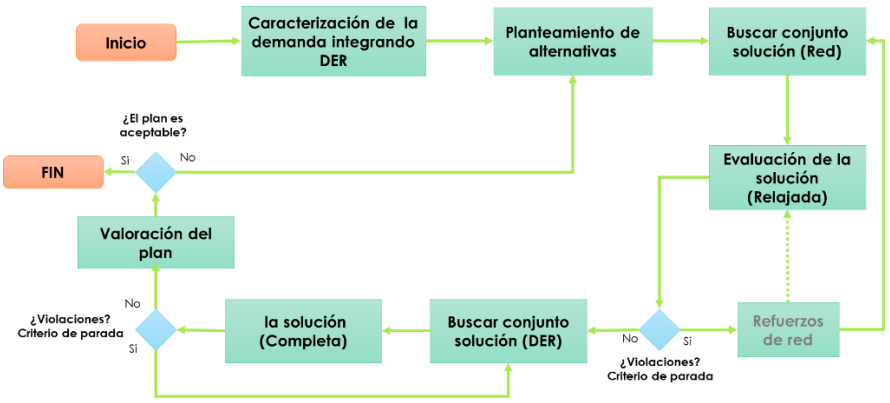

Fig. 1. Diagrama metodología propuesta

En la etapa siguiente se plantean las alternativas de expansión del sistema de distribución, calculando los costos asociados a cada alternativa y los requerimientos mínimos para su instalación, así como las restricciones de expansión asociadas a la capacidad máxima de los alimentadores nuevos y existentes, y los límites de expansión utilizando recursos energéticos distribuidos. Posteriormente, se relaja el problema de planeamiento y se busca la solución al mismo usando alternativas de expansión de la red como cambio de alimentadores y transformadores o nuevas instalaciones. En esta etapa se pueden sobrepasar en cierta medida las restricciones del problema, como los flujos en los alimentadores y los límites de tensión, bajo el supuesto que las mismas pueden aliviarse en etapas posteriores. Una vez encontrada una solución aceptable para el planeador, se procede a la etapa siguiente; en caso en que no se encuentre una solución

aceptable, es necesario regresar a la etapa de planteamiento de nuevas alternativas. Finalmente, se procede a solucionar el problema completo, esta vez utilizando todas las alternativas DER. En esta etapa, se consideran todas las restricciones asociadas a la expansión de la red, obteniendo el plan de inversión definitivo.

4 Modelo De Optimización

El modelo de optimización consiste en minimizar el Valor Presente Neto (VPN) del plan de inversión, calculado a partir del valor presente de la inversión realizada en cada periodo t ($\mathrm{EG_t}$). Las inversiones son traídas a valor presente usando una tasa de retorno mínima aceptable para el operador de red TIO.

$$\min_{alt\ exp} \sum_{t=t_1}^{T} \left(\frac{\mathrm{EG_t}}{(1+\mathrm{TIO})^{t-t_1}} \right) (2)$$

La inversión realizada en cada periodo $\mathrm{EG_t}$, es el resultado de la suma del costo de inversión en alternativas de red $EGRED_t$, Costo de inversión en DER $EGDER_t$, el costo de demanda Flexible $EGDFE_t$, y costos de operación del sistema $EOSIS_t$ como se expresa a continuación:

$$EG_t = EGRED_t + EGDER_t + EGDFE_t + EOSIS_t (3)$$

El costo de inversión en alternativas de red $EGRED_t$, es igual a la sumatoria sobre el número total de candidatos de expansión C, de la variable binaria nc que toma un valor de 1 cuando se ejecuta una obra y 0 en caso contrario, multiplicado por $EGNCred$, correspondiente al costo de inversión en cada refuerzo o instalación en la red (alimentadores, transformadores, subestaciones, transferencias de carga, etc.).

$$EGRED_t = \sum_{c=1}^{C} \mathrm{nc} * \mathrm{EGNCred} \ (4)$$

El costo de inversión en Recursos Energéticos Distribuidos es igual al costo de inversión en almacenamiento $EGALM$, mas costo de inversión en generación distribuida $EGGD$. Teniendo en cuenta que en ambientes de mercado el Operador de Red puede tener limitaciones para invertir en activos de generación.

$$EGDER_t = EGALM_t + EGGD_t (5)$$

A su vez, el costo de inversión en almacenamiento para cada periodo es igual a la variable continua $\mathrm{alm_{n|t}}$, que se refiere a la cantidad de almacenamiento instalada en cada nodo en el periodo t en kW, multiplicado por el costo de instalación. El costo de inversión en generación distribuida a es igual a la capacidad en generación distribuida instalada en cada nodo $\mathrm{gd_{n|t}}$ por el costo de instalación CGD_n.

$$\mathrm{EG}DER_{\mathrm{t}} = \sum_{\mathrm{n}=1}^{\mathrm{N}} \left(\mathrm{alm}_{\mathrm{n|t}} \cdot \mathrm{C}ALM_{\mathrm{n}}\right) + \left(\mathrm{gd}_{\mathrm{n|t}} \cdot \mathrm{C}GD_{\mathrm{n}}\right) (6)$$

Adicionalmente, el costo de contar con demanda flexible para el distribuidor $EGDFE$, es igual a la sumatoria sobre el número de nodos del costo asumido por el usuario para participar en demanda flexible (medidores inteligentes, controladores automáticos, comunicaciones, etc).

Finalmente, la expansión del sistema de distribución debe responder a límites técnicos en busca de preservar la seguridad y confiabilidad, tales como límites inferiores y superiores de tensión en todos los nodos, V_{min} y V_{max}, limites superiores de sobrecarga en los alimentadores S_{maxi} y las ecuaciones del flujo de carga para sistemas radiales expresados a continuación.

$$V_{min} \leq V_n \leq V_{max} \; \forall \; n \; (7)$$

$$S_{li} < S_{maxi} \; \forall \; li$$

$$P_{n+1} = P_n - P_{lin} - k_n R_n \frac{P_n^2 + Q_n^2}{V_n^2}$$

$$Q_{n+1} = Q_n - Q_{li} - k_n X_n \frac{P_n^2 + Q_n^2}{V_n^2}$$

$$\left|{V_{n+1}}^2\right| = {V_n}^2 - 2k_n(R_n \cdot P_n + X_n \cdot Q_n) - (R_n^2 + X_n^2)\frac{P_n^2 + Q_n^2}{V_n^2}$$

Como se evidencia, el problema de planeamiento es un problema no lineal entero mixto, que resulta dificil de resolver por metodologias deterministicas, principalmente si se desea encontrar la solucion atendiendo a las restricciones expuestas por el flujo de potencia. Por tal motivo, se usa un algoritmo que combina dos de las metaheuristicas poblacionales mas utilizadas en la actualidad para resolver problemas de planeamiento, como lo son los algoritmos geneticos AG y la optimizacion por enjambre de particulas PSO. Si bien no es posible garantizar que la solucion encontrada por el algoritmo sea la solucion optima, si es posible encontrar soluciones aceptables para el inversionista, mejorando la informacion utilizada para la toma de decisiones, respecto al plan de inversión.

En primer lugar se utiliza un algoritmo genetico, para encontrar una solucion aceptable respecto a las alternativas de expansion tradicionales de naturaleza binaria. Posteriormente, se utiliza PSO para encontrar una solucion respecto a la instalacion de DER, para solucionar los problemas de la red. Este proceso se repite en todas las etapas de planeamiento. En la Fig. 2 se muestra el diagrama de flujo del algoritmo de optimización.

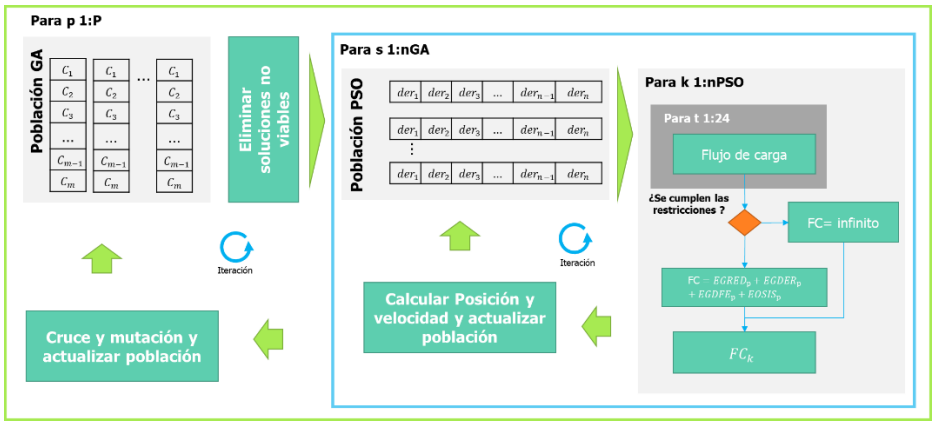

Fig. 2. Diagrama modelo de optimización

5 Caso de estudio y resultados

La metodología propuesta, es aplicada a un caso de prueba en un sistema IEEE de 33 nodos, como se muestra en la Fig. 3. Caracterizado por un crecimiento de la demanda que requiere expansión de la red de distribución, tanto por violaciones de tensión en los nodos finales del sistema, como sobrecarga en los nodos iniciales. Los datos utilizados en el estudio son extraídos de [6]. El problema de planeamiento consiste en encontrar el plan de inversión en un horizonte de 5 años, que garantice la operación segura y confiable del sistema ante cualquier condición de carga, considerando la penetración de generación distribuida en todos los nodos, así como la posibilidad de instalar DER por parte del inversionista.

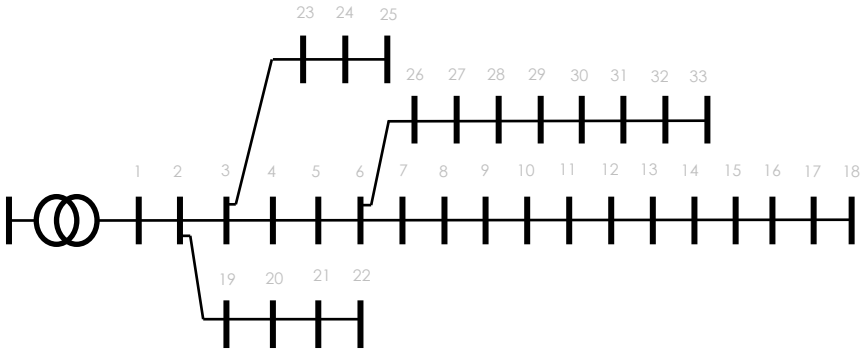

Fig. 3. Sistema IEEE 33 nodos radial

En la Fig. 4. se muestra la sensibilidad de la penetración de generación distribuida de acuerdo con el periodo de retorno para el usuario final. Evidenciando el efecto en la demanda de energía anual como en el comportamiento horario de la carga. Dicho

per[14]iodo de retorno puede ser modificado para diferentes periodos de tiempo, teniendo en cuenta el uso de incentivos financieros a este tipo de instalaciones y la reducción de costos experimentada por estas tecnologías en los últimos años.

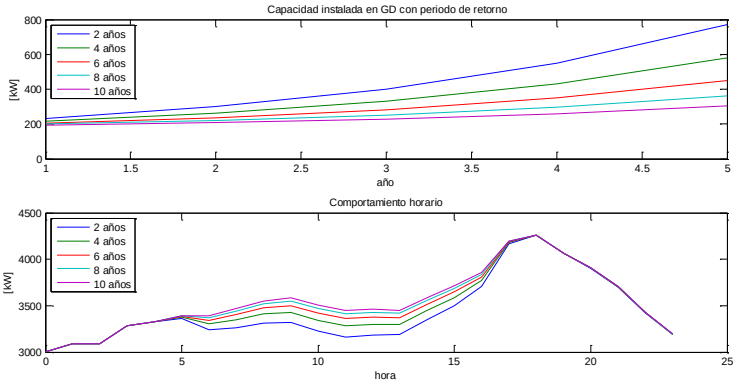

Fig. 4. Penetración de Generación Distribuida en un periodo

El impacto horario de la penetración de generación distribuida se muestra en la Fig. 5. con un efecto incremental a medida que crece la penetración, disminuyendo la demanda promedio diaria. No obstante, la demanda pico del sistema permanece sin variaciones, debido a la indisponibilidad de la fuente primaria. Por esta razón, a pesar del alivio de los requerimientos del sistema en términos de energía, las necesidades de expansión derivadas de la atención en horas pico permanece igual.

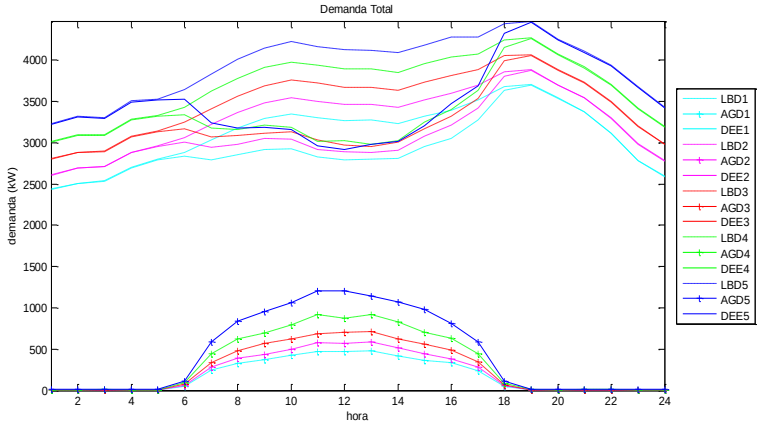

Fig. 5. Efecto horario de la generación distribuida

Como resultado al aplicar la metodología en el caso de estudio, se obtiene el plan de inversión durante el periodo de studio, como se muestra en la Fig. 6. Donde se muestra

la capacidad en DER, necesaria en cada nodo para cada periodo del horizonte de planeamiento, vale la pena resaltar que estas instalaciones pueden provenir de plantas de generación distribuida con la capacidad de generar en horas pico y bajo el control del operador de red, sistemas de almacenamiento o contratos de respuesta de la demanda.

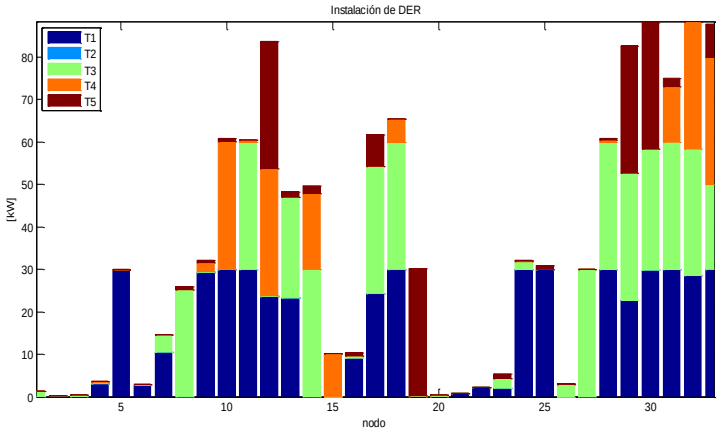

Fig. 6. Instalación de DER

En la Fig.7. Se observa las tensiones durante todo el horizonte de planeamiento, en caso en que no se intervenga la red, evidenciando violaciones a los límites establecidos bajo varias condiciones de operación, especialmente en los nodos entre el 9 y el 18 y entre el 28 y el 33.

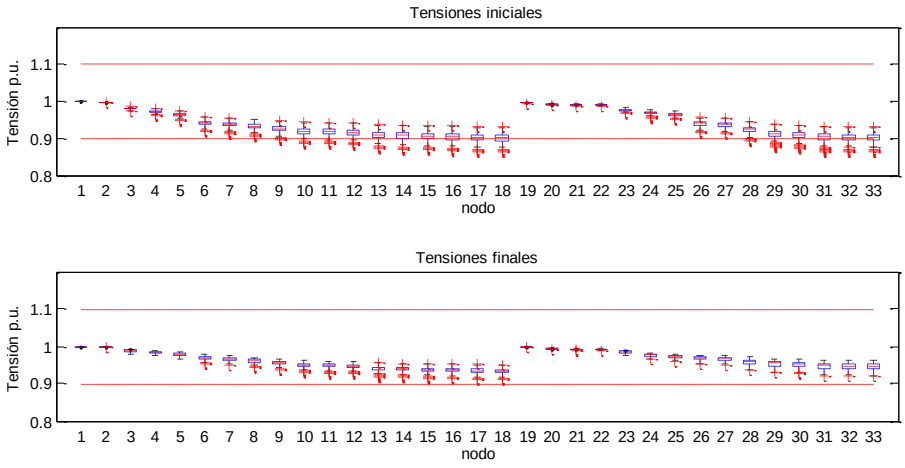

Fig. 7 Comparación de las tensiones

En la Fig 8. se muestra las tensiones en todo el horizonte de planeamiento, después de ejecutar el plan de inversión propuesto; escenario en el cual no se presentan violaciones a los límites establecidos.

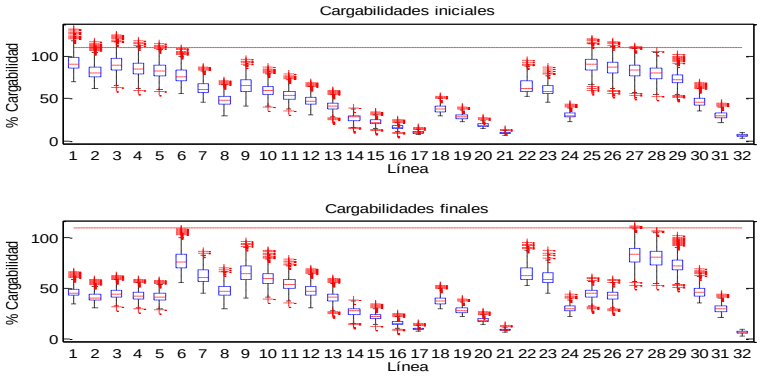

Fig. 8 Comparación de cargabilidades

El comportamiento horario de los DER en el horizonte de planeamiento se muestra en la Fig. 9. Evidenciando una reducción de los picos de demanda, consumo que es trasladado a otras horas del día, manteniendo el consumo de energía promedio.

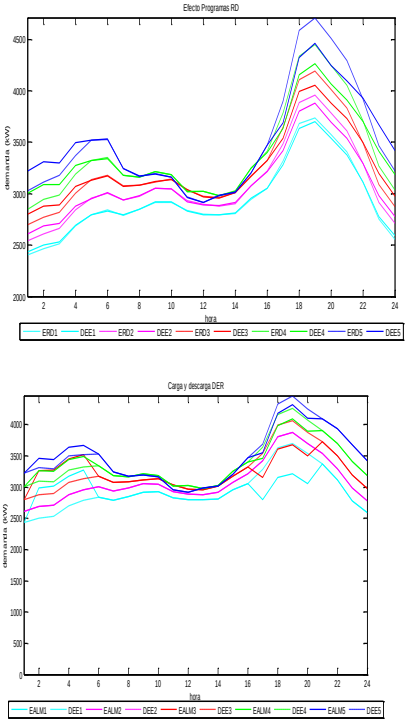

Fig. 10 Efecto del almacenamiento y de los programas RD

6 Conclusiones

La metodología propuesta fue aplicada para la expansión de la red de un sistema de distribución de prueba IEEE de 33 nodos, encontrando reducciones entre 25 % y 35 % de la inversión, en el periodo de planeamiento, ocasionada por evitar o atrasar expansión de la red. Adicionalmente, se encontraron beneficios provenientes de la flexibilidad de instalación y posibles.

La integración de las nuevas alternativas de expansión, principalmente las asociadas a la operación del sistema, demanda cambios en el planeamiento de la expansión de las redes de distribución, tales como la incorporación de modelos probabilísticos y la introducción de metodologías de gestión del riesgo en la selección de alternativas; es decir, debe ser elegido el plan de expansión con un nivel de riesgo tolerable para el planeador.

Contar con un plan de expansión cubriendo la totalidad de los riesgos, requiere grandes inversiones en infraestructura, ya que resulta imperioso considerar el peor escenario; esto es, cuando los recursos energéticos distribuidos están fuera de servicio, tanto las baterías estáticas como los vehículos eléctricos estén realizando su ciclo de carga; y se presente el pico de demanda convencional. Bajo este escenario la demanda de energía eléctrica aumentaría indiscriminadamente, y resultaría inviable la expansión del sistema de distribución para atender la demanda, manteniendo niveles tarifarios asequibles para los usuarios finales.

References

1. A. Camero and E. Alba, “Smart City and information technology: A review,” *Cities*, vol. 93, pp. 84–94, 2019.
2. S. Zhu, D. Li, and H. Feng, “Is smart city resilient? Evidence from China,” *Sustain. Cities Soc.*, vol. 50, p. 101636, 2019.
3. S. Montoya-Bueno, J. I. Muñoz-Hernández, and J. Contreras, “Uncertainty management of renewable distributed generation,” *Journal of Cleaner Production*. 2015.
4. C. Sepulveda, M. Resener, S. Haffner, and L. A. Pereira, “Computational model for the analysis of distributed generation in systems including smart grids,” in *2015 IEEE PES Innovative Smart Grid Technologies Latin America, ISGT LATAM 2015*, 2016, pp. 405–410.
5. A. Rastgou, S. Bahramara, and J. Moshtagh, “Flexible and robust distribution network expansion planning in the presence of distributed generators,” *Int. Trans. Electr. Energy Syst.*, 2018.
6. J. Liu, H. Cheng, P. Zeng, L. Yao, C. Shang, and Y. Tian, “Decentralized stochastic optimization based planning of integrated transmission and distribution networks with distributed generation penetration,” *Appl. Energy*, vol. 220, pp. 800–813, 2018.
7. K. Spiliotis, S. Claeys, A. R. Gutierrez, and J. Driesen, “Utilizing local energy storage for congestion management and investment deferral in distribution networks,” in *International Conference on the European Energy Market, EEM*, 2016, vol. 2016–July.
8. C. K. Das, O. Bass, G. Kothapalli, T. S. Mahmoud, and D. Habibi, “Overview of energy storage systems in distribution networks: Placement, sizing, operation, and power quality,” *Renew. Sustain. Energy Rev.*, vol. 91, pp. 1205–1230, 2018.

9. A. S. Brouwer, M. van den Broek, W. Zappa, W. C. Turkenburg, and A. Faaij, “Least-cost options for integrating intermittent renewables in low-carbon power systems,” *Appl. Energy*, vol. 161, pp. 48–74, 2016.
10. S. M. de Oca, P. Belzarena, and P. Monzón, “Benefits of optimal demand response in distribution networks in a competitive retail market,” in *2017 IEEE URUCON*, 2017, pp. 1–4.
11. J. Molina, D. Sánchez, L. Buitrago, and S. Giraldo, “Demanda Activa para la mitigacion de gases de efecto invenadero,” *Colomb. Intel.*, 2018.
12. S. Montoya-Bueno, J. I. Muñoz-Hernández, and J. Contreras, “Uncertainty management of renewable distributed generation,” *Journal of Cleaner Production*. Elsevier Ltd, University of Castilla - La Mancha (UCLM, INEI), Avda. Camilo José Cela, s/n, 13071 Ciudad Real, Spain, 2016.
13. W. Lyzwa and M. Wierzbowski, “Load duration curve in the long-term energy mix optimization,” in *International Conference on the European Energy Market, EEM*, 2016, vol. 2016–July.
14. T. Kulms, A.-K. Meinerzhagen, S. Koopmann, and A. Schnettler, “Development of An Agent-based Model for Assessing the Market and Grid Oriented Operation of Distributed Energy Resources,” in *Energy Procedia*, 2017, vol. 135, pp. 294–303.

IPN Sustainability Program: Solar Photovoltaic Electricity Generation and Consumption Reduction

P.J. Escamilla-Ambrosio[1[0000-0003-3772-3651]], M.A. Ramírez-Salinas[1[0000-0002-9376-2893]], O. Espinosa-Sosa[1], G. Gallegos-García, M. Morales-Olea[2] and Luis Hernández-Callejo[3[0000-0002-8822-2948]]

[1] Instituto Politécnico Nacional, Centro de Investigación en Computación, Ciudad de México, Mexico
[2] Fundación INBA A.C., Ciudad de México, Mexico
[3] Universidad de Valladolid (UVa), Campus Duques de Soria, C.P. 42004, Soria, España
pescamilla@cic.ipn.mx

Abstract. As part of the energy sustainability program intended to reduce the carbon footprint of the National Polytechnic Institute, solar photovoltaic electricity generation systems along with electricity consumption reduction actions have been implemented in three entities. These actions were implemented in accordance with recommendations defined by environmental committees and considering the diagnoses of baseline energy consumption. This work reports the quantification of the savings generated by the implementation of operational measures of technological substitution and solar photovoltaic electric power generation. The foregoing includes a process of identification of the baseline of electricity consumption, the replacement of infrastructure and equipment of high energy consumption with equipment of low consumption and environmental impact, as well as the installation of technology for the generation of electrical energy by renewable sources. Three solar photovoltaic systems were installed, replacement of luminaires, replacement of hand dryers and replacement of obsolete air conditioning equipment. It was found that on average the reduction in monthly electricity consumption is 31% with the consequent economic savings. Regarding the reduction of the carbon footprint, an impact on non-generation of tonnes of CO2 equivalent amount 37% quantified with reference to the generation before the implementation of the operational and power generation measures. This is equivalent to not having generated 18.31 tCO2e per month. This work describes the activities carried out and the methodology used to calculate the savings found, both in energy consumption, economic, and in reducing the carbon footprint.

Keywords: Energy Sustainability, Photovoltaic System, Carbon Footprint.

1 Introduction

As part of the energy sustainability and carbon footprint reduction project at the National Polytechnic Institute (IPN, from Instituto Politécnico Nacional, in Spanish) [1], a pilot program was implemented in 3 instances: Computer Research Center (CIC,

from Centro de Investigación en Computación, in Spanish), Center for Innovation and Technological Development in Computing (CIDETEC, from Centro de Investigación y Desarrollo Tecnológico en Cómputo, in Spanish) and Higher School of Computing (ESCOM, from Escuela Superior de Cómputo, in Spanish).

The project seeks to establish policies that facilitate the transition of the IPN education system to a sustainable development model, which promotes the incorporation of innovations and technological developments in the area of equipment, furniture and work instruments, to reduce the impact on the environment of its daily operation.

In this work technological substitutions and generation of electrical energy from a renewable energy source, which were implemented at 3 units of IPN, are presented. These actions aim to reduce the environmental impact, the carbon footprint and reduce the consumption and dependence of electricity generated by fossil fuels.

The information of the results generated from the initial approach and corresponding monitoring of the project is presented, as well as the analysis of the data generated through the activation of the technological platform refereed to as "Strategic System for Evaluation and Performance of Sustainability" (SEEDS, from Sistema Estratégico de Evaluación y Desempeño de la Sostenibilidad, in Spanish), implemented at CIC, CIDETEC and ESCOM buildings, which were equipped with the infrastructure that allows the use of alternative and sustainable energy.

CIC is located at Av. Juan de Dios Bátiz s / n esq. Miguel Othón de Mendizábal, Col. Nueva Industrial Vallejo, Mayor Gustavo A. Madero, C.P. 07738, Mexico City, Mexico. See Fig. 1. In its infrastructure CIC has a building with a total constructed area of 9,768.8 m^2, the property is 20 years old, it houses a total population of 383 users, the operation of the building is from Monday to Sunday, at a schedule of 07:00 am to 9:00 p.m., although it is an open-door building for its users, that is, it is functional 24 hours a day, 365 days a year.

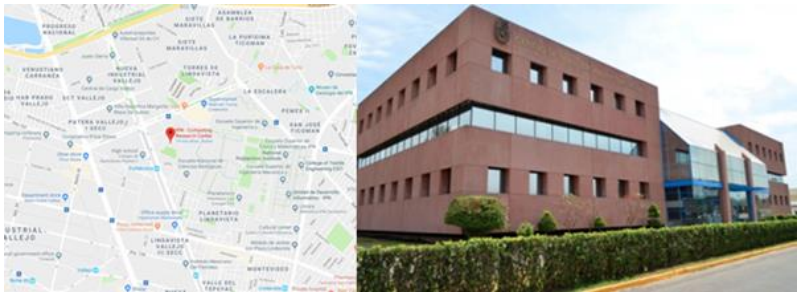

Fig. 1. Location and view of CIC.

CIDETEC is located at Av. Juan de Dios Bátiz s / n esq. Miguel Othón de Mendizábal, Col. Nueva Industrial Vallejo, Mayor Gustavo A. Madero, C.P. 07700, Mexico City, Mexico. See Fig. 2. In its infrastructure, CIDETEC has a building with a total constructed area of 2,563.26 m2, the property is 12 years old, it houses an approximate population of 174 users, the operation of the building is from Monday to Sunday, at a schedule of 07:00 am to 9:00 p.m., although it is an open-door building for its users, that is, it is functional 24 hours a day, 365 days a year.

Fig. 2. Location and view of CIDETEC.

ESCOM is located at Av. Juan de Dios Bátiz s / n Col. Nueva Industrial Vallejo, Mayor Gustavo A. Madero, C.P. 07738, Mexico City, Mexico. See Fig. 3. In its infrastructure ESCOM has 5 buildings with a total constructed area of 17,172.71 m^2, the property is 25 years old, has a total of 386 fixed users and 2800 variable users (students), the operation of the building is from Monday to Saturday, at 07:00 am to 10:00 pm.

Fig. 3. Location and view of ESCOM.

2 Baseline of electricity consumption and replacement of infrastructure.

In order to determine the baseline of electricity consumption in the three units considered, the following actions were carried out: a) activation of the SEEDS technology platform; b) installation of an electrical energy consumption monitoring network; c) replacement of infrastructure and equipment; d) installation of PV electricity generation systems, and e) quantification of energy, economic and environmental savings. These actions allowed monitoring the consumption of electrical energy through the installation of equipment for the measurement and processing of data, through a technological tool, which facilitated informed decision-making in the implementation of strategic projects that promote sustainable development.

2.1 Activation of the SEEDS Technology Platform

SEEDS is a software platform designed to support decision makers and administrators in the transition towards a model of sustainable development in organizations. Through programs developed for mobile and web environments, SEEDS allows to obtain the baseline of different sustainability variables, and evaluate performance in different intervention cycles. Furthermore, SEEDS allows entities the designing and monitoring of the effectiveness of improvement actions with respect to different sustainability variables, prioritizing the analysis of the consumption of electric energy and water usage, also as electricity energy generation. This software platform was installed in three instances of IPN in order to analyze and display information on the consumption of electricity and water, as energy generation, in real time, though an interactive web interface. The platform collects data through two systems:

1. Meters. The information is incorporated, from meters of electricity and water consumption, as electricity generation, in real time, to a database for processing and querying indicators in a web interface. This system has an API (Application Program Interface) to perform queries from other systems that have access permissions, for example, an Android application or other web system that request these data.
2. Logs. Module that allows to create logbooks with the information fields required to maintain a process of measuring the consumption of electricity and water, as well as electricity generation and the pattern of waste production.

SEEDS has a web interface for entering and consulting information. With the activation of SEEDS it was possible to integrate data that allow to know the pattern of resources consumption, in real time, identifying savings possibilities with the implementation of operational actions for the consumption of electric energy. By having data to define the quantification of electric power consumption, it was possible to establish indicators and goals related to the variables of sustainability based on a baseline of energy consumption. An example of the electricity consumption in a day at CIC, as registered in the SEEDS platform, is shown in Fig. 4.

Fig. 4. Electricity consumption as registered in the SEEDS platform at CIC on 2018-12-18.

2.2 Installation of the Electrical Energy Consumption Monitoring Network

The installed monitoring network had seven basic components, I. energy consumption meters, II. water consumption meters, III. analog transmission antennas, IV. systems for data acquisition, V. systems for information processing, VI. components for sending data and VII. Information display systems. The equipment that was installed in the entities seeks to innovate with the use of technological tools to facilitate decision-making in projects focused on saving resources and improving the quality of energy. The general architecture of the monitoring network is shown in Fig. 5. The first step consisted of the installation of the electricity and water meters in the general connections, in the cases that were necessary, transmitting and receiving antennas were enabled to send the information to the data acquisition system. These meters were then connected to the data acquisition system to enable the reception and sending of the electric and water consumption records; data is sent according to the type of connection available (ethernet, Wi-Fi or 3G). A screen in the local monitoring system was installed so that general users could monitor the consumption of electricity and water in real time.

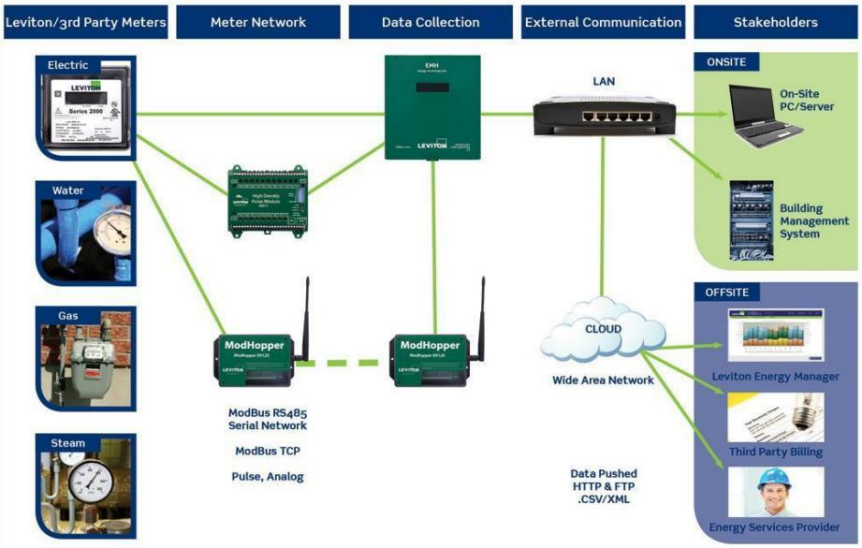

Fig. 5. Diagram of network architecture (source: Leviton, 2017 [2]).

2.3 Replacement of Infrastructure and Equipment

The installation of energy saving equipment in each of the IPN instances included several actions: replacement of high-energy consumption luminaires by low-energy consumption LED luminaires, replacement of high-energy consumption hand dryers with low-energy consumption hand dryers, replacement of obsolete and high-energy consumption air conditioning with low-energy consumption air conditioning system, installation of solar PV powered luminaries, among other actions. A summary of the

actions carried out in each instance is given in Table 1. A view of some of the installed equipment is shown in Fig. 6.

Table 1. Summary of the replaced Equipment.

Instance	Replaced equipment	Quantity
CIC	Luminaire, hand dryers and air conditioning	2,048 LED luminaires 12 hand dryers 1 air conditioner
CIDETEC	Hand dryers, presence sensors, luminaires and smart bars	6 hand dryers 11 presence sensors 337 LED luminaires 30 smart bars
ESCOM	Solar LED luminaires, luminaires, photocells and time-curlers	441 PV luminaires 200 LED luminaires 50 photocells 50 timers

Fig. 6. Replacement of luminaries, PV luminaries and low consumption hand drier.

2.4 Baseline of electricity consumption

The averaged electrical energy consumption (KWh) per day, per month and per year, at CIC, CIDETEC and ESCOM were obtained using data collected by the installed monitoring network and registered in the SEEDS platform. It should be mentioned that the data used correspond to a period of four months (November-December 2018 and January-February 2019). The results obtained are summarized in Table 2. As can be seen, the most power-hungry instance is CIC, this is mainly because this Centre host a Computing Site which is operational 24 hrs, the 365 days of the year.

Table 2. Averaged, daily, monthly and annual electricity consumption.

Instance	Averaged daily consumption (KWh)	Averaged monthly consumption (KWh)	Averaged annual Consumption (KWh)
CIC	2,285	68,453	821,435
CIDETEC	276	8,279	99,348
ESCOM	1,383	41,341	496,094

3 Installation of Solar PV Electricity Generation Systems.

In order to reduce the consumption of electric energy, and to reduce the carbon footprint, the company Greensun [3], carried out the design of the projects and performed the installation of three solar PV electricity generation systems, one in each of the instances considered (CIC, CIDETEC, ESCOM). Table 3 presents a summary of the Installed solar PV systems. Figs. 7 to 9 show some views of the installed PV systems in each of the instances considered. The total power generation capacity considering the three FV systems is 126.72 KW, with a total of 352 PV panels and 7 inverters.

Table 3. Solar PV systems installed at CIC, CIDETEC and ESCOM.

Characteristic	CIC	CIDETEC	ESCOM
Generation power	66.96 KW	15.12 KW	44.64 KW
Number of PV panels, brand, power	186, Canadian Solar CS3U, 360 W	42, Canadian Solar CS3U, 360 W	124, Canadian Solar CS3U, 360 W
Number of inverters, brand, power	3, Fronius Symo, 22.7 KW	1, Fronius Symo, 15 KW	3, Fronius Symo, 22.7 KW
Daily average power generation	280.9 KWh	63.4 KWh	187.24 KWh
Annual power generation	102.52 MWh	23.14MWh	68.34MWh
Daily electricity consumption (SEEDS)	2,285 KWh	276 KWh	1,383 KWh
Percentage of demand covered	12.29%	22.97%	13.53%

Fig. 7. Solar FV system installed at CIC-IPN.

Fig. 8. Solar FV system installed at CIDETEC-IPN.

Fig. 9. Solar FV system installed at ESCOM-IPN.

4 Quantification of Savings

In this section the quantification of electricity savings, cost savings and reduction of carbon footprint are presented. These savings are due to the implementation of operational measures including PV electricity generation and technological replacement of energy-hungry equipment. These savings were calculated using data of electricity consumption corresponding to the months of November 2018, December 2018, January 2019 and February 2019. The quantifications of the electricity savings in each instance considered are shown in Table 4. The quantifications of the corresponding economic savings in each instance considered are shown in Table 5. Finally, the quantification of the reduction of the carbon footprint in each instance considered are shown in Table 6. Notice that in the case of the carbon footprint, values are obtained in tonnes of carbon dioxide equivalent (tCO2e) [4]. Also, it is necessary to specify that the carbon footprint and savings were calculated considering only the electricity consumption and electricity savings due to PV electricity generation and technology substitutions.

According to the data provided by the Energy Regulatory Commission (CER) of the Mexican Federal Public Administration as a regulatory body on energy matters and with the opinion of the Secretary of Environment and Natural Resources (SEMARNAT), established that the National Electric System Emission Factor for 2017 is 0.527 tonnes of CO2 / MWh.

Hence, the calculation of the reduction in the number of tonnes of CO2 equivalent (tCO2e) is a direct function of the total electricity consumption of the IPN instances, specified in MegaWattsHora.

Table 4. Quantification of electricity savings at CIC, CIDETEC and ESCOM.

Instance	Average monthly consumption before the implementation of savings measures (KWh)	Average monthly consumption after the implementation of savings measures (KWh)	Average monthly savings in KWh	% Average monthly electricity savings
CIC	68,453	54,632.34	13,820.66	20.19
CIDETEC	8,279	3,551.76	4,727.24	57.1
ESCOM	41,341	34,177.92	7,163.08	17.33
TOTAL	118,073	92,362.02	25,710.98	31.54

Table 5. Quantification of economic savings at CIC, CIDETEC and ESCOM.

Instance	Average monthly cost for electricity consumption before the implementation of savings measures (MXN)	Average monthly cost for electricity consumption after the implementation of savings measures (MXN)	Average monthly economic savings in MXN	% Average monthly economic savings
CIC	68,453	54,632.34	13,820.66	20.19
CIDETEC	8,279	3,551.76	4,727.24	57.1
ESCOM	41,341	34,177.92	7,163.08	17.33
TOTAL	118,073	92,362.02	25,710.98	31.54

With the use of the monitoring network and through the SEEDS platform, the electricity consumption in MegaWatts / Month was obtained for the months of October, November and December 2018, as well as for the months of January, February and March of 2019, for the three instances considered (CIC, CIDETEC, ESCOM). In the months of April to December 2019, an average estimated consumption value of the previous months measured with the monitoring network was used and the savings obtained due to operational measures of technological substitution and energy generation were subtracted, this is:

$$CME = Average\ (CMA\_SMT)\ -AED\_LSAA-EGVPS \quad (1)$$

where:
CME = Estimated Monthly Consumption
CMA_SMT = Previous Months consumption obtained through monitoring network
AED_LSAA = Estimated Savings LSAA Devices (Luminaires, Dryers, Air Conditioning)
EGVPS = Energy Generated Via Solar Panels

Table 6 shows the results obtained, which are also plotted in Fig. 10. The global savings are summarized in Table 7.

Table 6. Quantification of carbon footprint reduction at CIC, CIDETEC and ESCOM.

Instance	Average monthly emissions before the implementation of savings measures (tCO2e)	Average monthly emissions after the implementation of savings measures (tCO2e)	Average monthly emissions reduction (tCO2e)	% Average monthly emissions reduction (tCO2e)
CIC	36.9	26.13	10.77	29.19
CIDETEC	4.44	1.86	2.58	58.11
ESCOM	20.78	15.82	4.96	23.87
TOTAL	62.12	43.81	18.31	37.06

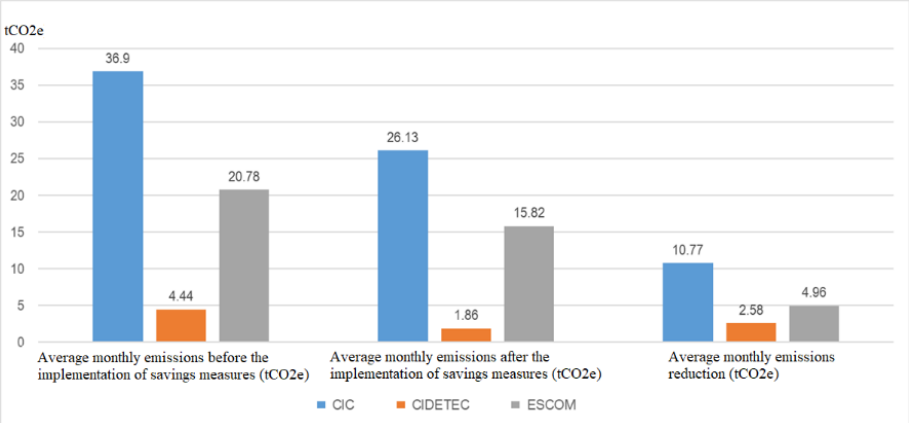

Fig. 10. Carbon footprint reduction at CIC, CIDETEC and ESCOM.

Table 7. Global savings at CIC, CIDETEC and ESCOM.

	Electricity consumption savings in KWh	Saving cost for electricity consumption in MXN	Reduction of emissions of tCO2
Overall monthly average savings	25,710.98	42,651.96	18.31
% Equivalent	31.54	35.45	37.06

5 Conclusions

Derived from the analysis of the information collected by the installed monitoring network and using the SEEDS platform, it was possible to perform the quantification of the savings generated by the operational measures of technological substitution and the implementation of PV systems for the generation of electricity from a renewable energy source in three IPN units, reducing the environmental impact, the carbon footprint and also reducing the consumption and dependence of electricity generated by fossil fuels.

The quantifications made indicate an average monthly savings in consumption of 25,710.98 KWh, corresponding to 31.54% of the average monthly electricity consumption. In economic terms, this is equivalent to an average monthly savings for electricity consumption costs of $ 42,651.96 (MXN), equivalent to 35.45% of the average monthly total cost per electricity consumption in the three IPN instances. Finally, in terms of the reduction of the carbon footprint, expressed in the non-production of equivalent tonnes of CO2 (tCO2e), it corresponds to 18.31 tCO2e, which represent 37.06% of the total generation of tCO2e before the implementation of the measures of technological substitution and generation of electric energy from renewable sources.

The reduction in the consumption of electric energy, as well as the corresponding economic savings and reduction of equivalent CO2 emissions quantified so far, and whose measurement is maintained in the temporality specified in this work, gives the guideline to continue monitoring the information through the SEEDS platform installed in three IPN instances. It will be necessary to obtain the statistics to ratify that the operational measures of technological substitution and electricity generation provide substantial savings to IPN. If the trend of the figures obtained so far continues, then there will be enough information to recommend the route to improve the performance of other IPN instances by the gradual incorporation of technologies for sustainable development.

Acknowledgments

This work was supported by Fondo Sectorial CONACYT-SENER Sustentabilidad Energética, under project grant 264087.

References

1. Coordinación Politécnica para la Sustentabilidad Homepage, https://www.ipn.mx/sustentabilidad/, last accessed 2019/09/01.
2. Leviton Homepage, https://www.leviton.com, last accessed 2019/09/01.
3. Greensun Homepage, http://www.greensun.com.mx, last accessed 2019/09/01.
4. The Carbon Trust: Carbon footprintin, online at https://www.carbontrust.com/resources/guides/carbon-footprinting-and-reporting/carbon-footprinting/#download-guide, last accessed 2019/09/01.

Implementation of a smart microgrid in a small museum: the Silk House

Luís Guilherme Aguiar Figueiredo[1,3][0000−0002−7085−4568], Wellington Maidana[1,2][0000−0002−5361−3850] and Vicente Leite[1,2][0000−0002−8790−519X]

[1] Instituto Politécnico de Bragança, Campus Santa Apolónia, Bragança, Portugal
[2] Research Center in Digitalization and Intelligent Robotics (CeDRI)
[3] Universidade Tecnológica Federal do Paraná, Cornélio Procópio, Paraná, Brasil
guilhermeaguiar_f@hotmail.com, maidana@ipb.pt, avtl@ipb.pt

Abstract. Microgrids are an alternative approach for the supply of energy integrating decentralized power sources, electrical loads, energy storage, and management in a local grid. The system has the capability of power control and energy management using communications' network between all devices, and is known as smart microgrid. This paper presents the implementation of an smart microgrid in the Silk House, a museum dedicated to dissemination of science located in Bragança, Portugal. It was funded by the Foundation for Science and Technology of Portugal under the SilkHouse Project. The goal is to transform the House of Silk in a self-sustainable museum contributing to the dissemination of renewable sources and new technologies for future buildings in smart cities. This work presents the context and requirements for the microgrid and describes the implementation of the renewable sources (photovoltaic and pico-hydro) and the SMA Flexible Storage System based on Sunny Island and Sunny Home Manager. This work also presents and analysis the first operating results since the start of operation at the end of July 2019.

Keywords: Microgrids · Renewable sources · Energy management.

1 Introduction

The worldwide need for more electricity results in a demand that grew at a rate of 2.9% in 2018, which is supplied by fossil fuels [1] [2]. Despite this growth, the use of fossil fuels has been debated continuously, nowadays, for its consequences, such as 2% carbon emissions growth - the highest in seven years [1]. Environmental concerns related to these issues have been changing the behavior on the use of energy sources, which is increasingly adopting the use of renewable sources to generate electricity and supply the growing demand. Renewable sources lead to an increase in world power generation, with the growth of 14.5% [1].

The main primary sources of renewable energy, among the many available, are solar, wind, and hydro. The distributed generation of this energy brings environmental, technical, and economic benefits to the consumers and the

distributions systems. Microgrids are a recent concept for the integration of renewable sources in the power grid.

A microgrid and the conventional distribution power system have basic differences [3]. The first has smaller generation capacity of the sources, the generated power is directly injected to the grid, and the sources are closer to the consumers. The concept of microgrid has several descriptions in the literature, but there is not a specific one adopted. In [3], a microgrid is essentially described as an active distribution network, because integrates distributed generation and different loads at the distribution voltage level. In [4] microgrid is described as an interconnected system of loads and a local generation that can operate independently of the power grid (off-grid) or is tied to it (on-grid). In short, microgrid is a distributed generation network, integrating renewable sources (or not), connected to loads (which are usually close to each other), with energy storage capacity, and with a management system (with higher or lower intelligence level), that can supply the electrical demand of a house, a building or a region. It may (or not) be connected to the conventional grid.

This paper presents the implementation of a smart microgrid in a small museum called Silk House. The microgrid integrates renewable sources, energy storage, and management system. It is connected to the main grid as an additional external source. The project aims to ensure the self-sustainability of the museum, in annual average terms. It will also be a showcase to spread to the society the use of local resources to produce renewable energy and the new technologies of microgrids for smart cities. The microgrid was installed, commissioned, tested, and is being monitored. The first results of its operation are shown and analyzed in this work.

2 Silk House

Silk House is part of the *Centro de Ciência Viva*, located in Bragança, in the north-eastern of Portugal. This place was used for dyeing silk in the 18th century and sometime later, during the 19th and 20th centuries was used as a mill. The Municipality of Bragança acquired the building in 1990 and restored it in 2006, maintaining the original constructive characteristics [5].

Nowadays, the place is a museum dedicated to the history of silk, with a permanent exhibit about it and to the dissemination of science, receiving about 11500 visitors per year. Exhibitions, lectures, and courses about several themes are frequent on-site.

The building is located in the historical center of the city, next to the Fervença river and conserves the historical architecture built of original stones. It has three levels, two galleries on the basement at river level, and a roof with ceramic tiles.

Before implementing the microgrid, the building's three-phase electrical system (400 V, 50 Hz) was powered by the mains, with a contracted power of 13.8 kW. The electrical loads are, basically, computers, monitors, multimedia projectors, heaters, air-conditioning system, a stereo system, and lighting. The regular operation of the museum is from Tuesday to Sunday, from 10 a.m. to 6 p.m.. It

closes on Mondays, but some essential loads remain powered. The average daily consumption is 45 kWh in normal working days, and the annual average is about 16000 kWh [5].

3 Previous microgrids developed

The SilkHouse Project - Development of a smart microgrid based on renewable energy sources and a monitoring system for the House of Silk - is promoted by the Polytechnic Institute of Bragança (IPB), in cooperation with four other partners: Bragança Ciência Viva Center, Cávado e Ave Polytechnic Institute, Guarda Polytechnic Institute and the company JG Instalações Elétricas. The project is funded by the European Union through the Foundation for Science and Technology, supported by the Municipality of Bragança.

The SilkHouse project development started in 2017 with the first conceptual design [6]. The microgrid design took into account the analysis of two places of the building for the energy potential: the roof and the original galleries used by the former mill. They revealed viability for renewable energy generation using endogenous resources: solar irradiance and water, respectively. The roof is used to generate photovoltaic (PV) energy. The water and galleries are used to generate hydropower taking advantage of the proximity of a small dam already available in Fervença river [5]. Thus, the Silk House was provided with a smart microgrid by integrating both energy sources and energy storage in a microgrid with a management system. The renewable sources and storage system were size considering the annual energy consumption of the building [7].

The project uses SMA technology and is based on the Sunny Island inverters and Sunny Home Manager. Previous experience, with a small microgrid held in a laboratory of the School of Technology and Management of the IPB, demonstrated the feasibility and flexibility of this technology [8] [9]. Based on these works and surveys aiming the application to the Silk House, it was designed the first schematic to the microgrid [6], as shown in Fig. 1. The following equipment composed the solution: three Sunny Island Inverters (SI), four Sunny Boy inverters (SB), one pico-hydro turbine, photovoltaic tiles, photovoltaic modules, battery bank, and an undefined control system [6].

The design was changed in a second phase. In fact, the use of PV tiles would be too expensive. On the other hand, tests achieved with 30 PV tiles (ZEP F10-U 9Wp) in the laboratory revealed the existence of shadow caused by the tiles themselves, in the morning and the afternoon [7]. Therefore, the project adopted high-efficiency PV modules instead of PV tiles.

Fig. 2 presents the second microgrid design composed by: three Sunny Island inverters, five Sunny Boy inverters, one Sunny Home Manager 2.0, twenty four 2 V batteries blocks to form a 48 V battery bank, eighteen PV modules, a water wheel for electricity generation, a pico-hydro turbine, electrical board with protections, and breaking devices [7].

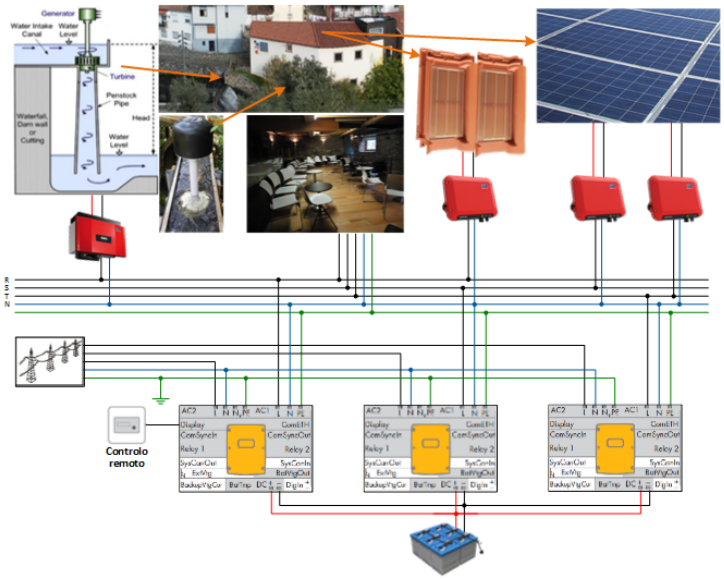

Fig. 1. First microgrid conceptual design [6].

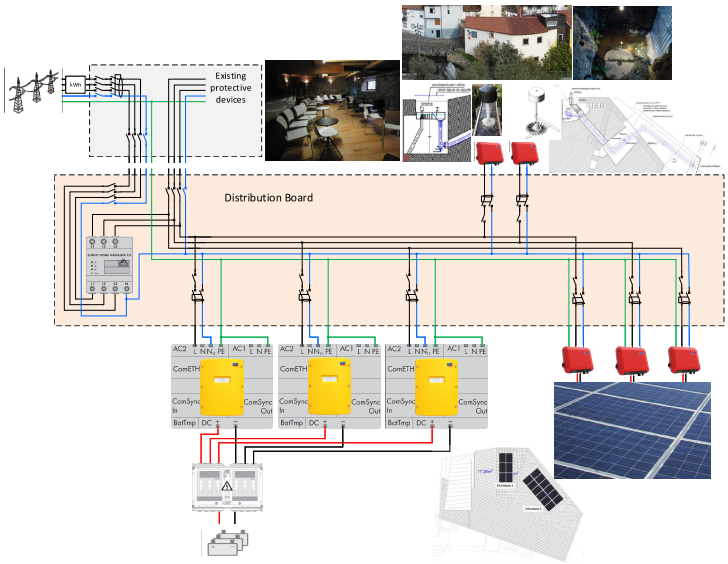

Fig. 2. Second microgrid conceptual design [7].

4 Microgrid implemented

The microgrid implemented in the House of Silk has some specific requirements considered during the project development. The first one is that the museum

is supposed to be self-sustainable. In other words, in annual average terms, the energy produced by the renewable sources must be equal to the energy consumed. Second, the electric grid must be an external energy source, but the energy injected into it must be zero. Hence, a third requirement is the energy storage in order to improve the self-consumption and self-sufficiency quotas [7] [10]. Fourth, the generated energy from renewable sources - photovoltaic and pico-hydro - should use innovative solutions. Indeed, the pico-hydro embraces an innovative approach, which will use a PV inverter and a microinverter as the interface between turbines' generators and the microgrid [11] [12]. Fifth, power management and monitoring system are required since this project is intended to be a permanent activity of the museum aiming the dissemination of the new technologies of microgrids for smart cities.

4.1 Silk House microgrid

This section introduces the smart microgrid developed according to the above requirements. The microgrid integrates distributed generation (PV and pico-hydro), energy storage based on the battery bank, management, and monitoring system. It is three-phase (400 V, 50 Hz) microgrid to supply the House of Silk loads.

The smart microgrid is based on the SMA Flexible Storage System with battery-backup and increased of self-consumption [13]. It is composed by three Sunny Island 4.4M, three PV inverters Sunny Boy 1.5, one Sunny Home Manager 2.0, two SMA Energy Meter, three strings of six Panasonic's PV modules VBHN325SJ47, one 300 W horizontal water wheel to recover the historical heritage of the former mill, one low-head turbine (LH400 from PowerSpout), one PV microinverter, one PV inverter, a battery bank consisting of twenty four VRLA 2 V battery's blocks Sonnenschein's batteries A602/625 Solar, battery fuse, electrical panel, automatic transfer switch, and protections. Fig. 3 presents a circuity overview of the smart microgrid implemented in the House of Silk and Fig. 4 shows the Silk House building with the PV modules installed and the microgrid devices. It is in full operation with the PV generation. By the time this work was written, the low-head pico-hydro system was being installed, and the water wheel was under construction.

The operation of the microgrid can be described as follows. The three-phase microgrid is the external electric grid whenever it is available. If the case of grid failure, the microgrid is established by the three Sunny Island (SI) 4.4M connected in a master-slave configuration. An automatic transfer switch is responsible by the external grid connection or disconnection [13]. The energy generated by the PV strings is injected into the microgrid, distributing the power by the three phases using three Sunny Boy 1.5.

When the generation is higher than the consumption, the excess of energy is stored in the battery bank by the three bi-directional battery inverters, SI. These inverters use the batteries to control the power flow and, thus, to improve self-consumption [14]. The active power generated by the inverters connected to the PV strings is limited by frequency control [15], as better explained later.

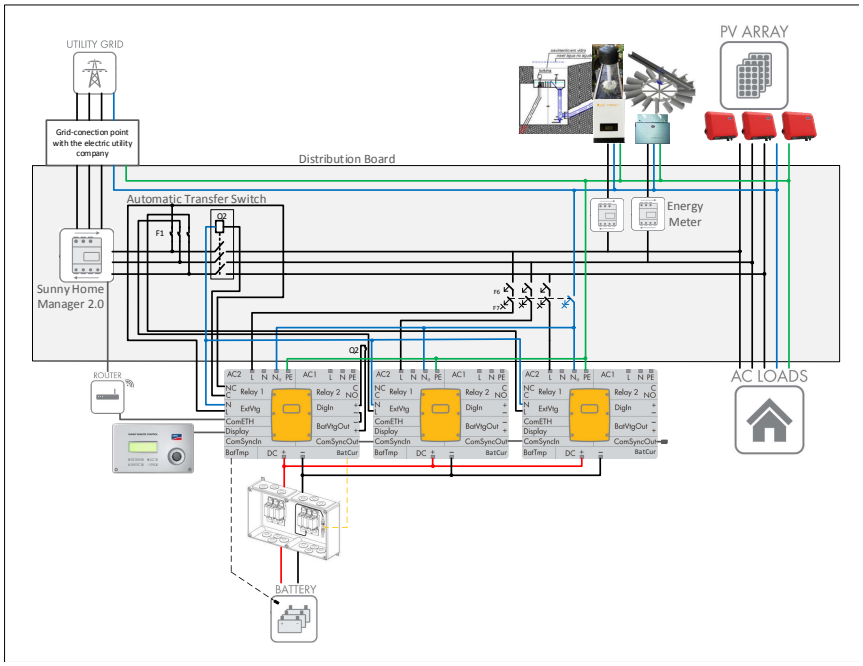

Fig. 3. Microgrid implemented in the Silk House.

Fig. 4. (a) Silk House, (b) Microgrid devices.

This happens whenever the generation is higher than consumption, the batteries are charged, and the energy fed into the external grid must be zero.

When the consumption is higher than the generation, the energy comes from the batteries and, if it is not enough, the remaining energy is purchased from the external grid to feed the loads. In case of grid failure, the microgrid is disconnected from the grid using the automatic transfer switch and starts working in stand-alone mode. In this operation mode, some hours of autonomy are available, but it strongly depends on the consumption, the generation, and

the battery bank state of charge. In this case, some loads can be automatically disconnected.

4.2 Photovoltaic system

The photovoltaic system consists of three strings with six PV modules each and was installed on the roof with a slope of 12º and two shadowless areas. The first is oriented South and the second is oriented Southwest. Taking advantage of this, the PV strings were divided by these two roof surfaces to improve the distribution of PV generation throughout the day. One PV string is oriented South and the other two are oriented Southwest. In the morning, the Southern oriented string starts the generation before than the Southwestern oriented ones, allowing a higher production. In the afternoon, the Southwestern oriented strings will extend their generation longer. These orientations make possible to improve the distribution of photovoltaic generation throughout the day, adjusting it to the opening hours of the museum.

The modules chosen are from Panasonic, model VBHN325SJ47, series HIT with 19.7% efficiency [16]. The maximum power (P_{max}) is 325 W, and the maximum total to the system is 5.85 kW. Each string is connected to a SMA Sunny Boy 1.5-1 VL 40 (SB) PV inverter [17] which, in turn, is connected to one of three phases (L1, L2, L3). This inverter is compatible with the active output power control by the microgrid frequency control, as explained later.

4.3 Pico-hydro system

The Silk House electric generation will be complemented, mainly in the winter periods, by two pico-hydro systems that are being installed. These systems are small-scale hydropower generation units up to 5 kW that converts the power of flowing water of a canal, river or stream in electricity [18]. These low power systems, but capable of producing energy 24 hours a day, unlike what happened until a few years ago, it is possible to use permanent magnet synchronous generators, with variable speed, depending on the flow rate and head [19] [20]. This happens because innovative results show that the energy produced can be harnessed using PV inverters, flexibly, and efficiently [19] [20]. Furthermore, those generators and PV string inverters and micro-inverters are, nowadays, off-the-shelf and widely available components used in wind and photovoltaic applications.

The installation of the hydroelectric plant results from the proximity of the Silk House of the river Fervença, the existence of a small dam (less than 10 m) and the hydraulic infrastructure of the old mill, channels, and galleries, which has been conserved. On the one hand, the adopted solution preserves the building's architecture and, on the other, it recovers the building's historical heritage by installing a horizontal water wheel to produce energy in place of the former mill [7]. There are two galleries available. The first, at the upper level, was used to install the microgrid equipment. The other, where the mill was located, a 300 W horizontal water wheel and a 1.2 kW low-head turbine (LH400 from PowerSpout)

are being installed. Two pipes were installed to capture water from the small dam and take it inside the gallery where the water wheel and turbine will be. The water is returned to the river 18 m downstream.

A PV microinverter from GWL Power [21] and a PV string inverter from Omnik, model Omniksol - 1.5k - TL2 [22], are used to connect the 300 W generator of the water wheel and the 1.2 kW generator of the low-head turbine to the microgrid, respectively. After extensive tests in the laboratory, the results show that the inverters presenting the best performance are not from SMA. Because of this, SMA Energy Meters must be used in order to account the energy produced by these renewable resources in microgrid energy management.

4.4 Microgrid power management

A smart system requires high-level control and a suitable communications' network. SMA technology has monitoring of the energy generated and also controls and regulates all the microgrid through a digital interface using the Internet portal Sunny Portal. The infrastructure should contain devices sharing the communications' network to turn the microgrid in a smart microgrid, being integrated into intelligent energy management.

SMA's devices have an integrated technology called Speedwire, which enables communication among each device used. It is a wired Ethernet communication for networks used in decentralized power generation, with a communication protocol optimized for PV systems [23]. The devices in this microgrid are connected to an Ethernet switch by UTP cables, which allows having Speedwire communication.

The Sunny Home Manager 2.0 (SHM) acts as a centralized energy manager in households with a PV system for self-consumption [24]. It receives data from other devices, as Sunny Boy and Sunny Island inverters and offers some functions which allow taking decisions about the microgrid.

The SHM carries out some important tasks [10], such as data collection of energy and power measured, energy monitoring via Sunny Portal presenting energy flows, energy management, dynamic limiting of the active power feed-in and support to self-consumption increase and its optimization.

The power management occurs when some decision of the microgrid is taken to control the generated energy. The SHM is capable of doing this and measuring the loads at the grid-connection point. This measure is presented in Sunny Portal, which also allows visualizing instantaneous data of the PV generation received via the integrated measuring device of the SB, the battery bank status connected to the SIs, and others SMA Flexible Storage System's devices connected to the local network.

An important parametrization of the microgrid is the limitation of active power supplied to the utility grid. This limit was set in 0 W (Zero Export), which means that the smart microgrid can not provide the generated energy to the utility grid and all the power should be stored or consumed by the microgrid loads (self-consumption system) [10].

When the generation is larger than the loads' consumption, efficient management is required of the microgrid power flow. The first step is to inject

the excess power into the battery bank. If it is fully charged, the SI detects this situation and increases the frequency of the microgrid in order to limit the output power the SB inverters. The control strategy adopted by SMA called "frequency-dependent control of active power" to limit the power generated whenever it is excessive. The SI increases the frequency of the microgrid above the nominal value (50 Hz). The PV inverter must be compatible with this control. In this case, when they feel the frequency increase, they start to reduce the active output power out. If the frequency continues to increase, PV inverters further reduce its active power nearly to 0 W, as shown in Fig. 5. The SB inverters continue to monitor the frequency. When it decreases, they start increasing their active power linearly to the available value [25]. Fig. 5 shows the active power control by frequency, and Table 1 shows an example of this frequency control.

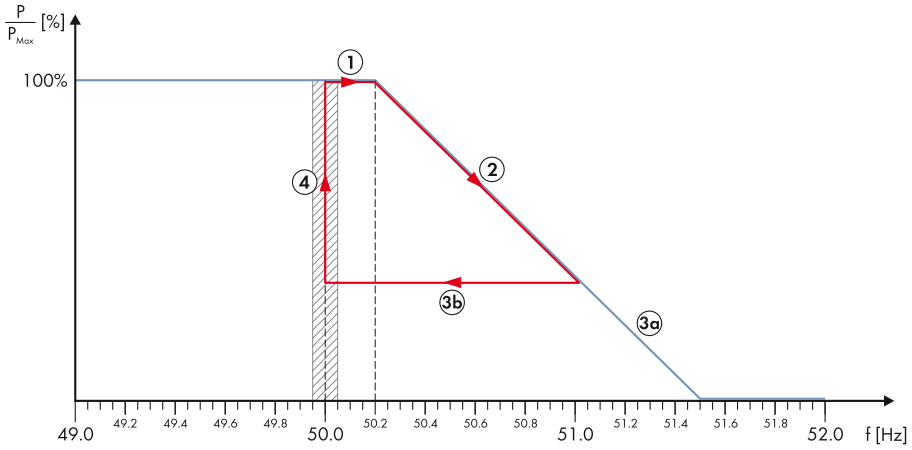

Fig. 5. Control of active power by frequency control [25].

Table 1. Example of the frequency values for the each positions in control of active power by frequency in Fig. 5.

Position	Stage	Frequency (Hz)
1	Normal operation	<50.2
2	Active power decreases linearly from maximum available power	>50.2
3a	Active power continues to decrease linearly up to 0 W	51.5>Freq.>50.2
3b	Frequency remains constant or returns to the nominal value PV inverter stops reducing active power	<51.5
4	Active power increases up to maximum available power	50.05

5 Analysis of operation

This section presents the first results obtained immediately following the implementation and commissioning of the microgrid in the Silk House. Now, it is possible to see the microgrid operation by analyzing several data and graphics obtained via Sunny Portal. The smart microgrid with PV generation is in operation since the end of July. The operation with pico-hydro generation will be available during the next months, once it is being installed.

Fig. 6 shows an energy balance, the temporal progress during the August 8th, 2019. The consumption graph shows when and from which sources the microgrid has been supplied with energy (photovoltaic, battery bank or utility grid). The generation graph shows when and how much energy was generated and how much is used for (direct consumption, battery charging, or greed feed-in).

On August 8th, 2019, the self-consumption rate was 100%, shown in Fig. 6, which means that all the energy generated was used on-site (for loads and battery-bank charging) and not fed into the utility grid as expected considering the requirements of this microgrid [26]. However, it should be noted that if the system allowed to feed into the utility grid, the self-consumption rate would be about 50 - 60% for this microgrid [7]. Direct consumption, which was 79%, corresponds to photovoltaic energy used directly in the loads. A minimum feed into the utility grid is inevitable and was 0.9 kWh feed-in. Table 2 presents some relevant data about the energy balance demonstrating the real operation of the microgrid on that day.

Table 2. Energy balance data of August 8th, 2019.

Balance	Energy (kWh)
Daily consumption	19.31
Daily yield	22.17
External Energy supply	0.09
Internal power supply	19.22
Battery discharging	1.60
Battery charging	4.60
Direct consumption	17.62
Self-consumption	22.11

Fig. 7 shows the production diagram of the three PV strings connected to the microgrid. It shows that the way they were installed, with different orientations, even though small, allows distributing better the energy generated throughout the day. It is worth mentioning this is important when the excess of power should be immediately consumed or stored, not supplied to the utility grid. The curves of SBs 2 and 3 show the PV generation prolongation between 6 p.m to 8 p.m., while the SB 1 generation is higher around 9 a.m.. During the rest of the day, the generation was the same to the three SB, i.e., PV strings.

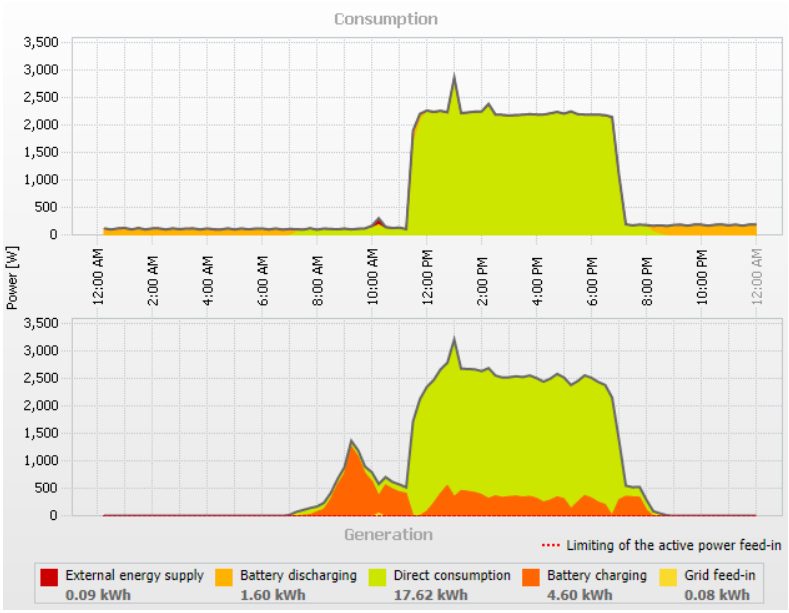

Fig. 6. Energy balance of August 8th, 2019.

In addition, the operation of active power control adopted by the frequency of the microgrid is also evident, as the maximum power generation was not achieved. This was because of the fact that consumption was lower than an electric generation.

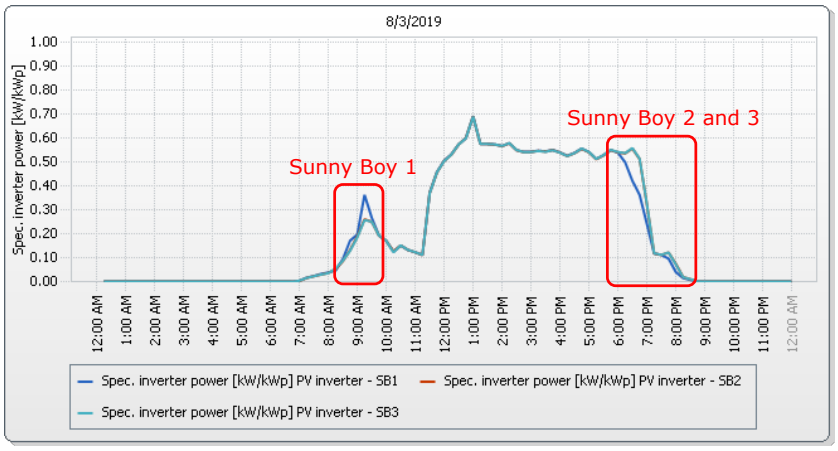

Fig. 7. Photovoltaic generation analysis of August 8th, 2019.

Fig. 8 shows PV generation during the week of August 2 - 8, 2019. On Mondays, the museum is closed and therefore has less consumption. This is visible on the curve of August 5^{th}, during which production was the lowest. That week, the three PV strings produced 255 kWh. It is worth remembering that PV generation depends on the consumption of the loads, and energy stored, and not just on the available solar radiation. This results from the control of the active power generated by frequency control, as there is no energy supplied to the utility grid.

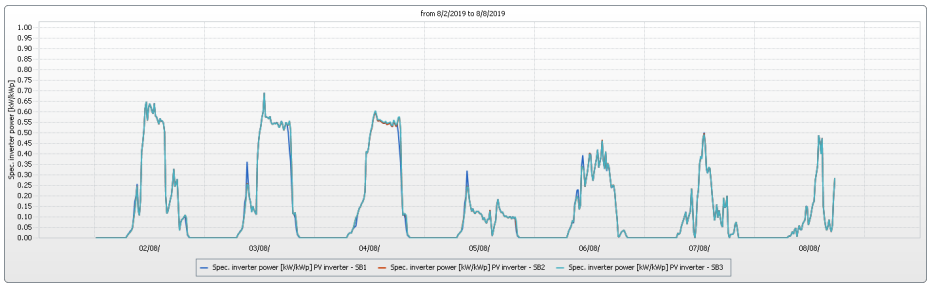

Fig. 8. Photovoltaic generation analysis during the week August 2 - 8, 2019.

An interesting data also available are the 174 kg avoided CO_2 during two weeks of operation. This information represents an avoided value of gas emissions into the atmosphere, given the operation of this building.

6 Conclusions

A smart microgrid was installed and commissioned in the Silk House. The Silk House of the Bragança Ciência Viva Center is a small museum dedicated to science dissemination located in Bragança, Portugal. It was carried out under the project SilkHouse funded by the Foundation of Science and Technology. This project aims to transform the House of Silk in a self-sustainable museum, in annual average terms, and contribute to the dissemination of renewable sources and new technologies for future buildings in smart cities.

The microgrid is based on SMA Flexible Storage System with battery-backup and increased self-consumption. The global system includes renewable energy generation, energy storage in a battery bank, energy consumption by the Silk House loads, power and energy management, and monitoring. The generation is obtained from local renewable resources: solar photovoltaic and pico-hydro, taking advantage of Fervença river and a small dam less than 10 m away. Pico-hydro systems are small-scale power plants (less than 5 kW). In the Silk House, they are a 300 W horizontal water wheel (to recover the historical heritage of a former mill) and a 1.2 kW low-head propeller turbine. These small plants are to be finished in the next months, and the rest of the microgrid was installed and

commissioned and is in full operation since the end of July 2019. The microgrid is connected to the utility grid as an external source but not for power injection. This paper presented the microgrid implementation and analyzed the first results of its operation

Acknowledgments

The authors would like to thank FCT (Foundation of Science and Technology, Portugal) for the financial support through the contract SAICT-POL/24376/2016 (POCI-01-0145-FEDER-024376); The Municipality of Bragança for its support; and the partnership between IPB and UTFPR (Federal University of Technology - Paraná) under the education and research program.

References

1. BP: BP Statistical Review of World Energy 2019. ed. 68. https://www.bp.com/content/dam/bp/business-sites/en/global/corporate/pdfs/energy-economics/statistical-review/bp-stats-review-2019-full-report.pdf. Last accessed 26 Aug 2019.
2. Fatima, H. Prabaharan, N. Palanisamy, A. Kalam, S. Mekhilef. and Justo, J. J. Justo:Hybrid-Renewable Energy Systems in Microgrids: Integration, Developments and Control. Woodhead Publishing, 2018.
3. IRE Series: Microgrids and active distribution networks. The institution of Engineering and Technology, 2009.
4. Farhangi, H: Smart Microgrids: Lessons from Campus Microgrid Design and Implementation. CRC Press, 2016.
5. Maidana, W. Leite, V. Ferreira, A. Queijo, L. Batista, J. Bonaldo, J. Golnçalves, E.:Design of a Self-sustainable System Based on Renewable Energy Sources for a Small Museum of Science Dissemination - the House of Silk. III Congresso Ibero-Americano de Empreendedorismo, Energia, Ambiente e Tecnologia, 12-14 July 2017.
6. Maidana, Wellington: Conceção de um Sistema Autossustentável para um Edifício de Divulgação de Ciência: A Casa da Seda. Master dissertation. Polytechnic Instute of Bragança, Bragança, Portugal, 2017.
7. Silva, M. Leite, V. Araújo, P. Simões, A. Dalmarco, I. Ferreira, A. Queijo, L.: Designing Innovative Home Energy Systems for Smart Cities: The Silk House Project. Ibero-American Congress of Smart Cities (ICSC-cities2018), September 26-27, 2018.
8. Leite, V. Ferreira, A. Batista, J. Couto, J.: Analysis of the Operation of a Microgrid with Renewable Distributed Generation. III Congreso Iberoamericano sobre Microrredes con Generación Distribuida de Renovables, 1-2 December 2015.
9. Leite, V. Ferreira, A. Batista, J.: On the Implementation of a Microgrid Project with Renewable Distributed Generation. I Congreso Iberoamericano sobre Microrredes con Generación Distribuida de Renovables, 23-24 September 2013.
10. SMA: Planning Guidelines SMA Smart home - The System Solution for Greater Independence. http://files.sma.de/dl/1353/SI-HoMan-PL-en-51.pdf. Last accessed 7 Aug 2019.
11. V. Leite, Â . Ferreira, J. Couto, and J. Batista, "Compatibility analysis of grid-connected pico-hydro systems using conventional photovoltaic inverters," in 2016 18th European Conference on Power Electronics and Applications (EPE'16 ECCE Europe), pp. 1–9, IEEE, 2016.

12. V. Leite, J. Couto, Â . Ferreira, and J. Batista, "A practical approach for grid-connected pico-hydro systems using conventional photovoltaic inverters," in 2016 IEEE International Energy Conference (ENERGYCON), pp. 1–6, IEEE, 2016.
13. SMA: Installation - Quick Reference Guide SMA Flxible Storage System with Battery Backup Function. ed. 3.3. https://files.sma.de/dl/20472/Ersatzstrom-IS-en-33W.pdf. Last accessed 9 Aug 2019.
14. SMA: Operating Manual - Sunny Island 3.0M/4.4M/6.0H/8.0H and Sunny Remote Control. ed. 3.3. https://files.sma.de/dl/17632/SI30M-44M-60H-80H-BE-en-33W.pdf. Last accessed 9 Aug 2019.
15. SMA: Planning Guidelines SMA Flexible storage system with battery-backup function. ed. 3.3. https://files.sma.de/dl/20472/Ersatzstrom-IS-en-33W.pdf. Last accessed 7 Aug 2019.
16. Panasonic: Photovoltaic module HIT VBHN330SJ47/VBHN325SJ47. https://eu-solar.panasonic.net/cps/rde/xbcr/solar_en/VBHN330_325SJ47_EN.pdf. Last accessed 6 Aug 2019.
17. SMA: Operating Manual - Sunny Boy 1.5/2.0/2.5. https://files.sma.de/dl/26198/SBxx-1VL-40-BE-en-13.pdf. Last accessed 6 Aug 2019.
18. Basar, M.F.Ahmad, A. Hasim, N. Sopian, K.:Introduction to the pico hydro power and the status of implementation in Malaysia. IEEE Student Conference on Research and Development, 283-288 (2011).
19. Leite, V. Ferreira, A. Couto, J. Batista, J.: Compatibility analysis of grid-connected pico-hydro systems using conventional photovoltaic inverters.18th European Conference on Power Electronics and Applications (EPE'16 ECCE Europe), 1-9 (2016).
20. Leite, V. Ferreira, A. Couto, J. Batista, J.: A practical approach for grid-connected pico-hydro systems using conventional photovoltaic inverters.IEEE International Energy Conference (ENERGYCON), 1-6 (2016).
21. GWL: GridFree Micro AC Direct Inverter DC-AC 230V. https://www.ev-power.eu/docs/pdf/GWL/GWL-MAC230A-Spec.pdf. Last accessed 25 Sep 2019.
22. Omnik: User Manual - Installation/Operation Omniksol-1k-TL2, Omniksol-1.5k-TL2, Omniksol-2k-TL2, Omniksol-2.5k-TL2-S, Omniksol-3k-TL2-S. https://www.omnik-solar.com/ueditor/net/upload/file/20190122/UserManual_Omniksol-1k&1.5k&2k&2.5k&3k-TL2-S_EN_built-in\%20card_V1.2_20190109.pdf. Last accessed 25 Sep 2019.
23. SMA: Technical Information - SMA Speedwire fieldbus. https://files.sma.de/dl/7680/Speedwire-TI-en-11.pdf. Last accessed 7 Aug 2019.
24. SMA: Operating Manual - Sunny Home Manager 2.0. ed 1.1. https://files.sma.de/dl/29870/HM-20-BE-en-11.pdf. Last accessed 9 Aug 2019.
25. SMA: Planning Guidelines - SMA Flexible Storage System with battery-backup function. ed 2.3. http://www.windandsun.co.uk/media/938530/sma-flexible-storage-system-with-battery-backup-planning-guidelines-v21.pdf. Last accessed 9 Aug 2019.
26. SMA: User Manual - Sunny Home Manager in Sunny Portal. https://files.sma.de/dl/15583/HoMan_Portal-BA-en-21.pdf. Last accessed 8 Aug 2019.

Heterogeneous data optimization for improving energy efficiency in smart buildings

Roberto Casado-Vara[1], David Garca-Retuerta[1] Alvaro Bartolom[1], Zita Vale[2], Fernando De la Prieta[1], and Javier Prieto[1]

[1] University of Salamanca, BISITE Research Group, 37008-Salamanca, Spain, {rober,alvarob96, dvid, fer, javierp}@usal.es

[2] GECAD – Research Group on Intelligent Engineering and Computing for Advanced Innovation and DevelopmentInstitute of Engineering, Polytechnic of Porto (ISEP/IPP), Porto, Portugal; ZAV@isep.ipp.pt

Abstract. As smart buildings use an extensive variety of IoT devices that collect different measurements from the environment in order to monitor the building, the topology can be influenced by the smart building sensors. An extensive variety of sensors imply that the retrieved data will be heterogeneous which can be turned into homogeneous data using complex networking and clustering techniques. We call this process 'IoT slicing'. So on, IoT slicing is based on generating a graph from scratch based on the smart building sensors topology and then visualizing layers from the clustering of the previously created graph. A case study using a smart building temperature control algorithm for evaluation is presented.

Keywords: IoT, Smart buildings, Algorithm design, Temperature control, Complex networks.

1 Introduction

Around 45% of the world's energy is used in the residential sector and 75% of buildings in the European Union (EU) are not designed according to any energy efficiency code [13]. Furthermore, the energy demand of the world is constantly increasing and the lack of solutions can lead to disastrous, global-scale consequences (Figure 1). This is why one of the world's biggest challenges is to increase energy efficiency in buildings and achieve a wide-spread development of smart-buildings. Nevertheless, the energy waste of residential and commercial buildings is still substantially large, due to the fact that current optimization techniques, applied to power systems, are affected negatively by the heterogeneous data gathered by IoT sensors.

Heterogeneous data often presents a series of problems such as low reliability and inaccurate information. Therefore, its use is likely to cause some erroneous results and, eventually, make the system ineffective. One of the foundations for developing an effective system is to preprocess the raw data and transform it into valid data. Consequently, the problem of inefficiency in smart buildings must be

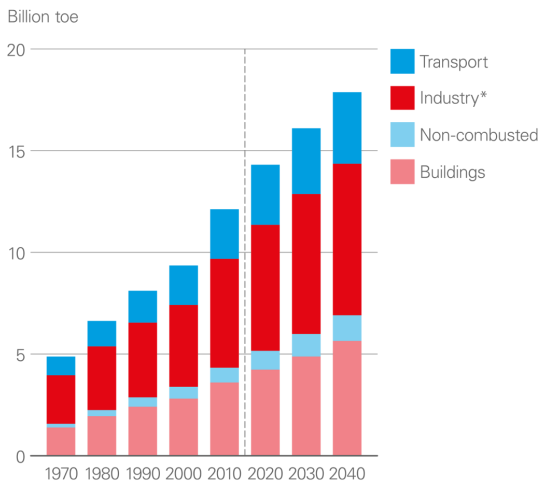

Fig. 1. Primary energy consumption by end-use sector.

dealt with focusing on its foundations; the use of heterogeneous data as inputs of the control systems techniques which are meant to optimise the energy systems of smart homes. Homogeneous data has the potential of increasing the accuracy and, so on, improving the performance of optimization algorithms. In order to achieve this, it is necessary to develop a schema which transforms the heterogeneous data into more reliable, homogeneous data. This schema has the ability of creating more efficient smart buildings [9, 10]. Hence the importance of researching in this field and developing new solutions for improving the monitoring and control task in smart buildings.

As the motivation of this work has already been stated, a detailed description is provided next. The transformation of heterogeneous data gathered by the IoT devices is transformed into homogeneous data according to the topology of the building and the characteristics of the IoT sensors. This proposal is based on the idea of dividing heterogeneous data into homogeneous data layers using a IoT slicing technique [6–8]. A temperature control algorithm has been used in this paper to evaluate the proposal. In addition, a case study is described, whose results show that the proposed algorithm outperforms other methods due to the use of a mixture of graph theory and clustering techniques.

This paper has the following structure: The details of the proposal are presented in Section 2; Section 3 introduces some simulations which results validate the proposal; lastly, Section 4 summarises the obtained results of the research and proposes future lines of work.

2 Network slicing model

This sections tackles the described inaccuracy problem, which emerges as a result of the implementation of temperature control algorithms in IoT nodes that collect heterogeneous data. This research presents a set of mathematical and artificial intelligence techniques with which we have developed an intelligent and self-adaptive model targeted at eliminating the inaccuracy of temperature control algorithms in all types of IoT networks. The scope of this model extends to the very fundamental process of data collection by the IoT nodes. These data are usually heterogeneous (i.e., the temperatures vary considerably from one area of the smart building to another; so do the collected temperature values). The designed model comprehends the following techniques or algorithms:

1. First, a graph is constructed in which the nodes are the IoT nodes and the edges of the graph are the doors or corridors that join those IoT nodes. Since a graph has been built of the IoT network, a complex network can then be built using this graph.
2. We then apply clustering algorithms using the temperature data collected by the nodes of the complex network (i.e., IoT nodes). In this way, heterogeneous data are separated into homogeneous clusters.
3. Next, a multiplex is built in which each of the layers represents one cluster.
4. Multiplex layers that have unconnected networks use virtual nodes to build a related network. In this way, the algorithms can be applied correctly in the next stages.
5. The control algorithms are applied depending on the intended use of the homogeneous data found in each of the layers.
6. Each layer is projected on to the complex network and the control signal is sent to each one of the actuators assigned to the IoT nodes.

2.1 Graph design module

The graph is constructed from the topology of the IoT nodes in the intelligent building. In this way, a graph is formed where the vertices of the graph are the IoT nodes and the edges of the graph are the physical connections between the rooms where the IoT nodes are located (i.e. there is no obstacle between any of the nodes). That is, if there is a door and a corridor between the rooms in which the IoT nodes are located, then there is an edge in the graph. The graph represents the heat transfer between the physically connected rooms. An illustrative example can be found in Fig. 2. This is how we build a graph from the IoT network. Now let's consider this graph as a complex network, also we consider non-directed graphs. Then, we create the *Laplacian matrix* of the graph as follows:

$$A = \begin{cases} 1 \text{ if } (i,j) \in E \\ t_i \text{ if node j = i } (t_i = \text{temperature of the i}th \text{ node}) \\ 0 \text{ otherwise} \end{cases} \tag{1}$$

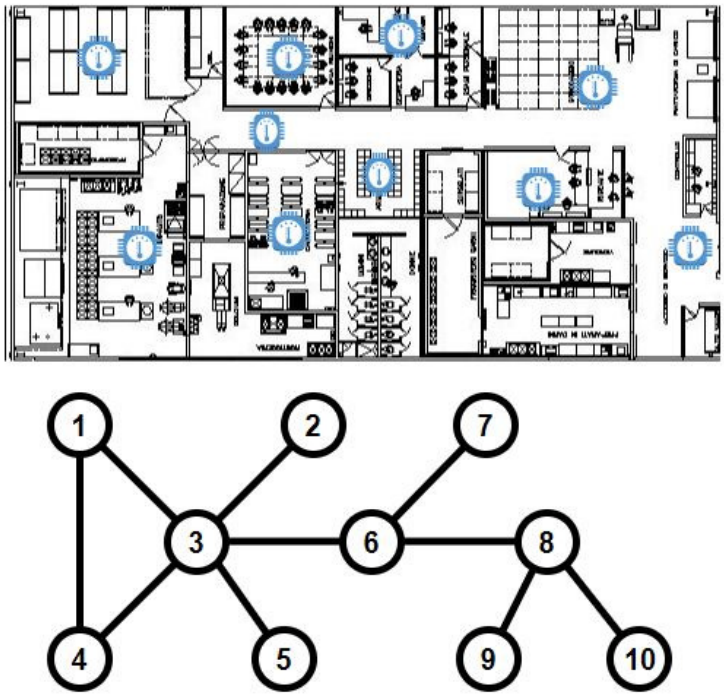

Fig. 2. Illustrative example of the construction of a graph based on the position of the IoT nodes on a map.

where E is the set of edge in the graph. In the example shown in Fig. 2, the *Laplacian matrix* is:

$$A = \begin{pmatrix} t_1 & 0 & 1 & 1 & 0 & 0 & 0 & 0 & 0 & 0 \\ 0 & t_2 & 1 & 0 & 0 & 0 & 0 & 0 & 0 & 0 \\ 1 & 1 & t_3 & 1 & 1 & 1 & 0 & 0 & 0 & 0 \\ 1 & 0 & 1 & t_4 & 0 & 0 & 0 & 0 & 0 & 0 \\ 0 & 0 & 1 & 0 & t_5 & 0 & 0 & 0 & 0 & 0 \\ 0 & 0 & 1 & 0 & 0 & t_6 & 1 & 1 & 0 & 0 \\ 0 & 0 & 0 & 0 & 0 & 1 & t_7 & 0 & 0 & 0 \\ 0 & 0 & 0 & 0 & 0 & 1 & 0 & t_8 & 1 & 1 \\ 0 & 0 & 0 & 0 & 0 & 0 & 0 & 1 & t_9 & 0 \\ 0 & 0 & 0 & 0 & 0 & 0 & 0 & 1 & 0 & t_{10} \end{pmatrix} \tag{2}$$

2.2 Clustering module

The temperature data collected by the IoT network of the smart building are normally heterogeneous. By applying a clustering algorithm, we will separate these data into groups of homogeneous temperatures. Gaussian Mixture Models

(GMMs) give us more flexibility than K-Means. With GMMs we assume that the data points are Gaussian distributed; this is a less restrictive assumption than the k-means algorithm uses the mean to form circular clusters. That way, we have two parameters to describe the shape of the clusters: the mean and the standard deviation. With an appropriate amount of component mixture, it is also possible to estimate almost all continuous probability density functions. Gaussian mixture density is defined as

$$p(x) = \sum_{k=1}^{K} \pi_k N(x|\mu_k, \Sigma_k) \tag{3}$$

where x is a d-dimensional random variable, $N(x|\mu_k, \Sigma_k)$ is a multivariate normal distribution with mean μ_k and covariance matrix Σ_k and π_k are the so-called mixing coefficients for the k components of the distribution $p(x)$ which have to satisfy $0 \leq \pi_k \leq 1$ and $\sum_{k=1}^{K} \pi_k = 1$ to form a convex combination of the mixture components [4]. An illustrative example is shown in Fig. 3. We apply this clustering technique to our 1-dimensional temperature array and the output is the graph with the clusters.

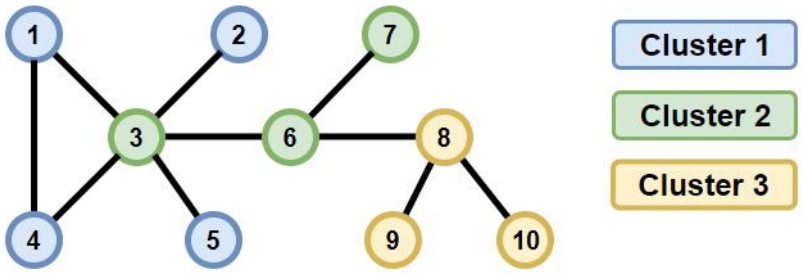

Fig. 3. Example of the application of the GMMs cluster technique to the graph with the temperatures of the IoT network.

2.3 Multiplex module and virtual network module

Multi-layer or multiplex networks can be defined as those that incorporate different connectivity channels, and describe systems that are interconnected with different categories of connection: each channel is represented by a sub-network or layer and the same node can have different types of interactions and a different neighborhood in each layer. Let's formalize the concept of multiplex networks or multilayer networks.

Multi-layer network is a couple $M = (G, E)$ where $G = \{G_\alpha, \alpha = 1, \ldots, M\}$

is a family of graphs $G_\alpha = (N_\alpha, L_\alpha)$ (i.e., layers of the multi-layer network) and $E = \{E_{\alpha\beta} \subset N_\alpha x N_\beta, \quad \alpha \neq \beta\}$ is the set of interconnections between the nodes of the different layers. The E elements are called cross-layers, the L_α elements are called interlayer connections. The set of nodes of each layer is denoted by $N_\alpha = \{n_1^\alpha, \cdots, n_{N^\alpha}^\alpha\}$ and the *Laplacian matrix* of each layer is denoted by $A^{[\alpha]}$.

Once the multiplex is constructed, the connection between each graph and its layer is verified. In case they are not connected, as many virtual nodes are created as necessary to link the graph with the layer i*th*. The virtual nodes are vertices of the graph of other layers, however we act as if it were in that layer for practical purposes . In this way, the graphs will be connected and the control algorithms can be applied subsequently. If there is only one element in a layer, as many vertices of other layers will be virtualized as the amount of edges of a node in the initial graph. In the *Laplacian matrix* we will represent a virtualized node as 1^*.

Applying this definition to the graph that we have constructed in the previous point, we are going to create a multiplex. Each one of the layers of the multiplex is going to be each one of the nodes of the graph that are in the same cluster. To assist in creating the multiplex we are going to create each of the adjacency matrices for each of the layers ($A^{[\alpha_1]}, A^{[\alpha_2]}$ and $A^{[\alpha_3]}$) as follows:

For instance, layer 1 of the multiplex contains only the IoT nodes 1, 2, 4 and 5. Also, we have to create a virtual node to virtualize the IoT node 3.

$$A^{[\alpha_1]} = \left(\begin{array}{ccccc|ccccc} t_1 & 0 & 1^* & 1 & 0 & 0 & 0 & 0 & 0 & 0 \\ 0 & t_2 & 1^* & 0 & 0 & 0 & 0 & 0 & 0 & 0 \\ 1^* & 1^* & t_3^* & 1^* & 1^* & 0 & 0 & 0 & 0 & 0 \\ 1 & 0 & 1^* & t_4 & 0 & 0 & 0 & 0 & 0 & 0 \\ 0 & 0 & 1^* & 0 & t_5 & 0 & 0 & 0 & 0 & 0 \\ \hline 0 & 0 & 0 & 0 & 0 & 0 & 0 & 0 & 0 & 0 \\ 0 & 0 & 0 & 0 & 0 & 0 & 0 & 0 & 0 & 0 \\ 0 & 0 & 0 & 0 & 0 & 0 & 0 & 0 & 0 & 0 \\ 0 & 0 & 0 & 0 & 0 & 0 & 0 & 0 & 0 & 0 \\ 0 & 0 & 0 & 0 & 0 & 0 & 0 & 0 & 0 & 0 \end{array}\right) \tag{4}$$

In the *Laplacian matrix*, each layer of the multiplex has been marked with lines. This way, the next step in the algorithm is to build each layer of the multiplex. Fig. 4 shows a multiplex which illustrates the above techniques.

3 Operation evaluation

In this section, we evaluate through a experimental case study the proposed method, which is about providing optimal data with the IoT slicing method. To demonstrate the efficiency of the IoT slicing technique the data quality algorithm will be used in this case study. In order to test the efficiency of this technique,

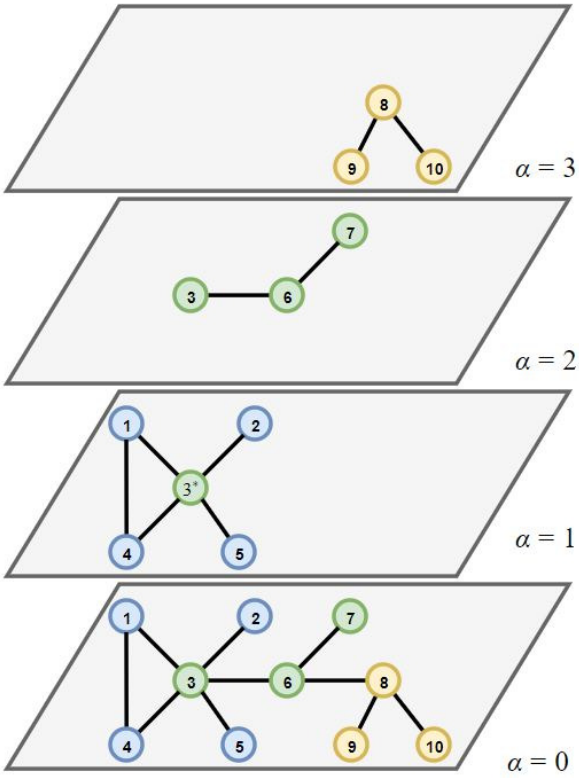

Fig. 4. Multiplex with 3 layers. In each of the layers are the IoT nodes that have similar temperatures according to the clustering algorithm used.

the results obtained by an algorithm in the two scenarios will be compared. In one scenario, the IoT slicing technique will be used to treat the data collected by the IoT devices and in the other, the data collected by the IoT devices will be used directly. In this case study, temperature data collected by the IoT devices in a smart building will be used.

3.1 Data quality algorithm case study

The algorithm chosen to test the efficiency of the IoT slicing method is the data quality algorithm designed by Casado *et al.* [5]. This algorithm compares the neighborhood temperature of the sensors using a cooperative game based on game theory to detect erroneous data and increase the quality of the data gathered by the sensors. In this algorithm, we expect neighborhood associations to democratically determine the temperature of the main sensor. To this end, coalitions are formed to determine the final temperature of the IoT node, which

is calculated according to whether or not they can vote in the process. Since the characteristic function, when the number is 1(0), each candidate can cast a vote (or not). s_i is the head IoT node with its temperature related t_{s_i}, the characteristic function is created like this:

1. The mean temperature of all IoT devices is determined in the first place:

$$T_{s_i}^k = \frac{1}{V}\sum_{i}^{V} t_{s_i} \tag{5}$$

   here $T_{s_i}^1$ represents the average temperature of the sensors neighbourhood s_i (including it) in the first iteration of the game, and V is the number of neighbours in the coalition.
2. The next step is to compute an absolute value for the temperature difference between the temperatures of each sensor and the average temperature:

$$\overline{T}_{s_i}^k = \left(\frac{1}{V}\sum_{i}^{V} \mid t_{s_i} - T_{s_i}^k \mid^2\right)^{\frac{1}{2}} \tag{6}$$

3. Use the variations in the temperature against the mean temperature $\overline{T}_{s_i}^k$ (see eq.(6)) a confidence interval is defined in the following way:

$$I_{s_i}^k = \left(T_{s_i}^k \pm t_{(V-1,\frac{\alpha}{2})}\frac{\overline{T}_{s_i}^k}{\sqrt{V}}\right) \tag{7}$$

   in Eq.(7) we use the Student's-t distribution with an error of 1%.
4. In this step we use a hypothesis test. If the temperature of the sensor lies in the interval $I_{s_i}^k$, it belongs to the voting coalition, otherwise, it is not in the voting coalition:

$$u^k(s_1,\ldots,s_n) = \begin{cases} 1 \text{ if } t_{s_i} \in I_{s_i}^k \\ 0 \text{ if } t_{s_i} \notin I_{s_i}^k \end{cases} \tag{8}$$

5. The characteristic function repeats this procedure iteratively until all IoT nodes in that iteration are part of the voting alliance. In each k iteration the following payoff vector of the coalition S_j (with $1 \leq j \leq n$ where n stands for the number of IoT nodes in the combination) at the step k ($PV(S_j^k)$) is available:

$$\begin{aligned} PV(S_j^k) &= (u^k(s_1),\ldots,u^k(s_n)) \\ \text{where } &\sum_{i}^{n} u^k(s_i) \leq n \end{aligned} \tag{9}$$

The stop condition of the game iterations is $PV(S_j^k) = PV(S_j^{k+1})$ the process end. That is, let $PV(S_j^k) = (u^k(s_1), \ldots, u^k(s_n))$ and let $PV(S_j^{k+1}) = (u^{k+1}(s_1), \ldots, u^{k+1}(s_n))$. The iteration process ends when both payoff vectors contain the same elements. This process is shown in the following equation:

$$\begin{cases} u^k(s_1) = u^{k+1}(s_1) \\ \vdots \\ u^k(s_n) = u^{k+1}(s_n) \end{cases} \tag{10}$$

So the game is able to define its solution in the next subsection.

4 Results

In this section we introduce the case study and the results obtained over the course of experiments. The data quality algorithm retrieves the data gathered from the IoT nodes and corrects them automatically.

4.1 General description of the experiment.

The validation phase took place in a smart building where the proposed model was to be implemented. At the time the IoT nodes measured the temperature, the desired temperature in the building was 23°C. A mesh was used to place the sensors on the surface with the help of laser levels, the IoT nodes were placed vertically, one in every section of the building. The temperature sensor had been collecting data at 5 minute intervals, for 8 hours in the same day. For the analysis we selected the data collected by the sensors in the following time interval 2019-07-22T08:30:00Z and ended on 2019-07-22T16:30:00Z. To test the efficiency of the data quality algorithm we provoked considerable temperature changes (our process) at 1 hour intervals to simulate random thermostat use (i.e., a group of people could select different temperatures on the thermostat of their office or labs rooms).

4.2 Case study results

The first thing we do is build the graph of the IoT network and apply the clustering algorithm. After applying the clustering algorithm, it can be observed how 3 clusters are formed. Therefore, the multiplex in Fig. 4 has got 3 layers. Thus, data is homogeneous. In this case study, non-connected graphs are formed on all layers of the multiplex using the data collected from the smart building. This is a common situation, and the algorithm self-corrects this by virtualizing all the required nodes for the graphs to be connected.

The results obtained from the comparison of the use of the control algorithm are presented in the Fig. 5. In this figure you can find the result of the application

of the data quality algorithm on heterogeneous data. In this case the data quality algorithm smoothes the data collected by the IoT network so that the data quality algorithm understood that the heterogeneous data were homogeneous. For this reason, the algorithm detects some temperatures collected by the IoT network and considers them outliers. Then the self-correcting algorithm corrects these values and the output of the data quality algorithm are homogeneous temperature data but this would not increase the energy efficiency as it does not use the information from the clusters to distinguish this information. On the other hand, using the technique proposed in this paper, through which heterogeneous data are transformed into homogeneous data with clustering techniques and complex networks, the energy efficiency of the IoT network is increased since the data collected by the IoT network by applying the control algorithm only acts for the homogeneous areas and thus maintains the temperature clusters as output of the data quality algorithm.

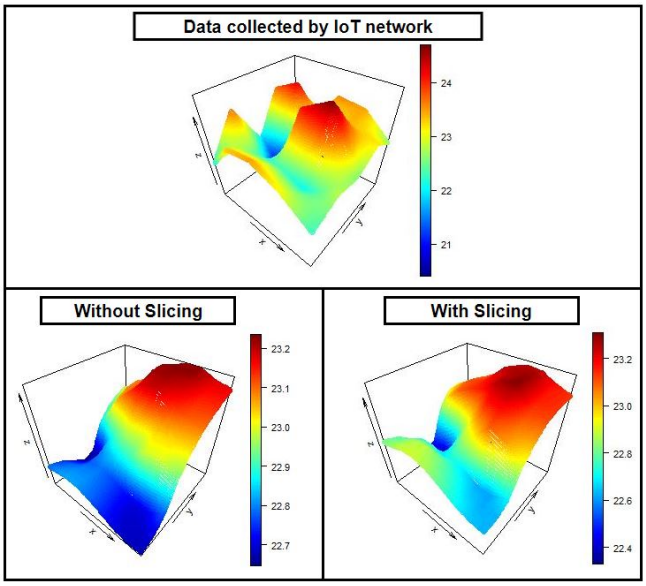

Fig. 5. The results obtained by the data quality algorithm are compared using the technique proposed in this article and without using the technique.

In both experiments, the algorithm we have used to test the efficiency of our new technique removes the outliers, but in the experiment that the IoT slicing smooth technique is not used the temperatures without considering the topology and uniformity of the smart building. Meanwhile, using the IoT slicing technique the smart building characteristics are considered, and when one uses data quality algorithm one obtains an output similar to data collected by the IoT devices but without wrong data (i.e., outliers). On a quantitative point of view, the final

Final temperature without slicing	Final temperature with slicing
$\begin{bmatrix} 22.98 & 23.07 & 23.19 & 23.22 & 23.17 \\ 22.90 & 23.08 & 23.21 & 23.19 & 23.13 \\ 22.67 & 22.84 & 23.01 & 23.04 & 23.03 \\ 22.69 & 22.77 & 22.76 & 22.70 & 22.77 \\ 22.78 & 22.81 & 22.78 & 22.70 & 22.67 \end{bmatrix}$	$\begin{bmatrix} 22.92 & 23.05 & 23.21 & 23.24 & 23.14 \\ 22.93 & 23.11 & 23.21 & 23.29 & 23.14 \\ 22.48 & 22.42 & 22.98 & 23.21 & 23.03 \\ 22.64 & 22.74 & 22.71 & 22.61 & 22.69 \\ 22.81 & 22.88 & 22.86 & 22.71 & 22.62 \end{bmatrix}$

Table 1. Final temperature in the case study in both experiments.

temperatures of the experiments done in the case study to validate the efficiency of the IoT slicing technique are presented in Table 1.

5 Conclusion

The evaluation results have shown that the proposed system can transform heterogeneous data into homogeneous data taking into account the topology and lack of uniformity of the intelligent building. The problem with the data collected by the IoT network is that the topology and non-uniformity of smart buildings are not considered. In this way, temperature control algorithms can be applied to these smart buildings, and the algorithm will smooth the entire temperature of the building considering only the comfort temperatures selected by the users (with thermostats). With the new IoT slicing technique proposed in this paper, the topology and non-uniformity of smart buildings are taken into account in order to transform heterogeneous data into homogeneous data. This implies a considerable increase in the functioning of the algorithms that use the data collected by IoT devices. In this paper, the effectiveness of this new technique is tested with a data quality algorithm developed by our research group with better results than expected in the research project.

Acknowledgment

This paper has been partially supported by the Salamanca Ciudad de Cultura y Saberes Foundation under the Talent Attraction Programme (CHROMOSOME project).

References

1. Lapillonne, B., Sebi, C., Pollier, K., & Mairet, N. (2012). Energy Efficiency Trends in Buildings in the EULessons from the ODYSSEE MURE project. ADEME. Retrieved December, 30, 2014.
2. Efficiency, E. (2009). Buildings energy data book. US Department of Energy.
3. Terroso-Saenz, F., Gonzlez-Vidal, A., Ramallo-Gonzlez, A. P., & Skarmeta, A. F. (2019). An open IoT platform for the management and analysis of energy data. Future Generation Computer Systems, 92, 1066-1079.

4. Bishop, C. M. (2006). Pattern recognition and machine learning. springer.
5. Casado–Vara, R., Prieto–Castrillo, F., & Corchado, J. M. (2018). A game theory approach for cooperative control to improve data quality and false data detection in WSN. International Journal of Robust and Nonlinear Control, 28(16), 5087-5102.
6. Shrivastava, R., Samdanis, K., & Sciancalepore, V. (2019). Towards service-oriented soft spectrum slicing for 5G TDD networks. Journal of Network and Computer Applications.
7. Srinivasan, M., & Murthy, S. R. (2019). Efficient Spectrum Slicing in 5G Networks: An Overlapping Coalition Formation Approach. IEEE Transactions on Mobile Computing.
8. Song, C., Zhang, M., Zhan, Y., Wang, D., Guan, L., Liu, W., ... & Xu, S. (2019). Hierarchical Edge Cloud Enabling Network Slicing for 5G Optical Fronthaul. Journal of Optical Communications and Networking, 11(4), B60-B70.
9. Casado-Vara, R., Chamoso, P., De la Prieta, F., Prieto, J., & Corchado, J. M. (2019). Non-linear adaptive closed-loop control system for improved efficiency in IoT-blockchain management. Information Fusion, 49, 227-239.
10. Casado-Vara, R., Novais, P., Gil, A. B., Prieto, J., & Corchado, J. M. (2019). Distributed Continuous-Time Fault Estimation Control for Multiple Devices in IoT Networks. IEEE Access, 7, 11972-11984.
11. Biswas, S., Das, R., & Chatterjee, P. (2018). Energy-efficient connected target coverage in multi-hop wireless sensor networks. In Industry interactive innovations in science, engineering and technology (pp. 411-421). Springer, Singapore.
12. Plageras, A. P., Psannis, K. E., Stergiou, C., Wang, H., & Gupta, B. B. (2018). Efficient IoT-based sensor BIG Data collectionprocessing and analysis in smart buildings. Future Generation Computer Systems, 82, 349-357.
13. Union, I. (2014). Communication from the Commission to the European Parliament, the Council, the European Economic and Social Committee and the Committee of the Regions. A new skills agenda for Europe (pp. 6-8). Brussels.

Desarrollo de un Gestor Inteligente de Redes TERmicas (GIRTER)

Jesús Samaniego[1], Manuel Andrés-Chicote[1], Andrea Gabaldón[1], Álvaro Corredera[1], José Hernández-García[1], Sofía Mulero[1], Luis A. Bujedo[1], Antonio Ferrer[2], Mª Rosario Heras[2], Alberto Díaz-Angulo[2], Silvia Soutullo[2], Alberto Castellanos[2], Fco. Javier Rey[3], Eloy Velasco[3], Julio San José[3], María Rey[3], Ignacio Bengoechea[4], José L. Bravo[4], Marta Otero[4], Roberto Carazo[5], Teresa Fernández[5], Sergio Lara[6], Gonzalo Real[6] y Manuel Salvador[6].

[1] CARTIF, Avda. Francisco Vallés 4, Boecillo, España
[2] CIEMAT, Avda. Complutense, 42, Madrid, España
3 Universidad de Valladolid, Paseo del Cauce s.n., Valladolid, España
[4]SEDICAL, Ribera del Carrión 4, Valladolid, España
[5]IDEAS TX Ingeniería, Calle El Sol, 5, 1ª Izda., Toro, España
[6]SOMACY, Edificio PRAE. Cañada Real 306, Valladolid, España
jessam@cartif.es

Resumen. Dentro del proyecto GIRTER se ha desarrollado un sistema de control con el que poder mejorar la explotación de Redes Térmicas de Distrito con poligeneración en las que hay tanto sistemas de producción despachables (calderas, cogeneraciones, etc.) como no despachables (energía solar, edificios prosumidores, calores residuales procedentes de industrias, etc.) intentando maximizar el aporte de energías limpias y de bajo coste a través de la reducción de la temperatura del anillo, adaptándola a la demanda prevista, la cual se determina mediante un servicio de predicción de demanda y considerando la gestión del almacenamiento tanto directo (en tanques) como indirecto (en la propia inercia del sistema).

Los principales avances del desarrollo GIRTER se basan en la aplicación de técnicas de predicción de demanda y modelos dinámicos simplificados implantados en el control, con los que caracterizar el comportamiento de las redes permitiendo la optimización en su gestión y control energéticos tanto desde el punto de vista medioambiental como económico

En el siguiente trabajo se muestran los avances conseguidos en dicho proyecto, el cual ha sido financiado en la convocatoria RETOS 2016 del Ministerio de Economía y Competitividad.

Palabras clave: Redes de distrito, predicción de demanda, polieneración.

1 Introduccion

Habitualmente la estructura de las redes térmicas de distrito actuales consiste en equipos de generación, en la mayoría de las ocasiones centralizados y basado en grandes calderas, un anillo de distribución y diversas cargas conectadas a dicho anillo a través de subestaciones intercambiadoras [1]. La regulación de estas redes de distrito, está basada en programaciones horarias de operación y ajuste de las consignas de generación, en función de la temperatura de impulsión y de retorno del anillo, siendo estas fijadas de manera rígida por el operador de la planta. Es habitual encontrarse redes en las que la temperatura de operación es constante y en valores elevados, realizando la modulación de la potencia en las subestaciones mediante regulación de caudal en el primario del intercambiador [2]. Los cambios bruscos y frecuentes en la consigna de temperatura del anillo, pueden llevar a problemas de tensiones acumuladas en la red, por tanto la aplicación de estrategias de modulación de la potencia mediante temperatura variable, deben ser realizadas con cambios progresivos y lentos siendo la predicción horaria de demanda, la herramienta adecuada para ello.

La evolución lógica de este tipo de generación va dirigida hacia la poligeneración renovable, por lo que se establece una necesidad de cubrir el hueco existente en el mercado a nivel de gestión de dicha poligeneración con sus particularidades y la integración con el comportamiento de la demanda.

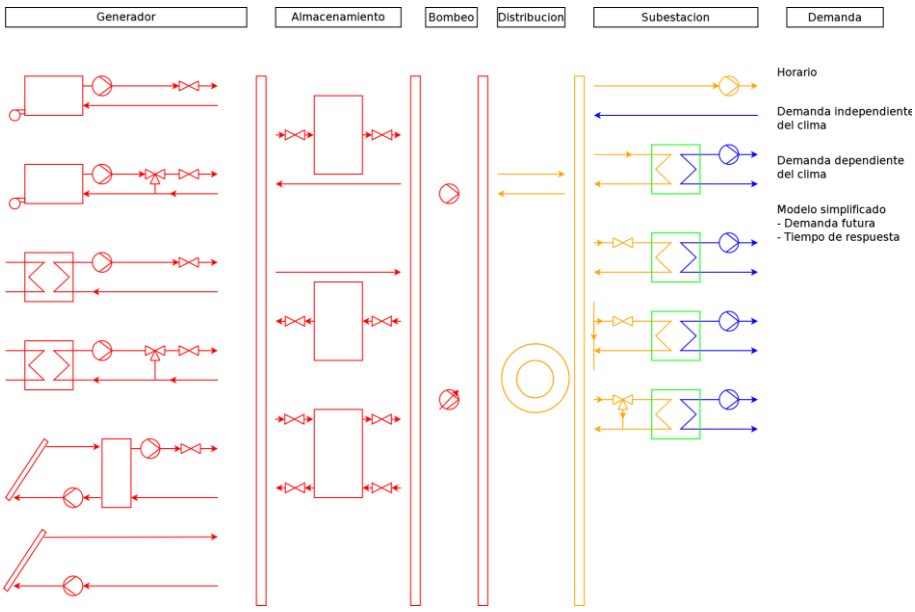

Fig. 1. Diagrama general de una red de distrito.

Destacar que se está produciendo un auge importante en el desarrollo de las redes de distrito, tanto nuevas, como en casos de rehabilitación energética de barrios con instalaciones existentes. En algunos casos se parte de una red previa centralizada en la que

se cambian los sistemas de generación [3], [4] pero en otros casos se dispone de un sistema de calefacción por edificios en los que se combinan sistemas obsoletos con otros más modernos [5] y en cuya rehabilitación se puede reducir el coste tanto de instalación como de operación, reutilizando parcialmente sistemas existentes de alto rendimiento, que pueden conectarse a la red ampliando el abanico de posibilidades de control o bien manteniendo un suministro dual. De este modo con bajas demandas un conjunto limitado de elementos distribuidos de alta eficiencia pueden permitir satisfacer la demanda completa o parcial como la opción más adecuada.

Una pieza clave en el aumento de penetración, rendimiento y fracción de uso de energías de baja entalpía como son las solares o las residuales, consiste en la reducción de la temperatura de operación del anillo. La existencia de instalaciones de energía solar para el suministro de agua caliente sanitaria son un elemento importante a considerar, sobre todo en el sur de Europa ya que en épocas estivales, en función del tamaño y la curva de demanda, pueden aportar un porcentaje importante de energía operando tanto centralizadas como distribuidas.

Dentro de esta estrategia, otro punto clave es el cálculo de la previsión de la demanda en un horizonte horario razonable y compatible con la velocidad de cambio del sistema, el cual dependerá fundamentalmente de su inercia y de la demanda a la que tenga que hacer la potencia de generación instalada.

En este escenario, la evolución lógica de las redes de distrito va dirigida hacia la poligeneración renovable, por lo que se establece una necesidad de cubrir el hueco existente en el mercado a nivel de gestión de dicha poligeneración con sus particularidades y la integración con el comportamiento de la demanda.

Dentro de este contexto, el proyecto GIRTER está desarrollando una estrategia de control que permita hacer frente a los nuevos retos a los que se tienen que enfrentar las redes de distrito: gestión de la poligeneración, reducción de temperatura de anillo, etc. apoyándose en: aplicación de modelos simplificados con los que poder estimar la demanda asociada a una previsión meteorológica y por otro lado, la correlación existente entre demanda que se puede satisfacer y la temperatura de anillo.

2 Descripción del sistema GIRTER

Aunque los equipos de control están aumentando su capacidad de cálculo, los controladores habituales basados en autómatas y PLCs disponen de una capacidad limitada de tiempo de ciclo para el cálculo de las señales de salida, por lo que la resolución de problemas en los que hay una gran cantidad de ecuaciones e incógnitas puede obligar a disponer de equipos muy potentes y costosos.

Por ello en GIRTER se decidió abordar el problema de control mediante el uso de modelos simplificados, los cuales dispongan de unos requerimientos de cálculo reducidos pero con niveles de precisión adecuados, en base a los cuales, se pueda mejorar los esquemas monolíticos de control actuales.

El estudio se ha orientado en dos direcciones: por un lado tener una caracterización dinámica del sistema en base a tiempos de respuesta de los elementos inerciales: depósitos, volúmenes de agua en tuberías, etc. y por otro lado una caracterización ener-

gética asociada a los edificios disponibles, los cuales van a marcar la demanda necesaria a cubrir y con ello, los requerimientos de potencia en la generación y temperatura necesaria en el anillo.

Como primer paso se ha hecho una revisión de los modelos más habituales de los diferentes elementos disponibles en las redes de distrito y se han comparado entre ellos o bien con datos reales de operación.

De esta forma se han seleccionado aquellos que combinan una precisión razonable con una carga matemática reducida, compatible con equipos de control de potencia media-baja.

El sistema trabaja partiendo de la previsión de climatología, siendo necesarias la temperatura ambiente y la radiación en un entorno de predicción que va desde una hora hasta las 6 horas.

A partir de un análisis de sensibilidad con diferentes variables edificatorias, se ha llegado a un modelo que es capaz de predecir la demanda de manera razonable con los valores de temperatura ambiente y radiación solar horarias, clasificando los edificios en base a dos parámetros básicos: el nivel de aislamiento, el cual es clave en la demanda invernal y por otro lado la superficie de acristalamiento, la cual tiene gran importancia en la demanda estival. En base a ello se han establecido 6 categorías de edificios considerando combinaciones de buen nivel de aislamiento y mal nivel de aislamiento frente a porcentajes de acristalamientos del 25, 50 y 75%.

Con los modelos de cada uno de los edificios de la red de distrito y la previsión meteorológica, se dispone de una previsión de demanda de calefacción.

La suma de las demandas de todos los edificios, indican las necesidades y por lo tanto la secuencia de calderas más adecuada.

Partiendo de datos de la subestación, se realiza una transformación de demanda a temperatura de forma que para cada edificio, se va a disponer de un valor de temperatura mínimo necesario para satisfacer su demanda y con los modelos de red, se estima los requerimientos de potencia para alcanzar la temperatura del anillo. El sistema GIRTER, en base a criterios de selección establecidos, selecciona el valor más adecuado de temperatura marcando la consigna con la que va a trabajar el anillo así como los requerimientos de potencia en el horizonte temporal próximo y por lo tanto las necesidades de generación.

3 Metodología de trabajo

Para llegar a las estrategias GIRTER, se han dado una serie de pasos encaminados la caracterización dinámica de los sistemas.

3.1 Especificaciones del sistema de gestión

Se ha realizado un modelo genérico de red de distrito en el entorno de simulación TRNSYS [6] con en el que se ha analizado:

- Los sistemas de generación centralizados de la red térmica.
- El modelo de subestación de intercambio entre red y edificios.
- El modelo de la demanda de los edificios.

- El modelo de la distribución y transporte de energía entre elementos de una red de distrito.
- La validación de los modelos simplificados de las estrategias de operación optimas.

Se ha establecido el interconexionado entre elementos y adaptado a las especificaciones y polivalencia de una red de distrito y se ha validado la consistencia del modelo.

De forma paralela se ha generado en Matlab® el modelo integral que implementa las ecuaciones de los modelos simplificados de comportamiento de los elementos de la red de distrito genérica, enlazando variables de entrada y salida y generando los elementos intermedios para evaluación del comportamiento.

El objetivo ha sido cuantificar la precisión de los modelos simplificados, y evaluar la integración con base de datos y elementos externos sometiendo a ambos a las mismas variables y control, y valorando el error cometido. A partir de los resultados, se han ajustado los parámetros iniciales de los modelos simplificados, mejorando su precisión.

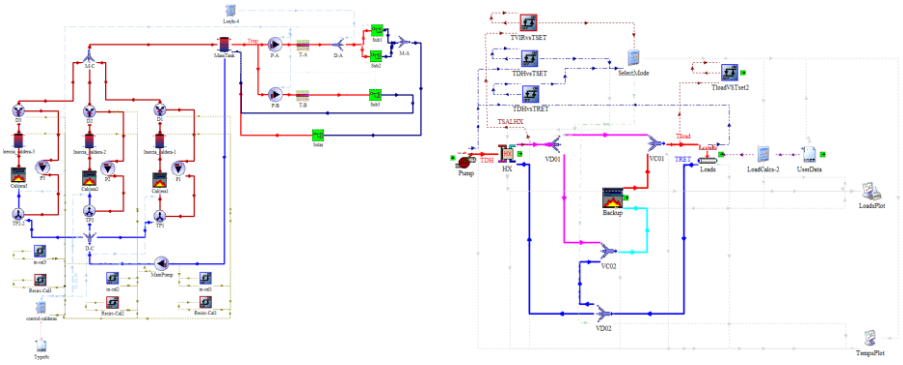

Fig. 2. Modelo TRNSY® de generación completo y detalle del modelo de subestación.

3.2 Desarrollo de estrategias inteligentes de operación.

Para establecer las especificaciones del sistema de gestión, se han estudiado los diferentes modos de control y estrategias que aparecen en la literatura y en proyectos europeos de redes de distrito (FLEXYNETS [7], STORM [8], etc.) y se han definido las variables de entrada y de salida del modelo más adecuadas para su implementación en el algoritmo de control final y su evaluación. Para poder valorar y comparar las distintas estrategias se han planteado una serie de indicadores y se han comparado con respecto a un caso base, el cual no tiene ningún tipo de control integrado.

Las estrategias parciales finalmente planteadas para su análisis, han sido:

- Estrategia 1 “Estudio de la secuencia de arranques”: Estudiar la secuencia de arranque y paro de las calderas locales para dar apoyo a los sistemas para cubrir la demanda solicitada y gestión de encendido de cargas, con el mínimo coste energético y económico. Se han analizado las inercias de los diferentes sistemas.

- Estrategia 2 “Disminución de la temperatura de anillo”: Operar con menor temperatura del anillo (mínimo 65ºC para garantizar 60ºC). En este caso se daría apoyo al ACS con las calderas locales en cada edificio. En operación real este valor puede que deba ser aumentado para garantizar la normativa antilegionella [9].
- Estrategia 3 “Integración de otras fuentes de generación”: Introducir sistemas renovables (solar) como apoyo al calentamiento de la red de distrito.

3.3 Evaluación bajo entorno de simulación dinámico

Se ha estudiado y analizado la manera de implementar las estrategias de operación establecidas anteriormente. Para ello se ha definido un caso base, bajo unas condiciones de contorno dadas, y sin ningún sistema de control, salvo el encendido de calderas cuando hay demanda, sin considerar ningún control predictivo de anticipación a la misma.

El modelo incorpora distintos modos de control en función de cada estrategia, y evalúa el comportamiento del sistema comparándolo con el de referencia bajo el entorno de TRNSYS.

Para comparar, se han analizado los resultados tanto energéticos como económicos de cada una de las estrategias adoptadas, para establecer cuáles son las más adecuadas para ejecutar en un entorno real operacional. Se han abordado los siguientes casos de estudio:

Estudio de tiempo de arranque de la red de distrito
Se han estudiado y simulado diferentes situaciones:

- Tiempo de arranque de calderas a diferentes temperaturas sin demanda conectada.
- Cubrir distintas demandas para distintas temperaturas iniciales del sistema, con calderas locales y cubriendo al menos el 70% de la demanda con red de distrito.
- Arranque retardado de calderas.

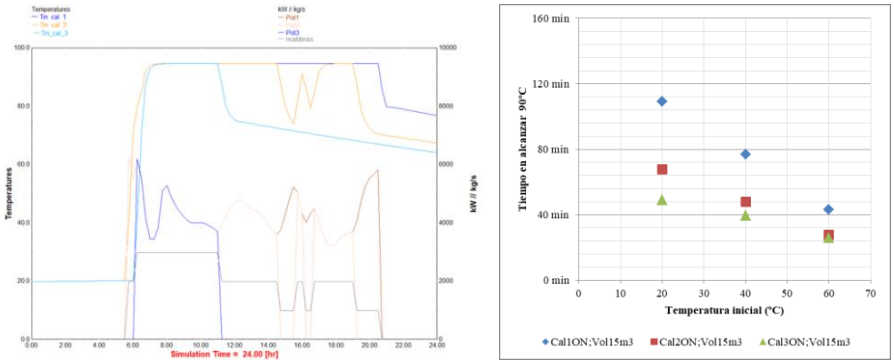

Fig. 3. Distribución de potencias, nº y temperaturas de caldera, con control GIRTER.

Disminución de la temperatura del anillo
Se han estudiado los siguientes supuestos:

- Reducir temperatura de suministro y apoyo con calderas locales.
- Reducción de temperatura de impulsión en radiadores

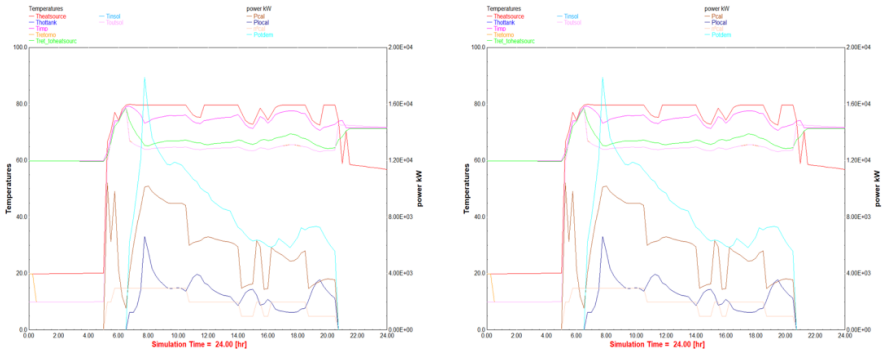

Fig. 4. Comportamiento de la red distribuyendo a 80ºC y a 65ºC.

Integración de otras fuentes renovables.
Se ha estudiado el porcentaje de apoyo de una instalación renovable solar a diferentes temperaturas de operación de la red de distrito.

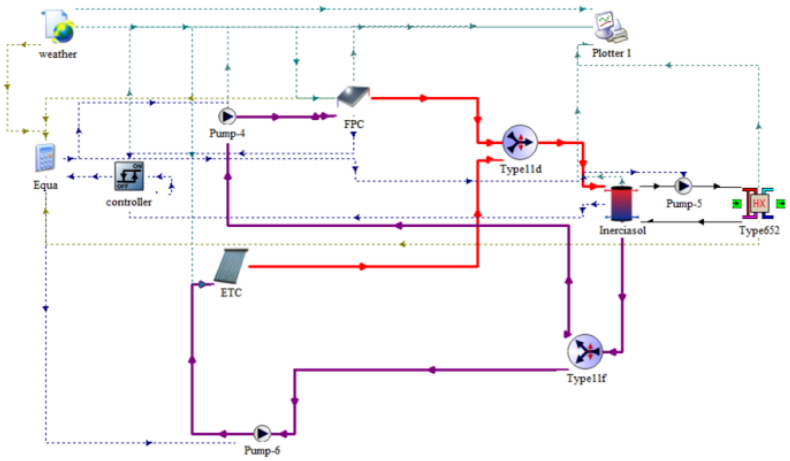

Fig. 5. Modelo de simulación de sistema solar térmico conectado a la red de distrito.

La Fig. 6 muestra los resultados de algunos de los casos de estudio bajo las mismas condiciones de contorno y para diferentes demandas pico de la red de distrito de estu-

dio. El caso base, al no anticiparse a la demanda, es el único que no cubre la demanda al 100%. El resto de casos son capaces de cubrir la demanda al 100%. En cuanto a los ahorros energéticos no existen diferencias significativas entre iniciar las calderas a la vez (caso: mismo horario de calderas) o a diferentes horas de forma escalonada, y no proporciona ahorros energéticos con respecto al caso base porque suministra el 100% de la demanda (suponiendo un consumo mayor que el base). El menor consumo energético (cubriendo el 100%) resulta ser el caso con dos calderas encendidas y cubriendo parte de la demanda (23%) con apoyo local distribuido y/o renovables. Los casos no son concluyentes pues dependen de las condiciones de contorno económicas, siendo necesario un análisis de sensibilidad más en detalle.

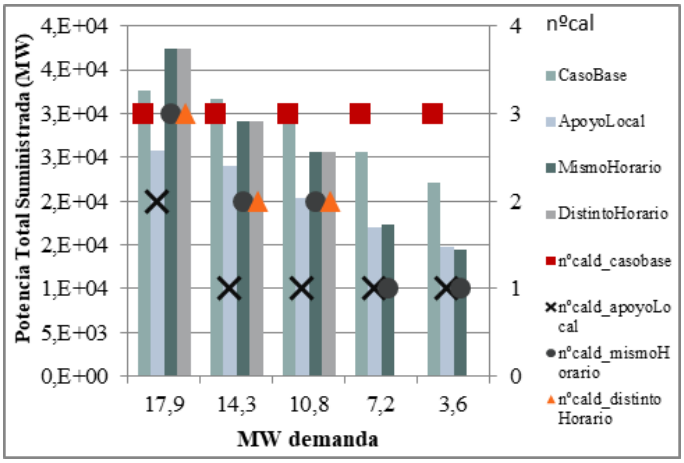

Fig. 6. Resultados simulación para una demanda pico de casi 18mw en el arranque (5 a 8 h) con diferente hora de arranque para cada calderas (distinto horario).

El análisis de los resultados de las diferentes simulaciones se ha concretado en un algoritmo de gestión final que es implementado en el controlador físico GIRTER, el cual, por un lado tiene en cuenta la inercia de los diferentes sistemas de la red y el volumen de agua en la distribución y establece, en función de la demanda estimada en las siguientes horas y el estado actual de la red de distrito, el momento de arranque y el número de calderas que deben estar en operación. Trata en cada momento de optimizar las condiciones de suministro, para lo cual establece la potencia y temperatura de suministro solicitada por cada subestación conectada a la red. El sistema establece que subestaciones piden mayor temperatura y analiza si son significativas sobre el total y si disponen de equipos auxiliares. En función de ello determina cual es la temperatura óptima de suministro y en que subestaciones debe dar apoyo el sistema auxiliar, consiguiendo con ello trabajar con la menor temperatura que minimice el coste energético y maximice la posible aportación de un sistema renovable u otra fuente de calor residual disponible.

4 Conclusiones y trabajos pendientes

GIRTER viene a mejorar los sistemas de gestión energética en redes de distrito, mediante una reducción en las pérdidas del sistema, así como una mejora en el aprovechamiento de las energías renovables y fuentes de baja entalpía disponibles.

Queda pendiente la implantación de los algoritmos desarrollados en el controlador así como el ajuste de los parámetros en operación.

Una pieza clave en el sistema GIRTER es la reducción de la temperatura de operación del anillo. En esta línea se está trabajando en la búsqueda de mejoras que refinen el establecimiento de la temperatura del anillo teniendo en cuenta condiciones de impacto de cargas en el criterio de decisión, de forma que puede haber edificios que marquen necesidades de temperatura elevadas las cuales puedan ser satisfechas por sistemas locales y por lo tanto sea más viable "sacarles" de la red de manera puntual.

5 Agradecimientos

El Proyecto GIRTER, Referencia RTC-2016-5800-3, es un Proyecto financiado por el Programa Estatal de Investigación, Desarrollo e Innovación Orientada a los Retos de la Sociedad, en el marco del Plan Estatal de Investigación Científica y Técnica y de Innovación 2013-2016 de la Agencia Estatal de Investigación (Ministerio de Economía, Industria y Competitividad), cofinanciado con Fondos FEDER.

El proyecto está liderado por SEDICAL acompañado por las empresas Ingeniería IDEAS TX y SOMACYL estando como centros de investigación CIEMAT, la Universidad de Valladolid y CARTIF.

Destacar el trabajo realizado por Cristina Cano sin cuyo esfuerzo el proyecto no habría sido igual. D.E.P.

6 Referencias

1. UPONOR, Guía de microrredes de distrito de calor y frío, Edición I.
2. ADHAC, Guía integral de desarrollo de proyectos de redes de distrito de calor y frío. Mayo 2012.
3. Proyecto REMOURBAN, http://es.remourban.eu, ultimo acceso 01/07/2019
4. Proyecto CITYFIED, http://es.cityfied.eu/, ultimo acceso 01/07/2019
5. Cristina Cano, Francisco José Valbuena García, Jesús Manuel Muñoz Martín, Francisco Javier Rey Martínez, Luis Manuel Navas Gracia: *Calefacción de distrito urbana con biomasa de la Universidad de Valladolid: Objetivo 20/20/20*. Congreso Nacional del Medio Ambiente CONAMA2014. http://www.conama2014.conama.org/web/index.php. ultimo acceso 01/07/2019.
6. TRNSYS: A transient Simulation Program (1990). Solar Energy Laboratory, University of Wisconsin, Madison WI.
7. Proyecto FLEXINETS, http://www.flexynets.eu/en/, último acceso 01/07/2019.
8. Proyecto STORM, http://www.storm-project.eu/, último acceso 01/07/2019.
9. Ministerio de Sanidad y Consumo, Real Decreto 865/2003, de 4 de julio, por el que se establecen los criterios higiénico-sanitarios para la prevención y control de la legionelosis.

Invernadero Fotovoltaico-es

Luis Hernández-Callejo[1[0000-0002-8822-2948]], Víctor Alonso-Gómez[1[0000-0001-5107-4892]], Marcia Eugenio-Gozalbo[1[0000-0002-7907-9780]], Elena Rico-Rodríguez[2[0000-0002-7872-6341]], Irene Huerta-Illera[2[0000-0002-5706-5273]] and Teodosio del-Caño-González[2[0000-0002-0328-4243]]

[1] Universidad de Valladolid, Campus Duques de Soria, 42004 Soria, Spain
[2]Onyx Solar Energy S.L., Rio Cea 1, 05004 Ávila, Spain
luis.hernandez.callejo@uva.es, L.H-C.; victor.alonso.gomez@uva.es, V.A-G.; marcia.eugenio@uva.es, M.E-G.; erico@onyxsolar.com, E.R-R.; ihuerta@onyxsolar.com, I.H-I.; tdc@onyxsolar.com, T.d-C-G.

Resumen. El proyecto "Invernadero Fotovoltaico-es" pretende demostrar la viabilidad técnica, económica, medio ambiental y energética de un invernadero, en el que se integran vidrios fotovoltaicos resultando un sistema de generación distribuida, para poder obtener la energía necesaria para el funcionamiento y la sostenibilidad del mismo. De esta forma, el invernadero realiza sus funciones de producción hortícola, mientras recupera la energía eléctrica necesaria para poder abastecer las necesidades de la microrred que lo conforma.

Keywords: Invernadero energético y sostenible, fotovoltaica integrada, microrred, silicio amorfo, BIPV

1 Introducción

En la actualidad, la mayor parte de la energía utilizada en el mundo proviene de combustibles fósiles [1]. Son ampliamente conocidos los daños que ocasionan al medio ambiente dichos combustibles durante su combustión, entre ellos por ejemplo cabe destacar la emisión de gases contaminantes, el calentamiento global y la contaminación del suelo.

El 40% de las emisiones de efecto invernadero, así como el 38% de la demanda energética global, proviene de los edificios [2]. El cambio climático es evidente y únicamente la aplicación de energías renovables en edificios y construcciones puede ayudar a reducir el consumo de combustibles fósiles y contribuir de este modo a un modelo energético global más sostenible [3].

La no dependencia de los combustibles derivados del petróleo hace que la mayoría de los países traten de incentivar el empleo de fuentes de generación renovable, para así, disponer de un mix energético más diversificado. España es uno de estos países que pretende diversificar sus fuentes de generación energéticas.

Entre las energías renovables, la tecnología solar fotovoltaica se presenta como una de las más interesantes, ya que la energía solar es un recurso disponible en cualquier parte del mundo y no tiene ningún coste [4]. En los últimos años, esta tecnología se ha

utilizado como material de construcción en edificios dando paso a lo que hoy en día se conoce como integración de energía solar fotovoltaica en edificios o BIPV [5]. Si además se lleva a cabo con generación distribuida (GD), rompiendo el paradigma de la generación centralizada y alejada de los puntos de consumo, estamos considerando un concepto de BIPV que puede resultar muy interesante, siendo el planteado en el presente proyecto.

Junto al concepto de BIPV de GD surge el concepto de microrred, que se define como el entorno con generación y demanda local, donde es preciso tratar de ajustar ambas, potenciando el consumo de energía proveniente de la microrred en detrimento de la energía proveniente de la red eléctrica [6]. Cuando la generación y el consumo se producen en un lugar próximos todos estos conceptos se fusionan (BIPV, GD y microrred).

El proyecto "Invernadero Fotovoltaico-es" pretende demostrar la viabilidad técnica, económica, medio ambiental y energética de un invernadero, en el que se integran vidrios fotovoltaicos resultando un sistema de GD, para poder obtener la energía necesaria para el funcionamiento y la sostenibilidad del mismo. De esta forma, el invernadero realiza sus funciones de producción hortícola, mientras recupera la energía eléctrica necesaria para poder abastecer las necesidades de la microrred que lo conforma.

Las necesidades energéticas de la microrred deberán de ajustarse a la realidad climática del emplazamiento en todo momento, tratando de hacer que la demanda energética pueda ser cubierta con la GD fotovoltaica disponible, intentando no olvidar que el proceso vital de la producción hortícola debe mantenerse a niveles óptimos.

El estudio de los diferentes grados de opacidad de los vidrios fotovoltaicos, así como las condiciones climáticas propias del emplazamiento y las necesidades vitales de la producción hortícola ecológica y sostenible, han sido fundamentales para el correcto desarrollo del proyecto "Invernadero Fotovoltaico-es".

Por tanto, y bajo las premisas de cultivos ecológicos, desarrollo sostenible, eficiencia energética y producción renovable, se ha desarrollado una integración fotovoltaica de GD en un prototipo que integra el paradigma asociado a los cultivos de invernaderos.

Es de esperar que este proyecto construya los cimientos de un futuro modelo energético sostenible, no agresivo con el medioambiente y potenciador de la economía local en el área de los invernaderos. Por tanto, este trabajo pretende mostrar el diseño e instalación del prototipo de invernadero fotovoltaico sostenible instalado en el Campus Universitario Duques de Soria de la Universidad de Valladolid (España) en Soria.

El proyecto "Aplicación de la tecnología fotovoltaica integrada en edificios (BIPV) para invernaderos agrícolas" con número de expediente 04/16/AV/0001 ha sido realizado en el marco del programa Proyectos de I+D en PYMES. Este proyecto ha sido financiado por el Fondo Europeo de Desarrollo Regional (FEDER) de la Unión Europea y la Junta de Castilla y León, a través del Instituto para la Competitividad Empresarial de Castilla y León (ICE), con el objetivo de potenciar la investigación, el desarrollo tecnológico y la innovación. El proyecto fue concedido a Onyx Solar Energy S.L., y en el que la Universidad de Valladolid actuó como parte subcontratada.

2 Objetivos generales y específico

El proyecto "Invernadero Fotovoltaico-es" consiste en la integración de energía solar fotovoltaica de GD en un invernadero, el cual pretende ser auto-sostenible y eficiente energéticamente, presentando un impacto medioambiental global positivo.
Por tanto, el invernadero se convierte en una infraestructura de medida y control sobre la que se han realizado distintas pruebas y análisis con el fin de establecer las bases técnicas y económicas para la creación de los "Invernaderos Fotovoltaicos" del futuro, siendo este el **objetivo principal** del proyecto.
Además, lo anterior se ha potenciado con el desarrollo del cultivo de manera ecológica, presentando el proyecto un nuevo paradigma de sostenibilidad en relación a los invernaderos.
Este invernadero, a modo de microrred, dispone de GD fotovoltaica, cargas pasivas y activas. Para ello, se han implementado elementos de sensorización y comunicación para la gestión y operación del mismo. Además, se han aplicado técnicas de producción agrícolas ecológicas y sostenibles.
A continuación, se enumeran los objetivos específicos derivados del desarrollo del proyecto "Invernadero Fotovoltaico-es", y que complementan al objetivo general:

- **BIPV en invernaderos**: este objetivo está estrechamente vinculado con el reto principal del proyecto y deberá ser minuciosamente estudiado. Para ello, se han abordado todos los aspectos necesarios para la correcta integración fotovoltaica en el invernadero. Entre ellos, cabe destacar los siguientes aspectos:
    - Sistemas de almacenamiento de la energía así como su gestión.
    - Tecnología fotovoltaica a utilizar.
    - Requisitos de diseño y características de los elementos individuales del sistema.
    - Viabilidad del sistema fotovoltaico a emplear.
    - Sistemas de fijación y anclaje que permitan optimizar una fácil integración de las soluciones constructivas en el invernadero.
    - Sistema constructivo modular con métodos de fabricación y montaje sencillos.
    - Otros.
- **Caracterización de vidrios fotovoltaicos**: desarrollo de modelos de simulación avanzados para la caracterización (activa y pasiva) de las tecnologías fotovoltaicas y los sistemas constructivos, así como establecer pautas generales de diseño en invernaderos que permitan obtener condiciones interiores adecuadas en función de la zona climática y el tipo de cultivo utilizado. En dicho invernadero se han cultivado y cultivarán diferentes producciones, las cuales necesitarán condiciones climáticas cambiantes, por lo que el ajuste del vidrio fotovoltaico a emplear es crucial para el desarrollo de la vida hortícola. Por tanto, el invernadero es una microrred, tratando de obtener la energía

necesaria para el funcionamiento de sus cargas interiores. El proyecto pretende probar diferentes grados de opacidad del cerramiento para obtener distintas condiciones ambientales en su interior, variando por tanto, la obtención de energía eléctrica para la microrred, todo ello conjugando las condiciones para la generación fotovoltaica con las condiciones de las necesidades vitales de la producción hortícola.

- **Sensórica ambiental:** las condiciones ambientales del interior del invernadero son fundamentales para el crecimiento de la producción hortícola deseada. Debido a que el proyecto "Invernadero Fotovoltaico-es" es un prototipo aplicable a diferentes emplazamientos y variadas producciones, es fundamental poder registrar las condiciones ambientales. Por tanto, se ha implementado la sensórica necesaria para la medida de condiciones ambientales, así como las variables eléctricas, precisando para su registro un datalogger.
- **Microrred:** tras la recuperación de la energía del fotón para su conversión en energía eléctrica, el resto de energía es preciso emplearla de manera óptima y eficiente para su uso dentro del invernadero. El principal uso de la energía de la microrred estará destinado a controlar: calefacción, temperatura mediante ventilación, humedad relativa, concentración de CO_2, etc.; para conseguir la sostenibilidad y auto-suficiencia, es preciso que la microrred pueda monitorizar y gestionar los recursos energéticos disponibles en la microrred.

La consecución de estos objetivos específicos, así como los generales, y sus acciones asociados permiten como resultado natural la realización del objetivo fundamental del proyecto: sentar las bases de los "Invernaderos Fotovoltaicos" del futuro.
Por último, es necesario destacar que con el desarrollo del presente proyecto se abre un nuevo mercado hacia un nuevo modelo de invernadero más sostenible y eficiente que ofrece un alto valor añadido.

3 Diseño y desarrollo del prototipo del invernadero

Se ha diseñado un invernadero innovador y versátil, de tal forma que pueda cubrir las necesidades ambientales de la producción planteada para su producción. En este sentido, el diseño del prototipo de invernadero fotovoltaico ha requerido de un estudio exhaustivo de las variables relacionadas con la optimización del mismo. Por tanto, ha sido necesario estudiar los distintos factores implicados como son los diferentes tipos y geometría de invernadero, climatología, tecnología fotovoltaica: silicio amorfo (a-Si) o silicio cristalino (c-Si), configuraciones de vidrio, sistemas constructivos de fijación, etc., en relación con los cultivos y sus necesidades y la producción energética principalmente.

Este análisis ha necesitado, por un lado, la recolección de distintos datos bibliográficos, el asesoramiento técnico de expertos en la temática de invernaderos así como la evaluación de las diferentes propiedades ópticas de los vidrios fotovoltaicos. Otro factor importante ha sido el emplazamiento seleccionado, ya que ha sido necesario un estudio de sombras a partir del "movimiento aparente del Sol".
Con el objetivo de poder realizar una comparativa de producción hortícola y poder obtener unos resultados con respecto al vidrio fotovoltaico instalado, se han diseñado y montado dos espacios iguales y juntos pero separados físicamente, donde uno de ellos tiene vidrio clásico y el otro vidrio fotovoltaico de silicio amorfo.
A partir de todo esto, el prototipo final ha sido instalado en las instalaciones de CEFIDEA (Centro Europeo para la Formación, Investigación y el Desarrollo de Energías Alternativas), ubicado en el Campus Universitario Duques de Soria de la Universidad de Valladolid (UVa), ver Figura 1.

Fig. 1. Vista general del prototipo "Invernadero Fotovoltaico-es". La mitad izquierda es con vidrio convencional y la derecha con vidrio fotovoltaico de silicio amorfo.

El sistema de cerramiento propuesto es de tipo modular y consiste en varios paneles de vidrio que se fijan sobre la estructura. Las características de los vidrios se han elegido de entre los módulos estándar disponibles fabricados por Onyx Solar en base a diferentes criterios, entre los que se incluyen:

- la superficie total del prototipo (aproximadamente 30 m2);
- mínimo número de vidrios necesarios con el objetivo de simplificar la estructura de soporte de los vidrios y reducir las zonas de sombra
- óptima relación de las dimensiones del invernadero (ancho, largo) y apropiado valor de la pendiente de la cubierta.
- el tipo de tecnología fotovoltaica empleada y el grado de transparencia

La sección no fotovoltaica está cubierta por módulos de vidrio convencional (no activos desde el punto de vista fotovoltaico) de dimensiones, propiedades mecánicas y térmicas (coeficiente de transferencia de calor) lo más similares posibles al vidrio

fotovoltaico. Esto facilitará la comparación de los resultados obtenidos en cada una de las zonas del invernadero, puesto que las diferencias entre los vidrios de ambas zonas serán mínimas (transparencia y comportamiento frente al paso de la luz principalmente).

Los módulos de vidrio fotovoltaico no pueden ser parte de las ventanas o accesos para la renovación de aire, ya que al estar conectados eléctricamente entre sí y al sistema de transformación y almacenamiento de la energía eléctrica, su movimiento está limitado.

Por lo tanto, la ventilación se realizará a través de los módulos no activos aprovechando los módulos con dimensiones y geometría diferente a la de los módulos estándar y dos módulos de la fila inferior de la cara norte que han sido diseñados como no PV específicamente para ser parte del sistema de ventilación.

El vidrio fotovoltaico elegido finalmente para el diseño del invernadero es el 034-BN-12450635-30-1, cuyas principales características se describen en la Tabla 1.

Tabla 1. Principales características del vidrio fotovoltaico.

Vidrio fotovoltaico	
Modelo	034-BN-12450635-30-1
Configuración:	Vidrio – vidrio (sin cámara inerte)
Dimensiones:	1245 x 635 x 7,96 mm (3,2 vidrio + 0,76 encapsulaste PVB + 4 vidrio)
Transparencia:	Vidrio incoloro con 30 % de transparencia
Tipo tecnología PV:	Silicio amorfo
Potencia nominal:	22 W por módulo//1298 W en total en toda la superficie activa (59 módulos)
Tratamientos especiales:	Sin tratamientos especiales

Tres de las cuatro vertientes del invernadero están cubiertas con vidrio fotovoltaico, concretamente serán el lado sur, norte y tejado. Al disponer de tres zonas fotovoltaicas, parece de sentido común tratar de agrupar los dispositivos fotovoltaicos en tres *arrays* diferentes. La Figura 2 muestra la configuración e interconexionado de las tres zonas de vidrios fotovoltaicos. Por motivos de diseño del regulador fotovoltaico, cada vidrio está conectado a un fusible propio, para posteriormente hacer las agrupaciones oportunas según el *array*. El esquema muestra igualmente la interconexión con el regulador fotovoltaico, y desde este dispositivo al conjunto de almacenamiento eléctrico disponible. Por último se puede observar la elección de un inversor para alimentar a las cargas en alterna, las cuales están formadas por los consumos del invernadero fotovoltaico.

La Figura 3 muestra el esquema de interconexión de los principales componentes de protección y control que conforman el cuadro. Este esquema se ha utilizado para realizar una instalación rápida y puesta a punto de los dispositivos.

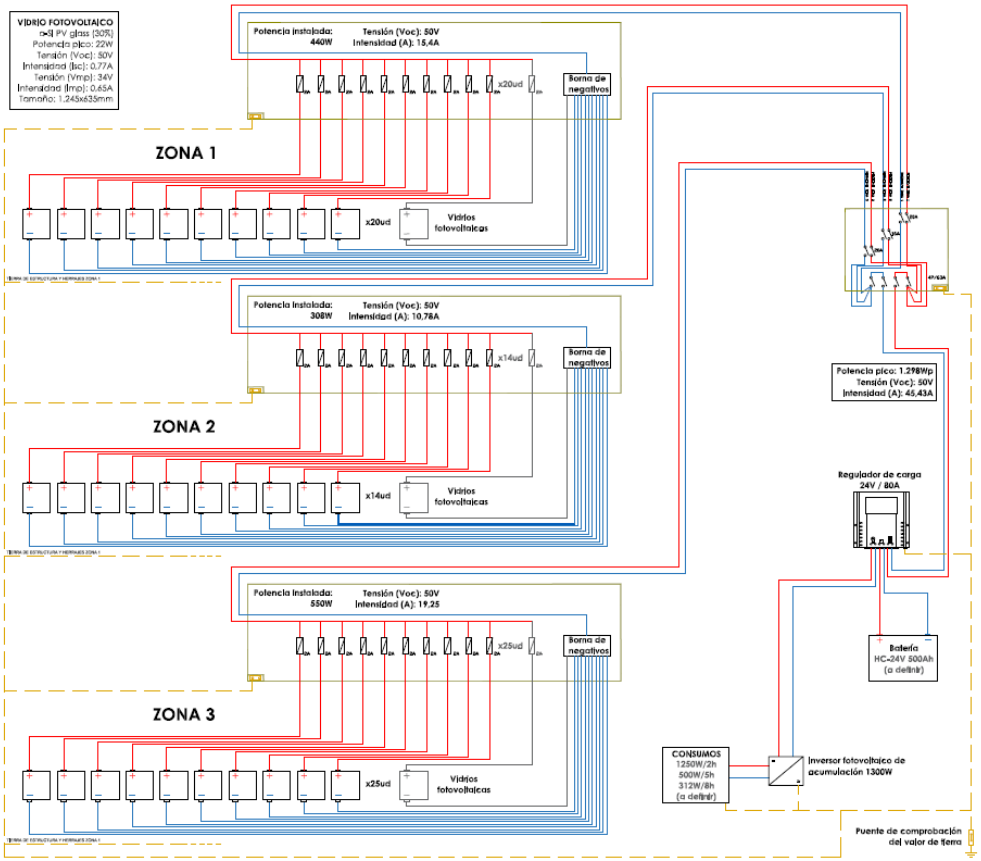

Fig. 2. Esquema de conexionado del sistema fotovoltaico y conectado a baterías mediante regulador e inversor.

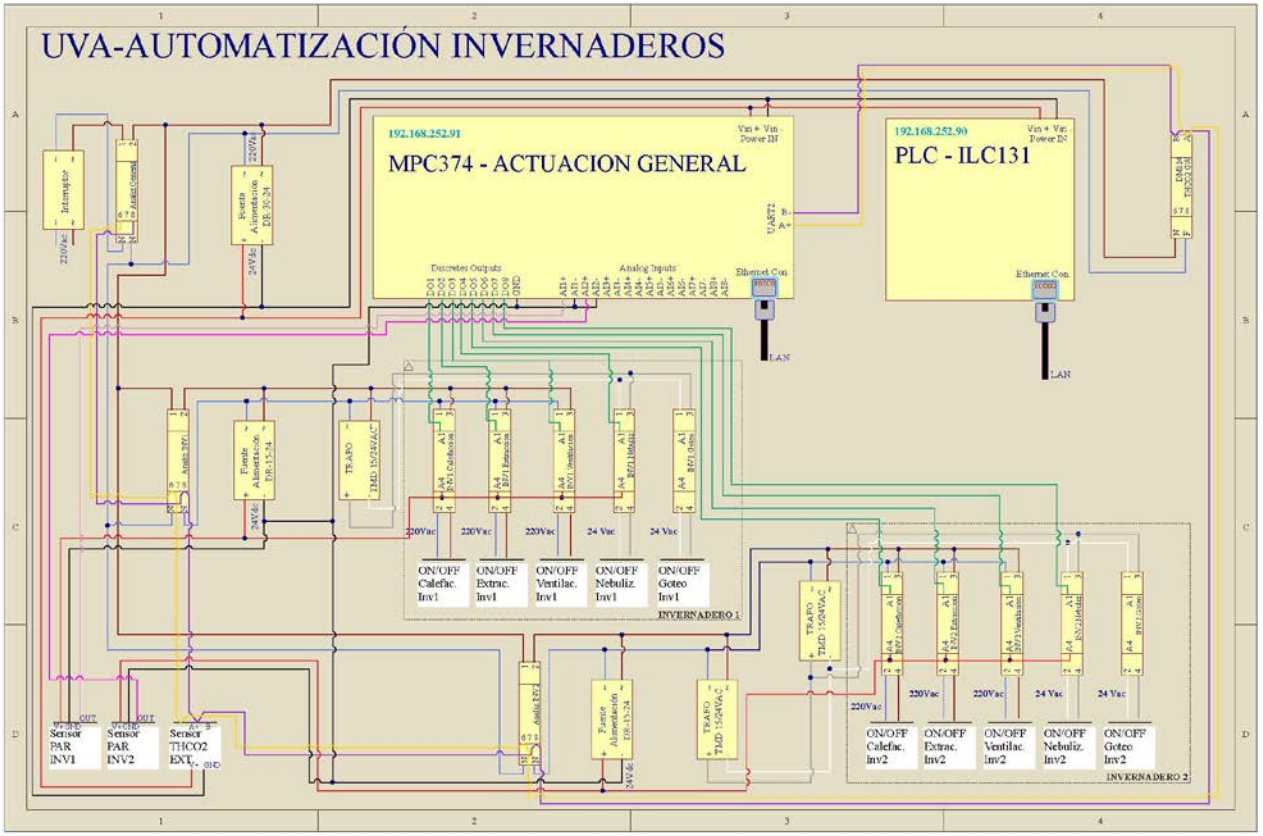

Fig. 3. Esquema de conexionado de PLC y datalogger, así como sensores y actuadores de ambos invernaderos.

4 Elementos de monitorización

En la Figura 4 se muestra un esquema aproximado del invernadero ubicado en el Campus Universitario Duques de Soria. El invernadero está separado en dos partes claramente diferenciadas, una de ellas con acristalamiento fotovoltaico y la otra sin él. Cada una de las secciones dispone de sus propios sensores para monitorización y los elementos de control.

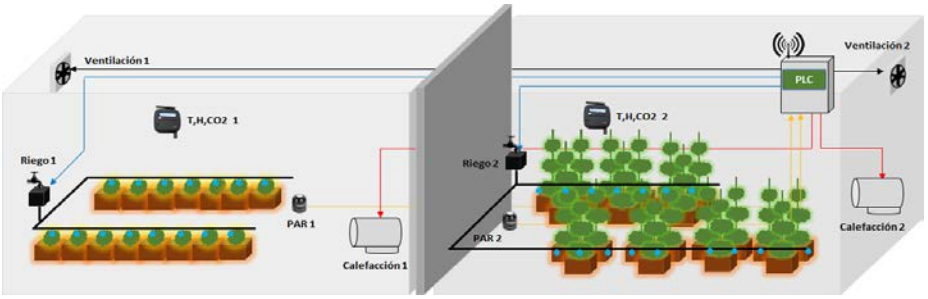

Fig. 4. Instalación del invernadero en Campus Universitario Duques de Soria. Fuente: elaboración propia.

El proyecto utiliza un sistema de monitorización modular, por lo cual el sistema de monitorización está compuesto de diferentes módulos de funcionamiento. El sistema de monitorización consta de los siguientes elementos:

- Un módulo de potencia formado por fuentes de alimentación y transformadores, encargado de alimentar todos los componentes del sistema. Representado como "Potencia" en la Figura 5.
- Un módulo de sensorización de los ambientes ("Sensores").
- Un módulo de almacenamiento de información ("Concentrador de datos").
- Un módulo de comunicación inalámbrica para la recepción de datos de los sensores inalámbricos ("Pasarela inalámbrica").
- Un módulo de control ("PLC").
- Un módulo formado por los actuadores del sistema ("Actuadores").

A modo de resumen, la Figura 5 muestra el diagrama de bloques del sistema monitorización integral.

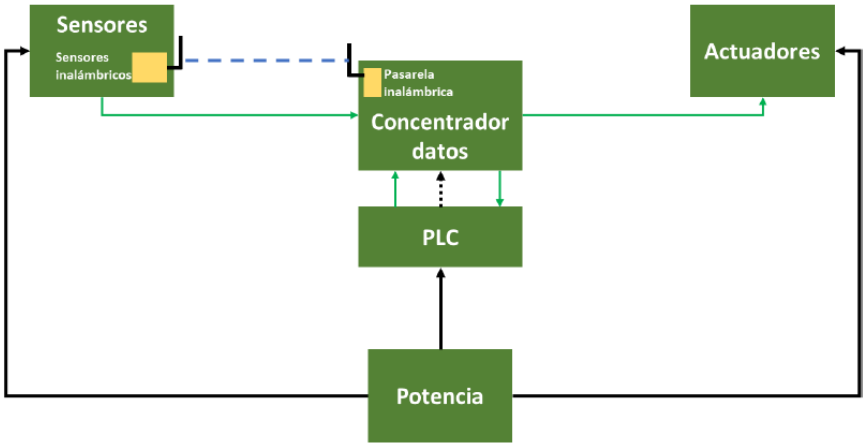

Fig. 5. Diagrama de bloques del sistema.

Los requisitos principales del sistema de monitorización instalado son los siguientes:

- El sistema debe monitorizar temperatura, humedad relativa y concentración de CO_2 en ambas secciones, así en el exterior.
- El sistema debe monitorizar la radiación PAR incidente sobre cada una de las secciones.
- El sistema debe monitorizar también el consumo eléctrico de cada sección de forma independiente.
- Los sensores serán capaces de comunicarse con el módulo de concentración de datos y el control.
- El sistema debe incluir un módulo de programación horaria para el sistema de riego por goteo.
- El sistema debe ser capaz de hacer un control basado en umbrales de funcionamiento de los siguientes parámetros:
    - Ventilación.
    - Extracción.
    - Calefacción.
    - Riego por nebulización.
- El sistema debe incluir actuadores de ventilación, extracción, calefacción y control de riego.
- El sistema debe permite actualizar las consignas en tiempo real.
- El sistema debe proporcionar una interfaz web diseñada a medida para la actualización y modificación de los umbrales de funcionamiento del sistema de control.

Puesto que uno de los objetivos del proyecto es analizar la diferencia de comportamiento entre cada sección del invernadero, se ha definido como escenario del proyecto el conjunto del invernadero a controlar, teniendo en cuenta que cada sección deberá

ser monitorizada y controlada de forma independiente. El escenario bajo estudio se caracteriza por:

- El invernadero está dividido en dos secciones con la misma geometría y equipamiento separadas mediante una pared para permitir aislar ambos ambientes.
- Ambas secciones están cubiertas de vidrio. Cada sección está cubierta por un tipo de vidrio diferente, estando una cubierta por vidrio convencional y la otra por vidrio fotovoltaico.
- Ambas secciones tienen una superficie de 15 m^2 aproximadamente.
- Ambas secciones carecen de ventilación natural.
- Ambas secciones están situadas de forma contigua, aunque
- Ambas secciones están controladas por el mismo cuadro eléctrico. De esta forma se economiza la instalación y facilita el cableado.
- Ambas secciones constan del siguiente equipamiento:
    - Sensor de temperatura, humedad relativa y CO_2 para interiores.
    - Sensor de radiación PAR.
    - Analizador de red para el análisis de consumo energético. Uno general para totalizar el consumo de ambas secciones más PLC y datalogger, y uno por cada una de las secciones. Por tanto, habrá tres analizadores de red.
    - Ventilador.
    - Calefactor.
    - Sistema de riego por goteo.
    - Nebulizador telescópico con 2 toberas.

Tomando como punto de partida los requisitos descritos, se procedió a realizar el diseño de un sistema monitorización capaz de adquirir los siguientes parámetros:

- Medición de la concentración de radiación fotosintéticamente activa en ambas secciones.
- Medición de nivel de CO^2 en el interior y el exterior del invernadero.
- Medición de nivel de temperatura en el interior y el exterior del invernadero.
- Medición de nivel de humedad relativa en el interior y el exterior del invernadero. Medición del consumo general del sistema y de cada una de las secciones de forma independiente.

5 Elementos de control

El sistema de control actúa sobre los siguientes sistemas de operación en cada una de las secciones del invernadero:

- Calefactor de hasta 1800 W de potencia.
- Ventilador parte de la ventilación forzada del sistema.

- Ventilador parte de la extracción forzada del sistema.
- Sistemas de riego por goteo.
- Sistema de riego por nebulización.

El principal elemento del sistema de control es el PLC. Este dispositivo es el encargado de establecer las reglas de control para asegurar que se cumplen los umbrales de funcionamiento del sistema, configurados previamente por el cliente. Tanto el concentrador de datos como el PLC están alojados en un mismo cuadro eléctrico de control que además incluye:

- Protección ante sobrecargas eléctricas.
- Las fuentes de alimentación del sistema.
- Los transformadores de alimentación de las electroválvulas.
- Los analizadores de red que caracterizan el comportamiento de las dos secciones en cuanto a consumo eléctrico. Como se ha dicho, también habrá un analizador que totalizará el consumo de todo el sistema (ambas secciones, datalogger, PLC, etc.).
- La pasarela de comunicación con los sensores inalámbricos.
- Contactores de control de las cargas del sistema de control de ambos invernaderos.
- Conectores para los sensores de ambos invernaderos.
- Conectores para los actuadores de ambos invernaderos.

La Figura 6 muestra un esquema del diagrama de bloques del sistema de control.

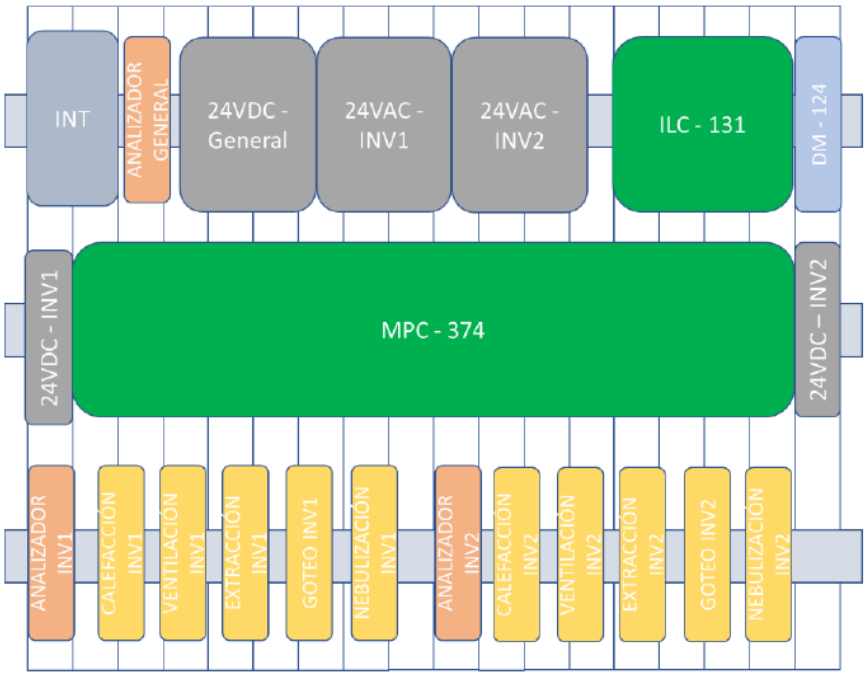

Fig. 6. Diagrama de bloques del sistema de control del invernadero.

6 Lazos de control y arquitectura del sistema

En las figuras siguientes (Figura 7 a Figura 11) se muestran los lazos de control a través de los cuales el PLC determinará qué actuaciones deben realizarse. El control está basado en umbrales, los cuales pueden ser actualizados, y de esta forma, las consignas de control podrán ser modificadas en base a las necesidades reales de cada cultivo a producir.

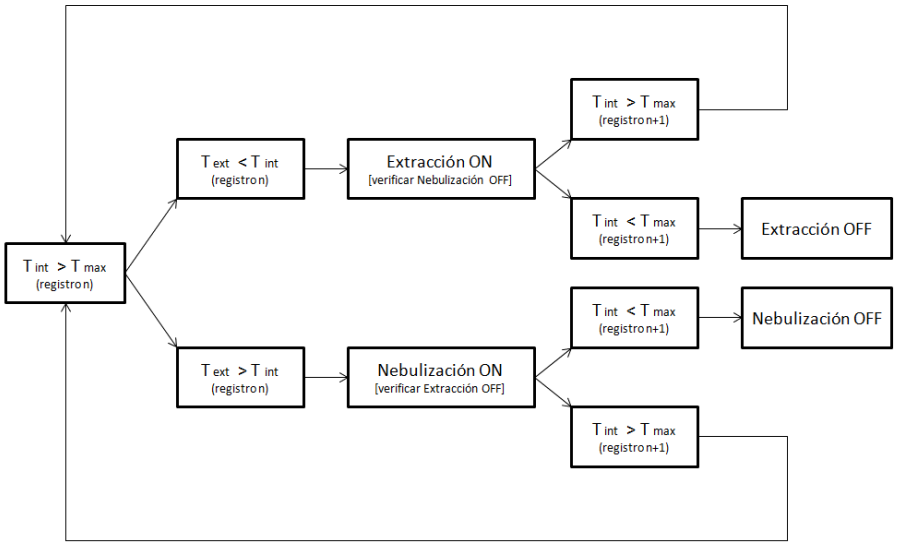

Fig. 7. Lazos de control cuando Tint > Tmax.

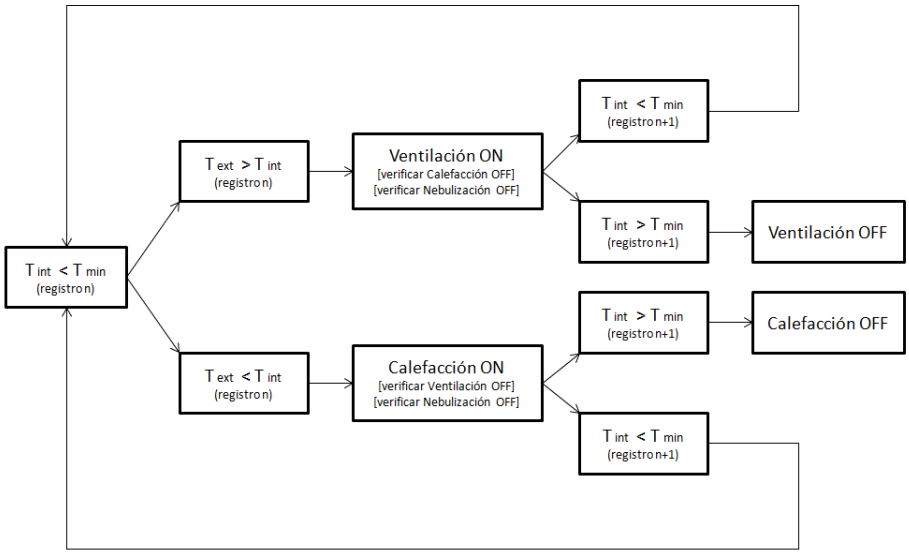

Fig. 8. Lazos de control cuando Tint < Tmin.

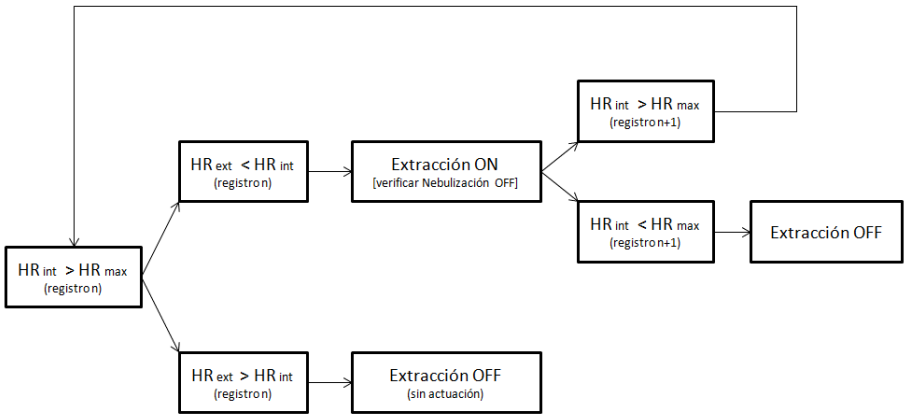

Fig. 9. Lazos de control cuando HRint > HRmax.

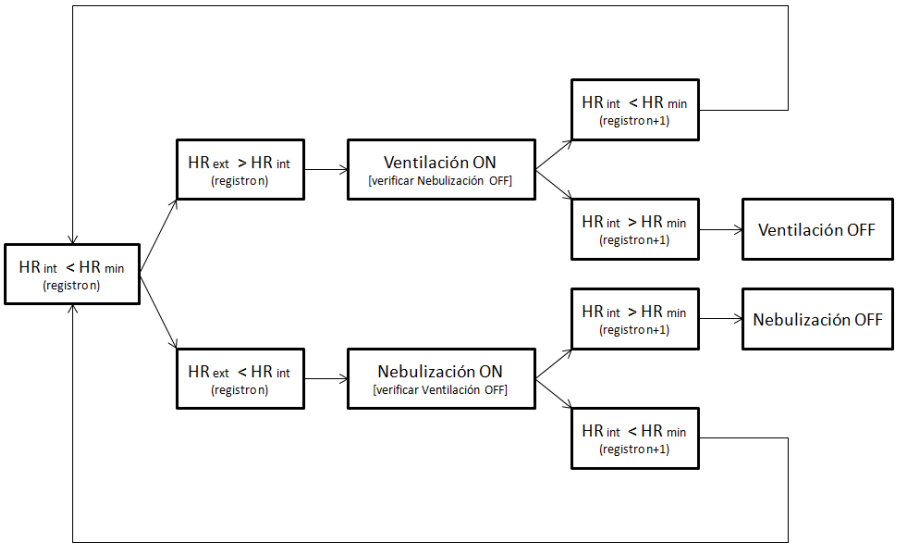

Fig. 10. Lazos de control cuando HRint < HRmin.

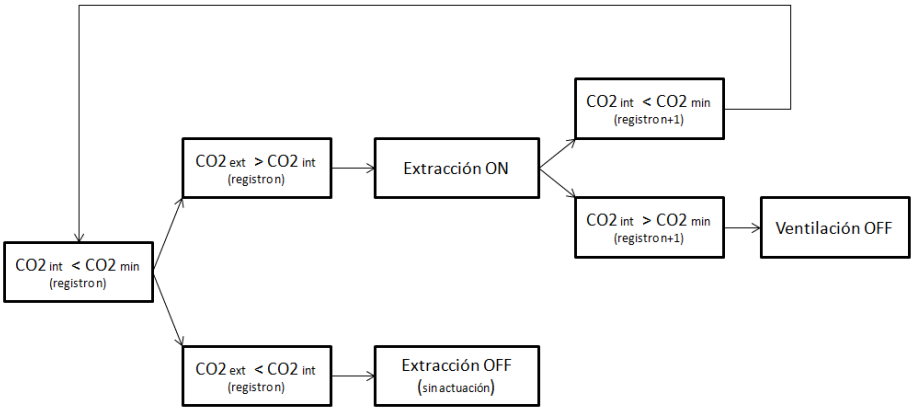

Fig. 11. Lazos de control cuando CO2int < CO2min.

Los sensores y actuadores seleccionados para este proyecto presentan diferentes tecnologías por lo que generan diferentes salidas. El concentrador de datos MPC-374 es capaz de adquirir simultáneamente tanto señales de sensores que presentan salidas analógicas, así como sensores que funcionan bajo protocolos de comunicación. A continuación, la Tabla 2 y Tabla 3 muestran las Entradas/Salidas de cada Sensor/Actuador.

Tabla 2. Tabla resumen de sensores.

Sensores	
Sensor	Salida
Temperatura, Humedad y CO_2 exterior	Modbus RTU
Temperatura, Humedad y CO_2 Interior	Modbus RTU
Radiación PAR	0-10 VDC
Analizador de red	Modbus RTU

Tabla 3. Tabla resumen de actuadores.

Actuadores	
Actuador	Entrada
Calefactor	0 - 230VAC
Ventilador	0 - 230VAC
Extractor	0 - 230VAC
Goteo	0 - 24VAC
Nebulizador	0 - 24VAC

Los sensores analógicos se conectan al puerto de entradas analógicas del MPC-374. Los datos de los sensores son adquiridos por medio de una conversión analógico-digital de 12 bits de resolución. Los datos adquiridos se almacenan en la memoria interna del datalogger estructurada como mapa de registros Modbus.
A continuación, la Tabla 4 detalla el mapa de registros Modbus correspondiente al puerto de entrada de canales analógicos.

Tabla 4. Mapa de registros Modbus correspondiente al puerto de entrada de canales analógicos.

MPC-374. 192.168.252.81				
ADDR Registro	Puerto	Sensor	Formato	Operación
4604	Analog input 1 - Voltage	PAR 1	Float 32	Read
4606	Analog input 2 - Voltage	PAR 2	Float 32	Read
4608	Analog input 3 - Current	--	Float 32	Read
4610	Analog input 4 - Current	--	Float 32	Read
4612	Analog input 5 - Current	--	Float 32	Read
4614	Analog input 6 - Current	--	Float 32	Read
4616	Analog input 7 - Current	--	Float 32	Read
4618	Analog input 8 - Current	--	Float 32	Read

Los sensores digitales (THCO2 interior y exterior) y los analizadores de red se conectan a un puerto de comunicaciones Modbus RTU, en concreto a la UART2. Los datos son adquiridos por una interfaz física RS485. Sobre esta interfaz se configura un cliente Modbus RTU. Los sensores son interrogados según el estándar marcado por este protocolo.
Los actuadores se conectan al puerto de salidas analógicas del MPC-374. Se trata de un puerto formado por salidas de control libres de potencial. Estas salidas atacan la bobina de cada uno de los contactores que encienden/apagan los actuadores según ordena el PLC. Las bobinas son atacadas con 24VDC. Este encendido/apagado se realiza acorde a las reglas de control programadas en el PLC.
El riego por nebulización es gestionado directamente por el puerto de salidas digitales incluido en el PLC ILC-131.
El riego por goteo no forma parte del sistema de control basado en umbrales. Es controlado de forma directa por el puerto de salidas discretas del MPC-374 con una programación horaria configurada en el MPC-374.
Una vez que las medidas de los sensores/actuadores se almacenan en el MPC-374 ya están disponibles para ser interrogadas por el PLC, SCADA o cualquier software que

haga la función de Máster de la red Modbus. El MPC-374, además de poder ser interrogado, ha sido configurado para enviar periódicamente la información almacenada por FTP.

7 Cultivos seleccionados y control de crecimiento

Con el propósito de evaluar experimentalmente cuál es el rendimiento de distintos tipos de cultivos hortícolas comunes, se decidió variar los cultivos en cada una de las plantaciones que se lleven a cabo en los próximos 2-3 años. Así, se han seleccionado los siguientes cultivos principales.

Ciclos de primavera-verano

Cultivos de la familia de las Solanáceas, en particular tomate (*Solanum lycopersicum*) y pimiento dulce (*Capsicum annuum*) (ver Tabla 5)
Cultivos de la familia de las Cucurbitáceas, en particular pepino (*Cucumis sativus*) y calabacín (*Cucurbita pepo*) (ver Tabla 5)
En asociación con éstos, se cultivará también:

- Lechuga (*Lactuca sativa*): es habitual asociar la lechuga con otras especies hortícolas, dada su tolerancia al sombreado y su rápido crecimiento, que permite cultivarla entre plantas de mayor porte sin que suponga una competencia significativa por nutrientes o implique otros efectos perniciosos. Se pueden intercalar entre las plantas de tomate, calabacín y pepino (ver Tabla 5).
- Ajo (*Allium sativum*): es un reconocido protector de otros cultivos. Se asocia favorablemente con pepino y muy favorablemente con lechuga, pimiento y tomate. Cabe a su vez considerar que entre los cultivos desfavorables están haba y judía.

La producción sostenible y ecológica aconseja el cultivo simultáneo de diferentes especies (*asociaciones*). En este caso, dado que el objetivo es determinar la influencia del vidrio fotovoltaico sobre el crecimiento y la producción de los cultivos, una situación ideal sería el cultivo de una sola especie, que evitaría distorsiones del crecimiento y la producción debidas a interferencias entre especies vecinas.
No obstante, ante la posibilidad de un eventual accidente -una plaga temprana de difícil control, por ejemplo- parece conveniente contar con al menos una especie con función protectora (ajo) y, en pro del aprovechamiento de recursos sin que suponga una competencia entre especies perniciosa para el cultivo principal, se cultivará también lechuga.

Tabla 5. Principales variables para los cultivos de ciclo de verano: Solanáceas y Cucurbitáceas.

	PRINCIPALES VARIABLES DE CONTROL			
	Temperatura (ºC)	**HR**	**Concentración CO_2**	**Radiación PAR**

		(%)	(ppm)	
TOMATE	Ópt.: 18 – 30 Mín. 10 Máx. 35	60 – 80	La concentración en aire debe ser ≥ 250	Floración – al menos 6 horas de luz diaria. Intensidad muy alta perjudicial
PIMIENTO	Ópt.: 18 – 25 Mín. 10 Máx. 35	50 – 70	La concentración en aire debe ser ≥ 250	–
PEPINO	Ópt.: 18 – 25 Mín. 15 Máx. 35	60 – 90	La concentración en aire debe ser ≥ 250	Poco exigente en cantidad de horas luz. Exigente en intensidad de luz
CALABACÍN	Ópt.: 20 – 30 Mín. 10 Máx. 35	65 – 80	La concentración en aire debe ser ≥ 250	–

Ciclos de otoño-invierno

Para el ciclo de otoño-invierno, (siembra y/o plantación en septiembre-octubre) se reduce de forma importante el número de especies hortícolas a cultivar, entre otras razones por necesidades de un fotoperiodo adecuado. Se plantarán los cultivos que a continuación se detallan.

Cultivos de la familia de las Leguminosas, en particular haba (*Vicia faba*) y guisante (*Pisum sativum*). Estos cultivos son considerados *mejorantes*: su implementación tiene como ventaja adicional que las especies de la familia Fabáceas (o Leguminosas) fijan el nitrógeno atmosférico en el suelo, siempre y cuando en sus raíces establezcan simbiosis con bacterias del género *Rhizobium*, que para ello deben estar presentes.

Las habas se desarrollan mejor en climas suaves que en los fríos. Temperaturas superiores a los 30 ºC entre la floración y el cuajado pueden provocar caída de flores y de vainas inmaduras, aumentando la dureza de estas, con la consiguiente pérdida de calidad. Toleran las heladas moderadas, incluso fuertes, pero de corta duración, siempre que no ocurran en flor. Prefieren suelos arcillo-limosos bien drenados, con pH neutros

o ligeramente alcalinos, aunque se adaptan a un amplio intervalo de pH (6,0 a 9,0) al igual que a suelos franco arenosos.

Las habas no tienen zarcillos, ni terminales ni foliares, por lo que no es planta de enrame; sus tallos, angulosos y fuertes, mantienen a la planta erecta sin necesidad de apoyos. Al no ser planta de enrame, el cultivo es sencillo, sin tutores ni apoyos, debiendo tenerse cuidado, si lo que se siembran son variedades de los grupos Aguadulce, Muchamiel, etc., de que las largas vainas no estén en contacto con el suelo.

Las habas son frecuentemente atacadas por pulgón, y puesto que no asocian bien con ajo ni cebolla, se recomienda incorporar otras plantas compañeras.

El cultivo de los guisantes se desarrolla entre 6 y 30 ºC, con temperaturas óptimas de desarrollo y reproducción comprendidas en los intervalos de 16-20 ºC para el día y 10-16 ºC para la noche. En general no soporta bien temperaturas superiores a los 30 ºC, influyendo negativamente sobre todo en la calidad del grano verde. Las variedades tradicionales (de grano) soportan bien las temperaturas invernales, pero evidentemente son un alto riesgo para el verdeo. Al igual que la mayoría de las leguminosas, los guisantes prefieren suelos de textura ligera o media bien drenados y aireados, con pH comprendido entre 6 y 7. Los suelos con altos niveles de calcio producen clorosis y endurecen el grano. Es un cultivo muy sensible a la compactación del terreno, reduciéndose el crecimiento y el área foliar, así como el número de flores en la planta.

En el caso del guisante cultivado, se distinguen dos subespecies: *elatius* y *sativum*, esta última con dos variedades botánicas: *arvense* y *sativum*; las variedades comerciales cultivadas en el mundo desarrollado pertenecen a esta última, si bien las de la arvense han sido y son forrajeras. Entre las variedades: (a) por el hábito de crecimiento las hay enanas, de medio enrame y de enrame, con altura de la planta desde 25 cm en las primeras hasta 300 cm en las últimas; (b) según la época de siembra: las hay de invierno y de primavera; y (c) por su ciclo productivo: de tempranas a tardías (de tres a cinco meses desde la siembra).

Otras opciones de cultivo en invernadero para el invierno podrían ser ajo, acelga, espinaca, brócoli y apio.

En cuanto al marco de plantación, se dejará un pasillo central que permita el paso y la manipulación de las plantas, a ambos lados del cual se ubican 2 líneas de cultivo, con espaciado entre plantas de 41-42 cm (ver Figura 12). El ajo se plantará en una línea de cultivo adicional al final de ambas mitades (desde el pasillo central). La lechuga se intercalará con las plantas de especies de mayor porte, y se cosecharán aproximadamente a mitad del ciclo biológico de éstas.

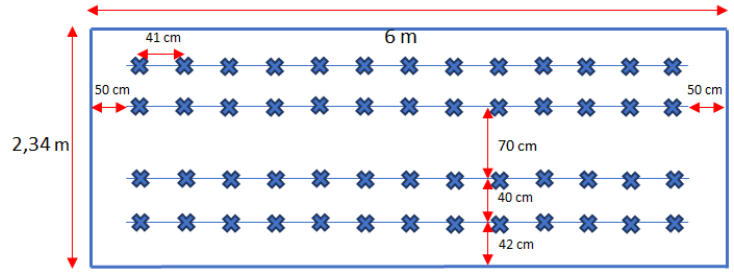

Fig. 12. Marco de plantación.

Para el estudio, tanto del crecimiento y desarrollo de las plantas, como finalmente de la producción de los cultivos, y por ende de las posibles diferencias generadas por la naturaleza de los dos materiales de cobertura del invernadero, el vidrio fotovoltaico y el convencional, se están observando los cultivos a razón de dos veces por semana. Se están tomando la medida de las variables mostradas en la Tabla 6.

Tabla 6. Indicadores de evolución comparada de los cultivos.

	Altura de la planta (cm)[1]	**Floración (días a la primera flor)[2]**	**Fructificación (días a la primera vaina)[3]**	**Peso de la parte comestible (gr)**
Tomate	x	x	x	x
Pimiento	x	x	x	x
Pepino		x	x	x
Calabacín		x	x	x
Haba	x	x	x	x
Guisante		x	x	x

(1) Frecuencia semanal
(2) Medida única
(3) Variable que se tomará a partir de maduración

Agradecimientos

El proyecto "Aplicación de la tecnología fotovoltaica integrada en edificios (BIPV) para invernaderos agrícolas" con número de expediente 04/16/AV/0001 ha sido realizado en el marco del programa Proyectos de I+D en PYMES. Este proyecto ha sido financiado por el Fondo Europeo de Desarrollo Regional (FEDER) de la Unión Europea y la Junta de Castilla y León, a través del Instituto para la Competitividad Empresarial de Castilla y León (ICE), con el objetivo de potenciar la investigación, el desarrollo tecnológico y la innovación.

Referencias

1. Aryanpur, V., Atabaki, M.S., Marzband, M., Siano, P., Ghayoumi, K.: An overview of energy planning in Iran and transition pathways towards sustainable electricity supply sector. Renewable and Sustainable Energy reviews, 112(September), 58-74 (2019).
2. Locker, C.R., Torkamani, S., Laurenzi, I.J., Jin, V.L., Schmer, M.R., Karlen, D.L.: Field-to-farm gate greenhouse gas emissions from corn stover production in the Midwetern U.S. Journal of Cleaner Production, 226(July), 1116-1127 (2019).
3. Lu, Y., Zhang, X-P., Huang, Z., Lu, J., Wang, D.: Impact of introducing penalty-cost on optimal design of renewable energy systems for net zero energy buldings. Applied Energy, 235(February), 106-116 (2019).
4. Hernández-Callejo, L., Gallardo-Saavedra, S., Alonso-Gómez, V.: A review of photovoltaic systems: Design, operation and maintenance. Solar Energy, 188(August), 426-440 (2019).
5. Chang, R., Cao, Y., Lu, Y., Shabunko, V.: Should BIPV technologies be empowered by innovation policy mix to facility energy transitions? – Revealing stakeholders´different perspectives using Q methodology. Energy Policy, 129(June), 307-318 (2019).
6. Hernández-Callejo, L.: A comprehensive review of operation and control, maintenance and lifespan management, grid planning and design, and metering in smart grids. Energies, 12(9), 1630-1680 (2019).

Machine learning data applied to monitoring PV systems: A case study*

D. J. Benavides[1,2][0000−0003−1624−8759], Paul Arévalo-Cordero[1,2][0000−0002−6721−1326], L. G. Gonzalez[2][0000−0003−1337−3829], Luis Hernández-Callejo[3][0000−0002−8822−2948], and F. Jurado[1][0000−0001−8122−7415]

[1] Universidad de Jaén, Campus Científico-Tecnológico de Linares, 23700 Jaén, Spain
[2] Universidad de Cuenca, Campus Tecnológico Balzay, 010107 Cuenca, Ecuador
[3] Universidad de Valladolid, Campus Universitario Duques de Soria, 42004 Soria, Spain
{djbp0001,wpac0001}@red.ujaen.es luis.gonzalez@ucuenca.edu.ec
luis.hernandez.callejo@uva.es fjurado@ujaen.es

Abstract. This paper develops an application model of machine learning and data mining for the monitoring of a photovoltaic installation of 35kW connected to public grid, based on the study of data mining on the power generated based on the meteorological variables influence of solar radiation and temperature of the area under study. The purpose of this paper is to evaluate the performance of the machine learning model to predict the energy production of three different photovoltaic systems, in response to the behaviour of the climatic variables of the area and also an analysis is made on the impact of cloudiness. On the other hand, it also includes the implementation of the resulting models through supervised learning in SCADA system, which will allow the operator to actively manage electrical grid, obtain reference values, compare the performance between systems, detect possible failures, etc. Achieving this, offer strategies in the simulation and real-time prediction of photovoltaic systems, in the concept applications of computational intelligence in energy systems.

Keywords: Machine learning · Photovoltaic · Monitoring · Real-time · SCADA.

1 Introduction

The integration of Renewable Energies (RE) in the electric grid intensifies the complexity for electric grid management to maintain service continuity and the production-consumption balance, due to the intermittent and unpredictable nature [6, 1]. Therefore, it is necessary to focus more on research and development in government and other levels to explore RE resources and meet energy needs globally [7]. The prediction in Photovoltaic (PV) production is necessary for the optimal integration of this technology in the existing power systems and is an

important factor for the operators of the electric grid. [1]. However, there are two main concerns about the implementation of PV systems in high penetration rates, intermittent nature and uncertainty of availability [3]. In addition, poorly functioning photovoltaic panels can cause gradual or rapid falls in the amount of energy generated. One study shows that it is possible to predict the daily power curve of a photovoltaic panel depending on the power curves of neighboring panels, by applying neural networks which allows monitoring the correct operation [4]. The precise forecast of PV production can mitigate the effects of energy quality that represent large quantities of distributed systems through the active management of electric grid and is an important feature that can help companies and operators in energy management and economic dispatch planning [1]. The power generated by a PV system at a given time is proportional to the solar radiation received by the Panel. However, the radiation varies due to the seasons and for several hours of the day, depending on the geographical location and orientation of the panel [4]. Therefore, it is important that the solar radiation and the corresponding energy production be predicted, so that the operator can acquire the appropriate measures and manage the intermittent [5]. Advanced data analysis applications with functionality and versatility allow managing energy system information to analyze and extract information, for example: improving energy quality, more efficient distribution, optimization, machine learning, among others. Under this same criterion the slogans are corrected as new information is known [2]. However, to obtain an acceptable model it is necessary to analyze a large amount of data for its training, considered thus an inconvenience in new systems and applications where this information is not yet available. Especially the technology of "Big Data" (BD) applied in the energy system that is currently in its initial stage and there is a long way to go [2]. There are several related studies of solar PV systems, from the point of view of modelling and simulation, however this behaviour in these systems is not always the same, because the climatic conditions are different in every part of the world. For this reason, it is necessary to carry out an additional study in real measured data to observe its behaviour under normal operating conditions. In this study, we present a model of prediction of the electric power (kW) generated by three different PV systems: polycrystalline, monocrystalline and tracking on an axis. Using machine learning techniques and data mining applied in SCADA (Supervisory Control and Data Acquisition) databases and climatic data obtained from the weather station, whose main objective is to establish a model using real-time indicators, which It will allow to establish a comparison between the real photovoltaic production compared to the photovoltaic production of the model. Finally, the results will be implemented in the SCADA system which will allow the operator to obtain a better reference and control over the production of photovoltaic energy.

2 Applications in energy management

There are many challenges ahead in terms of the BD Technology of smart grids, such as: data integration and storage, real-time data processing technology, data compression, great technology data visualization and privacy and data security [2]. In Fig. 1, shows some current applications of BD and "Machine learning" Focused in terms of RE management for smart cities, among which are: design, optimization, operation, control, Monitoring, supervision, issues of economic dispatch, Government, etc. [8]. All these topics can be analyzed from a database of a registrar, through machine learning and its derivatives. Thus promising, different applications in the field of energy management with sources of RE and storage systems correctly distributed in smart grids for a sustainable development.

Machine learning methods have been used to solve complicated practical problems in different areas and are becoming increasingly popular today [9]. For example, the energy system presents some important challenges for microgrid and power management of smart grids [10]. A study using the data mining algorithm "Decision Tree" with a black box model based on *Radom Forest* proposes the detection and classification of microgrid faults. [2]. In the community

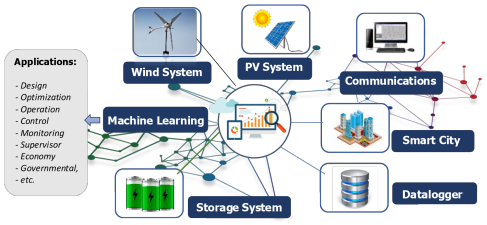

Fig. 1. Machine learning applications in energy systems

of solar forecasts, numerous investigations have been dedicated to the development of models that generate point forecasts, also called *deterministic forecasts* [5]. A machine learning algorithm to predict diffuse horizontal irradiance and behavioral sensitivity analysis for meteorological variables was used in the city of Hong Kong from 2008 to 2013, with excellent results. The proposed model would be appropriate for estimating long-term diffuse solar radiation, studying climate change and developing the typical meteorological year in Hong Kong. In addition the study presents the possibility of applying in places with similar climates [11].

3 Case study

Fig. 2, shows the location of the energy laboratory for the case study [12]. Located in the area $GTM - 5$ with geographic coordinates (-2.8919, -79.0385),

solar positioning is also observed from 7:00am - 7:00pm. The calculation of the position of the Sun is based on the equations that *J.J. Mi-chalsky* detailed in "Astronomical Algorithms". Being located near the equatorial line, the trajectory of the Sun in the place is directly elevated at midday during the days of the equinox. In addition, each daylight lasts about 12 hours, however, it also presents other problems that will be analyzed later. An example of data analysis

Fig. 2. Solar positioning during the day

and tools applied to the modeling and simulation of a photovoltaic system of this study is presented in [13], Its structure consists of 4 stages, in data acquisition, modeling and simulation, validation and finally its applications. In this study its application for monitoring out in more detail by comparing with the SCADA system, considering the databases PV system and the weather station. In Fig. 3, the structure of the machine learning application example in a mentioned PV system is described. Considering its study from the database generated by the SCADA datalogger.

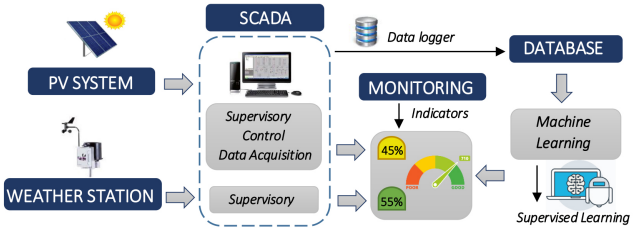

Fig. 3. Example of machine learning application in a PV system

3.1 PV System

The Photovoltaic System (PVS) consists of 136 panels of 250Wp of the Atersa brand, 60 of the monocrystalline type (15kW), 60 of the polycrystalline type (15kW) and 16 of the polycrystalline type with tracking on an axis (5kW). Each system is connected to a separate DC/AC inverter with the public grid [12].

3.2 Weather Station

Weather station located in the study area and at the same level of the photovoltaic installation, obtains the climatic information of the zone corresponding to the variables of solar radiation (W/m^2), ambient temperature ($°C$), relative humidity (%), precipitation (cm), wind speed (m/h), wind direction (°) and wind gust (m/h). These variables are assigned a sampling frequency of 1 minute.

3.3 Database

The database is created with the variables mentioned above and stored in the server's datalogger through the *Datalogging and Supervisory Control Module* and the Database connectivity tool of *LabVIEW 2015* software with the communication interface through *NI OPC servers*. In this way, the value of the variables is acquired and their conversion from analogue to digital signals for later viewing and storage.

3.4 Monitoring

The main objective of this research focuses on this point. It proposes an application model in the monitoring of this PV installation. Analyze the information of the database and its implementation in the SCADA system, as a support or help in the event that there are faults in the electrical system or measurement errors, by means of indicators relating the variables of the PV system and weather station, in this way it allows the operator to improve the security and reliability in the system.

3.5 SCADA System

The SCADA allows the control of the PV system in activation and disconnection of the DC/AC inverters, from electric grid, it also allows the supervision of the electrical variables of current, voltage and power in DC, current, voltage, power, (active, reactive and apparent) in AC of each PV system. Data acquisition is performed by means of measuring sensors and network analyzers, connected by means of a PLC through Modbus communication that allow reading/writing and storing the information in the local server [12].

4 Machine learning

Computing power that increases drastically and the reduction of the hardware cost, some new information extraction methods have been proposed and developed. Machine learning is a branch of artificial intelligence and deals with the construction and study of systems that can learn from data sets by giving computers the ability to learn without being explicitly programmed [6]. Machine

learning identifies knowledge and patterns in data, which is currently considered one of the most useful techniques for extracting information [2]. Machine learning algorithms use computational methods to "learn" information directly from the data without relying on a predetermined equation as a model [14]. In general, there are nine most used machine learning algorithms, "including k-means, Linear Support Vector Machines (LSVM), Logistic Regression (LR), Locally Weighted Linear Regression (LWLR), Gaussian Discriminant Analysis (GDA), Back-propagation Neural Network(BPNN), Expectation Maximization (EM), Naive Bayes (NB) and Value-Added Tax (VAT). Each of the algorithms has its own characteristics and can be used under different scenarios" [2]. Several methodologies based on artificial intelligence such as machine learning, Genetic Algorithm (GA) and Neural Networks (NN) have been proposed and applied for the modeling and forecasting of solar irradiance [9]. Although the main drawback of neural networks is the long training time and many parameters that require the intervention of the user [3].

It is also important to consider that a greater amount of data and relevant information (data mining) with respect to a better study topic will be the possibilities of finding an appropriate application model. Considering the objectives on the application of the case study. Data analysis is projected through *supervised learning*, that is, creating a predictive model from known input and response data. In this type of learning two categories of algorithms are used: *classification* destined to databases that include qualitative values (words) and *regression* for quantitative (numerical) databases. Based on the numerical characteristics of the databases obtained from the SCADA system, it will be used in the *regression* category for the analysis. Fig. 4 shows the workflow to establish an ideal model defined under two criteria in *training* and *application phases*. In the *training phase* to effectively apply a learning technique to a performance function, it must be subdivided into 4 stages: initially enter the database, then perform a preprocessing (filters, statistical summary, cluster analysis), then define the category of supervised learning (classification or regression) and finally the model is obtained. In the *application phase*, the new database is entered, the preprocessing is performed again, the model obtained in the training phase is applied to identify the important characteristics and architectural parameters of each model, to define the predictive model. Finally, evaluate the performance of the model [14, 1].

4.1 Training phase

In the application of a predictive model for the estimation of solar energy, the databases of both the PV system and weather station will be studied under a same sampling rate corresponding to one year, which allows to establish a correct relation of variables of equitable way. Before applying a learning algorithm to the model it is necessary to perform a preprocessing, where the database must be analyzed, for example in SCADA systems it is very frequent the loss of information from a record, either in errors of measurements of the sensors or

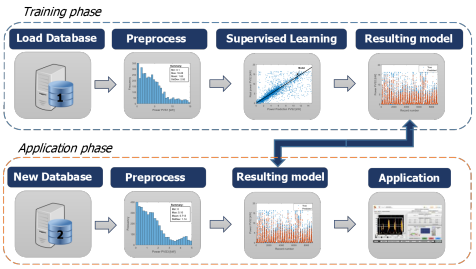

Fig. 4. Ideal workflow of Machine Learning [14]

in the discretization processing of analog reading variables. For this reason, it is necessary to be familiar with all the variables in the database, in order to verify some type of irregularities. An effective method in the case that the database has lost values, is to replace its value by the average of the previous and subsequent data in the registry.

The ideal methodology for developing optimal models of machine learning for predictions of PV energy should include a training phase (one-year), a validation phase (per month) and a test phase (per month), as shown by a similar study in [1]. Fig. 5 shows the production of PV power (kW) defined as a variable to be predicted under the supervised learning criterion. The records correspond to a one-month test database (43200x3 data) for the PVS1, PVS2 and PVS3 systems. The maximum generation limit for PVS1, PVS2 is 15kW and for PVS3 is 5kW. This power is limited by the inverters connected to the power grid. In this way it is possible to observe the differences in the electrical generation by the three PV systems. The PVS3 (5kW) differs from other systems, due to its structure of solar tracking on an axis, which allows to obtain a better use of solar energy. An average percentage increase of 15 % is estimated for the same installed power capacity with respect to the fixed system in a study conducted during the test phase for the month of July 2018. The prediction of PV

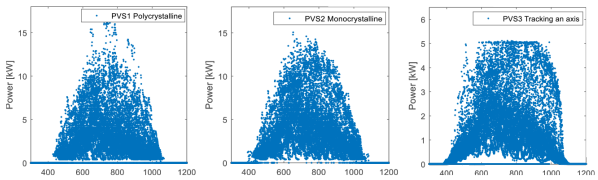

Fig. 5. Power generated during one month (July 2018) (a) PVS1, (b) PVS2, (c) PVS3

generation depends largely on the study of the behavior of the system, because it plays an important role in the operational management of power grids. [10]. The data of the weather station as a function of the variable to predict Power

PVS1, are shown in Fig. 6. It is possible to observe its correlation with the variables of solar radiation, temperature, relative humidity, wind speed, wind gust and precipitation respectively. A possible linear regression model can be clearly observed with respect to the variable of solar radiation. Another point of interest is the inverse relationship between the parameters of temperature and relative humidity. On the other hand, the variables of wind speed, wind gust, wind direction and rainfall do not show a pattern of interest in the model. This analysis can also be observed when constructing the correlation matrix between the aforementioned variables, as established in a preliminary study in [13]. In the

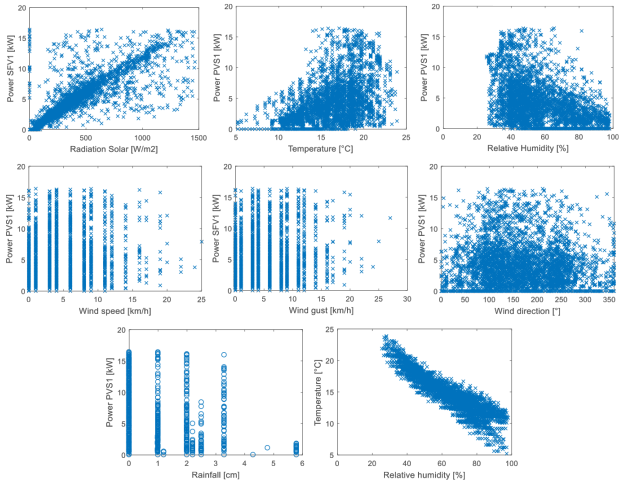

Fig. 6. Power PVS1 according to the variables of the weather station (a) Solar radiation,(b) Temperature,(c) Relative humidity,(d) Wind speed,(e) Wind gust, (f) Wind direction, (g) Rainfall and (h) Temperature vs RH

database corresponding to weather station, *solar radiation* and *temperature* are defined as the most influential variables on the photovoltaic prediction models, as detailed in a preliminary study in [13]. Fig. 7a shows the behavior of the temperature of the maximum and minimum values during the 24 hours of the day corresponding to the month of August 2018 (test phase). An average of variations between $8-22°C$ can be observed and it is possible to define a model of the temperature by means of the "sum of sine" function defined in Equation (1) [13]:

$$f(t) = 16.21 \cdot \sin(1.362 \cdot t + 0.6172) + 2.787 \cdot \sin(9.649 \cdot t + 2.118) \qquad (1)$$

Where, $f(t)$ represents the approximate value of the temperature in the study area and "t" corresponds to the record variable (hour-minutes). In addition, it is possible to observe that the temperature decreases in the night hours and

increases its maximum values with the solar radiation data during the midday hours. A machine learning study for the prediction of the solar radiation of the PV system, shows that it is possible to obtain a model with great approximation, using the forecast parameters the variables of temperature, relative humidity, wind speed and irradiance [9]. Using a model it has been established that there is a large percentage of data below the curve of the solar radiation limit values $g(t)$, according to Equation (2), where "t" indicates the number of records (value between 0 - 290 for the example), obtained through machine learning in Matlab:

$$g(t) = 477.5 \cdot \sin(0.0017 \cdot t + 1.345) + 276.75 \cdot \sin(0.0498 \cdot t + 0.371) + 723.25 \cdot \sin(0.0249 \cdot t - 2.16) \quad (2)$$

Fig. 7a and Fig. 7b, show the results of the application of Equations (1) and (2), together with the values of temperature and solar radiation respectively, corresponding to the month of August 2018 (test phase). Although, in this study

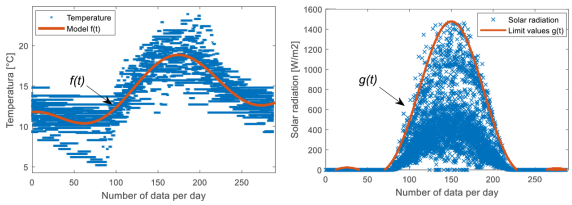

Fig. 7. (a) Temperature and (b) Solar radiation, during one month weather station (Test phase -August 2018)

it is necessary to consider an important factor of cloudiness, since according to the State Agency of Metrology (SAMET) the areas of maximum cloudiness are in the equatorial zone and between 60 and 70°. A single cloud that passes can bring the energy production of a solar farm from the total production to the minimum and return to the whole in a matter of minutes or even seconds [5]. This information can be seen in Fig. 8a where there is a large amount of solar radiation data that drastically change during daylight hours. This effect directly affects the production of energy in PV systems. Fig. 8b shows the power generated by the three photovoltaic systems under study, under practically zero cloud conditions. Mitigation measures for large drops in solar radiation, such as response to demand, storage and scheduling within an hour can only be maximized with accurate and reliable forecasting [5]. In Table 1, the results of the application of some models are described in terms of cloudless conditions on the power curve of the PVS1, PVS2 and PVS3 systems. Defined by means of the adjustment parameters of the sum of squares due to error SSE and the root of the mean square error RMSE. This process was carried out using the tool Curve Fitting Toolbox^{TM} software of MATLAB, on the models that best described the curvature based on the functions of "*Fourier*", "*Gaussian*" and "*Sum of Sine*",

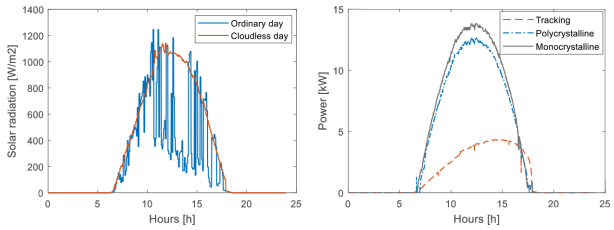

Fig. 8. (a) Impact of cloudiness on radiation, (b) Photovoltaic power PVS1, PVS2 and PVS3 (clear day)

all of the 4th order and considering as variable only the time (hours-minutes).

Table 1. Application of models for PVS1 systems, PVS2 and PVS3, clear weather

	Fourier 4^{th}		**Gaussian** 4^{th}		**Sum of Sine** 4^{th}	
Description	**SSE:**	**RMSE:**	**SSE:**	**RMSE:**	**SSE:**	**RMSE:**
PVS1	**98.24**	**0.262**	81.21	0.239	96.89	0.261
PVS2	**109.10**	**0.276**	76.28	0.231	113.90	0.283
PVS3	83.04	0.241	58.93	0.203	**97.28**	**0.261**

Next, the function models for cloudiness are described and the values of the coefficients are detailed in Table 2:

– PVS1 (General model Fourier 4th):

$$\begin{aligned} PVS1_{Cloudless}(t) = a_0 + a_1\cos(t\cdot w) + b_1\sin(t\cdot w) + \\ a_2\cos(2t\cdot w) + b_2\sin(2t\cdot w) + a_3\cos(3t\cdot w) + \\ b_3\sin(3t\cdot w) + a_4\cos(4t\cdot w) + b_4\sin(4t\cdot w) \end{aligned} \tag{3}$$

– PVS2 (General model Fourier 4th):

$$\begin{aligned} PVS2_{Cloudless}(t) = a_0 + a_1\cos(t\cdot w) + b_1\sin(t\cdot w) + \\ a_2\cos(2t\cdot w) + b_2\sin(2t\cdot w) + a_3\cos(3t\cdot w) + \\ b_3\sin(3t\cdot w) + a_4\cos(4t\cdot w) + b_4\sin(4t\cdot w) \end{aligned} \tag{4}$$

– PVS3 (General model Sum of Sine 4th):

$$\begin{aligned} PVS3_{Cloudless}(t) = a_1\sin(b_1\cdot t + c_1) + a_2\sin(b_2\cdot t + c_2) + \\ a_3\sin(b_3\cdot t + c_3) + a_4\sin(b_4\cdot t + c_4) \end{aligned} \tag{5}$$

Table 2. Coefficient of the equations

	PVS1 (Fourier 4^{th})	**PVS2** (Fourier 4^{th})	**PVS3** (Sum of Sine 4^{th})
$a_0 =$	4.27	4.682	-
$a_1 =$	-5.76	-6.396	3.227
$a_2 =$	1.256	1.443	0.3615
$a_3 =$	0.0464	0.1421	1.297
$a_4 =$	0.255	0.2201	0.307
$b_1 =$	-3.192	-3.348	0.166
$b_2 =$	2.052	2.21	0.8523
$b_3 =$	0.3879	0.4118	0.4889
$b_4 =$	-0.5591	-0.6314	1.12
$c_1 =$	-	-	-0.6329
$c_2 =$	-	-	-5.416
$c_3 =$	-	-	-5.124
$c_4 =$	-	-	-3.941
$w =$	0.2971	0.2964	2.540

A comparison between the photovoltaic generation of the PVS1, PVS2 and PVS3 systems of a completely clear day versus the result of the application of the Equations (3), (4), (5) respectively are presented in figure Fig. 9. This shows that for days of low cloudiness, it is possible to establish a model based on the variable "time" (hours of the day) only with an excellent approximation as a special case.

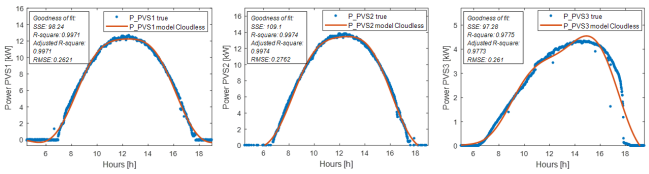

Fig. 9. Results of the application of the models, clear weather (a) PVS1 (b) PVS2 (c) PVS3

4.2 Validation phase

Now, considering the effects of cloudiness in this study, it can be seen that it is not possible to define a model only with the variable "time", it is necessary to find patterns with respect to the meteorological variables described above. For this reason, linear regression models are defined below using temperature and solar radiation as input variables of the functions.

– PVS1 Polycrystalline equation (83.27%)

When applying the *linear regression model* with the variables of *solar radiation* and *temperature*, a correlation coefficient of 0.8327 was established, which demonstrates an acceptable value in the model. In Equation (6), the power generated from the PVS1 is presented as a function of the variables of solar radiation (W/m^2) and temperature ($°C$). Fig. 10a shows the approximation of the real value and the prediction result during the *training phase*, where the values outside the line of the model represent in large part the effects caused by the crossing of clouds in the area. Subsequently, the results are presented in the *validation phase* (See Fig. 10b). It is possible to observe a good approximation to the real values. Under this same analysis criteria will develop for PVS2 and PVS3 in Equations (7) and (8) respectively below:

$$P_{PVS1}(rad, temp) = 0.0088 \cdot rad + 0.0999 \cdot temp - 1.1393 \tag{6}$$

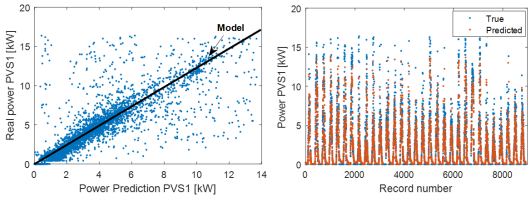

Fig. 10. (a) Regression model applied to PVS1, (b) Phase validation PVS1

– PVS2 Monocrystalline equation (82.36%)

$$P_{PVS2}(rad, temp) = 0.0096 \cdot rad + 0.1162 \cdot temp - 1.3018 \tag{7}$$

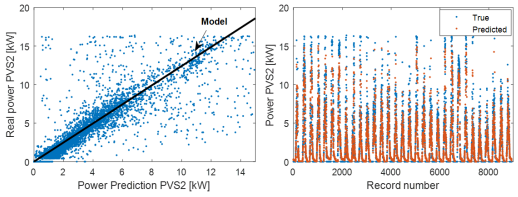

Fig. 11. (a) Regression model applied to PVS2, (b) Phase validation PVS2

– PVS3 Tracking on an axis equation (85.76%)

$$P_{PVS3}(rad, temp) = 0.0037 \cdot rad + 0.0225 \cdot temp - 1.1745 \quad (8)$$

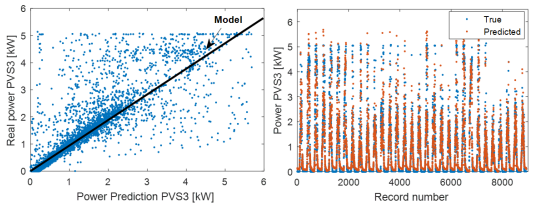

Fig. 12. (a) Regression model applied to PVS3, (b) Phase validation PVS3

4.3 Application to SCADA

The forecast of the power output of the PV systems is necessary for the proper functioning of electric grid or the optimal management of the energy flows that occur in the PV system [6]. Therefore, it is very important to integrate a monitoring system in real time, which guarantees the safety in operation and the control of the electrical systems supervised by the SCADA. Under this concept, the linear regression models developed in this study will be integrated. It should be noted that in order to develop a monitoring system in real time, it is necessary to study the corresponding database. Carry out all the steps to approximate the real value with the prediction, once the model is formulated under all possible considerations and cases, the model can be applied. An electric operator must ensure a precise balance between electricity production and consumption at any time. This is often very difficult to maintain with a conventional and controllable energy production system, mainly in small or non-interconnected systems [6]. Therefore, it is necessary to cover the term of real time, although to be able to apply a predictive model in real time, a previous analysis of databases is required. Later its application is possible including the equations of the resulting models in the SCADA system. Enter the measurements in real time, that is, the SCADA carries out the measurement, discretization and calculation in the corresponding formula of the model. Fig. 13 shows the implementation of the study carried out, with the integration of equations 1 to 8, corresponding to the prediction of temperature $f(t)$ and the limits of solar radiation $g(t)$. Photovoltaic production on cloudless days: $PVS1_{Cloudless}(t)$, $PVS2_{Cloudless}(t)$ and $PVS3_{Cloudless}(t)$. Photovoltaic production on ordinary days: $P_{PVS1}(rad, temp)$, $P_{PVS2}(rad, temp)$) and $P_{PVS3}(rad, temp)$. The input parameters corresponding to time (t), solar radiation (rad) and temperature $(temp)$, These parameters are acquired in real time from the SCADA system, then they enter the equation models and return the calculated prediction value.

The evaluation of the models will be obtained by means of a percentage indicator “meter” which is assigned to compare between the real value of power and the value of the prediction, in such a way that, if its value is lower than 20% (any assigned value) implies that there is a difference of 20% in the photovoltaic production of the real value and the prediction, which must be considered by the operator of the electrical system. Under these circumstances, an alarm indicator has also been implemented, in the case of similar situations. On the other hand, the temperature model $f(t)$, it can be used to verify the measurement status of that variable. Similarly, the solar radiation limit model $g(t)$, it allows checking the status of the measurement sensor, that is, verifying that the measurement value does not exceed the value of the resulting model at the set time.

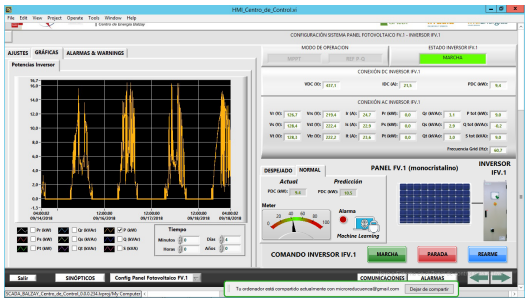

Fig. 13. Example of machine learning application in SCADA

5 Conclusions

As industrial development increases, automation and processes generate more data and information and require analysis, interpretation and communication. Therefore, this study has demonstrated the application of machine learning techniques in the analysis of real data and the development of predictive models. Considered a key field of application in future technologies.

The factor of cloudiness in the area and the impact generated in energy production were analyzed, as a response has been defined some models applicable on clear days, where it is possible to predict the photovoltaic power of the three systems studied. The regression models have also been defined for the prediction in ordinary days based on solar radiation and temperature with an excellent approximation. According to the ideal workflow for machine learning applications, it has been concluded with the implementation of the prediction models of photovoltaic systems in the SCADA system, available in electrical system operator monitoring applications to guarantee greater reliability, operation and control of these PV systems.

This work has been developed as an example of computer intelligence application based on machine learning techniques and data mining. Demonstrating

its wide variety and development in the field of energy management and its importance in smart grids.

References

1. S. Theocharides and G. Makrides and G. E. Georghiou and A. Kyprianou, "Machine learning algorithms for photovoltaic system power output prediction," 2018 IEEE International Energy Conference (ENERGYCON), pp. 1-6, June 2018.
2. Chunming Tu and Xi He and Zhikang Shuai and Fei Jiang, Big data issues in smart grid – A review, Renewable and Sustainable Energy Reviews, vol. 79, pp.1099 - 1107, November 2017.
3. T. T. Teo and T. Logenthiran and W. L. Woo and K. Abidi, "Forecasting of photovoltaic power using regularized ensemble Extreme Learning Machine," 2016 IEEE Region 10 Conference (TENCON), G., pp. 455-458, November 2016.
4. T. Huuhtanen and A. Jung, "PREDICTIVE MAINTENANCE OF PHOTOVOLTAIC PANELS VIA DEEP LEARNING," 2018 IEEE Data Science Workshop (DSW), pp. 66-70, June 2018.
5. Hugo T.C. Pedro and Carlos F.M. Coimbra and Mathieu David and Philippe Lauret, "Assessment of machine learning techniques for deterministic and probabilistic intra-hour solar forecasts," Renewable Energy, vol. 123, pp. 191 - 203, August 2018.
6. Cyril Voyant and Gilles Notton and Soteris Kalogirou and Marie-Laure Nivet and Christophe Paoli and Fabrice Motte and Alexis Fouilloy, "Machine learning methods for solar radiation forecasting: A review," Renewable Energy, vol. 105, pp. 569 - 582, May 2017.
7. Kurien, Caneon and Kumar, Ajay, "Scope of Artificial Intelligence Techniques for Exhaust Emission Prediction of CI Engines and Renewable Energy Applications," International Conference on Advances in Computing Applications (ICACA-18), pp. 456-461, February 2018.
8. Sunil Kr. Jha and Jasmin Bilalovic and Anju Jha and Nilesh Patel and Han Zhang, "Renewable energy: Present research and future scope of Artificial Intelligence," Renewable and Sustainable Energy Reviews, vol. 77, pp. 297 - 317, September 2017.
9. Jiaming Li and John K. Ward and Jingnan Tong and Lyle Collins and Glenn Platt, "Machine learning for solar irradiance forecasting of photovoltaic system," Renewable Energy, vol. 90, pp. 542 - 553, May 2016.
10. Manoja Kumar Behera and Irani Majumder and Niranjan Nayak, "Solar photovoltaic power forecasting using optimized modified extreme learning machine technique," Engineering Science and Technology, an International Journal, vol. 21(3), pp. 428 - 438, June 2018.
11. Siwei Lou and Danny H.W. Li and Joseph C. Lam and Wilco W.H. Chan, "Prediction of diffuse solar irradiance using machine learning and multivariable regression," Applied Energy, vol. 181, pp. 367 - 374, November 2016.
12. J. L. Espinoza and L. G. González and R. Sempértegui, "Micro grid laboratory as a tool for research on non-conventional energy sources in Ecuador," 2017 IEEE International Autumn Meeting on Power, Electronics and Computing (ROPEC), pp. 1-7, November 2017.
13. D. J. Benavides and F. Jurado and L. G. González, "Análisis de datos y herramientas aplicadas al modelado y simulación de un sistema fotovoltaico en Ecuador," Enfoque UTE, vol. 9, pp. 1 - 12, December 2018.
14. MATLAB, "MATLAB Machine Learning," https://es.mathworks.com/solutions/machine-learning.html, 2018/08/21.

Contribution of the wind turbine based on a special alternative current generator to the production of positive energy

Chems eddine Rouabhia[1], Abdelkarim Bouras[2], Slimane Bouras[3] and Nassim eddine Haouem[3]

[1] Electromechanical Engineering Laboratory, Department of Electromechanical, Badji Mokhtar University Annaba, Algeria
[2] Electromechanical Systems Laboratory, Badji Mokhtar University Annaba, Algeria
[3] The industrial risks, C.N.D, S.O.M.M Laboratory, Badji Mokhtar University Annaba, Algeria

karim.bouras@hotmail.com

Abstract. The priority of smart cities with positive energy is the control of the energy demand and the flexibility of consumption, the energy planning and the innovative management of the electrical network.
In this context, this research focuses on the study of a conversion system of wind energy advocating a particular machine design. The latter has as a stator, a direct current machine inductor and as a rotor, a wound rotor. The alternative electrical energy produced is poured into the utilitarian grid through its three rotor rings. Considering the instability of the wind, this WRAG (Wound Rotor Alternative Generator) multipolar generator has the advantage of adapting a variety of voltages for each imposed speed just by varying a low intensity excitation current at the level of the inductor.
Even if the use of a mechanical multiplier and an electronic power for this wind turbine remains necessary, they will be smaller size and therefore less expensive. Thus, the reduction of mechanical and electrical losses will contribute to the increase of the lifetime of our wind system. The aerogenerator presented in this work can contribute as an inexpensive and robust alternative solution for a small power wind energy conversion chain operating in isolated sites. The work is validated by experimental readings on a WRAG of 3 kVA.

Keywords: Electrical Energy, Wind Energy, Alternative Generator, Mechanical Multiplier, EMF.

1 Introduction

Generally, there are three main families of wind turbines: asynchronous machines, synchronous machines and machines with special structures [1–6]. Generators (dynamos and alternators) operate on the principle of producing the alternating current due to the variation of the magnetic field. The brushes, acting as a switch, take the current from the rotor when it is at the correct polarity. For the dynamo, the rotor rotating in a fixed magnetic field that produces the current. All the current must go

through the collector. In an alternator, it is the rotor that produces a rotating magnetic field and the fixed stator produces the current. Because of its relatively low cost and its maintenance [7, 8], the self-excited squirrel-cage asynchronous generator, in autonomous operation, appears as a very interesting solution, compared to other types of machines such as DFAG (Doubly-fed asynchronous generator) and the SG (synchronous generator). Asynchronous electrical machines are relatively simple, robust and less demanding in terms of maintenance and therefore not expensive. Although their robustness is slightly diminished by the presence of rings and brooms system, at least for the DFAG, the benefit of variable speed operation is a sufficient advantage for the use of this type of machines. Numerous studies have shown the interest of the variable speed in wind energy, even in the small wind turbine where the extra cost caused by the variable speed (because of the power electronics and additional regulation) is offset by the surplus production [9–13]. Only, regardless of the type of asynchronous machine used, the presence of a mechanical speed multiplier and an electronic interface is essential. The alternative low power aerogenerator that we recommend can help to be an intermediate solution. The WRAG has a ring rotor coupled to the network (or to the load). As a stator, it has a direct current machine inductor. This solution will be effective and less expensive, since it is less demanding in terms of size of the speed mechanical multiplier and of electronic converters.

This is the consequence that, from the start, there is a relatively lower speed ratio with the availability of a significant EMF (electromotive force) induced in the rotor. The advantageous exploitation of this wind system based on the WRAG is concretized by the fact of producing an adequate tension, by adjusting a compensatory magnetic flux at each weakening of the wind speed, only by injecting a DC current that does not exceed the unit at the level of the excitation.

The validation of this study was performed on a 3 KVA wound rotor alternative current generator (WRAG), involved in a wind system of small power at the isolated site of Adrar region in the Algerian Sahara for local positive energy needs. This machine offers a good compromise between the speed variation range and sizes the mechanical (Multiplier) and electronic (Rectifier and Inverter) converters [14, 15].

This study will focus on the performance of this WRAG machine dedicated to the wind system based on data provided by the wind map of the region.

2 Theoretical Background

2.1 Generalities

Today's small wind turbines are mostly 3 blade horizontal axis machines equipped with permanent magnet alternators and a passive orientation device.

Currently, for great depth drilling, the aerogenerator option is preferred, coupled with an electric pump that is more reliable than mechanical pumping [16–20]. To operate with minimal efficiency, a wind system requires an average annual wind speed of at least 4 m/s. However, having high speeds is not enough. Indeed, it is im-

portant to have, throughout the year, a number of hours during which the wind speed is high.

2.2 Basic Parameters For Calculating The Wind Turbine

To characterize a wind sensor, and especially its efficiency, three main operating parameters are considered [21], the specific speed λ which is expressed as the ratio of the peripheral speed (at the end of the blade) U = ω R with the speed V of wind:

$$\lambda = \frac{U}{V} = \frac{\omega R}{V} \quad (1)$$

With, ω the rotation speed of the turbine and R the extreme radius of the blade. The quantity λ indicates whether the turbine is fast (λ >3) or slower (λ <3). Not to mention that a high speed of rotation has bad consequences that are related to noise.

The power coefficient C_p, depending on wind speed and rotation speed, has a maximum value of 0.592 defined by Betz.

The coefficient of the torque, which indicates the performances of the wind sensor through the parameters C_p and C_c, is written as the ratio of the engine torque C_m which is exerted on the output shaft of the wind turbine. $C_m = P_m / \omega$ with the aerodynamic torque C_a.

$$C_c = \frac{C_m}{C_a} = \frac{C_p}{\lambda} \quad (2)$$

2.3 Formulation Of The Power Of The Wind System

The mechanical power P_{mg} available on the shaft of the electric generator, considering the ratio of the speed multiplier K, is expressed by:

$$P_{mg} = \frac{1}{2} C_p(\lambda)\left(\frac{R\Omega_2}{KV_1}\right)\rho\pi R^2 V_1^3 \quad (3)$$

Where: Ω_2 is the rotational speed after multiplier.

The mechanical power recovered by the wind turbine can be written simply:

$$P_{Turbine} = \frac{1}{2} C_p \rho\pi R_p^2 V_w^3 \quad (4)$$

Where:

C_p is the aerodynamic power coefficient;

$\rho = 1.3 Kg / m^3$, density of the air;

$R_p = 1.2$ m, turbine radius;

V_w is the wind speed.

Figure 1 present the characteristic of the mechanical power provided by the turbine of the wind system contributes easily to the determination of the electric power that will be provided by the generator according to the wind speed $P_{él} = f(V_{wind})$.

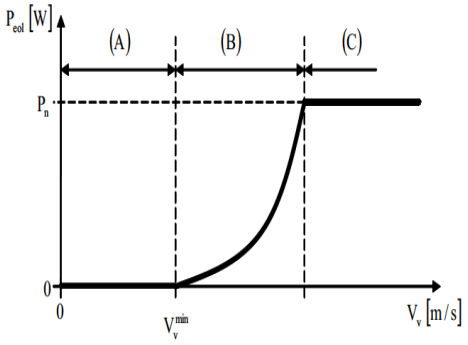

Fig. 1. Electric power of a wind turbine: A- start, B- Production zone, C- Power limitation.

The machine we are going to experiment shows the typical characteristics of a 3 blade wind turbine with wind speeds of less than 9 m/s. After operating the wind map and considering the average yield, the practical formula for a fast horizontal axis wind turbine is as follows:

$$P = 0{,}2\, D^2\, V^3 \tag{5}$$

Where: P is expressed in Watts, D is the diameter in meters and V is the wind speed in m/s.

Generally, the dimensioning of the generator is based on its useful electrical power deduced from the conversion of the mechanical power at the entrance of the machine. The latter requires the calculation of the turbine diameter and the sufficient wind speed to convert the wind energy.

The mechanical multiplier, and the calculation of its various elements, is deduced from the number of revolutions necessary for the generator to deliver the desired power.

All of these forces result in the appearance of a global alternative electromotive force (E) at the terminals of the rotor winding which is proportional to the intensity of the fixed inductor field (Stator) and to the speed of rotation of the engine Ω.

$$\mathrm{E} = \omega.\Phi = \mathrm{p}\,\Omega\Phi \tag{6}$$

With: the flow of the inductor is: $\Phi_s = k\, I_{exc}$

p: is the number of pairs of poles, k: is a constant of the electric machine and I_{exc} the intensity of the excitation direct current.

3 Test Bench

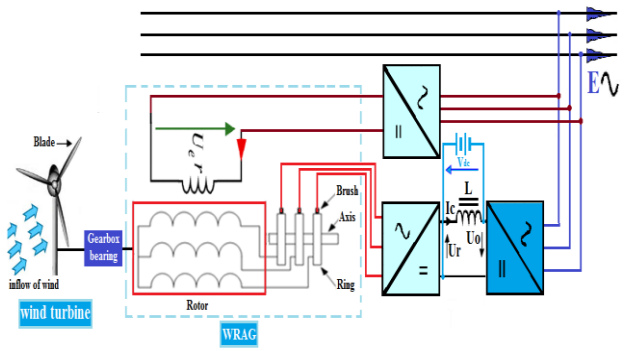

Fig. 2. WRAG wind turbine conversion chain.

In order to carry out an experiment on our WRAG wind system (Fig. 2) and to adapt it to the Adrar wind site, we used a group of electric machines (Fig. 3) consisting of a variable speed direct current motor with separate excitation coupled to the wound rotor alternative current generator (WRAG).

Fig. 3. Test bench: WRAG 3 KVA.

Table 1 present the characteristics of the electrical machines involved in the test bench are as follows:

Table 1. Nominal characteristics of electrical machines.

Type of Machines	Direct current motor	Alternative current Generator
Power	3 Kw	3 KVA
Voltage	220 V	~220 V
Intensity	10 A (induced)	~7.5A (Rotor)
Speed	1500 rpm	1500 rpm

Pairs of poles (p)	2	2
Direct current excitation	1.2 A	0.75A
DC voltage excitation	220 V	190 V
cos φ	-	0.8

The sampling of the speed is achieved by means of an alternative current tacho-generator (TG) with a coefficient: $\gamma = 8$ volts / 1000 rpm.

4 Experimental Results And Discussion

4.1 Mechanical Calculation And Application Of WRAG For The Adrar Site

Equipped with a horizontal axis turbine with a diameter D = 7.24 m and driven at a specific average speed (Adrar region) V = 6.25 m/s, our aerogenerator will have a transmitted mechanical power: $P_{mec} = 0.2.\ 7.242.\ 6.253 = 2560$ W.

The electric power delivered by the WRAG is: $S_{nom} = 3$ KVA, cos φ = 0.8 and $P_{él}$ = S.cos φ = 2400 Watts, for a turbine with D = 7.24 m and the wind speed V = 6.25 m/s.

To satisfy the nominal speed (Table 1) of the shaft of our generator $n_G = 1500$ rpm and adapt it to the speed 16.5 rpm of the large shaft of the turbine, there must be a mechanical speed multiplier with a factor G = 90. For the case of the Adrar site, it is in October and December that the monthly speed is the lowest of the year with 5.8 m/s in Table 2.

Table 2. The monthly wind speeds for Adrar and the corresponding EMF (Eg) at WRAG terminals with $I_{exc} = 0.75$ A, and φ = constant.

Month	Wind: V_m (m/s)	WRAG: n (rpm)	EMF: E (Volt)
January	6.2	1186.6	215
February	6.4	1224.88	218
March	6.5	1244.019	222
April	6.5	1244.019	222
May	6.9	1320.57	230
June	6.1	1167.464	212
July	6.7	1282.296	228
August	6.2	1186.6	215
September	6	1148.325	205
October	5.8	1110.047	195
November	5.9	1129.186	202
December	5.8	1110.047	198
V average/year	6.25	1196.17	218

Therefore, at the entrance of WRAG, the speed will be 1377.69 rpm and induce at its terminals an EMF approximating 240 V.

By acting only on the excitation current I_{exc} to decrease the flux, the voltage 220 V can be maintained without going through the inverter presented in Table 3 that illustrates the EMF's obtained experimentally at the terminals of the generator when it varies with the current of excitation of the inductor (or stator) and the speed of rotation of which we give the correspondence on the side of the turbine that is the wind speed.

Table 3. The wind speeds and the corresponding EMF's obtained experimentally.

WRAG n (rpm)	Wind V_m (m/s)	EMF of WRAG E (Volt)	
		$I_{exc.}$ = 0.5 A	$I_{exc.}$ = 0.75 A
600	3.135	80	100
700	3.657	90	115
1000	5.225	130	175
1200	6.27	160	215
1400	7.31	190	250
1500	7.83	220	270
600	3.135	80	100

In conclusion, for Adrar and similar sites, the WRAG can provide the necessary voltage to the local distribution network without the intervention of the inverter.

4.2 Features and Discussion

The figure 4a gives the EMF's delivered by the alternative current generator when the magnetic field of the inductor is acted on by means of the excitation current and by setting the maximum speed of 1500 rpm corresponding to 7.83 m/s for the wind.

Figure 4b shows the EMF's that WRAG can provide for a wide range of wind speeds and a steady flow.

Figure 5 shows the mechanical power at the entrance of the alternative generator WRAG for different wind speeds.

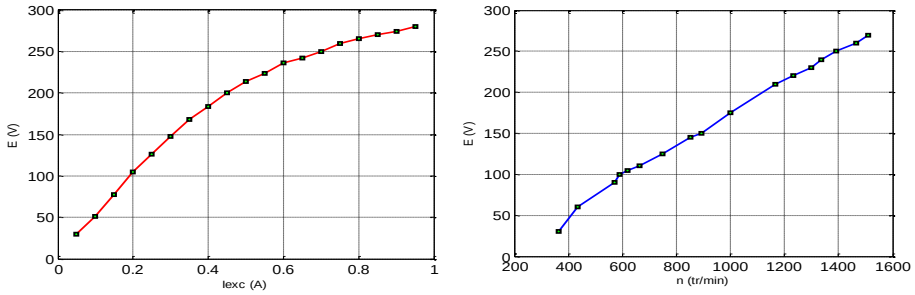

(a) (b)

Fig. 4. Vacuum features: (a) $E = f(I_{exc})$, (b) $E = f(n)$ for a flow Φ = constant.

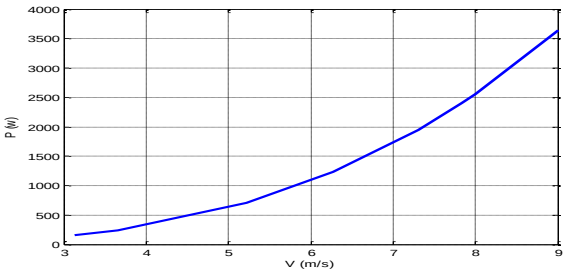

Fig. 5. Mechanical power of the WRAG according to the monthly wind speeds (ADRAR) in m/s for different excitation currents.

Figures 6 and 7 show the curves of the EMF obtained at the terminals of the generator at each set speed and with the variation of the stator flux (Inductor). If we fix a 220 volts EMF, we notice that for some speeds we can override the electronic converters for the supply of the load.

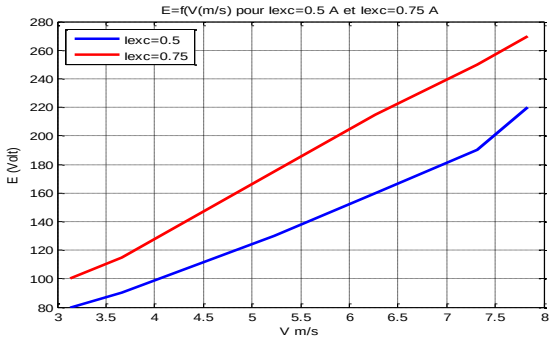

Fig. 6. Characteristic of E (V) for different inductor flows.

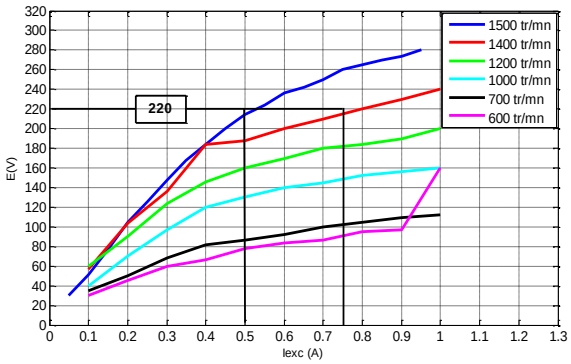

Fig. 7. Vacuum characteristics of E (I_{exc}) for different speeds.

EMF's (E (V) $\leq$ 220 V) obtained for I_{exc} varying from 0.5 A to 0.8 A for the speed range of WRAG going from 600 rpm to 1500 rpm and corresponding to V = (3.135 m/s – 7.83 m/s).

Consequently, E / 0.5 A = (60 V – 220 V) and E / 0.75 A = (90 V – 270 V).

We notice in Table 4 that it is enough to excite the generator with a rated current of 0.75 amperes to have a rather high voltage availability without using the inverter. This justifies, in our opinion, dimensioning gain in terms of electronic components.

When we observe the wind speeds and the resulting EMF we also see that we can save on the multiplier size, for its application on the site of Adrar or a similar site, the WRAG of our study requires only one multiplier with a coefficient G = 90.

Table 4. Voltage differences (ΔV) for different speeds with the nominal voltage of 220 V.

V(m/s)	3.135	3.657	5.225	6.27	7.31	7.83
n (tr/min)	600	700	1000	1200	1400	1500
I_{exc} (A)			0.75			
E (Volt)	90	102.5	148	182	215	260
Δ (Volt)	130	117.5	72	38	5	- 40

The value of Δ (Volt) and its sign indicate the lack to be added or subtracted in weber by acting on the excitation in the range (0.5 A – 0.75 A).

5 Conclusion

Small power wind systems dedicated to smart cities and isolated sites continue to grow around the world. The experimental results obtained for our machine are satisfactory. They can attest that, in this low-power range, the WRAG we propose can be an important alternative to other conventional wind turbines. The technical progress acquired to date and, above all, the gain in mechanical and electronic sizing (mechanical shaft, gears and converters) resulting from the design of this special alternative

current generator, largely contribute to making WRAG more competitive, less expensive and more profitable in front of the dual feed machine and the synchronous machine.

The keys to energy efficiency were provided by the data, the way it is acquired and the form in which it is returned. Thus this wind system and real-time data help to achieve sustainable technology goals aimed at providing better services.

References

1. Wood, D.: Small Wind Turbines. In: Sathyajith M., Philip G. (eds) Advances in Wind Energy Conversion Technology. Environmental Science and Engineering 2016. Springer, Berlin, Heidelberg (2016).
2. Ackermann, T.: Wind power in power systems. 2nd edn. Wiley, New Jersey, USA (2012).
3. Banos, R., Manzano-Agugliara, F., Montoya, F.G., Gil, C., Alcayde, A., Gomez, J.: Optimization methods applied to renewable and sustainable energy. A review, Renewable and Sustainable Energy Reviews Elsevier 15(4), 1753–1766 (2011).
4. Shanker, T., Singh R.K.: Wind energy conversion system. A review Students Conference on Engineering and Systems (SCES), pp. 1–6 (2012).
5. Patel, M.R.: Wind and Solar Power Systems. 2nd edn. CRC Press, USA (2005).
6. Boldea, I.: Synchronous Generators, the electrical generators handbook. 2nd edn. CRC Press, Taylor & Francis Group, USA (2006).
7. Carlin, P.W., Laxson, A.S., Muljadi, E.B.: The History and State of Art of Variable-Speed Wind Turbine Technology. National Renewable Energy Laboratory. Colorado, USA (2001).
8. Dev Shukla, R., Singh, A., Singh, S.P.: Generators for variable speed wind energy conversion systems: a comparative study. I J E S C C international science press 3(2), 103–117 (2012).
9. Muyeen, S.M.: Wind Energy Conversion System. Green Energy and Technology. Springer, London (2012).
10. Sheeba Percis, E., Ramesh, L., Nalini, A., Venmathi, M., Sujatha, K.: Comparative analysis of variable speed wind energy conversion systems. International Conference on Sustainable Energy and Intelligent Systems (SEISCON). Chennai, India, pp. 159–162 (2011).
11. Pali, B.S., Vadhera, S.: Renewable Energy Systems for Generating Electric Power: A Review. 1st IEEE International Conference on Power Electronics. Intelligent Control and Energy Systems (ICPEICES). Delhi, India (2016).
12. Djamai, M., Kasbadji Merzouk, N.: Wind farm feasibility study and site selection in Adrar. Algeria Science Direct. Energy Procedia 6(1), 136–142 (2011).
13. Creg.: Potentiel éolien en Algérie, Adrar (2015).
14. Tazil, M., Kumar, V., Bansal, R.C., Kong, S., Dong, Z.Y., Freitas, W., Mathur, H.D.: Three-phase induction generators: an overview. IET, Electric Power Applications 4(2), 75–89 (2010).
15. Wizelius, T.: Developing wind power projects: theory and practice Earthscan. London, UK (2007).
16. Schmidhofer, A., Weiss, H.: Optimization of Power Electronics for small Stand alone wind power stations. 10th European Conference on Power Electronics and Applications EPE'03. Toulouse, France, pp. 1–6 (2003).

17. Nachat, N., Farrag, M.E.: Operation of Stand-Alone Self-Excited Induction Generator Supported by Energy Storage Systems for Small Scale Wind Energy Generation. 2nd International Universities Power Engineering Conference (UPEC). Heraklion, Greece (2017).
18. Lascu, C., Boldea, I., Blaabjerg, F., Chen, W.: A class of flux observers for doubly-fed induction generators used in small power wind generation systems Energy Conversion. Congress and Exposition (ECCE), IEEE. Denver, CO, USA (2013).
19. Okedu, K.E., Takahashi, R., Tamura, J., Muyeen, S.M.: Comparative study on current and voltage controlled voltage source converter based variable speed wind generator. 2nd International Conference on Electric Power and Energy Conversion Systems (EPECS), pp. 1–6 (2011).
20. Farrag M.E., Ghanim, P.A.: Analysis of the Dynamics Performance of Self-Excited Induction Generators Employed in Renewable Energy Generation. Energies 7(1), 278–294 (2014).
21. Sørensen, J.N.: The general momentum theory for horizontal axis wind turbines. Springer, USA (2015).

Potential for thermal water desalination using microgrid and solar thermal field energy surpluses in an isolated community

J. A. Aguilar-Jiménez[1,*[0000-0001-7094-9893]], N. Velázquez[1], R. Beltrán[2], L. Hernández-Callejo[3,*], R. López-Zavala[1,4], E. González-San Pedro[1,4]

[1] Center for Renewable Energy Studies, Engineering Institute, Autonomous University of Baja California, Mexicali, Mexico.
a1116072@uabc.edu.mx
[2] Advanced Materials Research Center, Chihuahua, México.
[3] Department of Agricultural Engineering and Forestry, University of Valladolid (UVA), Campus Universitario Duques de Soria, 42004 Soria, Spain
luis.hernandez.callejo@uva.es
[4] Faculty of Engineering, Autonomous University of Baja California, Mexicali, Mexico.

Abstract. In this work, we present the study of seawater desalination potential using the energy surpluses of a microgrid based on renewable energies and a thermosolar absorption cooling system, installed in the isolated community of Puertecitos, Mexico and its primary school, respectively. Given the profile of electricity demand of the community in winter and the non-need for air conditioning, both systems can be used for the desalination of seawater, a resource greatly needed in the region because of the scarcity that is presented. Using the software TRNSYS and Aspen Plus, the simulation of the generating systems was carried out, activating a multiple-effect seawater desalination system during a typical week of February with measured data of electrical consumption. The results show that, with the energy available from both systems, it is possible to desalinate 2,500 kg/day of water with a thermal consumption of 25 kW, during 6 hours daily operation. The electrical energy supplied by the microgrid contributes four times more to the desalination of water than the thermal solar field. With this production, it is possible to satisfy the basic requirements of hygiene, hydration and food for 25 people.

Keywords: Microgrid, Solar Energy, Desalination, Isolated Community.

1 Introduction

Water scarcity is a global problem that has taken on great importance among public and private institutions. The United Nations incorporates it in the Sustainable Development Goal 6, mentioning that this resource, in sufficient quantity and quality, is essential for all aspects of life [1]. The decline in the availability of this resource is the result of several factors, such as the increase in world population, living standards and the pollution of water deposits; projections estimate that they will reach critical levels within

the first half of this century. [2]. It is for this reason that the efforts of scientists should be directed towards solving this problem, proposing new technologies that are more efficient, use renewable energies and can be applied in regions where there is a shortage of water.

The only methods to increase water supply are through desalination and reuse [3]. Of these two, seawater desalination offers a virtually unlimited and consistent supply of high quality water [4]. Desalination uses large amounts of energy to remove pure water from a salt water source [5]. Kalogirou [6] estimated that the production of 1,000 m^3 per day of fresh water requires 10,000 tons of oil per year. This is significant if the price of energy is expensive and populations with water needs cannot afford it.

The integration of desalination processes to solar concentration plants is today the best alternative to solve simultaneously the problems of water scarcity and exhaustion of fossil fuels [2]. Furthermore, if we relate that the regions where water is needed present a good solar resource and, in addition, can be found close to the sea, it becomes an attractive and sustainable combination. Using solar energy, the desalination process can be carried out in two ways, using electrical energy in reverse osmosis equipment, or thermally in multiple-stage flash (MSF), multiple-effect desalination (MED) or humidification/dehumidification systems [7, 8]. Although MSF systems predominate in the market [9], MED technology has improved and now has efficiency levels higher than MSF [10].

Numerous works have been carried out seeking to make desalination processes more efficient by using renewable energies as the source of activation, in which the studies carried out on the Almeria Solar Platform with a 14-effect solar MED system are highlighted [11–14]. López-Zavala *et al* [15] proposed the coupling of an absorption cooling system to a desalination system through internal energy integration. With that configuration, the cooling system was 19.44% more efficient, while producing 838 L/day of fresh water with the same amount of energy supplied. Mata-Torres *et al* [16] analyzed energetically the coupling of a MED system with a Rankine cycle for the simultaneous production of water and electrical energy, finding that largest MED plant sizes achieve the lowest unit exergy cost of electricity and water under all the conditions evaluated.

On the other hand, seawater desalination systems have been analyzed and implemented in isolated regions being activated with renewable energies [17–19]. Astolfi *et al* [20] mention that solar power plants and desalination units can be integrated synergistically as long as their programming is optimized by an advanced energy management system. They also conclude that the combination of two solar plants, such as photovoltaic (PV) and thermal, allows to take advantage of the characteristics of both; the first for its low costs of electricity production during periods of high insolation, while thermal systems extend the hours of operation using thermal energy storage.

Puertecitos, Mexico, is a coastal community isolated from the national electricity grid that has generators based on renewable energy. However, in the region there is a serious problem with access to fresh water, a service that is in high demand among the population due to the low quality of life. For this reason, this paper presents a study of the potential for desalination of seawater in the community by means of a multi-effect desalination system, using the energy capacity during the winter season of the genera-

tors installed, a period in which they are partially or completely stopped. This is intended to satisfy the basic requirements of clean water to the maximum possible number of residents, improving their quality of life and taking advantage of the energy waste of the renewable energy systems of the community.

2 Renewable Energy Systems Installed in the Community

The community of Puertecitos is located in the state of Baja California, Mexico. (30°21'19.7" N, 114°38'26.3" W) and it's a village isolated from the national power grid. It has a variable number of residents, mainly due to weather conditions, availability of public services and fishing seasons, the latter is the predominant work activity. Since it does not have electricity service, the Autonomous University of Baja California designed and installed a microgrid based on renewable energy to meet basic requirements, such as conservation of perishable foods, public lighting and air conditioning of spaces [21]. This system has 55.2 kW of photovoltaic modules, a 5 kW wind turbine, a 75 kVA diesel generator and a 522 kWh lead-acid battery bank, as shown in Fig. 1.

Fig. 1. Microgrid of the community of Puertecitos, Mexico.

In the same community of Puertecitos there is a primary school for the children who live there. This consists of four classrooms, where one is dedicated to preschool. However, the school suffers from a high rate of academic desertion due to the factors mentioned above, together with the high environmental temperatures present in the summer, which make it impossible to give classes under suitable comfort conditions. Since they did not have air conditioning systems or the economic resources to acquire them, besides not being able to pay the price of electricity from the microgrid, an absorption cooling system activated by solar thermal energy was installed [22], seeking that the school has the necessary comfort conditions for students to carry out their activities properly, reducing academic desertion or eventually leaving the community for lack of basic education. The system consists of a field of solar thermal collectors with 110.25

m^2 of caption area, which store thermal energy in a tank of 12 m^3 of capacity for subsequent use in an absorption water cooling machine of 35 kW, as shown in Fig. 2.

Fig. 2. Thermosolar absorption cooling system of 35 kW capacity installed in the primary school of Puertecitos, Mexico.

2.1 Operation in Winter Season

The climate in the community of Puertecitos differs greatly depending on the season. In the winters temperatures can reach close to 0°C, while summers record temperatures in the order of 45°C, with peaks of up to 50°C in the shade. This causes a very different profile in the demand for electricity between these seasons. In the summer, when there is a need for air conditioning due to high temperatures, community demand can be up to five times greater than expected in winter. When dimensioning a system for the production of electrical energy, the problem of determining the appropriate size of the plant occurs; if the community's demand for summer is taken as a reference, the plant will be oversized for the winter period; on the other hand, if it is dimensioned with the winter demand, it will be very limited for the electrical needs of the hot months. The sizing study must contemplate a cost-benefit analysis between demand and production and storage capacity, including different generators and energy storage systems.

Fig. 3 shows the predicted electricity demand of the community studied, based mainly on a socioeconomic study carried out on the population and extrapolated to a total of 20 houses, providing enough energy to have an acceptable quality of life [21]. During the first months of the year there is a demand of no more than 15 kW, mainly for public lighting, refrigerators, domestic lighting and entertainment. However, as ambient temperatures rise, forecasted demand tends to rise to a peak of around 60 kW in August, mostly due to the use of air-conditioning equipment to deal with high temperatures. During the months of September to December demand returns to its lowest levels. It was decided to install a 60 kW electrical system based on renewable energy and the energy shortfall during the critical months was covered by the diesel generator. In

this way, a greater amount of economic resource could be allocated to a larger energy storage system. This resulted in a shortage of electricity for a short period of time per year, remedied with conventional energy, while the remaining time there is an excess of energy production by photovoltaic and wind generators.

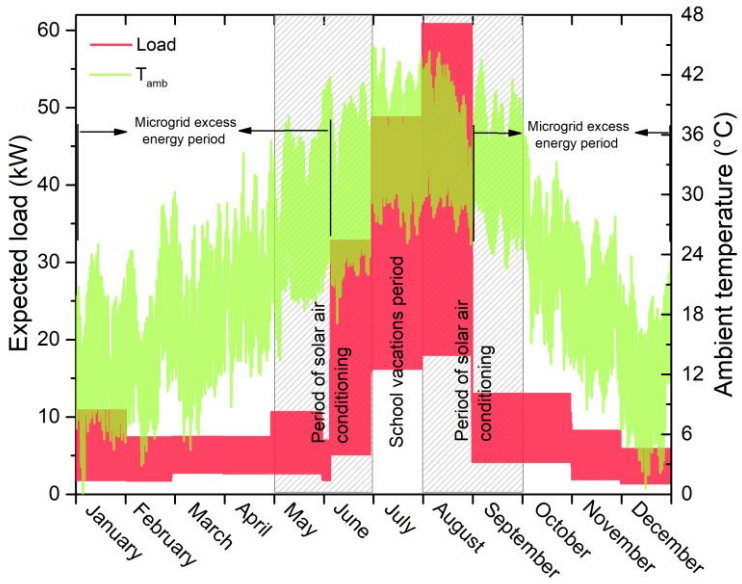

Fig. 3. Annual variation of the electric demand forecast for the community of Puertecitos and ambient temperature, where the periods of excess production of electric energy and use of the thermosolar absorption cooling system of the primary school are indicated.

On the other hand, the community primary school's thermosolar absorption cooling system has something similar to its operation. The need for air conditioning in the classrooms due to the region's high temperatures is present in the May-June and August-September periods, since July is considered a vacation period, as shown in Fig. 3, so the system will operate alone for four months of the year. During the remaining eight months there is no specific work defined, wasting the heating capacity of the solar field or the air conditioning of the absorption machine.

2.2 System for the Use of Energy Surpluses and Seawater Desalination

In the region there is a serious problem for the acquisition of clean water. The easiest way to obtain this resource is in a well 32 km away from the community, which is also overexploited and with high salinity indexes. In a direct questioning with the population of Puertecitos, they defined clean water as the second most desirable service in the community, only after electricity and even more desired than public health or safety services.

Taking into account the above, and seeking to take advantage of existing facilities in the community, such as the microgrid and field of solar thermal collectors, without affecting their main functions (meet the electricity needs and air conditioning of the classrooms of the school, respectively), it is proposed to evaluate the capacity of desalination of seawater in Puertecitos using surplus electricity from the microgrid and field of solar collectors during the periods mentioned above. In this way, the technical feasibility would be analyzed to provide this basic service so required in the region, without altering the current operation of the plants.

Fig. 4 presents the schematic diagram of the proposed seawater desalination system in the community. During the months in which the energy storage batteries are at their maximum capacity, the instantaneous electric demand of the community is being satisfied and there is still plenty of energy, this will be used to activate electrical resistances inside the thermal energy storage tank (TEST) of the thermosolar cooling system, converting electrical energy into thermal energy and transferring it to the TEST. The field of solar thermal collectors, during the months when there is no need to cool the classrooms of the school, will be working to increase the thermal energy of the TEST. With the energy supplied by the two systems, a MED system will be activated.

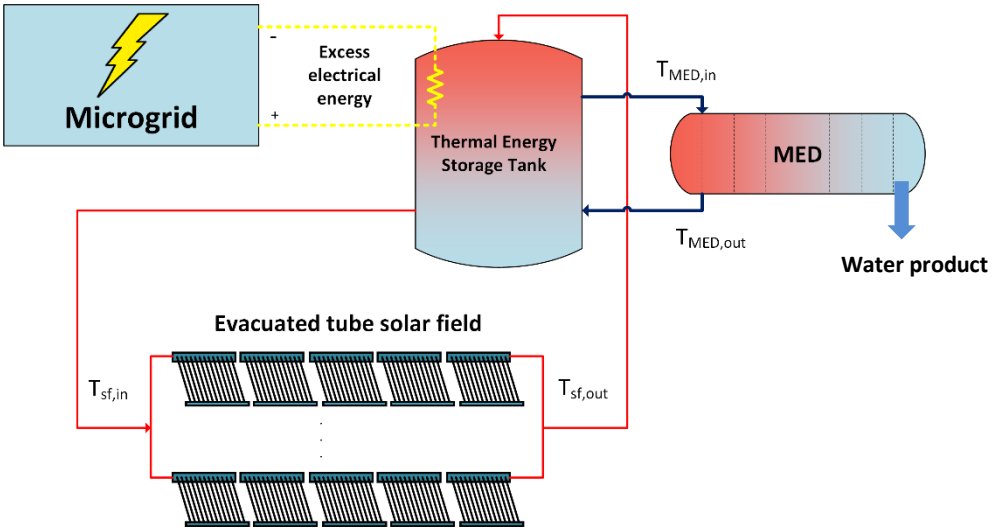

Fig. 4. Schematic diagram of the proposed system for the desalination of seawater using the surplus energy of the microgrid and thermosolar cooling of the community of Puertecitos.

3 Methodology

For the feasibility analysis of the proposal, the TRNSYS software was used to simulate the solar heating and microgrid systems, while Aspen Plus was used for the MED system. TRNSYS has a library of "types" programmed with mathematical models validated from a great amount of equipment, among them renewable technologies such as

photovoltaic modules and solar collectors, which, interconnected with other programmed control modules or other processes, form a system that can be analyzed in a semi dynamic state. The advantage of this software is that it can use meteorological databases typical of the locality of study, so the analysis is carried out under more real operating conditions, subject to environmental variations, such as temperature, radiation and wind speed, among others.

The microgrid, solar collectors' field and storage tank, as well as the dynamics of control and operation of the general system, were simulated in TRNSYS since their performance depends directly on solar radiation conditions and temperatures, in addition to being also used as references for decision making regarding the operation of the global system. The meteorological information used in the simulation study represents a typical year, based on average measurements over the last 10 years. On the other hand, the MED system is simulated in Aspen Plus software due to its advantages in terms of databases of thermodynamic properties and heat transfer of a large number of substances, which facilitate the resolution of mathematical models used in their blocks, representative of physical and chemical processes.

The characteristics of the systems installed in the Puertecitos community, as well as those of the proposed MED system, are presented in Table 1. This information is declared in the TRNSYS blocks to calculate the available heat for the activation of the desalination system. In the case of the microgrid, field of thermal solar collectors and TEST, the information supplied to the simulator is that provided by the manufacturer of the equipment, as well as it is considered that the mathematical models used in TRNSYS are validated. The MED system developed in Aspen Plus was based on the experimental results of a 14-effect plant and validated with experimental results presented by Palenzuela *et al* [13] and can be found at [15]. It is important to mention that the absorption system is not in operation due to the temperatures present during the simulation period, so only the field of solar collectors was taken as a study system. Also, as previously mentioned, the excess of electrical energy produced by the microgrid was taken into account. The amount of available energy was quantified in-situ and declared as input values in the simulator developed in TRNSYS.

The following considerations were taken into account in the simulation study in order to simplify the mathematical resolution of the proposed system:

- Semi-dynamic state in TRNSYS with simulation periods of 25 minutes.
- No heat loss from the equipment or piping was considered, only the heat transfer to the environment due to the temperature difference of the TEST and the solar collector field.
- Pressure drops in equipment and pipes were not considered.
- Since there is no direct link between the TRNSYS software and Aspen Plus, they were analyzed separately.
- The MED system was dimensioned based on the maximum usable thermal load of the TEST, looking for an operation for defined periods of time.

Table 1. System characteristics

Solar collector	
Brand/model	Suntask/SHC24
Collector type	Evacuated tube with CPC reflector
Number of tubes	24
Aperture area	4.41 m^2
Optical efficiency (a_0)	0.668
First order efficiency coefficient (a_1)	1.496 W/m^2*K
Second order efficiency coefficient (a_2)	0.005 W/m^2*K^2
Fluid	Water
Mass flow	0.02 $kg/s*m^2$
Number in series	5
Number of loops	5
Thermal energy storage tank	
Volume	12 m^3
Height	2.5 m
Material	Fiberglass
Insulation thickness	0.025 m
Loss coefficient	1.4 W/m^2*K
Fluid	Water
Microgrid system	
Brand/model	Solartec S72MC6-300
Power	300 W
Number of modules	184
Wind generator	5 kW
Inverter	Kehua 100 kVA
Controller	Kehua SPC348150-M
Batteries	2 V, 1,500 Ah each
Number of batteries	172 connected in serie
Diesel generator	75 kVA
Multiple-effect desalination system	
Number of effects	14
Thermal energy input	25 kW
Top brine temperature	70°C
Condensation temperature	35°C
Fresh water production	2,490 kg/h

4 Results

In order to carry out the feasibility study of seawater desalination with the excess energy of the microgrid and the entire solar heater field, a week of February was considered (period of 750-885 h per year) where the environmental conditions of radiation and temperature allow a stable operation of the system, as can be seen in Fig. 5. As it is a winter week, the present temperature allows the air conditioning systems to be switched

off, both the school's thermosolar absorption and the domestic electrical systems, which is why an energy surplus is expected from the microgrid and the availability of using the school's collector field for the desalination of seawater. However, the global solar radiation available does not exceed 700 W/m^2 and the hours of use of the resource are less than would be expected in summer, reducing the amount of solar energy that can be acquired during the day.

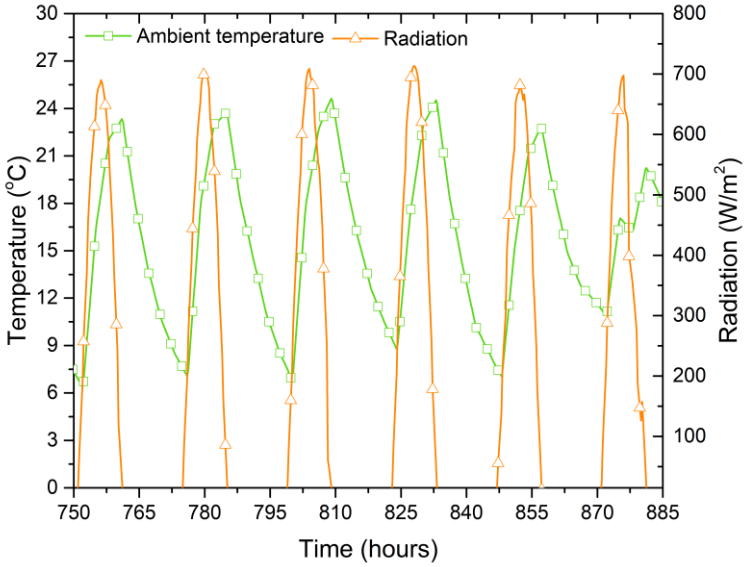

Fig. 5. Variation of ambient temperature and global radiation in the region of study during a week in February.

Fig. 6 presents the operating dynamics of the Puertecitos community microgrid, as well as the electrical demand profile and the electrical energy surplus. This information corresponds to data measured in the community during the aforementioned analysis period. It can be seen that, during the whole week studied, there is a surplus of electrical energy due to low-demand. The first day begins with the state of charge (SOC) of the storage system in the order of 0.8, due to the discharge of the same during the night; as the solar resource increases and the production of the photovoltaic field satisfies the instantaneous demand of the community, the excess energy is used to charge the batteries to their maximum. When the storage system reaches a SOC of 1.0, the electrical surplus is used to activate the electrical resistances within the TEST.

On the first day, due to the community's demand profile, a maximum of 27 kW of transferred energy was obtained for only a short period of time, giving a total of 49 kWh of harnessed energy. However, the rest of the days, after fully charging the battery bank, potencies in the order of 38 kW were reached, equivalent to an average daily energy of 96 kWh, the result of integrating the instantaneous power during the period of time presented, represented by the shaded area under the curve. It should be noted

that, being winter season, the storage system in batteries does not fall below 0.8 of its SOC during the night period, allowing the use of excess energy for the desalination of seawater.

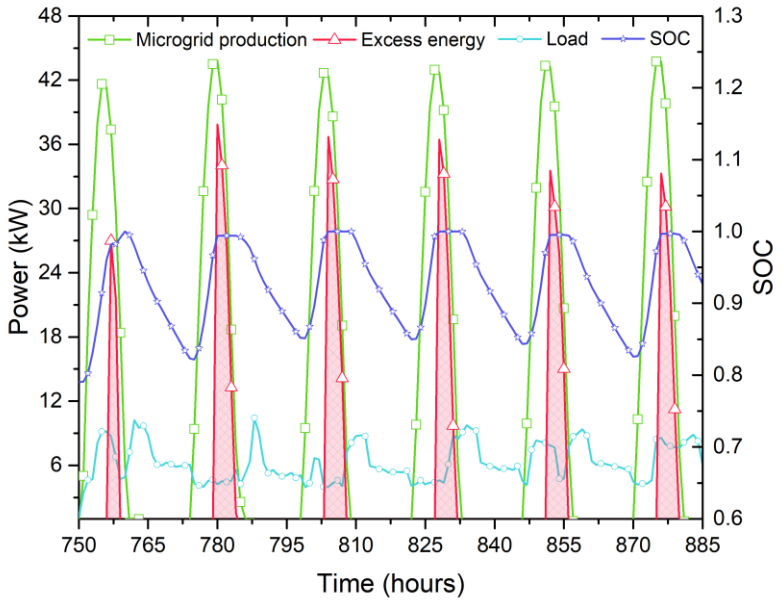

Fig. 6. Dynamics of electrical energy production by the microgrid, excess of energy due to the low demand of the Puertecitos community and SOC of the batteries of the system.

On the other hand, the field of thermal solar collectors of the cooling system is available in its entirety to be used as a medium for the activation of the MED system, together with the energy coming from the microgrid. Under the environmental conditions mentioned above, Fig. 7 shows the behavior of the solar thermal collection system during the analysis week. The output temperature of the solar field, $T_{out,sf}$, is directly influenced by the input temperature, $T_{in,sf}$, and the available solar radiation, and indirectly related to the temperature of the TEST. This can reach 95 °C during the solar mid-day, which is the set point defined as the maximum operating limit. The decrease in $T_{in,sf}$ is due to the fact that the solar heating system is not in operation for the night period. The thermal power supplied by the collector field increases with respect to the increased solar radiation, having a maximum of up to 35 kW at mid-day. This energy is transferred in its totality to the TEST to be used by the MED system.

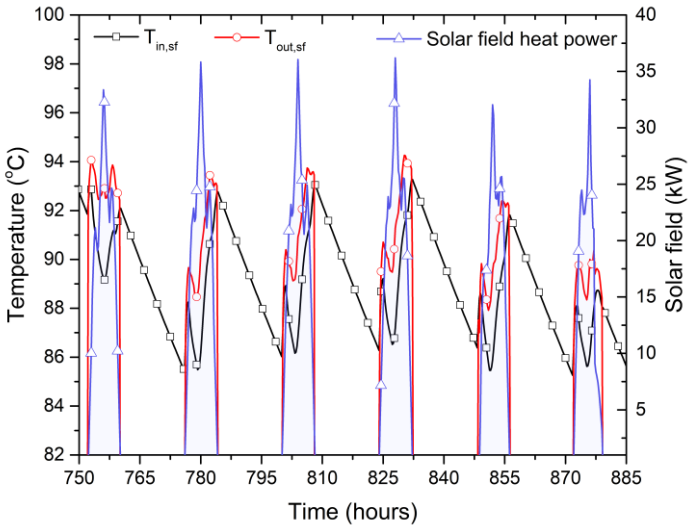

Fig. 7. Behavior of the solar thermal system of the Puertecitos school used in the seawater desalination system.

Given the amount of energy available, both from the excesses of the microgrid and the collector field, Fig. 8 shows the production of clean water calculated by the proposed system. The MED will run for a period of 6 h daily, starting at 9:00 and ending at 15:00, as this allows a programmed operation throughout the week without affecting the operating temperature and TEST conditions, as well as using only the daily energy supplied by the generators. On the other hand, if you have a longer daily operation, the system will not be able to return to the initial conditions of temperature and stored energy of the TEST, affecting the quality of the energy and the subsequent days of operation. Using the energy of the two systems, it is possible to produce 414 kg/h of desalinated water during the 6 hours a day, using 25 kW as thermal energy to activate the MED, giving a total of approximately 2,500 kg per day and a weekly accumulated of 17,500 kg.

It also presents the scenario in which only the solar field is available, without considering the electrical surpluses of the microgrid. For this case, during the same period of operation, it is possible to use a constant thermal power of 12 kW without negatively influencing the conditions of the TEST and, for a new capacity and design of the MED, it is capable of producing approximately 1,183 kg daily of desalinated water with a weekly accumulated of 8,305 kg. This results in a 52.5% reduction in water desalination when using only the thermal solar field, or seen in another way, the electrical excesses of the microgrid contribute two times more to the production of desalinated water than the entire solar collector field. Considering the recommendations of the World Health Organization [23], the quantity of 2,500 kg/day of desalinated water can satisfy the basic needs of food, hydration and hygiene of 25 residents of the community of Puertecitos, while using only the energy of the solar field satisfies the water requirements for 5 residents.

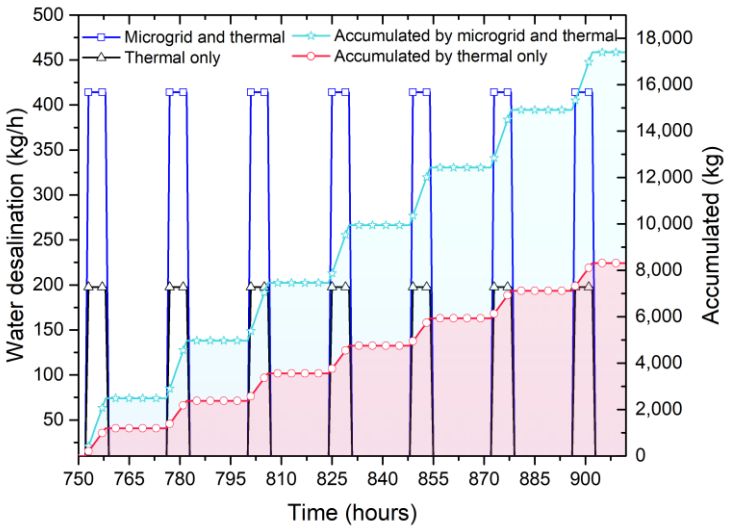

Fig. 8. Production rate of desalinated water and accumulated during the week of analysis.

5 Conclusions

A study was conducted to determine the potential for seawater desalination in the isolated community of Puertecitos, Mexico, using a multi-effect thermal desalination system to provide this scarce service in the region. This population has a microgrid based on renewable energy and, given that the profile of demand differs greatly depending on the seasonal season, we seek to take advantage of excess electricity in the winter period. In addition, a field of thermal solar collectors belonging to an absorption cooling system installed in the primary school of the community is available, which for eight months is without use because no air conditioning is needed in the classrooms.

Considering a week in February as the study period, the system was simulated using the TRNSYS and Aspen Plus software, based on the profile of electricity demand measured in the community, and the following was found:

- Using the energy surplus of the microgrid and the entire solar thermal field, it is possible to desalinate water using a MED system with a production of 2,500 kg/day.
- The thermal consumption of the MED system is 25 kW, being possible to maintain its operation for 6 h/day, during the period from 9:00 to 15:00.
- Using both generators, a weekly production of approximately 17,500 kg of water is obtained, while using only the field of solar collectors this decreases to 8,305 kg weekly.
- The excess energy of the microgrid contributes two times more to the desalination of water than the solar thermal field.
- According to the World Health Organization, it is possible to meet the basic hygiene, hydration and nutritional needs of 25 people with calculated water production.

Acknowledgments

The authors acknowledge CONACYT-SENER-SUSTENTABILIDAD ENERGÉTICA for the support received through the project P09 of CEMIE-Solar as well as a graduate scholarship for J. Armando Aguilar-Jiménez. The authors also acknowledge the CYTED Thematic Network "CIUDADES INTELIGENTES TOTALMENTE INTEGRALES, EFICIENTES Y SOSTENIBLES (CITIES)" no 518RT0558.

References

1. Nations, U.: Sustainable Development Goal 6 Synthesis Report on Water and Sanitation. United Nations, New York (2018). https://doi.org/10.1126/science.278.5339.827.
2. Palenzuela, P., Alarcón-Padilla, D.-C., Zaragoza, G.: Concentrating Solar Power and Desalination Plants. Springer International Publishing, Cham (2015).
3. Shannon, M.A., Bohn, P.W., Elimelech, M., Georgiadis, J.G., Marĩas, B.J., Mayes, A.M.: Science and technology for water purification in the coming decades. Nature. 452, 301–310 (2008). https://doi.org/10.1038/nature06599.
4. Phillip, W.A., Elimelech, M.: The Future of Seawater Desalination: Energy, Technology, and the Environment. Science (80-.). 333, 712–717 (2011).
5. Qiblawey, H.M., Banat, F.: Solar thermal desalination technologies. Desalination. 220, 633–644 (2008). https://doi.org/10.1016/j.desal.2007.01.059.
6. Kalogirou, S.A.: Seawater desalination using renewable energy sources. Prog. Energy Combust. Sci. 31, 242–281 (2005). https://doi.org/10.1016/j.pecs.2005.03.001.
7. Valero, A., Uche, J., Serra, L.: La desalación como alternativa al plan hidrológico nacional. , Zaragoza (2001).
8. Tariq, R., Sheikh, N.A., Xamán, J., Bassam, A.: An innovative air saturator for humidification-dehumidification desalination application. Appl. Energy. 228, 789–807 (2018). https://doi.org/10.1016/j.apenergy.2018.06.135.
9. IDA: Worldwide Desalting Plants Inventory. (2006).
10. Zheng, H., Zheng, H.: Solar Desalination System Combined With Conventional Technologies. In: Solar Energy Desalination Technology. pp. 537–622. Elsevier (2017). https://doi.org/10.1016/B978-0-12-805411-6.00007-5.
11. Chorak, A., Palenzuela, P., Alarcón-Padilla, D.C., Ben Abdellah, A.: Experimental characterization of a multi-effect distillation system coupled to a flat plate solar collector field: Empirical correlations. Appl. Therm. Eng. 120, 298–313 (2017). https://doi.org/10.1016/j.applthermaleng.2017.03.115.
12. Palenzuela, P., Alarcón-Padilla, D.C., Zaragoza, G.: Experimental parametric analysis of a solar pilot-scale multi-effect distillation plant. Desalin. Water Treat. 57, 23097–23109 (2016).

https://doi.org/10.1080/19443994.2016.1180481.
13. Palenzuela, P., Hassan, A.S., Zaragoza, G., Alarcón-Padilla, D.C.: Steady state model for multi-effect distillation case study: Plataforma Solar de Almería MED pilot plant. Desalination. 337, 31–42 (2014). https://doi.org/10.1016/j.desal.2013.12.029.
14. Chorak, A., Palenzuela, P., Alarcón-Padilla, D.-C., Abdellah, A. Ben: Energetic evaluation of a double-effect LiBr-H2O absorption heat pump coupled to a multi-effect distillation plant at nominal and off-design conditions. Appl. Therm. Eng. 142, 543–554 (2018). https://doi.org/10.1016/J.APPLTHERMALENG.2018.07.014.
15. López-Zavala, R., Velázquez-Limón, N., González-Uribe, L.A., Aguilar-Jiménez, J.A., Alvarez-Mancilla, J., Acuña, A., Islas, S.: A novel LiBr/H2O absorption cooling and desalination system with three pressure levels. Int. J. Refrig. 99, 469–478 (2019). https://doi.org/10.1016/J.IJREFRIG.2019.01.003.
16. Mata-Torres, C., Zurita, A., Cardemil, J.M., Escobar, R.A.: Exergy cost and thermoeconomic analysis of a Rankine Cycle + Multi-Effect Distillation plant considering time-varying conditions. Energy Convers. Manag. (2019). https://doi.org/10.1016/j.enconman.2019.04.023.
17. Kershman, S.A., Rheinländer, J., Gabler, H.: Seawater reverse osmosis powered from renewable energy sources - Hybrid wind/photovoltaic/grid power supply for small-scale desalination in Libya. Desalination. (2003). https://doi.org/10.1016/S0011-9164(02)01089-5.
18. Kyriakarakos, G., Dounis, A.I., Rozakis, S., Arvanitis, K.G., Papadakis, G.: Polygeneration microgrids: A viable solution in remote areas for supplying power, potable water and hydrogen as transportation fuel. Appl. Energy. (2011). https://doi.org/10.1016/j.apenergy.2011.05.038.
19. Bognar, K., Blechinger, P., Behrendt, F.: Seawater desalination in micro grids: An integrated planning approach. Energy. Sustain. Soc. 2, 1–12 (2012). https://doi.org/10.1186/2192-0567-2-14.
20. Astolfi, M., Mazzola, S., Silva, P., Macchi, E.: A synergic integration of desalination and solar energy systems in stand-alone microgrids. Desalination. 419, 169–180 (2017). https://doi.org/10.1016/j.desal.2017.05.025.
21. Aguilar-Jiménez, J.A., Velázquez, N., Acuña, A., Cota, R., González, E., González, L., López, R., Islas, S.: Techno-economic analysis of a hybrid PV-CSP system with thermal energy storage applied to isolated microgrids. Sol. Energy. 174, 55–65 (2018). https://doi.org/10.1016/j.solener.2018.08.078.
22. Aguilar-Jiménez, J.A., Velázquez, N., López-Zavala, R., González-Uribe, L.A., Beltrán, R., Hernández-Callejo, L.: Simulation of a Solar-Assisted Air-Conditioning System Applied to a Remote School. Appl. Sci. 9, 3398 (2019). https://doi.org/10.3390/app9163398.
23. Bartram, J., Howard, G.: Domestic Water Quantity , Service Level and Health. World Health Organization (2003). https://doi.org/10.1128/JB.187.23.8156.

Some results about the sensitivity of the thermal conductivity of the ground and the design temperatures for the heat transfer fluid in the design of low enthalpy geothermal systems.

Ignacio Martín Nieto[1[0000-0003-3984-7228]], Cristina Sáez Blázquez[1[0000-0002-5333-0076]], Arturo Farfán Martín[1] and Diego González-Aguilera [1[0000-0002-8949-4216]]

[1] Department of Cartographic and Land Engineering, University of Salamanca, Higher Polytechnic School of Avila, Hornos Caleros 50, 05003, Avila, Spain.

Abstract. In the design of large geothermal installations, accurate knowledge of the thermal characteristics of the ground is very important. An erroneous estimation of the thermal conductivity of the geological environment can make our project a failure, because there are large differences between the correct drilling lengths for different values of this parameter. Apart from an exact knowledge of the thermal conductivity of the ground, there is another way to mitigate this negative effect, it is to reduce the restriction of the thermal fluid's working temperature. This work shows how there is an attenuation of the sensitivity of drilling length of the well field against thermal conductivity when we allow lower operating temperatures in the geothermal fluid.

Keywords: Design of the well field, Thermal conductivity, Temperature restrictions.

1 Introduction.

In the present global environment of decarbonization policies, climatization systems based on electrical energy may become more and more important soon [1]. In this scenario, low enthalpy ground source heat pump geothermal systems (GSHP) may become an important part in the new configuration of the energy use in domestic and big scale heating/cooling installations.

This is due to the wide range of locations where these systems may work and because of the great efficiency in the use of electrical energy they are capable of (it´s common to obtain four units of thermal energy from the ground spending only one unit of electrical energy, this is called coefficient of performance (COP) four) [2].

In this work we are presenting some results in order to highlight the importance of several parameters when designing our low enthalpy geothermal system. It´s intended to show the great differences between systems designed for the same thermal needs when considering different approaches to obtain the thermal conductivity of the ground and different temperature low end limits for the heat transfer geothermal fluid.

We can think about a low enthalpy geothermal system as a mix of three different parts: the well field, the heat pump system and the distribution system. Let´s talk briefly about them:

- The well field: is where the ground loops are located. The quantity and depth of the boreholes, as well as the drilling methods, are quite important issues in the designing process of these systems.
- The heat pump system: the heat pump and all the devices related. The heat pump is necessary in low enthalpy geothermal systems due to the low temperature of the ground. It´s strongly dependent on the thermal needs of the project.
- The distribution system: It´s where the heat/cool from the ground is transferred to the building. Several methods exist like underfloor heating, radiators or forced-air systems.

We can assume that the heat pump and the distribution systems are designed properly. Their design does not depend on the ground and fluid conditions, just on the thermal needs of the building. So, we are focusing on the well field, the only sensitive part of the system to the ground thermal properties and the fluid temperature conditions.

In this work we will present some results obtained while designing a geothermal system. We have found huge differences between the well fields obtained, under different conditions of thermal conductivity of the ground and different working temperatures of the thermal fluid in the ground loops.

The starting point of the project was to design a GSHP system as an integral climatization system for the Higher Polytechnic School of Avila (belonging to the University of Salamanca). Starting from the annual thermal needs of this building, the Earth Energy Designer software (EED) [3] was used to design the well field with the thermal conductivity of the ground obtained from the geological data of the place. Then a thermal response test (TRT) was carried out in a geothermal borehole drilled in the area where the future well field will be located to obtain the real thermal conductivity of the ground. With the new thermal conductivity obtained from the TRT, the design of the well field was processed again with the same software.

Finally, for both thermal conductivities, changes were made in the working temperature of the fluid (in the design process) in order to observe the change in the design of the well field. All these results are exposed throughout this work and some conclusions are detailed at the end of it.

2 Thermal needs and first design.

For simplicity, having no practical influence on our work, we will limit the information about the project´s building to its thermal needs and its annual distribution. Both will remain the same in all cases.

The thermal needs of the building have been established in **1440.431 MWh /per year.** With an annual distribution showed in the table below (these data are included with the intention that the calculations became reproducible).

Table 1. Thermal needs of the project, annual distribution.

Month	Fraction	Energy (MWh)
January	0.155	223.27
February	0.148	213.18
March	0.125	180.05
April	0.099	142.60
May	0.064	92.19
June	0	0
July	0	0
August	0	0
September	0.061	87.87
October	0.087	125.32
November	0.117	168.53
December	0.144	207.42

From here we will carry out a first design of the project using geological maps and scientific bibliography [4] to estimate the thermal conductivity of our well field.

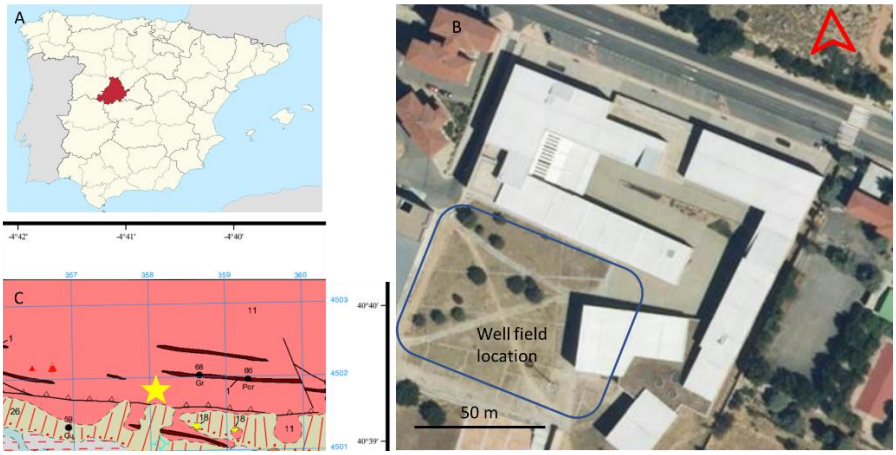

Fig. 1. A and B, location of the project. C geological environment [5].

From [5] we can conclude that we are in a granitic environment composed by Adamellites with great compactness and a very narrow altered zone near the surface

(around 5 to 10 meters). From Robertson´s survey on thermal conductivity from felsic rocks [4], We will estimate a thermal conductivity of the ground in 2.1 W/m·K.

In granite type rock environments, hammer drilling with air is the ideal technique. However, if the ground is not compact enough, we can find several problems (subsidence, entrapment of the hammer, etc.). Because of the very narrow altered zone expected, this will be the drilling method.

We have chosen a double loop system with thermal grouting material to enhance the performance of each borehole (thermal conductivity of the grouting material: 2.41 W/m·K). The area for the well field consists on a 50×70 square meter surface, with no other restrictions for the location of the boreholes applicable. A bore diameter of 110 mm has been selected; the type of tubes chosen are made of polyethylene PE-100 with 32mm in diameter. Some spacers will be used to maintain the tubes far enough to avoid thermal contact between them.

The thermal fluid chosen is a mixture of Propylene glycol (33%) with water, with a freezing point well below our working temperatures.

With all this the optimization process of the software shows this configuration for the well field as optimal:

Table 2. Optimal well field configuration in the first design.

Nº of boreholes	Space between them (m)	Borehole depth (m)	Total drilling length (m)
26	8	292	7603

According to [6], a 25-year modelling test have been performed on fluid temperatures to be sure we sure safe from soil exhaustion with that well field design.

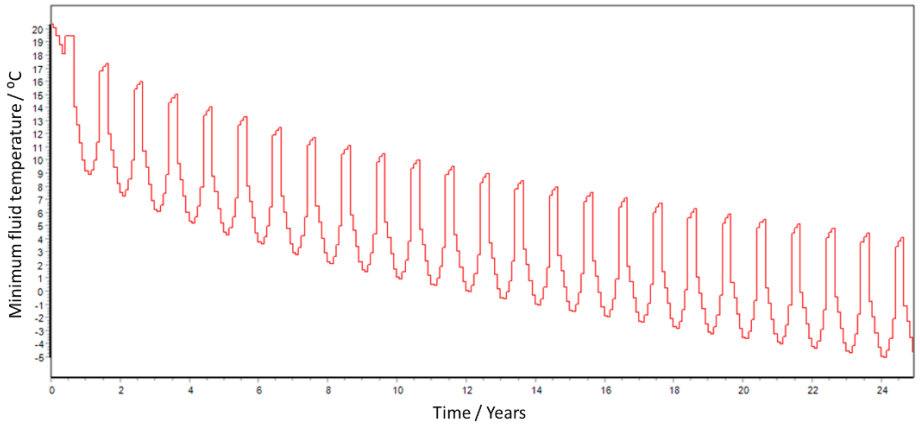

Fig. 2. Geothermal fluid temperature evolution.

As we can see in fig. 2. The minimum temperature keeps itself above the minimum design temperature of -5 ºC during the 25 years' period.

3 Thermal Response Test and re-design with the results.

As geothermal boreholes constantly exchange heat with the ground, the thermal conductivity of the surrounding rock is of great importance. This property can be determined through laboratory and/or field measurements (in situ), but when the design of the geothermal system must be based on the thermal conductivity of a given location, the measurements in situ are a better approximation. This is due to factors that can alter the conditions of heat transfer, such as the presence of altered rocks around the well, the convection of groundwater, etc.

Thermal response tests (TRTs) are commonly used to estimate borehole thermal conductivity. The usual injection TRT consists of circulating heated fluid (usually water) in a closed loop down the borehole. During the test, fluid temperatures are measured at the ground heat exchanger inlet and outlet, along with the flow rate. Theses measured values are then analyzed by analytical or numerical models with the aim of calculating thermal conductivity and borehole thermal resistance [7,8].

The TRT test has been performed in a borehole located in the well field of the project. The thermal conductivity obtained for the ground surrounding this borehole should be the one of the whole well field due to the existence of the same geological environment.

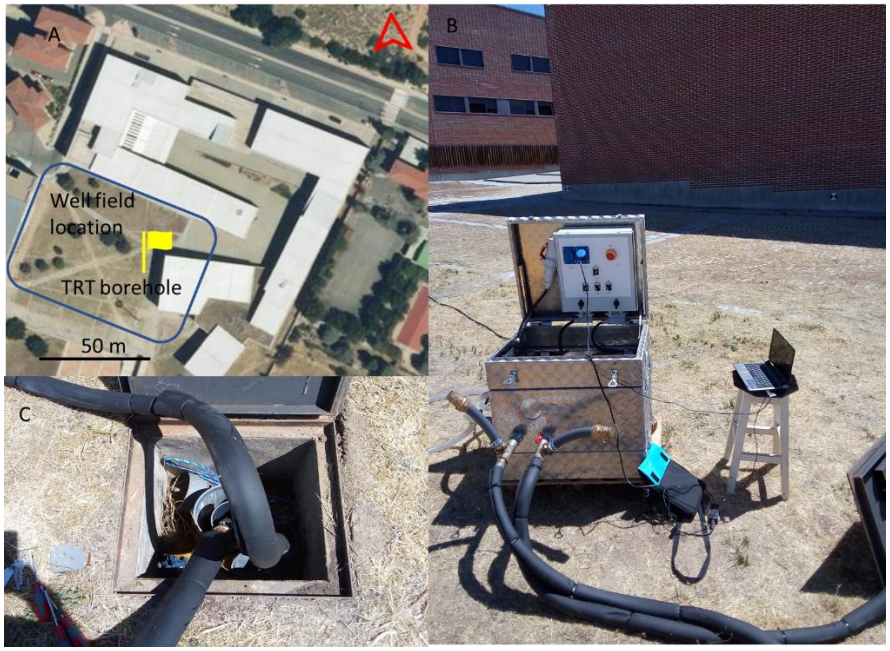

Fig. 3. A TRT borehole location. B TRT device ready to start. C borehole closed loop connected to the TRT device.

The TRT duration have been done following the regulation [9], the minimum duration of the TRT can be estimated by Equation (1).

$$T(s) = 5r^2/\alpha \quad (1)$$

With:

$$\alpha = K_e / C_v \quad (2)$$

Where:

r = borehole radius (m).
K_e = estimated thermal conductivity (W/m·K).
C_v = volumetric heat capacity (J/ K· m^3).

By applying eq. (1) and (2) we obtain: **T(s) = 72891.56 s = 20.25 h.** Despite this value, the test was extended through **43 hours** in order to ensure system stability.

Once we have taken the TRT data, we proceed to obtain the thermal conductivity in the vicinity of our borehole.

3.1 Thermal conductivity calculation.

The calculation of the thermal conductivity of the ground based on the thermal response test in Europe uses the radiant line approach [10]. According to the infinite line-source model, the thermal conductivity parameter can be obtained from the constant power rate and the slope of the temperature variation in time [11,12]. The interpretation of TRT results relies on a first-order approximation to linearize the mentioned infinite line-source model, neglecting the early measurements (those early measurements correspond to the transient response of the borehole).

$$k = \frac{Q}{4b\pi H} \tag{3}$$

where:

Q = heat flux (kW/min)
b = slope (K/min)
H = borehole length (m)

In figures 4 and 5 we can see the results from the TRT:

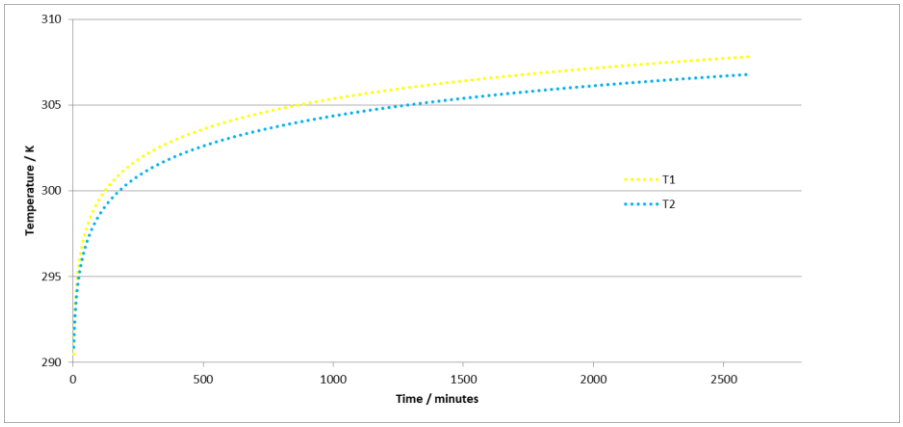

Fig. 4. Evolution of inlet (T1) and outlet (T2) temperatures registered during the TRT.

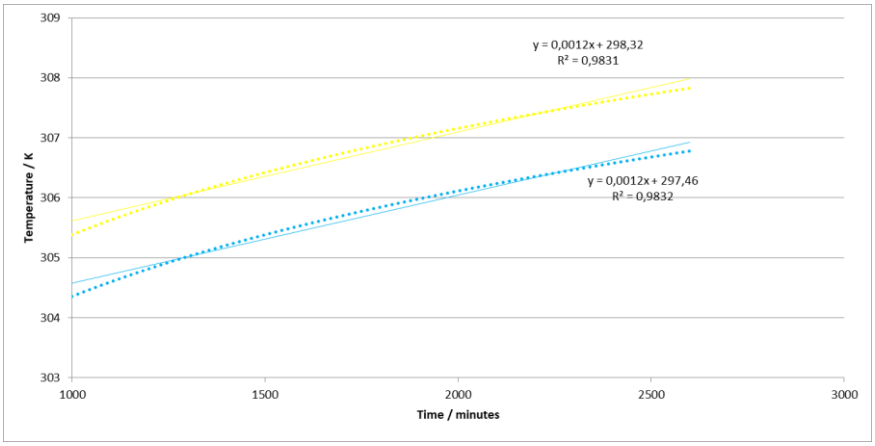

Fig. 5. Equation of the linear approximation to temperature registers (1000 first minutes neglected).

From figure 5, we can see that the slope of the linear approximation is the same for T1 and T2, such that the calculation of the thermal conductivity parameter is identical for both cases. When applying Equation (3), the following values were considered: b = 0.0012 K/min, H = 290 m and Q = 5.625 W/min (power injection rate of the TRT during the essay (9000 W) / time of the linear approximation (1600 min)). Thus, the global thermal conductivity of the borehole from TRT results takes a value of **1.56 W/m·K.**

With this value of the thermal conductivity of the ground, we are going to re-design the well field using again the EED software (all other parameters remain the same). In table 3 we can see the resulting design of the well field.

Table 3. Optimal well field configuration in the re-design.

Nº of boreholes	Space between them (m)	Borehole depth (m)	Total drilling length (m)
72	7	290	20905

Again, according to [6], a 25-year modelling test have been performed on fluid temperatures to be sure we sure safe from soil exhaustion with the present well field design. Figure 6 shows the result of the modelling:

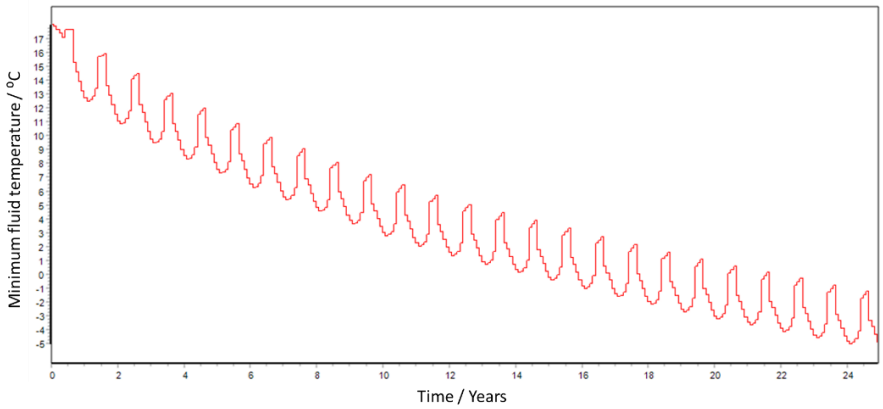

Fig. 6. Geothermal fluid temperature evolution.

We can see in figure 6, that in the modeling of the cold temperature of the geothermal fluid, it is never below -5 ºC. So, the well field seems well designed.

4 Decrease in fluid temperature restriction.

The detailed analysis of results will come later. However, at first glance, a comparison between the total drilling length proposed before and after the TRT may seem very different.

The previous results have been obtained with a temperature restriction of the thermal fluid consisting of not lowering -5 ºC. There is a way to get the total drilling length in the well field to decrease, and, that there is no such a marked difference in the designs for different thermal conductivities. Thus, we reduce the risk of depleting the subsoil thermal energy if we are wrong in estimating this property. The solution may be to reduce that temperature restriction.

We have re-designed our project for a temperature restriction of -10 ºC, and for both thermal conductivities (the one estimated and the one obtained with the TRT). These are the results:

Table 4. Optimal well fields configuration in the re-designs with the new temperature restriction.

Thermal conductivity (W/m·K)	Nº of boreholes	Space between them (m)	Borehole depth (m)	Total drilling length (m)
2.1	22	10	287	6320
1.56	30	7	292	8751

Of course, this has its disadvantages. When the operating temperature of the fluid decreases, the heat pump performance also decreases (between 15 and 30% according to some manufacturers).

5 Analysis of results and conclusions.

Regarding thermal conductivity, we can say that the design of the well field is very sensitive to this parameter. Just look at the huge differences in total length in the designs summarized in table 5:

Table 5. Optimal well fields configurations with restriction at -5 ºC.

Thermal conductivity (W/m·K)	Nº of boreholes	Space between them (m)	Borehole depth (m)	Total drilling length (m)
2.1	26	8	292	7603
1.56	72	7	290	20905

Of course, as we see in Table 4, the lower the temperature restriction, the less pronounced this difference is.

This difference in the size of the well field makes it necessary to know as accurately as possible, what are the thermal characteristics of the land where the project will be located. otherwise we may end designing a failed project.

As for the decrease in fluid temperature restriction, this may be a solution to lower the initial costs of the geothermal project. But of course, it will be accompanied by a higher energy expenditure of the installation. We also have to take into account that you have to choose the heat pump and the thermal fluid so that they are compatible with the new working conditions.

References

1. Directive (EU), 2019. 2018/410 Of the European Parliament and of the Council of 14 March 2018 Amending Directive 2003/87/EC to Enhance Cost-effective Emission Reductions and Low-carbon Investments, and Decision (EU) 2015/1814.
2. Self, S. J., Reddy, B. V., & Rosen, M. A. (2013). Geothermal heat pump systems: Status review and comparison with other heating options. Applied energy, 101, 341-348.
3. EED software created by BLOCON, 2019. Company Dedicated to Create Software About Heat Transfer and Ground Heat. https:// buildingphysics.com/eed-2/.

4. Robertson, E.C., 1988. Thermal properties of rocks. U. S. Geological Survey Open-File Report 88-441. pp. 97.
5. Geological and Mining Institute of Spain (IGME), 1972–2003. Geological National Mapping (MAGNA) 531.
6. UNE-EN 100715-1. Diseño, ejecución y seguimiento de una instalación geotérmica somera, sistemas de circuito cerrado vertical. (2014).
7. Pasquier, P. Interpretation of the first hours of a thermal response test using the time derivative of the temperature. Appl. Energy 2018, 213, 56–75.
8. Raymond, J.; Therrien, R.; Gosselin, L. Borehole temperature evolution during thermal response tests. 7Geothermics 2011, 40, 69–78.
9. UNE-EN ISO 172628:2017. Geotechnical Investigation and Testing. Geothermal Testing. Determination of Thermal Conductivity of Soil and Rock Using a Borehole Heat Exchanger; International Organization for Standardization: Geneva, Switzerland, 2017.
10. Mogensen, P. (1983). Fluid to duct wall heat transfer in duct system heat storages. Document-Swedish Council for Building Research, (16), 652-657.
11. Ingersoll, L.R.; Plass, H.J. Theory of the ground pipe heat source for the heat pump. Heat. Pip. Air Cond. 1948, 119–122.
12. Carslaw, H.S.; Jaeger, J.C. Conduction of Heat in Solids, 2nd ed.; Clarendon Press: Oxford, UK, 1959.

Centralized flexibility services for distribution system operators through distributed flexible resources

Sara Barja-Martinez[1], Pol Olivella-Rosell[1], Pau Lloret-Gallego[1] and Roberto Villafafila-Robles[1]

Centre d'Innovació Tecnològica en Convertidors Estàtics i Accionaments (CITCEA-UPC), Departament d'Enginyeria Elèctrica, ETS d'Enginyeria Industrial de Barcelona, Universitat Politècnica de Catalunya, Avinguda Diagonal, 647, Pl. 2, 08028 Barcelona, Spain,
sara.barja@upc.edu

Abstract. Under the context of smart grids within smart cities, increasing distributed generation, consumer empowerment and emerging flexibility services, distribution system operators could benefit by activating flexibility in distribution grids to avoid deploying new infrastructures and grid overloading. The solution offered by this work is an energy management system algorithm capable of activating flexibility behind the prosumer main meter during constrained periods. Therefore, the distribution system operator could compensate grid congestion during high consumption or production periods and increase their renewable generation hosting capacity by using behind-the-meter flexibility during peak production periods.

Keywords: smart grids, smart cities, distribution grid, flexibility, energy management system, centralized optimization

1 Introduction

The presence of more intermittent distributed generation and the empowerment of consumers are forcing the power system to evolve and adapt its operation to these changes. Past electrical system was mainly based on centralized, dispatchable and predictable generation that provided flexibility at transmission level to the electrical system to balance generation and demand. However, the increasing installation of distributed renewable generation is transforming the generation side in a more variable and intermittent source of energy. At the same time, the European Commission has presented a package of measures to ensure that consumers are active and central players on the energy markets of the future [1]. In this sense, the use of flexibility from the demand side can boost the involvement of prosumers in the energy system and make them a valuable asset in the electrical market. The proper management of available flexibility, both in generation and demand side, can help to compensate the lack of certainty of renewable sources.

In addition, electric vehicles (EV) and heat pumps have a strategic role in reducing greenhouse gas emissions and they are a key component of the transition to a low carbon economy [2]. However, its widespread use is increasing the demand of electricity, which may cause the need to upgrade the electricity infrastructure. The introduction of flexibility services can also be used as a more efficient alternative to reinforce the distribution grid, reducing or postponing infrastructure investment needs [3].

The use of flexibility for congestion management in the distribution grid is currently being widely investigated and there are some undergoing initiatives trying to standardize and provide common understanding of flexibility usage in the distribution grid. As an example, Universal Smart Energy Framework (USEF) Foundation created a detailed framework to provide an integral market design for the trading of flexible energy use [4]. However, optimization strategies are not covered as they can be different for each flexibility operator based on its own requirements and characteristics. Regarding optimization strategies, [5] proposes a method to employ the flexibility service from EV and heat pumps for real-time congestion management through an optimal power flow. In contrast, authors in [6] presented an optimization framework for the use of customers flexibility aggregation participating in the wholesale power market and the regulation capacity market. Moreover, in [7] an optimization problem is formulated considering battery degradation cost and using a decomposed solution approach with the alternating direction method of multipliers (ADMM) instead of commonly adopted centralised optimization to reduce the computational burden and time, and then reduce scalability limitations.

This paper presents a centralized energy management system algorithm that provides flexibility from prosumers to distribution system operators (DSOs) during constrained periods in order to avoid grid congestion or other related grid failures. The suggested approach has been developed under the INVADE project [8], which aims to design a flexibility management system using batteries that supports the distribution grid and electricity market while coping with grid limitations, high penetration of renewable energy and EV. The main contribution of this paper is the development of a robust algorithm capable of activating the maximum flexibility available to meet the DSO flexibility request (FR) at minimum cost behind the prosumer main meter when needed to avoid grid congestion during high consumption or production periods at distribution level.

The remainder of the paper is organized as follows: Section 2 describes the developed framework. The mathematical formulation problem is outlined in Section 3. The case study and its results are presented in Section 4. Ultimately, conclusions are presented in Section 5.

2 System description

The optimization problem description and the architecture implemented is based on the INVADE H2020 [8] project. The result of this project will be an integrated platform enabling flexible management algorithms. It will be applied to public

and private EV charging stations, households and mid-size customers to offer flexibility services to DSOs, BRPs and prosumers.

The three main actors involved in the present work and what role each one of them play is described below:

Distribution system operator : requests and purchases flexibility to the aggregator in order to avoid grid congestion and gives the corresponding financial compensation to the aggregator.

Aggregator : receives flexibility requests from the DSO and flexibility offers from the prosumers that are part of its portfolio. It is responsible for activating the flexibility requested by the DSO at minimum cost.

Prosumer : is the flexibility provider. Each prosumer aims to minimize its electricity bill by optimizing the used of batteries and photo-voltaic (PV) generation, but this optimized baseline consumption can be altered if the DSO needs to avoid a failure in the distribution grid in a certain period. The aggregator will economically reward the prosumer for modifying his optimized baseline.

The relationship and how these 3 main actors interrelate among each others is shown in Fig. 1.

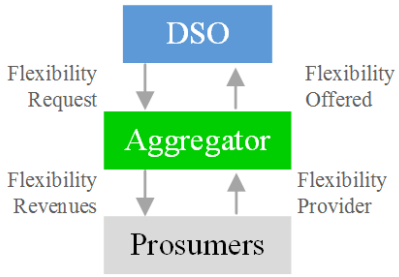

Fig. 1. Local flexibility market agents outline

Decisions are taken centrally. The aggregator will try to satisfy the DSO flexibility request at the lowest possible cost within its portfolio. This approach has a two way communication, which means that local data is available as an input to the optimization algorithm and the central system has direct control on the local flexible electric devices [9].

2.1 Flexibility Services

Flexibility services can be classified in function of the flexibility customer. The three main flexibility customers are listed in Table 1 along with what kind of

Flexibility customer	Flexibility Service
Distribution system operator	Congestion management
	Voltage / Reactive power control
	Controlled islanding
Balance responsible party	Day-ahead portfolio optimization
	Self-balancing portfolio optimization
Prosumer	Hourly tariff optimization
	kW max control
	Self-balancing

Table 1. Main flexibility customers and their flexibility services.

flexibility services they can demand. In order to describe the flexibility services, the INVADE project [10] and article [11] are used as reference.

The present study focuses on the DSO and prosumer flexibility service. Prosumers aim to minimize their electricity bill, while the DSO requests then flexibility needed to operate properly the distribution grid, within the safe operation zone.

2.2 DSO flexibility requests

The DSO flexibility requests are the minimum required amount of active energy variation with respect to the aggregated prosumer baseline optimization to avoid grid overloading. Negative flexibility request values mean decreasing generation or increasing demand while positive flexibility request is defined as increasing generation or decreasing demand. Table 2 summarizes these definitions.

FR <0	**FR >0**
$\downarrow$ *generation*	$\uparrow$ *generation*
$\uparrow$ *consumption*	$\downarrow$ *consumption*
Charge batteries	Discharge batteries

Table 2. Description of the DSO flexibility requests

The proposed flexibility algorithm flow chart is described in Fig. 2 and it is based on [7]. The algorithm starts by minimizing each prosumer electricity bill using their flexibility devices: distributed batteries and PV generation. The optimization result is the aggregated baseline optimized, which is the sum of each of the optimized consumption prosumer sites. The following step is to check whether the portfolio has enough flexibility to meet the DSO requests: the aggregator executes the aggregated level flexibility offer (ALFO) optimization problem. In case the flexibility requested could not be activated, it would deliver as much as possible. The aggregator sends to the DSO a flexibility offer and if

the DSO accepts it, the aggregated level flexibility management (ALFM) optimization problem is then carried out, which will provide the flexibility asked to the DSO at minimum cost.

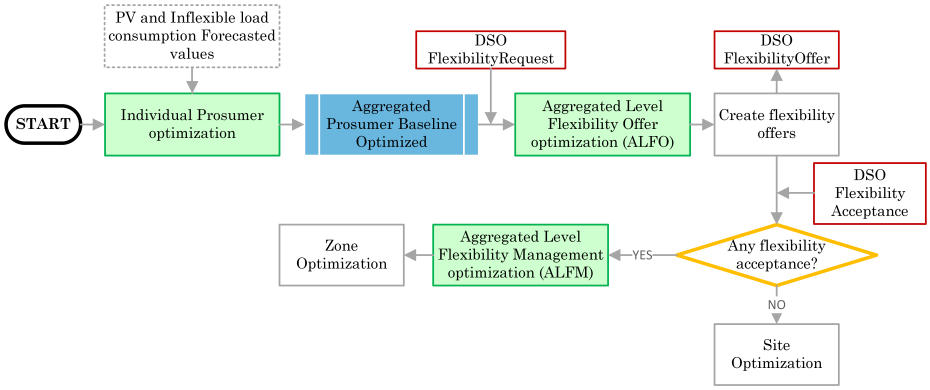

Fig. 2. DSO flexibility service flowchart

2.3 Flexibility Sources

Flexibility in the distribution grid can come from different distributed energy sources, mainly grouped by three types: loads, storage units, and renewable generation. All these flexible sources that can provide the amount of flexibility requested by the DSO are listed and described below:

Demand-side response: prosumers are provided with a financial incentive to turn down or turn off non-essential processes at times of peak demand or high energy prices, depending on what you want to minimize or maximize, helping the grid to balance supply and demand without the need for additional generation to be used.

Energy storage systems: electricity systems face an increased need for flexibility and a fundamental pillar in terms of flexibility are batteries, whose main potential is to help to deal with the high volatility of distributed renewable energy resources. Energy can be stored when there is a surplus of renewable energy generation. This energy can then be used at a time when its needed.

Distributed Energy Resources: they are electric generation units located within the electric distribution system at or near the end user. Electricity is generated locally, minimizing transportation losses.

3 Mathematical problem formulation

This problem is executed in three main steps: first, an individual optimization of each of the prosumers is carried out. The aggregated prosumer baseline optimized is used as an input to the ALFO optimization problem. Once the flexibility offer is calculated by the aggregator and accepted by the DSO, the ALFM optimization problem is carried out and it will provide the flexibility service to the DSO.

3.1 Individual prosumer flexibility service optimization problem

Prosumer objective function and constraints are defined as follows: The prosumer optimization function (1a) aims to reduce the electricity bill by minimizing the amount of energy purchased to the grid χ_t^{buy}, taking into account the revenues for injecting electricity to the grid χ_t^{sell}, maximizing the generation of renewable energy resources and minimizing the flexibility cost ζ_t^{flex}, which is the minimum amount of money that the prosumer is willing to save in order to activate a flexibility source (1b).

Equation (1c) represents the internal energy balance behind each prosumer smart meter: the total electricity imported from the grid, the optimized production from PV generation units $\psi_t^{gen,r}$ and the energy discharged by batteries σ_t^{dis} must be equal to the electricity exported to the grid, the consumption from inflexible load units W_t^{inflex} and the energy charged in batteries σ_t^{ch} for each period of time.

Binary variables δ_t^{buy} and δ_t^{sell} are introduced in equation (1d) in order to ensure that it is not possible to sell and buy electricity in the same period. They are set to 1 if the customer is buying (importing) or selling (exporting); else 0.

The amount of electricity bought (1e) and sold (1f) in each period of time must be less or equal to the maximum energy export capacity of each site per period, according to the terms stipulated in the retail contract.

$$\min_{\chi,\zeta} \quad \sum_{t\in T}(P_t^{retail,buy}\chi_t^{buy}P_t^{VAT} - P_t^{retail,sell}\chi_t^{sell} + \zeta_t^{flex}) \tag{1a}$$

$$\text{s.t.} \quad \zeta_t^{flex} = P_t^{gen,r}(W_t^{gen,r} - \psi_t^{gen,r}) + P_t^{b,ch}\sigma_t^{ch} + P_t^{b,dis}\sigma_t^{dis}, \tag{1b}$$

$$\psi_t^{gen,r} + \sigma_t^{dis} + \chi_t^{buy} = \chi_t^{sell} + \sigma_t^{ch} + W_t^{inflex}, \tag{1c}$$

$$\delta_t^{buy} + \delta_t^{sell} \leq 1, \tag{1d}$$

$$\chi_t^{buy} \leq \delta_t^{buy} X^{max,import}, \tag{1e}$$

$$\chi_t^{sell} \leq \delta_t^{sell} X^{max,export} \tag{1f}$$

3.2 DSO flexibility service optimization problem

The aggregator has to ensure that there is enough flexibility available in his portfolio to meet the DSO flexibility request. The DSO purchases this available flexibility and gives the corresponding economic compensation to the prosumer through the aggregator. Once the flexibility offer sent by the aggregator is accepted by the DSO, the ALFM optimization problem is be executed.

The objective function (2a) is to minimize the aggregator operational cost of meeting DSO flexibility request. $W_{p,t}^{baseline,opt}$ is the aggregated baseline consumption after the individual prosumer optimization. Constraints (2b) (2c) ensure that the activated amount of flexibility is less or equal to the positive and negative FR, respectively. Constraints (2d) and (2e) avoid the rebound effect, which can cause new load peaks before or after the FR activation.

$$\min_{\chi,\zeta} \quad \sum_{t\in T}\sum_{p\in P}(P_t^{retail,buy}\chi_{p,t}^{buy}P_t^{VAT} - P_t^{retail,sell}\chi_{p,t}^{sell} + \zeta_{p,t}^{flex}) \tag{2a}$$

$$\text{s.t.} \quad \chi_{p,t}^{buy} - \chi_{p,t}^{sell} \leq W_{p,t}^{baseline,opt} - FR_t \qquad \forall FR_t > 0, \tag{2b}$$

$$\chi_{p,t}^{buy} - \chi_{p,t}^{sell} \geq W_{p,t}^{baseline,opt} - FR_t \qquad \forall FR_t < 0, \tag{2c}$$

$$\chi_{p,t}^{buy} \leq max(W_{p,t}^{baseline,opt}), \tag{2d}$$

$$\chi_{p,t}^{sell} \leq max(W_{p,t}^{baseline,opt}) \tag{2e}$$

3.3 Distributed Flexible Resources constraints

Energy Storage System constraints Distributed storage units can provide flexibility to the electrical grid by charging or discharging batteries to meet a flexibility request made by the DSO in a given period of time.

The behaviour of the battery is then formulated. The variable σ_t^{soc} in (3) indicates the current battery state of charge (SOC). With the aim to represent a more accurate battery model, the mathematical formulation has into account efficiency factors for storing η^{ch} and delivering electricity η^{dis}. Energy storage units can meet both, negative and positive DSO flexibility requests by charging σ_t^{ch} or discharging σ_t^{dis} the batteries, respectively. Both are variables in this problem.

$$\sigma_t^{soc} = \sigma_{t-1}^{soc} + \sigma_t^{ch}\cdot\eta^{ch} - \frac{\sigma_t^{dis}}{\eta^{dis}} \qquad \forall t \in T \tag{3}$$

In order to preserve and extend the battery life-time, σ_t^{soc} must be between a minimum O^{min} and a maximum O^{max} energy limit value (4):

$$O^{min} \leq \sigma_t^{soc} \leq O^{max} \qquad \forall t \in T \tag{4}$$

Equations (5)(6) limit the maximum energy charged Q^{ch} and discharged Q^{dis} by battery per period .

$$\sigma_t^{ch} \leq \frac{Q^{ch}}{N^{hour}} \qquad \forall t \in T \tag{5}$$

$$\sigma_t^{dis} \leq \frac{Q^{dis}}{N^{hour}} \qquad \forall t \in T \tag{6}$$

Equation (7) makes sure that the energy charged σ_t^{ch} is linearly decreased.S_b^{ch} is the threshold in charging process. The same happens with the discharging energy σ_t^{dis} (8).The lower threshold to limit the energy output is S_b^{dis}.

$$\sigma_t^{ch} \leq \frac{-Q^{ch}}{1 - S^{ch}}\left(\frac{\sigma_t^{soc}}{O^{max}} - 1\right) \qquad \forall t \in T \tag{7}$$

$$\sigma_t^{dis} \leq \frac{Q^{dis}}{S^{dis}} \frac{\sigma_t^{soc}}{O^{max}} \qquad \forall t \in T \tag{8}$$

The total battery degradation cost ζ^{bat} is taken into account (9). $P^{b,ch}$ is the degradation price for charging 1 kWh. The discharging degradation cost has been already included in the charging cost.

$$\zeta^{bat} = \sum_{t \in T} P^{b,ch} \cdot \sigma_t^{ch} \qquad \forall t \in T \tag{9}$$

Photo-voltaic reducible generation constraints The optimized PV scheduled production $\psi_t^{gen,r}$ must be between 0 and the PV baseline electricity generation $W_t^{gen,r}$. The price for reducing the PV generation is set high to maximize the renewable generation.

$$0 \leq \psi_t^{gen,r} \leq W_t^{gen,r} \qquad \forall \ t \in T \tag{10}$$

The total cost for reducing the PV generation is given by $\zeta^{gen,r}$. $P^{gen,r}$ is the price for disconnecting a PV generation unit.

$$\zeta^{gen,r} = \sum_{t \in T} P^{gen,r} \cdot (W_t^{gen,r} - \psi_t^{gen,r}) \qquad \forall \ t \in T \tag{11}$$

4 Case Study

A case study where the aggregator provides a flexibility service to the DSO and prosumer in the Spanish energy market is proposed. The aggregator controls the flexible energy sources of its portfolio, which is formed by 31 prosumers located in Austin, Texas. Real load consumption and PV generation data from different households have been provided by DataPort Inc. Street [12].

The present case study covers a planning horizon of 3 days, divided into 15-minutes time intervals and starting at April 1st of 2019 at 00:00h. All the distributed storage units in the aggregator's portfolio begin and end at half their maximum capacity. The Spanish tariff market is applied in the present optimization problem and the elecricity tariff chosen for buying electricity from the grid is the PVPC (Precio Voluntario para el Pequeño Consumidor), because

price changes hourly. There is no economic remuneration for selling electricity to the grid. All prosumers have a contract power equal to 10 kW.

This work seeks to decide the optimal usage and scheduling for the utilization of the households's flexible devices in order to offer a flexibility service to the DSO when requested, for which they will be remunerated financially, while minimizing their individual electricity bill.

This section demonstrates the applicability of the developed DSO flexibility service algorithm for a zone level optimization, using the prosumer aggregated flexibility.

4.1 Prosumer optimization results

The aggregated result of each individual prosumer optimization is shown in Fig. 3. The lower horizontal axis shows the number of periods of the optimization horizon while the upper axis gathers these intervals in 3 days, for a better visual understanding. A negative energy value represents an electricity input to the system, such as PV generation and batteries discharging. A positive energy value refers to consumption as inflexible loads and batteries charging. Both, generation and consumption, must have the same amount of energy in order to meet the energy balance (1c).

Batteries charge when there is an excess of PV generation and discharge mainly in periods with no solar production and more expensive electricity prices (see periods 30 and 125 for example). The accumulated battery state of charge (SOC) is 155 kWh at the beginning and at the end of the time horizon, as indicated by the restriction imposed. The SOC helps to better understand the inertia of the batteries behaviour. The baseline is defined as the energy purchased minus the energy sold to the grid. Looking at the aggregated baseline optimized, it can be seen that there is an excess of generation injected to the grid between the intervals 159-163 and a high consumption during periods 216-223 and 284-288. The DSO will ask for flexibility in those time intervals in order to avoid grid congestion during high consumption or production periods. The execution time of the 31 individual optimizations in series was 31.19 seconds with an Intel(R) Core(TM) i5-7400 processor and 8GB of RAM.

4.2 Zone maximum flexibility available

The result obtained after the individualized optimization of each prosumer is the aggregated optimized baseline demand. Immediately, the DSO receives a notification of this aggregated optimized baseline demand of all its customers per zone [7] and based on this information, the DSO generates the FR with the aim of maintaining the electrical grid within the safe operation zone. Fig. 4 shows the aggregated optimized baseline demand and the DSO flexibility requests. The DSO needs to increase consumption (sends a negative FR) from periods 157 to 163 due to an excess of generation in the grid caused by the PV production. In periods 216 to 223 and 283 to 287, the DSO asks to reduce consumption (sends a positive FR) to avoid a grid overload. FRs are sent to the aggregator and

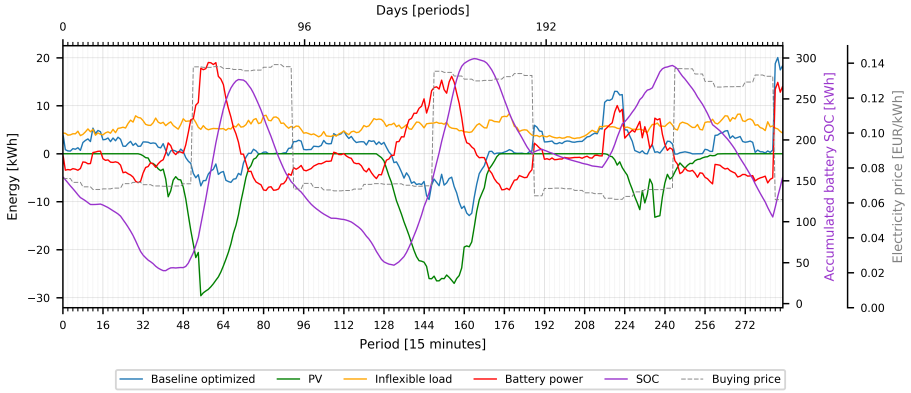

Fig. 3. Aggregated individual prosumer optimization results. Source: Pecan Street Inc. Dataport 2019.

then executes the ALFO optimization problem as it is formulated in [7]. It is verified that there is enough flexibility in the aggregator's portfolio, therefore it is possible to offer all the flexibility requested by the DSO. Following the scheme in Fig. 2, the aggregator creates and sends a flexibility offer to the DSO, which accepts.

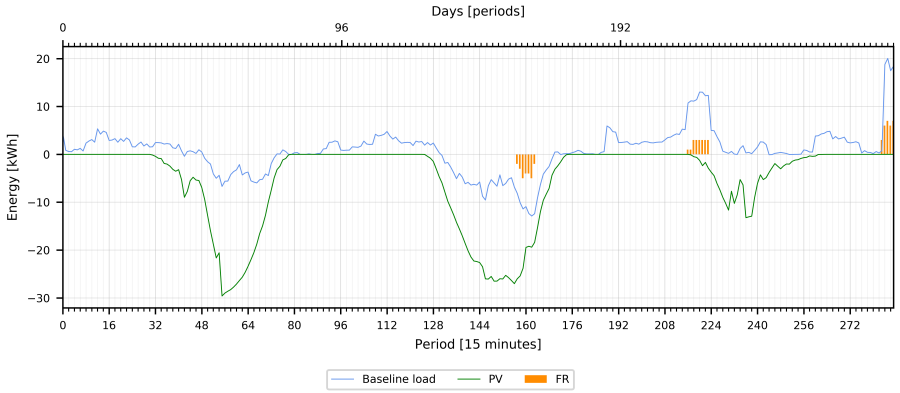

Fig. 4. Zone level optimization flexibility requests. Source: Pecan Street Inc. Dataport 2019.

4.3 Zone optimization results

The aggregated prosumer baseline optimization and the optimized battery power obtained in the previous individual prosumer optimization are the input of the ALFM optimization problem.

The result of the minimum cost centralized optimization is shown in Fig. 5. The activated flexibility is the same as the requested, since the portfolio has enough available flexibility. The only flexibility source are distributed batteries, as the reduction of PV production is severely penalised. It is observed that in periods where the DSO requests to increase the consumption due to an excess of PV generation (see 159-163 periods), the ALFM battery power increases regarding the baseline battery power. The opposite happens when the DSO requests a baseline load reduction: the ALFM battery power decreases in contrast to the battery power baseline because batteries charge has been reduced. The total cost for activating the flexibility is 64.72 €. The execution time of the centralized optimization problem was 33.21 seconds with an Intel(R) Cotre(TM) i5-7400 processor and 8GB of RAM.

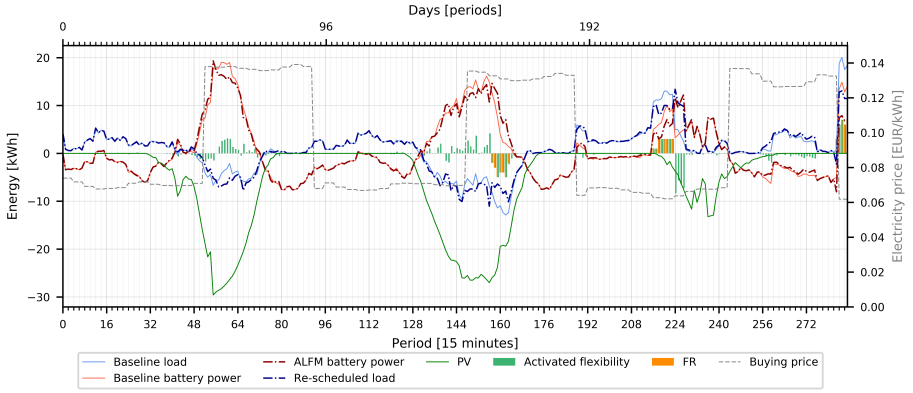

Fig. 5. ALFM optimization problem results under the DSO flexibility requests. Source: Pecan Street Inc. Dataport 2019.

5 Conclusions

It can be concluded that the centralized optimization algorithm proposed performs as it is expected: when the DSO requests a negative FR, this means increase consumption or reduce production, distributed batteries take advantage to charge during these time intervals. On the other hand, when the distribution grid is overloaded and a positive FR is required, some distributed storage units discharge to increase the generation in the grid to match the demand.

6 Acknowledgment

We thank Pecan Street Inc. Dataport database for providing real households data. This work has been supported by the INVADE H2020 project (2017-2019), which has received funding from the European Union's Horizon 2020 research and innovation program under Grant Agreement No. 731148, and by *Ministerio de Ciencia, Innovacin y Universidades* under the project RTI2018-099540.

References

[1] EC. *Clean Energy For All Europeans Communication*. Tech. rep. 2016.

[2] Martina K. Linnenluecke, Jianlei Han, Zheyao Pan, et al. "How markets will drive the transition to a low carbon economy". In: *Economic Modelling* 77 (2019), pp. 42 –54. ISSN: 0264-9993. DOI: https://doi.org/10.1016/j.econmod.2018.07.010. URL: http://www.sciencedirect.com/science/article/pii/S0264999318304619.

[3] European Distribution System Operators for Smart Grids (EDSO). *Flexibility: The role of DSOs in tomorrow's electricity market*. Tech. rep. 2014, pp. 1–16. URL: http://www.edsoforsmartgrids.eu/wp-content/uploads/public/EDSO-views-on-Flexibility-FINAL-May-5th-2014.pdf.

[4] USEF Foundation. "USEF: The framework explained". 2015.

[5] S. Huang and Q. Wu. "Real-Time Congestion Management in Distribution Networks by Flexible Demand Swap". In: *IEEE Transactions on Smart Grid* 9.5 (2018), pp. 4346–4355. ISSN: 1949-3053. DOI: 10.1109/TSG.2017.2655085.

[6] A. Roos, S. Ø. Ottesen, and T. F. Bolkesjø. "Modeling Consumer Flexibility of an Aggregator Participating in the Wholesale Power Market and the Regulation Capacity Market". In: *Energy Procedia* 58 (2014). Renewable Energy Research Conference, RERC 2014, pp. 79 –86. ISSN: 1876-6102. DOI: https://doi.org/10.1016/j.egypro.2014.10.412. URL: www.sciencedirect.com/science/article/pii/S1876610214017792.

[7] P. Olivella-Rosell, F. Rullan, P. Lloret-Gallego, et al. "Centralised and Distributed Optimization for Aggregated Flexibility Services Provision". In: *arXiv preprint arXiv:1907.08125* (2019).

[8] *INVADE H2020 Project Grant Agreement 731148*. 2017. URL: https://h2020invade.eu (visited on 10/20/2017).

[9] S. Widergren k. Kok. "A Society of Devices: Integrating Intelligent Distributed Resources with Transactive Energy". In: *IEEE power and Energy Magazine* 14 (2016), pp. 34–45.

[10] P. Lloret-Gallego, P. Olivella-Rosell, G. T. Berger, et al. *INVADE D4.1 Overall INVADE architecture*. Tech. rep. 2017. DOI: 10.5281/zenodo.853241. URL: https://doi.org/10.5281/zenodo.853241.

[11] P. Olivella-Rosell, P. Lloret-Gallego, . Munn-Collado, et al. "Local Flexibility Market Design for Aggregators Providing Multiple Flexibility Services at Distribution Network Level". In: *Energies* 11.4 (2018). ISSN: 1996-1073. DOI: 10.3390/en11040822. URL: www.mdpi.com/1996-1073/11/4/822.

[12] *DataPort Data Base*. https://dataport.cloud/. [Online; accessed 15-July-2019]. 2018.

Uso de seguidores solares para la optimización de producción energética solar fotovoltaica bajo condiciones del trópico.

Hugo Sánchez[1 [0000-0002-4122-1382]], Carlos Meza[1 [0000-0002-7374-505X]], Sebastián Romero Tencio[1], and Kenneth González[1]

Instituto Tecnológico de Costa Rica, Cartago 30101, Costa Rica,
husanchez@itcr.ac.cr,
http://www.tec.ac.cr

Resumen Los seguidores solares son sistemas que optimizan la producción de energía en un sistema solar fotovoltaico. Son utilizados especialmente en latitudes donde el rango de posición del sol, a lo largo del año, es amplio. No obstante han sido poco explorados en otras latitudes. Para el caso de Costa Rica la variación de la posición del sol a lo largo del año no es amplio, comparado con otras latitudes. El presente trabajo, muestra los principales resultados analíticos y las primeras pruebas sobre la utilización de un seguidor solar de un eje y su respectiva comparación con un sistema fotovoltaico cuyo módulo se encuentra a una inclinación fija.

Keywords: Instalación fotovoltaica · seguidores solares · Rendimiento Energético.

1. Introducción

El informe número 23 del Estado de la Nación 2017 menciona que, según un análisis del Instituto Costarricense de Electricidad (ICE) en Costa Rica las fuentes de energía con mayor potencial de aprovechamiento son la hidroeléctrica y la solar [1] . En los últimos años, el país está pasando por un cambio significativo en la legislación energética de producción fotovoltaica y con ello una mayor afinidad por parte de los usuarios finales al uso de esta tecnología. Por tanto, la experimentación con nuevos tipos de sistemas bajo las condiciones del país es vital para la búsqueda de nuevas tendencias tecnológicas como métodos de producción de energía.

Varios estudios han trabajado sobre la estimación de la eficiencia sobre el uso de seguidores solares, mostrados en [2], [3],[4] y [5]. Sin embargo, existen pocas referencias sobre la utilización de seguidores solares bajo condiciones del trópico, salvo algunas excepciones expuestas en [6] y [7]. Cabe destacar que no existe ninguna publicación sobre el uso de seguidores solares en Costa Rica. Una de las primeras hipótesis planteadas es que, dada la cercanía al Ecuador y a la relativa estabilidad del clima a lo largo de un año, el uso de este tipo de sistemas no resulta viable para Costa Rica.

Por tanto, se procedió con la implementación de uno de estos sistemas en el *Laboratorio de Sistemas Electrónicos para la Sostenibilidad* (SESLab) ubicado en el ITCR, para generar información relevetante sobre la viabilidad del uso de esta tecnología.Se realizó una comprobación teórica y una implementación para obtener datos experimentales, con el objetivo de responder a la pregunta sobre si estos sistemas se pueden usar en Costa Rica. Los principales resultados son mostrados en el presente artículo.

2. Geometría Solar y Seguidores Solares

Una de los principales objetivos de diseño de sistemas solares fotovoltaicos, es garantizar que los rayos solares incidan de forma perpendicular a la superficie del generador [8]. Sin embargo, la posición relativa del sol respecto a un punto sobre la superficie terrestre no es constante durante el año, dados los movimientos de traslación y rotación de la Tierra respecto al Sol. La figura 1 muestra la distribución de dicho movimiento.

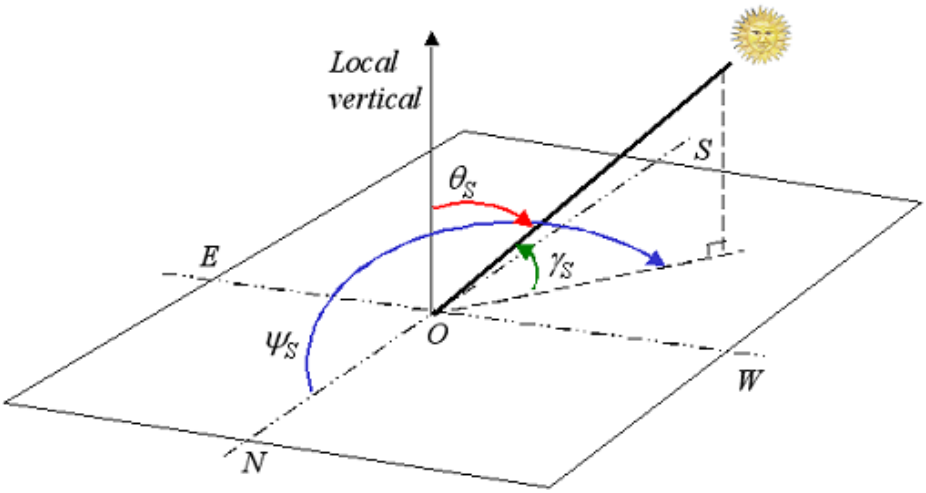

Figura 1. Cambio en la posición del Sol respecto a punto en la superficie terrestre. [9]

Como se puede apreciar existen dos movimientos del sol referentes a un punto fijo en el plano terrestre.

- Diario: Diariamente el sol tiene un movimiento de este (por las mañanas) hacia el oeste (por las tardes).
- Estacional: El sol tiene un movimiento que varía de acuerdo a la época del año. En el caso de Costa Rica, el sol se encuentra más hacia el Sur en diciembre y comienza a subir hasta encontrarse de forma perpendicular (en

abril). Continua hacia el norte en los meses de mayo, junio y julio, para comenzar su reorientación hacia el sur en el mes de agosto.

Como se puede observar, el movimiento es variable respecto a un punto en la superficie terrestre. Si se coloca el panel en una posición fija, no es posible garantizar la máxima producción energética de dicho generador fotovoltaico. A partir de los tipos de movimientos existen dos tipos de seguidores solares:

- Seguidores de un eje: Siguen al sol en un sólo movimiento, ya sea de forma diaria o de forma estacional. Son más comunes los seguidores solares que siguen el movimiento del sol de este a oeste
- Seguidores de dos ejes: Siguen el movimiento del sol, en los dos tipos de movimiento. Son ampliamente utilizados en latitudes del norte, dado su desempeño [10]

3. Diseño de experimento

Se procedió a la realización de un experimento sobre el uso de seguidores solares de un eje bajo las condiciones de Costa Rica que serán presentadas a continuación.

3.1. Modelado Teórico

Se procede con el planteamiento dos modelos matemáticos. El primero presenta una relación sobre la radiación que puede percibir un panel solar en Costa Rica si se encontrará de forma perpendicular, descrito en la siguiente expresión:

$$Rad = 1140 - \frac{7{,}6tanh^{-1}\left(\frac{tan(\frac{7{,}5(h-12)}{2})}{\sqrt{B(n)^2-A(n)^2}}\right)(A(n)-B(n))}{\sqrt{B(n)^2-A(n)^2}} + C \quad (1)$$

La radiación percibida, bajo el mismo caso pero en una superficie horizontal, está modelada por:

$$Rad = (1140A(n) + 57)h + 76B(n)sen(15(h-12)) \quad (2)$$

En ambos casos se realizó la sustitución de variables, descrita por:

$$A(n) = sen(\delta)sen(\phi) \quad (3)$$

$$B(n) = cos(\delta)cos(\phi) \quad (4)$$

Donde δ representa la declinación solar y ϕ representa la latitud del sitio de estudio.

A partir de dicho modelo matemático se realizó una simulación para comparar el rendimiento teórico que se puede obtener con un seguidor solar de un eje,

utilizando varios días del año. La figura 2 muestra los resultados obtenidos en dicha simulación, donde se observa que en el caso de un seguidor solar existe un aprovechamiento de captación energética de un 30 % respecto a la posición de un panel fijo.

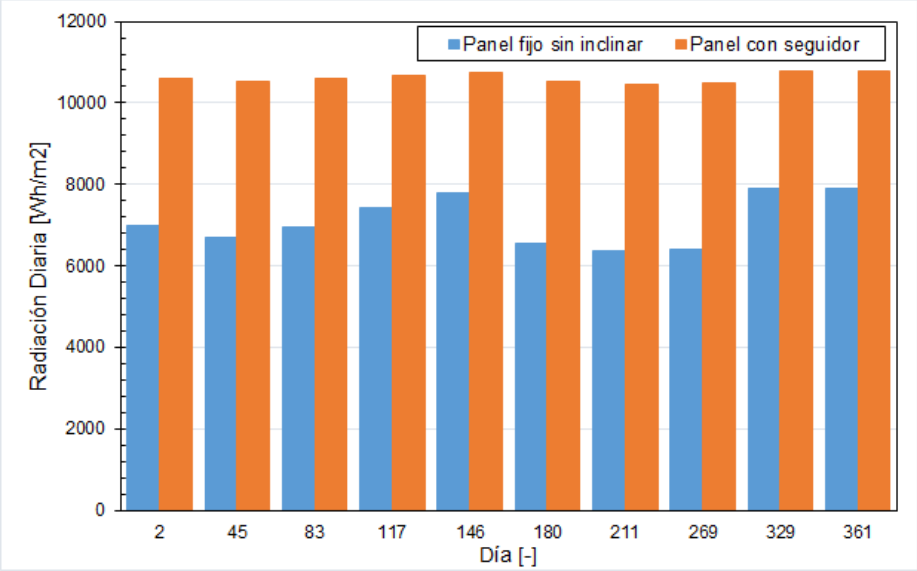

Figura 2. Simulación modelado teórico eficiencia de un sistema de seguidor solar

3.2. Implementación

Con el objetivo de realizar una validación experimental de los resultados mostrados en la figura 2 se procede a realizar una estructura para medir la eficiencia del panel solar. Dicho sistema se observa en la figura 3.

Para el caso del seguidor solar y su comparación con un panel en el plano horizontal se utiliza un panel solar *CanadianSolar CS6P-255* conectado a un microinversor *Aurora ABB-Microinverter 250W*. Una vez implementada ambas plantas (seguidor y panel fijo) se ejecutan adquisición de datos de los principales paramétros eléctricos, para ambos sistemas. En una segunda parte del experimento (Noviembre de 2017) se procedió con la realización de cambios en los algoritmos de control, que permitieran una optimización en el seguimiento solar.Los principales resultados se muestran en la Figura 4.

Un resumen de los resultados obtenidos, se puede apreciar en la Figura 5 donde se observa calcula el rendimiento energético de la planta (kWh/kW). Se logra apreciar una mejora de un 22 % en comparación con un panel fotovoltaico colocado de forma horizontal.

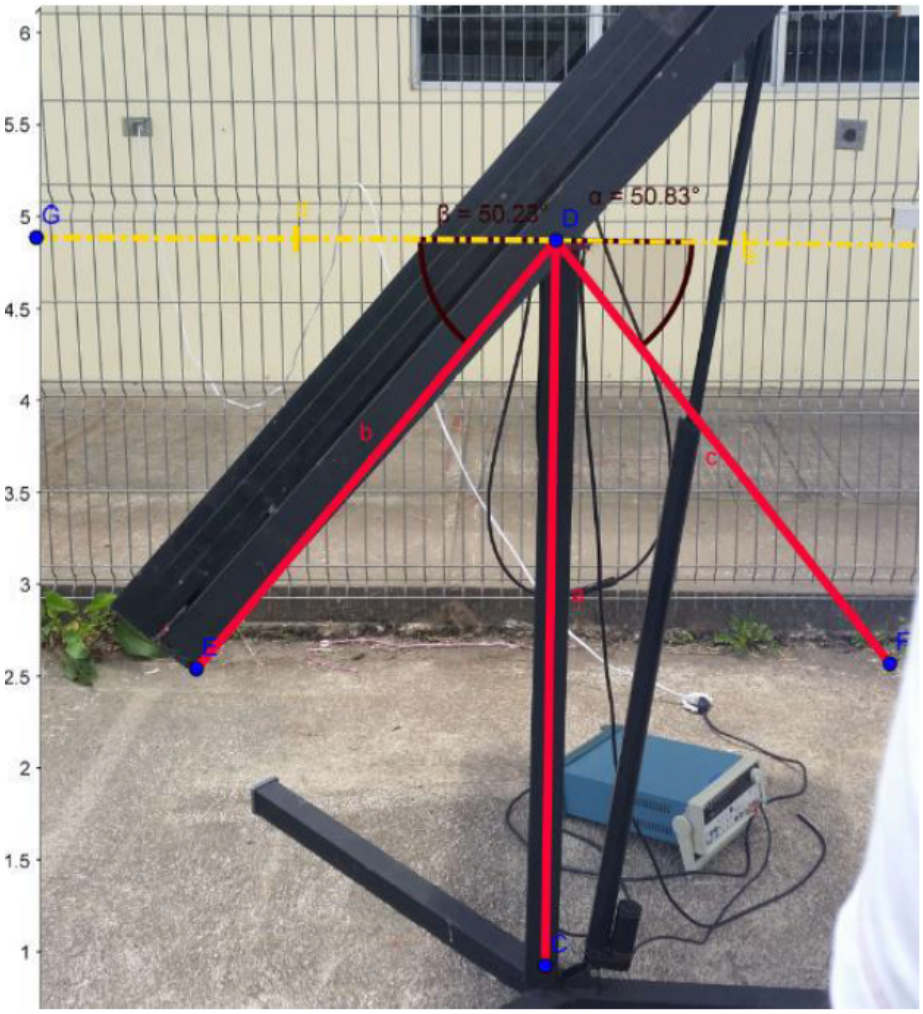

Figura 3. Seguidor solar de un eje implementado para la mediciones

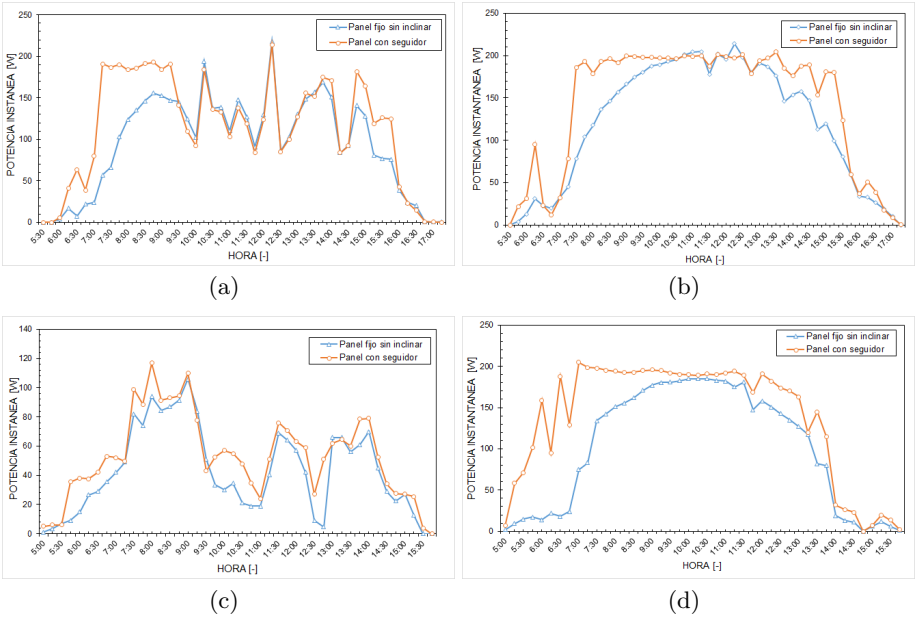

Figura 4. Comparación de datos para un seguidor de panel fotovoltaico y un panel horizontal fijo para los días 4(a) 15 de mayo de 2016 y 4(b) 16 de mayo de 2016 4(c) 2 de Noviembre de 2017 y 4(d) 6 de noviembre de 2017

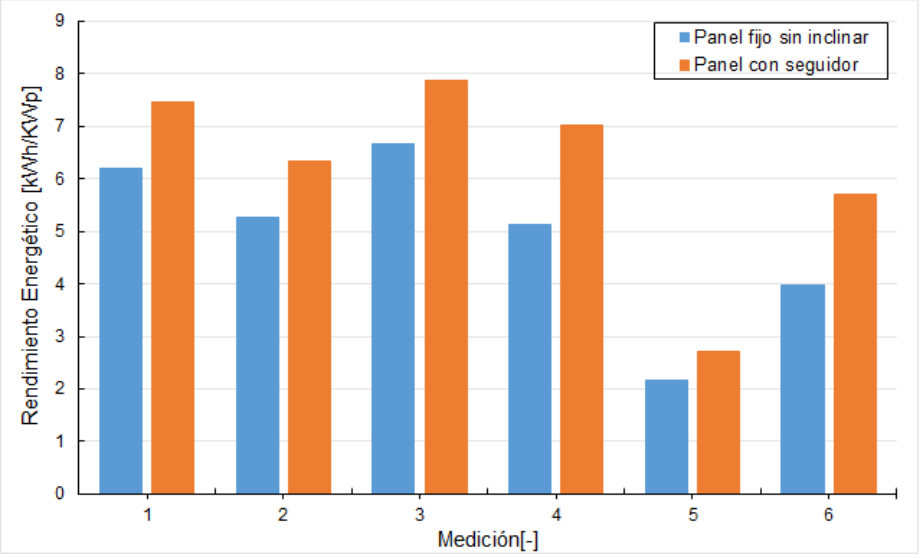

Figura 5. Comparación del rendimiento energético del seguidor solar y su comparación con un panel en posición fija

4. Viabilidad Financiera

En base a los resultados obtenidos en la sección anterior, se procedió a realizar un caso de estudio para analizar la eventual viabilidad económica del proyecto. En este caso, se tomó como referencia una instalación de 8,8kW ubicada en el campus del Tecnológico de Costa Rica con los siguientes parámetros mostrados en el Cuadro 1.

Cuadro 1. Parámetros de entrada simulación de viabilidad finaciera sistema de seguidor solar

Parámetro	Valor
Vida Útil de proyecto	25 años
Degradación	0,7 Anual
Escudo Fiscal	30 %
Inflación	5 % anual
Costo	1,5 USD /W

Además en la figura 6 se observa una curva que refleja el Retorno de Recuperación de la Inversión (ROI) para ambos escenarios.

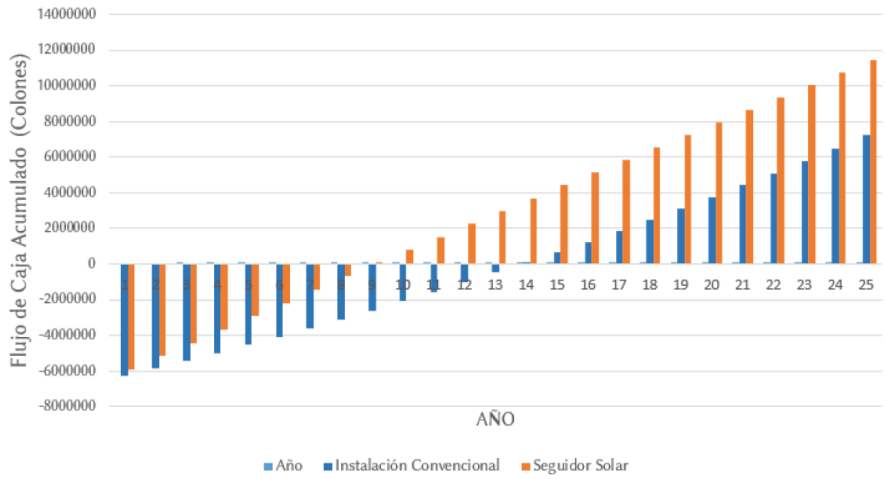

Figura 6. Comparación de las curvas de retorno de la inversión para un sistema de seguidor solar vs un sistema solar fijo

El Cuadro 2 muestra los principales resultados financieros obtenidos para los proyectos simulados.

Cuadro 2. Parámetros de entrada simulación de viabilidad finaciera sistema de seguidor solar

Parámetro	Sistema seguidor Solar	Sistema de Panel fijo
Retorno de la Inversión	7 años 2 meses	12 años 3 meses
Valor actual neto	11 481 60,97 colones	7 229 969,82 colones
Tasa Interna de Rendimiento	12 %	7 %

De la tabla anterior es posible observar como los sistemas de seguidores solares, a pesar de contar con una inversión inicial mayor y un costo anual más elevado de mantenimiento, presentan una mayor viabilidad económica que los sistemas de panel fijo, gracias a la generación adicional de electricidad que presentan. A su vez, el incremento de la potencia en el sistema puede significar una reducción de los costos de operación. De igual forma, la inversión en el uso de las tecnologías permitirá un mayor decremento en la curva de aprendizaje, volviendo estos sistemas más rentables, desde el punto de vista financiero.

5. Conclusiones

Con la aproximación de un modelo matemático, fue posible comprobar que el uso de seguidores solares por ángulo horario presentan un aprovechamiento de 35 % más de la radiación captada, en comparación con un panel solar fijo en el plano horizontal.
Situación que motivó el desarrollo de una planta experimental para la generación de mediciones experimentale. Mediante las mediciones experimentales se observa un crecimiento en el rendimiento energético de un 20 % en promedio para un sistema de seguidor solar por ángulo horario, en comparación con un panel solar fijo en el plano horizontal.Lo cual muestran una mejora en la eficiencia de recolección de la energía. La mejora en el diseño del seguidor solar o la utilización del mecanismo para un sistema inclinado de forma perpendicular al sol permitiría un mayor radio de recolección de energía para el sistema. El uso de seguidores solares no optimiza la producción en un escenario de baja radiación. Lo cual no garantiza la misma rentabilidad presentada para días nublados. Sin embargo, ésta es una de las líneas de trabajo a futuro, para conocer la relación de aprovechamiento de energía en función del índice de nubosidad y con ello, tener una mayor idea sobre el aprovechamiento en áreas con un mayor porcentaje de radiación difusa.
El uso de seguidores solares automatizados, de al menos un eje, presenta una mayor rentabilidad financiera en comparación a los paneles en posición fija, en este caso bajo las condiciones del mercado para Costa Rica. Dado que las condiciones técnicas pueden plantearse como similares para el resto del trópico, se pueden suponer que la rentabilidad financiera también es buena. Sin embargo, estará sujeta a las condiciones de cada mercado eléctrico como lo es el precio de consumo por kWh, los subsidios de energía renovable y las políticas para la

utilización de este tipo de sistemas.
Con el presente trabajo, se presenta una primera idea sobre la rentabilidad que puede presentar el uso de sistemas bajo las condiciones del trópico. Si bien es cierto, no presentan los mismos grados de eficiencia a los reportados en latitudes más alejadas del trópico, si presentan un incremento razonable. Lo cual motiva a la generación de más casos de estudios y variaciones que permitan entender el potencial real para el uso de estos sistemas.

Referencias

1. Programa Estado de la Nación. *Vigésimo Tercer Informe Estado de la Nación en Desarrollo Humano Sostenible.*Programa Estado de la Nación. San José, 2017.
2. Khan, M. T. A., Tanzil, S. S., Rahman, R., Alam, S. S. . Design and construction of an automatic solar tracking system. In Electrical and Computer Engineering (ICECE), 2010 International Conference on (pp. 326-329). IEEE (2010, December).
3. Mousazadeh, H., Keyhani, A., Javadi, A., Mobli, H., Abrinia, K., Sharifi, A.A review of principle and sun-tracking methods for maximizing solar systems output. Renewable and sustainable energy reviews, vol. 13(8), pp. 1800-1818.(2009)
4. Al-Mohamad, Ali. Efficiency improvements of photo-voltaic panels using a Sun-tracking system. Applied Energy, vol. 79, no 3, p. 345-354.(2004)
5. Saravanan, C.; Pannerselvam, M. A.; Christopher, I. William. A novel low cost automatic solar tracking system. Int. J. Comput. Appl. vol. 31, p. 62-67.(2011)
6. Rahman, Abdul Malek Abdul, et al. The performance of three different solar panels for solar electricity applying solar tracking device under the Malaysian climate condition. Energy and Environment Research, vol. 2, no 1, p. 235. (2012).
7. Guardado, D.H.; Rivera, V. E.; Implementación de seguidor solar en dos ejes para el Sistema Fotovoltaico de la Escuela de Ingeniería Eléctrica de la UES. Tesis Doctoral. Universidad de El Salvador. (2012)
8. Huang, B. J., et al. Performance evaluation of solar photovoltaic/thermal systems. Solar energy, vol. 70, no 5, p. 443-448. (2001)
9. Mines. Paris Tech, Solar Geometry. http://www.oie.mines-paristech.fr/Valorisation/Outils/Solar-Geometry/ (2018)
10. Huang, Bin-Juine, et al. Improving solar PV system efficiency using one-axis 3-position sun tracking. Energy Procedia, 2013, vol. 33, p. 280-287.

Modelos de generación Hibrido-Marina con almacenamiento de volante de inercia

Mónica Alonso[1], Brenda Rojas[1], Hortensia Amarís[1], Juan de Santiago[2]

[1] Universidad Carlos III de Madrid. 28911 Madrid. España
[2] Universidad de Uppsala, Uppsala, Suecia
monica.alonso@uc3m.es

Abstract. El presente trabajo propone un nuevo sistema de control de instalaciones marinas para mejorar el suavizado de la potencia de salida mediante la hibridación de las mismas con un sistema de almacenamiento de energía mediante flywheel (FESS). El control propuesto está formado por tres etapas: en la primera se agrega la potencia de salida de varios generadores marinos, a continuación, se realiza un filtrado de la potencia, y finalmente se controla la energía almacenada en el FESS para mejorar la calidad de la potencia entregada a la red. El modelo propuesto se ha validado empleando los datos de producción real de una instalación real situada en Lysekil (Suecia). Los resultados obtenidos muestran una reducción del 85% en la potencia máxima entregada a red, así como una reducción del 76% en la relación entre la potencia máxima y media a la salida de la instalación. Además, las pérdidas de potencia activa se ven reducidas en un 51% mejorando la eficiencia de la red eléctrica. Finalmente, la instalación híbrida propuesta es capaz de seguir una consigna impuesta por el operador de red, presentándose ante la red de distribución como un nuevo recurso distribuido capaz de ofrecer servicios auxiliares al operador de la red.

Keywords: energía marina, sistemas de almacenamiento mediante flywheel (FESS), recurso distribuido.

1 Introducción

Uno de los principales retos a los que se enfrenta actualmente la humanidad es el cambio climático y el calentamiento global, siendo el sector energético uno de los principales pilares en el que las energías renovables tienen un papel fundamental. La energía marina representa el 0.24% [1] de las energías renovables[3], con una potencia estimada de 92 PWh/year [2] . Sin embargo, teniendo en cuenta que el agua ocupa el 70% de la superficie de la tierra, de la cual océanos, mares y bahías acumulan el 96.54% de la cantidad de agua en la tierra, la energía marina se presenta como una gran alternativa para la generación de energía eléctrica en el futuro. En la actualidad, hay 1.7 GW de instalaciones marinas en construcción y 0.5 GW en instalaciones comerciales conectadas a red. La falta de grandes plantas marinas hace difícil predecir el futuro de esta tecnología. Sin embargo, se estima un gran crecimiento de la energía marina para el año 2020, alcanzándose valores de 838 GW y 16,2 GW en instalaciones marinas con fuente las olas o las mareas respectivamente.

La Fig. 1 muestra el potencial marino a nivel mundial, expresado en kW por unidad de longitud, donde la longitud se mide en la cresta de la ola o a lo largo de la dirección de la costa, así como la potencia total estimada en los diferentes continentes (en GW) [4]. Las mejoras localizaciones para la generación marina son aquellas que presentan un potencial entre 20 kW/m y 70 kW/m, y se encuentran, principalmente, en las latitudes comprendidas entre los 30º y 60º de cada hemisferio. Como el origen de las olas está en el viento, y el viento surge como consecuencia de los cambios de temperatura, los cambios térmicos experimentados en las diferentes estaciones del año afectarán a la producción de energía marina. Puesto que los cambios estacionales son menores en el hemisferio Sur, las costas de América del Sur, África y Oceanía son las que presentan mayor potencial marino. Esta menor variación en el recurso disponible permite optimizar mejor el funcionamiento de los generadores, al aumentar el número de horas en las que el recurso marino es aquel para el que la instalación ha sido diseñada.

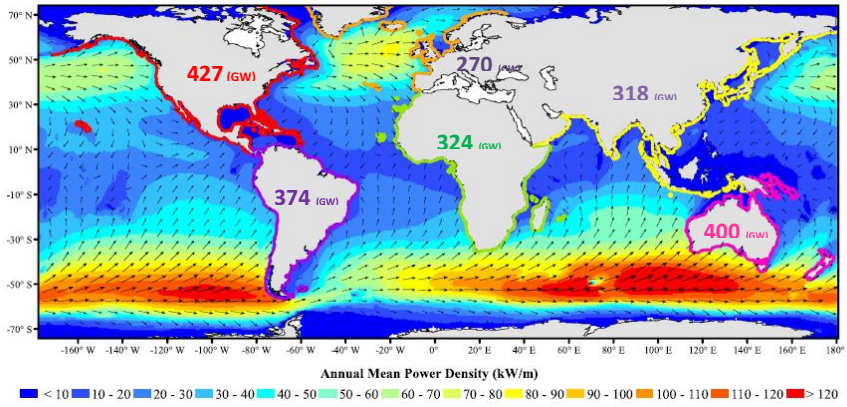

Fig. 1. Densidad media anual de recurso marino [4]

Entre las características de la energía marina destacan:

- La disponibilidad del recurso marino, su densidad de energía, así como la fiabilidad de las predicciones, con respecto a otras tecnologías renovables como la solar y eólica. Se puede considerar la energía marina como un segundo tipo de energía solar, ya que las olas surgen como consecuencia del viento, y este, a su vez de los cambios de temperatura. Así, una intensidad solar de 0.1-0.3 kW/m2 es transformada en una intensidad de flujo de potencia de 2-3 kW/m2 en el plano vertical en la dirección de la ola [5].
- Teniendo en cuenta la relación directa que existe entre la demanda de energía eléctrica y la temperatura, así como la que existe entre la energía solar y marina, la producción de energía eléctrica mediante esta tecnología se presenta como una buena alternativa a la hora de seguir la curva de demanda estacional de los consumidores [6.].
- Atendiendo al ratio de producción anual, los convertidores marinos trabajan el 90% de las horas del año, muy superior al 20-30% de generación de otras tecnologías renovables, como la solar y eólica [7].

Sin embargo, no todo son ventajas en el campo de la energía marina:

- La integración en red y la calidad de suministro se encuentran entre los principales retos a los que se enfrentan las instalaciones marinas. Ambos retos están directamente relacionados con la variabilidad del recurso marino.
- Las instalaciones marinas suelen estar localizadas en puntos alejados de los grandes centros de consumo y se conectan a redes débiles de distribución que presentan problemas de regulación de tensión, corrección del factor de potencia o mitigación de armónicos, que las actuales instalaciones marinas no son capaces de corregir.

Por lo tanto, a pesar de todas las ventajas que presenta la energía marina y la gran disponibilidad de recurso, es necesario superar una serie de retos para mejorar los desarrollos actuales de extracción e integración en red, así como el coste de las instalaciones [8]:

- En cuanto a los requerimientos de conexión a red no existen actualmente códigos de red específicos para la integración de las instalaciones de generación marina, por lo que se están aplicando los desarrollados para las instalaciones eólicas. Sin embargo, debe tenerse en consideración la gran variabilidad de la potencia de salida que inyectan las instalaciones marinas en red lo que los diferencia de otro tipos de instalaciones. En primer lugar, y dada la gran oscilación en la potencia de salida de las instalaciones marinas, es necesario determinar si las restricciones establecidas en los códigos de red pueden tener en cuenta distintos valores de potencia media o de potencia pico. Además, fruto de la variabilidad en la generación eléctrica de las instalaciones marinas no es posible aplicar directamente los requerimientos de rampas de generación empleados en otras tecnologías de energías renovables.
- En cuanto al comportamiento dinámico de las máquinas y a la estabilidad de la red, el impacto de la gran variabilidad en la potencia de salida de un pequeño generador marino puede ser muy superior al impacto de un gran generador eólico cuya potencia de salida presente un menor porcentaje de oscilación por lo que el tamaño de la máquina eléctrica no puede emplearse como criterio en el desarrollo de los códigos de red.
- Para impulsar el desarrollo de la energía marina y reducir los costes asociados a la misma se están empleando sistemas híbridos en los que la energía marina se instala cerca de los parques eólicos off-shore, de manera que es posible compartir el punto de conexión a red.

Por todo lo expuesto anteriormente, debe hacerse una gran inversión en el desarrollo de la energía marina de manera que pueda ser una generación fiable para el sistema eléctrico al que se conecta, a la par de reducir los costes de las instalaciones. Si la energía marina consigue finalmente despegar como energía alternativa en la generación de energía eléctrica, en el año 2050 el 10% de la energía consumida por el continente europeo podría ser suministrada por la tecnología marina.

En el presente trabajo se desarrolla un modelo de una instalación híbrida que combina tecnología marina con un sistema de almacenamiento mediante volente de inercia

(Flywhell Enery Storage System, FESS). El modelo propuesto es capaz suavizar la potencia de salida de una instalación marina, dotando a dicha instalación de la capacidad de regulación de su potencia de salida, de manera que pueda participar en la operación del sistema de distribución al que se encuentra conectado, ofreciendo al operador de red la posibilidad de seguir una consigna de potencia dada.

2 Infraestructuras de generación de energía Marina

La primera patente relacionada con la conversión de la energía marina en eléctrica data de 1799, desarrollada por Pierre-Simon Girard. Sin embargo, no es hasta la década de 1940 cuando Yoshio Masuda realizó los primeros estudios de producción de energía Marina que impulsaron su desarrollo como una tecnología competitiva. A pesar de que en 2009 se había alcanzado el millar de patentes relacionadas con la extracción de energía a partir del recurso marino [9], la energía marina se encuentra todavía en un estado inicial de desarrollo. En los andares de la energía marina varios programas de R&D [10]–[14], proyectos de investigación [15]–[17], y de desarrollo de la tecnología marina [2], [12], [18], [19]. Los requisitos en las etapas iniciales de desarrollo de la energía marina requieren llevar a cabo estudios en condiciones de ondas regulares [20]–[24]. Sin embargo, una vez que se ha alcanzado una solución óptima bajo esas condiciones, datos correspondientes a ondas reales deben ser empleados para demostrar la eficacia de los métodos desarrollados [22], [27]–[29].

La transformación del recurso marino en energía eléctrica se realiza a través de 3 procesos principales: captación del recurso (front end interface), transformación del recurso (power take off conversion, PTO) y generación de electricidad, tal y como muestra la Fig. 2.

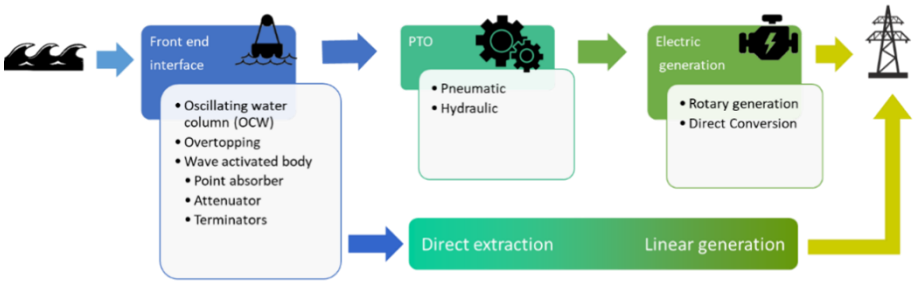

Fig. 2. Transformación de recurso marino en energía eléctrica.

Al igual que sucede con otras tecnologías renovables, existen numerosos dispositivos wave energy converters (WEC). Los sistemas WEC se pueden clasificar de acuerdo a la localización de las instalaciones, captación del recurso marino y la transformación del mismo en electricidad.

Atendiendo a la localización de la instalación, la profundidad del lecho marino establece 3 tipos de instalaciones: shoreline u onshore, para las instalaciones localizadas en la línea de la costa, nearshore y offshore.

2.1 Clasificación de los sistemas WEC de acuerdo a la Captación del recurso marino: Front end interface

En cuanto al sistema de captación del recurso, existen numerosos desarrollos en este campo que se pueden agrupar en 3 categorías principales, Fig. 3:

- oscillating water column (OCW), son considerados los primeros dispositivos empleados en la conversión del recurso marino en energía eléctrica. Están compuestos por una cámara parcialmente sumergida que permite crear una columna de agua cuya altura sube o baja en función del movimiento de las olas. Estos dispositivos suelen emplearse en las instalaciones cercanas a la costa y pueden estar anclados a las rocas del litoral o presentarse anclados al fondo marino.
- overtopping, son dispositivos compuestos por una estructura semi sumergida capaz de almacenar agua cuando las olas la rebasan. La presión ejercida por la columna de agua dentro de la estructura activa una turbina marina conectada a un generador de electricidad.
- wave activated body (WAB), pueden clasificarse en attenuators, point absorber and terminators. Los WAB son dispositivos dotados de una boya que flota sobre las olas de la superficie marina. El movimiento perpendicular de la boya con respecto al lecho marino activa la transformación de la energía contenida en las olas en energía eléctrica.

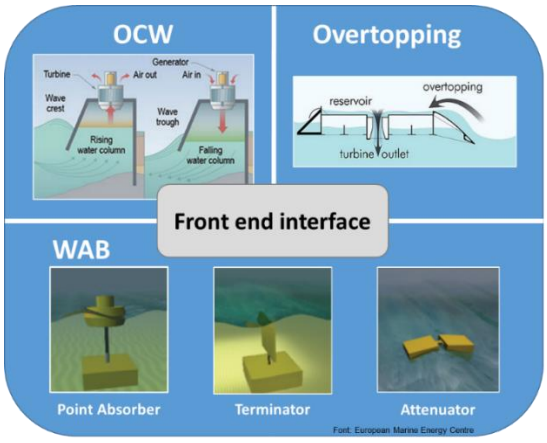

Fig. 3. Tipos de Front end interface [28]

2.2 Clasificación de los sistemas WEC de acuerdo al Power Take off conversión (PTO)

Finalmente, atendiendo a la conversión entre el movimiento mecánico inducido por las olas y la generación de electricidad se pueden considerar 4 tipos de tecnologías de transmisión, Fig. 4:

- neumática, empleados en aquellas instalaciones en las que el movimiento de las olas implica un movimiento de masa de aire dentro de una cámara. Este tipo de instalaciones empleará, por tanto, OCW para la captación del recurso marino.
- hidráulica, las instalaciones de PTO hidráulicas son las más extendidas porque presentan mayor facilidad en el control y rectificación de la potencia de salida de la instalación. Existen dos tipos de sistemas de transmisión hidráulicos: los que utilizan turbinas para convertir el movimiento de las olas en movimiento mecánico y los que disponen de un dispositivo de transformación y almacenamiento de energía hidráulica.
- Existe una última configuración de PTO en la cual la conversión de la energía marina en eléctrica se realiza en el mismo dispositivo, son los direct drive systems, que emplean principalmente como captador de energía de las olas los point absorber. Estos sistemas no disponen de dispositivos mecánicos intermedios para la generación de electricidad, como en el caso de los PTO neumáticos e hidráulicos, por lo que son mucho más sencillos, estructuralmente hablando, presentan menos pérdidas y por lo tanto mayor
- eficiencia en su funcionamiento. Aunque es posible emplear generadores rotativos en la transformación de la energía marina en eléctrica, dada la baja velocidad de variación de las olas y la gran fuerza que transmiten al generador, los generadores lineales de baja velocidad son más adecuados para tal fin. Los generadores lineales se encuentran unidos directamente a la boya para la generación de electricidad.

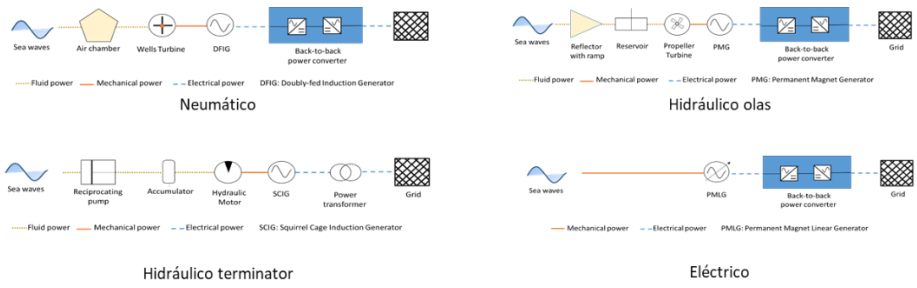

Fig. 4. Tipos de conversión marina-electricidad [28]

3 Suavizado de la potencia de salida de las instalaciones de energía marina

La transformación de la energía marina en eléctrica se puede dividir en 3 pasos fundamentales que comprenden los procesos de: absorción del recurso marino, transmisión de potencia marina y generación de energía eléctrica. Sin embargo, el recurso empleado por las instalaciones marinas es no controlable e intermitente Esta gran variabilidad en la potencia de salida de las instalaciones marinas hace necesaria una cuarta etapa, en el proceso de conversión de la energía marina en energía eléctrica, que realice un acondicionamiento de la señal de salida de la instalación. Esta etapa es especialmente importante en las instalaciones que emplean direct drive wave energy converters, ya que no existe una etapa mecánica entre la absorción del recurso marino y la generación de electricidad que pueda absorber las oscilaciones provocadas por el movimiento de las olas.

Por todo lo anteriormente expuesto, la integración en red es uno de los grandes retos a los que se enfrenta la energía marina. Sin sistemas de suavizado (Power Smoothing Systems, PSS) las variaciones en la producción de salida de las instalaciones marinas se propagan a la red eléctrica a la que se conectan provocando fluctuaciones de la frecuencia de red, problemas de flicker y harmónicos, así como violación de los límites térmicos de los elementos empleados en la conexión on-shore de estas instalaciones [29]. Es importante destacar, además, que las instalaciones marinas suelen estar conectadas on-shore a redes débiles que no son capaces de mantener la calidad de servicio establecida por los operadores de red cuando se vierte la energía generada por las unidades WEC.

Para mejorar la potencia de salida de las instalaciones marinas se han utilizado diferentes técnicas que pueden clasificarse en función del uso o no de sistemas de almacenamiento. En cuanto a las técnicas que no emplean almacenamiento en las unidades WEC:

- La primera aproximación para generar una potencia de inyección a red con menos oscilaciones de potencia consiste en la agregación de la potencia generada por un conjunto de unidades WECs de un parque marino conectadas en el mismo punto de conexión de red. Los estudios realizados en [30] muestran que, la agregación de las potencias de salida de una wave farm es mayor cuando se trabaja con ondas regulares que cuando se emplean ondas medidas en una instalación real.
- Las unidades WEC se conectan a la red eléctrica mediante dispositivos electrónicos. El control activo del sistema PTO mediante estos dispositivos permite mejorar la potencia de salida de una instalación marina conectada a red [31].
- Adicionalmente, se pueden usar instalaciones híbridas (formadas por parques eólicos off-shore con instalaciones de generación marina) para mejorar la potencia eléctrica de salida inyectada a red por las instalaciones marinas [29].
- En el caso de instalaciones cuyo PTO es hidráulico, es posible reducir las oscilaciones de potencia de salida de la instalación utilizando acumuladores de agua a nivel del mar en el sistema hidráulico.

En cuanto a las instalaciones que emplean sistemas de almacenamiento para suavizar la potencia de salida de las instalaciones marinas cabe destacar:

- Condensadores. En [25] se emplea el convertidor de potencia de la instalación para controlar la carga y descarga de los condensadores y minimizar así las oscilaciones de la potencia de salida de la instalación. Los autores de [32] han demostrado que el tamaño del condensador depende del tamaño de la instalación, por lo que el uso de condensadores queda restringido a plantas de pequeña potencia.
- En [33] se han empleado supercapacitores para mejorar la potencia de salida de una instalación marina en laboratorio, cuya entrada eran ondas regulares de tensión.

Finalmente, para mitigar a corto plazo las elevadas fluctuaciones de la potencia de salida de las instalaciones marinas es necesario emplear dispositivos capaces de realizar numerosos ciclos de carga y descarga y dispongan de una densidad de potencia elevada, este es el caso de los volantes de inercia.

4 Instalación de energía marina “Lysekil Research Site”

4.1 Localización

Atendiendo a la clasificación establecida por [34] la instalación marina de Lysekil (Lysekil Research Site, LRS) (Suecia) se puede incluir dentro del grupo de las “pre-commercial stage gate requirements test sites”. La instalación se encuentra situada en la costa occidental de Suecia, a 100 km al suroeste de la ciudad de Gotëborg y 2 km de la costa de la ciudad de Lysekil, ocupando una superficie de 40.000 m2 entre a las coordenadas (58º 11’ 850’’N 11º 22’ 460’’E) y (58º 11’630’’N 11º 22’’ 460’’E), en las que el fondo marino se encuentra a unos 24-25 metros y unas condiciones óptimas para el anclaje de las WEC [35]. La localización de la instalación de Lysekil se encuentra rodeada de islas lo que permite tener buen estado de la mar, incluso en los meses de invierno, con una densidad de energía de 2.6±0.3 kW/m [36]. La Fig. 5 muestra la localización de la instalación, así como el estado del mar en las proximidades de la LRS.

LRS comenzó su andadura en 2003 y las primeras medidas del estado del mar se tomaron en abril de 2004. La primera boya, conocida como L1, se instaló en marzo de 2006 conectándose mediante un cable de 2.9 km a la subestación de medida en la isla de Hermanö al sur de la LRS. En 2009 se instalaron dos nuevas WEC, L2 y L3, que junto con la L1 se conectaban a una subestación marina para volcar la energía generada a la red [37]. Junto con las WEC se instalaron, en 2007, 21 boyas medioambientales cuya misión era medir el impacto de las unidades WEC en el entorno marino de la instalación y vice versa. Entre 2009 y 2010 se instalaron 5 nuevas unidades WEC conocidas como L4, L5, L7, L8 y L9. En 2015 con 3 nuevas WEC (L10, L11 y L12) y desde noviembre de ese año se encuentra conectada a red with an installed capacity of 200 kW [37]. En la actualidad, más de 10 modelos de WEC han sido analizados en LRS [38]. El LRS se completa con una torre de medida instalada en verano de 2008 a 150 metros de LRS. La torre de medida está dotada de una cámara que permite realizar una

correlación entre las imágenes tomadas del movimiento de las olas y la tensión de salida de la instalación.

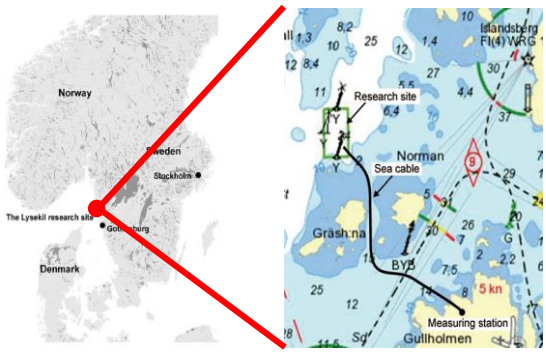

Fig. 5. Localización y estado del mar en la instalación marina de Lysekil [28]

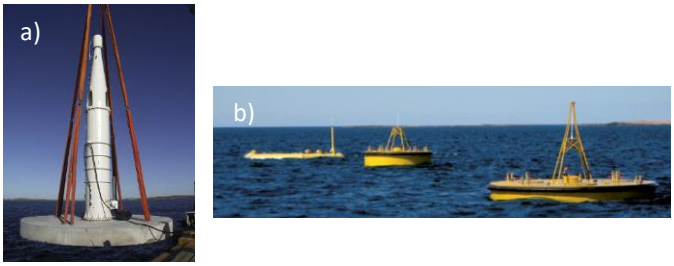

Fig. 6. Generadores lineales y boyas de LRS.

4.2 Tecnología empleada

En LRS se emplean point absorbers para extraer la energía de las olas, mientras que la conversión de la energía marina en energía eléctrica se realiza mediante un generador lineal (DDLG). El movimiento de las olas es transmitido desde el point absorber hasta el translator del generador mediante un cable. Para mejorar la operación de los generadores en condiciones extremas del mar, las unidades WEC están dotadas en unos resortes en la parte superior que limitan el movimiento del translator dentro de la cavidad del DDLG. Puesto que el LRS es una instalación de investigación varios DDLG and tipología de boyas han sido empleadas como se puede ver en las Fig. 6.a y 6.b respectivamente [39].

4.3 Subestación marina

La instalacion LRS se conecta a red a través de una subestación marina, con una potencia de 96 kVA, y un cable de 2.9 km, para la configuración de las primeras unidades WEC [40]. Los generadores disponen de una dump load de 12 Ω que se encarga de disipar la energía generado por las unidades WEC cuando se encuentran desconectadas de la subestación.

La tensión de salida de cada WEC es rectificada en un convertidor a través de un puente de 6 diodos. En la etapa de continua de la subestación marina, las tres unidades WEC se interconectan en paralelo. La tensión alterna, con frecuencia 50 Hz, a la salida del inversor se eleva a la tensión de red (1000 V) mediante un transformador Y-Y con regulación de tomas (80-100-125-180-250/1000 V). Los elementos que conforman la subestación están confinados en un contenedor de 3 m^3 rellenos de nitrógeno y con una presión de 3 bar.

La subestación marina se completa con un sistema auxiliar, un circuito resonante y una estación de medida. La función del sistema auxiliar es distribuir la generación de las unidades WEC entre los sistemas de control y los breakers del sistema. Dicha instalación auxiliar es alimentada por los generadores WEC o, en su defecto, puede ser alimentada desde el sistema on-shore. El circuito resonante permite aumentar la producción de la instalación. Por último, la estación de medida está dotada de diferentes cargas que permiten estudiar el comportamiento del LRS y controlarlo de forma remota.

5 Instalación híbrida marina-FESS para suavizado de potencia de salida

5.1 Datos de entrada

Para validar el modelo de instalación híbrida marina-FESS desarrollado se han empleado datos reales de la instalación marina de Lysekil correspondientes a las 22 horas del 20 de julio de 2009. Los datos han sido facilitados por la universidad de Uppsala y pertenecen a tres generadores lineales. La muestra está compuesta por la tensión de cada una de las fases y la potencia de salida rectificada de cada uno de los generadores. La figura 7 muestra los datos disponibles para los primeros 20 segundos de la muestra del generador L1.

5.2 Descripción general de la instalación híbrida

La estructura general de la instalación híbrida marina-FESS propuesta para el suavizado de la potencia de salida se muestra en la figura 8 y está compuesta por los siguientes bloques:

- Granja marina: compuesta por 3 generadores marinos lineales (wave energy converters, WEC's), modelados a partir de las medidas recogidas en la instalación de Lysekil (Fig. 8, bloque amarillo) [38].

- Etapa de filtrado: cuyo objetivo es crear la señal de referencia del FESS, que permita almacenar la energía proveniente de las oscilaciones de la potencia generada o entregar energía en función de la necesidad del suavizado de la potencia de salida (Fig. 8, bloque verde).
- Sistema de almacenamiento dinámico (Kinetic Energy Storage System, KESS): compuesto por un voltante de inercia de alta velocidad conectado a la etapa de continua de la instalación, (Fig. 8, bloque azul).
- Inversor DC/AC: el control del inversor permite suavizar la potencia de salida de la instalación híbrida (Fig. 8, bloque gris).
- Transformador marino: encargado de elevar la tensión de salida de la instalación marina y evacuar la potencia suavizada al punto de conexión a red.

La instalación híbrida marina-FESS desarrollado es capaz de trabajar en sistemas de potencia aislados o conectados a red.

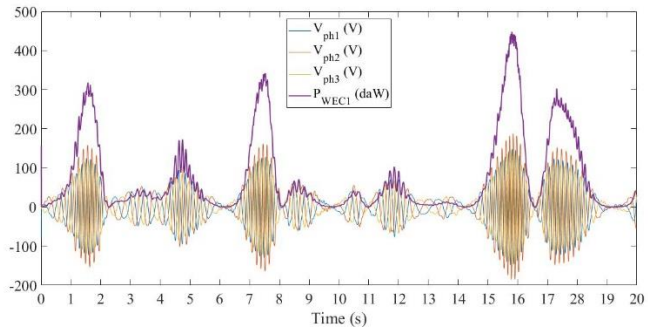

Fig. 7. Tensiones de fase y potencia de salida del generador L1 de LRS.

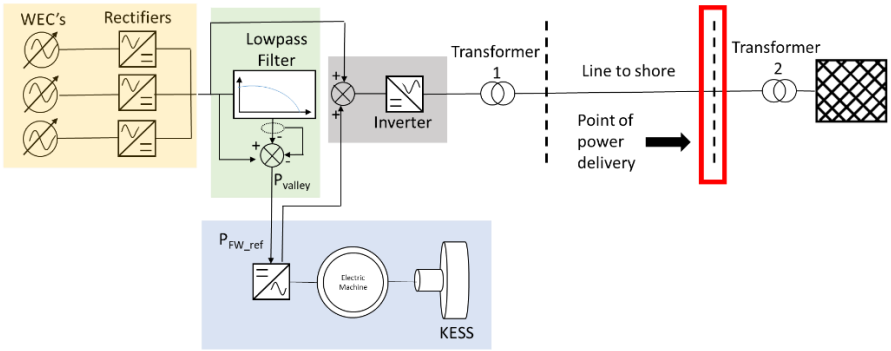

Fig. 8. Diagrama de la instalación híbrida marina-FESS de LRS.

6 Suavizado de la potencia de salida de la instalación "Lysekil Research Site"

En el proceso de suavizado de la potencia de salida de la instalación híbrida marina-FESS del emplazamiento de Lysekil se compone de tres etapas:

- En la primera etapa se realiza un primer suavizado de la potencia de salida de la instalación mediante la agrupación de la potencia de salida de las tres unidades marinas.
- La segunda etapa es la etapa de filtrado en la que se determina la potencia que va a ser almacenada en el FESS.
- Finalmente, en la tercera etapa se realiza el llenado de valle de la potencia de salida de la instalación mediante la energía almacenada en el FES. Esta última etapa permite a la instalación híbrida marina-FESS seguir una señal de consigna impuesta por el operador de red para una operación óptima de la red.

La Fig. 9 muestra la salida de la instalación híbrida marina-FESS para la hora de estudio en la que el operador de la red ha impuesto a la instalación híbrida una consigna de 2 kW. La curva azul de la Fig. 9 muestra la potencia de salida tras el rectificador del conjunto de los generadores marinos, es decir, la potencia entregada en la primera etapa del suavizado. La curva roja de la Fig. 9 muestra la potencia suavizada entregada por la instalación conjunta marina+FESS a la red. Como se puede observar en dicha figura, el Sistema híbrido marino-flywheel es capaz de entregar en el 95% de la hora de estudio la consigna de potencia establecida por el operador de red.

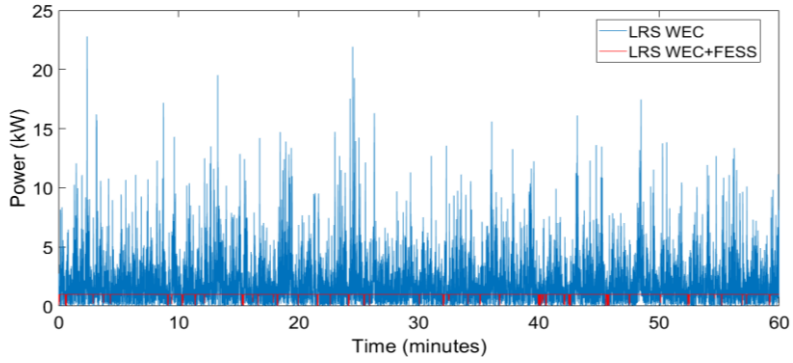

Fig. 9. Potencia de salida de las WEC (azul) y seguimiento de consigna de red del conjunto WEC+FESS (roja).

La Fig. 10 es una ampliación de la Fig. 9 para el periodo de tiempo comprendido entre los instantes 8.8 y 9.5 seg, en ella se muestra un detalle de la potencia salida de las WECS, la potencia entregada a red, así como el estado de carga del flywheel. En la figura 37 se puede observar que en aquellos instantes de tiempo en los que el flywheel no dispone de energía almacenada, la instalación híbrida no es capaz de seguir la con-

signa establecida por la red, entregando en esos casos la potencia resultante de la primera etapa de suavizado, lo que pone de manifiesto la necesidad de regular la energía almacenada en el flywheel.

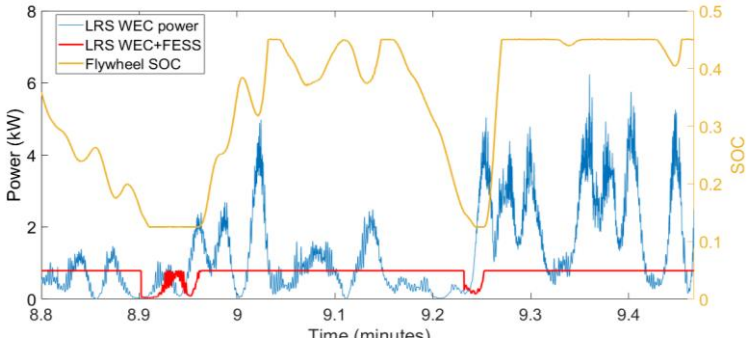

Fig. 10. Detalle de potencia de salida de las WEC (azul), WEC+FESS (roja) y estado de carga del FESS (naranja).

La Tabla 1 recoge un resumen de los KPIs de los principales estudios realizados en el presente apartado para mejorar la señal de salida de la instalación marina de Lysekil: la energía entregada a la red (E_{red}), la potencia máxima entregada a red ($P_{red\_máx}$), la potencia media de la hora entregada a red (P_{red_media}), el ratio entre la potencia máxima y la media ($P_{red\_máx}/P_{red\_media}$) y la desviación típica estándar de la potencia entregada a red en la hora de estudio.

Tabla 1. Resultados de las diferentes etapas del proceso de suavizado

	E_{red} (kWh)	$P_{red\_máx}$ (kW)	P_{red_media} (kW)	$P_{red\_máx}/P_{red\_media}$	Desviación $estándar_{Potencia}$
WEC asociación	3.4	45.58	3.40	13.39	0.96
Filtro	2.5	9.23	2.52	3.66	0.58
WEC-FESS	2.9	9.23	2.91	3.17	0.49

Como se puede apreciar en los resultados recogidos en la tabla 4.4, la etapa de filtrado es capaz de reducir considerablemente los picos de potencia de la hora de estudio. Sin embargo, es necesario la combinación de la agrupación de los generadores marinos (WEC), la etapa de filtrado y el empleo del FESS para reducir a la mitad la desviación estándar de la potencia de salida, y por consiguiente mejorar el suavizado de la potencia entregada por la instalación híbrida marina-FESS a la red.

7 Conclusiones

En el presente trabajo se modela una instalación híbrida marina-FESS para mejorar el suavizado de la potencia de salida de una instalación marina. El modelo propuesto se ha validado a partir de los datos de producción real de tres generadores marinos de la instalación de Lysekil (Suecia). Los resultados obtenidos muestran que el empleo de un volante de inercia es una buena alternativa para suavizar la potencia de salida de la instalación marina. Así la instalación híbrida es capaz de reducir en un 85% los picos de potencia entregada a red, en un 76% la relación entre la potencia máxima y media a la salida de la instalación, y en un 51% las pérdidas de energía en el proceso de evacuación de la generación al punto de conexión a red, mejorando así la eficiencia de la red eléctrica. La hibridación de la instalación marina con el FESS permite a dicha instalación mejorar la calidad de la potencia entregada en el punto de conexión a red, así como seguir una consigna de operación impuesta por el operador de la red de distribución a la que se encuentra conectada. El modelo híbrido marino-FESS propuesto es capaz por tanto de actuar ante el operador de la red de distribución como una unidad de generación distribuida controlable que puede ofrecer al operador de red servicios auxiliares de control de tensión.

References

1. E. Agency, World Energy Outlook 2016, Organization for Economic Cooperation and Development (OECD), Tech. Rep., 2016.
2. H.-W. S. et al., World Energy Resources: Marine Energy 2016, World Energy Council, Tech. Rep., Mar. 2017. https://www.worldenergy.org last accessed 2018/09/04.
3. How much water is there on earth, from the usages water science school, https://water.usgs.gov/edu/earthhowmuch.html, last accessed 2018/09/04.
4. Gunn, K., Stock-Williams, C. Quantifying the global wave power resource, Renewable Energy me 44, Pages 296-304 (2012).
5. Falnes, J, A review of wave-energy extraction, Marine Structures 20 (4), Pages 185-201 (2007).
6. Clément, A., et all, Wave energy in Europe: current status and perspectives, Renewable and Sustainable Energy Reviews 6 (5), Pages 405-431 (2002).
7. Pelc, R. and Fujita, R. M. Renewable energy from the ocean.Mar. Policy, 26(6), 471–479 (2002).
8. Blavette, A. et all. Grid Integration of Wave and Tidal Energy. 5. 10.1115/ OMAE2011-49953 (2011).
9. Titah-Benbouzid, H., Benbouzid, M. An Up-to-Date Technologies Review and Evaluation of Wave Energy Converters. INTERNATIONAL REVIEW OF ELECTRICAL ENGINEERING-IREE, 10 (1), pp.52-61 (2015).
10. Callaghan, J. and Boud, R. Future marine energy. results of the marine energy challenge: Cost competitiveness and growth of wave and tidal stream energy, Carbon Trust (2006).
11. R. A. Board, “Marine renewables: Current status and implications for r&d fund-ing and the marine renewables deployment fund”, London, Renewables Advisory Board, 2008
12. D. Vannuci, Wp3 technologies state of the art, 2011

13. Renewable Energy boem, https: //www.boem.gov/Renewable-Energy, last accessed 2018/09/04.
14. Energy Department Announces Investment in Wave Energy Test Facility, https://www.energy.gov/articles/ energy - department - announces - investment - wave - energy - test – facility, last accessed 2018/09/04.
15. A. Curvers and J. Pierik, “Wp 3: Technologies state of the art”, ECN Report, 2011
16. Orecca – Project, https://cordis. europa.eu/project/rcn/94058_es.html, last accessed 2018/09/04.
17. The Project meygen, http : / / www.meygen.com/the-project/, last accessed 2018/09/04.
18. F. d. O. Antonio, “Wave energy utilization: A review of the technologies”, Renewable and sustainable energy reviews 14 (3), pp. 899–918 (2010).
19. N. Khan, A. Kalair, N. Abas, and A. Haider, “Review of ocean tidal, wave and thermal energy technologies”, Renewable and Sustainable Energy Reviews 72, 590–604 (2017).
20. P. Moreno-Torres, M. Blanco, G. Navarro, and M. Lafoz, “Power smoothing sys-tem for wave energy converters by means of a supercapacitor-based energy stor-age system”, in Power Electronics and Applications (EPE’15 ECCE-Europe), 2015 17th European Conference on, IEEE, pp. 1–9 (2015).
21. A. Çelik and A. Altunkaynak, “Experimental and analytical investigation on cham-ber water surface fluctuations and motion behaviours of water column type wave energy converter”, Ocean Engineering 150, pp. 209–220 (2018).
22. Z. Zang, Q. Zhang, Y. Qi, and X. Fu, “Hydrodynamic responses and efficiency analyses of a heaving-buoy wave energy converter with pto damping in regular and irregular waves”, Renewable Energy 116, pp. 527–542 (2018).
23. G. Tampier and L. Grueter, “Hydrodynamic analysis of a heaving wave energy converter”, International Journal of Marine Energy 19, pp. 304–318 (2017).
24. D. Yurchenko and P. Alevras, “Parametric pendulum based wave energy con-verter”, Mechanical Systems and Signal Processing 99, pp. 504–515 (2018).
25. M. Melikoglu, “Current status and future of ocean energy sources: A global re-view”, Ocean Engineering 148, pp. 563–573 (2018).
26. D. Xu, R. Stuhlmeier, and M. Stiassnie, “Assessing the size of a twin-cylinder wave energy converter designed for real sea-states”, Ocean Engineering 147, 243–255 (2018).
27. Z. Han, Z. Liu, and H. Shi, “Numerical study on overtopping performance of a multi-level breakwater for wave energy conversion”, Ocean Engineering 150, 94–101 (2018).
28. Rojas Delgado, Brenda. Active Control of Smart Grids. Carlos III University PhD dissertation, 2019.
29. X. Zhao, Z. Yan and X. Zhang, "A Wind-Wave Farm System With Self-Energy Storage and Smoothed Power Output," in IEEE Access 4, 8634-8642 (2016).
30. Performance Composites Ltd. Mechanical properties of carbon fibre composite materials Data Sheet.
31. Barranger, J. (1965). Hysteresis and eddy-current losses of a transformer lamination viewed as an application of the Poynting theorem - NASA-TN-D-3114.
32. Bolund, B.; Bernhoff, H.; Leijon, M. Flywheel energy and power storage systems. Renew. Sustain. Energy Rev. 11, 235–258 (2007).
33. Moreno-Torres, P.; Blanco, M.; Navarro, G.; Lafoz, M. Power smoothing system for wave energy converters by means of a supercapacitor-based energy storage system. In Proceedings of the 2015 17th European Conference on Power Electronics and Applications (EPE’15 ECCE-Europe), Geneva, Switzerland, pp. 1–9, 8–10 September 2015.
34. IEA-OES. International Energy Agency Implementing Agreement on Ocean Energy Systems, OES-IA, Annual Report 2009. IEA-OES executive committee, 2009.

35. C. Boström, 'Electrical Systems for Wave Energy Conversion', PhD dissertation, Acta Universitatis Upsaliensis, Uppsala, 2011.
36. R.Waters, J. Engström, J. Isberg, and M. Leijon. Wave climate off the Swedish west coast. Renewable Energy 34(6), 1600–1606 (2009).
37. A. Brito e Melo and J. L. Villate, Annual Report 2016. The Executive Committee of Ocean Energy Systems, pp. 1–188 (2016)
38. Lysekil Wave Energy Site u.s. department of energy, https://tethys.pnnl.gov/annex-iv-sites/lysekil-wave-energy-site, last accessed 2018/06/05.
39. C. Boström, 'Electrical Systems for Wave Energy Conversion', PhD dissertation, Acta Universitatis Upsaliensis, Uppsala, 2011.
40. Erik Lejerskog, Cecilia Boström, Ling Hai, Rafael Waters, Mats Leijon, Experimental results on power absorption from a wave energy converter at the Lysekil wave energy research site, Renewable Energy 77, Pages 9-14 (2015).

Cities transformation through Positive Energy Districts: MAKING-CITY project.

Fredy Vélez[1] [0000-0003-0764-1321], Cristina de Torre Minguela[1], Cecilia Sanz[1]

[1] CARTIF Centro Tecnológico. Boecillo, Valladolid, Spain.
frevel@cartif.es

Abstract. This paper presents a MAKING-CITY project overview that is focused to address the cities transformation through positive energy districts. MAKING-CITY is a large-scale demonstration project aiming at the development of new integrated strategies to address the urban energy system transformation towards low carbon cities, with the positive energy district (PED) approach as the core of the urban energy transition pathway. Currently city energy plans are starting to be designed with a 2030 horizon. MAKING-CITY will address methodologies to support cities in their long term (2050 vision) urban planning towards an adequate energy transition, paving the way of the planning, implementation and up-scaling process. Cities of Groningen (Netherlands) and Oulu (Finland) will act as lighthouses. These cities are currently working intensively in ambitious transformation planning. Both have committed to deploy a demonstration of at least one positive energy district. León (Spain), Bassano del Grappa (Italy), Kadiköy (Turkey), Poprad (Slovakia), Vidin (Bulgaria) and Lublin (Poland) are the follower cities. All of them have assumed a huge commitment to develop a solid execution project of Positive Energy District and foster high level of replication of the solutions demonstrated in Groningen and Oulu.

Keywords: Energy efficiency, urban regeneration, positive energy district, sustainability cities, smart cities.

1 Introduction

Cities, whatever their size is, are essential actors in fighting climate change. According to the COP21 Paris Agreement, cities around the world are taking steps to promote renewable energy, support electric vehicles, change streetlights to energy-saving LEDs, slash emissions from buildings and acting as a host of other measures. Just within the more than 80 megacities that make up the C40 cities [1], members have taken more than 10,000 climate actions, as this organization reported in 2015. In 2016, the organization's "Deadline 2020" report [1] indicated that cities alone can reduce 5% of the world's global emissions, contributing to meet the Paris Agreement, and in concert with other tiers of government and the private sector, they can potentially contribute to reduce 46% [2].

UN SGD11 [3] aims by 2030 to enhance inclusive and sustainable urbanization, and capacity for participatory, integrated and sustainable human settlement planning

and management in all countries, besides substantially increase the number of cities adopting and implementing integrated policies and plans towards inclusion, resource efficiency, mitigation and adaptation to climate change.

Therefore, the reference time-horizon is 2030 (12 years ahead), that could be considered as a mid-term planning. On the contrary, longer term energy planning in cities has been normally evaded. Only few incipient studies in big cities, like London with a long-term vision in mobility [4] or the more general Goteborg 2050 [5] plan, have analyzed this long term horizon. There is a clear need to be systematically learning from the past, but planning also the future, updating continuously the cities strategies with a combined vision deployed in three levels: longer-term vision, mid-term strategy and short-term execution plans.

The term energy transition [6] designates a significant change for an energy system at long-term, that could be related to one or a combination of changes related to structure, scale, economics, and energy policy. Usually referred as a change in the state of the whole energy system in opposition to individual changes in energy technologies or fuel sources [6], historical energy transitions can be mentioned. For example the resource depletion triggered by technological innovations that lead to shifting to new energy sources in the 19th Century like kerosene or other petroleum-derived products.

Urban planning has been performed without considering mixed-use districts and buildings have been built individually, irrespective of the surrounding buildings. But, these heterogeneous districts and RES local energy production need to be seen as the key element contribute to sustainable cities, once both are locally interconnected and managed [7]. Therefore, an interdisciplinary design process is needed, in order to not only reduce consumption of those districts but also to allow an interchange of energy flows within the limits or even export energy outside its limits.

A useful approach is to work from the district and building point of view, where this “micro-level” can be analysed, addressing new concepts to foster and support the energy transition, as for instance the idea of Positive Energy Districts (PED), as a fully scalable way to progress in the city transformation in systematic way, consolidating sustainable changes while the way is paved for further advances.

To sum up, MAKING-CITY project aims to achieve evidences about the actual potential of the PED concept, as foundation of a high efficient and sustainable route to progress beyond the current urban transformation roadmaps through two cities demosites and 6 six follower cities.

2 Project Overview

Coordinated by CARTIF, MAKING-CITY is a large-scale H2020 Smart Cities and Communities demonstration project aiming at the development of new integrated strategies to address the urban energy system transformation towards low carbon cities, with the Positive Energy District (PED) approach as the core of the urban energy transition pathway. The MAKING-CITY consortium brings together expertise from 34 partners of across Europe (see **¡Error! No se encuentra el origen de la referencia.**): 9 city councils, 5 universities, 4 research centres, 4 clusters and foundations, 4

rental housing administrators, 4 SMEs, 3 energy companies, and one construction firm. The insights of Groningen (Netherlands) and Oulu (Finland), as "lighthouse cities", will be adopted by the six follower cities of Bassano del Grappa (Italy), Kadiköy (Turkey), León (Spain), Lublin (Poland), Poprad (Slovakia) and Vidin (Bulgaria).

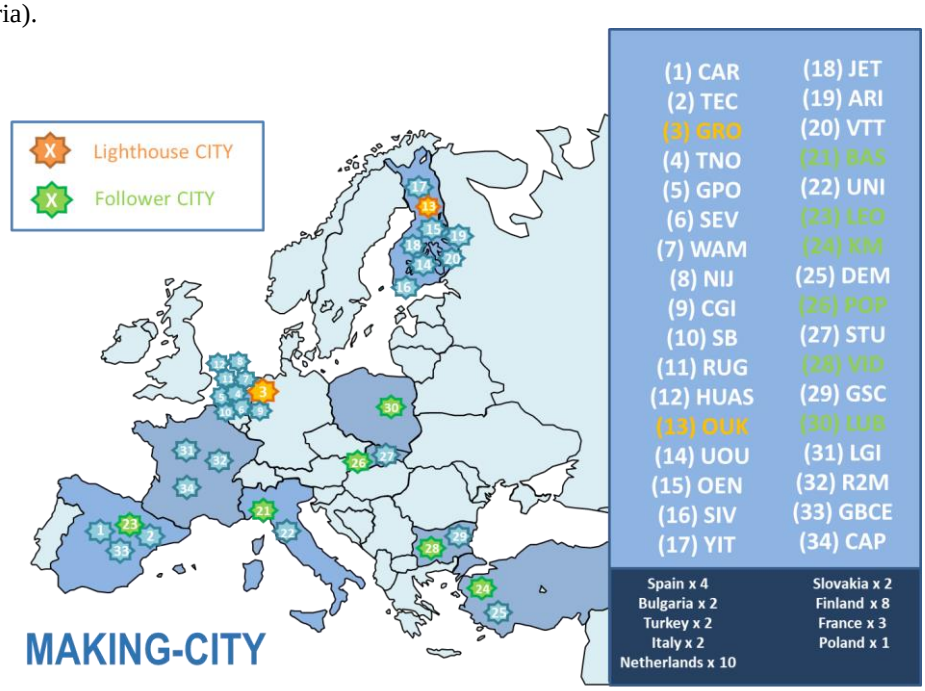

Fig. 1. Origin of the consortium members.

As the main goal, MAKING-CITY wants to apply the PED approach as the core of the urban energy transition, with the districts producing more energy than what they consume. The project's set of solutions includes positive energy buildings, renewable energy systems, energy sharing, electric mobility and smart IT. Furthermore, MAKING-CITY focuses on non-technical solutions such as effective policy innovation, business models, new regulations and standards, or actions to increase energy awareness among citizens. One of the key elements of MAKING-CITY is a strong collaboration and knowledge transfer between the cities, triggering public and private investments in the developed energy solutions. The project will also foster the growth of new sustainable start-ups and small businesses, creating up to 4000 new jobs. Therewith MAKING-CITY will not just contribute to mitigating climate change but also improve quality of life of the local citizens and stimulate the economy.

In other words, the project is intensively focused on achieving evidences about the actual potential of the PED concept, as foundation of a high efficient and sustainable route to progress beyond the current urban transformation roadmaps.

The Positive Energy Block concept is already integrated in the Action 3.2 Smart Cities and communities of the Energy Union and Set Plan, that aims at net–zero-

energy/emission districts (ZEED) that will strongly contribute to COP21 targets. A further step to this ZEED concept is the consideration of "positive energy districts (PED) [8]". These districts consist on delimited areas of buildings and public spaces where the total annual energy balance is positive, therefore the area will deliver, in average, an energy surplus to be shared with other urban or peri-urban zones. The total annual energy balance is the energy taken from outside the district against the energy delivered on-site (whatever the energy carrier). Achieving positive energy balance means that the energy delivered by the district must be higher that the energy supplied from outside. Since all energy carriers must be considered as potential energy inputs or outputs, just primary energy units can be used in the calculations to merge all of them. Therefore, in PED's the balance of primary energy consumed and delivered by the district must be positive. This consideration requires an intensive energy generation on-site, playing renewables (e.g. solar, geothermal…) a key role together with very efficient generation equipment (e.g. heat pumps, CHP...). Besides, a very low consumption is critical, so retrofitting actions for old buildings or ambitious designs of new ones to achieve high performance buildings are essential, integrating advanced materials, control systems, energy storage, etc. Both aspects, renewables on site and low consumption properly combined can led energy performance beyond the buildings codes and attractive business cases, thus fostering a faster energy transition. A schematic diagram to sum up the PED concept is shown in Fig. 2

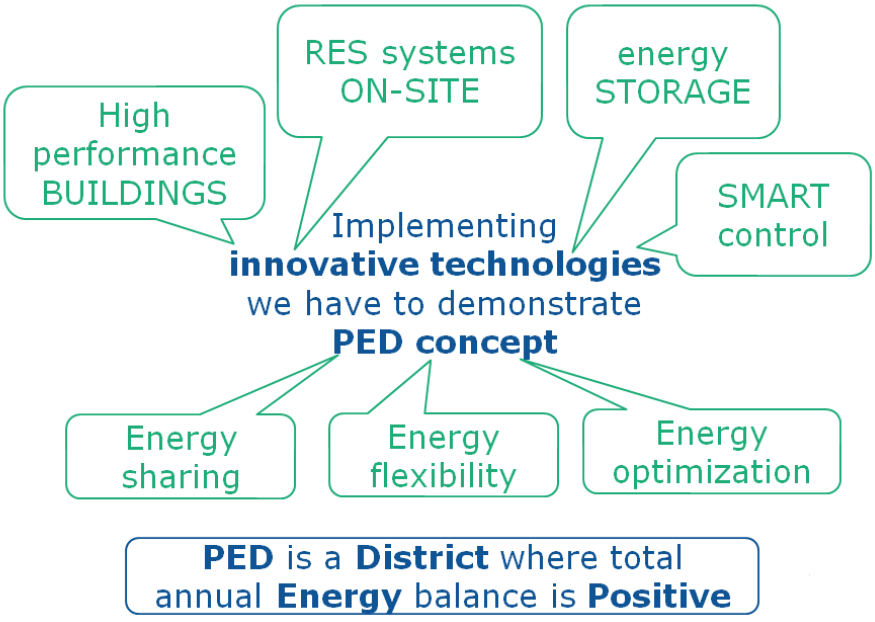

Fig. 2. Positive Energy District concept.

Positive Energy Districts of various sizes are expected to be used as innovation-pushing "seeding points" to showcase in highly concentrated form the integration of all the aspects that are needed for net–zero- energy/emission districts. Although many references about the individual concept of positive-energy building or positive home concept can be found in the state of the art (even others such as the smart energy zones approach, that is the general strategy of the city of Groningen) a small number of evidences about the actual performance and benefits of this new global PED concept can be found, like the Hikari district in Lyon [9]. According to this, PED claims for an extensive demonstration and validation action to consider this innovative concept as a reference to guide the energy transition in cities.

3 Demosites

3.1 Demonstration of Positive Energy Districts in lighthouse cities

Cities of Groningen (Netherlands) and Oulu (Finland) are the lighthouses. These cities are front-runners in the urban energy system transformation and provide a powerful added value to the project objectives addressing a set of demonstrations of technologies and solutions in representative areas of the cities that become Positive Energy Districts.

Groningen

Groningen will address the transformation of two districts in PEDs, one in North and other one in Southeast (see Fig. 3 a, b).

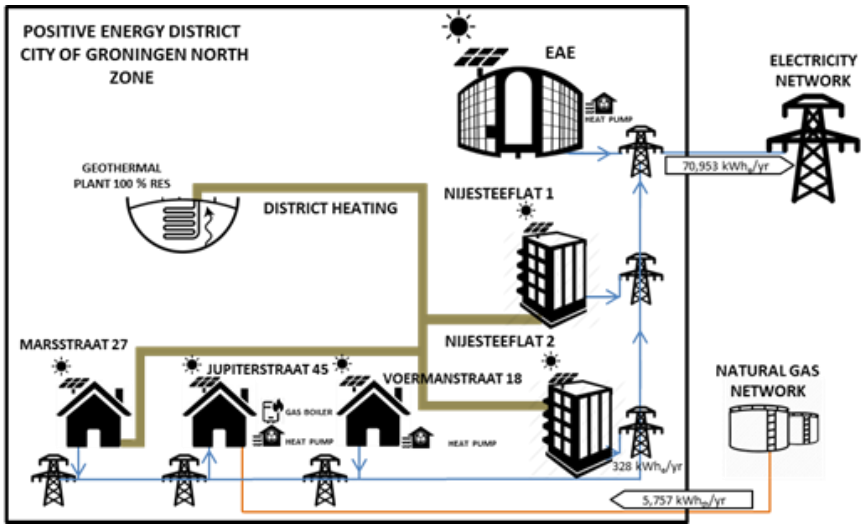

(a)

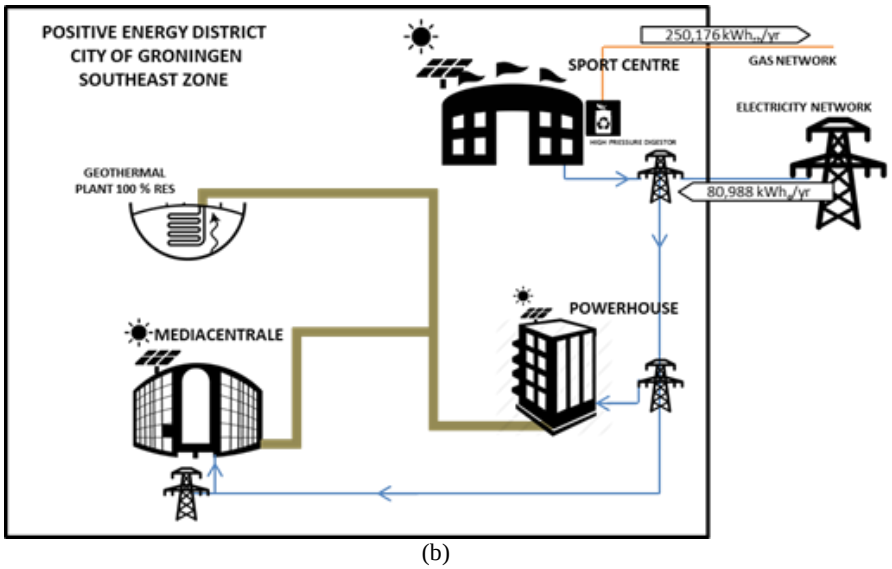

(b)

Fig. 3. Energy flows among buildings in Groningen PEDs. North (a) and Southeast (b), respectively

Groningen North and Groningen South are the two districts selected to implement the PED concept developed in the MAKING-CITY project. Several infrastructure typologies are represented in both urban areas: residential buildings bordering a university campus, industrial and tertiary blocks, public facilities. Part of the residential area in Groningen North was built in the 1960's while the vast majority of Groningen South is relatively new, constructed around the 1980's.

Overall, the PED implementation in Groningen North and Groningen South involves the retrofitting of residential buildings to reduce building energy consumption (as for instance high performance insulation, efficient windows, heat recovery facilities smart thermostats and sensors to real-time measuring of energy consumption and advanced energy management systems) in order to maximise infrastructure performance. On the other hand, the main foundation of the achievement of the PEDs is an intensive use of RES, mainly a district heating 100 % based on geothermal energy, a biogas plan in one of the buildings (high pressure digester) and an extensive installation of PV facilities for distributed electricity generation on site. Solar panels will be installed on the roofs of some buildings and car parks. In addition, solar thermal panels will support geothermal heat pumps which are directly connected to the geothermal district heating system. The surplus of thermal energy produced by some residential buildings will be stored and used during energy demand peaks. Finally, biogas technology will be used to collect and "digest" -under high pressure and thanks to bacteria-, waste and waste water produced by public sport and catering facilities. A special focus will be made on cycling and electric mobility. For instance, an existing cycling lane will be converted into a "SolaRoad" by the integration of solar panels in its surface able to produce around 60,000 kWh yearly. Moreover, smart charging

stations for electric vehicles will be installed and directly connected to the current grid and impact in the grid will be analysed in order to demonstrate that a potential roll up of these vehicles will be properly assumed by the existing grid infrastructure if PED concept is properly validated

The boundaries of the districts involve many buildings. Only a limited number of them will be part of the definition of the PED, creating the seed of a further scaling up on the basis of this first approach. Several building typologies have been selected, individual residential, high-rises and tertiary buildings (6 in North and 3 in Southeast) that ensure an easy upscaling.

The positive annual energy balance will be achieved due to the high ratio of PV panels installed and the almost zero demand of thermal energy from outside in the North area and the thermal energy surplus in the Southeast delivered through the district heating and gas network. Groningen North PED will export outside the district 70 MWhe/yr of electricity and will import 5.5 MWhth/yr of thermal energy (natural gas), for a total balance in primary energy units of 170 MWhp/yr exported outside the district. Groningen Southeast PED will export 250 MWhth/yr of thermal energy and will import 80 MWhe/yr of electricity for a total balance in primary energy of 97 MWhp/yr exported outside the district. So both districts have been designed to have a positive annual energy balance.

Oulu

Oulu plans to develop a PED in the area of Kaukovainio on the basis of the very high efficiency geothermal heat pumps and PV panels. Located 3 km away from the city center, this urban area gathers nearly 4,700 inhabitants and is mainly dominated by high-rise buildings and individual houses. The PED approach aims at revitalising the district by attracting more residents and families, fostering a community spirit, advancing equality between population groups, and promoting sustainability.

The main facility is a centralized heat pump that supplies energy to a low temperature district heating and integrates a PV plant to supply part of the electricity to operate the system (see Fig. 4). All buildings (4 residential and one shopping mall) will be connected to the district heating, and particularly the shopping mall will host a high performance heat pump, based on CO_2 tech, hybrid solar panels, PV panels and geothermal for seasonal storage (on summer, the extra energy produced will be redistributed into the district network (heating and hot water), or stored for winter energy demand peaks), that due to the high COP (6) is able to supply energy to the district heating network and reach positive annual energy balance. EV will be also considered. Some charging points will be installed in the shopping mall to analyse the charging impact on the grid and plan the necessary measures to support this new consumption. The annual positive energy balance will be reached by means a high energy surplus on the energy production of high performance heat pumps, distributed through the district heating outside the district. Oulu PED will export 1,020 MWhth/yr of thermal energy through the district heating and will import 518 MWhe/yr of electricity, for a total balance in primary units of 80 MWhp/yr exported to outside the district, so, has been designed to have a positive annual energy balance.

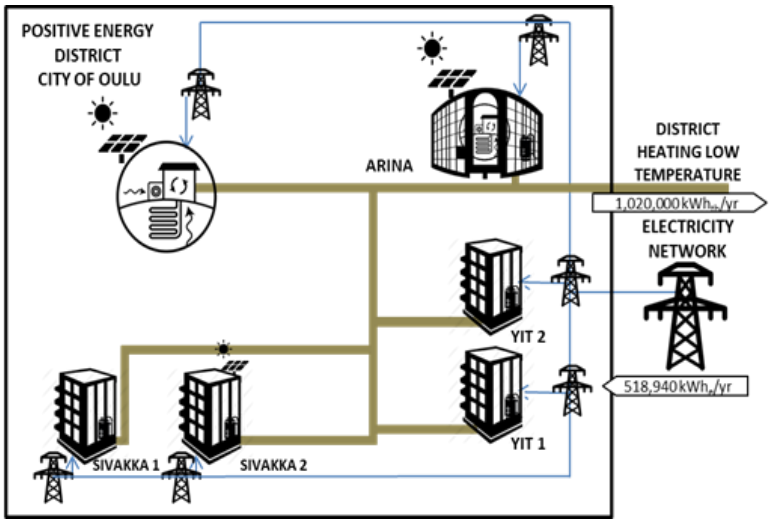

Fig. 4. Energy flows among buildings in Oulu.

3.2 Replication of Positive Energy Districts in follower cities

Six cities will act as followers, León (Spain), Bassano del Grappa (Italy), Kadiköy (Turkey), Poprad (Slovakia), Vidin (Bulgaria) and Lublin (Poland). They compose a geographical, socio-economic and cultural well-balance regarding the lighthouses. MAKING-CITY will address replication goals by means of two main actions:

- Designing a positive energy district in each follower until the level of execution project, defining the general approach of the PED (boundaries and goals), engaging citizens and stakeholders, selecting suitable technologies for increase energy efficiency and local energy production, and finally designing the link among buildings to share energy and supply outside.
- Developing a replication plan oriented to upscale and replicate the solutions demonstrated in the lighthouse and lesson learnt in the above-mentioned designing process.

Follower cities description are:

Bassano del Grappa
In Bassano del Grappa, three districts have been selected to replicate the PED concept developed in MAKING-CITY: Sant'Eusebio, Merlo and San Vito**.** Energy management using smart building energy controllers and the exploitation of existing renewables installations (mostly solar energy) will be part of the core actions undertaken.

León
Entrevias is a group of 5 separated neighbourhoods located at the north of León representing 21,2% of the city's population: La Inmaculada, Cantamilanos, Asuncion, San

Esteban, Las Ventas and San Mamés. With a high density, these districts were built during the 1940's and 1950's to house industrial workers.

A poor isolation of buildings makes today the PED replication applicable in these neighbourhoods through the retrofitting of buildings and the use of biomass and geothermal technology as sources of energy, among others. The final objective is to improve energy efficiency of public facilities located in the 5 districts selected plus to improve and reduce energy consumption for many dwellers.

Vidin

Two neighbourhoods have been selected to replicate the PED concept developed in the MAKING-CITY project. The first one is made of a variety of facilities (public schools and kindergartens, a train station, residential buildings…) while the second one (located closed to the city centre), is mostly dominated by residential housing.

As one of the 6 "Followers cities" part of MAKING-CITY, Vidin aims at replicating the PED approach mainly by the retrofitting of residential buildings (windows, better heating systems…). This will maximise infrastructure performance and reduce energy consumption. Another key objective is the integration of renewable energy sources (solar panels and thermal solar panels) into the current grid in order to achieve self-sufficient energy production.

Poprad

In Poprad, the PED replication will be carried out in 6 different districts (Zapad I & II, Juh I, III, IV & VI, and Centrum). Diversity of infrastructure defined these neighbourhoods: housing blocks, public schools, and central heating stations built at different times.

Main actions to replicate the PED concept developed by MAKING-CITY are:

- the retrofitting of buildings (high efficient insulation, new windows…)
- the installation of smart building energy controllers to better anticipate energy demand and consumption
- the implementation of solutions to connect buildings together and share renewables facilities extra energy production

Kadikoy

Kadıköy aims at reducing its carbon gas emissions by 20% in 2020, and by 40% in 2030 (2015 Paris Agreement). Two highly urbanised neighbourhoods have been selected to replicate the PED concept developed in the MAKING-CITY project: Hasanpaşa and Caferağa.

Main actions to replicate the PED concept carried out in the MAKING-CITY project are:

- the retrofitting of buildings (windows, high efficient insulation…)
- the installation of solar panels on the roofs of some buildings and car parks
- the use of solar thermal panels to produce hot water

Lublin

Located in the Wieniawa district, the two areas selected to replicate the PED concept elaborated in MAKING-CITY are both a mix between public and residential buildings: schools, universities, cultural centre, municipal offices…

In Poland, Lublin was the first city to introduce a "green civic budget". The city committed to reduce by 23% its gas emissions and by 9,5% its energy consumption in the 2008 Low Carbon Economy Plan.

The PED replication developed by the MAKING-CITY partners will mainly include:

- the retrofitting of buildings (windows, high efficient insulation…)
- the installation of more renewables power stations and their connection to the entire district
- the implementation of an intelligent urban lighting management system

4 Expect results

Three PED full monitored and six PED near to be implemented: As main results during the duration of the project (five years), three PEDs (two in Groningen and one in Oulu) will be operated in real conditions, and the launch of another 6 in the cities that "follow" the project. Each of the eight cities involved in the project will have designed their city plans by including the PED concept in them and encouraging them to the fullest to meet the environmental commitments.

A surplus of 348 MWh/year is expected to be obtained in the PED of the lighthouse cities of the MAKING-CITY project. After two years of monitoring that will be carried out in its final stage, it will be possible to confirm the final surplus obtained, as well as analyze usage patterns that facilitate replicability in the districts identified as potential PEDs in the cities that follow the project.

Guidelines to design and calculate PED: Likewise, a methodology for the design and evaluation of PEDs will be developed, which will be compiled as a guide for easy monitoring by cities outside the project, which will maximize its impact, as well as its replicability contributing to the transformation of cities in more sustainable environments.

In general terms, the results expected with the project are:

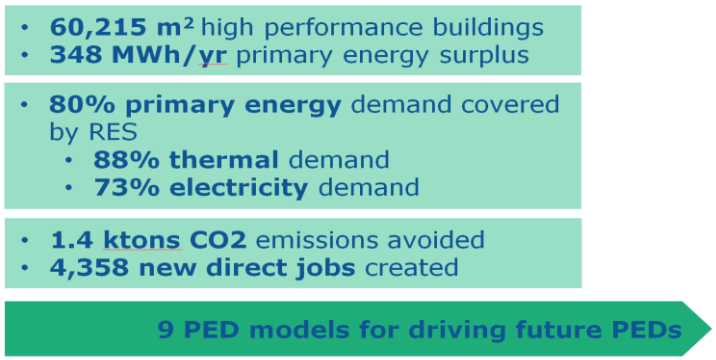

5 Conclusions

The MAKING-CITY project sets the guidelines to be followed to include the concept of positive energy districts in the development of city planning, contributing to reach 100 framed PEDs as the objective of the SETPlan by 2025 [8]. PEDs require flexibility in energy consumption patterns that users will implement based on the web services that cities offer them. The business models that will arise around this energy flexibility must satisfy all the agents involved in the exchange, and this will be possible thanks to the real-time monitoring that will allow the combination of a complete measurement system and a versatile data platform.

6 Acknowledgements

Authors acknowledge the financial support of the HORIZON 2020 program from the European Union under Research Contract No. nº 824418.

References

1. C40 CITIES Initiative homepage, www.c40.org, last accessed 2019/08/20
2. PLACE (Thomson Reuters Foundation) homepage, http://citiscope.org/story/2017/explainer-what-paris-agreement-climate-change-and-what-does-it-mean-cities, last accessed 2019/08/15
3. United Nations Sustainable Development Goals homepage, www.un.org/sustainabledevelopment/, last accessed 2019/08/22
4. The Transportation Research Board homepage, https://trid.trb.org/view/1319762, last accessed 2019/08/15
5. Aumnad P.: Futures studies' backcasting method used for strategic sustainable city planning. Futures 43 (7), 707-714 (2011).
6. IRENA (International Renewable Energy Agency) homepage, www.irena.org/energytransition, last accessed 2019/08/25
7. Monti, A., Pesch, D., Ellis, K., & Mancarella, P.: Energy positive neighborhoods and smart energy districts: methods, tools, and experiences from the field. Academic Pres 2016
8. EIP-SCC European Innovation Partnership on Smart Cities and Communities homepage, http://eu-smartcities.eu/initiatives/71/description, last accessed 2019/08/25.
9. AGC Glass Europe homepage, https://www.agc-yourglass.com/agc-glass-europe/gb/en/positive_energy/hikari/project.html, last accessed 2019/08/01.

Battery Energy Storage System Dimensioning for Grid Applications According to Power Quality and Battery Ageing

Jorge Nájera *[0000-0002-3396-0062], Marcos Lafoz [0000-0002-8196-8958], Gustavo Navarro [0000-0002-5169-9080], and Jorge Torres [0000-0001-7524-9925]

Centro de Investigaciones Energéticas, Medioambientales y Tecnológicas, 28040 Madrid, Spain
jorge.najera@ciemat.es

Abstract. Smart cities account for smart grids that, in absence of energy storage systems, are potentially weak. Batteries are suitable for being implemented in a smart grid and enhance the reliability and flexibility of the network. However, selecting the proper battery for a smart grid requires a dimensioning process in terms of energy and power which is not a straightforward process. This paper proposes a dimensioning methodology and applies it to a study case in a simulation environment with a fully parametrized weak grid and realistic load profile. Results show that there is an optimum design in terms of power and energy in order to prevent the grid from suffering low voltage excursions and frequency deviations while extending the battery lifetime.

Keywords: Battery Energy Storage Systems, Distribution networks, Frequency deviations, Voltage Excursions.

1 Introduction

Storing large amount of energy in a competitive way is one of the main technological challenges of the present [1]. Among the extensive amount of energy storage technology applications, battery energy storage systems (BESSs) for transmission and distribution (T&D) networks and smart grids support is one of the prominent and leading uses [2]. Its benefits encompass the majority of the electricity value chain, including peak shaving and continuity of supply for customers, ancillary and power quality services for transmission and distribution system operators (TSOs & DSOs), and flexibility and curtailment minimization for renewable generation companies, among many other benefits [3].

Smart cities account for smart grids, which integrate high shares of renewable energy and decentralized generation and consumption. The uncertainty and variability of renewable sources, the reduced inertia of the system due to the low number of traditional generation plants, the high line impedances in urban areas, and the enormous quantity of devices connected through an inverter make smart grids weak, i.e., changes in power production or consumption induce unacceptable variations in frequency, voltage levels,

voltage unbalance, and harmonic distortion, among other electric variables [4, 5]. Hence, smart grids imperiously need energy storage systems, typically BESSs, to provide flexibility and reliability, while ensuring a safety operation and optimum control of the network.

However, choosing a battery for grid applications is not a straightforward issue. Battery manufacturers offer a wide variety of solutions, and selecting an appropriate battery requires a precise dimensioning process in terms of energy and power.

In the literature, batteries for grid services have been dimensioned by using a Primal-Dual Interior Point Method [6], aiming to reinforce the grid when there is a high penetration of electric vehicles and avoid low voltage levels. Moreover, a brute force calculation following several grid frequency constraints is applied in [7] in order to enhance the integration of wind power and improve the reliability of the grid. Another brute force analysis is applied in [8] for dimensioning PV-batteries, considering incentive and selling price conditions.

This work proposes a battery dimensioning methodology that focuses on eliminating frequency and voltage level variations that exceed the operability thresholds. Moreover, this paper considers battery ageing as a final step for comparing different configurations. Hence, battery owners and DSOs interests are both considered with this approach. This methodology is applied for a study case with a weak grid, realistic consumption data and primary and secondary frequency regulation.

The paper is organized as follows: Section 2 describes the simulation models used during the methodology. Section 3 presents the dimensioning methodology and power quality indicators. Finally, an application example is presented in Section 4, while conclusions are given in Section 5.

2 Distribution network, load, and BESS modelling

In order to analyze power quality in an electric network equipped with BESS, a simulation tool is needed. The mathematical and simulation models, which are used in the last section to exemplify the methodology application, are described next. Three main models are considered: a grid, a load and a BESS. The more accurate and complete the model is, the more information can be obtained from it. However, model parameters are difficult to determine, especially in the case of the battery and weak grid. Hence, a set of few parameters easily calculated have been selected for each model, which represent with sufficient accuracy and simplicity the behavior of each component.

2.1 Distribution network model

A 50 Hz - 400 $V_{ph\text{-}ph}$ network is used in this work as a distribution grid and is schematized in **Fig. 1**. The network model consists of three main components: a grid model, a load model, and a BESS model. Load and BESS models are detailed in subsections 2.3 and 2.4 respectively. The network model inputs the required parameters for each component, and outputs frequency, active and reactive power, and currents and voltages for each node. Simulation outputs are registered each second.

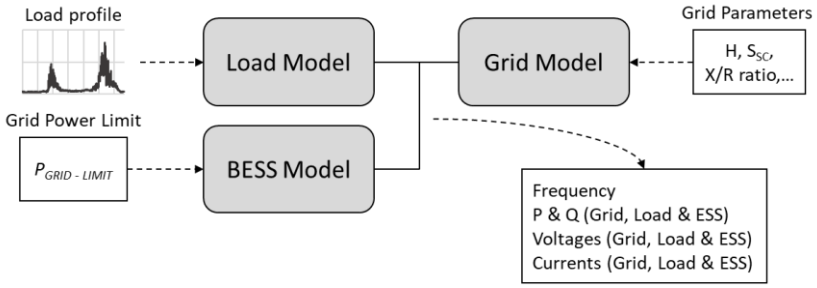

Fig. 1. Schematic diagram of the study case network model (parameters, inputs and outputs).

2.2 Grid model

The grid model is a three-phase controlled voltage source with variable frequency. Frequency variations are computed as in [9], i.e., as a function of the active power demanded by the load and the power delivered by the ESS. Besides, primary and secondary regulation are both considered when calculating frequency deviations.

$$2H \cdot \frac{df}{dt} = P_{ESS} - P_{LOAD} - D \cdot f + R_1 + R_2 \quad (1)$$

$$\frac{dR_1}{dt} = \frac{1}{T_{R1}} \cdot \left(-\frac{f}{R} - R_1\right) \quad (2)$$

where H is the mechanical inertia constant, R_1 is the response of the primary frequency control, R_2 is the response of the secondary frequency control, R is the aggregate speed drop for primary regulation, D is the load sensitivity to frequency variations, and T_{R1} is the frequency insensitivity of the speed governors. Secondary frequency regulation dynamics are modelled as in [10].

The grid model is fully parametrized as a weak distribution network, and the parameters are shown in **Table 1**. The mechanical inertia constant, the aggregate speed droop for primary regulation, and the load sensitivity have been estimated as suggested in [11] and [12]. Moreover, short circuit power (S_{SC}) and X/R ratio are obtained from [13] and [14] respectively.

Table 1. Grid model parameters

Parameter	Value
H	4 s
S_{SC}	1000 kW
X/R ratio	0.8
D	0.04
R_1	1/20

2.3 Load model

The load model consists of a PQ model, so it demands an externally defined profiles of P and Q, which are the inputs of the model. Typical daily individual consumptions for can be obtained with the software LoadProfileGenerator developed in [15], which simulates the behavior of the household occupants, so individual household power profiles can be obtained. Power profiles are obtained for 24 h on 1 second basis, they are randomly generated, and are all different.

For the application example presented in the last section of this work, a settlement of 20 households with a power factor equal to 0.95 is selected. Besides, a typical summer day and a typical winter day are considered.

For the analysis performed in this work, individual household consumptions are aggregated into a three-phase load with no unbalance between phases. Thus, power profiles for the load model for both a typical summer day and a typical winter day are shown in **Fig. 2**.

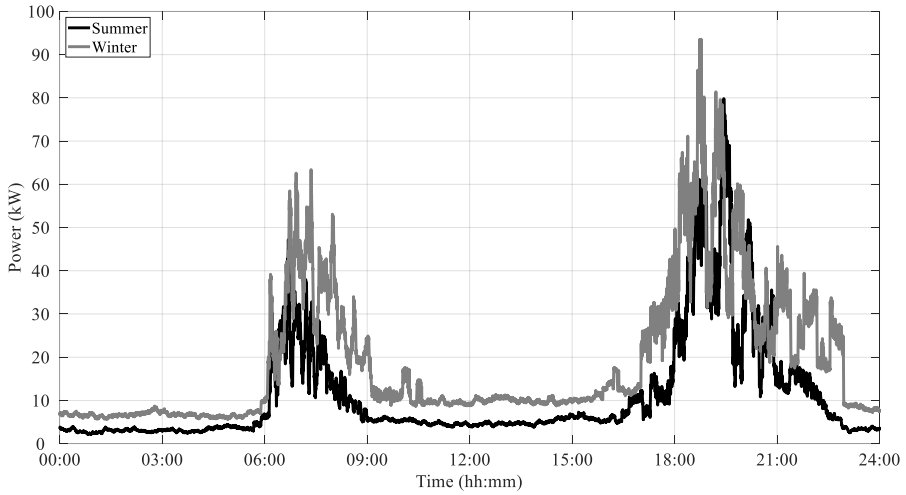

Fig. 2. Load power profiles for typical days in summer and winter.

2.4 BESS model

The BESS model is a controlled P source. The BESS control aims to limit the grid power contribution. In this way, less power flowing through the grid implies less losses, lower voltage drops, and less frequency variations since the BESS matches a percentage of the power demanded by the load. BESS control algorithm behaves in the following way: if the power delivered by the grid to satisfy the load demand and the losses is below a set point $P_{GRID\ -\ LIMIT}$, the BESS charges if possible. However, if the power demanded by the load and the grid exceeds $P_{GRID\ -\ LIMIT}$, the BESS will provide the extra power.

$$\text{If} \quad (P_{LOAD} + P_{LOSS}) > P_{GRID-LIMIT} \rightarrow P_{ESS} = P_{LOAD} + P_{LOSS} - P_{GRID-LIMIT} \tag{3}$$

$$\text{If} \quad (P_{LOAD} + P_{LOSS}) \leq P_{GRID-LIMIT} \rightarrow P_{ESS} = 0 \; or \; Charge \; mode \tag{4}$$

The lithium-ion battery model used in this paper is a modification of the Mathworks model in the SimPower toolbox from MATLAB Simulink, which has been previously published in [16]. The equivalent circuit is based on the Shepherd model [17], which was developed and validated in [18]. In this paper, the battery model is based on the one described in [19], including thermal dependencies and modelling the internal resistance as two different resistances, ohmic and polarization resistance, the latter being dependent on the State of Charge (SoC). The battery model equivalent circuit is represented in **Fig. 3**. Further information about the battery runtime-model is provided in [16] and [19].

The battery aging model included in the model for this work neglects calendar aging [20]. An aging model for this chemistry was developed in [21], based on experimental results, and the capacity loss can be calculated as follows:

$$Q_{loss} = (a \cdot T^2 + b \cdot T + c) \cdot \exp\left((d \cdot T + e) \cdot C_{rate}\right) \cdot Ah \tag{5}$$

where Q_{loss} is the lost capacity in Ah, C_{rate} is the charge/discharge current with respect to the nominal capacity, and Ah is the capacity that has been extracted and/or injected into the battery.

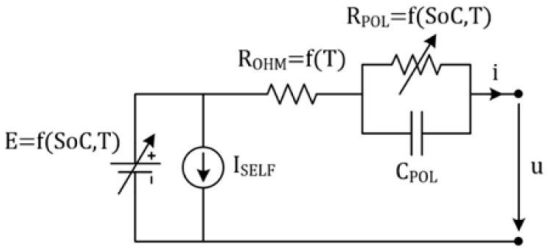

Fig. 3. Battery Equivalent Circuit [21].

The commercial battery cell selected for the application example presented in this paper are of are of $LiNi_xCo_yMn_zO_2$ chemistry and has a rated capacity of 55 Ah and a nominal voltage of 3.7 V [22].

3 BESS dimensioning methodology

3.1 ESS Dimensioning Premises

The BESS dimensioning methodology developed for this work follows four premises:

Premise 1. Power demanded by customers must be fully covered.

This premise implies that both BESS (P_{ESS}) and the electrical grid (P_{GRID}) must cover the customers demand (P_{LOAD}) and the losses (P_{LOSS}).

$$P_{ESS} + P_{GRID} = P_{LOAD} + P_{LOSS} \quad (6)$$

Premise 2. Network parameters must remain within the correct operability limits.

Network parameters include voltage levels, frequency deviation, unbalance between phases, and harmonic distortion among others. The analysis performed in this paper focuses on voltage levels and frequency deviation, assuming a balanced condition with no harmonic distortion. Thus, being voltage and frequency parameters dependent on the power flow across the network and on the power balance between generation and consumption, it is crucial that P_{GRID}, which is limited by the BESS control variable $P_{GRID\text{ - }LIMIT}$, does not overcome the threshold that implies frequencies and voltages out of the correct operability range.

In order to find the solutions of $P_{GRID\text{ - }LIMIT}$ and analyze its effect on voltage levels and frequency, a parametrical analysis is needed. Several values of $P_{GRID\text{ - }LIMIT}$ are tested in order to define the different scenarios. Power quality indicators for a correct operability are defined in subsection 3.3.

Premise 3. BESS power and energy must be sufficient to avoid that P_{GRID} overcomes $P_{GRID\text{ - }LIMIT}$.

The power and energy of the BESS must be sufficient to inject the required P_{ESS} into the grid during the peak periods when $(P_{LOAD} + P_{LOSS}) > P_{GRID\text{ - }LIMIT}$. Moreover, the ESS should be fully recharged during the off-peak periods, i.e., while $(P_{LOAD} + P_{LOSS}) < P_{GRID\text{ - }LIMIT}$.

Premise 4. BESS lifespan must be maximized.

Among the valid solutions of BESSs that comply with premises 1 to 3, the one that suffers less degradation is selected as final solution.

3.2 Steps for the BESS dimensioning methodology

In order to be compliant with the four premises already defined, the BESS dimension methodology aims to find a BESS that eliminates frequency excursions and voltage level deviations, while keeping battery ageing at its lowest. The critical parameter is $P_{GRID\text{ – }LIMIT}$, since the BESS control that determines its power charge/discharge profile is based on this value. The BESS dimensioning methodology follows the flow chart illustrated in **Fig. 4**.

Step 1. Define Test Cases.

The first step consists on defining the different load conditions and values of $P_{GRID\text{ - }LIMIT}$, i.e., the different scenarios that are going to be analyzed. Different scenarios will lead to different BESS configurations and sizes, as well as different ageing.

Step 2. Select, simulate, and analyze voltage levels and frequency for each test case.

After defining the scenarios, the different values of $P_{GRID-LIMIT}$ and load conditions inputs the network model described in section 2, so the simulation can be performed. Once the simulation is completed, voltage levels and network frequency are analyzed, and the next scenario is selected to start a new simulation.

Step 3. Calculate P_{ESS} and E_{ESS}, and select the BESS configuration.

If voltage and frequency along the simulation are within the correct operation thresholds, the required BESS power and energy are calculated. Then, according to the E_{ESS} profile, a BESS configuration can be obtained. Moreover, the charge/discharge profile of the BESS is obtained from the simulation.

Step 4. Calculate BESS lifespan, and final decision.

Finally, a BESS ageing test is performed with the correspondent charge/discharge profile. Final solution is made based on the technical performance and an economic evaluation, which is not performed in this work.

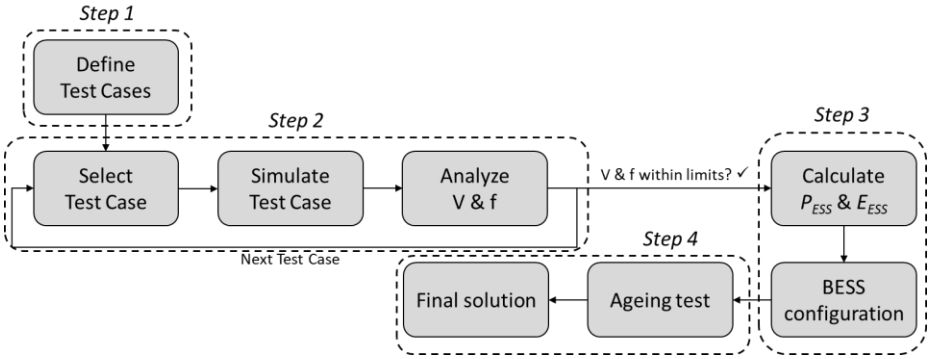

Fig. 4. Flow chart of the ESS dimensioning methodology.

3.3 Power Quality Indicators

As aforementioned, the criteria for selecting a valid BESS is that both grid voltage and frequency should remain within the correct operability thresholds established by the network codes. European standard EN50160 [23] establishes the voltage and frequency characteristics of electricity supplied by public electricity networks, including the distribution grids deployed in urban areas.

Regarding voltage levels, EN50160 determines that phase-to-neutral voltages averaged every minute should be compliant with the following boundary:

$$0.9\ pu < U < 1.1\ pu \tag{7}$$

Concerning frequency two thresholds are established, one related to “alert state” and one to “emergency state”. The system is considered to be in “alert state” if frequency

remains within "alert state" limits for a time interval greater than 5 min. For shorter periods of time, frequency is considered acceptable:

Normal operation: $49.9\ Hz < f < 50.1\ Hz$

Alert state: $49.8\ Hz < f < 49.9\ Hz$ or $50.1\ Hz < f < 50.2$ (8)

Emergency state: $f < 49.8\ Hz$ or $f < 50.2\ Hz$

4 Application Example

In order to present how the methodology described in the previous section is applied to a real case, an application example is provided. Grid, Load and BESS model described in section 2 are used, with the parameters and load consumption detailed in section 2 as well. The same structure of steps as in subsection 3.2 is followed for this application example:

Step 1. Define Test Cases.

The test cases defined for the study case simulations are listed in **Table 1**. 14 scenarios are defined, 7 for a typical summer day and 7 for a winter day. Summer scenarios will implement the summer load profile shown in **Fig. 2**, and winter scenarios will implement the winter load profile. Considering a base power equal to 100 kVA, the BESS control variable $P_{GRID\ -\ LIMIT}$ changes between scenarios in steps of 0.1 pu (10 kW).

Table 2. Simulation scenarios conducted in this paper

Scenario	$P_{GRID\ -\ LIMIT}$	Season
S1	0.1 pu	Summer
S2	0.2 pu	Summer
…	…	…
S7	0.7 pu	Summer
SN	No limit	Summer
W1	0.1 pu	Winter
W2	0.2 pu	Winter
…	…	…
W7	0.7 pu	Winter
WN	No limit	Winter

Step 2. Select, simulate, and analyze voltage levels and frequency for each test case.

MATLAB Simulink SimPowerSystems is used to perform the simulations, based on the load, BESS, and grid model explained in section 2.

Voltage and frequency analysis are also carried out with MATLAB. For both summer and winter scenarios, voltage excursions, frequency alert and frequency emergency events measured per minute are displayed in **Fig. 5** and **Fig. 6**.

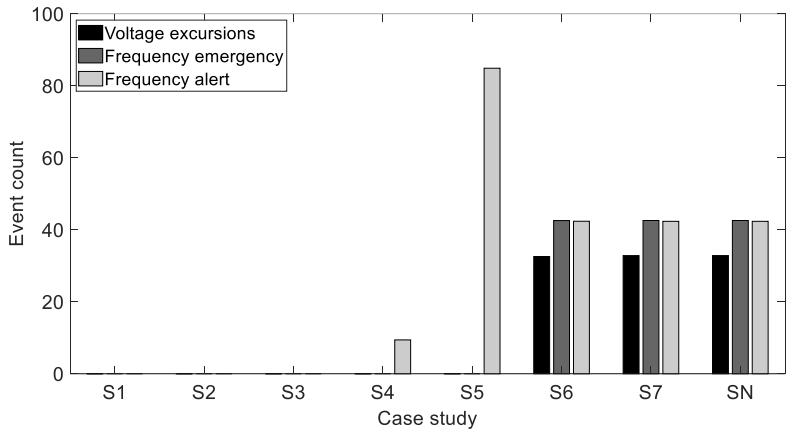

Fig. 5. Voltage and frequency events for summer scenarios.

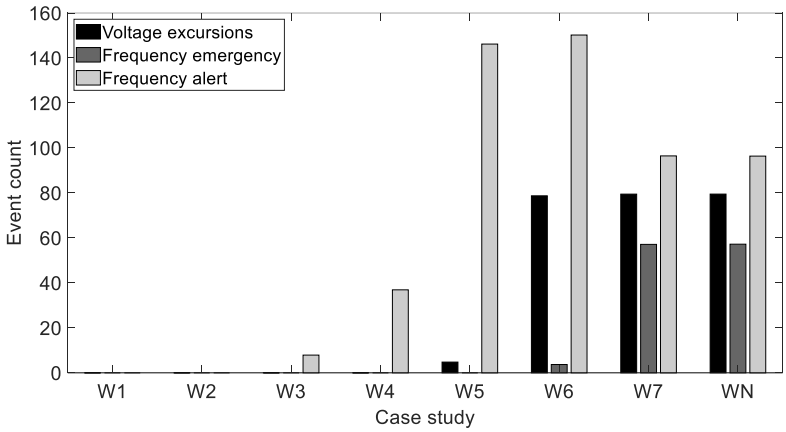

Fig. 6. Voltage and frequency events for winter scenarios.

As expected, voltage excursions and frequency deviations are more numerous for winter than for summer scenarios, since the load profile (**Fig. 2**) is higher for the former ones. Besides, frequency emergency events and voltage excursions events increase as the contribution from the grid increases, which is also expected since a higher power from the grid implies higher voltage drops across the lines, higher losses, and steeper variations in power generation since the grid is in charge of matching a higher percentage of the load's power. It is noticeable that scenarios with a grid power limit of 0.6 and higher show no appreciable difference for summer scenarios, which indicates that

small BESSs are not able of improving power quality conditions at all on the grid. A similar behavior can be seen for scenario W7.

High frequency alert events in scenarios S5, W5 and W6 indicate that the events that were considered as emergency state for scenarios S6 and W7, are now within the alert state limits, since a higher contribution from the BESS prevents frequencies to fall below the state alert threshold.

As a result of Step 2, only scenarios S1, S2, S3, W1 and W2 are compliant with the power quality standards defined in subsection 3.3.

Step 3. Calculate P_{ESS} and E_{ESS}, and select the BESS configuration.

Apart from the analysis carried out in Step 2, the simulation model outputs power, energy and charge/discharge current profiles for the BESS. In order to calculate the BESS configuration in terms on number of cells in series and number of cells in parallel, the charge/discharge profile in terms of energy is applied, so the BESS should store the minimum amount of energy to finish the cycle. For this application example, a BESS nominal voltage of 400 V has been selected, which, according to the battery data from section 2.4, results in 108 cells in series to reach the target voltage. The number of cells in parallel will be the minimum number to reach the value of $E_{ESS\,max}$ obtained from the simulation. For sake of example, BESS configuration calculation for scenario S3 is detailed:

$$E_{108s} = 108\ cells \cdot 55\ Ah\ \cdot 3.7\ V = 21.98\ kWh \tag{9}$$

$$N_{parallel} = 35.51\ kWh\ for\ S3\ /\ 21.98\ kWh = 1.61 \rightarrow 2 \tag{10}$$

According to premise 3, the BESS must be fully recharged during off peak periods. Considering energy charge/discharge profiles, BESS for scenarios S1 and W1 are not able to be fully recharged; the power available for recharging is quite low in those two scenarios, since the grid is limited to 0.1 pu and during off peak periods the grid also takes care of the load power demand. Results for $P_{ESS\,max}$, $E_{ESS\,max}$, and BESS configuration are summarized in **Table 2**.

Step 4. Calculate BESS lifespan, and final decision.

Applying the runtime model and ageing model described in subsection 2.4, cycling ageing simulations can be performed. Since the charge/discharge cycle follows a whole day (24 h), the ageing model outputs the BESS lifespan in days until it reaches a capacity decay of 20%, which is considered by most manufacturers as the BESS end of life (EOL) and results in a need for replacement. Battery ageing results are also summarized in **Table 2**.

According to the results, those scenarios where the BESS works with the lowest C_{rate}, i.e., with the lowest current per parallel branch are the ones that present longer lifespan. The lowest C_{rate} are achieved by the BESS that are oversized in terms of energy. As happened for the BESS configuration calculation for scenario S3 in Step 3, selecting 1 branch of cells in parallel is insufficient to store the required energy, but selecting two branch exceeds it by far. For scenario S3, 35.51 kWh are required, and

the minimum BESS configuration that can store that amount of energy is 108s 2p, account for 44 kWh.

Table 3. Application example results summary

Scenario	Fully recharged?	$P_{ESS\,max}$ (kW)	$E_{ESS\,max}$ (kWh)	BESS config.	Days for 20% Q_{loss}
S1	No	69.8	99.54	108s 5p	1290
S2	Yes	59.8	60.47	108s 3p	1282
S3	Yes	49.8	35.51	108s 2p	1886
W1	No	83.5	181.39	108s 9p	2941
W2	Yes	73.5	122.19	108s 6p	1258

Final solution should be made upon the criteria of the BESS owner and/or operator, although a cost-benefit analysis should be performed in order to complete the methodology presented in this paper. Results arose that bigger BESS last longer since they work with lower C_{rate}; however, a bigger battery severely increases the upfront cost of the equipment, so an economic evaluation is needed in order to evaluate this considerations.

5 Conclusion

This paper presents a BESS dimensioning methodology for grid applications that considers power quality and battery ageing. It aims to maintain frequency and voltage levels within the correct operability thresholds, while maximizing the battery lifespan and delaying the need for battery replacement. Hence, the proposed methodology has potential interest for BESS owners, both companies and particulars, TSOs and DSOs.

Simulation models for the BESS and the distribution network, including load modelling and primary and secondary frequency regulation, are described and implemented.

Four premises are defined as a baseline for BESS selection: power demanded by customers must be fully covered, network parameters must remain within the correct operability limits, BESS power and energy must be sufficient to avoid that P_{GRID} overcomes $P_{GRID\,-\,LIMIT}$, BESS must be fully recharged in a 24 hour cycle, and BESS lifespan must be maximized.

In order to demonstrate how to implement the proposed methodology, as well as to analyze the results arose from it, a settlement of 20 households together with a fully parametrized weak network is considered as a study case. Moreover, a typical summer day and a typical winter day have been considered for modeling the settlement consumption. Then, 14 scenarios are defined, with different values of $P_{GRID\,-\,LIMIT}$.

Results show that there are different configurations of BESS that allow for a correct operability of the grid in terms of frequency and voltage levels, since voltage excursions, frequency alert and frequency emergency events are eliminated. Out of those BESS configurations, an ageing analysis is performed.

It is also true that, in order to find the most suitable solution, the whole range of $P_{GRID\text{-}LIMIT}$ together with different Li-ion BESS commercial chemistries should be considered. Moreover, power electronics behavior and its control, which have not been considered for this work, should be taken into consideration for a complete analysis.

BESS owners and designers should perform a study like the one proposed in this work in order to find the most suitable solution for their grid application, which should include, in the final stage, a translation into economical terms for maximizing benefits.

References

1. Horizon 2020 - Energy. https://ec.europa.eu/programmes/horizon2020/en/area/energy
2. Bauer, D., Bauer, T. P., Bedel, L., Bergins, C., Bubeck, R., Budenberg, T., ... & Zunft, S. (2017). Joint EASE/EERA recommendations for a European energy storage technology development roadmap. European Association for Storage of Energy (EASE).
3. EASE - Storage Applications. http://ease-storage.eu/energy-storage/applications/
4. Gielen, D., Gorini, R., Wagner, N., Leme, R., Gutierrez, L., & Prakash, G. (2018). Global Energy Transformation: A Roadmap to 2050. International Renewable Energy Agency (IREA): Abu Dhabi, Vereinigte Arabische Emirate, 76.
5. Fang, X., Misra, S., Xue, G., & Yang, D. (2011). Smart grid—The new and improved power grid: A survey. IEEE communications surveys & tutorials, 14(4), 944-980.
6. Held, L., Krämer, H., Zimmerlin, M., Suriyah, M. R., Leibfried, T., Ratajczak, L., ... & Konermann, M. (2018, September). Dimensioning of battery storage as temporary equipment during grid reinforcement caused by electric vehicles. In 2018 53rd International Universities Power Engineering Conference (UPEC) (pp. 1-6). IEEE.
7. Etherden, N., & Bollen, M. H. (2013). Dimensioning of energy storage for increased integration of wind power. IEEE Transactions on Sustainable Energy, 4(3), 546-553.
8. Mulder, G., Six, D., Claessens, B., Broes, T., Omar, N., & Van Mierlo, J. (2013). The dimensioning of PV-battery systems depending on the incentive and selling price conditions. Applied energy, 111, 1126-1135.
9. Villalba, I., Blanco, M., Pérez-Díaz, J. I., Fernández, D., Díaz, F., & Lafoz, M. (2018). Wave farms grid code compliance in isolated small power systems. IET Renewable Power Generation, 13(1), 171-179.
10. Egido, I., Fernández-Bernal, F., Rouco, L., Porras, E., & Sáiz-Chicharro, Á. (2004). Modeling of thermal generating units for automatic generation control purposes. IEEE transactions on control systems technology, 12(1), 205-210.
11. Ulbig, A., Borsche, T. S., & Andersson, G. (2014). Impact of low rotational inertia on power system stability and operation. IFAC Proceedings Volumes, 47(3), 7290-7297.
12. Kundur, P., Balu, N. J., & Lauby, M. G. (1994). Power system stability and control (Vol. 7). New York: McGraw-hill.
13. Etxegarai, A., Eguia, P., Torres, E., Iturregi, A., & Valverde, V. (2015). Review of grid connection requirements for generation assets in weak power grids. Renewable and Sustainable Energy Reviews, 41, 1501-1514.
14. Alizadeh, S. M., Ozansoy, C., & Alpcan, T. (2016, September). The impact of X/R ratio on voltage stability in a distribution network penetrated by wind farms. In 2016 Australasian Universities Power Engineering Conference (AUPEC) (pp. 1-6). IEEE.
15. Pflugradt, N. D. (2016). Modellierung von wasser und energieverbräuchen in haushalten.

16. Nájera, J., Moreno-Torres, P., Lafoz, M., de Castro, R., & R Arribas, J. (2017). Approach to hybrid energy storage systems dimensioning for urban electric buses regarding efficiency and battery aging. Energies, 10(11), 1708.
17. Shepherd, C. M. (1965). Design of primary and secondary cells II. An equation describing battery discharge. Journal of the Electrochemical Society, 112(7), 657-664.
18. Tremblay, O., Dessaint, L. A., & Dekkiche, A. I. (2007, September). A generic battery model for the dynamic simulation of hybrid electric vehicles. In 2007 IEEE Vehicle Power and Propulsion Conference (pp. 284-289).
19. Moreno-Torres Concha, Pablo. Analysis and Design Considerations of an Electric Vehicle Powertrain regarding Energy Efficiency and Magnetic Field Exposure. Doctoral Dissertation. Universidad Politécnica de Madrid, 2016.
20. Barré, A., Deguilhem, B., Grolleau, S., Gérard, M., Suard, F., & Riu, D. (2013). A review on lithium-ion battery ageing mechanisms and estimations for automotive applications. Journal of Power Sources, 241, 680-689.
21. Wang, J., Purewal, J., Liu, P., Hicks-Garner, J., Soukazian, S., Sherman, E., ... & Verbrugge, M. W. (2014). Degradation of lithium ion batteries employing graphite negatives and nickel–cobalt–manganese oxide+ spinel manganese oxide positives: Part 1, aging mechanisms and life estimation. Journal of Power Sources, 269, 937-948.
22. Kokam, Technical Specification: SLPB100255255HR2.
23. Markiewicz, H., & Klajn, A. (2004). Voltage Disturbances–Standard EN 50160. Copper Development Association, IEE Endorsed Provider, Wroclaw University of Technology.

Heat islands and green roofs in Bus Rapid Transit stations. Study Case: Line 1, Aburra Valley

[1.] Quijano R, [1] Dominguez J[2] Quijano JP [3]

[1] Universidad Nacional de Colombia. Facultad de Minas. Escuela Procesos y Energía. Carrera 80 #65-223, Medellín Colombia. rquijano@unal.edu.co

[2] Ministerio de Ciencia e Innovación. CIEMAT. Departamento de Energía. División de Energías Renovables. Av. Complutense, 22. 28040, Madrid (España). javier.dominguez@ciemat.es

[3]The University of Newcastle, University Drive,Callaghan, NSW 2308, Australia. Juan.quijanobaron@uon.edu.au

Abstract. The center of Medellín is the area with the highest surface temperature in the Aburrá valley, where the effect of the heat islands is a product of the large vehicle fleet. Between 2014 and 2015, the number of cars in the city grew 3.1 percent from 1,234,946 to 1,273,223, which includes an increase of 4.1 percent in cars and 2.1 percent in motorcycles. In the last decade, the increase in vehicles in the Aburrá Valley has been significant: 67 percent more cars, 280 percent more motorcycles, 54 percent more taxis and buses, and 50 percent more trucks. Although public transport is constituted by 2% of buses and less than 1% of Bus Rapid Transit (BRT)-Metroplús, these generate considerable emissions of greenhouse gases and energy consumption: 2,606,333 Ton / year of CO_2, 10,176 Ton / year of CH4 and 63 Ton / year of N2O and a consumption of 37,784 Tera Joule / year. Because of the emissions, reflection of solar radiation from road constructions and the lack of natural vegetation, temperatures can reach 31.3 ° C.

In this investigation, we use the EFERVERDE model and the ENVIMET tool for the simulation of green roofs and walls in the Plaza Mayor station of the BRT Metroplús System, Line 1, which is located in an area with hight temperature. The results showed a reduction in air temperature of 2.0 degrees Celsius, fixation of 12,127 Ton / year of CO_2 (decrease in 65.72 Ton / year of CO_2) and savings of 16,307 kWh / year in electrical energy, which represents an annual electricity cost reduction of around € 20,465 euros. This methodology can be applied to other stations the BTR lines of the city or other cities with similar characteristics.

This work presents a continuation of the methodological development to improve people's quality of life of whose commute in urban areas of high pollution. The purpose is to reach the sustainability of the city and minimize the risk of diseases associated with heat islands: stress, fatigue and bronchial respiratory diseases.

Keywords: Energy Efficiency, Green Roofs, CO_2 Emissions Reduction, Heat Islands, EFERVERDE.

Introduction

Medellín, capital of the department of Antioquia, is the most populated city in the state and the second in Colombia. The city is located in the Aburrá Valley, in the Andes mountain range, becoming the largest western Andean urban center. It is located at coordinates 6° 13′55″ N - 75 ° 34′05″ W and has a total area of 328 km² of which 110 km² are urban land and 218 km² are rural land. The elevation of Medellín varies between 1,800 and 1,500 meters above sea level with the Nutibara and Volador hills located in the middle of the city. It has a daily temperature that ranges between 12° C and 30° C, these being constant during the year, and an average annual rainfall of 1,656 mm. The winds are soft and constant, blowing mainly in a north-south direction [1].

This project seeks to simulate the implementation of green roofs and living walls where their use has a contrasting effect in terms of temperature and pollution reduction. The objective is to model the implementation of these systems in an area of the city that coincides with the nerve points of the city, which presents the phenomenon of heat islands, high population density and significant effects on people's sense of well-being.

1.1 CO_2 emissions from fuel consumption in the city of Medellin

The air quality in Medellín has deteriorated in recent years. Red alert levels have been generated at different times of the year, especially the time of transition from dry weather to rainy season in the months of March, April, October and November in the years 2015, 2016, 2017 and 2018 [20]. The increased use of the car and the unique topographic and meteorological characteristics of the Aburrá Valley contribute to higher concentrations of pollutants harmful to public health [2].

The greenhouse gas emissions for 2014 generated by mobile sources in the city of Medellin were 2'606,333 Ton / year of CO_2, 10,176 Ton / year of CH4 and 63 Ton / year of N2O. Cars and trucks produced most of these greenhouse gases, while the fuels that generated the highest carbon dioxide emissions were gasoline and diesel. Gasoline and vehicular gatural gas were responsible for the majority of methane emissions, while more than 60% of nitrous oxide was the product of gasoline [3]. For the same year, the Aburrá Valley had other pollutants such as 154,447 Ton / year of carbon monoxide CO, 16,306 Ton / year of nitrous oxides NOx, 3,264 Ton / year of sulphurous oxides - SOx, 15,214 Ton / year of volatile organic compounds - VOC and 1,465 Ton / year of particulate material less than 2.5 microns $PM_{2.5}$ [4].

1.2 Heat Islands

Urban Heat Island is a term that refers to the characteristic heat of the atmosphere and surface in urban areas compared to its undeveloped environments [5]. When analyzing the information of weather stations in the city of Medellín, there are many differences in the temperatures of the neighborhoods. The hottest are located in the center of the city (La Candelaria, El Chagualo, San Benito, among others) and in the northern part of the Medellín River bank (La Toscana, Boyacá-Las Brisas, Moravia, Santa Cruz).

The coldest neighborhoods are located in the high parts of the surrounding mountains (Altos del Poblado, San Lucas, La Sierra, March 8, Oriente, Santo Domingo Savio, San José de la Cima, Carpinelo, Picacho, among others).

Heat islands generate different effects and consequences for the environment and people's quality of life. The main effect of the heat island is the increase in temperature and thermal sensation, accompanied by the reduction of humidity and less probability of occurrence of rainfall in the area. Thermal shocks in summer and the decrease in air circulation increase the concentration of particulate matter PM_{10} and $PM_{2.5}$ affecting the health of people, especially the vulnerable population such as children, the elderly and people with respiratory diseases [6]. There is also a greater expenditure of water, both for human consumption and for irrigation and cooling activities, thus generating greater energy consumption to alleviate the effects of microclimate. Likewise, because of using cooling systems, the emission of residual heat and the emission of greenhouse gases such as CO_2 are increased.

1.3 Green roofs and living walls

Green roofs and living walls are systems in which the construction structure incorporates plants. This concept is relatively new, it is used for facades and internal walls. They consist of pre-cultivated panels or geotextile felts that support the vegetation. The plants that are used can adapt to grow vertically such as: upholsteries, ferns, small shrubs, flower perennials and others [7]. Green roofs and living walls are widely used to reduce the effects of temperature, CO_2 fixation and dampen the pollution present in heat islands.

Methodology

The methodology is based on the simulation and evaluation of green roofs and living walls in points on the stations of line 1 of the massive METROPLUS system. First, the system station was determined from a multicriteria comparison, to select the one that would generate the most benefits after the implementation of green roofs and living walls. Subsequently, the potential location and plant species to be used were established. Next, the benefits of these structures were calculated in terms of avoided carbon dioxide emissions, demand and analysis of electric energy savings (through the LEAP model) and their economic assesment. Finally, the ENVIMET software was used to simulate the effects of green roofs and living walls on temperature [4]. The steps described above follow the modeling methodology called Energy Efficiency and Green Walls - EFERVERDE [8].

For the selection of the study case, a multicriteria evaluation analysis of four stations of Line 1 of the Bus Rapid Transit –BRT) is performed (see Figure 1). These stations were selected because they were in the areas with the highest heat concentration as a consequence of the heat islands. The station to be studied is determined by the highest

score by weighting the variables of temperature, pollution, radiation, heat islands, vegetation cover and population density.

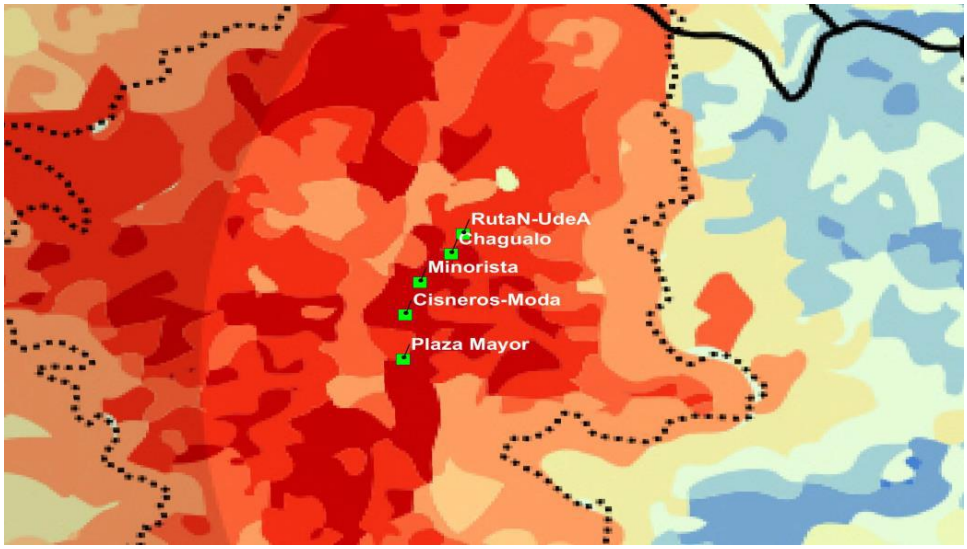

Figura 1. Location stations under study and overlap with heat islands. Source: Martínez, A. (2017).

The design of the green roofs is done by determining the available area for plant location and selecting the plant species. The available area is conducted by evaluating the size of the ceilings of the station and the dimensions of the walls, and the selection of the species is made based on the methodology proposed by Bolaños and Moscoso [9]. This consists of characterizing the species and giving them a score of 0 to 3; being 0 unfit, 1 the least fit and 3 the fittest. At the end, the species with the highest score prove to be the best for the system. The species used for the analysis are:

Sp 1: Clorophytum comosum (cinta)
Sp 2: Hedera helix (English ivy)
Sp 3: Duranta Erecta (Gold edge)
Sp 4: Geranium 'Johnson's Blue' (Geranium)
Sp 5: Celosia (Amaranthaceae)

The estimation of energy efficiency and CO_2 sequestration was carried out based on the methodology of the intergovernmental panel on climate change - IPCC [10]. The calculation of energy efficiency is based on the electrical power of the air conditioner that would be necessary at the station. Additionally, the thermal variation of people entering and leaving the station and an average use of 8 hours per day is calculated. The estimation of avoided emissions is based on the emission factors used in the EXTERNEE project [11] for a combined cycle plant. This is based on the Termo Sierra power plant, located in the middle Magdalena Antioqueño, with a value of 400 gr / kWh

of CO_2. The CO_2 uptake of the species selected for the system, took into account the plant species and the photosynthesis pathway (C3, C4 or CAM).[12]

The simulations of temperature and CO_2 concentrations were carried out with the free version of the ENVIMET program [13]. This software simulates temperature dynamics over time, based on input environmental variables. Additionally, it considers the type of material that composes the facades and roof. Notice that the program does not directly simulate the plants, so these are coupled to the wall from materials that approximate their behavior. Simulations of the station were carried out with the current structure and with a horizontal and vertical plant systems.

Results

1.4 Study case selection

The results of the multicriteria evaluation of four stations: Cisneros, Retail, Chagualo and Plaza Mayor are shown in Table No.1. As the main objective of the project is the reduction of the heat island, a higher percentage is given to the temperature, which varies between 27° and 31° C. Pollution refers to PM_{10} and $PM_{2.5}$ particulate material. Values between 51.8 and 58.22 µg / m³ were obtained for PM_{10} and between 19.92 and 22.83 µg / m³ for $PM_{2.5}$. Pollution was estimated as an average of the value obtained and weighted with the maximum allowed value for the air quality standard: 75 µg / m³ for PM_{10} and 37 µg / m³ for $PM_{2.5}$. The radiation was taken the UV index, which was assumed as 10 for the entire city. For the heat island criteria, the coincidence with the station with the highest temperature zones presented in Figure 1 was evaluated [14]. The vegetal cover was calculated with the Geovisor of the city of Medellín and the population density was determined from the Administrative Planning Department of the city. It was determined that the station that could generate a greater impact after the implementation of green roofs and living walls is Plaza Mayor.

Table 1. Matrix for station choice. Source: own calculation.

	Station	**Temperature**	**Pollution**	**Radiation**	**Heat Island**	**Vegetal Cover**	**Urban density**	**Total**
	Weight	**25%**	**12%**	**12%**	**25%**	**16%**	**10%**	**100%**
Plaza Mayor	Value	10	6.3	10	10	10	10	**9.6**
	Weighted	2.5	0.8	1.2	2.5	1.6	1	
	Value	9	9	10	10	1.9	5	**7.8**

Cisneros	Weighted	2.25	1.1	1.2	2.5	0.3	0.5	
Minorista	Value	10	8	10	10	7.4	8	**9.1**
	Weighted	2.5	1.0	1.2	2.5	1.2	0.8	
Chagualo	Value	9	6.2	10	10	9.4	2.5	**8.4**
	Weighted	2.3	0.74	1.2	2.5	1.50	0.25	

1.5 Study area description

The center of the city of Medellín, specifically the Plaza Mayor transport station, is the area that has been selected as a case study in this investigation. This place is among the highest surface temperature zones of the Aburrá Valley, that is, where the effect of heat islands is notorious [15]. Additionally, this place suffers from problems such as low vegetation density, use of materials on roads that absorb and reflect solar radiation (e.g. concrete and asphalt) and roads with high vehicle flow. It has also been shown that urban heat islands are increased by high population density, which in our case study was 300 dwellings per hectare by year 2010 and which has been increasing over the years [16].

The Plaza Mayor Station (see Figure 2) is the ninth station of the integrated Bus Rapid Transit -BRT-METROPLÚS transport system, on the L1 line that starts in the west of Medellín and ends in the Aranjuez neighborhood. It is located on the avenue of the railway, in the middle of the International Center for Conventions and Exhibitions Plaza Mayor and La Plaza de La Libertad in Medellín [8].

Figure 2. Plaza Mayor station. Recovered from Mapgis

The station has pedestrian access with access to a direct ramp to the Plaza Mayor convention center and the administrative complex of the Alpujarra. Inside the station there is a main hall 100 meters long and approximately 6 meters wide, whose floor is made of smooth cement with guide arrangements for blind personnel and signage adjacent to

each access door to the bus system. Its geographical location is located at coordinates 75°34’31,264’’ W - 6°14’37,260’’ N, occupying a total area of 680 m² (see Figure 3).

Figure 3. Plaza Mayor station plan. Recovered from Mapgis

1.6 Design and location of green roofs

The Plaza Mayor station has some ornamental plants arranged in the access areas and its structure is composed of vertical columns, exterior walls and ceiling beams [17]. In the proposed design of green roofs and walls, 80-90% of the roof and 54% side walls (100 linear meters of wall) of the station are proposed. Additionally, it is proposed to use a strategic distribution of windows in the roofs, approximately 6-8% of the roof of the station, to ensure a comfortable amount of light during daylight hours and a system of pocket-type walls of polymeric materials to support plants with a height of 3 m.

For the selection of plant species, it is important to take into account the orientation of the walls with respect to the sunrise and sunset to determine their sunstroke. The most suitable wall for the intervention are in front of the railroad avenue, these sides have southeast and northwest orientation respectively and six (6) hours average of sunshine.

Once the relevant analysis has been carried out in the matrix, it is concluded that the most suitable plants for green walls are Duranta Erecta (Gold edge) and Celosia (Amaranthaceae). The first is native to America and belongs to the family of verbenáceas, fast growing with the need for full light, which is ideal for the location of the walls to intervene since they are constantly exposed to sunlight. The second is a tropical plant native to Asia, Africa and America, belonging to the Amaranthaceae family, they are fast growing, their flowers can be yellow, orange, red and pink, and just like the Duranta Erecta they prefer to be in full light. A posible third alternative is the Thunbergia which is a vine plant native to India that stands out for its blue flowers. It is a very fast growing plant, it has very flexible stems and rounded leaves. The plant needs full sun exposure or minimum semi-shade but it does not resist frost.

1.7 Calculation of energy efficiency, avoided emissions and CO_2 fixation

The energy efficiency calculations yielded a total gross saving of 164.3 MWh / year represented in the non-use of air conditioners. This is due to the comfort obtained by green roofs and walls [18] [8], and likewise, the emission of 65.72 tons of CO_2 / year is avoided by reducing the use of electrical energy. In terms of costs, this represents a saving of € 20,465 euros per year.

The CO_2 uptake was 33.23 kg per day, equivalent to 12,127 Ton CO_2 per year. This took into account that the system consists of 6645 plants, which absorb between 2 and 5 grams of CO_2 [14], and which have a photosynthesis type C4. This CO_2 fixation path makes them more efficient and resistant to dry and hot conditions.

1.8 Temperature and CO_2 simulations

The simulations were held for the first quarter of 2019 between 9:00 am to 1:00 pm. Each simulaton time of one hour equals four real hours, so each simulation took 16 hours in real time. Figure 4 shows the two-dimensional plan of the Plaza Mayor station. A total area of 957 m² was simulated, corresponding to the roof 540 m² and 417 m² corresponding to the sides.

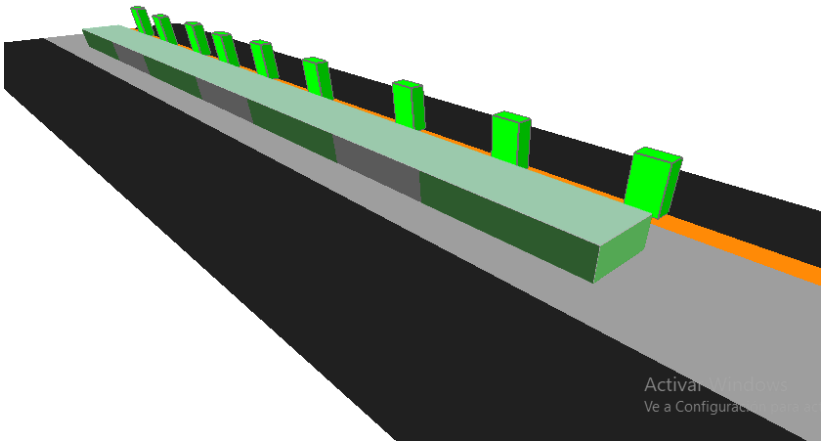

Figure 4. Simulated Plaza Mayor station display.

Figure 5 and Figure 6 images compare the behavior of the air temperature at 1:00 pm at a height of 3.7 meters for the stage with and without green roofs and walls. The simulation with the roof and green wall yields as a minimum temperature value of 24.30° C and maximum of 26.13° C, while the simulation that does not include the roof and green wall, the temperature range varies between a minimum of 25.34° C and a maximum of 27.03° C. Consequently, the green wall can generate a temperature reduction of up to 2.0 ° C. Likewise, it can be seen that the temperature decrease in the area

around the square is about 1° C and in the closest area of the wall, the temperature distribution is less uniform, given the cooling effect that it produces.

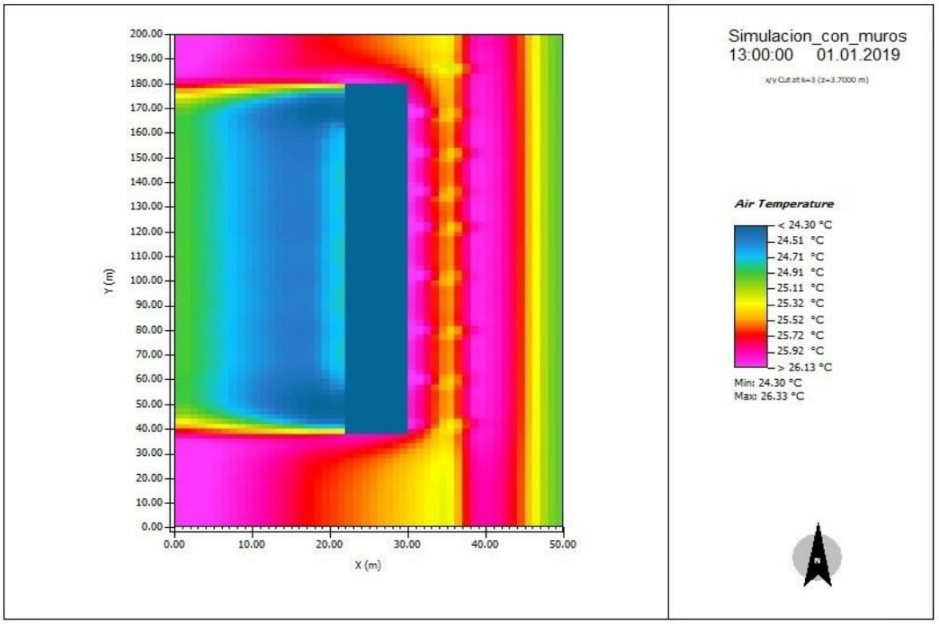

Figure 5. Simulation behavior of air temperature with the green wall/roof

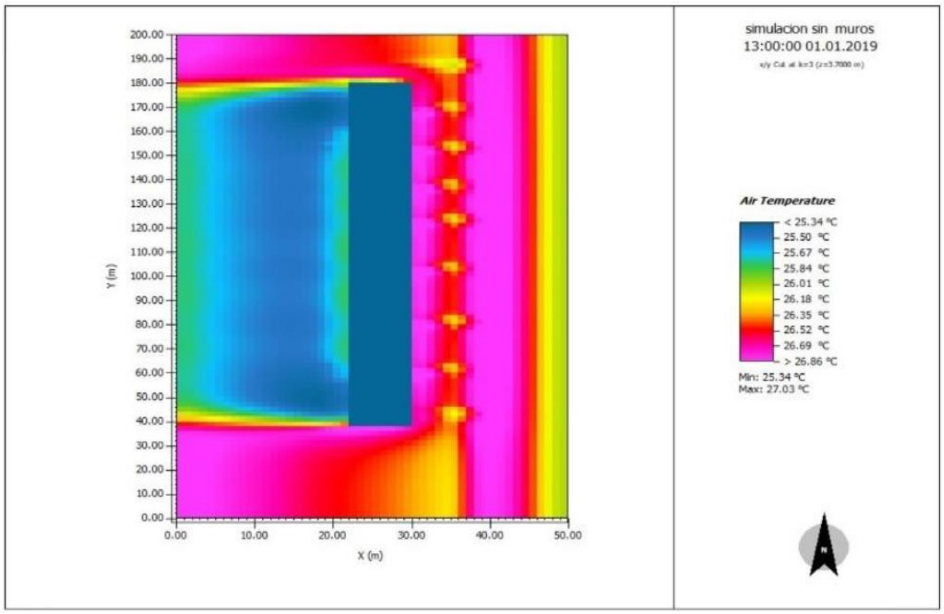

Figure 6. Simulation behavior of air temperature without the green wall/roof

Figure 7 shows that with the implementation of the green roof and wall, a reduction in CO_2 concentration is achieved. On the tracks and surroundings of the Plaza Mayor station, the concentrration pass from 409.49 ppm to 414.70 ppm with green walls and roofs, to a scenario from 413.83 ppm to 421.33 ppm of CO_2 without walls and green roofs.

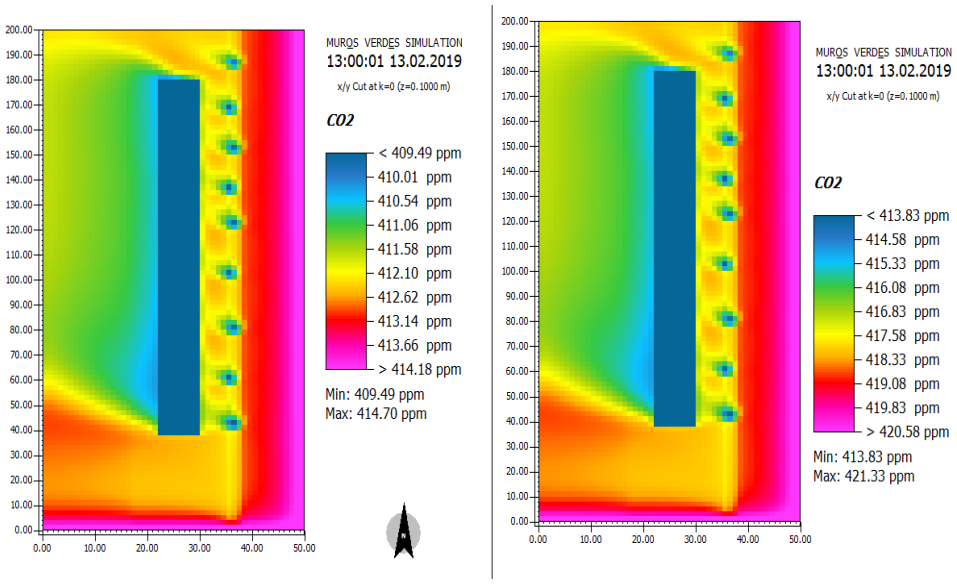

Figure 7. Simulation of the behavior of the point pollution of ppm of CO_2. Left: with green walls and ceilings. Right: no walls and green roofs.

Conclusions

It is clear that the implementation of the roof and green wall produces the mitigation of the effects that are generated by the heat islands: decrease in temperature, reduce energy costs, avoid CO_2 emissions, fix atmospheric CO_2 and improve the quality of life. The ambient temperature in the area is reduced by up to 2.0 ° C degrees Celsius while fixing 33.23 kg of CO_2 per day. In energy efficiency, 164.3 Mwh / year of electricity are saved, representing a saving of € 20,465 euros per year. Additionally, the emission of 65.72 tons of CO_2 / year is avoided, which can be an opportunity to negotiate CO_2 in international markets or receive assistance from global organizations that support this type of projects. The concentration of CO_2 in the surroundings is reduced from 421.33 to 414.7 ppm of CO_2, meaning an improvement in the quality of greenhouse gases. The aesthetics and perception of the area could be improved even thoug it is a densely populated, polluted and congested area. Implementation of green roof and

wall produces an improvement in the quality of life and minimizes the risk of diseases associated with heat islands, such as stress, fatigue and bronchial respiratory diseases.

ACKNOWLEDGEMENTS

We acknowledge the students from the Faculty of Mines of the National University of Colombia, Medellín, group six, for their work "Mitigation of heat islands by ecodesigns in metroplus stations", of the Engineering Projects Seminar: Angélica Maria Lizarazo Pérez, Alvaro Diego Bedoya Zapata, Jonathan Gallego Vélez, Santiago Cadavid Gutierrez, Sergio Arango Rincón, Tomas David Marcilia Burgos, Maria Angélica Ortega Camargo, Valeria Rosa Morelos De Fex and the tutor Alejandra Herrera for her contribution in the preliminary simulation of the green wall.

References

[1] Alcaldía de Medellín [online] Recuperado https://www.medellin.gov.co/irj/portal/medellin

[2] Camino de la Política para Mejorar la Calidad de la Aire Urbano en Medellín, Colombia, Observatorio de Politicas Públicas del Consejo de Medellín. Junio de 2017

[3] Área Metropolitana del Valle de Aburrá - Universidad Pontificia Bolivariana. (2014). Actualización del inventario de emisiones atmosféricas del Valle de Aburrá.

[4] Roldán, Luis Miguel. "Novedad En El Plan de Contingencia Ambiental." *Medellín Cómo Vamos*, February 6, 2017. http://www.medellincomovamos.org/que-tan-nuevo-es-el-plan-de- contingencias-atmosfericasdelamva/.

[5] Ángel, L., Ramírez, A., & Domínguez, E. (2010). Isla de calor y cambios espacio-temporales de la temperatura en la ciudad de Bogotá. Rev. Acad. Colomb. Cienc, 34(131), 173-183.

[6] Guindon, S. M., & Nirupama, N. (2015). Reducting risk from urban heat island effects in cities. Natural Hazards, 77(2), 823-831.

[7] Carrera Acosta, A. (2011). Sistemas vegetales verticales. Universidad Politécnica de Madrid. Recuperado de http://oa.upm.es/10204/2/TESIS_MASTER_ALVARO_CARRERA_ACOSTA.pdf

[8] Quijano R, Dominguez J Quijano JP. EFERVERDE, Modelo de Eficiencia Energética y muros verdes, Eficiencia Energética y reducción de temperatura mediante muros verdes en islas de calor, ponencia, Universdad de Valladolid, Soria España, septiembre 2018

[9] Bolaños-Silva, T., & Moscoso-Hurtado, A. (2011). Consideraciones y selección de especies vegetales para su implementación en ecoenvolventes arquitectónicos: una herramienta metodológica. Revista Nodo, 5, 5–20. Recuperado de https://dialnet.unirioja.es/servlet/articulo?codigo=3736189

[10] Panel Intergubernamental de Cambio CLimatico [online] Recuperado www.ipcc.ch/home_languages_main_spanish.shtml

[11] ExternE-Methodology [online] Recuperado http://www.externe.info/externe_d7/

[12] Mota, C., Alcaráz López, C., Iglesias, M., Carvajal, M., & Martínez Ballesta, M. C. (s.f.). Investigación sobre la absorción de CO_2 por los cultivos más representativos de la región de Murcia. Recuperado de http://www.lessco2.es/pdfs/noticias/ponencia_cisc_espanol.pdf

[13] ENVI_MET is a software company with a service portfolio including cities & health, trees & vegetation, building & climate and wind & sun. [online] Recuperado https://www.envi-met.com/
[14] Trujillo Uribe, S. (2012). Estimación de temperatura superficial en el Valle de Aburrá mediante técnicas de percepción remota.
[15] Martínez, A. (2017). Islas de calor en el área urbana del valle de Aburrá. Tesis de maestría. Universidad Nacional de Colombia – Sede Medellín. Recuperado de http://bdigital.unal.edu.co/57837/1/1039453046.2017.pdf
[16] López, F., Nieto, D., & Arias, C. (2010). Relaciones entre el concepto de movilidad y la ocupación territorial de Medellín. Revista EIA, (13), 23–37.
[17] Sistema Bus Rapid Transit –BRT – METROPLÚS. https://metroplus.gov.co/empresa/organigrama/mapas
[18] R Quijano, J, Domínguez, y S, Botero, (2012) MODERGIS Application: Integrated simulation platform to promote and develop renewable sustainable energy plans, Colombian case study, Renewable and Sustainable Energy Reviews 16 (2012) 5176–5187, Vol 16, Issue 1, ISSN – 1364-0321.

Impact on a microgrid using different storage systems under three energy dispatch control

Paul Arévalo[1,2] [0000-0002-6721-1326], D. J. Benavides [1,2] [0000-0003-1624-8759], Juan Leonardo-Espinoza[3] [0000-0002-7450-2084], Luis Hernández-Callejo[2] [0000-0002-8822-2948] and Francisco Jurado[1] [0000-0001-8122-7415]

[1] Universidad de Jaén, Campus Científico-Tecnológico de Linares, 23700 Jaén, Spain
[2] Universidad de Cuenca, Campus Tecnológico Balzay, 010107 Cuenca, Ecuador
[3] Universidad de Valladolid, Campus Universitario Duques de Soria, 42003 Soria, Spain
{wpac0001,djbp0001}@red.ujaen.es, juan.espinoza@ucuenca.edu.ec, luis.hernandez.callejo@uva.es,fjurado@ujaen.es

Abstract. This paper presents the simulation of a renewable energy microgrid composed of: photovoltaic system, wind turbines, hydrokinetic turbines, diesel generator and energy storage systems. Three types of energy control have been used: cycle charging, load following and combined dispatch in order to study the impact on the system against different demand behaviors, different storage systems have been used (lithium ion batteries, lead acid and flow of redox vanadium, hydraulic pumping system and supercapacitor). For each case, the net present cost, the cost of energy and CO_2 emissions are studied in order to determine the impact on the microgrid. The results show that: when using the load following control, the net present cost and energy cost are lower using the pumped hydroelectric energy storage. On the other hand, the system with the lowest CO_2 emissions is lead acid batteries when using the combined cycle control. Finally, the wind turbines have presented the greatest variation of the net present cost with respect to the capital cost, all the results have been obtained using Homer software.

Keywords: Microgrid, Energy Control, Storage, Modeling

1 Introduction

The global electricity demand is constantly growing due to current technological development. However, there must be sustainable development without compromising the environment. For this reason, research related to electricity generation through renewable technologies is paramount. Many studies have shown that electric power generation is more efficient using more than one technology simultaneously. In addition, a wide variety of tools and computational methods have been used to determine the different behaviors that hybrid systems have according to the conditions of each place [1]–[8]. For example, in references [9]–[18], explain the operation and optimization by software of a hybrid system composed of Photovoltaic (PV) - Wind Turbines (WT) energy, showing positive results. In addition, in reference [19] different storage technologies have

been considered for the PV-WT system, the results have shown that Lithium Ion and Cadmium Nickel batteries could be as competitive as those of Acid Lead if their investment cost decreases. It is clear that, the type of renewable generation technology will depend on the resources present in the place of study and the technological development they possess. Another source of renewable generation under study is Hydrokinetics Turbines (HKT), since not needing the construction of civil works is a good option. In the references [20], [21] a study of optimization of a hybrid system (PV-HKT) has been carried out with novel results, lead acid batteries and fuel cells have been used in order to reduce the operation of the diesel generator. In addition, several authors highlight the performance of hydrokinetic turbines in hybrid systems, generally their use is based on water pumping systems [22]–[29].

Being technologies currently studied, the optimization problem is evident and every time several authors recommend its use. That is why, this study presents an analysis related to the optimization of a microgrid composed of PV/WT/HKT, in order to determine new behavior patterns in these systems. Additionally, three energy control systems have been developed: Load Following (LF), Cycle Charging (LC) and Combined Dispatch (CD) using the Homer pro computational tool, in each type of control, the operation of a diesel generator is modified according to weather conditions at every moment of time. In addition, this study goes further by analyzing the effects produced by different Energy Storage Systems (ESS) on the microgrid such as: lead acid batteries, lithium ion batteries, redox vanadium batteries, supercapacitors and pumping systems. Each of ESS, has been investigated in [19], lead acid batteries are the most used in several analyzes due to their versatility and low cost. However, lithium-ion batteries are a good option for acid lead replacement since they have a higher life expectancy and energy density [30]–[34]. On the other hand, references [35]–[38] have shown that Vanadium Redox flow batteries (VRF) have characteristics that can be used in renewable systems due to their rapid response to load fluctuations and their long life expectancy. ESS composed of supercapacitors in order to soften the power peaks produced by a system and storage by pumping for large-scale loads are new. However, there are several studies that demonstrate its advantages in renewable systems [39]–[48]. It is for this reason that, the originality of this document lies in the analysis of the impact of each ESS on the microgrid (PV-WT-HKT), using parameters such as: Net Present Cost (NPC), Cost of Energy (COE), CO_2 emissions. The results are presented and analyzed in the document.

2 Metodology

In this article, the input variables are: (radiation, wind and river speed) and customers load for one year, as shown in sections 2.1 and 2.2. Using the Homer software, it is possible to sizing optimization of microgrid through simulations, in section 2.3 a mathematical representation of the components formed by the microgrid has been made. It is important to mention that the models are idealized. In this case, the input variables for each component are: capital and maintenance costs, fuel cost, battery minimum SOC and system life expectancy. Afterwards, simulations have been carried out by choosing the type of control (CC, LF and CD) that have been explained in section 2.4. The output variables are: power of each component of the microgrid, NPC, COE, CO_2

emissions calculated through thousands of simulations, the software calculates the optimal technical-economic result presented in section 2.5. Finally, in section 3 the conclusions of the article have been discussed, indicating aspects and final considerations of the document.

2.1 Background

The daily energy load of consumers is considered a National University of Education (UNAE) located in southern Ecuador, shown in Fig. 1. Demand data has been provided by the University the demand is similar to a residential load. The area has constant temperatures throughout the year, therefore the average annual demand has not presented variations. The loads are mostly resistive, and there have been no high variations in demand.

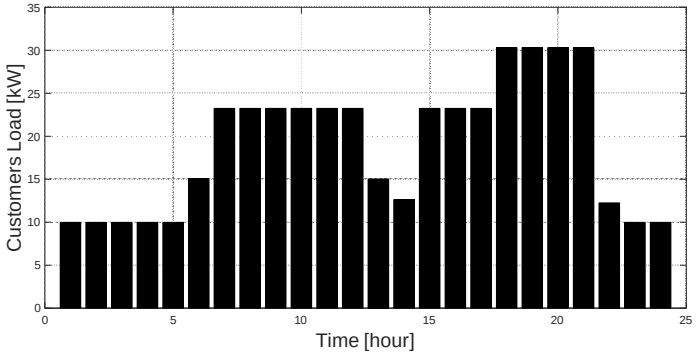

Fig. 1. Electric demand daily

2.2 Renewable Resources

The University is located near a river and a mountain range, there are renewable resources that can be used (wind, speed river and solar radiation). The global solar radiation is show in Fig. 2, the wind speed in Fig. 3 and the river speed in Fig. 4 respectively, Data were taken from the weather station with a sampling rate of one hour for one year.

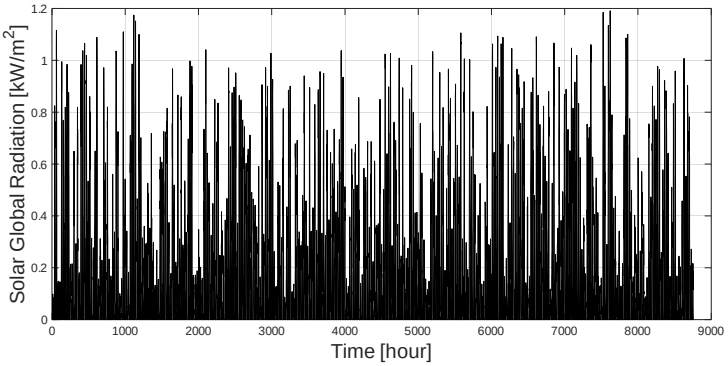

Fig. 2. Global solar radiation [kW/m^2]

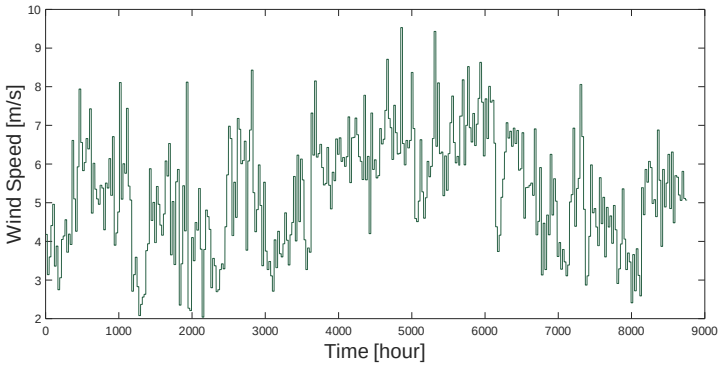

Fig. 3. Annual average wind speed in (m/s)

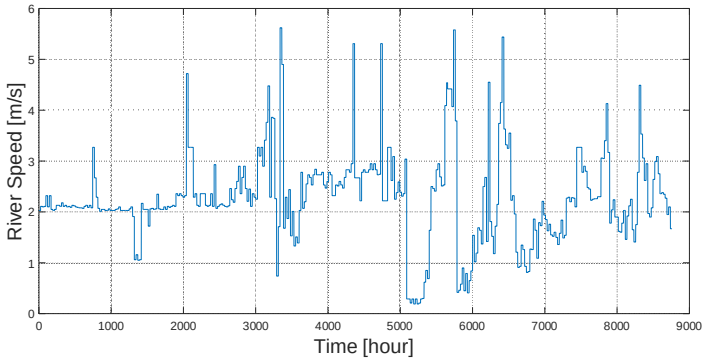

Fig. 4. Annual average river speed in (m/s)

2.3 Modeling of systems

The renewable components and storage system are shown in Fig. 5, a mathematical model has been made for the simulation of each one of them.

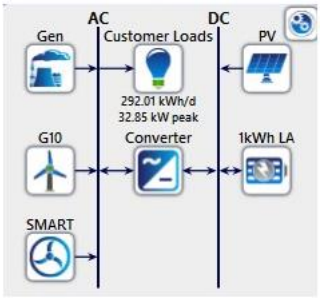

Fig. 5. Microgrid components under study (HOMER)

2.3.1. Modeling of PV Array

The Equation (1) shows the output in the PV system [49]:

$$P_{PV} = Y_{PV} * f_{PV} * \left(\frac{\bar{G}_T}{\bar{G}_{T,\,STC}}\right) * [1+\alpha_P * (T_c - T_{c,STC})] \quad (1)$$

Where:

Y_{PV} = the rated capacity of the PV array, meaning its power output under standard test conditions [kW].

f_{PV} = the PV derating factor [%], in this study is considered 80%

$\bar{G}_T$ = the solar radiation incident on the PV array in the current time step [kW/m^2]

$\bar{G}_{T,\,STC}$ = the incident radiation at standard test conditions [1 kW/m^2]

α_P = the temperature coefficient of power [%/°C], in this case -0.37 %/°C

T_c = the PV cell temperature in the current time step [°C]

$T_{c,STC}$ = the PV cell temperature under standard test conditions [25 °C]

2.3.2. Modeling of Hydrokinetic turbine

The power of the hydrokinetic turbine is given by Equation (2) [20].

$$P_{HKT} = \frac{1}{2} * \rho w * A * v^3 * C_{p,H} * \eta_{HKT} \quad (2)$$

Where: P_{HKT} is the power of the hydrokinetic turbine (HKT), (ρw) is the water density in kg/m^3, HKT performance coefficient ($C_{p,H}$), combined HKT-generator efficiency (η_{HKT}), HKT area (A) in m^2, water flow velocity (v) in m/s and time (t) in seconds.

2.3.3. Modeling of wind turbine

The available power of each wind turbine is given by Equation (3):

$$P_{WT} = k_1 * C_p * (\alpha_i) * v_i^3 \quad (3)$$

Where: P_{WT} Is the nominal power limit of the wind turbine, $k_1 = (\pi\rho R^2/2)$, ρ is the air density, R is the radius of the rotor, C_p is the power coefficient and v_i the wind speed [50].

2.3.4. Modeling of the diesel generator

The fuel consumption for the production of electricity is calculated according to Equation. (4) [49], [51].

$$F = F_{0,dg} * Y_{dg} + F_{1dg} * P_{dg} \quad (4)$$

Where, F es the fuel consumption, F_0 the intercept coefficient of the fuel curve is (0.000205m^3/h), F_1 is the slope of the fuel curve (0.00025 m^3/h/kW), Y_{dg} (kW) is the nominal capacity of the generator and P_{dg} (kW) is the electrical power. The lowest calorific value of diesel fuel is 43.2 MJ/kg with a density of 820 kg/m^3 [51]. The Duty Factor (DF), (kWh/start-stop/year) is the ratio of power generation of the supplementary primary motors to the total start stop and can be calculated using Equation. (5), where is the number of start-stop [52].

$$DF = \frac{P_{dg}}{N_{s/s}} \quad (5)$$

2.3.5. Modeling of Batteries

Equation. (6) determines the maximum load power of the storage system (battery) [49].

$$P_b(t) = \frac{k*Q_1(t)*e^{-k} + Q(t)*k*c*(1-e^{-k*\Delta t})}{1-e^{-k*\Delta t} + c*(k*\Delta t - 1 + e^{-k*\Delta t})} \quad (6)$$

Where: $Q_1(t)$ is the energy available at the beginning of the operating interval in the minimum SOC. In the case of Lead Acid batteries (LAB) this value is 40%, in Li-Ion batteries it is 20% and those of VRF is 0%, the maximum SOC for the three systems will be 100% considering idealized models. $Q(t)$ Is the total energy at the beginning of the passage of time, c is the ratio of the storage capacity of each system, k is the constant energy storage rate, and Δt is the time interval, more detailed calculations can be found from HOMER help manual [53].

2.3.6. Modeling of supercapacitor

Energy stored (joules) in a supercapacitor can be calculated using the Equation (7):

$$E = \frac{1}{2} C*V^2 \quad (7)$$

Where: E is the energy stored in joules, C is the capacitance in farads, and V is the voltage. In this case, the idealized battery model has been used [54].

2.3.7. Modeling of pumped storage hydropower

The flow rate is the amount of water (m^3/s) that flows in or out, the energy storage capacity of a pumped hydroelectric system is calculated using Equation (8):

$$E = 9.81 * \rho_{water} * V_{res} * h_{head} * \eta \quad (8)$$

Where:

E = is the energy stored in joules.

ρ_{water} = is the density of water usually about 1000 kg/m^3.

V_{res} = is the volume of the reservoir in cubic meters, in this case 1000 m^3

h_{head} = is the head height in meters, in this study 100 m.

η = is the efficiency of the energy conversion, and must consider losses like turbine efficiency, generator efficiency, and hydrodynamic losses, usually 90% [53].

2.3.8. Modeling of Inverter DC/AC

In this study an inverter is used to connect the DC buss with the AC current, by equation (9) the power of the load side is determined [30].

$$P_0(t) = P_i(t) * \eta_{inv} \quad (9)$$

Where: $P_0(t)$ is the power output of the inverter, $P_i(t)$ is the input power of the inverter and η_{inv} is the efficiency of the inverter, in this case 96%. The capacity of the inverter is automatically selected by the software. The input power of the inverter will be formed by the power of the PV system, power of the fuel cell and the power of the battery system.

2.4 Energy Control

2.4.1. Dispatch strategy Load Cycle

This type of control has the objective of charging the batteries through the diesel generator when there is a deficit of energy from the renewable sources, in such a way that the battery has the capacity to supply the demand, the operating algorithm is indicated in Fig. 6.

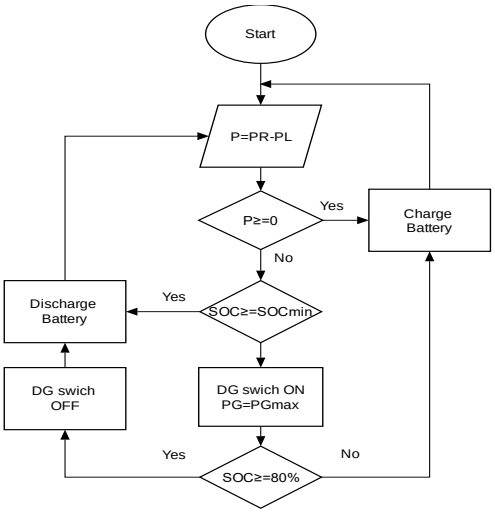

Fig. 6. Cycle charging control (LC)

Where: P is a designated variable, PR is the total renewable output power formed by the PV system including the power of the hydrokinetic system, PL is the power of the load, SOC is the state of charge of the battery, DG is the diesel generator and PG the power of the diesel generator.

At the beginning of the cycle there is a power balance between generation and demand, PR = PL.

If, ($P \geq 0$) there is excess energy, charge the batteries.

If, ($P < 0$) the system does not have the capacity to supply the demand so you must obtain the missing power from the battery system only if ($SOC \geq SOC_{min}$).

If, ($SOC < SOC_{min}$) start the diesel generator, $PG = PG_{max}$, ensuring that the batteries are charged in the shortest possible time, when $SOC \geq 80\%$ (early ensures energy supply through the ESS), the diesel generator is turned off [49], [55].

2.4.2. Dispatch strategy Load Following

In this type of control the starting of the diesel generator will have as a priority to supply the demand and not to charge the batteries as in the previous case, the algorithm is shown in Fig. 7.

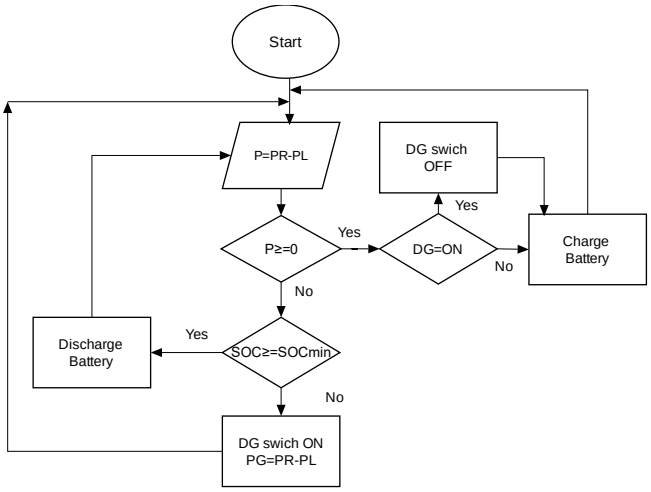

Fig. 7. Load Following control (LF)

P is a designated variable, PR is the total renewable output power, PL is the power of the load, SOC is the state of charge of the battery, DG is the diesel generator and PG the power of the diesel generator.

Initially the ideal conditions are (PR = PL), if there is an excess of electricity, that is; ($P \geq 0$), the system must charge the batteries ensuring that the diesel generator is at rest, in case of having less renewable power than required by the load, ($P < 0$), the storage system must provide the missing power in case of being in a state of charge greater than or equal to the minimum depending on each type of battery, if not, must start the diesel generator only to supply the load, providing the necessary energy, the diesel generator is switched off when the generation of renewable power is greater than the power requiered by the load, it is then that the battery is charged, with the excess of energy coming from renewable sources [49], [55].

2.4.3. Combined Cycle Dispatch Strategy

In this type of control, the system must be able to operate under the type of dispatch that is most economical according to the operating conditions existing at each moment, the logic of this type of dispatch is shown in Fig. 8.

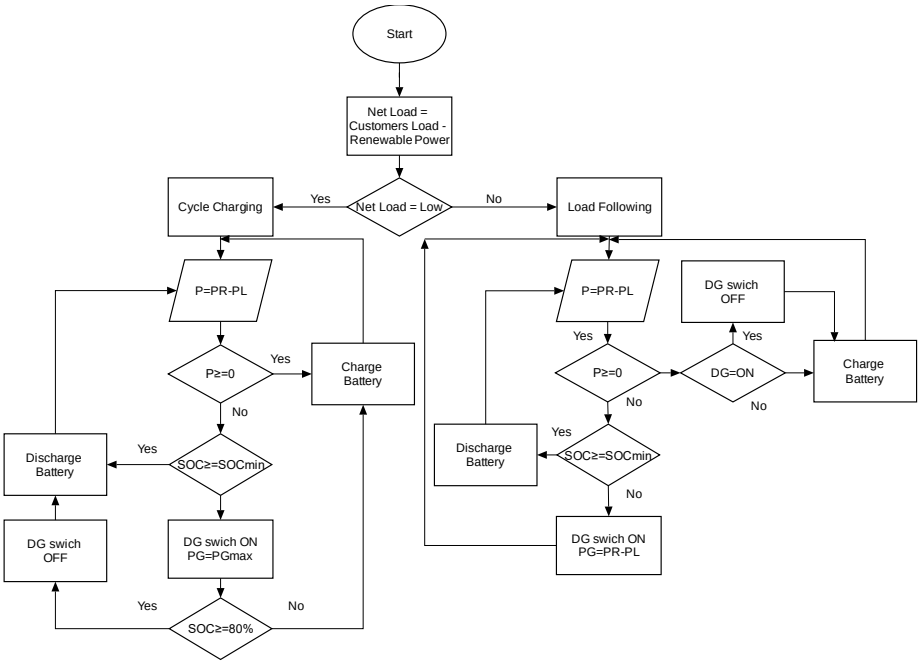

Fig. 8. Combined Cycle Dispatch Strategy (CD)

The decision of the controller depends on the cost of energy production. Depending on the system conditions, the controller must choose between the cycle charging and load following controls. Because customers load is random as well as renewable generation, the combined dispatch strategy uses the current net charge (consumer load - renewable power) to make a decision. The controller must use the cycle charging strategy if the current net load is low, approximately less than 20% of the total load power. On the contrary, if the current net load is high the controller must choose the load following strategy. Homer optimizes each of the options to meet the demand by comparing the cost of charging the battery with the diesel generator with the cost of charging the battery using excess renewable energy [55].

2.5 Results and comments

The simulation of the microgrid has been performed in the Homer software, in each case the best possible performance in the system has been obtained, therefore the net present cost NPC in each case is the lowest. The LC, LF and CD energy control strategies have been used to analyze the behavior of the microgrid with different energy storage systems (lead acid, li-ion, VRF batteries, pumped hydroelectricity and supercapacitor). The results show that: the analysis with respect to NPC and COE are observed in Fig. 9 and 10 respectively, to the load control cycle, the system with NPC and COE. In contrast, the lower NPC and COE present the supercapacitor and pumped hydroelectricity in LF control. On the other hand, use the following load control, the highest NPC and COE as the acid lead storage system, the lowest NPC and COE has the hydraulic pumping system. Similarly, using the combined control cycle, lead-acid batteries show even more

their NPC and COE compared to the previous cases, and the lower NPC and COE costs are maintained in the hydraulic pumping system.

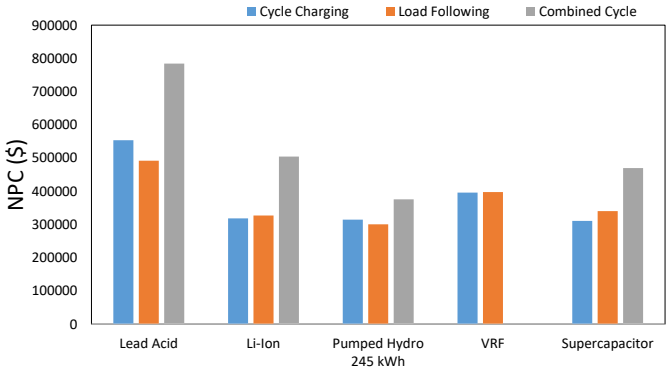

Fig. 9. Variation of net present cost (NPC) in different operating conditions

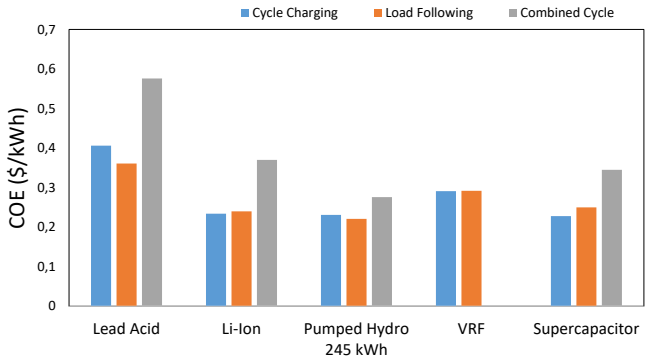

Fig. 10. Variation of cost of energy (COE) in different operating conditions

In Fig. 11 the three types of control have been compared with respect to the different storage systems with the following results: with the cycle charging control system, the systems that provide the greatest amount of CO_2 are: the supercapacitor and the VRF. On the other hand, lead acid batteries emit the least CO_2. Using the load following control changes the result since, the systems with the highest CO_2 emission are: lead acid, VRF and supercapacitor with similar values, on the other hand the system with the lowest emissions is pumped hydro. Similarly, using the combined cycle it can be seen that the emissions produced by lead acid batteries have decreased considerably and pumped hydro emissions have increased, the other systems still have high CO_2 emissions. These results are the product of the type of ESS, its response time to load peaks and the state of charge of each system.

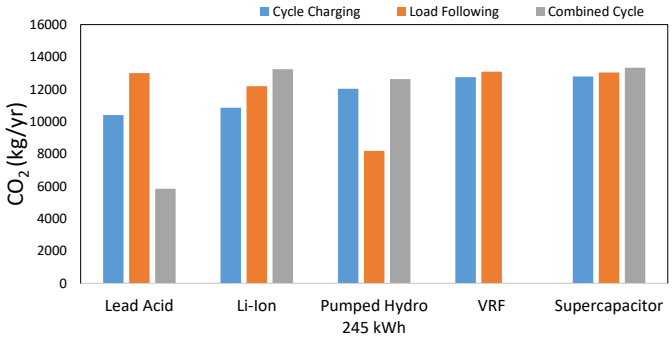

Fig. 11. Variation of CO_2 in different operating conditions

3 Conclusions

In this study the best storage system could be the pumped hydro for its best results. However, the results could vary depending on the type of load and the future growth of demand. However, the geological conditions necessary for this type of storage should be determined, since an approximated model has been used. The supercapacitor could be an eligible solution. Though, there are no high load variations to justify this type of storage. Applications where VRF batteries would be optimal should require high power density, in this case it is not required. After all, the results have indicated the possibility of using them without violating any restrictions. On the other hand, lead acid batteries could be used as an old and easily manufactured technology. Nonetheless, Lithium Ion batteries have presented lower levels of pollution and cost. Therefore, Li-Ion is the recommended technology for this case, considering the different points of view discussed. Finally, in future studies, indices such as: excess energy, renewable penetration and unmet load should be analyzed. In addition, sensitivity analyzes will be carried out considering variables such as: time step, capital cost and minimum SOC batteries, verifying more accurately the impact on the microgrid.

REFERENCES

[1] F. K. Abo-Elyousr and A. Elnozahy, "Bi-objective economic feasibility of hybrid microgrid systems with multiple fuel options for islanded areas in Egypt," *Renew. Energy*, vol. 128, pp. 37–56, Dec. 2018.

[2] H. J. Vermaak, K. Kusakana, and S. P. Koko, "Status of micro-hydrokinetic river technology in rural applications: A review of literature," *Renew. Sustain. Energy Rev.*, vol. 29, pp. 625–633, Jan. 2014.

[3] M. Castañeda, A. Cano, F. Jurado, H. Sánchez, and L. M. Fernández, "Sizing optimization, dynamic modeling and energy management strategies of a stand-alone PV/hydrogen/battery-based hybrid system," *Int. J. Hydrogen Energy*, vol. 38, no. 10,

pp. 3830–3845, Apr. 2013.

[4] O. Djelailia, M. S. Kelaiaia, H. Labar, S. Necaibia, and F. Merad, "Energy hybridization photovoltaic/diesel generator/pump storage hydroelectric management based on online optimal fuel consumption per kWh," *Sustain. Cities Soc.*, vol. 44, pp. 1–15, Jan. 2019.

[5] L. Olatomiwa, S. Mekhilef, M. S. Ismail, and M. Moghavvemi, "Energy management strategies in hybrid renewable energy systems: A review," *Renew. Sustain. Energy Rev.*, vol. 62, pp. 821–835, Sep. 2016.

[6] R. Siddaiah and R. P. Saini, "A review on planning, configurations, modeling and optimization techniques of hybrid renewable energy systems for off grid applications," *Renew. Sustain. Energy Rev.*, vol. 58, pp. 376–396, May 2016.

[7] A. H. Fathima and K. Palanisamy, "Optimization in microgrids with hybrid energy systems – A review," *Renew. Sustain. Energy Rev.*, vol. 45, pp. 431–446, May 2015.

[8] S. Bahramara, M. P. Moghaddam, and M. R. Haghifam, "Optimal planning of hybrid renewable energy systems using HOMER: A review," *Renew. Sustain. Energy Rev.*, vol. 62, pp. 609–620, Sep. 2016.

[9] M. Belouda, M. Hajjaji, H. Sliti, and A. Mami, "Bi-objective optimization of a standalone hybrid PV–Wind–battery system generation in a remote area in Tunisia," *Sustain. Energy, Grids Networks*, vol. 16, pp. 315–326, Dec. 2018.

[10] K. Anoune, M. Bouya, A. Astito, and A. Ben Abdellah, "Sizing methods and optimization techniques for PV-wind based hybrid renewable energy system: A review," *Renew. Sustain. Energy Rev.*, vol. 93, pp. 652–673, Oct. 2018.

[11] M. J. Khan, A. K. Yadav, and L. Mathew, "Techno economic feasibility analysis of different combinations of PV-Wind-Diesel-Battery hybrid system for telecommunication applications in different cities of Punjab, India," *Renew. Sustain. Energy Rev.*, vol. 76, pp. 577–607, Sep. 2017.

[12] I. V, S. V, and L. R, "Resources, configurations, and soft computing techniques for power management and control of PV/wind hybrid system," *Renew. Sustain. Energy Rev.*, vol. 69, pp. 129–143, Mar. 2017.

[13] A. S. Al Busaidi, H. A. Kazem, A. H. Al-Badi, and M. Farooq Khan, "A review of optimum sizing of hybrid PV–Wind renewable energy systems in oman," *Renew. Sustain. Energy Rev.*, vol. 53, pp. 185–193, Jan. 2016.

[14] A. Haghighat Mamaghani, S. A. Avella Escandon, B. Najafi, A. Shirazi, and F. Rinaldi, "Techno-economic feasibility of photovoltaic, wind, diesel and hybrid electrification systems for off-grid rural electrification in Colombia," *Renew. Energy*, vol. 97, pp. 293–305, Nov. 2016.

[15] A. Maleki, M. Ameri, and F. Keynia, "Scrutiny of multifarious particle swarm optimization for finding the optimal size of a PV/wind/battery hybrid system," *Renew. Energy*, vol. 80, pp. 552–563, Aug. 2015.

[16] S. Sinha and S. S. Chandel, "Review of recent trends in optimization techniques for solar photovoltaic-wind based hybrid energy systems," *Renewable and Sustainable Energy Reviews*, vol. 50. pp. 755–769, Oct-2015.

[17] A. Mahesh and K. S. Sandhu, "Hybrid wind/photovoltaic energy system developments: Critical review and findings," *Renew. Sustain. Energy Rev.*, vol. 52, pp. 1135–1147, Dec. 2015.

[18] V. Khare, S. Nema, and P. Baredar, "Solar–wind hybrid renewable energy system: A

review," *Renew. Sustain. Energy Rev.*, vol. 58, pp. 23–33, May 2016.

[19] A. Kaabeche and Y. Bakelli, "Renewable hybrid system size optimization considering various electrochemical energy storage technologies," *Energy Convers. Manag.*, vol. 193, pp. 162–175, Aug. 2019.

[20] J. Lata-García, F. Jurado, L. M. Fernández-Ramírez, and H. Sánchez-Sainz, "Optimal hydrokinetic turbine location and techno-economic analysis of a hybrid system based on photovoltaic/hydrokinetic/hydrogen/battery," *Energy*, vol. 159, pp. 611–620, Sep. 2018.

[21] J. Lata-Garcia, F. Jurado-Melguizo, H. Sanchez-Sainz, C. Reyes-Lopez, and L. Fernandez-Ramirez, "Optimal sizing hydrokinetic-photovoltaic system for electricity generation in a protected wildlife area of Ecuador," *Turkish J. Electr. Eng. Comput. Sci.*, vol. 26, no. 2, pp. 1103–1114, 2018.

[22] K. Kusakana, "Optimization of the daily operation of a hydrokinetic–diesel hybrid system with pumped hydro storage," *Energy Convers. Manag.*, vol. 106, pp. 901–910, Dec. 2015.

[23] K. Kusakana, "Energy management of a grid-connected hydrokinetic system under Time of Use tariff," *Renew. Energy*, vol. 101, pp. 1325–1333, Feb. 2017.

[24] K. Kusakana and H. J. Vermaak, "Cost and Performance Evaluation of Hydrokinetic-diesel Hybrid Systems," *Energy Procedia*, vol. 61, pp. 2439–2442, Jan. 2014.

[25] K. Kusakana, "Techno-economic analysis of off-grid hydrokinetic-based hybrid energy systems for onshore/remote area in South Africa," *Energy*, vol. 68, pp. 947–957, Apr. 2014.

[26] S. P. Koko, K. Kusakana, and H. J. Vermaak, "Optimal power dispatch of a grid-interactive micro-hydrokinetic-pumped hydro storage system," *J. Energy Storage*, vol. 17, pp. 63–72, Jun. 2018.

[27] K. Kusakana and H. J. Vermaak, "Hydrokinetic power generation for rural electricity supply: Case of South Africa," *Renew. Energy*, vol. 55, pp. 467–473, Jul. 2013.

[28] D. Kumar and S. Sarkar, "A review on the technology, performance, design optimization, reliability, techno-economics and environmental impacts of hydrokinetic energy conversion systems," *Renew. Sustain. Energy Rev.*, vol. 58, pp. 796–813, May 2016.

[29] K. Kusakana, "Feasibility analysis of river off-grid hydrokinetic systems with pumped hydro storage in rural applications," *Energy Convers. Manag.*, vol. 96, pp. 352–362, May 2015.

[30] B. K. Das and F. Zaman, "Performance analysis of a PV/Diesel hybrid system for a remote area in Bangladesh: Effects of dispatch strategies, batteries, and generator selection," *Energy*, vol. 169, pp. 263–276, Feb. 2019.

[31] M. Ghorbanzadeh, M. Astaneh, and F. Golzar, "Long-term degradation based analysis for lithium-ion batteries in off-grid wind-battery renewable energy systems," *Energy*, vol. 166, pp. 1194–1206, Jan. 2019.

[32] R. G. Charles, M. L. Davies, P. Douglas, I. L. Hallin, and I. Mabbett, "Sustainable energy storage for solar home systems in rural Sub-Saharan Africa – A comparative examination of lifecycle aspects of battery technologies for circular economy, with emphasis on the South African context," *Energy*, vol. 166, pp. 1207–1215, Jan. 2019.

[33] S. Hajiaghasi, A. Salemnia, and M. Hamzeh, "Hybrid energy storage system for

microgrids applications: A review," *Journal of Energy Storage*, vol. 21. pp. 543–570, Feb-2019.

[34] C. Liu, Y. Wang, and Z. Chen, "Degradation model and cycle life prediction for lithium-ion battery used in hybrid energy storage system," *Energy*, vol. 166, pp. 796–806, Jan. 2019.

[35] A. Parasuraman, T. M. Lim, C. Menictas, and M. Skyllas-Kazacos, "Review of material research and development for vanadium redox flow battery applications," *Electrochim. Acta*, vol. 101, pp. 27–40, Jul. 2013.

[36] P. Alotto, M. Guarnieri, and F. Moro, "Redox flow batteries for the storage of renewable energy: A review," *Renew. Sustain. Energy Rev.*, vol. 29, pp. 325–335, Jan. 2014.

[37] B. K. Das, Y. M. Al-Abdeli, and M. Woolridge, "Effects of battery technology and load scalability on stand-alone PV/ICE hybrid micro-grid system performance," *Energy*, vol. 168, pp. 57–69, Feb. 2019.

[38] B. Zakeri and S. Syri, "Electrical energy storage systems: A comparative life cycle cost analysis," *Renew. Sustain. Energy Rev.*, vol. 42, pp. 569–596, Feb. 2015.

[39] A. Abdelkader, A. Rabeh, D. Mohamed Ali, and J. Mohamed, "Multi-objective genetic algorithm based sizing optimization of a stand-alone wind/PV power supply system with enhanced battery/supercapacitor hybrid energy storage," *Energy*, vol. 163, pp. 351–363, Nov. 2018.

[40] L. W. Chong, Y. W. Wong, R. K. Rajkumar, and D. Isa, "An adaptive learning control strategy for standalone PV system with battery-supercapacitor hybrid energy storage system," *J. Power Sources*, vol. 394, pp. 35–49, Aug. 2018.

[41] L. Kong, J. Yu, and G. Cai, "Modeling, control and simulation of a photovoltaic /hydrogen/ supercapacitor hybrid power generation system for grid-connected applications," *Int. J. Hydrogen Energy*, Jun. 2019.

[42] L. W. Chong, Y. W. Wong, R. K. Rajkumar, and D. Isa, "An optimal control strategy for standalone PV system with Battery-Supercapacitor Hybrid Energy Storage System," *J. Power Sources*, vol. 331, pp. 553–565, Nov. 2016.

[43] K. Sun, K.-J. Li, J. Pan, Y. Liu, and Y. Liu, "An optimal combined operation scheme for pumped storage and hybrid wind-photovoltaic complementary power generation system," *Appl. Energy*, vol. 242, pp. 1155–1163, May 2019.

[44] M. Miao, Z. Wu, S. Lou, and Y. Wang, "Research on Optimizing Operation of Hybrid PV Power and Pumped Hydro Storage System," *Energy Procedia*, vol. 118, pp. 110–118, Aug. 2017.

[45] A. Rathore and N. P. Patidar, "Reliability assessment using probabilistic modelling of pumped storage hydro plant with PV-Wind based standalone microgrid," *Int. J. Electr. Power Energy Syst.*, vol. 106, pp. 17–32, Mar. 2019.

[46] G. Notton, D. Mistrushi, L. Stoyanov, and P. Berberi, "Operation of a photovoltaic-wind plant with a hydro pumping-storage for electricity peak-shaving in an island context," *Sol. Energy*, vol. 157, pp. 20–34, Nov. 2017.

[47] B. Xu, D. Chen, M. Venkateshkumar, Y. Xiao, and Y. Xing, "Modeling a pumped storage power integration to a hybrid power system with solar-wind power and its stability analysis," *Energy Procedia*, vol. 158, pp. 6225–6230, Feb. 2019.

[48] C.-L. Chen, H.-C. Chen, and J.-Y. Lee, "Application of a generic superstructure-based formulation to the design of wind-pumped-storage hybrid systems on remote islands,"

Energy Convers. Manag., vol. 111, pp. 339–351, Mar. 2016.

[49] P. Arévalo, D. Benavides, J. Lata-García, and F. Jurado, "Energy Control and Size Optimization of a Hybrid System (Photovoltaic-Hidrokinetic) Using Various Storage Technologies," *Sustain. Cities Soc.*, p. 101773, Aug. 2019.

[50] S. Siniscalchi-Minna, F. D. Bianchi, M. De-Prada-Gil, and C. Ocampo-Martinez, "A wind farm control strategy for power reserve maximization," *Renew. Energy*, vol. 131, pp. 37–44, Feb. 2019.

[51] F. Khalid, I. Dincer, and M. A. Rosen, "Thermoeconomic analysis of a solar-biomass integrated multigeneration system for a community," *Appl. Therm. Eng.*, vol. 120, pp. 645–653, Jun. 2017.

[52] A. Askarzadeh, "Distribution generation by photovoltaic and diesel generator systems: Energy management and size optimization by a new approach for a stand-alone application," *Energy*, vol. 122, pp. 542–551, Mar. 2017.

[53] "HOMER CALCULATIONS." [Online]. Available: https://www.homerenergy.com/products/pro/docs/3.11/homers_calculations.html. [Accessed: 08-Feb-2019].

[54] D. N. Luta and A. K. Raji, "Optimal sizing of hybrid fuel cell-supercapacitor storage system for off-grid renewable applications," *Energy*, vol. 166, pp. 530–540, Jan. 2019.

Technical Comparison of Specific Software Used in the Design of Ground Source Heat Pump Systems

Cristina Sáez Blázquez[1] [0000-0002-5333-0076], Ignacio Martín Nieto[2][0000-0003-3984-7228], Arturo Farfán Martín[3] and Diego González-Aguilera[4] [0000-0002-8949-4216]

[1] TIDOP Group, Department of Cartographic and Land Engineering, University of Salamanca, Higher Polytechnic School of Avila, Hornos Caleros 50, 05003 Avila, Spain
u107596@usal.es

Abstract. An accurate design of a ground source heat pump system is crucial to ensure the future operation of the geothermal installation. PC-programs usually constitute the most optimal and quick solution for the dimensioning of the mentioned systems. In this regard, Earth Energy Designer *(EED)* software is frequently used by specialized users for the design of closed vertical geothermal loops. Based on the weaknesses detected on this program and the enhanced knowledge of the geothermal operation from different research studies, a new geothermal tool, GES-CAL, has been developed. In this way, the principal objective of this study is to evaluate this new software and to compare the results of both PC-programs. This comparison derives from the application of both tools in the calculation of the same study case. Results obtained in this research show that GES-CAL software is an accurate and valid alternative for the design of all heat exchanger configurations, especially for those installations placed in the region of Ávila. EED, is however, recommended for the calculation of high power geothermal systems that require an exhaustive analysis of the ground and heat carrier fluid behavior.

Keywords: ground source heat pump system, EED, GES-CAL.

1 Introduction

Ground source heat pump technologies that directly use the heat of the ground are counted among the most sustainable choices for space heating [1-2]. Heat is extracted from the ground at a relatively low temperature which is then increased through the heat pump and use in a heating system. Depending on the way of using the working fluid, these systems are commonly classified as open or closed systems. In the first place, open systems use groundwater as heat carrier fluid brought to the heat pump through an extraction borehole. Closed systems are characterized by the use of a mixture of water-glycol as working fluid and heat exchangers located in the underground (either in a horizontal, vertical or oblique fashion).

Focusing on the last group (closed systems) for being the most frequent configuration, the correct design of the heat exchangers is crucial to ensure the future operation of the system. PC-programs constitute a quick and reasonably sound dimensioning of

ground source heat pump systems [3-5]. In this context, Earth Energy designer *(EED)* is one of the most accessible and user-friendly programs that allows an accurate design of the final geothermal schema. Despite the large number of advantages of EED software, it only enables the dimensioning of vertical closed loop systems, that is to say, horizontal and helical heat exchanger configurations are not considered by EED.

With the aim of dealing with a broader range of possibilities, this research also considers the use of a new approach, GES-CAL software, which allows the design of all the possible heat exchanger configurations. The development of this new tool is based on the results and conclusions of already published research works [6-12].

This research is focused on evaluating and comparing both geothermal programs (EED and GES-CAL) from their application on a particular study case with identical input data. In the following sections, EED and GES-CAL software are described and applied for the calculation of a shallow geothermal system to supply the energy demand of a certain space. Sections 2 and 3 describe the process of calculation of both software, section 4 presents the principal results when using the programs and finally, section 5 contains the main conclusions of the manuscript.

2 Materials and method

As mentioned in the introductory section, the objective of this work is the comparison of the specific geothermal software, EED and GES-CAL. These programs are described below as well as the particular case where they have been implemented.

2.1 Brief description of the geothermal software

Earth Energy Designer (EED)

This PC-program, developed by Blocon *(Buildingphysics.com)*, is typically used in the design of vertical borehole heat exchangers in a ground source heat pump system. Algorithms are derived from modeling studies with a numerical simulation model that results in analytical solutions of the heat flow with several possibilities of geometry and borehole patterns.

Fig. 1. Earth Energy Designer main window.

First of all, the user must introduce some information concerning the ground, climatic conditions, space energy demand and geothermal components and configuration. After the introduction of these initial data, EED software is capable of providing the final schema of the system in terms of borehole's number and drilling length and the evolution of the temperature of the heat carrier fluid over the installation lifetime.

Table 1 includes the principal strengths and weaknesses found when using EED software.

Table 1. Strengths and weaknesses of EED software.

EED software	
Strengths	**Weaknesses**
Quick and easy use	
Simulation of the ground and fluid behavior over the system operation	Only vertical heat exchangers
Possibility of selecting different drilling schemas	It does not allow the calculation of the space energy demand
Different range of restrictions for the heat carrier fluid temperature	Manual dimensioning of the heat pump power
Multiple solutions for the final well field design	Standard properties for the geological formations

GES-CAL

GES-CAL software is created by some members of the TIDOP Research Unit from the University of Salamanca (registration of the intellectual property 00/2019/3318). The development of this software is linked to the need of improving some modules of EED. Despite its first version is specifically designed for the dimensioning of ground source heat pump systems in the region of Ávila (Spain), it can be also implemented in any other location.

Calculations of this PC-program are based on the recommendations of IDAE *(Institute for the diversification and energy saving)* [13] and the results of previous research works [6-12]. The mentioned researches allowed establishing the most appropriate working conditions concerning the ground thermal characterization, building energy demand, grouting material and besides the fact that GES-CAL allows the selection of the most usual heat exchanger configurations (vertical, horizontal or helical designs).

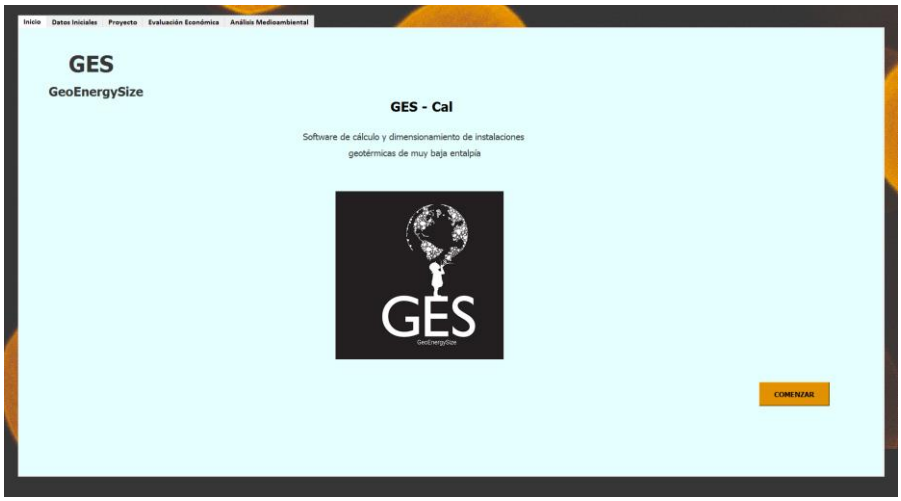

Fig. 2. GES-CAL main window.

Table 2. Strengths and weaknesses of GES-CAL software.

GES-CAL software	
Strengths	**Weaknesses**
Quick and easy use	It does not provide simulations of the fluid temperature evolution
Vertical, horizontal and helical configurations	The first version is specially developed only for the region of Ávila (Spain)
Enhanced thermal characterization of the ground	Geological information limited to the aforementioned area
It allows the calculation of the space energy demand	It is not recommended for high power installations, above 70 kW [14]
Automatic calculation of the final heat pump power	
Economic and environmental evaluation	

2.2 Input data

The application of the software described above has been focused on the determination of geothermal schema to cover the heating demand of a particular study case. Table 3 shows the characteristics and conditions of the mentioned case.

Table 3. Information of the building where the ground source heat pump systems is planned to be installed.

Space information	
Area	100 m^2
Height	4 m
Location	Ávila (Spain)
Building type	Single family house
Year of construction	2018
Available ground dimension	20 x 20 m
Geology	Granitic formations

3 Calculation process

3.1 EED

Before using EED, the energy demand of the building must be determined since this software does not include a specific module for its calculation. For this reason, the energy demand was calculated by the use of an external tool based on the regulation UNE-EN 13790:2011 [15]. Thus, as Figure 3 shows, the heating energy demand for the building of the study is 36.590 kWh/year.

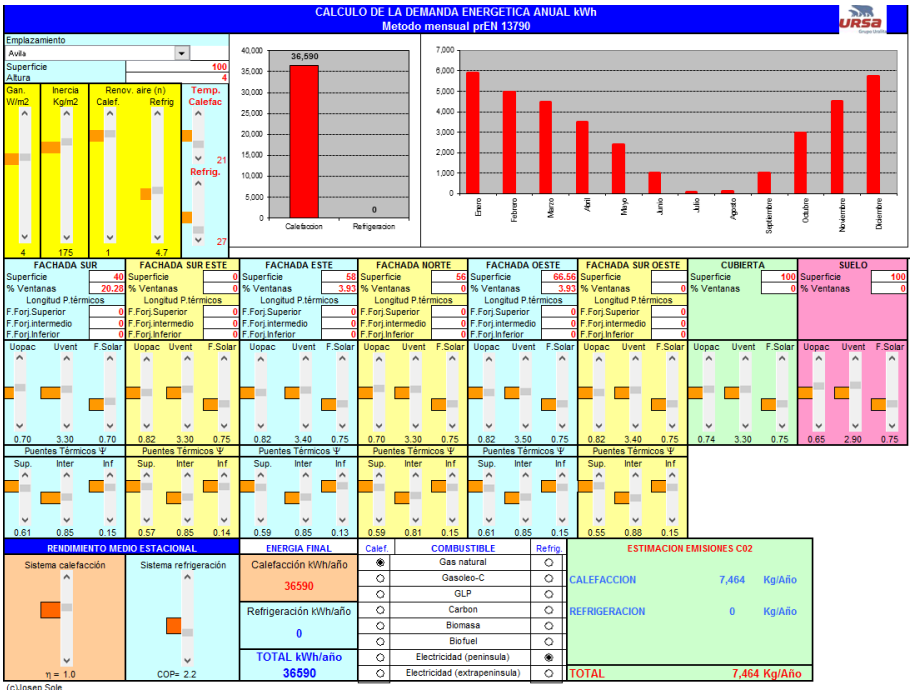

Fig. 3. Calculation of the building energy demand.

Once the energy demand is known, the following steps involve the introduction of several input data in EED software.

- Ground properties: EED provides standard thermal values for a set of geological formations. As the building is located in a granitic environment, the parameters corresponding to this formation are selected. Regarding the ground superficial temperature, this software does not include the region of Ávila, so a similar climatic area was selected.

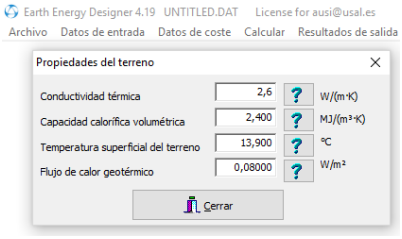

Fig. 4. Selection of the ground properties in EED.

- Heat exchanger configuration: selection of the vertical design (simple-U, double-U or coaxial), drilling characteristics and grouting material.

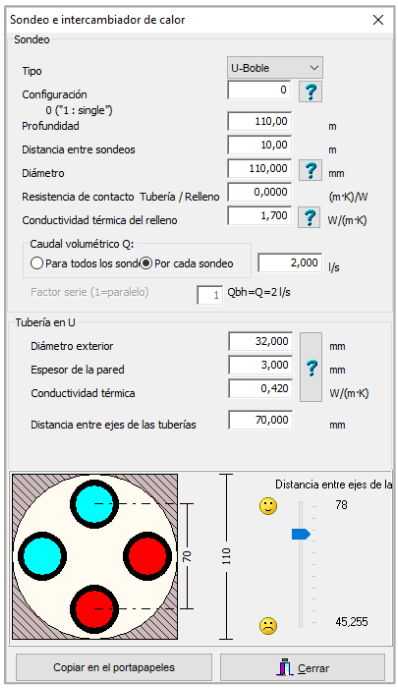

Fig. 5. Heat exchanger configuration in EED.

- Base and peak demand: introducing the building energy demand (previously calculated), EED provides the initial heat pump power that must be oversized by the user and introduced in the software.

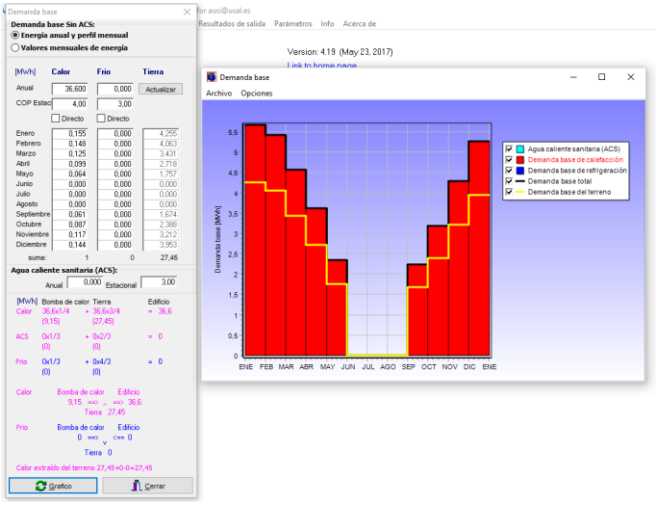

Fig. 6. Base and peak demand in software EED.

- Schema of the ground source heat pump system: the final result of EED software is the dimensioning of the drilling configuration; number of boreholes and total drilling length (Fig.7) as well as the evolution of the working fluid temperature (Fig.8). EED provides multiple drilling schemas so the user selects one of them.

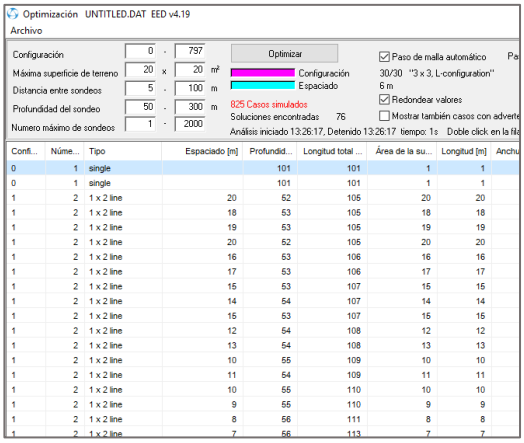

Fig. 7. Configuration of the well field by EED.

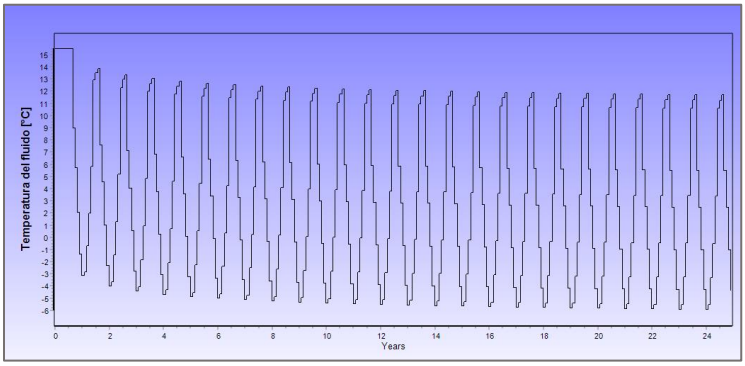

Fig. 8. Evolution of the working fluid temperature in EED.

3.2 GES-CAL

GES-CAL software incorporates a module for the calculation of the space energy demand based on the area, height, orientation and year of construction. In this way, the energy demand was automatically determined by this program and, as can be observed in Fig. 9, it takes the value of 36.680,80 kWh/year.

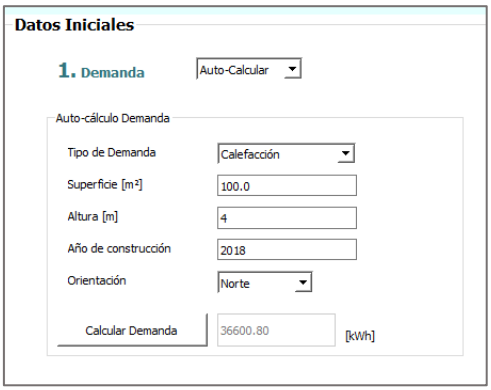

Fig. 9. Module to calculate the energy demand of the building in GES-CAL.

- Heat pump dimensioning: GES-CAL is capable of automatically defining the final heat pump power without additional user calculations.

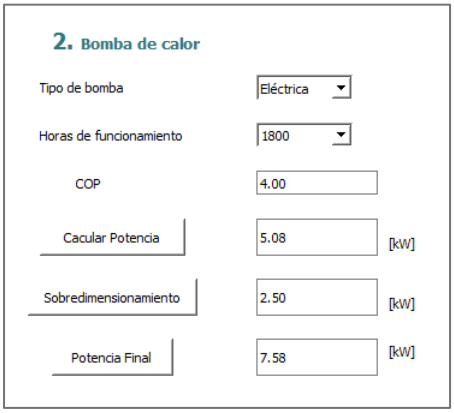

Fig. 10. Heat pump dimensioning in GES-CAL.

- Ground properties, heat exchangers and grouting material: as GES-CAL is specifically designed for the region of Ávila (location of the building of this research), it allows selecting the area of the province where the building is located (Fig.11). Once selected the area, GES-CAL automatically introduces the thermal properties of the ground. In addition to the ground information, heat exchanger configuration and grouting material must be defined by the user. Although GES-CAL considers the three most important designs, in this research the vertical double-U tubes are selected with the aim of keeping the same conditions in both programs. Grouting material is also the same in both assumptions.

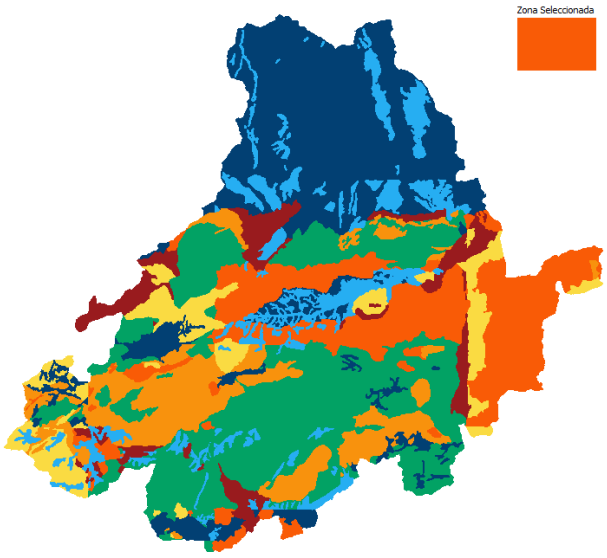

Fig. 11. Selection of the area of study in GES-CAL.

- Well field design: once all the initial data are defined, GES-CAL provides the final configuration of the well field, offering three possible alternatives (Fig.12).

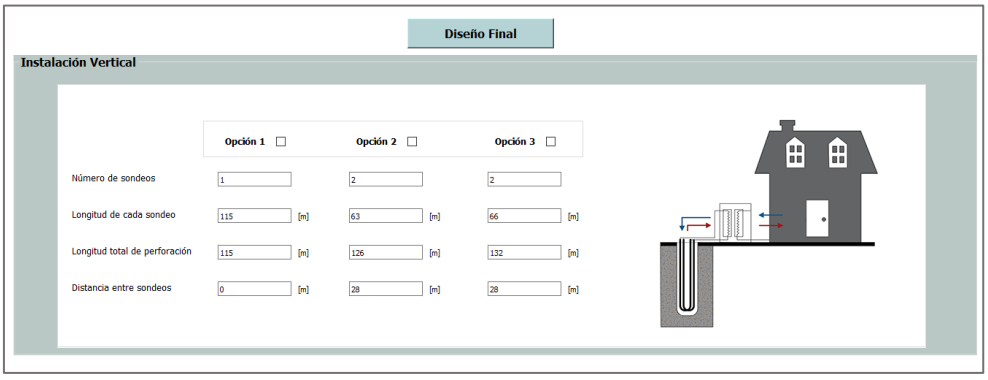

Fig.12. Final design of the well field by GES-CAL.

- Economic and environmental evaluation: GES-CAL also offers the possibility of estimating the initial investment of the system and its operational costs. It also compares the economic evolution of the ground source heat pump system compared to other energy sources (Fig.13).

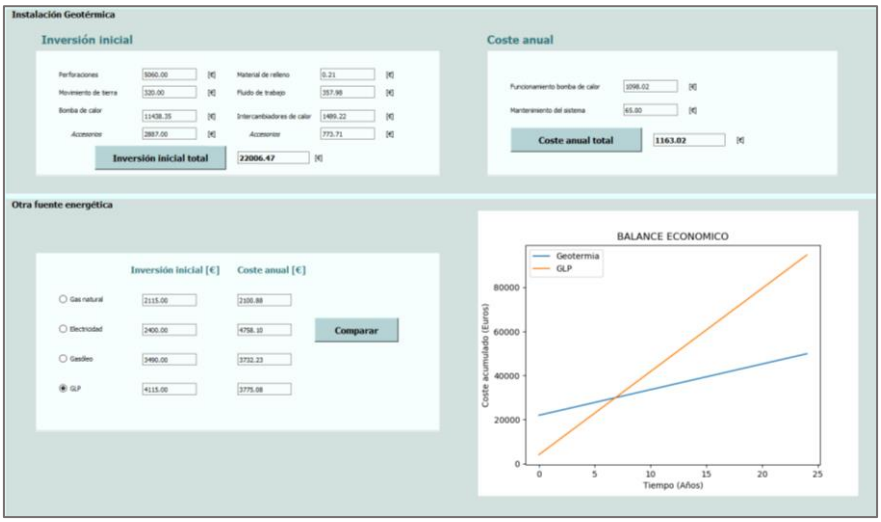

Fig. 13. Economic evaluation of the ground source heat pump system in GES-CAL.

As shown in Figure 14, this software additionally calculates the emissions of greenhouse gases associated to the use of the geothermal system during the whole lifetime period and compares it with the emissions of other energy sources.

Fig. 14. Environmental evaluation of the geothermal system in GES-CAL.

4 Results and discussion

This research solves the configuration of the well field in a ground source heat pump system from two different procedures; the commonly used EED and the new software

GES-CAL. From the calculation of both PC-programs (detailed in the previous section) the final schema of the geothermal system for the case presented in this work is included in Table 2.

Table 3. Configuration of the geothermal systems obtained from EED and GES-CAL.

	EED	**GES-CAL**
Number of boreholes	1	1
Borehole length	101 m	115 m
Total drilling length	101 m	115 m
Distance between boreholes	0	0
Heat pump nominal power	5.08 kW	5.08 kW
Minimum fluid temperature	-6°C	0°C

Observing the results of the above Tab. 3, the final schema of the geothermal system is, in general terms, quite similar applying one or another software. Going into more detail, the following subsections thoroughly compare the results of both programs from different points of view.

4.1 Well field design

Selecting the first option suggested by EED and GES-CAL, the number of boreholes required in the well field is the same for both assumptions. Regarding the borehole length and total drilling length, it is slightly higher when using GES-CAL. This fact derives from the different fluid temperature restrictions considered in the calculation of both programs.

4.2 Working fluid temperature

EED offers the possibility of analyzing the evolution of the heat carrier fluid temperature during a certain period of time (usually 25 years). This evaluation is crucial to avoid the ground freezing and to guarantee the right operation of the system in the mentioned period. For the study case presented in this research, the evolution of the fluid temperature (shown in Fig. 8) allows knowing the minimum temperature value that the fluid will have over the system operation.

Concerning GES-CAL software, its calculations are based on a conservative minimum fluid temperature value (0°C) ensuring in this way, a proper working cycle of the installation without ground freezing. This restriction contributes to a higher dimensioning of the drilling length compared to EED results.

4.3 Heat pump configuration

As mentioned in the previous sections, in EED software, user must define the final heat pump power of the system to complete the design of the well field. This final power needs to be oversized in order to deal with unexpected variations in the energy demand or errors in the global system operation.

GES-CAL, however, includes a specific module (Fig. 10) that directly provides the final heat pump power required in the system so the user does not need to make extra calculations.

4.4 Ground characterization

EED software uses standard values to define the thermal properties of the ground for a series of geological formations. These values are an approximation to the real one and, in this sense; some imprecisions are included in the global calculations.

The first version of GES-CAL, developed for the region of Ávila, is capable of providing precise information about the ground thermal conductivity thanks to the conclusions of previous researches on this area. Results of this program are, therefore, adjusted to the real thermal conditions of the ground.

4.5 Heat exchangers geometry

As explained above, EED only considers the use of vertical heat exchangers (single-U, double-U and coaxial). Although these designs are the most common ones, horizontal and helical configurations are also implemented in a large number of occasions. For this reason, the new tool, GES-CAL, has been developed with the aim of enabling the dimensioning of the geothermal system when using vertical, horizontal or helical heat exchangers.

5 Conclusions

A new approach used for the design of closed shallow geothermal systems is presented in this work. The validity of this new PC-program (GES-CAL) has been evaluated through its application on a particular study case. Results of this software have been compared to the ones obtained from the use of EED in the same initial conditions. Assuming that EED is experienced software whose foundation derives from simulations of the working fluid behavior, some statements about the applicability of the alternative tool GES-CAL, can be deduced:

- GES-CAL software constitutes an optimal solution for the design of shallow geothermal systems especially for those ones located in the region of Ávila. The accuracy of the results obtained from the use of this program is considerably high accu-

racy since calculations derive from the thermal characterization of the ground in that region.

- Despite GES-CAL does not enable the simulation of the working fluid temperature, calculations consider a conservative temperature restriction that ensures a proper response of the ground during the whole system operation.

- The range of use of GES-CAL allows the dimensioning of all the most frequent heat exchangers configurations that EED software does not include.

- In addition, GES-CAL offers the possibility of evaluating the geothermal systems in economic and environmental terms. It calculates the initial investment of the installation, the operational costs and the greenhouse gases emission associated to its use. Finally, this module is capable of comparing the geothermal systems in relation to alternative energy sources.

- GES-CAL means an intuitive and quick tool that facilitates and simplifies the dimensioning of shallow geothermal systems, that is to say, a non-specialized user could use it in a simple way.

- For the design of high power geothermal installations in different regions, EED software is still the best solution for a more precise calculation. The simulation of the fluid temperature plays an essential role to avoid the ground freezing, especially in these high power systems.

- In conclusion, this work emphasizes the need of promoting the use of renewable energies as the geothermal one on the basis of Smart Cities and energy savings. Future works will be directed to the enhancement of the global low enthalpy geothermal systems operation by the search of new alternatives and solutions.

References

1. Rybach, L., Mongillo, M. Geothermal sustainability – a review with identified research needs. Geothermal Resource Council Transactions 30, 1083–1090, (2006).
2. Saner, D., Juraske, R., Kübert, M., Blum, P., Hellweg, S., Bayer, P. Is it only CO_2 that matters? A life cycle perspective on shallow geothermal systems. Renewable and Sustainable Energy Reviews 14, 1798–1813, (2010).
3. Nagano, K., Katsura, T., Takeda, S., Development of a design and performance prediction tool for the ground source heat pump system. Applied Thermal Engineering 26, 1578–1592, (2006).
4. Li, X., Chen, Z., Zhao, J., Simulation and experiment on the thermal performance of U-vertical ground coupled heat exchanger. Applied Thermal Engineering 26, 1564–1571, (2006).
5. Gao, Q., Li, M., Yu, M., Experiment and simulation of temperature characteristics of intermittently-controlled ground heat exchanges. Renewable Energy 35, 1169–1174, (2010).
6. Cristina Sáez Blázquez, Arturo Farfán Martín, Pedro Carrasco García, Luis Santiago Sánchez Pérez, Sara Jiménez del Caso. "Analysis of the process of design of a geothermal installation", Renewable Energy 89, 1-12 (2016).
7. Cristina Sáez Blázquez, Arturo Farfán Martín, Ignacio Martín Nieto, Pedro Carrasco García, Luis Santiago Sánchez Pérez, Diego González Aguilera. "Thermal conductivity map of the Avila region (Spain) based on thermal conductivity measurements of different rock and soil samples", Geothermics 65, 60–71 (2017).
8. Cristina Sáez Blázquez, Arturo Farfán Martín, Ignacio Martín Nieto, Pedro Carrasco García, Luis Santiago Sánchez Pérez and Diego González-Aguilera. "Efficiency Analysis of the Main Components of a Vertical Closed-Loop System in a Borehole Heat Exchanger", Energies 10, 201-216; Special Issue "Low Enthalpy Geothermal Energy" (2017).
9. Cristina Sáez Blázquez, Arturo Farfán Martín, Ignacio Martín Nieto and Diego González-Aguilera. "Measuring of Thermal Conductivities of Soils and Rocks to Be Used in the Calculation of A Geothermal Installation", Energies 10, 795-813 (2017).
10. Cristina Sáez Blázquez*, Arturo Farfán Martín, Ignacio Martín Nieto, Pedro Carrasco García, Luis Santiago Sánchez Pérez, Diego González-Aguilera. Analysis and study of different grouting materials in vertical geothermal closed-loop systems, Renewable Energy 114, 1189-1200, (2017).
11. Cristina Saez Blazquez, David Borge-Diez, Ignacio Martin Nieto, Arturo Farfan Martin, Diego Gonzalez-Aguilera, Technical optimization of the energy supply in geothermal heat pumps. Geothermics 81, 133‑142 (2019).
12. Cristina Sáez Blázquez, Ignacio Martín Nieto, Arturo Farfán Martín, Diego González-Aguilera and Pedro Carrasco García, Comparative Analysis of Different Methodologies Used to Estimate the Ground Thermal Conductivity in Low Enthalpy Geothermal Systems. Energies 12 (9), 1672 (2019).
13. IDAE, Institute for the diversification and energy saving, Diseño de sistemas de intercambio geotérmico en circuito cerrado. Guía técnica, Ahorro y Eficiencia Energética en Climatización, (2010).
14. UNE-EN 100715-1. Diseño, ejecución y seguimiento de una instalación geotérmica somera, sistemas de circuito cerrado vertical. (2014).
15. UNE-EN ISO 13790:2011. Eficiencia energética de los edificios. Cálculo del consumo de energía para calefacción y refrigeración de espacios. (ISO 13790:2008).

Impacto del autoconsumo fotovoltaico sobre las instalaciones de carga del vehículo eléctrico ubicadas en aparcamientos públicos

V. Canals, E. Alcover, A. Salas, R. Pujol-Nadal, V. Martínez-Moll, J. L. Rosselló, B. Mas

Universidad de las Isla Baleares, Palma, Ctra. Valldemossa km 7.5, Campus UIB, Islas Baleares ES07122, España
v.canals@uib.es

Abstract. El presente trabajo aborda el impacto energético y económico que conllevará la incorporación del autoconsumo fotovoltaico (PV) en su modalidad de excedentes acogidos a compensación, en el marco del RD244/2019, en aparcamientos públicos que presten servicios de carga de vehículos eléctricos (EV). Presentándose las diferentes metodologías desarrolladas e integradas en una herramienta encargada de: planificar estadísticamente el número de plazas de estacionamiento necesarias para un determinado nivel de penetración del EV basándose en datos históricos de la facturación individualizada de los estacionamientos, estimar la demanda energética relacionada con la carga a intervalos de un minuto de forma estadística simulando un parque móvil de EV representativo, y estimar la generación de una instalación fotovoltaica conectada a red tomando en cuenta diferentes efectos limitadores de la generación (sombras, ensuciamiento de las placas, efecto de la temperatura ambiente, rendimiento del inversor). Finalmente, se describe el módulo de facturación para instalaciones con una tarifa de acceso 3.0A acogidas a la modalidad de autoconsumo con excedentes compensados. Concretamente se analizan dos escenarios de generación fotovoltaica mediante la instalación de diferente número de marquesinas PV provistas de puntos dobles de carga en modo 3 en un aparcamiento ubicado en el centro de Palma de Mallorca, tomando en cuenta la evolución de los niveles de penetración del EV para los próximos 5 años. Los resultados muestran como con bajas penetraciones del EV, como es un 2,35%, los incrementos en la demanda y la facturación energética son relevantes, alcanzando un 45,82% y un 34,39% respectivamente. Mientras que los diferentes escenarios de autoconsumo PV conllevaran reducciones significativas del termino de energía y en el importe de la factura energética, alcanzado un 29,74% y un 20,08% respectivamente. Ahora bien, en ninguno de los casos analizados los ahorros alcanzados permiten amortizar las inversiones a realizar en un periodo razonable.

Keywords: Electric vehicles, Parking lot, Renewable energy, Solar energy, Statistical methods, Monte Carlo simulation.

1 Introducción

Las naciones acordaron en la convención de las Naciones Unidas (UN) sobre el Cambio Climático, celebrado en Paris en el año 2015, reducir las emisiones a fin de limitar el aumento de la temperatura media del planeta a largo plazo a un máximo de 2ºC sobre los niveles preindustriales [1]. Esto conlleva irremediablemente una reducción de las emisiones de los gases de efecto invernadero (GEI), y más concretamente las emisiones de CO_2, el más común de los GEI emitidos por las actividades humanas en términos de cantidades liberadas a la atmosfera e impacto sobre el calentamiento global del planeta. Los objetivos de reducción de un 70% de las emisiones de CO_2 para el año 2050 en comparación a las emisiones de 2015 [2], requieren de la transformación del sistema energético global. Dicha transformación solo pude conseguirse con un despliegue masivo de fuentes de energía renovables (eólica, fotovoltaica, solar térmica…), en el cual se involucren todos los niveles de la sociedad – desde los gobiernos, comunidades, hasta los diferentes sectores públicos y privados.

En este marco, el sector del transporte de pasajeros y mercancías representa un 25% del consumo energético mundial [3]. Siendo el petróleo (gasolina y diésel) y los otros combustibles líquidos (GNL, GLP, Biocombustibles, entre otros) las principales fuentes de energía vinculadas a dicho sector, que son las grandes responsables de la polución en las ciudades modernas y de la lluvia acida [4]. Por ello, muchos países están buscando reemplazar los vehículos de combustión interna por otros mucho más ecológicos [5]. Como son los vehículos híbridos enchufables (PHEV) y los vehículos eléctricos puros (EV), a priori más respetuosos con el medio ambiente y que presentan costes de operación muy inferiores [6]. Ahora bien, esta transición requiere de una infraestructura eléctrica capaz de satisfacer la demanda asociada a la carga de los EV [7], y con unas emisiones asociadas de GEI inferiores a las que producirían el conjunto de vehículos de combustión interna a sustituir [8]. En consecuencia, la infraestructura eléctrica y su gestión [9] jugarán un papel crucial en el despliegue del EV [6]. Por ello, tanto gobiernos nacionales como locales están trabajando para adaptar las ciudades a las nuevas necesidades de la movilidad eléctrica, apoyando la repotenciación de líneas eléctricas y subvencionando el despliegue de las infraestructuras de carga [10]. Donde la infraestructura de carga para el EV en el espacio público es un factor esencial para la adopción por parte de los consumidores de los vehículos eléctricos [11, 12], aunque su implementación pública aún carece de viabilidad financiera, por lo que el sector público debe tomar la iniciativa en su despliegue [13].

Todo ello, en el marco de la transición energética en curso que conllevará la masiva penetración de fuentes renovables, principalmente de origen fotovoltaico (PV) en ámbitos urbanos relacionado con el autoconsumo. Donde la generación PV se caracteriza por un suministro de energía no despachable y variable en el tiempo, mientras que la demanda de carga de los EV se caracteriza por cargas controlables y capacidad de almacenamiento de energía, con lo cual tiene sentido combinar la carga de los EV con la generación PV [14]. Por un lado, la carga de los vehículos eléctricos puede ayudar a la red eléctrica a mantener el equilibrio entre la oferta y la demanda, lo que permitirá una mayor penetración de las energías renovables [15]. A su vez, la producción energía de origen PV también podría posibilitar una mayor penetración de los vehículos eléctricos,

al no conllevar un aumento significativo de la demanda neta si los EV se cargan desde la PV. Aunque su integración deberá realizarse con sumo cuidado para no comprometer a estabilidad de la red eléctrica [16, 17], relacionada con la variabilidad de la generación PV [13] y el aumento de la demanda puntual que puede conllevar la carga de los EV.

A su vez, los aparcamientos para EV provistos de energía solar fotovoltaica pueden desplegarse en superficie en prácticamente en cualquier lugar que disponga de una infraestructura eléctrica básica, como son: centros comerciales, estaciones de trenes y autobuses, universidades, aparcamientos públicos y privados, … Siendo el diseño típico de los aparcamientos solares para EV el de estacionamientos en batería recta u oblicua, con una superficie cada uno de entre 12-15 m^2, cubiertos por paneles solares que a su vez están soportados en el aire mediante unas estructuras metálicas o de madera; debajo de las cuales se ubican las diferentes estaciones de carga de los vehículos eléctricos. Siendo su disposición habitual la de grupos de dos filas de estacionamientos en paralelo separados por un vial de circulación entre medias [18].

El presente trabajo analiza el beneficio energético y económico que conllevaría la incorporación de la generación fotovoltaica en modalidad de autoconsumo con excedentes acogidos a compensación [19], recogido en el RD244/2019 recientemente aprobado en España, sobre la demanda de las instalaciones de carga de EV ubicadas en aparcamientos públicos, que con actuales los niveles de penetración del EV carecen de viabilidad financiera. Pero que desde el sector público se ha tomado la iniciativa de su implantación para impulsar la transición energética en el ámbito de la movilidad. Concretamente se analiza el impacto energético y económico sobre un aparcamiento en superficie ubicado en el centro de Palma de Mallorca, operado por la Sociedad Municipal de Aparcamientos Públicos (SMAP) del ayuntamiento de dicha ciudad, para los niveles de penetración del EV previstos para los próximos 5 años a nivel de la comunidad autónoma de las Islas Baleares.

Para ello, se ha partido de una herramienta numérica desarrollada por los autores a requerimiento de la SMAP para planificar las necesidades de nuevas infraestructuras de carga y el impacto energético que estas conllevaran sobre la demanda base de los diferentes aparcamientos públicos de Palma de Mallorca. A partir de los datos referentes a la facturación individual (importe, duración, hora de entrada y salida) del conjunto estacionamientos a lo largo del año 2017 (año de referencia). A dicha herramienta se le ha incorporado para este trabajo sendos módulos de estimación la generación fotovoltaica y de estimación de la facturación de energética en modalidad de autoconsumo con excedentes acogidos a compensación. El modulo destinado a estimar la generación de una instalación fotovoltaica toma en cuenta parámetros del rendimiento de placas e inversor, así como la ubicación de los paneles y de los obstáculos, afín de incorporar el efecto de las sombras sobre la generación.

El presente trabajo se estructura de la siguiente forma: en la segunda sección se presenta brevemente la metodología desarrollada para estimar los niveles de penetración del EV en el parque móvil de la Islas Baleares para los próximos 5 años. En la tercera sección se describe brevemente la estructura y la metodología propia que incorpora la herramienta desarrollada por los autores para la planificación de las infraestructuras de carga de EV y su demanda energética específica sobre la curva base de las instalaciones,

y finalmente combinada con la generación fotovoltaica que tendría asociada un aparcamiento solar con un numero de paneles e inversores dados, asociados a una pérgola fotovoltaica.

En la cuarta sección se presenta una descripción detallada del aparcamiento sobre el que se desarrolla el presente estudio, así como el conjunto de resultados asociados a la demanda energética y los costes energéticos asociados de la carga del EV para diferentes escenarios de penetración del EV y de la potencia fotovoltaica pico instalada. Finalmente, en el apartado de conclusiones se discuten en detalle los resultados obtenidos y sus implicaciones prácticas en el despliegue de aparcamientos solares destinados a la carga de EV.

2 Evolución de la penetración del EV

Disponer de una previsión de la evolución de la incorporación del vehículo eléctrico en el parque móvil, con un horizonte de al menos 5 años, es fundamental para establecer las prioridades y horizontes en el desarrollo de las infraestructuras de carga del EV y su impacto energético asociado. Ante la falta de previsiones oficiales nacionales e internacionales al respecto, se ha optado por predecir evolución de la penetración del vehículo eléctrico en el parque móvil de las Islas Baleares. Para ello se ha partido de datos históricos de las matriculaciones/ventas anuales de turismos a nivel nacional, y de datos históricos de la flota turismos a nivel la comunidad autónoma de las Islas Baleares (número de vehículos en circulación, ventas y bajas anuales) disponibles en la web de la *Dirección General de Tráfico* (DGT), y de la serie temporal de ventas de EV y PHEV mensuales a nivel nacional para el período comprendido entre el 01/01/2014 al 31/05/2018, provista por la *Asociación Española de Fabricantes de Automóviles y Camiones* (ANFAC) [20]. A partir de las serie histórica de ventas mensuales de vehículos eléctricos y mediante un modelo estadístico Box-Jenkins de la familia *AutoRegressive Integrated Moving Average* (ARIMA), implementado sobre MATLAB® , específico para la previsión de series temporales a partir de observaciones pasadas de la propia serie y los errores previos de la previsión [21] se ha estimado las ventas mensuales de vehículos eléctricos (EV + PHEV) hasta diciembre de 2023. Para ello se han identificado los parámetros idóneos que modelan la serie temporal de ventas de EV+PHEV, cabe remarcar los modelos ARIMA muy sensible a variaciones de estos parámetros. El modelo se suele expresar como ARIMA (p, d, q) donde los parámetros *p*, *d* y *q* son números enteros que indican el orden de las diferentes componentes del modelo. Donde *p* establece el orden del coeficiente no estacional auto regresivo (AR), *d* establece el orden del término no estacional integrativo (I), y finalmente *q* establece el orden del término de la media móvil no estacional (MA). Expresándose el modelo como:

$$Y_t = \left(\phi_0 + \sum_{i=1}^{p} \phi_i \Delta^d Y_{t-1}\right) + \left(Y_t - \Delta^d Y_t\right) + \left(\varepsilon_t - \sum_{i=1}^{q} \theta_i \varepsilon_{t-1}\right) \quad (1)$$

Donde “d “se corresponde al número de diferencias o derivadas a realizar para convertir la serie temporal de entrada en estacionaria, los términos $\phi_1, \dots, \phi_p$ son los coeficientes de la parte autoregressiva del modelo, los términos $\theta_1, \dots, \theta_p$ son los coeficientes de la parte de medias móviles del modelo, ϕ_o es una constante, ε_t es el término del error, y

$\Delta Y_t = Y_t - Y_{t-1}$ representa el resto entre el valor de salida de la serie temporal en el instante *t* y el instante anterior *t-1*.
Concretamente el modelo implementado es un *Seasonal AutoRegressive Integrated Moving Average* (SARIMA), a fin de incorporar el efecto de la estacionalidad de la venta de vehículos a lo largo del año en el modelo. Una vez analizada la serie temporal e identificadas sus componentes básicas, se ha implementado un modelo con una $\phi_o = 0$, un número de diferencias igual a *d=1* a fin de convertir la serie temporal en estacionaria, un término de la media móvil no estacional de orden *q=1*, y finalmente un término estacional de periodo 12 (meses) y orden unitario del *Seasonal Moving Average* SMA=1, periodo que se corresponde con un año. Los resultados de la previsión de las ventas mensuales de EV+PHEV se ha integrado anualmente a fin de estimar las ventas anuales para los próximos 5 años, que se presentan en la Tabla 1.

Tabla 1. Previsión de la cuota de mercado del vehículo eléctrico en España, para el periodo (2018-2023).

Año	Estimación de ventas anuales de turismos	Previsión de ventas anuales de EV+PHEV	Cuota de mercado del EV+PHEV
2018	926.427	14.016	1,50%
2019	926.427	23.427	2,50%
2020	926.427	39.883	4,26%
2021	926.427	67.898	7,25%
2022	926.427	115.592	12,34%
2023	926.427	196.787	21,01%

Finalmente, a partir de la estimación de la cuota de mercado eléctrico y los valores medios del volumen de la flota de turismos de las islas baleares, el número de matriculaciones, el número de bajas, todas ellas obtenidas de la web de la DGT [22], se ha procedido a estimar la penetración del vehículo eléctrico en el parque móvil de las Islas Baleares para el periodo 2018-2023, en la Tabla 2.

Tabla 2. Previsión de la penetración del vehículo electico en la flota de turismos de las Islas Baleares, para el periodo (2018-2023).

Año	Volumen de la flota de turismos	Matriculaciones anuales de turismos	Bajas anuales de turismos	Previsión de matriculaciones de EV+PHEV	EV+PHEV en circulación	Penetración del EV+PHEV en la flota de turismos
2018	659.702	30.538	25.174	458	1.053	**0,16%**
2019	659.702	30.538	25.174	763	1.817	**0,28%**
2020	659.702	30.538	25.174	1.301	3.117	**0,47%**
2021	659.702	30.538	25.174	2.214	5.331	**0,81%**
2022	659.702	30.538	25.174	3.768	9.100	**1,38%**
2023	659.702	30.538	25.174	6.416	15.516	**2,35%**

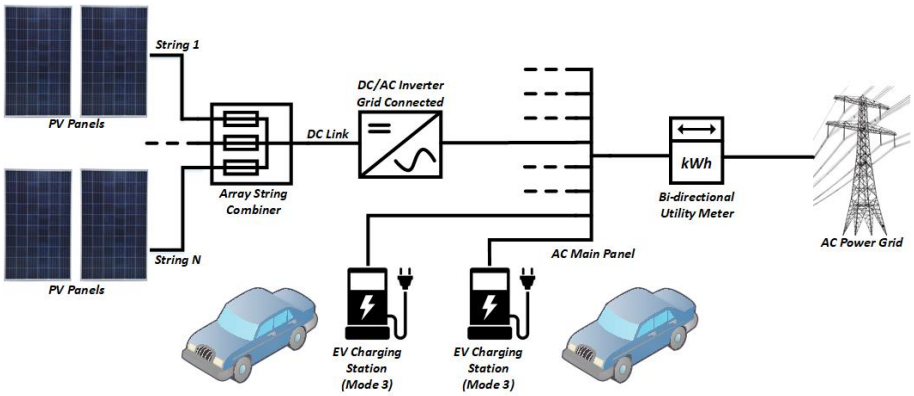

Fig. 1. Arquitectura del sistema de generación PV conectada a red, para dar soporte a la carga del EV.

Siendo los datos de penetración de EV+PHEV presentados en la Tabla 2 para la comunidad autónoma de las Islas Baleares para el periodo 2019-2023, los que usaran para estimar el impacto energético de la carga del vehículo eléctrico en el presente trabajo.

3 Planificación y estimación de la demanda del EV

La carga de los EV en la Unión Europea (UE) se rige por unos estándares electrotécnicos IEC 92196 y SAE J1772 [23, 24] que establecen las características de los conectores de carga y los modos en los que debe desarrollarse esta, mientras que el estándar IEC 61851 [25] establece las características de las infraestructuras de carga del EV y sus parámetros de compatibilidad electromagnética. Con respecto a los conectores de carga, la gran mayoría de fabricantes de vehículos eléctricos europeos y más recientemente los japoneses han optado para la carga AC en monofásica y trifásica por el conector Mennekes (tipo 2) en modo 3 (dando soporte a la carga normal/lenta, semi-rápida y rápida). Sin embargo, la tendencia de los fabricantes a medio plazo es la de optar por la carga en DC en modo 4 (dando soporte mayoritariamente a la carga semi-rápida y rápida), a fin de retirar el circuito cargador AC/DC del interior de los vehículos y dar soporte a la implantación del *Vehicle-to-Grid* (V2G), para la que los EV de fabricantes europeos harán uso de conectores para carga combina CCS (compatible físicamente con el Mennekes pero que además incorpora tomas para la carga en DC), mientras que los fabricantes japoneses mayoritariamente incorporarán conectores CHAdeMO. En cuanto al modo de carga de los EV, la mayoría de fabricantes han optado por implementar recargas lentas en AC modo 3 (10A-32A@230V_{AC}) y rápidas (>40kW) en DC modo 4. Mientras que las recargas AC semi-rápidas (16A-32A@400V_{AC}) son implementadas actualmente por solo dos fabricantes, Renault y BMW. Finalmente, remarcar que los fabricantes han reservado la carga lenta en Modo 2 (10A@230V_{AC}) para la carga de emergencia.

Concretamente la metodología que se presenta en este trabajo se ha enfocado a analizar la demanda de la carga AC normal/lenta y semi-rápida en modo 3 de los EV en un rango de potencias de carga de [2,3-22kW] en aparcamientos públicos en régimen de rotación, para un rango de niveles de penetración del EV relativamente bajos [0-2,35%] que son los que se esperan para el próximo lustro. Por ello, y unido al coste infinitamente superior de las estaciones de carga DC en modo 4 frente a las AC en modo 3; hacen a día de hoy innecesaria e inviable económicamente su instalación en aparcamientos públicos de rotación. Por lo que respecta a la generación de energía en el aparcamiento se ha optado por analizar una instalación fotovoltaica conectada a red, compuesta por un número dado de paneles fotovoltaicos (PV) cuyos strings en DC se interconectarán a uno o varios inversores, encargados de la convertir la tensión DC a la tensión y frecuencia AC de la red eléctrica interior; sobre la cual se interconectarán las diferentes estaciones de carga de los EV en modo 3 y el resto de servicios de la instalación interior, como se presenta en la Fig. 1.

3.1 Metodología

La metodología propuesta se ha implementado en una herramienta sobre MATLAB®, encargada de planificar las infraestructuras de carga y estimar su demanda energética, que a su vez es soportada por 8 sub-módulos que implementan partes específicas de la metodología desarrollada. Cabe remarcar que la metodología implementa en su núcleo un algoritmo Montecarlo que realizará una simulación, minuto a minuto, del aparcamiento para una serie temporal de 10 repeticiones del año de referencia (2017). A su vez, en la Fig. 2 se presenta la arquitectura de la herramienta desarrollada, detallando la interconexión de los diferentes sub-módulos y los flujos de información. La metodología desarrollada en cada uno de los sub-módulos se presenta a continuación:

Análisis y Modelado de la Ocupación del Aparcamiento
Este sub-módulo se encarga de ajustar la distribución estadística de los periodos de estacionamiento y el diagrama horario de ocupación media para el aparcamiento, para dos periodos anuales (temporada alta y baja). Todo ello a partir de la información histórica de facturación de los estacionamientos individuales (tickets de estacionamiento) de los años 2016 y 2017, que se carga mediante un fichero externo. Para conocer la distribución de los periodos de estacionamiento se construye el histograma de las duraciones de estacionamiento para intervalos de 10 minutos en un rango de [0, 2000] minutos, eliminando así periodos de estacionamiento atípicos. Cuya forma resigue perfectamente una distribución continua como la de Weibull $W_e(x;\lambda,k)$, definida dos parámetros; el parámetro de forma $k>0$ y el parámetro de escala de la distribución $\lambda>0$. Los cuales se determinan sobre los datos normalizados del histograma anteriormente construido, mediante un método de mínimos cuadrados. Mientras que el diagrama de ocupación horaria media del aparcamiento por periodo, se construye determinando el número medio de vehículos que inician y finalizan su estacionamiento en una determinada franja horaria a lo largo de un determinado periodo; en este caso se ha establecido también dos periodos anuales.

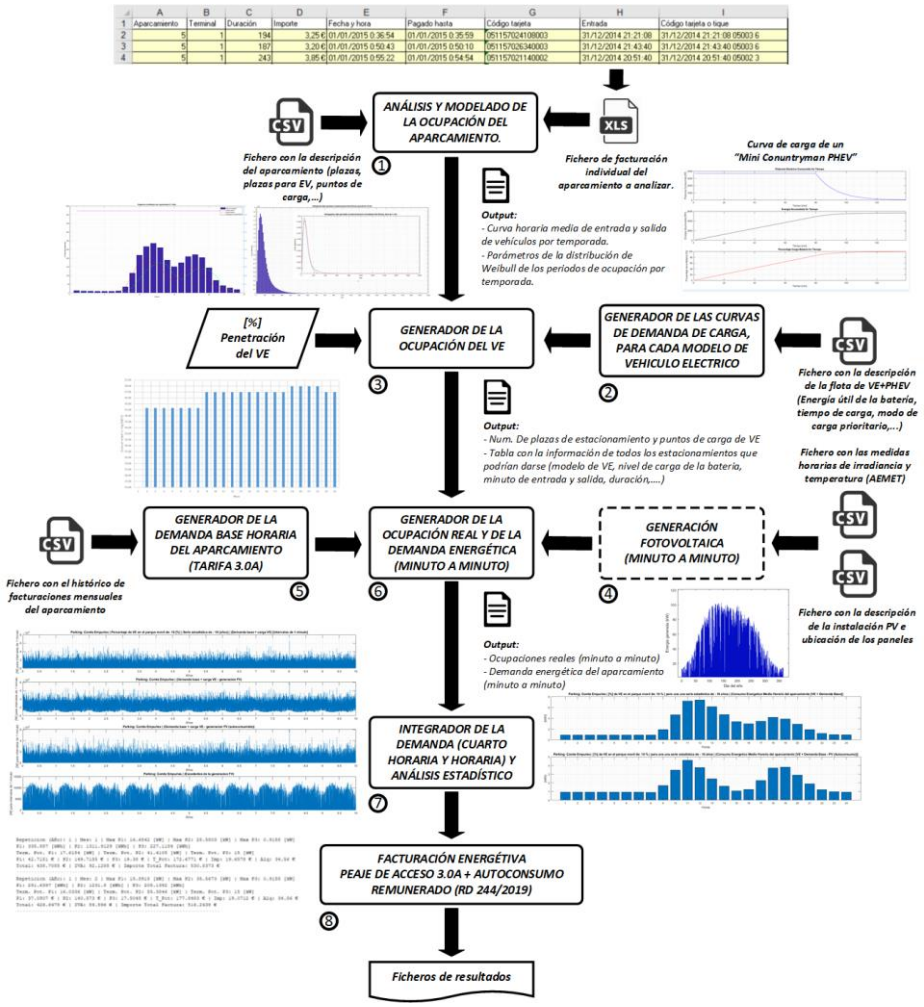

Fig. 2. Arquitectura de la herramienta de planificación y estimación de la demanda del EV.

Generador de Curvas de la demanda de carga

Genera las curvas de carga de las baterías de los vehículos que conforman la flota conformada de EV. Concretamente el parque móvil se incorpora mediante un fichero externo en el cual se incorporar una columna para cada EV que conforma la flota, en la cual se detallan: el porcentaje absoluto de penetración el modelo en el parque móvil, la energía útil de la batería, el tiempo de carga y la potencia nominal de carga del vehículo, además de otros parámetros. Concretamente el parque móvil usado en este trabajo se ha conformado con 10 vehículos, 5 son eléctricos puros y 5 híbridos enchufables como se muestra en la Tabla 3, cuyo porcentaje de penetración se ha establecido acorde al actualmente existente en el parque móvil eléctrico nacional.

Tabla 3. Características de los vehículos que conforman la flota EV

Modelo	[%] Penetración en la flota EV nacional	[%] Penetración del modelo en la flota EV	[kWh] Energía útil de la batería	[kW] Potencia nominal de carga	[min] Tiempo de carga
Renault Zoe Z40	8,71	21,44	41	17,28	189
Nissan Leaf e+	6,88	16,93	40	6,60	410
BMW i3	5,06	12,45	27.2	11	195
Renault Kangoo ZE	3,90	9,60	33	7,36	315
Nissan e-nv200	3,98	9,78	40	6,60	410
Mitsubishi Outlander PH	7	16,97	13,8	3,68	271
Volkswagen Golf GTE	1,50	3,68	8,7	3,68	188
Mercedes GLC 350e	1,37	3,37	6,2	3,68	147
BMW 225ex	1,44	3,55	5,7	3,68	139
Mini Countryman PHEV	0,91	2,33	5,7	3,68	139

A partir de estos datos, la metodología genera la curva de demanda (AC) de la estación de carga modo 3 vinculada a la batería de litio-ión de cada uno de los vehículos de la flota. Concretamente, la metodología desarrollada pretende emular la demanda asociada a la carga de la batería, mediante una función a dos tramos. Un primer tramo a potencia nominal constante $P_{car}(t_i) = P_{car\_nom}/60$ y una segunda a potencia variable que decrecerá exponencialmente $P_{car}(t_i) = P_{car\_nom}e^{-at}/60$. Que se iniciará cuando la energía que resta para finalizar la carga t_{rest} es inferior a la energía que se cargaría a potencia nominal en una hora, el método ajusta el parámetro "a" de la función exponencial negativa de la potencia nominal mediante integración numérica, a fin que la energía restante se cargue en dicho periodo.

Generador de la Ocupación del EV

Determina la ocupación del EV a partir del valor de penetración del EV en el parque móvil y de los datos de ocupación horaria media del aparcamiento, que proveerán el número medio de entradas/estacionamientos de vehículos para todos los intervalos horarios del periodo de evaluación. Entonces la metodología propuesta generará tantos números uniformemente distribuidos $U(0,1)$ como vehículos se prevé que accedan al aparcamiento en un determinado intervalo horario, para determinar si el vehículo que ha accedido al aparcamiento es eléctrico o no; concretamente si el valor del número aleatorio generado es menor al valor de penetración del EV se considerara que ha accedido un EV. De esta forma la metodología reproduce la componente estocástica que tiene asociado el estacionamiento real de vehículos. Seguidamente para cada EV que acceda al aparcamiento se generaran tres nuevos números aleatorios. El primero consistirá en un numero aleatorio uniformemente distribuido $U(1,60)$ y encargado de fijar aleatoriamente el minuto a lo largo del intervalo horario en el que el vehículo accederá

al aparcamiento. Mientras que el segundo se generará mediante un generador de números aleatorios que sigue una distribución de Weibull $t_{est} = W_e(\lambda, k, U(0,1))$, y fijará aleatoriamente la duración del estacionamiento característica del aparcamiento. Mientras que el tercero usará un generador aleatorio uniformemente distribuido $U(0,1)$ que servirá determinar el modelo de EV que ha accedido al aparcamiento.

Finalmente, la metodología determina los percentiles P_{99} y $P_{99.6}$ de la serie horaria de ocupaciones del EV de todo el periodo de evaluación, a fin de establecer los requerimientos de plazas de estacionamiento y estaciones de carga de EV.

Generación Fotovoltaica

Para poder estimar la generación PV con precisión es fundamental disponer de datos meteorológicos de calidad de la ubicación o de alguna estación meteorológica cercana a ella. Para ello se hará uso de datos horarios de la irradiancia solar horizontal global (*DGI*), la irradiancia solar difusa horizontal (*DHI*) y la irradiancia directa normal (*DNI*) y temperatura ambiental, todos ellos provistos por la Agencia Estatal de Meteorología (*AEMET*) para el año de referencia; que en esta aplicación se ha establecido como el año 2017. A su vez, para evaluar la irradiancia incidente sobre los diferentes orientaciones e inclinaciones de los paneles fotovoltaicos, que conforman una instalación PV, es fundamental conocer la posición del sol en cada instante. Para este propósito, se ha incorporado el algoritmo de la *Plataforma Solar de Almería* (*PSA*) [26] para la determinación de la altitud, azimut y declinación solar para cualquier momento del año. Entonces, a partir de la posición solar y las medias horarias de irradiancia aplicando métodos geométricos puede determinarse la irradiancia difusa (ID_{if}) que incidirá sobre un panel fotovoltaico dado, tomando en cuenta su orientación e inclinación. Obteniendo la radiación directa sobre el plano horizontal multiplicando la irradiancia directa normal (*DNI*) por el seno la elevación solar, y conociendo el ángulo que forman el panel PV respecto a la posición del sol, se puede fácilmente determinar la cantidad de irridiancia que incidirá perpendicularmente (*ID*) sobre el panel PV. Donde la irradiancia aprovechable (GI_{ef}) por un panel/modulo fotovoltaico vendrá dada por la suma de las componentes directa efectiva (ID_{ef}) y difusa efectiva ($IDif_{ef}$), como se muestra en la siguiente expresión:

$$GI_{ef} = IDif_{ef} + ID_{ef} \tag{2}$$

A su vez, el modelado de la respuesta óptica o *Incidence Angle Modifier* (IAM) del captador fotovoltaico se han obtenido mediante herramienta web OTSun [28, 29].

Seguidamente para determinar la cantidad de energía generada por un panel PV dada una irradiancia es fundamental incorporar un parámetro que modele el grado de ensuciamiento del panel PV. Ya que la suciedad altera las propiedades ópticas angulares de los paneles a la vez que reduce la transmitancia del cristal/material protector del panel [27], limitando tanto la irradiancia directa ID_{ef}, como la difusa $IDif_{ef}$. Por lo que respecta al rendimiento de la conversión de la irradiancia incidente a energía eléctrica en los paneles fotovoltaicos, se ha optado por la incorporación de un modelo que determina la potencia P_{DC} de salida de los módulos PV que toma en cuenta la temperatura. Al depender directamente el rendimiento de las células fotovoltaicas de la temperatura a la que se haya en cada instante el módulo PV. Concretamente, para este efecto se ha

optado por el modelo *Sandia PV Array Performance Model* (*SAPM*) [30], que toma en consideración la metodología de instalación de los paneles. Finalmente, para determinar la potencia eléctrica P_{AC} entregada por el inversor a la red se ha optado por el modelo de *PVWatts* del *NREL* [31] que propone para la estimación del rendimiento del inversor una función empírica escalada de acuerdo a la eficiencia nominal del inversor PV. A su vez, el módulo de generación fotovoltaica desarrollada toma en consideración las sombras debidas a los obstáculos colindantes a la instalación.

Generador de la Demanda Base Horaria

Para la generar la curva base se parte de un fichero externo provisto de la información de diversas facturaciones mensuales, incorporando para cada una de ellas una fila con toda la información de las facturas históricas del suministro eléctrico para un peaje de acceso 3.0A ($P_{cont} \geq 15kW@400V_{AC}$), en la cual se detallarán: periodo de facturación mensual, potencia contratada para los periodos de facturación horaria P1/P2/P3, energía activa consumida mensualmente por periodo. Para finalmente estimar el consumo medio horario, y minuto a minuto del aparcamiento.

Generador de la Ocupación Real y de la Demanda Energética

Determina la ocupación real del aparcamiento, una vez se ha fijado el número de plazas de aparcamiento y estaciones para el EV. Para a continuación determinar la demanda energética asociada a la de la carga del EV. Para ello metodología empieza ordenando de forma ascendente la tabla con la información de cada uno de los estacionamientos de EV en función del minuto de inició del estacionamiento. Seguidamente se crean dos matrices unidimensionales, de tantos elementos como minutos del periodo de evaluación. La primera almacenara la ocupación real minuto a minuto de las plazas de EV, incrementando su valor en una unidad entre el minuto de entrada del vehículo en el aparcamiento y su salida, mientras que el número de vehículos estacionados no exceda el número de estacionamientos prefijado anteriormente; en tal caso se descartara el estacionamiento. Mientras que en la segunda matriz se incrementará con la potencia instantánea consumida por la carga del EV en el periodo prefijado para el estacionamiento. Finalmente, este módulo combina las diferentes demandas energéticas (curva base, demanda del EV, generación PV) para su posterior análisis.

Integrador de la Demanda

Se encarga de integrar la demanda energética de los energética en periodos cuatro horarios y horarios, para su posterior análisis y evaluación de la facturación eléctrica.

Facturación Energética

Se encargara de calcular la factura energética mensual [32] para un peaje de acceso 3.0A, tipología habitual de los aparcamientos públicos de rotación. Cabe destacar, que no existe un mercado regulado para la tarifa vinculada a un peaje de acceso 3.0A; donde el gobierno español marca el precio de los peajes de acceso para potencia y el consumo, pero cada comercializadora puede aplicar el margen de comercialización y las condiciones contractuales (como compromisos de permanencia) que crea convenientes. Es

una tarifa que utiliza siempre discriminación horaria en tres periodos: P1 (Punta), P2 (Plan) y P3 (Valle); y cada período le corresponde una franja horaria diaria donde el coste de la energía y de la potencia contratada es diferente. Las tarifas integradas en la herramienta se presentan en la Tabla 4, las cuales también incorporan el termino de alquiler de los equipos (414,72€/año), el impuesto sobre la electricidad (5,11%) y el IVA (21%)

Tabla 4. Tarifa de acceso 3.0A

Tarifa / Rango de potencia	[€] Termino potencia P1	[€] Termino potencia P2	[€] Termino potencia P3	[€] Termino energía P1	[€] Termino energía P2	[€] Termino energía P3
Tarifa 1 / 15 a 30 kW	41,95	25,17	16,78	0,1272	0,1141	0,0853

Los cálculos del termino de energía re realizan a partir de la energía consumida horariamente, mientras que los cálculos del termino de potencia se realizaran a partir de la potencia contratada en cada uno de los periodos de facturación y la potencia demandada cuarto-horariamente registrada por el maximetro. A su vez, se he integrado en este sub-módulo el autoconsumo para instalaciones de generación ($P \leq 100kW$) en su modalidad de autoconsumo con excedentes con compensación simplificada, recientemente introducida en el RD244/2019 [19], que introduce una variante del balance cero que en vez de compensar los [kWh] consumidos y producidos propone una compensación económica asimétrica mensual. Donde los [kWh] inyectados a la red se pagarán según acuerdo de compensación de excedentes con la comercializadora para cada periodo, en un rango de entre [0,04-0,05 €/kWh]; en este trabajo se ha tomado un precio de 0,04018 €/kWh para los tres periodos. A su vez, si el importe producido es igual o mayor al consumido el valor del termino de energía será de 0 €; lo que implica regalar el excedente al sistema.

4 Resultados

La metodología desarrollada se ha aplicado sobre el aparcamiento de *Comte d'Empúries* ubicado en las coordenadas (*39°34'38,9"N | 2°39'16,3"E*) en el centro de Palma de Mallorca, Fig. 3a, y orientado hacia el noroeste, Fig. 3b. Las 83 plazas de este aparcamiento son operadas por la *SMAP* en régimen de rotación, de lunes a sábado con un horario de las 7 a las 22h. El aparcamiento actualmente no dispone de ninguna plaza de estacionamiento ni infraestructura de carga que de soporte al EV. A su vez, el aparcamiento tiene asociada una tarifa de acceso 3.0A con una potencia contratada de 15kW para los tres periodos de facturación, y un consumo energético medio anual de 8.022 kWh. Todo ello lo hace idóneo para abordar el análisis del impacto energético y económico que conllevaría la incorporación de un autoconsumo fotovoltaico, en su modalidad de "*excedentes acogidos a compensación*", en la estrategia de despliegue de in-

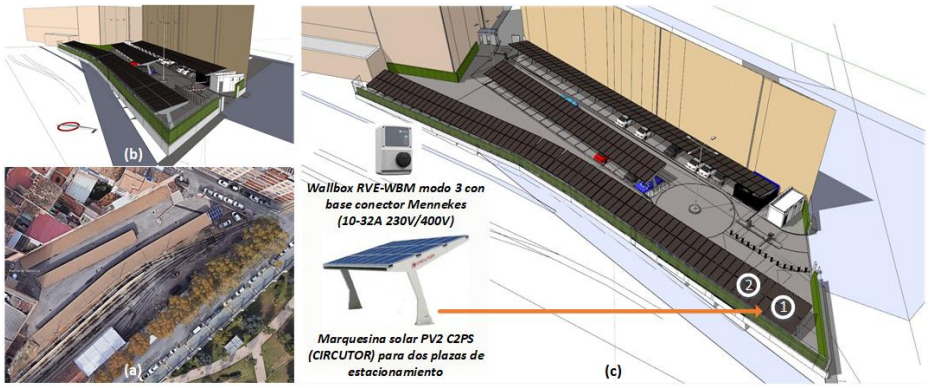

Fig. 3. a: Ubicación del aparcamiento. b: Orientación del aparcamiento. c: Descripción e ubicación de las marquesinas solares.

fraestructuras de carga y estacionamiento para el EV que está impulsando el sector público. Concretamente se analizan dos escenarios de autoconsumo fotovoltaico tomando en cuenta la evolución anual de los niveles de penetración del EV para los próximos 5 años y las infraestructuras de carga que se prevén instalar. Puesto que su evolución debería impactar significativamente sobre el termino de potencia de la factura energética.

4.1 Planificación y Análisis Energético

La planificación de las infraestructuras de carga del EV es la fase previa a cualquier análisis energético y/o económico que se quiera llevar a cabo, con la metodología propuesta. Para ello se ha estimado el número de estaciones de carga y plazas de estacionamiento de EV necesarias para dar soporte al número de estacionamientos de EV cubiertos por los percentiles P_{99} y $P_{99.6}$ que se darán con los niveles de penetración EV para los próximos 5 años. Como puede apreciarse en la *Fig. 4a*, tanto si se opta por una planificación basada en el percentil P_{99} o el percentil $P_{99.6}$ en los próximos 5 años se requerirá de 2 plazas de estacionamiento y estaciones de carga de EV, para dar soporte a la demanda del estacionamiento de EV. A su vez, los dos escenarios planteados de generación fotovoltaica consistirán en la instalación de 1 o 2 marquesinas modelo PV2 del fabricante Circutor, cuyas especificaciones se presentan en la Tabla 5, según se muestra en la Fig. 3c. Ambos escenarios cumplen con los requerimientos de plazas y estaciones de carga para el periodo analizado.

Tabla 5. Parámetros asociados a los dos escenarios de autoconsumo PV

Escenario	Núm. Módulos PV (270 W_p)	[kW_p] Potencia PV	Núm. Inversores x [kW] $P_{Nominal}$	Núm. Plazas / Núm. Estaciones de carga modo 3
1: 1 x Marquesina PV2-2	15	4,05	1 x 3,70	2 / 1
2: 2 x Marquesina PV2-2	30	8,10	1 x 7	4 / 2

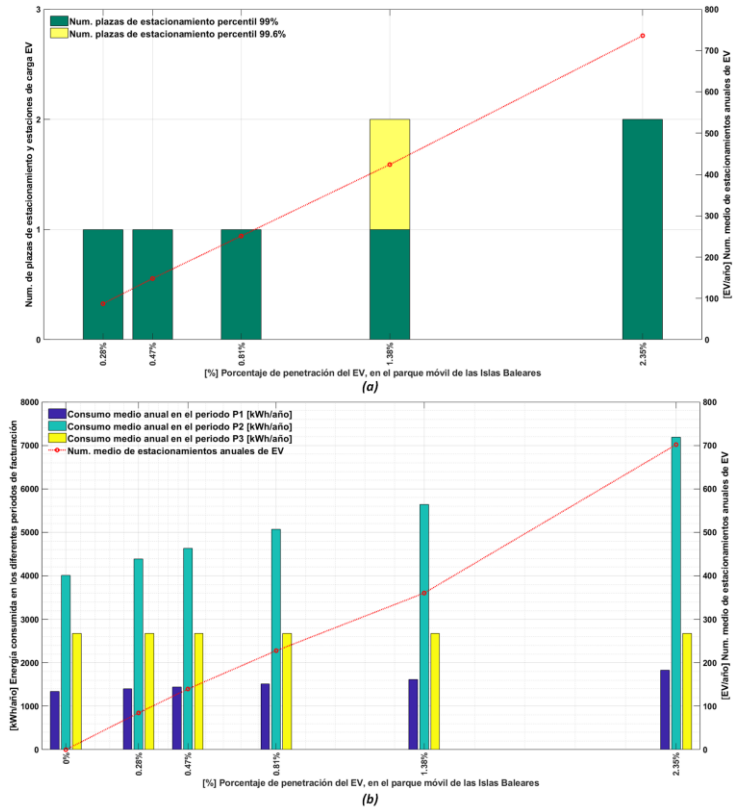

Fig. 5. a: Planificación de los requerimientos de plazas y estaciones de carga de EV. b: Impacto de la penetración del EV sobre la demanda energética, para los diferentes periodos de facturación.

A continuación, la metodología procede a estimar la demanda energética base del aparcamiento combinada con la asociada a la carga de los EV en función del nivel de penetración anualmente establecido, en intervalos de minuto a minuto. Para posteriormente integrarlos en periodos cuarto-horarios y horarios que servirán de demanda energética de referencia, para posteriores análisis. Concretamente, si analizamos la evolución de la demanda energética anual por periodo horario de facturación y el número medio de estacionamientos anuales de EV en función del nivel de penetración del EV, Fig. 4b. Donde la demanda energética total (P1+P2+P3) se verá incrementada en tan solo 5 años en un 45,82%. A su vez, la demanda energética actual del periodo P1 (18-22h) se verá incrementada entre un [36-39%], la del periodo P2 (8-18h y 22-24h) entre un [79-82%], y la del periodo P3 (00-08h) se mantendrá prácticamente inalterada. Los resultados obtenidos para el periodo P3 se deben a que el estacionamiento permanece cerrado en el periodo de las 22h a las 07h. Mientras que el mayor incremento de la demanda se dará en el periodo P2, hecho a tener muy presente en el supuesto que se pretenda modificar la contratación energética. Seguidamente, la metodología estima la demanda energética

incorporando los dos escenarios de autoconsumo PV para los diferentes niveles de penetración del EV; obteniendo así las demandas energéticas combinadas por periodo de facturación (cuarto-horarios y horarios), y sus respectivos percentiles P_{99} y picos de la demanda. A fin de facilitar la interpretación de los resultados obtenidos, las demandas para los diferentes escenarios de penetración de EV y autoconsumo PV se presentan en la Tabla 6 de forma porcentual con respecto a la demanda base del año 2017 de referencia para este aparcamiento.

Tabla 6. Demanda energética del aparcamiento para los diferentes escenarios de autoconsumo PV

Sin aporte PV/ Penetración del EV	**(2017) 0%**	**(2019) 0,28%**	**(2020) 0,47%**	**(2021) 0,81%**	**(2022) 1,38%**	**(2023) 2,35%**
Num. Plazas / Estaciones carga	0/0	1/1	1/1	1/1	1/1	2/2
Dem. Anual P1 [kWh]	1.337	4,92%	7,95%	13,14%	20,64%	36,81%
Dem. Anual P2 [kWh]	4.011	9,42%	15,42%	26,44%	40,54%	79,34%
Dem. Anual P3 [kWh]	2.674	0%	0%	0%	0%	0,04%
Dem. Anual Total [kWh]	***8.022***	***5,53%***	***9,03%***	***15,41%***	***23,71%***	***45,82%***
P_{99} Dem. Cuarto-horaria [kWh]	0	1,69	4,60	6,20	7,52	9,88
Pico Dem. Cuarto-horaria [kWh]	0	5,42	7,52	8,28	10,13	14,39
P_{99} Dem. Horaria [kWh]	0	2,85	4,20	4,99	6,39	8,28
[Escenario 1]: 1 x Marquesina PV2-2 → (4,05 kWp)						
Dem. Anual P1 [kWh]	1.337	3,43%	6,65%	9,72%	19,44%	36,61%
Dem. Anual P2 [kWh]	4.011	-38,31%	-33,96%	-23,87%	-11,34%	24,59%
Dem. Anual P3 [kWh]	2.674	0,00%	0,00%	0,00%	0,00%	0,00%
Dem. Anual Total [kWh]	***8.022***	***-18,67%***	***-15,96%***	***-10,40%***	***-2,52%***	***18,31%***
P_{99} Dem. Cuarto-horaria [kWh]	0	1,32	3,22	4,80	6,57	9,10
Pico Dem. Cuarto-horaria [kWh]	0	4,86	5,98	7,52	9,44	13,67
P_{99} Dem. Horaria [kWh]	0	2,15	3,22	4,40	5,41	7,66
[Escenario 2]: 2 x Marquesinas PV2-2 → (8,10 kWp)						
Dem. Anual P1 [kWh]	1.337	3,60%	5,55%	10,26%	19,14%	39,05%
Dem. Anual P2 [kWh]	4.011	-43,50%	-39,65%	-31,91%	-21,83%	6,82%
Dem. Anual P3 [kWh]	2.674	0,00%	0,00%	0,00%	0,00%	0,00%
Dem. Anual Total [kWh]	***8.022***	***-21,24%***	***-18,98%***	***-14,33%***	***-7,81%***	***9,83%***
P_{99} Dem. Cuarto-horaria [kWh]	0	0,92	2,38	4,60	6,19	8,28
Pico Dem. Cuarto-horaria [kWh]	0	4,37	5,40	7,52	8,28	12,34
P_{99} Dem. Horaria [kWh]	0	1,44	2,70	4,03	4,88	7,32

Los resultados presentados muestran a todas luces como la incorporación de generación PV en régimen de autoconsumo tiene un efecto beneficio, reduciendo la demanda energética global. Alcanzando el escenario 1 una reducción de la demanda media del

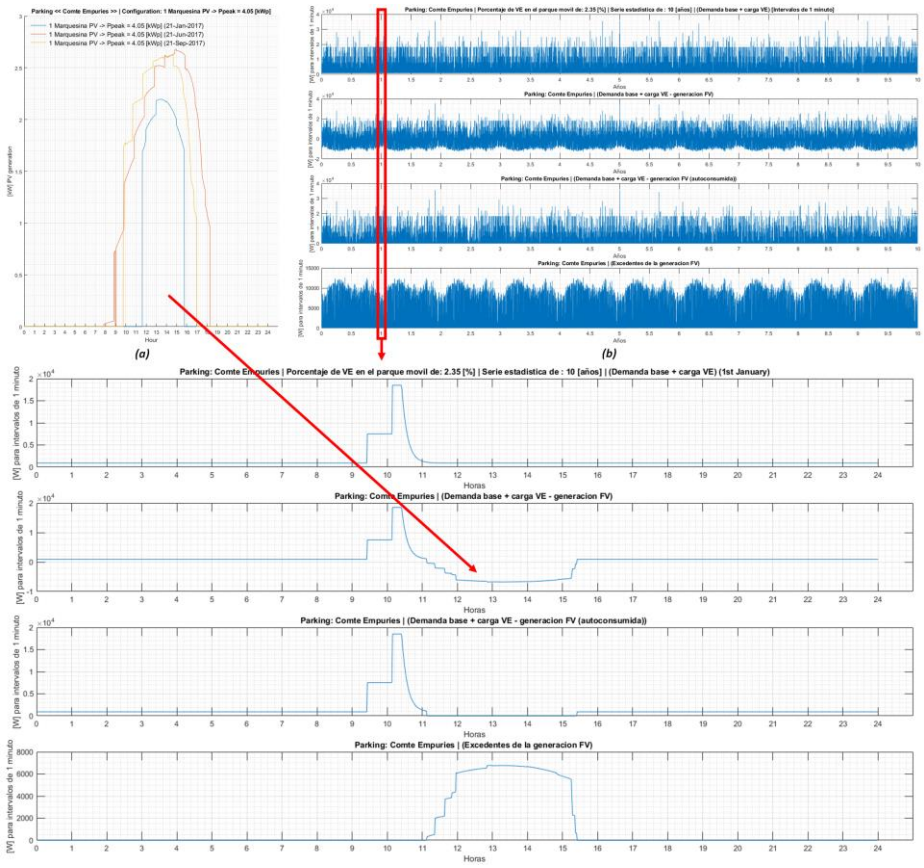

Fig. 6. a: Generación minuto a minuto de la marquesina PV nº 1, para diferentes fechas. b: Demandas y generaciones minuto a minuto para una penetración de 2,35% del EV, y el escenario 2 de autoconsumo PV.

25,81% para los diferentes niveles de penetración del EV, mientras que el escenario 2 incrementa esta reducción hasta el 29,74%. Concretamente la máxima reducción con respecto a la demanda se ha alcanzado para el escenario 2, con un 21,24% base para una penetración del EV del 0,28%. Concentrándose la mayor parte de los ahorros energéticos en el periodo P2 (08-18h). A su vez, en el periodo P1 (18h-22h) la aportación solar tan solo alcanza a contener ligeramente el incremento de la demanda. Este hecho se debe principalmente a la ubicación del aparcamiento, confinado entre edificios y con presencia árboles en su parte sur, actualmente despejada, lo que provoca que las sombras limiten el aporte solar al periodo P1, como puede apreciarse en la Fig. 6a. A su vez, para penetraciones *≤1%* del EV en el parque móvil se obtienen reducciones semejantes de la demanda anual para los dos escenarios de autoconsumo PV. Mientras que a medida que la penetración del EV aumenta *>1%*, y por consiguiente la demanda energética aumenta, se aprecia como el escenario 2 de autoconsumo PV aporta mayores reducciones de la demanda energética.

Ahora bien, este hecho está vinculado a que la reducción de la demanda proviene del autoconsumo, es decir de la resta de potencia instantánea demanda con la generada para cada instante de tiempo, como se muestra en la Fig. 6b. Mientras que los excedentes, energía generada que no pueden auto-consumirse instantáneamente no puede descontarse de la demanda energética global para un determinado periodo de facturación de acuerdo con el RD244/2019, como si sucede con el balance neto en otros países de la UE [30]. En el caso español el excedente se descuenta monetariamente del importe de la demanda hasta que esta se haga cero para un periodo mensual de facturación eléctrica, siendo el balance entre importe de compra de la energía y el de venta completamente asimétrico, como se discutirá en la siguiente sub-sección.
Finalmente, si se analiza la evolución del percentil P_{99} de la demanda energética cuarto-horaria se puede apreciar como con los escenarios 1 y 2 de autoconsumo PV se consigue reducir de media 0,95kWh y 1,60kWh respectivamente del valor de la demanda energética sin aporte PV. Lo cual es sumamente interesante al estar vinculada la demanda cuarto-horaria con la potencia registrada por el maxímetro de la instalación (ubicado en el contador bidireccional, Fig. 1); que en el modelo facturación eléctrica española [26] es usada para determinar el termino de potencia de la instalación, que en el supuesto que sea superior al 105% de la potencia contratada por periodo será el que se facture finalmente.

4.2 Análisis Económico

La determinación del coste de la factura energética que llevará asociado el despliegue de las infraestructuras de carga de EV en modo 3 para diferentes niveles de penetración EV, es la fase previa a estimar los ahorros asociados a los dos escenarios de autogeneración PV contemplados en el presente trabajo. Para posteriormente abordar los costes asociados al despliegue combinado de las infraestructuras de carga y el autoconsumo PV con objeto de evaluar la viabilidad económica de la inversión a realizar.

A partir de la información vinculada con tarifa de accesos que tiene contratada el aparcamiento y las demandas energéticas obtenidas en la sección anterior se ha procedido mediante el sub-módulo de facturación a determinar el importe anual de la facturación energética (agregando las facturaciones mensuales del aparcamiento). Para facilitar el análisis posterior de los costes energéticos evaluados par los diferentes niveles penetración del EV y que se muestran en la Tabla 7, se ha optado por presentar los importes energéticos desglosados en euros para el escenario *sin aporte de PV*; mientras que los escenarios de autoconsumo PV se presentan de forma porcentual con respecto a los costes energéticos del año de referencia (2017).
Los resultados que se presentan en la tabla anterior muestran a todas luces como, inclusos pequeñas penetraciones del EV en el parque móvil implicaran argumentos significativos en el importe de la factura energética. Por ejemplo, en tan solo cinco años, 2023, la factura energética del aparcamiento se verá incrementada en un 34,39% con solo un 2,35% de penetración de EV. Concretamente, el escenario 1 de autoconsumo PV alcanzara de media un ahorro de la factura energética para los diferentes niveles de penetración del EV del 13,25%, mientras que para el escenario 2 el ahorro aumenta hasta el 20,08%. A su vez se aprecia como el incremento del coste de los términos de energía y potencia son prácticamente idénticos. Esto se debe a que el término de potencia de la

factura energética crece al superar la demanda cuarto-horaria la potencia contratada para los diferentes periodos. Que estadísticamente es más probable que se dé al aumentar el número de medio de cargas/estacionamientos de EV.

Tabla 7. Facturación energética asociada a la demanda energética del aparcamiento para los escenarios de autoconsumo PV

Sin aporte PV/ Penetración del EV	***(2017)*** ***0%***	***(2019)*** ***0,28%***	***(2020)*** ***0,47%***	***(2021)*** ***0,81%***	***(2022)*** ***1,38%***	***(2023)*** ***2,35%***
ΔTermino de energía [%]	855,99€	6,01%	9,16%	15,57%	25,59%	51,33%
ΔTermino de potencia [%]	1.258,52€	4,65%	6,59%	9,08%	13,60%	33,66%
Importe factura [€/año]	***3.191,18***	***3.330,95***	***3.396,40***	***3.506,01***	***3.687,42***	***4.288,72***
ΔImporte factura anual [%]	0	4,38%	6,43%	9,87%	15,55%	34,39%
[Escenario 1]: 1 x Marquesina PV2-2 → (4,05 kWp)						
ΔTermino de energía [%]	855,99€	-30,16%	-27,21%	-21,27%	-11,79%	12,30%
ΔTermino de potencia [%]	1.258,52€	3,11%	4,82%	7,09%	11,26%	29,99%
Importe factura [€/año]	***3.191,18***	***2.923,31***	***2.982,63***	***3.083,46***	***3.252,99***	***3.814,22***
ΔImporte factura [%]	0	-8,39%	-6,54%	-3,38%	1,94%	19,52%
Importe Excedentes [€/año]	0	86,58	85,58	83,46	80,93	73,26
Importe Energía regalada [€/año]	0	0	0	0	0	0
[Escenario 2]: 2 x Marquesinas PV2-2 → (8,10 kWp)						
ΔTermino de energía [%]	855,99€	-50,19%	-47,18%	-41,16%	-33,58%	-13,25%
ΔTermino de potencia [%]	1.258,52€	2,64%	3,08%	7,02%	10,39%	25,85%
Importe factura [€/año]	***3.191,18***	***2.716,22***	***2.755,70***	***2.883,65***	***3.019,29***	***3.486,08***
ΔImporte factura [%]	0	-14,88%	-13,65%	-9,64%	-5,39%	9,24%
Importe Excedentes [€/año]	0	236,51	232,82	228,57	221,84	204,92
Importe Energía regalada [€/año]	0	0	0	0	0	0

Con respecto al impacto del autoconsumo PV sobre la facturación energética se parecía claramente una drástica reducción del termino de energía en la facturación para los dos escenarios de autoconsumo PV. Alcanzando para el escenario 2 una reducción del 50% del termino de energía respecto al del año de referencia. Mientras que el impacto sobre el termino de potencia es prácticamente imperceptible para niveles ≤1,38% de penetración del EV, conteniendo dicho termino en un pequeño porcentaje. Ahora bien, para niveles >1,38% de penetración del EV el impacto sobre el termino de potencia es más visible. Aunque en ningún caso se alcanzan reducir estos valores al nivel del año de referencia. Este hecho se debe a que tanto el autoconsumo PV como el estacionamiento y carga de los EV son procesos estocásticos, que van variando aleatoriamente con el tiempo, lo que implica que gran parte del tiempo se supere la potencia contratada para determinados periodos de facturación.

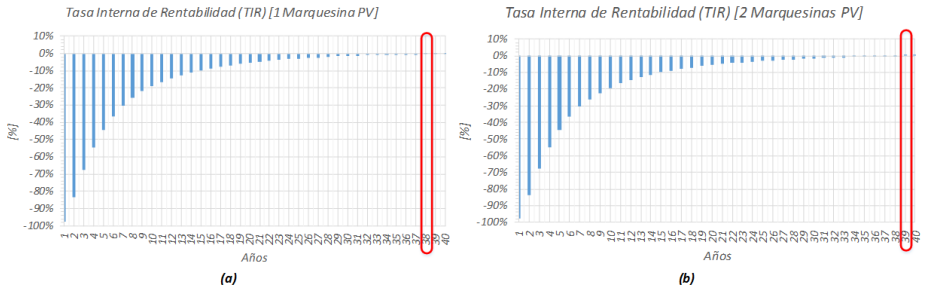

Fig. 7. a: Tasa Interna de Rentabilidad para el escenario 1 de autoconsumo PV. b: Tasa Interna de Rentabilidad para el escenario 2 de autoconsumo PV.

Con respecto a la idoneidad de los dos escenarios PV, ninguno de ellos genera energía suficiente para ningún nivel de penetración del EV para alcanzar a compensar el término de energía mensual, y por ello verse obligado a regalar los excedentes de generación a la red de distribución. Ahora bien, el escenario 1 de autoconsumo PV presenta unos importes anuales por los excedentes PV, que no han podido ser autoconsumidos, muy inferiores a los del escenario 2. Esto hace pensar que el escenario 1 es a priori mucho más óptimo que no el escenario 2. Debido a que la modalidad de autoconsumo con excedentes acogidos a compensación, recogido en el RD244/2019, está enfocado al autoconsumo directo plateando una compensación asimétrica para los excedentes de generación. Que, a la práctica conlleva tener que se tengan que generar 3 kWh para compensar 1 kWh de demanda no auto-consumida. Lo que implica que para instalaciones con una demanda base pequeña, como es el caso del aparcamiento analizado, no tenga sentido instalar gran cantidad generación PV, ya que difícilmente podrá ser absorbida por la instalación, y la venta de excedentes no parece a priori económicamente interesante.

Tabla 8. Detalle de los costes asociados al despliegue de las infraestructuras de carga y de autoconsumo PV.

Escenarios	***1 x Marquesina PV2-2***	***2 x Marquesina PV2-2***
Importe Marquesina + estación carga [€]	12.395,62	21.468,84
Importe Obra Civil [€]	2.528,74	2.807,48
Importe Instalación Eléctrica [€]	1.800,00	1.800,00
Otros (Transporte y Legalización) [€]	1.000,00	2.000,00
Importe de la Inversión [€]	***17.724,36***	***28.076,32***

Una vez, evaluados los ahorros asociados para los dos escenarios de autoconsumo PV se procederá a analizar la viabilidad económica de cada uno de ellos. Donde se espera que los ahorros energéticos permitan sufragar la inversión de la instalación PV y de las estaciones de carga. Concretamente la inversión a realizar para cada uno de los escenarios se presenta desglosada en la Tabla 8. A partir del importe del a inversión y los

ahorros presentados en la Tabla 7 se evaluará la *Tasa Interna de Retorno* (TIR) con objeto de estimar la viabilidad económica del despliegue de los dos escenarios de autoconsumo PV. Los resultados obtenidos del TIR para los dos escenarios de autoconsumo PV para un periodo de 40 años, se presentan en la Fig. 7. En dicha figura se apreciar cómo se requieren 38 años para amortizar el escenario 1 de autoconsumo PV y 39 años para amortizar el escenario 2. Lo que indica a todas luces que el despliegue de estas infraestructuras a cargo de los ahorros energéticos es inviable. Lo que resulta chocante si se comparan estos periodos con los de las plantas de generación PV conectadas a red que están actualmente entre los 5 y 8 años.

5 Conclusiones

En este trabajo se ha presentado una metodología para la planificación de las infraestructuras de carga de los EV y la estimación de su demanda energética asociada. Que ha servido de base para la estimación del impacto económico y energético que conllevaría la incorporación de diferentes escenarios de autoconsumo PV para dar soporte a la carga de los EV, en el periodo de los próximos 5 años, en el aparcamiento público de "*Compte d'Empuries*" operado en régimen de rotación por la SMAP, y ubicado en el centro de Palma de Mallorca. Para ello, inicialmente se ha abordado una metodología estadística para la previsión de la serie temporal de penetraciones del EV en el parque móvil, para los próximos 5 años; obteniendo valores de penetración comprendidos entre [*0,28-2.35%*] para dicho periodo. Que han servido de datos de partida para la estimación de la demanda energética del aparcamiento, para los dos escenarios de autoconsumo PV. Para finalmente determinar sus costes energéticos asociados.

Los resultados obtenidos muestran como la incorporación de generación PV en régimen de autoconsumo tiene un efecto beneficio al reducir la demanda energética global compensando en gran medida el aumento de demanda energética vinculada con la carga del EV. Donde el autoconsumo PV de 4,05kWp ha alcanzado una reducción de la demanda media del 25,81% para los diferentes niveles de penetración del EV, mientras que el autoconsumo PV de 8,10kWp ha alcanzado una reducción de la demanda media del 29,74%. Concentrándose la mayor parte de los ahorros en el periodo de las 8-18h, donde se concentra la generación PV.

A su vez, análisis del impacto económico de la penetración del EV han mostrado como bajos niveles de penetración del EV llevan asociados incrementos significativos de los costes energéticos. Donde una penetración del 2,35% del EV conllevará un incremento del 34,39% de la factura energética. A su vez, el autoconsumo PV de 4,05kWp alcanzará de media un ahorro del 13,25% de la factura energética para los diferentes niveles de penetración del EV, mientras que el autoconsumo PV de 8,10kWp el ahorro crecerá hasta el 20,08%. Concretamente los resultados muestran como el autoconsumo PV resulta ser un mecanismo efectivo para mitigar el incremento del coste de la factura energética, impactando esencialmente sobre el término de energía, al menos para los niveles actuales de penetración del EV. A su vez, los resultados arrojan que el escenario de autoconsumo más interesante, para un aparcamiento con una demanda base pequeña

como es el caso, es el compuesto por tan solo marquesina PV al no tener sentido práctico instalar mayores potencias PV. Ello debido a que modalidad de autoconsumo con excedentes acogidos a compensación, recogido en el RD244/2019, está enfocada al autoconsumo directo penalizando los excedentes de generación mediante una compensación asimétrica de la generación frente a la demanda.

Finalmente, se ha analizado la viabilidad de sufragar la inversión para el despliegue de los dos escenarios de autoconsumo PV en base a los ahorros energéticos; resultando en ambos casos inviable. Por ello, el despliegue de este tipo de infraestructuras solo será viable mediante ayudas o inversiones públicas encaminadas al despliegue de una infraestructura pública de estaciones de carga suficiente para dar soporte a transición hacia una movilidad sostenible.

6 Agradecimientos

Este trabajo ha sido financiado en parte por el Ministerio de Economía, Industria y Competitividad de España (MINECO) en virtud de los proyectos TEC2017-84877-R y ENE2015-68339-R, y por la UE a través de los Fondos Regionales de Desarrollo Europeo (FEDER). Así como por el programa iberoamericano de ciencia y tecnología para el desarrollo (CYTED), bajo el proyecto de red 518RT0558 titulado *Ciudades Inteligentes Totalmente Integrales, Eficientes y Sostenibles* (CITIES).

Referencias

1. UNFCCC Secretariat (2015) Synthesis report on the aggregate effect of the intended nationally determined contributions, FCCC/CP/2015/7. Paris
2. IRENA, IEA (2017) Perspectives for the Energy Transition: Investment Needs for a Low-Carbon Energy Transition
3. DOE, EIA, Office of Energy Analysis (2016) International Energy Outlook 2016, With Projections to 2040. Energy Dept.; Energy Information Administration; Office of Energy Analysis
4. Fazelpour F, Vafaeipour M, Rahbari O, Rosen MA (2014) Intelligent optimization to integrate a plug-in hybrid electric vehicle smart parking lot with renewable energy resources and enhance grid characteristics. Energy Convers Manag 77:250–261. https://doi.org/10.1016/j.enconman.2013.09.006
5. Amini MH, Boroojeni KG, Cheng Jian Wang, et al (2016) Effect of electric vehicle parking lots' charging demand as dispatchable loads on power systems loss. In: 2016 IEEE International Conference on Electro Information Technology (EIT). IEEE, pp 0499–0503
6. Tulpule PJ, Marano V, Yurkovich S, Rizzoni G (2013) Economic and environmental impacts of a PV powered workplace parking garage charging station. Appl Energy 108:323–332. https://doi.org/10.1016/j.apenergy.2013.02.068
7. Kintner-Meyer M, Schneider K, Pratt R (2006) Impact assessment of plug-in hybrid vehicles on electric utilities and regional US power grids. Part 1: Technical analysis

8. Duvall M Environmental assessment of plug-in hybrid electric vehicles (PHEVs) : greenhouse gas emissions and air quality impacts of PHEVs. In: The PHEV 2007 conference : where the grid meets the road. Winnipeg, MB (Canada)
9. Alsabaan M, Alasmary W, Albasir A, Naik K (2013) Vehicular Networks for a Greener Environment: A Survey. IEEE Commun Surv Tutorials 15:1372–1388. https://doi.org/10.1109/SURV.2012.101912.00184
10. IEA – International Energy Agency (2019) Global EV Outlook 2019: Scaling up the transition to electric mobility
11. Levinson RS, West TH (2018) Impact of public electric vehicle charging infrastructure. Transp Res Part D Transp Environ 64:158–177. https://doi.org/10.1016/j.trd.2017.10.006
12. Wood EW, Rames CL, Muratori M, et al (2017) National Plug-In Electric Vehicle Infrastructure Analysis. Golden, CO (United States)
13. Nunes P, Figueiredo R, Brito MC (2016) The use of parking lots to solar-charge electric vehicles. Renew Sustain Energy Rev 66:679–693. https://doi.org/10.1016/j.rser.2016.08.015
14. Nunes P, Farias T, Brito MC (2015) Day charging electric vehicles with excess solar electricity for a sustainable energy system. Energy 80:263–274. https://doi.org/10.1016/J.ENERGY.2014.11.069
15. Fattori F, Anglani N, Muliere G (2014) Combining photovoltaic energy with electric vehicles, smart charging and vehicle-to-grid. Sol Energy 110:438–451. https://doi.org/10.1016/j.solener.2014.09.034
16. Poullikkas A (2015) Sustainable options for electric vehicle technologies. Renew Sustain Energy Rev 41:1277–1287. https://doi.org/10.1016/j.rser.2014.09.016
17. Romo R, Micheloud O (2015) Power quality of actual grids with plug-in electric vehicles in presence of renewables and micro-grids. Renew Sustain Energy Rev 46:189–200. https://doi.org/10.1016/j.rser.2015.02.014
18. Amini MH, Moghaddam MP, Karabasoglu O (2017) Simultaneous allocation of electric vehicles' parking lots and distributed renewable resources in smart power distribution networks. Sustain Cities Soc 28:332–342. https://doi.org/10.1016/j.scs.2016.10.006
19. Ministerio para la Transición Ecológica (2019) Real Decreto 244/2019, de 5 de abril, por el que se regulan las condiciones administrativas, técnicas y económicas del autoconsumo de energía eléctrica. Madrid, Spain
20. Asociación Española de Fabricantes de Automóviles y Camiones (ANFAC) (2017) Informe anual ANFAC 2016. Madrid
21. Box GEP, Jenkins GM, Reinsel GC, Ljung GM (2015) Time Series Analysis: Forecasting and Control, 5th Edition. Wiley
22. Dirección General de Trafico (DGT) (2016) Parque de vehículos - Tablas Auxiliares Anuario - 2016. Madrid
23. SAE (2010) SAE J1772: Electric Vehicle and Plug in Hybrid Electric Vehicle Conductive Charge Coupler
24. IEC (2011) IEC 62196-2 ed1.0: Plugs, socket-outlets, vehicle connectors and vehicle inlets - Conductive charging of electric vehicles
25. IEC (2010) IEC 61851-1 ed2.0: Electric vehicle conductive charging system – Parts 1, 21, 23, 24

26. Blanco-Muriel M, Alarcón-Padilla DC, López-Moratalla T, Lara-Coira M (2001) Computing the solar vector. Sol Energy 70:431–441. https://doi.org/10.1016/S0038-092X(00)00156-0
27. Duffie JA, Beckman WA (2013) Solar Engineering of Thermal Processes: Fourth Edition
28. Pujol-Nadal R, Martínez-Moll V, Moià-Pol A, et al (2016) OTSun Project: Development of a Computational Tool for High-Resolution Optical Analysis of Solar Collectors. In: Proceedings of EuroSun2016. International Solar Energy Society, Freiburg, Germany, Germany, pp 1–11
29. Pujol-Nadal R, Bonnín-Ripoll F, Martínez-Moll V, Cardona G (2018) Simulación óptica de captadores solares mediante la herramienta web OTSun. In: Solar AE de E, Energía II (eds) Energía limpia y gestionable para tod@s. Libro de Actas del XVI Congreso Ibérico y XII Congreso Iberoamericano de Energía Solar. SAPT Publicaciones Técnicas, S.L., pp 151–158
30. King DL, Boyson WE, Kratochvil JA, et al (2004) Photovoltaic Array Performance Model. In: Sandia National Laboratories. pp 2004–3535
31. Dobos A (2014) PVWatts Version 5 Manual. Golden, CO (United States)
32. Ministerio de Industria Energía y Turismo (2014) Resolución de 23 de mayo de 2014, de la Dirección General de Política Energética y Minas, por la que se establece el contenido mínimo y el modelo de factura de electricidad. Madrid, Spain

A Solid-state Smart Switch for Controlling the Electrical Energy Flow Provided by Three Different Power Sources

Pedro Banuelos-Sanchez[1][0000-0001-5502-2993], Jose Luis Vazquez-Gonzalez[1][0000-0002-2368-3786], Ruben Alejos-Palomares[1][0000-0002-8732-4686], and Luis Garcia-Santander[2][0000-0002-6474-6528]

[1] Universidad de las Americas Puebla, Puebla, 72810, MEXICO
[2] Universidad de Concepción, Concepción, 4089100, CHILE
pedro.banuelos@udlap.mx

Abstract. This paper presents a Smart Switch implemented with Silicon Controlled Rectifiers (SCRs), an arduino, and a raspberry PI for electrical energy savings. The purpose of the smart switch, based on voltage detection, is to have the ability to switch the electrical energy from an initial power source to a cheaper power supplier. This paper provides the details of an experimental prototype where a voltage drop, greater than 10 %, in a power source provokes to switch to another available power source, keeping a constant voltage to a load. Experimental results verify the performance of the experimental smart switch where the nominal AC voltage is 120 V and a frequency of 60 Hz.

Keywords: Smart Switch, Smart Grids, Power Converters, Power Quality.

1 Introduction

The electric utility industry is probably the largest and most complex industry in the word. It is related to generation, transmission, distribution, and utilization of electrical energy. In the past, utilities generated and delivered electric power to a specific area. The transmission system was built to deliver power from a utility's generator across town to its distribution company. The increase of customers meant an increase of generators and transmission lines. But, customers kept increasing; the electric grid became complex to supply the required energy. Coal, oil, and gas were the main fuel resources to generate electricity. Once again, population kept increasing. Recently, new fuel energies emerged, but this time, clean energies, ecofriendly energies. The traditional unidirectional radial distribution system is in transition to a multidirectional distribution system due to the increase of generation sources and customers.

Facing the huge problem represented by global warming and a tremendous customer's demand, electrical energy has been generated by using renewable energies. The undeniable advantage of these sources is their resilience; they are replenished as they are consumed. Solar, wind, hydro, geothermal, and biomass are the most common renewable energies. For instance, photovoltaic (PV) energy can be almost generated everywhere, and this energy can be integrated to the main distribution system without the

need of the transmission system, reducing the cost of electrical systems. But the grid becomes complex. Hundreds of small generators are participating in the generation of the total energy. The integration of renewable energies makes the traditional distribution networks to face many challenges.

The International Energy Agency (IEA) defines a Smart Grid as " an electricity network that uses digital and other advanced technologies to monitor and manage the transport of electricity from all generation sources to meet the varying electricity demands of end-users. Smart grids co-ordinate the needs and capabilities of all generators, grid operators, end-users and electricity market stakeholders to operate all parts of the system as efficiently as possible, minimizing costs and environmental impacts while maximizing system reliability, resilience and stability" [1]. The concept of Smart Grid is to provide customers with a stable and reliable power, even if there is a lot of generators and consumers. Smart grid manages a two-way communication capabilities and information flow. It has information from the providers and from the consumers of electric power. Customers can emit their power requirements to the providers. The users become active players to improve the use of electrical energy.

Power electronics converters take a preponderant place in energy conversion and smart grid's information. PV systems generate DC voltage, then, it is necessary to use an inverter to convert from DC to AC power energy. Depending on the type of distribution network, a single-phase or a three-phase inverter has to be used to integrate PV energy to the mains [2, 3, 4]. Not only PV systems use power electronics converters, wind energy should be also regulated. The faster the wind blows, the wind turbine rotates faster and the more electricity is generated. An AC/DC/AC converter regulates varying AC voltage to a fix in amplitude and frequency AC voltage [5, 6, 7]. In the case of smart grid, power converters are used to control the energy flow depending on the bidirectional data. Smart grids must replace traditional electric systems. Conventional systems cannot continue bearing the highly increasing demand of electrical energy.

2 The power converter

An AC/AC converter, or voltage controller, is a converter that controls the voltage, current and consequently the power to an AC load from an AC power supply. Power electronics switches connect or disconnect the load to the source depending on the required action. In phase control scheme, the switches are connected at a delay angle between 0° to 180 °. Figure 1a shows a single-phase AC/AC converter with a resistive load. If the delay angle is α, then the load voltage is as shown in Figure 1b. The average load voltage is always zero as the source voltage. However, the rms load voltage has changed. The load voltage is no longer equal to the source voltage. Varying the delay angle, the rms load voltage changes and then the output power.

The heart of an AC/AC converter is the Silicon Controlled Rectifier (SCR). When a SCR is forward biased and a pulse signal is applied to the SCR's gate, the SCR is on, allowing the load to be connected to the source at the required needs. If the delay angle is 0°, the load voltage is always the same as the input voltage; even, the average and the rms load voltage are equal to the input voltage. The SCR allows the load to be

connected or disconnected to the source when it is required; for example, when an important voltage drop happens, the SCRs can disconnect the load.

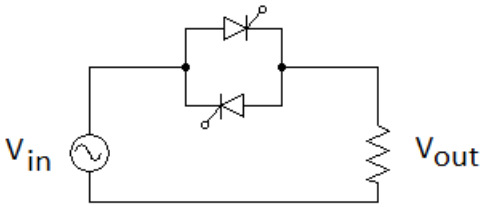

(a)

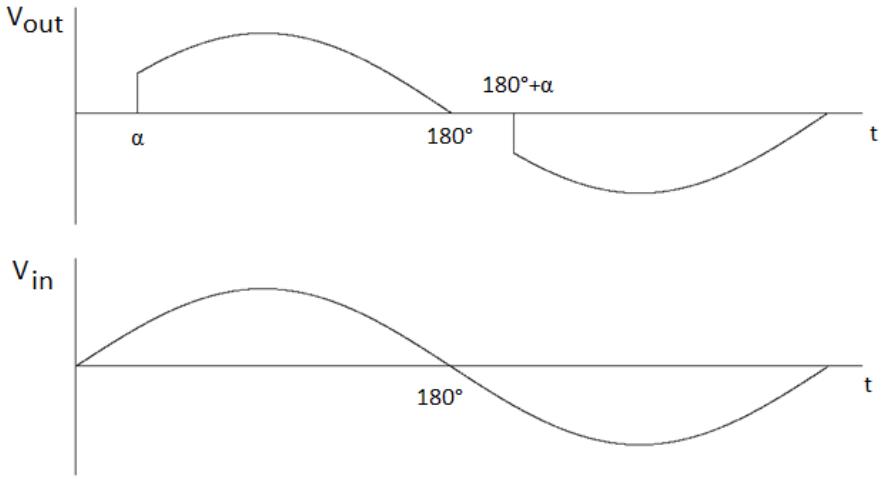

(b)

Fig. 1. (a) AC/AC converter with resistive load. (b) Output and input voltage with a delay angle of α degrees.

3 Proposed circuit

A voltage controller can be used to control the energy flow from the source to the load. Depending on our needs, the SCRs are connected or disconnected. If we want to control the power delivered to the load, we can change the delay angle of the SCRs. However, a voltage controller, as shown in figure 1, can be used to connect the load to a different

power source. In a modern power system, as we have said, the electrical energy is no longer generated by just one generation facility. The integration of renewable energies allows to the consumers to have the possibility to select which power source is the cheapest in a specific moment of time. When there is sunlight, it is possible that the energy provided by a PV generator is cheaper than that generated by a thermoelectric facility. The consumers would have the opportunity to choose which facility is better for them. Smart grid can accomplish this task.

Figure 2 shows the proposed smart switch, which is composed by S1, S2, and S3 simple bidirectional switches. In this case, three different power sources, or three different electrical facilities, are considered: V_1 represents the energy coming from a wind turbine; V_2 is the voltage generated by a PV system, and V_3 is the conventional fossil fuel voltage generated. Suppose that the final consumer needs electrical energy at 10 pm. At this moment, there is no sunlight, then, there is no V_2 source. Suppose there is no wind at that precise time, meaning that V_1 source is OFF too. Then, the consumer has to purchase the electrical energy just from the conventional generator. Switch S3 is then ON while S1 and S2 are OFF.

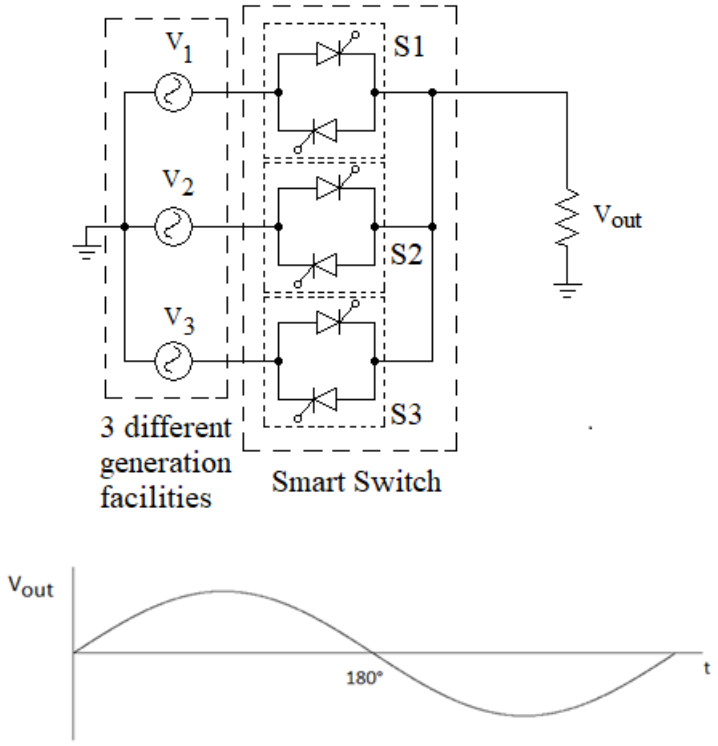

Fig. 2. A smart switch used to select the cheapest energy provider.

Now consider that the consumer has electrical needs at 10 am. This means that there is sunlight, and probably, the wind is blowing up. In this case, the three generators are ready to supply the required energy. By the use of the smart switch shown in figure 2, the consumer has the ability to choose which provider is the best option. If the electrical facility V_2 is located closer to the consumer, the cost of the electrical energy can be cheaper. Switch S2 is ON while V_2 is the cheapest energy. A similar situation occurs when the cheapest energy comes from the wind generator. Switch S1 is now ON, while witches S2 and S3 are OFF. The smart switch allows the consumer to choose the cheapest energy at a precise moment depending on generation, transmission, and distribution costs. The increasing integration of renewable energies to the mains can be faced by the use of smart technologies as the proposed smart switch.

The proposed smart switch uses an Arduino and a Raspberry PI transmitter/receiver to control the information. Depending on a real time database, the Raspberry emits a signal to connect the cheapest power supply to the load. Figure 3(b) shows the triggering circuit of the bidirectional switch. Optocoupler MOC3023 isolates digital signals, coming from the raspberry, to the power system. This type of optocoupler configuration allows to control any AC powered load. The bidirectional switches are capable of conducting in both halves of an AC cycle with zero-crossing detection, Fig. 3(a), allowing the load to receive full power. Fig. 3(a) shows the zero-crossing detector. When the AC signal goes from positive to negative or negative to positive, a pulse signal is generated and the raspberry reads it. The optocoupler 4N25 isolates the raspberry to the power AC signal. The load receives a complete AC cycle all the time long.

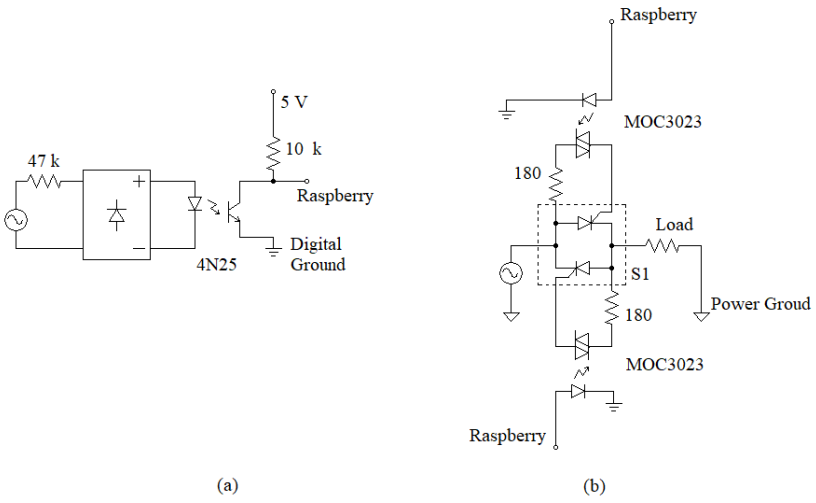

Fig. 3. (a) Zero-crossing detector. (b) Triggering circuit of the bidirectional switches, in this case, just for the switch S1.

4 Experimental Results

A smart switch as shown in figure 2 was implemented to test its the operability. The experimental Smart Switch was tested when three different power sources are available to supply electrical energy to just one load. For this case, we suppose that if one of the sources is ON, the load should be ON. When two or three sources are ON, the load is always ON but the electrical energy is supplied by a specific source as shown in Table 1. For example, if sources 1, 2, and 3 are ON, the smart switch selects the source 1 as the voltage provider. But if source 1 and source 2 are OFF, and source 3 is ON, then, the electrical energy is provided by source 3. When the voltage source drops more than 10 %, we are also considering that the source is OFF. The possible combinations shown in Table 1 were tested. The load was always ON and the smart switch selected the right power source. This test was made because we didn't have enough information to conform a database representing the cost of the electrical energy in a specific period of time.

Table 1. Possible combinations to select the source feeding the load.

Source 1	Source 2	Source 3	Source feeding the load	Load
OFF	OFF	OFF	--	OFF
OFF	OFF	ON	Source 3	ON
OFF	ON	OFF	Source 2	ON
OFF	ON	ON	Source 2	ON
ON	OFF	OFF	Source 1	ON
ON	OFF	ON	Source 1	ON
ON	ON	OFF	Source 1	ON
ON	ON	ON	Source 1	ON

The experimental prototype used a three-phase power supply, representing three different power sources. For our case, it means that the three voltages have the same frequency and voltage amplitude relative to a common reference but with a phase difference of one third of a cycle between each. We have intentionally reduced the voltage of one or more of the sources as suggested by Table 1. The smart switch selected the correct source when the others sources were OFF.

Figure 4 shows the load voltage (yellow line) and the source 2 voltage (blue line). In this case, source 3 was initially supplying energy to the load. We have reduced the voltage of source 3. The smart switch detected the voltage reduction. After a short time, it switched from source 3 to source 2. Load voltage is equal to zero for a short period of time (yellow line in the figure). It means that the smart switch detected the voltage was crossing the zero, and then, it waited to the next complete cycle to provide energy to the load. The difference on phase of 120° between both sources is evident in the figure.

Figure 5 shows source 2 voltage (blue line), load voltage (yellow line), and the pulse of zero-crossing detector. The pulse is necessary to synchronize the SCRs delay angle. For this example, the delay angle was 0° all the time. We didn't control the amount of power delivered to the load. We just needed to choose the power source where the rms voltage and frequency were constant; for our case, 120 Vrms and 60 Hz, respectively.

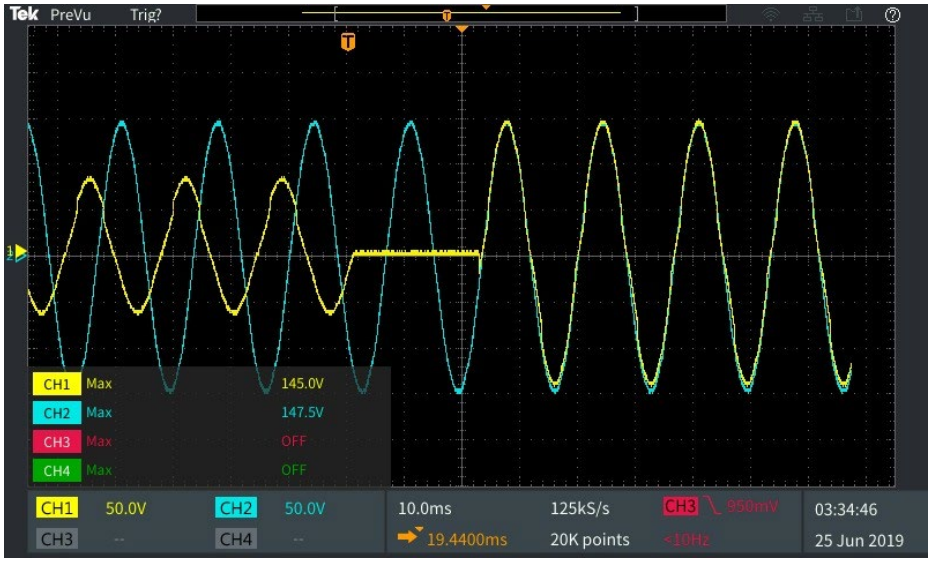

Fig. 4. Load voltage (yellow line) switched from source 3 to source 2 (blue line).

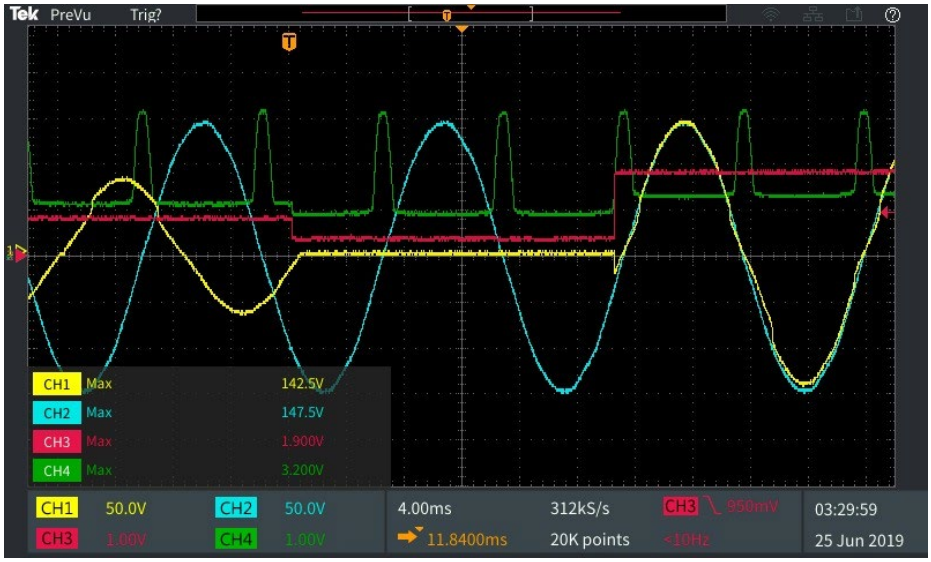

Fig. 5. Load voltage (yellow line) switched from source 3 to source 2 (blue line). The pulse of zero-crossing detector is indicated in green line.

5 Conclusions

A simple smart switch was implemented and tested. An AC load drained energy from 3 different power sources, once at a time. When the supplying source experienced a voltage drop, the smart switch changed from that source to a source where the voltage and frequency where unperturbed. This action was done automatically. The implemented smart switch can be also used to select a voltage provider offering the cheapest electrical energy. For this case, a complete database is necessary. That's the future work to be done.

References

1. IEA Homepage, http://www.iea.org/publications/freepublications, last accessed 2019/08/08
2. T.C.Y. Wang, Zhihong Ye, Gautam Sinha, Xiaoming Yuan: Output filter design for a grid-interconnected three-phase inverter. In: IEEE 34th Annual Conference on Power Electronics Specialist, 2003, PESC'03. Vol. 2, pp. 779-784. Publisher: IEEE (2003).
3. Satoshi Nagai, Keisuke Kusaka, Jun-ichi Itoh: FRT capability of a single-phase grid-connected inverter with minimized interconnected inductor. In: 2017 IEEE Applied Power Electronics Conference and Exposition (APEC). pp. 2802-2809. Publisher: IEEE (2017).
4. Ke Chen, Zhikun Huang, et al: Cascaded iH6 multilevel inverter with leakage current reduction for transformerless grid-connected photovoltaic system. In: IEEE 12th International Conference on Power Electronics and Drive System (PEDS). Publisher: IEEE (2017).
5. Kotb B. Tawfig, A. F. Abdou, E. E. EL-Kholy, S. S. Shokrall: Application of matrix converter connected to wind energy system. In: 8th International Middle East Power Systems Conference (MEPCON). Publisher: IEEE (2016).
6. Adel Mehdi, Abdelmalek Boulahia, Houssam Medouce, Hocine Benalla: Induction generator using AC/DC/AC PWM converters and its application to the wind-energy systems. In: Eurocon 2013. Publisher: IEEE (2013).
7. Abdelmalek Boulahia, Khalil Nabti, Hocine Benalla: Direct Power Control for AC/DC/AC Converters in Doubly Fed Induction Generators Based Wind Turbine. In: International Journal of Electrical and Computer Engineering (IJECE). Vol. 2, No. 3. pp. 425-432. (2012).

Multiobjective household energy planning using evolutionary algorithms

Giovanni Colacurcio[1], Sergio Nesmachnow[1],
Jamal Toutouh[2], Francisco Luna[3], and Diego Rossit[4]

[1] Universidad de la República, Uruguay,
{giovanni.colacurcio,sergion}@fing.edu.uy

[2] Massachusetts Institute of Technology, USA
toutouh@mit.edu

[3] Universidad de Málaga, Spain
flv@lcc.uma.es

[4] Universidad Nacional del Sur, Argentina
diego.rossit@uns.edu.ar

Abstract. This article presents the advances in the design and implementation of a recommendation system for planning the use of household appliances, focused on improving energy efficiency from the point of view of both energy companies and end-users. The system proposes using historical information and data from sensors to define instances of the planning problem considering user preferences, which in turn are proposed to be solved using a multiobjective evolutionary approach, in order to minimize energy consumption and maximize quality of service offered to users. Promising results are reported on realistic instances of the problem, compared with situations where no intelligent energy planning are used (i.e., '*Bussiness as Usual*' model) and also with a greedy algorithm developed in the framework of the reference project. The proposed evolutionary approach was able to improve up to 29.0% in energy utilization and up to 65.3% in user preferences over the reference methods.

1 Introduction

Energy management is a crucial issue in nowadays societies. Many strategies have been proposed to guarantee an increased access to the energy resources at affordable costs for citizens, while ensuring the preservation of natural resources and the protection of the environment [15].

For implementing effective energy management policies, innovative technologies must be integrated in easy-to-use and efficient systems, which must include specific features to be useful for both energy companies and citizens. In order to be applied by energy companies, management systems must include capabilities for performing realistic simulations, controlling, and planning the electricity market. From the point of view of citizens, system must provide easy-to-use applications to monitor and manage the energy consumption at household level.

The capabilities of monitoring, controlling, and managing the energy consumption and generation are very important to provide good quality of service (QoS) and user experience, especially when considering the emphasis on citizen engagement, environment protection, and economic considerations, under the novel paradigm of smart cities [4].

Residential buildings significantly contribute to the total energy used in the world. According to statistics from the USA Energy Information Administration, the average household in the USA and Canada uses about 12,000 kWh of electricity. In Europe the figure is less than 10,000 KWh, but also significant. Some household appliances make the biggest contributions to consumption, including heaters and air conditioning (40–45%), electronic and kitchen appliances (∼30%), water heaters (15%–20%), and cooling (5%–10%) [16]. Energy utilization patterns are not too different in developing countries, where the impact of energy consumption is also very important.

The related literature indicates that systems based on planning the use of *deferrable appliances* allow improving energy efficiency at domestic level [12,14]. Deferrable appliances are those whose demand for energy can be postponed or interrupted (such as dishwashers, washing machines, etc.), causing a negligible impact on the QoS provided to users. This is an important approach that takes into account the different prices of electricity and the availability of (non-storable) energy from renewable sources.

In this line of work, this work presents the application of evolutionary algorithms (EAs) to solve the problem of planning the use of household appliances considering user preferences. A multiobjective approach is considered, aiming at simultaneously maximizing user satisfaction (evaluated in terms of the QoS offered according to the specified preferences) and minimizing the total energy consumed, which is directly related to the total cost of the electricity bill for the user. The main results indicate that the proposed approach is able to find appropriate plannings that improve over situations where no intelligent energy planning are used (i.e., '*Bussiness as Usual*' model) and also with a greedy algorithm previously proposed in the framework of the reference project.

The main contributions of this research are: *i)* formulating a novel multiobjective household energy planning problem accounting for user satisfaction and energy consumption; *ii)* devising a specific EA to address the problem, using a linear aggregation approach for the objectives; and *iii)* evaluating the proposed evolutionary approach over realistic scenarios, built by using real data of household energy consumption from well-known repositories.

The research reported in this article is developed in the context of the Cloud Computing for Smart Energy Management (CC-SEM) project [6,7], which proposes building an integrated platform for smart monitoring, controlling, and planning energy consumption and generation in urban scenarios. The project integrates cutting-edge technologies (Big Data analysis, computational intelligence, Internet of Things, High Performance Computing and Cloud Computing) and specific hardware for energy monitoring/controlling built within the project.

The article is organized as follows. Section 2 presents the formulation of the multiobjective household energy consumption planning and a review of related works. The proposed evolutionary approach for household energy planning is described in Section 3. The experimental analysis is reported in Section 4. Finally, Section 5 presents the conclusions and the main lines of future work.

2 The household energy planning problem

This section introduces the household energy planning problem, the multiobjective formulation addressed in this article, and a review of related works.

2.1 General considerations

The goal of the study is to develop a system to help end-users to take appropriate decisions concerning the use of household appliances in a given planning period (e.g., daily, weekly, etc.). The problem consists in scheduling the use of different household appliances to minimize the electric bill, taking into account the end-user preferences, electricity prices, and the available contracted power.

The planning period is divided in slots considering the user preferences. For every slot, each user can indicate a value that represents the priority of using a certain appliance in that time. Higher values of priority represent a higher desire of using the appliance. In case that users do not indicate their preferences, machine learning is applied to infer preferences from the analysis of historical utilization data. Classification methods can also be applied to characterize the household power consumption, regarding neighboring houses and socio-economical data, such as for other public services [10].

The problem formulation assumes that the energy cost is known for each time interval. These values are publicly available from the energy companies, for example from the National Electricity Company (UTE) in Uruguay. Also, the maximum contracted power for each user is known, from the contract details provided by the energy company. The contracted maximum power can only be surpassed by a small amount (up to 30%) in a short period of time, without causing a short circuit. Schedules that includes such a surplus are penalized.

2.2 Problem formulation

The multiobjective version of the household energy planning problem addressed in this article considers the following elements:

- a set of users $U = (u_1 \dots u_N)$, each user represents a house in a city;
- a set of time slots $T = (t_1 \dots t_M)$ in the planning period;
- a set of domestic appliances $L = (l_1 \dots l_K)$ for each user;
- a function $E : U \rightarrow \mathbb{N}$, where $E(u_i)$ indicates the maximum electric power contracted by user u_i;
- a penalty term ρ applied to those users that surpass the maximum electric power contracted;

- a function $D : L \times U \rightarrow \mathbb{N}$, where $D(l_k, u_i)$ indicates the average time of utilization of appliance l_k for user u_i;
- a function $C : T \rightarrow \mathbb{N}$, where $C(t_j)$ indicates the utilization cost (per kW) of the energy in time t_j;
- a function $P : L \rightarrow \mathbb{N}$, where $P(l_k)$ indicates the power (in kWh) consumed by appliance l_k;
- and a function $UP : U \times L \times T \rightarrow \mathbb{N}$, where $UP(u_i, l_k, t_j)$ indicates the preference of user u_i to use the appliance l_k at time t_j;

Lets consider the binary variable x^i_{kj}, that indicates if appliance l_k of user u_i is turn on at time t_j; and function $y(x^i_{kj})$ that indicate the time period in which appliance l_k of user u_i is turned on continuously (without intermediate turn off) from time t_j: $y(x^i_{kj}) = m - j$ with $m = \max r / \forall h \in (j, r)\ x^i_{kh} = 1$

The problem proposes finding a planning function $X = \{x^i_{kj}\}$ for the use of each household appliance that simultaneously maximizes the user satisfaction defined in Eq. 1 (given the users' preference functions) and minimize the total energy consumed (see Eq. 2).

$$f(X) = \sum_{i=1}^{N} \sum_{j=M}^{T} \sum_{k=1}^{K} UP(u_i, l_k, t_j) \times \delta^i_{kj} \tag{1}$$

$$\text{with } \delta^i_{kj} = \begin{cases} 1 \text{ if } y(x^i_{kj}) \geq D(l_k, u_i) \\ 0 \text{ otherwise} \end{cases}$$

$$g(X) = \sum_{i=1}^{N} \sum_{j=M}^{T} \sum_{k=1}^{K} x^i_{kj} \times C(t_j) \times P(l_k) + \rho \times \psi^i_{kj} \tag{2}$$

$$\text{with } \psi^i_{kj} = \begin{cases} P(l_k) - E(u_i) \text{ if } P(l_k) - E(u_i) \geq 0 \\ 0 \quad \text{otherwise} \end{cases}$$

Two scenarios are defined for defining the penalty model used for those situations in which the household consumption exceeds the maximum power contracted. The first scenario (*soft penalty*) is when the user exceeds the maximum power contracted for less than 30% of it. This is the maximum value of energy consumption that can exist without a short circuit occurring. In that case, the solution is penalized by a 30% of ρ. The second scenario (*hard penalty*) is when the user exceeds the maximum power contracted in a value greater than or equal to 30%. Therefore, that plannings are penalized entirely by the penalty term ρ.

Function UP considers the energy consumption measurements of electrical devices reported by Kolter and Johnson [5]. For each minute of the day, in the period of a month, the user preference is defined considering how many times each appliance was turned on for each appliance at that minute.

Function D uses consumption values of user appliances from a representative day. The duration of using for the appliance was studied, defined as the number of consecutive minutes in which it remained powered on [2].

2.3 Related works

The analysis of the related literature allows identifying several hardware- and software-based methods for household energy consumption characterization and planning. The main related works are reviewed next.

The main line of work related to the proposed research has been developed by Soares et al., who studied the household electricity demands and categorized a set of appliances, according to their use and management strategies that can be applied to them [13]. An initial work [14] introduced a model based on integer non-linear programming for energy utilization planning, with the aim of reducing cost. The authors applied an EA to minimize the cost of invoice and violations to the maximum contracted power. The EA allowed to reduce up to 40% the energy cost for the users with respect to a reference scenario without demand management. Later, the authors proposed minimizing cost and maximizing user satisfaction [12], which is the main motivation for the work proposed in our research. Results showed that the cost reduction was 22–24%. However, no trade-off solutions were computed, so different users with equal contracted power and equal preferences should adapt to the same planning. Additionally, no studies were carried out in different urban levels (buildings, neighborhoods, etc.) or used real data.

Our previous work [11] presented a hardware and software platform for intelligent monitoring and planning of energy consumption in homes. The proposed system integrates a hardware controller for energy efficiency, a communication protocol to improve data transmission, and a software module for planning and managing household devices. The proposed solution was implemented applying the Internet of Things (IoT) paradigm, allowing the integration of computational intelligence techniques. A greedy algorithm was proposed for planning, considering user preferences and a maximum allowed power consumption. Results showed that it is possible to reduce the energy consumption of a water heater to 38.9% and that two water heaters and an air conditioner can be optimized simultaneously without reducing QoS. These results suggest that the proposed approach is useful for energy consumption planning in homes.

Bilil et al. proposed a characterization of household appliances and a dynamic planning method for collaborative microgrids [1]. Two multiobjective optimization problems were studied, accounting for the activation and power profiles of appliances. A simulation procedure was applied to generate the instances of these problems and NSGA-II was used to solve them. The instances consisting in 40 microgrids that includle a flexible deferrable appliance, such as a water heater, and a non-flexible one (i.e., dishwasher). For the experiments, a residential load curve based on U.S. user profiles was used. The results showed that the load curve can indeed become very flat by applying the proposed bi-level multiobjective optimization scheduling approach.

The analysis of the related works indicates that there is room to contribute with solutions focused on the development of systems to implement the management of domestic demand through the integration of IoT technologies and computational intelligence algorithms.

3 The proposed EA for household energy planning

This section describes the proposed EA to solve the household energy planning problem.

3.1 Evolutionary algorithms

EAs are stochastic techniques that emulate natural evolution to solve optimization, search, and learning problems. They are useful for solving complex real-world problems in multiple application areas [9].

An EA is an iterative technique (each iteration is called *generation*). In each generation, probabilistic operators are applied on a set of individuals (the *population*). The initial population is generated by applying a random procedure or using a specific heuristic for the problem to be solved. Each individual encodes a tentative solution to the problem and has a *fitness* value that determines its suitability to solve the problem. The goal of the EA is to improve the fitness of individuals in the population. In order to achieve this objective, *evolutionary operators* are applied iteratively, such as the *recombination* of parts of two individuals and the random *mutation* of an individual's coding. These operators are applied to individuals selected according to their fitness, thus guiding the EA toward tentative solutions of higher quality that replace old individuals. The stop criterion usually involves a fixed number of generations, a quality level on the fitness of the best individual, or detecting convergence. The EA returns the best solution found in the iterative process, taking into account the fitness function considered for the problem. Algorithm 1 presents the generic schema of an EA with a population P.

Algorithm 1 Schema of an evolutionary algorithm.

```
1: initialize(P(0))
2: t←0                                          ▷ generation counter
3: while not stop criterion do
4:     evaluate(P(t))                           ▷ evolutionary cycle
5:     parents←selection(P(t))
6:     children←variation operators(parents)
7:     newpop←replacement(children,P(t))
8:     t++
9:     P(t)←newpop
10: end while
11: return best individual found                ▷ best fitness value
```

In this article, a traditional EA using a linear aggregation approach is used to solve household energy planning problem. Although the aggregation approach is often outperformed by Pareto-based methods for multiobjective optimization, it is a common approach in the literature, because of two main advantages: i) it is suitable for multiobjective optimization problems with a convex Pareto front, and ii) it is computationally efficient, so it is recommended when the times available to perform the planning is short [3].

3.2 The proposed EA for household appliances planning

The main features of the proposed EA for household appliances planning are described next.

Solution encoding. A problem-specific encoding is used to represent solutions. The proposed encoding considers for each user a vector $X = (x_0, x_1, \ldots, x_T)$, where T is the total number of timesteps (i.e., minutes) in the planning period. Each element x_j in the encoding is a vector of binary values $x_j = (b_1, b_2, \ldots, b_L)$, where L is the number of appliances considered in the planning and each value b_i indicates if the appliance is on on timestep j.

Fig. 1 presents an example of solution encoding for an instance of the problem considering five appliances. In the example, at timestep (minute) i, appliances #1, #2, and #5 are ON, while appliances #3 and #4 are OFF.

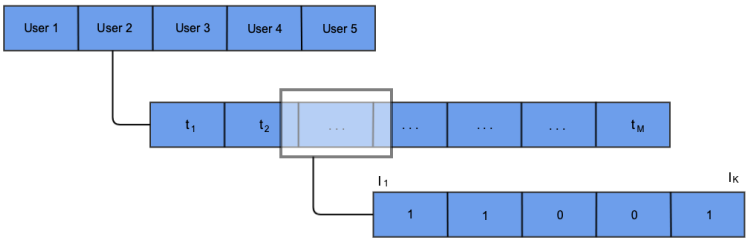

Fig. 1: An example of the proposed solution encoding.

Fitness assignment. The fitness function of the proposed EA corresponds to an linear aggregation of the power consumption and user satisfaction functions: $F = \alpha \times f(X) - \beta \times g(X)$. Several combinations of weights (α, β) were studied in order to properly weight each objective function and provide a useful search pattern. The main results of the analysis are reported in Section 4.3. The combination that allowed computing the best results was ($\alpha = 0.65$, $\beta = 1$).

Initialization. The population of tentative solutions is initialized by applying a randomized method that assigns to each appliance a probability $\gamma = 0.6$ (value tuned in preliminary experiments) to be ON at each time step, following a discrete non-uniform distribution. Assigning a slightly larger probability to each appliance to be ON than to be OFF allows starting the evolutionary search for a more diverse set of solutions. The value of γ was set to provide an equal pressure to both objectives, considering the weights defined in the previous paragraph.

Selection. The standard tournament selection was applied in the proposed EA. Preliminary experiments demonstrated that tournament selection provides an appropriate selection presure to guide the search. After a preliminary configuration analysis, the size of the tournament was set to two individuals, and the best of them is selected.

Evolutionary operators. Ad-hoc evolutionary operators were conceived to provide efficacy and diversity to the search, working with the proposed solution encoding. The proposed evolutionary operators are:

- *Recombination.* An ad-hoc version of the Single Point Crossover operator was conceived to recombine solutions. A cutting point is selected for each user and a new planning is created for each user, using information from the first parent (before the cutting point) and from the second parent (after the cutting point). Fig. 2 presents an example of the application of the proposed recombination operator between two solution for a problem instance with three users and six appliances for each user.

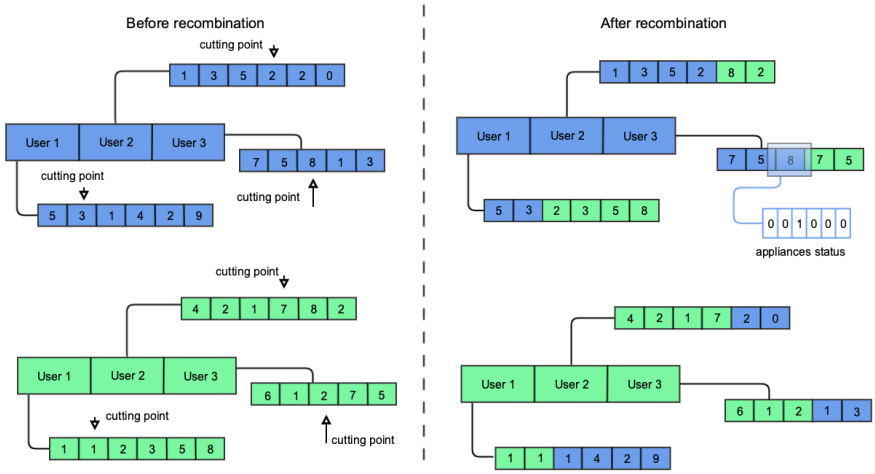

Fig. 2: An example of the proposed recombination operator.

Mutation. The mutation operator modifies the current state of an appliance. First, a specific time interval is randomly selected for every user, according to a uniform distribution. An appliance is then randomly selected (applying a uniform distribution) from all belonging to that user, and its state is changed (on/off or viceversa). Fig. 3 presents an example of the mutation operator.

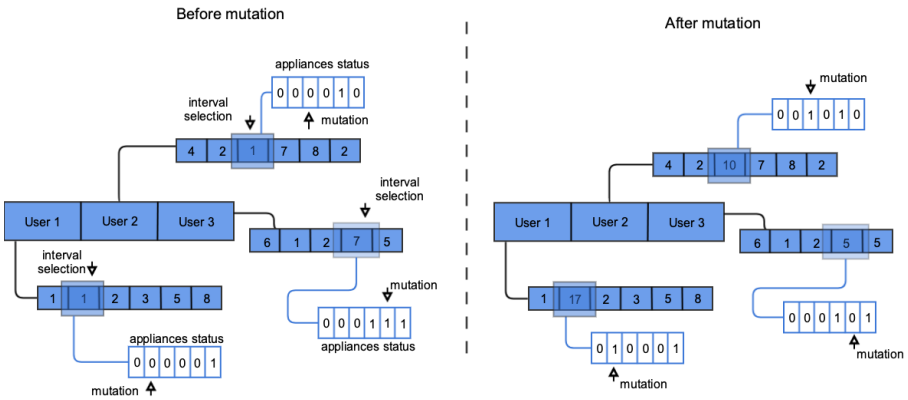

Fig. 3: An example of the proposed mutation operator.

3.3 Development and execution platform

The evolutionary approach was implemented using the ECJ library, a Java-based evolutionary computation system developed at George Mason University (`cs.gmu.edu/~eclab/projects/ecj`). ECJ includes easily modifiable classes for solving optimization problems. The experimental evaluation was performed on a Dell Power Edge server, Quad-core Xeon E5430 processor at 2.66GHz, 8 GB RAM, from Cluster FING, Universidad de la República, Uruguay [8].

4 Experimental analysis

This section presents the experimental analysis of the proposed EA for household energy consumption planning.

4.1 Problem instances

A set of problem instances was build using real data.

Raw energy consumption data for appliances were obtained from the REDD dataset [5], sampled every three seconds for a period of one month. Appliances included in the problem instances were selected considering: i) the categorization of household appliances according to their operating profiles and purposes [14]; ii) the average and maximum time of use of each appliance; and iii) several other parameters, including the number of activations and energy consumption measurements, the number of houses where each appliance is present, the frequency of activation, etc. Six appliances were selected: dishwasher, microwave, dryer, air conditioning, oven, and refrigerator. The planning period is one day.

Energy consumption data in the REDD dataset was averaged over intervals of 15 minutes, and the resulting values were analyzed to define the preferences of using each appliance for each user. The overall energy consumption data were studied for each day. One representative weekday and one representative weekend day was determined for each appliance, in order to define the daily power consumption in each case. Real energy prices from the National Electricity Company (UTE) in Uruguay (`https://portal.ute.com.uy`), considering an average residential plan (contracted power of 3.7 kWh) were used.

Six problem instances were generated (Table 1) accounting for different number of users, appliances, and consumption patterns (weekday/weekend).

Table 1: Proposed problem instances

#	*name*	*users*	*appliances in the instance*	*consumption pattern*
1	small.1 (s1)	2	(2,3)	weekday
2	small.2 (s2)	2	(2,3)	weekend
3	medium.1 (m1)	4	(4,4,3,2)	weekday
4	medium.2 (m2)	4	(4,4,3,2)	weekend
5	large.1 (l1)	6	(5,5,4,4,3,2)	weekday
6	large.2 (l2)	6	(5,5,4,4,3,2)	weekend

4.2 Baseline algorithms for results comparison

Two baseline strategies were implemented for evaluating the results of the proposed EA for household appliances planning: a greedy algorithm and a Business-as-Usual (BaU) planning strategy, which are described next.

Greedy planning strategy. Greedy algorithms iteratively build solutions based on a taking optimal local decisions in each step. A greedy algorithm from the literature [11] was adapted for baseline comparison. The proposed strategy searches the best time intervals to switch on each appliance d_k, according to the user satisfaction and cost , considering the linear aggregation fitness function using $\alpha = 0.65$, $\beta = 1$ (Algorithm 2).

Algorithm 2 Greedy algorithm for household appliances planning

```
procedure IntervalMaxPrefCost(initMin,u_i,d,X)
    prefCost ← 0; duration ← 0
    for (m=initMin; m< t_M; m++) do
        if duration < D(d, u_i) then
            if Σ_{k=1}^{K} x^i_{km} × P(d_k) + P(d) < E(u_i) then
                prefCost ← prefCost + α × UP(u, d, m) − β × C(m)
                duration ← duration + (t_{m+1} − t_m)
            else
                prefCost ← 0
                duration ← 0
            end if
        else
            return [m, prefCost]                          ▷ interval found
        end if
    end for
    return [m, prefCost]                                  ▷ no interval found
end procedure

X ← 0⃗
for (i = 1; i ≤N; i++) do                                 ▷ for each user
    for (k=1;i≤K;k++) do                                  ▷ for each appliance
        prefCost ← 0; bestPrefCost ← -1; bestmin ← 0      ▷ search best interval
        for (m=t_1; m< t_M − D(d_k, u_i); m++) do
            [min, prefCost] = IntervalMaxPrefCost(m, d_k, u_i, X)
            if prefCost > bestPrefCost then
                bestPrefCost ← prefCost
                bestmin ← min
            end if
        end for
        for (m=bestmin −D(d_k, u_i); m ≤ bestmin; m++) do
            x^i_{km} ← 1                                  ▷ set appliance ON
        end for
    end for
end for
```

BaU planning strategy. The BaU strategy proposes assigning ON times to each appliance without planning. These plannings have good user preference values, but suboptimal cost values.

4.3 Linear aggregation fitness function

The analysis considered the candidate values $\alpha \in \{0.3, 0.65, 0.75, 1.0\}$ and $\beta \in \{0.3, 0.5, 1.0\}$. The EA was executed over three medium-size instances of the problem (two, four, and six devices). Table 2 reports the mean and interquartile range (IQR) of the best fitness value computed in 30 independent executions of the proposed EA for the three instances solved, using the studied configurations.

Table 2: Best fitness values computed using different values of (α, β)

α	β	instance #1		instance #2		instance #3	
		median	IQR	median	IQR	median	IQR
0.3	0.3	15.81	1.09	179.83	0.55	132.35	6.68
0.3	0.5	11.02	1.54	167.94	2.03	110.10	4.54
0.3	1.0	4.27	6.39	128.55	28.66	54.82	13.56
0.5	0.3	34.06	0.81	311.32	28.66	253.95	5.11
0.5	0.5	26.75	1.06	298.80	23.71	224.47	12.21
0.5	1.0	13.53	10.28	269.83	26.03	175.11	40.39
0.65	0.3	47.28	2.08	409.91	1.76	342.66	6.57
0.65	0.5	39.87	0.83	398.45	1.34	316.32	8.40
0.65	1.0	25.48	6.12	369.21	3.91	257.55	39.03
0.75	0.3	54.85	2.79	475.64	0.39	405.86	10.03
0.75	0.5	48.52	3.20	462.74	35.73	373.95	4.11
0.75	1.0	30.18	3.43	433.82	3.23	304.31	21.64
1.0	0.3	81.21	4.41	640.62	0.59	548.20	5.64
1.0	0.5	71.46	4.55	628.42	2.76	524.55	9.10
1.0	1.0	52.05	2.89	597.33	0.24	454.48	20.50

Fig. 4 presents a trade-off analysis of solutions computed using different values of (α,β) for instance #3 (results are representative of those obtained for other instances). The combination (0.65,1.0) allows computing the best trade-off solutions regarding user satisfaction and total energy/price.

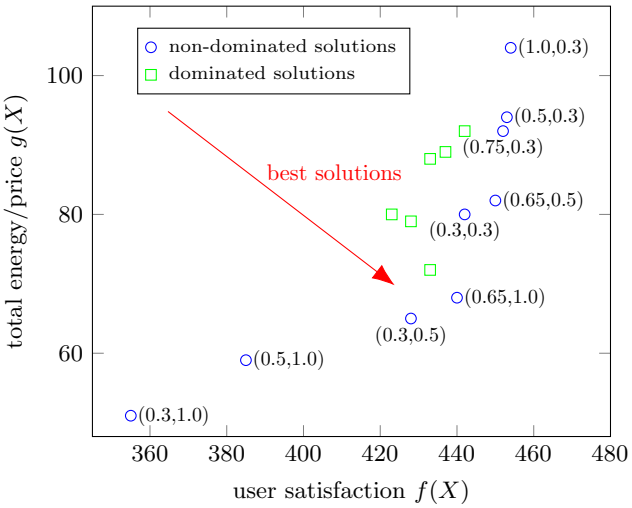

Fig. 4: Trade-off analysis of solutions computed using different values of (α,β)

4.4 Parametric configuration analysis

EA parameters must be adjusted to determine the configuration that allows computing the best results. The analysis was performed over three problem instances, different from those used in the evaluation to avoid bias. After an initial evaluation, the population size was fixed at 150 individuals.

Three relevant parameters of the proposed EA were studied: number of generations used as stopping criterion (G), recombination probability p_C and mutation probability p_M. Candidate values for each parameter were: $p_C \in \{0.1, 0.25, 0.5\}$; $p_M \in \{0.1, 0.05, 0.01\}$; and $G \in \{2500, 5000, 10000\}$. All combinations of parameter values were studied by performing 50 independent executions of the proposed EA for the three problem instances considered in the analysis. The metric considered in the analysis was the linear aggregation fitness function defined in the previous subsection.

The methodology for selecting the best configuration included: i) the Shapiro-Wilk statistical test was applied to check normality, taken as a null hypothesis that the results followed a normal distribution; as p-values less than 0.05 were obtained, the null hypothesis was discarded and it was assumed that the fitness results follow a non-normal distribution; ii) the Friedman's rank test was applied, taken as a null hypothesis that the fitness distributions for the different configurations were not different, as p-values less than 0.05 were obtained, the null hypothesis was discarded and the results significantly differ from each other.

Table 3 reports the fitness values computed in the parameter setting experiments for a representative problem instance. Overall, the best results (i.e., largest fitness median and also lower IQR) were obtained using configuration #11 (values $G = 10000$, $p_C = 0.1$, and $p_M = 0.1$). Henceforth, these values were used in the validation experiments of the proposed EA.

Table 3: Parameter setting results for the proposed EA

configuration (G, p_C, p_M)	*fitness*		*configuration* (G, p_C, p_M)	*fitness*	
	median	*IQR*		*median*	*IQR*
(2500, 0.1, 0.01)	7.88	10.45	(10000, 0.5, 0.1)	40.27	7.61
(5000, 0.1, 0.01)	38.74	11.71	(2500, 0.25, 0.1)	40.73	7.01
(10000, 0.1, 0.01)	40.04	6.98	(5000, 0.25, 0.1)	41.64	6.76
(2500, 0.5, 0.01)	9.26	11.17	(10000, 0.25, 0.1)	40.72	8.67
(5000, 0.5, 0.01)	39.22	9.37	(2500, 0.1, 0.05)	39.60	6.97
(10000, 0.5, 0.01)	39.28	9.88	(5000, 0.1, 0.05)	40.22	9.23
(2500, 0.25,0.01)	9.06	9.22	(10000, 0.1, 0.05)	40.58	7.95
(5000, 0.25,0.01)	39.39	10.18	(2500, 0.5, 0.05)	38.66	7.39
(10000, 0.25,0.01)	38.69	11.76	(5000, 0.5, 0.05)	39.59	10.07
(2500, 0.1, 0.1)	41.77	8.88	(10000, 0.5, 0.05)	40.79	11.62
(5000, 0.1, 0.1)	41.30	8.46	(2500, 0.25, 0.05)	38.17	10.32
(10000, 0.1, 0.1)	**42.57**	**6.46**	(5000, 0.25, 0.05)	41.67	8.38
(2500, 0.5, 0.1)	40.62	7.22	(10000, 0.25, 0.05)	41.00	8.44
(5000, 0.5, 0.1)	41.28	8.65			

4.5 Experimental results

Table 4 reports the median of the best fitness computed by the EA and the comparison with the reference algorithms (greedy and BaU). The relative improvement on fitness values (Δ_f) and on each objective function (Δ_{cost}, Δ_{pref}) over each reference algorithm refA is computed as $\Delta = (f(\text{EA}) - f(\text{refA}))/f(\text{refA})$.

Table 4: Experimental results: fitness values and improvements of the proposed EA over the baseline greedy algorithm and the BaU strategy.

instance	f(EA)	*greedy*				*BaU*			
		f	Δ_f	Δ_{cost}	Δ_{pref}	f	Δ_f	Δ_{cost}	Δ_{pref}
weekday									
small.1	14.1	11.0	28.3%	22.6%	56.2%	-7.6	284.6%	81.1%	16.0%
medium.1	340.0	239.4	42.0%	27.2%	65.3%	69.5	388.9%	77.9%	19.4%
large.1	407.8	347.9	17.2%	20.8%	47.3%	-187.1	317.0%	70.6%	22.0%
weekend									
small.2	323.7	252.1	28.4%	25.1%	44.9%	67.4	383.1%	76.6%	25.8%
medium.2	253.4	197.2	28.5%	29.0%	48.1%	153.8	64.7%	60.6%	20.8%
large.2	369.8	351.9	5.1%	19.7%	37.4%	-299.9	224.2%	72.2%	31.6%

Results in Table 4 indicate that the proposed EA is able to improve significantly over the greedy algorithm regarding the fitness values.

Considering the baseline results computed by the proposed greedy algorithm, improvements of up to 42.0% were obtained in instance medium.1. Results also suggest that consumption patterns during the weekend are harder to plan for the EA, as the improvements over the greedy algorithm reduced to 5.1% in instance large.2. This can be explained due to the interactive utilization of household appliances in weekends, when people are at home a significantly larger periods than in weekdays. Regarding the improvements on user satisfaction and cost, the plannings computed by the proposed EA allow reducing more than 20% the electric bill, and preferences improve more than 40% in all the studied scenarios.

The EA computed significantly cheaper plannings than those of BaU, which systematically failed to provide good cost values, indicating that users do not take the correct decisions to turn on home appliances in this regard, and they can benefit of having an automated planning offered by a recommendation system. In addition, preferences on the solutions computed by the EA were 16–31% better than BaU. The obtained improvements over a BaU strategy are consistent with results reported in previous works for a reduced subset of home appliances (air conditioner and water heater) [11].

The obtained results suggest that the proposed evolutionary approach is accurate for computing household energy consumption plannings accounting for both energy costs and user satisfaction at the same time. The proposed approach is a first step towards designing an intelligent recommendation system for end-users.

5 Conclusions and future work

This article presented an evolutionary approach to address the problem of household energy planning, as a first approach to develop an automated recommendation system for end-users. This is a relevant problem for both energy companies and citizens under the novel smart city paradigm.

A mathematical formulation for the problem was proposed, considering the optimization of user preferences and energy consumed/cost. A specific EA was proposed to solve the problem, simultaneously optimizing both criteria using a linear aggregation multiobjective function and ad-hoc evolutionary operators.

A set of six realistic problem instances built using real data were considered in the experimental evaluation of the proposed EA. The analysis compared the EA results with two baseline planning methods (greedy and business-as-usual).

The experimental results showed that the proposed EA is able to compute accurate plannings, accounting for significant improvements on the problem objectives. Regarding the baseline greedy algorithm, improvements of up to 42.0% were obtained in the proposed multiobjective function, accounting for an average reduction of more than 20% in the energy consumption (and thus, on the electric bill) and preferences improved more than 40% in all the studied scenarios. Regarding the BaU strategy, the EA computed significantly cheaper plannings and user preferences improved up to 31%, in line with previous results from our research group.

The obtained results suggest that the proposed evolutionary approach is accurate for computing household energy consumption plannings accounting for both energy costs and user satisfaction at the same time. Overall, the proposed algorithm showed to be effective for addressing the considered optimization problem. The analysis demonstrated that users can significantly benefit of having an automated planning offered by a recommendation system.

The main lines for future work are related to study explicit multiobjective algorithms to solve the problem, in order to compute several trade-off solutions at the same time. The problem formulation can be extended to include the noisy nature of user preferences in order to define an uncertainty optimization problem. In this regard, robust evolutionary approaches should be studied to solve this problem variant. Finally, new real problem instances can be generated, especially using data from the National Electricity Administration (UTE), in Uruguay.

References

1. Bilil, H., Aniba, G., Gharavi, H.: Dynamic appliances scheduling in collaborative microgrids system. IEEE Transactions on Power Systems 32(3), 2276–2287 (2016)
2. Chavat, J., Graneri, J., Nesmachnow, S.: Energy disaggregation of household appliances based on pattern consumption similarities. In: Iberoamerican Congress on Smart Cities (2019)
3. Coello, C., Van Veldhuizen, D., Lamont, G.: Evolutionary algorithms for solving multi-objective problems. Kluwer Academic, New York (2002)

4. Deakin, M., Al Waer, H.: From intelligent to smart cities. Intelligent Buildings International 3(3), 140–152 (2011)
5. Kolter, J., Johnson, M.: Redd: A public data set for energy disaggregation research. In: Workshop on Data Mining Applications in Sustainability. vol. 25, pp. 59–62 (2011)
6. Luján, E., Otero, A., Valenzuela, S., Mocskos, E., Steffenel, L., Nesmachnow, S.: Cloud Computing for Smart Energy Management (CC-SEM Project). In: Smart Cities, Communications in Computer and Information Science, vol. 978. Springer, Cham (2019)
7. Luján, E., Otero, A., Valenzuela, S., Mocskos, E., Steffenel, L., Nesmachnow, S.: An integrated platform for smart energy management: the CC-SEM project. Revista Facultad de Ingeniería (2019)
8. Nesmachnow, S.: Computación científica de alto desempeño en la Facultad de Ingeniería, Universidad de la República. Revista de la Asociación de Ingenieros del Uruguay 61(1), 12–15 (2010)
9. Nesmachnow, S.: An overview of metaheuristics: accurate and efficient methods for optimisation. International Journal of Metaheuristics, 3(4), 320–347 (2014)
10. Nesmachnow, S., Baña, S., Massobrio, R.: A distributed platform for big data analysis in smart cities: combining intelligent transportation systems and socioeconomic data for montevideo, uruguay. EAI Endorsed Transactions on Smart Cities 2(5), 153478 (2017)
11. Orsi, E., Nesmachnow, S.: Smart home energy planning using IoT and the cloud. In: IEEE URUCON (2017)
12. Soares, A., Antunes, C., Oliveira, C., Gomes, A.: A multi-objective genetic approach to domestic load scheduling in an energy management system. Energy 77(1), 144–152 (2014)
13. Soares, A., Gomes, A., Antunes, C.: Categorization of residential electricity consumption as a basis for the assessment of the impacts of demand response actions. Renewable and Sustainable Energy Reviews 30, 490–503 (2014)
14. Soares, A., Gomes, A., Antunes, C., Cardoso, H.: Domestic load scheduling using genetic algorithms. In: European Conference on the Applications of Evolutionary Computation. pp. 142–151 (2013)
15. Turner, W., Doty, S.: Energy management handbook. The Fairmont Press (2007)
16. U.S. Energy Information Administration (EIA): Energy use in homes, https://www.eia.gov/, June 2018

ELECTROMOBILITY: A REVIEW ON ELECTRIC VEHICLE TECHNOLOGIES AND POTENTIALITIES FOR THE BRAZILIAN SCENARIO

Danielle Rodrigues de Moraes[1], Ronney Arismel Mancebo Boloy[1] and Gisele Maria Ribeiro Vieira[1]

[1] Grupo de Pesquisa em Empreendedorismo, Energia, Meio Ambiente e Tecnologia - GEEMAT. Centro Federal de Educação Tecnológica Celso Suckow da Fonseca, Rio de Janeiro, Brazil.
danirdmoraes@gmail.com

Abstract. The current article, in the review form, aims to gather information and studies recently developed by several researchers regarding the energy-environmental viability associated with the expansion of electric vehicles (VEs) in Brazil. Aspects and classifications of VEs are explained in order to provide information for a better understanding of the use of this technology in the transportation sector. From the bibliographical review, it was possible to verify that most models and types of VEs have both viable autonomy and charging battery time, and also favor the mitigation of direct emissions of greenhouse gases to the environment, however, there is a certain gap in studies on the environmental impact in terms of ecological efficiency, CO_2 equivalent and indicator of pollution of life-cycle. Therefore, current potentials and challenges are addressed with suggestions and discussions to advance knowledge in electromobility area. The country has several policies to encourage the production and use of ethanol, such as tax differentiation and the provision of financing lines for the sector, which are of prime importance for the propagation of Hybrid Electric Vehicles (PHEVs) with flex fuel technology, Fuel Cell Electric Vehicles (FCEVs) and Fuel Cell Hybrid Electric Vehicles (FCHEVs), recognized as the best options for the Brazilian scenario, which has a mostly renewable electrical matrix. It is hoped that this review will strengthen the studies related to the environmental viability of the use of electric vehicles in the Brazilian transportation sector, specifically PHEVs, FCEVs e FCHEVs fueled with ethanol.

Keywords: Electromobility, Electric Vehicle, Environmental Impact.

1 Introduction

Electromobility plays an important role in the decarbonization of the transport sector, being promising to mitigate the climate changes caused by global warming from massive greenhouse gas emissions, also is a valuable tool for the development of mobility in smart cities. A smart city should perform well in the economy, people, government, mobility, environment and life, based on the intelligent combination of resources and

activities of self-determined, independent and conscious citizens. [1] Therefore, the purpose of a smart city is to form a virtuous cycle of urban systems, to create a better living, working, rest and entertainment environment, exploiting natural resources in a wise and sustainable manner, always based on the use of new technologies, such as electric vehicles. [2]

Between the years 1832 and 1839, the first prototype of electric transport, powered by non-rechargeable primary cells, was invented by Robert Anderson. After that, several prototypes were developed, but none had the required suitability due to the low efficiency of the electric motor and the lack of practicality in the recharge of its battery. Later, between 1856 and 1881, DC motors and rechargeable batteries underwent a series of advances, the credit of which was given to developers Werner Siemens, Antonio Pacinotti and Zénobe Gramme. [3] Gaston Planté and Camille Faure were responsible for increasing the storage capacity of the battery, which triggered the commercialization of electric vehicles in France and in Great Britain from the 80's. [4] In 1897, in the New York City, the first Electric Vehicle (EV) was introduced in the category of electric taxi, which after three years of its launching was already responsible for 28% of the road fleet. Despite this, Internal Combustion Engine Vehicles (ICEV) were introduced to the market by Henry Ford in 1908, falling down the popularity of VEs, driven mainly by lower ICEV production and maintenance costs. [3]

At the 21st Conference of the Parties (COP21) of the United Nations Framework Convention on Climate Change (UNFCCC) in Paris, an agreement was reached among the member countries with the central objective of strengthening the global response to the threat of climate change and calling for action impact of these changes. [5] In other words, the message that the Paris Agreement brings is that the world is willing to change its way of generating and consuming energy by investing in renewable sources and technology so that its generation and consumption become increasingly sustainable. In this perspective, the decarbonization of the transport sector becomes essential for the achievement of this objective. However, the pace of introduction of electromobility in transport and the ascendancy of new vehicular technological routes are critical uncertainties that affect various energy chains, industrial and their respective stakeholders: automotive, oil, bioenergy, electricity, transport, cities, consumers and citizens. [6]

The implementation of EVs is growing worldwide, both pure electric and hybrid (propulsion by electric motor and internal combustion). There are still EVs powered by hydrogen cell, and EVs powered by external cables, present in public transport networks, such as Light Rail Vehicles (LRVs) in the city of Rio de Janeiro, Brazil. In the study by Souza et al. (2018), the comparative evaluation of the environmental lifecycle of conventional vehicles with different fuel options, plug-in hybrid and electric vehicle options was made, aiming to recognize the possibility of a sustainable transport system in Brazil. The results showed that the scenario where the ICEV is fueled with gasoline has a greater contribution to global warming, and, in turn, the pure electric vehicle was responsible for much smaller environmental impacts, followed by the ICEVs fueled with ethanol. [7]

However, the main concerns about the use of EVs in the transport sector are associated with the environmental impact; in addition, EVs face some challenges in their development and applications, in order to contribute to the efficiency and sustainability of smart cities. This article aims to gather information and recent studies on the autonomy, loading time and carbon dioxide emissions of the different types of EVs available in the market. A discussion is held about the challenges and potentialities of EVs in order to offer knowledge and information to the scientific community, considering Brazilian Scenario. It is worth mentioning that the article brings important contributions to scientific development in the area of electromobility.

2 Electric Vehicles: Concepts, Challenges and Potentialities

An electric vehicle uses one or more electric motors, either partially or completely, for propulsion, which makes it recurrent to the designation of these vehicles as "zero emissions", because they hardly emit atmospheric or noise pollutants. Electricity is the fuel that powers electric vehicles, being obtained in several ways, such as: I- connecting directly to the external source of electricity, either by plugs or overhead cables; II- using the regenerative braking mechanical energy when braking the vehicle; III- by means of an electromagnetic induction system; IV- or through the reaction of oxygen, hydrogen and water in a fuel cell. [5,8,9]

In the latter, the oxygen source that supports the occurrence of this reaction is the atmospheric air itself, on the other hand, the necessary hydrogen can be obtained in two ways: when supplied directly by an external source and stored in a tank; or through the use of the fuel cell, example of Solid Oxide Fuel Cell (SOFC), where the chemical reaction that produces hydrogen from ethanol takes place. [8] The regenerative braking system consists of the use of energy that would be lost in the form of heat in conventional braking systems during the deceleration, contributing to increase the energy efficiency of vehicles that use it. [9] The electromagnetic induction system dispenses physical connections between the EV and the charging station, since it uses the concepts of electromagnetism to recharge with the help of induction coils installed inside the EV and in the station itself. Because it is a relatively new technology in the market, recharge by electromagnetic induction still presents some disadvantages, as the low efficiency when compared to the mechanisms by conduction (plugs or aerial cables). However, its main benefits are durability and safety during use. [3]

This electricity is stored in chemical batteries that power the electric motor, except for Fuel Cell Electric Vehicles (FCEVs). Older EVs used lead acid batteries, while newer ones used lithium-ion batteries. [10] The lithium-ion batteries were developed to meet the most diverse specifications, from the use of different chemical compounds, nevertheless, batteries of this type have already reached their maturity, beginning the search for new alternatives for storage systems of electrochemical energy with higher energy density, safety and longer life-cycle. [3] An alternative is the lithium-sulfur battery, which offers greater energy density compared to the lithium-ion battery, in addition to greater reliability, a wider operating temperature range and lower production costs due to the availability of sulfur. [11]

The EVs not only contribute to direct mitigation of greenhouse gas emissions, but also on indirect emissions, when considering gradual substitution of electrical vehicles fleet, the same fleet that, nowadays in Brazil, is found majorly composed by internal combustion vehicles. [12]. According to Baran & Legey's studies [13], the use of electricity in Brazilian's private transports would be responsible for about 40,7% reduction on gasoline consumption to 2030, followed by a 31,3% increase on electricity consumption. Although the reduction of gasoline consumption presents as a good alternative for CO_2 emission reduction released by the transportation sector, said alterations couldn't be considered totally positive, since it isn't known if Brazilian's electric matrix will be able to count with the necessary support to the call of increased demand for electricity.

The main peculiarities of the Brazilian scenario are: the diversification of the electric matrix, including a relevant percentage of renewable energy sources; and its leadership in the production and use of biofuels, with emphasis on policies to encourage ethanol consumption, which is currently widely used in flex fuel vehicles and blends with gasoline in a percentage above 25%. [8,14,15]

Regarding the Brazilian electric matrix, considering that the country is the largest global producer of sugarcane, it started to produce electricity from the waste generated during the various uses of sugarcane, said bioelectricity. In 2016, bioelectricity accounted for 8.2% of the Brazilian electricity matrix, with more than 85% of this production using as input the residues of the sugarcane industry. [14] This shows that the Brazilian power matrix is based mostly on renewable energy sources, where hydraulics added to biomass, wind and solar, account for 83.2% of all energy generated in the country in 2018, according to the National Energy Balance (Brazilian Energy Balance - BEN) carried out by the Brazilian Energy Research Company, Empresa de Pesquisa Energética (EPE), in conjunction with the Ministry of Mines and Energy. [15] This percentage is above the world average where, according to the International Energy Agency (IEA), only 24% of the world's electricity matrix comes from renewable sources, taking 2016 as the base year. [16]

Currently, the country has several public policies to encourage the use and production of biofuels, among which we can cite the establishment of the National Biofuels Policy, through Federal Law no. 13.576, promulgated on December 26, 2017, which aims to increase the participation of several biofuels in the Brazilian energy matrix, such as ethanol, biodiesel, biogas and aviation biokerosene. [17] In the specific case of ethanol, it has been the target of several governmental actions favorable to its use and production, such as: an increase in the percentage of anhydrous in gasoline, which increased from 25% to 27% in March 2015; the recomposition of the rate of the Contribution of Intervention in the Economic Domain (CIDE) on gasoline to R$ 0.10/ liter, since 2015, whereas on hydrated ethanol it has been kept at zero since 2004. [14]

However, in making an analysis of the positive and negative environmental impacts of using EVs, it is important to be aware of the sources of energy used to generate the electricity that will feed it, as well as the fuels to be used in hybrid electric vehicles, considering that each type of fuel emits different volumes of polluting gases. Other factors that can be considered are pollution indicator, particulate matter and ecological efficiency.

2.1 Battery Electric Vehicle (BEV)

There are several categories of electric vehicles on the market. The Battery Electric Vehicle (BEV) is the one whose main source of energy is electricity from an external source. Thus, all BEVs are inserted in the category Plug-in Electric Vehicle (PEV), as they need to connect to the power grid. The types of charging according to the charging levels are: Level I, has its typical use in homes and work places and uses alternating current at 127 volts; Level II, even typical use of Level I chargers, but with voltage between 220-240 volts; Level III, used to denote vehicles that have both Level I and Level II inputs separately; and, finally, the fast charger whose charging occurs predominantly in public places, operating in AC and DC voltage and up to 600 volts. [12].

Table 1 explained some recent models of PEVs with their respective recharge time, full range in kilometers and battery capacity in kWh. It is noted that the 2014 Tesla Model S Long Range and 2018 Tesla Model X 75D electric vehicles have greater autonomy, proportional to the longer battery charge time, this is due to the greater weight of the vehicle and larger size of the battery for storage of the vehicle. electricity.

Table 1. Some Plug-in Electric Vehicles (PEVs) available in the market.

Vehicle Model	Battery Capacity Size (kWh)	Weight (kg)	PEV Range (km)	Charging Time (Level II; Fast Charger)	Source
2018 Ford Focus Electric	33.5	1643	185	5.5 hours; 33 minutes	[18,19]
2018 Tesla Model X Long Range	75	2458	523	12 hours; 15 minutes	[18,20]
2019 Nissan Leaf	40	1557	241	8 hours; 40 minutes	[18,21]
2019 Chevrolet Bolt	60	1616	383	9.5 hours; 30 minutes	[18,22]
2019 Tesla Model S Long Range	75	2214	595	12 hours; uninformed	[18,23]

According to Teixeira & Sodré [24], if 5% of the Brazilian fleet of vehicles were replaced by EVs, the increase in electricity consumption would be 9.73 TWh/day, equivalent to 1.1% of all consumption in the country. In another scenario, where 100% of the vehicle fleet would be exchanged for electric vehicles, this increase in electricity consumption would be around 19.4%, with a daily demand growth of around 194.55 TWh/day. The impacts of this change are expected to be environmentally positive, considering that about 83.2% of the electricity matrix in Brazil comes from renewable sources such as hydroelectric, biomass, sugarcane and derivatives, wind, solar and geothermal. [15] According to Souza et al. [7], the BEV technology presents better results on the environmental impacts in relation to the categories: POP

(Photochemical Oxidant Formation Potential), ACP (Potential Acidification) and ETP (Eutrophication Potential) due to the Brazilian energy matrix.

The BEVs do not produce exhaust emissions, however, it is possible to identify greenhouse gas (GHG) if we consider the entire product life-cycle management and energy that feeds. Thus, it is possible to identify GHG emissions that are indirectly inherent in the production and use of BEVs and electric vehicles in general. Still, EVs emissions are typically lower than the ICEVs run on gasoline, ethanol or diesel, for example, especially if the electricity that feeds comes from renewable sources such as wind power or hydroelectric power plant. [7] According to Teixeira & Sodré [24], the CO_2 emission factor inherent to Brazilian's electric matrix is smaller than in countries such as China and Romania. Therefore, it can be claimed that a BEV in Brazil will have lesser GEE emissions inherent to its circulation than a BEV circulating in China's and Romania's streets.

According to studies conducted by the United States Department of Energy's National Renewable Energy Laboratory, batteries designed for electric vehicles can last up to 15 years in moderate climates and slightly less in severe climates. [25] BEVs typically use lithium-ion batteries, while hybrid nickel-metal batteries are generally used to power Hybrid Electric Vehicles (HEVs) because of their relatively low cost. [7]

2.2 Hybrid Electric Vehicle (HEV)

In the category of PEVs are also inserted some hybrid electric vehicles, whose propulsion occurs by the action of both electric motors and internal combustion. Such hybrid vehicles can be dimensioned in series - when the internal combustion engine is used to produce the electricity that feeds the electric motor, which is the main motor - and in parallel, where the two motors are used for propulsion. [12] Vehicles designated as Hybrid Electric Vehicle (HEV), the pure hybrids, have the main engine internal combustion, while the electric motor only increases the efficiency of vehicles by providing low-power traction. [8] Thus, HEV is a parallel hybrid, in which electricity for the electric motor is supplied by the regenerative braking system. [26]

According to projections made by EPE (Brazilian Energy Research Company), the participation of hybrid vehicles in the Brazilian fleet will represent less than 1% in 2026. For this projection were considered only hybrid vehicles, being assumed as flex fuel hybrids from 2021. [6] In the case of Brazil, there is an advantage related to the diffusion of hybrid vehicles of the flex fuel type, since they do not require so many technological changes, without the need for further changes in the fuel supply infrastructure. In addition, it is worth noting the important role played by biofuels in the country's economy.

An example of HEV available on the market is the Toyota Yaris Hybrid, whose emissions revolve around 0.075 kg of CO_2 per kilometer, according to data obtained by the Vehicle Certification Agency of the United Kingdom in the year 2018, which is a small value compared with the emissions of a Toyota Corolla (ICEV), whose direct emissions turn around 0.23 kg of CO_2 per kilometer. [12,27] It uses a nickel-metal hydride battery and is fueled only by gasoline, which does not fit into the flex

fuel category. [28]. However, if we are to consider the emissions of greenhouse gases that occur throughout the life-cycle of the HEV powertrain, we will have around 27.5 tons of CO_2 equivalent, yet this value is lower than that obtained for the ICEV powertrain emissions, with just under 35 tons of CO_2 equivalent throughout its entire life-cycle. [29]

2.3 Plug-in Hybrid Electric Vehicle (PHEV)

Within the PEV category, there are the Hybrid Plug-in Electric Vehicles (PHEV), whose internal combustion engine is also the main one, however, these differ from the HEV because of the possibility of receiving electricity from an external source, being a parallel hybrid just like the previous one. "PHEV also shows similar characteristics to BEV, mainly due to the use of lithium-ion batteries, which promotes higher values in the Human Toxicity Potential (HTP) and ADP (Abiotic Depletion Potential) categories, but a lower weight of batteries with respect to BEV, the PHEV demonstrates slightly better results for these categories." [7]

Table 2 shows some models of PHEVs available in the market, where all have values close to total autonomy, which is due to the parallel use of electric motors and internal combustion. All have the possibility to act only in electric mode.

Table 2. Some Plug-in Hybrid Electric Vehicles (PHEVs) are available in the market.

Vehicle Model	EV Mode Driving Range (km)	Total Driving Range (km)	Charging Time (At 240V)	Source
2019 Hyundai Ioniq	46	1013	2.3 hours	[18,30]
2019 Toyota Prius Prime	40	1029	2 hours	[18,31]
2019 Ford Fusion Energi	41	981	2.6 hours	[18,32]

With the internal combustion engine being primarily responsible for the propulsion of PHEVs, consequently there will be direct GHG emissions, which will vary according to the type of fuel used to power it. For example, the Hyundai Ioniq Plug-in Hybrid emits about 0.026 kg of CO2 per kilometer, which is quite small compared to the emissions of a Toyota Yaris Hybrid, whose direct emissions are around 0.075 kg of CO_2 per kilometer wheeled. [27] When considering the entire PHEV powertrain life-cycle, its emissions are around 25 tons of CO_2 equivalent, which is among the values obtained for HEVs (approximately 27.5 tons of CO_2 equivalent) and ICEVs (approximately 35 tons of CO_2 equivalent). [29]

2.4 Extended Range Electric Vehicle (E-REV)

In addition to HEV and PHEV, there are still the Extended Range Electric Vehicles (E-REV), whose electric motor acts as the main motor and is powered by an external

source of electricity. The role of the internal combustion engine in this type of vehicle is simply to maintain a minimum level of battery charge, making the E-REV longer range and autonomy by providing power to a generator.

An example of E-REV available on the market is the BMW i3 REx, which operates with 180 km electric autonomy, so the Autonomy Extender is automatically activated when the battery level is low, extending the range by up to 150 km. That is, its internal combustion engine (ICE) is used as a generator to recharge the battery. In a public direct current charging station, recharge up to 80% occurs in 39 minutes. [33]

According to the survey conducted by the UK Vehicle Certification Agency in 2018, the direct emissions of the BMW i3 REx revolve around 0.012 kg of CO_2 per kilometer, a very optimistic value compared to the emissions of ICEVs. [27] Lower emission values for E-REVs are observed when comparing them to ICEs because of their relatively low engine dependency on internal combustion, as it is possible to travel certain distances under zero emissions circumstances until the battery needs recharge and fuel combustion starts, and because of this the capacity of E-REVs tanks is usually less than that of ICEVs.

2.5 Fuel C ell Electr ic Vehicles (FCEV)

Electric vehicles of the type Fuel Cell Electric Vehicles (FCEV), usually powered by hydrogen fuel cell, combine hydrogen and atmospheric oxygen to produce electricity to feed him. "The conversion of hydrogen gas into electricity produces only water and heat as by-products, which means they do not present exhaust emissions" [8] or zero direct emissions of carbon dioxide. "If compared to other types of VEs, VCE has autonomy superior, [...] guaranteed by hydrogen cells that make them more suitable for use in vehicles that travel long distances and also for users who do not have plug-in access in their homes." [12]

Depending on the production method for producing hydrogen feed FCEVs can generate GHG, yet the total emissions that occur throughout the life-cycle of the vehicle concerned are much smaller than the conventional emissions from gasoline or diesel vehicles. [34] Although FCEV has been significantly researched, there are some obstacles to its commercialization as the hydrogen storage and supply infrastructure, and production costs, as oil prices are still more affordable. [26]

A FCEV example available in the market is the Toyota Mirai, whose autonomy for the 2016 model is around 502 kilometers, and battery nickel-metal hydride type with a capacity of 1.7 kWh. [18] With regard to the life-cycle of the FCEV powertrain, where it is assumed that it depends entirely on the hydrogen produced by the steam reforming of methane, about 27.5 tons of CO_2 equivalent are generated, the value of which is similar obtained for HEVs (mentioned in item 2.2). [29]

2.6 Fuel C ell Hybrid Electric Vehicles (F CHEV)

The modification of the FCEV powertrain gave rise to a new configuration called the Fuel Cell Hybrid Electric Vehicle (FCHEV). This type of vehicle architecture adopts another Fuel Cell Supporting Energy Storage System (ESS), so they can be used as

ESS batteries or capacitors, as these can be charged and discharged based on demand and power supply. [8]

Still according to Wei Tan, Shekhar Das, Yatim [8], possible problems are related to the size of the energy converter, weight and reliability, as well as converter efficiency, electromagnetic interference, output voltage and current ripples are some important factors. The 2019 Honda Clarity Fuel Cell is one of the FCHEVs available in the world market, operating autonomously of approximately 579 kilometers, and lithium-ion battery with capacity of 1.7 kWh. [18]

2.7 Road Powered Electric Vehicle (RPEV)

Also, worth mentioning is the Road Powered Electric Vehicle (RPEV), which receives electricity through directly connected external cables, whether above the vehicle - such as trolley buses and trucks in ports and electrified roads - or below - such as Light Rail Vehicles (LRVs). [12] The RPEV are present in public transportation networks, such as the LRV Carioca in the city of Rio de Janeiro, Brazil. Because they are all-electric models, they have zero GHG emissions, being a great alternative in terms of mitigating the negative environmental impacts caused by the public transportation sector.

According to the recommendations and public policy implications made by EPE in 2018, in order to achieve the decarbonization goal of the transportation sector, the country must prioritize mass transportation (BRT, LRV and subway), flex fuel hybrid vehicles, electric vehicles in the captive and commercial fleet niches in urban centers, electric vehicles to fuel cells based on biofuels and gas. [6] However, it is not enough to only invest in EVs in the public transport network, since a mesh that does not meet the demand for urban mobility of a metropolis ends up causing an increase in the fleet of individual vehicles, thus increasing the amount of emissions atmospheric per capita.

3 Conclusion and Suggestions

Many parameters should be studied for decision making associated with the use of EVs in the transportation sector, especially in smart cities. In this paper the following parameters were addressed: autonomy, loading time and direct carbon dioxide emissions. Each of these parameters are important for the development and dissemination of EVs. As discussed, responding to the main objective of this article, several studies developed by researchers show that EVs have, on average, autonomy, loading time and direct emissions of carbon dioxide relevant to their use in the urban transportation network. However, in environmental issues, it is perceived that most of the studies point to scientific insufficiency involving parameters such as: ecological efficiency, carbon dioxide equivalent emissions, pollution indicator, when considered the life-cycle, specially to the hybrid EVs fueled with ethanol. This observation is not surprising when analyzing the considerations adopted in studies published in the scientific community on the subject.

Brazil has a unique characteristic in relation to several countries that have progress in the use of VEHs, since 84.4% of all electric energy consumed in the country comes from renewable sources [13]. However, the infrastructure for the fast charger of pure electric vehicles is very small, which favors the use of hybrid electric vehicles, among which are: PHEVs flex fuel, FCEV and FCHEV recognized as the best options to the Brazilian scenario, where there is a diverse and mostly renewable electrical matrix.

The choice of ethanol-fueled hybrid vehicle is justified by the fact that they combine the best characteristics of conventional and purely electric vehicles (high energy efficiency, greater autonomy and lower direct GHG emissions), as well as the country's policy of encouraging the use of biofuels, which contributes to a significant reduction in the levels of regulated emissions and, mainly, of greenhouse gases.

Therefore, it is expected that this article in the form of a review will lead to increasing efforts for the development and dissemination of EVs, particularly the hybrids that contribute to greater mitigation of GHG emissions in the Brazilian urban transport network, especially in smart cities, in addition to open new paths for policies to encourage the use of EVs in the country.

The following are suggestions for strengthening the environmental criteria that allow greater fidelity in decision making regarding the dissemination and use of hybrid electric vehicles:

a) Development of ecological efficiency studies considering the life-cycle;
b) Determination of carbon dioxide equivalent emissions;
c) Determination of the pollution indicator.

The suggestions made are important and remarkable contributions, able to strengthen the qualification and quantification of the environmental impact of the use of hybrid electric vehicles in smart cities, mainly in Brazil.

Acknowledgments. The authors be very grateful to the financial support provided by the Iberoamerican Program of Science and Technology for Development (CYTED) with the project Smart Cities Totally Comprehensive, Efficient and Sustainable (CITIES). (Process number: 518RT0557).

References

1. Giffinger R, Haindlmaier G, Kramar H, 2010. City-ranking of European medium-sized cities. Urban Research & Practice. 3, 299–312.
2. Weisi F U, Ping P, 2014. A Discussion on Smart City Management Based on Meta-Synthesis Method. Management Science and Engineering. 8, 68-72.
3. Ying Yong J et al., 2015. A review on the state-of-the-art technologies of electric vehicle, its impacts and prospects. Renewable and Sustainable Energy Reviews. 49, 365-385.
4. Muneer T et al., 2015. Energetic, environmental and economic performance of electric vehicles: Experimental evaluation. Transportation Research Part D. 35, 40-61.
5. United Nations (UN). Paris Agreement. Paris, http://unfccc.int/files/essential_background/convention/application/pdf/english_paris_agreement.pdf, last accessed 2019/06/26.

6. Empresa de Pesquisa Energética (EPE). Eletromobilidade e Biocombustíveis. Brasil, 2018. [cited 2019 20/06/2019] Available from: http://www.epe.gov.br/pt
7. Souza L L P et al., 2018. Comparative environmental life cycle assessment of conventional vehicles with different fuel options, plug-in hybrid and electric vehicles for a sustainable transportation system in Brazil. Journal of Cleaner Production. 203, 444-468.
8. Tan C W, Das, H. S., Yatim, A H M, 2017. Fuel cell hybrid electric vehicles: A review on power conditioning units and topologies. 76, 268-291.
9. Zhang J et al., 2015. Mechanism analysis and evaluation methodology of regenerative braking contribution to energy efficiency improvement of electrified vehicles. Energy Conversion and Management. 92, 469-482.
10. Rezvanizaniani S M, Liu Z, Chen Y, Lee J, 2014. Review and recent advances in battery health monitoring and prognostics technologies for electric vehicle (EV) safety and mobility. Journal of Power Sources. 256, 110-124.
11. Fotouhi A et al., 2016. A review on electric vehicle battery modelling: From Lithium-ion toward Lithium–Sulphur. Renewable and Sustainable Energy Reviews. 56, 1008-1021.
12. Fundação Getúlio Vargas (FGV). Carros Elétricos, 2017. Editora: Accenture. ISSN 2358-5277.
13. Baran R, Legey L F L, 2013. The introduction of electric vehicles in Brazil: Impacts on oil and electricity consumption. Technological Forecasting & Social Change. 80, 907-917.
14. Empresa de Pesquisa Energética (EPE). Ministério de Minas e Energia (Brasil) (MME). CENÁRIOS DE OFERTA DE ETANOL E DEMANDA DE CICLO OTTO E DEMANDA DE CICLO OTTO 2018-2030. Brasil, 2018. [cited 2019 20/06/2019] Available from: http://www.epe.gov.br/pt
15. Empresa de Pesquisa Energética (EPE). Ministério de Minas e Energia (Brasil) (MME). Balanço Energético Nacional 2019 – Relatório Síntese, 2019. [cited 2019 29/09/2019] Available from: http://www.epe.gov.br/pt/publicacoes-dados-abertos/publicacoes/balanco-energetico-nacional-2019
16. International Energy Agency (IEA). Statistics; Total Primary Energy Supply (TPES) by source, 2016. [cited 2019 26/06/2019] Available from: https://www.iea.org/statistics/
17. BRASIL, 2017. Lei Federal nº 13.576 de 26 de dezembro de 2017. Dispõe sobre a Política Nacional de Biocombustíveis (RenovaBio) e dá outras providências.
18. U. S. Department of Energy (EPA). Find and Compare Cars, 2018-2019. [cited 2019 26/06/2019] Available from: https://www.fueleconomy.gov/feg/findacar.shtml
19. Ford. Focus Electric - Models & Specs, 2018. [cited 2019 26/06/2019] Available from: https://www.ford.ca/cars/focus/models/focus-electric/
20. Tesla Motors. Model X, 2019. [cited 2019 26/06/2019] Available from: https://www.tesla.com/modelx
21. Nissan USA. 2019 Nissan Leaf Specs, 2019 [cited 2019 26/06/2019] Available from: https://www.nissanusa.com/electric-cars/leaf-2019/compare-specs.html#modelName=S
22. Chevrolet. 2019 CHEVROLET BOLT EV SPECIFICATIONS, 2019. [cited 2019 26/06/2019] Available from: https://media.chevrolet.com/media/us/en/chevrolet/vehicles/bolt-ev/2019.tab1.html
23. Tesla Motors. Model S, 2019. [cited 2019 26/06/2019] Available from: https://www.tesla.com/models
24. Teixeira A C R, Sodré J R, 2018. Impacts of replacement of engine powered vehicles by electric vehicles on energy consumption and CO_2 emissions. Transportation Research Part D. 59, 375-384.

25. Neubauer J S, Wood E, Pesaran A. U. S. National Renewable Energy Laboratory. United States, 2015. A Second Life for Electric Vehicle Batteries: Answering Questions on Battery Degradation and Value.
26. Hannan, M. A., Azidin, F. A., Mohamed, A., 2014. Hybrid electric vehicles and their challenges: A review. Renewable and Sustainable Energy Reviews. 29, 135-150.
27. Vehicle Certification Agency (United Kingdom). New Car Fuel Consumption & Emissions Figures, 2018. [cited 2019 26/06/2019] Available from: https://carfueldata.vehicle-certification-agency.gov.uk
28. Toyota. Toyota Yaris Hybrid; Modelos e Especificações, 2019. [cited 2019 26/06/2019] Available from: https://www.toyota.pt/new-cars/yaris/index/specs#/
29. International Energy Agency (IEA). Global EV Outlook 2019, 2019. [cited 2019 26/06/2019] Available from: https://webstore.iea.org/global-ev-outlook-2019
30. Hyundai. 2019 Hyundai Ioniq Hybrid; Features & Specifications, 2019. [cited 2019 26/06/2019] Available from: https://www.hyundaiusa.com/ioniq-hybrid/specifications.aspx?%20specs
31. Toyota. 2019 Toyota Prius Prime; Full Specs, 2019. [cited 2019 26/06/2019] Available from: https://www.toyota.com/priusprime/features/mpg/1235/1237/1239
32. Ford. Models & Specs; 2019 Ford Fusion Energi Titanium, 2019. [cited 2019 26/06/2019] Available from: https://www.ford.com/cars/fusion/models/fusion-energi-titanium/
33. BMW. Modelos e Preços; BMW i3, 2019. [cited 2019 26/06/2019] Available from: https://www.bmw.com.br/pt/all-models/bmw-i/i3/2017/autonomia-carregamento-eficiencia.html
34. Center for Climate and Energy Solutions. Hydrogen Fuel Cell Vehicles. Virginia, United States, 2015.

IIoT: Gestión de la Temperatura y la Humedad en el Proceso de Fermentado del Té Negro

Adriana P. Quiñones[1[0000-0001-9377-9508]], Diego A. Godoy[1[0000-0002-7445-7375]], Eduardo O. Sosa[2[0000-0002-0160-301X]], Santiago H. Bareiro[1[0000-0002-3060-5217]]

[1]Centro de Investigación en Tecnologías de la Información y Comunicaciones (CITIC). Universidad Gastón Dachary, Av. López y Planes 6519, 3300 Posadas - Argentina

[2]Secretaría de Investigación y Posgrado (SECIP). Facultad de Ciencias Exactas, Químicas y Naturales, Universidad Nacional de Misiones. Félix de Azara 1552, 3300 Posadas- Argentina

{paolaqui;diegodoy;hbareiro}@citic.ugd.edu.ar,
eososa@unam.edu.ar

Abstract.
En el proceso productivo del té negro existen parámetros que se deben mantener bajo estricto control para así asegurar una calidad del producto acorde a la demanda internacional. En este trabajo se presenta un prototipo con tecnologías capaces de determinar en tiempo real la humedad y temperatura del producto en proceso. Mediante estos dispositivos se establece un análisis comparativo con valores de humedad de la masa de producto que se encuentra en la cinta de fermentado. Con ello se puede llegar a prescindir tomas de muestras, análisis de laboratorio, especialistas; como así también de la aplicación de conocimientos empíricos aplicados por personal de las fábricas. En este estudio, el contenido de humedad del té negro se ha determinado mediante la técnica de equilibrio de humedad relativa utilizando sensores. En estos últimos se calibraron y establecieron ecuaciones para mejorar la precisión. El prototipo es una herramienta que combina la interdisciplinariedad de las ciencias, principalmente la química básica, la química de alimentos, la ingeniería electrónica con sus componentes de hardware innovadores y la ingeniería en informática. De ésta manera se integran estos saberes en un solo componente que brinda información determinante para la toma de las decisiones que darán como resultado información acerca de la buena, media o baja calidad del té negro elaborado.

Keywords: Internet Industrial de las Cosas, Sensores Inalámbricos, fermentado del Té

1 Introducción

El té es un arbusto de la familia de las Teáceas, que crece hasta 10 o 15 metros de altura. Posee hojas perennes, flores blancas y fruto capsular. Con la denominación genérica de té, se entiende exclusivamente el producto obtenido por el procesamiento conveniente de las yemas, hojas jóvenes, pecíolos y tallos tiernos de la especie Camellia sinensis L. Según el Código Alimentario Nacional Argentino [1], el té destinado

a la preparación de infusiones y puede clasificarse en cuatro tipos: Té o Té negro, Té verde, Té tipo Oolong, y Té rojo. El presente trabajo tiene relación directa con el primero de esta clasificación es decir, la producción de té negro, que corresponde al producto obtenido mediante marchitado, enrulado, fermentado y secado de las yemas, hojas jóvenes, pecíolos y tallos tiernos.

La zona productora de té en Argentina, comprende a las provincias de Misiones con el 95,2 % de la producción y el Noreste de la provincia de Corrientes, con el restante 4,8%. Estas dos zonas son las que poseen las condiciones agroecológicas específicas para la producción [2]. Los productores son alrededor de 6.000 y la superficie cultivada es de cerca de 42.400 hectáreas. Solamente el 5% del indicado es consumido en el mercado interno, destinándose lo demás a la exportación. De esto se desprende principalmente la necesidad de los productores de mantener la calidad del producto destinado al mercado externo.

La elaboración del té negro comienza al marchitar los brotes, produciendo la ruptura de las células con maquinarias apropiadas, lo cual produce un jugo que reacciona con las enzimas propias de la especie. El proceso siguiente es la fermentación, en el cual es indispensable controlar la humedad y temperatura por un tiempo determinado, para conservar las características especiales del producto: aroma, color, intensidad, viveza, etc. En el proceso siguiente es necesario inactivar las enzimas y quitar el contenido de agua existente en el material procesado. El contenido de humedad del té afecta la calidad y durabilidad del producto.

Debido a la falta de practicidad que presenta el sistema actual de medición de temperatura. las empresas únicamente lo implementan en el proceso de secado. Puesto que para poder acceder a certificaciones buenas prácticas de manufactura (BPM) [3] se requiere obligatoriamente de un registro frecuente de la temperatura en dicha etapa de elaboración.

En la manufactura del té negro el proceso de fermentado es una etapa crítica ya que de no realizarse correctamente afecta a la calidad del lote, produciendo efectos irreversibles. Tales efectos cambiarán el aroma, color y sabor del producto final, elementos fácilmente identificables en una catación cotidiana. En el primer caso el té no llega a cocinarse y en el segundo se supera la temperatura recomendada. En empresas pequeña y mediana envergadura el monitoreo de temperatura y humedad se llevan a cabo de forma manual, personas idóneas toman un puñado de la materia prima (Fig. 1), y en base a su conocimiento empírico determinan el estado de las variables (temperatura-humedad).

A partir de la subjetividad del idóneo se realiza la toma de decisión que modifica las condiciones del proceso de fermentado afectando la calidad del lote que se está elaborando, como así también de los procesos previos y posteriores a él.

Las decisiones que se toman durante el proceso son diversas, como ejemplo se mencionan: la reclasificación de la materia prima, no permitir el ingreso al proceso de la misma por su baja calidad, la modificación de la velocidad de la cinta transportadora y de los ventiladores, tanto del proceso de enrulado como de fermentado, la modificación del estado del aspersor de agua del fermentado y por último la temperatura del horno del proceso de secado. Cabe resaltar que la operación incorrecta podría

acarrear desperdicios de energía, lo que impactaría negativamente en el costo de producción.

Fig. 1. Método para medir la humedad en el sólido de la hoja que se encuentra en el proceso de Fermentado.

Actualmente en la mayoría de las industrias se realiza el testado de forma manual (Fig. 1), por personas idóneas. Por ello la variable humedad del sólido suele arrojar valores inexactos.

La disponibilidad del agua en un alimento se podría medir analizando la movilidad molecular del alimento o estudiando la capacidad de difusión de los solutos y como se modifica la viscosidad en el microambiente al que está sometido dicho alimento. Ambos métodos no son viables en industrias de la región: el primer método requiere de equipos costosos de difracción y resonancia magnética, es decir por la aparatología necesaria; y el segundo método por su influencia no deseada en la estabilidad de los alimentos que se someten a tal medición.

Por lo que actualmente, se emplea el método tradicional para conocer la actividad de agua contenida en el alimento en momentos específicos y sin cumplir con el objetivo de poder brindar información útil al elaborador.

La dificultad viene dada porque el proceso de fermentado dura entre 40 minutos y 2 horas y el método tradicional para conocer la humedad en el sólido requiere de 12 horas aproximadamente.

Las pocas empresas que realizan dichos controles lo hacen tomando muestras del lecho de fermentado. Estas son aisladas herméticamente para conservar las mismas condiciones de humedad hasta que son recibidas en un laboratorio. En dicho lugar se procede al pesado de las muestras y se las introduce de 6 a 12 hs aproximadamente en una estufa a temperatura constante. Luego se vuelven a pesar y la diferencia en el peso es la cantidad de humedad en el sólido que contenían dichas muestras.

Contar con un sistema de monitoreo práctico y automatizado es un aspecto trascendente para mejorar la calidad del té que se produce en la región.

La utilización de WSN para aplicaciones industriales es de mucho interés en la actualidad. Se diferencia de su aplicación en las redes administrativas, dado que el entorno industrial es impredecible pero a la vez agresivo a la funcionalidad de las WSN, considerando las variaciones constantes en la temperatura, presión, humedad, presencia de equipos pesados, etc. [4].

El objetivo de este proyecto fue diseñar y construir una solución tecnológica de Internet de las Cosas en entornos industriales [5] que monitoree la humedad en el sólido de manera instantánea y remota, sin la necesidad de muestreos y análisis de laborato-

rios, ni especialistas, utilizando dispositivos diseñados específicamente para medir temperatura y humedad relativa.

2 Trabajos relacionados

En esta sección se presentan trabajos relacionados que se detallan a continuación.

En este estudio [6], el contenido de humedad del té Oolong se midió mediante la técnica de equilibrio de humedad relativa (HR). El equilibrio de humedad relativa y temperatura de los materiales y del té se midieron utilizando sensores destinados a tal fin. Los sensores se calibraron y se establecieron mediante ecuaciones para mejorar la precisión. El contenido de humedad se calculó utilizando un modelo de equilibrio de contenido de humedad. El error del contenido de humedad determinado con este método estuvo dentro de 0.5% w.b. a humedad <15% w.b. El análisis de incertidumbre reveló que el rendimiento del sensor de humedad tuvo un efecto significativo en la precisión de la determinación de la humedad.

En este trabajo [7], se investigó el comportamiento de secado de las hojas de té verde en un secador de gabinete de varias bandejas. Se desarrolló un modelo matemático para predecir el contenido de humedad y la temperatura de las hojas de té verde y también la humedad y la temperatura del aire de secado, en las bandejas de la secadora. Cada bandeja se consideraba como un lecho fijo de hojas de té. El modelo propuesto se resolvió, después de dividir la cama en una serie de capas delgadas, utilizando un método de diferencia finita y una técnica de prueba y error. Los contenidos de humedad de equilibrio y los valores de difusividad de humedad, usados en el modelo matemático, fueron estimados y comparados para el té verde, usado en este estudio. Las predicciones del modelo mostraron un buen acuerdo (ERM inferior al 5%) con los datos experimentales, obtenidos del secado de hojas de té verde en un secador doméstico de tres bandejas a 60 y 70 ° C. Se investigó el efecto de la velocidad del aire de secado, la temperatura y el número de hojas de té verde en cada bandeja sobre el comportamiento de secado del té verde en la secadora.

Este trabajo [8] es una continuación del trabajo [6]. Se estableció un generador de flujo dividido propio para calibrar dos tipos de sensores eléctricos de humedad. La humedad de referencia estándar se calculó a partir de la temperatura del punto de rocío y la temperatura del bulbo seco de aire medida por un monitor de espejo enfriado. Este generador de flujo dividido podría producir resultados consistentes de los resultados de medición de HR. La incertidumbre del estándar de referencia aumentó con los valores de HR. La incertidumbre combinada con las ecuaciones de calibración adecuadas varió de 0,82% a 1,45% HR para sensores de humedad resistivos y 0,63% a 1,4% para sensores de humedad capacitivos, respectivamente. Este generador de flujo dividido propio y el método de calibración son baratos, ahorran tiempo y son fáciles de usar. Por lo tanto, el enfoque propuesto se puede aplicar fácilmente en los laboratorios de investigación.

El presente trabajo se destacada de los anteriores por transformar un sistema tradicional de medición de temperatura y humedad del ambiente en una implementación basada en Wireless Sensor Network (WSN) capaz de calcular la humedad del sólido

que se está analizando de manera instantánea y remota, sin la necesidad de muestreos y análisis de laboratorios, ni especialistas, utilizando dispositivos diseñados para medir temperatura y humedad relativa. Además de ofrecer la funcionalidad de integrar esta red de sensores a un middleware para generar una interface de usuario amigable para la toma de decisiones.

3 Metodología

3.1 Plataforma de hardware utilizado

Como plataforma base para el proyecto se han utilizado equipos con un módulo principal iSense [9]. El hardware iSense se proporciona junto a un firmware operativo y de red modular, permitiendo la generación de aplicaciones pequeñas pero completas; proveyendo una base sólida para el desarrollo rápido de aplicaciones. Brinda una API C++ para el nodo hardware, funcionalidades de sistema operativo y una amplia variedad de protocolos de red.

El sistema de software iSense incluye un número variado de servicios y protocolos listos para usar, tales como ruteo, sincronización de tiempo y programación “en el aire”. Integra un procesador Jennic JN5139 con un sistema radial de 2,4 GHz compatible con normas IEEE 802.15.4, con ancho de banda de 250 kbit/s, 192kB de ROM, 96kB of RAM, así como una variada posibilidad para la utilización de periféricos analógicos y digitales. Como módulo en la tarea en planta industrial se ha utilizado el “Weather Sensor Module” de iSense [10] capaz de medir presión atmosférica, temperatura y humedad relativa, alimentándose de dos baterías AA. (Fig. 2).

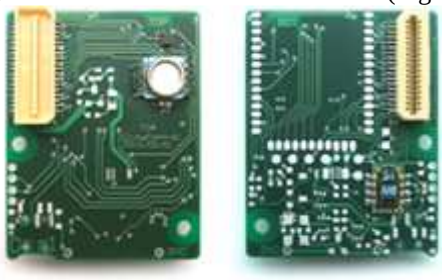

Fig. 2. Weather Sensor Module de iSense

3.2 Herramientas de software utilizadas

El hardware iSense utilizado en la capa de infraestructura, proporciona un conjunto de herramientas de software que incluyen: Sistema operativo, bibliotecas y códigos fuentes desarrollados en lenguaje C++.

Este conjunto de herramientas provee un variado número de servicios y protocolos listos para usar, lo cual permite el desarrollo rápido de aplicaciones pequeñas pero complejas.

Entre las herramientas de software utilizadas se encuentran: herramientas de compilación (make, cmake, g++), compilador ba-elf (para micro controladores Jennic), plataforma de desarrollo Eclipse, firmware iSense (Biblioteca para desarrollo iSense), iShell (herramienta para análisis, programación y operación sobre nodos).

Se ha utilizado también una plataforma de solución middleware, desarrollado previamente en una investigación de [11].

3.3 Calibración de los sensores

A fin de asegurar a la planta industrial la calidad del servicio prestado por los sensores, y en un trabajo conjunto con el Programa "Yerba Mate" de la Facultad de Ciencias Exactas, Químicas y Naturales de Universidad Nacional de Misiones, se realizó la calibración de cada uno de los equipos a utilizar. La graduación se realizó sobre los valores obtenidos de temperatura y humedad relativa.

Para analizar la relación de ámbas variables, en cada uno de los sensores, se introdujeron en microclimas con valores conocidos y controlados de temperatura y humedad, [12]. Donde luego se compararon los valores obtenidos con el establecido experimentalmente.

La dificultad mayor fue la de introducir a los sensores en ambientes con valores de humedad conocida; como es intuitivo pensar al estar en una habitación con un aire acondicionado encendido, dentro de un horno, dentro de una heladera o un congelador la humedad del ambiente cambiará, pero el problema es que su valor no será conocido.

Durante el calibrado de temperatura, los valores indicados por un termómetro de mercurio de laboratorio fueron comparados con los valores indicados por los nodos sensores, no existiendo indicativo de diferencias significativas entre ambos métodos.

En cuanto al calibrado de los nodos sensores referentes a la humedad relativa, se generaron tres microclimas utilizándose una estufa a 40ºC constantes. Se introdujeron en los ambientes distintas sales, las que poseen la propiedad de fijar el porcentaje de humedad de los ambientes respectivos (Tabla 1).

Tabla 1. Porcentaje de humedad relativa según el tipo de sal utilizada a 40°C de temperatura

Sal	Humedad (%)
Cloruro de Litio	11,21
Cloruro de Magnesio	31,60
Cloruro de Cobalto	55,48
Nitrato de Sodio	71,00
Cloruro de Potasio	82,32

Como ejemplo indicamos aquí los resultados obtenidos de someter un nodo a tres microclimas y los valores obtenidos (Tabla 2).

Tabla 2. Calibrado de humedad relativa de los Sensores

Sal utilizada	Humedad (%)	
	Medido	Nominal
Cloruro de litio	15,3	11,2
Cloruro de cobalto	49,8	55,5
Cloruro de potasio	68,4	82,3

Luego de someter a los nodos a tres microclimas se obtuvieron 6 valores por cada nodo con los cuales mediante una interpolación lineal se determinó la función de calibración que coincide con una recta que realizará la corrección respectiva a los valores de humedad relativa.

De la interpolación de los valores medidos se ha determinado para el sensor 0x1ca1 que la función de calibración se condice con una recta con valores correspondientes a -9,6094 a la ordenada al origen y 1,3321 de pendiente. A continuación, se despliegan las tres funciones que permitieron asegurar a la planta fabril que los valores que expone el sistema de monitoreo son fiables.

Una vez obtenidas las curvas de calibración se reprograman cada uno de los dispositivos dando utilidad a la característica principal de los nodos que es su capacidad de cómputo. Cuando el cliente reciba la información de la humedad será un valor calibrado por lógica. En el mismo momento en que se realiza la captura del dato se corrige este valor y luego se arma la trama que se enviará desde del nodo final al nodo concentrador de la red.

4 Arquitectura de la solución propuesta

Como se ha expuesto a lo largo del trabajo, el problema consiste en monitorear los valores del entorno del lecho de fermentado y conseguir un sistema que conociendo los valores relativos calcule la humedad de las hojas que están en uno de los procesos de la elaboración del té negro (Fig. 3).

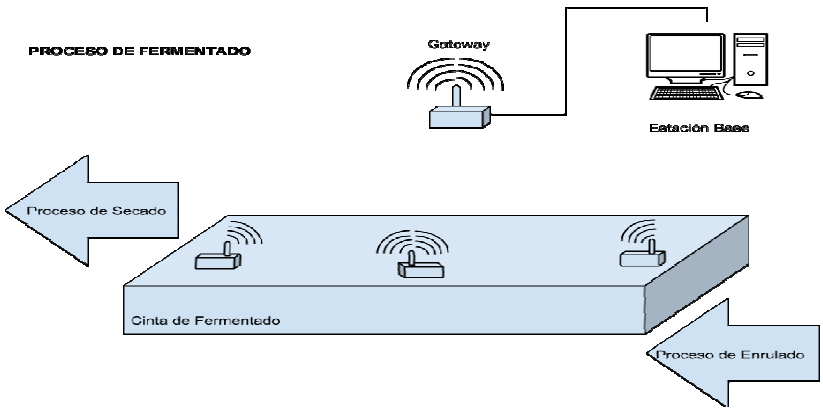

Fig. 3. Componentes del sistema de monitoreo en el entorno Industrial.

La arquitectura propuesta implica que los datos medidos de la WSN del ambiente industrial lleguen a un usuario final que puede estar en diversos lugares. Para conseguirlo existen tres capas: la primera es la red inalámbrica, la segunda es la estación base y por último las vistas del cliente (Fig. 4).

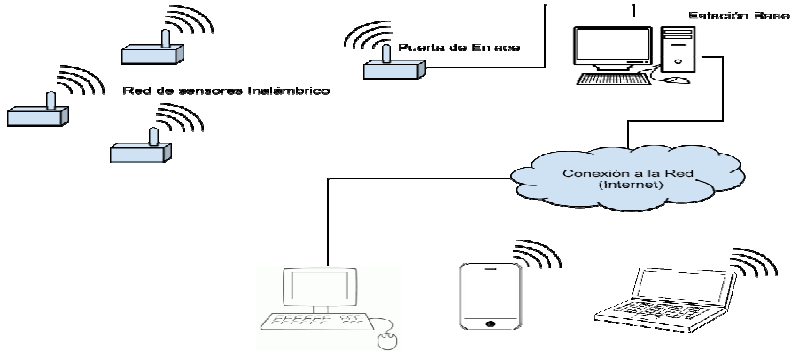

Fig. 4. Arquitectura en tres capas del sistema de monitoreo.

Como se puede observar en la Fig.4 los nodos se comunican con el software que se ejecuta en la estación base a través de la correspondiente puerta de enlace. Tratándose de una red con topología en estrella el Gateway tiene las características de nodo concentrador.

En la estación base se utiliza un middleware que será el responsable de capturar los datos de la WSN y escribirlos en una base de datos. Además, se desarrollará una vista para el usuario que consultará al middleware los valores obtenidos por la red de sensores.

En la primera capa de esta arquitectura se requirió la implementación de nodos finales y un nodo de la WSN sumidero. Para ambos se desarrollaron programas y mediante ellos los datos capturados pueden llegar a la segunda capa.

La programación de los nodos que denominamos finales logra su objetivo cuando las unidades medidas del entorno llegan hasta el nodo concentrador de la red. Para ello realizan un conjunto de tareas a saber: conocer al nodo concentrador de la red, identificar el momento en el cual deben realizar la medición del estado de las variables, armar un paquete de datos con las mediciones y enviar el paquete de datos al destino correcto.

En la segunda capa estación base se utilizó un middleware que proporciona un enlace entre dos aplicaciones independientes: la WSN de un lado y un software de visualización del otro. Además permite visualizar mediante un servicio web los valores requeridos sin tener que atender a las características específicas de las bases de datos

El back end del middleware es el responsable de lanzar un aplicativo que está en ‘espera activa’ escuchando uno de los puertos USB de la estación base, la percepción que tiene del dispositivo conectado es la de un ‘archivo de texto’ siendo lecturas y escrituras las tareas que se pueden realizar, es así como este aplicativo recibe como una cadena de caracteres los paquetes de datos recibidos de las WSN la cual luego de

procesada es guardada en una base de datos. Estos paquetes recibidos de la red, pueden consultar en distintos formatos de datos interoperables como XML y Json.

La tercera capa de la arquitectura que es la vista del usuario que interactúa con el front end del middleware utilizando un navegador Web. Este último enviará una consulta al middleware solicitando el inicio de la comunicación, a partir de ese momento la aplicación del usuario podrá interactuar con el middleware y viceversa. Las solicitudes enviadas al middleware ocasionarán un procesamiento sobre los datos almacenados en la base de datos, abstrayendo a la vista de usuario por completo de cómo se recolectaron esos datos devolviendo generalmente una respuesta que el front end recibe y expone al usuario de una forma entendible para este.

5 Pruebas realizadas

Para la realización de pruebas se utilizaron cinco nodos sensores en total. Un único nodo conectado a la estación base con la función de puerta de enlace, recibiendo los datos de los otros cuatro sensores que medían temperatura y humedad. De los cuales, los tres primeros se encontraban directamente en el lecho. El cuarto o último nodo se lo expuso a la intemperie para tener una referencia de las condiciones fuera de la nave.

La ubicación de los nodos corresponde a las necesidades de control que se tienen en el proceso que se está evaluando. El primer punto de control fue ubicado a la salida del proceso de enrulado, es decir a la entrada del proceso de fermentado (Fig. 5) para conocer las condiciones iniciales. De esta manera se pudo evaluar y modificar los procesos previos al fermentado, como ser: la recepción y clasificación de la materia prima, el enrulado y el proceso de marchitado.

Fig. 5. Cinta transportadora al final del proceso de enrulado y principio del proceso de fermentado.

El segundo nodo se ubicó exactamente en la mitad del proceso (Fig. 6) siendo éste el punto más importante pues en esta instancia aún se pueden modificar las variables de humedad y temperatura del lecho (activando o desactivando los aspersores de agua, aumentando o disminuyendo la velocidad de la cinta transportadora, aumentan-

do o disminuyendo el espesor de colchón de hojas o encendiendo y apagando los ventiladores).

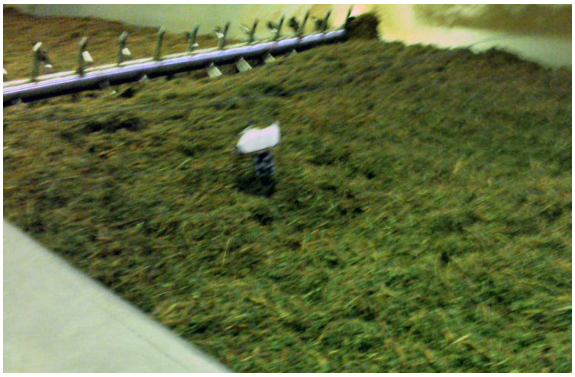

Fig. 6. Cinta transportadora a la mitad del proceso de fermentado.

Por último se instaló un mote al final del proceso de fermentado (Fig. 7), que permite obtener la información necesaria para determinar la temperatura del horno en la próxima etapa denominada secado.

Fig. 7. Cinta transportadora al final del proceso de fermentado y al inicio del secado.

Además, se adicionó en un sensor a mitad del lecho en contacto directo con la masa de té que está en el fermentado y que acompañó todo el recorrido de la cinta para determinar la temperatura en el sólido.

La ubicación exacta donde se colocó este sensor fue a cinco centímetros de la cinta transportadora con té por encima y por debajo; midiendo de esta forma la temperatura de la masa de té, ya que el equipo se encontraba en equilibrio con dicha masa. Cabe aclarar que no se tuvieron en cuenta los valores de humedad que éste identificaba por hallarse herméticamente protegido. Al momento que se realizo la prueba se alcanzó una temperatura ambiente exterior de 28°C a las 20:00hs.

Entre la tarde y la media noche de un día de verano, en Misiones Argentina existe un descenso en la temperatura. Esta es la razón para estudiar el comportamiento de la cinta de fermentado en dicho momento. Se la identifica como una franja horaria donde resulta difícil mantener constante los valores requeridos y en ocasiones es recomendable detener la elaboración, debido a que dicho descenso de temperatura afecta de manera negativa hasta convertir en inutilizable todo el lote de té.

Se pudo observar que a las 22:40 hs, antes de la instalación del sistema de monitoreo el té al tacto al principio del proceso estaba caliente con aspecto a falto de humedad. Sin embargo al momento de empezar a monitorear la cinta de fermentado la masa al tacto ya se percibía fría.

Las consecuencias negativas de la transición antes mencionada se ven reflejadas en la primera hora del monitoreo (Fig. 8 y Fig. 9) donde el proceso inicia con temperaturas que alcanzan los 33°C y el 80% de humedad. Sabiendo que deberían mantenerse valores de 27°C y 100% de humedad respectivamente.

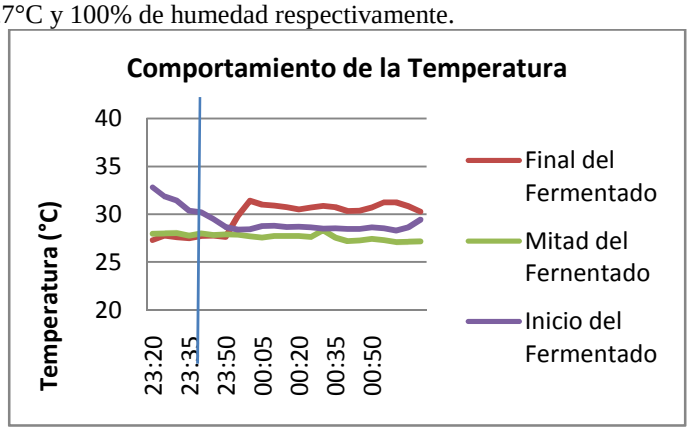

Fig. 8. Momento en que los nodos sensores detectaron valores óptimos de temperatura en la elaboración.

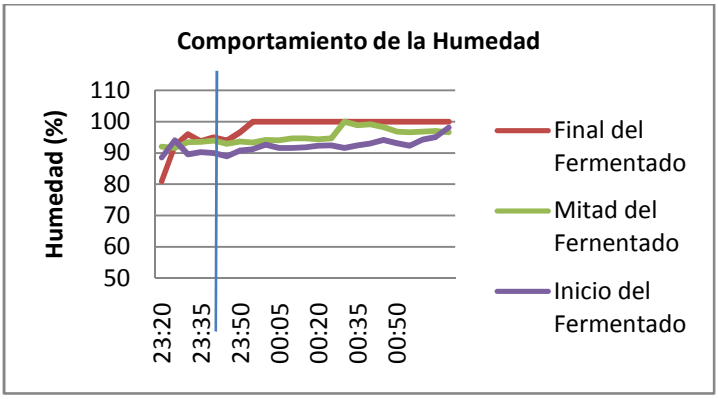

Fig. 9. Momento en que los nodos sensores detectaron valores óptimos de humedad en la elaboración.

En esta evaluación se pudo comprobar que el conocimiento del idóneo se corresponde con los valores óptimos detallados en las bibliografías (Fig. 10 y Fig. 11). Se capturó un momento en el cual las condiciones de elaboración eran buenas y el sistema de monitoreo certifica este hecho.

A las 23:55 se realizó el testado de la calidad del té que se estaba elaborando. El personal encargado toma un puñado de la masa que estaba al principio de la cinta de fermentado y al presionarlo se pudo observar que entre los dedos de su mano se filtraba líquido. Fue satisfactorio comprobar que el sistema de monitoreo en ese momento describía 28°C y 93% de humedad (Fig. 10 y Fig. 11). La cinta de fermentado continuó su recorrido hasta que el té evaluado alcanzó al segundo hito de control (Fig. 10 y Fig. 11), en este caso el sensor ubicado en la mitad de la cinta describió 27°C y 98% de humedad.

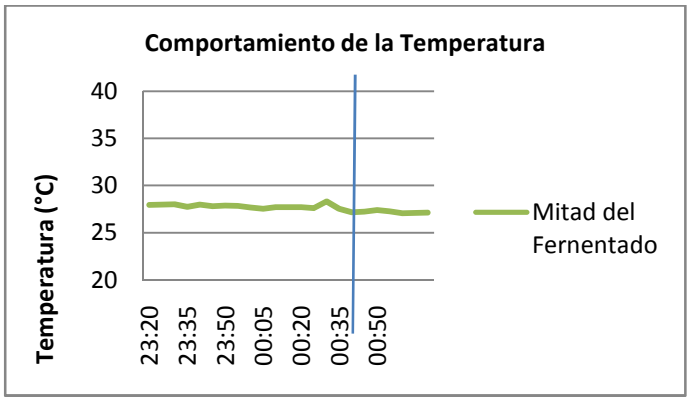

Fig. 10. Comportamiento de la temperatura en la mitad del lecho de fermentado. Elaboración propia.

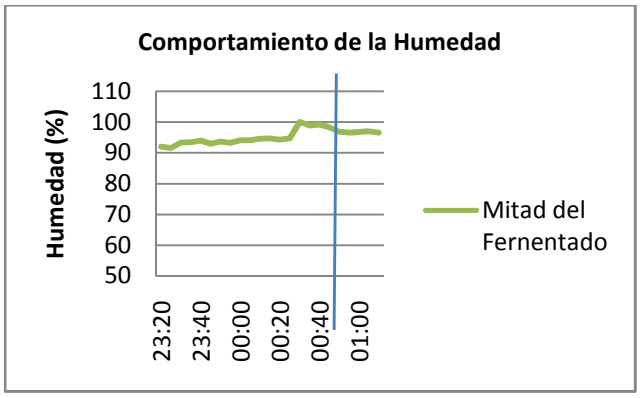

Fig. 11. Comportamiento de la humedad en la mitad del lecho de fermentado. Elaboración propia.

El tiempo del proceso de fermentado en esta prueba tuvo una duración de una hora. El té que ingresó a las 23:10 hs. con características no deseadas (por haber sido elabo-

rado con temperaturas que exceden lo recomendable) es el que está en el tercer hito de control a las 00:10hs. (Fig. 12) describiendo también valores no deseados en el final del proceso de fermentado.

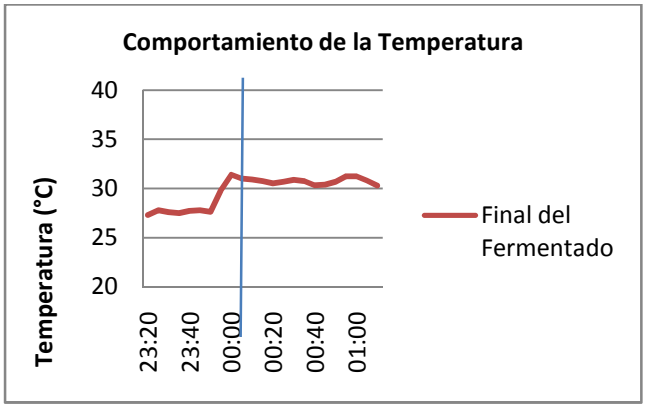

Fig. 12. Comportamiento de la temperatura en el final del lecho de fermentado.

Este conjunto del cual se hace referencia como de mala calidad es considerado de esta manera por haber sido elaborado con altas temperaturas, pero valores correctos de humedad en el fermentado (Fig. 13).

Por haber sido elaborado con valores de humedad altos acarrea que en el siguiente proceso “el secado” se eleve la temperatura del horno proporcionándole la característica de quemado a dicho conjunto. No es identificado como óptimo, debido a los valores de temperatura desviados y se puede comprobar su falta de calidad basado en la visual y el tacto del experto.

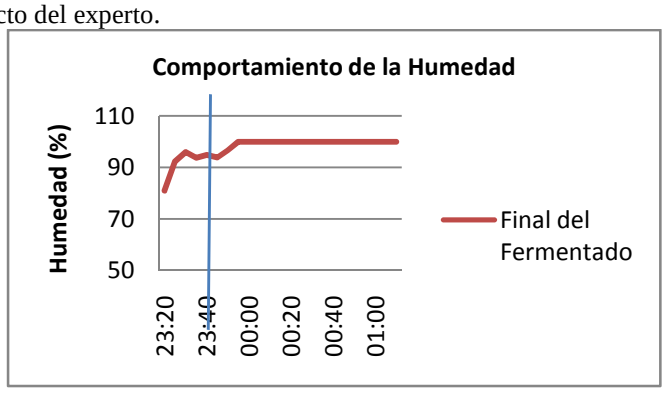

Fig. 13. Comportamiento de la humedad en el final del lecho de fermentado.

6 Conclusión

El prototipo construido se presentó en el contexto de una industria en la provincia de Misiones y resultó innovador y de gran apoyo a la toma de decisiones del personal que trabaja en pos de lograr la mejor calidad del producto elaborado.

La red de sensores inalámbricos en esta investigación resultó una potente herramienta en el monitoreo de ambientes fabriles.

Conocer la proporción de agua que poseen los alimentos en la actualidad es una tarea difícil, integrando saberes de varias ciencias como: la ingeniería en alimentos, la ingeniería química, la ingeniería en electrónica y la ingeniería en informática se logró desarrollar un prototipo capaz de exponer la humedad de la hoja que se encuentra en el proceso de fermentado para la elaboración del té negro.

Se puede decir que el prototipo reemplaza de manera eficiente al proceso anterior, que solamente les permitía conocer dicho valor varios días después de haber tomado las muestras, como también al operario que se basa en el tacto y la visual para determinar las condiciones de las hojas que pasan por el proceso.

Queda expuesto que el monitoreo de las variables críticas en el desarrollo de la industria tealera mejora en gran medida la calidad del té negro ya que permite mejorar las condiciones competitivas del sector elaborador en la provincia de Misiones.

La conexión remota nos permitió un monitoreo en tiempo real desde cualquier parte del mundo a través de internet, lo cual aparte de eficaz convierte a este prototipo en una solución eficiente.

Las WSN son una de las tecnologías fundamentales en la Internet de las cosas, y representa la expansión de Internet al mundo real, permitiendo acceder a indicadores que pueden ser consultados en línea.

La proyección sugerida para este trabajo es la construcción de un sistema de actuadores que proceda a activar o desactivar los aspersores de agua, aumentar o disminuir la velocidad de las cintas transportadoras, como así también el espesor de los colchones de hojas y por último encender o apagar los ventiladores de cada línea.

En el momento de escalar el prototipo se podría pensar en ampliar el proyecto a conocer el comportamiento termodinámico de la cinta transportadora, involucrando mayor cantidad de sensores, una decena o cientos. De esta manera se podría detectar sectores de la cinta transportadora que requieren de mayor mezcla o zonas frías que lote tras lote afectan la calidad de la elaboración. En ese momento sería interesante evolucionar en el método de comunicación de los nodos. Se propone trabajar sobre comunicaciones multisalto logrando que los nodos lleguen al nodo sink de manera inteligente.

Se propone la combinación de las WSN y de la tecnología RFID (Identificación por radio frecuencia), para lograr registrar medidas medioambientales, parámetros de calidad y seguridad alimentaria en un sistema de trazabilidad contundente. La tecnología RFID es considerada el sistema más efectivo para implantar un sistema real de trazabilidad.

Por último, se propone extender el monitoreo a los procesos previos del fermentado y unificar la información ya existente del proceso posterior. De esta manera se podría obtener un control de toda la elaboración.

7 Bibliografía

[1] ANMAT - Administración Nacional de Medicamentos, Alimentos y Tecnología Médica. (2016) Código Alimentario Nacional. [Online]. http://alimentosargentinos.gob.ar/HomeAlimentos/Marco_Regulatorio/codigo_alimentario_argentino.php

[2] Ministerio de Agricultura, Ganadería y Pesca. (2016, diciembre) Panorama de la Cadena del Té en la Argentina. [Online]. https://www.economia.gob.ar/peconomica/docs/SSPE_Cadena%20de%20Valor_Te.pdf

[3] Argentina; Ministerio de Economía y Obras y Servicios Públicos; Secretaría de Agricultura, Pesca y Alimentación; Subsecretaría de Alimentación, "Alimentos argentinos," 2017. [Online]. http://www.alimentosargentinos.gov.ar.

[4] International Society for Automation. (2012) Industrial Wireless Sensor Networks:Trends and developments. [Online]. http://tiny.cc/l3c3ww

[5] V.Güngör and Gerhard Hancke, *Industrial Wireless Sensor Networks: Applications, Protocols, and Standards.*, 1st ed.: CRC Press, 2017. ISBN 9781138076204.

[6] Andrew Chen, Chen Hsuan-Yu, and Chen Chiachung, "Use of Temperature and Humidity Sensors to Determine Moisture Content of Oolong Tea," *Sensors - Open Access Journal*, vol. 14, no. ISSN 1424-8220, pp. 15593–15609, Agosto 2014. doi: https://doi.org/10.3390/s140815593.

[7] Shomali Abbas and Abbasi Souraki Behrooz, "Experimental investigation and mathematical modeling of drying of green tea leaves in a multi-tray cabinet dryer.," *Heat and Mass Transfer Journal*, vol. ISSN 1432-1181, pp. 1-15, Junio 2019. doi: https://doi.org/10.1007/s00231-019-02662-6.

[8] Chen Ling-Hsi and Chen Chiachung, "Uncertainly Analysis of Two Types of Humidity Sensors by a Humidity Generator with a Divided-Flow System.," *Sensors - Open Access Journal*, vol. 18, no. ISSN 1424-8220, p. 637, Febrero 2018. doi: https://doi.org/10.3390/s18020637.

[9] Coalesenses GmbH. (2015) Bridging the gap between virtuality and reality. [Online]. http://www.coalesenses.com

[10] coalesenses GmbH. (2013) iSense Weather Sensor Module. [Online]. http://goo.gl/hoypi

[11] Diego Alberto Godoy, Eduardo Omar Sosa, and Rebeca Díaz Redondo, "Internet De Las Cosas: Middleware De Gestion De Datos De WSN," in *13ª Conferencia Ibero Americana WWW/Internet y Computación Aplicada*, Florianópolis, 2015.

[12] Paola Quiñones, Diego Alberto Godoy, and Eduardo O. Sosa, "Redes Inalámbricas De Sensores: Una Experiencia En La Industria Del Té.," in *42 JAIIO*, Córdoba, Argentina., 2013, pp. 161-171. ISSN 1850-2776.

SCALE: Smart Cities Advanced Learning*

Joaquín Adiego Rodríguez[1], Natalia Martín Cruz[2] y Manuel Barrio Solórzano[1]

[1] Dpto. Informática (ATC, CCIA, LSI)
Universidad de Valladolid, España
{jadiego,mbarrio}@infor.uva.es
[2] Dpto. Organización de Empresas y Comercialización e Investigación de Mercados
Universidad de Valladolid, España
ambiela@eco.uva.es

Resumen. SCALE es un proyecto financiado por la Unión Europea a través del programa Erasmus+ cuyo objetivo es diseñar, desarrollar y validar un programa de formación en competencias relacionadas con Smart Cities, común a todas las disciplinas que este concepto abarca, incluyendo un programa de movilidad para apoyar la adquisición de competencias de los becarios en el área de Smart Cities, así como para promover la colaboración del mundo empresarial y la educación y formación superior.

Conceptos clave: Nuevos planes de estudio, métodos educativos, desarrollo de cursos de formación innovadores, superación de desajustes de competencias (básicas/transversales), cooperación internacional, relaciones internacionales, cooperación para el desarrollo.

1 Introducción

La Unión Europea (UE) está especialmente preocupada por el desarrollo de una estrategia de crecimiento urbano "inteligente" para las ciudades de la UE. Cada vez son más los ejemplos de proyectos piloto de Smart City que se desarrollan en las ciudades en colaboración con empresas que implementan soluciones innovadoras para mejorar la calidad de vida y la sostenibilidad de los entornos urbanos.

El concepto multidisciplinar de Smart Cities, junto con la alta demanda de innovación en este sector, supone un reto en el ámbito de la educación superior. Es necesaria una colaboración más estrecha entre estas empresas que trabajan en proyectos de innovación y generación de ciudades inteligentes, y la educación superior, que debe dotarles de personal con las habilidades y competencias exigidas en este sector.

El proyecto SCALE (Smart Cities Advanced Learning) ofrecerá a los egresados una formación complementaria para dotar al estudiante de determinadas competencias

* Referencia del proyecto: 2018-1-ES01-KA203-050168

Cofinanciado por el programa Erasmus+ de la Unión Europea

transversales, como la innovación, la organización y planificación, el pensamiento analítico, la creatividad, etc. Por otro lado, permitirá que las empresas que trabajen en el ámbito de Smart Cities sean más competitivas porque contarán con personal mejor preparado. Por último, facilitará que las ciudades y empresas puedan implementar proyectos innovadores y exitosos en Smart Cities con la ayuda de los estudiantes durante sus pasantías.

2 El Proyecto SCALE

El Proyecto *"SCALE: Smart Cities Advanced Learning"* es un proyecto financiado por la Unión Europea a través del programa Erasmus+ para la cooperación para la innovación y el intercambio de buenas prácticas mediante alianzas estratégicas para la educación superior. La duración del mismo es dos años, concretamente del 1 de diciembre de 2018 al 30 de noviembre de 2020.

De acuerdo con el programa de modernización de los sistemas de enseñanza superior europeos, la economía del conocimiento necesita personas con la combinación adecuada de cualificaciones: competencias transversales, cibercapacidades para la era digital, creatividad y flexibilidad y una sólida comprensión del ámbito elegido. Para maximizar la contribución de los sistemas de educación superior europeos al crecimiento inteligente, sostenible e inclusivo, se necesitan reformas en el fortalecimiento del triángulo del conocimiento entre la educación, la investigación y las empresas, y este proyecto se dirige directamente a lograr esta colaboración triangular para el intercambio de conocimientos y planes de aprendizaje.

Este proyecto reforzará el mencionado triángulo del conocimiento, vinculando la educación y la investigación con las empresas de las ciudades inteligentes, dotando a los graduados de los conocimientos y competencias básicas que necesitan para tener éxito en ocupaciones de alta cualificación, como las que requiere el sector de las ciudades inteligentes. La elaboración de los contenidos formativos se basará en las competencias y habilidades reales que necesita este sector, y tanto las universidades como las empresas colaborarán en el desarrollo de un curso de formación sobre competencias transversales de las ciudades inteligentes, estrechando el diálogo, la comunicación y el entendimiento entre los actores relevantes del sector de las ciudades inteligentes.

SCALE se basa en el valor y la eficiencia que el aprendizaje basado en el trabajo puede proporcionar a la educación superior. El desarrollo de proyectos realmente innovadores en las ciudades inteligentes durante las prácticas garantizará una inversión, un rendimiento y una eficacia sostenibles en la educación superior.

2.1 El consorcio

El consorcio del proyecto lo componen siete socios provenientes de 3 países (España, Alemania y Austria), existiendo un equilibrio entre universidades y empresas que trabajan en el campo de las ciudades inteligentes, lo que fomentaría el triángulo del conocimiento. Los miembros del consorcio tienen experiencia y antecedentes en estrategias

y servicios de cooperación entre ciudades inteligentes y entre universidad y empresa. La experiencia y competencia que los socios aportan al proyecto es la siguiente:

La Universidad de Valladolid (España), que lidera el proyecto, es muy activa en el sector o Ciudades Inteligentes. De hecho, la Universidad lidera acciones de investigación y formación en el campo de las ciudades inteligentes, principalmente en Informática, IoT y Big Data.

Fachhochschule des Mittelstands (FHM) GmbH - Universidad de Ciencias Aplicadas de Bielefeld (Alemania). Tienen una oferta específica en títulos relacionados con Smart Cities.

La Universidad FH Joanneum (Graz, Austria) actúa como imediador entre la sociedad, la industria y la ciencia. La FHJ es una de las universidades más importantes de Austria, con sus programas de estudios altamente especializados a nivel universitario.

WUSMED (España) es una red de Universidades en Europa y el Mediterráneo. Esta organización es una de las promotoras de uno de los doce programas de máster en Europa relacionados con Smart Cities[†], que se inició en el curso 2013/2014.

Premium Research (España) es la principal empresa creada en relación con la Universidad de Valladolid para gestionar la transferencia tecnologica TIC (incluidas las Ciudades Inteligentes) y la promoción de alianzas de innovación con la industria.

Energie Impuls OWL e.V. en Bielefeld (Alemania) son las energías renovables y la eficiencia energética, y aporta al proyecto esta importante área de trabajo en el campo de las ciudades inteligentes.

Innovation Service Network GmbH (Austria) apoya los procesos de innovación y aprendizaje basados en la multitud[‡], pero también ofrece conferencias y seminarios sobre gestión de la innovación.

[†] http://smartcitiesmaster.udg.edu/en/
[‡] www.neurovation.net/www.1000x1000.at

3 Descripción

La UE, para desarrollar una estrategia de crecimiento urbano "inteligente" para las ciudades, promueve la Asociación Europea para la Innovación en Ciudades y Comunidades Inteligentes (EIP-SCC) que reúne a ciudades, industria y ciudadanos para mejorar la vida urbana a través de soluciones integradas más sostenibles. Esto incluye la innovación aplicada, una mejor planificación, un enfoque más participativo, una mayor eficiencia energética, mejores soluciones de transporte y el uso inteligente de las tecnologías de la información y la comunicación (TIC), entre otras.

Sobre esta base, se desarrollan cada vez más ejemplos de proyectos piloto de Smart City en ciudades como Lyon, Vigo, Ámsterdam y Edimburgo. Estos proyectos se llevan a cabo en colaboración con empresas como IBM, Schneider Electric o Siemens que implementan soluciones innovadoras para mejorar la calidad de vida y la sostenibilidad de los entornos urbanos. Empresas, investigadores y autoridades también colaboran en eventos mundiales como el Smart City Expo World Congress que reúne a más de 400 ciudades de todo el mundo, más de 200 empresas, 400 ponentes y las principales instituciones y expertos en transformación urbana.

El concepto multidisciplinar de Smart City plantea un reto en el ámbito del aprendizaje permanente debido a los siguientes problemas:

- Necesidad de alinear la investigación y la formación en la realidad multidisciplinar de las ciudades inteligentes.
- Falta de una estrategia metodológica de aprendizaje permanente.
- Falta de colaboración real y efectiva entre empresas y universidades.
- Desajuste de los contenidos de la formación impartida por los centros de enseñanza superior o los proveedores privados de formación especializados para colmar el déficit de cualificaciones y competencias que necesita el mercado.

Para los licenciados es necesario que tengan la combinación adecuada de capacidades: competencias transversales, cibercapacidades para la era digital, creatividad y flexibilidad y una sólida comprensión del campo elegido. Algunas de estas habilidades son aportadas por las universidades, pero las competencias transversales como la innovación, el trabajo en equipo, la organización y planificación, el pensamiento analítico, la creatividad, etc. no están cubiertas por los títulos oficiales y están adquiriendo una gran relevancia en el campo de las ciudades inteligentes.

Es necesario desarrollar un programa de formación común, diseñado por las instituciones pertinentes del sector de las ciudades inteligentes, con el fin de satisfacer las necesidades de la industria que deberían ponerse en práctica en forma de prácticas en colaboración entre la educación superior y el resto de las partes interesadas.

El objetivo del proyecto SCALE es diseñar, desarrollar y validar un programa de formación en competencias relacionadas con Smart Cities, común a todas las disciplinas que este concepto incluye, incluyendo un programa de movilidad para apoyar la adquisición de competencias de los becarios en el área de Smart Cities, así como para promover la colaboración del mundo empresarial y la educación y formación superior.

La metodología para lograr este objetivo parte de una investigación sobre las competencias de las ciudades inteligentes, comunes a todas las disciplinas y campos. Se

elaborará un programa de formación sobre estas competencias que estará abierto a estudiantes y personal de universidades y empresas, socios o no del proyecto, siempre que estudien o trabajen en el campo de las ciudades inteligentes.

Al mismo tiempo, se identificarán proyectos innovadores de Smart Cities para ser transferidos y puestos en práctica en otro contexto, en otras ciudades y en otros países. Estos proyectos serán llevados a cabo por un estudiante en forma de prácticas en colaboración en un país socio, con el fin de poner en práctica las competencias adquiridas en Smart Cities.

El proyecto SCALE potenciará las prácticas de estudiantes de licenciaturas y másteres relacionados con Smart Cities porque adquirirán las competencias necesarias en el campo, las empresas serán más competitivas porque contarán con personal mejor preparado y las ciudades y empresas implementarán proyectos innovadores y exitosos en Smart Cities con la ayuda de los estudiantes durante sus pasantías. De manera más específica, se plantean las siguientes metas:

- Adaptar los sistemas de aprendizaje permanente a los retos de las ciudades inteligentes, mejorando la relación entre la universidad y la industria y el conjunto de los mecanismos de aprendizaje permanente.
- Apoyar el desarrollo de competencias en la educación superior en el ámbito de las ciudades inteligentes con el fin de desarrollar un enfoque transversal, desarrollar habilidades relacionadas con la creatividad, la innovación y el trabajo en equipo multidisciplinar.
- Fomentar la generación de proyectos innovadores dentro de la comunidad que combinen ciencia, conocimiento y modelos de negocio de diferentes sectores para diseñar productos y servicios innovadores.

3.1 Hechos diferenciadores

El proyecto SCALE se está desarrollando mediante un consorcio equilibrado de universidades y empresas relacionadas con las ciudades inteligentes tanto en el ámbito de la educación como en el de la industria. Todos los socios colaborarán para un mismo objetivo desde diferentes perspectivas, realizando un estudio sobre las competencias y las habilidades que demanda el mercado, la identificación de los desajustes entre la oferta y la demanda del mercado laboral, los nichos de mercado, las proyecciones de carrera, las preferencias en materia de redes y el interés general de las partes interesadas.

Hasta la fecha no existe ninguna iniciativa europea que se enfrente a los retos de las ciudades inteligentes que exija un ajuste importante en la educación superior, en la relación entre la Universidad y todos los mecanismos de aprendizaje a lo largo de toda la vida con la industria relacionada con las ciudades inteligentes.

Los estudiantes universitarios también se deben formar para trabajar en empresas altamente innovadoras que combinen ciencia, conocimiento y modelos de negocio de diferentes sectores, diseñando productos y servicios que respondan a las necesidades de una nueva generación de clientes en Ciudades Inteligentes que evolucionan continuamente y que se ven afectadas por el cambio global, los avances tecnológicos y la globalización.

La adaptación de los sistemas de educación superior y formación debe hacerse desde una doble perspectiva:

- Completar los planes de estudio basados en la demanda específica de la industria de las ciudades inteligentes.
- Desarrollar un nuevo modelo de innovación para la cooperación Universidad-Empresa que pueda basarse en un flujo de trabajo bilateral capaz de combinar el enfoque científico multidisciplinar y las competencias de innovación con la ciudadanía.

SCALE se basa en una comunidad de personas (profesionales, estudiantes, trabajadores, profesores, investigadores, personal universitario, etc.) de muchas organizaciones diferentes inspiradas en un enfoque de aprendizaje bottom-up, colaborativo y de innovación. El proyecto incorporará un innovador programa de pasantías ya desarrollado en proyectos anteriores, y asegurará la estrecha colaboración entre las instituciones de educación superior y de aprendizaje permanente, por un lado, y la industria y las empresas, por otro. Este programa de pasantías se fomentará durante y después del proyecto, y lo podrán utilizar otros sectores educativos y económicos.

El proyecto se cimienta en la investigación, colaboración y participación directa de todos los actores relacionados con Smart Cities, y se basa en las siguientes necesidades reales:

- Competencias comunes relacionadas con Smart Cities.
- Identificación de proyectos de ciudades inteligentes, fomentando el intercambio de buenas prácticas entre los países socios.
- Desarrollo de prácticas colaborativas, que permitirán a los becarios acceder de una manera más efectiva y directa al mercado laboral con el apoyo continuo de los profesores y profesionales que les darán tutoría durante las prácticas.

4 Resultados esperados

Las instituciones educativas (universidades), los proveedores de aprendizaje permanente y otras organizaciones que trabajan en la educación y formación de Smart Cities tendrán una oferta educativa relacionada con ésta, más adaptada a las nuevas demandas del mercado, y ofrecerán una mejor educación con una conexión más amplia con la industria. Intercambiarán conocimientos y retos comunes, así como recibirán información sobre el desarrollo de proyectos concretos en el campo de las ciudades inteligentes, que les proporcionará información relevante para ofrecer una educación de calidad y adecuada.

Los estudiantes se beneficiarán del curso de formación on-line desarrollado en el proyecto, y tendrán más oportunidades en el mercado laboral relacionado con Smart Cities, aumentando su nivel de empleabilidad. Debido a su participación en la investigación, el curso de formación on-line se ajustará a sus motivaciones y necesidades.

La industria de las ciudades inteligentes y las partes interesadas en el proyecto contarán con personal mejor preparado, con las competencias y habilidades necesarias en el sector, además de los conocimientos técnicos.

Las ciudades se beneficiarán del proyecto ya que estarán al tanto de las últimas tendencias e innovaciones en el campo de las ciudades inteligentes, y de aquellas que puedan ser abordadas de forma común por las ciudades europeas, en el sentido de que el proyecto las ofrecerá en forma de prácticas y que esta información estará disponible en la página web del proyecto.

SCALE generará una comunidad que llegará a los grupos objetivo con campañas de difusión, productos y eventos.

BiciTEC: Sistema de préstamo de bicicletas en el campus universitario del Tecnológico de Costa Rica

Carlos Meza[1][0000−0002−7374−505X], Alina Rodríguez[2][0000−0003−2115−4976], Raquel Mejías[2][0000−0003−3312−2699], Estefanía Prahl[1], Mainor Lizano[1], and María Eugenia Quesada[2]

[1] SESLab, Escuela de Ing. Electrónica, Instituto Tecnológico de Costa Rica, Cartago, Costa Rica
cmeza@tec.ac.cr
[2] GASEL, Instituto Tecnológico de Costa Rica, Cartago, Costa Rica
alirodriguez@tec.ac.cr

Resumen Los sistemas de bicicletas compartidas tienen una relevancia significativa en un esquema de movilidad sostenible para ciudades inteligentes. Por un lado, ofrecen un servicio de transporte individual de bajo costo pero flexible para que el ciudadano pueda realizar trayectos cortos, complementándose muy bien con los servicios de transporte público regulares. Por otro lado, la utilización de dispositivos electrónicos con capacidad de procesamiento y comunicación en cada una de las bicicletas, dota al sistema de la capacidad de generar redes móviles y capturar datos de importancia para la gestión de la ciudad. El Instituto Tecnológico de Costa Rica ha decidido desarrollar su propio sistema de bicicletas compartidas con el objetivo de mejorar la situación de transito vehicular en su campus y de probar soluciones innovadoras en los sistemas electrónicos que están empotrados en cada una de las 73 bicicletas del proyecto. En este trabajo se presentan los principales subsistemas del proyecto y se resalta su potencial importancia en centros urbanos.

Keywords: Bicicletas compartidas · Movilidad sostenible · Internet de las cosas

1. Introducción

Los grandes problemas de tráfico en Amsterdam motivaron al diseñador industrial holandés Luud Schimmelpennick a idear el primer sistema de bicicletas compartido. Este programa se denominó “Plan de Bicicletas Blancas” y fue implementado en los años 60s [5], logrando descongestionar el centro de Amsterdam y continuando con la promoción de la utilización de bicicletas en todo el país.

La congestión vehicular es hoy en día un problema en las principales ciudades del mundo. Más aún, es la flota vehicular que opera con combustibles fósiles una de las principales causas de la contaminación del aire y la generación de gases de efecto invernadero. Es por ello que en los últimos años se ha experimentado un

incremento a nivel mundial en el desarrollo de sistemas de bicicletas compartidas. Según [11] existen al menos 468 ciudades en el mundo que tienen implementado un sistema de bicicletas compartidas.

Un programa de bicicletas compartidas es un componente fundamental en un sistema de movilidad integrado sostenible, ya que representa un complemento para el uso de vehículos propios así como de transporte público regular. Presenta ventajas únicas, algunas de las cuales se enumeran a continuación:

- Una bicicleta compartida se puede usar por varias personas en un mismo día, lo cual optimiza el uso del recurso y minimiza su huella de carbono.
- El servicio es más flexible y permite atender necesidades muy diversas de distintas categorías de usuarios. Por ejemplo, puede ser utilizado para transportarse al trabajo o a los centros de educación o para realizar visitas turísticas en una ciudad.
- Es un medio de transporte de emisión nula durante su uso.
- Permite aliviar el tráfico.
- Atiende las necesidades de transporte individual que el transporte público regular no puede atender.
- Permite atender necesidades de transporte en trayectos cortos a un costo significativamente menor que otros medios de transporte público individual. Por ejemplo, el taxi por su estructura de costos, es muy caro para trayectos cortos.
- Aumenta la salud en sus usuarios [4].
- No hay tiempo de espera o preocupación sobre estacionamientos.

Desde el "Plan Bicicleta Blanca" los servicios de bicicleta compartida han experimentado importantes avances, los cuales son normalmente catalogados en generaciones tal y como se detalla a continuación ([14]):

- **Primera Generación:** Las bicicletas, identificadas de forma única con un diseño especial, son distribuidas sin costo alguno entre los potenciales usuarios. No existe un control sobre la ubicación de las bicicletas.
- **Segunda Generación:** Integra estaciones de entrega y devolución. Las bicicletas se encuentran únicamente en las estaciones. Existe un costo bajo por el uso de las bicicletas. No existe un control sobre el tiempo de uso de la bicicleta.
- **Tercera Generación:** Integra tecnologías de la información y comunicación. Las estaciones de entrega y devolución tienen un kiosco para interactuar con el usuario. Se conoce y controla el tiempo de uso de las bicicletas.
- **Cuarta Generación:** Integra un sistema para la distribución y relocalización de bicicletas ya sea utilizando candados inteligentes o estaciones móviles.

Uno de los mayores desafíos para la operación efectiva de los sistemas de bicicletas compartidas es mover las bicicletas de las estaciones saturadas a las vacías [15]. Varios trabajos como [1–3,6,7,9,13,15] se concentran en el desarrollo de modelos de predicción de uso para determinar dónde ubicar las estaciones y cómo realizar su relocalización.

Por otro lado, la integración de tecnologías de la información y comunicación en el sistema de bicicletas compartidas está permitiendo el estudio de nuevas funcionalidades. Así por ejemplo, en [10] se propone el uso de las bicicletas para recolectar información sobre calidad del aire en aquellos sitios por donde se transita con ellas. Prist en [12] propone utilizar las bicicletas y las estaciones como nodos de un sistema de comunicación y medición interconectado. De esta forma cada bicicleta puede llevar un registro de su posición, nivel de batería y comunicar esta información entre todos los nodos. En [8] se propone usar acelerómetros en las bicicletas compartidas para poder sintetizar información sobre el estado de la carretera.

Los sistemas de bicicletas compartidas no sólo permiten mejorar las condiciones de tránsito de la ciudad sino que pueden ser utilizados como nodos móviles para contribuir con la digitilación de entornos urbanos inteligentes. Es por ello que en el Instituto Tecnológico de Costa Rica se está implementando un proyecto propio de bicicletas compartidas. Este proyecto ha sido diseñado e implementado de forma completa por personal de la Institución con el objetivo de poder utilizarlo como un entorno para experimentar funcionalidades adicionales en su funcionamiento.

El presente trabajo describe los principales elementos del programa de préstamo de bicicletas del Instituto Tecnológico de Costa Rica, denominado BiciTEC.

2. Proyecto BiciTEC

Al igual que muchas ciudades, el campus central del Instituto Tecnológico de Costa Rica presenta problemas de tránsito vehicular y de falta de puestos de estacionamiento. El campus ha duplicado su extensión y existen varios conjuntos de edificios separados por hasta tres kilómetros. Esta situación ha hecho necesario proponer un plan de movilidad sostenible cuyo proyecto principal es el desarrollo de un sistema de biciletas compartidas universitario.

BiciTEC es el sistema de bicicletas compartidas del Instituto Tecnológico de Costa Rica y permite que estudiantes activos utilicen, sin costo alguno, alguna de las 73 bicicletas disponibles para tal fin. Las bicicletas no pueden ser utilizadas fuera del campus y se prestan por un periodo de 30 minutos. La forma en que el estudiante solicita la bicicleta es por medio de una aplicación para teléfono móvil.

Las bicicletas utilizadas para el proyecto fueron fabricadas para una frecuencia de uso elevada en entornos urbanos. En la figura 1 se muestra una fotografía de las biciletas seleccionadas. Estas bicicletas además requieren poco mantenimiento, lo cual reduce los costos operativos del proyecto.

Las bicicletas cuentan con un candado electrónico que fue diseñado y ensamblado en el Tecnológico de Costa Rica. Integra un microprocesador que puede ser utilizado como nodo en una red de sensores móviles. Para la primera etapa del proyecto, la funcionalidad de nodo ha sido desactivada. Más información sobre el candado se presenta más adelante.

Figura 1: Bicicletas utilizadas para BiciTEC

Las estaciones de despacho y devolución de bicicletas son infraestructuras normalmente costosas que requieren de obra civil y alimentación eléctrica, no siempre disponible en los sitios en donde se deben colocar las bicicletas. Por otro lado, tal y como se menciona en [3, 7, 13, 15] es difícil determinar la ubicación y la cantidad óptima de bicicletas que debe tener cada estación. Es por ello que se ha decidido diseñar una estación ligera, de bajo costo y de fácil reubicación. Las estaciones que se utilizan en el proyecto BiciTEC se muestran en la figura 2.

2.1. Sistema automático de recepción y despacho de bicicletas

Cada bicicleta porta un candado electrónico diseñado y ensamblado por personal del Instituto Tecnológico de Costa Rica. Este candado se encuentra entre la rueda trasera y el asiento tal y como se muestra en la Figura 3. Una foto de la parte interna de este candado se puede observar en la Figura 4.

Cada estación tiene conectada un cable metálico con una clavija (ver figura 5) que se inserta dentro del candado electrónico, el cual está firmemente sujetado a la bicicleta. Cuando las bicicletas están estacionadas el candado y la clavija están sujetos. Cada bicicleta posee un código QR que, al ser escaneado por el dispositivo móvil de un usuario registrado, desbloquea la clavija y permite utilizar la bicileta por 30 minutos. Al llegar a la estación el usuario debe conectar la clavija al candado y dar por terminado el préstamo.

El candado posee un sistema electrónico empotrado que, utilizando tecnología Bluetooth de bajo consumo, puede comunicarse con un dispositivo móvil por medio de una aplicación diseñada para tal fin. Esta aplicación se comunica con

Figura 2: Fotografía de las estaciones de BiciTEC

Figura 3: Imagen de la bicicleta con el candado

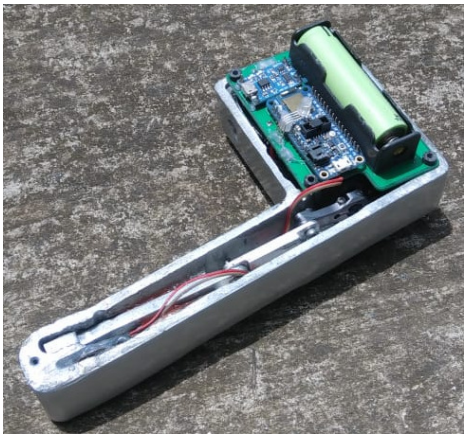

Figura 4: Fotografía del interior del candado inteligente

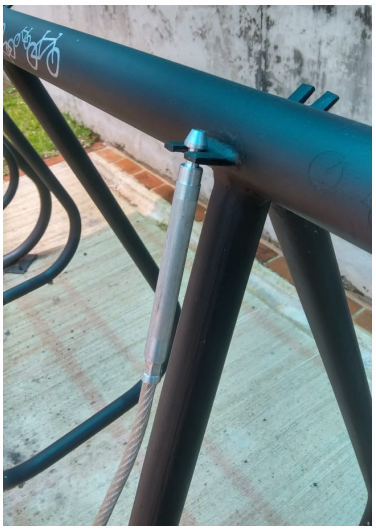

Figura 5: Fotografía de la clavija usada para asegurar las bicicletas a las estaciones

un servidor de la universidad que valida la información de los usuarios y registra los préstamos y otras estadísticas de interés.

La figura 6 muestra el diagrama de bloques del sistema electrónico para BiciTEC. Se distinguen cuatro elementos principales:

- Dos paneles solares fotovoltaicos ubicados en el guardabarros posterior de la bicicleta que se utilizan para alimentar el sistema electrónico.
- Un candado electrónico por bicicleta que consta de los siguientes subsistemas:
  - Unidad de procesamiento de potencia para cargar la batería del sistema electrónico por medio de los paneles fotovoltaicos.
  - Batería de iones de litio recargable.
  - Un sistema electrónico con microprocesador para realizar todas las tareas lógicas para la comunicación, desbloqueo y activación de alarmas.
  - Alarma sonora para indicar que se ha vencido el tiempo de préstamo.
  - Mecanismo electromecánico de bloqueo para asegurar o liberar la clavija.
  - Modulo de comunicación Bluetooth para la interacción con el dispositivo móvil.
- Teléfono móvil con una aplicación para gestionar el sistema del candado.
- Servidor en la nube que se encarga de autorizar usuarios y registrar lo datos de uso.

2.2. Aplicación móvil

El usuario realiza solicitudes de reserva de bicicletas por medio una aplicación móvil que debe descargar e instalar en su teléfono. La aplicación permite abaratar

Figura 6: Diagrama de bloques de los elementos electrónicos de BiciTEC

los costos del proyecto, ya que el candado accesa la información de la base de datos del servidor de la Universidad por medio del internet del teléfono. Así mismo, se puede utilizar el GPS del teléfono móvil para obtener datos sobre la ruta seguida por el usuario. Las figuras 7a, 7b, 7c, 8a y 8b muestran las principales funciones que el usuario puede realizar en su dispositivo móvil.

Al abrir la aplicación móvil el usuario debe registrase con sus credenciales de estudiante tal y como se indica en la pantalla de la figura 7a. Una vez dentro de la aplicación un menú indica las distintas acciones que el usuario puede realizar (ver Figura 7b), éstas son,

- Alquilar bicicleta: función para alquilar bicicleta. Al ingresar esta opción se activa la cámara del dispostivo móvil para que el usuario lea el código QR de la bicicleta que se desea utilizar. Una vez seleccionada la bicicleta y autorizado el usuario éste tiene 30 minutos para utilizar la bicicleta tal y como se le indica en la pantalla de la figura 7c. Cuando faltan 5 minutos para la caducidad del tiempo de préstamo el usuario verá una pantalla como la mostrada en la figura 8a. Si el tiempo se agota, el candado emitirá un sonido constante y el estudiante deberá ponerse en contacto con los administradores del programa para desactivarlo.
- Reportar bicicleta: función para reportar averías y bicicletas en mal estado.
- Mi usuario: brinda información sobre la distancia recorrida con la bicicleta y las emisiones de CO_2 evitadas tal y como se muestra en la pantalla de la figura 8b.

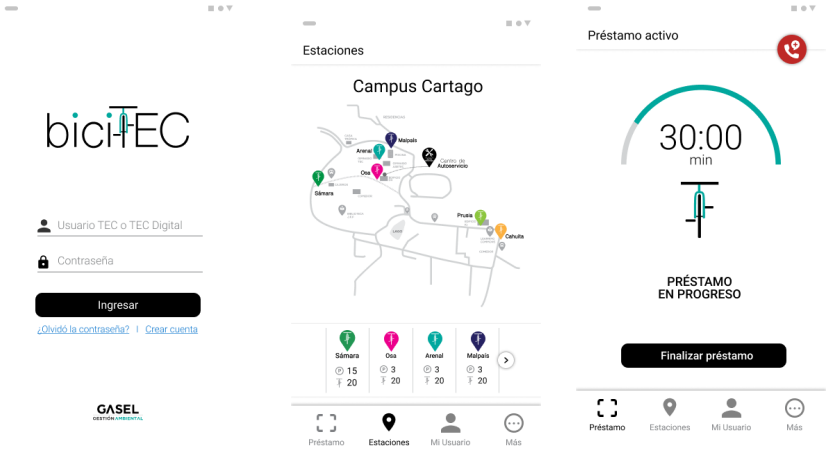

(a) Pantalla para el registro de usuarios (b) Menú de la aplicación (c) Pantalla préstamo activo

Figura 7: Pantallas de la aplicación para la solicitud de bicicletas compartidas -

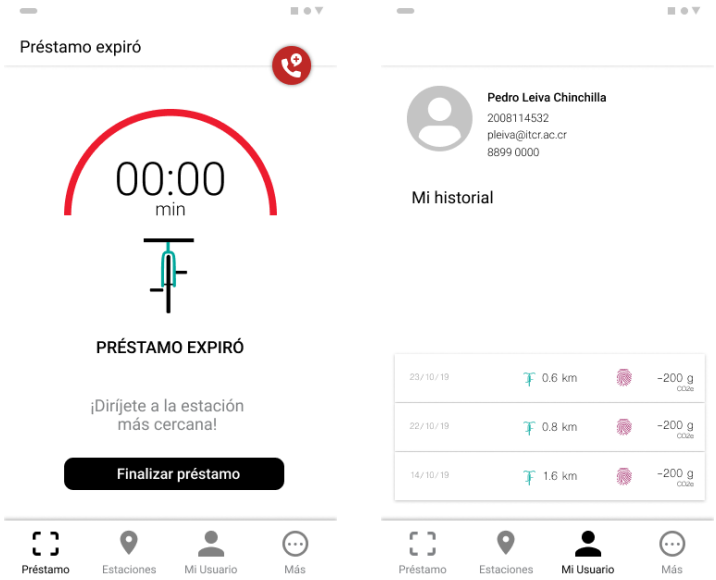

(a) Pantalla cuando se está por vencer el préstamo (b) Pantalla sobre información de usario

Figura 8: Pantallas de la aplicación para BiciTEC

3. Conclusiones y trabajo futuro

Durante el desarrollo del proyecto BiciTEC se ha podido verificar que el uso de sistemas electrónicos empotrados con capacidad de procesamiento reducen significativamente sus costos. La utilización de un candado electrónico con estaciones ligeras representa una ahorro significativo en comparación con las estaciones que integran el sistema de sujeción en su estructura. Así mismo, la utilización de los recursos (conexión a internet, GPS) del dispositivo móvil del usuario simplifica y reduce los costos del sistema electrónico empotrado en la bicicleta.

En una segunda etapa se estará dotando al candado electrónico de la capacidad de interconectarse con otros candados para conformar una red inalámbrica de sensores móviles. Dicha red puede utilizarse para la monitorización de distintas variables del campus como por ejemplo calidad del aire.

Referencias

1. Cagliero, L., Cerquitelli, T., Chiusano, S., Garza, P., Xiao, X.: Predicting critical conditions in bicycle sharing systems. Computing **99**(1), 39–57 (2017)
2. Cheng, Y.X., Jiang, Y.H., Yang, J.: A Research about Shared-Bicycle Time and Space Distribution Model. Proceedings - 2017 16th International Symposium on Distributed Computing and Applications to Business, Engineering and Science, DCABES 2017 pp. 223–226 (2018)
3. Dali, L., Mladenic, D.: BICIKELJ: Environmental data mining on the bicycle. Interfaces (ITI), Proceedings of the ITI 2012 pp. 331–336 (2012)
4. Fuller, D., Gauvin, L., Kestens, Y., Morency, P., Drouin, L.: The potential modal shift and health benefits of implementing a public bicycle share program in Montreal, Canada. International Journal of Behavioral Nutrition and Physical Activity **10**, 2–7 (2013)
5. Furness, Z.M.: "Put the Fun Between Your Legs!": The Politics and Counterculture of the Bicycle. Ph.D. thesis, University of Pittsburgh (2006)
6. Guo, T.Y., Zhang, P., Shao, F., Liu, Y.S.: Allocation optimization of bicycle-sharing stations at scenic spots. Journal of Central South University **21**(8), 3396–3403 (2014)
7. Hamon, R., Borgnat, P., Flandrin, P., Robardet, C.: Networks as signals, with an application to a bike sharing system. 2013 IEEE Global Conference on Signal and Information Processing, GlobalSIP 2013 - Proceedings pp. 611–614 (2013)
8. Iwasaki, J., Yamamoto, A., Kaneda, S.: Road information-sharing system for bicycle users using smartphones. 2015 IEEE 4th Global Conference on Consumer Electronics, GCCE 2015 pp. 674–678 (2016)
9. Liu, J., Li, Q., Qu, M., Chen, W., Yang, J., Xiong, H., Zhong, H., Fu, Y.: Station site optimization in bike sharing systems. Proceedings - IEEE International Conference on Data Mining, ICDM pp. 883–888 (2016)
10. Liu, X., Xiang, C., Li, B., Jiang, A.: Collaborative bicycle sensing for air pollution on roadway. Proceedings - 2015 IEEE 12th International Conference on Ubiquitous Intelligence and Computing pp. 316–319 (2016)
11. Oliver O'Brien: Bike Share Map. `https://bikesharempa.com/`, Accesado: 2019-08-28

12. Prist, M., Freddi, A., Longhi, S., Monteriu, A., Antonini, P.: Wireless sensor network based management system for electric bicycle-sharing. EEEIC 2016 - International Conference on Environment and Electrical Engineering pp. 1–6 (2016)
13. Schlote, A., Chen, B., Sinn, M., Shorten, R.: The effect of feedback in the assignment problem in shared bicycle systems. 2013 International Conference on Connected Vehicles and Expo, ICCVE 2013 - Proceedings pp. 960–961 (2013)
14. Shaheen, S.A., Guzman, S., Zhang, H.: Bikesharing in europe, the americas, and asia: past, present, and future. Transportation Research Record **2143**(1), 159–167 (2010)
15. Zhang, J., Pan, X., Li, M., Yu, P.S.: Bicycle-sharing system analysis and trip prediction. Proceedings - IEEE International Conference on Mobile Data Management pp. 174–179 (2016)

Urban data analysis for the public transportation system of Montevideo, Uruguay

Renzo Massobrio and Sergio Nesmachnow

Universidad de la República, Uruguay
{renzom,sergion}@fing.edu.uy

Abstract. This article presents a study of the public transportation system in Montevideo, Uruguay, following a data science approach. More than 20 million records from the Intelligent Transportation System (ITS) are analyzed in order to characterize mobility in the city. Several useful pieces of information are obtained through data analysis, related to tickets sold, patterns of smart card utilization, most used bus lines and stops, and socioeconomic insights about passengers behavior. Practical case studies are also presented: anomaly detection in space and time, and a study of potential safety hazards due to reckless driving. The work reported in this article constitutes one of the first steps towards using data from the ITS in Montevideo to understand mobility in the city.

Keywords: data science · public transportation · smart cities

1 Introduction

Public transportation plays a major role in urban mobility, as they are the most efficient, sustainable, and socially fair mode of transportation [9]. Understanding the interaction between citizens and public transportation systems is paramount in order to design and implement policies aimed at improving mobility.

Modern *smart cities* take advantage of technology to improve urban services [6]. Urban traffic and transportation systems are addressed under the paradigm of smart cities, in what is referred to as *smart mobility* [3]. Related to this concept are Intelligent Transportation Systems (ITS), which use technology to develop and enhance transportation. In addition to improving mobility, ITS allow collecting large volumes of urban data [7]. Large repositories of data offer a unique opportunity to gain valuable insights into the mobility of citizens [12]. In this context, urban data analysis arises as a tool to extract meaningful information from raw urban data to help decision-making processes in cities.

In 2010 an urban mobility plan was implemented in Montevideo, Uruguay, with the goal of restructuring and modernizing public transportation [1]. Under this plan, public transportation in the city was integrated into a unified system, which incorporates many of the characteristics common to ITS. Buses were equipped with on-board GPS units and ticket selling machines operated with smart cards. These devices represent new sources of urban data, which have a huge potential to help authorities understand mobility in Montevideo.

This article presents a characterization of the use of the transportation system through urban data analysis, along with a series of case studies of potential use for these rich data sources. The article is organized as follows. Next section describes the data analysis process in smart cities. Section 3 describes the public transportation system in Montevideo, Uruguay. Specific case studies are described and analyzed in Section 4. Finally, Section 5 presents the conclusions and the main lines for future work.

2 Data analysis in smart cities

This section introduces ITS in the context of smart cities, and urban data analysis as an efficient tool to extract meaningful information from urban data. Then, a brief review of related works in the literature is presented.

2.1 Smart cities and ITS

The paradigm of smart cities proposes taking advantage of information and communication technologies to improve the quality and efficiency of urban services [6]. Smart devices embedded into traditional physical systems deployed on cities, generate vast volumes of data for the analysis. Extracting insights from the gathered data is crucial to improve decision-making in cities and to achieve quality improvements and increase the efficiency of public services.

Related to smart mobility, ITS integrate synergistic technologies, computational intelligence, and engineering concepts to develop and improve transportation. Automatic Vehicle Location (AVL) systems automatically determine and communicate the geographic location of a moving vehicle [17]. The transmitted locations of a fleet of vehicles can be collected at a central server to overview and control the group of vehicles. Due to its widespread availability, low cost, and precision, the most common technology to determine the location of vehicles in AVL is GPS. AVL technology is frequently incorporated in ITS and provides a rich source of data, as it can help to monitor and control the QoS provided by the transportation system to users.

Automatic Passenger Counters (APC) are electronic devices that can be incorporated to moving vehicles to record boarding and alighting data [5]. This technology is a major improvement over traditional manual passenger counts or surveys. Several implementations of this concept have been proposed including infrared lights in doorways of vehicles, scales to measure weight changes, and CCTV cameras coupled with computer vision software. The data generated by these systems allow identifying use patterns by linking boarding and alighting data with stop or station location [8].

Automatic Fare Collection (AFC) [4] automate the ticketing system on public transportation. AFC are comprised of fare media, devices to read/write onto these media, communication technologies, and back office systems. Contactless smart cards have become the de facto technology in AFC systems. AFC systems

generate highly valuable data that can be processed to extract useful metrics for both day-to-day operation and long-term planning of transportation systems.

The development of smart tools that use data gathered by ITS has risen in the past years. These tools rely on efficient and accurate data processing (even in real-time), which poses an interesting challenge from the technological perspective. The methodology for analyzing sources of urban data to gain valuable insights to describe and improve the life of citizens is described next.

2.2 Urban data analysis

Data analysis is the process of collecting and processing raw data to extract meaningful information that provides supporting evidence for conclusions and helps decision-making processes. Multiple workflows have been proposed to describe the process of data analysis, and techniques under a variety of names have emerged in different fields of knowledge at both academia and industry.

The data analysis process starts and ends in the current reality. In urban contexts, the analysis starts with collecting raw data from a city and ends with communicating findings that can help stakeholders to shape the reality of that city to improve the quality of life of its citizens. In between, the data analysis process is comprised of several phases. Firstly, raw collected data must be processed. This phase include several tasks such as placing data into structures (e.g., tables), inspecting datasets, and cleansing data to detect missing or inaccurate records. After data processing, Exploratory Data Analysis (EDA) is performed [15]. This phase may lead to detecting further inaccuracies in the data and potentially requiring further cleansing. After EDA, statistical models and algorithms are applied to identify relationships between the studied data [11]. Finally, results are interpreted and communicated, mostly using visualization. When dealing with urban data, effectively communicating results is crucial, thus, the visualization phase is described in more depth in the following paragraphs.

2.3 Related work

The advantages of using data analysis for social transportation have been studied in a thorough manner in the general review of the field developed by Zheng et al. [18]. The authors discussed the use of several sources of information, including vehicle mobility (e.g., GPS coordinates, speed data), pedestrian mobility (e.g., GPS and WiFi signals from mobile devices), incident reports, social networking (e.g., textual posts, user location), and web logs (e.g., user identification, comments). In the review, the advantages and limitations of using each source of data were discussed. Several other novel ideas to improve public transportation were also reviewed, including applying *crowdsourcing* techniques for collecting and analyzing real-time or near real-time traffic information, and using *data-based agents* for driver assistance and human behavior analysis. Finally, a data-driven social transportation system that integrates all the previous concepts and improves traffic safety and efficiency was proposed.

More related to the data analysis research included in this article, many works have studied urban mobility using smart card data from AFC in public transportation systems.

Bagchi and White [2] discussed the role of smart card data for travel behavior analysis. The transportation systems of Southport, Merseyside and Bradford in England were studied. The authors performed a simple study focused on the average number of trips and transfers made by passengers. The turnover rates were analyzed to identify the number of active users in the system. The research concluded that smart card data allow obtaining much larger samples than surveys to characterize transportation systems. However, certain information (e.g., purpose of traveling) cannot be inferred from these data. Thus, the authors conclude that smart card transactions are not an alternative to traditional data collection methods, but a useful complementary source of data.

Utsunomiya et al. [16] studied access and usage patterns of passengers in the transportation system of Chicago, US. The authors discussed the analysis using smart card sign-ups and transactions data, identifying the major issues encountered as well as general recommendations. The potential uses for smart card data were classified in categories: service planning, demand forecasting, pricing and fare policy definition, and market research. Seven days of recorded transactions were studied to analyze walking access distances, frequency of daily travel patterns, and passenger behavior by residential area. Frequent errors were due to missing transactions and incorrect bus route identification. In order to deal with these inconsistencies, the authors proposed combining smart card data with passenger counts and vehicle location from APC and AVL systems.

3 The public transportation system in Montevideo

This section presents the public transportation system in Montevideo, Uruguay, and the urban data analysis process to characterize its usage.

3.1 Overview of the city and transportation system

Montevideo is the capital city of Uruguay, and extends to an area of only 530 km^2. Despite accounting for only 0.3% of the total surface of the country, nearly 40% of the total population lives in Montevideo.

The public transportation in Montevideo (Sistema de Transporte Metropolitano, STM), is comprised of 1528 buses operated by four private companies. The bus network consists of 145 main bus lines and 4718 bus stops, Bus lines have different variants, accounting for outward and return trips, as well as shorter versions of the same line. The total amount of bus lines when considering each variant individually is 1383. Figure 1 shows the bus lines that comprise STM according to data provided by [14].

Passengers of the public transportation system in Montevideo can use smart cards to pay for their tickets without physical money. STM smart cards are contact-less cards which are linked to the identity of the owner. Two different

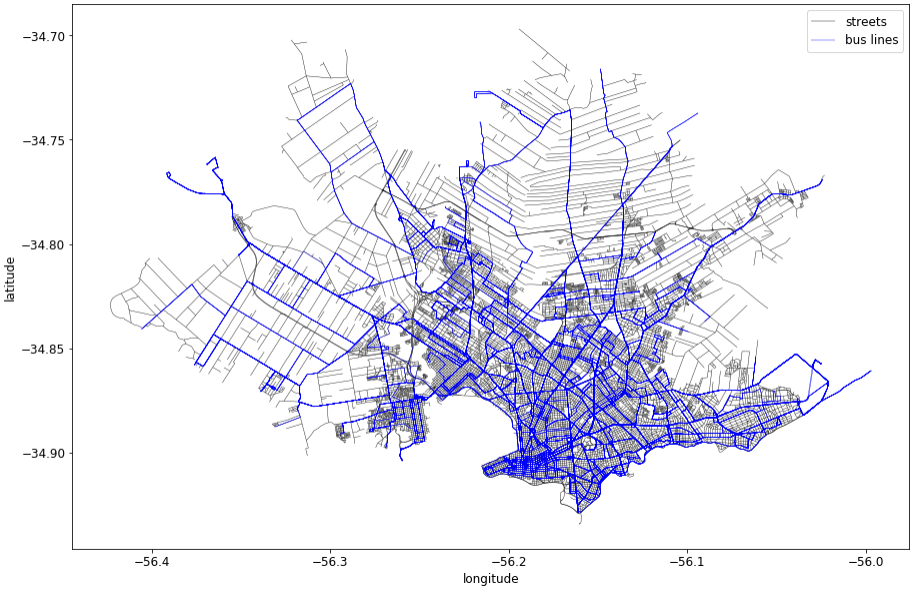

Fig. 1. Bus lines in STM

types of bus tickets are available which allow bus transfers: *one-hour* and *two-hours* tickets. One-hour tickets allow boarding up to two buses within an hour, while two-hours tickets grant unlimited bus transfers within a period of two hours. The fare scheme supports transfers between any bus line at any bus stop.

3.2 Data collection and cleansing

Data collection. Many state agencies and local governments have web interfaces for publishing open data. In this context, the most useful web interface was the geographic information site at Intendencia de Montevideo (`www.sig.montevideo.gub.uy`), which holds geographic data of Montevideo including base maps, socioeconomic indicators, and transportation network data.

Besides using open data publicly available, the analysis included data regarding STM accessed through a collaboration between our research group and IM. The sources of these data are the AVL and AFC systems integrated in buses of the STM. The data corresponding to the full set of records of GPS bus location and bus ticket sales payed with STM cards during 2015 was released for research purposes. These large datasets comprise over 150 GB of raw data.

The bus location dataset contains information about the position of each bus in STM, sampled every 10 to 30 seconds. Each location record holds the following information:

- a unique bus line identifier.
- a unique trip identifier to differentiate trips of the same bus line.
- GPS coordinates.

– instant speed of the vehicle.
– time stamp when the GPS measure was taken.

Ticket sales data contain records related to each STM transaction made, including the following fields:

– trip identifier for the sale, which allows linking to the bus location dataset.
– GPS coordinates at the moment of the STM card validation.
– bus stop identifier.
– time stamp at the moment of the STM card validation.
– unique STM card identifier, hashed for privacy purposes.
– number of passengers traveling with the same STM card.
– leg number, for multi-leg trips that include transfers.

For the sake of clarity, the reported results correspond to tickets sold during May 2015. Pre-hoc analysis of the complete dataset showed that this month is representative of the full dataset.

Data cleansing. Data cleansing is a mandatory step in data analysis that strives to detect and correct corrupt or inaccurate records [13]. Due to the lack of a backup source of information, records that appeared to be corrupted were simply filtered and deleted, according to the actions described next.

Vehicle location using GPS is prone to errors from a variety of sources. The most frequent error was records having a fixed value for both latitude and longitude, pinpointing to the middle of the Atlantic Ocean. Most likely, this was caused by an error message of the GPS unit being misinterpreted as a valid coordinate during data recording. 932.176 records suffered from this issue, accounting for nearly 4.6% of the total dataset. Additionally, 29.432 records corresponded to locations outside Montevideo. However, the dataset also holds the identifier of the boarding bus stop of each transaction, registered by the on-board GPS unit. Thus, even though the GPS measure at the moment of the transaction may fail, the boarding bus stop can be accurately determined from previous measures. Consequently, the bus stop identifier is more reliable than the raw GPS measure when defining the starting point of each trip.

Regarding time stamps of transactions, 74 sales corresponding to May 1^{st} were filtered, since they correspond to Labour Day, a public holiday in which the transportation system is mostly inoperative. Those transactions represent a clear outlier from the remainder of the dataset. Similarly, only one transaction occurring on May 31^{st} was present in the dataset. As a consequence, during the data analysis process, the month of May represents STM transactions occurring between May 2^{nd} 00:00:00 to May 30^{th} 25:59:59 of 2015.

Some transactions had trip identifiers which were not present in the GPS records. Since these records cannot be linked to their corresponding bus line, the 1634 records with this issue were discarded. Similarly, 22 transactions made with the same STM card during the same trip were detected in the original dataset. This might be explained by a synchronization problem between the bus and the centralized server where transactions are recorded.

Since the dataset corresponds to sales from 2015, some transactions refer to bus lines that were modified or no longer exist. These transactions (36.030 records) were also filtered from the dataset. Finally, 274.011 records were filtered, corresponding to transactions with identifiers of bus stops which were not part of the bus line route corresponding to the sale.

In summary, the complete data cleansing process consisted in filtering 311.772 out of a total of 20.359.835 records, accounting for 1.53% of the original dataset.

3.3 Characterizing public transport utilization

This section presents the results from the data analysis process to describe the use of the transportation system in Montevideo from several perspectives.

Cardholders. The sales dataset holds transactions made with 654.228 STM cards. The public transportation system allows several passengers to travel together using the same STM card. Table 1 reports the number of passengers traveling with the same STM card. The vast majority of passengers use their personal STM card, with over 97% of transactions corresponding to individual ticket sales.

Table 1. Number of passengers traveling with the same STM card

# passengers	*total*	*percentage*
1	19494451	97.24%
2	510043	2.54%
3	36454	0.18%
4	5468	0.03%
5+	1647	0.01%

Another interesting aspect that can be studied through data analysis is the frequency of use of the transportation system. Table 2 reports descriptive statistics of daily and monthly transactions per STM card. The *mean* number of transactions is reported, along with the standard deviation (*std*), the minimum (*min*) and the maximum (*max*) values, and the 25^{th} (*Q1*), 50^{th} (*Q2*), and 75^{th} (*Q3*) percentiles. The 50^{th} percentile corresponds to the median of the distribution of transactions per STM card. Monthly statistics consider all transactions done by each cardholder during May 2015. Daily transaction statistics only consider days for which at least one transaction was made.

When looking at monthly figures, cardholders perform over 30 transactions on average, nearly one transaction per day. However, the standard deviation is large, indicating a significant difference between regular and sporadic users of the public transportation system. The median of the monthly transactions is 22, nearly one transaction per working day in the month. Regarding daily use, the average cardholder performs 2.78 transactions each day that uses the transportation system. Figure 2 presents an histogram of daily transactions per STM card, considering only cards that made up to 10 transactions within the

Table 2. Descriptive statistics of daily and monthly use of STM cards

	STM transactions	
	daily	*monthly*
mean	2.78	30.65
std	1.53	28.14
min	1	1
Q1 (25%)	2	8
Q2 (50%)	2	22
Q3 (75%)	4	47
max	54	528

same day in order to remove outliers. Most cardholders perform two transactions per day, which probably correspond to direct trips used for commuting. It is interesting to observe that more cardholders perform four rather than three transactions. This might be explained by passengers commuting to work using a trip involving a transfer, thus, two transactions correspond to the outward trip and the remaining two transactions to the return trip.

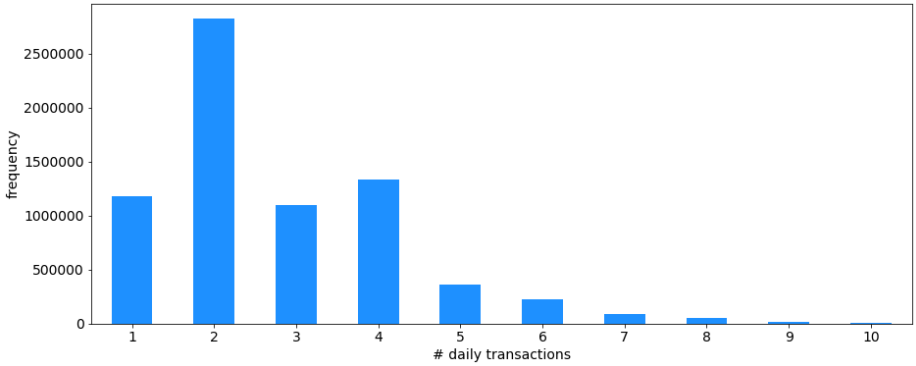

Fig. 2. Histogram of daily transactions per STM card during May 2015

A few interesting applications arise when looking at outliers within the STM use statistics. On the one hand, cardholders with very low activity can be identified by their card ID. For instance, in the studied dataset 15.440 cardholders performed only a single trip during the whole month of May 2015. Targeted marketing campaigns could be designed to encourage disengaged citizens to use the public transportation system more frequently. On the other hand, cardholders with large number of transactions can also be identified. In the studied dataset a single card was found to perform 54 transactions within the same day. Through data analysis, authorities may further investigate these situations in order to identify possible abuses to the rules of the transportation system.

Transactions per bus trip. Grouping STM transactions by their corresponding trip identifier provides a rough estimate for the number of boardings on each trip. Figure 3 presents a histogram of the number of transactions per trip. On average, 39.70 transactions are made in each bus trip (std: 28.16). The largest value encountered was a single trip with 249 transactions. It is worth noting that passengers might also board without using a STM card, so these figures represent a lower bound on the total number of boardings for each trip. Taking into account the capacity of the buses operating in Montevideo, the largest values may indicate overcrowding in some of the bus lines of the transportation system.

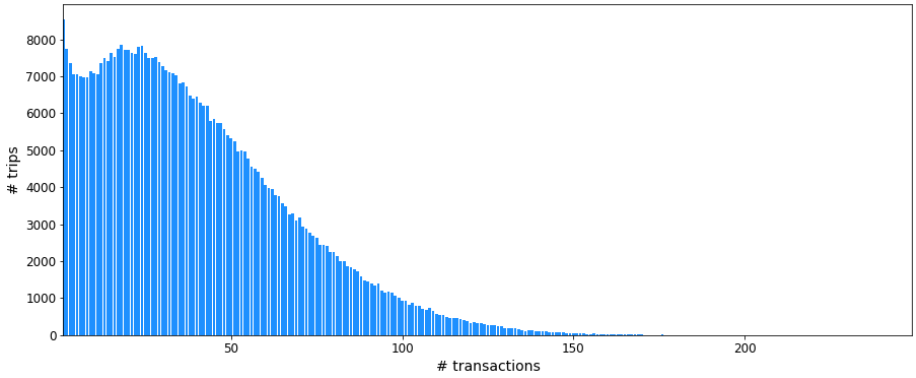

Fig. 3. Histogram of transactions per bus trip during May 2015

Most used bus lines. Data analysis over the transaction data can be used to identify the most popular as well as the most underused bus lines. Figure 4 shows the ten most used bus lines. Some of the lines overlap since they correspond to different variants of the same line (e.g., outward and return lines). For each line the regular name (i.e., the name appearing in the front of the bus) is indicated in the map, along with its variant code indicated in parenthesis. The most used bus line is 183, closely followed by 181. Both lines connect the neighborhood of La Teja, located in the west side of Montevideo, with Pocitos, located in the south by the coastline. It is interesting to notice that none of the ten most used bus lines go into the city center.

Spatiotemporal analysis of transactions. The spatial and temporal dimensions of sales data can be combined, in order to gain insights that might not be evident when studying each dimension independently. Figure 5 shows an aggregated visualization of the spatiotemporal distribution of sales in Montevideo during May 2015. In this visualization the hours of the day are used as categories. Each transaction occurring at a given pixel in the image is categorized according to its time stamp. Then, the color of the pixel is set considering the amount of transactions on each category. The color mapping, which is detailed

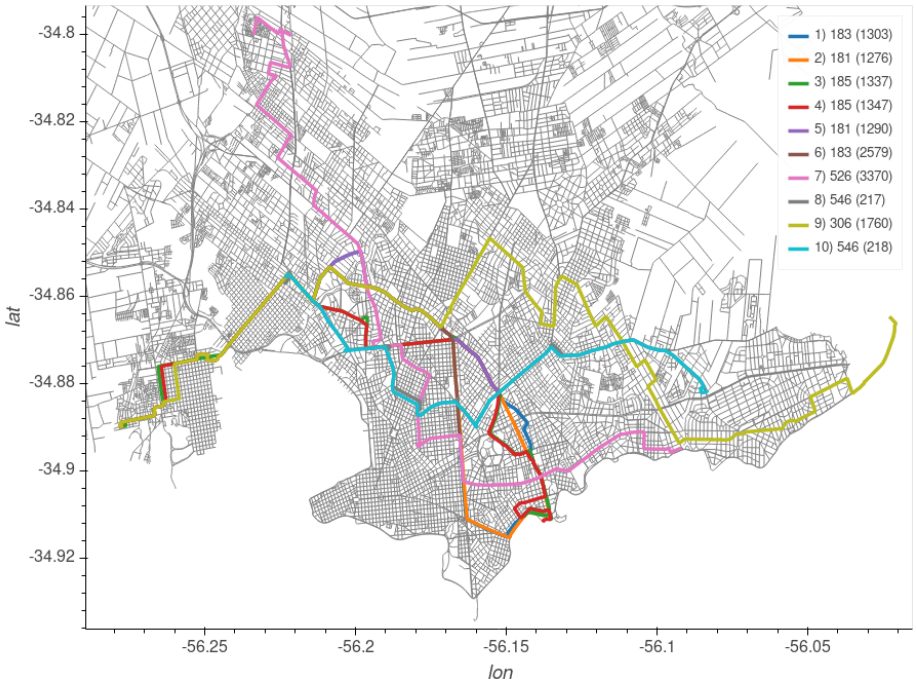

Fig. 4. Top 10 bus lines with most STM card transactions during May 2015

in the visualization, corresponds roughly to: red (12 a.m.), yellow (4 a.m.), green (8 a.m.), cyan (12 p.m.), blue (4 p.m.), purple (8 p.m.), and back to red, since hours and colors are both cyclic.

Firstly, it is observed that the city center has a prevalent blueish tone in the visualization. This corresponds to most transactions taking place between noon and the afternoon. This is consistent with the fact that many offices and public entities are located in this area of the city, thus, most transactions correspond to people commuting from the city center back to their homes by the end of the office-hours.

Another interesting fact arising from the spatiotemporal analysis of STM transactions is the clear difference between areas near the coast and areas farther away. It can be clearly observed that areas away from the coastline appear with more yellow and greener tones whereas areas closer to the coast have predominantly blue tones. This means that the majority of STM transactions in areas farther away from the coast occur earlier in the day than those near the coast. This can be explained by people commuting early in the day from these areas to workplaces located closer to the city center.

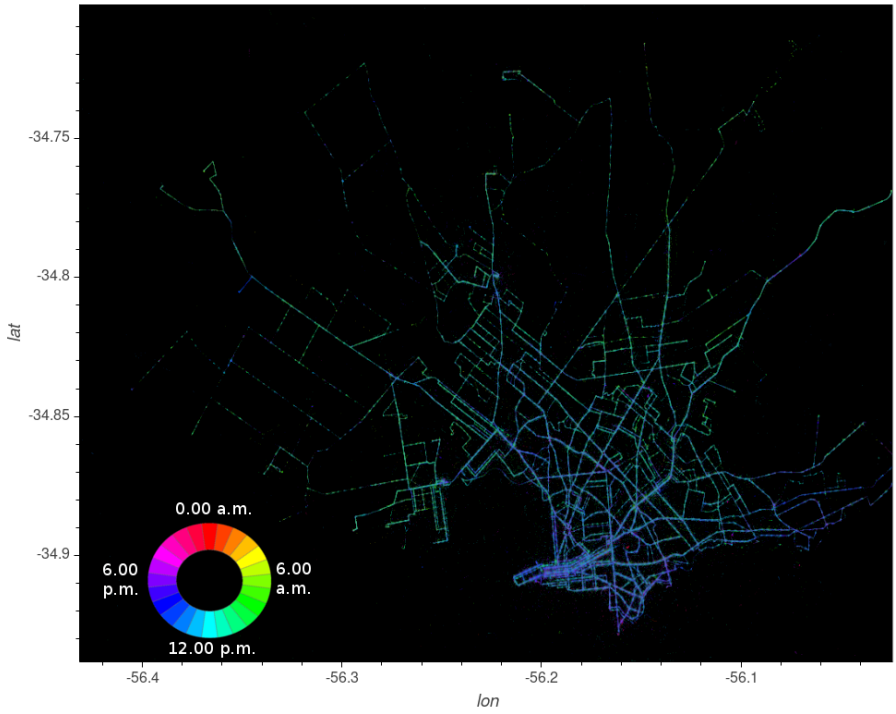

Fig. 5. Spatiotemporal distribution of trips in Montevideo during May 2015

4 Case studies: unexpected events and safety

This section outlines a series of case studies of uses of urban data analysis to detect special events and safety hazards within the public transportation system.

4.1 Anomaly detection in the spatial dimension

Geolocation data of sales transactions can be used to detect abnormal situations in the transportation system. As an example, Figure 6 shows a heatmap of transactions, along with the streets (in gray) and the bus lines (in blue). Two clusters of sales records (labeled A and B) appear in a street where no bus routes run. This represents a detour of one or more bus lines from their predefined routes. This may be due to an exceptional circumstance (e.g., road works) or due to a periodic event occurring certain days of the week (e.g., a flea market). Authorities can take advantage of this type of analysis to identify anomalies and make appropriate changes to bus routes and schedules.

4.2 Anomaly detection in the time dimension

The time stamp of sales can be used to identify abnormal use patterns in the transportation system. Figure 7 shows an aggregated visualization of combined

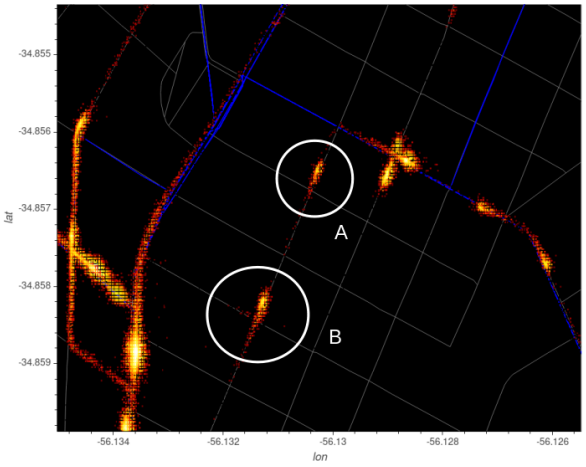

Fig. 6. Anomaly detection: example of detour. The blue lines represent bus routes. A and B are two clusters of transactions which occurred outside of the bus network.

spatial and temporal information of smart card transactions data. A small cluster of pixels in red can be observed in the map (indicated with a circle), which correspond to a group of sales occurring approximately at midnight. This pattern significantly differs from the rest of the dataset. Given the location of these records, near an outdoor venue, the transactions probably correspond to a special event (e.g., a concert) taking place at night in this venue. In these occasions, bus companies usually assign buses to allow citizens to return to their homes at the end of the event. Authorities can use urban data analysis to identify special events taking place in the city and implement strategies that improve the mobility of those attending these events.

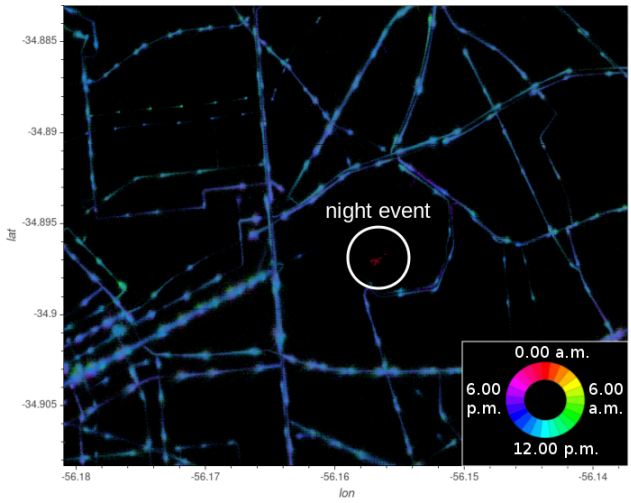

Fig. 7. Anomaly detection: example of event at midnight near an outdoor venue.

4.3 Driving behavior and safety

Another interesting use for information is to analyze the spatial distribution of sales. Figure 8 shows a heatmap of transactions occurring in one-way streets. Arrows indicate the direction of each street and bus stops are represented using blue circles. The visualization shows that the spatial distribution of sales is skewed with respect to the location of the bus stops: more transactions occur after the location of the bus stop than before. This uneven distribution is probably caused by drivers moving the bus before all the boarding passengers validate their smart cards. This might represent a safety issue, since passengers are standing while validating their cards.

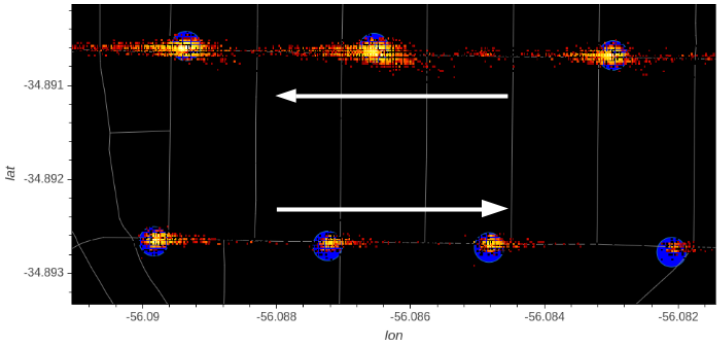

Fig. 8. Spatial distribution of transactions with regards to stop location: one-way streets

Figure 9 shows a heatmap of transactions near a roundabout, where a large number of transactions take place within the roundabout. Again, passengers are standing and validating their smart cards while the bus is moving. In fact, this might represent an even more serious issue, when drivers are also in charge of operating the smart card terminal. Driving and selling tickets at the same time is a risky behavior, frequently seen among bus drivers in Montevideo. The studied data provide evidences that support these observations. Authorities can use this type of data analysis to audit driving behavior, improving the safety of passengers and drivers of the transportation system.

5 Conclusions and future work

Under the paradigm of smart cities, ITS have emerged to take advantage of information and communication technologies to improve public transportation. ITS allow collecting massive amounts of urban data, which can be used to extract meaningful information to help decision making in cities. This article studied data from the ITS in Montevideo, Uruguay, to characterize mobility in the city.

The results reported in this article account for more than 20.4 million bus tickets sold using smart cards. During a data cleansing process, 1.53% of the records were filtered due to inconsistencies. Several insights were obtained through data analysis of the studied dataset, including: number of passengers traveling

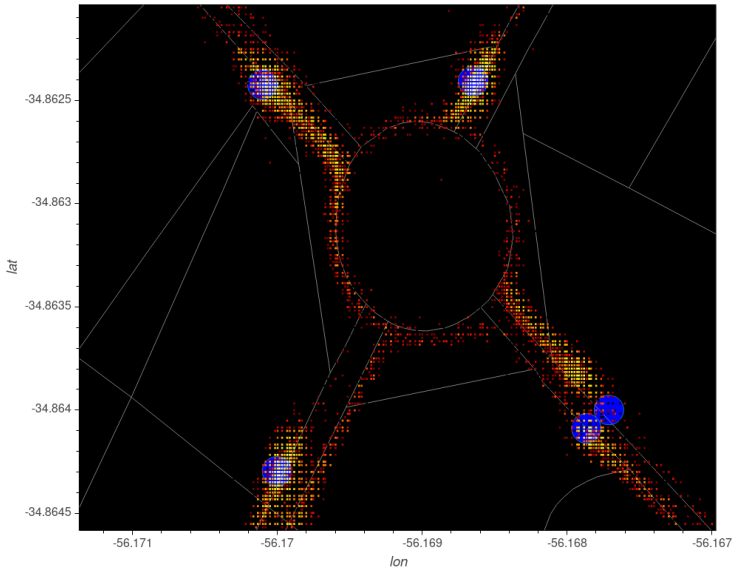

Fig. 9. Spatial distribution of transactions with regards to stop location: roundabout

with the same smart card, frequency of use of the smart cards, number of bus transfers, number of transactions per bus trip, and most used bus lines and stops. A spatiotemporal analysis was also performed which revealed that citizens from areas farther away from the coastline start trips earlier than those near the coast.

Finally, some practical case studies on the use of data analysis on ITS data were presented, including: anomaly detection in space (to identify bus detours), anomaly detection in time (to identify events in the city), and a characterization of potential safety hazards due to reckless driving. Such analysis are useful for characterizing different aspects of mobility in smart cities [10, 12].

The work reported in this article constitutes one of the first steps towards using data from the ITS in Montevideo to understand mobility in the city. As such, many lines of research remain to be explored in order to extract more and richer information that can be used to improve the public transportation system.

The data analysis reported in this article mainly focused in understanding the interaction between passengers and the transportation system. However, the available data sources offer the potential to study other very interesting aspects of mobility in the city. For instance, location data from AVL systems could be used to further study the QoS offered to citizens by the transportation system in terms of punctuality, frequency of lines, and load of passengers with regards to the bus capacity. Additionally, speed information of buses could be used to characterize the streets of the city and identify bottlenecks. This information could be used as input when designing new lines or re-designing existing ones.

Finally, it is worth noting that this work used ITS data from 2015. Since that year, the use of smart cards to pay for tickets has risen significantly. The proposed approach should be applied to recent ITS data when it becomes available publicly.

References

1. Abreu, P., Vespa, J.: Plan de Movilidad. Online: http://www.montevideo.gub.uy/sites/default/files/plan_de_movilidad.pdf (2018-12-30) (2010)
2. Bagchi, M., White, P.: The potential of public transport smart card data. Transport Policy **12**(5), 464–474 (2005)
3. Benevolo, C., Dameri, R.P., D'Auria, B.: Smart mobility in smart city. In: Torre, T., Braccini, A.M., Spinelli, R. (eds.) Empowering Organizations. pp. 13–28. Springer International Publishing (2016)
4. Blythe, P.: Improving public transport ticketing through smart cards. In: Proceedings of the Institution of Civil Engineers-Municipal Engineer. vol. 157, pp. 47–54 (2004)
5. Boyle, D.K.: Passenger counting systems. Transportation Research Board (2008)
6. Deakin, M., Waer, H.A.: From intelligent to smart cities. Intelligent Buildings International **3**(3), 140–152 (2011)
7. Figueiredo, L., Jesus, I., Tenreiro, J., Ferreira, J., Martins, J.: Towards the development of intelligent transportation systems. In: IEEE Intelligent Transportation Systems. pp. 1206–1211 (2001)
8. Furth, P., Hemily, B., Muller, T., Strathman, J.: Using archived AVL-APC data to improve transit performance and management. Tech. Rep. 113, Transit Cooperative Research program-Transportation Research Board (2006)
9. Grava, S.: Urban Transportation Systems. McGraw-Hill Professional Publishing (2000)
10. Hipogrosso, S., Nesmachnow, S.: Sustainable mobility in the public transportation of Montevideo, Uruguay. In: II Iberoamerican Congress on Smart Cities (2019)
11. Judd, C., McClelland, G., Ryan, C.: Data analysis: A model comparison approach. Routledge (2011)
12. Nesmachnow, S., Bana, S., Massobrio, R.: A distributed platform for big data analysis in smart cities: combining Intelligent Transportation Systems and socioeconomic data for Montevideo, Uruguay. EAI Endorsed Transactions on Smart Cities **2**(5), 1–18 (2017)
13. Rahm, E., Do, H.H.: Data cleaning: Problems and current approaches. IEEE Data Engineering Bulletin **23**, 3–13 (2000)
14. Servicio de Geomtica - Intendencia de Montevideo: Lneas de Transporte (2012), [Data file] Online: http://geoweb.montevideo.gub.uy/geonetwork/srv/es/metadata.show?uuid=307ffef2-7ba3-4935-815b-caa7057226ce (2018-12-30)
15. Tukey, J.: Exploratory Data Analysis. Addison-Wesley Publishing Company (1977)
16. Utsunomiya, M., Attanucci, J., Wilson, N.: Potential uses of transit smart card registration and transaction data to improve transit planning. Transportation Research Record: Journal of the Transportation Research Board **1971**, 119–126 (2006)
17. Zhao, Y.: Vehicle location and navigation systems. Artech House Publishers (1997)
18. Zheng, X., Chen, W., Wang, P., Shen, D., Chen, S., Wang, X., Zhang, Q., Yang, L.: Big data for social transportation. IEEE Transactions on Intelligent Transportation Systems **17**(3), 620–630 (2016)

Development of a Wireless Sensors Network using IoT for Monitoring Fervença River's Water Quality

João V. Peroni[1,2,3], Estefânia Gonçalves[1], Ivone Fachada[1], Thadeu Brito[2], Vicente Leite[2], Ana I. Pereira[1,2], José Lima[2,4]

[1] Centro Ciência Viva de Bragança, R. Beato Nicolao Dinís 35, 5300-252 Bragança, Portugal.
{jalmeida, ifachada, egoncalves}@braganca.cienciaviva.pt
[2] Research Centre in Digitalization and Intelligent Robotics, Instituto Politécnico de Bragança, Bragança, Portugal.
{brito, avtl, apereira,jllima}@ipb.pt
[3] Universidade Tecnológica Federal do Paraná, Av. Monteiro Lobato, s/n - Jardim Carvalho, Ponta Grossa - PR, 84016-210, Brasil.
[4] Instituto de Engenharia de Sistemas e Computadores, Tecnologia e Ciência, R. Dr. Roberto Frias, Porto, Portugal.

Abstract. This work presents the development of a Wireless Sensors Network (WSN) based on the Internet of Things (IoT) technology, in order to monitor Fervença River's water on physical and chemical parameters, to evaluate anthropogenic effects in its quality. The WSN is located in the city of Bragança, Portugal, and consists of four measurement points to cover all the extension of the river, from the spring to the mouth. The sensors will communicate with a gateway and store the collected data in a cloud server using LoRaWAN technology, which has the possibility of establishing long-range communications, low energy consumption and low vulnerability to interferences. In these locations, the physical and chemical parameters of the water will be measured, namely pH, temperature, electrical conductivity and dissolved oxygen. Together with the data coming from a macroinvertebrate's analysis done regularly by the Bragança Ciência Viva Science Center, it is expected to compare the obtained values with the ones presented by the Portuguese Legislation, which establishes the optimal levels for aquaculture life support, assessing whether the river water presents an acceptable quality environment for biodiversity, and promoting actions in the society to improve the quality of the river's water. The collected data will be also available for the visitors of Silk House of Bragança Ciência Viva Science Center in the form of an interactive exhibit, being an instrument for science dissemination and environmental education.

Keywords: Internet of Things, Wireless Sensors Network, Monitoring System, Water Quality, Science Dissemination.

1 Introduction

Assuring good river water's quality is of utmost importance to maintain the biodiversity and ecologic quality of the system. In rivers that cross urban environments or small communities, it is possible to observe the anthropogenic effects in the water quality [1].

Fervença River is a border affluent of river Sabor, has its spring located in the Fontes Barrosas village and crosses the Bragança city, being one of the main hydric resources for farming activities in the small communities of the region. It is also an extensive source of biodiversity in its waters and the riverside, inside and outside of the city's territory [2].

The health of the ecosystem in the region is strongly influenced by the quality of Fervença River's water, since it is inhabited by several species of aquatic life and establishes the necessary conditions for terrestrial and semiaquatic life maintenance, thus it is crucial for monitoring and treating its waters in order to avoid the negative effects of human activities. In Fig. 1 is demonstrated the current state of Fervença River next to Quinta dos Figueiredos, where it is possible to see the growing foam. The foam can be an indicative of increased phosphorus levels in the water, caused by the use of fertilizers and municipal and industrial wastewater [1], hence the necessity of monitoring the river's water parameters with the aim of improving its quality.

Fig. 1. Fervença River next to Quinta dos Figueiredos [2].

The river monitoring system relevance is enhanced by the fact that Fervença River flows into the Sabor river, one of the most tributaries of the Douro River in Portugal. The Douro river is one of the most important rivers of the Iberian Peninsula, being of high importance to measure the parameters to account the effects of human activities in the Douro basin.

Parallel to the proposed real time physicochemical parameters measurement to infer the anthropogenic effects in the river's water, it is recommended to monitor the concentration of nutrients (nitrogen and oxygen), which tends to raise due to the domestic and agriculture effluents poured into the river. It is also common to analyze the existence of benthic macroinvertebrates since these are sensitive species and are excellent indicators of pollution levels [2].

In Portugal there is specific legislation that defines the parameter levels to identify the good river water quality vary according to its destination, that can be for human consumption, farming, seaside, or water that supports aquatic life, being the latter the case of Fervença River [3].

Fervença river crosses several villages in Trás-os-Montes region, and it is difficult to manually collect water in different points, simultaneously. The WSN with low power consumption and long range communication it is capable of providing real time information which will be extracted from different points of the river. The use of most recent and innovative technologies in IoT is an essential aspect of this project, enabling easy communication and interaction within the WSN for its use in Smart Cities [4].

A Smart City is a new concept where urban environments are experienced with new communication technologies for urban management aiming social and environmental improvements. "*IoTs are designed to support the Smart City vision, which aims at exploiting the most advanced communication technologies to support added-value services for the administration of the city and for the citizens*" [4]. In this context, WSNs are major assets on data acquisition in real time, with several low-powered sensors located in the region to collect data [4].

The system presented in this paper has the objective of developing a WSN with the goal of monitoring the physical and chemical parameters of Fervença River in different locations, using the IoT technologies to allow real time data collection with low cost and low energy consumption, being a complement of existing projects that are being developed for better usage of available natural resources.

The Fervença River monitoring system is made under the *SilkHouse* [5] and *Natureza Virtual* projects, which have the objective of restructuring the Silk House with new interactive modules for the interpretation of natural values, which analyze the region's resources and transform them into museological points of interest, promoting valorization and efficient management of the hydric resources, increasing the scientific and cultural resources available in the museum.

The project is being developed for the permanent exhibition of the Silk House - Bragança Ciência Viva Science Center (Fig. 2) an interactive science museum located in Bragança, Portugal, which has the mission of promoting science education and knowledge in a dynamic and interesting way for people of all ages [6]. The data collected will also be available for the local authorities and visitors through a web application, in order to have a bigger impact on the population awareness on the importance of improving environmental quality.

Fig. 2. Fervença River, in front of the Silk House – Bragança Ciência Viva Science Center. July 15, 2019.

With this work it is expected to better analyze the consequences of human activities in the quality of the waters of Fervença River, provide reliable data to research development in the field, promote environmental awareness to the residents and Bragança Ciência Viva Science Center visitors, and support actions from the competent authorities in improving the hydric resource quality and consequently the well-being of the environment and the population. The aesthetic factor is also relevant in the expected results of the system, since improving the river water quality will also value the real estate business in the region, attracting more people to live close to the river and the city's historic center.

This paper is organized as follows: The first Section presents an introduction of the study development. The Section 2 describes the proposed river monitoring system characterization, with the definition of the parameters that will be measured in order to get information about the river quality, and the definition of the locations where the measurements will take place for the system to cover all of the extension of the river, from the spring to the mouth. The Section 3 presents the implementation of the river monitoring system describing the expected results and the main difficulties of the proposed system. The last section presents the conclusions and future approaches.

2 River Monitoring System Characterization

The development of the system starts with the definition of the parameters to be measured, the level of information that can be extracted from the data collected, and also the data collection intervals defined.

Once the parameters and intervals were defined, the measurement locations were determined in order to allow a comparison of the human activities in the river water's

quality. After defining the locations where the measurements will take place, the technology that best fits the project was chosen in order build the system with the highest efficiency, reliability and lowest cost possible.

2.1 Definition of the Parameters

To analyze the quality of the available water resources in the Fervença River, four physicochemical parameters were defined to be measured to obtain information about the anthropogenic effects in its surroundings.

To define the river's water quality, the most commonly used methodology is to measure the water's parameters in seasonal campaigns with a given interval (monthly or trimester) [7]. Since the proposed system has the objective of real time data acquisition, a time interval of 1-hour has been defined between each measurement. The expectations are that parameters will not vary significantly between two consecutive measurements. In the proposed river monitoring system four parameters are measured, namely temperature, pH, electrical conductivity and dissolved oxygen.

Temperature. The water temperature, measured in ºC, has average values in the range between 0ºC and 30ºC, presenting seasonal variations. An increase in the average river water temperature may indicate industrial discharges and other changes in the water system [9]. According to the Portuguese Legislation the temperature measured in the downstream should not exceed 1,5ºC (salmon water)/3ºC (cyprinid water) of the natural river temperature, and thermic discharges should not exceed 28ºC [3].

The annual temperature variation might be responsible for the geographic variation and the presence/absence of benthic macroinvertebrates and is an important factor in the physical and biotic characteristics of rivers [9].

In higher temperatures, the river's capacity of metabolizing organic products without reducing the oxygen concentration is reduced and is also responsible for raising the speed in which nutrients in dissolved solids, like phosphorus, are converted in readily available sources. This implicates on the river water's eutrophication since the algae and phytoplankton will find more available nutrients that will allow them to grow, thus increasing the oxygen consumption rates, raising the organic matter and lowering the dissolved oxygen concentration in the water [9]. For these quoted effects of temperature in a river's water, it is important to measure it in regular intervals.

pH. The pH values demonstrate how acid or alkaline the water is, being a variable that "influences the aquatic ecosystems by affecting the physiology of several species" [8]. According to the legislation, the maximum pH levels of the river water should be between 6 and 9.

Electrical Conductivity. The maximum/minimum electrical conductivity levels are not explicitly defined by the Portuguese Legislation, but this parameter can be a secondary indicator of total suspended solids, which should be a maximum of 25 mg/l [3]. The more suspended solids, the easier it is for the water to conduct electricity, and the

electrical conductivity is high. High levels of suspended solids will reduce the solar light penetration capacity, affecting the benthic macroinvertebrates [9]. Electrical conductivity is measured in $\mu S/cm^2$, and values that are above 100 $\mu S/cm^2$ may indicate the presence of polluting agents in the environment [2]. To have better information about the pollution levels in the river's water, this parameter should be observed in regular intervals.

Dissolved Oxygen. Oxygen is essential for guaranteeing the life of aerobic beings, and the reduction of the dissolved oxygen levels have a negative impact on the ecosystem and on the biodiversity of the aquatic environment [2]. The dissolved oxygen in the water is also correlated to the nitrogen levels. When in low concentration, the oxygen causes an inhibition in the nitrification process, allowing nitrogen to be accumulated on the environment [8]. According to the legislation, the maximum admitted values for dissolved oxygen should be between 50% and 100% mg/l O_2 [3]. Thus this parameter should be measured together with the ones quoted previously in order to evaluate the biodiversity capacity of the river's water.

2.2 Definition of the Locations

It is known that for large rivers, distances about 10 km is enough to detect variations in the water quality parameters [9]. Since the data collected has the main objective of correlating the anthropogenic effects on the river water, it was defined four measurement points with distances that differ 3 to 10 km from each other, in which all the parameters will be measured in the time defined on Section 2.1, to compare the same characteristics in different locations with different levels of human interaction with the river.

The locations in which the measurements will take place are defined as shown by Fig. 3 and the motivations for the choices are explained below.

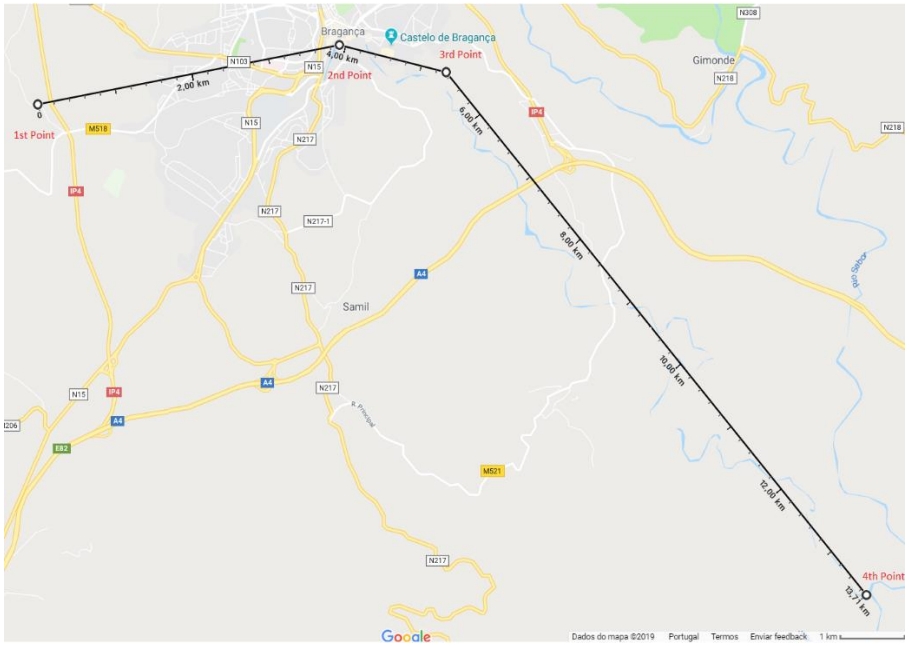

Fig. 3. Defined locations for data acquisition [10].

1st Point: In the River's Source. The first measurement point will be next to the river's source, where it will have little contact with human activities. On this point, the water parameters are expected to be the closest to the ideal levels and will be the comparative point where the water quality should present its best state. If the measurements show otherwise, it is possible to create an alert for the river's spring quality.

2nd Point: In the Bragança Polis Park. The measuring point located inside the Silk House of the Bragança Ciência Viva Science Center, in the Bragança Polis Park, plays a strategical part in the science dissemination purpose of the project, being visible to the visitors who can learn about the system and the technology used in the development. It is also located in the middle of the city and close to the historic center, where the contact with human activities is most observed.

3rd Point: After the Wastewater Treatment Facility. Bragança has a wastewater treatment facility called ETAR, and it plays a crucial part in keeping the water parameters in acceptable levels. Measuring the parameters after the facility is important to compare the values of the water before and after the quality assurance processes, and also to ensure that the water is being treated properly.

4th Point: In the Mouth of the River. It is necessary to measure the water parameters in the downstream of the river to evaluate the quality of the water that will flow into

the Sabor river and then the Douro river, measuring the human activities effects on the region's river basin.

2.3 Definition of the WSN Communication Technology

The Fervença River has a considerable size and has some of its extension located in areas of thorny access. With these characteristics, a regular communication network will be difficult to install and perform maintenance due to the need for long cabling in geographically uneven areas. Therefore, a WSN is the best technology choice for this case.

The WSN consists of several sensors measuring the parameters and sending the collected data, in real time, to a cloud storage server through a gateway. The sensors are located in open areas, the distance from the sensors to the gateway is in the order of kilometers. With these characteristics, the optimal communication network is a Low Power Wide Area Network (LPWAN), which offers "*low power consumption, low transceiver chip cost and large coverage areas*" [11].

Smart Cities are complex ecosystems with intensive use of information and communication technology, and several efforts have been made to integrate IoT with smart city environments. Several protocols are being used to transport data between devices and back-end servers, some specialized in low coverage and higher transmission rates such as ZigBee, Bluetooth, IEEE 802.11p, and some specialized in high coverage and interoperability, such as LoRaWAN [12].

The chosen LPWAN technology for this application was LoRaWAN, for the lower transceiver market prices and easier connectivity in higher distances [13], allied to the low energy consumption. The logical topology of the system is the star topology, illustrated by Fig. 4, where the sensors communicate to the gateway, and the gateway is responsible for collecting and sending the data to the cloud storage system, where the visual application will access and show it to the Silk House visitors.

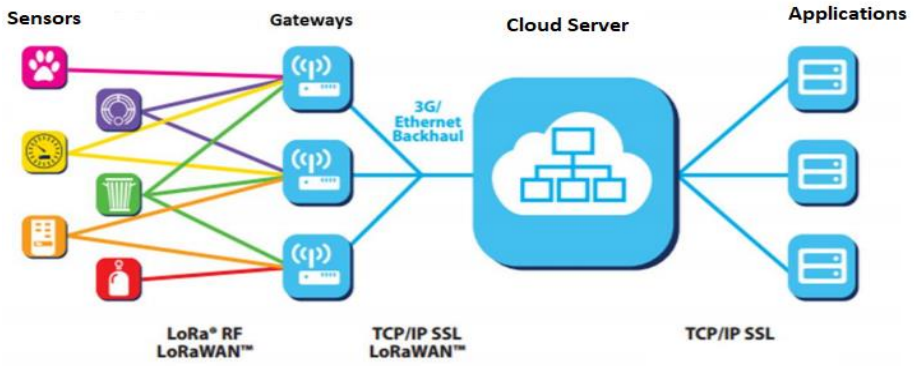

Fig. 4. LoRaWAN Logical Topology [13].

Since the collected data is made of bytes of information collected in 1-hour intervals, the low data transmission rate (maximum of 50kbps) of LoRa technology is adequate for this application [14].

LoRa technology uses a Chirp-Spread-Spectrum (CSS) modulation and operates in non-licensed ISM bands (868MHz in Europe). LoRaWAN has encouraging results in recent projects and ensures a network coverage in problematic areas if multiple gateways are used. The topography and building density also play significant roles in signal propagation, in particular when used in closed spaces [15].

Low power consumption is one of the most important features of LoRaWAN protocol, since the sensor nodes will be located in locations of large distance from each other, making the maintenance of the system more difficult. Therefore, having a sensor that will work for several months using a single power source allows easier implementation and lowers the maintenance efforts.

The LoRa technology has as targets projects where the end devices need low power consumption (battery-powered), higher transmission rate is not needed, and the end nodes are located in a long distance from each other. LoRa is commonly used in smart sensors technologies in health monitoring, smart metering, industrial applications and environmental monitoring [16], and for those reasons LoRa was the chosen technology for this system.

Recent studies indicate that LoRaWAN has shown a good performance in Smart Cities applications. In fact, LoRaWAN is an open source protocol that allows interoperability between a range of devices, also due to its simplicity of use, the possibility of scalability, high range, low energy consumption and the security of information. Smart Cities applications, water monitoring, waste collection and transportation technology are usually made using battery powered sensors which transmit low amount of data, and LoRaWAN was developed to meet these requirements [17].

3 River Monitoring System Implementation

The system's main objectives are science dissemination, environmental education concerning water quality and collecting data that will support decision making in improving the Fervença River's water quality, as well as being part of an interconnected city with information stored in cloud servers for anyone to have access to, using state of the art technology to improve the well-being of the citizens and the environment.

The parameters measured by the sensors will be displayed as part of the Silk House main interactive exhibition and will be available for all the visitors of the museum, being an instrument for environmental education. The innovative IoT technology LoRa is strategically chosen to increase the population's contact with new knowledge and state of the art approaches for device communication.

One of the four measuring points will be located inside the Silk House in order to be visible to the visitors and together with an explanatory overview of the system, aim to stimulate the curiosity about science and technology, being part of a science dissemination structure.

The observed river's water parameters are expected to be analyzed together with the competent authorities in order to create coordinated action plans with the objectives of improving the water quality, with expected results of supporting en1vironmental balance, social well-being for the citizens of Bragança and tourists, and ensuring that the river basin of Fervença has a good quality water source.

The data will be shown in the form of time graphs, with the parameters and period set separately, exemplified in Fig. 5. The data will be presented together with a 3D modelling of the devices, to give the viewers a more immersive experience about the technology used in the system.

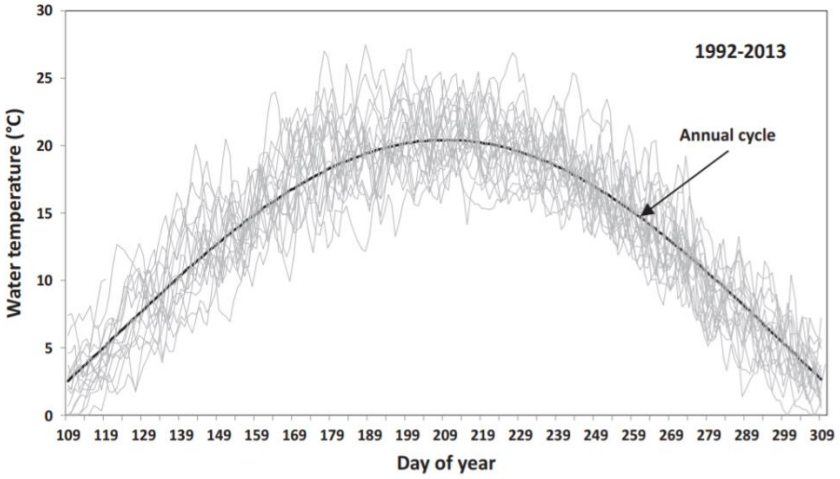

Fig. 5. Example of data visualization in web application [18].

Fig. 5 also illustrates that river parameters monitoring is usually made in a high sampling period (years or decades) in order to observe changes in the mean values and correlate to external factors. A web-based real-time monitoring will be a great asset in collecting more samples and reducing efforts to do so in the same time period.

Since the sensors will be located in the open space, in the middle of the river, one of the greater challenges of the implementation will be to deal with vandalism and theft, therefore the sensors used in the development of this work should have the lowest cost possible in order to assure the possibility of replacing lost pieces of the sensor modules if needed.

3.1 Communication Technology Prototypes

In order to evaluate the choice of communication technology, a prototype system was built using as gateway a Raspberry Pi 3B with a LoRa Shield connected to the network by an Ethernet cable, Fig. 6 illustrates the gateway prototype. To send data to the gateway prototype, two communication modules with the DHT11 sensor were designed. This sensor measures air humidity and temperature.

Fig. 6. Gateway prototype. August 22, 2019.

In the first sensor module, the data collected by the sensor will be transmitted using the RFM95W LoRa transceiver, illustrated in Fig. 7, connected to an Arduino UNO. "*The RFM95W 868MHz transceivers feature the long-range LoRa™ modem that offers ultra-long range spread spectrum communication and high interference immunity while minimizing current draw*" [19]. The wiring diagram used in the development of the first module is illustrated by Fig. 8.

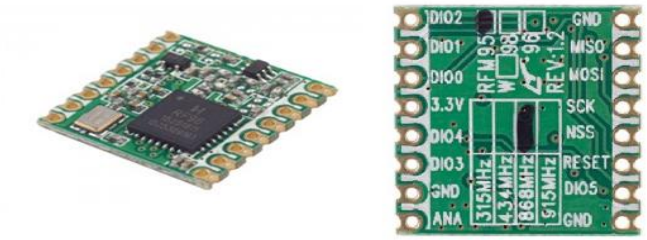

Fig. 7. LoRa transceiver RFM95 [19].

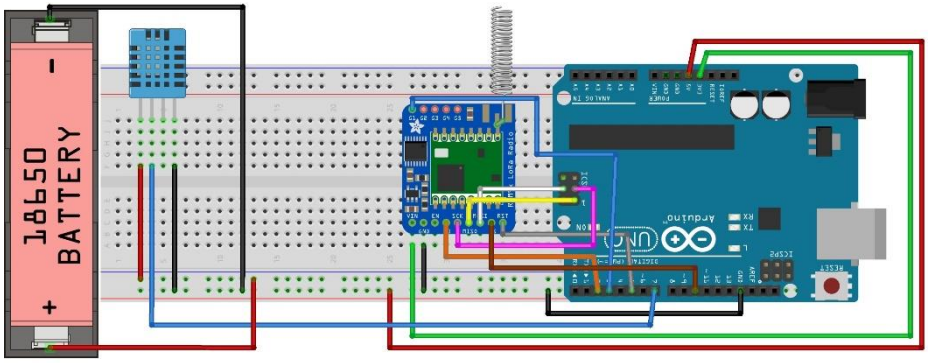

Fig. 8. Wiring diagram of test module nº 1. August 25, 2019.

In the second sensor module, the same DHT11 sensor was used, but connected to an Arduino MKR 1300, which already have embedded LoRa technology. The wiring diagram for the second sensor module is illustrated by Fig. 9.

Both test modules were configured to send the collected data in every 30 seconds. Test module nº 1 was configured to communicate with port 1 and test module nº 2 was configured to communicate with port 0, in order to eliminate the possibility of signal interference between the two modules.

The test modules and the gateway were turned on and were distanced apart while the data send was checked regularly in the defined interval, in order to check the maximum distance that allowed the communication between modules and the gateway.

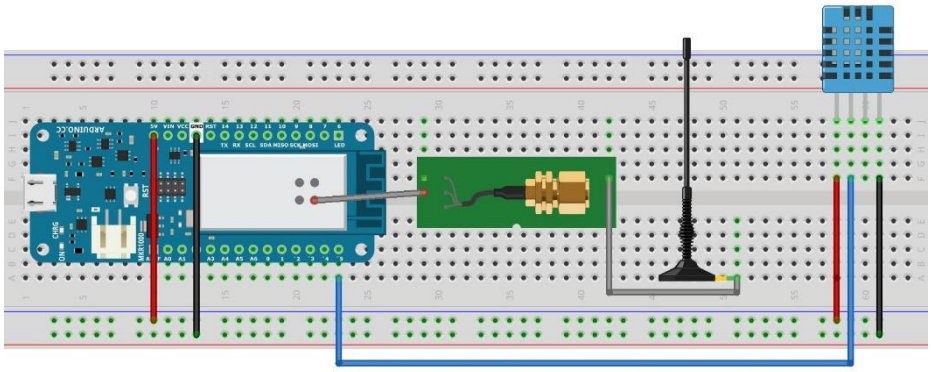

Fig. 9. Wiring Diagram of Test Module nº 2. August 25, 2019.

The two test modules communicated with the gateway and successfully sent the collected data to the server, as illustrated by Fig. 10. This test is considered only the region of the second point, defined in Section 2.2. Using a more powerful antenna with an outdoor LoRa gateway located in a higher, interference-free location, it is possible to provide a higher communication coverage area to cover the four measurement points defined in this project.

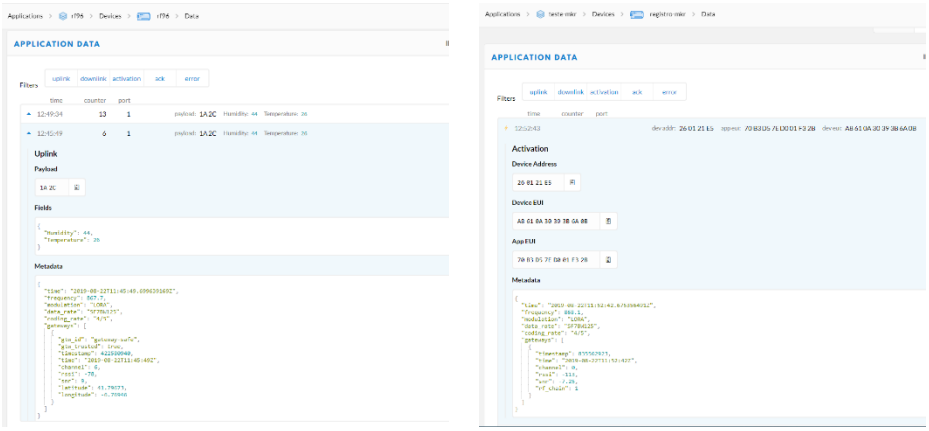

(a) Data sent by RF96. (b) Data sent by MKR1300.

Fig. 10. Communication results of test module nº 1 and nº 2. August 22, 2019.

4 Conclusions and Future Work

This paper presents the development of a WSN used for river water quality control and monitoring using IoT technologies for real-time communication and applied in environmental education, science dissemination and quality control of the aquatic ecosystem life support. The system was designed to be part of the interactive exhibit for the Silk House museum of the Bragança Ciência Viva Science Center, where the data collected in the different measurement points will be available for the visitors, together with an explanatory summary of the system and a sensor node.

The greatest challenge in implementing this system is dealing with vandalism and theft, since the sensor nodes will be located in open areas and remote locations, inside the river's water. The system is scalable, and other parameters can be measured in the future with the installation of different sensors, or other measurement points can be added to the system in order to have more information available to compare. This work will be integrated with the monitoring and control system of the SilkHouse Project [5]. It includes a smart microgrid integrating several measuremts such as power and energy flos.

The project was structured based on the need for collecting data on the Fervença River's water to improve its quality. The river has been previously restored in the

POLIS project, concluded in 2006 [20], but the means to demonstrate the efficiency of the POLIS project are still absent, and the developed river monitoring system is expected to be an asset to provide data and determine if the actions on the improvement of the water's quality are being efficient and well implemented.

Acknowledgements

This work has been supported and developed under the Natureza Virtual project, supported by the Fundação "la Caixa".

References

1. Conley, D., J., Paerl, H., W., Howarth, R., W., Boesch., D., F., et al. Controlling Eutrophication: Nitrogen and Phosphorus. Science. Vol. 323. (2009).
2. Rodrigues, V. C. R.: Rio Fervença: Efeitos da Perturbação no Ecossistema. Escola Superior Agrária, Instituto Politécnico de Bragança (2013).
3. Ministério do Ambiente. Decreto-Lei n.o 236/98. Diário da República - I SÉRIE-A, nº 176 (1998).
4. Zanella, A., Bui, N., Castellani, A., Vangelista, L., Zorzi, M. Internet of Things for Smart Cities. IEEE Internet of Things journal, Vol. 1, No. 1. (2014).
5. Maidana, W., Leite, V., Ferreira, A., Queijo, L., Et al. Design of a Self-sustainable System Based on Renewable Energy Sources for a Small Museum of Science Dissemination - the House of Silk. III Congresso Ibero-Americano de Empreendedorismo, Energia, Ambiente e Tecnologia. Portugal (2017).
6. Ciência Viva Homepage, https://www.cienciaviva.pt/centroscv/rede/regulamento.asp, last accessed in 2019/07/30
7. Abreu, C., H., M., Cunha, A., C., Water quality and trophic index in tropical riverine ecosystem under environmental impact. Eng. Sanit. Ambient. vol.22 no.1 Rio de Janeiro (2017).
8. Silva, A.E.P., Angelis, C. F., Machado, L. A. T. Influência da precipitação na qualidade da água do Rio Purus. Anais XIII Simpósio Brasileiro de Sensoriamento Remoto, Florianópolis, Brasil (2007).
9. Silveira, M. P. Aplicação do Biomonitoramento para Avaliação da Qualidade da Água em Rios. Centro Nacional de Pesquisa de Monitoramento e Avaliação de Impacto Ambiental, Empresa Brasileira de Pesquisa Agropecuária (2004).
10. Google Maps, https://www.google.pt/maps/@41.7747952,-6.7479757,13.21z, last accessed 2019/08/02.
11. Petäjäjärvi, J., Mikhaylov, K., Yasmin, R., Et al. Evaluation of LoRa LPWAN Technology for Indoor Remote Health and Wellbeing Monitoring. 10th International Symposium on Medical Information and Communication Technology (2016).
12. Mehmood, Y., Ahmad, F., Yaqoob, I., Adnane, A., Et al. Internet-of-Things-Based Smart Cities: Recent Advances and Challenges. IEEE Communications Magazine, (2017).
13. Teixeira, G., B., Almeida, J., V., P. Rede Lora® E Protocolo Lorawan® Aplicados Na Agricultura De Precisão No Brasil. Trabalho de Conclusão de Curso (Bacharelado em Engenharia Eletrônica) - Universidade Tecnológica Federal do Paraná. Ponta Grossa, (2017).
14. Adelantado, F., Vilajosana, X., Tuset-Peiro, P. Et.al. Understanding the Limits of LoRaWAN. IEEE Communications Magazine (2017).

15. Wixted, A. J., Kinnaird, P., Larijani, H., Et al. Evaluation of LoRa and LoRaWAN for Wireless Sensor Networks. 2016 IEEE Sensors (2017).
16. Augustin, A., Yi, J., Clausen, T. Townsley, W. M., A Study of LoRa: Long Range & Low Power Networks for the Internet of Things. Enabling the Move from Wireless Sensor Networks to Internet of Things and Cyber-Physical Systems (2016).
17. Loriot, M., Aljer, A., Shahrour, I., Analysis of the use of LoRaWan technology in a Large-Scale Smart City Demonstrator. Laboratory of Civil Engineering and geo-Environment, (2017).
18. Caissie, D., Thistle M., E., Benyahya, L., River temperature forecasting: case study for Little Southwest Miramichi River (New Brunswick, Canada). Journal des Sciences Hydrologiques, (2017).
19. Botnroll Homepage. https://www.botnroll.com/pt/rf-lora/2600-rfm95-m-dulo-lora-868mhz.html. Last accessec 2019/08/10.
20. Câmara Municipal de Bragança, https://www.cm-braganca.pt/pages/273, last accessed 2019/07/30.

Movilidad Urbana Sostenible: Microgrids de base hidráulica: Proyectos Sinfín Energy

José Luis Suarez Sierra[1,2,3]; Eva Martínez García[4]; Mar Alonso Martínez[5]; Higinio Rubio Arnaldo[6].

[1] CEO de Red Táctica y de Táctica Desarrollo Industrial S.L., C/Los Prados,166 (33.203), Gijón-Asturias; jlsuarez@tacticaindustrial.com

[2] Profesor del Área de Ingeniería de Construcción de la Universidad de Oviedo, Gijón-Asturias; suarezjose@uniovi.es

[3] Director Técnico de Sinfín Energy, C/Los Prados,166 (33.203), Gijón-Asturias; jlsuarez@sinfinenergy.com

[4] Investigadora del Área de Ingeniería de Construcción de la Universidad de Oviedo, Gijón-Asturias; emartinezg@uniovi.es

[5] Profesora del Área de Ingeniería de Construcción de la Universidad de Oviedo, Gijón-Asturias; mar@constru.uniovi.es

[6] Ingeniero de Proyectos en Táctica Desarrollo Industrial S.L., C/Los Prados,166 (33.203), Gijón-Asturias; hrubio@tacticaindustrial.com

Resumen

Durante las últimas décadas, la sociedad ha asumido el reto de hacer frente al problema medioambiental. El desarrollo de dispositivos generadores de energía renovable ha ido progresivamente en aumento, tanto en cantidad como en eficiencia, haciéndose más competitivos en el mercado, pero teniendo aún algunos obstáculos que afrontar.

Siguiendo la línea de los avances de aprovechamientos energéticos en entornos urbanos y la filosofía de "*Smart Microgrid*", basado en la producción distribuida, se desarrolla en el presente proyecto, un método de obtención energética basado en energía renovable de base hidráulico.

Derivado del extendido uso de energías de origen renovable y la integración de consumos que reduzcan la huella de carbono, surgen cada vez más vehículos de naturaleza eléctrica, cuya filosofía sólo quedará completa si la energía generada es de origen renovable. Integrado en este ámbito aparece el programa ESBH, cuyo objetivo es la implantación de un sistema de recarga para vehículos eléctricos, basado en energía microhidráulica. Se trata de la implantación de tecnologías que permitan generar energía utilizando los recursos naturales disponibles en cada ubicación.

Las tecnologías básicas de generación energética de este proyecto será el Tornillo de Arquímedes, turbina que aprovecha pequeños saltos naturales de agua; aunque actualmente se están desarrollando otro tipo de turbinas como la de flujo cruzado, para la explotación de bajos caudales y saltos más grandes; o las bombas que trabajan como turbinas (denominadas así por sus siglas en inglés PAT's), capaces de ser implementadas en zonas de alta presión (como, por ejemplo, instalaciones de roturas de presión o tuberías presurizadas).

Este trabajo pretende no sólo afrontar el reto de la implantación de energías renovables, sino posicionarlas como un elemento fundamental en la promoción de la movilidad urbana sostenible, a través de la creación de estaciones de recarga de vehículos eléctricos, alimentadas por fuentes de energía de base hidráulica, generadas y almacenadas en el mismo punto de recarga.

El despliegue de estas infraestructuras sostenibles potenciará la utilización del vehículo eléctrico, ya que no solo se garantiza el origen "verde" de la energía, sino que se podrá desarrollar una red de estaciones de recarga de alta potencia, que permitirá la utilización de sistemas de recarga "rápida" o incluso "ultrarrápida", independientes de las posibles fluctuaciones en la demanda de electricidad de la red nacional.

Keywords: Microrred, Turbinas, Energía Renovable, Tornillo de Arquímedes, Eficiencia, Movilidad Sostenible.

Introducción

Las últimas décadas de crecimiento global han determinado que el desarrollo económico de un país o región se encuentra estrechamente ligado con su consumo energético. Para afrontar las necesidades energéticas actuales en una sociedad altamente digital y concentrada en ciudades con cada vez mayor densidad, se hace imprescindible el planteamiento de una red de abastecimiento fiable, que sea capaz de proveer, con suficiente potencia, las diferentes demandas tanto urbanas como suburbanas.

Ante el progresivo cierre de las grandes instalaciones de generación eléctrica que hacen uso de combustibles fósiles, y la dificultad de implementar grandes estaciones de generación de base renovable, se plantea un nuevo paradigma energético, basado en que la generación y su consumo se deberían situar en el mismo lugar, permitiendo crear sistemas más sencillos, sostenibles y eficientes.

Este tipo de redes inteligentes serán capaces de integrar sistema de producción a tamaño micro o pico (potencias por debajo de 1 MW), ya sean pequeños saltos de agua, zonas de alta irradiación solar, derivaciones térmicas procedentes de calefacción o refrigeración urbana centralizados, etc. Queda evidenciada, de esta manera, la necesidad de implantar sistemas de almacenamiento, tan diversos y sostenibles como los sistemas de producción energética.

La infraestructura asociada a la construcción de este tipo de sistemas se apoya en la interoperabilidad de los propios sistemas. Esta integración hace posible una capacidad de respuesta a la demanda de abastecimiento, una comunicación entre distintos puntos de la red o micro-red para compensación de carga y demanda, una integración puntual de distintos sistemas de producción renovable, capacidad de almacenamiento para mejora de la eficiencia del sistema y una interoperabilidad y seguridad de infraestructura (véase figura 1), que convierte esta metodología en una de las óptimas para un desarrollo global equilibrado.

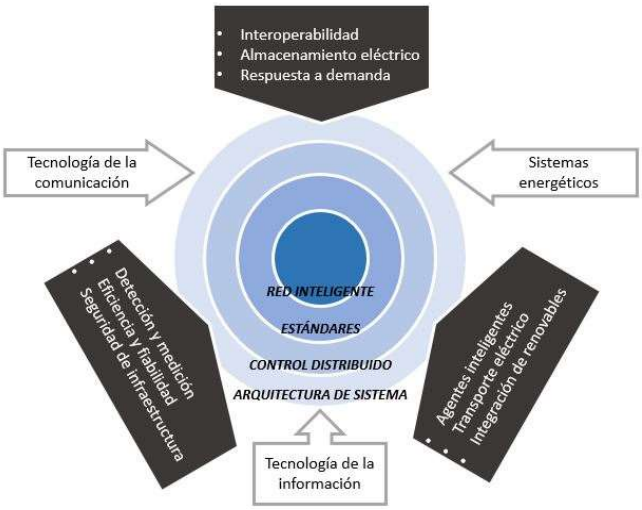

Fig. 1. Esquema básico de los medios que constituyen una smartgrid.

Derivada de la idea de creación de redes inteligentes de abastecimiento, aparece una jerarquía de implementación de subsistemas. Esta pirámide (figura 2), definida por BC-Hydro, categoriza una serie de posibles aplicaciones de redes inteligentes a corto y medio plazo, según su utilidad para el sistema global o para el cliente final. El presente proyecto intenta hacer realidad algunas de las posibles aplicaciones aunándolas en un mismo sistema de funcionamiento.

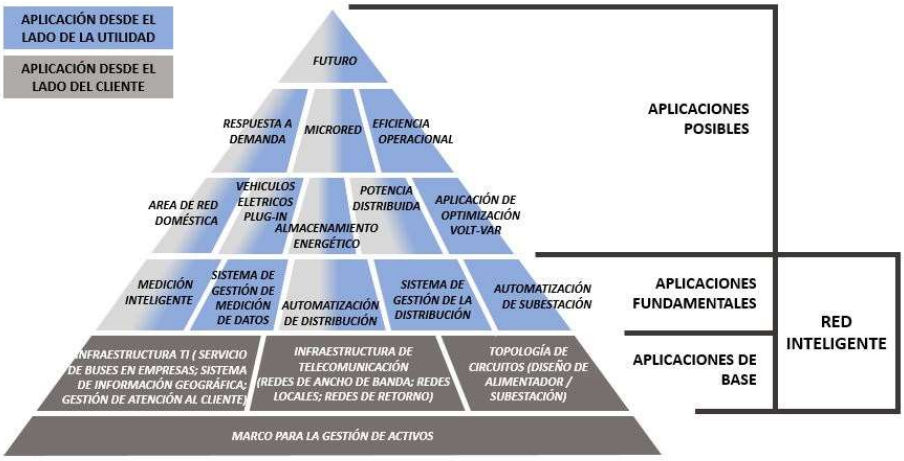

Fig. 2. Piramide jerarquizada de los subsistemas y elementos de una smartgrid.

La potencia hidráulica de pequeños saltos es históricamente conocida como un recurso de generación renovable capaz de crear energía sin necesidad de embalsar o retener agua mediante una presa. Esta tecnología emplea habitualmente cursos naturales o ríos con saltos de hasta aproximadamente 6 metros de altura para producir energía.

Los requisitos técnicos y de calidad incrementan habitualmente cuando las turbinas aumentan de tamaño. Las máquinas de reacción destinadas a pequeños saltos, suelen ser:

- Ruedas hidráulicas tradicionales
- Rodetes (Kaplan, Francis,…)
- Tornillos de Arquímedes (PAT's)

Se ha podido comprobar, en estudios realizados, que los dispositivos para pico generación (con rangos comunes de 300W hasta 5 kW) y micro generación (5-100 kW), disponen de un gran número de localizaciones donde pueden ser implantadas con diferentes objetivos: formando parte de un sistema conectado independiente facilitando energía para aplicaciones específicas (red en isla), o dando servicio a pequeñas comunidades a través de generación distribuida.

Desde el punto de vista mecánico, existen tres variables que controlan el proceso de cálculo y eficiencia para este tipo de sistemas, encontrándose relacionadas a través de la ecuación de Bernoulli:

- P: presión generada

- H: altura de presión existente/ aprovechable
- V: velocidad del agua a través del sistema

En la tabla 1, se recogen las ecuaciones de las presiones estática y dinámica que interviene en este proceso.

Table 1. Tabla presiones influyentes en tecnologías de aprovechamiento de base hidráulica.

Ps (Presión estática)	Pd (Presión dinámica)
$\triangle P \mid \triangle zrg$ $\eta > 70\%$	$\frac{1}{2}r\triangle v^2$ $\eta < 40\%$

La presión (P) y altura (H) se corresponden con la presión estática, y han sido identificadas como las variables óptimas para un mecanismo de recurso hidráulico, obteniendo altos rendimientos (alrededor del 70% o superior), con respecto a las eficiencias que ofrecen las tecnologías hidráulicas de reacción, con rendimientos totales que oscilan en torno al 40%. En la figura 3 se recogen los tipos de turbinas hidráulicas existentes más habituales.

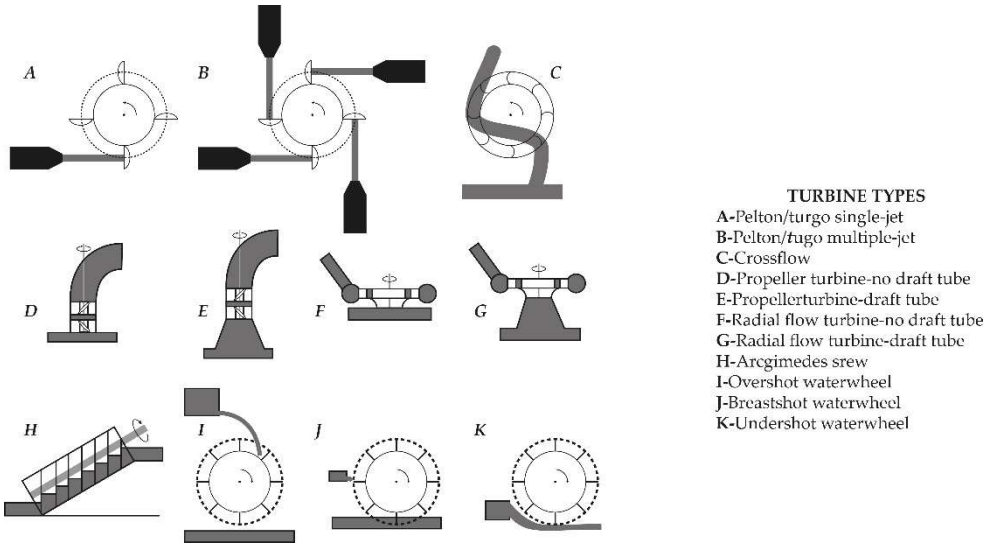

Fig. 3. Tipologías de turbinas hidráulicas.

La tecnología que se propone en el presente proyecto está basada no tanto en la impulsión como en la acción, obteniendo fuerzas mecánicas de torsión como consecuencia de la presión ejercida por el peso del agua sobre la turbina. Con un mínimo impacto sobre el medio ambiente, este tipo de turbinas tienen muy bajos costes de instalación y requieren de mínima obra civil para su instalación, pudiendo incluso aprovecharse áreas

ya construidas para fines similares, como salidas de aguas de refrigeración industriales, estaciones de tratamiento de aguas, antiguos molinos de agua, etc.

De esta manera, el uso de turbinas de pequeño salto, especialmente las de tipo tornillo de Arquímedes, permiten su aplicación en industria, extrayendo energía de pequeños cursos o efluentes de agua de diferente procedencia, en base a un reducido coste e implementación de escasa obra civil, y reduciendo así el periodo de amortización de la inversión.

Tornillo de Arquímedes

1. Análisis y diseño

El tornillo de Arquímedes es una de las máquinas más antiguas que se encuentra en uso en la actualidad. Este dispositivo atmosférico, que fue desarrollado para elevar el agua con propósitos de irrigación y drenaje, también se usa en la extracción de potencia hidráulica, como consecuencia de un proceso de ingeniería inversa.

El tornillo de Arquímedes funciona con el peso del agua que se desplaza a través del tornillo, haciéndolo girar y, mediante acoplamiento a un generador, produciendo electricidad. Sus dimensiones geométricas (diámetro y longitud del tornillo) dependen fuertemente de las características del salto de agua a turbinar (altura y caudal), y se encuentra afectado por el incremento de pendiente.

Una de sus principales ventajas es su bajo impacto ambiental. Debido a sus dimensiones y a la baja velocidad de rotación, la turbina en funcionamiento no dificulta el paso de peces (pudiendo etiquetarse bajo la tipología de “fishfriendly”), pudiendo descender de manera segura a través de los álabes del rotor. Las partes lubricadas del mecanismo, tampoco afectan a los ecosistemas implicados y la obra civil requiere escasos materiales y movimiento de tierras.

La variable principal de funcionamiento de la turbina es la altura de presión del agua, así que puede considerarse como una turbina de presión estática. El agua contenida entre los álabes de la turbina es la que hace que ésta se mueva, asemejando su funcionamiento al de los cangilones de un molino hidráulico. Teóricamente no existen pérdidas, y toda la energía potencial contenida en el caudal turbinado se extrae, se considera pues una máquina 100% eficiente.

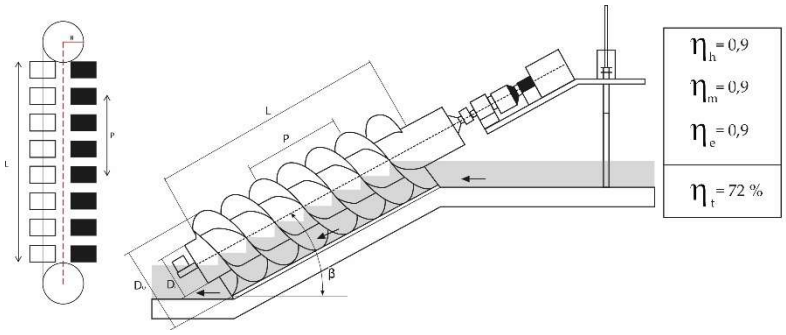

Fig.4. Características geométricas del Tornillo de Arquímedes.

En la realidad, las eficiencias mecánica, eléctrica e hidráulica se encuentran cerca del 90%, tal como se aprecia en la figura 4. Como resultado de los diferentes rendimientos, se obtiene una eficiencia total mayor del 70%.

A pesar de la compleja geometría de los álabes y de volumen de llenado de los "cangilones", el análisis y la simulación numérica realizados permiten simplificar la formulación de la eficiencia del tornillo. Se puede afirmar que el rendimiento se reduce por pérdidas volumétricas derivadas de fugas hidráulicas por la holgura entre los álabes y el canal.

2. Instalación

Una vez verificados el análisis y diseño de la máquina hidráulica, se procede con la obra civil y su instalación en la industria de Solvay (Cantabria). Esta implantación es la primera infraestructura de generación de este tipo, constitutiva del primer peldaño en la construcción de una microrred energética de base hidráulica destinada a la carga de vehículos eléctricos.

El cauce de agua aprovechado proviene de los efluentes de la planta de tratamiento de la industria de Solvay. Véase figura 5.

Fig. 5. Ejecución obra civil cauce Solvay.

La instalación ha sido acometida por la empresa SINFÍN ENERGY, y consiste en la instalación de dos tornillos de Arquímedes de 35 kW cada uno, 70 kW instalados en total, con un diámetro de 2.5 m entre puntas del álabe.

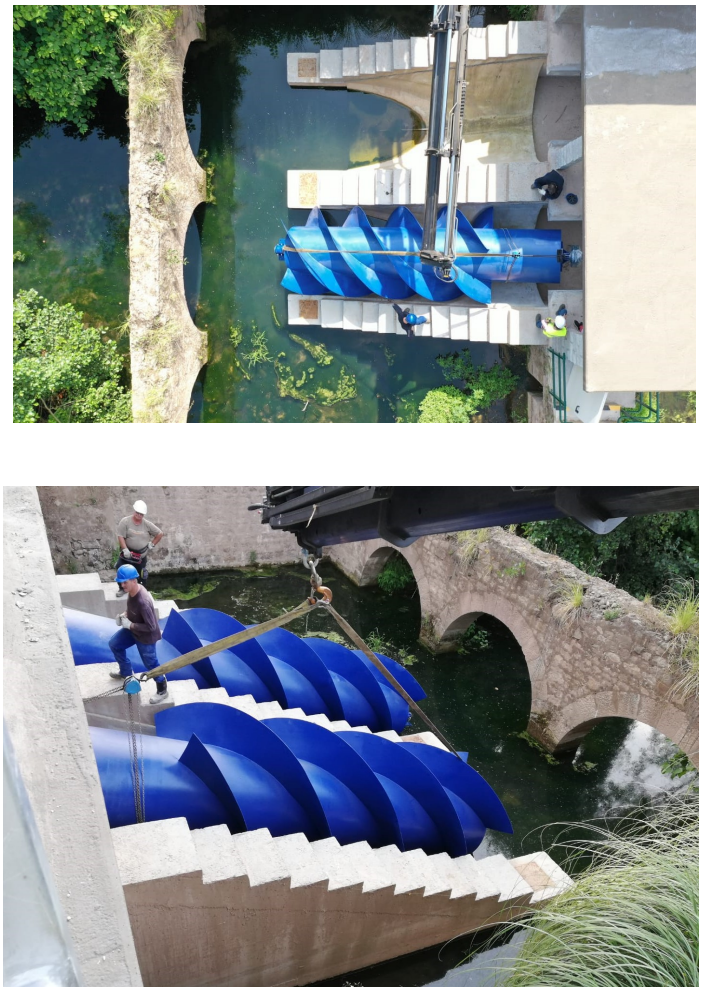

Fig. 6. Instalación de las turbinas tipo tornillo de Arquímedes instaladas en obra.

Se ha hecho uso del canal existente realizando una obra civil de pequeña entidad para su emplazamiento. Esta instalación produce electricidad que puede ser utilizada para reabastecer procesos de la propia planta o carga de vehículos eléctricos de los empleados de la central.

Una evaluación de costes globales tras su instalación y puesta en marcha, refleja que uno de los porcentajes más elevados corresponde con la partida de turbina hidráulica y el sistema de regulación y control, tal como se aprecia en la figura 7.

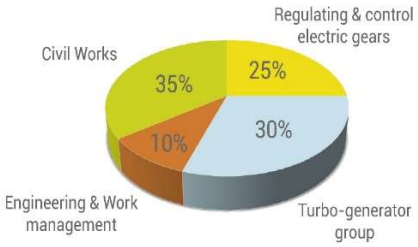

Fig. 7 Resumen porcentual de gastos por partida ejecutada.

3. Movilidad Urbana Sostenible. Microrredes de base renovable.

Uno de los retos de las sociedades desarrolladas en entornos urbanos es evolucionar hacia modelos económicos de movilidad de bajo consumo en carbono y menor consumo energético, bajo las premisas de la economía circular y sostenible. Desde el punto de vista del transporte, debe garantizarse una respuesta a las necesidades sociales, económicas y medio ambientales con las mínimas repercusiones negativas.

En este contexto, la electrificación del sector transporte juega un papel de gran importancia para la consecución de la descarbonización del sistema energético, será crucial para vehículos de corta y media distancia, así como para el transporte público y los vehículos de reparto usados en entornos urbanos. Al igual que sucede con el parque de vehículos eléctricos, el número de estaciones de carga aumenta anualmente.

En este sentido, las infraestructuras de carga de vehículos eléctricos son indispensables para su penetración en el mercado. Además, garantizar la disponibilidad de puntos de carga es también esencial para conseguir una transición hacia una energía más limpia.

La movilidad eléctrica permitirá ahorro en términos económicos, cuidado del medio ambiente en términos ecológicos y la eficiencia energética en términos de optimización de recursos, actuando de agente normalizador de la demanda energética: aumentando el consumo de la red en los horarios de menor demanda energética, se conseguiría aplanar dicha curva.

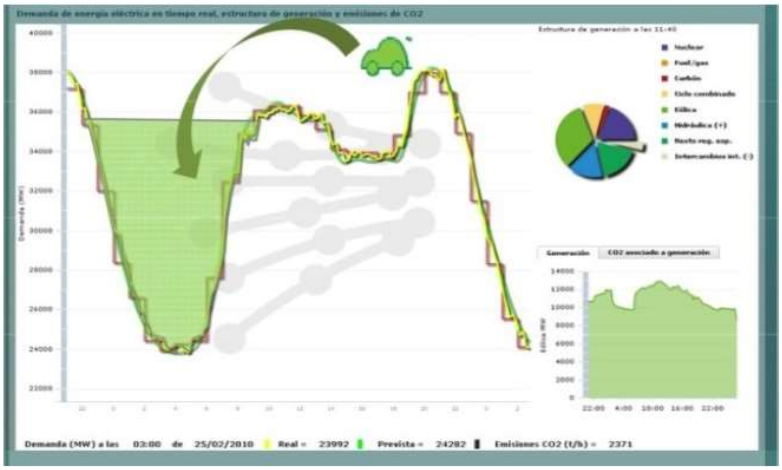

Fig. 8 Curva de demanda energética. Fuente Informe Global Electric Vehicle (2017).

Sin embargo, si se cumplen las perspectivas de futuro, el número de vehículos eléctricos desplegados a lo largo del mundo a medio y largo plazo requerirán una potencia muy superior a la actual, por lo que se necesitarán desarrollar nuevas infraestructuras de producción, almacenamiento y distribución de energía.

De esta manera, el desarrollo y penetración de vehículos eléctricos se está viendo condicionado, como se ha explicado, por la capacidad de progreso tecnológico de los modos de carga y almacenamiento de energía. Cuanta mayor sea la demanda de carga de vehículos eléctricos, mayor será el impacto en las redes de distribución de baja tensión existentes, pudiendo tener como consecuencia, a nivel general, un envejecimiento acelerado de la red o provocar, incluso, interrupciones del servicio.

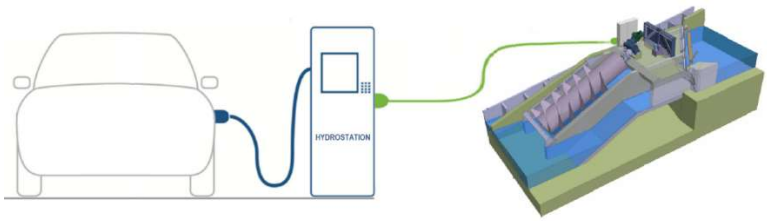

Fig. 9 Esquema del sistema de microrred propuesto.

La implementación de sistemas tipo µGs (abreviatura de microGrids), incluyen todos los elementos necesarios: generación, almacenamiento y carga de baterías en una misma instalación. La característica principal de este sistema es que, debido a independencia de las redes de distribución eléctrica, permite ofrecer servicios de recarga rápida o ultrarrápida del vehículo, adaptando el tiempo de servicio a las necesidades de los usuarios. Otro de las principales ventajas de este tipo de sistemas es el conocido con el término "Well-to-Wheels" ("del Pozo a las Ruedas", en español), que recoge y cuantifica los gases de efecto invernadero emitidos desde la producción de la energía hasta su uso en el automóvil.

Por tanto, una de las formas que existe para garantizar una reducción de los gases de efecto invernadero a cero es a través de la generación de energía de base renovable, suponiendo una energía limpia (energía verde) en todo su ciclo de vida, desde la generación hasta su consumo a nivel de usuario.

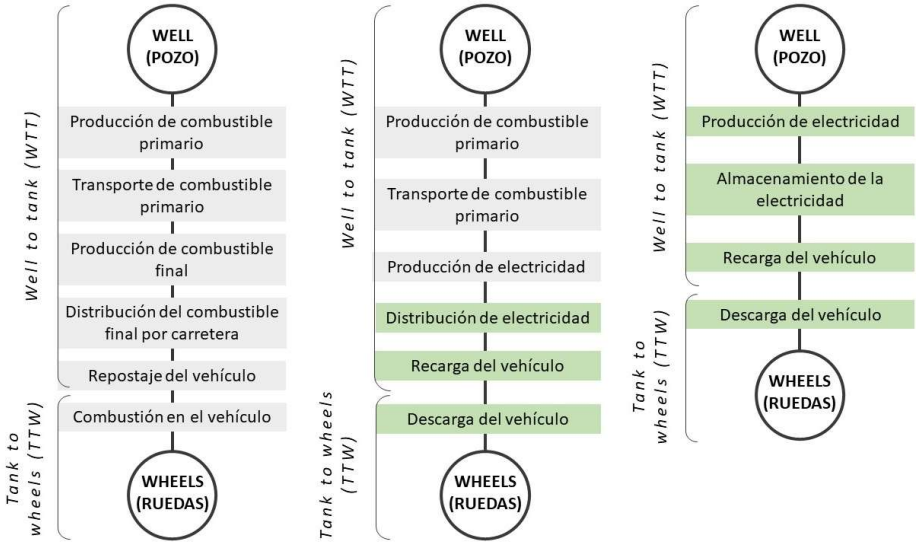

Fig. 10 Análisis Well-to-Wheels (del pozo a las ruedas). A la izquierda, ciclo de vida de la energía para un vehículo MCIA. En el medio, ciclo de vida de energía de base no renovable para un vehículo eléctrico. A la derecha, ciclo de vida de la energía de base renovable para un vehículo eléctrico (sistema propuesto).

Bajo este contexto, se está llevando a cabo el plan de actuación a través de la línea de proyectos "e-Mover", que trata de afrontar este reto a través del desarrollo de tecnologías de almacenamiento para la generación de energía renovable y almacenamiento sostenible en las diferentes escalas de transporte que se dan en el ámbito urbano: desde los equipos de trabajo municipales hasta el transporte colectivo.

Fig. 11 Cartel de la línea de proyectos "e-Mover".

Dentro de esta línea de proyectos, cabe destacar también el proyecto "Lanzaderas", cuyo objetivo es la implantación de un transporte colectivo de alumnos entre los distintos módulos de la Escuela Politécnica de Ingeniería de Gijón, a través de un girobús eléctrico, motorizado por energía 100% renovable gracias a distintos sistemas de microgeneración ubicados en sus paradas.

4. Conclusiones

Las turbinas de microgeneración son dispositivos eficaces, que ejercen de pilar básico para el desarrollo de microrredes en entornos urbanos, potenciando la movilidad urbana sostenible bajo las premisas de la economía circular y el medio ambiente.

El tornillo de Arquímedes no es una tecnología emergente sino ya real, capaz de aprovechar la presión estática de pequeños saltos de agua, dándole además una gran versatilidad por la posibilidad de no incurrir en grandes costes por obra civil, lo que influye en un bajo período de retorno del capital invertido. Además, esta tecnología

permite reutilizar la energía de aguas cuyo ciclo de vida industrial ya ha finalizado (como las aguas de refrigeración o las plantas de tratamiento), y es respetuosa con la fauna circundante (fish-friendly).

Por otro lado, cabe destacar que Sinfín Energy es la primera empresa que ha desarrollado y optimizado la tecnología del tornillo de Arquímedes para aprovechamiento de fuentes de energía renovable de base hidráulica, implementando la primera turbina de este tipo conectada a la red. Asimismo, Sinfín Energy, a través del plan de actuación "e-Mover", trata de estudiar la implantación de este tipo de sistemas a todos los niveles de transporte urbano, habiendo posibilitado técnicamente el desarrollo de microrredes eficientes y seguras, fomentando así la movilidad urbana sostenible, e introduciéndose dentro del nuevo contexto tecnológico de la sociedad actual.

Referencias

1. Chris Rorres, The Turn of the screw. **January 2000**, *Journal of hydraulic engineering*.
2. S.J. Williamson.; B.H. Stark; J.D. Booker; Low head pico hydro turbine selection using a multi-criteria analysis. **2012**; ELSEVIER.
3. Clean Energy Solutions Ltd.; Low Head Hydro Technologies and the need for greater uptake and implementation in the UK; BHA AC, **2007**. www.cleanenergysolutions.co.uk
4. GreenBug Energy Inc. Emergent Hydro Workshop. Presented by Tony Bouk – VP Business Development, **2011**.
5. Gerald Müller; James Senior. Simplified theory of Archimedean Screws; Journal of Hydraulic Research Vol.47, No. 5, **2009**. pp. 666–669 ; doi:10.3826/jhr.2009.3475; © 2009 International Association of Hydraulic Engineering and Research.
6. Future Energy Yorkshire. Archimedes' screw: Copley Hydropower Generator, a case study. www.fey.org.uk
7. Arantza Fernández Prada, Diseño de Tornillos de Arquímedes para su funcionamiento como turbinas microhidráulicas. Universidad de Oviedo, Proyecto Fin de Carrera Nº 3131461, **December 2014.**
8. MSc Christos Charisiadis; An introductory presentation to the "Archimedean Screw" as a Low Head Hydropower Generator, 2015. Leibniz Universität Hannover.

Control of a bidirectional single-phase grid interface for electric vehicles

Matheus Montanini Breve[1,2] [0000-0003-0599-3892] and
Vicente Leite[2] [0000-0002-8790-519X]

[1] Universidade Tecnológica Federal do Paraná, Cornélio Procópio, Brazil
matheus.m.breve@gmail.com,
[2] Research Centre in Digitalization and Intelligent Robotics (CeDRI)
Instituto Politécnico de Bragança, Portugal
avtl@ipb.pt.

Abstract. The number of electric vehicles is expected to increase exponentially in the next decade. This represents a huge potential for grid support, such as energy storage in their batteries, with advantages for grid operators and for customers. For this purpose, flexible power interfaces are required. This paper presents a simulation of a bidirectional single-phase power interface between an electric vehicle battery and the grid. The proposed system is fully simulated and counts with features such as vehicle-to-grid, vehicle-to-home and grid-to-vehicle. All power flow and the controllers for these modes of operation are described in detail. The simulation was developed in a Software-in-the-Loop scheme to facilitate a future physical implementation with a Hardware-in-the-Loop platform. The proposed system was extensively tested via simulation, the results proving the system is stable, able to change operation modes smoothly and definition of the exchanged active and reactive powers.

Keywords: Bidirectional Interface, Electric Vehicle, V2G, V2H

1 Introduction

According to estimations from the International Energy Agency (IEA) around 120 million electric vehicles (EV) will be on the road globally by 2030 [1]. Thus, EVs might serve as a distributed energy storage system that can be integrated with the electric grid [2–4].

This integration was first devised in 1997 [2] and has since been frequently referred as vehicle-to-grid (V2G) technology [3], with its various aspects being analyzed in depth by many authors [5–8]. If V2G technology is adopted by the majority of EV owners, it has the potential to be not only useful to grid operators, but to customers as well. Enabling information and power exchange between grid operators and electric vehicles owners would allow customers to optimize charging based on electricity prices, for example. Grid operators, on the other hand, could benefit from an additional grid stabilization source, which could prove useful in a scenario where the usage of photovoltaic energy and wind energy is also growing.

The possibility of a bidirectional power flow could also be used to power homes during short electricity shortages and electric grid instabilities, technology called Vehicle-to-Home (V2H). Vehicle-to-Home is one of the features built in the latest model of the aforementioned Nissan Leaf [9]. V2H could help reduce consumption of grid power in periods of the day when demand is highest and thus costlier, or simply as a backup power supply in case of emergencies. This technology, explored for example in [10, 11], could become important taking into account the expanding connectivity between home appliances in a Smart Home scenario and the growing number of households with renewable energy sources, like photovoltaics (PV).

In this context, this paper presents the simulation of a bidirectional single-phase power interface between an electric vehicle and the grid with MATLAB® and Simulink. The presented system counts with features such as grid-to-vehicle (G2V) for battery charging, vehicle-to-grid (V2G) for grid support and vehicle-to-home (V2H), as well as allowing seamless transitions between these operation modes. The simulation is assembled in a Software-in-the-Loop (SiL) scheme with the power and control structures simulated in the discrete domain and with different simulation rates. This allows for future testing in a Hardware-in-the-Loop (HiL) platform, for which only small parameter adjustments are needed.

The paper is divided in five sections, the first being a brief introduction about concepts such as V2G and V2H and their relevance. The second section contains details on the implemented system structure, such as the control algorithms employed and power topology used. The third section explains the computational model created in Simulink and the simulation results are listed in the fourth section. The fifth and last section contains the conclusions.

2 System Structure

The power structure chosen to accomplish the integration of an electrical vehicle with the electric grid is arranged in a dual-stage configuration and composed of five parts. This structure is the most commonly employed [12] and counts with two dedicated power processors, similar to the structure employed in [10, 13, 14]. The parts are:

- Vehicle, represented as a battery;
- Bidirectional DC/DC converter (BDC);
- Bidirectional single-phase voltage-source inverter (BADC or VSI);
- Output filter to reduce current harmonic distortion;
- Grid and common-coupling point (CPP).

A simplified block diagram of the proposed system structure can be seen in Figure 1. The connection lines between the blocks represent the bidirectional nature of the power flow in the system.

2.1 Power Topology

Figure 2 shows the power topology of the bidirectional interface in greater detail. The bidirectional DC/DC converter (BDC) is a power converter that alternates

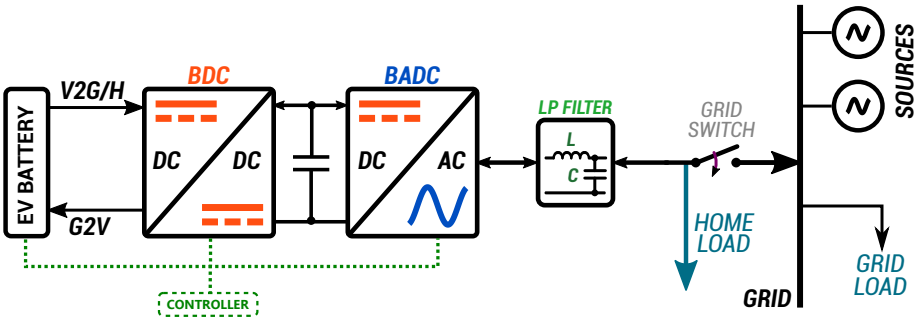

Fig. 1. Proposed system structure

between two modes of operation, step-down (buck) and step-up (boost) modes, respectively charging (G2V) and discharging the battery (V2G and V2H).

The bidirectional single-phase voltage-source inverter (BADC) is a full-bridge inverter with two IGBT inverter legs and free-wheel diodes. The output filter is a low-pass LC filter to lower the harmonic distortion in the inverter current output waveform. The grid is represented by an AC source with capability of exchanging any given amount of active and reactive power, thus acting as an infinite bus. The common-coupling point represents where home loads can be connected to and the point which, after a grid fault condition is detected, remains energized in case the V2H feature is enabled.

The power structure is controlled by two control algorithms, the BDC and BADC control algorithms. Table 1 contains a summary of the system operation modes and the control targets of the BDC and BADC control algorithms.

Table 1. Summary of system operation modes and the respective control targets of the DC/DC and DC/AC converters

Operation modes			Control target	
Mode	**Grid tied**	**Battery**	**BDC**	**BADC**
G2V	Yes	Charging	CV and CC charging	DC bus voltage
V2G	Yes	Discharging	DC bus voltage	P and Q
V2H	No	Discharging	DC bus voltage	AC voltage

2.2 BDC Control Structure

The BDC control strategy can be divided in three subsystems, as shown in Figure 3.

The "*Charging Current Reference Generator (G2V)*" subsystem generates a battery current reference, I_B^*, to control the charging current in G2V mode. The

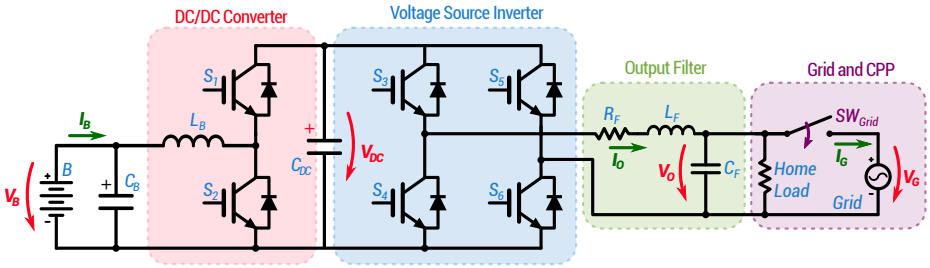

Fig. 2. Proposed power structure

battery charging current is determined by two charging modes, constant current (CC) and constant voltage (CV). In CC charging mode the current reference $I^*_{B_{\mathrm{CC}}}$ can be set to equal the maximum or a given percentage of the battery nominal charge current. In CV charging mode a PI controller generates a battery current reference, $I^*_{B_{\mathrm{CV}}}$, to maintain the battery voltage constant.

The "*Discharging Current Reference Generator (V2G/H)*" subsystem contains a PI controller that will determine the battery current needed to maintain the DC link voltage constant at a set voltage. This V_{DC} control method is used both in V2G (grid-connected) and V2H (grid-isolated) modes.

The "*Battery Current Controller*" subsystem controls the BDC PWM duty cycle to maintain the battery current at the setpoint, in turn given by the two aforementioned subsystems. It contains a PI controller comparing the battery current reference I^*_B, given by the two aforementioned subsystems, and the measured battery current value I_B, generating a BDC control signal. This signal is converted to a PWM signal generator to drive the IGBT gates in the BDC converter to achieve the desired battery current.

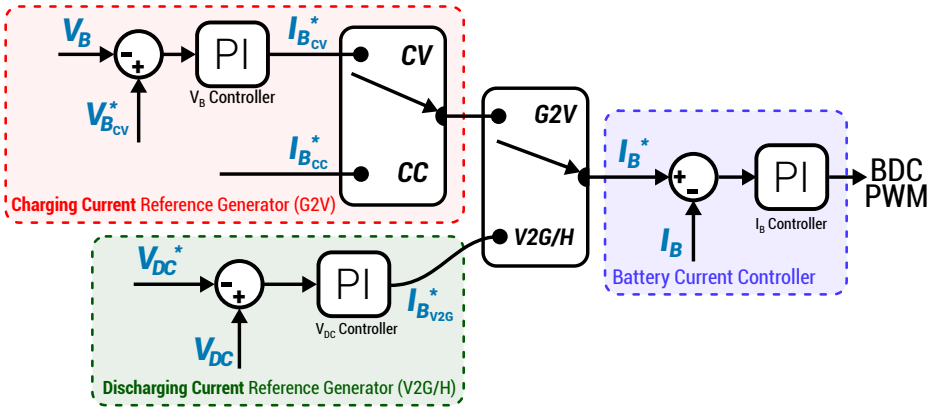

Fig. 3. Proposed BDC control structure

2.3 BADC Control Structure

The BADC control algorithm can be subdivided in two different modes: the grid-connected and grid-isolated modes.

Grid connected modes include the G2V and V2G operation modes. An overview of the grid-connected control algorithm is shown in greater detail in Figure 4. The system operating in G2V mode is responsible for controlling the battery charging current and voltage. In V2G mode it controls the active and reactive power exchange with the grid. The control algorithm of the two grid-connected operation modes are explained as it follows:

- **V2G mode**: in V2G mode, the active and reactive power are set externally by P_{REF} and Q_{REF}. Since the active power delivered to the grid is proportional to the output current d-component, i_d, and the reactive power proportional to the output current q-component, i_q, converting these power quantities into the desired dq-components of the output current requires power calculations in dq-theory. These calculations result in dq-current references, i^*_{Od} and i^*_{Oq}, which are fed into classical PI controllers, that in turn give out V'_d and V'_q, called voltage demand values [15].
- **G2V mode**: in G2V mode the VSI is responsible for maintaining the DC link voltage constant, acting similar to the BDC in V2G mode. In this mode a PI controller compares the DC link voltage, V_{DC}, with the reference value, V^*_{DC}, and generates the needed current to be extracted from the grid and injected into the DC link I^*_{DC} to maintain the DC bus voltage constant. An unitary power factor is also maintained, since the q-component of the grid current is kept null, unless reactive power compensation while charging the battery is needed. Thus, in this mode there is a 180º phase difference between the VSI voltage and current output.

As displayed in Figure 4 the dq-current controllers only calculate the demand values V'_d and V'_q. In order to obtain the true V_d and V_q values, a process called decoupling is necessary. Decoupling takes into account the dynamics of the inverter AC-side, including output filter. Signals such as θ_{PLL} and $||V_G||_{\mathrm{PLL}}$ represent respectively the grid voltage phase and amplitude, needed for grid synchronization. These signals are calculated via a Phase-Locked Loop (PLL) based on the structure devised in [16].

2.4 Grid-isolated mode (V2H)

The transition from grid-connected to grid-isolated mode is activated following the detection of a grid fault by the grid fault detection module. This module detects large frequency or amplitude variations in the grid voltage and, if the manually-defined thresholds are surpassed, it sends a signal ordering the disconnection from the grid, opening the grid switch as shown in Figure 1. If the grid-isolated mode is allowed, the system control algorithm changes following the fault detection and it starts operating in grid-forming mode, also called grid-isolated mode, disconnecting itself from the grid.

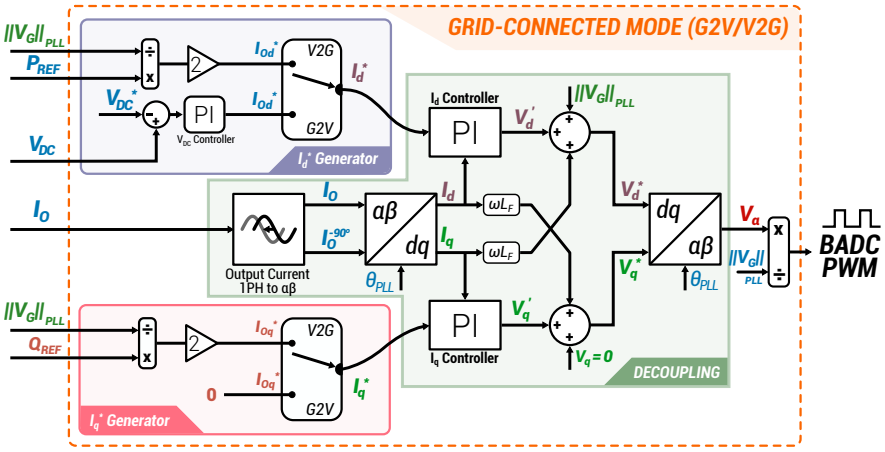

Fig. 4. Proposed BADC current control structure in grid-connected modes

In grid-isolated mode (V2H) the VSI must be controlled with a fixed sinusoidal voltage reference, since grid synchronization is not possible, being the system responsible for generating a grid. This voltage reference in V2H mode is obtained via the system represented in Fig. 5.

This system uses a fixed frequency reference, 50 Hz, to generate a signal ωt via a discrete integrator. The maximum value of ωt is limited 2π, that is, 360^o, given that the integrator is reset when ωt reaches this value. An initial phase, θ_0, given by a PI controller for re-synchronization with the grid, is added to the resulting signal and the sum $\omega t + \theta_0$ is converted into a sinusoidal reference with a 230 V RMS value. The peak voltage is divided by the DC link voltage to obtain the PWM reference signal corresponding to a 230V RMS output.

The voltage output requires a closed-loop control as shown to ensure a steady V^*_{RMS} voltage regardless of the load, up to the specified inverter power limits. The controller output is limited to a $\pm 5\%$ variation to prevent over-voltage conditions.

2.5 Grid re-synchronization

In the event of grid reconnection in stand-alone (V2H) mode, the VSI output might be at a different frequency or out-of-phase in relation to the grid voltage and thus a grid re-synchronization strategy is required. For that, an initial phase, θ_0, is given by a PI controller. The controller compares and reduces the difference between the grid and output phase by altering the initial phase value, which is added to the resulting signal generator. The phase difference is calculated by converting the grid and output phase signals into sinusoidal signals and then the difference between them. This results in another sinusoidal signal, whose amplitude relates to the phase difference. This way it is possible to define a threshold value and, if the calculated RMS value, that is, the difference, is lower than the threshold the system reconnects itself with the grid, thus enabling seamless transition between grid-isolated and grid-connected operation modes.

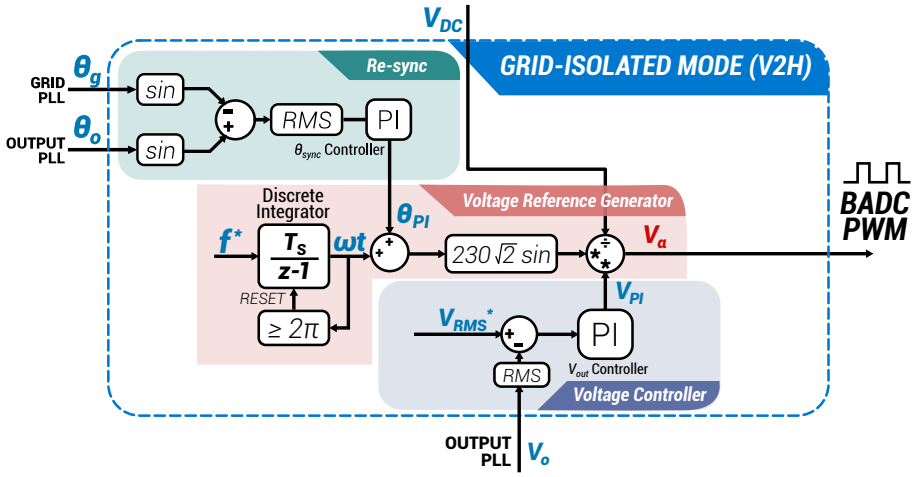

Fig. 5. Voltage reference generator in grid-isolated (V2H) mode

3 Computational System Model

This section concerns the methods and materials used to create a computational model (Figure 6) of the power structure as shown by Figure 7 and the respective control algorithms as displayed in Figure 8.

Figure 6 shows that the main parameters are set externally, that is, an external user or higher-hierarchy controller can determine the operation mode while grid-connected (G2V/V2G), the power to be exchanged with the grid (power references), if the grid-isolated mode (V2H) is allowed and if the system is enabled. This reflects a the context in which higher-hierarchy controllers determine the needed V2G services, that is, what each vehicle with this system will provide.

The simulation of the system was carried out with the software MATLAB® and Simulink by MathWorks, as well as the *Specialized Power Systems* library under Simscape.

The power structure was developed and simulated in the discrete domain with a simulation step time of 2 μs (500 kHz). The power structure is shown in Figure 7.

The control algorithms are simulated with a longer simulation step time of 100 μs (10 kHz) and are displayed in Fig. 8. Thus, the simulation was developed in a Software-in-the-Loop (SiL) scheme to facilitate a future physical implementation with a Hardware-in-the-Loop (HiL) platform.

The computational model reflects the experimental platform found in the Polytechnic Institute of Bragança (IPB), that counts with a real-time control interface based on the dSPACE DS1103 Controller Board and IGBTs switches in the PM75RLA120 power module with a maximum switching frequency of 10 kHz, the frequency used to simulate the power system representation.

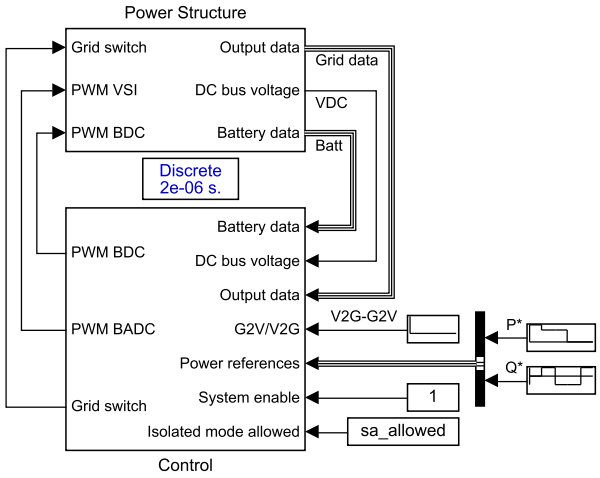

Fig. 6. SiL system representation modelled in Simulink

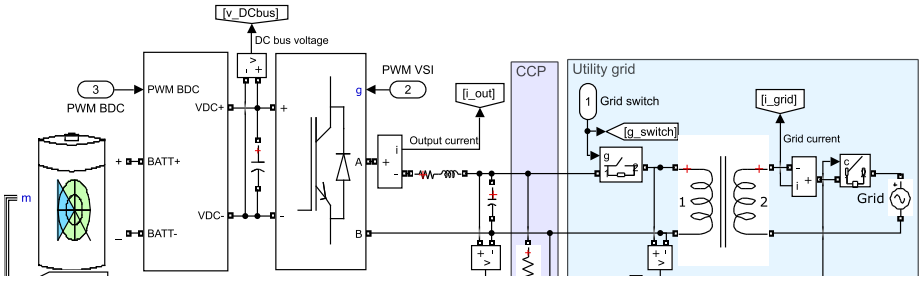

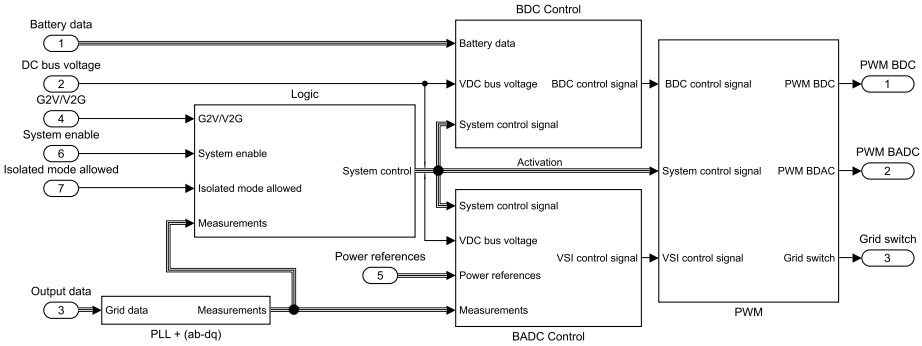

Fig. 8. Control structure modelled in Simulink

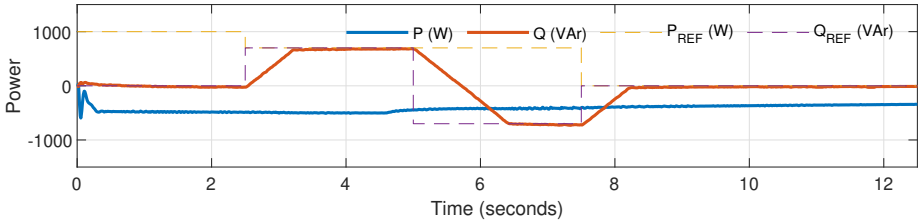

Fig. 9. Power references and measured power in G2V mode

4 Computational Results

The following results demonstrate the different system modes of operation, including operation while connected to an electric grid, thus including V2G and G2V operation modes with varying power references, as well as the V2H operation mode and the transitions between the main modes of operation.

4.1 Operation in grid-to-vehicle (G2V) mode

During continuous G2V operation the grid current phase is opposed to that of the voltage, that is, a 180 degrees phase difference. In this simulation the active and reactive power references were also varied during the simulation to show operation in 4 different power combinations:

- CC charging mode and null reactive power;
- CC charging mode and 700 VAr;
- CV charging mode and -700 VAr;
- CV charging with null reactive power.

Since the active power withdrawn from the grid is defined by the battery charging algorithm - approximately 490 W in constant-current mode, the active power reference is given either by the CC or CV charging schemes.

The active power in G2V mode is not set externally, but rather internally by the battery charging controller. This can clearly be seen in Figure 9 where the power reference line does not have any influence on the power being withdrawn from the grid to charge the battery. A change between different charging modes can also be seen at the 5 seconds mark, showing the change from a CC to a CV charging scheme. The reactive power can be set externally and, thus, the system can simultaneously charge the battery and act as an active power factor corrector if needed.

Figure 10 shows the current and voltage outputs in 3 power combinations while operating in G2V mode.

4.2 Operation in vehicle-to-grid (V2G) mode

In this simulation the active and reactive power references were varied during the simulation. The simulation lasts 12.5 seconds and shows the system operating in

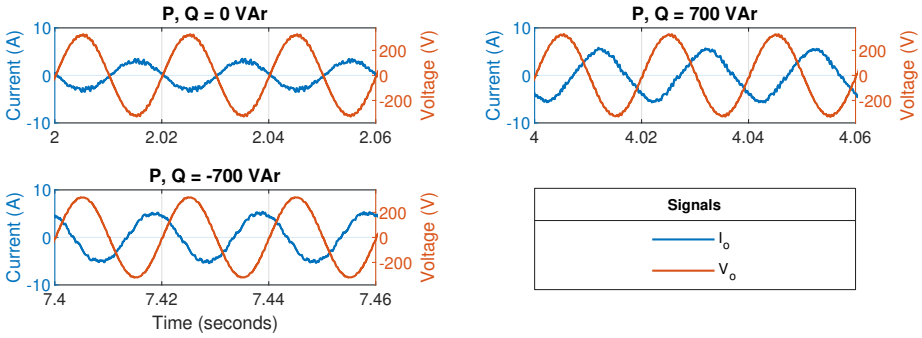

Fig. 10. VSI output current waveform in G2V mode

5 different power combinations, reflecting the existence of an external controller to determine the needed power in a micro-grid, for example. The tested power combinations are listed as it follows:

- 1000 W and null reactive power;
- 700 W and 700 VAr;
- 700 W and -700 VAr;
- 0 W and -700 VAr;
- 0 W and 700 VAr.

Figure 12 shows the results obtained in this mode of operation. It shows the power references set externally, that is, the active and reactive powers desired, and the measured power exchanged with the grid, which follow these external parameters. The results prove that the system is able to operate in two power quadrants, that is, with positive active power - delivered to the grid - and either consuming or injecting reactive power.

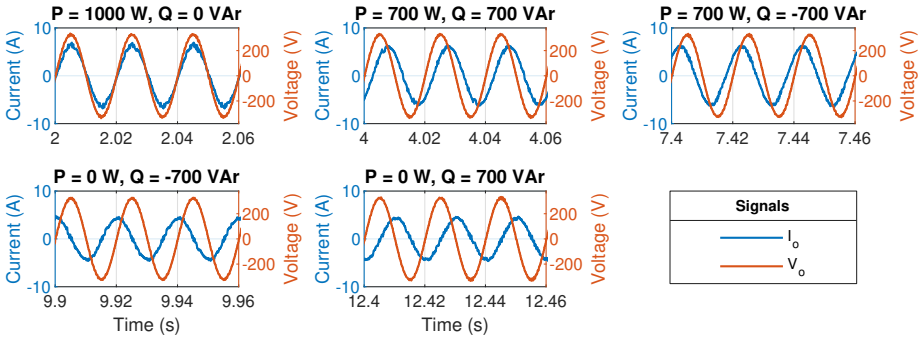

Fig. 11. VSI output current waveform in V2G mode

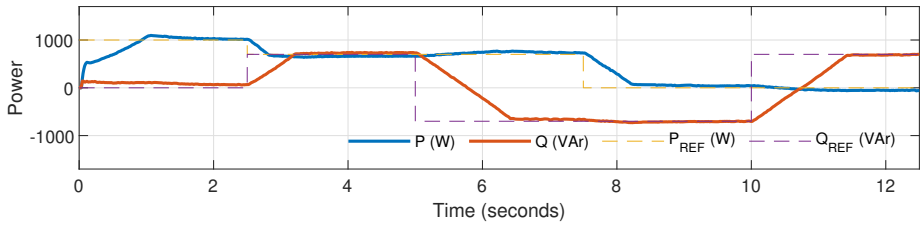

Fig. 12. Active and reactive power at VSI output and their reference values in V2G operation mode

4.3 Grid-tied operation mode transitions

The following results, visible in Figures 13 and 14, prove the system capability of switching between V2G and G2V operation modes maintaining system stability. All the switching operations are only performed when the output current crosses zero in order to reduce transients.

Figure 13 exhibits the VSI output current waveform, output power, DC link voltage and the battery voltage and current during the transition from G2V to V2G. The transition is requested at the 2 seconds mark, but executed at the next current zero crossing. Fig 13 shows the transition of the current phase in relation to the grid voltage, from being in-phase before the 2 seconds mark and becoming in opposite phase after the 2 seconds mark.

Figure 14 exhibits the VSI output current waveform, output power, DC link voltage and the battery voltage and current during the transition from V2G to G2V. The transition is requested at the 2 seconds mark, but executed at the next current zero crossing. Fig. 14 shows the transition of the current phase in relation to the grid voltage, from being in opposite phase before the 3 seconds mark and becoming in-phase after the 3 seconds mark.

4.4 Seamless Transition - From stand-alone to grid-connected

This subsection contains the results obtained by simulating the system grid-isolated feature (V2H), including the seamless transition and smooth grid re-synchronization strategy after a grid reconnection is detected. For this test the grid voltage was set to be leading 45 degrees compared to the V2H voltage reference.

Figure 15 shows more details of the re-synchronization and transition processes from V2H to V2G and Figure 16 from V2H to G2V. Both figures display the output and grid phases, the error between them, the grid status, the current and voltage waveforms and the power output during these test conditions.

The transition from V2H to grid-tied operation modes is always executed when a voltage zero-crossing is detected to ensure a smooth transition. Complete re-synchronization takes approximately 3.2 seconds starting after detecting the grid presence for G2V and 1 second for V2G.

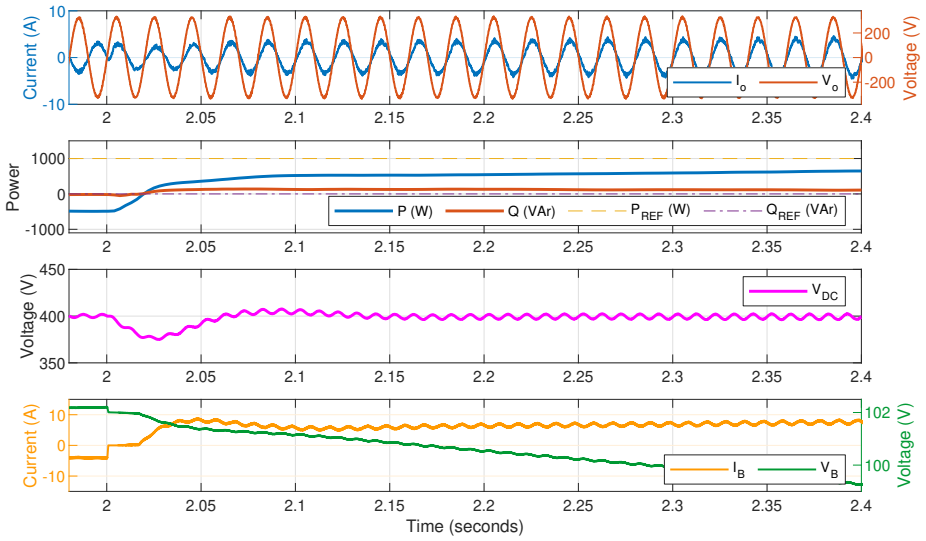

Fig. 13. VSI output current waveform, output power, DC link voltage and battery voltage and current during transition from G2V to V2G.

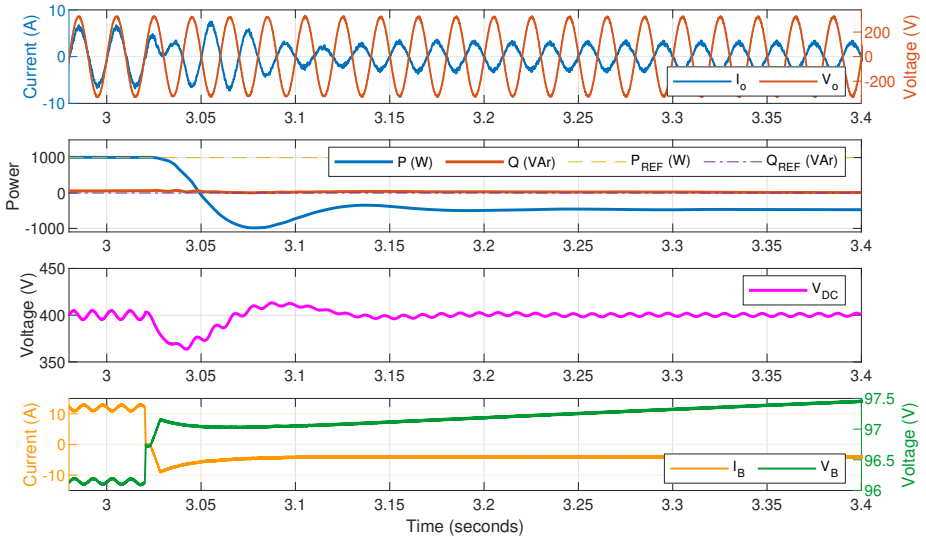

Fig. 14. VSI output current waveform, output power, DC link voltage and battery voltage and current during transition from V2G to G2V.

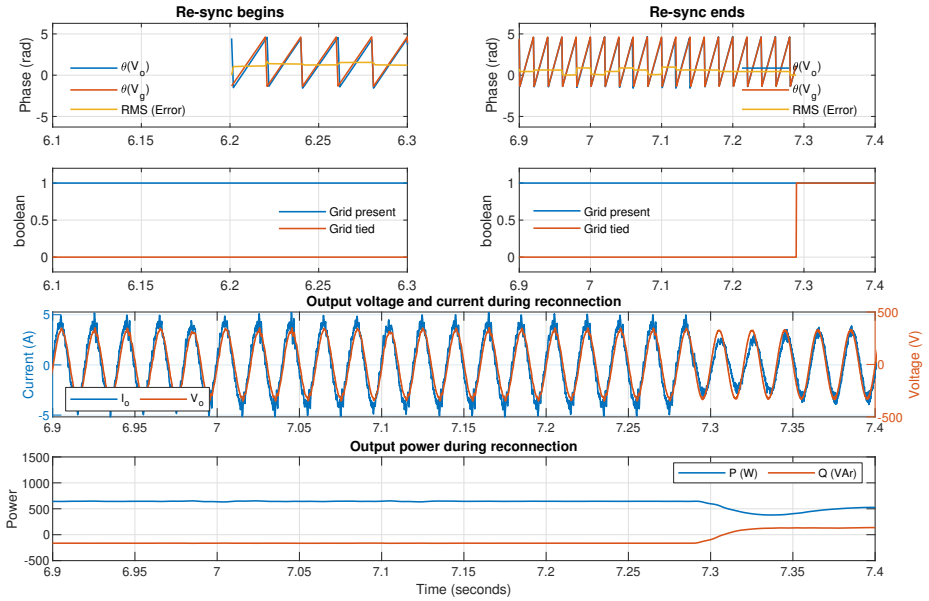

Fig. 15. Re-synchronization and transition from grid-isolated (V2H) to grid-tied V2G mode.

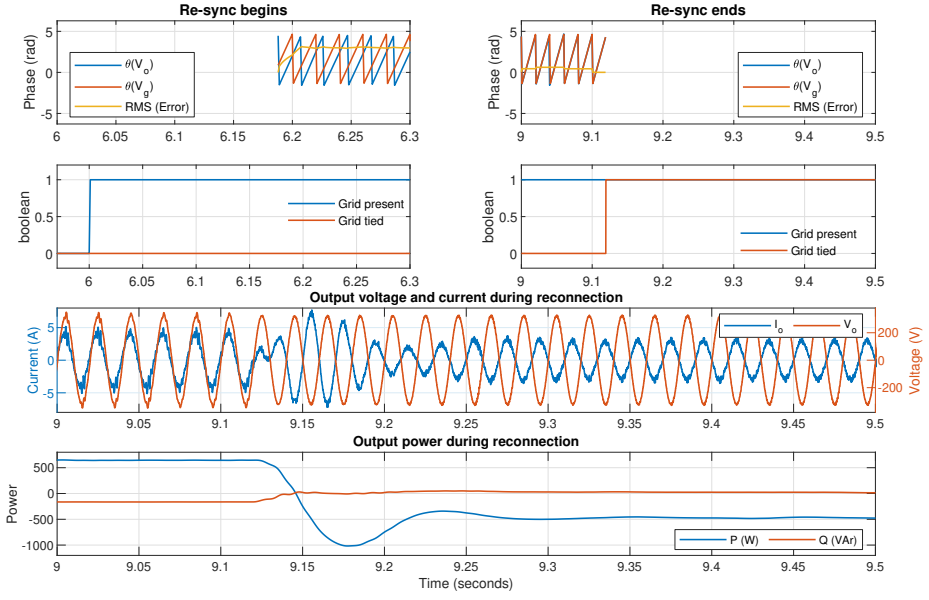

Fig. 16. Re-synchronization and transition from grid-isolated (V2H) to grid-tied G2V mode.

5 Conclusions

The implementation of a single-phase bidirectional power interface between an electric vehicle battery and the grid was successful, based on the achieved computational presented in this paper. Tests were performed in the simulation to extensively test the system and prove it is stable under different operation conditions and with varying power references. The system proved capable of dealing well with external requests or events such as mode transitions or grid faults as well, maintaining stability and with small transients.

Since the proposed system is controlled externally, that is, an external user is able to set the active and reactive power to be exchanged, decide whether the battery should be charged or discharged and if the grid-isolated mode is permitted, the proposed system is useful in the context of higher-hierarchy controllers to determine the needed V2G services. This way it is possible for grid operators or aggregators, for example, to determine which service each vehicle will provide, controlling numerous vehicles as a fleet and coordinating, based on other factors such as current battery levels, state of health, user preferences, the duration and type of services to be provided.

A simulation-validated system in which all these features are packed together, that is, battery charging in two different modes (G2V), grid support (V2G), grid-isolated (V2H), reactive power compensation, as well as allowing manual selection of the operation mode and switching between them smoothly, is not found in any of the literature cited within this document.

Besides that, the simulation here presented was developed in a Software-in-the-Loop scheme, thus, physical implementation of the system with a Hardware-in-the-Loop becomes a natural next step, being part of the planned future works related to this paper. The physical implementation will be performed with the experimental platform found in the IPB, that counts with a real-time control interface based on the dSPACE DS1103 Controller Board.

Summary of Acronyms G2V - grid-to-vehicle; V2G - vehicle-to-grid; V2H - vehicle-to-home; BDC - bidirectional DC/DC converter; BADC - bidirectional DC/AC converter; VSI - voltage-source inverter; CC - constant current; CV - constant voltage; HiL - Hardware-in-the-Loop; SiL - Software-in-the-Loop

References

1. International Energy Agency: Global EV Outlook 2018: towards cross-modal electrification, https://webstore.iea.org/global-ev-outlook-2018
2. Kempton, W., Letendre, S.E.: Electric vehicles as a new power source for electric utilities. Transportation Research Part D: Transport and Environment 2(3), 157 – 175 (1997), http://www.sciencedirect.com/science/article/pii/S1361920997000011
3. Kempton, W., Tomić, J.: Vehicle-to-grid power fundamentals: Calculating capacity and net revenue. Journal of Power Sources 144(1), 268 – 279 (2005)
4. Kempton, W., Tomić, J.: Vehicle-to-grid power implementation: From stabilizing the grid to supporting large-scale renewable energy. Journal of Power Sources 144(1), 280 – 294 (2005)

5. Sovacool, B.K., Axsen, J., Kempton, W.: The Future Promise of Vehicle-to-Grid (V2G) Integration: A Sociotechnical Review and Research Agenda. Annual Review of Environment and Resources 42(1), 377–406 (2017)
6. Tan, K.M., Ramachandaramurthy, V.K., Yong, J.Y.: Integration of electric vehicles in smart grid: A review on vehicle to grid technologies and optimization techniques. Renewable and Sustainable Energy Reviews 53, 720 – 732 (2016)
7. Mwasilu, F., Justo, J.J., Kim, E.K., Do, T.D., Jung, J.W.: Electric vehicles and smart grid interaction: A review on vehicle to grid and renewable energy sources integration. Renewable and Sustainable Energy Reviews 34, 501 – 516 (2014)
8. Ferdowsi, M.: Plug-in hybrid vehicles - a vision for the future. In: 2007 IEEE Vehicle Power and Propulsion Conference. pp. 457–462 (9 2007)
9. Nissan: Vehicle to Home Electricity Supply System, https://www.nissan-global.com/EN/TECHNOLOGY/OVERVIEW/vehicle_to_home.html
10. Pinto, J.G., Monteiro, V., Gonçalves, H., Exposto, B., Pedrosa, D., Couto, C., Afonso, J.L.: Bidirectional battery charger with grid-to-vehicle, vehicle-to-grid and vehicle-to-home technologies. In: IECON 2013 - 39th Annual Conference of the IEEE Industrial Electronics Society. pp. 5934–5939 (11 2013)
11. Vittorias, I., Metzger, M., Kunz, D., Gerlich, M., Bachmaier, G.: A bidirectional battery charger for electric vehicles with V2G and V2H capability and active and reactive power control. In: 2014 IEEE Transportation Electrification Conference and Expo (ITEC). pp. 1–6 (6 2014)
12. Sharma, A., Sharma, S.: Review of power electronics in vehicle-to-grid systems. Journal of Energy Storage 21, 337 – 361 (2019)
13. Leite, V., Ferreira, A., Batista, J.: Bidirectional vehicle-to-grid interface under a microgrid project. In: 2014 IEEE 15th Workshop on Control and Modeling for Power Electronics (COMPEL). pp. 1–7 (6 2014)
14. Zgheib, R., Al-Haddad, K., Kamwa, I.: V2G, G2V and active filter operation of a bidirectional battery charger for electric vehicles. In: 2016 IEEE International Conference on Industrial Technology (ICIT). pp. 1260–1265 (3 2016)
15. Samerchur, S., Premrudeepreechacharn, S., Kumsuwun, Y., Higuchi, K.: Power control of single-phase voltage source inverter for grid-connected photovoltaic systems. In: 2011 IEEE/PES Power Systems Conference and Exposition. pp. 1–6 (3 2011)
16. Ciobotaru, M., Teodorescu, R., Blaabjerg, F.: A new single-phase PLL structure based on second order generalized integrator. In: 2006 37th IEEE Power Electronics Specialists Conference. pp. 1–6 (6 2006)

Citizen Participation in the Context of Smart Cities

Jorge J. Gómez Sanz, Carla Cubillos, and Juan Pavón

Universidad Complutense
28040 Madrid, Spain
http://grasia.fdi.ucm.es
{jjgomez, carlacub, jpavon}@ucm.es

Abstract. Smart cities are closer to be a daily reality thanks to the advances in the Internet of Things, Big Data, and Artificial Intelligence technologies. However, few voices have shown concern about what it means for the citizens. In this work, we try to analyze, what an inclusive smart city is, and what aspects can be accounted to put people first. The analysis identifies the participation of citizen as a major element to help in this direction. However, participation has not improved as much as expected with the advent of new communication technologies. The paper proposes ramifying the participation of citizens. As an example, the paper proposes using text adventure development kits to build a survey tool in form of a text adventure game.

Keywords: Smart Cities · Inclusiveness · E-Governance · gamification

1 Introduction

The world population that lives in urban cities will probably reach 70% by 2050 [6]. This is a big challenge for our cities. Not only due to the environmental, energetic, transport, communication, and infrastructure impact, but the social consequences as well. Different population groups have different needs that the city should, at least, be aware of. When these groups are not participating in governance decisions and their positions are not considered, we risk ending in disadvantageous situations for others. Even social exclusion in the worst cases. Older people are specially sensitive to this problem because of their documented technology aversion and the risk of impairments due to the aging process.

The notion of smart cities appears in the 90s as an answer to the urban growth and its implications for the daily living [3,11,39,17]. Some authors complain the development of these cities is still being made attending more to technology than to the people [39]. Nevertheless, the European Commission has been promoting policies for the development of inclusive smart cities manifesto, claiming citizens have to be central [30]. Both views divide smart city definitions between those pushing the role of technology (hard domains) and those where technology is secondary (soft domains) [3].

In order to put people first, citizen participation should be encouraged. Citizen involvement in smart cities has to do with participatory processes and how Information and Communication Technologies (ICT) enable them. At the same time, ICT is promoting new ways of governance, bringing the e-governance [38] and the debate on smart governance in smart cities [17]. Despite the expectations, research results show that the new ICT methods effectiveness is similar to conventional surveys, the data quality lower, and does not prevent bias or exclusion of participants [12].

It seems a greater understanding of the participatory processes and how they are performed is necessary. A frequently cited theory on citizen participation is the ladder of participation [8]. This first vision established three categories with levels within: no participation (therapy, manipulation), degrees of tokenism (placation, consultation, informing), and degrees of citizen power (citizen control, delegated power, partnership). Garau [22] collects the different ways in which the ladder has appeared since its initial formulation in 1969 and connects its current form with the concept of *participatory planning*. Authors are revising this model and proposing specific ways in which ICT tools can help [43].

The definition of the participatory process goal is subject of discussion as well. Research has proposed evaluation frameworks [42], but, at the same time, smart cities research have produced ways to evaluate a smart city project itself while integrating social aspects. This is the case of the Quadruple Helix (QH) model [11].

In this paper, we pursue the concept of *inclusive smart city* which implies, among others, the development of technologies that allow all persons, regardless of their condition, to reach a better quality of daily living, greater participation in their community, and full accessibility to all the spaces and deployed services.

The current state of the art of technology has promoted the realization of massive participation of citizens through Information and Communication Technology (ICT). Nevertheless, the performance of the methods applied so far does not improve conventional surveys' drop out rate and even provides with lower quality data [12].

This paper contributes to the concept of the inclusive collaborative platform by deepening in the meaning of inclusiveness and how to account it in the context of a smart city. The conclusion is that participation is the key to advance in this area. Also, the paper contributes with an analysis of how ICT is contributing to increase citizen participation. As a result, the paper proposes gamifying the consultation in order to increase the quality of the data and reducing the drop out rate [41].

The document is organized as follows. Section 2 studies the related work on smart city evaluation models and tools. Section 3 evaluates enabling technologies for evaluating smart cities performance in what respect to social aspects. Based on those technologies, section 4 proposes a method and a tool to create consultation processes that increase the participation of citizens. An example is presented in section 5. The paper finishes with section 5.

2 Pursuing the Inclusive Smart City

Despite the popularity of the concept, there still no consensus on what is a smart city [3,28,33]. Many authors hypothesize that, depending on the background of the discipline, the country, or the point of view of the proposers, definitions change[3,5,36,31,40]. Some disciplines emphasize the dimension of equipment and devices, the inter-connectivity among them in computerized platforms or the incorporation of optimization elements of the devices or the deployed services; while others emphasize the political dimension: governance, participation; or social: economic growth, energetic sustainability, better quality of live. This same diversity of concepts can be appreciated as we distinguish between different categories such as technology, people, and community [3,35].

In summary, it is possible to notice two divergent perspectives: a reductionist technological conceptualization, widely criticized, cited before; and a broader conceptualization of a sustainable smart city, more holistic [5,10,11,39]. Far from its assimilation as a digital city, a virtual city or ubiquitous city, a smart city is characterized by the human component, the people [3] and, broadly, the persons in the context of the community [35], involving them in economic, social, environmental, and cultural development.

Understanding what is a smart city is basic first step in order to discuss citizen participation methods. Nevertheless, rather than looking for more definitions, this section goes the other way around: looking for factors to address in any smart city. The working hypothesis is that taking into account this information can help understanding the goal a particular inclusive citizen participation initiative should pursue.

Inclusiveness and other social aspects do appear in the reviewed indicators. Nevertheless, collected examples refer to the evaluation of already completed developments, not early participatory discussions on how to bring an improvement in an inclusive way.

2.1 Reviewing Smart City Indicators

A leading set of indicators adopted in the European smart city vision is the "wheel of Cohen". It is integrated by six axes: smart economy, smart mobility, smart environment, smart people, smart life, and smart governance [14,18,45]; each one of the six components or dimensions has three sub components called *working areas*. Hence, there are 18 working areas with a total of 62 indicators. One of them is *smart people*, which is composed by sub-dimensions of education, creativity, and inclusive society. An integral definition of an inclusive smart city must focus into all of these dimensions, considering that all these axes, as a whole, contribute significantly towards the growth and sustainability of the city.

This view is supported by Berardi y Dangelico [3] who make an exhaustive revision of the smart city concept, concluding that none of the definitions so far did include the term *social*. Furthermore, they infer that the lack of consensus can be originated by the fact that the concept of a smart city has been applied to two domains that seem irreconcilable: (1) Hard domains in which ICT can play a

crucial role such as buildings, power grids, natural resources, water management, waste management, mobility, and logistic; (2) Soft domains where the application of ICT is not so decisive such as education, culture, and political innovations, social inclusion and governance [3]. Also, they remark that it is necessary to consider that, regardless of the different visions and priorities in a city, integral development of hard and soft aspects is necessary.

As Paskaleva et al. [39] indicated, despite the discourse of citizen/user-centered approaches, the level of empowerment and social participation of all stakeholders is still limited. Most implemented smart cities initiatives, even the most successful, are still assuming that social and urban development is a consequence of technological interventions. Hence they not perform actions aimed at the participation of citizens in the design and implementation of smart cities. That is, for example, the case of Glasgow or Barcelona. On the other hand, the Amsterdam Smart City program greatly depends on the active participation of the community (bottom-up participating approach). Nevertheless, it still presents some barriers to reach an inclusive vision, such as the lack of elements that facilitate the dissemination and use of data by the community[11,45].

Paskaleva et al. [39] examined how data governance appears in the smart city agenda focused on sustainability of the three cities belonging to the international Triangulum project: Eindhoven, Manchester, and Stavanger. They retrieved documents and material from academic publishers and the project site. Also, they performed a survey to stakeholders living in those cities. The survey contained 18 open-ended questions about five key decisions domain of data governance.

Other studies based their analysis on the application of the *Fourth Helix Model* also known as the *Quadruple Helix Model* (QH model). As Borkowska and Osborne [11] remarks, the QH model is an extended version of the triple helix model of innovation (TH) developed by sociologist Etzkowitz and Leyesdorff in the 1990s, that refers to a interplay between three actors, academia, government and industry, in creating knowledge-based economies and foster social development. The QH model adds a fourth helix or stakeholder, civil society, and combines a top-down and bottom-up approaches to innovation. This was supossed to represent going from a technological innovation approach to a user-oriented or user-centred innovation approach [7].

According to Arnkil et al. [7] it is more useful to talk about different QH models situated along a QH continuum; hence they constructed four different types of QH models -only as ideal-type models-, adequate to provide examples of the possible application of QH. Those types are a) the TH + users model, b) the Firm-centered living lab model, c) the Public-sector-centred living lab model, and d) the Citizen-centered model.

2.2 Measuring Smart City Indicators

Despite the technology involved in the development of smart cities, evaluating one is mainly a manual/assisted process. The methods applied in the revised studies to evaluate indicators aspect are diverse, but belong to one of two groups. On the one hand, there is the systematic qualitative analysis of the literature and

documents generated by the initiative. On the other hand, there are traditional surveys to be answered by involved stakeholders, workshops, focus group, or simply improvised/planned routes [4] through the city while taking pictures and writing down notes [36].

Cohen's wheel applications examples can be found in Bifulco et al. [10], which focus on participative approaches to innovation and city governance. They explore three smart cities in Europe (Amsterdam, Barcelona and Helsinki) through a qualitative content analysis with NVivo software on official documents to analyze the living labs initiatives of the project partners. More recently, Joss et al. [28] examined key texts related to 27 cities worldwide, using a webometric method to measure hit counts produced by searching for the term smart city. Then, they selected 346 online texts and analyzed them quantitatively (co-occurrence analysis) and qualitatively (concordance analysis) using AntConc software, an analysis toolkit for corpus linguistic research.

QH model evaluation examples are similar. Borkowska and Osborne [11] focused their study on the fourth QH model element, civil society. They analyzed the extent to which civil society was involved in the planning, implementation and evaluation of the Glasgow Future City Demonstrator initiative in the UK. As a method, the authors applied four indicators to analyze documentary evidence with the aims to asses the benefits of introducing the QH model into technological initiatives. Indicators were: 1) supporting participation of citizens in the process of decision-making; 2) implementing technological innovation which positions citizens as active users; 3) implementing technological innovation which aims to benefit the community; 4) evaluating technological innovation (based on needs and experiences of citizens).

Also based on the QH model, Chetta et al. [16] present an experimental method tested in the city of Lecce (Italy). In their study authors introduce a vision of the city as a Living Lab where the public is assigned an active role; they explore how the stakeholders (Government, University, Industry, and Citizens), with the support of technological innovation, co-design and co-create integrated services to improve accessibility and social inclusion. They described the implementation of an ICT tool, a web application developed to support citizens active participation called "Lecce 2019-Idea Management System (IMS)".

In another research, the same authors [23] present an audit tool for assessing the quality of urban spaces, in terms of accessibility and walk-ability, called the survey "Conditions of Practicable Environments" (SCOPE). The tool combines secondary, digitized data analysis and on-street surveys to estimate factors determining the potential of the public space to support children's independent activities. The assessment procedure consists of five stages: selection and characterization of the case study; structuring of the evaluation; selection of indicators; data collection and evaluation of indicators; and scoring and aggregation of the indicators.

2.3 Participation Indicator

All of the approaches towards an intelligent inclusive smart city give maximum importance to participation, which we associate to the inclusiveness of a smart city project.

A greater participation implies a lower risk of building a project whose side effects potentially harm or disturbs a part of the population.

In the field of smart cities, QH model involves the participation of people, as users, in the process of design and implementation of public services as well as in the elaboration of policies of regional development or urbanism [7]. Furthermore, this model is in line with the Europe 2020 strategy towards intelligence, sustainable, and inclusive growth [7]. Also, this participation should acknowledge diversity, avoiding segregation of minorities, and trying to eliminate those barriers that make harder such participation, physical or digital [37].

Despite the participation in the governance seems to attract greater attention in the literature, and that the participation has been considered when designing some smart cities, the person dimension is hardly considered. As Oliveira and Kofuji [36] point out, it is even rarer finding studies relative to accessibility and urban digital infrastructure that, in their opinion, it would configure an inclusive smart city. They remark the need of designing products, services, and devices that permit the accessibility of people to all places, information, and services, not only the accessibility of those without impairments.

The accessibility, as a right acknowledged by the UN, it is an instrumental right, since it enables the participation and autonomy. Therefore, it should be seen in a wide sense, beyond the barriers that make more difficult the inclusion of people with functional diversity. Also, they physical, digital, and information/communication barriers should be considered, specially those limiting the participation and autonomy of other persons.

Nevertheless, it is still challenging the inclusion of people with impairments (through assisting technologies, design for all) in terms of accessibility and participation [36,37]. Also, in a lower degree, involving vulnerable or excluded collectives [4,23].

Smart cities, to be inclusive, need to answer the need of persons that inhabit them. Specially those that are part of the most vulnerable groups. Hence, the design and implementation of services and technologies developed will have to monitor who access to them, who don't, and why reason.

The concept of accessibility is non trivial. Geurs and Van Wee [24] determined the notion of accessibility as a social indicator, identifying four components in the accessibility that interact between themselves: the use of terrain, the transport, the time, and the individual. The last is crucial since it represents the features of the persons that influence in their level of accessibility: the needs, the capabilities, and opportunities. The inclusive smart cities need to cover the needs and increment the skills, as well as favoring the economic and social opportunities of the subjects.

There is no doubt that social inclusion is one of the dimensions more relevant to the smart city [3]. Nevertheless, we have seen this notion does not exist in any

theoretical development, technological applications developed for this notion, or even experiences in inclusive smart cities.

3 Technologies applied to Participatory Planning

Leaving aside the characterization of inclusive smart cities, there is still the problem in how to massively increase the participation through technology. A line of work that has explored the collaboration of ICT and participatory methods is *Participatory Planning* in the context of Geographical Information Systems (GIS). The Public Participation GIS (PPGIS), Participatory GIS, and Volunteered Geographic Information methods are participatory processes where the geographic information is nuclear [13]. PPGIS/PGIS promote inclusion, looking for scarcely represented population groups. PPGIS uses random sampling of participants, digital mapping technology and promotes spatial data quality. PGIS uses purposing sampling, non-digital mapping technology and spatial data quality is secondary. VGI accounts events where citizens co-work with geographic information and chooses volunteers with special interest in GIS.

PPGIS is envisioned frequently as an advanced surveying method. Response rates in five different published studies with random household sampling averages 13% when using internet based methods, while paper-based approaches average 30% in 11 studies [13] . This means the PPGIS have similar success rates from survey response rates. And incentives, e.g. vouchers for participating, only raised modest increases.

Web-based PPGIS applications tend to reuse mapping applications and use text questionnaires to which users answer by tagging places on the map and writing comments [9] . In theory, this can be used along the development of a whole urban plan, but it has been applied mainly in early planning stages [13].

Citizen involvement is crucial and not so common. Gil et al. [25] reviews thirteen platforms for citizen participation in decision making processes and classifies them into three categories: government-to-citizen (G2C), citizens-to-government (C2G), government-to-business(G2B), and government-to-government (G2G) services. This is another way of seeing the participation ladder, where the G2C are mostly for consultation (middle tier in the ladder) and C2G implies different degrees of citizen empowerment (higher tier in the ladder).

The technologies used in the thirteen reviewed platforms are diverse [25]: forum with post scoring capabilities (top rated ideas are discussed), form based (e.g. to notify defects in streets combined with GPS coordinates, to collect ideas, to inform about flooding progress in risky areas, to map the occurrence of violence acts), GIS systems (e.g. open-street map), or online 3D games (e.g. second life and leaving comments within the game, virtual world to explore a part of the city and take decisions as in a game).

Falco and Kleinhans similarly review Digital Participatory Platforms (DPPs) implementations and identify 113 active DPPs [20]. Means used to interact with citizens include: "opinion maps, surveys, discussion forums, budget allocation, simulation design, voting and ranking of ideas, analytic, map-based and geo-

located inputs for collaborative mapping such as comments, pins, and other geographical features, crowdfunding, exporting in different formats for further analysis (shape files, csv, kml), importing and media uploading, sharing on other social networking sites such as Facebook and Twitter" [20]. Authors remark the importance of map-based and geo-visualization tools for citizen engagement.

Above mentioned tools can be combined together with classical methods. For instance, the DemoCU framework [44] uses classical (focus group method) and web-based participatory tools. It combines them in a process t. The web-based tool in [44] was map based and was used during four months by consulting the information available from the tool and answering a questionnaire. The questionnaire was filled in by 140 citizens.

The scale of PPGIS is significantly higher than traditional methods with a lower budget. Using tools available from the browser is an advantage with respect paper based or workshop based techniques, but it does not guarantee success. Early works in participatory processes recognized five factors that influenced the success of a participatory method [42]: early involvement of the citizens, independent participation, transparency, representativeness, and influence. Following these criteria can increase the success of a PPGIS initiative [29] but does not guarantee inclusiveness. The experiment in Helsinki [29] involved 3745 participants (a 1% of the population) and there were some collectives underrepresented, such as older people.

The quality and representativeness of results from PPGIS has been addressed already. In the context of GIS, these methods provide higher response rates, lower spatial quality, and still a participation bias risk [12]. Previous PPGIS research determined that random sampling is not representative of the general public since there is a bias towards older more educated male participants with higher incomes. And volunteer sampling is even more biased. Online panels alleviate this problem but bring lower data quality and uncertainty about the representativeness of the panel.

The inclusiveness of PPGIS has been considered too in [26]. The exclusion risk of some collectives, such as older people or other groups with low computer skills or lack of access to computers, is studied. Older adults find issues like lack of experience, concentration, spatial abilities or memory deficiencies, not to mention motor issues related with aging, such as tremors or arthritis, or sensory capabilities. As result, they suggest usability tests for this kind of tools and issue some recommendations on what items to pay attention to.

4 Towards a Method and Tool that Increases Participation

To address better the inclusiveness in smart cities, based on existing research, this section proposes a tool and a method that focuses the barriers identified in the literature, namely obtaining a greater participation than with a survey and increasing the inclusiveness of the surveying method.

The working hypothesis is that a greater participation than in a regular survey could be achieved by a game-based experience. The inclusiveness would be increased by means of a simpler interface, including guidance within the tool, and providing information little by little to the surveyed. Literature already shows the gamification of a survey and showing questions in more original formats should induce a greater answer quality, lower drop out rates, and greater respondent satisfaction [41].

The proposal is not a holistic one in the same sense as [43]. It intends to complement the information obtained from regular methods in an alternative way and, by now, it is an experiment to obtain experimental data about how well game-based surveys work.

The paper proposes a game-based survey will offer the individual a story to play in form of a graphical adventure that recreates situations meaningful for the authorities that want to perform the above-mentioned consultation.

This should potentially create a greater connection with the surveyed individual. Rather than answering questions, the tool intends to create an immersive feeling that allows the surveyed individual to understand better the background of the questions. It requires more time than a regular survey, but it is a method that provides more information per individual and a more positive reward. It is not only the answer to questions, but the actions of the individual while playing what could be analyzed.

The method is oriented specifically to build the material upon which the tool is based. It is necessary due to the complexity of the surveying material.

4.1 Exploring The Gamification of Surveys

From the possible ways to gamify consultation processes, the one proposed here is based on text-adventures. Text-adventures have been used for education [15] though they have been replaced in the last decade with modern game engines that work in 3D or by point-and-click adventures [27].

A combination of text a 2D visuals may achieve a reasonable immersion experience at a reasonable price. Immersion implies attention, an emotional state in response to the story, and a mental construction of the plot [19]. This immersion is greater in 3D games, but in text adventure games could be scored as average [19]. Augmenting the sensory input (e.g. using 3D and voices) may not necessarily create a more immersive experience [21].

Graphic adventures are games that are essentially combines text and graphics to involve the reader in a story. Though graphic adventures have been displaced by other gaming genres, there are available several development kits to easily create them. The one used in this work is Renpy [1]. Renpy is a software that facilitates the creation of text-adventures with custom made interaction methods. Besides, the created games can be built upon different platforms: web, mobile, and desktop platforms. This facilitates reaching a wider audience.

The game is a novel-like story where the reader is presented with an interactive story. The working hypothesis is that by building this story using the case

study information, a greater engagement will be achieved and information with a greater quality will be collected.

Within the game, different statements are added to collect information about the actions of the character. The goal is to build a portfolio of the actions of the volunteers and then analyze their behavior in this context, as in game analytics [34].

The use of real photographs is expected to stimulate the players and to make them more convinced about the experience. This method is very cheap and dialogues are quite straightforward to elaborate. Collecting information from the application is easy as well. Plain Python statements deliver the information to a server where they are stored for later consultation.

About the age barrier, it is harder to overcome. People between 23 to 45 are more likely to answer electronic surveys [2]. This is a barrier to be overcome through recommendations on the [32] and the use of warm colors and combinations of large icons. Again, the use of pictures and short messages should facilitate the adoption by people with low experience with technology. Also, we expect the diversity in the deployment platforms for this Renpy software helps reaching at least one media that is frequently used by the respondents.

4.2 Planning the experiment

To determine in what ways the quality of the daily living of people is altered, it is necessary to have the opinion of those that would benefit or prejudice from those improvements, specially those with special accessibility needs.

The study of the indicators from section 2 should give clues on what areas a smart city project affects. The study of each indicator is linked with the preparation of the massive consultation itself.

This massive survey would be part of a multi-method approach, combining classic offline techniques and online ones that could be performed in parallel. Among such techniques we consider: Document analysis techniques (e.g. revision of bibliography, content analysis, reports, or statistical data, among others); qualitative techniques (participatory census, open interviews, focus group, delphi method, to cite some); quantitative techniques (detailed analysis of the different mentioned sources to measure the interest of each actuation of the project).

The application of previously cited methods helps to model the massive survey. The preparation of the survey includes what questions to make and how to make them. In the case of text adventures, it is necessary to prepare a script that describes the characters that will be impersonated by the respondents. This script should allocate actions that help to collect the necessary information.

Given that there are different stakeholders in a smart city project, it should be expected either several stories, one per stakeholder, or a few complex one combining perspectives from different actors.

5 A brief case study introduction

The problem studied for this example is the case of the Politics and Sociology Faculty in the Universidad Complutense of Madrid. The goal is to find out how to use the different spaces in the faculty, perhaps as co-creation places inside or outside the building.

The problem is still an open one. Some uses have already been applied, such as the case of the market garden "La oprimida" (the oppressed). We include this one, since it is known how it came to exist, and reflex upon the process that led to decide this initiative was the one needed and not other.

This problem involves different stakeholders: professors, students, maintenance staff (they take care of the spaces), administrative staff (they validate what uses of the building spaces are economically sustainable), and building caretakers (they prepare rooms for the lectures and will be involved in the daily operation of the spaces). To understand the different backgrounds, different stories could be elaborated, one per stakeholder.

In this case, we focus on the case of the student. Our character in the game goes through different situations that forces us to decide what to do. The daily living activities programmed in the game makes the player visit the different relevant places (e.g. the parking lot in figure 1) and ask questions when sufficient information has been supplied.

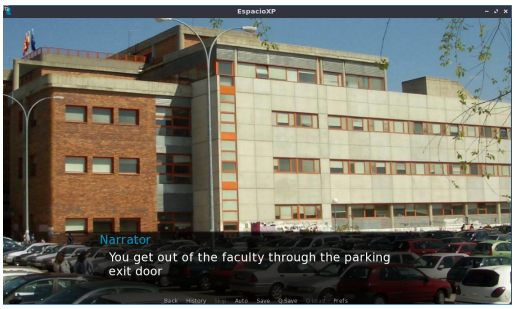

Fig. 1. The character of the game gets out of the building

In the figure 2, the avatar of the game is programmed to ask us to explore the different spaces to get an idea of the possibilities. Inside the building, the student sees faculty corridors, classrooms, meeting rooms, auditoriums, the cafeteria, and the "agora" (an open auditorium connected to the main building).

When exploring the outside, we are guided to the market garden option. As in PPGIS, some project require complex input from the user. Figure 3 illustrates how the user suggests a position for the location of the market garden. This is made after the user is forced to travel through the locations, inspecting the pictures and recreating a walk from the faculty to the bus. In this case, we

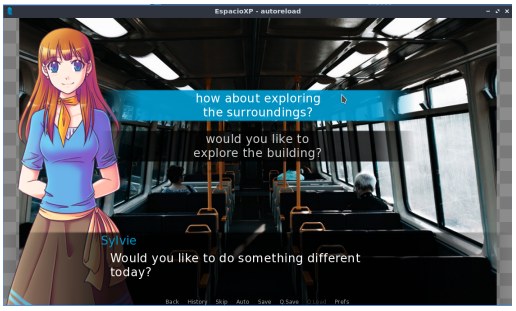

Fig. 2. Our guest in the game asks us to choose what to do now

are interested in knowing which location, from the available ones, stakeholders prefer. Therefore, one of the situations requires placing a garden somewhere around the faculty.

Fig. 3. An interaction example where the player picks a place in the map to allocate a garden

Besides obtaining specific information, such as the location of the market garden from figure 3, the interaction with the tool will generate additional activity information. For instance, how long did the respondent took to move from one place to another in the game, if the respondent explored all the options, which ones where explored first, to cite some. This information can help understanding better the answers provided by the respondent. Also, we expect a greater quality in the answers because respondents will process more information before answering. This is also a risk, since it will take more time to answer and this may increase the drop rate. We expect field experiments will answer this and generate additional empirical information.

6 Conclusions

The paper has introduced the citizen involvement problem in decision making processes in the context of smart cities. In particular, it has been addressed the e-governance problem and how citizens could participate. Different methods have been surveyed concluding that most of them are in fact surveys presented in different formats, including online ones, but that achieve similar ratio of respondents despite the format.

The paper has proposed to explore the use of mixed graphical adventures to obtain information from citizens. This alternative should create a greater engagement than a regular survey and provide with information on how the respondents performed during the experiment. The technology used for this tool was based on a software specialized in the creation of game adventures that can be ported to multiple platforms.

Acknowledgements

This work was possible thanks to the funding from: "Diseño colaborativo para la promoción del bienestar en ciudades inteligentes inclusivas" (TIN2017-88327-R); the thematic network "CIUDADES INTELIGENTES TOTALMENTE INTEGRALES, EFICIENTES Y SOSTENIBLES" (518RT0558), funded by CYTED (Programa Iberoamericano de Ciencia y Tecnología para el Desarrollo), and "Research Thematic Network on Smart Cities" (TIN2016-81766-REDT) funded by Spanish Ministry for Economy and Competitiveness.

References

1.
2. Alam, I., Khusro, S., Rauf, A., Zaman, Q.: Conducting surveys and data collection: From traditional to mobile and sms-based surveys. Pakistan Journal of Statistics and Operation Research **10**(2), 169–187 (2014)
3. Albino, V., Berardi, U., Dangelico, R.M.: Smart cities: Definitions, dimensions, performance, and initiatives. Journal of urban technology **22**(1), 3–21 (2015)
4. Annunziata, A., Garau, C.: Understanding kid-friendly urban space for a more inclusive smart city: The case study of cagliari (italy). In: International Conference on Computational Science and Its Applications. pp. 589–605 (2018)
5. Anttiroiko, A.V., Valkama, P., Bailey, S.J.: Smart cities in the new service economy: building platforms for smart services. Ai & Society **29**(3), 323–334 (2014)
6. Arata III, H.J., Hale, B.L.: Smart bases, smart decisions. The Cyber Defense Review **3**(1), 69–78 (2018)
7. Arnkil, R., Järvensivu, A., Koski, P., Piirainen, T.: Exploring quadruple helix outlining user-oriented innovation models (2010)
8. Arnstein, S.R.: A ladder of citizen participation. Journal of the American Institute of planners **35**(4), 216–224 (1969)
9. Babelon, I., Ståhle, A., Balfors, B.: Toward cyborg ppgis: exploring socio-technical requirements for the use of web-based ppgis in two municipal planning cases, stockholm region, sweden. Journal of Environmental Planning and Management **60**(8), 1366–1390 (2017)

10. Bifulco, F., Tregua, M., Amitrano, C.C.: Co-governing smart cities through living labs. top evidences from eu. Transylvanian Review of Administrative Sciences **13**(50), 21–37 (2017)
11. Borkowska, K., Osborne, M.: Locating the fourth helix: Rethinking the role of civil society in developing smart learning cities. International Review of Education **64**(3), 355–372 (2018)
12. Brown, G.: A review of sampling effects and response bias in internet participatory mapping (ppgis/pgis/vgi). Transactions in GIS **21**(1), 39–56 (2017)
13. Brown, G., Kyttä, M.: Key issues and research priorities for public participation gis (ppgis): A synthesis based on empirical research. Applied geography **46**, 122–136 (2014)
14. Caragliu, A., Del Bo, C., Nijkamp, P.: Smart cities in europe. Journal of urban technology **18**(2), 65–82 (2011)
15. Cavallari, B., Heldberg, J., Harper, B.: Adventure games in education: A review. Australasian journal of educational technology **8**(2) (1992)
16. Chetta, V., Marasso, L., Giangreco, E., Storelli, D., Camillò, A., Turrisi, G., Antonucci, G., Barile, M., Centrone, B., Papadia, D., Francesco, S.: Idea management system for smart city planning. Interdisciplinary Studies Journal (ISJ) (01 2014)
17. Chourabi, H., Nam, T., Walker, S., Gil-Garcia, J.R., Mellouli, S., Nahon, K., Pardo, T.A., Scholl, H.J.: Understanding smart cities: An integrative framework. In: 2012 45th Hawaii international conference on system sciences. pp. 2289–2297. IEEE (2012)
18. Cohen, B.: The smartest cities in the world 2015: Methodology. urlhttps://www.fastcompany.com/3038818/the-smartest-cities-in-the-world-2015-methodology (2014), accedido 19-03-2019
19. Dillon, T.: Adventure games for learning and storytelling. UK, Futurelab Prototype Context Paper, Adventure Author (2005)
20. Falco, E., Kleinhans, R.: Digital participatory platforms for co-production in urban development: A systematic review. In: Crowdsourcing: Concepts, Methodologies, Tools, and Applications, pp. 663–690. IGI Global (2019)
21. Gander, P.: Two myths about immersion in new storytelling media. Lund University (1999)
22. Garau, C.: Citizen participation in public planning: A literature review. International Journal of Sciences **1**(12), 1–24 (2012)
23. Garau, C., Annunziata, A., Coni, M.: A methodological framework for assessing practicability of the urban space: The survey on conditions of practicable environments (scope) procedure applied in the case study of cagliari (italy). Sustainability **10**(11), 4189 (2018)
24. Geurs, K.T., van Wee, B.: Accessibility evaluation of land-use and transport strategies: Review and research directions. Journal of Transport Geography **12**(2), 127–140 (2004)
25. Gil, O., Cortés-Cediel, M.E., Cantador, I.: Citizen participation and the rise of digital media platforms in smart governance and smart cities. International Journal of E-Planning Research (IJEPR) **8**(1), 19–34 (2019)
26. Gottwald, S., Laatikainen, T.E., Kyttä, M.: Exploring the usability of ppgis among older adults: challenges and opportunities. International Journal of Geographical Information Science **30**(12), 2321–2338 (2016)
27. Hainey, T., Connolly, T.M., Boyle, E.A., Wilson, A., Razak, A.: A systematic literature review of games-based learning empirical evidence in primary education. Computers & Education **102**, 202–223 (2016)

28. Joss, S., Sengers, F., Schraaven, D., Caprotti, F., Dayot, Y.: The smart city as global discourse: Storylines and critical junctures across 27 cities (2018)
29. Kahila-Tani, M., Broberg, A., Kyttä, M., Tyger, T.: Let the citizens map—public participation gis as a planning support system in the helsinki master plan process. Planning Practice & Research **31**(2), 195–214 (2016)
30. Kakderi, C.: Inclusive smart cities: a european manifesto on citizen engagement. retrieved january 4, 2018 (2017)
31. Khanna, R., Kaur, H.: Smart cities – the future of world. International Journal of Advanced Research in Computer Science **8**(4) (2017)
32. Lumsden, J., Flinn, S., Anderson, M., Morgan, W.: What difference do guidelines make? an observational study of online-questionnaire design guidelines put to practical use. In: People and Computers XIX—The Bigger Picture, pp. 69–83. Springer (2006)
33. Manitiu, D.N., Pedrini, G.: Urban smartness and sustainability in europe. an ex ante assessment of environmental, social and cultural domains. European Planning Studies **24**(10), 1766–1787 (2016)
34. Medler, B.: Generations of game analytics, achievements and high scores. Eludamos. Journal for Computer Game Culture **3**(2), 177–194 (2009)
35. Nam, T., Pardo, T.A.: Conceptualizing smart city with dimensions of technology, people, and institutions. In: Proceedings of the 12th Annual International Digital Government Research Conference on Digital Government Innovation in Challenging Times. pp. 282–291 (2011)
36. de Oliveira Neto, J.S., Kofuji, S.T.: Inclusive smart city: an exploratory study. In: International Conference on Universal Access in Human-Computer Interaction. pp. 456–465. Springer (2016)
37. de Oliveira Neto, J.S., Kofuji, S.T.: Inclusive smart city: Expanding design possibilities for persons with disabilities in the urban space. In: 2016 IEEE International Symposium on Consumer Electronics (ISCE). pp. 59–60 (2016)
38. Palvia, S.C.J., Sharma, S.S.: E-government and e-governance: definitions/domain framework and status around the world. In: International Conference on E-governance. pp. 1–12. No. 5 (2007)
39. Paskaleva, K., Evans, J., Martin, C., Linjordet, T., Yang, D., Karvonen, A.: Data governance in the sustainable smart city. In: Informatics. vol. 4, p. 41. Multidisciplinary Digital Publishing Institute (2017)
40. Pipan, T.: Interactive tangible planning support systems and politics of public participation. Urbani izziv **29**, 63–78 (2018)
41. Roberts, C.: Participation and engagement in web surveys of the general population: An overview of challenges and opportunities. Tech. rep., ESRC; National Centre for Research Methods (2013)
42. Rowe, G., Frewer, L.J.: Public participation methods: A framework for evaluation. Science, technology, & human values **25**(1), 3–29 (2000)
43. Stratigea, A., Papadopoulou, C.A., Panagiotopoulou, M.: Tools and technologies for planning the development of smart cities. Journal of Urban Technology **22**(2), 43–62 (2015)
44. Stratigea, A., Somarakis, G., Panagiotopoulou, M.: Smartening-up communities in less-privileged urban areas—the democu participatory cultural planning experience in korydallos—greece municipality. In: Smart Cities in the Mediterranean, pp. 85–111. Springer (2017)
45. Zygiaris, S.: Smart city reference model: Assisting planners to conceptualize the building of smart city innovation ecosystems. Journal of The Knowledge Economy **4**(2), 217–231 (2013)

Assessing Optimal Placement Algorithms of Phasor Measurement Units for State Estimation

Hatim G. Abood[1][1], Ghassan A. Salman[1] and Hassan Al-Saadi[2]

[1] College of Engineering, University of Diyala, Baqubah, Iraq
[2] Shool of Electrical and Electronic Engineering, University of Adelaide, Australia
[1] hatim.abood@gmail.com

Abstract. Power System State estimation utilizes the available measurements to estimate the state of the system, which is necessary for modern power grids. Hence, obtaining an accurate and stable state estimator is the main objective to most of the meter placement studies that are related to the state estimation. However, Smart Grids have recently started employing advanced meters such as the Smart meters and the Phasor Measurement Units (PMUs). However, a clear majority of the existing PMUs placement algorithm discards the quality of the state estimation solution and focus only on achieving a completely observable system. This leads to creating non-realistic meter configuration as the power systems have already their own measurement set, and hence, the optimal placement algorithms should concern the normal configuration of the power networks before suggesting a new scheme. This paper investigates the validity of the existing optimal placement techniques and their response to the requirements of the state estimation solution and provides suggestion to the practical placement strategies. The paper compares 25 of the top-cited papers in the research area of PMU optimal placement and assess the objectives of these papers in terms of the power system state estimation.

Keywords: Measurement Redundancy, Meter Placement, Observability, Phasor Measurement Unit (PMU).

1 Introduction

The operation of the power system State Estimation (SE) is employed by the Energy Management System (EMS) as a part of the wide-area monitoring and control activities [1]. The state of a power system includes the voltage magnitudes and the phase angles of the all the system's buses [2]. The estimated states facilitate the decisions of the monitors regarding the different contingency events. However, the state estimator using the iterative Weighted Least Square (WLS) problem that is sensitive to round-off errors and it is affected by the types and the numbers of the measurements. Hence, an accurate SE needs optimal meter placement strategies.

The state estimator utilizes the available measurements set for producing the state estimation solution. If the available measurements are sufficient to estimate the state of each bus, the system is declared to be observable [3]. The conventional measurements

set can be measured by the power injection (active/reactive) meters, the power flow (active/reactive) meters, the voltage meters, and the current magnitude meters. The state estimator gathered the measurements from different locations in the power system via SCADA system. However, the conventional meters are not efficient regarding the robust monitoring, the contingency conditions, and the dynamic state estimation. Hence, recently, the Phasor Measurement Units (PMUs) became highly demanded by the power systems applications, especially, the Smart Grids applications [4]. In addition to the EMS, the Distribution Management System (DMS) became necessary for the active distribution grids. The PMU provides accurate and instantaneous measurements using the GPS. However, optimal placement strategies need to be achieved for determining the optimal numbers and locations of those expensive devices, i.e., the Optimal PMU Placement (OPP) [5].

The problem of OPP has been investigated in an enormous number of articles in terms of several power systems applications [5], [6]. However, most of the available OPP studies have no concerns about the quality of the SE solution; even that articles hold the "state estimation" in their titles [7]. Moreover, they do not consider the available conventional measurements in the power system. Rather, most OPP studies try to re-design the configuration of the meter from scratches.

This paper is part of a multi-stage research that focuses on the discrepancy between implementing robust and accurate power system state estimators for the modern distribution systems and the studies that discard the multi-objective problem of the PMUs placement. Accordingly, this paper presents a critical review and comparisons to available placement algorithms and their optimization constraint. Moreover, the mathematical background of SE solution, the derivation of the OPP algorithm, and the different objective functions are presented in this paper.

2 Formulation of WLS State Estimator

The conventional nonlinear WLS state estimator is based on the following formula [8]:

$$z = h(x) + \varepsilon \tag{1}$$

where z is the measurement vector, x is th state vector, $h(x)$ is a nonlinear vector function, ε is theerror vector.

The solution of (1) is the WLS estimation of x. The aim is to obtain the value of estimated state x that minimize $J(x)$. Hence, the objective function can be rewritten as follows [9-11]:

$$J(x) = (z - H(x))^T W (z - H(x))$$

The solution is subjected to the first-order optimality condition, which is:

$$\underset{x}{H^T} W[z - H(x)] = 0$$

where H_x is the measurements Jacobian matrix. However, the H_x is used in early in the linear state estimation. In linear (non-iterative) the Jacobian matrix is used directly in (1) instead of $h(x)$. That means all the collected measurements are stable and as accurate as the PMU and not a time varying. This is the first objection that turns the OPP to be a non-realistic optimization approach [12]. Thus, linear state estimation sacrifices the accuracy [12],[13]. Nevertheless, the final form of both the state estimators is the same:

$$G(x^k)\Delta x^k = H^T R^{-1} [z - h(x^k)] \quad (2)$$

where x^k refers to the value of state x at the kth iteration and $G(x^k)$ is known as the gain matrix for the kth iteration. The gain matrix should be square, positive definite and symmetrical for observable systems [11].

3 Objectives of PMU Placement Studies

Utilizing the advance PMUs with their communication channels need to be justified. Hence, it is agreed that the OPP is a multi-objective problem and, thus more than one constraint should be considered in the optimization algorithm [15]. This section focuses on the common objectives of the OPP problem relevant to the state estimation.

3.1 Power System Observability

Achieving a complete observability for the power systems is the main objective of any meter's placement algorithm. However, regarding the state estimation problem, there are two types of observability can be implemented, the numerical observability and the topological observability [16]. The numerical observability of a power system is achieved when the Jacobian matrix has a full rank, which is equal to the state vector. However, this analysis might complicate the placement algorithm due to the rank checking that requires building the measurements Jacobian matrix.

On the other hand, the most efficient approaches of observability assessment is the topological one since it is a graph-based process. Hence, the observability status can be identified without the full Jacobian matrix. The configuration of the power system and its connectivity reflect the necessary PMUs configuration. From the Graph-Theory perspective, if all the buses and the lines of a power system are included in a graph $G(N, B)$ such that N is the graph nodes, and B is the graph branches, the power system is declared to be observable topologically [17].

On the other hand, the topological observability can be achieved using a minimal number of PMUs when using the electrical circuits' laws. The Ohm's law and Kirchhoff's laws (KCL and KVL) can substitute many missing measurements, and thereby. That means, the vertices and the nodes of $G(N,B)$ can be observed either directly, or indirectly using the measured quantities of the adjacent buses/branches [19]. In this approach, the directly observable buses/branches belong to the nodes connected to the PMUs [18]. The indirectly observable buses/branches are those can be deduced from the available real-time measurements. The electrical circuits' laws as follows [19]:

Rule 1: Any bus can be observable if it is connected to a PMU bus. This is determined by the Ohm's and KCL laws.

Rule 2: Any branch between two observed buses is, in turn, observable (Ohm's law).

Rule 3: Any branch current can be computed using KCL law if all the incident branches are measured.

Regarding the optimal placement algorithms for a complete observability, the following procedure, which starts with connectivity matrix, is the most used in the literature:

$$C_{i,j}=\begin{cases}1 & , \text{ if } i=j \text{ or if } i \text{ and j are connected} \\ 0 & , \text{ otherwise}\end{cases}$$

where C is the connectivity matrix that reflects the system's configuration. Then, the placement algorithm is as follows; this placement algorithm can be named as the connectivity-based optimization [19], [20]:

$$min \sum_1^N p_i$$

$$s.t. \;\; C.P \geq \bar{\mathrm{R}}$$

$$P = [p_1, p_2, \dots, p_n]^T$$

$$p_i \in \{0,1\}$$

where P is a decision vector whose entries are zero and ones based on the presence of PMUs and $\bar{R}$ is a small natural value (such as one or two) that refers to the number of times each bus is observed by a PMU. For increasing the local redundancy, in the case of contingency, the value of $\bar{R}$ can be two or three. The final solution of PMU placement problem is based on the number of ones that appear in the x vector. However, this placement approach aims to obtain bus/branch combinations that make the whole system monitored by the PMUs only.

The above constraint can be employed to express the required level of the measurements' redundancy which crucial for contingency analysis. This can be carried out easily by changing the value of to be more than one, which refers to more redundant PMUs. However, the optimal solution should satisfy the f (p) such that.

$$f(p) = N_{bus} - N_{obv} = 0 \tag{3}$$

where N_{obv} refers to the observable buses which is eventually should be equal to the buses number. indented.

3.2 Contingency and Measurement Redundancy

Placement of PMUs for contingency purposes seems to be irrelevant to the state estimation; yet, in the OPP it is associated with the redundancy rate which is, in turn, related to the measurements used for the state estimation. Any robust meter placement configuration needs to consider the case of meters failure, single power line outage, and outages of multiple lines. The available solution for meters and line outages is to increase the PMUs numbers or to changes their location in such a way that increases the

measurements redundancy [21], [16,22]. The measurements redundancy aims to provide more meters for the same quantity. Increasing the local redundancy can be beneficial in the case of failure, but it contributes to the numerical instability of the SE solution [17]. Thus, this is the bad impact of most of the optimistic PMUs placement techniques. This process may be influential by increasing the required numbers of PMUs in the large-scale networks.

3.3 Requirements of Security and Bad Data Detection

This objective is essential for improving the quality of the SE solution. Nevertheless, the top-cited articles of PMUs placement rarely consider this aim as one of their fitness function constraints [5]. However, recently, the placement studies started considering the Bad Data Detection (BDD) and the cyber-attack as constraints in their objective functions [23]. Yet, the studies concern facilitating the BDD mainly come as incremental PMUs placement algorithms, i.e., not an explicit OPP problem.

4 Comparative Case Studies

The authors explored the top-cited literature associated with the OPP problem in state estimation as those papers have attached the research topics of thousands of papers. The comparative study of this paper is based on the top 25 papers that have published under the title of "optimal phasor measurements placements for state estimation" and other similar titles. According to the authors' investigations, around 5000 articles are based on those 25 papers. Thus, they influence the trends of the OPP studies dramatically.

The main observation is that all the most cited papers are interested in the observability problem as the objective function of the PMU placement algorithms. Table 1 illustrates the major features of the articles are related to this study. However, different types of observability (numerical and topological) have been investigated in those papers. Therefore, other placement objectives that are discussed in section 3 have a marginal appearance in the pioneer papers.

On the other hand, Table 2 shows statistics about the algorithms that have been employed in the most cited papers. It is obvious that most of the paper uses the algorithm of section 2. Although the search has been extended to include any PMU placement literature, the concentration of the most cited papers is one optimizing the PMUs configuration based on the most-connected bus/branch technique of section 2.

Table 1. Main objectives of top-cited papers.

Articles with connectivity-based optimization algorithms	Articles consider other optimization objectives	Articles consider BDD
[17], [24–45] (All)	[26], [28], [30–31], [33–35], [36], [40]	[30], [33], [40]

Table 2. Main objectives of OPP studies.

Paper	Observability	Contingency	Quality and BDD
[17]	✓		
[24]	✓		
[25]	✓		
[26]	✓	✓	
[27]	✓		
[28]	✓	✓	
[29]	✓		
[30]	✓		✓
[31]	✓	✓	
[32]	✓		
[33]	✓		✓
[34]	✓	✓	
[35]	✓	✓	
[20]	✓		
[36]	✓	✓	
[37]	✓		
[21]	✓	✓	
[38]	✓		
[39]	✓		
[40]	✓	✓	✓
[41]	✓		
[42]	✓	✓	
[43]	✓	✓	
[44]	✓		
[45]	✓		

5 Conclusion

This paper provides a critical review to the studies of the optimal PMU placement in terms of the state estimation problem. Moreover, comparisons of the characteristics of the placement algorithms of the most cited papers are presented in this paper. The comparisons show that the common optimistic philosophy of the OPP problem cannot respond efficiently respond to the requirements of the grown smart grids. Thus, incremental placement strategies are recommended for more comprehensive placement algorithms.

References

1. M. E. Baran and A. W. Kelley, "State estimation for real-time monitoring of distribution systems," Power Systems, IEEE Transactions on, vol. 9, pp. 1601-1609, 1994.
2. C. N. Lu, J. H. Teng, and W. H. E. Liu, "Distribution System State Estimation," IEEE Transactions on Power systems, vol. 10, pp. 229-240, February 1995.
3. B. Xu and A. Abur, "Observability analysis and measurement placement for systems with PMUs," presented at the Power Systems Conference and Exposition, 2004. IEEE PES 2004.
4. A. G. Phadke, "SYNCHRONIZED PHASOR MEASUREMENTS - A HISTORICAL OVERVIEW," presented at the Transmission and Distribution Conference and Exhibition 2002:Asia Pacific. IEEE/PES 6-10 Oct. 2002.
5. N. M. Manousakis, G. N. Korres, and P. S. Georgilakis, "Taxonomy of PMU Placement Methodologies," Power Systems, IEEE Transactions on, vol. 27, pp. 1070-1077, May 2012.
6. H. G. Abood and V. Sreeram, "A review on phasor measurement units placement for state estimation studies," in Power Engineering Conference (AUPEC), 2014 Australasian Universities, 2014, pp. 1-6.
7. W. Jiang and V. Vittal, "Optimal Placement of Phasor Measurements for the Enhancement of State Estimation," in Power Systems Conference and Exposition, 2006. PSCE '06. 2006 IEEE PES, Oct. 29 2006-Nov. 1 2006, pp. 1550-1555.
8. M. E. Baran, J. Zhu, H. Zhu, and K. E. Garren, "A METER PLACEMENT METHOD FOR STATE ESTIMATION," IEEE Transactions on Power systems, vol. 10, pp. 1704-1710, August 1995.
9. J. J. Grainger and W. D. Stevenson, Power system analysis vol. 621. New York: McGraw-Hill, 1994.
10. A. Abur and A. G. Exposito, Power System State Estimation Theory and Implementation: CRC Press, 2004.
11. F. C. Schweppe and J. Wildes, "Power System Static-State Estimation, Part I: Exact Model," Power Apparatus and Systems, IEEE Transactions on, vol. PAS-89, pp. 120-125, 1970.
12. D. A. Haughton and G. T. Heydt, "A Linear State Estimation Formulation for Smart Distribution Systems," Power Systems, IEEE Transactions on, vol. 28, pp. 1187-1195, 2013.
13. H. G. Abood, V. Sreeram, and Y. Mishra, "A new algorithm for improving the numerical stability of power system state estimation," IEEJ Transactions on Electrical and Electronic Engineering 14, no. 3 (2019): 358-365.
14. S. C. Tripathy, D. S. Chauhan, and G. D. Prasad, "State estimation algorithm for ill-conditioned power systems by Newton's method," International Journal of Electrical Power & Energy Systems, vol. 9, pp. 113-116, 4// 1987.
15. S. Chakrabarti, E. Kyriakides, G. Ledwich, and A. Ghosh, "Inclusion of PMU current phasor measurements in a power system state estimator," Generation, Transmission & Distribution, IET, vol. 4, pp. 1104-1115, 2010.
16. S. M. Mazhari, H. Monsef, and A. Fereidunian, "A Multi-Objective PMU Placement Method Considering Measurement Redundancy and Observability Value Under Contingencies," Power Systems, IEEE Transactions on vol. 28, pp. 2136-2146, 2013.
17. T. L. Baldwin, L. Mili, M. B. J. Boisen, and R. Adapa, "Power system observability with minimal phasor measurement placement," Power Systems, IEEE Transactions on, vol. 8, pp. 707-715, May 1993.
18. B. Xu and A. Abur, "Observability analysis and measurement placement for systems with PMUs," in Power Systems Conference and Exposition, 2004. IEEE PES, 10-13 Oct. 2004, pp. 943-946.

19. H. G. Abood, V. Sreeram, and Y. Mishra, "Optimal placement of PMUs using river formation dynamics (RFD)," in 2016 IEEE International Conference on Power System Technology (POWERCON), 2016, pp. 1-6.
20. B. Gou, "Optimal placement of PMUs by integer linear programming," IEEE Transactions on power systems, vol. 23, pp. 1525-1526, 2008.
21. S. Chakrabarti, E. Kyriakides, and D. G. Eliades, "Placement of synchronized measurements for power system observability," IEEE Transactions on Power Delivery, vol. 24, pp. 12-19, 2009.
22. M. Esmaili, K. Gharani, and H. A. Shayanfar, "Redundant observability PMU placement in the presence of flow measurements considering contingencies," Power Systems, IEEE Transactions on, vol. 28, pp. 3765-3773, 2013.
23. A. Majumdar and B. C. Pal, "Bad Data Detection in the Context of Leverage Point Attacks in Modern Power Networks," IEEE Transactions on Smart Grid, vol. PP, pp. 1-1, 2016.
24. K.-S. Cho, J.-R. Shin, and S. H. Hyun, "Optimal placement of phasor measurement units with GPS receiver," in Power Engineering Society Winter Meeting, 2001. IEEE, 2001, pp. 258-262.
25. F. J. Marin, F. Garcia-Lagos, G. Joya, and F. Sandoval, "Genetic algorithms for optimal placement of phasor measurement units in electrical networks," Electronics Letters, vol. 39, pp. 1403-1405, 2003.
26. B. Milosevic and M. Begovic, "Nondominated sorting genetic algorithm for optimal phasor measurement placement," IEEE Transactions on Power Systems, vol. 18, pp. 69-75, 2003.
27. B. Xu and A. Abur, "Observability analysis and measurement placement for systems with PMUs," in Power Systems Conference and Exposition, 2004. IEEE PES, 2004, pp. 943-946.
28. X. Bei, Y. J. Yoon, and A. Abur, "Optimal placement and utilization of phasor measurements for state estimation," PSERC Publication, pp. 05-20, 2005.
29. R. F. Nuqui and A. G. Phadke, "Phasor measurement unit placement techniques for complete and incomplete observability," IEEE Transactions on Power Delivery, vol. 20, pp. 2381-2388, 2005.
30. J. Chen and A. Abur, "Placement of PMUs to enable bad data detection in state estimation," IEEE Transactions on Power Systems, vol. 21, pp. 1608-1615, 2006.
31. J. Peng, Y. Sun, and H. F. Wang, "Optimal PMU placement for full network observability using Tabu search algorithm," International Journal of Electrical Power & Energy Systems, vol. 28, pp. 223-231, 2006.
32. M. Hajian, A. M. Ranjbar, T. Amraee, and A. R. Shirani, "Optimal placement of phasor measurement units: Particle swarm optimization approach," in Intelligent Systems Applications to Power Systems, 2007. ISAP 2007. International Conference on, 2007, pp. 1-6.
33. W. Jiang, V. Vittal, and G. T. Heydt, "A distributed state estimator utilizing synchronized phasor measurements," IEEE Transactions on Power Systems, vol. 22, pp. 563-571, 2007.
34. C. Rakpenthai, S. Premrudeepreechacharn, S. Uatrongjit, and N. R. Watson, "An optimal PMU placement method against measurement loss and branch outage," IEEE transactions on power delivery, vol. 22, pp. 101-107, 2007.
35. S. Chakrabarti and E. Kyriakides, "Optimal placement of phasor measurement units for power system observability," IEEE Transactions on power systems, vol. 23, pp. 1433-1440, 2008.
36. B. Gou, "Generalized integer linear programming formulation for optimal PMU placement," IEEE Transactions on Power Systems, vol. 23, pp. 1099-1104, 2008.
37. F. Aminifar, C. Lucas, A. Khodaei, and M. Fotuhi-Firuzabad, "Optimal placement of phasor measurement units using immunity genetic algorithm," IEEE Transactions on power delivery, vol. 24, pp. 1014-1020, 2009.

38. A. G. Phadke, J. S. Thorp, R. F. Nuqui, and M. Zhou, "Recent developments in state estimation with phasor measurements," in Power Systems Conference and Exposition, 2009. PSCE'09. IEEE/PES, 2009.
39. F. Aminifar, A. Khodaei, M. Fotuhi-Firuzabad, and M. Shahidehpour, "Contingency-constrained PMU placement in power networks," IEEE Transactions on Power Systems, vol. 25, pp. 516-523, 2010.
40. S. Chakrabarti, E. Kyriakides, G. Ledwich, and A. Ghosh, "Inclusion of PMU current phasor measurements in a power system state estimator," IET generation, transmission & distribution, vol. 4, pp. 1104-1115, 2010.
41. J. De La Ree, V. Centeno, J. S. Thorp, and A. G. Phadke, "Synchronized phasor measurement applications in power systems," IEEE Transactions on Smart Grid, vol. 1, pp. 20-27, 2010.
42. R. Emami and A. Abur, "Robust measurement design by placing synchronized phasor measurements on network branches," IEEE Transactions on power systems, vol. 25, pp. 38-43, 2010.
43. A. Ahmadi, Y. Alinejad-Beromi, and M. Moradi, "Optimal PMU placement for power system observability using binary particle swarm optimization and considering measurement redundancy," Expert Systems with Applications, vol. 38, pp. 7263-7269, 2011.
44. M. Hajian, A. M. Ranjbar, T. Amraee, and B. Mozafari, "Optimal placement of PMUs to maintain network observability using a modified BPSO algorithm," International Journal of Electrical Power & Energy Systems, vol. 33, pp. 28-34, 2011.
45. D. H. Tungadio, J. A. Jordaan, and M. W. Siti, "Power system state estimation solution using modified models of PSO algorithm: Comparative study," Measurement, vol. 92, pp. 508-523, 2016.

The Influence of Facility Location on the Sustainability of Smart Cities: Current Literature Analysis

Eduardo do Carmo Marques[1,3] Vanessa de Almeida Guimarães Guimarães [2,3]

[1] Polytechnic Institute of Bragança, Campus of Santa Apolónia, Bragança 5300253, Portugal
[2] Alberto Luiz Coimbra Institute of Engineering Graduate and Research, Rio de Janeiro 21941450, Brazil
[3] Celso Suckow da Fonseca Federal Center, Angra dos Reis. 522,23953030 Rio de Janeiro, Brazil
eduardo.dc.marques@alunos.ipb.pt
vguimaraes@id.uff.br

Abstract. The theme "Smart Cities" has been a subject very much addressed over the last few years in the literature and especially in major world organizations. The big search for modern urban infrastructure depends on a few factors to make it work better, one of which is the facility location in which involving intermodal terminals and basic transportation services to society. However, the sustainable aspect must be a condition allied with this content.
Based on this theme, this research aims to investigate the most recent studies involving facility location reconciled sustainability themes and smart cities, in order shown and analyze the most recent studies in area and how can they help in concept of smart cities. As results, is that in the bibliographic search the scarcity in the literature is remarkable studies that can involve the three pillars of sustainability, and that number is around 7% of all reports have been studied smart cities. However, the inclusion of facility location and intermodality improved in environmental and social aspects the life of the population as can be analyzed in the studies that were investigated in this article

Keywords: Smart Cities, Facility Location, Sustainability.

1 Introduction

The concept of smart cities has been used a lot in congresses, public and private forums and in international companies [1]. The expression “smart” has become an important symbol of the century XXI, together with this the “sustainability” is a worldwide concern, facts that make the importance of these two assumptions for the actual days.

For the term smart cities there are some definitions that best describe the actual context of the word, among them, “smart city is the that one who utilize the technology for provide the best urban services, improve the quality life of the citizens and transform the relationship with local entities, citizens, companies, easing the life mode” [1],

"Smart city as a high-tech intensive and advanced city that connects people, information and city elements using new technologies in order to create a sustainable, greener city, competitive and innovative commerce, and an increased life quality" [2], "Smart Cities initiatives try to improve urban performance by using data, information and information technologies (IT) to provide more efficient services to citizens, to monitor and optimize existing infrastructure, to increase collaboration among different economic actors, and to encourage innovative business models in both the private and public sectors" [3], and many others.

It's possible to see in many different definitions, the authors used familiar words like "sustainable"; "improve the citizens life" and "increase economic", these three terms send us to the triple bottom of sustainability (See Fig. 1).

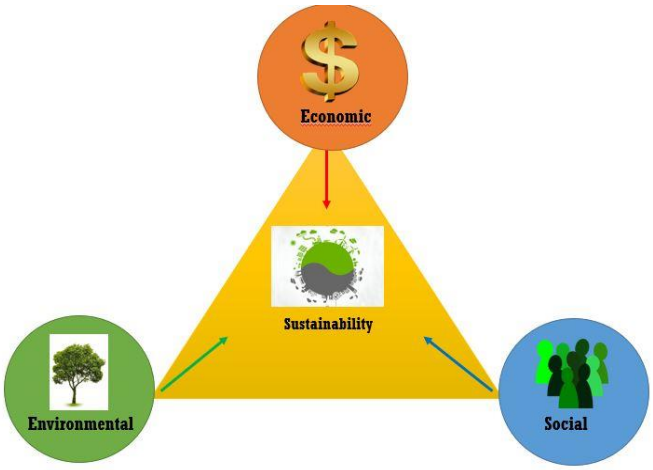

Fig. 1. Structure of tripe bottom line: social, environmental and social

However, it's not simple design sustainable a smart city, and harder than this is the researchers introduce these criteria in a facility location model. The problems of localization relate to a decision make deciding where to position resources that best meets the stablished criteria for the organizations regarding the demand points [4].

That problem involves as mentioned before the transport infrastructure, and according to [5] a good transport infrastructure describe a characteristic of a smart cities. Beside this, one of the sectors which has more importance in the facility location context and has too a big impact in social/environmental dimension is the transport [6].

Transport is a fundamental activity for the economic development of a country or region, as it allows the flow of goods between dispersed production and consumption zones. In countries with large territorial extension, this sector becomes even more important due to its continental dimension and the distribution of its productive activities [6].

It is common sense, for big cities, an efficient transport system it's essential for the movement of citizens and facilities between different points.

Studies also point out that the urban population has grown a lot over the years, the graphic below (See Fig. 2) shows some data, which represent in 2015 the world urban population is 54% in total, and in 2050 they going to arrive 2/3 of the total with 6,3 billions of people will live in the cities.

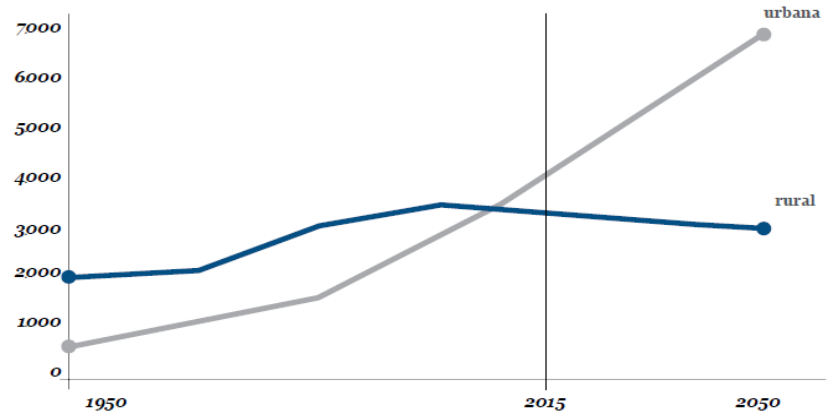

Fig. 2. World urban and rural population (1950-2050) [1]

With this population growth, cities increasingly need to meet the growing demand in subways, bus stops, train stations, among others. The above factor mentioned, based on other conditions, it is possible to say that the economic weight of cities will continue to grow. The 600 largest cities will contribute more than 60% of world gross domestic product by 2025,while in 2007 they accounted for 50% [1].

This economic importance in cities can directly impact the environmental scenario. Over 50% of CO_2 emissions are estimated to be from sources derived from transport, urban and residential energy consumption (heating, air conditioning) [7].

For the author Loo et al [8], electricity and transport fuel are identified as the main causes of carbon emission and consumption of non-renewable resources in cities.

More recently, low-carbon transport has been considered not only a key to achieving an overall carbon emission target per year, but as a fundamental policy and planning principle [8].

Thinking about the aspects with the population growth in the cities and the need for new environmental policies combined with transport, the present study is fused in this theme in order to show the importance of the success of the facility location in transport based on a smart city.

2 Objectives and Methodology

Dirks and Keeling [9] emphasize the importance of the integration of a city's various systems ("facilities") like transportation, energy, education, health care, buildings, physical infrastructure, food, water, and public safety in creating a smart city. Such facilities may be linked to products, factories, freight (such as intermodal terminals and hubs), passenger (integration terminals), and citizen services (parking lots, schools).

The table 1 is below presented with the main components and aspects of a smart city. It is seen that for the mobility of a smart city it is necessary to consider the logistic integration and the infrastructures, besides in the environmental dimension efficiency and sustainability are pointed, main keywords of this study.

Based on this, the main objective of this report is to draw up recent studies involving the key words "facility location", "sustainability" and "smart cities" in order to identify and measure how the social, environmental and economic dimension has been incorporated into ease location issues for a smart city.

Table 1. Components of a smart city and related aspects

Components of a smart city	Related aspect of urban life
Economic	Industry
People	education
Governance	e-democracy
Mobility	logistics & infrastructures
Environment	efficiency & sustainability
Living	security & quality

Table 2. Description of Web Database of Science Search

Criteria	Font size and style
Topic	TS = ("facilit* locatio* Smar* Citie* Sustanaibl*" OR "facilit* locatio* Smar* Citie* Sustanaibilit*")
Database	Web of Science, Current Contents Connect, Derwent Innovations Index, KCI, Russian Science Citation Index and SciELO Citation Index
Allotted time	2018-2019
Refinement	None, meaning the search included articles from all areas registered in WoS
Search date	July 18, 2019 at 2:50 pm

Table 2 above presents the search methodology. A methodology was used, which we classify as a scientometric search in order to identify patterns and qualitative and quantitative aspects of scientific productions. The theoretical framework of this research was taken from the scientific website Web of Science, due to its scope and coverage [10], between the years 2018-2019. in order to analyze the latest qualitative trends on the subject.

3 Results

Based on the keywords presented above, the search was delimited to identify the studies that addressed the theme sustainability, transport and facility location.

In this sense, searches were made starting from a more encompassing term "Smart Cities" to a refining of "Smart Cities Facility Location" or "Sustainable Smart Cities Transport", and other terms of search. In the years between 2018-2019, searching the subject smart cities, were found in total 4327 studies.

When refining went into research that included the topic sustainability in smart cities, the number of productions found was a total of 344. This represents that only a percentage of approximately 7% of the total smart city's studies over this period of years have done this kind of analysis.

Of these 344 studies, only 52 study the influence of transport sustainable criteria in smart cities. This represents 1,2% of total research in the area, and with the main theme of this investigation, which is the facility location, only 2 articles were found. The fig.3 bellow shows the representativeness of searches graphically.

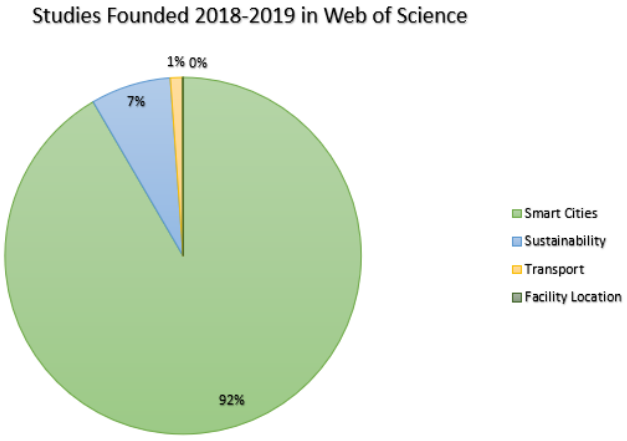

Fig. 3. Number of publications with the keyword's smart cities, sustainability, transport and facility location (2018-2019)

\

Among the studies that can include transportation, sustainability and smart cities, the most cited are magazine searches; *Tranportation Research Part A – Policy and Practice* (2), *Sustainable Cities and Society* (4), *Sustainability* (7), *Journal of Cleaner Production* (2). These five magazines represent 27% of the principal researches (see Fig. 4.).

The main countries identified in the studies are most European countries, being them, Scotland, Spain, France, Germany, Australia, China, Canada among others.

With the main theme of the present research "facility location", were found two articles with the following titles; "*City-hubs for smarter cities: The case of Lille "Eura-Flandres" interchange*" from the authors Odile Heddebaut and Floridea di Ciommo published on *European Transport Research Review* (2018) and the second article is; "*Sustainable Zoning, Land-Use Allocation and Facility Location Optimisation in Smart Cities*" from the authors Ahmed WA Hammad, Ali Akbarnezhad, Assed Haddad and Elaine Garrido Vazquez published on Energies (2019).

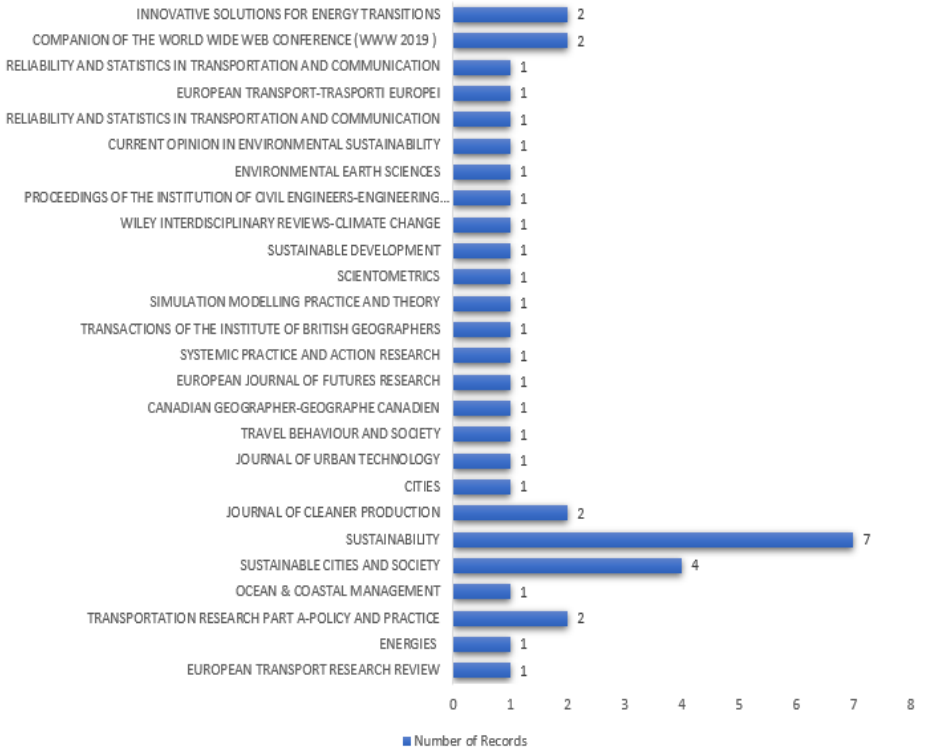

Fig. 4. Number of records by scientific journals involving sustainability, transportation and smart cities.

It's important to see, the articles are divided into different categories within the same subject. This means that there are articles inserted in the environmental dimension, these studies suggest that urban areas are the biggest consumers of natural resources

increasingly scarce, and in this sense there is a need to make cities more and more sustainable [9-11].

In addition, other studies are found that address systemically certain subjects, among them we can mention elements linked to information and communication technology. These studies aim to characterize a smart city from the efficient use of information and communication.

The next section will discuss the two articles found that address the main subject of this research, analyzing how facility location can be efficient in the concept of smart cities.

4 Analysis and Discussion

As previously mentioned, two articles were found that address the main theme of the present research. The first analysis to be done is from the study "*City-hubs for smarter cities: The case of Lille "EuraFlandres" interchange"* published on 27 December of 2017.

This paper has a very good feature related to the subject of intermodality, because it really shows that the importance of transportation infrastructure is a crucial point in characterizing a smart city.The main focus of this study is on the impact on social organization and in the conception of transport intermodal infrastructures.

That paper in the present case is part of a European research project in which 27 interchanges have been studied in nine European countries.

The focuses on the case study of the Lille metro service in France, with two main train stations, analyzing the socio-economic impact enabling a better place for smart city.

The methodology applied was to determine the number of interactions between intermodal transport exchanges and their respective environmental effects and establishing a method of potentiation for their characteristics in terms of function and logistic dimension (demand, number of modes of transport, service and facility, city location)

The key points for a smart city according to the authors [14] are the transport network in cities networks must be associated with fluidity, comfort and environmental care.

This can be associated with one of the most important concepts for a smart city is the concept of smart mobility that prioritizes clean and non-motorized transport, saving costs, reducing CO_2 emissions and increasing community efficiency [5, 12].

From the authors' point of view an excerpt that emphasizes the importance of intermodality is "Intelligent mobility and good use of transport infrastructures contribute to a smart city, transport intermodality is a specific structure that enables this "smart mobility""

The principal function of an interchange is to easily transfer from one mode of transport to another, the main idea is to facilitate intermodal transfers, increase the sustainable transport mode use, and reduce the journey time, increasing the quality of service. It is essential to make interchanges attractive places in order to reach or maintain a good level of public transport use.

In this sense, measures oriented to improve public transport service quality are required, such as reducing the transfer inconvenience and providing a seamless travel experience [5, 13]. Moreover, total travel time directly influences trip choices. Good connectivity at public transport stops and stations is critical to overall transportation network effectiveness [5, 14].

To better exemplify the purpose of the study, (see Fig. 5) as presented in the article shows the three main functions of a city hub and how they should interact in such a way that timelessness, facility location, and sustainable concepts involving social, environmental, and economic dimensions can be incorporated into a smart city.

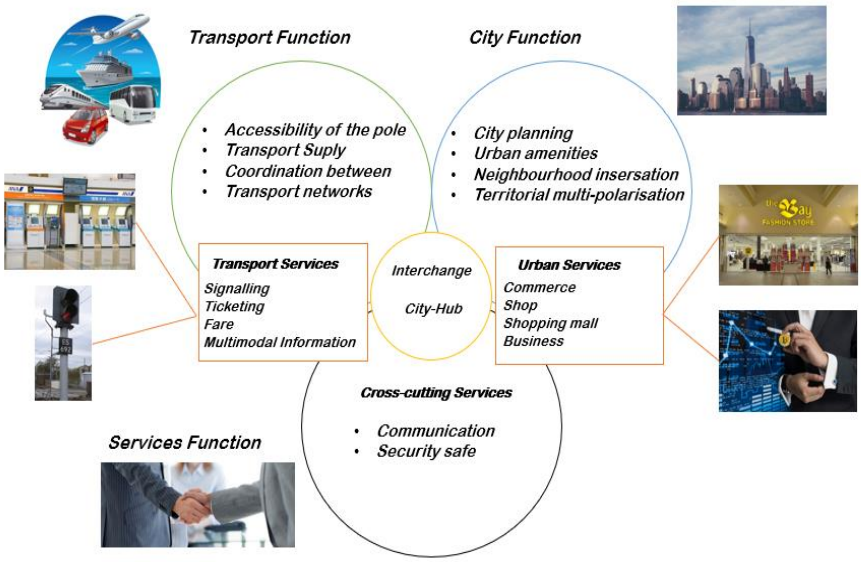

Fig. 5. The three dimensions of a city-hub [5, 15]

In the study by Euraflanders a typology is established that captures different exchanges and a scheme to score their characteristics in terms of function and logistic dimensions (demand, number modes of transport, services and facilities, city location) and its local restrictions as previously mentioned.

This typology divides into two groups, among them the first group of aspects (Dimension A) is related to the internal and logistic functions of an exchange, including transport elements of the exchange and the services and facilities necessary to comply with the transfer works correctly. This dimension determines the size of terminal building.

The second group (dimension B) includes the external aspects of the city environment that affects how the building could be. This dimension includes the location of the exchange within the city and whether the exchange plan conflicts with the existing land uses in the surrounding area.

The scores are given as follows. The values given in dimension A determine the need for space: size of the interchange. Total score less than 4 requires a Small exchange.

Scores 5 to 7 indicate the need for a Medium, while greater than 8 means that the exchange It should be quite large, making it an urban landmark.

The dimension B aspect can be negative, positive or neutral, thus modifying the previous scores and the type of necessary exchange.

Table 1 below shows how the score distribution was performed in the article.

Table 2. Interchange Dimensions: Function and Logistics, Local Constraints [14]

Dimension A Function and Logistics	Levels	Need for space	Score
Demand (users/day)	<30,000	Low	1
	30,000-120,000	Medium	2
	>120,000	High	3
Modes of Transport	Dominant - Bus	Low	1
	Dominant - Rail	Medium	2
	Several modes and lines	High	3
Services and Facilities	Kiosks, vending machines	Low	1
	Several shops and basic facilities	Medium	2
	Integrated shopping mall with all facilities	High	3
Dimension B Local constraints	*Levels*	*Upgrading level*	*Value*
Location in the City	Suburbs	Less	-
	City acess	Neutral	0
	City Centre	More	+
Surrounding area features	Non-supporting activities	Less	-
	Supporting activities	Neutral	0
	Strongly supporting activities	More	+
Development plan	None	Less	-
	Existing	Neutral	0
	Existing and including intermodality in the area	More	+

As a result, the study found that a good exchange could increase between 7% and 20% the use of intermodal modes and public transport. The development Euraflanders could attract audiences and active-mode users with a real decrease in car use, contributing to an environmentally friendly city, one aspect of smart cities.

However, additional research is needed to measure the effective participation of Euraflandre's customers and the role of Euralille CBD residents to help improve these aspects of the smart city. In fact, the smart aspects of a transport interchange are closely

related to modal change, the environment and health impacts. All these aspects are key features for a HUB-city, such as consistency of schedules, orientation, use of waiting time, comfort during waiting time, all aspects that make a City-HUB smarter and contribute to a Smart city. This study can show how the intermodality and location of facilities is potentially part of the smart elements that makes up a smart city.

For the second study involving the proposed themes, entitled "*Sustainable Zoning, Land-Use Allocation and Facility Location Optimization in Smart Cities* "published April 5, 2019, addresses the following theme: Examine the applicability of a mathematical framework to improve the sustainability of decisions involved in zoning, land use allocation, and location of facilities within smart cities.

A mathematical optimization structure is proposed, which links to other platforms in cities to optimize zoning, land use allocation, new building locations and infrastructure investment decisions work smartly cities. Multiple objective functions are formulated to optimize social, economic and environmental aspects considerations in the urban space.

Following the theme discussed in the introduction, It is well known to area researchers who estimate that nearly 55% of the world's population currently resides in urban areas with an estimate of which rates increase to 70% by 2050 [19].

So increasingly the concept of smart cities becomes important to be able to integrate more and more and more people effectively.

Second [16, 17], the decision making in the planning and operations of smart cities should be structured around the main considerations, namely strategic and tactical decisions. Within the strategic decision-making area, this includes good city planning that includes an intelligent location of its operating facilities, including schools, hospitals and others [16, 18].

The focus of this study is on the concept of smart city location planning. A proposed approach can be divided into three main areas: (i) the need to create a framework for building a smart city with zero where zoning and land use can be used;

(ii) a location of buildings in smart cities and investment decisions regarding expansion existing network structure and capacity, which involves a consideration of attributes influences the decision to position buildings such as schools, hospitals and offices; and (iii) the determination of the restrictions imposed on these location decisions based on the triple end result sustainability, through the objective of defining social, environmental and economic cost objectives functions.

As a result, three main decisions that form an essence of urban planning and design in smart cities are targeted: a saber, how decisions made regarding zone allocation and how participation of buildings in the region, such as expansion decisions related to road structure and expansion of the capacity of existing links on the network (if any).

The structure proposed in this study is to ensure the efficiency urban zoning planning and design, building smart city location and transportation networks, provision of smart city layout and location planning.

As mentioned earlier in this study three main decisions, that form the essence of urban planning and design in smart cities are directed: namely, decisions regarding the allocation of zones and the allocation of buildings to sites in the region, expansion

decisions related to the city's road structure and the expansion of the capacity of existing links on the network (if it already exists).

The main concept introduced through the developed structure is the vital integration of the three decisions into a single model that simultaneously optimizes the decision-making process involved.

Given that an important consideration in smart cities is to ensure effective and robust mobility decision-making to improve the transport of goods and people. To allow this to happen, a multiobjective optimization model is developed, based on a two-level structure. The two-level structure is required to model decision spaces. Of the model's two main decision makers: urban planners and transport network users.

The importance of generating sustainable solutions for the triple bottom line Sustainability is also accounted for by considering objective functions in optimizing developed model, focusing on the environmental, social and economic impacts of infrastructure decisions made.

As shown (see Fig. 6), the procedure returns to the optimization model, whose associated parameters are updated in response to induced changes and a new solution is generated.

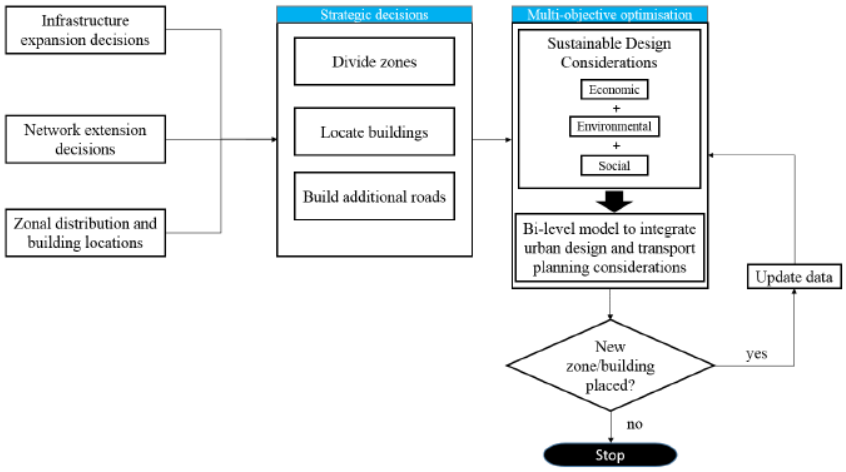

Fig. 6. Proposed framework for planning in smart cities [19].

The main decision variables in the mathematical model propose from this study is the upper level are: (i) the location decision, represented by the binary variable z f s and which equals 1 if building f is placed in location s, and 0 otherwise; (ii) the binary variable yij, which specifies whether link (i, j) is constructed or not; and (iii) the continuous variable fij, which indicates whether an existing link of the network is expanded or not.

As stated earlier the mathematical model of this study involves the formulation of three objective functions; Each function targets a specific sustainability measure. The first modeled equation is a proxy for the social pillar of sustainability; minimizes the total noise pollution experienced in each area of the Smart city. Noise is generated by

the buildings to be positioned in the region as measured by the by a parameter or variable. The second equation addresses the economic aspect of sustainability, where the cost of building buildings in urban areas, Cs, is minimized

The ultimate objective function, the third equation, considers minimizing total carbon emissions of users in the traffic network. The third equation is responsible for emissions from different transport modes, which is multiplied by the distance of network links, dij; the flow of the links, xij; and travel time on network links, which considers congestion impacts on the roads.

As a result of this study the social factor (which is one of the scarcest dimensions in scientific productions in this segment), presented as a response that the noise pollution in the region was minimized; as

environmental factor, carbon emissions in the transport network have been minimized; and as an economic factor, the construction cost of buildings was minimized.

The proposed model was applied in a realistic case example for urban structure design. of a smart city.

The lexicographic approach highlighted cost variations of up to 52% when carbon emissions are prioritized by decision makers.

5 Conclusion

As a conclusion of this study it is possible to perceive several important aspects, the first one is that in the bibliographic search the scarcity in the literature is remarkable. Studies that can involve the three pillars of sustainability: economic pillar, social and environmental is hard to found and this is observed when performing the research and only 7% of articles founded correlated the sustainaility with smart cities.

About the search methodology performed in this work, it is possible to make improvements in terms of refinement and database, in which other databases could be consulted for the search. In addition, datamining software could better assist in the search. However, the search results were few satisfactory, since only 2 articles were found in the search period. This reinforces the idea that matters in this area need greater attention and visibility as they have a major influence on the success of transport.

Regarding the results, as mentioned earlier, the literature is shallow. However, two articles were found that fit the search objective and found the main subjects proposed here.

Other point to consider is that when it starts to involve transport and location of facilities it is not always easy to measure the socio-environmental dimensions, however the works presented here can unite both themes to move towards more sustainable policies.

Another factor is that the location of facilities as seen in the analysis of the two articles is a key factor to promote intermodality, integration, flow, and better dynamic localization / allocation strategies and operational.

Without this perception it is very complicated to think of a smart city that does not involve reasoning such as: What will be the best location for a school or hospital to serve the population more sustainably?

It is these types of issues that lead us to understand that the transport junction and facility location are terms inherent in each other and walk side by side so that the dynamics of intermodality can be optimized.

Finally, the need for issues involving sustainability concepts in recent years has grown, showing that the world has been moving in this direction, it is for this purpose that the proposed study seeks to show the the importance of social and environmental criteria in the concept of smart cities has become very important and demonstrate how excellent transport dynamics associated with facility location can influence and a lot in current development.

For future studies, the suggestion is a broader search, including articles, papers and dissertations, in order to analyze the entire scientific scope and quantify new studies and trends. As a basis, the idea is to propose a mathematical model of location of facilities that proposed, intermodality and sustainability.

With this research it has been realized that, despite all the worldwide road to new environmental policies and planning, this is still a major challenge in mathematical models and how to incorporate them into real day to day applications. As a suggestion, studies in this segment need to be better proposed to contribute more and more to smart cities.

References

[1] M. A. Cunha, E. Przeybilovicz, J. F. M. Macaya, and F. B. P. dos Santos, "Smart cities: transformação digital de cidades." Programa Gestão Pública e Cidadania, 2016.

[2] T. Bakıcı, E. Almirall, and J. Wareham, "A smart city initiative: the case of Barcelona," *J. Knowl. Econ.*, vol. 4, no. 2, pp. 135–148, 2013.

[3] M.-L. Marsal-Llacuna, J. Colomer-Llinàs, and J. Meléndez-Frigola, "Lessons in urban monitoring taken from sustainable and livable cities to better address the Smart Cities initiative," *Technol. Forecast. Soc. Change*, vol. 90, pp. 611–622, 2015.

[4] M. G. de Oliveira, "Sistema de Localização de Facilidades," *Apostilas Pesqui. Operacional*, p. 89, 2012.

[5] V. de A. Guimarães, "Modelagem matemática para localização-alocação de centros de integração logística considerando as demandas par-a-par." Dissertação de mestrado em Engenharia de Transportes. PET/COPPE/UFRJ: Rio de Janeiro, 2015.

[6] V. de Almeida Guimarães and G. M. Ribeiro, "MODELAGEM MATEMÁTICA PARA LOCALIZAÇÃO DE CENTROS DE INTEGRAÇÃO LOGÍSTICA," 2015.

[7] Cetreforcities, "Smart Cities," 2014. [Online]. Available: https://www.centreforcities.org/wp-content/uploads/2014/08/14-05-29-Smart-Cities-briefing.pdf. [Accessed: 21-Sep-2019].

[8] B. P. Y. Loo and F. du Verle, "Transit-oriented development in future cities: towards a two-level sustainable mobility strategy," *Int. J. Urban Sci.*, vol. 21, pp. 54–67, 2017.

[9] S. Dirks and M. Keeling, "A vision of smarter cities: How cities can lead the way into a

prosperous and sustainable future," *IBM Inst. Bus. Value*, vol. 8, 2009.

[10] X. Chen, "The declining value of subscription-based abstracting and indexing services in the new knowledge dissemination era," *Ser. Rev.*, vol. 36, no. 2, pp. 79–85, 2010.

[11] D. Genari, L. F. da Costa, T. P. Savaris, and J. Macke, "Smart Cities e o desenvolvimento sustetável: revisão e perspectivas de pesquisas futuras," *Rev. Ciências da Adm.*, vol. 20, no. 51, pp. 69–85, 2018.

[12] I. Zubizarreta, A. Seravalli, and S. Arrizabalaga, "Smart city concept: What it is and what it should be," *J. Urban Plan. Dev.*, vol. 142, no. 1, p. 4015005, 2015.

[13] C. Fernández, F. Manyà, C. Mateu, and F. Sole-Mauri, "Approximate dynamic programming for automated vacuum waste collection systems," *Environ. Model. Softw.*, vol. 67, pp. 128–137, 2015.

[14] O. Heddebaut and F. Di Ciommo, "City-hubs for smarter cities. The case of Lille 'EuraFlandres' interchange," *Eur. Transp. Res. Rev.*, vol. 10, no. 1, pp. 1–14, 2018.

[15] C. Manville *et al.*, "Mapping smart cities in the EU," 2014.

[16] S. Hernandez, A. Monzon, and R. de Oña, "Urban transport interchanges: A methodology for evaluating perceived quality," *Transp. Res. Part A Policy Pract.*, vol. 84, pp. 31–43, 2016.

[17] H. Iseki and B. D. Taylor, "Style versus service? An analysis of user perceptions of transit stops and stations," *J. Public Transp.*, vol. 13, no. 3, p. 2, 2010.

[18] C. Richer, "L'émergence de la notion de pôle d'échanges, entre interconnexion des réseaux et structuration des territoires," 2008.

[19] A. W. A. Hammad, A. Akbarnezhad, A. Haddad, and E. G. Vazquez, "Sustainable zoning, land-use allocation and facility location optimisation in smart cities," *Energies*, vol. 12, no. 7, 2019.

[20] T. Bektas, T. G. Crainic, and T. Van Woensel, "From managing urban freight to smart city logistics networks," 2015.

[21] A. W. A. Hammad, D. Rey, and A. Akbarnezhad, "A Bi-level mixed integer programming model to solve the multi-servicing facility location problem, minimising negative impacts due to an existing semi-obnoxious facility," in *Data and decision sciences in action*, Springer, 2018, pp. 381–395.

Modelo de administración sustentable para microrredes aisladas: caso de estudio Puertecitos, México

N. Velázquez[1], J. A. Aguilar-Jiménez[1], J. Rivas[1], R. Cota[1], E. González[1], R. López-Zavala[1], L. Hernández-Callejo[2]

[1] Centro de Estudios de las Energías Renovables, Instituto de Ingeniería, Universidad Autónoma de Baja California, Mexicali, México.
nicolas.velazquez@uabc.edu.mx
[2] Universidad de Valladolid, Campus Universitario Duques de Soria, 42004 Soria, España

Abstract. Las microrredes con energías renovables nos permiten desarrollar sistemas de generación eléctrica sustentables, con los cuales se puede combatir la marginación de las comunidades aisladas. En este trabajo primeramente se presenta la metodología que se sigue para la detección de las comunidades en estado de marginación y se realiza un análisis de los diferentes modelos de gestión energética, posteriormente se muestra cómo se lleva acabo el desarrollo de sistemas de generación eléctrica sustentables con microrredes para comunidades aisladas. El modelo de organización de Sociedad Cooperativa con Participación Estatal fue desarrollado e implementado en la comunidad de Puertecitos, Ensenada, Baja California, México. La sostenibilidad de los Sistemas Eléctricos Sustentables de las comunidades aisladas depende directamente de un modelo de gestión energética que considere los aspectos económicos, sociales y culturales de la comunidad, así como del compromiso de las instituciones gubernamentales involucradas.

Keywords: Microrred, Energías Renovables, Comunidades aisladas.

1 Introducción

Para conseguir un crecimiento equitativo de la población es indispensable incorporar el sector rural y urbano-marginal al proceso de desarrollo del país. Ambos grupos marginales necesitan de las mismas posibilidades y servicios básicos para desarrollar sus capacidades sociales y económicas. Sin embargo, muchas de estas poblaciones se encuentran en regiones aisladas sin acceso a energía eléctrica y servicios de salud, los cuales son básicos y necesarios para contar con una calidad de vida adecuada. Claro está que los países más electrificados son los más desarrollados y, por ende, los que gozan de una mejor posición social y económica. En estos países se tiene la convicción de que la energía eléctrica es una herramienta que requiere la población para el desarrollo de sus actividades productivas y mejora de su calidad de vida, atendiendo sus necesidades de comunicación, alumbrado y principalmente para el desarrollo de sus actividades agropecuarias, artesanales, comerciales e industriales [1], sin dejar de lado la conservación de alimentos y confort térmico.

La electrificación rural en México es un problema nacional que se debe de atacar. La Comisión Federal de Electricidad (CFE) estima que en México existen poco más de millón y medio de personas sin acceso a la electricidad [2]; si bien no es un porcentaje alto, sí representa una gran cantidad de habitantes sin este servicio público. El principal factor que predomina en esta inaccesibilidad eléctrica es el lugar remoto en que se encuentran las comunidades, ya que para la CFE no le es económicamente viable llevar el servicio a estos pequeños pueblos, dada la gran inversión que tendría que hacer por la ampliación de la red.

Dados los problemas que se tienen al tratar de llevar energía eléctrica a todos los rincones del planeta, en la actualidad se han desarrollado tecnologías capaces de producir este servicio en el mismo lugar donde se necesita, es decir, instalar generadores de energía en el centro de consumo, sin la necesidad de una interconexión a la red de transmisión eléctrica [3]. A esto se le llama electrificación descentralizada o generación distribuida. El sistema más comúnmente adoptado consiste en la instalación de generadores eléctricos en base a combustibles fósiles, como lo son la gasolina y el diésel ya que, de primera instancia, el costo de inversión inicial es bajo, pero el asociado a la operación es muy elevado [4], lo cual, en conjunto con las condiciones económicas de las poblaciones marginadas, vuelve imposible su operación continua. Un claro ejemplo de esto es la comunidad del Ejido Delicias, ubicada en el tramo carretero San Felipe-Puertecitos, en el estado de Baja California, México. Donde se cuenta con una población de 80 personas (20 viviendas) y su asentamiento se encuentra a 41 km de distancia de la Red Eléctrica Nacional (REN), obligándolos a producir su propia energía para satisfacer necesidades básicas, como lo son conservación de alimentos, alumbrado, aire acondicionado, entre otros. Cada vivienda aporta alrededor de $450 MX (aproximadamente 23 USD, 24 €) mensuales sólo por dos horas diarias de electricidad, lo cual se destina únicamente a la compra de diésel para la operación de un generador eléctrico.

Es fácil comprender lo costoso que es generar energía eléctrica con combustibles fósiles durante 24 horas del día en regiones aisladas. Otras fuentes de energía muy importantes son las energías renovables, las cuales aprovechan los recursos presentes en el medio ambiente para su conversión energética, como lo son la radiación solar, viento, energía potencial de masas de agua, calor geotérmico, entre otras. Estas, a diferencia de los combustibles fósiles, no producen contaminantes cuando se utilizan, por eso también se les conoce como energías verdes.

Actualmente existe la tecnología para generar energía eléctrica a partir de las energías renovables, pero el éxito de su implementación depende en gran medida del modelo de gestión energética, ya que se han instalado muchos sistemas de generación eléctrica aislados basados en energías renovables y han fracasado por no implementar un modelo de gestión energética que considere los aspectos culturales, sociales y económicos de las comunidades.

Se han desarrollado modelos de gestión donde el gobierno (municipal, estatal o federal) o gobierno en conjunto con las comunidades se encargan de la administración y operación y mantenimiento del sistema de generación eléctrica de las comunidades [5], pero no se ha logrado desarrollar un modelo de gestión sostenible a largo plazo. Akinyele et al [6], analizando proyectos de electrificación rural fallidos en Nigeria, proponen un modelo de implementación de microrredes aisladas basado en los principios

fundamentales de la sostenibilidad y experiencias propias de los autores. En el modelo se toma en cuenta la situación social, técnica, económica, ambiental y política, con el fin de lograr microrredes sustentables. Domenech et al [7] realizaron la instalación de microrredes en comunidades remotas de Perú utilizando distintas fuentes de energías renovables, donde la tecnología adecuada en cada área de acuerdo a sus necesidades y potencial energético fue evaluada. Este proyecto llevó electrificación a 58 casas, un centro de salud, una escuela y otros consumidores. La operación y mantenimiento de los sistemas fue realizada en conjunto con un modelo de administración comunal especialmente planteado para esta comunidad, basado en las características de la población.

Para resolver la problemática descrita, en este trabajo se propone satisfacer las necesidades de energía eléctrica de las comunidades aisladas con microrredes que utilizan energías renovables y un modelo de gestión comunitario, lo cual fue implementado en la comunidad de Puertecitos, Ensenada, Baja California, México.

2 Metodología para la detección de comunidades e implementación de microrredes

Con el enfoque de utilizar las energías renovables para combatir la marginación de las comunidades aisladas y después de hacer un estudio de viabilidad técnico económica para la electrificación de dichas comunidades, comparando las opciones; 1) extender la red eléctrica convencional, 2) generación eléctrica con diesel y 3) microrred con energías renovables, se encontró que, si la comunidad está a 35 km o más alejada de la red eléctrica convencional, la mejor opción es la microrred [8]. En la Fig. 1 se muestra la secuencia que se sigue para la detección de las comunidades en estado de marginación y el desarrollo de sistemas de generación eléctrica sustentables con microrredes, así como su modelo de gestión energética.

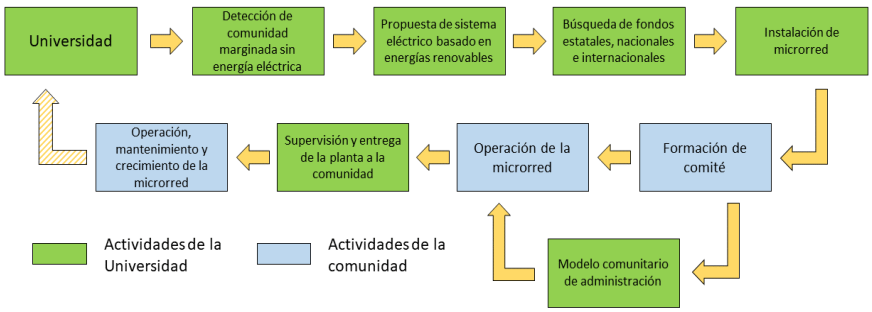

Fig. 1. Metodología para el desarrollo del sistema de generación eléctrica sustentable.

La metodología descrita en la Fig. 1 está compuesta por tres etapas:

1. Detección de comunidades: La comunidad ideal para la instalación de una microrred seria aquella que se encuentre alejada de la red eléctrica convencional, deben vivir familias que se encuentren organizadas y que tenga un recurso natural explotable o

una actividad productiva que pueda detonarse con la existencia de un servicio eléctrico de calidad. Habitualmente son comunidades sin servicios de electricidad, agua potable, drenaje, recolección de basura, transporte y telefonía. En esta primera etapa se realiza un estudio de viabilidad técnica y económica de las diferentes opciones para la electrificación de las comunidades aisladas y se justifica el Sistema de Generación Eléctrica Sustentable.

2. Diseño e implementación de la microrred: Considerando la disponibilidad de los recursos energéticos renovables, la posible demanda de energía eléctrica, las tecnologías y recursos económicos disponibles, el poder de pago de las familias, aceptación de la tecnología por parte de los miembros de la comunidad, entre otros, se procede al dimensionamiento e implementación de la microrred.
3. Desarrollo del modelo de gestión para sistemas aislados: Una vez localizada la comunidad en estado de marginación y conseguir los recursos económicos para el Sistema Eléctrico Sustentable, se procede a realizar un estudio social, económico y cultural de la comunidad para desarrollar el modelo de gestión energética y el diseño de la microrred de acuerdo a las características particulares de la comunidad. En esta etapa se realiza las siguientes actividades:

- Visita guiada a la comunidad.
- Encuesta socioeconómica.
- Encuesta de opinión.
- Base de datos sobre las condiciones socioeconómicas de los habitantes y aparatos eléctricos disponibles.

3 Modelos de gestión para sistemas aislados

Los modelos de gestión para sistemas aislados actuales están basados en los siguientes *paradigmas de la sostenibilidad* [5, 9]:

- La asistencia técnica como criterio único de sostenibilidad
- La rentabilidad económica.
- La opción multicriterio o integradora

Con los paradigmas de la sostenibilidad se busca consolidar lo técnico, definir lo económico, ser responsable con el medio ambiente y fortalecer lo social (empoderar a las comunidades).

Los *modelos de gestión energética* que se han implementado en sistemas aislados hasta ahora, tienen las siguientes características:

- De tipo Municipal, no están capacitados para el manejo de servicios, se politizan rápidamente y se pierden los objetivos iniciales.
- De tipo Estatal, generalmente se incurre en paternalismo, se hacen inversiones sin análisis realistas (social, económico, técnico) y esta propenso a los cambios políticos.

- De tipo Comunal, es de todos y es de nadie, no existen responsabilidades claras ni reglas establecidas. Si no se desarrolla un buen modelo, con el tiempo la comunidad se desorganiza y pierde interés.
- De tipo Cooperativo, se convierte en el botín para algunos grupos internos, no cuenta con un marco legal claro.
- De tipo Privado, es más manejable, se puede adaptar al marco legal vigente, hay experiencias sostenibles, pero se encárese el servicio.

Los *criterios básicos* que se aplican en los modelos de gestión son:

- Se aprovecha los recursos locales (naturales y humanos).
- Se define la propiedad y la instancia de administración.
- Evaluación de la capacidad y voluntad de pago.
- Diagnóstico, consenso, participación, toma de decisiones.
- Se promueve el criterio empresarial en el manejo de energía (tarifas, contratos, etc.).
- Se incentiva el desarrollo de habilidades y destrezas (capacitación).
- Se fortalece la organización local.
- Se desarrolla el concepto de uso racional de energía.

Para la implementación de los modelos de gestión energética se desarrollan los siguientes *instrumentos*:

- Esquema tarifario
- Reglamentos sobre el servicio
- Contrato usuario – empresa
- Manual de operación
- Capacitación (usuarios, operadores, autoridades)
- Fiscalización

Ya que la finalidad es proporcionar un sistema para la generación de energía renovable que ayude al desarrollo económico y social de la comunidad aislada y que perdure con el paso de los años, fue necesario plantear un esquema de administración y operación y mantenimiento de la microrred en el que la universidad pueda heredar el proyecto a la población y fungir solamente como asesor técnico. A este esquema se le llamó "Modelo de Administración Comunitario Autosustentable" y se aplicó a la comunidad de Puertecitos y su microrred.

Esto permitió que la universidad no interviniera en la administración, operación y mantenimiento de la microrred, y que dejara planteado el modelo para que la misma población, propietarios del proyecto, la mantengan en óptimas condiciones. Eso no significa que la universidad no aporte con la asesoría técnica y administrativa si es que la comunidad la necesitara, ya que la institución educativa cuenta con la facultad de dar soporte en futuros incrementos de capacidad instalada, rediseño de circuitos, modificaciones del banco de baterías y actualizaciones al modelo de administración comunitario, entre otros aspectos técnicos.

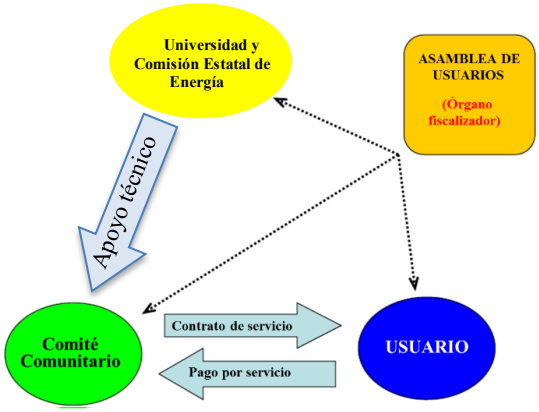

Fig. 2. Esquema de modelo de gestión.

4 Caso de estudio: Microrred de Puertecitos, México

La comunidad de Puertecitos, Ensenada, Baja California, México (30°21'19.7" N, 114°38'26.3" O), es un pueblo pesquero aislado de la REN (Fig. 2), donde habitan alrededor de 20 familias con un alto índice de marginación social ya que, al no contar con los servicios básicos de electrificación, agua potable y salud, las condiciones de vida son muy deplorables y, en conjunto con las altas temperaturas ambientales de la temporada de verano de hasta 50°C, la necesidad de aire acondicionado, conservación de alimentos y medicamentos se vuelve primordial. Es aquí donde el Centro de Estudios de las Energías Renovables (CEENER) del Instituto de Ingeniería de la Universidad Autónoma de Baja California (UABC), en conjunto con distintas instituciones públicas y privadas, nacionales e internacionales, llevaron a cabo la instalación de una microrred con base a energías renovables para proporcionar energía eléctrica a la sección de la comunidad más necesitada.

Fig. 3. Comunidad de Puertecitos, Ensenada, Baja California, México.

Una vez localizada la comunidad en estado de marginación y conseguir los recursos económicos para el Sistema Eléctrico Sustentable de Puertecitos, se procedió a realizar un estudio social, económico y cultural de la comunidad para desarrollar el modelo de gestión energética y el diseño de la microrred de acuerdo a las características particulares de la comunidad de Puertecitos. Considerando la disponibilidad de los recursos energéticos renovables, la posible demanda de energía eléctrica, las tecnologías y recursos económicos disponibles, el poder de pago de las familias, aceptación de la tecnología por parte de los miembros de la comunidad, entre otros, se procedió al dimensionamiento de la microrred y al desarrollo del modelo administrativo y operativo de la misma. En la tabla 1 y Fig. 4 y 5 se muestran las características de los componentes de la microrred o Sistema Eléctrico Sustentable de Puertecitos.

Table 1. Componentes de la microrred instalada en Puertecitos, B. C., México.

Equipo	Capacidad
Sistema fotovoltaico Solartec	55 kW
Aerogenerador Liten	5 kW
Generador diésel de 480V CA	75 kVA
Banco de baterías selladas de 1500 AH c/u	522 kWh
Controlador de carga solar con MPPT	55 kW
Controlador de carga eólico	7 kW
Inversor eólico	7 kW
Inversor principal @480V CA	100 kVA
Transformador principal	112 kVA
Transformador cuarto de control	15 kVA
Transformadores reductores	50 kVA
Interfaz de monitoreo	N/A

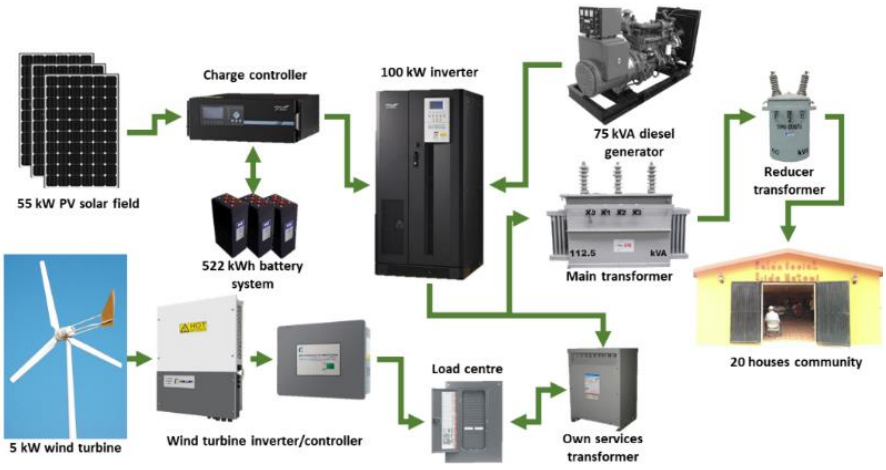

Fig. 4. Diagrama esquemático de la configuración de la microrred.

Fig. 5. Fotografía de la microrred de Puertecitos.

4.1 Modelo de gestión propuesto para la comunidad de Puertecitos

El propósito del modelo de gestión o modelo de organización es tener una administración, operación, mantenimiento, e inclusive crecimiento sostenible del Sistema de Generación Eléctrica Sustentable de Puertecitos. Para lograr lo anterior fue necesario realizar un estudio socioeconómico y cultural de la comunidad para desarrollar el modelo de gestión energética de acuerdo a las características particulares de la comunidad. Con dicho estudio se tomó en cuenta todos los aspectos sociales al instalar la planta de generación eléctrica con energías renovables y se promovió su aceptación de forma sostenible, considerando sobre todo los siguientes aspectos:

- Situación actual de la comunidad.
- Condiciones socioeconómicas de los hogares.
- Generación y consumo de energía eléctrica.
- Posición de la comunidad con respecto a la prestación del servicio de electricidad.
- Análisis FODA.

El modelo de organización propuesto para el Sistema de Generación Eléctrica Sustentable de Puertecitos es bajo la figura jurídica de Sociedad Cooperativa de Participación Estatal. Las principales razones para seleccionar dicho modelo son:

- Cuenta con una base legal ya definida lo que acelera la planeación de actividades en el corto plazo y facilita la resolución de conflictos en el largo plazo.
- Permite el registro de la Sociedad en convocatorias públicas para solicitud de fondos gubernamentales.
- Fomenta la participación comunitaria sin dejar de lado atribuciones que le permitan al gobierno estatal (Comisión Estatal de Energía) asegurar el buen funcionamiento de la Sociedad y el servicio de electricidad.
- Permite el manejo de recursos por medio de una cuenta bancaria con cheques controlables y tarjetas de débito limitadas.

No es posible presentar en este artículo la totalidad de los documentos desarrollados, por lo que se enfocará en algunos aspectos de la constitución y reglamento del modelo de organización propuesto.

4.2 Constitución

- El servicio de energía eléctrica se otorgará bajo la figura jurídica de Sociedad Cooperativa de Participación Estatal.
- Esto permitirá que la Comisión Estatal de Energía (CEE) y la Comunidad puedan desarrollar sus actividades de manera conjunta y con una base legal definida en la Ley de Sociedades Cooperativas.
- La Comunidad desempeñaría las funciones requeridas para mantener el servicio de electricidad funcionando y la CEE en conjunto con la Universidad (UABC) las de soporte y fiscalización.

El acta constitutiva consta de 90 artículos que hablan de los siguientes aspectos:

- Constitución, domicilio, duración y objeto
- Los socios
- Capital social
- Entradas y salidas de recursos económicos
- Registro de actividades, contabilidad y del ejercicio social
- Administración, representación y auditoría
- Fiscalización
- Disolución y liquidación
- Disposiciones generales

4.3 Reglamento

El objetivo del reglamento es regular y asegurar el aprovechamiento, mantenimiento, reparación y mejoramiento del servicio de energía eléctrica, en beneficio de los habitantes de la localidad.
La aplicación del presente reglamento les corresponde a las siguientes autoridades:

- Al presidente del Consejo Administrativo
- A la Asamblea
- A las autoridades fiscalizadoras

El reglamento comprende los siguientes apartados:

- Definiciones
- Condiciones para la entrega del servicio
- Aspectos técnicos del servicio
- Derechos y obligaciones del usuario
- Derechos y obligaciones de la distribuidora
- Condiciones comerciales

5 Resultados

Antes de la puesta en marcha del sistema, existía un gran escepticismo por el proyecto debido a las malas experiencias adquiridas con autoridades locales. Sin embargo, cuando se inició el suministro de energía eléctrica, la población cambió repentinamente de actitud. Fue entonces cuando se logró concluir el ciclo metodológico presentado en la Fig. 1, entregando el proyecto al comité de la comunidad.

Ya que no se contaba con un servicio de energía eléctrica continua y confiable en la comunidad, al iniciar operaciones la microrred no se esperaba que se utilizaran una gran cantidad de equipos electrodomésticos en los hogares de los habitantes y que, a medida que avanzara el tiempo, se fueran adquiriendo hasta el límite máximo establecido.

En la Fig. 6 se muestra la cantidad de energía eléctrica suministrada por la microrred a la comunidad durante todo un año completo de mediciones. Para tal registro se utilizó el equipo Fluke 1735 Power Logger. El inicio operativo de la micrrored fue en febrero, un mes en el que las temperaturas ambientales no eran tan elevadas, por lo que no era necesario el encendido del aire acondicionado y, por ende, la demanda de energía de la comunidad no superaba los 9 kW. A medida que avanzaban los meses la demanda se incrementaba debido a distintos factores, como lo es el incremento de la temperatura ambiental y la adquisición de nuevo equipos electrodomésticos. Para el mes de mayo a julio las temperaturas presentes en la comunidad obligaban a tener encendidos los equipos de aire acondicionado, por lo que la demanda se incrementó en gran medida, al grado de que la generación eléctrica basada en energías renovables no era suficiente para soportar periodos de 24 horas continuas de suministro, provocando colapsos energéticos. Cada vez eran más prolongados los periodos sin energía eléctrica a medida que avanzaban los días, hasta que en el mes de agosto se detuvo su operación completa para evitar dañar al banco de baterías por las sobredescargas.

Para el mes de diciembre el sistema se reestableció, y en la actualidad sigue operando con normalidad teniendo un mejor control con la generación-demanda-almacenamiento.

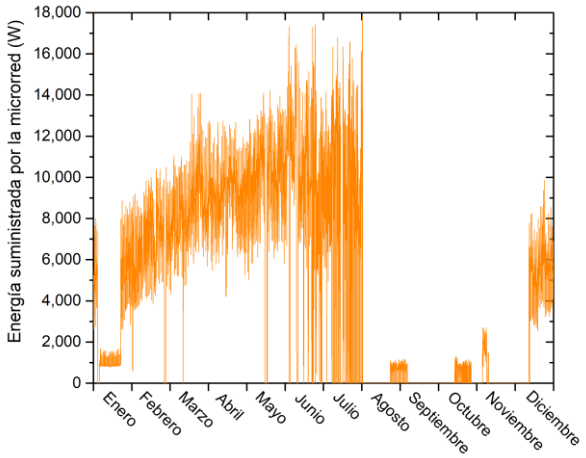

Fig. 6. Energía eléctrica suministrada por la microrred durante un año.

Por otro lado, el modelo de administración sustentable propuesto cumplió con las expectativas; durante los cuatro años operativos el comité realiza sus actividades de medición del consumo energético, facturación, cobro y mantenimiento del sistema, creando una bolsa económica para futuras expansiones y/o reemplazos de equipos.

6 Conclusiones

La instalación de Sistemas Eléctricos Sustentables con microrredes, se puede utilizar como punta de lanza para el desarrollo social y económico de las comunidades aisladas en estado de marginación. La sostenibilidad de los Sistemas Eléctricos Sustentables de las comunidades aisladas depende directamente de un modelo de gestión energética que considere los aspectos económicos, sociales y culturales de la comunidad, así como del compromiso de las instituciones gubernamentales involucradas. El reto más importante que se tiene en la electrificación de las comunidades aisladas no está en la parte técnica, la sostenibilidad depende mucho de los aspectos sociales y culturales de las comunidades.

Agradecimientos

Los autores agradecen a la Red Temática de la CYTED "CIUDADES INTELIGENTES TOTALMENTE INTEGRALES, EFICIENTES Y SOSTENIBLES (CITIES)" nº 518RT0558

Referencias

1. Ministerio de Electricidad y Energía Renovable: Electrificación rural con energías renovables, https://www.energia.gob.ec/electrificacion-rural-con-energias-renovables/.
2. CFE: Comisión Federal de Electricidad, http://saladeprensa.cfe.gob.mx/boletines/show/8328/.
3. Aguilar-Jiménez, J.A., Velázquez, N., Acuña, A., Cota, R., González, E., González, L., López, R., Islas, S.: Techno-economic analysis of a hybrid PV-CSP system with thermal energy storage applied to isolated microgrids. Sol. Energy. 174, 55–65 (2018). https://doi.org/10.1016/J.SOLENER.2018.08.078.
4. Cota-Soto, R., González-San Pedro, E., Velázquez-Limón, N.: Microrredes aisladas, el futuro sustentable de la electrificación rural. In: Carreón Diazconti, C., Ahumada Valdez, S.E., and Ramírez Barreto, M.E. (eds.) Avances en Investigación Ambiental en la UABC: Conociendo Nuestro Ambiente 2016. pp. 148–166. Universidad Autónoma de Baja California (2016).
5. Alvial-Palavicino, C., Garrido-Echeverría, N., Jiménez-Estévez, G., Reyes, L., Palma-Behnke, R.: A methodology for community engagement in the introduction of renewable based smart microgrid. Energy Sustain. Dev. 15, 314–323 (2011). https://doi.org/10.1016/j.esd.2011.06.007.
6. Akinyele, D., Belikov, J., Levron, Y.: Challenges of microgrids in remote communities: A STEEP model application. Energies. 11, 1–35 (2018). https://doi.org/10.3390/en11020432.
7. Domenech, B., Ferrer-Martí, L., Lillo, P., Pastor, R., Chiroque, J.: A

community electrification project: Combination of microgrids and household systems fed by wind, PV or micro-hydro energies according to micro-scale resource evaluation and social constraints. Energy Sustain. Dev. 23, 275–285 (2014). https://doi.org/10.1016/j.esd.2014.09.007.

8. Cota Soto, R.: Estudio y evaluación de microrredes para comunidades aisladas, https://drive.google.com/open?id=1m0iWnZVIOusNnCm43YHHyyDK1LQta9C7, (2017).
9. Van Acker, V., Szablya, S.J., Louie, H., McLean Sloughter, J., Pirbhai, A.S.: Survey of energy use and costs in rural Kenya for community microgrid business model development. Proc. 4th IEEE Glob. Humanit. Technol. Conf. GHTC 2014. 166–173 (2014). https://doi.org/10.1109/GHTC.2014.6970277.

Estrategia para la implementación de iniciativas sostenibles en ciudades universitarias ejemplificada con el Complejo Solar del TEC de Costa Rica

Carlos Meza[1][0000−0002−7374−505X], Hugo Sánchez[1][0000−0002−4122−1382], Francisco Monge[1], Julio Morera[2], and Abel Mendez[3][0000−0001−8038−7839]

[1] Escuela de Ing. Electrónica, Tecnológico de Costa Rica, Cartago, Costa Rica
cmeza@tec.ac.cr
[2] Escuela de Ing. Electromecánica, Tecnológico de Costa Rica, Cartago, Costa Rica
[3] Escuela de Ing. Computación, Tecnológico de Costa Rica, Cartago, Costa Rica

Resumen La realidad de la crisis climática requiere de nuevos modelos de desarrollo sostenible y de la integración, compromiso y trabajo en conjunto de gobiernos, industria privada, sociedad civil y academia. A lo largo de la toda la historia, las universidades han jugado un papel transcendental en el desarrollo de conocimiento y su posterior transferencia. Los campus universitarios son comunidades que se asemejan a pequeñas ciudades en donde las autoridades universitarias deben atender tareas similares a las que se enfrenta un gobierno municipal o ayuntamiento. Las ciudades universitarias representan un excelente laboratorio para probar soluciones innovadoras que permitan reducir el impacto ambiental de las actividades que allí toman lugar. No obstante, la temporalidad y falta de previsión de todos los elementos en los proyectos que se implementan en el campus hace que tengan resultados poco satisfactorios o que eventualmente se abandonen. En este artículo, se plantea la estrategia utilizada en el Instituto Tecnológico de Costa Rica para la implementación de instalaciones solares fotovoltaicas en sus campus. Dicha estrategia ha sido diseñada a partir de las experiencias adquiridas en proyectos pasados y en un estudio bibliográfico de proyectos similares. De esta forma, se pretende contribuir a la sistematización y sostenibilidad de iniciativas innovadoras en ciudades universitarias.

Keywords: Campus Verde · Unviersidad Sostenible · Energía fotovoltaica

1. Introducción

En muchos campus universitarios trabajan, habitan y transitan estudiantes, profesores y diverso personal de apoyo a la academia. Estos campus representan pequeñas ciudades en donde es normal que las mismas autoridades universitarias gestionen los sistemas de recolección de residuos y de aprovisionamiento de agua

y electricidad, entre otros. En este sentido, las universidades representan microciudades y por lo tanto excelentes laboratorios para poner en práctica soluciones sostenibles que puedan ser extrapoladas a un mayor centro urbano.

Profesores e investigadores de distintas universidades han documentado sus experiencias relacionadas con la implementación de sistemas innovadores en ciudades universitarias con el fin de hacerlas más sostenibles. Por ejemplo, Shukla en [25], describe el proceso de diseño y construcción de un complejo sistema de compostaje, de un sistema de recolección de agua y de una instalación fotovoltaica aislada. Estas actividades fueron implementadas en el campus universitario de la Universidad de Gurajat Vidaypith, India. En esta misma línea García en [10] describe el proceso de implementación de varios proyectos energéticos que lograron mejorar la eficiencia energética en la Universidad de Concepción, Chile, reduciendo de forma importante su factura eléctrica. Otras iniciativas similares han sido reportadas en [9, 13, 21, 22, 30].

Las instalaciones solares fotovoltaicas son una de las alternativas que se pueden implementar para reducir las emisiones de carbono de una ciudad universitaria. Una instalación fotovoltaica tiene un bajo impacto ambiental además de no generar contaminantes durante su operación. Por otro lado, los costos cada vez más bajos de los sistemas fotovoltaicos permiten que sean utilizados como una medida de ahorro en la factura eléctrica. De acuerdo con [14] en 2018 el costo de los paneles fotovoltaicos fue de 0.22 USD/W lo cual representó una reducción de su costo del 90 % con respecto al año 2009. De acuerdo a Radhakrishnan en [21] uno de los proyectos más exitosos dentro del programa de "Campus Verde" de la *National University* fue la implementación de una instalación solar fotovoltaica en su campus de Costa Mesa, California, Estados Unidos. Dicha instalación tiene una capacidad de 852 kWp y ha permitido reducir la factura del campus en un 85 %. Varios autores como por ejemplo en [20, 24–26, 29], también reportan proyectos fotovoltaicos en campus universitarios. Su ubicación en ciudades universitarias permite, además de la reducción de los costos en electricidad , ser utilizados para actividades académicas como por ejemplo el estudio de los efectos de la temperatura en su eficiencia [29], su integración en sistemas híbridos o microrredes eléctricas [1, 7, 12, 15, 16] o su utilización en actividades docentes [3, 4, 9].

A pesar de las múltiples iniciativas y experiencias en el desarrollo de soluciones tecnológicas para hacer más sostenibles y eficientes las ciudades universitarias aún existen importantes desafíos que se deben atender. Shukla en [25] enumera los siguientes problemas relacionados con la implementación de proyectos en campus universitarios:

- Coordinación inadecuada entre los grupos interesados. Es normal la falta de coordinación entre varios grupos, como la administración, el personal docente, los investigadores y los estudiantes, lo cual dificulta la comprensión de la utilidad de los dispositivos amigables con el medio ambiente implementados en el campus. Esto sucede con excepción de aquellos individuos involucrados en el proyecto, los cuales, no obstante, normalmente tienen un tiempo finito dedicado al proyecto.

- Exposición insuficiente de los proyectos debido a falta de interés, preocupación y visualización de oportunidades y beneficios.
- En los proyectos no se toma en cuenta su mantenimiento y monitorización. Siempre ha sido fácil iniciar un proyecto o introducir una nueva solución, pero la dificultad radica en mantenerlo, ya sea por que no se tomó en cuenta dentro de los costos del proyecto o porque no existe personal con los conocimientos y las habilidades técnicas para hacerlo.

Situaciones similares son expuestas en [6,21], en donde se afirma que la mayoría de los trabajos que tratan sobre campus verdes y sostenibles son principalmente anecdóticos y no se basan en un proceso metodológico definido.

El presente trabajo propone un esquema organizativo para el desarrollo sostenible de campus verdes. Más específicamente, se presenta el caso de las instalaciones solares fotovoltaicas que están siendo desarrolladas en los campus del Instituto Tecnológico de Costa Rica (TEC) dentro de un programa denominado Sostenibilidad TEC que propone, diseña y supervisa la ejecución de proyectos innovadores relacionados con eficiencia energética dentro de los campus del Instituto Tecnológico de Costa Rica. De esta forma, con este artículo se pretende aportar a la sistematización del desarrollo y mantenimientos de iniciativas sostenibles en ciudades universitarias.

2. Campus Verdes y Sostenibles

El modelo económico para el desarrollo ha cambiado de forma radical en los últimos años. Dada la urgencia de la crisis climática, el modelo económico ha pasado de asumir que el planeta cuenta con recursos ilimitados y con una capacidad suficiente de absorber la contaminación, a una mitigación de los problemas y a la generación de ciudades más elásticas y resistentes, esto es, con capacidad de adaptarse a condiciones cambiantes, [6]. Dada la situación actual, existe una necesidad clara de utilizar un modelo de desarrollo económico que sea más sostenible manteniendo un equilibrio entre el consumo eficiente de recursos, la disminución del impacto ecológico y la calidad de vida de los habitantes [27]. Ante ello, los centros de educación superior son instrumentos que puede ayudar a acelerar el proceso de transición [4,9].

Una de las primeras iniciativas conjuntas de los centros de educación superior fue la declaración de Talloires. Establecida en 1990 esta declaración consiste en un plan de acción de 10 puntos que los firmantes se comprometen a seguir para incorporar la sostenibilidad y la alfabetización ambiental en sus actividades docentes, de investigación, en las operaciones y la divulgación [2]. A marzo de 2019, 507 universidades de 57 países distintos han firmado la declaración de Talloires. Luego de esta declaración le han sucedido al menos 9 declaraciones más que profundizan o extienden los compromisos de las universidades firmantes [28]. A pesar de las buenas intenciones de estos tratados algunos autores, como por ejemplo [5,28], ponen en duda su efectividad en los casos en los cuales las universidades participantes no complementen sus compromisos con planes de trabajo para alcanzarlos.

Una de las razones por las cuales es difícil comparar el éxito de las experencias en iniciativas sostenibles en los campus es la diversidad en la definición de "universidad sostenible". Para efectos de este artículo, se tomará la definición propuesta por [31] y también adoptada en [6, 8, 23], entre otros:

> Una **universidad sostenible** es *"una institución de educación superior que aborda, involucra y promueve, a nivel local, regional o global, la minimización de los efectos negativos ambientales, económicos, sociales y de salud generados en el uso de sus recursos para cumplir con sus funciones de enseñanza, investigación, divulgación, vinculación y administración de forma tal que facilite la transición de la sociedad hacia un estilo de vida sostenible"* [a].

[a] la traducción de la definición es de los autores del presente trabajo.

De esta forma, un campus verde o sostenible es el espacio físico en donde una universidad desarrolla sus resultados teóricos para implementar el concepto de universidad sostenible [6]. Implica planificación, tareas de operación y mantenimiento y el uso del campus como un laboratorio vivo en donde existe participación de estudiantes para el desarrollo de los proyectos.

3. Propuesta de plan de acción para el desarrollo de iniciativas sostenibles en Campus Verdes

Desde el 2010, el Instituto Tecnológico de Costa Rica ha desarrollado de forma sistemática iniciativas de eficiencia energética y energías renovables en sus campus [11, 17, 18]. A partir de estas experiencias y aquellas reportadas por diferentes autores (e.g. [6, 8, 10, 19, 21, 23, 25, 31]) se identificaron el siguiente conjunto de actividades que se sugiere ejecutar a la hora de desarrollar una iniciativa en el campus:

- Administrativas y de gestión:
  - Enmarcar las iniciativas en un programa u oficina adscrito a una entidad del gobierno universitario de alta jerarquía, como por ejemplo una rectoría o vicerrectoría.
  - Identificar y asegurar los fondos y el recurso humano necesario para la concepción, desarrollo, puesta en marcha, operación y mantenimiento de la iniciativa.
  - Vincular desde el inicio a todos las oficinas y actores que estarán involucrados en la concepción, desarrollo, puesta en marcha, operación y mantenimiento de la iniciativa.
  - Asegurar que los actores involucrados tengan los conocimientos y las habilidades necesarias para desarrollar la labor asignada.
- Académicas:
  - Identificar, potenciar y promover las actividades de docencia, investigación y difusión que se puede realizar con la iniciativa.

- Vinculación:
  - Identificar, potenciar y promover las actividades de vinculación con el sector productivo y con instituciones internacionales que permite la iniciativa a desarrollar.

En las siguientes secciones se ejemplifica el plan de trabajo propuesto para el caso de las instalaciones fotovoltaicas implementadas en los campus del Instituto Tecnológico de Costa Rica.

4. Complejo Solar TEC: Instalaciones fotovoltaicas en los campus del Instituto Tecnológico de Costa Rica

Una de las primeras acciones realizar por parte del programa de Sostenibilidad TEC es el desarrollo de instalaciones fotovoltaicas que permitan la generación de investigación y transferencia de conocimiento con miembros de la comunidad institucional y el sector productivo. Entre los proyectos a destacar se encuentran:

- Instalación fotovoltaica de 30 kWp en el techo del edificio de Rectoría, en el Campus Tecnológico Central de Cartago.
- Instalación fotovoltaica de 20 kWp de piso, en el Campus Tecnológico Local San Carlos, al norte de Costa Rica.
- Instalación fotovoltaica para la evaluación de desempeño de 400 kWp en el Campus Tecnológico Central de Cartago.
- Instalación fotovoltaica aislada de 6.8 kWp para evaluar sistemas de almacenamiento de energía en el Campus Tecnológico Central de Cartago.

Estas instalaciones presentan tres objetivos principales:

- Reducir la factura eléctrica de la Institución.
- Contribuir con los indicadores necesarios para conseguir y mantener el certificado de la carbono neutralidad de los campus.
- Servir de apoyo y casos de estudio para programas de formación regular (grado y postgrado) y educación continua.
- Fortalecer la vinculación con el sector empresarial nacional e internacional.
- Servir para la generación de estudios comparativos y de evaluación de desempeño y para el desarrollo de tecnología, de forma tal que permita la consecución de productos científicos como ponencias, artículos en revistas y propiedad intelectual.

A continuación se presentan las principales características de las instalaciones fotovoltaicas de los campus del Instituto Tecnológico de Costa Rica.

Cuadro 1. Características generales instalación 30 KW_p FV Edificio de Rectoría, Campus Central

Potencia nominal instalada (kW_p)	29.7
Cantidad de paneles instalados	108
Tecnología celdas solares	Policristalinos
Superficie de Instalación(m2)	185
Factor de Rendimiento (%)	82.9
Producción Anual Promedio (MWh)	40.71
Rendimiento Energético (kWh/kW_p)	1 396.1
Puesta en marcha	23 marzo, 2017

4.1. Instalación fotovoltaica de 30kW_p de techo Edificio de Rectoría, Campus Tecnológico Central de Cartago

Esta es la primera de las instalaciones en ser conectada por el programa de Sostenibilidad TEC. La principales características del sistema se detallan en el Cuadro 1

Esta instalación fue ubicada en el edificio principal de la universidad, con el objetivo de abastecer en un 100 % la demanda eléctrica de dicho edificio. La distribución de los paneles se encuentran en las fachadas norte y sur del edificio, por lo que a su vez el sistema funciona para el estudio de perdidas por orientación, mediante una comparación 1 a 1 de los paneles. Además las conexiones eléctricas se encuentran divididas en tres sistemas de acondicionamiento de potencia:

- Inversor de cadena con potencia nominal de 10kW
- Inversor de cadena con potencia nominal de 6kW
- 36 microinversores con una capacidad de 250W cada uno.

La Figura 1 muestra una vista aérea de la instalación realizada en el edificio de Rectoría.

4.2. Instalación fotovoltaica de piso 20kW_p campus Tecnológico Local de San Carlos

De forma simultánea a la instalación del edificio de rectoría, se procedió al diseño e instalación de un sistema fotovoltaico con estructura en tierra en el campus de San Carlos, ubicado en la zona norte de Costa Rica.

La principales características del sistema se detallan en el Cuadro 2

La Figura 2 muestra una vista de las instalaciones de piso realizadas en San Carlos.

4.3. Instalaciones fotovoltaicas para la evaluación de desempeño de 400 kWp, Campus Tecnológico Central de Cartago

Actualmente (agosto 2019) se encuentra en desarrollo varias instalaciones fotovoltaica con una capacidad a condiciones estándares de prueba (STC) de

Figura 1. Vista aérea planta fotovoltaica edificio de Rectoría

Cuadro 2. Características generales instalación FV Campus San Carlos

Potencia nominal instalada (kW_p)	19.4
Cantidad de paneles instalados	72
Tecnología celdas solares	Policristalinos y Monocristalinos
Superficie de Instalación(m2)	125
Factor de Rendimiento (%)	77.7
Producción Anual Promedio (MWh)	28.69
Rendimiento Energético (kWh/kW_p)	1 475.6
Puesta en marcha	31 mayo, 2017

Figura 2. Vista sistema fotovoltaico de piso en San Carlos

400 kWp. Estas instalaciones tienen distintos tipos de paneles fotovoltaicos, conectados en distintas configuraciones y se encuentran tanto en tejado como en superficie. El cuadro 4.3 muestras las principales características de esta instalación.

Características generales instalación FV 400kW

Potencia nominal instalada (kWp)	400
Cantidad de paneles instalados	1200
Tecnología celdas solares	Policristalinos,Monocristalinos, PERT
Superficie de Instalación(m2)	13 000
Factor de Rendimiento (%)	Por determinar
Producción Anual Promedio (MWh)	560(estimado)
Rendimiento Energético (kWh/kWp)	por determinar
Puesta en marcha Puesta en marcha	Noviembre 2019

Figura 3. Vista sistema fotovoltaico sobre edificio de aulas

4.4. Gestión administrativa

Para la coordinación del proyecto se creó un programa institucional denominado Sostenibilidad TEC que estuvo inicialmente adscrita a la Rectoría y luego a la Vicerrectoría de Administración. El programa tiene un presupuesto asignado y está subordinado al Vicerrector de Administración. Se decidió integrar el programa Sostenibilidad TEC dentro de esta vicerrectoría para facilitar las gestiones de desarrollo, puesta en marcha y mantenimiento de las instalaciones solares fotovoltaicas.

Figura 4. Vista sistema se fotovoltaico sobre edificio de Fundación Tecnológica

Figura 5. Vista de sistema fotovoltaico en Laboratorio de Sistemas Electrónicos para la Sostenibilidad

Figura 6. Trabajos en instalación sobre piso

El programa de Sostenibilidad TEC tiene como objetivo proponer, diseñar y supervisar la implementación de proyectos de eficiencia energética, siendo los proyectos más relevantes las instalaciones fotovoltaicas del Campus. Este programa trabaja de forma coordinada con la Unidad de Gestión Ambiental y Seguridad Laboral (GASEL), la cual está a cargo de todas las iniciativas relacionadas con reducir el impacto ambiental de las actividades propias de la Universidad. Algunas de las actividad que ha realizado GASEL son el programa de gestión de residuos, la prohibición de los plásticos de un sólo uso en el campus y la consecución de la carbono neutralidad en los campus de la universidad, entre otros. GASEL es también una instancia de la Vicerrectoría de Administración.

Una parte importante en la gestión administrativa del proyecto fue la identificación de los actores dentro de la universidad que deben ser integrados e informados sobre el mismo. A continuación la lista de las entidades que fueron identificadas e integradas en el desarrollo de las instalaciones fotovoltaicas de los campus:

- Departamento de Administración del Mantenimiento: Unidad de la universidad que tiene a cargo todas las tareas de mantenimiento de las edificaciones en el campus. Con ellos se identificaron las tareas y presupuesto estimado para realizar las tareas de mantenimiento. Se brindó una capacitación sobre sistemas fotovoltaicos al personal de este departamento con el objetivo de que tuvieran conocimiento de las tareas involucradas en la operación y mantenimiento de una instalación solar.
- Dirección de Cooperación: Unidad de la Vicerrectoría de Investigación encargada de proponer y revisar convenios con empresas u otras instituciones. Con esta oficina se redactaron y firmaron varios convenios de cooperación con los actores externos al TEC que se detallan más adelante en este texto.

- Unidad de Gestión Ambiental y Seguridad Laboral: Unidad encargada de desarrollar la estrategia para obtener y mantener la carbono neutralidad en los campus de la universidad. Los datos de generación de energía fotovoltaica son facilitados a ellos para que sean considerados dentro de los ahorros en emisiones.
- Departamentos académicos: Se obtuvo colaboración para la etapa de diseño de las instalaciones de las escuelas de Ing. Ambiental, Ing. Electrónica, Ing. Electromecánica e Ing. en Computación. Se informó al personal docente de estas Escuelas sobre las características de la instalación para que fueran utilizados en sus cursos, tal y como se detalla más adelante en este documento.
- Programa de Investigación en Energías Limpias: es un programa de la Vicerrectoría de Investigación que reúne a varios investigadores de la universidad que desarrollan investigaciones en energías limpias. Se informó sobre las características de la instalación y se promovió el desarrollo de investigaciones que utilicen esta infraestructura.

Como se observa, se procuró contar con representantes del sector administrativo, docente, de investigación y de vinculación de la universidad.

4.5. Labores académicas

Una parte fundamental de las instalaciones fotovoltaicas es su componente académico, es por ello que se creó una coordinación académica con tiempo asignado para trabajar con los departamentos académicos de la universidad para generar talleres, cursos y prácticas que han uso de las instalaciones fotovoltaicas.

Esta gestión fue fundamental para que las autoridades y la comunidad universitaria no percibieran las instalaciones como un proyecto con una duración finita sino como un medio para apoyar las labores docentes.

Programas de grado y postgrado Actualmente, las instalaciones fotovoltaicas se están utilizando para los siguientes programas académicos:

- Licenciatura en Ingeniería en Electrónica: proyectos de tesis de licenciatura y para prácticas en el curso “Sistemas Fotovoltaicos” y “Procesamiento Electrónico de Potencia”.
- Licenciatura en Ingeniería en Mantenimiento Industrial: proyectos de tesis de licenciatura. Se está elaborando un curso en “Energías Renovables” que tendría prácticas que utilicen las instalaciones.
- Licenciatura en Ingeniería Ambiental: proyectos de tesis de licenciatura. Visitas para el curso Administración de Energía.
- Licenciatura en Ingeniería en Computación: proyectos de tesis de licenciatura relacionados con visión artificial y bases de datos.
- Maestría en Ciencia y Tecnologías para la Sostenibilidad: proyectos de tesis de maestría y para los cursos “Conversión y Almacenamiento de Potencia”, “Energías Renovables” y “Energía Fotovoltaica”.
- Doctorado en Ingeniería: proyectos de tesis doctorales.
- Doctorado en Ciencias para el Desarrollo: proyectos de tesis doctorales.

Programas de educación continua El Instituto Tecnológico de Costa Rica tiene la posibilidad de ofrecer programas de educación continua orientados a complementar la formación de ingenieros y en algunos casos técnicos superiores. Un porcentaje de los ingresos recibidos por estos programas es asignado a la unidad que los imparte. Desde el 2015 se utilizan las instalaciones fotovoltaicas de la Institución para impartir dos programas de educación continua. Una parte del dinero recibido por estas capacitaciones es usada para la operación y mantenimiento de las instalaciones, lo cual asegura su sostenibilidad financiera. Actualmente se ofrecen dos programas:

- Especialización en Sistema Fotovoltaicos: es un programa de educación continuada que permite a técnicos superiores e ingenieros complementar su formación adquiriendo nuevos conocimientos y habilidades en el diseño, análisis, instalación y operación de sistemas fotovoltaicos. Los contenidos y la metodología de enseñanza de este programa han sido seleccionados, generados y adaptados para la realidad de la comunidad latinoamericana, especialmente en aquellas regiones ubicadas en el Trópico. Este programa se implementó en el 2015 gracias al apoyo económico de la Agencia de Cooperación Alemana (ver Figura 7) y se ha impartido a más de 250 personas en Costa Rica, El Salvador, Honduras y Nicaragua.

Figura 7. Primera Generación del Programa en Sistemas Fotovoltaicos, Junio 2015

- Programa de Análisis Financiero para Sistemas Fotovoltaicos: ofrece las bases para la realización de análisis financiero a corto plazo de proyectos fotovoltaicos a partir de insumos técnicos cercanos a la realidad. El contenido de este programa incluye las principales consideraciones técnicas en un proyecto solar fotovoltaico y su relevancia para un análisis financiero, el punto de equilibrio operativo y el estado de flujos de efectivo, métodos de evaluación de proyectos (período de recuperación, rentabilidad contable, Valor Actual

Neto (VAN), Tasa Interna de Retorno (TIR) así como la evaluación financiera desde diferentes escenarios y supuestos. Finalmente se trabaja con las variables macroeconómicas y el riesgo en los proyectos de inversión.

Investigación En coordinación con el Programa de Investigación en Energías Limpias y las Escuelas de Ing. en Electrónica, Ing. en Computación e Ing. Electromecánica, se ha elaborado una estrategia para el desarrollo de proyectos de investigación utilizando las instalaciones solares fotovoltaicas del campus. En la figura 8 se muestra un mapa mental de dicha estrategia, en donde se puede observar que la orientación de la investigación esta en el control y optimización de sistemas, la identificación de parámetros y el diagnóstico de fallas. Por ejemplo, la figura 9 muestra el proceso de reconocimiento de paneles en imágenes aéreas para ser utilizadas en sistemas de realidad aumentada que faciliten las tareas de mantenimiento e identificación de fallas. Por otro lado, la figura 10 ilustra el proceso de identificación de ensuciamiento por medio de procesamiento de imágenes.

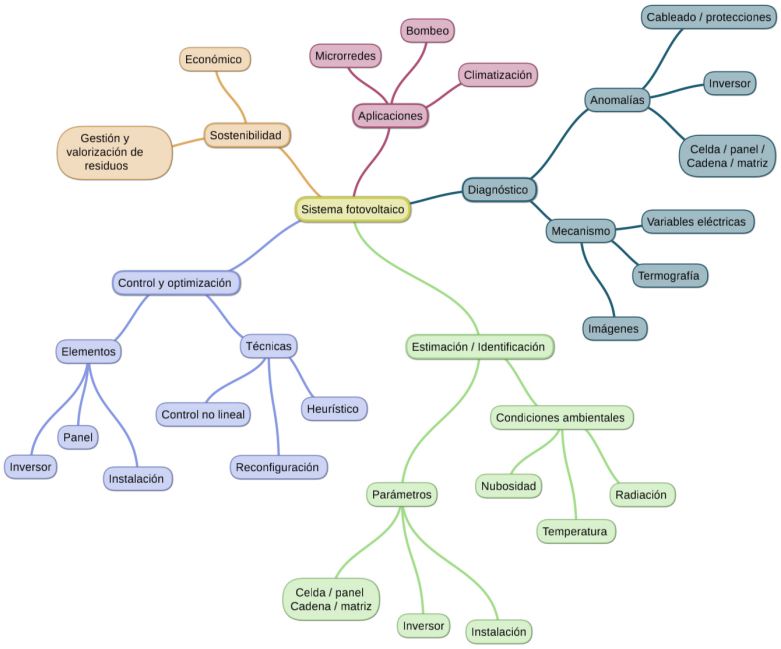

Figura 8. Mapa mental de las investigaciones que se realizan en el conjunto de instalaciones fotovoltaicas del campus del Instituto Tecnológico de Costa Rica

Figura 9. Caputra de pantalla de reconocimiento de paneles solares en imágenes aéreas.

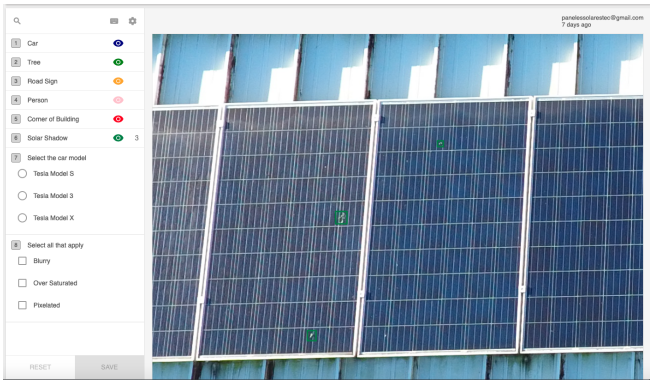

Figura 10. Captura de pantalla del entrenamiento del algorimo para identificación de anormalidades.

4.6. Labores de vinculación

El conjunto de instalaciones fotovoltaicas ha permitdo concretar las siguientes vinculaciones con el sector productivos:

- se ha firmado un convenio de colaboración con la empresa que proporcionó los equipos del conjunto de instalaciones solares de 400 kW. Dicho convenio permitió a la universidad adquirir los paneles a un precio significativamente menor al de mercado mientras que la empresa obtuvo más exposición de su marca y sus servicios. Además se acordó compartir información con la empresa sobre las investigaciones realizadas en la instalación. La empresa también participará en las reuniones semestrales que se realizarán para discutir las actividades de formación y de investigación que se realizarán en las instalaciones. Se espera que con la participación de la empresa en las reuniones se tenga conocimiento de primera mano de las situaciones y problemas que ocurren en la práctica con instalaciones solares en el país y la región.
- Se está capacitando a una empresa de limpieza de naves industriales para que extiendan sus servicios para dar mantenimiento a instalaciones solares de grandes superficies. Con ellos se están probando la efectividad de sustancias que permitan crear películas hidrofóbicas en la superficie del panel, además de la evaluación de sistemas robotizados semiautónomos para limpieza de paneles.
- Con una empresa de instrumentación científica se estarán realizando capacitaciones y talleres de monitorización de desempeño y ensuciamiento según la norma IEC-61724.

5. Conclusiones

Los campus universitarios representan lugares idóneos para la puesta en marcha de soluciones novedosas que permitan facilitar la transición hacia un modelo económico sostenible de bajo impacto ambiental. No obstante, para que éstas iniciativas novedosas sean sostenibles es necesario desarrollarlas desde una perspectiva integral tomando en cuenta aspectos académicos, administrativos y de vinculación con el sector externo universitario. En este artículo se ha presentado un plan de acción integral que ha sido implementado de forma exitosa para el desarrollo de varias instalaciones fotovoltaicas en los campus del Instituto Tecnológico de Costa Rica. De esta forma, se espera aportar a discusión sobre la necesidad de sistematizar la implementación de soluciones innovadoras de bajo impacto ambiental en ciudades universitarias. Es de opinión de los autores que dicha sistematización es fácilmente extrapolable a centros urbanos.

Referencias

1. Angelim, J.H., Affonso, C.M.: Energy management on university campus with photovoltaic generation and BESS using simulated annealing. 2018 IEEE Texas Power and Energy Conference, TPEC 2018 **2018-Febru**, 1–6 (2018)

2. Association of University Leaders for a Sustainable Future: Talloires Declaration. http://ulsf.org/talloires-declaration/, accesado: 2019-08-28
3. Axaopoulos, P.J., Fylladitakis, E.D.: Photovoltaic engineering e-learning applications developed for remote laboratory experimentation systems. International Journal of Energy and Environmental Engineering **5**(1), 1–10 (2014)
4. Baltazar, J., Osório, S., Guerra, D.A., Dutra, L., Beatriz, N., Schwinden, C.: Energy Efficiency in the Adoption of Renewable Energies in Schools. In: Implementing Campus Greening Initiatives, pp. 183–201. Springer International Publishing (2015), http://link.springer.com/10.1007/978-3-319-11961-8
5. Bekessy, S., Samson, K., Clarkson, R.: The failure of non-binding declarations to achieve university sustainability: A need for accountability. International Journal of Sustainability in Higher Education **8**(3), 301–316 (2007)
6. Bellantuono, N., Pontrandolfo, P., Scozzi, B., Dangelico, R.M.: Assessing Resources and Dynamic Capabilities to Implement "Green Campus"Project. In: The Contribution of Social Sciences to Sustainable Development at Universities, pp. 213–227. Springer International Publishing (2016), http://link.springer.com/10.1007/978-3-319-26866-8
7. Bourahla, N.A., Benghanem, M., Bouzeboudja, H.: Conception and Analysis of a Photovoltaic Microgrid in the USTO Campus. Proceedings of 2018 3rd International Conference on Electrical Sciences and Technologies in Maghreb, CISTEM 2018 pp. 1–6 (2019)
8. Choi, Y., Oh, M., Kang, J., Lutzenhiser, L.: Plans and living practices for the green campus of portland state university. Sustainability **9**(2), 252 (2017)
9. Eggleston, C.M.: Renewable Energy on Campus at the University of Wyoming. In: Implementing Campus Greening Initiatives, pp. 103–111. Springer International Publishing (2015), http://link.springer.com/10.1007/978-3-319-11961-8
10. García, L.: Hacia una Universidad de Concepción Sustentable: Implementación de Proyectos Energéticos. In: Ciudades Inteligentes Totalmente Integrales, Eficientes y Sostenibles, pp. 295–306. Editorial Universidad de Santiago de Cali (2018)
11. Guzman-Hernandez, T.d.J., Araya-Rodríguez, F., Castro-Badilla, G., Obando-Ulloa, J.: Uso de la energía solar en sistemas de producción agropecuaria: producción más limpia y eficiencia energética. Tecnología en Marcha **30**(5), 46–56 (2016)
12. Hernández-Callejo, L., Latorre, M., Obregón, L.: Electric Microgrid in Smart Cities: CEDER-CIEMAT a case of study. In: Ciudades Inteligentes Totalmente Integrales, Eficientes y Sostenibles, pp. 295–306. Editorial Universidad de Santiago de Cali (2018)
13. Inarejos, R., Rodríguez, A., López, G., Alvarez-Campana, M., Avilés, C.: Análisis de la huella de carbono de la ETSIT de la UPM y propuesta de mejora basada en datos de la plataforma IoT Smart CEI Moncloa. In: Ciudades Inteligentes Totalmente Integrales, Eficientes y Sostenibles, pp. 660–674. Editorial Universidad de Santiago de Cali (2018)
14. IRENA, I.: Renewable power generation costs in 2019 (2018)
15. Ke, B.R., Ku, T.T., Ke, Y.L., Chuang, C.Y., Chen, H.Z.: Sizing the battery energy storage system on a university campus with prediction of load and photovoltaic generation. 2015 IEEE/IAS 51st Industrial and Commercial Power Systems Technical Conference, I and CPS 2015 pp. 1–12 (2015)
16. Khan, K.S., Ullah, Z., Khan, B., Sami, I., Ali, S.M., Mehmood, C.A.: Assessment of hybrid off-grid wind photovoltaic system: A case study of university campus. ICECE 2017 - 2017 International Conference on Energy Conservation and Efficiency, Proceedings **2018-Janua**, 16–21 (2018)

17. Meza-Benavides, C.: Seslab promueve e investiga en energías renovables. Investiga. TEC (14), ág–12 (2012)
18. Morales, S., Meza, C.: Experiencias e iniciativas para promover la eficiencia energética y las energías renovables en el entorno universitario. In: IV Congreso Brasileiro de Eficiência Energética (2011)
19. Némoz, S.: Smart Campus: Recent Advances and Future Challenges for Action Research on Territorial Sustainability. In: Implementing Campus Greening Initiatives, pp. 313–323. Springer International Publishing (2015), http://link.springer.com/10.1007/978-3-319-11961-8
20. Oliveira, I.C., Rosa, A.C., Bonatto, B.D., Arango, H., Pereira, J.L., Ribeiro, P.F.: Analysis of economic return of the installation of photovoltaic panels at the campus of the Federal University of Itajubá. SBSE 2018 - 7th Brazilian Electrical Systems Symposium pp. 1–6 (2018)
21. Radhakrishnan, B.D., Viswanathan, S.: National University's Integrted Approach Towards Sustainable-Green Campus: Leadership, Curriculum, and Outreach. In: Implementing Campus Greening Initiatives, pp. 75–91. Springer International Publishing (2015), http://link.springer.com/10.1007/978-3-319-11961-8
22. Rodríguez, R., Radel, M., Cubero, A., Vázquez, F.: UCO Smart Campus, an intelligent environment for the university community. In: Ciudades Inteligentes Totalmente Integrales, Eficientes y Sostenibles, pp. 872–886. Editorial Universidad de Santiago de Cali (2018)
23. Saleh, A.A., Mohammed, A.H., Abdullah, M.N.: Critical success factors for sustainable university: A framework from the energy management view. Procedia-Social and Behavioral Sciences **172**, 503–510 (2015)
24. Seres, I., Farkas, I.: Development of A10 kWp Photovoltaic System — Efficiency Analysis. Proceedings of ISES World Congress 2007 (Vol. I – Vol. V) pp. 1652–1656 (2009)
25. Shukla, N., Khimani, R.: On the Way to Greening of the University. In: Implementing Campus Greening Initiatives, pp. 229–549. Springer International Publishing (2015), http://link.springer.com/10.1007/978-3-319-11961-8
26. Skorpil, J., Scerba, E., Dvorsky, E., Hejtmankova, P.: PV Generators in the Czech Republic and at the WBU in Pilsen — Application, Research, Education, Perspective. Proceedings of ISES World Congress 2007 (Vol. I – Vol. V) pp. 1567–1571 (2009)
27. Suni, A., Corr, M., De, S.: The Role of the University in Promoting Photovoltaic Usage in Brazil. In: Implementing Campus Greening Initiatives, pp. 229–549. Springer International Publishing (2015), http://link.springer.com/10.1007/978-3-319-11961-8
28. Sylvestre, P., McNeil, R., Wright, T.: From talloires to turin: A critical discourse analysis of declarations for sustainability in higher education. Sustainability **5**(4), 1356–1371 (2013)
29. Tamaneh-Nyah, C., Mukwekwe, L.: An investigation on the effect of operating temperature on power output of the photovoltaic system at University of Namibia Faculty of Engineering and I.T campus. 2015 3rd International Conference on Digital Information, Networking, and Wireless Communications, DINWC 2015 pp. 22–29 (2015)
30. Valbuena, F., González, M., Gutiérrez, C.: Edificios inteligentes para ciudades inteligente: el edificio I+D+i del Campus de Soria. In: Ciudades Inteligentes Totalmente Integrales, Eficientes y Sostenibles, pp. 710–726. Editorial Universidad de Santiago de Cali (2018)

31. Velazquez, L., Munguia, N., Platt, A., Taddei, J.: Sustainable university: what can be the matter? Journal of Cleaner Production **14**(9-11), 810–819 (2006)

On Campus Smart Energy Services enabled by the Smart CEI Moncloa IoT Platform

Pedro Moura[1][0000-0003-4852-2812], Gregorio López[2][0000-0001-9954-3504], José Ignacio Moreno[3][0000-0002-1770-1853], Manuel Alvarez-Campana[3][0000-0003-2747-9798], Julio Berrocal[3][0000-0001-6822-0921]

[1] Institute of Systems and Robotics, Dep. of Electrical and Computer Engineering, University of Coimbra, Polo II, 3030-290 Coimbra, Portugal
[2] Institute for Research in Technology (IIT), ICAI School of Engineering, Comillas Pontifical University, Calle de Alberto Aguilera, 25, 28015 Madrid, Spain
[3] Departamento de Ingeniería de Sistemas Telemáticos, Universidad Politécnica de Madrid, Avenida Complutense 30, 28040 Madrid

Abstract.
University campuses are not only responsible for high energy demand, but also set examples for the community by implementing energy sustainability projects. In such context, in 2013, Universidad Politécnica de Madrid (UPM) launched the UPM City of the Future initiative. One of the main projects within this initiative was the design, development and deployment of an IoT-based platform which allowed for the experimentation and evaluation of Smart City services in the Moncloa Campus of International Excellence (CEI Moncloa).
This paper proposes the optimization of the energy consumption and renewable energy generation in a set of buildings of the ETSIT-UPM Campus by using photovoltaic solar panels on the facades and roofs of buildings and the incorporation of actuators to allow intelligent control of lighting and air conditioning.
First, an analysis of the consumption in a complete year cycle and the evaluation of current carbon footprint is developed. From this point, the capacity of the buildings to generate energy by means of photovoltaic cells which cover up to 44% of current demand is assessed, as well as the impact of energy storage solutions. Such options lead to a total decrease of the carbon footprint, ensuring the required consumption levels to be qualified as nZEB. In order to ensure such monitoring and control, the IoT-based platform deployed in the CEI Moncloa campus was used, and new energy services to be included in the future were proposed. These services, to be implemented on the IoT-based platform Smart CEI Moncloa, are based on real-time monitoring to ensure a higher matching between local generation and demand, as well as to reduce cost and ensure a significative reduction of carbon footprint.

Keywords: IoT Platform, Solar photovoltaics, Energy Efficiency, Energy Storage, Monitoring and Control.

1 Introduction

University campuses are normally constituted by large buildings responsible for high energy demand. The challenges associated with high energy costs and environmental impacts are clear motivations to achieve efficiency and suitability goals. Additionally, University buildings are also important as demonstration sites for new technologies and systems.

This paper presents the considered options of energy sustainability in the set of four buildings that constitute the Escuela Técnica Superior de Ingenieros de Telecomunicación of the Universidad Politécnica de Madrid (ETSIT-UPM). Located at the Campus of International Excellence in Moncloa (University City of Madrid), ETSIT is a national and international reference center in the field of teaching, research and technological development and innovation in the area of Information and Communications Technology (ICT).

The four buildings of the ETSIT are constituted by a series of classrooms, teaching or research laboratories and offices of professors and researchers:

- Building A (Sanz Mancebo) – building with the largest number of classrooms and student laboratories, as well as some teachers' offices, main hall, meeting room, evaluations room, assembly hall, library, canteen, student clubs, secretariat and directors' board.
- Building B (García Redondo) – building with other classrooms, some student laboratories and numerous research laboratories and professors' offices (the building is connected to building A by means of an elevated corridor known as "the accelerator").
- Building C (López Araujo) – this building communicates with building B and is mainly constituted by research laboratories, and professors' offices, but also by the museum and a second assembly hall (attached to this building is the Solar Energy Institute).
- Building D – this is the most recent building, it is connected to building A and is conceived in part as a business incubator, but it also contains more research laboratories and offices.

The development of ETSIT's teaching and research activity entails a significant consumption of energy resources. Therefore, this paper deals with the options to achieve more sustainable use of energy. This entails identifying two areas of action aimed at reducing the carbon footprint: the incorporation of renewable energy sources and the use of an intelligent system to control air conditioning and lighting. In order to ensure such monitoring and control, the IoT-based platform deployed in the CEI Moncloa campus is used. Furthermore, the paper discusses the implementation of new energy services in the IoT-based platform.

The remainder of the paper is structured as follows. Section 2 presents the characterization of the electricity demand, the sizing and design of the photovoltaic generation and storage systems and the evaluation of their contribution to the reduction of the carbon footprint. Then, Section 3 presents the IoT-based platform deployed in the CEI

Moncloa campus and the future energy services to be implemented. Finally, Section 4 summarizes the paper, emphasizing its main conclusions and presenting future developments.

2 Electricity Demand and Generation

2.1 Electricity Demand

In 2018 the buildings presented an electricity demand of about 4.4 TWh/year. Since the building has an area of 44.020 m^2 this corresponds to a specific consumption of 99.96 kWh/m^2 year. Fig. 1 presents the variation of the electricity consumption of the building during the year. As can be seen, the consumption does not present major variations, with the exception of August, which presents a much lower consumption due to the holiday's period. The maximum electricity consumption (in July) is 40% higher than the minimum (in August). However, excluding August, such variation is reduced to only 20% (the standard deviation is reduced from 31.46 MWh to 23.75 MWh). The highest consumptions are achieved in the Summer, due to the high impact of the cooling demand. This is confirmed by observing the variations of the average minimum and maximum temperature, being an increase of the maximum temperature associated with a demand increase. The same occurs, but with lower impact, on the low values of minimum temperature.

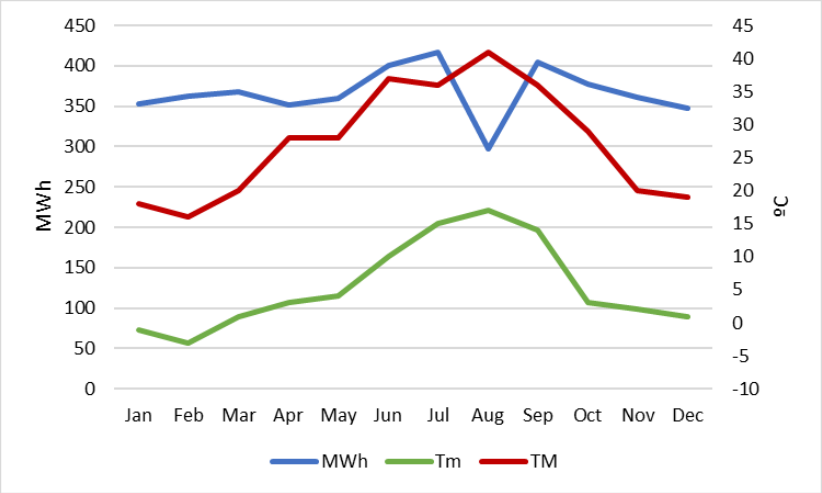

Fig. 1. Monthly electricity demand, minimum (Tm) and maximum temperature (TM) in 2018

2.2 Renewable Generation

In order to evaluate the potential for photovoltaic (PV) generation of the ETSIT buildings, the available areas and orientations were measured using Google Earth. All buildings have the same orientation, which is similar to the ideal orientation. An orientation with the main facade of the building facing South is preferable to take advantage of solar passive gains in the building, as well as to photovoltaic generation, since the PV panels should ideally be oriented to South. The buildings are not perfectly oriented to the South, but there is only an angle of 7.8º. Therefore, the PV panels can have the same orientation of the building, facilitating their integration, since a 7.8º angle only reduces the average generation in less than 0.5%.

It was then considered the use of 270 W PV panels with dimensions of about 0.992 x 1.64 m. In order to maximize the generation and taking into account the location, a tilt angle of 38º was considered. Therefore, the roof area occupied by each panel is about 1.273 m^2. Considering the use of 50% of the available area, in order to ensure the spacing to avoid shadowing and enable other uses of the roof, it is possible to install 3856 panels, as presented in Table 1.

Table 1. Available area and PV panels that can be installed in each building.

Building	Area m^2	PV Area m^2	Panels #
A	5731	2866	2250
B	1395	698	548
C	1244	622	488
D	1453	727	570
Total	9823	49125	3856

However, in building C, there are already PV panels installed in three different levels of the facade. The generation of such panels was taken into account in the assessment and a similar structure was considered for buildings B and A The system installed in building C has 352 PV panels, and keeping the same dimensions, systems with 150, 144 panels were considered for buildings A and B, respectively. Therefore, Table 2 presents the total number of panels, as well as the associated peak power.

Table 2. Quantity of PV panels and power.

Building	Roof #	Facade #	Total #
A	2250	150	2400
B	548	144	692
C	488	352	840
D	570	0	570
Total	3856	646	4502

The PV system was then designed and simulated using Sunny Design [1], considering the meteorological data of Madrid, using an annual total global irradiation of 1,655.16 kWh/m²a.

In order to evaluate the self-consumption of the generated energy, the electricity consumption records of the building in 2018 were used with a time interval of 15 minutes. Fig. 2 presents examples of the load profiles during the first week of February, July, and August. As can be seen, the electricity demand during the weekend is much lower than in weekdays and the demand during August is much lower than in other months due to the summer holidays. The high demand at night is justified by the use of the building by students and researchers during such period. Such diagrams are going to be taken into account to evaluate the matching between the PV generation and consumption.

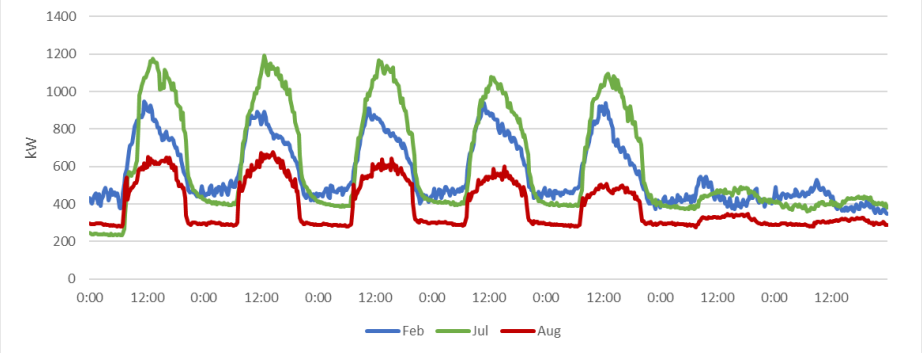

Fig. 2. Load profiles during one week in February, July and August

The main characteristics of the designed PV system are presented in Table 3. As can be seen, the system has 4502 PV panels ensuring a peak power of about 1.22 MWp and a nominal AC active power of 1.17 MW, due to the 72 inverters. The annual energy generation is, on average, 1,935 MWh, with a performance ratio of 86.2%.

Table 3. Characteristics of the PV system.

Total number of PV modules	4502
Peak power	1.22 MWp
Number of PV inverters	72
Nominal AC power of the PV inverters	1.17 MW
AC active power	1.17 MW
Active power ratio	96.2 %
Annual energy yield	1,935.89 MWh
Energy usability factor	99.99 %
Performance ratio	86.2 %

Table 4 presents the distribution of the PV generation and assesses the self-consumption, self-generation, and self-sufficiency in the buildings. As can be seen, from the

total generation of 1,936 MWh, 1,606 MWh are used in the buildings (83% of the generated energy), as self-consumption and 330 MWh have to be injected into the grid (due to the high generation in periods of low demand). Therefore, 2,792 MWh have to be purchased from the grid, in order to ensure the total demand of 4,398 MWh. The generation is equivalent to 44% of the demand, but to compensate the grid feed-in, the energy purchased from the grid is 63.5%, leading to a self-sufficiency of 36.5%.

Table 4. Distribution of PV energy and consumption.

Annual energy consumption	4,398 MWh
Annual energy yield	1,936 MWh
Grid feed-in	330 MWh
Purchased electricity	2,792 MWh
Self-consumption	1,606 MWh
Self-consumption quota (in % of PV energy)	83.0 %
Self-generation (in % of energy consumption)	44.0 %
Self-sufficiency quota (energy consumption in %)	36.5 %

Fig. 3 presents the variation of the PV generation, self-consumption, and grid feed-in throughout the year. As expected, the generation is higher during summer, leading to higher self-consumption levels. Regarding the grid feed-in, there is a high increase in August due to the low demand and high generation level.

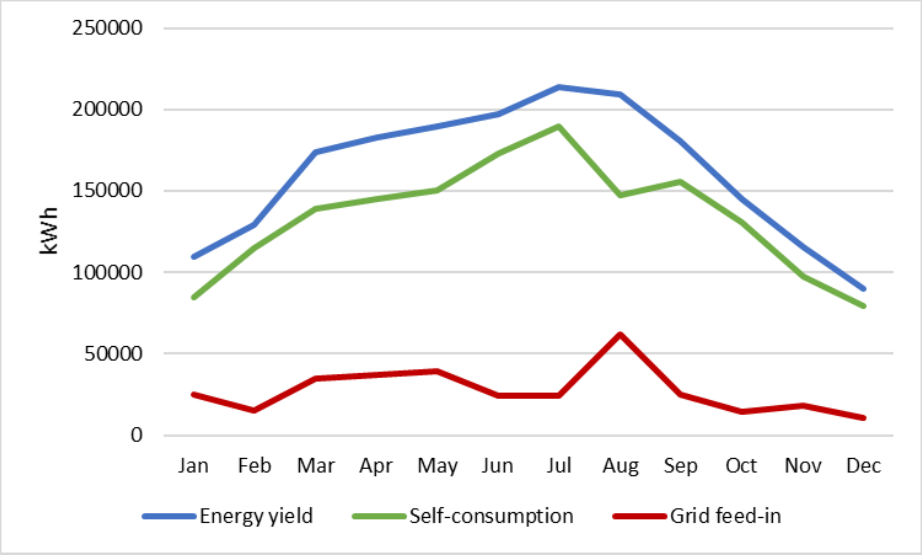

Fig. 3. Variation of the PV generation, self-consumption and grid feed-in

2.3 Energy Storage

A storage system was also considered with the objective to increase the matching between PV generation and consumption, therefore reducing the grid feed-in. An energy storage system with lithium-ion batteries with a total capacity of 480 kWh with a minimum state of charge of 20% and a round trip of 95% was considered, being the impact presented in Table 5. As can be seen, despite the high energy storage capacity the impact on the self-consumption is not high, being achieved an increase of only 3.6% due to a reduction on the grid feed-in of 67 MWh. This is justified by the low daily use of the battery.

Unlike what happens in residential buildings, where there is typically a daily cycle, charging the surplus during the day to be used at night, in this case most days do not present a generation surplus. The generation surplus is concentrated in the weekend, being the battery mainly used to store such surplus in order to be used on Monday. This leads to an annual nominal energy throughput of the battery of only 139. Therefore, only from the self-consumption point-of-view, such storage system is not cost-effective. However, the capacity not used to store generation surplus can be used to store electricity from the grid in periods of lower cost, in order to minimize the costs with the purchased electricity, as presented in [2].

Table 5. Distribution of PV energy and consumption (scenario with energy storage).

Annual energy consumption	4,398 MWh
Annual energy yield	1,936 MWh
Grid feed-in	263 MWh
Purchased electricity	2,732 MWh
Self-consumption	1,673 MWh
Self-consumption quota (in % of PV energy)	86.4 %
Self-generation (in % of energy consumption)	44.0 %
Self-sufficiency quota (energy consumption in %)	37.9 %

2.4 Carbon Footprint

The norm ISO 14064 was used to the evaluation of the carbon footprint. The evaluation considers the year of 2018 and the total surface of the four ETSIT buildings, which is 44,020 m^2 [3], and a total number of 3057 users (including students and employees) [4].

The evaluation considers direct emissions (due to the use of fuels in the buildings) and indirect emissions (due to the consumption of electricity generated outside the building). In addition to electricity, the buildings use natural gas and the considered emission factors were the standard emission factor for Spain defined by the Covenant of Mayors, which are 0.44 tCO_2/MWh to electricity and 0.202 tCO_2/MWh to natural gas [5]. The used conversion factor of electricity to primary energy was 2.6 [6].

Table 6 presents several performance indicators for the building, such as the CO_2 emissions, carbon footprint, primary energy consumption and specific primary energy consumption. As can be seen, the buildings have a carbon footprint of 16.46 gCO2/pax*m^2 and specific primary energy consumption of 291.29 kWh/m^2year.

Table 6. Performance indicators.

Source	Final Energy (MWh/year)	CO_2 Emiss. (t CO_2/Year)	Carbon Foot. (gCO_2/paxm^2)	Primary Ener. (MWh/year)	Specific P. E. (kWh/m^2year)
Electricity	4,398	1,935	14.38	11,435	259.76
Natural Gas	1,388	280	2.08	1,388	31.53
Total	5,798	2,215	16.46	12,823	291.29

Considering the designed PV system, the net electricity consumption decreases to about 2,462 MWh/year, therefore decreasing the carbon footprint to 10.13 gCO_2/pax*m^2 and the specific primary energy consumption to 176.95 kWh/m^2year (Table 7), achieving a reduction of 39%.

Table 7. Performance indicators (including PV generation).

Source	Final Energy (MWh/year)	CO_2 Emiss. (t CO_2/Year)	Carbon Foot. (gCO_2/paxm^2)	Primary Ener. (MWh/year)	Specific P. E. (kWh/m^2year)
Electricity	2,462	1,083	8.05	6,401	145.41
Natural Gas	1,388	280	2.08	1,388	31.53
Total	3,850	1,364	10.13	7,789	176.94

However, energy sustainability should not be only ensured with more (renewable) generation, being fundamental to increase energy efficiency in order to decrease the baseline consumption. One important option can be the reduction of lighting consumption. In this type of buildings, lighting typically represents 30% of electricity consumption. The replacement of the actual conventional systems by LEDs typical ensures about 63% of savings [2], representing in this case 831 MWh/year. Such option can decrease the carbon footprint to 7.42 gCO_2/pax*m^2 and the specific primary energy consumption to 127.85 kWh/m^2year (Table 8), achieving a reduction of 56%.

Table 8. Performance indicators (including PV generation and lighting),

Source	Final Energy (MWh/year)	CO_2 Emiss. (t CO_2/Year)	Carbon Foot. (gCO_2/paxm^2)	Primary Ener. (MWh/year)	Specific P. E. (kWh/m^2year)
Electricity	1,631	718	5.33	4,240	96.32
Natural Gas	1,388	280	2.08	1,388	31.53
Total	3,019	998	7.42	5,628	127.85

This numbers can be compared with the requirements to achieve a nearly zero energy buildings (nZEB) definition. EU states shall draw up national plans for increasing the number of nearly zero-energy buildings, which should include a numerical indicator in primary energy expressed in kWh/m^2 year. Spain has not yet defined a numerical indicator for nearly zero energy buildings, but the buildings will most likely need to comply with class A [7], which requires, for office buildings, a maximum primary energy consumption of 175 kWh/m^{2}year [8]. Therefore, with the designed PV system and energy savings due to lighting refurbishment the buildings can ensure the required consumption levels to be qualified as nZEB.

3 IoT Platform

3.1 Current Services

The Smart CEI Moncloa was deployed within the context of the UPM City of the Future initiative. It is an IoT platform that currently offers two services [9]:

- people flow monitoring,
- and environmental monitoring.

There are quite a few techniques to perform people flow monitoring (e.g., based on radiofrequency, cellular technologies, GPS, Bluetooth or Wi-Fi) [10]. In the case of Smart CEI Moncloa, this service is provided by means of Wi-Fi tracking, using low-cost Wi-Fi sensors based on Raspberry Pi. The software running in these sensors have been specifically developed for the Smart CEI Moncloa platform and allows scanning all Wi-Fi channels and recording the MAC addresses of the Wi-Fi-compliant devices (e.g., smartphones, tablets, laptops) in the region of coverage, storing them appropriately anonymized. To be more precise, these Wi-Fi sensors scan each of the Wi-Fi channels from both the 2,4 GHz and the 5 GHz bands during a configurable amount of time (currently, 250 ms), read the header of the radio IEEE 802.11 packets (e.g., data packets or probe requests) in its region of coverage, record the sender MAC addresses and store a hash of them.

For the environmental monitoring service, the Smart Citizen Kit (SCK) [11] is used. The SCK are based on Arduino and incorporate a shield board which includes sensors for temperature, humidity, light, noise level, and air quality (notably, CO and NO_2). These devices are adapted to be able to take these measurements both indoors and outdoors.

As shown in Fig. 4, the Smart CEI Moncloa currently includes 52 Wi-Fi sensors (9 of them deployed in the ETSIT-UPM) and 25 environmental sensors (3 of them deployed in the ETSIT-UPM).

The Smart CEI Moncloa has been used and further developed in a remarkable number of BSc and MSc thesis, as well as in research works. Among the latter, it is worthwhile to mention [10], where the huge amount of data stored from the Wi-Fi tracking devices of the ETSIT-UPM during a whole year are used for analyzing time and occupancy, position of people, and identification of common behaviors. In addition, [12] proposes the combination of the data coming from both services in the ETSIT-UPM to improve energy efficiency, and so reduce environmental footprint, by controlling the

light in certain places of the ETSIT-UPM based on the occupancy and light measured by the Smart CEI Moncloa platform.

Engineering schools	Number of sensors	
	Wi-Fi tracking	Environmental
1. Telecommunications	9	3
2. Forestry I	3	2
3. Forestry II	3	2
4. Rectorate	4	2
5. Civil	3	2
6. Agricultural I	3	2
7. Agricultural II	5	2
8. Aeronautical & Aerospace	5	2
9. Naval & Marine	3	2
10. Architecture I	4	2
11. Architecture II	2	-
12. Health Science & Sport	3	2
13. Industrial	5	2
Total	52	25

Fig. 4. Summary of the sensors currently deployed in Smart CEI Moncloa [9]

3.2 New Services

Using the actual infrastructure, several new services were designed to be implemented in the near future, related to the electricity demand and renewable generation monitoring, control and demand flexibility.

Electricity Demand and Renewable Generation Monitoring
The most important information to be included in the platform, from the energy perspective, is the variation of the electricity demand (total and by building). The demand is already being monitored and the information is available online at [13]. Therefore, such information can be easily integrated into the platform.

Besides the load diagram, the platform could provide more data and services. Based on the load diagram several statistics can be provided, such as energy consumption, maximum and minimum power during the current day. Then, an overview of the evolution of such parameters can be provided enabling the comparison between the previous days, weeks and months.

One important use for such information can be the detection of abnormal situations, for instance, if the minimum power during the previous weeks has not presented major variations and then suddenly such value increases this means that additional equipment is now operating in periods of time without major activity in the building. This can be caused by the installation of new equipment or by abnormal functioning of existing equipment (damaged equipment or in permanent operation). The same can be done regarding any sudden increase in energy consumption or maximum power. However, in

such situations, the values should be only compared considering working days and differentiating the weeks with and without classes.

Other interesting services could be the comparison of the variation of the electricity demand with the variation of the Wifi activity. The Wifi activity is correlated with the number of users [9] and a higher number of users leads to higher electricity demand.

The data from the environmental data can also be important to assess the variation of consumption. For instance, the variation of the temperature can be compared with the variation in electricity demand in order to evaluate the impact of the temperature on the electricity consumption.

Like electricity consumption, it would be important to present in the platform the variation of the PV generation in the buildings. The information from the actual PV systems are already available at [13] and such information can be easily integrated into the platform.

Such statistics can also be very useful for maintenance purposes. Most PV systems are constituted by serial strings of PV panels with one central inverter. Then, when one PV panel presents any malfunction, this is going to affect all the other PV panels connected to the same inverter, leading to a strong reduction of the generation. Therefore, such situations must be corrected as soon as possible, being important to have tools to automatically detect it. A simple way to implement this detection is to analyze the variation of the generation of the various PV systems. If only one PV system presents a reduction of the generation for one day when compared with the previous day, this is not due to any reduction of the solar radiation, since such reduction would affect all PV systems. Therefore, to detect it, the generation of the PV systems can be compared with the generation during the previous day (or an average of some previous days). If any PV system presents a reduction that is much higher than any other systems, the platform can send an alarm.

The temperature provided by the environmental data can also be useful. Typical silicon PV panels have a temperature coefficient of about -0.4 to -0.5%. This means that for every degree Celsius above 25, the power output from the array would drop by that percentage. Then, the temperature data can also be used to evaluate the impact on the PV generation level.

The platform can also provide information about the carbon footprint. Based on the previously mentioned data on energy consumption and generation, using the specific emission factors, the emissions associated with the energy consumed (discounted by the generated energy) can be assessed. The evolution in real-time can be presented, as well as the accumulated emissions during the day, week or month.

Another parameter that can be presented is the share of the local renewable generation on the total demand. The matching between the generation and consumption can also be provided, by providing information about the variation of the self-consumption and self-sufficiency shares.

Control and Demand Flexibility

The smart control of HVAC systems can also be included in the platform in the near future, using SONOFF Pow devices to implement it [14]. This can be done in several circumstances, for instance, when a very high peak load is detected, or when the local

generation presents a high reduction (for instance due to the passage of clouds by the PV system).

The temperature data can also be used to decide if the control of HVAC can have a relevant impact on the comfort conditions. Another option is to implement the control based on the variation of the electricity tariff, for instance ensuring the pre-heating of the building to take advantage of lower tariffs.

The data from the consumption monitoring in the systems controlled by the SONOFF Pow devices can also be presented, being useful to observe the variation of consumption caused by the control.

All in all, the SONOFF actuators will leave the door open to develop automatic algorithms to increase energy efficiency and reduce environmental footprint.

4 Conclusions and Future Work

As other University Campus, the Moncloa Campus is constituted by large buildings with high electricity consumption. This is the case of ETSIT-UPM, which is constituted of four buildings with a total area of 44.020 m^2. With an electricity demand of about 4.4 TWh/year and a natural gas consumption of about 1.4 TWh/year, the buildings have a carbon footprint of 16.46 gCO2/pax*m^2 and a specific primary energy consumption of about 292 kWh/m^2year.

Therefore, in order to reduce the carbon footprint, the potential of the buildings for PV generation was assessed, being designed a PV system with 1.22 MWp able to ensure a generation level equivalent to 44% of the actual electricity demand. The design also includes lithium-ion batteries with a total capacity of 480 kWh with the objective to increase the self-consumption to 86.4%. Such storage system can also be used to ensure a minimization of electricity costs, by storing energy in the periods with the lowest cost. Other considered option was the increase of energy efficiency by replacing the actual conventional systems by LEDs. The implementation of such an option can decrease the carbon footprint to 7.42 gCO_2/pax*m^2 and the specific primary energy consumption to 127.85 kWh/m^2year, ensuring the required consumption levels to be qualified as nZEB.

In order to ensure the optimization of all resources, the use of ICT is crucial. Therefore, new energy services were designed, in order to be implemented in the near future on the IoT-based platform Smart CEI Moncloa. Such services are based on the real-time monitoring of electricity demand and generation, and the assessment of data in order to detect abnormal situations, provide information to increase the efficiency and the control of resources to ensure a higher matching between local generation and demand, as well as to reduce cost and ensure a significative reduction of carbon footprint.

Finally, when assessing the costs and benefits of undertaking the investment required to deploy the proposed system, the benefits that it would bring from the point of view of research must be taken into considerations. All in all, a platform like this represents a remarkable test bench which would allow evaluating innovative proposals, which may result in research funding and scientific publications.

Acknowledgments

This research has been partly funded by the Carolina Foundation through the mobility scholarship programme for Portuguese university lecturers and researchers, and by the Sustainable Campus Program at the Universidad Politécnica de Madrid for the year 2019, within the RES2 + U Sustainable Campus (Responsible, Sustainable, Social and University) platform.

References

1. SMA, “Sunny Design Pro”, https://www.sunnydesignweb.com, last accesse 2019/07/15
2. Paula Fonseca, Pedro Moura, Humberto Jorge and Aníbal de Almeida (2018) "Sustainability in university campus: options for achieving nearly zero energy goals", International Journal of Sustainability in Higher Education, Vol. 19 No. 4, pp. 790-816
3. UPM, “Portal de transparencia de la UPM: Inmovilizado material. Superficies a 31/12/2017: https://transparencia.upm.es/economico/relacion_bienes_inmuebles, last accessed 2019/07/15
4. UPM, “Portal de transparencia de la UPM.: Infraestructuras y recursos de la ETSIT UPM”, http://www.upm.es/transparencia/, last accessed 2019/07/15
5. Covenant of Mayors, “The Emission Factors”, https://www.eu-mayors.eu/IMG/pdf/technical_annex_en.pdf, accessed at 2019/07/15
6. BPIE, “Nearly Zero Energy Buildings Definitions Across Europe”, May 2015
7. RenoZEB, “RenoZEB Market Assessment”, September 2018.
8. Alex Ciurana, "Calificaciones Energeticas y Edificios nZEB”, https://www.congresoiener.com/pdf/ponencias-2018/sesion-5B-04-Calificaciones%20energeticas%20y%20edificios%20Nzeb%20-%20PGI.pdf, last accessed 2019/07/15
9. Manuel Alvarez-Campana *et al.* (2017), “Smart CEI Moncloa: An IoT-based Platform for People Flow and Environmental Monitoring on a Smart University Campus”, Sensors 17 (12), 2856
10. Javier Andión *et al.* (2018), “Smart Behavioral Analytics over a Low-Cost IoT Wi-Fi Tracking Real Deployment”, Wireless Communication and Mobile Computing, vol. 2018, Article ID 3136471, 24 pages
11. Smart Citizen Kit: https://smartcitizen.me/, last accessed 2019/08/12
12. Ramón Inarejos *et al.* (2018), “Análisis de la huella de carbono de la ETSIT de la UPM y propuesta de mejora basada en datos de la plataforma Smart CEI Moncloa”, 1st Ibero-american Congress of Smart Cities – ICSC-CITIES 2018, pp. 660-674, Soria, Spain.
13. UPM, “Monitorización”, http://monitoring.robolabo.etsit.upm.es/, last accessed 2019/07/15
14. ITEAD, “Sonoff Pow WiFi Switch With Power Consumption Measurement”, https://www.itead.cc/sonoff-pow.html, last accessed 2019/07/15

Low-cost illumination system for photovoltaic devices validation at the control and constant irradiance

Bhishma Hernández-Martínez[1[0000-0001-5577-209X]], Luís Hernández-Callejo[1[0000-0002-8822-2948]], Sara Gallardo-Saavedra[1[0000-0002-2834-5591]], Víctor Alonso-Gómez[1[0000-0001-5107-4892]] and Jose Ignacio Morales-Aragonés[1[0000-0002-9163-9357]]

[1] University of Valladolid, Campus Universitario Duques de Soria, Spain
bhishma.hernandez@alumnos.uva.es, B.H.;
luis.hernandez.callejo@uva.es, L.H-C.;
sara.gallardo@uva.es, S.G-S.;
victor.alonso.gomez@uva.es, V.A-G.;
ziguratt@coit.es, J.I.M.

Abstract. To advance on research in photovoltaic (PV) systems, there is a multitude of measurements and experiments that should be performed. Experiments should be accomplished in a controlled environment in order to obtain useful information that could be compared. Weather supposes variations on the solar irradiation that cannot be controlled and make it difficult to compare experiments under the same working conditions. To overcome these limitations, a low-cost illumination system for PV devices has been developed and validated. This allows the characterization of PV devices indoor, independently of the external irradiance conditions.

Keywords: illumination, photovoltaic measurements, artificial sun.

1 Introduction

Renewable technologies are considered as clean sources of energy and optimal use of these resources minimize environmental impacts, produce minimum secondary wastes and are sustainable based on current and future economic and social societal needs and the Sun is the source of all energies [1].

Despite there are some challenges to face, PV systems are the most demanded today. Its easy installation and reduced cost make them very attractive worldwide [2].

The PV cell and the PV module must be inspected continuously [3-4], some of these inspection techniques are: thermography [5], electroluminescence [6] and measurements using I-V curves [7].

The measurement of I-V curves is the most direct way to obtain information on the efficiency of the PV module [8-9]. The information from this measurement technique is essential to decide regarding the faults in the PV module [10].

This technique requires special environmental conditions, specifically temperature and irradiance. The effect of clouds and low irradiance means that I-V devices do not

work properly. Therefore, this work focuses on the design and implementation of an artificial sun. In this way, the I-V technique will not depend on the environmental conditions, and can be performed with the device proposed in this work.

2 Methodology and resources

2.1 Solar irradiance

To perform experiments on the field is important to understand responses on real conditions. Result difficult to reproduce exact same working conditions from day to day, even from one minute to the following one. Solar irradiance which is the main excitation to the majority of PV experiments depends on weather conditions. It is not possible control the weather variations which change randomly. The method used in field measurements is registered irradiance and temperature parameters.
Unfortunately, is very difficult to maintain constant the irradiance values in order to compare experiments and results. Figure 1 represents the solar irradiance values that we could register one day that we would like to perform experiments with PV modules.
There are two different approaches to the variability of irradiation. The first is, only could perform experiments a few days in one year to ensure small solar irradiation variability. Second, we should apply mathematical models to normalize measured values. On that case information is manipulated and potentially lose accuracy on information.

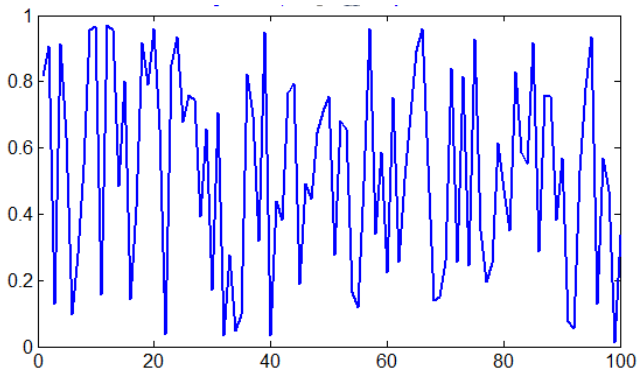

Fig. 1 Solar irradiance of 100 minutes from a random day.

The solar spectrum is composed of a complex mixture of wavelengths and amplitudes. There are devices that create illuminations with a very similar spectrum to the sun's spectrum. The cost of those devices sometimes is some thousand dollars. To small investigation teams maybe this cost is not acceptable. Figure 2 shows the solar spectrum measured.

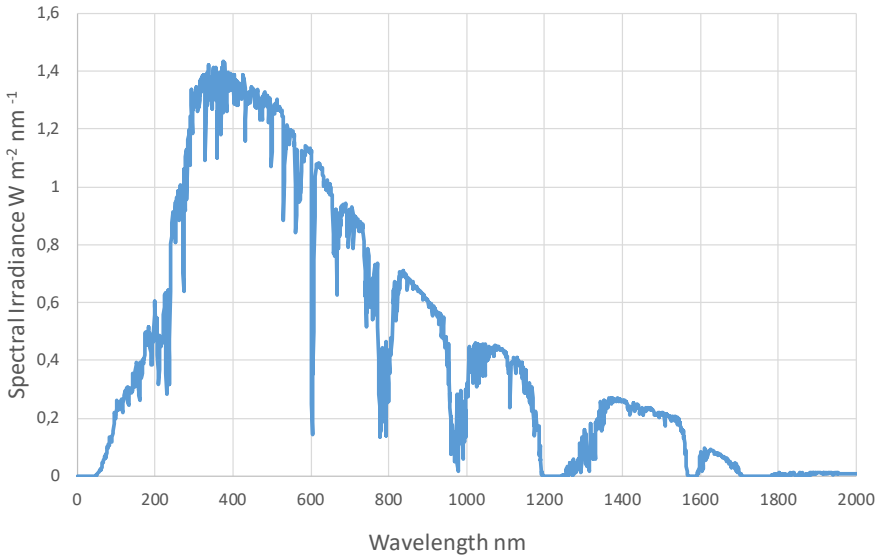

Fig. 2 Solar spectrum AM 1.5 Direct circumsolar $[\frac{W}{m^2 * nm}]$.

2.2 Photovoltaic devices.

The response of PV devices (PV cells, PV modules…) is adapt to the solar wavelength that we could observe on earth surface. The specific response of each device is different and has a relation with the technology used to manufacture it.

Figure 3 represents solar excitation and crystalline silicon PV cell response used to convert solar irradiation on electricity. Figure 4 is represented the total energy from the sun and the PV cells capability to acquire it. Different technologies will have different efficiencies. As bigger is the capability to transform wavelengths on electricity, bigger is the efficiency that the PV device has. Tandem cells that use different technology on the different semiconductor layer, are designed to increase the usable energy capture on the PV cell.

Field experiments take advantage of the direct solar spectrum, but assume the potential differences that could be on solar irradiation due to variations that are created due to weather conditions.

Comparing Figure 3 and Figure 4, we could see the performance of crystalline PV silicon cells and how it is adapted to the solar spectrum.

Field experiments should include the information the variation created by different working conditions. Obtained results to be provided difficult to correlate to each others due to not full control working conditions. Equations to normalize results reduce the accuracy and include an unspecified uncertain level.

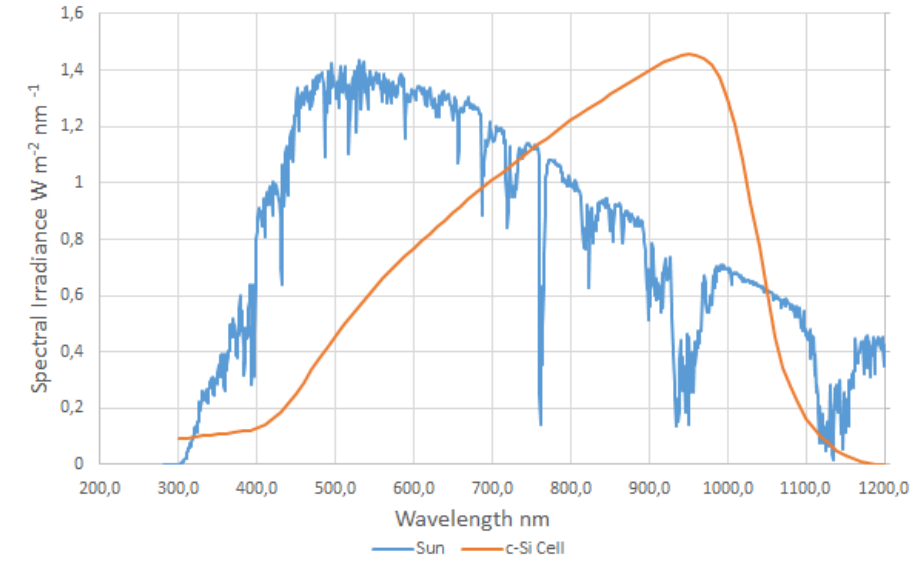

Fig. 3 Solar spectrum AM 1.5 Direct circumsolar $[\frac{W}{m^2 * nm}]$ and crystalline silicon response.

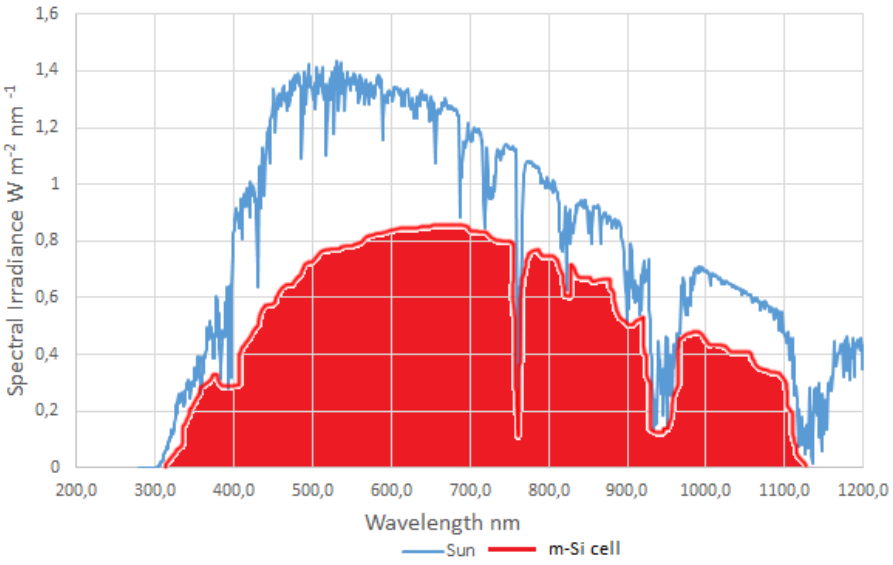

Fig. 4 Solar spectrum AM 1.5 Direct circumsolar $[\frac{W}{m^2 * nm}]$ and energy usable for silicon PV cells.

2.3 IRIS. The low-cost illumination system

Understanding limitations that are inherent to field measurements and, defining real needs for the desired test to perform on PV devices. The investigation team decided to develop a simple illumination device, centered on 850 nm wavelength irradiation (see Figure 5).

The excitation that IRIS (as we call the developed lamp) is different from the solar spectrum. Illumination created has a narrow wavelength and high irradiance on it. However, the response that we measure in some experiments performed on solar cells and solar panels demonstrate that the develop illumination system is used for most of them.

Low-cost lamp designed, has a fan device to ensure thermal stability and current drivers to ensure constant current. Both parameters should be under control and constants. It is important to control the temperature because it will be impacting the wavelength. The current applied to LED will be impacting radiation. Figure 6 presents the radian flux for different current values applied to the LED.

The system designed is easily scalable. It provides the capability to grow and assembles one lamp to the next creating tessellation. It includes the capability to enable or disable lamps and trimming the current value to simulate as we desire different flux radiation. The layout is designed to install other LEDs that could provide different wavelength. It is thought of that way to be flexible for future requirements.

The shape that the device has (see Figure 7), is equal to the PV cell shape. It provides the possibility to be adapted directly to 15cmx15cm PV solar cell. The tessellation will be then on squares of 15x15cm size.

It is important to understand the power requirements that the device has. The power consumption is 67.5W (25V@ 2.7Amps) per lamp. To illuminate a full PV module of 72 cells, cell by cell, it will be needed around 5 kW. It means that the system will need 200 A.

The irradiance created could be bigger than irradiance registered on the earth's surface. It could be modulated using a trimmer or modifying the distance between the PV device and the lamp.

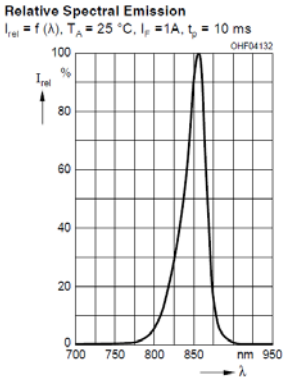

Fig. 5 Spectrum provided by developed low-cost lamp.

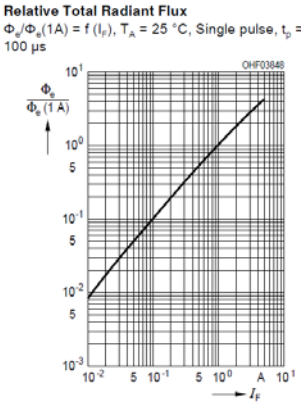

Fig. 6 Irradiation provided by the developed low-cost lamp**.**

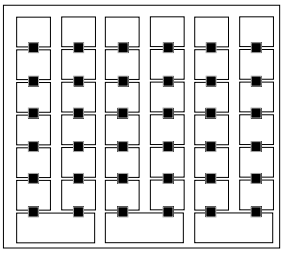

Fig. 7 The shape of the developed low-cost lamp.

Figure 8 shows a low-cost lamp frontal view. It is composed of 42 power LED used to create uniform radiation con PV devices.

Fig. 8 Frontal view, low-cost lamp.

3 Results

Results obtained on preliminary measurements demonstrate that low-cost lamps designed cover illumination needs that the investigation team has. We are able to implement experiments and perform it any time ensuring results under the same working conditions. The climatic chamber will control temperature conditions and low-cost lamp will create the irradiation needed. Having under control both parameters it is possible to create hundreds of experiments which results will be correlated easily.

The low-cost lamp is not replacing field experiments but, help us to identify phenomenon and experiments that really needs to be implemented in the field. The new device brings us the opportunity to advance faster on investigations and ensure constant working conditions.

The illumination capabilities, thanks to the developed device, bring the capability to control working conditions create high intense irradiations and repeat as much as is needed.

Table 1 shows the results obtained on different tests perform. The excitation capability needed to be provided by the sun is covered by the low-cost lamp. We could create bigger irradiances placing closer the PV cell under test to the low-cost illumination lamp, creating higher irradiance than the irradiance on earth surface.

	Voc[mV]	**Isc[A]**	**Irradiance [W/m2]**	**Distance to**
Solar illumination	562	1.57	736	∞
Low cost lamp illumination	583	1.89	809	15 cm

Table 1 Results obtained testing PV cells under real and laboratory working conditions.

Fig. 9, Fig. 10 and Fig. 11 correspond with images from experiments performs with low-cost lamp prototype. Fig. 9 and Fig. 10 presents the current value provided by the cell under low-cost illumination and the irradiance parameter measured. Fig. 11 corresponds with the current measures and solar irradiance registered during the test.

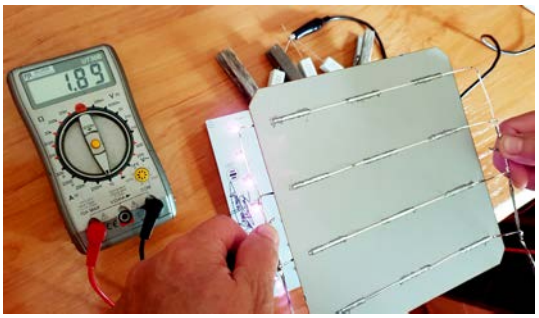

Fig. 9 Short circuit current measured using low-cost lamp.

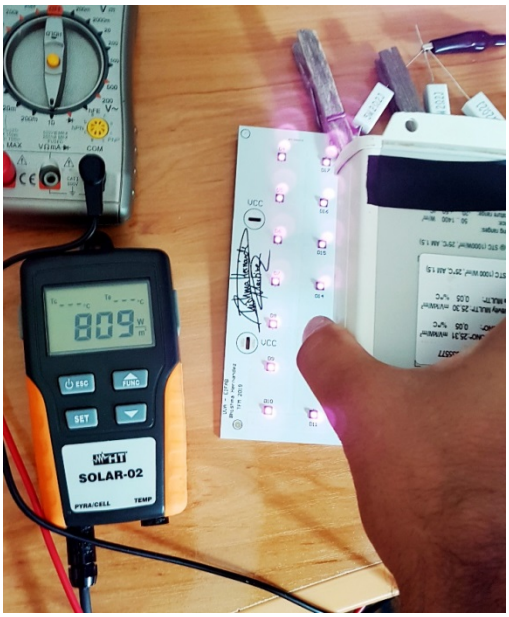

Fig. 10 Irradiation measured at 15 cm from low-cost lamps.

Fig. 11 Irradiances and short circuit current measured on field test.

4 Conclusions

The creation of own illumination, bring the capability to generate working conditions with controlled constant illumination during 24/7. Unhook testing itself from excitation permit to clean testing procedures and obtain comparable values from different units under test.

Field testing is not replaced by low-cost lamps but. However, developed low-cost lamps enlarge testing time and improve quality on measurements due to constant and controlled irradiation used as excitation from low-cost lamps.

Acknowledgments

The authors thank the CYTED Thematic Network “INTELLIGENT CITIES FULLY INTEGRAL, EFFICIENT AND SUSTAINABLE (CITIES)” nº 518RT0558. In addition, the work has been possible thanks to the "DOCTOR-PV" project Ref .: RTC-2017-6712-3, which has been funded by the “Ministry of Industry, Economy and Competitiveness, State R + D + i Program Oriented to the Challenges of the Society (Collaboration Challenges)”.

References

[1]. Panwar, N.L., Kaushik, S.C., Kothari, S.: Role of renewable energy sources in environmental protection: A review. Renewable and Sustainable Energy Reviews, 15(3), 1513-1524 (2011).
[2]. Katiraei, F., Romero-Aguero, J.: Solar PV integration Challenges. IEEE Power and Energy Magazine, 9(3), 62-71 (2011).
[3]. Gallardo-Saavedra, Hernández-Callejo, L., Duque-Pérez, O.: Quantitative failure rates and modes analysis in photovoltaic plants. Energy, 183(September), 825-836 (2019).
[4]. Hernández-Callejo, L., Gallardo-Saavedra, S., Alonso-Gómez, V.: A review of photovoltaic systems: Design, operation and maintenance. Solar Energy, 188(August), 426-440 (2019).
[5]. Gallardo-Saavedra, Hernández-Callejo, L., Duque-Pérez, O.: Image resolution influence in aerial thermographic inspections of photovolotaic plants. IEEE Transactions on Industrial Informatics, 14(12), 5678-5686 (2018).
[6]. Kropp, T., Schubert, M., Werner, J.H.: Quantitative Prediction of Power Loss for Damaged Photovoltaic Modules Using Electroluminescence. Energies, 11(5), 1172-1186 (2018).
[7]. Wu, L., Chen, Z., Long, Ch., Cheng, S., Lin, P., Chen, Y., Chen, H.: Parameter extraction of photovoltaic models from measured I-V characteristics curves using a hybrid trust-region reflective algorithm. Applied Energy, 232(December), 36-53 (2018).
[8]. Gallardo-Saavedra, Hernández-Callejo, L., Duque-Pérez, O.: Analysis and characterization of PV module defects by termographic inspection. Revista Facultad de Ingeniería, 93(Oct-Dec), 92-104 (2019).
[9]. Chen, Z., Lin, W, Wu, L., Long, Ch., Lin, P., Cheng, S.: A capacitor based fast I-V characteristics tester for photovoltaic arrays. Energy Procedia, 145(July), 381-387 (2018).

[10]. Sarikh, S., Raoufi, M., Bennouna, A., Benlarabi, A., Ikken, B.: Fault diagnosis in a photovoltaic system through I-V characteristics analysis. In: *2018 9th International Renewable Energy Congress (IREC)*, 20-22 March 2018, Hammamet (Tunisia).

Tecnológico de Costa Rica: Primer Universidad Estatal Carbono Neutral de Costa Rica

Alina Rodríguez Rodríguez[1(✉)][0000-0003-2115-4976], Raquel Mejías Elizondo[1][000-0003-3312-2699] y Carolina Vindas Chacón[1][0000-0001-9171-345X]
[1]Instituto Tecnológico de Costa Rica, Cartago, Costa Rica.
{alirodriguez,rmejias}@itcr.ac.cr,cvindas95@gmail.com

Resumen. Con una población de 8400 estudiantes y 1400 colaboradores, el Instituto Tecnológico de Costa Rica, ubicado en la provincia de Cartago, se convierte en el año 2018 en la primera universidad estatal de Costa Rica en alcanzar la certificación carbono neutral; reafirmando así, el compromiso del país por ser una nación sostenible. Este proceso implicó el desarrollo de un sistema de gestión que, entre muchos aspectos, consiguiera integrar los objetivos de la Universidad bajo un concepto de sostenibilidad; que a su vez lograra ser incorporado en la cultura de los futuros profesionales del país. La implementación de este sistema se fundamenta en los criterios establecidos a través del Programa País y la Norma INTE B5:2016. Comprende el desarrollo del inventario de emisiones y remociones de gases con efecto invernadero, el marco documental del sistema de gestión ambiental, así como, el plan de gestión y cuantificación de las reducciones para el periodo en análisis. Los resultados estimaron para el primer año una emisión de 1076,86 toneladas de CO_2e, de las cuales 521,76 T de CO_2e fueron removidas por las coberturas forestales que se conservan dentro del campus, 1,60 T de CO_2e se redujeron 555, 1 T de CO_2e fueron compensadas mediante Unidades Costarricenses de Compensación (UCCs). Concluyendo que un sistema de gestión como el desarrollado, puede considerarse un modelo clave para el desarrollo de ciudades sanas y sostenibles.

Palabras claves: Carbono neutral, sistema de gestión ambiental, inventario de gases con efecto invernadero.

1 Introducción

En la última década, la temperatura del planeta ha alcanzado cifras nunca antes registradas. Según la Administración Nacional Oceánica y Atmosférica de los Estados Unidos (NOAA) el mes de julio del 2019 fue el más caluroso en los últimos 140 años, provocando que el nivel de hielo marino del Ártico y el Antártico descendieran a mínimos históricos [1]. Este fenómeno, mejor conocido como cambio climático, se produce por la alteración del balance energético del sistema climático, a raíz de una variación en la concentración de los gases con efecto invernadero en la atmósfera [2].

La afectación del cambio climático tiene implicaciones sobre los ecosistemas, los seres vivos, las actividades humanas y la salud de las personas, esta última con resultados agudos o crónicos que denotan una alta carga de enfermedad y mortalidad, así como un aumento en los gastos de atención sanitaria y costos de la protección social [3]. Es así como el fenómeno se convierte en uno de los mayores desafíos que enfrenta la sociedad moderna, recibiendo cada vez más atención en todo el mundo, principalmente en la reducción de las emisiones de los gases con efecto invernadero (GEI) y en la adaptación al mismo [4].

Como consecuencia, los gobiernos han concertado acuerdos nacionales e internacionales para afrontar el problema. En el año 1979 se desarrolla la primera Conferencia Mundial sobre el Clima, en la cual se expusieron las señales iniciales del aumento de GEI, su relación con las actividades antropogénicas y su principal consecuencia: el aumento de la temperatura de la atmósfera mundial. A mediados de la década de 1980, la Organización Meteorológica Mundial (OMM) y el Programa de las Naciones Unidas para el Medio Ambiente (PNUMA) crearon el Panel Intergubernamental sobre el Cambio Climático (IPCC), el cual tiene como objetivo evaluar el conocimiento científico para la comprensión del aumento de la temperatura del planeta, conocer los factores que ocasionan el cambio climático, así como las consecuencias ambientales y socioeconómicas para establecer estrategias que mitiguen sus efectos [5].

En el caso de Costa Rica, las medidas de mitigación que el país ha puesto en marcha se pueden categorizar como ambiciosas, ya que buscan la carbono neutralidad a nivel nacional. Es así como, el Ministerio de Ambiente y Energía oficializa en el año 2018 el Programa País Carbono Neutral 2.0, como parte de los esfuerzos que realiza Costa Rica en su rol de líder en materia ambiental, y en consecuencia con los objetivos de mitigación del país en el contexto de la Estrategia Nacional de Cambio Climático y los compromisos internacionales establecidos en la Contribución Nacionalmente Determinada (NDC) y el Acuerdo de París [6].

El programa se crea bajo modalidad voluntaria, con el objetivo de brindar un mecanismo para reconocer la adecuada gestión de las emisiones de GEI a organizaciones públicas y privadas, con el fin de apoyar los compromisos del país en materia de acción climática. La norma establece que las organizaciones que deseen obtener el reconocimiento carbono neutral deben elaborar su inventario de emisiones y remociones de gases con efecto invernadero (GEI), cumplir con todos los requisitos de la norma INTE B5 y compensar las emisiones que no sean posibles de reducir [6].

Por su parte, la norma INTE B5 "Norma para demostrar carbono neutralidad", es publicada por el Instituto de Normas Técnicas de Costa Rica y establece los requisitos

que debe cumplir una organización que tenga como objetivo ser cero emisiones de CO_2e. Tiene como referencias las normas ISO 14064-1, ISO 14064-2, ISO 14064-3, ISO 14065 e ISO 14069 [7]. En cuanto a las formas de compensación, mediante el Decreto 37926 – MINAE es oficial el Mercado Doméstico de Carbono y las Unidades Costarricenses de Compensación. El Fondo Nacional de Financiamiento Forestal (FONAFIFO) es el ente autorizado para vender dichos créditos de carbono a nivel nacional [8].

1.1 Alcanzar la Carbono Neutralidad

Para lograr la carbono neutralidad, una organización debe medir las emisiones y remociones netas de carbono equivalente, reducir las emisiones y compensar las emisiones residuales [7]. Para ello, la tasa de emisiones de GEI antropogénicas necesita ser controlada y gestionada de modo que no supere la tasa de secuestro de carbono [9]. Reducir las emisiones de GEI es posible mediante una mejora en la eficiencia energética, la introducción de cambios que permitan aumentar la demanda de tecnologías limpias para el sector de energía y transporte, así como, la adecuada gestión de los residuos sólidos [10].

No obstante, la disminución de emisiones de GEI está ligada a múltiples factores naturales, socioeconómicos, tecnológicos y políticos, por lo que es necesario que sean complementadas con mecanismos de captura de CO_2 [11]. La remoción o captura de CO_2 en forma natural se da mediante las plantas, las cuales lo absorben de la atmósfera mediante el proceso de fotosíntesis. En este proceso usan energía del Sol, CO_2 y agua para producir materiales orgánicos vegetales. Los bosques de rápido crecimiento son los únicos capaces de capturar cantidades significativas de CO_2, pues, un bosque maduro produce este gas mediante la respiración y la descomposición de plantas muertas [12].

Cabe señalar, que alcanzar la carbono neutralidad implementando únicamente mejoras internas para la reducción de GEI es imposible, ya que toda actividad genera impacto ambiental. Por esta razón surge la compensación voluntaria de emisiones como estrategia de gestión. Para lo cual, las organizaciones pueden optar por el apoyo a la protección de bosques, cambios tecnológicos en empresas y/o generación de electricidad con fuentes renovables [13]. Actualmente instituciones financieras como bancos y sociedades de gestión de fondos de reforestación venden créditos de carbono a clientes comerciales e individuales que desean reducir y compensar su huella de carbono. Estos créditos tienen como objetivo proporcionar un valor monetario tangible para las emisiones de CO_2, creando incentivos para productores y consumidores [12].

Para calcular la carbono neutralidad, el protocolo de Gases con Efecto Invernadero (GHG Protocol), establece la separación de las emisiones en tres alcances principales [14]:

- Alcance I: El alcance uno se refiere a las emisiones directas. Estas emisiones son aquellas provenientes de fuentes propias o controladas por la organización. Por ejemplo, emisiones provenientes de hornos, calderas o vehículos.

- Alcance II: Comprende las emisiones indirectas. Se derivan del consumo de energía eléctrica, así como de la utilización de calor o vapor suministrados por un externo.
- Alcance III: Abarca otras emisiones indirectas, las cuales corresponden a emisiones resultantes de actividades de la organización, pero que sus fuentes no pertenecen ni son controladas por la misma. Puede incluir emisiones relacionadas con la manufactura realizada por terceros a cuenta de la organización, así como subcontratos, arrendamientos o franquicias.

Para determinar las emisiones de GEI relacionadas a cada alcance es necesario conocer el consumo en cada actividad, seleccionar el factor de emisión asociado (según método de nivel 1) y estimar la cantidad de CO2e multiplicando los consumos por el factor correspondiente [2, 15]. En Costa Rica, el Instituto Meteorológico Nacional (IMN) es la entidad que elabora los inventarios nacionales de GEI, avala los factores de emisión para cada fuente en el país, y establece que los GEI a considerar en el territorio nacional son los incluidos en el Protocolo de Kioto: CO2, CH4, N2O, HFC, PFC y el SF6 [16].

A manera de resumen, la carbono neutralidad se define mediante la siguiente ecuación [7]:

$$\sum E - \sum R - \sum C = 0 \quad (1)$$

Donde:

E: medición o estimación verificable de las emisiones totales y/o remociones del año o periodo al que corresponde el inventario.

R: disminución de emisiones de GEI lograda por la organización mediante la implementación de acciones a través del tiempo, dentro del periodo de reporte.

C: mecanismo de nivelación para todo el inventario de GEI mediante la adquisición de reducciones de GEI generadas por una tercera parte.

Parte fundamental de la gestión para la carbono neutralidad consiste en el desarrollo de un sistema de gestión ambiental. En el cual la organización debe desarrollar, aplicar y documentar un procedimiento para el recálculo de su año base o inventario de GEI posteriores, que le permita considerar cambios en los límites operativos, propiedad y control de las fuentes o sumideros de GEI. Debe mantener, procedimientos de gestión de la información que aseguren la coherencia con el uso futuro del inventario de GEI y revisiones rutinarias para aseverar la exactitud y cobertura total del mismo, permitiendo también identificar y corregir los errores y las omisiones [7].

La Sede Central del Tecnológico de Costa Rica cuenta con más de 1400 funcionarios y una población estudiantil que supera los 8400 estudiantes, de los cuales, cerca del 6% habita permanentemente en residencias ubicadas en la Universidad. En relación con su área, el campus posee una extensión de 0,9 km^2, abarcando más de 90 edificios de aulas, estructuras de más de 4 pisos, laboratorios, campos agropecuarios, servicios de alimentación, servicios médicos, espacios administrativos e instalaciones deportivas como gimnasio, cancha multiuso, plaza de fútbol, pista de atletismo, piscina y cancha de béisbol [17]. Por su parte, Costa Rica cuenta con 473 distritos, de los cuales, el 70% poseen una población igual o inferior a la sede en estudio, con superficies, en algunos casos, menores a 1 km^2 [18].

Según la información anterior universidades como el Tecnológico de Costa Rica, siendo una de las más grandes del país, puede ser equiparable con algunas comunidades nacionales, con requerimientos y necesidades similares, tales como transporte, servicios médicos, seguridad, gestión de residuos, gestión del recurso hídrico, producción de energía, servicios de alimentación, áreas de recreación para la comunidad. Por esta razón, las soluciones a problemas de movilidad, inseguridad y contaminación desarrolladas en la Institución, pueden servir de ejemplo para las comunidades locales. De este modo, se plantea que un adecuado sistema de gestión ambiental con enfoque universitario puede replicarse a los modelos de desarrollo de comunidades y ciudades sostenibles en Costa Rica, fungiendo como apoyo para la toma de decisiones en los asentamientos humanos.

2 Materiales y Métodos

2.1 Definición del Caso de Estudio

El estudio fue desarrollado en la sede central del Instituto Tecnológico de Costa Rica (ITCR), ubicado en la provincia de Cartago, cantón Central, distritos Oriental y Dulce Nombre. Esta es una institución nacional autónoma de educación superior universitaria, la cual tiene como funciones principales la docencia, investigación y extensión de la tecnología y la ciencia para el desarrollo del país.

2.2 Definición del Alcance

El proyecto se desarrolló a partir de la creación de un sistema de gestión para la carbono neutralidad (SGCA) orientado a la Sede Central. De acuerdo con el Programa País, los límites organizacionales deben ser consolidados por medio del enfoque de control operacional [6]. Por lo tanto, la cuantificación de emisiones se realiza dentro de los límites operativos de la Universidad sobre los cuales tiene capacidad de tomar decisiones mediante la selección de políticas operativas.

Se considera como límites operativos las emisiones directas (alcance I) e indirectas (alcance II) de los gases con efecto invernadero. Además, se incluyen otras emisiones indirectas (alcance III) correspondientes a viajes aéreos y generación de residuos sólidos no valorizables enviados al relleno sanitario. La inclusión de estas últimas se debe a que en inventarios de GEI preliminares representan aproximadamente el 50% del total de emisiones.

2.3 Cuantificación del Inventario de Emisiones y Remociones

La metodología utilizada en la cuantificación de emisiones y remociones es la referenciada en la Norma para Demostrar la Carbono Neutralidad, la cual está basada en la ISO-14064-1 que a su vez se fundamenta en el GHG Protocol. De manera general se utilizó como metodología de cálculo la aplicación de factores de emisión documentados

o método 1 y para los viajes aéreos se utilizó la calculadora de Organización Internacional de Aviación Civil (ICAO) para la determinación de las emisiones correspondientes. Cabe destacar que el estudio considera las emisiones, remociones y reducciones del año 2017, el cual se contempla como el año base.

Para las fuentes de remoción se utilizó la metodología propuesta en la norma INTE-DN-03:2016 y el Manual de Buenas Prácticas para Usos del Suelo, Cambios del Uso del Suelo y Forestal del IPCC. Las categorías utilizadas para calcular las cifras de remoción corresponden a: bosque secundario, cortinas rompevientos, plantaciones forestales y árboles dispersos.

2.4 Selección y Recopilación de Datos de la Actividad

Para la selección y recopilación de datos de la actividad se confeccionaron registros para las fuentes: consumo de electricidad, consumo de combustible en calderas, plantas generadoras de electricidad, maquinaria, gas licuado de petróleo, aplicación de agroquímicos, uso de extintores, uso de lubricantes, uso de refrigerantes y viajes aéreos. Las fuentes que no se controlan mediante registros son el combustible de la flotilla vehicular y la generación de residuos sólidos. La primera se recopila mediante el uso de un software institucional. En el caso de la generación de residuos sólidos no valorizables, se utilizó como referencia pesajes internos y corroborados con estudios de composición de residuos sólidos desarrollados por la Unidad Institucional de Gestión Ambiental y Seguridad Laboral del ITCR.

2.5 Selección de Factores de Emisión

Con respecto a los factores de emisión, se utilizaron los propuestos por el IMN para las fuentes de consumo eléctrico, combustible, refrigerantes, extintores, agua residual, lubricantes en vehículos y residuos sólidos no valorizables. En el caso de agroquímicos, y lubricantes en motores de dos tiempos se usaron los factores de emisión recomendados por el IPCC en su versión 2016. Las emisiones generadas por los viajes aéreos, no se calcularon mediante la utilización de un factor de emisión como tal, sino que se aproximaron mediante la calculadora de emisiones del ICAO. En el caso del factor de emisión del acetileno, este se calculó mediante un balance de masas según la ecuación 2:

$$1\ kg\ C_2H_2 * \frac{2\ mol\ C_2H_2}{2*26\ kg\ C_2H_2} * \frac{4\ mol\ CO_2}{2\ mol\ C_2H_2} * \frac{44\ kg\ CO_2}{1\ mol\ CO_2} = 3.38\ \text{kg}\ CO_2 \quad (2)$$

Las emisiones de GEI se calcularon según lo establecido por el GHG Protocol [14], siguiendo la ecuación 3.

$$Emisión = CG * FE * PCG \quad (3)$$

Donde:

CG: Consumo o generación de la fuente de emisión
FE: Factor de emisión
PCG: Potencial de calentamiento global.

Existen excepciones en cuanto al cálculo del agua residual y los agroquímicos, el cálculo para estos se establecen las siguientes ecuaciones [19].

Agua Residual

$$CO_2e = FE_{CH_4} * \frac{\text{kg DBO}}{\text{L}} * Q * 365 * PC_{CH_4} * \frac{1}{1000} \quad (4)$$

Donde:

CO2e = Dióxido de Carbono equivalente (ton / año)
FE_{CH4} = Factor de emisión de CH_4 de generación de agua residual
kg DBO / L = Máximo anual de la DBO a la entrada de la PTAR
Q = Caudal promedio por año (L / año)

Agroquímicos

Emisiones Directas.

$$N_2O_{aportes} = N * F_{emisión} * \frac{44}{28} \quad (5)$$

Donde:

N = Cantidad de nitrógeno aplicado (kg N / año)
$F_{emisión}$ = Factor de emission de N_2O de aportes de N (kg N_2O-N / kg N)
N_2Oaportes= Emisiones de N2O producido por aportes de N(kgN_2O)

Emisiones Indirectas. Debido a la volatilización y a la lixiviación.

$$\text{Emisiones Indirectas} = N_2O_{volat} + N_2O_{lixiv} \quad (6)$$

$$N_2O_{volat} = N * Fr_{volat} * FV_{emisión} * \frac{44}{28} \quad (7)$$

$$N_2O_{lixiv} = N * Fr_{lixiv} * FL_{emisión} * \frac{44}{28} \quad (8)$$

Donde:

N = Cantidad de N aplicado (kg N / año)
N_2O_{volat} = Emisiones de N_2O por volatilización (kg N_2O)
Fr_{volat} = Fracción de N volatilizado (kg N volatilizado / kg N)
$FV_{emisión}$ = Factor de emission de N_2O de volatilización (kg N_2O-N / kg N volatilizado)
N_2O_{lixiv} = Emisiones de N_2O por lixiviación (kg N_2O)
Fr_{lixiv} = Fracción de N lixiviado (kg N lixiviado / kg N)
$FL_{emisión}$ = Factor de emisión de N_2O de lixiviación (kg N_2O-N / kg N lixiviado)

Dióxido de carbono equivalente.

$$CO_{2eq} = (N_2O_{aportes} + N_2O_{volat} + N_2O_{lixiv}) * PC_{N_2O} * \frac{1}{1000} \quad (9)$$

Donde:

CO_2 = Dióxido de carbono equivalente (Ton / año)

PC_{N2O} = Potencial de calentamiento global

Finalmente, el inventario de emisiones se construyó usando la aplicación de hojas de cálculo Microsoft Excel. Incluyendo para cada fuente de emisión de GEI identificada los factores de emisión necesarios para el cálculo, la clasificación de las fuentes según su alcance y los totales de las emisiones para estas.

2.6 Determinación de la Compensación

La metodología seleccionada para compensar las emisiones de gases con efecto invernadero corresponde a las Unidades Costarricenses de Compensación (UCC) de FONAFIFO. La compensación se determinó mediante la siguiente ecuación:

$$C = E - R - Re \quad (10)$$

Donde:

C = Compensación de las emisiones de GEI (Ton CO_2eq / año)

E = Emisiones de GEI (Ton CO_2eq / año)

R = Reducciones de GEI (Ton CO_2eq / año)

Re = Remociones de GEI (Ton CO_2eq / año)

2.7 Desarrollo del Plan de Gestión de Reducciones

El desarrollo del plan de gestión de reducciones se hizo conforme a lo establecido por la Norma para demostrar la Carbono Neutralidad y se definió un plazo de 5 años para su ejecución. Este plan se dividió por fuente de emisión y se tomaron en cuenta las siguientes secciones: objetivo, meta, medidas, actividades, responsable, metodología de cuantificación, indicadores de seguimiento, métodos de control, presupuesto, supuestos, estimación de la disminución en toneladas de dióxido de carbono equivalente y el cumplimiento.

2.8 Cuantificación de las Reducciones

La metodología de cuantificación de las reducciones se desarrolló siguiendo los requisitos que menciona la Norma INTE B5:2016 Norma para Demostrar la Carbono Neutralidad. A continuación, se presenta la metodología empleada para los proyectos de reducción cuantificados en el año 2017.

Compra y Utilización de Carros Híbridos en la Unidad de Transportes. Para el cálculo de las reducciones de GEI asociadas al uso de carros híbridos en la Unidad de

Transportes, se registró el kilometraje de dichos vehículos y se calculó las emisiones de estos, usando como indicador los gramos de dióxido de carbono por kilómetro, además se compararon estas emisiones con las que se hubiesen generado con el vehículo que se reemplazó en la flotilla, dichos indicadores se obtuvieron del sitio web Fuel Economy. La resta de las emisiones que se habrían producido con los vehículos convencionales y las emitidas por los vehículos híbridos representa la reducción correspondiente a dicha medida.

Instalación de Paneles Fotovoltáicos en el Edificio de Rectoría. A partir lectura realizadas a los medidores eléctricos de la Institución se registró la energía anual producida por los paneles solares instalados en el Edificio de Rectoría. Las reducciones en dióxido de carbono equivalente se calcularon mediante la siguiente ecuación:

$$CO_2eq = \frac{Producción(kWh)}{año} * FE_{CO_2} * PC_{CO_2} * \frac{1}{1000} \quad (11)$$

Donde:

CO_2eq = CO_2 equivalente reducido (ton / año)
FE_{CO2} = Factor de emisión de CO_2 del consumo eléctrico (kg CO_2eq / kWh)
PC_{CO2} = Potencia de calentamiento global

3 Resultados

3.1 Fuentes de Emisión y Remoción

Las fuentes de emisión de GEI responden a actividades académicas e institucionales, debido a esto presentan características específicas tales como la fluctuación dependiendo del periodo lectivo y el constante aumento debido al crecimiento de la Universidad. A continuación, en el Cuadro 1 se muestran las fuentes de emisión identificadas, según su alcance.

Cuadro 1. Fuentes de emisión de gases con efecto invernadero para el ITCR, Sede Central.

Alcance	Fuente
Alcance I (emisiones directas)	Combustibles fósiles
	Refrigerantes
	Lubricantes
	Agroquímicos
	Extintores
	Generación de agua residual
Alcance II (emisiones indirectas)	Electricidad
Alcance III (otras emisiones indirectas)	Residuos sólidos
	Viajes aéreos

En relación con los combustibles fósiles, el consumo se deriva de 7 componentes: flotilla institucional, plantas de emergencia, calderas, maquinaria, consumo de gas licuado de petróleo, acetileno y dióxido de carbono. Los dos últimos utilizados en procesos de soldadura, tanto por el Departamento de Administración de Mantenimiento como por otras carreras afines a procesos mecánicos. Cabe mencionar que las calderas son utilizadas en el desarrollo de la docencia, por lo que no representan un consumo significativo de combustible.

En cuanto a las fuentes de remoción, el campus central del ITCR cuenta con 4 categorías:

- Bosque secundario: El Campus Central cuenta con 16,1 ha de bosque natural. Sin embargo, no todo el terreno se encuentra en las mismas condiciones por lo que se decidió estratificar según categorías diamétricas en los siguientes bosques: de regeneración, Las Ninfas y Toyogres.
- Cortinas rompevientos: Corresponden a grupo de árboles distribuidos de forma lineal o similar cuya copa frondosa sirve para detener el paso directo del viento. En el Campus hay 0,13 ha correspondientes a esta categoría. Para homogenización en el análisis de datos se decidió estratificar por especie.
- Plantaciones forestales: Hace referencia a arboledas forestales creadas mediante plantación y/o sembrado en procesos de repoblación forestal o reforestación. El Campus cuenta con 5,9 ha correspondientes a esta categoría. Para homogenización en el análisis de datos se decidió estratificar por especie.
- Árboles dispersos: Son árboles aislados en el Campus producto de remanentes de bosque que pudieron quedarse durante la construcción de edificios o limpias de sitios. Comprenden un área de 41,95 ha, que corresponden a un aproximado de 31 especies arbóreas distintas.

3.2 Reporte de Emisiones

En el Cuadro 2 se presentan las emisiones de gases con efecto invernadero, por tipo de gas y alcance, según corresponde.

Cuadro 2. Resumen de las emisiones por tipo de gas y alcance.

	Toneladas							
GEI	CO_2	CH_4	N_2O	R410	R22	R507	R134	CO_2e
Alcance I	374,58	40,24	6,40	14,08	3,40	4,49	7,67	450,85
Alcance II								223,79
Alcance III		176,28						402,22
Total	374,58	216,52	6,40	14,08	3,40	4,49	7,67	1076,86

En la Figura 1 se muestra el aporte porcentual de cada una de las actividades en la totalidad del inventario de emisiones, aquellas que no se muestran en el gráfico es debido a que representan menos del 1% del total del inventario de emisiones. Como se

observa, las fuentes predominantes corresponden a viajes aéreos, el consumo de combustible en la flotilla vehicular, los residuos sólidos y el consumo de energía eléctrica.

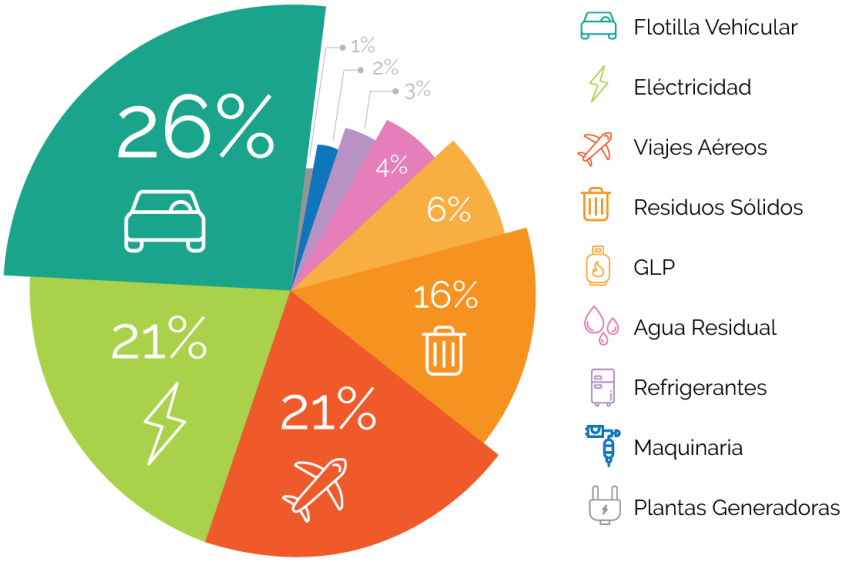

Fig. 1. Aporte porcentual de cada fuente al total del inventario de GEI. (Fuente: Elaboración propia)

En cuanto al indicador de desempeño, este se calcula tomando como coeficiente de productividad la cantidad de estudiantes y funcionarios de la Sede Central. Obteniendo de esta forma un valor de 0,118 toneladas de CO_2e por persona. Este valor se asemeja al obtenido por la Universidad Nacional de Costa Rica de 0,143 en el año 2014, dado que ambos estudios coinciden en la mayoría de las fuentes de emisión analizadas, así como en los factores utilizados debido a la similitud del contexto geográfico.

3.3 Reporte de Remociones

En el Cuadro 3 se presenta el total de remociones alcanzadas por tipo de cobertura.

Cuadro 3. Remociones por tipo de cobertura.

Cobertura	Remociones 2017 CO_2(t)
Bosque Natural	241,04
Plantaciones Forestales	109,26
Cortinas Rompevientos	169,29
Árboles Dispersos	2,17
Total	521,76

3.4 Plan de Gestión de las Reducciones

Como parte del sistema de gestión para la carbono neutralidad se estableció un plan de gestión de reducciones con un periodo de implementación del año 2017 al 2021. El plan incluyó 3 fuentes de emisión: consumo de energía eléctrica, consumo de combustibles fósiles y generación de residuos sólidos. La priorización de las fuentes se realizó analizando su aporte al total de emisiones y la factibilidad de implementación de las medidas.

En cuanto al consumo de energía eléctrica, se planteó la instalación de sensores ultrasónicos en aulas y oficinas, instalación de sensores de presencia para los aires acondicionados, creación de directrices institucionales de eficiencia en instalación de aires acondicionados. Además, se inició la construcción de un complejo solar que abastezca en aproximadamente el 30% del consumo eléctrico de la Institución y que además sirva de laboratorio para el incremento de la investigación en este campo.

Para la disminución del consumo de combustibles fósiles, se planteó la adquisición de vehículos híbridos o eléctricos, capacitación a los choferes en conducción eficiente, creación de directrices institucionales de eficiencia en la movilidad y adquisición de maquinaria eléctrica.

Finalmente, se plantearon como medidas para la gestión de residuos sólidos: mejoras en la separación de aquellos que son valorizables, como la eliminación de basureros y el remplazo por más contenedores para su clasificación, desarrollo de un programa de capacitación a toda la población universitaria (estudiantes y funcionarios), declaración de la Institución libre de plástico de un sólo uso, desarrollo de un plan de reducción de uso de papel y el diseño de un sistema para el tratamiento de los residuos orgánicos.

3.5 Reducción de GEI

La Institución implementó medidas durante el año 2017 que se enfocaron en reducir emisiones de tres de las fuentes con mayor aporte: consumo de combustibles fósiles, consumo de energía eléctrica y generación de residuos sólidos. Sin embargo, algunas medidas de reducción no se consideraron en el cálculo por encontrarse ya incluidas en el inventario de GEI, dado que, para este caso el año base coincide con el año de reporte.

Las medidas consideradas para el periodo 2017 corresponden a la sustitución de 4 vehículos convencionales por vehículos híbridos y la instalación de tres sistemas fotovoltaicos. En el Cuadro 4, se muestran las emisiones reducidas durante el periodo del estudio.

Cuadro 4. Reducciones cuantificadas en el año 2017.

Medida	Toneladas de CO_2e
Compra de vehículos híbridos	0,20
Instalación de paneles fotovoltaicos	1,49
Total	1,60

3.6 Compensación de GEI

Se estimó una compensación correspondiente a 555,1 toneladas de CO_2e utilizando Unidades Costarricenses de Compensación de FONAFIFO.

3.7 Cálculo de la Carbono Neutralidad

Resulta importante recalcar que, al tratarse de una neutralización del año en estudio, el valor de las reducciones es cero, ya que las mismas se encuentran implícitas en el valor de emisiones**.** En el Cuadro 5 se presentan los datos utilizados para el cálculo de la carbono neutralidad.

Cuadro 5. Datos para el cálculo de la carbono neutralidad

Dato	Toneladas de CO_2e
Emisiones	1076,86
Remociones	521,76
Reducciones	1,60
Compensación	555,1

Los datos del Cuadro 4 se sintetizan en la ecuación 1 para el cálculo de la carbono neutralidad.

$$555{,}1 - 0 - 555{,}1 = 0$$

3.8 Sistema de Gestión para la Carbono Neutralidad (SGCN)

En un SGCN es fundamental la trazabilidad de la información, la cual se logra con la correcta documentación de las evidencias. Por esta razón, el sistema propuesto se divide en dos grandes secciones: documentación y evidencias. La primera está compuesta por el marco documental de los procedimientos, registros, inventario de GEI y plan de gestión de las reducciones. Mientras tanto, las evidencias deben representar todo aquello que necesite ser corroborado y trazable.

En cuanto al Manual del SGCN, este plantea la estructura general del sistema, teniendo entre sus secciones: la guía para la cuantificación del inventario de emisiones y remociones; la gestión de las reducciones; la compensación de las emisiones de GEI, la gestión de la información y la declaración de la carbono neutralidad. En relación con los procedimientos se definieron 16 de 3 tipos: emisiones, remociones y, control y seguimiento.

Cabe resaltar que, el Inventario Nacional de GEI realizado en el año 2012 determinó que a nivel país, las fuentes de emisión de mayor impacto corresponden al sector transporte y de residuos. Demostrando que resultados obtenidos en la Universidad no se alejan de la realidad nacional. Por esta razón, el SGCN se presenta como una guía para la gestión de políticas y acciones que permitan controlar las emisiones antropogénicas de GEI en comunidades y ciudades del país.

4 Conclusiones

- El inventario de emisiones de GEI corresponde a 1076,86 toneladas de CO_2e que se traduce en un valor per cápita de 0,118 toneladas de CO2e.
- Las fuentes de emisión con mayor contribución al inventario de emisiones corresponden de mayor a menor a consumo de combustible, viajes aéreos, consumo de electricidad y generación de residuos sólidos no valorizables.
- Se removieron 521,76 toneladas de CO_2e a partir de las coberturas de bosque secundario, plantaciones forestales, cortinas rompevientos y árboles disperses.
- Se lograron reducir 1,60 toneladas de CO_2e a través de medidas orientadas a la reducción en el consumo de combustibles fósiles y de energía eléctrica.
- Para lograr la carbono neutralidad se realizó la compensación de 555,1 toneladas de CO_2e mediante las Unidades Costarricenses de compensación del Fondo Nacional de Financiamiento Forestal.
- El desarrollo del sistema de gestión para la carbono neutralidad que permitió la gestión de la documentación y el aseguramiento de la trazabilidad de la información, fue de vital importancia para lograr ser la primer universidad pública carbono neutro de Costa Rica.
- Un sistema de gestión como el desarrollado puede considerarse un modelo replicable para el desarrollo de ciudades sanas y sostenibles en Costa Rica.

Referencias

1. NOAA National Centers for Environmental Information.: State of the Climate: Global Climate Report for July 2019. (2019).
2. IPCC: Climate Change 2007 - The Physical Science Basis: Working Group I Contribution to the Fourth Assessment Report of the IPCC. Cambridge University Press, Cambridge, United Kingdom and New York, NY, USA. (2007). ISBN 9780521705967
3. Useros Fernández, J: Climate change and its effects on the human health. Anales de la Real Academia de Medicina y Cirugía de Valladolid. 51, 23-54 (2014). ISSN 0210-6523
4. Meyer, M., Weigel, B.: Climate Change and Transportation Engineering: Preparing for a Sustainable Future. Journal of Transportation Engineering. 137, 393-403 (2011). doi: 10.1061/(ASCE)TE.1943-5436.0000108
5. Jara González, C.: Alternativas para la reducción de emisiones de CO2 del sector doméstico del municipio de Santa María de Palautordera. Universidad Politécnica de Catalunya (2010).
6. Ministerio de Ambiente y Energía: Programa País Carbono Neutralidad 2.0., Costa Rica (2018).
7. Norma para demostrar la Carbono Neutralidad. Instituto de normas técnicas de Costa Rica, Costa Rica (2016).
8. Salgado, L., Dumas, M., Feoli, M., Cedeño, M.: Mercado Doméstico Voluntario de Carbono de Costa Rica: Un instrumento hacia la C-Neutralidad, San José, Costa Rica (2017). ISBN 9789968794596
9. Mathur, M., Awasthi, S.: Carbon neutral village/cluster: A conceptual framework for envisioning. Current Science. 110, 1208-1215. (2016). doi 10.18520/cs/v110/i7/1208-1215
10. J. Rojas Wang:. Residuos sólidos y calentamiento global – Parte 1. CEGESTI, 254, 1–3. (2014).

11. Vargas, A., Yáñez, A.: La captura de carbono en bosques ¿una herramienta para la gestión ambiental?. Gaceta ecológica. 5-18 (2004). ISSN-e 14052849
12. Gevorkian, P.: Carbon dioxide sequestration and carbon trading economics. In: Alternative energy systems in building design. pp. 421-430. McGraw-Hill, New York (2010). ISBN 9780071625241
13. J. Rojas Wang.: La compensación de emisiones y los mercados de carbono. CEGESTI, 145, 1-4. (2011).
14. World Business Council for Sustainable Development, World Resources Institute.: The Greenhouse Gas Protocol: A Corporate Accounting and Reporting Standard. World Business Council for Sustainable Development, Geneva, Switzerland (2004). ISBN 1569735689
15. Vásquez, L., Iriarte, A., Almeida, M., Villalobos, P.: Evaluation of greenhouse gas emissions and proposals for their reduction at a university campus in Chile. Journal of Cleaner Production. 108, 924-930 (2015). doi: 10.1016/j.jclepro.2015.06.073
16. IMN Cambio Climático, http://cglobal.imn.ac.cr, last accessed 2019/07/01
17. Campus Tecnológico Central Cartago, https://www.tec.ac.cr/sedes/sede-central-cartago, last accessed 2019/08/01.
18. Instituto Nacional de Estadísticas y Censos: X Censo Nacional de Población y VI de Vivienda 2011: Características Sociales y Demográficas. 1st edn. INEC, San José, Costa Rica (2012). ISBN 9789968921961
19. IPCC.: 2006 IPCC Guidelines for National Greenhouse Gas Inventories. Prepared by the National Greenhouse Gas Inventories Programm, Eggleston, S., Buendia, L., Miwa, K., Ngara, T., Tanabe, K. (eds). Institute for Global Environmental Strategies, Hayama, Japón (2016). ISBN 9291693200

Nature Based Solutions for Cities Resilience: opportunities for action in Madrid

Oquendo-Di Cosola Valentina[1], Sánchez Adán[1], Olivieri Lorenzo[1], Olivieri Francesca[1].

[1] Department of Construction and Technology in Architecture, Universidad Politécnica de Madrid. ETS Arquitectura. Avda. Juan de Herrera, 4. 28040 Madrid, Spain.

Abstract. Nature-Based Solutions (NBS) can turn nature into a tool for environmental, social, and economic innovation to meet the challenges of climate change. Fostering these solutions from the European Union agenda would allow Europe to be part of today's growing market for NBS. This requires a combination of technical, financial, governance, regulatory, and innovation aspects. In this work, we reflect on the scientific, technical, and political implications of NBS in cities, with a focus on the context of the city of Madrid. We explore the different regulations that consider these solutions as instruments for mitigating and adapting urban areas to climate change by identifying measures that drive these initiatives. Also, we identified potential barriers and opportunities to escalate the implementation of these solutions. From the results we conclude that: (1) the quantification of the effects and benefits of nature-based solutions in urban environments would allow establishing their value and potential as tools to increase the resilience of cities (2) due to monitoring, public administrations can have a clear idea of the effectiveness of these solutions and evaluate their development and promotion in local plans; (3) private companies that commercialize the technologies involved can use the monitoring data to provide reliability on the functioning of the different solutions; (4) investors, with evaluation indicators, can assess the profitability of the investment in these solutions. To reach its goals, the development and replicability of NBS must take into account all stakeholders to contribute to achieving all dimensions of sustainability.

Keywords: Nature-Based Solutions, Sustainable cities, Innovation, Climate change.

1 Introduction

1.1 Innovation through Sustainable Development Objectives (ODS)

In 2015, 193 member states of the United Nations unanimously adopted Agenda 2030 for Sustainable Development, made up of 17 Sustainable Development Goals (SDGs) and 169 goals to be achieved by 2030 [1]. These universally applicable goals set quantitative results in the three dimensions of sustainable development: social, economic, and environmental. They address critical issues related to human

development such as energy poverty, climate change, economic development, protection of ecosystems, and cities. However, this agenda has been more ambitious and comprehensive than the previous ones, since it integrates dimensions that had been absent until now, such as governance, gender equity, and peace.

The international community, through the 2030 agenda, has changed its vision of how to tackle development problems. This approach implies taking on challenges on a global scale in a much more complex and interdependent world, which in turn involves significant resource management. This requires the collaboration of different actors in society - governments, citizens, investors, civil society - seeking to connect demand with action. The transition to a more desirable world for all must go beyond independent initiatives and partial approaches and must be characterized by a new perspective that encompasses the growth of the entire economy [2].

Cities play a fundamental role in the set of actions planned to achieve the Sustainable Development Goals. Any vision of the future that seeks to design sustainable scenarios that consider social, economic, and environmental aspects must analyse the context in which it finds itself. By 2050 it has been estimated that more than half of the world's population will live in large cities, with more than 90% of urban expansion in developing countries [3]. The interpretation of these data leads to estimate that the rate of growth of cities will be 1 million people each week. This becomes one of the biggest challenges of the 2030 agenda since population growth is intrinsically related to energy consumption and the emission of pollutants.

Cities occupy only 3% of the earth's surface and account for 80% of energy consumption and around 75% of the planet's CO_2 emissions. Many cities are also highly vulnerable to climate change and natural disasters mainly due to their location, so strengthening adaptation and mitigation to the vast consequences of massive city development is crucial to avoid negative socio-economic impacts.

With the Agenda 2030 and the Sustainable Development Goals, countries have committed themselves to set a goal for prosperity, peace, and partnerships in favour of moving towards a stable and long-term development scenario. To achieve this, not only are technological developments or scientific advances needed, transformations are needed that develop technologies capable of promoting public and private investments and stimulating governance mechanisms.

In response to this scenario, the Sustainable Development Solutions Network, in its report, 2019 [4], refers to six main changes to achieve the SDGs, based on two cross-cutting principles. The first is related to governments and the need to ensure that each change promoted is designed by and to encourage equity and social inclusion, applying particularly to public services and infrastructure. The second argues that any transformation must reduce humanity's vulnerability, i.e., the environmental footprint, resource use, and pollution caused by human well-being.

Within the 6 transformations, the promotion of SDG11 - Sustainable cities and communities - stands out, which within its action contemplates cities, towns, and communities that require investments in infrastructure and services that grant resilience

to climate change. Although this is a concrete objective, its impacts indirectly affect all SDGs, mainly those related to transport, urban development, and water resources [4].

The increasing importance of cities is a fact against which we cannot oppose, as demonstrated by the creation of the New Urban Agenda, and, in turn, the European Urban Agenda. Sociologist and economist Saskia Sassen state that "cities will be more important than states" [5], which highlights an important milestone in the future development of global urban policy and the need to find innovative answers to the problems identified, for which no less solution is available today.

As for research and the principal funding programmes, both at European level (Horizon Europe) and the state level in Spain (State Research Plan 2021 - 2027) are based on an approach supported by large missions. This approach is being promoted by the European Commission [6,7] and has been theorised by Mariana Mazzucato [8,9], professor of Economics of Innovation and Public Value at University College London (UCL), who states that based on innovative policies, oriented to one or more concrete missions, ambitious objectives can be defined and long-term policies defined.

These missions oriented towards sustainability in the urban environment will require investment in areas such as energy, transport, nutrition, health, and waste reduction. This approach offers a massive opportunity to increase the impact of research and innovation, capture the collective intelligence, and make real progress in complex challenges. Whether it is to achieve lower pollution levels in congested cities, have access to digital technologies that improve public services.

A crucial element within this theory of innovation in cities is the support for experimentation, risk-taking, original and creative thinking, aimed at finding new solutions to existing problems. This requires interdisciplinary academic work from the intersection between knowledge sectors, the collaboration between different segments of the industry, public-private partnerships, and civil society, to identify cross-cutting solutions to complex problems.

Due to their complexity and the fundamental role they play in the transition towards a more desirable future, cities offer us an extraordinary scenario to develop experimental research based on interdisciplinary approaches. As cities are places where negative social and environmental impacts occur, issues such as air pollution and climate change have a direct impact on public health, such as cardiorespiratory diseases, rising temperatures, among others.

According to forecasts and meteorological reports, the current climate will be characterized over the long term by the predominance of extreme weather events, as well as, a general increase in temperatures and a decrease in rainfall. This is why addressing current needs in terms of adaptation and mitigation of impacts, without losing sight of the context of climate change, is part of the main objective.

NBS appear as solutions that promote the transition to healthier, more resilient, sustainable, and inclusive city models.

1.2 Nature-Based Solutions: goals and challenges

Climate change is affecting ecosystems, and, in this scenario, future environmental challenges are expected to increase [10]. The densification of cities, the degradation of soils, and natural areas are part of the challenges we face today. These processes lead to the biodiversity loss and the biological processes necessary for the survival of the planet.

If these challenges are seen as opportunities for innovation, NBS can achieve biodiversity conservation, but also bring environmental, economic, and social benefits, and foster climate change mitigation and adaptation [11].

The term Nature-Based Solution emerge around the year 2000 as a perspective of the relationship between people and nature, focusing specifically on the use of nature to address social and environmental challenges such as climate change. The European Commission defines them as "those that can turn nature into opportunities for social, economic and environmental innovation" [11]. However, the affirmation of the concept as a means of providing solutions to the problems posed by climate change is very recent [12].

They are actions capable of interpreting complex processes of nature, such as the absorption of carbon dioxide, the treatment and management of rainwater, the fixation of atmospheric particles, among others, to reduce environmental risks and achieve human well-being. Therefore, maintaining and improving the natural capital is the principle of this type of solutions.

The idea that nature brings benefits to society has been developed and used in different contexts, although always focused on the concept of sustainability and the ability to provide services from the management of their natural resources. This concept has also been contemplated in environmental policies and initiatives over the last few decades, but it has also shaped research programmes, such as the European Union's Research Framework Programmes (Horizon 2020) [13] which have incorporated narratives on biodiversity and services aligned with the Sustainable Development Objectives [1]. The current calls dedicate a significant part of the funds to the recovery of elements of the urban ecosystem, with an important emphasis on the NBS, foreseeing the monitoring of the pilot experiences to quantify their benefits [14].

According to a group of experts from the European Commission [11], nature-based solutions should be developed within the framework of 4 main objectives and 7 actions in the field of research and innovation. These include "(I) urban regeneration through nature-based solutions; (II) nature-based solutions for improving well-being in urban areas; (III) establishing nature-based solutions for coastal resilience; (IV) multi-function nature-based watershed management and ecosystem restoration; (V) nature-based solutions for increasing the sustainable use of matter and energy; (VI) nature-based solutions for enhancing the insurance value of ecosystems; (VII) increasing carbon sequestration through nature-based solutions". These actions would lead to the

promotion of international cooperation in the development of sustainable solutions that would help Europe achieve its objectives of sustainable urbanisation, adaptation and mitigation of climate change, risk management, and resilience.

Taking advantage of the momentum of major problems to bet on change seems to be the way forward, facing the current challenges from the knowledge and the development of alliances between governments, companies, and investors. Today there is a real awareness of the value of nature, and the growing number of international organizations, policy initiatives for conservation and sustainability is proof of this.

2 Evaluating the effectiveness of Nature-Based Solutions

The impact and effectiveness of nature-based solutions can be analysed from three main concepts including quantification of the benefits obtained, mapping and evaluation of the profitability of these solutions, and finally the capacity to integrate different sectors of society and assimilate it into their city management policies.

2.1 Monitoring and analysis

One of the most important challenges for NBS is to make its effects tangible. They have several benefits aimed at achieving objectives and actions within their context, varying in scale from a micro-level of the building, a meso-level of an entire city or country, or a macro-level of the entire planet. [15]. A possible way to quantify their effects may be to evaluate through the impact they exert on a given space, identifying indicators.

Taking into account that resilience is based on two main concepts, adaptation as the ability to react to a stimulus such as climate change, and mitigation as the possibility of improving the current state of a factor, such as the reduction of greenhouse gas emissions or the absorption of carbon dioxide, the case of NBS can be considered as an adaptation of the two concepts in a single solution.

Therefore, taking into account the different scales of action and capabilities of these solutions it is possible to assess the impact through:

- Increase of green areas for the evaluation of, carbon absorption and improvement of air quality [16–20], reduction of temperatures [21–25], and acoustic absorption [26–30];
- Increase the use of façades and plant covers to mitigate the effect of urban heat island, through the management of shade and the effect of evapotranspiration of plants and substrate [24,31–37].
- Reduction of emissions and energy consumption through the study of solutions that contribute to the energy balance of buildings [21,38–42].

2.2 Economic valuation: NBS as a business model

NBS are a form of ecological innovation that seeks to solve climate change from mitigation and adaptation to its effects on cities and people, such as air quality, loss of

biodiversity, urban heat island effect among others. Part of these solutions, as mentioned above, has to do with green infrastructures that adapt to the current grey infrastructure, such as façades and green roofs, rainwater recycling systems, parks, and forests, etc.

Each of these solutions can provide a unique service and value for each of the components of society, whether economic, environmental, or social.

From an economic point of view, nature-based solutions can be interpreted as natural capital, which provides services and value to current ecosystems-issues [43]. These services can be classified into three categories according to The Economics of Ecosystems and Biodiversity (TEEB) [44]; first, they provide "*provisioning services*", such as food, biomass, pure water, and medical resources; Secondly, they offer "*regulating services*", such as regulation of temperature, air quality, protection of things, noise reduction, reduction of carbon in the atmosphere and purification of water; finally, they provide "*cultural services*" through recreation in public spaces and psychological well-being for people.

The idea that innovation can be part of a business model has been extensively studied [45–47], distinguishing three main areas: the value proposition for customers in the form of service; the way that value is delivered, in other words, partners; and the component that captures value, i.e. revenues and costs.

These concepts translated into NBS, specifically, those related to buildings, facades, and roofs, as well as those related to water management can establish a sustainable business model.

An example of this is the green roofs, which provide insulation and protection to buildings, which leads to maximizing energy efficiency. For the owner of a building, the investment in this type of solutions will be felt if one takes into account the reduction in expenses related to the climate control, as well as those of maintenance. Also, these solutions can use the building's water, heat, and organic waste to maintain themselves. This type of technology can be developed in the model of passive solutions for reducing energy consumption, recycling rainwater, improving air quality, increasing biodiversity, among others.

However, these benefits are difficult to capture through private investments, so their monitoring and quantification would establish a framework for profitability and investment.

Another important example would be the management of water flows in densely urbanized areas. Water management through nature-based solutions provides a solution to prevent flooding in cities, as opposed to creating a grey infrastructure based on pipelines. Sustainable drainage systems can generate numerous benefits, however, the lack of quantification of these benefits becomes a barrier to diffusion in cities and adaptation by authorities.

The obstacles faced by NBS are largely economic, and this is linked to the ability to capture the value or service they offer. The success of innovation through nature can go hand in hand with the quantification of its benefits and the public-private investment connected to the real knowledge of added value.

2.3 Policy implications

The insertion of these solutions in cities depends to a great extent on a new model of governance, i.e. coordination between administrations is essential when it comes to tackling problems that affect society. This is proposed in the European Urban Agenda [48], through the establishment of global and integrated strategies that provide solutions to common objectives.

Part of these strategies could be materialized in the rise of new organizations in the form of innovation laboratories driven by the local administration that allow to prototype and evaluate actions and solutions that in turn respond to current challenges and are developed in open collaboration with the citizenry. The development of technology and interdisciplinary collaboration can be transformed based on acceleration towards the resilience of cities.

However, there are several options through which policy-makers at a local, regional, or national level can encourage innovation in NBS in cities. Whether through long-term financing in collaboration with private enterprise; the establishment of an accounting framework for the services offered by nature, such as improving air quality; and the development of public-private partnerships with incentives that benefit all actors - academia, business, government - in order to give value to NBS that allows them to integrate into government decision-making.

Indicators such as the growth rate for jobs related to green infrastructure, access to energy from renewable sources, the percentage of total area of green spaces, the reduction in insecurity rates linked to the recovery of degraded spaces, the levels of population exposed to outdoor air pollution, wastewater treatment, the percentage of solid waste recycling, the proportion of renewable energy, and the investment capacity of public-private cooperation, can be instruments of public policies for quantifying the effectiveness of these solutions.

3 Nature-Based Solutions in practice: the case of Madrid city

3.1 Government and regulations

Today, urban nature has acquired the character of an instrument for adapting the city to the effects of climate change. In the international context and at European level, different cities are developing programmes for integrating nature into urban contexts as a means of adapting cities to climate change [49–51].

In relation to these plans, the commitments made by Madrid City Council on climate change have been on the rise, demonstrating this through adherence to the European New Covenant of Mayors initiative, participation in the Paris Conference of the Parties (COP21), adherence to international networks such as the network of cities for climate C40, and the development of concrete plans for the implementation of solutions based on nature and the improvement of air quality.

In order to identify threats and the vulnerability of the city of Madrid to climate change, the Directorate General for Sustainability and Environmental Control carried out an analysis of vulnerability to climate change in the city of Madrid [52], based on the Energy and Climate Change Plan of the city of Madrid - Horizon 2020, which identifies the main climatic trends and the impacts derived from which the city will have to face throughout this century. This includes a decrease in rainfall, an increase in average monthly and annual temperatures, as well as an increase in the duration of heatwaves. These alterations can affect public health and the loss of biodiversity. In addition to increasing atmospheric pollution, decreasing reserves of water resources, and increasing the risk of flooding by torrential rains.

To respond to these challenges, the Energy and Climate Change Plan establishes a strategic framework for developing a low-carbon city, which promotes energy efficiency and the use of renewable energies, the optimisation of municipal energy and environmental management, and the planning of adaptation to climate change.

Recognizing the importance of the need to make progress in measures included in coordinated municipal policies, the *Madrid + Natural* plan emerged [53]. To promote the development of green urban infrastructures that offer services and benefits to the city. The program is structured on three scales: the building, the neighbourhood, and the city, in such a way that the actions lead to specific and common objectives. Among those that stand out are the improvement of the energy behaviour of buildings, the regulation of rain flow, the availability of green spaces, the mitigation of the urban heat island effect, the improvement of air quality, and the monitoring of facilities in order to quantify the cost-benefit, maintenance, and operation of these solutions.

This program is part of Measure 29: Adaptation to Climate Change of *Plan A: Plan de Calidad del Aire y Cambio Climático de la Ciudad de Madrid*, a tool for reducing atmospheric pollution, contributing to the prevention of climate change and defining adaptation strategies [54]. It is structured around 4 axes: sustainable mobility, urban regeneration, adaptation to climate change, and citizen awareness and collaboration with other administrations; and it demonstrates the ecological vision of the city, both in terms of mobility and awareness of citizenship, as well as in the rehabilitation of buildings, public spaces, local energy production, water management and the renaturalization of the city.

Within the framework of the programmes and initiatives described above, and with the premise that the city needs to establish new models of relationship with climate and

the environment, the following is a series of case studies developed in the city of Madrid and coordinated from the Universidad Politécnica de Madrid, which establish as their main objective to introduce NBS as a tool for mitigation and adaptation to climate change.

3.2 Case studies

The following are different research projects whose main objective is to quantify the effects on buildings and the urban environment of different NBS, through the use of developed predictive models, the use of specific computer tools and the analysis of data obtained from the monitoring of several experimental case studies installed in the city of Madrid.

Several variables are analysed in detail:

- Energy efficiency
  - To quantify, by monitoring and data analysis, the effect provided by vertical gardens on the indoor thermal conditions of a building.
  - To quantify, by predictive models, the energy behaviour of façades and plant roofs, the effect that the installation of a plant roof and roof would provide on the internal thermal conditions of a building and its energy demand.

- Reduction of temperatures at street level
  - To quantify the effect of different Nature-Based Solutions in reducing outdoor temperatures at street level during the warm season.

- Reduction of air pollutants
  - To quantify the effect of a tower with vegetation in the absorption of polluting gases and the capture of suspended particles.

- Sustainable use of rainwater in the built environment
  - To quantify the effect of a circular system for integrated water management in built environments on the temporary retention of runoff water and the elimination of pollutants.

Energy efficiency through analysis of experimental data: vertical gardens on itdUPM.

The study is being carried out in the maintenance building of the Escuela Técnica Superior de Ingeniería Agronómica, Alimentaria y de Biosistemas (ETSIAAB) of the Universidad Politécnica de Madrid, the current headquarters of the Centro de Innovación en Tecnología para el Desarrollo Humano (itdUPM).

The building has been remodelled in 2016 to be transformed into the headquarters of itdUPM and has been constituted as an experimental building that seeks to promote sustainable development within a program of new strategies and technologies. The building dates back to 1960 and takes place in a physical space that until then had occupied space for offices and storage of maintenance staff. It is a free-standing rectangular building with approximate dimensions of 21.38m x 9.35m. Posse two floors: basement and ground floor, each floor of 199.90m2 built, with a height of 4.70m. The total surface of the building is 399.80m2. The proposal to requalify the building is based on the integration of a plant envelope that occupies part of the south, east and west facades, is developed with the use of a module made of recyclable plastic, belonging to the systems of continuous non-hydroponic plant facades, with organic substratum; this system allows savings in water consumption and low use of fertilizers. These modules have standard dimensions and have been coupled to create a uniform surface that can be incorporated into the metal skin.

The metal skin has been made through a ventilated façade in three of the four walls of the building (south, east, and west) and consists of modules 2.4m long x 0.6m high, supported on vertical uprights. These uprights placed every 2.4m, do not rest on the ground but are anchored to the envelope of the existing building using metal plates screwed to the wall. Each upright rest at three points on the wall. This metal façade with its structure allows the vertical garden modules to be placed on top of it, making it very quick to install. The vertical garden modules are made up of pre-cultivated panels fixed to the metal enclosure. These façades currently cover an area of 11.25m2 on the south façade, 6.25m2 on the east façade and 10m2 on the west façade.

The system used is a commercial product *Biofiver* [55], which has the following characteristics:

- Size: 50cm x 50cm x 10cm
- Weight (without plants): 2 Kg
- Number of floors/m2: 48
- Static system: simple anchorage
- Irrigation system: integrated exudate pipe
- Module material: recyclable polyethylene
- Substrate: organic (coconut, peat, humus clays)

The system is composed of two three-dimensional polyethylene structures between which is a layer of hydrophilic layer for the distribution and drainage of water from irrigation. One of the structures is filled with a substrate for cultivation, and the other remains empty generating a hollow space for air circulation. The irrigation system is internal and is performed through a self-compensating drip, which produces that the water is always in motion generating a humid environment. This system has been developed to reduce dependence on water and fertilizers, as well as the costs of maintenance and computer systems for the control of the optimum operation.

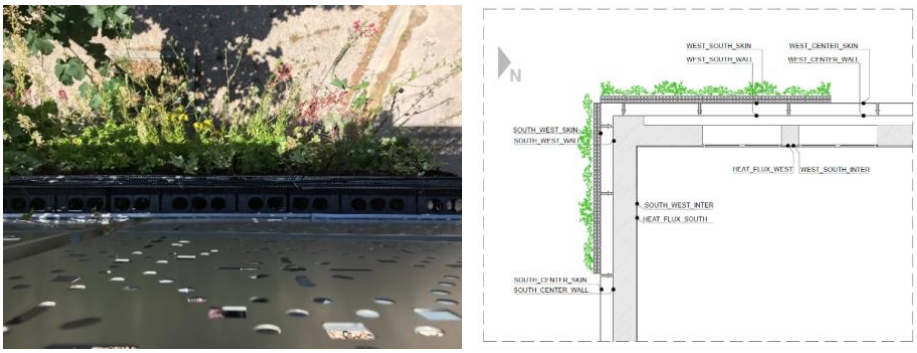

(a) **(b)**

Fig. 1. (a) Vegetable façade top view; (b) position of measurement sensors

A weather station, a system of temperature and heat flow sensors has been installed to monitor the thermal behaviour of the facades of the plant. Thermocouples type K, with an error range between 0.1°C and 0.3°C, are installed in different layers of the south and west facades, both in vegetated and non-vegetated areas. They are connected to a distribution system that allows information to be collected every minute, which can be displayed on the itdUPM website. The Hukseflux thermal sensors were used to monitor the heat flow, installed inside the building's permanence spaces, two on the south façade (one on the vegetated side and one on the unvegetated side) and two on the west façade (one on the vegetated side and one on the unvegetated side). Sensors are passive sensors that do not need energy and remain connected to a data logger that displays the measurement results, which can also be viewed on the web. The weather station has been installed at the southwest end of the roof of the building, near the two guarded facades, and is the Davis Vantage Pro2 Wireless w/24-Hour Fan Aspirated Radiation Shield.

This experiment aimed to compare the temperatures registered in the facades using two types of solutions – a living wall system and a metallic envelope -. The variables considered in the study were external temperature (ºC), relative humidity (HR%), and surface temperatures. For the analysis was considered a database with a period of 12 months that allows identifying the behaviour of the solutions during different seasons. For each station, the maximum or minimum temperature recorded was chosen, which gives results about the performance under extreme conditions.

Results have been set up into two categories, reduction of temperatures and maximum temperature time lag.

For example, as for the reduction of the temperatures (Fig. 2-3) shows the peaks between the metallic skin and the vegetal façade, which in most cases is due to the evapotranspiration of the vegetation. From the maximum temperature recorded on a sunny summer day, the increase in the temperature of the internal surface of the vegetated façade about the external temperature varies between 1ºC and 8ºC, while the vegetated façade fluctuates between 9ºC and 13ºC.

As for the external surface temperatures, the vegetated façade maintains constant temperatures similar to the external temperature with an average of 28ºC, while the metallic skin exceeds in a range of up to 26ºC the external temperature.

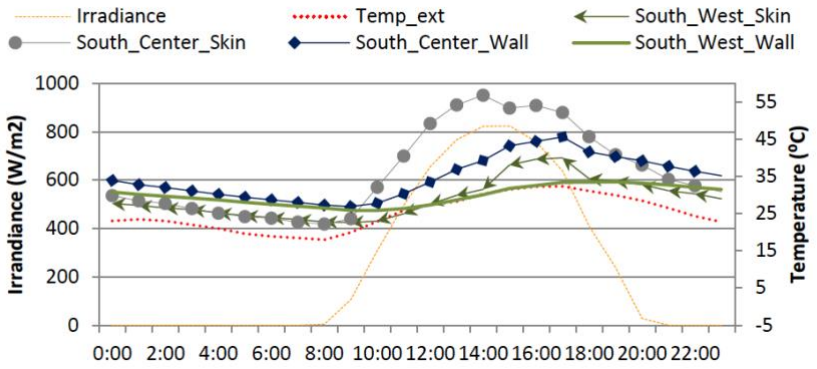

Fig. 2. Irradiance and temperature values recorded on a sunny summer day with the higher external temperature on the south facade

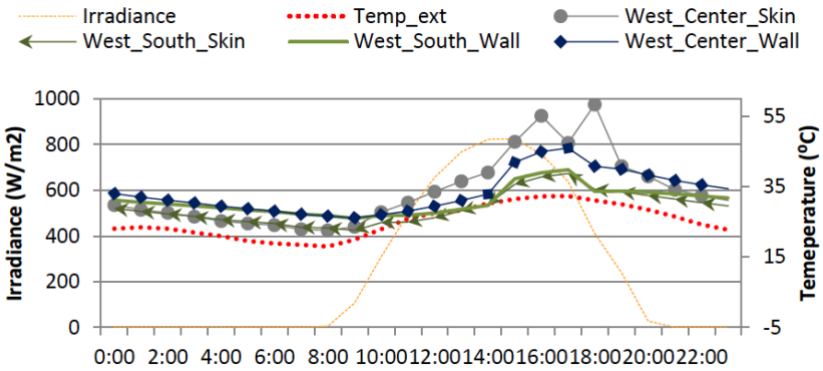

Fig. 3. Irradiance and temperature values recorded on a sunny summer day with the higher external temperature on the west façade

This research was aims to analyse the effects of vegetation as a building envelope, based on a modular vegetation system constituted by plants and an organic substrate. The results obtained show the ability of vegetation to reduce temperatures and the transmission of heat flows to the interior of the building, particularly during the summer.

Reduction of temperatures at street level: renaturation of Matadero.

This second case study is part of the Matadero Acción Mutante project an initiative carried out by Matadero in collaboration with a group of researchers from the UPM, the Sub directorate General for Energy and Climate Change, and the Directorate General for Intervention in Urban Landscape and Cultural Heritage of the Madrid City Council and other agents such as architects, engineers, artists, botanic, etc., which aims to raise awareness of the environmental crisis with strategies for mitigation and adaptation to climate change and through the relationship culture-nature.

The exterior space of the enclosure occupies 34330 m2, so it is significant to think about treating these spaces that form part of the complex. The spaces without vegetation and shade suffer enormously from extreme temperatures and especially the heat waves that are occurring more and more frequently in Madrid. It is for this reason that Matadero has become a case study to apply Nature-Based Solutions and thus test responses to adapt to climate change while transforming Matadero in a friendlier and fresher space. The NBS will be the result of a creative process involving five artists from different parts of the world.

As a first step of the work, in the summer of last year five sensors were installed in different external spaces of Slaughterhouse or near it for the measurement of temperatures and humidity of the air in the current state, before the interventions of urban naturalization (Fig.2) The sensors used were the HOBO MX2301A Temperature/RH Data Logger [56].

Fig. 4. Location of the sensors, from the top right clockwise: Plaza de Legazpi, Plaza de acceso, Calle Matadero, Casa del Lector (north access), "No huerto".

Reduction of air pollutants: modules for urban air cleaning (*MUAC*).

This case study is based on the installation and monitoring of two identical experimental prototypes of the *MUAC* (*Modules for Urban Air Cleaning*) tower with vegetation. The first was installed in October 2018 in the vicinity of the former maintenance building of the Escuela Técnica Superior de Ingeniería Agronómica, Alimentaria y de Biosistemas (ETSIAAB) of the Universidad Politécnica de Madrid, current headquarters of the Centro de Innovación en Tecnología para el Desarrollo Humano (itdUPM); and the second will be installed in the vicinity of the Escuela Técnica Superior de Ingenieros Industriales (ETSII) of the Universidad Politécnica de Madrid in autumn 2019.

The MUAC vegetation tower is an air decontamination device that reproduces the biological and microbiological purification processes carried out in forests. It is 2.8m high and has a square floor plan of 0.7m on each side, with a total surface area of 0.49m_2. The tower is made up of 16 vegetated panels of the Biofiver system, described in the previous case.

Air purification is carried out both outside and inside the tower. Outside, the vegetation leaves capture and absorb suspended particles (PM2.5/PM10), in addition to generating a gas exchange (CO_2 for O_2) through the photosynthesis process. Inside, the air is filtered through a system where the roots and microorganisms that inhabit the substrate absorb and feed on contaminating gases such as COx, NOx, O_3 or SOx.

Fig. 5. A prototype of the MUAC installed at the entry of the itdUPM headquarters.

The system has been designed to easily adapt to different types of environments and climates, using native vegetation for this purpose. Also, the *MUAC* is equipped with an autonomous energy system that, through a photovoltaic panel and a storage battery, allows it to operate 24 hours a day, even in conditions in which there is no connection to the electrical network. The electrical energy is used to supply both the irrigation system and the air circulation system inside the tower.

The two vegetation towers are equipped with two types of sensors for the measurement of suspended particles and polluting gases. These are the Uhooair sensors, which measure NOx, COx, COVx, O3, PM2.5, etc. (Table 1) and Purpleair sensors, which measure particles in suspension PM 0.3, 0.5, 1.0 2.5 and 10 µm (Table 2) tower, where the composition of the air is measured after the decontamination process.

	Temperature	RH	PM2.5	Carbon Dioxide	TVOC	Carbon Monoxide	Nitrogen Dioxide	Air Pressure	Ozone
Units	°C / °F	%	µg/m^3	ppm	ppb	ppm	ppb	mBar	ppb
Range	-40°C / -40°F to 85°C / 185°F	0 to 100	0 to 200	400 to 10.000	0 to 1000	0 to 1000	0 to 1000	300 to 1100	0 to 1000

Resolution	0.1 °C	1%	0.1 µg/m³	1 ppm	1 ppb	1 ppm	1 ppb	1 mBar	1 ppb
Tolerance	± 0.3°C	± 3%	± 20 µg/m³ or ± 20%	± 50 ppm or ± 3%	± 5%, based on the types of VOC in the air	± 10 ppm	± 5%	± 1 mbar	± 5%

Table 1. Actual measurement values by sensor type (Source Uhooair.com)

Laser Particle Counters	
Type	(2) PS5003
Range of measurement	0.3, 0.5, 1.0, 2.5, 5.0, & 10 µm
Counting efficiency	50% at 0.3µm & 98% at ≥0.5µm
Effective range (PM2.5 standard) *	0 to 500 µg/m³
Maximum range (PM2.5 standard) *	≥1000 µg/m³
Maximum consistency error (PM2.5 standard)	±10% at 100 to 500µg/m³ & ±10µg/m³ at 0 to 100µg/m³
Standard Volume	0.1 Litre
Single response time	≤1 second
Total response time	≤10 seconds

Table 2. Actual measurement values of PM particles (Source purpleair.com)

The monitoring period shall be one year (limited to the lifetime of the measurement sensors). The data obtained will be used to measure the efficiency of the system, in addition to allowing us to estimate the impact that the implementation of towers would have on the urban fabric of cities.

Sustainable use of rainwater in the built environment: *Bluebloqs* circular system.

This case study deals with a circular system of rainwater, which is in the process of evaluating the installation area in the city of Madrid, including the Torre Caleido, in the northern financial district of the Castellana, in the city of Madrid.

This last case study consists of the installation and monitoring of the *Bluebloqs* system. It is an innovative solution developed by the Dutch Start-up Field Factors for the management and sustainable use of rainwater in the built environment, which integrates natural techniques for the retention, treatment, storage and reuse of rainwater in a circular system of flexible implementation in urban design, with the aim of restoring the natural water cycle in cities.

Bluebloqs biofilter is a modular system that combines hybrid technology using biological purification, using the proven purification power of wetland plants (68-72), as well as mineral purification using sand filters (73-77) to achieve highly efficient water treatment. *Bluebloqs* integrates natural purification processes in a controlled environment, eliminating the need for large infrastructures or chemical substances.

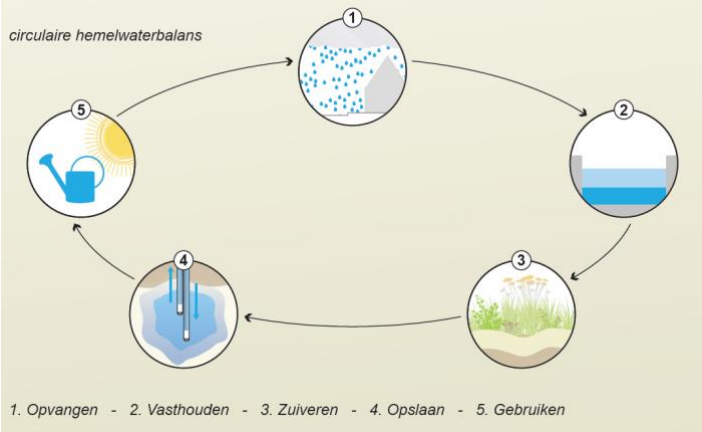

Fig. 6. Water cycle in the *Bluebloqs* system.

The system has distribution channels and water level and flows control mechanisms. The biofilter can be adapted to remove specific contaminants: organic matter, metals, and high levels of nitrogen usually found in runoff water (samples of water quality are currently analysed weekly, with results showing purification of more than 90% of impurities). The biofilter is optimized to work in combination with technologies for water injection and extraction in aquifers, guaranteeing high levels of water quality to comply with infiltration regulations and avoiding obstruction of facilities.

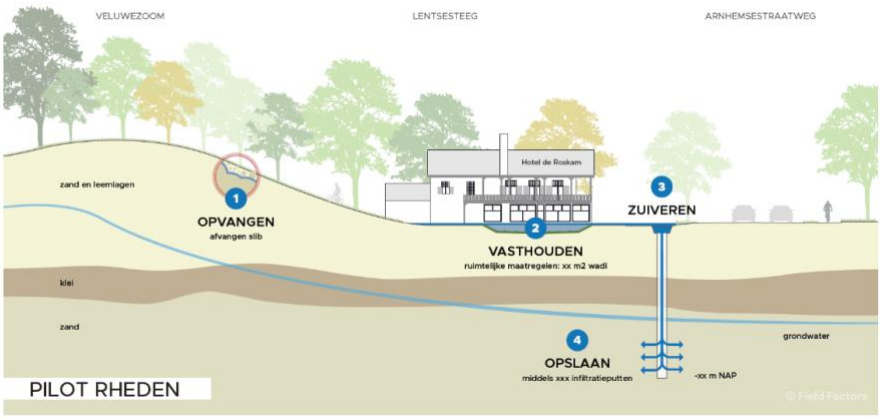

Fig. 7. Scheme of the pilot system installed in Rheden.

Bluebloqs presents a comprehensive solution for multiple challenges in water management. First, it aims to prevent flooding. The urban space is full of buildings and infrastructure that limit the infiltration of rainwater into the terrain. Bluebloqs makes use of the natural capacity of the subsoil to purify and store excess rainwater. This slows runoff infiltrates surface water and recharges groundwater levels, providing the retention capacity needed to prevent flooding.

Secondly, it contributes to combating drought. Longer periods of drought, loss of infiltration, and exponential population growth force us to use drinking water differently. With *Bluebloqs,* rainwater can be used when it's needed most: in times of drought. By creating a high-quality local water source, purified water stored in the subsoil can be used for numerous applications, including water parks, sports fields, and gardens, combating the heat, stabilizing surface waters and for industrial processes.

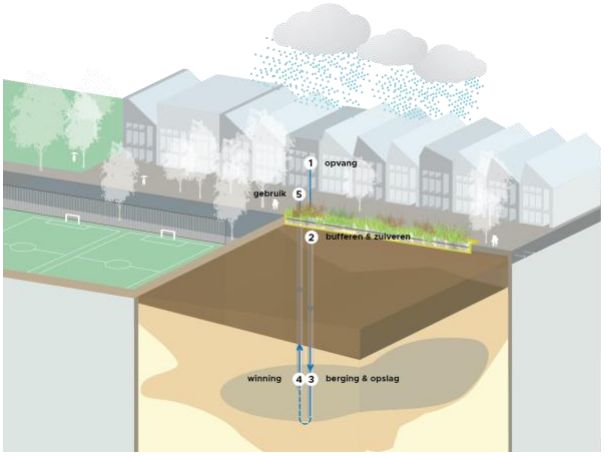

Fig. 8. Representation of the *Bluebloqs* system in a residential environment.

Finally, improving water quality. Urban currents carry pollutants present on the surface and in the environment, especially in large cities. Pavements, roofs, and the use of the environment emit pollutants that include metals, nutrients, and pathogens. To make safe use of rainwater and avoid the dispersion of pollutants, it must be treated.

Bluebloqs makes use of natural purification systems, removing organic matter, solids, metals, and nitrogen levels typically found in urban runoff.

4 Conclusions

The main objective of the study carried out is to demonstrate the importance of quantifying the benefits of nature-based solutions in buildings and the urban environment. At the same time, it proposes the use of innovative and replicable technologies as possible answers to some of the problems derived from climate change in urban areas, identifying adaptation and mitigation strategies.

From the critical evaluation of the current European context and that of the city of Madrid, as well as from the different case studies in development, it is concluded that the potential benefits and beneficiaries of the results of this project are:

- The quantification of the effects and benefits of nature-based solutions in urban environments would allow establishing their value and potential as tools to increase the resilience of cities;
- Public administrations, which on the basis of the data obtained will be able to have a clear idea of the efficiency of the different solutions and assess how they can be taken into account in the development and promotion of local plans for adaptation and mitigation of climate change;
- Private companies that commercialize the technologies involved in the study will be able to use the results of the analysis to provide their clients with reliable data on the functioning of these technologies;
- Potential investors who, based on the data available, will be able to evaluate the profitability of the investment.

The work developed in the case studies presented is considered to be part of the thematic priorities of the State Plan for Scientific and Technical Research and Innovation and the H2020 programme. It is also considered that the project responds to the guidelines established by the new European programme Horizonte Europa and by the new State Research Plan 2021-2027.

Acknowledgments.

This research has been partly funded by the Sustainable Campus Program at the Universidad Politécnica de Madrid for the year 2019, within the RES2 + U Sustainable Campus (Responsible, Sustainable, Social and University) platform.

References

[1] U. Nations, Sustainable Development Goals (SDG), (n.d.).
[2] J. A. Alonso, T. Riesgo, and J. Romero, Seminario UPM: Alinear la investigación con los ODS: una oportunidad de financiación, 2018. http://www.upm.es/Investigacion/difusion/SeminariosUPM/eventosAnteriores?id=d3f6482bc3ca7610VgnVCM10000009c7648a____&prefmt=articulo&fmt=detail.
[3] ONU-Habitat, Las ciudades y el cambio climático: orientaciones para políticas, 2011. https://unhabitat.org/books/las-ciudades-y-el-cambio-climaticoorientaciones-para-politicas-spanish-language-version/.
[4] Sustainable Development Solutions Network, Sustainable Development Report 2019, 2019.
[5] S. Sassen, Los estados se están empobreciendo demasiado, ABC. (2013). https://www.abc.es/cultura/20131024/abci-saskia-sassen-ciencias-sociales-201310241558.html.
[6] E.I.T.C. Strategy, Transformation in time, 2019.
[7] E.I.T.C. Strategy, Call to action: call for Proposals for Climate Action, 2019.
[8] M. Mazzucato, Mission-Oriented research and Innovation in the European Union, 2018. doi:10.2777/36546.
[9] D. Roberts, The Green New Deal, explained , Vox.Com. (2018) 1–32. https://www.vox.com/energy-and-environment/2018/12/21/18144138/green-new-deal-alexandria-ocasio-cortez%0Apapers3://publication/uuid/FAFC4EA4-32A2-4267-ACD4-2276D3433164.
[10] B.Z. Dagmar Schröter, Wolfgang Cramer, Rik Leemans, I. Colin Prentice, Miguel B. Araújo, Nigel W. Arnell, Alberte Bondeau, Harald Bugman, Timothy R. Carter, Carlos A. Gracia, Anne C. de la Vega-Leinert, Markus Erhard, Frank Ewert, Margaret Glendining, Joanna I, Ecosystem Service Supply and Vulnerability to Global Change in Europe, 2005. doi:10.1126/science.1115233.
[11] European Commission, P.O. of the E. Union, Nature-based solutions & re-naturing cities. Final report of the horizon 2020 expert group on 'Nature-based solutions and re-naturing cities' (full version), 2015. doi:10.2777/765301.
[12] IUCN, 2012 IUCN Annual report: Nature+ Nature-Based Solutions, 2012. doi:10.1111/epp.12066.
[13] European Commission, Horizon 2020, (n.d.). https://ec.europa.eu/programmes/horizon2020/en.
[14] N. Mestre, NBS: (No más) soluciones (tan) basadas en la naturaleza. Metabolismos, ecosistemas y otra naturaleza envasada., (n.d.) 46–51.
[15] C.M. Raymond, B. Pam, M. Breil, M.R. Nita, N. Kabisch, M. de Bel, V. Enzi,

N. Frantzeskaki, D. Geneletti, M. Cardinaletti, L. Lovinger, C. Basnou, A. Monteiro, H. Robrecht, G. Sgrigna, L. Munari, C. Calfapietra, An Impact Evaluation Framework to Support Planning and Evaluation of Nature-based Solutions Projects, 2017. doi:10.13140/RG.2.2.18682.08643.

[16] S. Charoenkit, S. Yiemwattana, Living walls and their contribution to improved thermal comfort and carbon emission reduction: A review, Build. Environ. 105 (2016) 82–94. doi:10.1016/j.buildenv.2016.05.031.

[17] L. Chen, C. Liu, R. Zou, M. Yang, Z. Zhang, Experimental examination of effectiveness of vegetation as bio-filter of particulate matters in the urban environment, Environ. Pollut. 208 (2016) 198–208. doi:10.1016/j.envpol.2015.09.006.

[18] A. Przybysz, A. Sæbø, H.M. Hanslin, S.W. Gawroński, Accumulation of particulate matter and trace elements on vegetation as affected by pollution level, rainfall and the passage of time, Sci. Total Environ. 481 (2014) 360–369. doi:10.1016/j.scitotenv.2014.02.072.

[19] R. Szep, R. Keresztes, G. Deak, F. Toba, M. Ghimpusan, The dry deposition of the PM10 and PM2.5to the vegetation and its health effect in the ciuc basin, Rev. Chim. 67 (2016) 639–644. https://www.scopus.com/inward/record.uri?eid=2-s2.0-84981347693&partnerID=40&md5=766b32d9f7eddb9138238176995ecc15.

[20] W. Kuttler, A. Strassburger, Air quality measurements in urban green areas - A case study, Atmos. Environ. 33 (1999) 4101–4108. doi:10.1016/S1352-2310(99)00151-X.

[21] N.C.N.H. Wong, A.Y. Kwang Tan, Y. Chen, K. Sekar, P.Y. Tan, D. Chan, K. Chiang, N.C.N.H. Wong, Thermal evaluation of vertical greenery systems for building walls, Build. Environ. 45 (2010) 663–672. doi:10.1016/j.buildenv.2009.08.005.

[22] L. Mariani, S.G. Parisi, G. Cola, R. Lafortezza, G. Colangelo, G. Sanesi, Climatological analysis of the mitigating effect of vegetation on the urban heat island of Milan, Italy, Sci. Total Environ. 569–570 (2016) 762–773. doi:10.1016/j.scitotenv.2016.06.111.

[23] S. Nadia, S. Noureddine, N. Hichem, D. Djamila, Experimental study of thermal performance and the contribution of plant-covered walls to the thermal behavior of building, Energy Procedia. 36 (2013) 995–1001. doi:10.1016/j.egypro.2013.07.113.

[24] A. Price, E.C. Jones, F. Jefferson, Vertical Greenery Systems as a Strategy in Urban Heat Island Mitigation, Water. Air. Soil Pollut. 226 (2015). doi:10.1007/s11270-015-2464-9.

[25] I. Karakounos, A. Dimoudi, S. Zoras, The influence of bioclimatic urban redevelopment on outdoor thermal comfort, Energy Build. 158 (2018) 1266–1274. doi:10.1016/j.enbuild.2017.11.035.

[26] A.M. Lacasta, A. Peñaranda, I.R. Cantalapiedra, Green streets for noise reduction, Nat. Based Strateg. Urban Build. Sustain. (2018) 181–190. doi:10.1016/B978-0-12-812150-4.00017-3.

[27] N. Fernández-Bregón, M. Urrestarazu, D.L. Valera, N. Fernandez-Bregon, M.

Urrestarazu, D.L. Valera, N. Fernández-Bregón, M. Urrestarazu, D.L. Valera, Effects of a vertical greenery system on selected thermal and sound mitigation parameters for indoor building walls, J. Food, Agric. Environ. 10 (2012) 1025–1027. doi:1025-1027. 2012.

[28] R. Bullen, F. Fricke, Sound propagation through vegetation, J. Sound Vib. 80 (1982) 11–23. doi:10.1016/0022-460X(82)90387-X.

[29] T. Van Renterghem, D. Botteldooren, K. Verheyen, Road traffic noise shielding by vegetation belts of limited depth, J. Sound Vib. 331 (2012) 2404–2425. doi:https://doi.org/10.1016/j.jsv.2012.01.006.

[30] M. Hornikx, T. Van Renterghem, The potential of vegetation for reducing road traffic noise at urban quiet sides, in: Proc. - Eur. Conf. Noise Control, 2012: pp. 949–954. http://www.scopus.com/inward/record.url?eid=2-s2.0-84866000235&partnerID=tZOtx3y1.

[31] A. Afshari, A new model of urban cooling demand and heat island—application to vertical greenery systems (VGS), Energy Build. 157 (2017) 204–217. doi:10.1016/j.enbuild.2017.01.008.

[32] D.H.S. Duarte, P. Shinzato, C. dos S. Gusson, C.A. Alves, The impact of vegetation on urban microclimate to counterbalance built density in a subtropical changing climate, Urban Clim. 14 (2015) 224–239. doi:10.1016/j.uclim.2015.09.006.

[33] C.Y. Jim, H. He, Estimating heat flux transmission of vertical greenery ecosystem, Ecol. Eng. 37 (2011) 1112–1122. doi:10.1016/j.ecoleng.2011.02.005.

[34] T.A. Moya, A. van den Dobbelsteen, M. Ottelé, P.M. Bluyssen, A review of green systems within the indoor environment, Indoor Built Environ. 0 (2018) 1–12. doi:10.1177/1420326X18783042.

[35] C. Bartesaghi Koc, P. Osmond, A. Peters, Evaluating the cooling effects of green infrastructure: A systematic review of methods, indicators and data sources, Sol. Energy. 166 (2018) 486–508. doi:10.1016/j.solener.2018.03.008.

[36] P.M.F. van de Wouw, E.J.M. Ros, H.J.H. Brouwers, Precipitation collection and evapo(transpi)ration of living wall systems: A comparative study between a panel system and a planter box system, Build. Environ. 126 (2017) 221–237. doi:10.1016/j.buildenv.2017.10.002.

[37] P. Panels, E. Cubi, N.F. Zibin, S.J. Thompson, J. Bergerson, Sustainability of Rooftop Technologies in Cold Climates, 20 (2015) 249–262. doi:10.1111/jiec.12269.

[38] Z. Azkorra, G. Pérez, J. Coma, L.F. Cabeza, S. Bures, J.E. Álvaro, A. Erkoreka, M. Urrestarazu, G. P??rez, J. Coma, L.F. Cabeza, S. Bures, J.E. ??lvaro, A. Erkoreka, M. Urrestarazu, Evaluation of green walls as a passive acoustic insulation system for buildings, Appl. Acoust. 89 (2015) 46–56. doi:10.1016/j.apacoust.2014.09.010.

[39] I. Susorova, M. Angulo, P. Bahrami, Brent Stephens, A model of vegetated exterior facades for evaluation of wall thermal performance, Build. Environ. 67 (2013) 1–13. doi:https://doi.org/10.1016/j.buildenv.2013.04.027.

[40] F. Olivieri, D. Redondas, L. Olivieri, J. Neila, Experimental characterization

and implementation of an integrated autoregressive model to predict the thermal performance of vegetal fa??ades, Energy Build. 72 (2014) 309–321. doi:10.1016/j.enbuild.2013.12.062.

[41] J. Alonso, F. Olivieri, J. Neila, C. Bedoya, Hygrothermal performance of vegetation on cladding and translucent fa?ade systems, PLEA 2011 - Archit. Sustain. Dev. Conf. Proc. 27th Int. Conf. Passiv. Low Energy Archit. (2011) 13–15.

[42] A.M. Omer, Renewable building energy systems and passive human comfort solutions, Renew. Sustain. Energy Rev. 12 (2008) 1562–1587. doi:10.1016/j.rser.2006.07.010.

[43] C. Nesshöver, T. Assmuth, K.N. Irvine, G.M. Rusch, K.A. Waylen, B. Delbaere, D. Haase, L. Jones-walters, H. Keune, E. Kovacs, K. Krauze, M. Külvik, F. Rey, J. Van Dijk, O. Inge, M.E. Wilkinson, H. Wittmer, Science of the Total Environment The science , policy and practice of nature-based solutions : An interdisciplinary perspective, Sci. Total Environ. 579 (2017) 1215–1227. doi:10.1016/j.scitotenv.2016.11.106.

[44] The Economics of Ecosystems and Biodiversity, The Economics of Ecosystems and Biodiversity, (n.d.).

[45] D.J. Teece, Business Models, Business Strategy and Innovation, Long Range Plann. 43 (2010) 172–174.

[46] O. Alexander, Clarifying Business Models: Origins, Present, and Future of the Concept, Commun. Assoc. Inf. Syst. (2005).

[47] T.S. Nicolai J Foss, Fifteen Years of Research on Business Model Innovation: How Far Have We Come, and Where Should We Go?, J. Manage. (2016).

[48] Habitat III Secretariat, United Nations, The New Urban Agenda, 2017. http://habitat3.org/wp-content/uploads/NUA-English.pdf.

[49] City of Zagreb, The City of Zagreb Development Strategy for the period leading up to 2020, (2017). https://www.zagreb.hr/UserDocsImages/gu za strategijsko planiranje/RSZG 2020 _ ENG_digital.pdf.

[50] Mairie de Paris, Paris Resilience Strategy, (n.d.).

[51] City of Melbourne, Emissions reduction plan for our operations 2016 - 2021, (2016). https://www.melbourne.vic.gov.au/about-council/vision-goals/eco-city/Pages/emissions-reduction-plan.aspx.

[52] W. Duván, Z. Ramírez, Ante El Cambio Climático, (2015).

[53] M. ambiente y movilidad-A. de Madrid, Madrid + Natural. Soluciones naturales para adaptarnos al Cambio Climático, n.d.

[54] Ayuntamiento de Madrid, Plan A: Plan de Calidad del Aire y Cambio Climático de la Ciudad de Madrid, n.d.

[55] Sistema Biofiver, (n.d.).

[56] ONSET, HOBO MX2301A Temperature/RH Data Logger, (n.d.).